

USAF-TPS-CUR-86-01

(1)

USAF TEST PILOT SCHOOL
PERFORMANCE
PHASE
TEXTBOOK
VOLUME I

AD-A170 957

DTIC
ELECTED
AUG 14 1986
S
A

"Approved for Public Release: Distribution is Unlimited"

DTIC FILE COPY

APRIL 1986

Vol 2-pt 1-AD-A170959
Vol 2-pt 2-AD-A170960

EDWARDS AFB, CALIFORNIA

Table of Contents

<u>Chapter</u>	<u>Page</u>
1 Introduction to Performance Analysis & Testing	
2 Fundamentals of Aerodynamics	
2.1 Introduction	2.1
2.2 The Atmosphere - Basic Properties.	2.1
2.2.1 Static Properties.	2.2
2.2.2 Temperature.	2.2
2.2.3 Density.	2.3
2.2.4 Equation of State.	2.4
2.2.5 Velocity	2.5
2.2.6 Viscosity.	2.5
2.3 Technical Notations and Definitions.	2.6
2.4 Aerodynamic Flight Regimes	2.7
2.5 Fluid Flow Equations	2.8
2.6 Aerodynamic Forces	2.11
2.6.1 Dimensional Analysis	2.12
2.6.2 Buckingham π Theorem	2.12
2.6.3 Turning Flow	2.16
2.7 Viscosity.	2.18
2.7.1 Coefficient of Viscosity	2.18
2.7.2 Nature of Viscosity.	2.20
2.7.3 Boundary Layer	2.24
2.7.4 Reynolds Number.	2.27
2.7.5 Boundary Layer Growth and Transition	2.30
2.7.6 Velocity Profiles.	2.33
2.7.7 Skin Friction.	2.34
2.7.8 Separation and Pressure Gradient	2.35
2.8 Summary.	2.39
3 Airfoil and Wing Theory	
3.1 Introduction	3.1
3.2 Airfoil Terminology.	3.1
3.3 Airfoil Section Designation.	3.3
3.3.1 Four-Digit Series.	3.4
3.3.2 Five-Digit Series.	3.4
3.3.3 The 1-series Airfoils.	3.6
3.3.4 The 6-series Airfoils.	3.7
3.3.5 The 7-series Airfoils.	3.8
3.3.6 Supersonic Section	3.9
3.3.7 Other Airfoil Designation Systems.	3.10
3.4 Wing Terminology	3.11
3.5 Aircraft Reference System.	3.14
3.6 Infinite Span Wing Theory.	3.15
3.7 Finite Span Wing Theory.	3.19
3.8 Aerodynamic Coefficients	3.22
3.9 Forces on an Aircraft.	3.23
3.10 Pressure Distribution.	3.24
3.11 The Lift Curve	3.29

Table of Contents (continued)

<u>Chapter</u>	<u>Page</u>
3.12 Zero Lift Line	3.31
3.13 Variables Affecting Lift Curve	3.31
3.13.1 Lift Curve Variation with Mach Number	3.32
3.13.2 Lift Curve Variation with Reynolds Number.	3.34
3.13.3 Lift Curve Variation with Wing Section	3.36
3.13.4 Lift Curve Variation with Wing Planform.	3.37
3.13.5 Lift Curve Variation with Aspect Ratio	3.38
3.14 Flight Test Lift Curve Determination	3.43
3.15 Variation in Stall Speed with Altitude	3.44
3.16 High Lift Devices.	3.46
3.16.1 Flaps	3.46
3.16.1.1 Trailing Edge Flaps.	3.46
3.16.1.2 Leading Edge Flaps	3.49
3.16.2 Boundary Layer Control (BLC).	3.50
3.16.2.1 Slot	3.50
3.16.2.2 Slat	3.51
3.16.2.3 Blowing and Suction.	3.52
3.16.2.4 Vortex Generators.	3.54
3.17 Aerodynamic Moments.	3.55
3.17.1 Symmetric Airfoils.	3.56
3.17.2 Cambered Airfoils	3.57
3.17.3 Properties of Moments	3.58
3.17.4 Variables Affecting $C_{m_{ac}}$	3.61
3.17.5 Summary	3.62
 4 Aerodynamic Drag	
4.1 Introduction	4.1
4.2 Skin Friction Drag	4.1
4.3 Pressure Drag.	4.4
4.3.1 Reynolds Number Effect on Pressure Drag	4.6
4.3.2 Boundary Layer Control	4.9
4.4 Profile Drag	4.9
4.5 Interference Drag.	4.14
4.6 Parasite Drag.	4.15
4.6.1 Drag Counts.	4.15
4.6.2 Equivalent Flat Plate Area	4.16
4.7 Induced Drag	4.17
4.7.1 Effect of Planform on Induced Drag	4.21
4.7.2 Effect of Load Factor on Induced Drag.	4.22
4.7.3 Reducing Induced Drag.	4.24
4.8 Wave Drag.	4.25
4.9 Miscellaneous Types of Drag.	4.26
4.9.1 Ram Drag	4.26
4.9.2 Cooling Drag	4.26
4.9.3 Trim Drag.	4.26
4.10 Total Drag	4.26
4.11 Summary of Major Drag Categories	4.27

Table of Contents (continued)

<u>Chapter</u>		<u>Page</u>
4.12	The Drag Polar	4.28
4.12.1	Variables Affecting Drag Coefficient	4.31
4.12.1.1	Drag Polar Variation with Mach	4.31
4.12.1.2	Drag Polar Variation with Reynolds Number.	4.32
4.12.1.3	Drag Polar Variation with Oswald's Efficiency Factor	4.33
4.12.1.4	Drag Polar Variation with Aspect Ratio	4.34
4.12.2	Effect of Flaps on the Drag Polar	4.35
4.12.3	Lift Drag Ratio	4.36
4.13	Flight Test Drag Polar Determination	4.38
4.14	Drag Effects on Level Flight Performance	4.40
4.15	Laminar Flow Airfoils.	4.46
5	Pitot-Static Fundamentals and the Standard Atmosphere	
5.1	Introduction	5.1
5.2	Divisions and Limits of the Atmosphere	5.1
5.3	Standard Atmosphere.	5.4
5.3.1	Equations for the Standard Atmosphere	5.6
5.3.2	The Measurement of Altitude	5.8
5.3.3	Pressure Variation with Altitude.	5.9
5.4	Altimeter Theory	5.12
5.5	Airspeed System Theory	5.14
5.5.1	Incompressible Airspeed Theory	5.14
5.5.2	Compressible True Airspeed Theory.	5.18
5.5.3	Calibrated Airspeed.	5.21
5.5.4	Equivalent Airspeed.	5.24
5.5.5	Determining V_t from Flight Test Data	5.24
5.6	Machmeter Theory	5.26
5.7	Instrument Error Theory and Calibration.	5.28
5.7.1	Pressure Lag Error	5.31
5.7.2	Position Error	5.32
5.7.2.1	Total Pressure Error	5.32
5.7.2.2	Static Pressure Error.	5.33
5.7.2.3	Definition of Position Error	5.35
5.7.2.4	Low Mach Effects	5.38
5.7.2.5	Medium Subsonic and Transonic Mach Effects	5.41
5.7.2.6	Supersonic Mach Effects.	5.43
5.7.2.7	Extrapolation of Results	5.43
5.7.2.8	Presentation of Position Error Correction	5.46
5.8	Pitot-Static System Types.	5.48
5.8.1	Fuselage Mounted Systems	5.48
5.8.2	Noseboom Systems	5.48
5.8.3	Wingboom Systems	5.49
5.8.4	Compensated Systems.	5.49
5.9	Free Air Temperature Measurement	5.49

Table of Contents (continued)

<u>Chapter</u>		<u>Page</u>
	5.9.1 Determination of Temperature Probe Recovery Factor.	5.53
5.10	Pitot-Static Calibration Tests	5.55
	5.10.1 The Tower Fly-by Test	5.55
	5.10.2 The Pacer Test.	5.57
	5.10.3 The Speed Course.	5.57
	5.10.4 Radar Method.	5.58
	5.10.5 Smoke Trail Method.	5.60
	5.10.6 Trailing Bomb Method.	5.60
	5.10.7 Trailing Cone Method.	5.62
	5.10.8 Data Cards.	5.63
	5.10.9 Techniques.	5.64
6	Supersonic Aerodynamics	
6.1	Introduction	6.1
6.2	Types of Ideal Gases	6.1
6.3	Aerodynamic Consideration of Compressible Flow.	6.2
6.4	One-Dimensional Flow Approximation	6.3
6.5	Total (Stagnation) Properties.	6.5
	6.5.1 Total Temperature.	6.6
	6.5.2 Total Pressure	6.8
	6.5.3 Total Density.	6.8
	6.5.4 Mathematical Relationships for Total Properties	6.8
6.6	Speed of Sound	6.9
6.7	Mach	6.11
6.8	Two-Dimensional Propagation of Sound Waves.	6.13
	6.8.1 Mach Angles.	6.13
	6.8.2 Activity Envelope.	6.15
6.9	Classification of Speed Ranges	6.16
6.10	Isentropic Flow.	6.16
6.11	Flow in Convergent-Divergent Streamtubes	6.21
	6.11.1 Flow at the Throat.	6.26
	6.11.2 Mass Flow in a Choked Streamtube.	6.29
	6.11.3 Local Sonic Conditions.	6.30
	6.11.4 M^*	6.31
	6.11.5 Area Ratio.	6.32
6.12	Normal Shock Waves	6.33
	6.12.1 Normal Shock Equations.	6.34
	6.12.2 Normal Shock Summary.	6.35
6.13	Supersonic Pitot Tube.	6.35
6.14	Oblique Shock Waves.	6.37
	6.14.1 Oblique Shock Relations	6.41
	6.14.2 Minimum and Maximum Wave Angles	6.43
	6.14.3 Relation Between θ and δ	6.44
	6.14.4 Mach Lines.	6.47
6.15	Isentropic Compression	6.47
6.16	Isentropic Expansion	6.49
6.17	Interaction of Wave Forms.	6.57
6.18	Two-Dimensional Supersonic Airfoils.	6.60

Table of Contents (continued)

<u>Chapter</u>		<u>Page</u>
6.19	Pressure Coefficient for Two-Dimensional Supersonic Airfoils and Infinite Wings	6.62
6.20	Thin Wing Theory	6.64
6.21	Supersonic Flow in Three Dimensions.	6.67
6.22	Three-Dimensional Supersonic Wings	6.69
6.23	Transonic Flow Regime.	6.71
	6.23.1 Thickness	6.73
	6.23.2 Supercritical Airfoils.	6.76
	6.23.3 Wing Sweep.	6.76
	6.23.4 Fuselage Shape and Area Rule.	6.79
	6.23.5 Transonic and Supersonic Control Surfaces.	6.84
6.24	Summary.	6.85
7	Aero Propulsion	
7.1	Introduction	7.1
7.2	The Flight Spectrum.	7.1
7.3	Principle of Jet Propulsion.	7.4
	7.3.1 The Basic Gas Turbine Engine	7.4
7.4	Engine Classification.	7.7
	7.4.1 The Ramjet Engine.	7.7
	7.4.2 The Turbojet Engine.	7.9
	7.4.3 The Turboprop or Turboshaft Engine	7.12
	7.4.4 The Turbofan Engine.	7.14
7.5	Thrust	7.17
7.6	Factors Affecting Thrust	7.21
	7.6.1 Ram Effect	7.22
	7.6.2 Altitude Effect.	7.23
7.7	Simple Cycle Analysis.	7.24
	7.7.1 Engine Station Designations.	7.24
	7.7.2 Basic Equations and Processes.	7.25
	7.7.3 The Ideal Cycle.	7.28
	7.7.3.1 Note on Temperature Measurements	7.31
	7.7.4 Thermal Efficiency	7.31
	7.7.5 Ideal Turbojet Performance	7.37
	7.7.5.1 Ideal Turbojet Cycle Analysis	7.38
	7.7.5.2 Propulsive Efficiency.	7.44
	7.7.5.3 Overall Efficiency	7.46
	7.7.5.4 Ideal Turbojet Trends: Net Thrust	7.46
	7.7.5.5 Ideal Turbojet Trends: Thrust Specific Fuel Consumption.	7.49
	7.7.6 Ideal Turbofan Performance	7.51
	7.7.6.1 Turbofan Operation	7.51
	7.7.6.2 Variation in TSFC of a Turbofan With Mach	7.55
	7.7.6.3 The Variable Cycle Engine.	7.56
	7.7.6.4 Ideal Turbofan Cycle Analysis	7.57

Table of Contents (continued)

<u>Chapter</u>		<u>Page</u>
	7.7.7 Comparison of the Cycle Turbojet and Turbofan Ideal Cycle	7.62
	7.7.8 Comparison of Turbojet and Turbofan Engines	7.62
7.8	Engine Components.	7.64
	7.8.1 Air Inlet Duct	7.65
	7.8.2 Diffuser	7.66
	7.8.2.1 Subsonic Diffuser.	7.66
	7.8.2.2 Subsonic Duct Losses	7.70
	7.8.2.3 Supersonic Diffusers	7.70
	7.8.2.3.1 Normal Shock Inlets	7.72
	7.8.2.3.2 Internal Compression Inlets	7.76
	7.8.2.3.3 External Compression Inlets	7.78
	7.8.2.3.4 Mixed Compression Inlets	7.79
	7.8.2.4 Mass Flow.	7.81
	7.8.2.5 Modes of Supersonic Diffuser Operation.	7.87
	7.8.2.6 Other Supersonic Diffuser Performance Parameters	7.89
	7.8.3 Compressors.	7.92
	7.8.3.1 General Thermodynamic Energy Analysis.	7.93
	7.8.3.2 Centrifugal Compressors.	7.95
	7.8.3.3 Axial Flow Compressors	7.98
	7.8.3.4 Principle of Operation and Basic Terms.	7.99
	7.8.3.5 Velocity Vector Analysis	7.100
	7.8.3.6 Dual Axial Compressors	7.103
	7.8.3.7 Compressor Performance Charts.	7.104
	7.8.3.8 Compressor Stall	7.106
	7.8.3.9 Methods of Increasing Stall Margin	7.108
	7.8.4 Combustion Chambers.	7.109
	7.8.4.1 Combustor Operation.	7.110
	7.8.4.2 Combustion Process and Efficiency.	7.112
	7.8.4.3 Fuel Control Units	7.114
	7.8.4.3.1 Digital Electronic Engine Control	7.114
	7.8.5 Gas Turbines	7.115
	7.8.5.1 Turbine Design Considerations.	7.117
	7.8.5.2 General Thermodynamic Analysis	7.119
	7.8.5.3 Velocity Vector Analysis	7.122
	7.8.5.4 Improvement of Turbine Inlet Temperature.	7.123
	7.8.5.4.1 Materials Considerations	7.123
	7.8.5.4.2 Turbine Blade Cooling.	7.124
	7.8.5.5 Engine Internal Temperature Control	7.128
	7.8.6 Exhaust Duct/Nozzle.	7.128
	7.8.6.1 Convergent Exhaust Nozzle.	7.128



Availability Codes	
Dist	Special
A-1	

Table of Contents (continued)

<u>Chapter</u>		<u>Page</u>
	7.8.6.2 Convergent - Divergent Exhaust Nozzle	7.129
	7.8.6.3 Variable Area Nozzles.	7.129
	7.8.6.4 Two-Dimensional Nozzles.	7.130
	7.8.6.5 Jet Nozzle Velocity.	7.130
	7.8.6.6 Nozzle Efficiency.	7.130
	7.8.7 Thrust Augmentation.	7.132
	7.8.7.1 The Afterburner.	7.132
	7.8.7.1.1 Afterburner Performance.	7.134
	7.8.7.1.2 Afterburner Screech Liners	7.136
	7.8.7.1.3 Rumble	7.137
	7.8.7.2 Water Injection.	7.137
	7.8.7.3 Summary of Thrust Augmentation Devices	7.138
7.9	Overall Engine Analysis.	7.139
	7.9.1 Effect of Humidity on Engine Performance.	7.142
	7.9.2 Thrust Horsepower.	7.142
	7.9.3 Specific Impulse	7.142
7.10	Engine Operational Characteristics	7.143
	7.10.1 Advantages and Disadvantages of the Turbojet	7.143
	7.10.2 Turboprop Characteristics	7.143
	7.10.2.1 The Turboprop Propellor.	7.146
	7.10.3 The Turbofan Engine	7.147
7.11	Propellor Theory	7.150
	7.11.1 Momentum Theory	7.152
	7.11.2 Blade Element Theory.	7.154
	7.11.3 Vortex Theory	7.156
	7.11.4 Propellor Performance	7.158
	7.11.5 Propellor Wind Tunnel Testing	7.160
	7.11.6 The Effects of Blade Geometry on Propellor Characteristics.	7.163
	7.11.6.1 Blade Width.	7.163
	7.11.6.2 Number of Blades	7.163
	7.11.6.3 Blade Thickness.	7.163
	7.11.6.4 Blade Section.	7.164
	7.11.6.5 Planform	7.164
	7.11.6.6 Blade Tips	7.164
	7.11.7 Shrouded Propellers	7.165
	7.11.7.1 Method of Singularities.	7.166
	7.11.7.2 Momentum Methods	7.167
	7.11.7.3 Other Methods.	7.168
	7.11.8 Shrouded Fans	7.168
	7.11.9 F.A.A. Certification Requirements	7.170
	7.11.10 Ground Testing	7.170
	7.11.11 Flight Testing	7.171
	7.11.12 Advanced Design Propellers	7.173
7.12	Propulsion System Testing.	7.175
	7.12.1 Propulsion Flight Test Categories.	7.175
	7.12.2 Installed Ground Tests	7.176
	7.12.2.1 Ground Starting	7.176
	7.12.3 Throttle Transients.	7.177
	7.12.4 Climbs and Descents.	7.180

Table of Contents (continued)

<u>Chapter</u>	<u>Page</u>
7.12.5 Airstarts.	7.180
7.12.6 Engine Handling and Response	7.184
7.12.7 Gas Ingestion.	7.185
 8 Takeoff and Landing Performance	
8.1 Introduction	8.1
8.2 Takeoff Theory	8.1
8.2.1 Method of Development.	8.1
8.2.2 Forces (Ground Phase).	8.2
8.2.3 Ground Roll Equation	8.3
8.2.4 Shortening the Ground Roll	8.4
8.2.5 Air Phase Equation	8.6
8.3 Landing Theory	8.7
8.3.1 Ground Distance Equation	8.7
8.3.2 Shortening the Landing Roll.	8.8
8.3.3 Air Distance Equation.	8.9
8.4 Corrections to Standard Conditions	8.10
8.4.1 Wind	8.10
8.4.2 Runway Slope	8.11
8.4.3 Thrust, Weight, and Density.	8.12
8.4.4 Pilot Technique.	8.13
8.4.5 Landing Data Corrections	8.14
8.5 Flight Test.	8.15
8.5.1 High Speed Taxi Tests.	8.16
8.5.2 Takeoff Tests.	8.16
8.5.3 Landing Tests.	8.17
8.5.4 Safety	8.17
8.5.5 Data Recording Methods	8.18
8.5.6 Standardization Technique.	8.19
8.5.7 Summary.	8.20
 9 Energy Concepts	
9.1 Introduction	9.1
9.1.1 Aircraft Performance Models.	9.1
9.1.2 Need for Nonsteady State Models.	9.2
9.2 Steady State Climbs and Descents	9.2
9.2.1 Forces Acting on an Aircraft in Flight.	9.2
9.2.2 Angle of Climb Performance	9.5
9.2.3 Rate of Climb Performance.	9.7
9.2.4 Time to Climb Determination.	9.10
9.2.5 Gliding Performance.	9.11
9.2.6 Polar Diagrams	9.14
9.3 Basic Energy State Concepts.	9.17
9.3.1 Assumptions.	9.17
9.3.2 Energy Definitions	9.18
9.3.3 Specific Energy.	9.18
9.3.4 Specific Excess Power.	9.19
9.4 Theoretical Basis for Energy Optimizations.	9.20
9.4.1 Maxima and Minima.	9.20

Table of Contents (continued)

<u>Chapter</u>		<u>Page</u>
	9.4.2 Basic Problems of the Calculus of Variations.	9.22
	9.4.3 Application of the Euler Equations.	9.23
9.5	Graphical Tools for Energy Approximation.	9.24
	9.5.1 Specific Energy Overlay.	9.25
	9.5.2 Specific Excess Power Plots.	9.27
9.6	Time Optimal Climbs.	9.31
	9.6.1 Graphical Approximations to Rutowski Conditions.	9.31
	9.6.2 Minimum Time to Energy Level Profiles	9.32
	9.6.3 Subsonic to Supersonic Transitions.	9.33
9.7	Fuel Optimal Climbs.	9.36
	9.7.1 Fuel Efficiency.	9.36
	9.7.2 Maneuver Energy	9.39
	9.7.3 Path Independent Maneuver Energy Diagrams.	9.39
	9.7.4 Path Dependent Maneuver Energy Diagram	9.40
	9.7.5 Maneuver Energy and Persistency.	9.41
	9.7.6 Comparison of Fuel Optimal and Time Optimal Paths	9.41
9.8	Maneuverability.	9.42
	9.8.1 Instantaneous Maneuverability.	9.42
	9.8.2 Sustained Maneuverability.	9.44
	9.8.3 Effect of Load Factor on P_s Contours.	9.45
9.9	Comparison Techniques and Tools.	9.47
	9.9.1 P_s Overlays.	9.47
	9.9.2 Differential P_s Charts	9.48
	9.9.3 P_s Versus Turn Rate.	9.50
	9.9.4 P_s Versus True Airspeed/Mach	9.53
	9.9.5 Rate-Radius Diagrams	9.57
9.10	Profile Optimization	9.60
	9.10.1 Maximum Range Climb	9.60
	9.10.2 Maximum Range for Given Fuel.	9.62
	9.10.3 Maximum Range at Fixed Throttle.	9.62
	9.10.4 Maximum Range Profile	9.63
9.11	Operational Applications to Transport Operations	9.65
9.12	Data Collection for Energy Methods	9.68
	9.12.1 Measurement Techniques.	9.68
	9.12.1.1 Pressure Methods	9.68
	9.12.1.2 Position Measurements.	9.69
	9.12.1.3 Optical Tracking (OT).	9.69
	9.12.1.4 Laser Tracking (LT).	9.69
	9.12.1.5 Acceleration Measurements	9.69
	9.12.2 Relative Merits	9.70
9.13	Climb and Descent Tests	9.71

Table of Contents (continued)

<u>Chapter</u>	<u>Page</u>
9.13.1 Sawtooth Climb Test	9.71
9.13.2 Level Flight Acceleration Test.	9.72
9.13.2.1 Method	9.73
9.13.2.2 Preflight Preparation.	9.73
9.13.2.3 Uses	9.74
9.13.2.4 Limitations.	9.74
9.13.3 Check Climb Test for Jet Aircraft.	9.74
9.13.3.1 Preflight Preparation.	9.75
9.13.3.2 Flight Techniques.	9.76
9.13.4 Reciprocating Engine Check Climb Test.	9.78
9.14 Summary.	9.78
 10 Turn Performance	
10.1 Introduction	10.1
10.2 The V-n Diagram.	10.1
10.2.1 Lift Boundary Limitation.	10.2
10.2.2 Structural Limitations.	10.2
10.2.3 g Limitation.	10.3
10.3 Pilot Limitations.	10.3
10.4 Thrust Limitations	10.3
10.5 Sustained Turn Performance	10.4
10.6 Forces in a Turn	10.4
10.7 Turning Performance Charts	10.7
10.8 Thrust and Drag Analysis in a Turn	10.12
10.9 Turning Performance Tests.	10.14
10.9.1 Stabilized Turn Method.	10.14
10.9.1.1 Stable g Method.	10.15
10.9.1.2 Constant Airspeed Method	10.15
10.9.1.3 Timed Turn Method.	10.15
10.9.2 Level Acceleration Method	10.16
 11 Cruise Performance	
11.1 Cruise Performance Theory.	11.1
11.2 Lift and Drag Functional Relationships.	11.2
11.3 Engine Parameter Functional Relationships.	11.6
11.4 Engine Thrust Curves	11.7
11.5 Engine-Airplane Functional Combinations.	11.9
11.6 Endurance, Jet Aircraft	11.12
11.7 Range, Jet Aircraft	11.15
11.8 The Cruise Climb.	11.19
11.9 Drag Polar Determination.	11.26
11.10 Variable Geometry and Dual Rotor Engines	11.26
11.11 Propeller-Driven Aircraft Cruise Theory	11.28

Table of Contents (continued)

<u>Chapter</u>	<u>Page</u>
11.12 Propeller - Driven Aircraft	
Endurance and Range	11.37
11.12.1 Range.	11.38
11.12.2 Endurance.	11.40
11.13 Cruise Performance Testing.	11.41
12 Data Reduction and Corrections to Standard Day	
12.1 Introduction.	12.1
12.2 Standard Conditions	12.1
12.2.1 Atmospheric Conditions.	12.1
12.2.2 Weight.	12.2
12.2.3 Center of Gravity (CG).	12.2
12.2.4 Wind.	12.3
12.2.5 Configuration	12.3
12.2.6 Schedules and Techniques.	12.3
12.2.7 Other Considerations.	12.3
12.3 Pitot-Static Data Reduction	12.3
12.3.1 Tower Fly-by Data Reduction	12.3
12.3.2 Pacer Data Reduction.	12.9
12.3.3 Radar Data Reduction.	12.10
12.3.4 Speed Course Data Reduction	12.11
12.4 Takeoff Data Reduction.	12.12
12.5 Energy Method Data Reductions	12.17
12.5.1 Excess Thrust	12.17
12.5.2 Determination of F_{ex}	12.19
12.5.3 Correction to Standard Conditions	12.20
12.5.4 Climb Performance Data Reduction Using Step-by-Step Method	12.20
12.5.4.1 General	12.20
12.5.4.2 Tapeline Altitudes.	12.21
12.5.4.3 True Speed and Thrust Correction.	12.24
12.5.4.4 $\Delta R/C$, Determination	12.27
12.5.4.5 Wind Correction	12.27
12.5.4.6 Accelerator Error	12.30
12.5.4.7 Weight Corrections.	12.31
12.5.4.8 Summary	12.33
12.5.5 Descent Performance Data Reduction Using Step-by-Step Methods.	12.34
12.5.5.1 Thrust Correction	12.34
12.5.5.2 Weight Correction	12.34
12.5.6 Standardization of Excess Thrust.	12.35
12.5.7 Level Acceleration and Sawtooth Climb Data Reduction.	12.37
12.5.8 Check Climb Data Reduction.	12.43
12.5.9 Turn Performance Data Reduction	12.52
12.6 Cruise Performance Data Reduction	12.54
12.6.1 Speed-Power Test, Constant W/6 Method	12.55
12.6.1.1 Preflight Preparation	12.56
12.6.1.2 In-flight Techniques.	12.59
12.6.1.3 W/6 Data Reduction.	12.60
12.6.1.4 Drag Polar Determination.	12.65
12.6.2 Range Cruise Control Test	12.66

Table of Contents (continued)

<u>Chapter</u>		<u>Page</u>
	12.6.2.1 Inflight Techniques	12.68
<i>Chapter 13 Data Analysis</i>	12.6.2.2 Ferry Range Data Reduction.	12.69
Appendix A	Glossary of Terms and Symbols	A.1
Appendix B	U.S. Standard Atmosphere, 1962	B.1
Appendix C1	Pitot-Static Position Error Relations	C.1.1
Appendix C2	Pitot-Static Charts	C.2.1
Appendix D	Charts of Interest for the USAF Test Pilot School	D.1
Appendix E	Distribution Tables	E.1
Appendix F	Derivations	F.1

List of Figures

<u>Figure</u>		<u>Page</u>
2.1	Flow of Air Through a Venturi.	2.8
2.2	Turning Flow Model	2.17
2.3	Deformation of a Solid Cube.	2.18
2.4	Laminar Flow Mechanism	2.19
2.5	Two Planes of Fluid.	2.20
2.6	Mechanism of Viscous Force Development	2.21
2.7	Developed Velocity Gradient.	2.22
2.8	Fully Developed Uniform Flow	2.22
2.9	Exaggerated Boundary Layer Thickness	2.25
2.10	Velocity Profile in the Boundary Layer	2.26
2.11	Development of the Boundary Layer.	2.27
2.12	Boundary Layer Transition Over a Flat Plate	2.32
2.13	Boundary Layer Velocity Profiles on a Flat Plate	2.33
2.14	Boundary Layer Velocity Profiles	2.35
2.15	Upper Surface Pressure Distribution on an Airfoil.	2.36
2.16	Change in Velocity Profile Due to Negative Pressure Gradient	2.37
2.17	Change in Velocity Profile Due to Positive Pressure Gradient	2.37
2.18	Effect of Adverse Pressure Gradient.	2.38
3.1	Airfoil Nomenclature	3.2
3.2	Aerodynamic Parameters	3.3
3.3	Examples of Common Airfoil Sections.	3.10
3.4	Reference Wing Area.	3.11
3.5	Mean Aerodynamic Chord Determination	3.12
3.6	Summary of Wing Geometric Characteristics.	3.13
3.7	Example Aircraft General Arrangement Diagram.	3.14
3.8	Development of Lift on a Circular Cylinder	3.16
3.9	Ideal Nonviscous Flow Past a Cambered Airfoil with Zero Circulation at an Angle of Attack.	3.18
3.10	Viscous Flow Past an Airfoil with Circulation at an Angle of Attack.	3.18
3.11	Wing Vortex System	3.19
3.12	Planform Effects on Lift Distribution.	3.21
3.13	Aerodynamic Forces and Moments	3.22
3.14	Forces on an Aircraft in Flight.	3.23
3.15	Airfoil Streamlines.	3.25
3.16	Pressure Distribution as a Function of Angle of Attack for Symmetric Airfoil.	3.26
3.17	Pressure Coefficient on a NACA 4412 Airfoil.	3.27
3.18	Airfoil Pressure Distribution.	3.28

List of Figures (Continued)

Figure		Page
3.19	Lift Curves for Symmetric and Cambered Airfoils.	3.29
3.20	Cambered Airfoil Pressure Distribution at Zero Angle of Attack	3.30
3.21	Zero Lift Line	3.31
3.22	Effect of Mach on the Lift Curve	3.33
3.23	Effect of Reynolds Number on the Lift Curve	3.34
3.24	Lift Characteristics of Typical NACA Airfoil Sections.	3.36
3.25	Planform Effects on the Lift Curve	3.38
3.26	Definition of Aspect Ratio	3.38
3.27	Arbitrary Wing Planform.	3.39
3.28	Typical Spanwise Lift Distribution	3.40
3.29	Upper and Lower Finite Wing Flow Fields.	3.41
3.30	Tip Vortices on a Wing	3.42
3.31	Effect of Aspect Ratio on the Lift Curve	3.43
3.32	Effect of Increasing Altitude on $C_{L_{max}}$	3.45
3.33	Basic Types of Trailing Edge Flaps	3.47
3.34	Effect of Trailing Edge Flaps on the Lift Curve	3.48
3.35	Various Leading Edge Flap Devices.	3.49
3.36	B-747 Variable Camber Leading Edge Krueger Flap	3.49
3.37	Krueger-Fowler Flap Configuration.	3.50
3.38	Fixed Slot	3.50
3.39	Fixed Slat	3.51
3.40	Movable Slat	3.52
3.41	Effect of Slots, Slats, or BLC on the Lift Curve	3.52
3.42	Boundary Layer Control	3.53
3.43	High Lift Devices.	3.53
3.44	Maximum Sectional Lift Coefficients.	3.54
3.45	Vortex Generators.	3.55
3.46	Symmetric Wing Section at Angle of Attack for Zero Lift	3.56
3.47	Variation of Moment Coefficient About the Aerodynamic Center with Angle of Attack for Symmetric and Cambered Airfoils	3.57
3.48	Cambered Wing Section at Angle of Attack for Zero Lift	3.58
3.49	Moments on an Airfoil.	3.59
3.50	Effect of Wing Reflexing	3.62
4.1	Skin Friction Curves for a Smooth Flat Plate.	4.4
4.2	Pressure Drag of Streamlined and Unstreamlined Bodies	4.5

List of Figures (Continued)

Figure		Page
4.3	Flow Past a Sphere at Low Mach	4.7
4.4	Drag Versus Velocity for a Smooth Sphere at Low Mach.	4.7
4.5	Variation of Sphere Drag Coefficient with Reynolds Number	4.8
4.6	Ideal Nonviscous Flow Past a Circular Cylinder.	4.10
4.7	Ideal Nonviscous Flow Pressure Distribution Around a Symmetric Wing Section at Zero Angle of Attack	4.11
4.8	Flow Past a Flat Plate Perpendicular to the Flow.	4.11
4.9	Flow Past a Flat Plate Parallel to the Flow.	4.12
4.10	Relative Drag of Various Nonlifting Aerodynamic Shapes at Low Mach	4.13
4.11	Interference Drag.	4.14
4.12	Bound Vortex on an Infinite Wing	4.17
4.13	Vortex Flow on a Finite Wing	4.18
4.14	Vertical Velocity Due to Vortex Flow on a Finite Wing	4.18
4.15	Induced Flow Field	4.19
4.16	Lift Distribution for Uniform Downwash Velocity.	4.21
4.17	Pressure Distribution on Supersonic Shape with Resultant Wave Drag	4.25
4.18	Drag Classification.	4.28
4.19	Basic Drag Polar	4.30
4.20	Effect of Mach on the Drag Polar	4.31
4.21	Variation of Drag Coefficient with Mach at Constant Lift Coefficient.	4.32
4.22	Effect of Reynolds Number on the Drag Polar	4.33
4.23	Effect of Oswald's Efficiency Factor on the Drag Polar	4.34
4.24	Effect of Aspect Ratio on the Drag Polar	4.35
4.25	Effect of Flaps on the Drag Polar.	4.35
4.26	Effect of Flap Operation on Drag Polar	4.36
4.27	Aircraft Lift-Drag Ratio	4.37
4.28	Lift-Drag Ratio for a Wing of Aspect Ratio 6 with a NACA 23012 Airfoil Section.	4.37
4.29	Flight Test Drag Polar Determination.	4.39
4.30	Variation in Drag Coefficient with Velocity for Stabilized Level Flight	4.41
4.31	Variation in Drag Coefficient with Mach for Stabilized Level Flight	4.42

List of Figures (Continued)

Figure		Page
4.32	Variation in Total Drag with Velocity for Stabilized Level Flight	4.43
4.33	Variation in Total Drag with Mach for Stabilized Level Flight	4.44
4.34	Drag Characteristics of an Early Supersonic Fighter	4.45
4.35	Comparison of Conventional Cambered and Laminar Wing Sections.	4.46
4.36	Laminar Flow Wing Section Drag Polar	4.48
5.1	Standard Atmosphere Temperature Lapse Rate with Altitude	5.3
5.2	Forces Acting on a Vertical Column of Air of Unit Area.	5.5
5.3	Pressure Variation with Altitude	5.10
5.3A	Standard Day and Test Day Pressure Variation With Altitude.	5.11
5.4	Altimeter Schematic.	5.14
5.5	Pitot-Static Schematic	5.15
5.6	Airspeed Indicator Schematic	5.24
5.7	Machmeter Schematic.	5.27
5.8	Airspeed Instrument Calibration.	5.30
5.9	Typical Subsonic Static Pressure Distribution on Aircraft Fuselage.	5.34
5.10	Detached Shock Wave in Front of Pitot-Static Probe	5.34
5.11	Low Mach C_p Effects on Pressure Coefficient.	5.39
5.12	Low Mach C_p Effects on Velocity Error.	5.39
5.13	Low Speed Altitude Position Error Correction	5.40
5.14	Low Speed Mach Position Error Correction	5.41
5.15	Indicated Mach Corrected for Instrument Error, M_{ic}	5.42
5.16	Velocity Position Error Illustrating Altitude and Mach Effects	5.43
5.17	Machmeter Position Error Correction as a Function of Instrument Corrected Indicated Mach	5.47
5.18	Total Temperature Sensor (Non De-Iced).	5.52
5.19	Total Temperature Sensor with Boundary Layer Control.	5.52
5.20	Subsonic Temperature Recovery Factor K_t	5.54
5.21	Temperature Recovery Factor Versus Mach.	5.54
5.22	The Tower Fly-By Line.	5.56
5.23	Speed Course	5.58

List of Figures (Continued)

<u>Figure</u>		<u>Page</u>
5.24	Radar Tracking Time History of Pace Pressure Survey	5.59
5.25	Radar/Smoke Trail Method	5.60
5.26	Typical Trailing Bomb.	5.61
5.27	Typical Trailing Cone.	5.62
5.28	Tower Fly-By Data Cards.	5.63
6.1	Total Pressure and Density for Reversible and Irreversible Processes.	6.7
6.2	Sound Wave Propagation from a Point Source	6.14
6.3	Convergent-Divergent Streamtube.	6.21
6.4	Comparison of Compressible and Incompressible Flow Through a Closed Tube.	6.25
6.5	Pressure and Mach Variation Through a Converging-Diverging Streamtube.	6.27
6.6	Pressure Adjustment Outside a Nozzle or Streamtube	6.28
6.7	Flow Properties in the Vicinity of a Normal Shock	6.34
6.8	Pitot Tube in Supersonic Flow.	6.36
6.9	Shock Process as Seen by Stationary Observer	6.38
6.10	Shock Process as Seen by Moving Observer	6.39
6.11	Supersonic Flow Into a Corner.	6.40
6.12	Analogy to Aid Understanding of Oblique Shocks	6.40
6.13	Analysis of Velocity Components Across an Oblique Shock.	6.42
6.14	Turning Angle as a Function of Wave Angle for Flow Through an Oblique Shock.	6.45
6.15	Wave Angle as a Function of Mach for Flow Through an Oblique Shock.	6.46
6.15	Wave Angle as a Function of Mach for Flow Through an Oblique Shock.	6.46
6.16	Isentropic Compression	6.48
6.17	Impossibility of Shock Formation Flow Turning Away From Itself.	6.50
6.18	Supersonic Flow Around a Corner	6.51
6.19	Supersonic Flow Around a Smooth Corner.	6.52
6.20	Turning Angle as a Function of Mach for Prandtl-Meyer Flow	6.56
6.21	Two Expansions	6.57
6.22	Two Compressions	6.58
6.23	Shock Followed by Expansion.	6.59
6.24	Expansion Followed by Shock.	6.59

List of Figures (Continued)

<u>Figure</u>		<u>Page</u>
6.25	Supersonic Flow Pattern and Distribution of Pressure	6.61
6.26	Double Wedge Airfoil in Supersonic Flow.	6.62
6.27	Approximate Equations for Supersonic Section Characteristics.	6.66
6.28	Stream Lines About a Cone.	6.67
6.29	The Flared Cone.	6.68
6.30	Flow in a Round Corner	6.69
6.31	Mach Cone Limits	6.70
6.32	Supersonic Tip Effects	6.71
6.33	Transonic Lift Coefficient Characteristics.	6.72
6.34	Transonic Flow Patterns.	6.74
6.35	Thin Wing Transonic Lift Coefficient.	6.75
6.36	Critical Pressure Coefficient and Critical Mach for Airfoils Different Thicknesses.	6.75
6.37	Comparison of Drag Rise Phenomena at Critical Mach	6.76
6.38	General Effects of Sweepback	6.77
6.39	Stall Characteristics of Tapered Swept Wing	6.78
6.40	Effect of Sweepback on Low Speed Lift Curve	6.79
6.41	Optimum Nose Shape	6.80
6.42	Equivalent Body of Revolution.	6.80
6.43	Benefits of Area Rule Application.	6.82
6.44	"Coke Bottle" Fuselage	6.83
6.45	Planform Effects and Control Surfaces	6.85
7.1	Continuous Level Flight Corridor	7.3
7.2	Typical Turbojet Engine Internal Pressure Variations.	7.7
7.3	Principal Elements of a Ramjet Engine	7.8
7.4	Principal Elements of a Turbojet Engine.	7.9
7.5A	Single Axial Compressor Turbojet	7.10
7.5B	Dual Axial Compressor Turbojet	7.10
7.6	Dual Axial Compressor Turbojet with Afterburner.	7.11
7.7	Principal Elements of a Turboprop Engine	7.12
7.8A	Single Axial Compressor: Direct Propeller Drive Turboprop	7.13
7.8B	Dual Axial Compressor: Direct Propeller Drive Turboprop.	7.13
7.9	Single Axial Compressor: Free Turbine Propeller Drive Turboprop.	7.14

List of Figures (Continued)

Figure		Page
7.10A	Principal Elements of a Turbofan Engine (Front Fan)	7.14
7.10B	Principal Elements of a Turbofan Engine (Aft Fan)	7.14
7.11	Schematic Diagrams of Turbofan Engines. (A) Courtesy Pratt & Whitney Aircraft Division of the United Aircraft Corp. (B) Courtesy Rolls-Royce (C) Courtesy Flight International	7.16
7.12	Air-Breathing Engine	7.18
7.13	Effect of Ram Pressure on Thrust.	7.23
7.14	Effect of Altitude on Flight	7.24
7.15	Single-Spool Turbojet Engine Station Designations	7.25
7.16	h-s Diagram for Air	7.29
7.17	Turbojet Engine Ideal Cycle	7.30
7.18	Ideal Turbojet Thermal Efficiency	7.35
7.19	Ideal Turbojet Thermal Efficiency	7.35
7.20	Thermal Efficiency Versus Net Work.	7.36
7.21	Ideal Cycle for the J-79 Turbojet (per lb of air) $V_0 = 230$ KTS, $T_0 = 40^\circ$, $H_0 = 16000$ ft	7.44
7.22	Propulsive Efficiency of Air-Breathing Engines	7.46
7.23	Ideal Turbojet Net Thrust	7.48
7.24	Ideal Turbojet Net Thrust	7.48
7.25	Ideal Turbojet Thrust Specific Fuel Consumption	7.50
7.26	Ideal Turbojet Thrust Specific Fuel Consumption	7.50
7.27	Effects of Fan Stage Design Variables on TSFC	7.53
7.28	Net Thrust Improvements with Bypass Ratio	7.54
7.29	Effect of Core Compression Ratio on Net Thrust for the Turbofan ($TIT = 2400^\circ R$ and $CR_c = 2$)	7.55
7.30	Effect of Core Compression Ratio on TSFC for the Turbofan ($TIT = 2400^\circ R$ and $CR_c = 2$)	7.55
7.31	Mach effects for an Actual Turbofan Engine.	7.56
7.32	h-s Diagram for the Fan Stage	7.58
7.33	Comparison of Net Thrust Versus Airspeed for the Turboprop, Turbofan, and Turbojet Engine.	7.64
7.34	Subsonic Diffuser	7.66
7.35	Diffuser Process on a T-s Plane	7.68
7.36	Variation of Total Pressure Ratio and Total Temperature Ratio for Various Values of Diffuser Recovery Factors Assuming a Normal Shock for Mach Greater than One	7.69
7.37	Two-Dimensional Inlets	7.71
7.38	Axisymmetric Inlet	7.72
7.39	Subsonic Diffuser Operating in a Supersonic Stream	7.73
7.40	Total Pressure Loss in Normal Shock Inlet	7.74
7.41	Normal Shock Inlet with Swallowed Shock.	7.75
7.42	Normal Shock Inlet with Expelled Shock.	7.76

List of Figures (Continued)

Figure		Page
7.43	Types of Supersonic Inlets (Reference)	7.77
7.44	Two Concepts Illustrating Variable Geometry	7.78
7.45	External Compression Inlet at Design Conditions	7.79
7.46	Multiple Shock Systems	7.80
7.47	Effect of Number of Shocks on Total Pressure Recovery	7.80
7.48	Typical Subsonic and Supersonic Diffusers	7.81
7.49	Subsonic Diffuser Operating on Design	7.82
7.50	No Title	7.84
7.51	Subsonic Diffuser with Several Demands for Inlet Air	7.85
7.52	Supersonic Ramp-Type Diffuser	7.85
7.53	Multiple Shock Inlet - Off-Design	7.86
7.54	Adjusting Inlet Area with Variable Ramp	7.87
7.55	A Conical Inlet at Zero Angle of Attack and Design Mach Showing Three Modes of Operation.	7.88
7.56	Effect of Boundary Layer Removal Depth on Total Pressure Recovery of Fuselage Side Inlet	7.91
7.57	Compressor Energy Balance	7.93
7.58	Ideal and Actual Adiabatic Compression Processes	7.93
7.59	Components of a Centrifugal Compressor.	7.96
7.60	Double-Entry Compressor Impeller.	7.97
7.61	Multistage Centrifugal Compressor	7.98
7.62	Components and Assembly of Axial Flow Compressor	7.99
7.64	Schematic Diagram of Compressor Blading Effects	7.102
7.65	Dual Axial Compressor or Twin-Spool System.	7.104
7.66	Typical Compressor Performance Chart.	7.105
7.67	The Can or Tubular-Type Combustion Chamber.	7.109
7.68	Typical Annular Combustion Chamber.	7.110
7.69	Schematic Diagram of Burner Cross Section	7.111
7.70	Ideal and Actual Combustion Process on h-s Plane	7.113
7.71	DEEC Variables.	7.115
7.72	Turbine Elements.	7.116
7.73	Turbine Inlet Blade Temperature Profile Limitations	7.118
7.74	Shrouded Turbine-Rotor Blades	7.119
7.75	Turbine Energy Balance	7.119
7.76	Ideal and Actual Adiabatic Turbine Expansion Process	7.120
7.77	Turbine Energy Transfer	7.122
7.78	Improvement in Turbine Blade Temperature Limits Due to Improved Metallurgical Techniques	7.123
7.79	General Turbine Blade Cooling Methods	7.125
7.80	Relative Effectiveness of Turbine Blade Cooling Methods	7.126
7.81	Chronological Improvement in Turbine Inlet Temperature as a Function of Turbine Blade Cooling	7.127

List of Figures (Continued)

<u>Figure</u>		<u>Page</u>
7.82	Conventional Convergent Exhaust Duct	7.129
7.83	Convergent-Divergent Exhaust Duct (Nozzle)	7.129
7.84	Comparison of Ideal and Actual Nozzle Expansion on a T-s or h-s Plane	7.131
7.85	Typical Afterburning Turbojet	7.133
7.86	h-s Diagram of a Turbojet Engine with Afterburner	7.135
7.87	Variation of Gas Properties Through a Turbojet Engine During Flight	7.139
7.88	T-s Diagram for Typical Turbojet Engines	7.140
7.89a	Comparative Net Thrust at Sea Level	7.145
7.89b	Comparative Thrust Specific Fuel Consumption	7.145
7.90	Typical P & WA PT2 or T34 Turboprop Performance	7.146
7.91	Propeller Blade Angle Variation	7.147
7.92	Relative Performance at Maximum Cruise	7.149
7.93	Relative Maximum-Continuous-Thrust Comparison During Climb	7.150
7.94	Sea Level Static Takeoff Thrust	7.150
7.95	Thrust Per Horsepower Versus Vehicle Speed	7.151
7.96	Propeller Momentum Theory	7.152
7.97	Propeller Blade Element Theory	7.155
7.98	Comparison of Calculated and Measured Thrust Distribution on a Propeller Blade	7.157
7.99	Representative Angle for Propellers	7.159
7.100	Typical Propeller Wind Tunnel Results.	7.160
7.101	Propeller Power Coefficient and Propeller Efficiency Curves	7.162
7.102	Propeller Efficiency and Variable Pitch Propellers	7.162
7.103	Propeller Characteristics of Various Types of Propellers	7.163
7.104	Sketches of a Shrouded Propeller	7.165
7.105	Thrust and Drag Increments of a Shroud with Forward Velocity	7.166
7.106	Shrouded Propeller/Q Fan	7.169
7.107	Static Thrust Measurements of Engine Propeller Combinations	7.171
7.108	Ducted Propulsor Performance	7.173
7.109	General Electric NASA Unducted Fan (UDF) Demonstrator Engine.	7.174
8.1	Takeoff Roll Forces.	8.2
8.2	Variation of Forces During Takeoff Ground Roll.	8.4
8.3	Variation of Forces During Landing Rollout.	8.9
8.4	Takeoff Data	8.18
9.1	Forces Acting on an Aircraft in Flight.	9.3
9.2	Rate of Climb.	9.4
9.3	Wind Effect on Climb Angle	9.5

List of Figures (Continued)

Figure		Page
9.4	T-38 Thrust and Drag	9.6
9.5	Typical Rate of Climb Performance.	9.9
9.6	T-38 Rate of Climb Performance	9.10
9.7	Time to Climb.	9.11
9.8	Forces Acting in a Glide	9.12
9.9	Effect of Weight on Glide Ratio.	9.13
9.10	Military Thrust Polar Diagram.	9.14
9.11	Family of Polar Diagrams	9.16
9.12	Maximum Value of a Function.	9.21
9.13	Specific Energy Overlay.	9.25
9.14	Alternative Specific Energy Overlays	9.26
9.15	F-104g 1g Specific Excess Power.	9.29
9.16	Effect of Increasing Drag, Increasing Load Factor, or Reducing Thrust.	9.30
9.17	Possible Aircraft Limits	9.31
9.18	Subsonic Climb Paths	9.33
9.19	Supersonic Climb Path.	9.34
9.20	F-104G Minimum Time to Energy Level Climb Path.	9.36
9.21	Minimum Fuel to Energy Level Climb Path	9.38
9.22	Path Independent Maneuver Energy Plot.	9.40
9.23	Comparison of Time Optimal and Fuel Optimal Paths	9.42
9.24	T-38 V-n Diagram	9.44
9.25	Effect of Load Factor on P _s Contours.	9.46
9.26	Illustration of Radial Acceleration for a Vertical Maneuver.	9.47
9.27	Typical P _s Overlay	9.48
9.28	Differential P _s Contours	9.49
9.29	Typical Overlay of P _s Contour.	9.50
9.30	P _s Versus Turn Rate.	9.51
9.31	Comparison of Turning Performance - Specified Altitude and Airspeed.	9.52
9.32	P _s Versus Turn Rate (Constant Mach, Various Altitudes)	9.53
9.33	P _s vs Mach Number at Specified G Loads, Specified Altitude	9.54
9.34	Rate of Turn vs Radius of Turn.	9.57
9.35	F-5E Turn Performance - 5,000 Feet	9.58
9.36	F-5E Turn Performance - 15,000 Feet.	9.59

List of Figures (Continued)

<u>Figure</u>		<u>Page</u>
9.37	F-5E Turn Performance -	
	30,000 Feet.	9.59
9.38	Maximum Range Glide Path	9.61
9.39	Maximum Range for a Given	
	Fuel at Fixed Throttle	9.63
9.40	Maximum Range for a Given	
	Fuel with Glide.	9.64
9.41	Comparison of Maximum Range	
	Profiles for a Given Fuel.	9.65
9.42	Profiles for 200 NM Range.	9.67
9.43	Sample Data Card	9.76
10.1	V-n Diagram.	10.1
10.2	Forces in a Turn	10.4
10.3	Turn Rate - Turn Radius	
	Relationships.	10.8
10.4	Turn Rate/Radius P Overlay.	10.9
10.5	Factors Affecting Turning	
	Performance.	10.10
10.6	Load Factor vs Mach	
	For a Sustained Turn	10.10
10.7	Sustained Turn Performance	
	Results.	10.11
10.8	Stabilized Turn Test Method.	10.15
10.9	Graphical Determination of E_s	10.17
10.10	Normalized Excess Thrust vs E_s	
	Mach	10.18
10.11	Excess Thrust Extrapolation.	10.19
10.12	Sustained g vs Mach.	10.20
11.1	Steady State Flight.	11.1
11.2	Drag Polar	11.5
11.3	Engine Thrust Curve,	
	100% RPM	11.7
11.4	Engine Thrust Curve,	
	95% RPM.	11.8
11.5	Engine Thrust Curve.	11.9
11.6	Corrected Thrust	11.11
11.7	Corrected Fuel Flow.	11.11
11.8	Thrust Required.	11.14
11.9	Fuel Flow.	11.18
11.10	Comparison of Cruise Climb	
	and Constant Altitude Flight	11.21
11.11	Specific Range	11.24
11.12	Determination of Optimum Mach	
	for Any Given Range Factor	11.25
11.13	Power Required for Level	
	Flight	11.31
11.14	Engine Horsepower Curve.	11.32
11.15	Linearized Power Required.	11.34
11.16	Power Required for Level Flight.	11.34
11.2	Drag Polar	11.37

List of Figures (Continued)

<u>Figure</u>		<u>Page</u>
11.17	Determination of Maximum Endurance and Maximum Range Airspeeds.	11.40
11.18	Standard Fuel Flow	11.42
11.19	Corrected Fuel Flow.	11.43
11.20	Fuel Flow.	11.44
11.21	Specific Range	11.45
11.22	Specific Range, One Altitude	11.46
11.23	Range Factor, All Altitudes and Weights.	11.47
12.1	Ground Block Pressure Altitude Plot.	12.4
12.2	Ground-Roll Takeoff Distance	12.16
12.3	Force Diagram.	12.17
12.4	Pressure (Altimeter Reading)	12.22
12.5	Wind Gradient Effect on Rate of Climb.	12.29
12.6	No Title	12.30
12.7	P_s Versus M from Level Accel	12.41
12.8	P_s Versus H and M from Level Accel	12.42
12.9	Climb Schedules from Level Accel Data.	12.43
12.10	Climb Performance Summary.	12.51
12.11	H_c as a Function of Gross Weight	12.57
12.12	H_c as a Function of Fuel Used.	12.58
12.13	Specific Range Versus Mach for Various Weight-Pressure Ratios	12.63
12.14	Range Factor and Mach Versus Weight-Pressure Ratio.	12.64
12.15	Drag Polar	12.65
12.16	Ferry Range.	12.71

List of Tables

<u>Number</u>		<u>Page</u>
2.1	Standard Sea Level Properties of Air	2.5
2.2	Flight Regime Definition	2.8
2.3	Dimensional Analysis Variables	2.14
3.1	Pressure Coefficient Relationships From Figure 3.18	3.28
6.1	Supersonic Wave Characteristics (6.2:213)	6.56
7.1	Summary of Thrust Equations	7.21
7.2	Ideal Turbojet Component Processes and Equations.	7.27
7.3	Effects of Compression Ratio on n_{TH} and W_N	7.36
7.4	Flight Conditions and Engine Parameters for J-79 Turbojet Analysis	7.38
7.5	Summary of Net Thrust Trends	7.47
7.6	Summary of TSFC Trends Ideal Turbojet	7.49
7.7	Flight Conditions and Engine Parameters for Converted J-79 Turbofan Analysis	7.57
7.8	Comparison of Results	7.62
7.9	Characteristics of the Turbofan Engine	7.63
7.10	Axial Flow Compressor Velocities	7.101
7.11	Variation Across a Typical Axial Flow Compressor Stage	7.103
7.12	Compressor Dimensionless Performance Ratios	7.105
7.13	Characteristics of Some Current U.S. and British Afterburning Turbojet Engines	7.136
7.14	Summary of Performance Data of Typical Thrust Augmentation Devices	7.138
7.15	Comparison of Propellor and Q Fan Characteristics	7.169
9.1	Mathematical Correspondence	9.23
9.2	Fuel Consumption for 200 MM Profiles	9.66

9.3	Rank Ordering of Measurement Techniques	9.70
-----	---	------

CHAPTER 1

INTRODUCTION TO AIRCRAFT PERFORMANCE
ANALYSIS AND TESTING

↙ Aircraft performance, in its most general sense, can be defined as the flight achievements an aircraft must execute for successful mission accomplishment. Obviously, expected performance parameters must be an integral part of the design process of an aircraft. Given certain performance expectations by the customer, the designer must make decisions regarding wing loading, power plant selection, airfoil selection, planform configuration, and myriad other considerations. All of these help to tailor the design to give the aircraft certain desired performance characteristics.

It is also certain that actual performance characteristics will not always be the same as those predicted by the designer. Herein lies the need for performance flight testing. Performance flight testing is defined as the process of determining aircraft performance characteristics, or in a more modern sense, evaluation of the energy gaining and losing capability of the aircraft. ↙

C Determination of aircraft performance parameters, whether expected or actual, are dependent upon our knowledge of certain fundamentals in several different scientific disciplines. In order to predict or measure an aircraft's performance, we must be able to estimate the aerodynamic forces involved. This requires knowledge of the properties and behavior of the fluid medium in which we operate, i.e., the earth's atmosphere.

Therefore, we must study atmospheric science, fluid dynamics, thermodynamics, subsonic aerodynamics, and supersonic aerodynamics. Performance prediction or measurement requires knowledge of the power plant/propulsion system characteristics of the aircraft. Hence, we must be familiar with the theory and operation of basic turbine and turbine variant engines, reciprocating internal-combustion engines, and propeller theory. We must also understand the basic measurements, instrumentation techniques, and equipment in order to gather the data needed to determine the various elements of an aircraft's performance. Finally, we must have knowledge of the structural limitations of the aircraft.

Once we have a background in these various fields of study, we can begin to answer questions about the aircraft's predicted or actual performance such as:

How fast will the aircraft fly?

How high will the aircraft fly?

How far and/or how long will the aircraft fly on a load of fuel?

How much payload can the aircraft carry?

How long a runway is required for takeoff and landing?

How fast will the aircraft climb?

How expensive is the aircraft to operate?

What is the aircraft's maximum sustained turn rate?

These are only some of the most important questions that must be answered.

We must determine the proper parameters to use in our analysis. As stated earlier, this is dependent upon the type of propulsion system the aircraft has. Reciprocating engines are normally rated in terms of power, and therefore certain characteristics of propeller driven aircraft are given in terms of power required versus power available. Turbine engines are normally rated in terms of thrust, and therefore it is more logical to analyze performance characteristics in terms of thrust available versus thrust required. Aircraft such as turboprops, turbofans, and rotary wing exhibit some characteristics of both types of power plants and must be analyzed accordingly.

Performance can be subdivided into steady state performance and accelerated performance. Steady state performance characteristics are normally determined by analysis of the basic thrust, weight, lift, and drag forces involved in a quasi-equilibrium condition, i.e., where the velocities and other flight path parameters are either constant or are changing so slowly that their rate of change can be neglected. For instance, top speed in level flight occurs at the high speed intersection of either power required versus power available or thrust required versus thrust available curves, depending upon the propulsion system. Steady state rate of climb is dependent upon the excess of power available over power required.

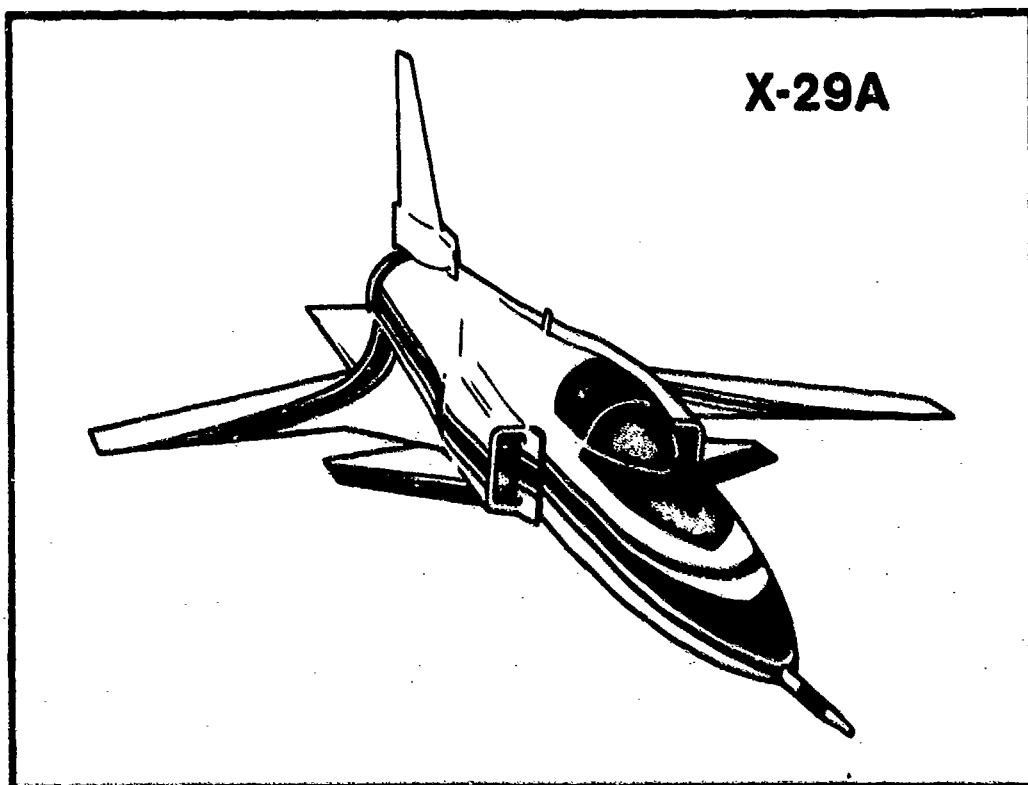
In accelerated performance analysis we must consider accelerations along and normal to the flight path in addition to the basic parameters used to

determine steady state performance characteristics. Failure to consider accelerated effects can often produce misleading results. For example, the steady state absolute ceiling of an aircraft can actually be exceeded by an accelerated maneuver known as a zoom climb in which there is partial conversion of the kinetic energy of the aircraft into potential energy, or altitude.

Performance flight testing is conducted with several fundamental purposes in mind other than determining the actual performance characteristics of an aircraft. In fact, it is also used to:

1. Determine if the aircraft meets specific contractual performance guarantees, or hard performance requirements as specified in the user generated Statement of Need (SON).
2. Provide data to construct aircraft flight manuals for use by operational aircrews.
3. Determine techniques and procedures to be used by operational aircrews to attain optimum aircraft performance.
4. Obtain research information to advance aeronautical science or to develop new flight test techniques.

As aircraft become more and more technologically sophisticated, it is almost certain that the future heralds the development of newer and better methods of aircraft performance prediction and determination. It is incumbent upon the experimental test pilot and flight test engineer to be in the forefront of that development. Such expectations can begin to be realized only if the test pilot and flight test engineer possess a working knowledge of the material contained within this manual.



CHAPTER 2

FUNDAMENTALS OF AERODYNAMICS

2.1 INTRODUCTION

Aerodynamics is one of the branches of theoretical physics. The science of aerodynamics concerns itself with the determination of the characteristics of airflow past bodies of various shapes. Once the flow pattern has been established, the aerodynamic forces acting on the body may be calculated.

The complex field of low speed (subsonic) aerodynamics--the bread and butter of aeronautical engineers for fifty years--essentially vanished from the research and development scene with the advent of the glamorous "space age." The last few years have seen a strong rebirth of interest in the field. Under the pressure of still unsolved problems, new applications, increasing requirements of both military and commercial vehicles, and VSTOL technology, subsonic aerodynamics is once again becoming a major research endeavor. Problems such as the prediction of wing stall, boundary layer control, and low speed flying qualities loom as difficulties that the techniques and knowledge of ten to fifteen years ago simply cannot handle.

Two essential ingredients of basic aerodynamics are the principles of fluid dynamics and thermodynamics. Because this text is intended for the use of flight test pilots and flight test engineers, these subjects will be handled in a limited fashion.

2.2 THE ATMOSPHERE - BASIC PROPERTIES

The earth's atmosphere at sea level is a mixture of several gases. The approximate percentage by volume of the main constituents is 78% nitrogen, 21% oxygen, 0 to 4% water vapor, and traces of argon and other rare gases. Almost all of the water vapor is concentrated in the lower ten miles of the atmosphere. Aside from this concentration, the mixture is practically homogeneous up to about 50 miles. Above this level, oxygen begins to dissociate under the influence of ultraviolet radiation from the sun. At still higher levels, nitrogen also dissociates.

There is no well defined upper limit to the atmosphere. Any upper limit is purely arbitrary and depends solely upon the definition of properties required to constitute an atmosphere. The atmosphere will be further discussed and the standard atmosphere defined in Chapter 5.

The aerodynamic forces and moments acting on an object are due primarily to the properties of the air mass through which it is moving (2.1:1). The usual properties which define an air mass will now be discussed.

2.2.1 Static Properties

Pressure is a measure of both speed and number of molecules per unit volume. In other words, pressure is the net result of all molecular motions. The static pressure of the air at any altitude within the earth's atmosphere is a result of the mass of air above that altitude. This mass of air under the gravitational attraction of the earth has weight.

$$W = mg$$

Pressure is a property expressed in terms of force (weight) per unit area. The symbol for pressure is P or p , and may be subscripted to indicate measurements under various conditions or locations.

The most common subscripts used throughout the textbook which apply to pressure and all the other air mass properties are:

a = ambient conditions

t = test conditions

∞ = free stream conditions

SL = standard sea level conditions

1, 2, 3, etc. = specific conditions

2.2.2 Temperature

Temperature is a measure of molecular motion. On an absolute scale, temperature is measured theoretically from that point where molecular motion ceases. There are two scales of absolute temperature: the Rankine and Kelvin scales. The two more widely known temperature scales, based on the boiling and freezing points of water, are the Fahrenheit and Centigrade scales. The symbol for temperature is a capital T and may be accompanied by any of the previously mentioned subscripts. The Fahrenheit and Rankine scales are

related through the expression

$$T(^{\circ}\text{R}) = T(^{\circ}\text{F}) + 459.67$$

Similarly, the relationship between Centigrade and Kelvin may be expressed as

$$T(^{\circ}\text{K}) = T(^{\circ}\text{C}) + 273.15$$

Absolute temperature must always be used in engineering calculations.

2.2.3 Density

The density of air is perhaps the property of greatest importance in the study of aerodynamics. Density is defined as mass per unit volume and is symbolized by the greek letter rho (ρ). Density decreases slowly with increasing altitude from the surface of the earth.

With respect to density, the field of aerodynamics is normally divided into two regimes: Incompressible Flow - flow at low velocities where changes in density of the air may essentially be neglected, and Compressible Flow - flow at velocities sufficiently high that density changes cannot be neglected (2.1:65). Definition of the dividing velocity between the two regimes requires that two other quantities commonly used in aerodynamics also be defined.

Speed of sound (a) is a function of absolute temperature and is defined by the relationship

$$a = \sqrt{\gamma RT}$$

Speed of sound is also called sonic velocity and is the velocity at which small disturbances are propagated through the atmosphere.

Mach (M) is a velocity divided by a characteristic speed of sound

$$M = \frac{V}{a}$$

Utilizing these definitions, we may state that the assumption of incompressible flow is usually valid up to $M = 0.3$.

2.2.4 Equation of State

For a large number of problems in aerodynamics, air can be treated as an ideal or perfect gas. A perfect gas is defined as one which is homogeneous, continuous, and nonviscous. For a perfect gas, the properties temperature, pressure, and density are related by the equation of state

$$P = \rho RT \quad (2.1)$$

It should be noted that pressure, temperature, and density are point properties and can have different values from one point to another. Thus, Equation 2.1 relates those properties at a point. The R in Equation 2.1 is known from thermodynamics and the kinetic theory of gases as the gas constant. Equation 2.1 closely describes the behavior of the atmosphere in the lower layers and is an adequate relationship for the portion of the atmosphere where aircraft performance data is of interest. However, when pressure is reduced to such a degree that the number of molecules in a given area is reduced to a point where uniform pressure no longer exists, Equation 2.1 is no longer valid. Because of the rarity of the atmosphere and the change in the mean molecular weight of the air due to dissociation, Equation 2.1 as given is not valid above 55 miles.

Three important ratios are used in aerodynamics for atmospheric property relationships. These ratios relate the ambient static property value to the sea level standard property value. They are

$$\delta(\text{delta}) = \frac{P_a}{P_{SL}} \quad \text{pressure ratio} \quad (2.2)$$

$$\theta(\text{theta}) = \frac{T_a}{T_{SL}} \quad \text{temperature ratio} \quad (2.3)$$

and

$$\sigma(\text{sigma}) = \frac{\rho_a}{\rho_{SL}} \quad \text{density ratio} \quad (2.4)$$

Through the Equation of State, Equation 2.1, it can be determined that

$$\delta = \sigma \theta \quad (2.5)$$

2.2.5 Velocity

Velocity is a measure of the motion of a fluid. Velocity is a vector quantity and has both magnitude and direction, and is also a point property.

2.2.6 Viscosity

Early aerodynamic theory neglected the fact that air is a viscous fluid. For many of the problems in aerodynamics, air may be treated as if it were, in fact, an inviscid fluid. However, for flow very close to an object in a region termed the boundary layer, the effects of viscosity must be accounted for. An in-depth discussion of viscous flow, including definitions of viscosity and the boundary layer, is found in Section 2.7 of this chapter.

Standard sea level values of the fundamental properties of air are summarized in Table 2.1.

TABLE 2.1

STANDARD SEA LEVEL PROPERTIES OF AIR

<u>Property</u>	<u>Symbol</u>	<u>Value (English)</u>	<u>Value (SI)</u>
Pressure	P	2116.22 lb/ft ²	$1.01325 \times 10^5 \text{ N/m}^2$
Temperature	T	59° F (519°R)	15°C (288.15°K)
Density	ρ	0.0023769 slugs/ft ³	1.2250 kg/m ³
Sonic Velocity	a	1116.4 ft/sec	340.3 m/sec
Viscosity	μ	$1.2024 \times 10^{-5} \text{ lb/ft sec}$	$1.7894 \times 10^{-5} \text{ kg/m sec}$
Gas Constant	R	1716 ft lb/slug °R	287 J/kg °K

2.3 TECHNICAL NOTATIONS AND DEFINITIONS

In the field of aerodynamics, certain terms are so frequently used that they have become part of the flight test vocabulary. Definition of many of the terms is also necessary to facilitate discussion of certain concepts in the remainder of this chapter and the rest of the textbook.

Ambient conditions (subscript a) are static atmospheric conditions which are normally the same as the corresponding free stream conditions.

Free stream conditions (subscript ∞) are atmospheric conditions measured remotely (theoretically an infinite distance) from an aerodynamic body which are out of the body's influence.

Dynamic pressure (q) is defined as

$$q = \frac{1}{2} \rho V^2$$

where ρ is density and V is true velocity.

Equivalent Airspeed (V_e) is defined as

$$V_e = V \sqrt{\sigma}$$

where V is true airspeed and σ is density ratio

Pressure coefficient (C_p or $\Delta P/q$) is defined as

$$C_p = \frac{P - P_\infty}{\frac{1}{2} \rho_\infty V_\infty^2} = \frac{P - P_\infty}{q_\infty}$$

or alternatively

$$C_p = \frac{2}{\gamma M_\infty^2} \left(\frac{P}{P_\infty} - 1 \right)$$

where P is the static pressure at some point and γ is the ratio of specific heats.

A streamline is a line whose tangent at any point represents the direction of the instantaneous velocity vector. In steady flow,

streamlines do not change with time, since succeeding particles follow the same path as that of previous particles (2.1:234).

Critical Mach (M_{cr}) is the aircraft flight Mach at which the air flowing over some part of the aircraft first reaches sonic velocity and shock waves begin to form on the aircraft at this point.

2.4 AERODYNAMIC FLIGHT REGIMES

There are many assumptions that can be made to simplify the very complex general aerodynamic flow problem. For low subsonic Mach, it can be assumed that air is an ideal, nonviscous, and incompressible gas. Using these assumptions, many two- and three-dimensional aerodynamic problems can be solved. These ideal subsonic solutions can often be modified to show the effects of viscosity (Reynolds number effects) and effects of compressibility (Mach effects).

For flow next to a surface, the viscosity of the air must be considered. Viscosity plays an important part in aerodynamic flow separation, stalls, and in the computation of skin friction drag.

For supersonic flow, air can be considered to be an ideal, nonviscous, but compressible gas. Using these assumptions, which are valid for flow away from surfaces, pressure distributions can be calculated for many aerodynamic shapes.

The transonic flight regime is extremely complicated. Both subsonic and supersonic flows exist simultaneously. The interaction between these two types of flow plus the viscous effects on the aircraft surface create a condition that defies direct mathematical analysis. There are several definitions of the transonic speed range; however, the most useful is that it begins when sonic flow (Mach 1.0) first occurs somewhere on the aircraft and ends when the flow is essentially supersonic.

Analysis of hypersonic flow requires a knowledge of all the above flight regimes. The high temperatures and low densities associated with hypersonic flow also require the consideration of air as a non-ideal, rarefied gas. Heat transfer effects which are negligible for subsonic, transonic, and supersonic flow must also be considered above Mach 5.0.

The Flight Regimes may be categorized as shown in Table 2.2.

TABLE 2.2

FLIGHT REGIME DEFINITION

<u>Flight Regime</u>	<u>Mach Range</u>
Subsonic	$0 < M < M_{cr} (\approx 0.7)$
Transonic	$0.7 < M < 1.2$
Supersonic	$1.2 < M < 5.0$
Hypersonic	$5.0 < M$

2.5 FLUID FLOW EQUATIONS

We must now investigate the effect that velocity has on the static properties of air. As a fluid moves, we shall examine the changes that take place in its properties along a streamline by using a device known as a venturi tube which is illustrated in Figure 2.1.

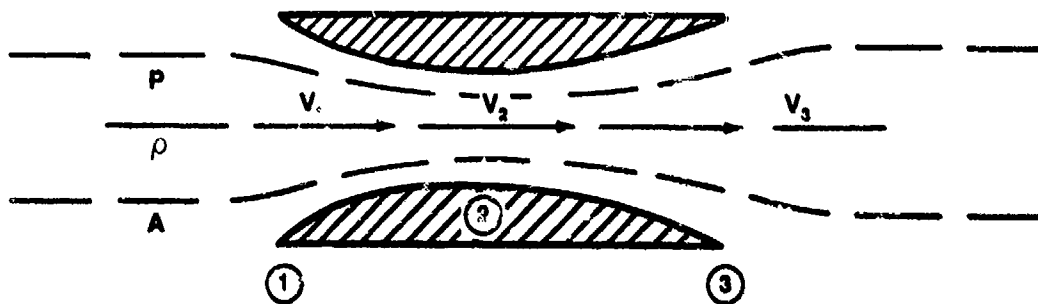


FIGURE 2.1. FLOW OF AIR THROUGH A VENTURI

From the law of conservation of mass, what enters the tube at Station 1 must exit at Station 3. The mass flow rate can be represented by the product ρAV at any station. Therefore, since mass is conserved,

$$\rho_1 A_1 V_1 = \rho_2 A_2 V_2 = \rho_3 A_3 V_3 \quad (2.6)$$

For the same mass of fluid to pass Station 2 as Station 1, the velocity and/or density must increase because the area has decreased. Considering the incompressible case where density is constant, Equation 2.6 between Stations 1 and 2 is

$$A_1 V_1 = A_2 V_2 \quad (2.7)$$

Solving this relationship for V_2 ,

$$V_2 = \frac{A_1}{A_2} V_1 \quad (2.7)$$

Since A_1 is larger than A_2 , V_2 must be greater than V_1 , by the ratio A_1/A_2 . This fundamental relationship (Equation 2.6 or 2.7) is known as the continuity equation. The relationship holds true for the compressible case and can be written for any two stations in the flow. If the average fluid properties for all streamlines far upstream are used, the relationship is also true across all streamlines in the flow. This principle also illustrates that for subsonic flow, the velocity is least where the streamlines are far apart, and as the velocity increases, the streamlines are closer together.

From Newton's Second Law

$$F = ma \quad (2.8)$$

we can derive a relationship known as the Euler or momentum equation.

$$dp = -\rho V dV \quad (2.9)$$

The derivation of this equation may be found in Appendix F.

This equation can be integrated between two points along a streamline for an incompressible, inviscid flow to yield

$$p_1 + \rho_1 \frac{V_1^2}{2} = p_2 + \rho_2 \frac{V_2^2}{2} \quad (2.10)$$

Since the Points 1 and 2 were completely arbitrary choices, the same equation must apply to conditions at any other points, therefore

$$p + \rho \frac{v^2}{2} = \text{constant} \quad (2.10)$$

This equation yields the relationship between pressure and velocity between any two points along a streamline in an incompressible, inviscid flow. The relationship does not hold true for compressible flow. However, we can integrate the Euler equation to get a more complicated relationship which does hold true for compressible flow when we have not assumed constant density for the integration process.

Another way to derive the Bernoulli equation, as this relationship is called throughout the literature, is to consider the flow from an energy standpoint.

We know from basic physics that the kinetic energy of a substance can be represented as

$$KE = 1/2 mV^2 \quad (2.11)$$

Since density (ρ) is defined as mass per unit volume, we can represent the kinetic energy of a unit volume of a flowing fluid by the relationship

$$KE = 1/2 \rho V^2 \quad (2.12)$$

The potential energy in a fluid can be thought of as the static pressure at some particular point. From the law of conservation of energy, we know that energy must be conserved as we move along a streamline through the venturi tube. Although there are other forms of energy, we need to consider only the potential energy due to the static pressure at a point along the streamline and the kinetic energy due to a point mass of air moving along the streamline. Therefore, we can say that

$$\text{Total Energy (TE)} = \text{Potential Energy (PE)} + \text{Kinetic Energy (KE)} \quad (2.13)$$

and must remain constant as we move from Station 1 to Station 2. We already

know that the velocity increased in moving from Station 1 to Station 2 from the derivation of the equation of continuity. Therefore, as the velocity increases along the streamline, the static pressure must decrease for the total energy to remain constant.

The kinetic energy term in Equation 2.10 is $1/2 \rho V^2$. This is the relationship previously defined as dynamic pressure and given the symbol q . Therefore, potential energy (static pressure) plus kinetic energy (dynamic pressure) is equal to a constant along a streamline. This constant value is termed the total pressure of the flowing air. This concept of total pressure is very important for compressible flow, and relationships for its use in this context are presented in Chapter 6.

The energy equation is needed to complete our inventory of basic equations of fluid flow. However, it is needed only for the compressible flow case and uses basic thermodynamic relationships. The thermodynamic relationships needed for compressible flow and the energy equation are discussed in Chapter 6, Supersonic Aerodynamics.

2.6 AERODYNAMIC FORCES

The fluid properties p , ρ , T , and V which have been defined and discussed fully define a flow field. The most practical consequence of the flow over an object is the generation of aerodynamic forces. These aerodynamic forces exerted by the airflow on the surface of an object immersed in an airstream stem from only two sources:

1. Pressure distribution on the surface
2. Shear stress distribution (friction) on the surface

Pressure exerted by the air on the surface of a solid object always acts normal to the surface. This surface pressure varies with location. The net unbalance of the varying pressure distribution over the surface creates an aerodynamic force. This resultant aerodynamic force is usually resolved into two components: one perpendicular to the relative wind and known as lift; the other parallel to the relative wind in the direction opposite to the aircraft motion, known as drag. The lift force is discussed in Chapter 3.

The shear stress, τ , is defined as the force per unit area acting tangentially on the surface due to friction. Shear stress is a point property and varies along the surface. The net unbalance of the surface shear stress distribution also creates a drag force on the body. So we see that pressure distribution contributes to both lift and drag on a body, but shear stress distribution contributes only to the drag force. Drag is fully discussed in Chapter 4.

Although the pressure and shear stress distributions are the primary source of aerodynamic forces, there exists a functional relationship with respect to the properties of the fluid and the properties of the body immersed in the fluid.

2.6.1 Dimensional Analysis (2.2:224, 225)

One common method used to obtain functional relationships between aerodynamic parameters is to use dimensional analysis. Data from two or more different environments may be compared if "dynamic similarity" exists. Dynamic similarity exists if appropriate dimensionless parameters are the same in two or more geometrically similar flow systems.

As the name implies, we are interested in dimensions fundamental to our study, i.e., mass (M), length (L), and time (T). To extend the analysis into the hypersonic regime, we would also have to include temperature, but we will confine our study to velocities less than hypersonic. The object of our endeavor is to obtain the most significant and independent dimensionless parameters for the particular physical system. One fact that must be noted is that we cannot determine how one dimensionless parameter will vary with another, only how to organize our experiments and plot our experimental data.

2.6.2 Buckingham π Theorem (2.2:2.24, 2.25)

The basis for the dimensional analysis technique is the Buckingham π Theorem. Buckingham speculated that for N number of variables in any equation such as

$$f(x_1, x_2, x_3, \dots, x_N) = 0 \quad (2.14)$$

and for k number of fundamental dimensions used to measure these variables,

then the equation may be expressed by a minimum of $N-k$ independent dimensionless groups. The total number of dimensionless groups is

$$\frac{N!}{[(k+1)!(N-k-1)!]} \quad (2.15)$$

These independent groups are designated $\pi_1, \pi_2, \pi_3, \dots, \pi_{N-k}$. Each of these groups ($N-k$) will consist of k quantities in common called repeating variables. These repeating variables must include all of the k fundamental dimensions. For a fluid system, the most significant groups will result if the repeating variables are chosen such that one is a geometric characteristic, one is a fluid property, and one is a flow characteristic. When the repeating variables are chosen, each one of the remaining original quantities is included with each one of the π groups. In order that the π groups be dimensionless, any one quantity in each may appear to the first power, and the others will appear to some unknown power which must be found. These powers are found by equating exponents of like fundamental quantity and solving using simultaneous equations.

The resultant aerodynamic force at a set angle of attack is a function of density, velocity, reference area, coefficient of viscosity, and speed of sound, or

$$f(F, \rho, V, S, \mu, a) = 0 \quad (2.16)$$

According to the Buckingham π Theorem, we have $N = 6$ variables of which there are $k = 3$ fundamental quantities -- mass (M), length (L), and time (T). Therefore, there are a minimum of $N-k = 3$ dimensionless groups, and the total number of dimensionless groups is 15. We will designate the groups as π_1, π_2 , and π_3 . Since we are concerned with aerodynamics, we will pick as our $k = 3$ repeating variables S for the geometric characteristic, ρ for our fluid property, and V for our flow characteristic. Then we may write

$$\pi_1 = f(S, \rho, V, F)$$

$$\pi_2 = f(S, \rho, V, a)$$

$$\pi_3 = f(S, \rho, V, \mu)$$

or considering only π_1 ,

$$\pi_1 = S^a \rho^b V^c F^1 \quad (2.17)$$

Each of these variables must now be represented in terms of their fundamental dimensions. These relationships are presented in Table 2.3.

TABLE 2.3

DIMENSIONAL ANALYSIS VARIABLES

<u>Variable</u>	<u>Dimension</u>
S	L^2
ρ	ML^{-3}
V	LT^{-1}
F	MLT^{-2}
a	LT^{-1}
μ	$ML^{-1}T^{-1}$

Substituting the fundamental dimensions into Equation 2.17

$$\pi_1 = (L^2)^a (ML^{-3})^b (LT^{-1})^c (MLT^{-2})^1$$

Recall that the π 's were defined as dimensionless groups. Therefore,

$$\pi_1 = L^0 M^0 T^0$$

or

$$L^0 M^0 T^0 = L^{2a} M^b L^{-3b} L^c T^{-c} M^1 L T^{-2}$$

or

$$L^0 M^0 T^0 = L^{(2a - 3b + c + 1)} M^{b+1} T^{-2-c}$$

Equating exponents of like dimensions

$$\begin{array}{ll} M: & b + 1 = 0 \\ T: & -c - 2 = 0 \\ L: & 2a - 3b + c + 1 = 0 \end{array} \quad \begin{array}{l} \therefore b = -1 \\ \therefore c = -2 \\ \therefore a = -1 \end{array}$$

$$\pi_1 = S^{-1} \rho^{-1} V^{-2} F$$

or

$$\pi_1 = \frac{F}{\rho V^2 S}$$

In place of using π_1 , which has little meaning, we can call this dimensionless quantity π the force coefficient, C_F . Therefore,

$$C_F = \frac{F}{\rho V^2 S} \quad (2.18)$$

Similarly, we can determine π_2 and π_3 as the Reynolds number, R_e , and the Mach, M . Thus,

$$C_F = f(R_e, M) \quad (2.19)$$

For varying angle of attack

$$C_F = f(R_e, M, \alpha) \quad (2.19A)$$

The dimensional analysis technique has only developed functional relationships. However, the results are extremely useful. These functional relationships will be used throughout the textbook to:

1. Present performance characteristics in a practical manner
2. Minimize flight test verification testing
3. Facilitate comparison between different aircraft or engine configurations
4. Develop standard day data reduction techniques

One important limitation should be kept in mind when using the results of any dimensional analysis: the functional relationships derived are only as good as the original assumptions. This means that all important variables must be included, assumed constants must stay constant, and limitations of simplifying assumptions on the analysis results must be understood.

Another functional relationship which can be developed by the use of dimensional analysis for an engine with one characteristic rotation speed and fixed design geometry and size is shown in Equation 2.20.

$$\frac{F_n}{\delta} = f \left(M, \frac{N}{\sqrt{\theta}} \right) \quad (2.20)$$

The parameter, F_n/S which is engine thrust divided by pressure ratio, is called a corrected thrust parameter. The parameter M is the Mach. The parameter $N/\sqrt{\theta}$, which is engine revolutions per minute (RPM) divided by the square root of the temperature ratio, is called a corrected RPM parameter. The functional relationship defined by Equation 2.20 has wide application in performance flight testing. Two conclusions which can be drawn from this functional relationship and will be discussed in detail in Chapter 11, Cruise Performance, are:

1. If at any two points in the operating envelope the Mach and corrected RPM parameter are the same, the corrected thrust parameter will be matched, and
2. If test Mach and standard day Mach are the same (they always are) and corrected RPM parameters are the same for test and standard conditions (they are for optimum cruise performance missions flown at a constant weight-pressure ratio), then test corrected thrust parameter is equal to standard corrected thrust parameter.

2.6.3 Turning Flow

Another mathematical model for aerodynamic forces results when the force required to turn a streamtube in incompressible, nonviscous flow is examined. Since the flow shown in Figure 2.2 is nonviscous, the magnitude of vector V_1 and V_2 is the same as shown in Equation 2.21.

$$|\vec{V}_1| = |\vec{V}_2| = V \quad (2.21)$$

Newton's second law can be written

$$F = m \Delta V \quad (2.22)$$

Since mass flow is constant, an expression for the magnitude of the force in Equation 2.22 can be written as

$$F = (\rho A V) |\Delta \vec{V}| \quad (2.23)$$

As shown in Figure 2.2

$$\Delta \vec{V} = \vec{V}_2 - \vec{V}_1 \quad (2.24)$$

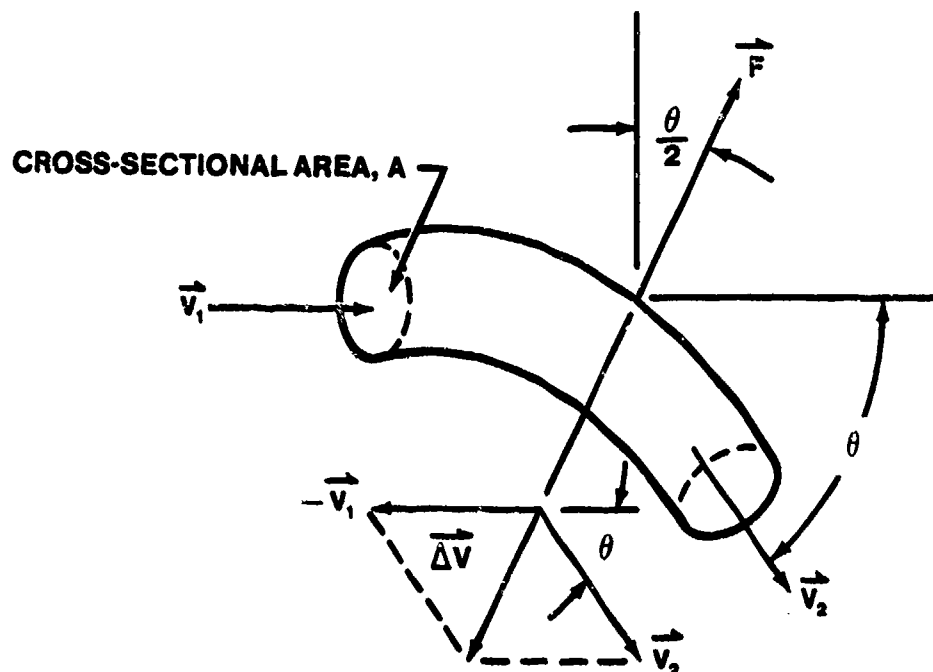


FIGURE 2.2. TURNING FLOW MODEL

From the law of cosines

$$|\Delta \vec{v}| = v \sqrt{2(1 - \cos \theta)} \quad (2.25)$$

Substituting Equation 2.25 into Equation 2.23 gives

$$F = \rho A v^2 \sqrt{2(1 - \cos \theta)} \quad (2.26)$$

which can be written using the definition of dynamic pressure as

$$F = 2 q A \sqrt{2(1 - \cos \theta)} \quad (2.27)$$

The angle between the resultant aerodynamic force and the vertical shown in Figure 2.2 can be found graphically or by trigonometry to be $\theta/2$.

Therefore, a momentum analysis using Newton's second law such as the one just performed can be used to determine a resultant aerodynamic force for any subsonic turning flow which can be similarly modeled. The geometry of the particular flow will determine the area, A , and turn angle θ , in Equation

2.27. This type of analysis gives good results for turning vanes and deflected jets.

2.7 VISCOSITY

Small as it is, air viscosity plays a major role in aerodynamics. Viscosity is normally thought of as associated with fluids or liquids. A highly viscous liquid is a very sticky one which pours slowly. By comparison, the viscosity of air is small. The failure of the early mathematical theories to describe real fluid flows was due to the fact that the theory neglected viscosity.

2.7.1 Coefficient of Viscosity

Suppose that a solid cube is attached at its base to a surface, and a force, F , is applied at its upper surface. The cube will deform slightly as shown in Figure 2.3.

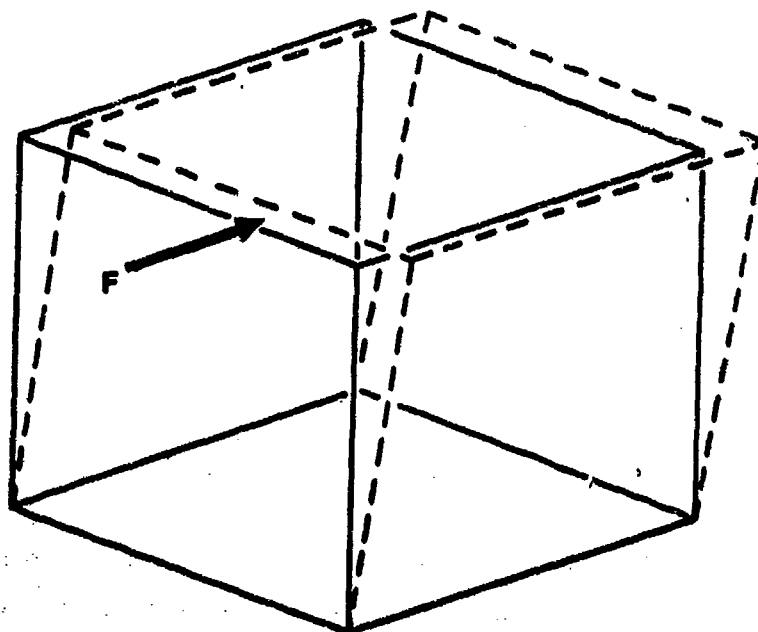


FIGURE 2.3. DEFORMATION OF A SOLID CUBE

For a solid, a "shear modulus" is defined in terms of a shearing stress divided by shearing strain or deformation. Thus,

$$\text{Shear Modulus, } E = \frac{\text{shear stress}}{\text{shear strain}}$$

But unlike a solid, a fluid will not sustain a shear under static conditions. Fluids often act as if they were layered, with one layer sliding over another and, by frictional effects, transmitting force to the adjacent layer. This is called laminar flow. This condition analogous to the elastic cube is shown in Figure 2.4.

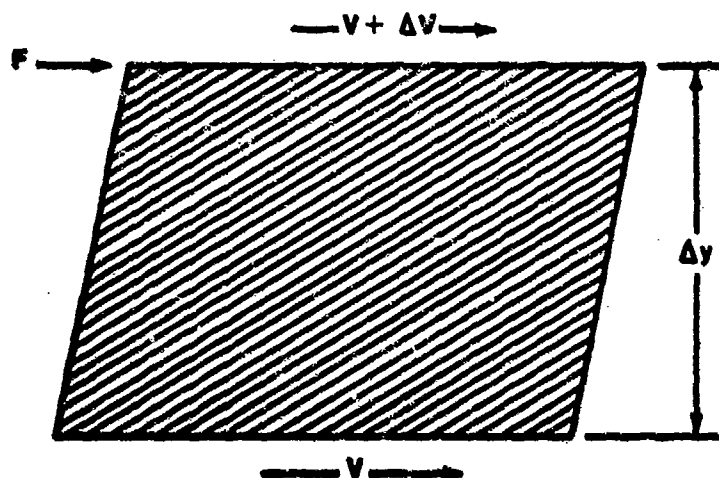


FIGURE 2.4. LAMINAR FLOW MECHANISM

As the upper face moves at a velocity, $V + \Delta V$, it drags the lower face along at a velocity, V , due to the presence of shear forces in the element. The difference in velocity, ΔV , through the thickness of the element, Δy , is proportional to the viscosity of the fluid. Thus, a proportionality constant μ can be written as

$$\text{Coefficient of viscosity, } \mu = \frac{\text{shear stress}}{\text{change of velocity/unit thickness}}$$

$$\mu = \frac{\text{shear stress}}{\text{velocity gradient}} = \frac{\tau}{\Delta V / \Delta y} = \frac{\tau}{dV/dy} \frac{\text{slugs}}{\text{ft-sec}} \quad (2.28)$$

So the coefficient of viscosity is considered a dynamic shear modulus. It is a measure of how easily one layer of a fluid slides over another layer, a measure of the resistance to flow. Newton first saw this fundamental relationship shown in Equation 2.29.

$$\tau = \mu \frac{dV}{dy} \quad (2.29)$$

where the coefficient of viscosity, μ , is the proportionality constant relating shear stress to velocity gradient. Fluids for which Equation 2.29 applies are called "Newtonian fluids" of which air is one.

2.7.2 Nature of Viscosity

In a gas, viscosity is caused by a momentum exchange between adjacent layers of molecules. The magnitude of the viscosity (or coefficient of viscosity) for a perfect gas may be shown by considering two planes of gas separated by a distance λ , defined as the mean transverse distance that the molecules travel between collisions as shown in Figure 2.5.

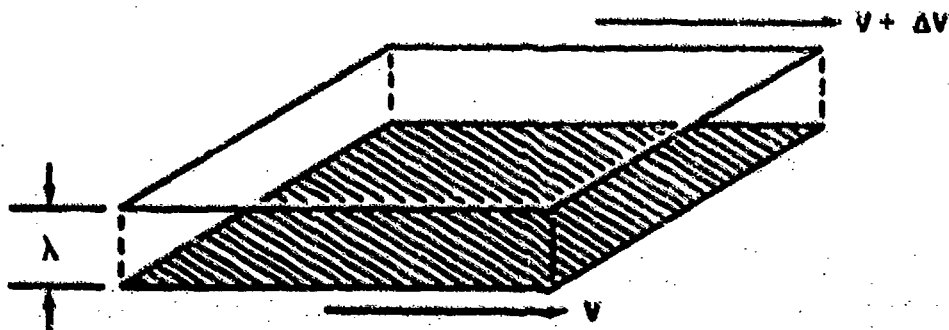


FIGURE 2.5. TWO PLANES OF FLUID

The lower plane is moving at a velocity of V and the upper plane moves at a velocity of $V + \Delta V$. Due to molecular agitation, there is a continual interchange of molecules from one plane to another. The low speed molecules from

the lower plane are accelerated upon reaching the upper plane; however, Newton's second law implies that there is an inertia force in a direction opposite to this acceleration. Conversely, there is an inertia force in this opposite direction due to the deceleration of molecules migrating to the lower plane from the upper plane. There results a shearing force per unit area (shear stress) which is a function of the transverse mean molecular velocity, the density, and the change in velocity.

Figure 2.6 further illustrates the mechanism by which viscous forces are developed. Consider two parallel streams of air having different velocities. Since the velocity of airstream A is greater than that of airstream B, the momentum of the molecules in stream A is greater than the momentum in stream B.

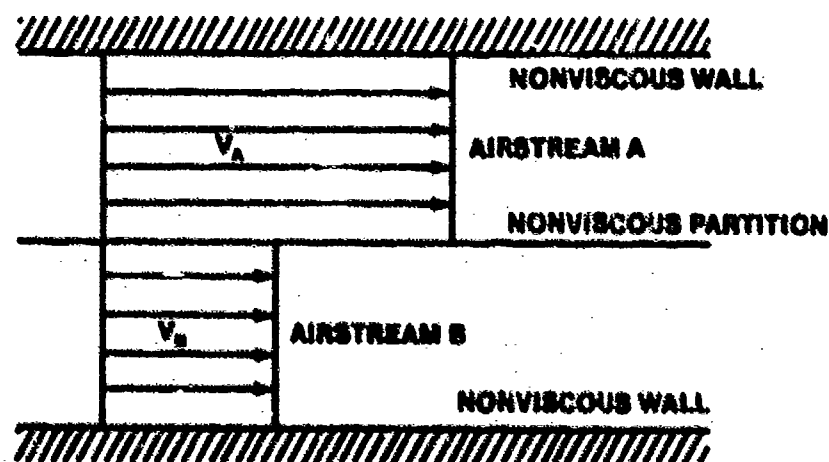


FIGURE 2.6. MECHANISM OF VISCIOUS FORCE DEVELOPMENT

Due to the random molecular motion, molecules from stream A wander over into stream B and vice versa. The same number of molecules go from A to B as go from B to A, so there is no net exchange of mass.

The average velocity of those molecules going from A to B is greater than the average velocity of those going from B to A. The molecules coming from stream A tend to increase the velocity and momentum of stream B, while the molecules of stream B tend to decrease the velocity and momentum of stream A. The stream velocities adjacent to the interface between streams A and B adjust to some average velocity, as shown in Figure 2.7, until there is no discontinuity in velocity between the two streams.

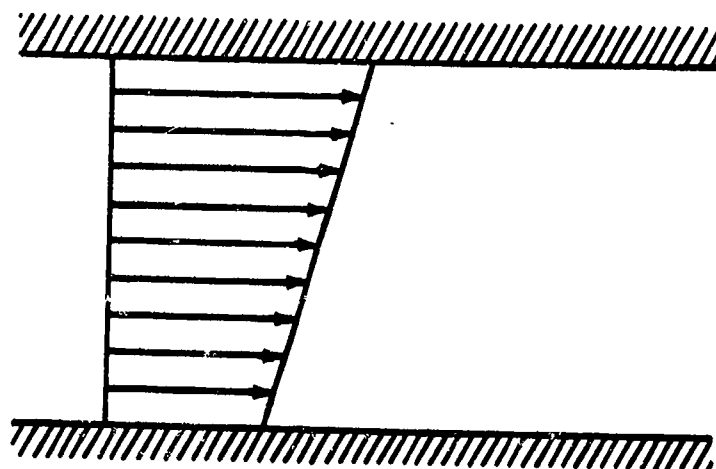


FIGURE 2.7. DEVELOPED VELOCITY GRADIENT

The end result of this process is fully developed uniform flow as shown in Figure 2.8.

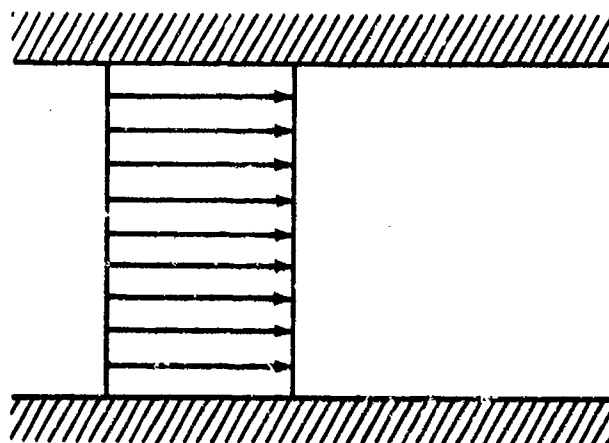


FIGURE 2.8. FULLY DEVELOPED UNIFORM FLOW

Thus, the mechanism that causes shear or viscous forces in a gas is proportional to the time rate of change of momentum.

$$\text{Viscous forces} = F = \frac{d(mV)}{dt} \quad (2.30)$$

and since the net mass exchanged is zero ($Vdm = 0$),

$$F = \frac{m}{dt} dV = \dot{m} \Delta V \quad (2.31)$$

Equation 2.31 shows that the viscous or shear force, F , is proportional to the rate at which the molecules pass from one stream to the other.

In a gas, temperature affects molecular activity. Shear stress is a function of the transverse mean molecular velocity, the density, and the change in velocity. From Kinetic Theory of Gases, the absolute temperature of a perfect gas is directly proportional to the kinetic energy of its molecules, and the coefficient of viscosity, μ , is proportional to the square root of the absolute temperature as shown in Equation 2.32.

$$\mu \propto \sqrt{T} \quad (2.32)$$

Actually for air the coefficient of viscosity varies more closely with the three-quarters power of the absolute temperature. For temperature in the range of interest for flight test, 390° to 610°R , the coefficient of viscosity may be expressed within ± 0.5 percent by the linear equation

$$\mu = (74.0 + 0.575 T) 10^{-9} \quad (2.33)$$

where T is temperature $^{\circ}\text{R}$ (2.3:11).

If standard day temperatures for sea level and 50,000 feet are inserted into Equation 2.33, it will be found that the coefficient of viscosity changes only about 20% between these altitude extremes. Density, on the other hand, changes about 87%. For this reason, the coefficient of viscosity is sometimes called a "weak" function of temperature in the literature. Often in aerodynamics it is taken to be a constant; however, this assumption must be made with caution. Contrary to intuition, viscosity is independent of pressure.

A liquid behaves in just the opposite way. Heating a liquid decreases its viscosity. Liquid viscosity is a function of intermolecular attraction, and the attractive force between molecules decreases as the distance between molecules increases; consequently, the liquid viscosity decreases. To visualize this phenomenon, envision what happens when maple syrup is poured on hot pancakes. Maple syrup is very thick and hard to pour from a bottle (high

viscosity). As soon as it touches the hot pancakes, it becomes thinner and flows easier (viscosity decreases).

Regardless of the mechanism by which viscous forces arise, whether from a momentum exchange as in a gas or from intermolecular attraction as in a liquid, they are manifested primarily as shear stresses transmitted between the various layers of the fluid or between the flowing fluid layer and a solid surface. Shear or viscous stresses normal to a surface are generally considered negligible in gases.

Viscous effects are responsible for two important phenomena encountered in the study of fluid flow. First, viscosity causes dispersing effects which tend to dissipate all disturbances in a flow such as pulsations, vortices, turbulence, jet wash, etc. An example is the reduction in the size of surface waves on water as they travel away from their source. Second, viscosity is primarily responsible for the formation of a boundary layer on the surface of a solid body in fluid flow.

2.7.3 Boundary Layer

The boundary layer is a thin sheet of retarded fluid immediately adjacent to the surface of a body immersed in a flowing fluid. It is caused by the shear stresses in the fluid which slow the molecules next to the surface to zero velocity. Von Karman suggested that this condition of zero velocity at the surface can probably be explained by the molecular or atomic structures of the solid and the fluid. Both consist of particles, atoms or molecules. The motion of the molecule in an airstream consists of a forward motion in the stream direction, on which a random motion is superposed. The atoms of the solid have a fixed mean position with empty spaces between. If the molecules enter the empty spaces of the solid, they lose their forward velocity by collision with the solid molecules; and, if they rebound, they return with random velocity without preference for any flow direction. Hence, Von Karman concluded that the average velocity of the airflow right at the surface is zero, or equal to the velocity of the solid when the solid is moving (2.4:74).

This leads to an important conceptual point in theoretical aerodynamics: a flow field can be split into two regions, one extremely thin region where friction is important, namely in the boundary layer near the surface, and another region of frictionless flow (sometimes called potential flow) outside

the boundary layer. It has already been pointed out that the Bernoulli equation can be applied anywhere in the flow field outside the boundary layer. This concept was first introduced by Prandtl in 1904, and it revolutionized modern theoretical aerodynamics (2.5:116).

It can be shown experimentally and theoretically that the pressure through the boundary layer in a direction perpendicular to the surface is constant. This is an important phenomenon. It is why a surface pressure distribution calculated from frictionless flow through use of the Bernoulli equation many times gives accurate results for the real-life (viscous) surface pressures; it is because the frictionless calculations give the correct pressures at the outer edge of the boundary layer, and these pressures are transmitted without change through the thin boundary layer right down to the surface. In Figure 2.9, on which the boundary layer thickness has been greatly exaggerated for clarity, the static pressures at Points 1 and 2 are the same.

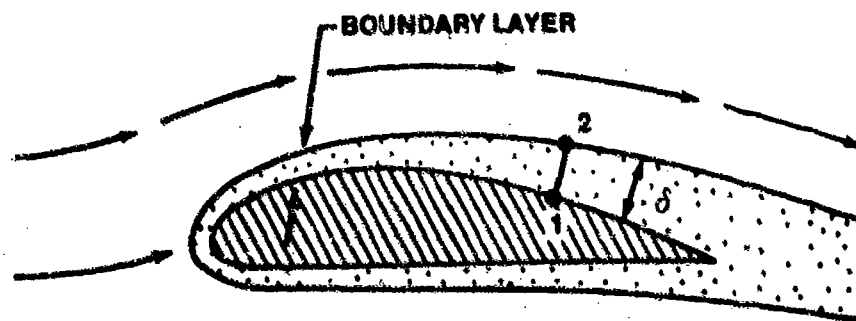


FIGURE 2.9. EXAGGERATED BOUNDARY LAYER THICKNESS (2.5:116)

The above statements are reasonable for slender aerodynamic shapes (like fuselages and airfoils); they do not hold for regions of separated flow over blunt bodies (2.5:116).

So as air flows over a body, a boundary layer is formed. At the surface, the velocity is zero. The viscosity of the fluid causes shear stresses which retard the velocity of the fluid near the surface. This shear stress decreases as distance from the surface increases until the viscous effects disappear and the velocity of the air becomes that of the free stream at the

top of the boundary layer. A typical velocity profile through the boundary layer is shown in Figure 2.10.

The characteristic features of the boundary layer velocity profile are:

1. A second-order curve shape indicating a decrease in velocity near the solid body with an associated loss of momentum.
2. Zero velocity at the surface of the solid body.
3. Local free stream velocity at the top of the boundary layer.

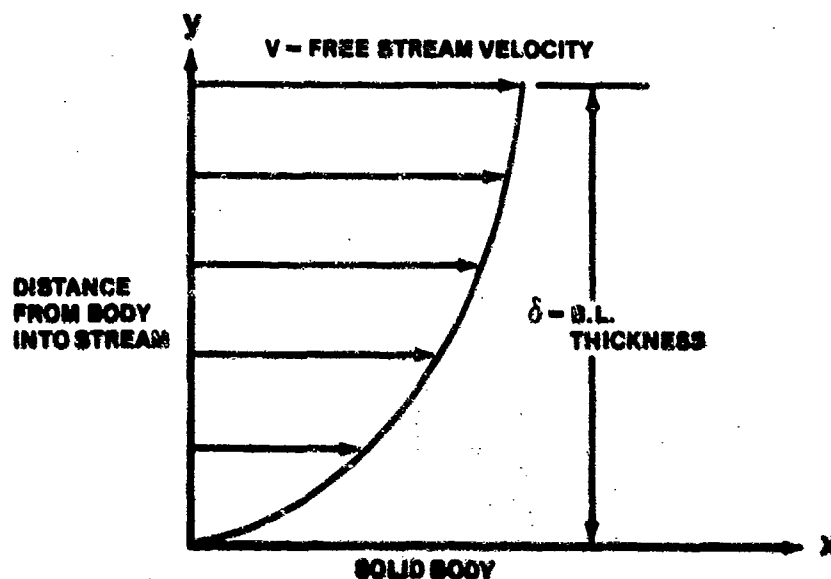


FIGURE 2.10. VELOCITY PROFILE IN THE BOUNDARY LAYER

The development of the boundary layer may be studied by periodically injecting drops of dye into a uniform liquid stream as it approaches and passes over a flat plate as in Figure 2.11. To observe a gaseous boundary layer, smoke may be injected into the gas or small cotton tufts may be attached to the surface to be studied.

Observing the resulting patterns, two characteristics common to the growth of all boundary layers are noted:

1. The boundary layer becomes thicker as the distance, x , from the leading edge of the body increases.

2. The velocity profile changes with increasing x distance.

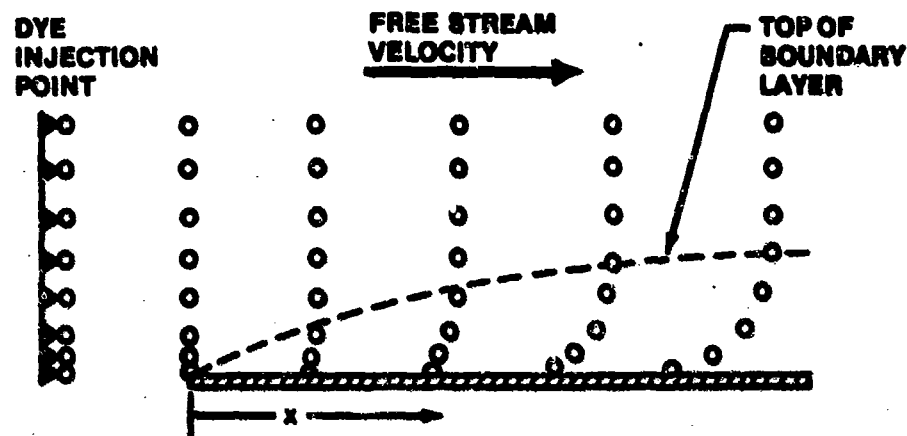


FIGURE 2.11. DEVELOPMENT OF THE BOUNDARY LAYER

The thickness of a boundary layer and velocity distribution in a boundary layer can often be predicted with a high degree of accuracy once the flow situation is completely described, that is, type of fluid, velocity of flow, geometric shape, and physical condition of the body, etc. This viscous flow in the boundary layer will be of concern when skin friction drag is studied. The concept of a nonviscous fluid where all viscous effects occur inside the boundary layer will become clearer as aerodynamic problems are discussed and the solutions of nonviscous problems are compared with experimental viscous (real-world) results.

2.7.4 Reynolds Number

The characteristics of a boundary layer in a flow depend on the combined effects of velocity, density, viscosity, distance from the leading edge, etc. The effect of the most important parameters is combined into a dimensionless parameter called Reynolds number, R_e .

The grouping of these terms and the physical interpretation was first observed by Osborne Reynolds, for whom the quantity was named. The Reynolds number is defined as

$$R_e = \frac{\rho V l}{\mu} = \frac{V l}{\nu} \quad (2.34)$$

Reynolds observed that when dye was injected into a fluid flow, a very straight, fine line persisted for a certain distance downstream. At this point, the flow became unsteady, causing the line to oscillate, until further downstream the flow became violently disturbed, causing the dyeline to dissipate completely.

From his experiments, he concluded that transition was directly related to the quantity $(\rho V l)/\mu$ for the fluid. This conclusion was not immediately obvious to Reynolds; in fact, it took many years of research and contemplation before he published his findings.

The flow prior to this transition is said to be laminar, that is, consisting of specific lamina with no cross flow currents between lamina to disturb the dye. The flow downstream of the transition is said to be turbulent, consisting of random cross flow and rotational currents which disperse the dye.

The transition region between these two conditions may be thought of as being part laminar and part turbulent. The significance of these two types of flow and their relationship to the parameter $(\rho V l)/\mu$ was probably not fully realized by Reynolds. However, the Reynolds number is very valuable when determining the aerodynamic properties of an aircraft and when applying wind tunnel data to full scale aircraft. The latter use is the reason that Reynolds number is often called a scaling factor.

A better physical grasp of the meaning of the Reynolds number is obtained if it is viewed in terms of the forces acting on the fluid of which there are four:

1. Inertia forces
2. Viscous forces
3. Pressure forces
4. Gravitational forces

Gravity usually has no noticeable influence on aerodynamic phenomena around a wing or fuselage and is neglected. That leaves three other forces which must balance in a force equation. The pressure force serves to balance the other two forces. Thus, it is enough to consider the viscous and inertia forces.

Reynolds postulated that the ratio of inertia forces to viscous forces was the governing similarity parameter needed to relate the flow patterns about geometrically similar objects in different flow fields.

$$\frac{\text{INERTIA FORCES}}{\text{VISCOUS FORCES}} = \frac{\frac{\Delta \text{MOMENTUM}}{\text{UNIT TIME}}}{\text{SHEAR STRESS} \times \text{UNIT AREA}} \quad (2.35)$$

Remember that shear stress, $\tau = \mu \, dv/dy$.

A dimensional analysis of Equation 2.35 yields an important result.

Let l = a characteristic length (like the distance back from the leading edge or chord length for an airfoil)

V = a characteristic velocity of the flow

ρ = a mass density of the flowing fluid

μ = coefficient of viscosity

m = mass (ρL^3)

t = time (L/V)

Substituting these units into Equation 2.35,

$$\frac{\frac{\Delta \text{MOMENTUM}}{\text{UNIT TIME}}}{\text{SHEAR STRESS} \times \text{UNIT AREA}} = \frac{\frac{d(mV)}{dt}}{\mu \frac{dv}{dy} A} = \frac{\frac{\rho L^3 V}{L/V}}{\mu \frac{V}{L} L^2} = \frac{\rho V l}{\mu} = R_e \quad (2.36)$$

Therefore, Reynolds number = $\frac{\text{Inertia Forces}}{\text{Viscous Forces}} = \frac{\rho V l}{\mu}$ = Similarity parameter

The term μ/ρ is called kinematic viscosity, ν , and is sometimes used in the Reynolds number equation. Thus, $R_e = V l / \nu$.

This concept is helpful when trying to understand the flow situation described by a Reynolds number for a laminar, transition, or turbulent

boundary layer. It may be said that laminar flow results when the viscous forces are large enough to overcome the oscillations caused by the dynamic forces, that is, low Reynolds number. Conversely, turbulent flow occurs when the dynamic forces become so large that they overcome the viscous damping forces, resulting in cross flow or turbulence, that is, high Reynolds number.

Transition is directly a function of the Reynolds number. When transition occurs in a certain measured distance, such as at $R_e = 530,000$ for flat, relatively smooth plates, this R_e is called the critical Reynolds number, $R_{e_{cr}}$. By increasing the velocity or density, or decreasing the viscosity, transition will occur in a shorter distance because $R_{e_{cr}}$ occurs sooner.

It should be noted that the critical Reynolds number also depends on two other variables, namely the initial turbulence in the fluid and the roughness of the surface over which the fluid is flowing.

2.7.5 Boundary Layer Growth and Transition

Many aerodynamicists, mathematicians, and theoreticians have devoted their lives to the study of the boundary layer phenomenon. One common goal was to be able to predict transition and describe the velocity profile throughout either a laminar or turbulent boundary layer on an object. Many mathematical theories have been proposed, many experiments performed, and many books, journals, and reports written. Still, no single equation defines the "general" boundary layer for any object.

Without going into detail, simple equations for computing laminar and turbulent boundary layer thicknesses will be presented to show the relative sizes of both. However, a brief discussion of the difference between laminar and turbulent flow is in order. In laminar flow, the fluid particles move along parallel streamlines with very little mixing. The only interaction between layers is the random molecular motion throughout the fluid. A "fluid particle" is considered to contain a very large number of molecules. Only a small momentum exchange occurs between layers in laminar flow since individual molecules are involved. However, when the flow is turbulent, entire fluid particles are intermingled, causing a large momentum exchange in the fluid.

The understanding of laminar and turbulent flow and the contribution of the Reynolds number to predicting transition can be used in this simple discussion of the boundary layer. As might be anticipated from Reynold's experiment, flow over a solid surface is ideally laminar until the $R_{e\text{ cr}}$ is reached (transition), after which the flow becomes turbulent.

The boundary layer grows thicker as the flow passes over the surface (Figure 2.11), and has a characteristic velocity profile (Figure 2.10). The shape and rate of growth of this velocity profile are dependent on whether the flow in the boundary layer is laminar or turbulent.

As a flow with uniform velocity approaches and passes over a smooth flat plate as shown in Figure 2.12, a laminar boundary layer develops which grows according to Equation 2.37 (2.1:311).

$$\delta_L = \frac{5.2x}{\sqrt{R_e}} \quad (2.37)$$

where

δ_L = laminar boundary layer thickness

x = the distance from the leading edge of the plate

R_e = Reynolds number based on the characteristic length, x

When the Reynolds number reaches the critical value, transition begins. In the transition region the flow is neither laminar nor turbulent but is mixed, with the lower portion being primarily laminar and the upper part being primarily turbulent.

A region of partial separation sometimes occurs near the surface but disappears once transition has been accomplished. In effect, the transition region is one in which the turbulent boundary layer is born and the laminar layer is shrinking to a fraction of its original size. On an airfoil, the transition region decreases in size with increasing Reynolds number. For typical values of in-flight Reynolds number, the region is small enough to be referred to as the transition point.

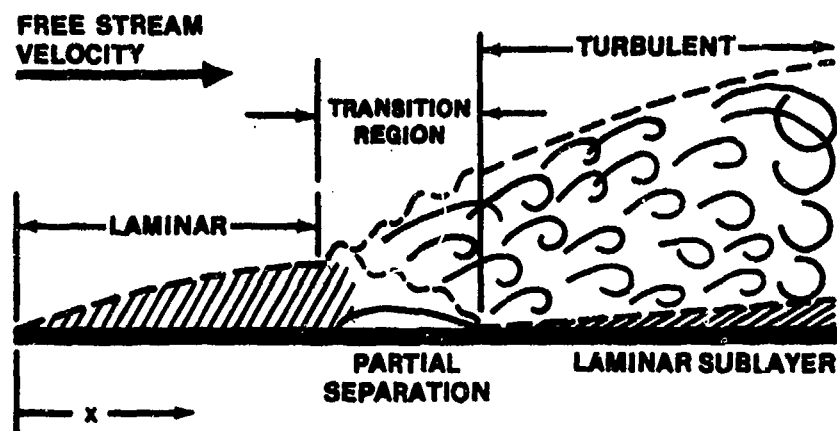


FIGURE 2.12. BOUNDARY LAYER TRANSITION OVER A FLAT PLATE

After transition, a laminar boundary layer continues to exist as a small sublayer next to the surface, with the velocity profile in the sublayer being nearly linear with a very steep gradient. This laminar sublayer is only on the order of one percent of the total boundary layer thickness (2.1:388).

A turbulent boundary layer on a flat plate grows rapidly according to Equation 2.38 (2.1:400).

$$\delta_T = \frac{0.37 x}{(R_e)^{0.2}} \quad (2.38)$$

where

δ_T = turbulent boundary layer thickness

x = the distance from the leading edge of the plate

R_e = Reynolds number based on the characteristic length, x

Experimental comparison of the rate of growth of the various types of boundary layers has shown that the turbulent boundary layer grows roughly ten times faster than the laminar boundary layer.

It should be noted that Equation 2.38 applies only to a turbulent boundary layer which has been turbulent effectively from the leading edge; if the layer is laminar for an appreciable distance, the problem becomes more

complicated and cannot be measured from some point between the leading edge and transition (2.1:401).

Normally, for smooth flat plates or smooth airfoils, a laminar boundary layer will initially form and transition to a turbulent boundary layer at the critical Reynolds number for the flow conditions. However, many factors can cause a turbulent boundary layer to initially form, e.g., surface roughness or flow turbulence.

2.7.6 Velocity Profiles

The velocity profiles in laminar and turbulent boundary layers show a very significant difference when the ratio of velocity in the boundary layer over free stream velocity is plotted versus the percentage of the boundary layer thickness as shown in Figure 2.13.

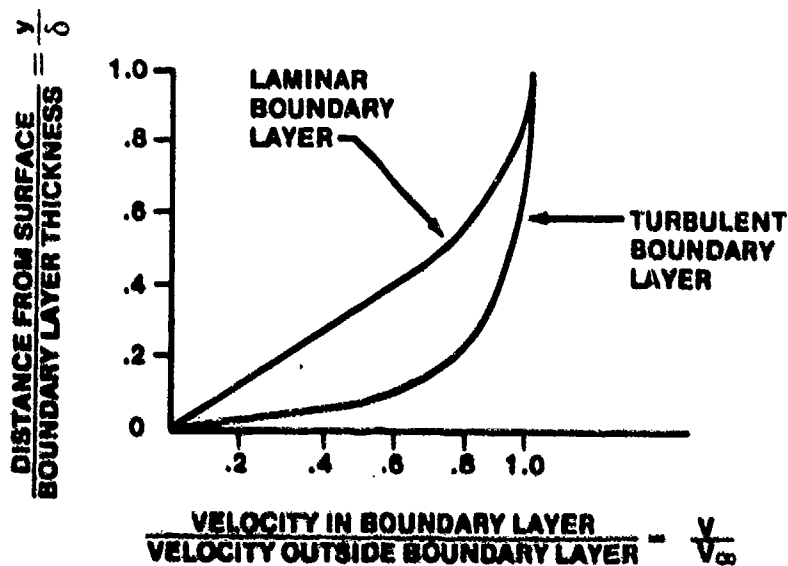


FIGURE 2.13. BOUNDARY LAYER VELOCITY PROFILES ON A FLAT PLATE

The magnitude of the velocity in the turbulent boundary layer is much greater than in the laminar boundary layer. The turbulent boundary layer has considerably more energy in the lower levels near the object's surface than a

corresponding laminar layer. This occurs because the turbulence mixes more of the high energy air from the upper levels into the lower levels.

2.7.7 Skin Friction

The velocity profile is the primary factor which determines the skin friction on a surface. The shear stress for laminar flow was given by Equation 2.29,

$$\tau = \mu \frac{dV}{dy} \quad (2.29)$$

and since the flow next to the surface is always laminar even when turbulent flow exists above it, the viscous resistance can be calculated. This calculation is possible because shear stresses in the boundary layer, other than those caused by the velocity gradient, dV/dy , at the surface, cannot be transmitted to the surface. Shear stresses in one layer of fluid affect only the adjacent layer of fluid. The velocity gradient at the surface is the only one needed to calculate the skin friction.

$$\text{Skin Friction} = \tau A = \mu A \left. \frac{dV}{dy} \right|_{\text{Surface}} \quad (2.39)$$

where A is the area the shear stress is acting upon. It can be seen that more skin friction is produced by a turbulent boundary layer than by a laminar boundary layer, since at the surface dV/dy is greater in a turbulent boundary layer as shown in Figure 2.14.

It appears almost universal in nature that systems with the maximum amount of "disorder" are favored. For aerodynamics this means that the vast majority of practical viscous flows are turbulent. The boundary layers on practical aircraft are turbulent with the exception of small regions near the leading edge. Consequently, the skin friction on these surfaces is the higher, turbulent value. For the aerodynamicist who is striving to reduce drag, this is unfortunate (2.5:120).

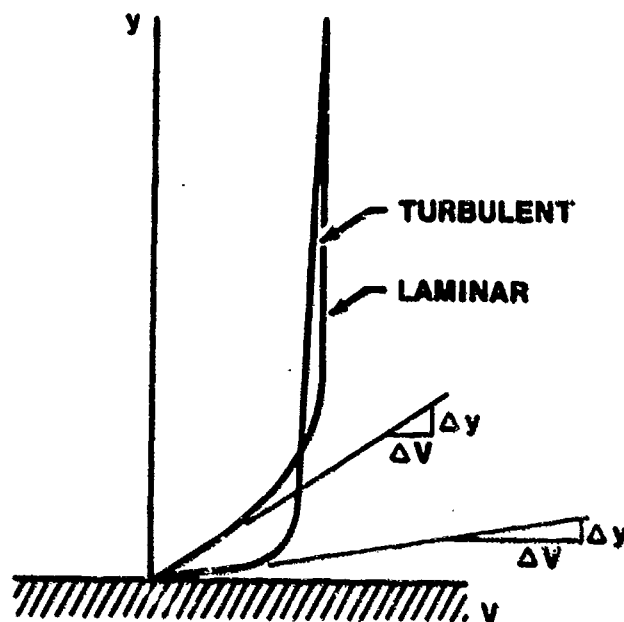


FIGURE 2.14. BOUNDARY LAYER VELOCITY PROFILES

While less skin friction is created on an object by a laminar boundary layer, attempts to maintain laminar flow are not usually practical because of separation problems. Turbulent boundary layers help prevent flow field separation. Quite frequently, separation and the resulting increase in pressure drag cause a much greater increase in the total drag on an object than does the increase in skin friction drag due to the normal formation of a turbulent boundary layer. Consequently, it cannot be said in general that either laminar or turbulent flow is preferable. Any preference depends on the specific application (2.5:133).

2.7.8 Separation and Pressure Gradient

When fluid flow no longer conforms to the geometric contour of a body, it is said that the flow has separated from the body. When separation occurs, the boundary layer detaches from the surface of the body. Separation is a function of the velocity gradient in the boundary layer. A steep velocity gradient at the surface helps prevent separation even though it increases the skin friction on the surface.

Sharp surface contours may cause separation, since the inertia of the moving fluid may cause it to flow away from the surface when attempting to negotiate a sharp corner. While this cause may be the most obvious, it is not the primary cause of separation, since corners sharp enough to produce separation are easily avoided on most aerodynamic shapes. On the other hand, at high angles of attack, the leading edges of some wings appear as a sharp corner to the airflow, causing leading edge separation. Obviously, this is a very undesirable characteristic.

The pressure gradient over an object in a flowing fluid is the primary cause of separation. The typical velocity profile in Figure 2.10 is altered somewhat when there is a pressure gradient along the object. The pressure gradient is defined as dP/dx ; that is, the pressure changes a given amount, dP , as the stream moves a length, dx , over a surface (dx is positive in the direction of flow).

A positive pressure gradient is one in which the pressure increases as x increases, whereas a negative pressure gradient is one in which the pressure decreases as x increases. An example of a negative pressure gradient is found over the forward upper surface of a wing while a positive gradient exists over the aft upper surface as shown in Figure 2.15.

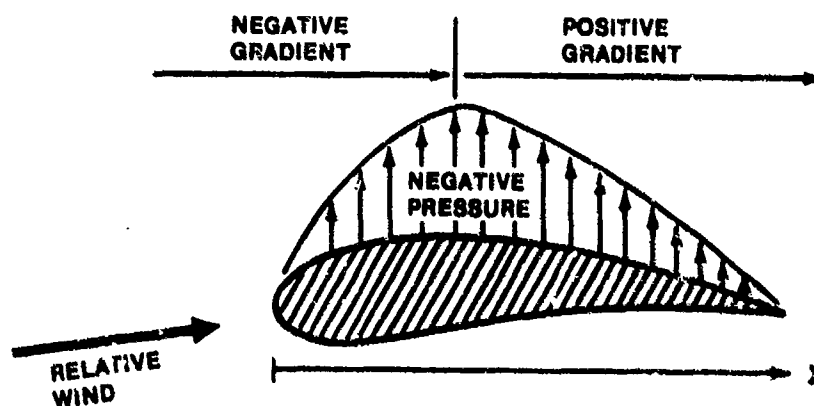


FIGURE 2.15. UPPER SURFACE PRESSURE DISTRIBUTION ON AN AIRFOIL

When the fluid in a boundary layer flows into a negative pressure gradient, that is, a region of lower pressure, it tends to accelerate, causing the velocity profile to increase or become fuller as shown in Figure 2.16.

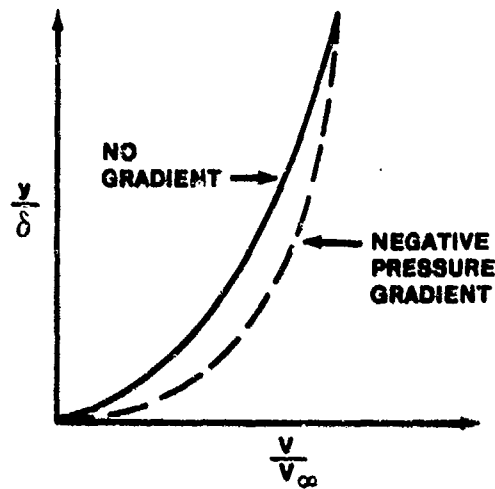


FIGURE 2.16. CHANGE IN VELOCITY PROFILE DUE TO NEGATIVE PRESSURE GRADIENT

For flow to continue into a positive pressure gradient, the kinetic energy of the fluid velocity must be dissipated. Therefore, the velocity in the boundary layer decreases when flowing into a positive pressure gradient. The longer the flow in a boundary layer acts against a positive pressure gradient, the thinner the velocity profile becomes as shown in Figure 2.17.

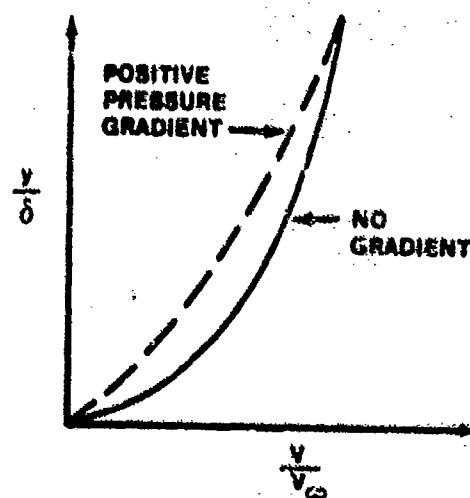


FIGURE 2.17. CHANGE IN VELOCITY PROFILE DUE TO POSITIVE PRESSURE GRADIENT

Velocity in the boundary layer will decrease due to a positive pressure gradient until the flow reverses direction. This reversal of flow direction, called separation, occurs at a point on the surface where the velocity gradient, dV/dy , equals zero. The effect of a positive pressure gradient on the velocity profile of a stream as it flows along a surface is shown in Figure 2.18.

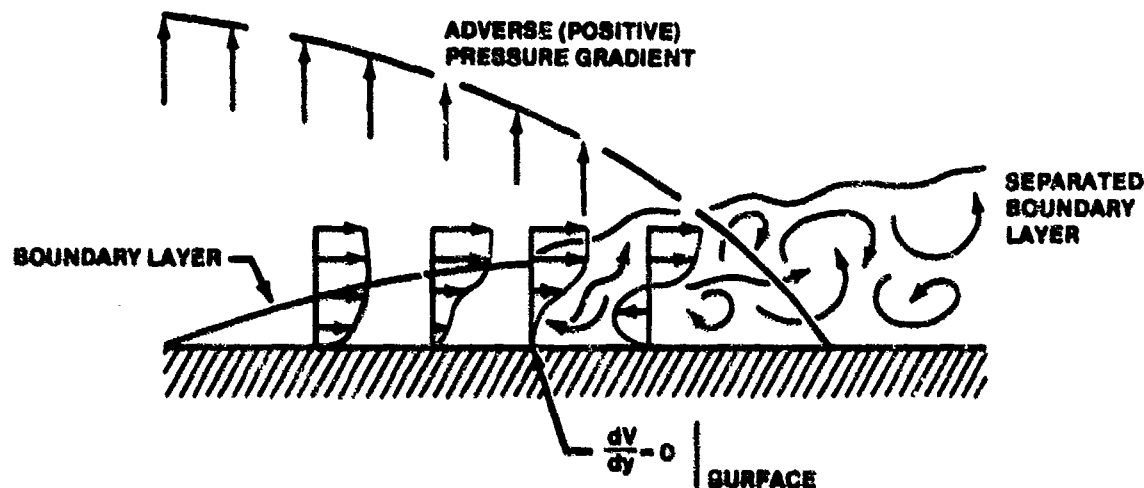


FIGURE 2.18. EFFECT OF ADVERSE PRESSURE GRADIENT

Separation will occur only due to a positive pressure gradient. It can be shown that separation will not occur due to a negative gradient. For this reason, a positive pressure gradient is often referred to as an adverse pressure gradient, since separation is an undesirable condition. By the same reasoning, a negative gradient is termed a favorable pressure gradient.

The fluid particles in the boundary layer must respond to the forces produced by this pressure distribution. On an airfoil between the forward stagnation point and the point of minimum pressure (maximum velocity), a boundary layer particle is pushed downstream by the favorable pressure gradient. But due to viscous effects, the particle is losing some energy, and by the time it reaches the point of minimum pressure, its momentum is less than it would have been if the flow were nonviscous.

As it continues on toward the trailing edge, it is literally going up a pressure "hill," but it starts with reduced momentum. So it must flow against

both an adverse pressure gradient and greater viscous force. With this combination of reduced momentum and retarding viscous force, it is inevitable that the particle will stop before reaching the trailing edge. Thus, it separates from the airfoil, forming a wake. The flow beyond this point shows "back flow" from the trailing edge moving toward the separation point, as shown in Figure 2.18.

To forestall separation of the boundary layer in the presence of an adverse pressure gradient, the boundary layer must have the highest possible kinetic energy. If a choice is available, a turbulent boundary layer is preferable to a laminar layer because the turbulent velocity profile shows higher local velocities near the surface.

2.8 SUMMARY

The relationships discussed in this chapter are the basis for the study of aerodynamic theory, and the practical application of this theory is the basis for all the elements of aircraft performance.

PROBLEMS

- 2.1 A flying wing with a chord of 12 ft is cruising at 400 ft/sec at 10,000 ft on a standard day. What is the flight Reynolds number based on wing chord length?
- 2.2 An F-15 is traveling at 700 KTAS at 60,000 ft on a standard day. What is the flight Mach?
- 2.3 What true velocity (ft/sec and kts) is an SR-71 maintaining at Mach = 3.0 cruise at 65,000 ft on a standard day?
- 2.4 A T-38 flying on a standard day stabilizes at 37,000 ft at 96 percent RPM at Mach 0.80. Later at another point in the mission, while performing aerobatics, the pilot notices that at 45,000 ft with his power set at 96% RPM, he is accelerating through Mach 0.8.
- a. Compute the flight dynamic pressure for the two points described above.
 - b. What is the equivalent airspeed at the 45,000 ft point described above?
- 2.5 An aircraft stabilizes at a pressure altitude of 30,000 ft in level unaccelerated flight. The ambient temperature at that level is measured to be -60°F . Is it a standard day? FIND: Ambient pressure in lb/ft^2 , δ , θ , and σ .

2.1 2.4×10^7 (No Units)

ANSWERS

2.2 1.22 (No Units)

2.3 1,718 kts; 2,905 ft/sec

2.4 a. 203 lb/ft^2 ; 138 lb/ft^2

b. 341 ft/sec

2.5 $\theta = 0.771$; $\delta = 0.297$; $\sigma = 0.385$ (No Units)

BIBLIOGRAPHY

- 2.1 Kuethe, Arnold M., and Chow, Chuen-Yen, Foundations of Aerodynamics: Bases of Aerodynamic Design, 3rd ed. New York: John Wiley & Sons, 1976.
- 2.2 FTC-TIH-70-1001, Performance, USAF Test Pilot School, 1973.
- 2.3 Dwinell, James H., Principles of Aerodynamics. New York: McGraw-Hill Book Company, Inc., 1949.
- 2.4 Von Karman, Theodore, Aerodynamics: Selected Topics in the Light of their Historical Development. Ithaca, NY: Cornell University Press, 1954.
- 2.5 Anderson, J.D., Jr., Introduction to Flight; Its Engineering and History. New York: McGraw-Hill Book Company, Inc., 1978.

CHAPTER 3
AIRFOIL AND WING THEORY

3.1 INTRODUCTION

Now that the fundamentals of aerodynamics have been introduced, we shall look at how lift is developed on airfoils and wings. Moment characteristics will also be studied.

Airfoils are simply a two-dimensional concept useful for the study of certain parameters which determine the characteristics of real, three-dimensional wings.

The wing is the primary aircraft component responsible for the development of lift. Other aircraft components such as the fuselage, nacelles, and tail can and do produce lift. However, these components are primarily of interest to the designer and will not be considered here. Application of lift production by the wing to the total aircraft will be considered.

Separation of lift and drag, which does not occur in nature, is done here to facilitate discussion. Drag will be thoroughly discussed in Chapter 4.

3.2 AIRFOIL TERMINOLOGY

The first step in the study of airfoils is to define an airfoil and other terms which describe its geometric and aerodynamic characteristics.

Airfoil (wing section) is a surface formed by a streamlined contour.

Chord Line is a straight line between the leading edge and trailing edge of the airfoil. The length of the chord line is generally given the symbol c .

Mean Camber Line is the line described by points which are equidistant from the upper and lower surfaces of the airfoil.

Camber is a measure of the curvature of an airfoil as evaluated by the height of the mean camber line above or below the chord line.

Thickness is the distance between the upper and lower surfaces of the airfoil.

Relative Wind (V or V_{∞}) refers to the motion of air relative to an airfoil and is equal and opposite to the forward velocity of the aircraft.

Angle of Attack (α) is the angle between the relative wind and the chord line.

Center of Pressure (cp) is a point on the chord of an airfoil through which the resultant aerodynamic force acts.

Resultant Aerodynamic Force (F or RAF) is the vector summation of all of the aerodynamic forces acting on an airfoil.

Lift (L) is the component of the resultant aerodynamic force perpendicular to the relative wind.

Drag (D) is the component of the resultant aerodynamic force parallel to the relative wind.

Aerodynamic Center (a.c.) is a point on the chord of an airfoil about which the moment coefficient is practically constant for all angles of attack.

Figure 3.1 is an illustration of the geometric characteristics defined above.

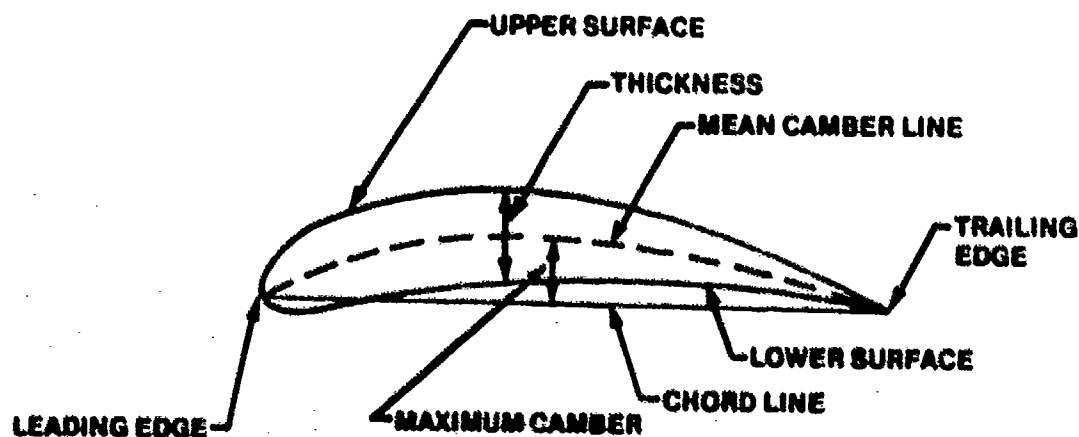


FIGURE 3.1. AIRFOIL NOMENCLATURE

In Figure 3.2, the aerodynamic characteristics are illustrated.

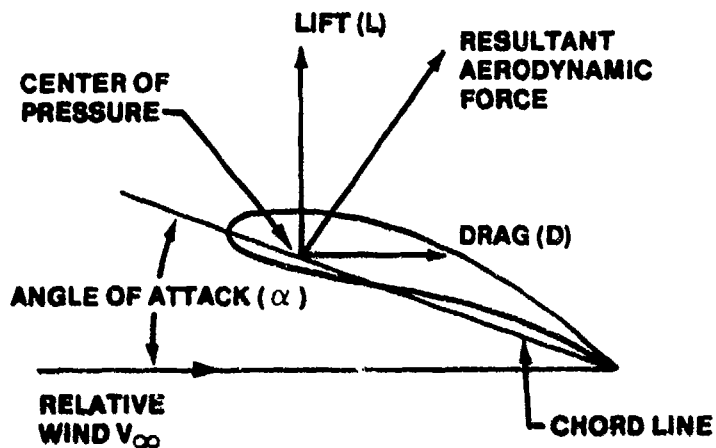


FIGURE 3.2. AERODYNAMIC PARAMETERS

3.3 AIRFOIL SECTION DESIGNATION

The geometric proportions of an airfoil section are conveniently expressed in terms of three main variables:

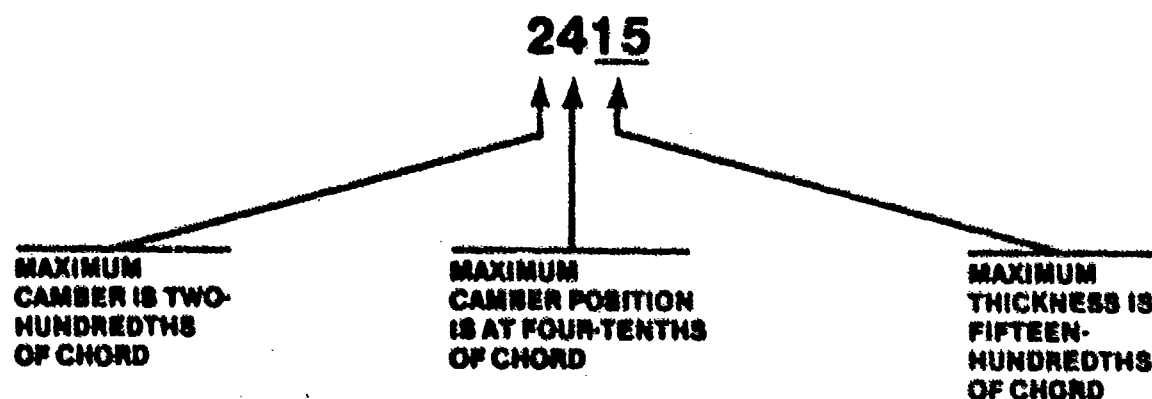
1. Shape of the mean line
2. Thickness
3. Thickness distribution

A great number of airfoil sections have been developed by experimenters in the United States and elsewhere. In order to provide a reliable basis for design, the NACA, in 1929, started development of a systematic series of sections that have since provided clear proof of the influence of changes in shape of the mean line and changes in thickness of the airfoil on aerodynamic characteristics. Basing the series upon the assumption that the thickness

distribution is the least important of the three previously mentioned variables, the NACA chose the average thickness distributions from two well-known, successful airfoil sections as a basis for a major part of their early tests: they were the Clark Y (U.S.A.) and the Gottingen 398 (German). By varying the percent thickness and shape of the mean line but keeping the thickness distribution fixed, two series of airfoil sections were developed, the original four and five digit series.

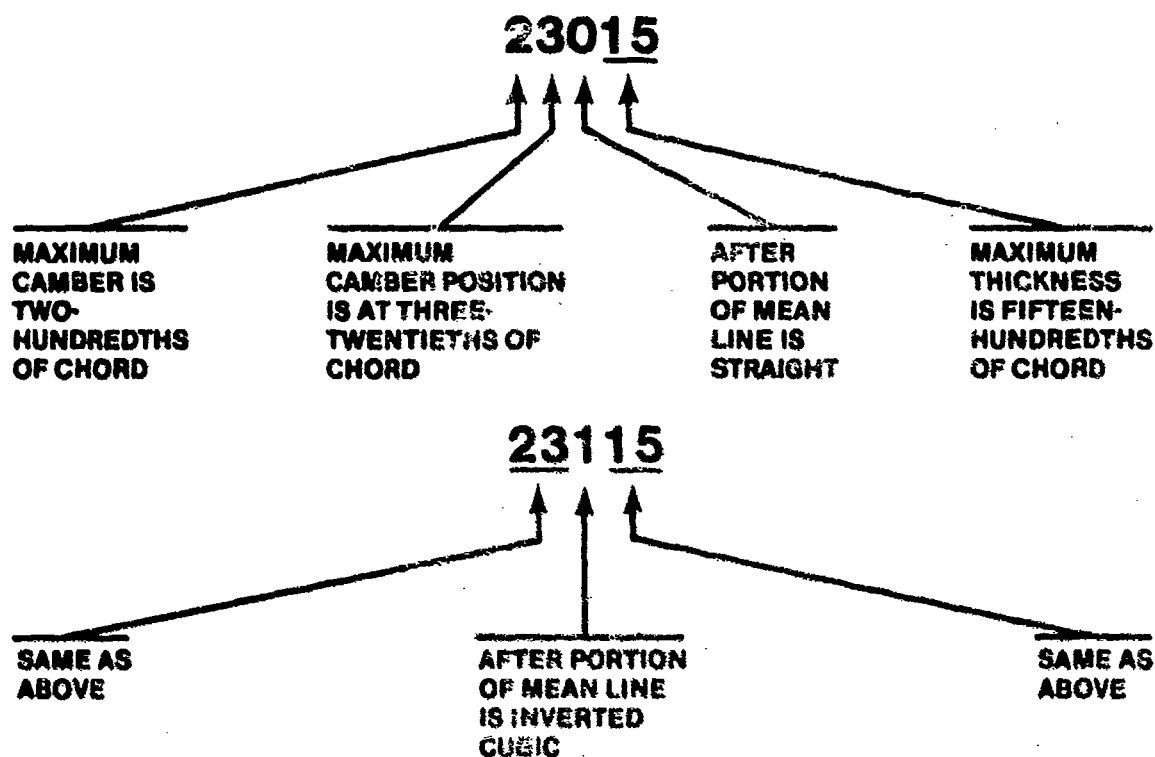
3.3.1 Four-Digit Series

The four-digit series is based upon a mean line defined by two second-degree parabolas that are tangent at the point of maximum camber. The code used to define the resultant contour of the airfoil is composed of four digits: the first gives the amount of maximum camber in percent of chord, the second gives the position of the maximum camber in tenths of chord, and the last two give the maximum thickness in percent of chord. The following example may clarify the preceding explanation



3.3.2 Five-Digit Series

The five-digit series has the same thickness distribution as the four digit series but is based upon a mean line defined by a cubic in the forward part of the airfoil, which becomes tangent either to a straight line or to an inverted cubic that forms the after portion. The designation for the five-digit series is somewhat similar to that for the four-digit series and may be shown by the following examples:

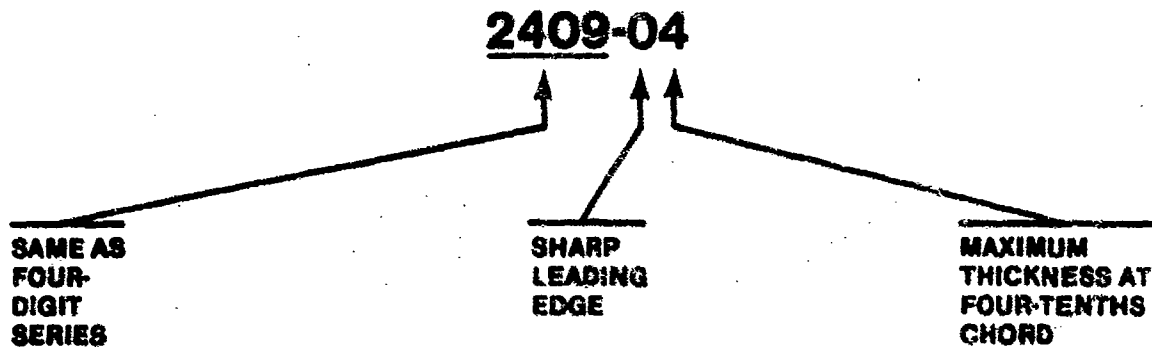


Theoretical considerations have indicated that by having the most negative pressure on an airfoil occur closer to the trailing edge than on the four- or five-digit series and by reducing the absolute value of the most negative pressure, the drag may be reduced and the high-speed characteristics improved. This led to several airfoil series that are characterized by a maximum thickness occurring somewhere in the vicinity of the mid-chord.

One of the earliest of this type was originally designed for desirable high-speed characteristics. It is a modified four-digit series in which the first four digits have their usual meaning, while a group of digits following a dash indicates thickness distribution. The first digit within this group indicates leading-edge radius according to the following:

- 0 designates sharp leading edge
- 3 designates one-fourth normal four-digit radius
- 6 designates normal four-digit radius
- 9 designates three times normal four-digit radius

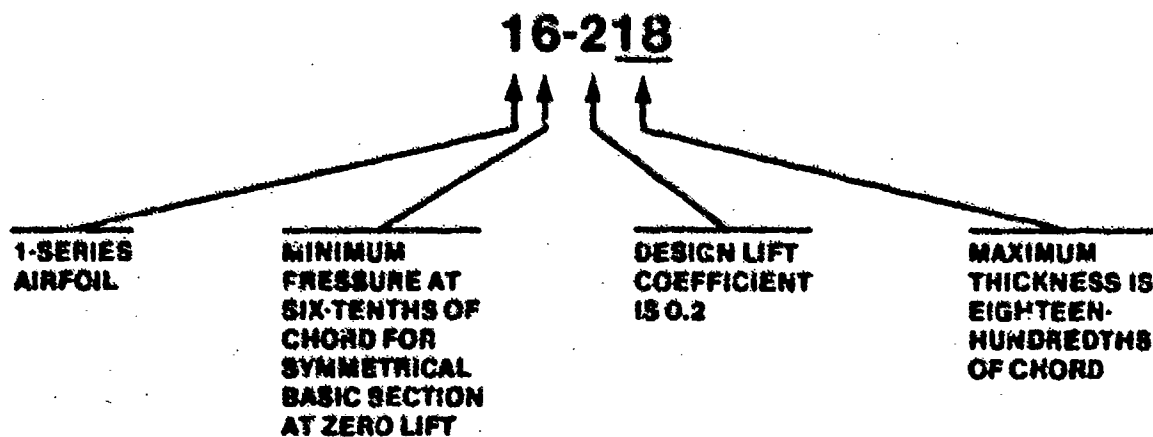
The second digit gives the position of the maximum thickness in tenths of chord. For example,



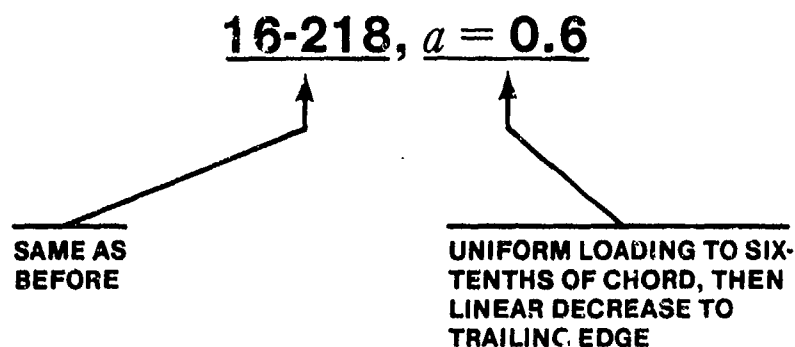
More extensive tests were subsequently run on other airfoils designed primarily for low drag characteristics, the most successful of which were the 1-series, 6-series, and 7-series. The numbering system is somewhat similar for these three groups, but each will be discussed separately.

3.3.3 The 1-series Airfoils

This group is defined as a symmetrical airfoil having a minimum (most negative) pressure occurring well back from the leading edge. Changes in airfoil characteristics within the series are then accomplished by changing the thickness and the shape of the mean line as in the four- and five-digit airfoils, the difference being that the airfoil is designed to give low drag at a particular angle of attack or lift coefficient. The second digit refers to the position of minimum pressure for the basic symmetrical section at zero lift, in tenths of chord. The digit after the hyphen refers to the design lift coefficient in tenths, and the last two digits refer to the maximum thickness in percent of chord. For example,



The mean line is usually curved in such a manner that it produces an approximately constant chordwise difference in pressure between upper and lower surfaces at the design lift coefficient, which produces an approximately constant load per inch on the chord. However, the mean line may be curved so as to produce an approximately constant load from the leading edge to the 60% percent chord, say, and then a linearly decreasing load to the trailing edge. This change in "loading" is indicated after the airfoil designation:

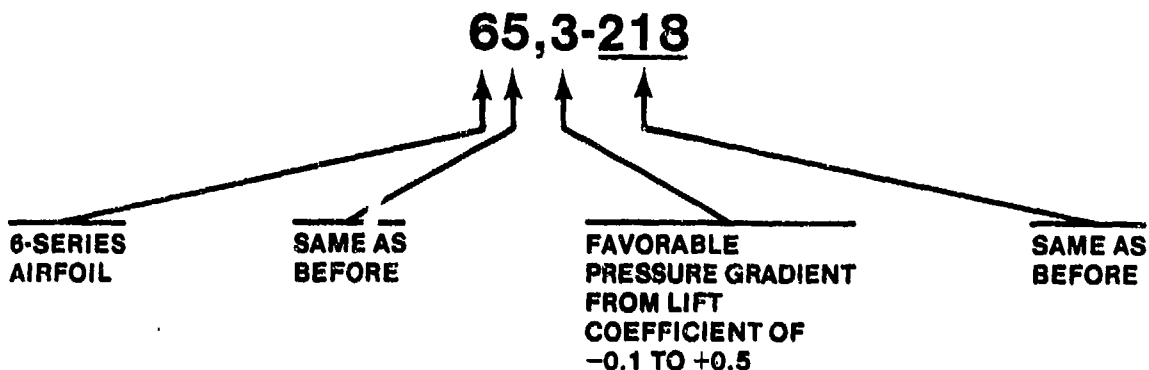


Frequently, if the loading is uniform so that $a = 1.0$, the load designation is deleted.

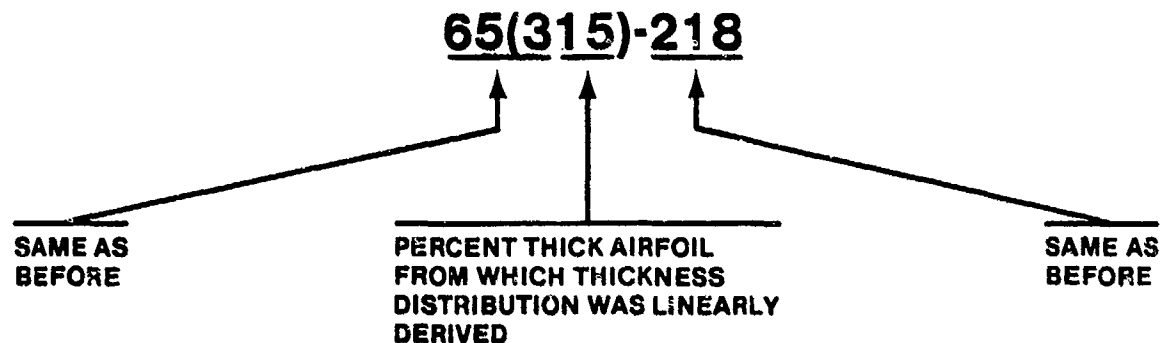
One of the most useful 1-series airfoils is the 16-() series, which is usually referred to as the 16-series.

3.3.4 The 6-series Airfoils

The system of designation is similar to that for the 1-series airfoils, but additional information is given by another number that shows the range of lift coefficients, in tenths, above and below the design lift coefficient, for which a favorable pressure gradient exists on both surfaces.



In contrast to all the preceding airfoils discussed, the thickness distribution of the above airfoil depends upon its maximum thickness. A second subgroup with a thickness distribution obtained by linearly varying all ordinates in proportion to the maximum thickness is designated as in the following example



A third subgroup is based upon a theoretical rather than individually derived (first subgroup) or linearly specified (second subgroup) variation in thickness distribution with maximum thickness. All digits have the same meaning as in the first subgroup. For example,

65₃-218

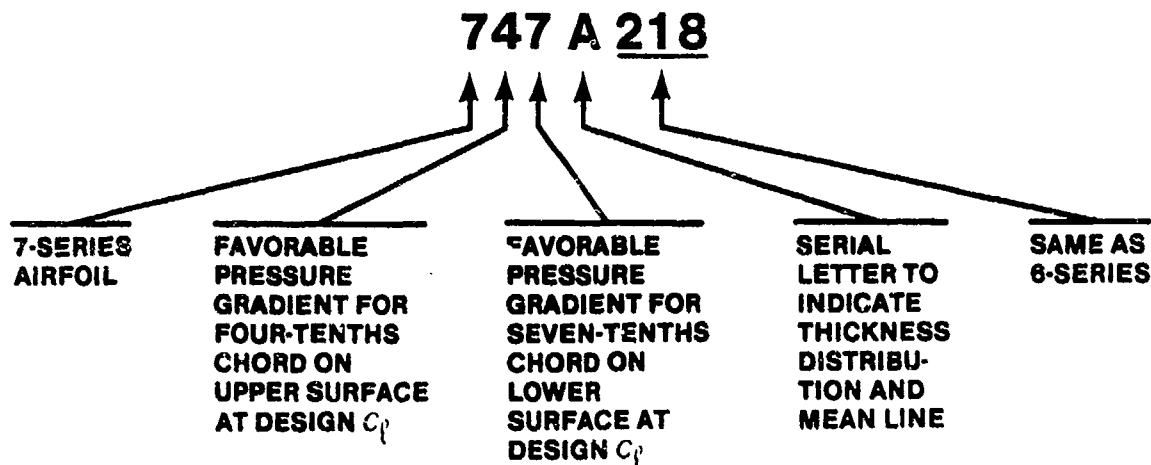
Again the above airfoil has a distribution of thickness that depends upon its maximum thickness. A fourth subgroup obtained by a linear variation like the second subgroup is specified like the second subgroup

65₍₃₁₅₎-218

All the 6-series airfoil symbols may be followed by a loading term as in the 1-series.

3.3.5 The 7-series Airfoils

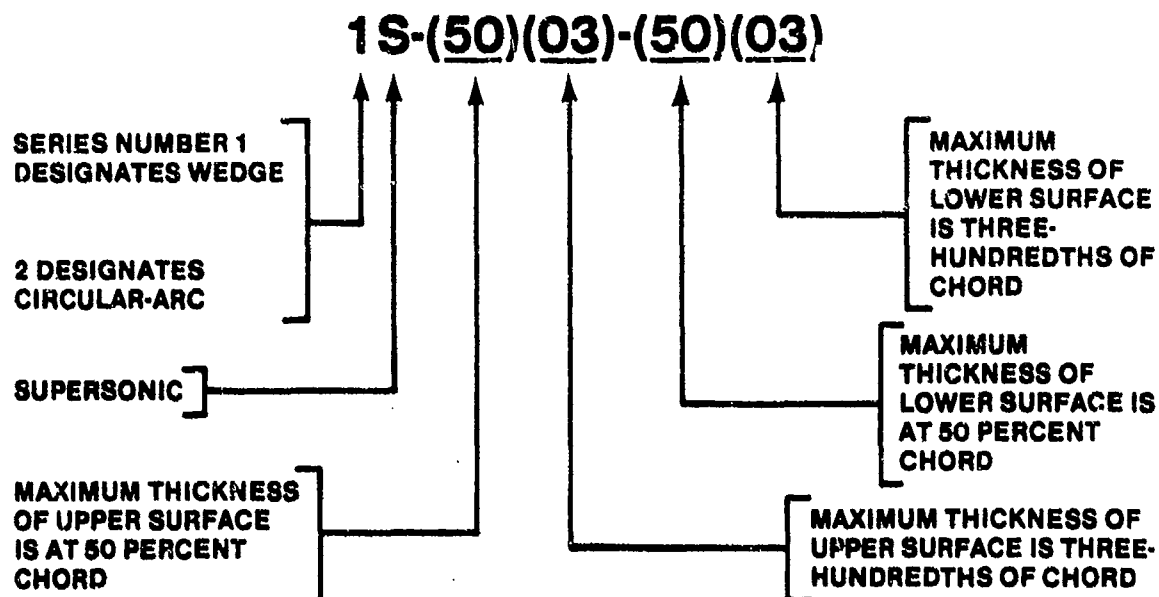
This series was designed to produce a minimum pressure at different percent chord on the upper and lower surfaces. For example,



All the 7-series airfoils have thickness distributions that are individually derived, hence do not vary linearly with maximum thickness.

3.3.6 Supersonic Sections

Supersonic flight poses problems that are entirely different from subsonic. A series of airfoils, based on theoretical considerations, has been developed by NACA. All airfoils are characterized by a knife-edge leading edge. The numbering system may best be illustrated by an example.



Examples of some common airfoils of the various groups described are depicted in Figure 3.3 (3.1:61-67).

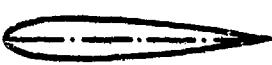




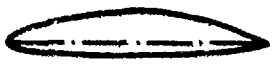
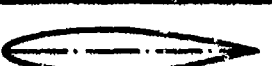
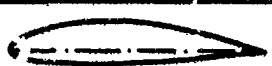
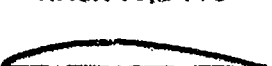
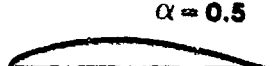
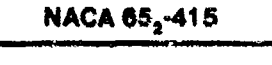
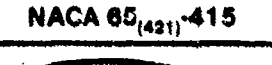
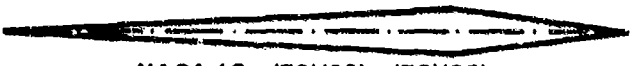
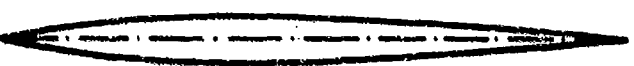
FOUR-DIGIT SERIES AIRFOILS	 NACA 0015	 NACA 4415
FIVE-DIGIT SERIES AIRFOILS	 NACA 23015	 NACA 23115
1-SERIES AIRFOILS	 NACA 16-015	 NACA 16-515
6-SERIES AIRFOILS	 NACA 65,2-015	 NACA 65(216)-415 $\alpha = 0.5$
	 NACA 65,2-415	 NACA 65(421)-415
7-SERIES AIRFOILS	 NACA 747A015	 NACA 474A415
SUPERSONIC AIRFOILS	 NACA 15-(70)(03)-(70)(03)	
	 NACA 28-(30)(03)-(30)(03)	

FIGURE 3.3. EXAMPLES OF COMMON AIRFOIL SECTIONS

3.3.7 Other Airfoil Designation Systems

This extensive coverage of the NACA airfoil designation system should not be construed to mean that it is the only system in existence. There are several other systems in existence. Examples are the Gottingen (German), the St. Cyr (French), and other types of systems and special airfoils developed in other countries and even by specific aircraft manufacturers.

The NACA system has been in existence for over 50 years, and many NACA airfoils are still used throughout the international aerospace industry.

3.4 WING TERMINOLOGY

The following terms are used to describe the geometric and aerodynamic characteristics of wings.

Wing Area (S) is the reference wing area used in computing aerodynamic coefficients. In the U.S., it is generally the main "trapezium" area as shown shaded in Figure 3.4.

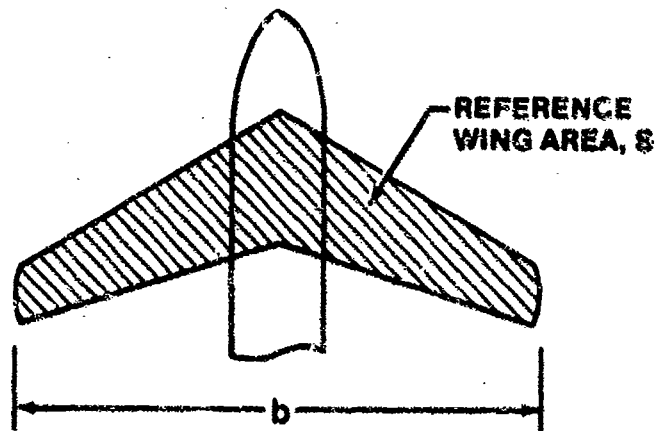


FIGURE 3.4. REFERENCE WING AREA

Wing Span (b) is also a reference dimension measured wingtip to wingtip as shown in Figure 3.4.

Mean Aerodynamic Chord (MAC) is a theoretical chord for an imaginary, straight, untapered wing which has the same force vectors as the actual wing throughout the speed range of concern. The true mean aerodynamic chord is difficult to compute for many modern aircraft wings since they can be tapered, swept, elliptical, or otherwise irregular, but can be calculated by the relationship

$$C_{mac} = \frac{\int_{-b/2}^{b/2} c^2 dy}{\int_{-b/2}^{b/2} c dy} = \frac{1}{S} \int_{-b/2}^{b/2} c^2 dy$$

In practice, it has been found that the MAC can be approximated geometrically as shown in Figure 3.5.

Taper Ratio (λ) is the ratio of the tip chord to the root chord of a wing.

Sweep Angle (Λ) is the angle the quarter chord line of the wing makes with a lateral line perpendicular to the fuselage reference line. Sweep aft is normally considered positive, and forward sweep is negative.

Aspect Ratio (AR) for any wing planform is defined as the ratio of the span squared to the area.

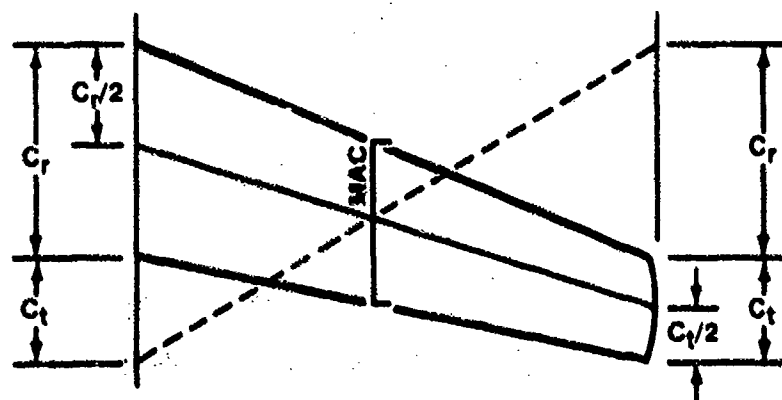
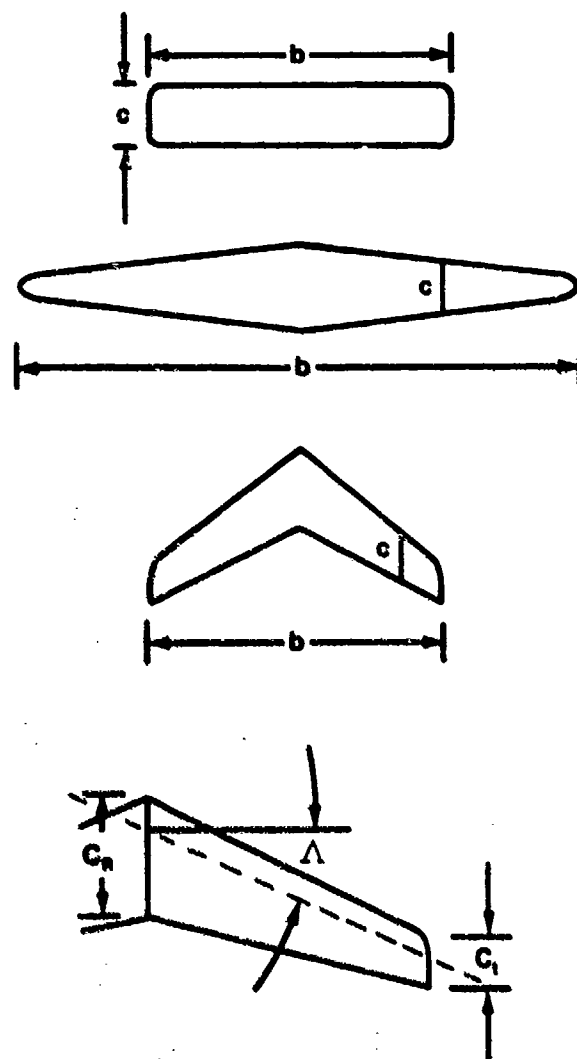


FIGURE 3.5. MEAN AERODYNAMIC CHORD DETERMINATION

Figure 3.6 summarizes geometric characteristics.



S - WING AREA, SQ FT
b - SPAN, FT
c - CHORD, FT

AR - ASPECT RATIO
 $AR = b/c$
 $AR = b^2/s$

C_R - ROOT CHORD, FT
C_t - TIP CHORD, FT
 λ - TAPER RATIO
 $\lambda = C_t/C_R$

Λ - SWEEP ANGLE, DEGREES

FIGURE 3.6. SUMMARY OF WING GEOMETRIC CHARACTERISTICS (3.2:62)

3.5 AIRCRAFT REFERENCE SYSTEM

Figure 3.7 illustrates a Water Line (W.L.), Base Line (B.L.), and Fuselage Station (F.S.) reference system. The reference system used in aircraft general arrangement diagrams is not standard among contractors. Some contractors refer to Water Lines as Fuselage Reference Lines (FRL). Lockheed picks a line about down the center of the fuselage as W.L. 100 and defines this line as the fuselage reference line. In almost all cases, these lines, or stations, are measured in inches from the base zero line. The F-104A base zero lines are shown in Figure 3.7 (3.3:35). Location of the F-104A MAC is shown using the system described above.

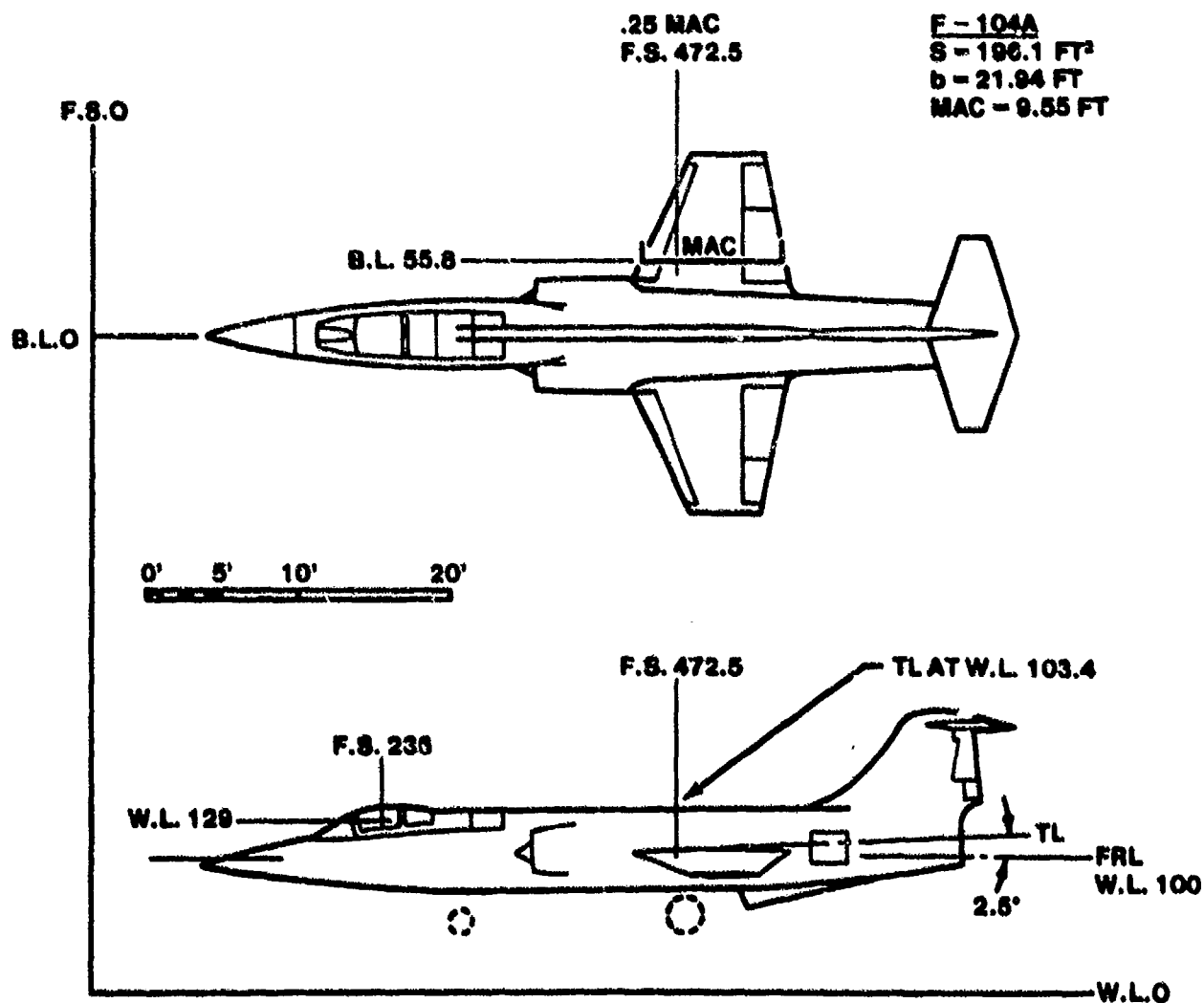


FIGURE 3.7. EXAMPLE AIRCRAFT GENERAL ARRANGEMENT DIAGRAM (3.3:35)

3.6 INFINITE SPAN WING THEORY

In 1878, Rayleigh studied the flow around a circular cylinder and found that, if the cylinder is exposed to a uniform flow or moves uniformly through a fluid at rest, d'Alembert's theorem applies, and there is no force acting on the cylinder. No lift and no drag exist. But, according to the Kutta-Joukowski theorem, the superposition of a circulatory flow upon a uniform flow produces a force perpendicular to the direction of the original flow, or perpendicular to the direction of motion of the cylinder.

If a clockwise circulatory motion is superimposed on the circular cylinder in the uniform stream, the streamline pattern shown in Figure 3.8 results. The velocity over the top of the cylinder is increased, and the velocity over the bottom of the cylinder is decreased. From the Bernoulli equation, there is a net upward force developed on the cylinder perpendicular to the uniform stream. A two-dimensional infinite wing can be represented mathematically in this fashion by a bound vortex which moves with the wing at the wing's aerodynamic center. Therefore, an infinite wing so represented develops lift perpendicular to the relative wind without creating drag (3.4:33).

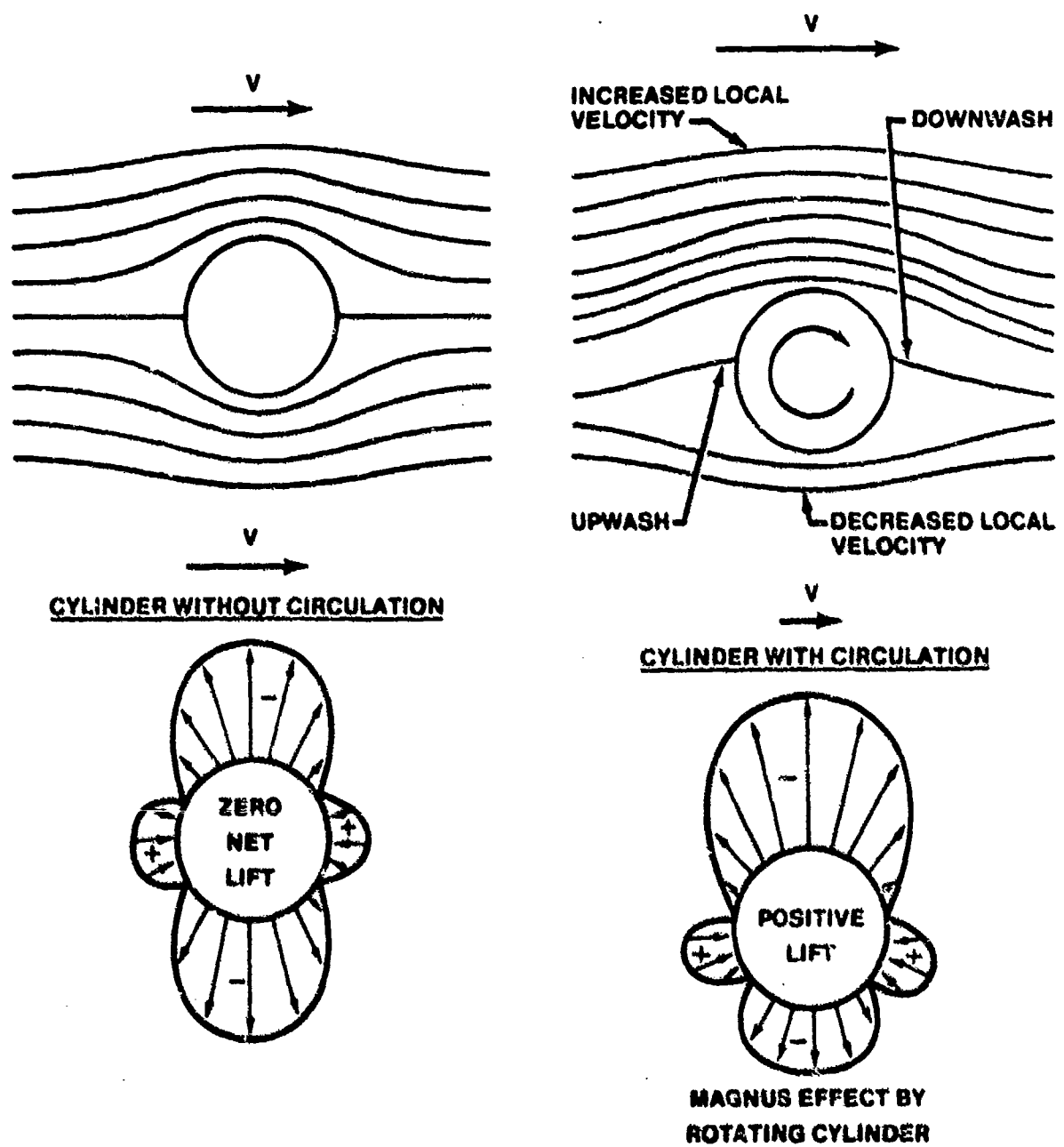


FIGURE 3.8. DEVELOPMENT OF LIFT ON A CIRCULAR CYLINDER (3.2:17)

In order to find the lift force on a practical shape such as an airfoil in fluid flow, it is necessary to know the value of the circulation. Theory indicates that the geometry of the body and the free stream velocity do not determine the value of the circulation (3.5:96).

In a viscous flow (however small the viscosity), the circulation is fixed by empirical observation. Experiments show that when a body with a sharp trailing edge (such as an airfoil) is set in motion, the action of the fluid viscosity causes the flow over the upper and lower surfaces to merge smoothly at the trailing edge; this circumstance, which fixes the magnitude of circulation around the body is termed the "Kutta condition."

In 1902, Kutta assumed that viscosity set the value of circulation even though he could not give a physical explanation for this phenomenon. Experiments at that time and since have shown that his assumption accurately corresponds to reality. Some years later, Prandtl gave a complete description of the physical mechanism by which circulation develops through use of his boundary layer theory. Boundary layer theory is beyond the scope of this course, but the essential feature of Prandtl's explanation is that even for enormous values of Reynolds number, shear stress remains finite and viscosity does not vanish. Even a very small value of viscosity is enough to prevent the back-flow around the sharp trailing edge of an airfoil toward the rear stagnation point as shown in Figure 3.9. Vorticity develops to cause the flow to merge smoothly at the trailing edge as described by the Kutta condition (3.6:37).



FIGURE 3.9. IDEAL NONVISCOS FLOW PAST A CAMBERED AIRFOIL WITH ZERO CIRCULATION AT AN ANGLE OF ATTACK (3.5:97)

The resulting circulation superimposed on the uniform free stream flow causes the velocity traversing the top of the wing to increase, and the velocity below the wing to decrease. According to the Kutta-Joukowski theorem, this produces a force perpendicular to the uniform free stream flow as shown in Figure 3.10. Therefore, an infinite wing with an airfoil cross-sectional shape develops lift perpendicular to the relative wind without creating drag.

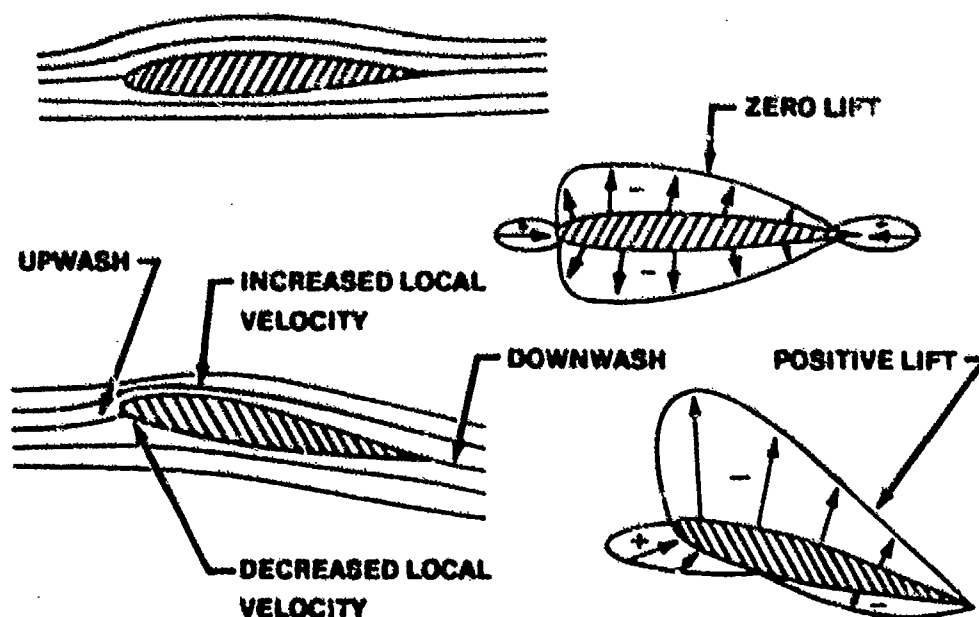


FIGURE 3.10. VISCOUS FLOW PAST AN AIRFOIL WITH CIRCULATION AT AN ANGLE OF ATTACK (3.2:17)

3.7 FINITE SPAN WING THEORY

Lanchester, in 1907, was the first man to attack the problem of a wing with a finite aspect ratio. He also had the idea that a wing must really behave like a vortex and induce a flow field around the wing. So he replaced the wing mathematically with a bound vortex at the wing's aerodynamic center; however, according to Helmholtz, a vortex cannot begin or terminate in the air. It must end at a wall or form a closed loop. Lanchester concluded that, if the bound vortex ends at the wingtip, the continuation must be a free vortex extending downstream from each wingtip. Lanchester's published drawing of a vortex system looks very much like that in Figure 3.11 (3.4:48).

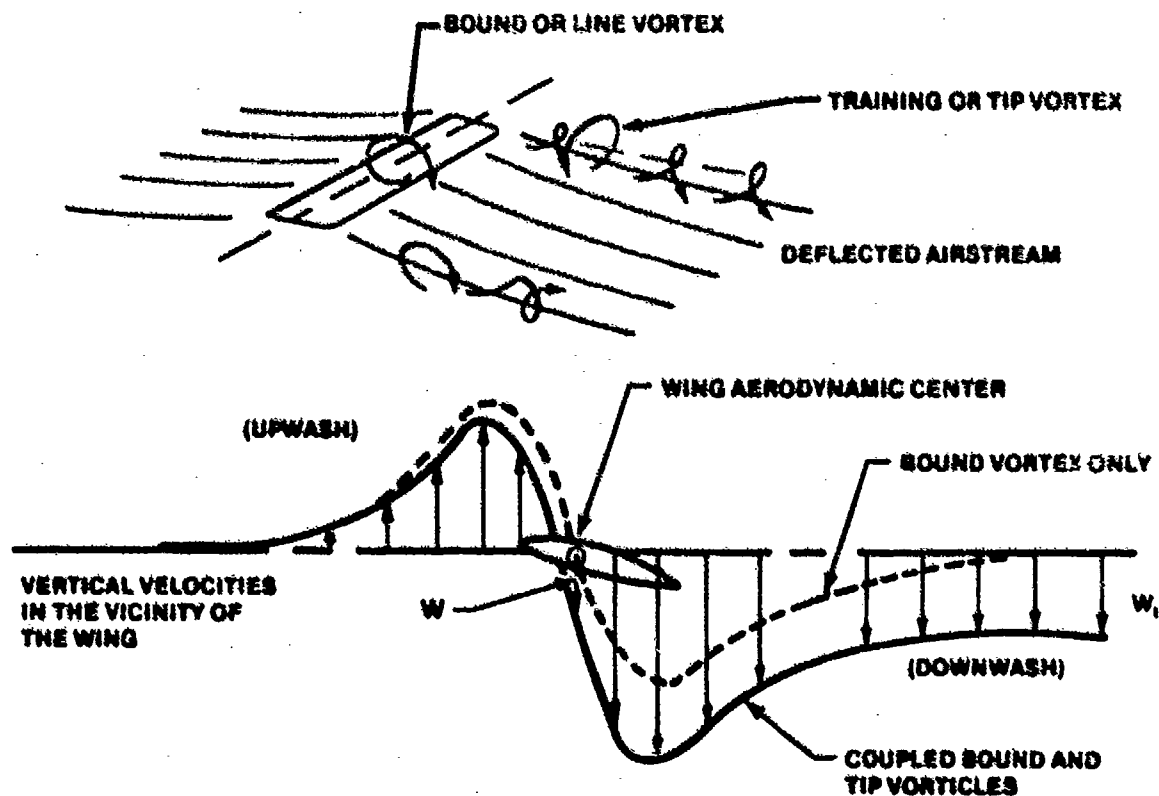


FIGURE 3.11. WING VORTEX SYSTEM (3.2:67)

The system of free vortices gives rise to a field of induced velocities in which each vortex sets up a circulatory motion of air. The vertical component of these induced velocities is called downwash (or upwash). Downwash occurs in the wing wake in the vicinity of the wing and, in particular, at the wing's aerodynamic center. Upwash occurs ahead of the wing and outboard of the wingtips. The momentum imparted to the air to direct it downward by the wing results in a reactive lift force on the wing. As the aircraft proceeds, air is continually deflected downwards and the momentum per unit time is equal to the lift force (3.4:50).

Lanchester was the first to point out that the kinetic energy of the downwash field represents the work necessary to sustain flight. One important consequence is that no work is necessary if the wing is infinitely long. Lanchester reasoned that given two wings with the same lift and same area but with different spans, the work is less for the longer wing than for the shorter (3.4:50).

Prandtl is credited with developing wing theory. He systematized Lanchester's ideas and developed a theory to solve two problems. First, if the distribution of lift along the wingspan is known, the flow pattern of the velocities and the energy necessary to obtain the lift distribution can be calculated. Second, the lift distribution along the span can be calculated when the geometry of the wing is given. Many methods have since been used to solve these two problems analytically (3.4:54).

Figure 3.12 illustrates representative lift distribution per foot of span for several different planforms. This illustration provides a basis for appreciating the effect of area distribution and taper along the span.

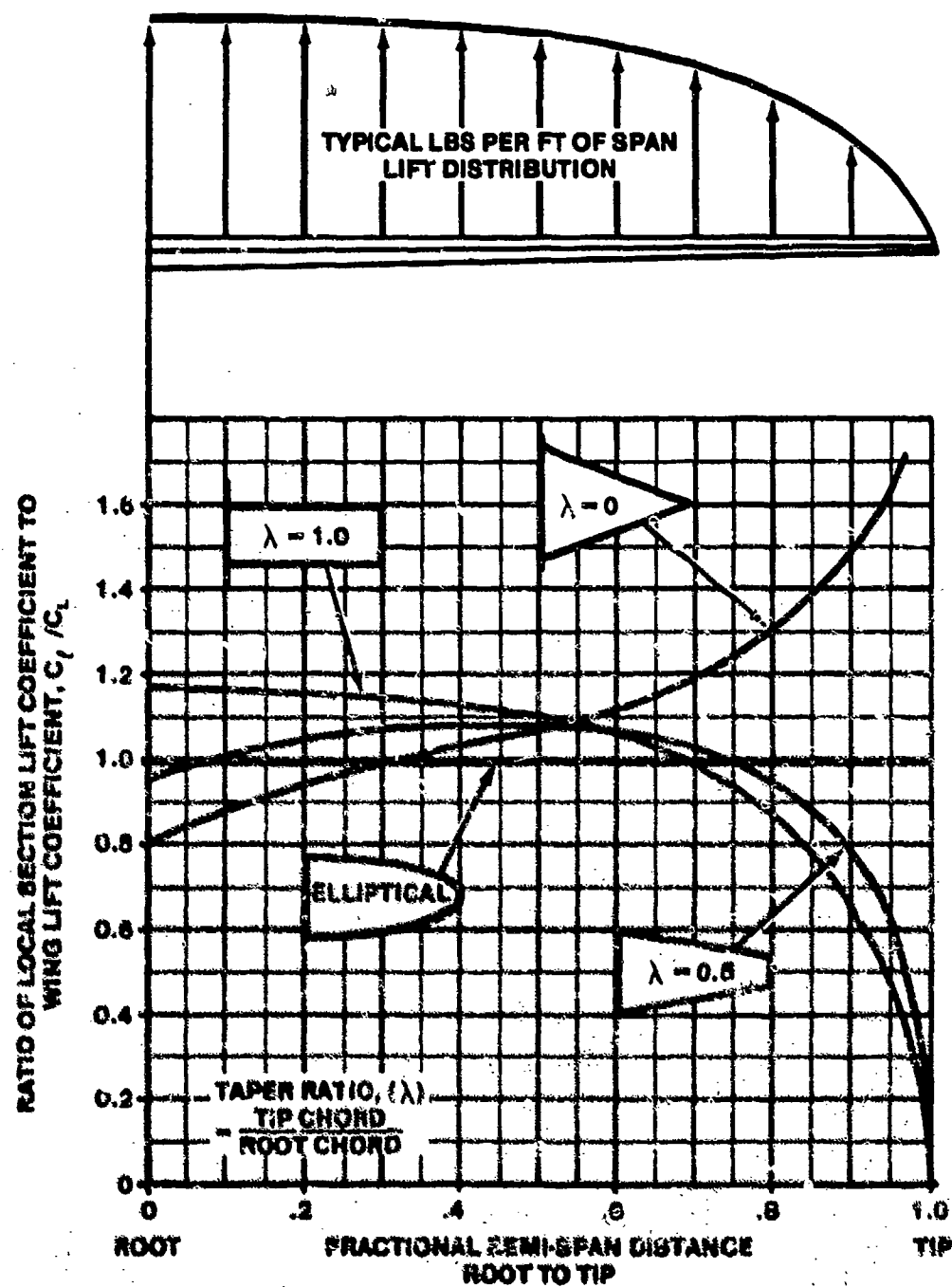


FIGURE 3.12. PLANTFORM EFFECTS ON LIFT DISTRIBUTION (3.2:75)

3.8 AERODYNAMIC COEFFICIENTS

The definitions of the primary aerodynamic coefficients C_L , C_D , and C_M follow directly from Equation 3.1 and Figure 3.13.

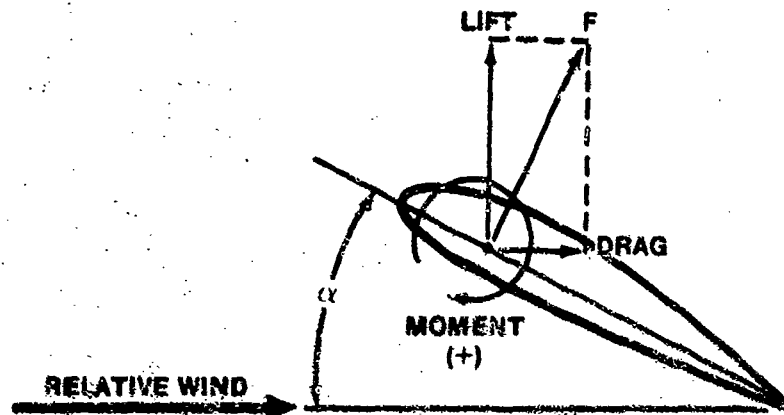


FIGURE 3.13. AERODYNAMIC FORCES AND MOMENTS

$$F = C_F qS \quad (3.1)$$

The definition of force coefficient follows from rearranging Equation 3.1 which was determined from dimensional analysis in Chapter 2 (Equation 2.18).

$$C_F = \frac{F}{qS} \quad (3.2)$$

Since lift and drag are defined as components of the resultant aerodynamic force, F , lift coefficient and drag coefficient are defined by Equations 3.3 and 3.4.

$$C_L = \frac{L}{qS} \quad (3.3)$$

$$C_D = \frac{D}{qS} \quad (3.4)$$

Assuming there is an aerodynamic moment as well as a resultant aerodynamic force, the moment coefficient can be defined as shown in Equation 3.5.

$$C_m = \frac{M}{qSc} \quad (3.5)$$

A nose-up moment is defined as positive as shown in Figure 3.13. Generally, a positively cambered airfoil section will generate a negative or nose-down moment.

Equations 3.3, 3.4, and 3.5 are used to determine C_L , C_D , and C_m directly from wind tunnel tests since S and c are known and D , L , M , and q can be measured. Throughout the literature, lower case subscripts are used to define airfoil section characteristics, i.e., C_l , C_d , and C_m . Upper case subscripts, C_L , C_D , and C_M , are used to define wing or total aircraft characteristics.

3.9 FORCES ON AN AIRCRAFT

For a simplified analysis, it will be assumed that all forces act through the center of gravity, cg , of the aircraft and that the cg is located at the center of pressure.

Because of aircraft symmetry about the x - y plane, the following concepts will be discussed in two dimensions, namely x and z , without losing generality. Reducing the flow situation to two dimensions is a common practice when discussing basic aerodynamics.

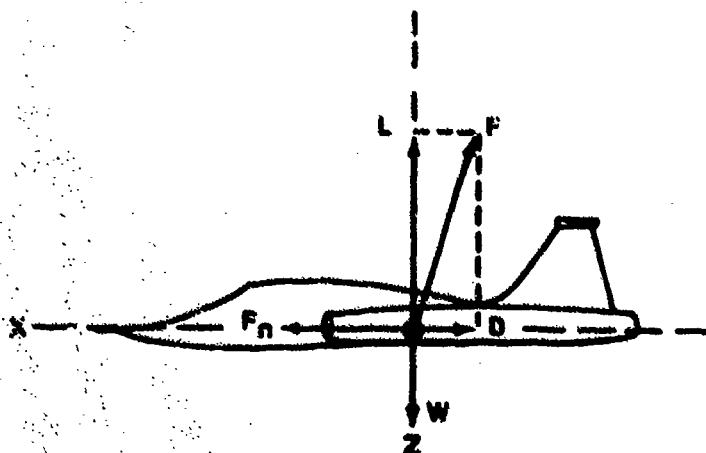


FIGURE 3.14. FORCES ON AN AIRCRAFT IN FLIGHT

The aircraft in Figure 3.14 is in stabilized level flight if Equations 3.6 and 3.7 are satisfied.

$$\begin{aligned}\Sigma F_z &= 0 \\ L &= W\end{aligned}\tag{3.6}$$

$$\begin{aligned}\Sigma F_x &= 0 \\ F_n &= D\end{aligned}\tag{3.7}$$

If net thrust, F_n , exceeds the drag, D , the aircraft will accelerate along a flight path and is said to have excess thrust.

$$F_{ex} = F_n - D\tag{3.8}$$

If the lift, L , is greater than the weight, W , the aircraft is said to be maneuvering and has an acceleration in a direction perpendicular to the flight path which is equal to the ratio of lift to weight force. This ratio is then defined as load factor, n , and is sometimes called "g" force.

$$n = L/W\tag{3.9}$$

The performance and flying qualities of an aircraft are directly related to the forces acting on the aircraft. Thrust is attributable to the power-plant(s) while lift and drag result from air flowing over and through the aircraft.

3.10 PRESSURE DISTRIBUTION

The previously discussed Bernoulli equation explains how aerodynamic forces are produced on a body in subsonic flight.

$$P + \frac{1}{2} \rho V^2 = \text{constant}\tag{3.10}$$

Since the total pressure is constant, if velocity increases, static pressure

must decrease; conversely, if velocity decreases, static pressure must increase.

Figure 3.15 shows typical streamlines and areas of increased and decreased velocity on an airfoil at a high angle of attack. Airflow accelerating across the top of the wing reduces pressure, and airflow decelerating underneath the wing increases pressure.

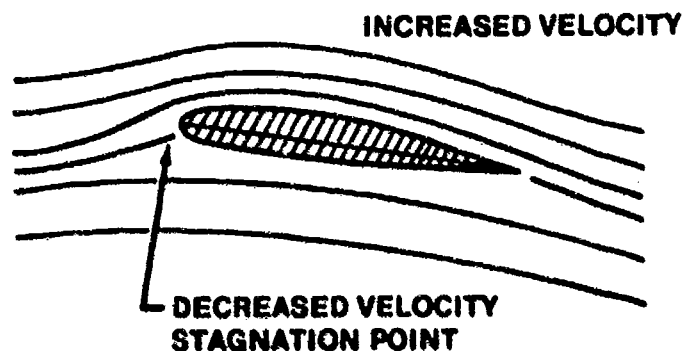


FIGURE 3.15. AIRFOIL STREAMLINES

Note in Figure 3.15 that the streamlines move closer together as velocity increases and further apart as velocity decreases. This is caused by the requirement for constant mass flow between streamlines.

Figure 3.15 also shows a well defined forward stagnation point where the average airflow velocity equals zero and the total pressure exists on the airfoil. This forward stagnation point is where the flow divides into flow over and under the wing.

Theoretically, nonviscous theory shows that there is also an aft stagnation point at the trailing edge of the airfoil; however, in practice, because of viscous effects, total pressure recovery is never actually achieved.

Figure 3.16 shows the pressure distribution caused by the streamline pattern. The pressure plotted is shown relative to the free stream static pressure. The outward arrows on top of the airfoil indicate pressure less

than free stream; therefore, an integration of each incremental pressure times its effective area results in a lift force. Unfortunately, this area of pressure less than free stream is sometimes called an area of "negative pressure" or "suction." This is a poor choice of terms from an engineering standpoint.

The inward arrows on the bottom of the airfoil indicate pressure greater than free stream; therefore, an integration of each incremental pressure times its effective area also results in a lift force.

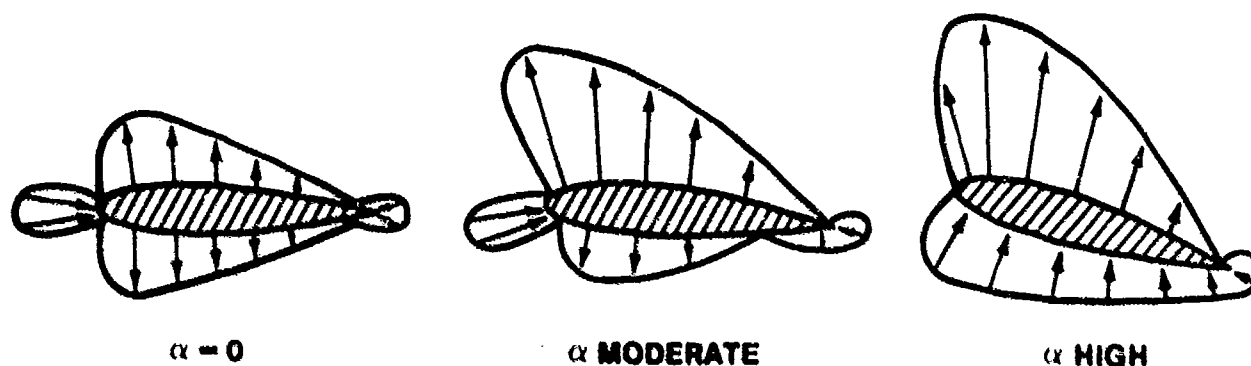


FIGURE 3.16. PRESSURE DISTRIBUTION AS A FUNCTION OF ANGLE OF ATTACK FOR SYMMETRIC AIRFOIL

The shape of the pressure distribution is a strong function of angle of attack and airfoil shape. Figure 3.16 shows how pressure distribution changes with angle of attack on a symmetric airfoil.

Figure 3.17 is a plot of calculated pressure distribution compared with the wind tunnel measured result. The theoretical result is from early two-dimensional circulation theory.

The pressure coefficient can be related to velocities around the airfoil using the Bernoulli equation. From the definition of pressure coefficient,

$$C_p = \frac{\Delta P}{q} = \frac{P - P_\infty}{q_\infty} \quad (3.11)$$

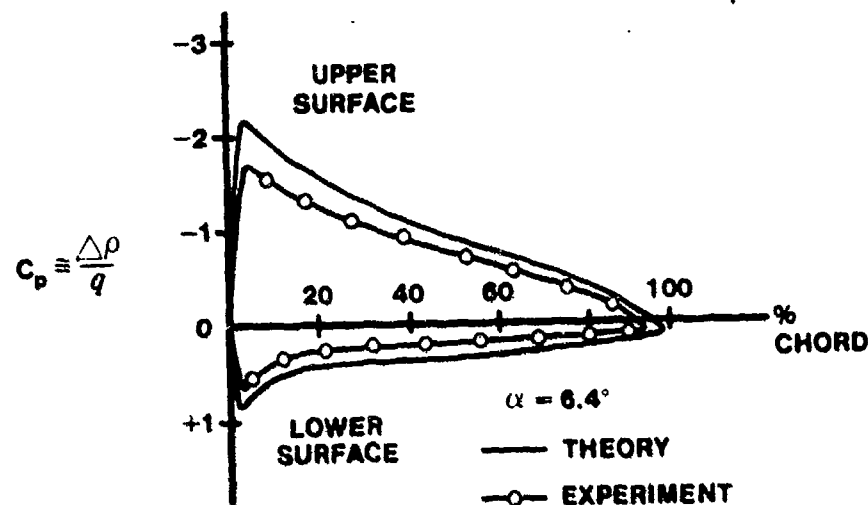


FIGURE 3.17. PRESSURE COEFFICIENT ON A NACA 4412 AIRFOIL

the Bernoulli equation, Equation 3.10, can be written in terms of the pressure, P , and dynamic pressure, q , at any given point on the airfoil as

$$P_T = P_\infty + q_\infty = P + q \quad (3.12)$$

Rearranging Equation 3.12 gives

$$P - P_\infty = q_\infty - q \quad (3.13)$$

Substituting Equation 3.13 into Equation 3.11 gives

$$C_p = \frac{q_\infty - q}{q_\infty} = 1 - \frac{q}{q_\infty} \quad (3.14)$$

Substituting the definition of dynamic pressure

$$C_p = 1 - \frac{\frac{1}{2} \rho V^2}{\frac{1}{2} \rho V_\infty^2} \quad (3.15)$$

Equation 3.15 simplifies to

$$C_p = 1 - (V/V_\infty)^2 \quad (3.16)$$

In subsonic flow, the pressure coefficient is a very complex function of the velocity around the airfoil; nevertheless, it can be related to a plot of pressure distribution like the one shown in Figure 3.17. Figure 3.18 shows points on the airfoil and flow areas corresponding to those shown in Table 3.1. Equations 3.11 and 3.16 were used to construct Table 3.1.

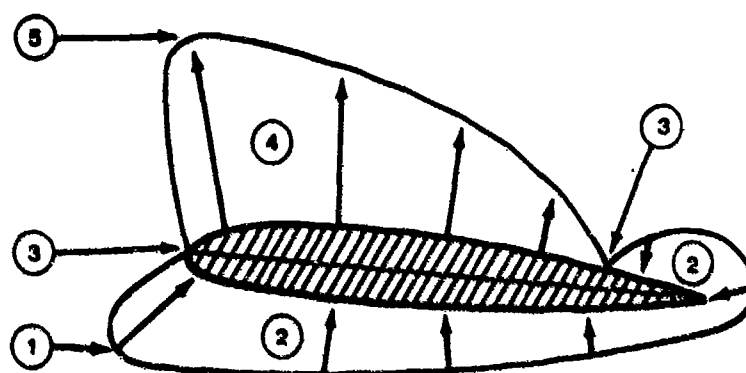


FIGURE 3.18. AIRFOIL PRESSURE DISTRIBUTION

TABLE 3.1. PRESSURE COEFFICIENT RELATIONSHIPS
FROM FIGURE 3.18

Area or Point	Velocity V	Pressure P	C_p
1	0	H	1.0
2	$<V_\infty$	$>P_\infty$	(+)
3	V_∞	P_∞	0
4	$>V_\infty$	$<P_\infty$	(-)
5	MAXIMUM	MINIMUM	MINIMUM (MOST NEG.)

Pressure coefficient is particularly useful for calculations in supersonic flight since it is constant along flat aerodynamic surfaces, and many supersonic wing sections have flat aerodynamic surfaces.

3.11 THE LIFT CURVE

A symmetrical airfoil at a zero angle of attack produces as much upward force as it does downward force so the C_L versus α curve for a symmetrical airfoil section shows zero lift at zero angle of attack. This is illustrated in Figure 3.19.

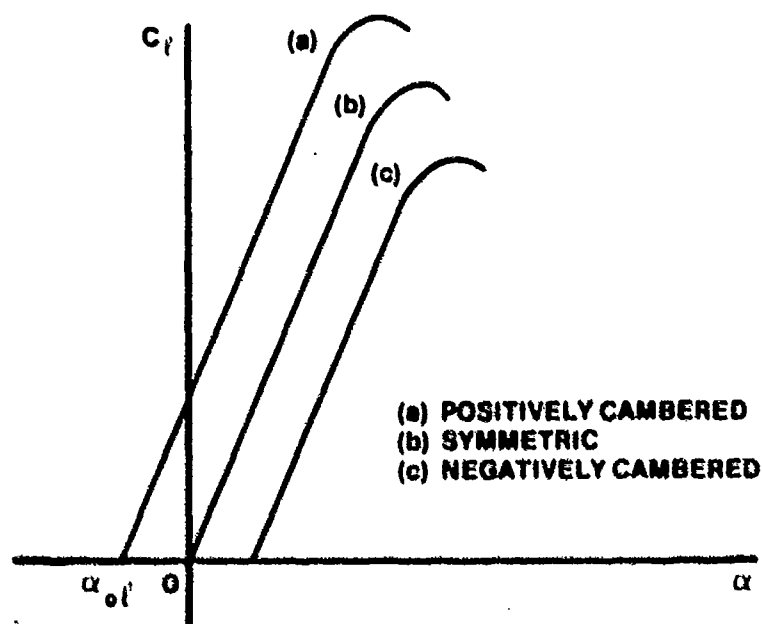


FIGURE 3.19. LIFT CURVES FOR SYMMETRIC AND CAMBERED AIRFOILS

A positively cambered airfoil, however, has no such symmetry at zero angle of attack and therefore produces lift, as shown in Figures 3.19 and 3.20. Consequently, the angle of attack required to produce zero lift, α_{OL} , is some negative angle which depends on the shape of the airfoil and amount of camber.

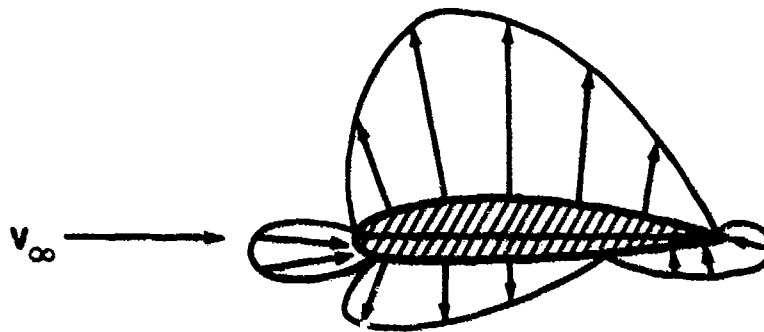


FIGURE 3.20. CAMBERED AIRFOIL PRESSURE DISTRIBUTION
AT ZERO ANGLE OF ATTACK

Even though the pressure distribution on an airfoil changes drastically with angle of attack, an important characteristic of the lift curve is that it is linear through most of its range except in the region of stall at maximum lift coefficient. Since it is linear, the slope is constant and is equal to

$$\frac{dc_L}{da} = a \quad (3.17)$$

The equation for the straight line portion of the lift curve (C_L versus a) can be written as

Symmetrical Airfoil

$$C_L = \frac{dc_L}{da} a = a a \quad (3.18)$$

or, in general for any airfoil

$$C_L = \frac{dc_L}{da} (a - a_{OL}) = a (a - a_{OL}) \quad (3.19)$$

Values of lift curve slope can have units of "per degree," and they are also given in dimensionless form as "per radian"; therefore, a typical lift

curve slope could be written

$$a = 0.10 \text{ per degree} = 5.73 \text{ per radian}$$

3.12 ZERO LIFT LINE

Frequently, it is convenient to reference the angle of attack to some line other than the chord line. Such a reference line is the zero lift line which is frequently used for flying quality work.

The zero lift line is defined as a line parallel to the relative wind and passing through the trailing edge of the airfoil when the airfoil is at zero lift as shown in Figure 3.21.

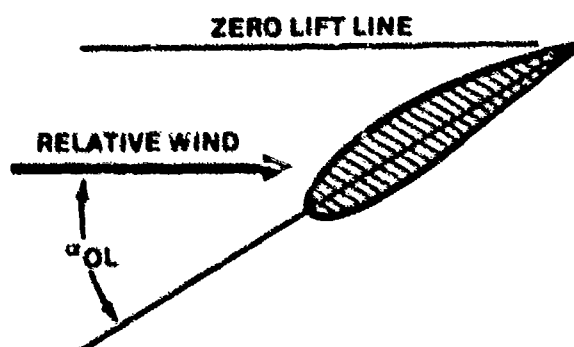


FIGURE 3.21. ZERO LIFT LINE

3.13 VARIABLES AFFECTING LIFT CURVE

It was shown in dimensional analysis that

$$C_L = f(M, R_e, \alpha) \quad (2.19A)$$

A conclusion drawn was that geometrically similar shapes compared at the same Mach, Reynolds number, and angle of attack have the same lift coefficient. The linear variations of lift coefficient with angle of attack have already been shown on the lift curve in Figure 3.19. Typical variations of the lift curve with Mach and Reynolds number will be shown in the following paragraphs. Variations in lift curve with wing section and planform

which affect the geometric similarity of aerodynamic bodies will also be shown. These are airfoil thickness, airfoil camber, wing planform shape, and aspect ratio.

3.13.1 Lift Curve Variation with Mach

Mach effects occur because air is a compressible fluid. While the compressibility of air is negligible at low speeds it becomes very important at speeds approaching Mach 1.0 and above.

As the velocity of the air increases over an airfoil, at low speeds there is a negligible change in the air density; however, at high speeds, a change in velocity causes a finite, non-negligible change in the air density. This effect can be seen from Equation 3.20 which will be derived in Chapter 6, Supersonic Aerodynamics.

$$\frac{dp}{\rho} = -M^2 \frac{dV}{V} \quad (3.20)$$

At low speeds ($M = 0.2$), a 10% increase in velocity causes a 0.4% decrease in the density. However, at high speeds ($M = 0.9$), a 10% increase in velocity causes a 6.4% decrease in the density. Thus, the compressibility of the air becomes significant as the Mach increases.

Since the Mach is a parameter which describes the magnitude of the effects of compressibility, the terms "compressibility effects" and "Mach effects" are used interchangeably.

The effect of compressibility on the lift coefficient can be seen from an equation proposed by Glauert for thin airfoils. Equation 3.21 which is applicable to the linear portion of the lift curve shows that the slope of the compressible lift curve increases with increasing Mach over the slope of the incompressible lift curve.

$$\left(\frac{dC_L}{d\alpha} \right)_{\text{Comp}} = \frac{1}{\sqrt{1 - M^2}} \left(\frac{dC_L}{d\alpha} \right)_{\text{Incomp}} \quad (3.21)$$

Equation 3.19 was derived earlier for the linear portion of the lift curve.

$$C_L = \frac{dC_L}{d\alpha} (\alpha - \alpha_{OL}) \quad (3.19)$$

If the $dC_L/d\alpha$ in Equation 3.19 is considered the "compressible" slope of interest, then Equation 3.21 can be substituted into Equation 3.19.

$$C_L = \left(\frac{1}{\sqrt{1 - M^2}} \right) \left(\frac{dC_L}{d\alpha} \right)_{Incomp} (\alpha - \alpha_{OL}) \quad (3.22)$$

Equation 3.22 shows that all of the lift curves pass through the angle of attack for zero lift shown in Figure 3.22.

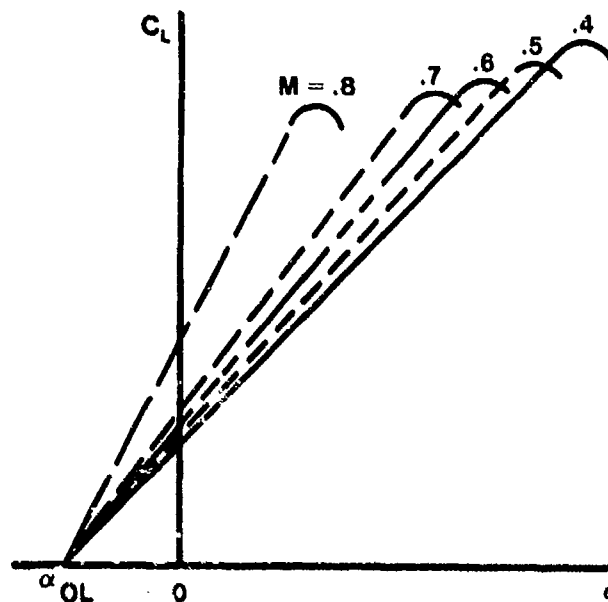


FIGURE 3.22. EFFECT OF MACH ON THE LIFT CURVE

Figure 3.22 shows the increase in lift curve slope with Mach, or that lift coefficient increases at the same angle of attack as Mach increases. This effect does not continue indefinitely because Equation 3.21 from which

it was derived is not good above the critical Mach, where shock waves begin to form on the airfoil surface. In fact, as will be shown in Chapter 6, Supersonic Aerodynamics, at supersonic speeds the trend is reversed (slope decreases).

Note also in Figure 3.22 that $C_{L_{\max}}$ decreases as Mach increases.

As a general rule this is true, although exceptions can be found. This is not indicated mathematically in the analysis given. It is determined by wind tunnel or flight testing. This discrepancy serves to indicate the limitations of the mathematical approach to the problems of flight, particularly in the transonic region (3.7:94).

3.13.2 Lift Curve Variation with Reynolds Number

Lift coefficient variation with Reynolds number is shown in Figure 3.23.

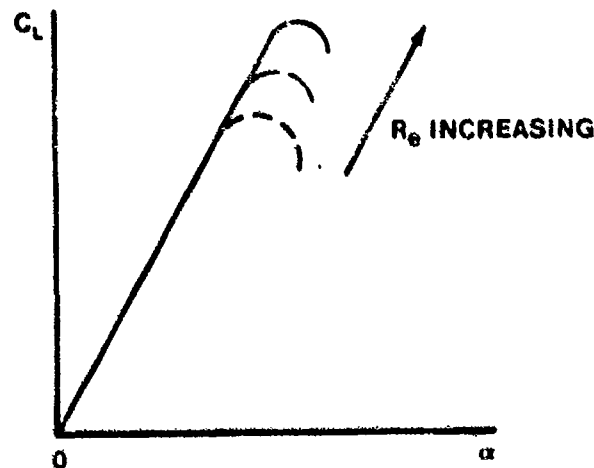


FIGURE 3.23. EFFECT OF REYNOLDS NUMBER ON THE LIFT CURVE

Reynolds number effects become significant at the high lift coefficients obtained when approaching the stall angle of attack for a given airfoil. It can be seen that the maximum C_L is obtained at the highest Reynolds number.

The Reynolds number describes whether the flow will be laminar or turbulent. The Reynolds number of the flow measured at different points in

the boundary layer along an airfoil describes how long the boundary layer will remain laminar and at what point there will be a transition to a turbulent boundary layer.

As the angle of attack is increased, turbulent flow in the boundary layer on an airfoil will resist separating from the surface longer than laminar flow, therefore creating more lift on the same airfoil. This effect follows directly from the discussion of separation and pressure gradient earlier in Chapter 2.

The pressure gradient over an airfoil surface describes at what point the boundary layer (whether laminar or turbulent) will separate from the surface. A compromise must be reached between laminar and turbulent boundary layers on an airfoil. The boundary layer on the upper portion of a typical airfoil is laminar at the leading edge extending rearward, then becomes turbulent and eventually separates from the airfoil toward the trailing edge.

Consider flow over an airfoil at a constant free stream Reynolds number. As the angle of attack of the airfoil increases, the local velocity in the boundary layer on the airfoil increases; hence, the local Reynolds number increases over the upper surface. The increase in velocity decreases the pressure on the upper surface, causing a larger adverse pressure gradient on the aft portion of the airfoil.

The increased local Reynolds number and pressure gradient cause transition to turbulent flow and separation to occur farther forward on the wing. This forward movement proceeds slowly as the angle of attack is increased through moderate angles (less than 8° to 10°) but increases rapidly at high angles.

Now, consider what happens to the aerodynamic lift at moderate to high angles of attack when the free stream Reynolds number is increased. An increase in the free stream Reynolds number represents an increase in the energy of the flow, i.e., since V^2 is a measure of kinetic energy. Because of this additional energy, the boundary layer becomes turbulent farther forward on the surface and is able to remain attached longer, separating nearer the trailing edge. Since there is less separation, the airfoil has a higher $C_{L_{max}}$. Even after the boundary layer has become completely turbulent, increasing Reynolds number still adds energy to the boundary layer and delays separation, i.e., the lift curve shown in Figure 3.23 will stay linear to higher angles of attack.

3.13.3 Lift Curve Variation with Wing Section

Figure 3.24 shows the lift characteristics of five typical NACA standard airfoil sections. One characteristic feature of all airfoil sections is that the slope of the various lift curves is essentially the same (3.2:29).

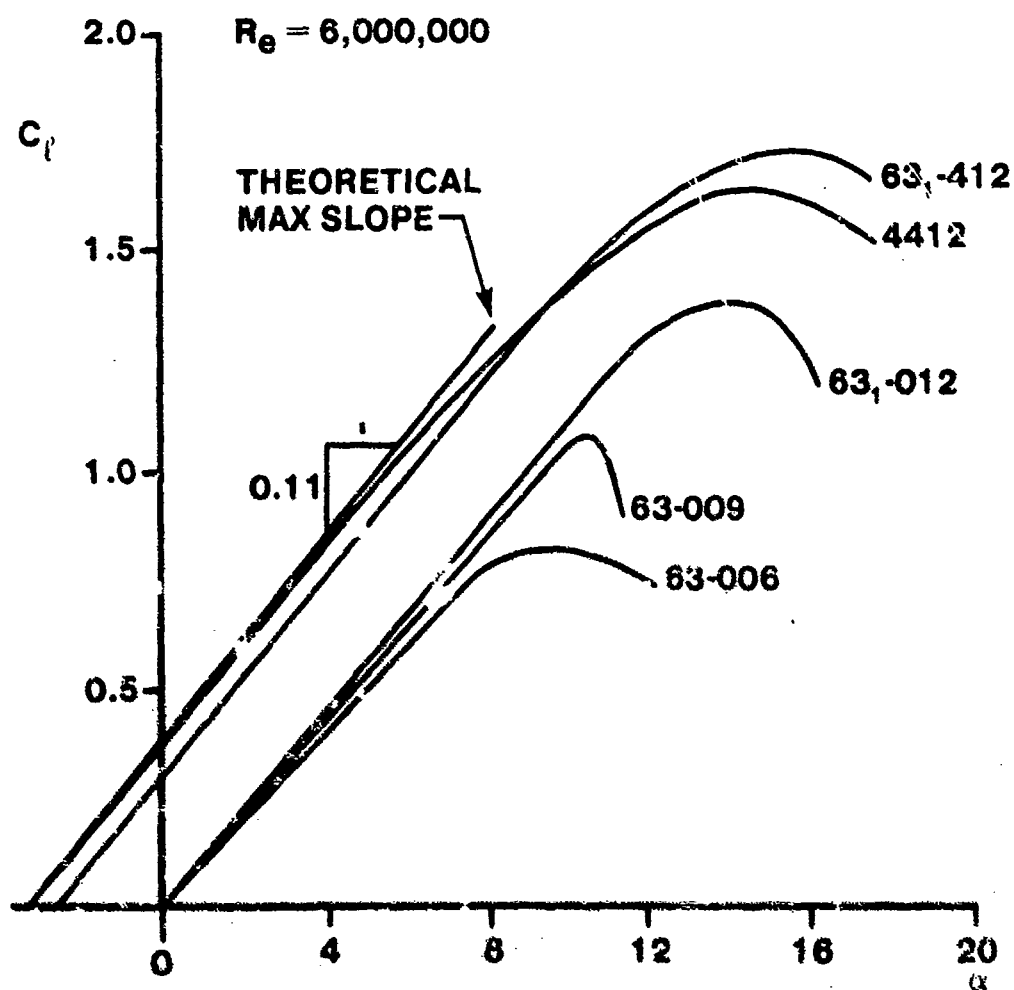


FIGURE 3.24. LIFT CHARACTERISTICS OF TYPICAL NACA AIRFOIL SECTIONS (3.2:28)

For each of the airfoils shown, the section lift coefficient increases linearly approximately 0.10 for each degree increase in angle of attack. For each airfoil, a 5° change in angle of attack would produce an approximate 0.5 change in section lift coefficient. Evidently, lift curve slope is not an important factor in the selection of an airfoil. Also shown on Figure 3.24 is the theoretical maximum lift curve slope, 2π per radian or 0.11 per degree (3.2:29).

An important lift property affected by airfoil shape is the section maximum lift coefficient, $C_{l_{\max}}$. The effect of airfoil shape on $C_{l_{\max}}$ can be appreciated by comparison of the lift curves for the five airfoils in Figure 3.24. The NACA airfoils 63-006, 63-009, and 63₁-012 are symmetric sections of increasing thickness in percent chord. The effect of thickness on $C_{l_{\max}}$ is obvious from these curves. The 12% thick section has a $C_{l_{\max}}$ approximately 70% greater than the 6% thick section (3.2:29).

The effect of camber is illustrated in Figure 3.24 by the lift curve of the NACA 4412 and 63₁-412 sections. Both airfoils have the same thickness and thickness distribution, but the 63₁-412 section has additional camber. The lift curves for these two airfoils show that increasing camber has a beneficial effect on $C_{l_{\max}}$. Note also that both of these cambered wing sections have considerably higher values of $C_{l_{\max}}$ than the three symmetric sections shown. The cambered NASA Whitcomb GA(W)-1 airfoil has also been shown to develop $C_{l_{\max}}$ values of nearly 2.0.

3.13.4 Lift Curve Variation with Wing Planform

It should be noted that all wings or aircraft do not have linear lift curve slopes. That is, the planform has a great effect on the slope of the curve. For instance, a delta wing, a highly swept wing, or a short straight wing will have a lift curve similar to that shown in Figure 3.25.

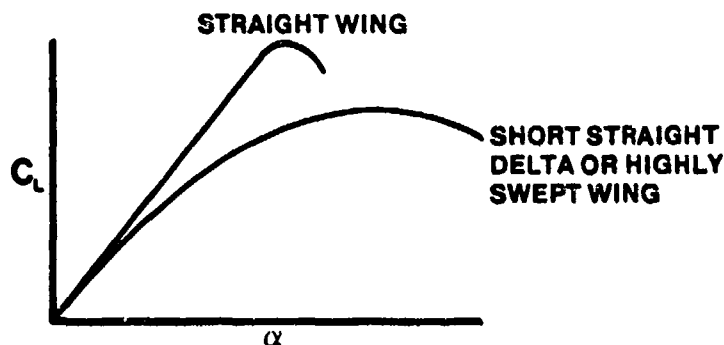


FIGURE 3.25. PLANFORM EFFECTS ON THE LIFT CURVE

Notice the well defined angle of attack for maximum C_L for the straight wing, while the other curve depicts a region of angles of attack for which the C_L is maximum. The F-106 and T-38 exhibit this type of C_L versus α curve. When the stall region of angle of attack is reached, no abrupt aircraft gyration is noticed (except a high rate of sink), and the angle of attack may be increased still further with no abrupt effects.

3.13.5 Lift Curve Variation with Aspect Ratio

Aspect ratio also affects the lift curve. A straight, rectangular airfoil is shown in Figure 3.26.

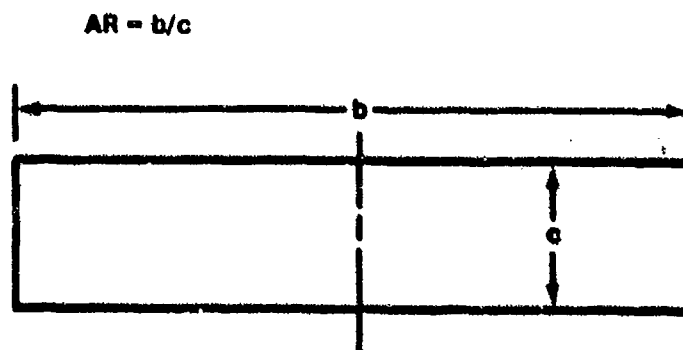


FIGURE 3.26. DEFINITION OF ASPECT RATIO

Not all wings are straight with a constant chord. The aspect ratio of any wing can be determined if the wing area and span are known. For example, the aspect ratio of the wing shown in Figure 3.27 is

$$AR = \frac{b^2}{S} = \frac{(20)^2}{150} = \frac{400}{150} = 2.67$$

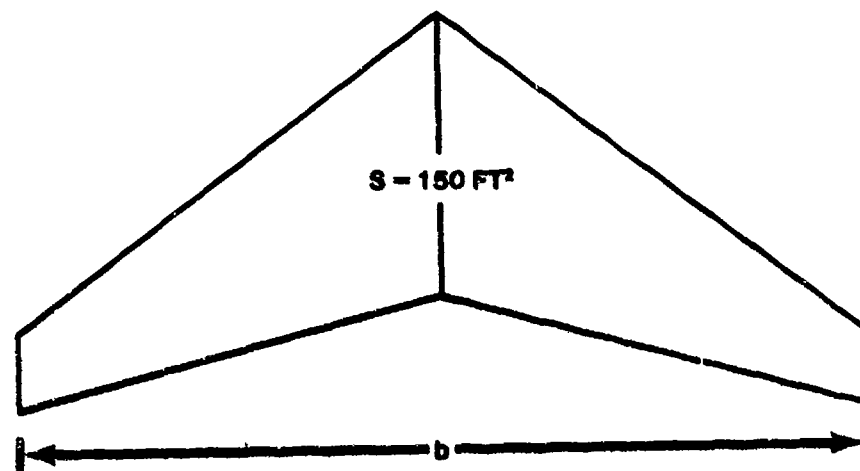


FIGURE 3.27. ARBITRARY WING PLANFORM

A wing of finite span does not develop the maximum possible lift for any given angle of attack because of tip losses. The airflow over a finite wing is extremely complex because of different pressure fields on the upper and lower surfaces. Generally, when the wing is lifting at moderate angles of attack, the pressure on the top surfaces is slightly lower than atmospheric, while the pressure on the lower surface is slightly higher than atmospheric. Air responds to pressure forces, always trying to flow from regions of high pressure to low pressure. Therefore, in flight, air spills out from below the wingtips and rushes up into the region of low pressure on the top of the wing. The pressures above and below the wingtip try to equalize, with the result that on the upper side of the wing, near the wingtips, the pressure is not quite as low as over the rest of the wing. By the same process, the positive pressure under the wing is not as high near the tips as under the inner portion of the wing because of this outward and upward flow.

Lift, which is due to the difference in air pressure between the lower

and upper surfaces of the wing, is not uniform across the span because of this loss of efficiency near the tips. A typical lift distribution along the span of a rectangular wing is shown in Figure 3.28.

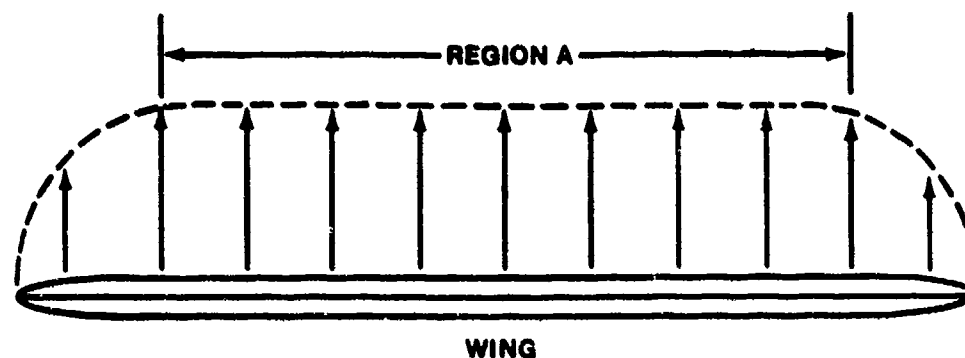


FIGURE 3.28. TYPICAL SPANWISE LIFT DISTRIBUTION

Note that the lift is essentially constant in the center of the wing, but decreases to zero at the tips. Intuition suggests that if a section were added to this wing at the middle, the overall efficiency of the wing would be increased. Region A would be extended approximately by the amount of the additional wing section. With the longer wing, the loss of lift near the tips will be a smaller percentage of the total lift. So in this elementary way, it should be apparent that aspect ratio is an important wing property. A wing so long that it has no wingtips at all is called an "infinite wing." It has infinite aspect ratio, no tip losses, and uniform lift across the span; but it is simply a tool of the theoretical aerodynamicist and wind tunnel analyst.

Since near the tips of a finite wing air is flowing outward, there is a small spanwise flow over the entire lower surface. When this flow is superposed on the primary rearward flow, a flow field results such as shown in Figure 3.29. Also shown in Figure 3.29 is the effect of the inward spanwise component on the flow field on the upper surface of the wing. This spanwise flow could not occur with the theoretical infinite wing since it has no wingtips.

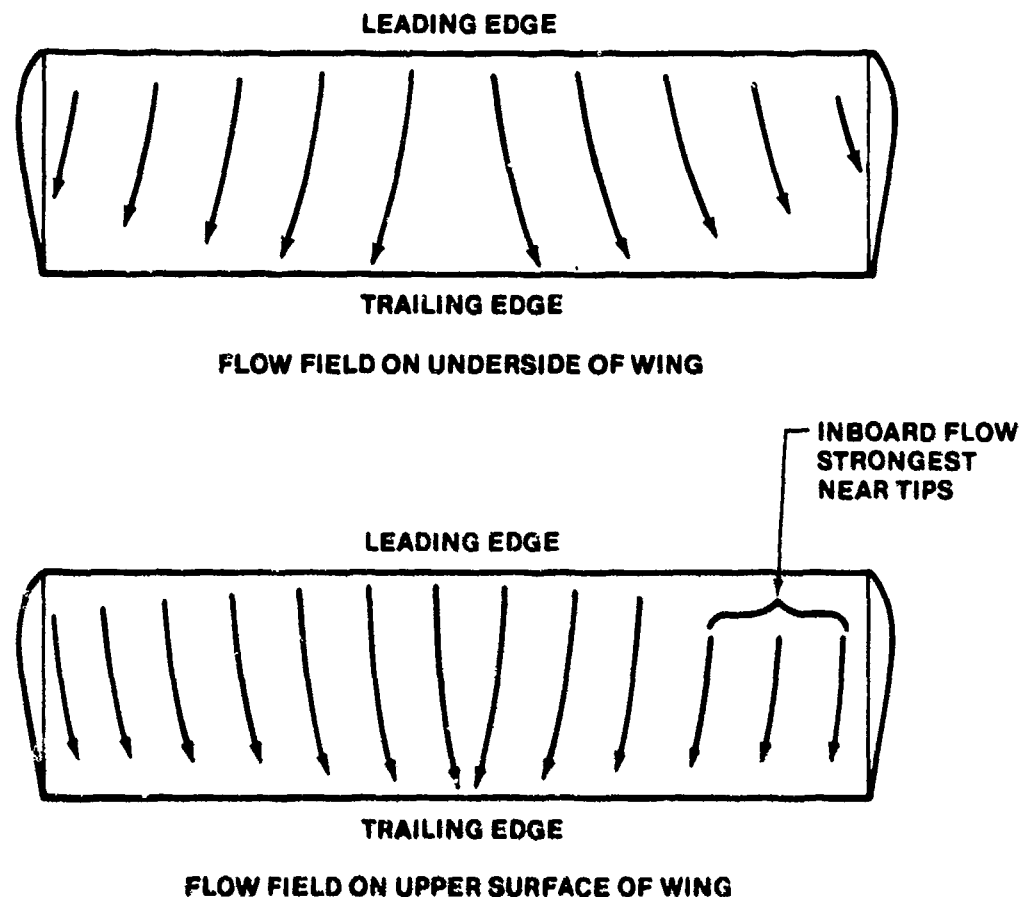


FIGURE 3.29. UPPER AND LOWER FINITE WING FLOW FIELDS

At any point on the trailing edge of the upper surface of the wing, a streamline of air is moving rearward, inward, and downward. And on the lower surface along the trailing edge, streamlines are moving rearward, outward, and downward. These streamlines from the upper and lower surfaces converge to form tiny vortices all along the trailing edge. These small vortices are entrained in the strong flow at the tips. The tip vortices are powerful air movements giving an upward motion to air outside the wingtip and a downward motion to air behind and inside the span. These tip vortices are shown in Figure 3.30.

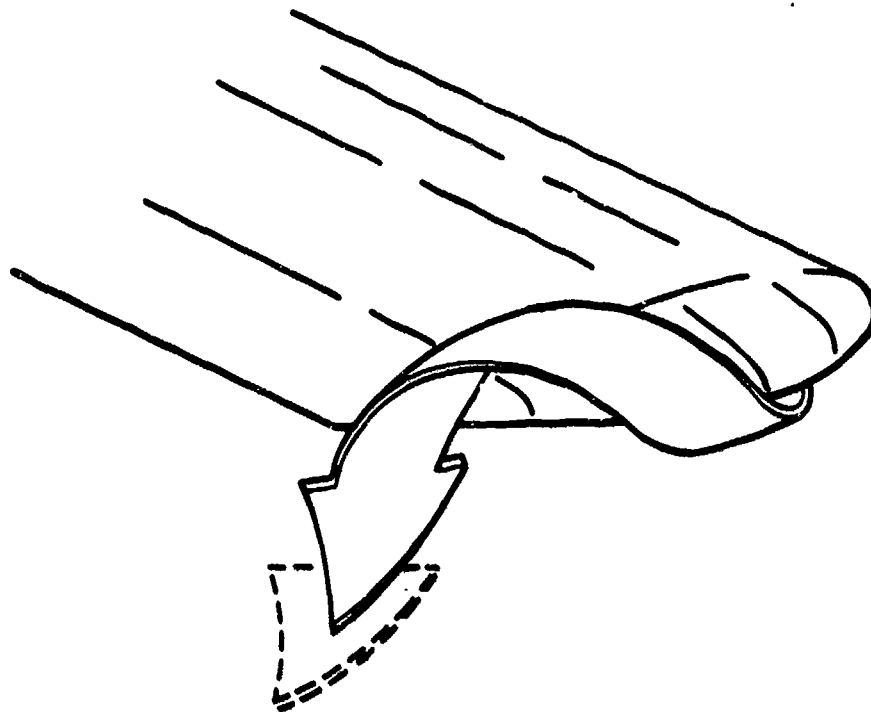


FIGURE 3.30. TIP VORTICES ON A WING

The result of tip losses then is a decrease in the wing's lifting ability. The shorter the span, the more area that is affected by these losses. Therefore, a low aspect ratio wing would have to be at a higher angle of attack to develop the same lift coefficient as a high aspect ratio wing of the same wing area. The effects of aspect ratio on the C_L versus α curve are shown in Figure 3.31.

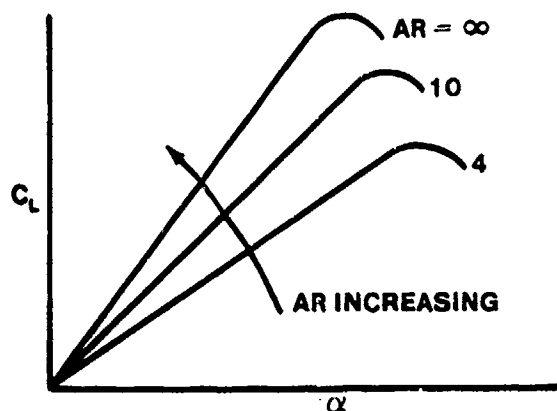


FIGURE 3.31. EFFECT OF ASPECT RATIO ON THE LIFT CURVE

3.14 FLIGHT TEST LIFT CURVE DETERMINATION

For determining the lift curve from flight test it is convenient to obtain the lift coefficient in terms of equivalent airspeed, or Mach.

The lift coefficient was defined as

$$C_L = \frac{L}{qS} \quad (3.3)$$

Using the definition of load factor and dynamic pressure, Equation 3.3 can be written

$$C_L = \frac{nW}{\frac{1}{2} \rho V^2 S} \quad (3.23)$$

Substituting the definition of equivalent airspeed and density ratio, Equation 3.23 can be written

$$C_L = \frac{nW}{\frac{1}{2} \rho_0 V_e^2 S} = \frac{841.5 nW}{V_e^2 S} \quad (3.24)$$

To find the lift coefficient in terms of Mach, the definition of Mach, the expression for determining the speed of sound, and the perfect gas law can be used to write Equation 3.23 as

$$C_L = \frac{nW}{1481 \delta M^2 S} \quad (3.25)$$

Equation 3.24 and 3.25 are used to determine lift coefficient from flight test. For example, in stabilized level flight load factor is equal to 1.0, and the weight can be determined by subtracting fuel used from aircraft start-engine gross weight. Equivalent airspeed (or pressure ratio and Mach) are readily obtained from calibrated pitot-static systems. Note, one advantage of Equation 3.24 is that it is independent of altitude. If the angle of attack is also measured during a series of stabilized, level flight points, then the lift curve can be determined. Equations 3.24 and 3.25 are useful for all sorts of subsonic aerodynamic analysis, such as the one which follows.

3.15 VARIATION IN STALL SPEED WITH ALTITUDE

As previously discussed, Reynolds number has a great effect on separation and therefore stall speed of an aircraft. This effect on stall speed can be illustrated if the Reynolds number is written using the definition of equivalent airspeed as shown in Equation 3.26.

$$R_e = \frac{\rho V_e l}{\mu} = V_e \sqrt{\rho} \left[\frac{\sqrt{\rho_0} l}{\mu} \right] = K V_e \sqrt{\rho} \quad (3.26)$$

Since viscosity, μ , is only a weak function of temperature, it varies little with altitude and so may be considered constant along with the other terms in brackets in Equation 3.26. Therefore, at the same V_e , Reynolds number decreases with increasing altitude as density decreases. Figure 3.32 shows the effect of increasing altitude on the lift curve and on $C_{L_{max}}$.

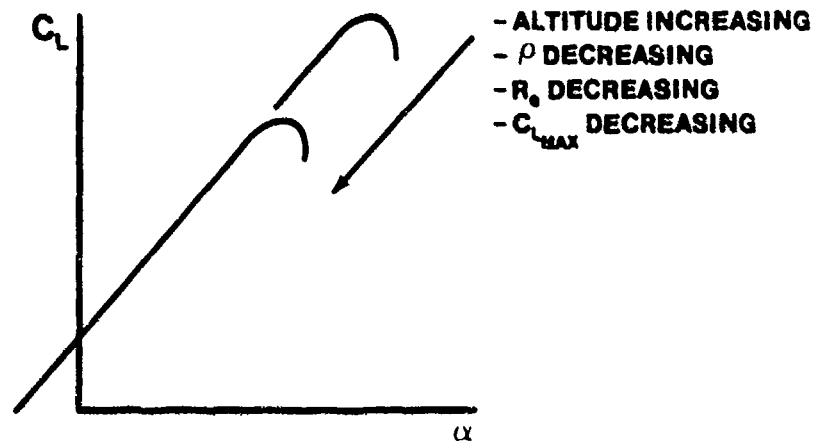


FIGURE 3.32. EFFECT OF INCREASING ALTITUDE ON $C_{L_{max}}$

There are several considerations which determine how stall speed is defined; however, the most commonly used definition is that it occurs at the equivalent airspeed corresponding to $C_{L_{max}}$.

Equation 3.24 can be written in terms of stall speed as

$$C_{L_{max}} = \frac{841.5 \text{ nW}}{(v_e)_{\text{Stall}}^2 S} \quad (3.27)$$

Rearranging, gives

$$(v_e)_{\text{Stall}} = \sqrt{\frac{841.5 \text{ nW}}{S C_{L_{max}}}} \quad (3.28)$$

Since Reynolds number decreases with altitude (density decreasing) and $C_{L_{max}}$ decreases as Reynolds number decreases, stall speed increases as altitude increases. This trend of stall speed increasing with altitude will be noticed in flight test when stalls are performed at low and high altitudes. Stall indicated airspeed will increase with increasing altitude, assuming indicated airspeed, calibrated airspeed, and equivalent airspeed all vary in the same manner.

Equation 3.28 also shows that for a given $C_{L_{\max}}$, stall speed increases with increasing aircraft weight and load factor and decreases if wing area is increased.

3.16 HIGH LIFT DEVICES

Basically, high lift devices are used to increase $C_{L_{\max}}$. Maneuvering, slow speed flight, and landing require high lift coefficients. Equation 3.28 shows that to obtain the lowest possible landing or final approach speed (typically 1.1 or 1.2 times stall speed), the maximum lift coefficient should be large.

$$\left(v_e \right)_{\text{Stall}} = \sqrt{\frac{841.5 \text{ } nW}{S C_{L_{\max}}}} \quad (3.28)$$

In order to provide lift coefficients greater than the maximum lift coefficient of a given airfoil, it is necessary to resort to special hardware. Devices of this type are slots, slats, boundary layer control (BLC), and flaps (both leading and trailing edge). Some of these devices are characteristically low speed devices, i.e., slots and BLC, while others are suitable for both high and low speed applications, i.e., flaps and slats. Numerous variations of these devices have been proposed and used on operational aircraft. Each type will be defined and their individual effects on an aircraft discussed briefly.

Basically, increasing the total lift of an airfoil can be accomplished by any one or combination of three methods. The first would be increase the wing area, the second, increase the camber of the wing, and the third would be to delay separation through some means of boundary layer control.

3.16.1 Flaps

Flaps are high lift devices which are basically hinged leading or trailing edge wing sections. They increase lift by increasing the camber or area of the wing.

3.16.1.1 Trailing Edge Flaps. Trailing edge flaps are normally 15% to 25% of the chord; although they can be found up to 40% chord.

Several arrangements are commonly used. The basic types of trailing edge flaps are shown in Figure 3.33.

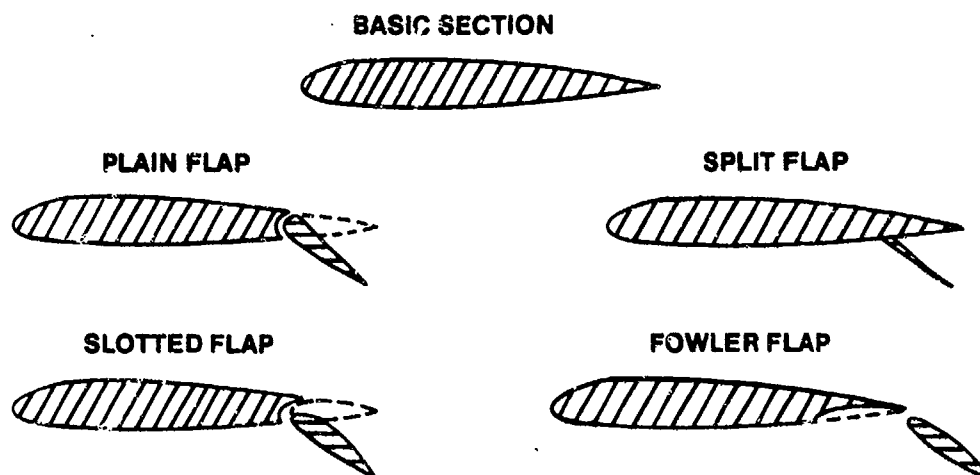


FIGURE 3.33. BASIC TYPES OF TRAILING EDGE FLAPS (3.2:40)

The plain (or simple) flap shown in Figure 3.33 is a simple hinged portion of the wing trailing edge. The split flap is essentially a plate deflected from the lower surface of the wing.

The slotted flap is similar to the plain flap, but the gap between the main wing section and flap leading edge is given a specific contour so that high energy air from the lower surface is ducted to the flap upper surface when the flap is deflected. The high energy air from the slot re-energizes the upper surface boundary layer and delays separation.

The fowler flap arrangement is similar to the slotted flap; however, when extended it lowers and translates aft, thus increasing wing area as well as camber. Because of the unique movement of this type of flap, the mechanism is quite heavy and complicated and therefore may not be practical for certain aircraft applications.

Figure 3.34 shows that all four basic trailing edge flap types provide a significant increase in $C_{l_{max}}$. As expected, the more complicated the flap arrangement, the larger the increase in $C_{l_{max}}$. Note that addition of flaps

does not change the lift curve slope but that the lift curve shifts parallel to itself for all four basic flap types shown. Therefore, any required value of lift coefficient occurs at a lower angle of attack.

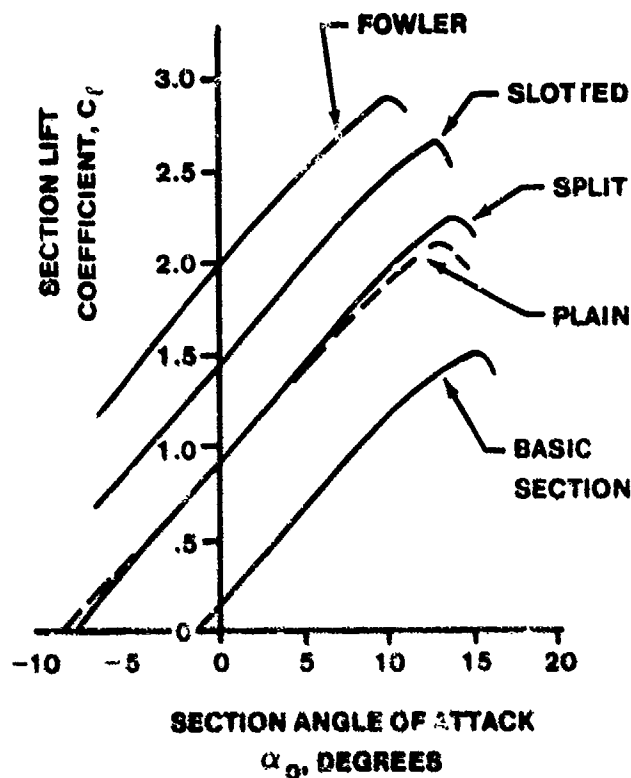


FIGURE 3.34. EFFECT OF TRAILING EDGE FLAPS ON THE LIFT CURVE (3.2:40)

The effectiveness of flaps on a wing configuration depends on many factors. One important factor is the amount of wing area affected by the flaps. Since a certain amount of wingspan is normally reserved for ailerons, the actual wing maximum lift properties will be less than that of the flapped two-dimensional section. Recently attempts (some more successful than others) have been made to increase total aircraft lift coefficient by using full-span flaps in conjunction with spoilers for roll control.

3.16.1.2 Leading Edge Flaps. There are many variations in the design of leading edge flaps. Many leading edge flaps also form leading edge slots when extended. Figure 3.35 illustrates several types of leading edge flap devices.

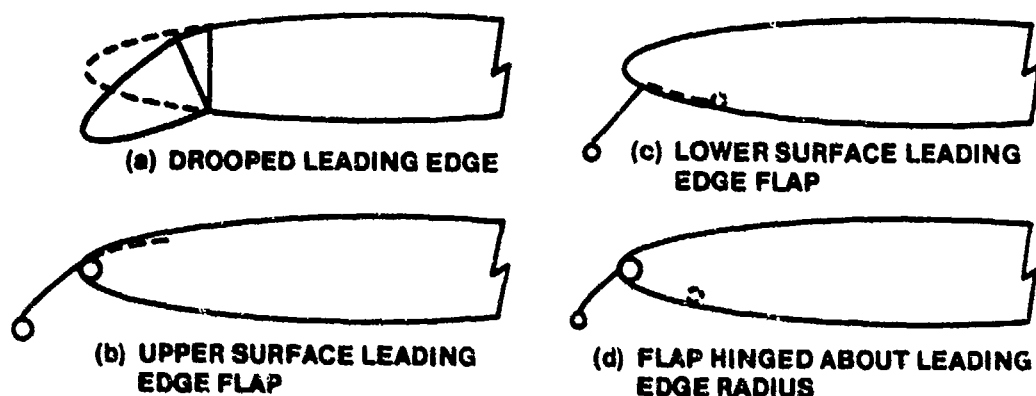


FIGURE 3.35. VARIOUS LEADING EDGE FLAP DEVICES (3.8:9-5)

A currently popular leading edge flap which pivots about the leading edge of the airfoil was introduced in 1942 and is referred to as a Krueger flap. Figure 3.36 is an illustration of a Krueger flap currently in operation. The obvious complexity of this device serves to point out that use of certain types of high lift devices is necessarily restrictive in application.

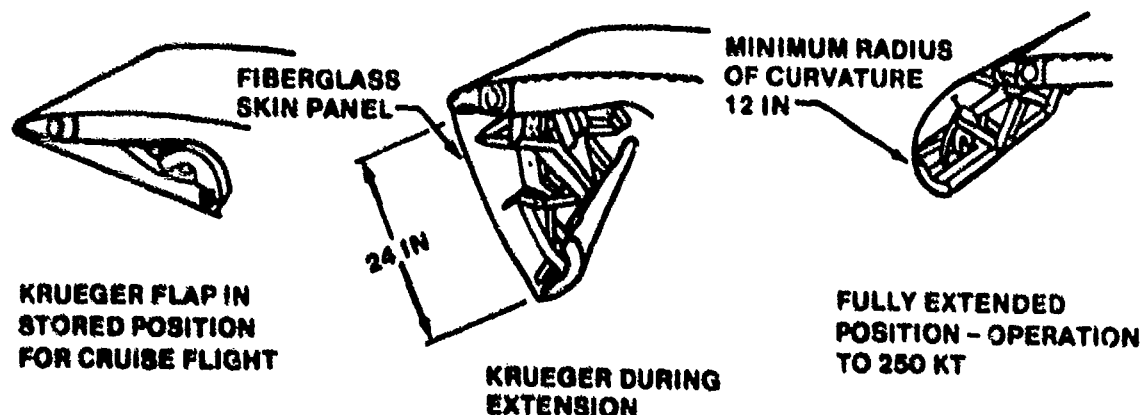


FIGURE 3.36. B-747 VARIABLE CAMBER LEADING EDGE KRUEGER FLAP (3.8:9-5)

The combination of a slotted-Krueger and a multi-sectioned-Fowler flap is shown in Figure 3.37.

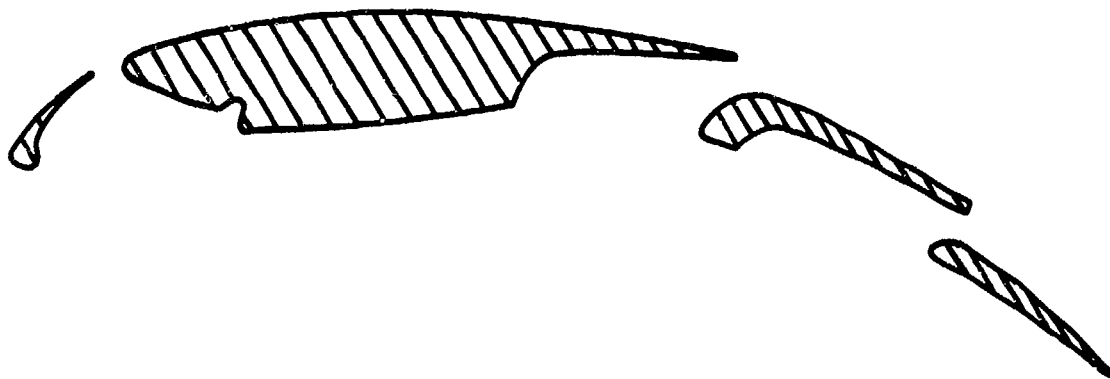


FIGURE 3.37. KRUEGER-FOWLER FLAP CONFIGURATION

3.16.2 Boundary Layer Control (BLC)

Slots and slats are aerodynamic means of affecting boundary layer control. Boundary layer control may also be accomplished by artificial means such as blowing air provided by a compressor over the wing or by drawing the low energy boundary layer through the surface of the wing by some suction device.

3.16.2.1 Slot. A fixed slot is in effect an aerodynamic boundary layer control device since it takes high energy air from the lower surface of the wing and ducts it through the wing into the low energy boundary layer on the upper surface, as shown in Figure 3.38.

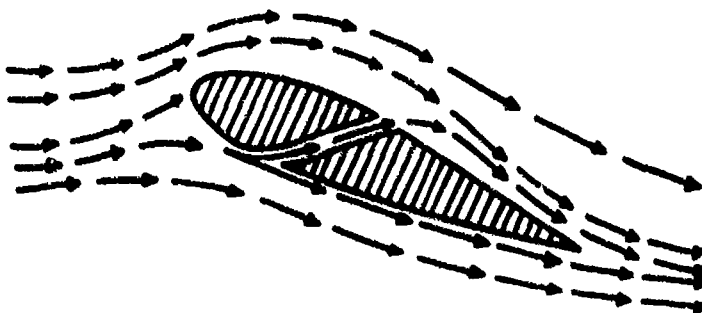


FIGURE 3.38. FIXED SLOT

In doing so, it delays separation and allows higher lift coefficients to be developed. A slot is relatively ineffective at low angles of attack but becomes very effective at high angles, thus improving the high lift characteristics without significantly compromising the low lift characteristics. Slots are used only on very slow speed aircraft since they cause very high drag at higher speeds.

3.16.2.2 Slat. A slat operates on the same principle as a slot except that it is located near the leading edge and acts like an additional airfoil in front of the basic airfoil. Its function is to direct air flow over the leading edge of the airfoil, as shown in Figure 3.39. Fixed slats also cause high drag at high speed.

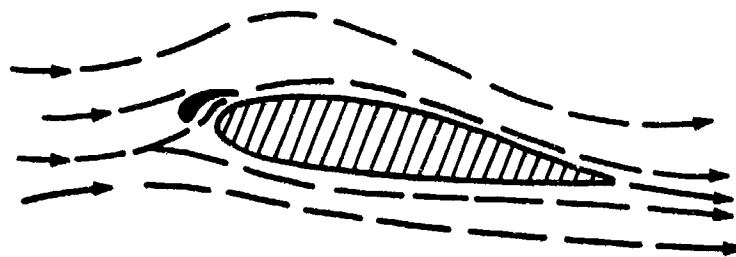


FIGURE 3.39. FIXED SLAT

A slat may also be of the movable type which remains retracted at high speed and extends at low speed and high angles of attack, as shown in Figure 3.40. This increases the wing area slightly as well as increasing the flow over the upper surface of the wing.

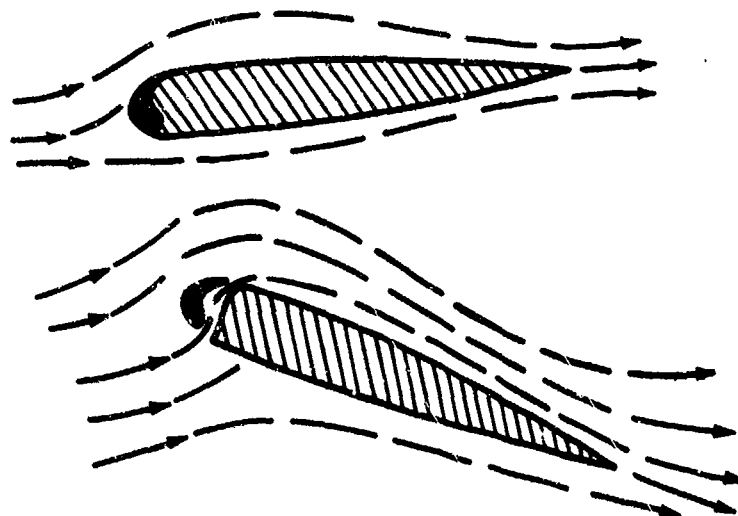


FIGURE 3.40. MOVABLE SLAT

The slot or extended slat simply delays stall to a higher angle of attack as shown in Figure 3.41.

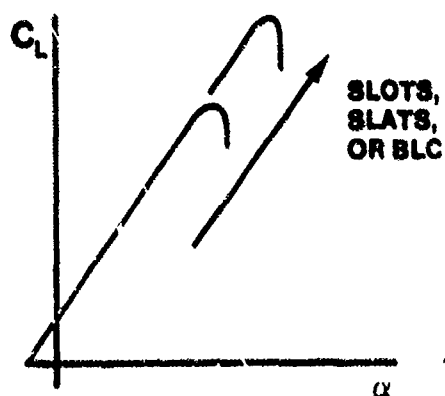


FIGURE 3.41. EFFECT OF SLOTS, SLATS, OR BLC ON THE LIFT CURVE

3.16.2.3 Blowing and Suction. Figure 3.42 illustrates boundary layer control techniques.

BLOWING BLC



SUCTION BLC



FIGURE 3.42. BOUNDARY LAYER CONTROL

Boundary layer control has exactly the same effect on the lift curve as does the use of slots or slats as shown in Figure 3.41.

Almost any combination of slots, slats, flaps, and BLC can be found today in modern aircraft designs. Slots or extended slats used alone increase maximum lift coefficient; however, they can produce undesirably high angles of attack at low speeds as shown in Figure 3.43. For this reason, slots or slats are usually used in conjunction with flaps since flaps provide a reduction in the maximum lift coefficient angle of attack. Figure 3.43 summarizes various high lift devices used together.

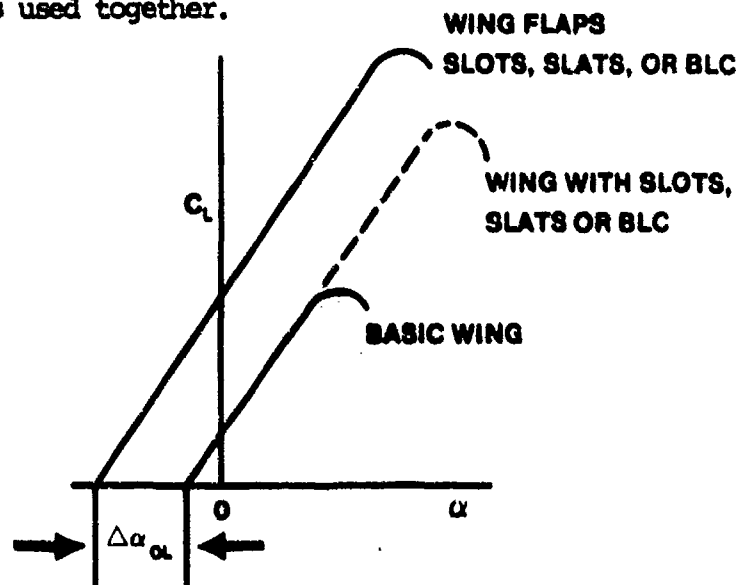


FIGURE 3.43. HIGH LIFT DEVICES

Figure 3.44 shows the maximum sectional lift coefficient generated by the various high lift devices on a typical NACA airfoil.

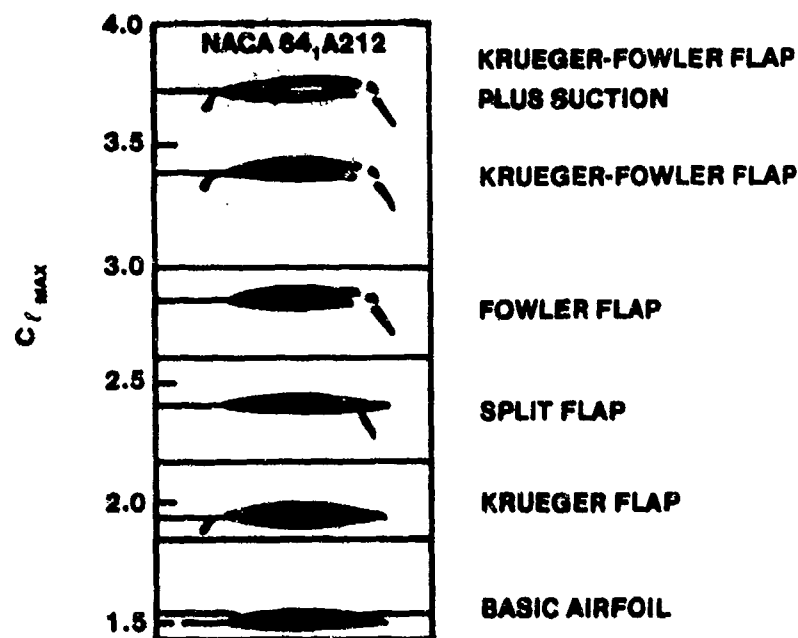


FIGURE 3.44. MAXIMUM SECTIONAL LIFT COEFFICIENTS (3.5:416)

3.16.2.4 Vortex Generators. Although they are not generally considered high lift devices, vortex generators also prevent separation aerodynamically. As shown in Figure 3.43, these devices are rows of small vanes placed perpendicular to the surface of an aircraft, each acting like a small wing whose wingtip vortex brings high energy air from outside the boundary layer down into the boundary layer, thus re-energizing it.

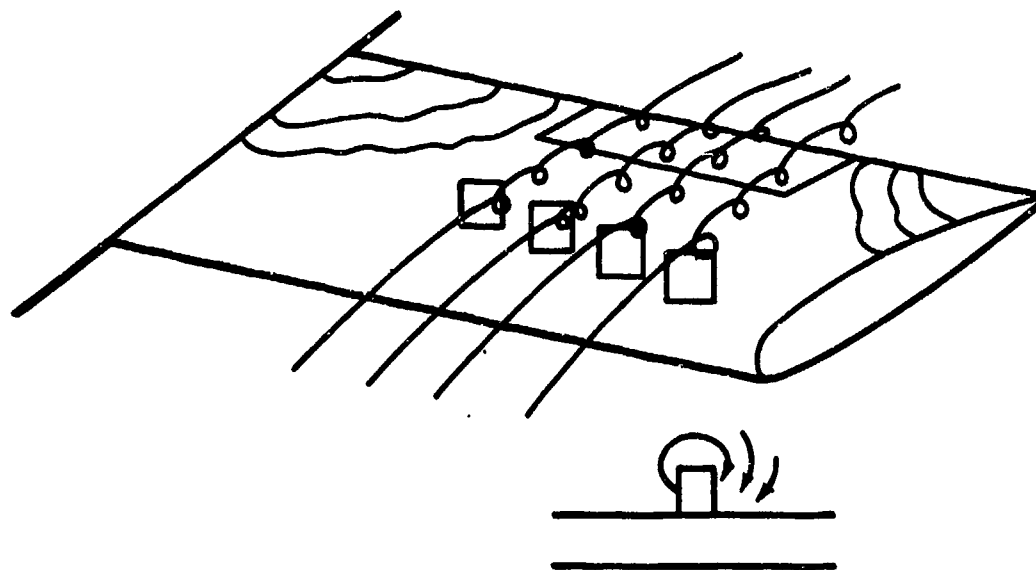


FIGURE 3.45. VORTEX GENERATORS (3.9:154)

Vortex generators normally add little toward increasing maximum lift coefficient. They are generally used to prevent local areas of separation such as in front of an aileron, which causes the flow over the aileron to stay attached to a higher angle of attack than the rest of the wing. The "strategic" placement of vortex generators is an art rather than a science.

3.17 AERODYNAMIC MOMENTS

It is appropriate that aerodynamic moments are the last major topic to be considered in this chapter since they are caused by lift and drag. Like lift and drag coefficients, pitching moment coefficient was defined earlier in Equation 3.5

$$C_m = \frac{M}{qSc} \quad (3.5)$$

For an airfoil, aerodynamic moments are most often expressed in terms of their value about the wing's aerodynamic center, ac . The aerodynamic center was defined earlier as the point on the chord about which the moment coefficient is practically constant for all angles of attack. The location of the aerodynamic center is generally considered to be constant. In fact, two-dimensional incompressible airfoil theory predicts the ac to be at the 25%

chord point for any airfoil regardless of camber, thickness, or angle of attack. Actual airfoils, which are subject to real fluid flow, may not have the ac at exactly 25% chord; however, its actual location is rarely forward of 23% or aft of 27% chord. For all practical purposes, the aerodynamic center can be assumed to be at 25% chord. In fact, much wind tunnel moment coefficient data are presented about 25% chord, and no attempt is made to precisely locate the aerodynamic center (3.1:118).

Moments are created on an airfoil by asymmetric upper and lower pressure distributions over the surface of the airfoil. The variables affecting pressure distribution are angle of attack, camber, and thickness. The effects of thickness can be eliminated immediately, since increasing the thickness causes identical increases in the pressure distribution on the upper and lower surfaces proportionately, so that there is no net contribution to the moment. Effect of angle of attack and camber will be discussed on symmetric and cambered airfoils individually.

3.17.1 Symmetric Airfoils

The angle of attack affects the moment on a symmetric airfoil directly. When angle of attack increases, lift increases, but the moment arm about any point remains constant since the center of pressure, c_p , remains stationary at about quarter-chord length behind the leading edge. The aerodynamic center is also stationary at quarter-chord.

Figure 3.46 illustrates a symmetric airfoil at angle of attack for zero lift, α_{OL} . Since a symmetric airfoil has no camber, the pressure distribution is symmetric, and there is no moment at α_{OL} about any point on the chord. The only moments created are those due to angle of attack.

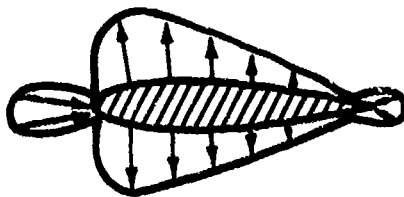


FIGURE 3.46. SYMMETRIC WING SECTION AT ANGLE OF ATTACK FOR ZERO LIFT (3.2:48)

Since there is no moment about any point on the chord at α_{OL} , there is no moment about the ac. If there is no moment about the ac at α_{OL} , and moments about the ac are constant with angle of attack, then the moment (and moment coefficient) about the ac for a symmetric wing section is always zero as shown in Figure 3.47.

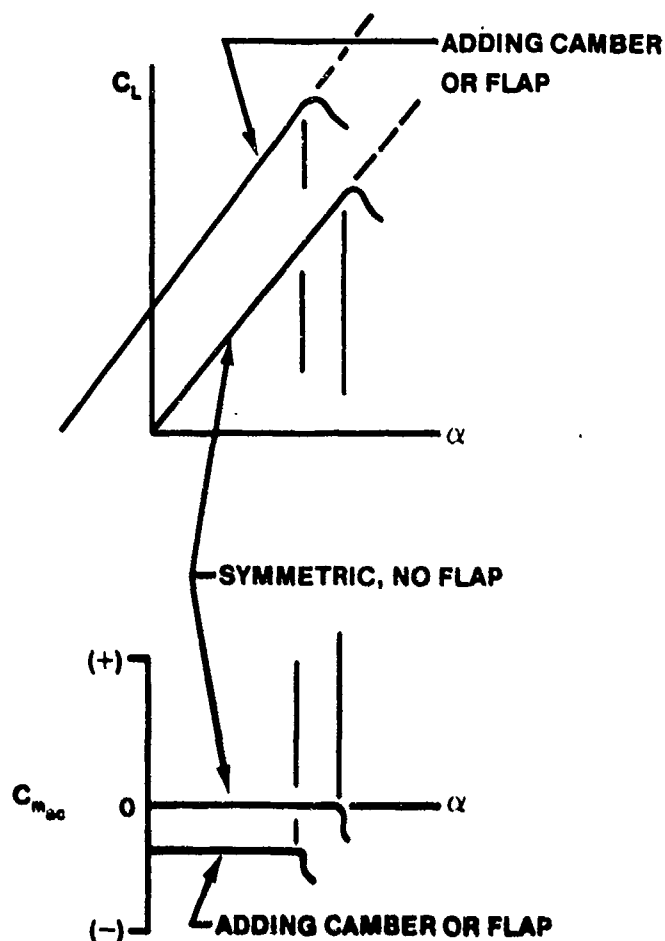


FIGURE 3.47. VARIATION OF MOMENT COEFFICIENT ABOUT THE AERODYNAMIC CENTER WITH ANGLE OF ATTACK FOR SYMMETRIC AND CAMBERED AIRFOILS

3.17.2 Cambered Airfoils

Angle of attack also affects the moment on a cambered airfoil directly; however, for cambered airfoils the cp location is not constant, but moves

forward with increasing angle of attack. The aerodynamic center for a cambered airfoil remains stationary at quarter-chord. Figure 3.48 illustrates a cambered airfoil at α_{OL} .

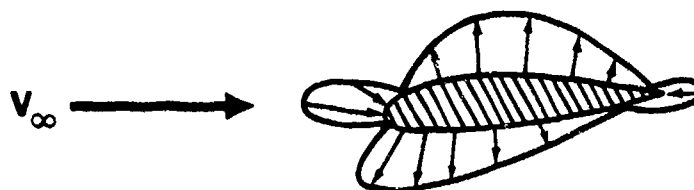


FIGURE 3.48. CAMBERED WING SECTION AT ANGLE OF ATTACK FOR ZERO LIFT (3.2:48)

The effects of camber are apparent from Figure 3.48. Since the airfoil is at α_{OL} , the sum of the aerodynamic forces perpendicular to the relative wind is zero; however, the pressure distribution is not symmetric, and there is a small resultant negative moment about the aerodynamic center. Since the moments about the ac are constant with angle of attack, the moment coefficient about the ac for a positively cambered wing is always a small negative constant. Since moments are additive, the total moment on a cambered airfoil is the sum of: moments due to camber and moments due to angle of attack. The moment coefficient about the ac for a cambered wing is shown in Figure 3.47.

3.17.3 Properties of Moments

Some useful insight into the properties of moments, as applied to an airfoil, is obtained from an expansion of the basic definition of the moment about some arbitrary point, n , on an airfoil as shown in Figure 3.49.

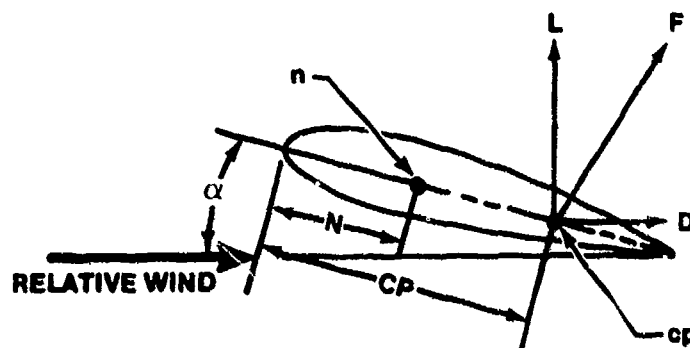


FIGURE 3.49. MOMENTS ON AN AIRFOIL

From Figure 3.49,

$$M_n = -L \cos \alpha (CP - N) - D \sin \alpha (CP - N) \quad (3.29)$$

Changing the distances N and CP to a percent of the chord, c , i.e.,

$$n = \frac{N}{c} \quad \text{and} \quad cp = \frac{CP}{c}$$

$$M_n = -L c \cos \alpha (cp - n) - D c \sin \alpha (cp - n) \quad (3.30)$$

Making a small angle assumption, that if an angle (measured in radians) is small, the cosine of the angle equals one, and the sine of the angle equals the angle, and assuming that the lift is of much greater magnitude than the drag,

$$\cos \alpha = 1$$

$$\sin \alpha = \alpha$$

$$L \gg D$$

then

$$M_n = -L c (cp - n) - (0) \quad (3.31)$$

To find C_{m_n} , divide M_n by $q c S$, obtaining

$$C_{m_n} = -\frac{L}{qS} (c_p - n) \quad (3.32)$$

$$C_{m_n} = C_L (n - c_p) \quad (3.33)$$

or, solving for c_p

$$c_p = n - \frac{C_{m_n}}{C_L} \quad (3.34)$$

Equation 3.34 is a general equation relating the percent chord location of two points, c_p , and an arbitrary point, n , to the moment coefficient about this arbitrary point, n , and the airfoil lift coefficient.

If n is the percent chord to the aerodynamic center of the airfoil ($n = ac$) then $C_{m_n} = C_{m_{ac}}$ and Equation 3.34 becomes

$$c_p = ac - \frac{C_{m_{ac}}}{C_L} \quad (3.35)$$

From Equation 3.35 it can be seen that for a symmetric airfoil where $C_{m_{ac}}$ is zero, c_p equals ac . This is the case since both c_p and ac are located at quarter-chord. If $C_{m_{ac}}$ is not zero, c_p becomes infinite at zero lift. Since $C_{m_{ac}}$ is constant and negative for positively cambered airfoils, c_p is always positive as C_L goes to zero. As C_L increases from zero, the c_p location approaches the ac at quarter-chord very rapidly since $C_{m_{ac}}$ is a very small negative constant.

Because the c_p is continually moving as C_L is varied, it is not a

convenient reference for aircraft stability and control analysis. A more useful expression for the moment coefficient about any point, n , is obtained when Equations 3.34 and 3.35 are equated.

$$n - \frac{C_{m_n}}{C_L} = ac - \frac{C_{m_{ac}}}{C_L} \quad (3.36)$$

or, rearranging Equation 3.36

$$C_{m_n} = C_{m_{ac}} + C_L (n - ac) \quad (3.37)$$

From Equation 3.37 it can be seen that the total moment coefficient on an airfoil is the sum of the constant $C_{m_{ac}}$ plus the moment caused by lift and that at zero lift the moment coefficient at any point along the chord equals $C_{m_{ac}}$.

Equation 3.37 is extremely convenient for flying quality analysis. In fact, in the longitudinal static stability course, it will be found that Equation 3.37 is used to represent the wing's contribution to the total aircraft equilibrium (balance) equation. More often than not, the arbitrary point, n , is taken as the aircraft center of gravity, cg , so Equation 3.37 is usually written

$$C_{m_{cg}} = C_{m_{ac}} + C_L (cg - ac) \quad (3.38)$$

3.17.4 Variables Affecting $C_{m_{ac}}$

Figure 3.47 shows that $C_{m_{ac}}$ is a constant for both symmetric and cambered wings, i.e., either zero or a negative constant. For most positively

cambered airfoils, the negative constant is small. Supercritical wing sections have a $C_{m_{ac}}$ about twice that of a conventional cambered section due to their aft loading.

Positive camber causes the negative moment coefficient shown in Figure 3.47. Increasing the camber increases this negative moment; therefore, lowering flaps creates a more negative moment coefficient since lowering flaps effectively increases wing camber. This effect of deflecting a flap is the same as that of increasing camber on the symmetric airfoil shown in Figure 3.47.

The reflexed wing shown in Figure 3.50 tends to reduce the effects of camber by creating a down load near the trailing edge of the wing. In fact, if enough reflex is incorporated in a wing either by an upward moving control surface or fixed reflex, the negative pitching moment due to camber can be completely overpowered. All tailless aircraft must have some means of adjusting the reflex of the wing for stability and control considerations.

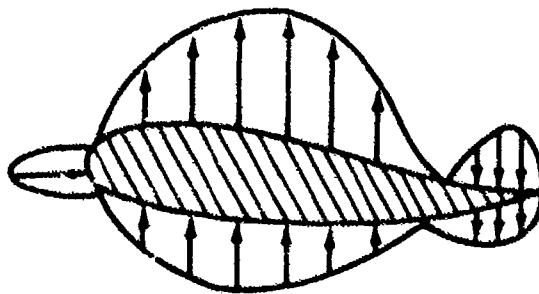


FIGURE 3.50. EFFECT OF WING REFLEXING

3.17.5 Summary

Equation 3.38 is a very useful moment coefficient expression used to relate airfoil moment coefficients to an aircraft cg.

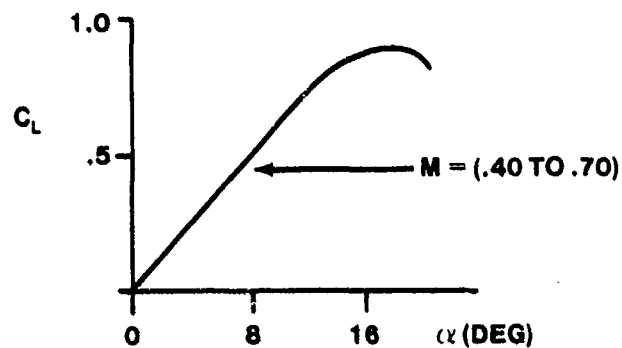
$$C_{m_{cg}} = C_{m_{ac}} + C_L (cg - ac) \quad (3.38)$$

In Equation 3.38, $C_{m_{ac}}$ is zero for symmetric airfoils, a negative constant for positively cambered airfoils, and can be "adjusted" to any desired value (zero, positive, or negative) by properly reflexing the airfoil trailing edge. For all practical purposes the aerodynamic center of any airfoil is located at the quarter-chord position.

The treatment of moments for the total aircraft is covered extensively in Flying Qualities.

PROBLEMS

- 3.1 A T-38 weighing 11,000 lb with a wing area of 170 ft^2 is stabilized in a 4-g turn at 20,000 ft on a standard day at an equivalent airspeed of 500 ft/sec. How much lift is the aircraft generating? What is the coefficient of lift (C_L)?
- 3.2 The RF-4C has a wing reference area of 530 ft^2 . If its wingspan is 38.41 ft, what is its aspect ratio?
- 3.3 Given the lift curve shown below, estimate the lift curve slope at a Mach of 0.9. Draw the estimated 0.9 Mach lift curve.



- 3.4 Find the pressure coefficient at Point P. The wing is traveling at 300 ft/sec on a standard day at sea level.



- 3.5 Plot changes in C_L vs α (symmetric airfoil) for:
- Increase in aspect ratio
 - Increase in Reynolds number
 - Extension of leading edge (LE) flaps
 - Extension of trailing edge (TE) flaps
- 3.6 The wing of an aircraft operating at 10,000 ft on a standard day has a stagnation point where the pressure is 100 lb/ft^2 higher than atmospheric pressure, and a maximum velocity point where the pressure is 200 lb/ft^2 lower than atmospheric. Assume that Bernoulli's equation applies.
- What is the free stream velocity in ft/sec?
 - What is the maximum tangential velocity on the wing surface in ft/sec?
 - Where on the wing is the static pressure a minimum?
- 3.7 A T-38 is flying at 40,000 ft on a standard day at 500 ft/sec TAS. What is the Bernoulli constant (total head) for this flight condition? How does this answer compare to the total pressure of 471 lb/ft^2 obtained when compressibility is considered? What is the aircraft's flight Mach?
- 3.8 On a standard day an aircraft with a wing area of 691 ft^2 and a wingspan of 58.8 ft is in stabilized level flight cruising at an altitude of 38,300 ft and at a true velocity of 400 kts. The aircraft weighed 50,000 lb at takeoff and has since burned 10,000 lb of fuel. The SAC pilot also consumed his three lb lunch immediately after takeoff. The ten engines on the aircraft are producing 300 lb of thrust each.
- What are the aircraft lift and drag coefficients for these flight conditions?
 - The same aircraft in preparation for landing has slowed down to an airspeed of 150 ft/sec (V_g) at a gross weight of 18,478 lb in cruise configuration and has stabilized in level flight. Each engine is now producing 166.3 lb of thrust. What are the aircraft lift and drag coefficients for these flight conditions?

ANSWERS

3.1 44,000 lb; 0.87 (No Units)

3.2 2.78 (No Units)

3.4 1.084 (No Units)

3.6 a. 338 ft/sec

b. 585 ft/sec

3.7 465 lb/ft^2 ; $M = 0.52$ (No Units); $\Delta = 1.27\%$

3.8 a. 0.40, 0.03 (No Units)

b. 1.00, 0.09 (No Units)

BIBLIOGRAPHY

- 3.1 Dwinell, James H., Principles of Aerodynamics. New York: McGraw Hill Book Company, Inc., 1949.
- 3.2 Hurt, H.H., Jr., Aerodynamics for Naval Aviators, NAVWEPS 00-80T-80, Office of the Chief Of Naval Operations Aviation Training Division, U.S. Navy, 1960.
- 3.3 Heffley, R.K., and Jewell, Wayne F., Aircraft Handling Qualities Data, Prospective NASA CR, Systems Technology, Inc., Hawthorne, CA, 1972.
- 3.4 Von Karman, Theodore, Aerodynamics: Selected Topics in the Light of their Historical Development. Ithaca, NY: Cornell University Press, 1954.
- 3.5 Kuethe, Arnold M., and Chow, Chuen-Yen, Foundations of Aerodynamics: Bases of Aerodynamic Design, 3rd ed. New York: John Wiley & Sons, 1976.
- 3.6 Millikan, C.B., Aerodynamics of the Airplane. New York: John Wiley & Sons, 1941.
- 3.7 Carroll, Robert L., The Aerodynamics of Powered Flight. New York: John Wiley & Sons, 1960.
- 3.8 Nicolai, Leland M., Fundamentals of Aircraft Design. Fairborne, OH: Domicone Printing Services, 1975.
- 3.9 Anon., Aerodynamics for Pilots, ATC Manual 51-3, Hq ATC, Randolph AFB, TX 78148, 1 Jul 1970.

CHAPTER 4
AERODYNAMIC DRAG

4.1 INTRODUCTION

If a vehicle is to fly, it must first overcome the resistance to its motion through the air. This resistive force, acting in a direction opposite to the direction of flight, is called aerodynamic drag.

A propulsion system, either propeller driven, jet, or rocket, carried in the vehicle produces thrust to overcome the drag force on the vehicle. If the propulsive force or thrust is just equal and in opposite direction to the drag force on the vehicle in flight, the vehicle is said to be in steady or equilibrium flight. If the thrust exceeds the drag, the vehicle will accelerate.

The drag on an aircraft can be considered as the sum of many component drags, such as the drag caused by the wings, fuselage, tail, etc. The aircraft designer is usually interested in component drags when estimating the total drag of a proposed aircraft. The wind tunnel engineer is also interested in component drags, values which he can measure experimentally on models in a wind tunnel. From these measurements, he attempts to predict the drag of a proposed or actual aircraft.

The flight test engineer is more interested in the total drag of an aircraft configuration, or in changes in total drag with changes in configuration, e.g., differences in drag between two different external store loadings. Total aircraft drag, rather than component drag, is the major consideration in aircraft performance determination. Total drag is what is normally determined from flight test measurements.

All aerodynamic forces are caused by pressure distribution due to pressure forces acting perpendicular to the aircraft surface or by shear stress distribution due to frictional forces acting tangentially to the aircraft surface.

4.2 SKIN FRICTION DRAG

Skin friction drag is drag caused by the viscosity of air flowing over the aircraft and is proportional to the shear stress on the aircraft surface caused by the airflow.

Skin friction drag has long been recognized as an important factor in

aircraft design. However, little emphasis was placed on reducing it, until the development of high speed subsonic and supersonic aircraft. The advent of high speed aircraft made skin friction drag a major concern, and the designs of modern day aircraft reflect the increasing importance placed on reducing this drag.

Skin friction drag on an aircraft is created on all of the surfaces of the airframe exposed to the airstream, that is, wing, fuselage, tail, etc. On aircraft with small wing surfaces, like the F-104, the skin friction drag on the fuselage surfaces is certainly greater than that on the wing surfaces. When discussing skin friction drag, the drag caused by the whole vehicle or object must be considered.

Skin friction drag is caused by viscosity which creates a boundary layer on aerodynamic surfaces. If there is no boundary layer attached to the object, that is, when separation has occurred, there is no skin friction drag on the object after the point of separation.

There are two basic ways to decrease the skin friction drag. Although impractical from the standpoint of total drag, one way to eliminate skin friction drag entirely is to detach the boundary layer from the object. This would create zero skin friction drag on the object, but would create a huge increase in drag due to separated flow far outweighing the benefits of zero skin friction drag.

A more practical method is to delay the transition from a laminar to a turbulent boundary layer, since less energy is available in a laminar boundary layer to create skin friction drag. This is extremely difficult to do because any small disturbance in the flow field can cause the boundary layer to transition from laminar to turbulent flow. Recall that more skin friction is produced in a turbulent boundary layer because of the greater velocity gradient at the surface.

Analytical expressions have been empirically developed for calculating the skin friction drag on some simple shapes. For example, Equation 4.1 can be used to calculate the total (both sides) skin friction drag on a smooth flat plate at zero angle of attack.

$$D = 2 C_f q S_{\text{plate}} \quad (4.1)$$

where S_{plate} is the flat plate's area. If the boundary layer is laminar, then an expression for skin friction coefficient developed in 1911 by Blasius is

$$C_f = \frac{1.328}{\sqrt{R_e}} \quad (4.2)$$

where Reynolds number is based on the length of the flat plate (4.1.313).

If the boundary layer is turbulent, then Equation 4.1 still applies where

$$C_f = \frac{0.072}{(R_e)^{0.2}} \quad (4.3)$$

and Reynolds number is based on the length of the flat plate.

Equations predicting the skin friction drag of a flat plate have very little flight test application; however, Equations 4.2 and 4.3 can be used to demonstrate two practical considerations for all aerodynamic surfaces.

1. A turbulent boundary layer does generate more skin friction drag than a laminar boundary layer. In fact, the turbulent skin friction drag coefficient is several times as large as the laminar coefficient.
2. It would appear from examination of Equations 4.2 and 4.3 that increasing Reynolds number at constant velocity always decreases skin friction drag since Reynolds number is in the denominator in both equations. This is not the case. If the boundary layer is turbulent and Reynolds number is increased, skin friction drag coefficient decreases. This is normally the case for real airfoils in-flight since they have primarily turbulent boundary layers. If the boundary layer is laminar and Reynolds number is increased and the boundary layer remains laminar, then skin friction drag coefficient decreases. If increasing Reynolds number causes the boundary layer to transition from laminar to turbulent flow, then skin friction drag increases. This phenomena is shown in Figure 4.1. Although Figure 4.1 shows analytical and wind tunnel data for a flat plate, airfoils behave similarly.

If the flow Reynolds number is increased to its critical value, transition from laminar to turbulent flow will occur, and skin friction drag will increase. Equation 4.2 only applies below a Reynolds number of 728,000, which is the critical Reynolds number determined experimentally for a flat plate.

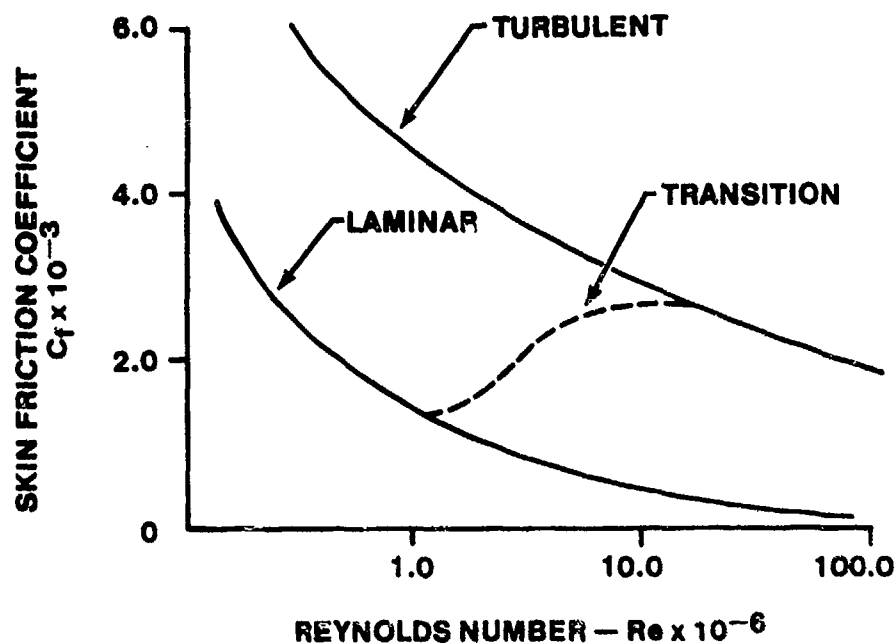


FIGURE 4.1. SKIN FRICTION CURVES FOR A SMOOTH FLAT PLATE

4.3 PRESSURE DRAG

Pressure drag arises because of the overall pressure distribution on an object. The difference between the forces caused by the high pressures on the forward portion and low pressures on the aft portion of the object is pressure drag. Pressure drag is sometimes called form or wake drag because its magnitude is proportional to the size of the wake produced behind an object.

Pressure drag always occurs in the real case. The total pressure is never completely recovered at the aft stagnation point, and there is always at least a small wake of separated flow behind any aerodynamic shape as in Figure 4.2.

Streamlining is used to delay flow separation as far aft on a body as possible, thereby allowing the pressures on the rear surface to approach those on the forward surface. The secret lies in the situation which arises when a boundary layer is required to flow from a region of low pressure to a region of higher pressure, that is, against an adverse pressure gradient. If the boundary layer flow separates, the pressure drag increases spectacularly. This situation is averted by streamlining.

The result of separation is that the pressure at the trailing edge never comes up to the stagnation pressure at the leading edge. Thus, there is a net pressure force in the aft direction. This retarding force is pressure drag.

It is proportional to (1) how low the pressure is in the separated region, and (2) the cross-sectional area in the wake. Both of these factors depend on how far aft the boundary layer travels before it separates. In turn, the separation point depends on (1) how steep the adverse pressure gradient is, and (2) how much energy is in the boundary layer.

At angles of attack below separation, pressure drag is considered to be independent of angle of attack; therefore, it is defined as occurring at angle of attack for zero lift. With blunt objects, the pressure drag is usually many times greater than the viscous skin friction drag and accounts for the comparatively large drag of unstreamlined forms.

Consider the three aerodynamic shapes in Figure 4.2, the streamlined object, the sphere, and the flat plate. All have the same circular frontal cross-sectional area and are immersed in the same air flow.

As expected, the streamlined object produces the least amount of pressure drag. Due to the streamlined shape of the object, the adverse pressure gradient behind the point of maximum thickness is very shallow, and the boundary layer follows the surface contour almost to the trailing edge. When

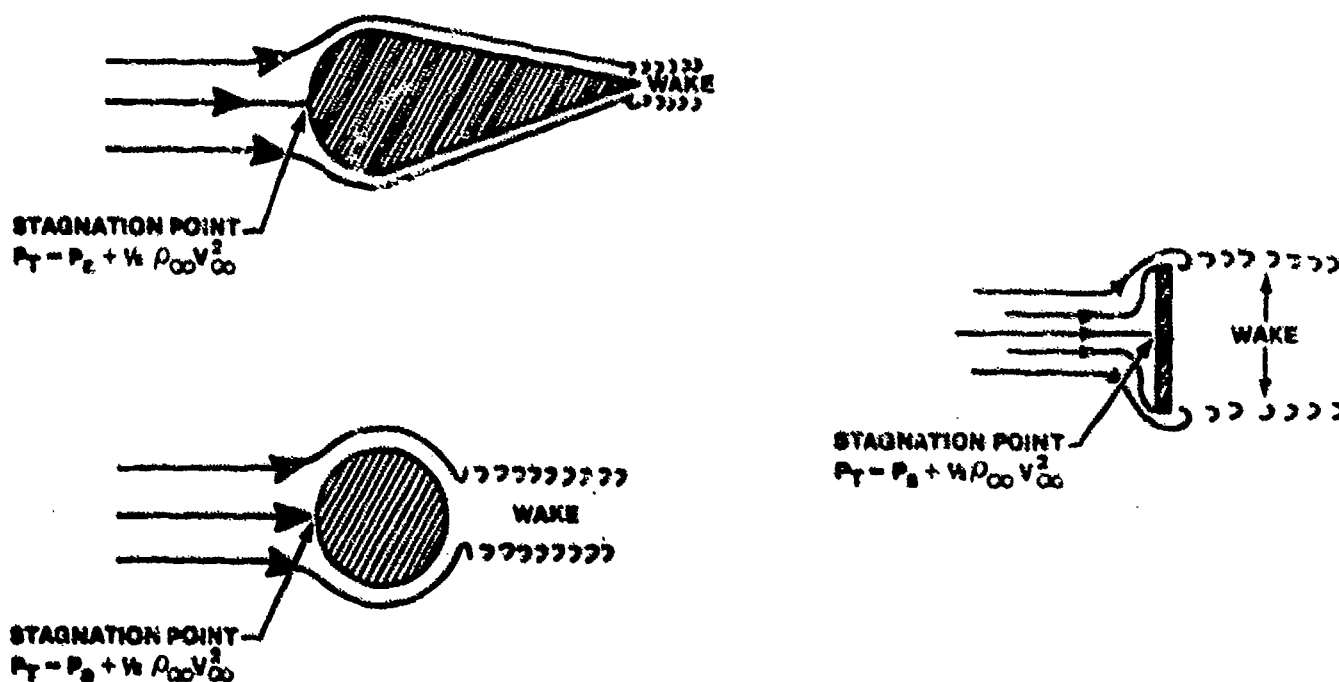


FIGURE 4.2. PRESSURE DRAG OF STREAMLINED AND UNSTREAMLINED BODIES

the energy in the boundary layer is no longer sufficient to overcome the shallow pressure gradient, the flow separates from the surface, forming a small wake. The size of this wake is an indication of how much dynamic pressure has been converted into static pressure before separation. Had all the dynamic pressure been converted into static pressure, no separation would have occurred and there would be no pressure drag. The small low pressure wake behind the streamlined object creates a pressure differential in a direction parallel to the flow. This pressure differential multiplied by the cross-sectional area of the wake is the pressure drag.

The sphere produces considerably more pressure drag than the streamlined object because the adverse pressure gradient on the back side of the sphere is quite steep compared to the pressure gradient on the back side of the streamlined object. The steep gradient dissipates the flow energy faster, causing separation to occur farther from the horizontal centerline of the sphere than on the streamlined object, creating a larger low pressure wake behind the sphere. The wake size behind a sphere is a function of Reynolds number.

Of the objects shown, the flat plate creates the greatest amount of pressure drag, since the adverse pressure gradient behind the plate has, in theory, an infinitely steep slope. The flow energy in the boundary layer cannot overcome this gradient, and the flow separates at the edges of the plate rather than making an abrupt 180° turn, leaving a very large low pressure wake behind the plate.

4.3.1 Reynolds Number Effect on Pressure Drag

Experiments using a sphere as the test object show a definite relationship between pressure drag and the particular Reynolds number of the flow. Consider the flow about the sphere in Figure 4.3. If the flow did not separate, the pressure on both the front and rear sides of the sphere would be equal, and there would be no pressure drag. However, due to a strong adverse pressure gradient after the 90° point, the flow does separate. Where the flow separates between the 90° and 180° points depends on the energy in the boundary layer. Obviously, an early separation will create a large wake and a large pressure drag.

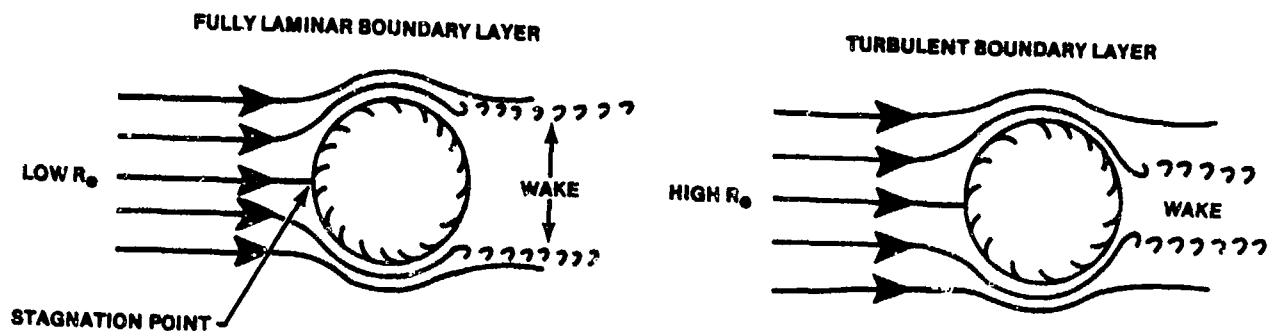


FIGURE 4.3. FLOW PAST A SPHERE AT LOW MACH

To forestall separation of the boundary layer in the presence of an adverse pressure gradient, a turbulent boundary layer is preferable to a laminar boundary layer since it has more energy as was explained earlier. As flow Reynolds number increases, the transition point moves forward around the surface because the critical Reynolds number is reached sooner. This fact has practical importance. For example, the drag of a smooth sphere increases with increasing airspeed up to a certain point, after which it decreases and then ultimately increases again as shown in Figure 4.4.

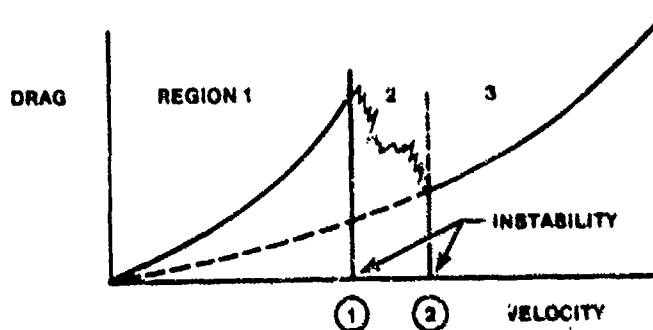


FIGURE 4.4. DRAG VERSUS VELOCITY FOR A SMOOTH SPHERE AT LOW MACH

In region 1, the flow is laminar over the sphere and separates near the shoulder. The drag is primarily pressure drag since a sphere is a "blunt" body. At speed 1 the transition point has moved to the shoulder and coincides

with the separation point. As the velocity increases further, the region of the transition flow overlaps the original separation point. The additional energy in the partially turbulent flow now helps the boundary layer go farther toward the aft end of the sphere before it stalls and separates. Thus, the pressure drag is reduced. Finally, when the velocity reaches point 2, transition is complete before the separation point is reached. Beyond point 2, the drag again increases with increased speed, but now along a more gentle curve.

Another way to look at the same problem is to examine sphere drag coefficient as a function of Reynolds number as shown in Figure 4.5.

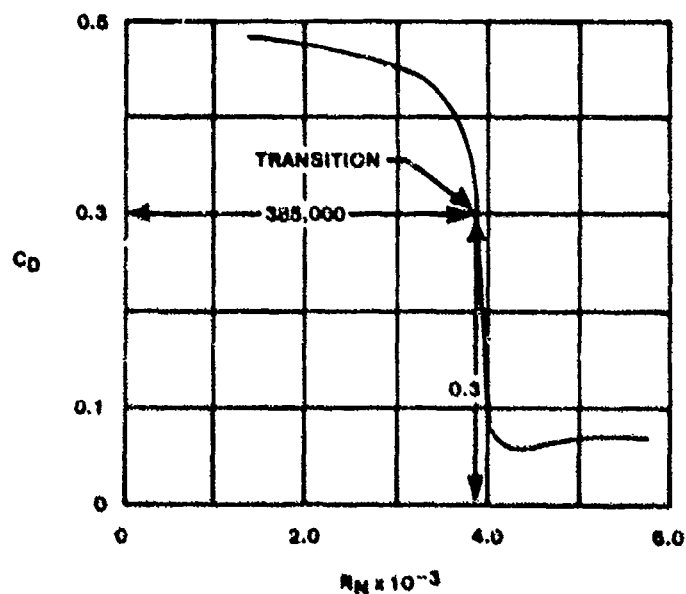


FIGURE 4.5. VARIATION OF SPHERE DRAG COEFFICIENT WITH REYNOLDS NUMBER (4.1:197)

Figure 4.5 clearly shows that as Reynolds number increases, transition from a laminar to a turbulent boundary layer causes a dramatic decrease in drag coefficient which results in a decrease in drag.

The ordinary golf ball operates at low Reynolds numbers and would have very high pressure drag if the boundary layer were laminar. The dimples force

the boundary layer to become fully turbulent and delay separation, thus greatly reducing the pressure drag of the ball. In the early days of the game, golf balls were smooth. But wind tunnel tests have shown that over the entire range of speeds at which golf balls leave the tee, the dimpled ball has less drag. The drag reduction is a major one. With a swing which drives a dimpled ball 230 yards in flight, a smooth ball is driven only 50 yards in experiments on a golf course.

While spheres are not shapes that are normally used on aircraft, the theory discussed concerning pressure drag and the effects of Reynolds number is directly applicable to aerodynamic shapes.

Turbulent boundary layers are more effective than laminar boundary layers in delaying separation. However, an aircraft surface would not be roughened (as in the case of the golf ball) to induce a turbulent layer because of the tremendous increase in skin friction drag that would result.

4.3.2 Boundary Layer Control

The aerodynamic and artificial means to delay separation also decrease pressure drag at high angles of attack, i.e., slots, slats, suction, and blowing. However, the primary purpose of boundary layer control as used in present day aircraft is to decrease stall speeds by delaying separation, and not to decrease pressure drag. The reason is that the energy required to effect a decrease in pressure drag through boundary layer control is usually more than the benefits gained from this drag decrease. In fact, because of operational considerations, high values of pressure drag are sometimes desirable in the power approach and landing configurations.

4.4 PROFILE DRAG

Profile drag is a measure of the resistance to flight caused by the air on the profile of the aircraft. This resistance to flight is the sum of skin friction and pressure drag. Profile drag is sometimes called boundary layer or viscous drag since neither skin friction nor pressure drag would occur if air were nonviscous. Since the viscosity of air is small, in 1783 the French mathematician, d'Alembert, assumed it could be neglected completely. This led him to the conclusion that if a body were moved through the air, and viscous

forces were neglected, the body would encounter no drag. This conclusion became known as "d'Alembert's Paradox" and was finally resolved by Prandtl in 1904. Figure 4.6 illustrates classical ideal nonviscous flow past a circular cylinder.

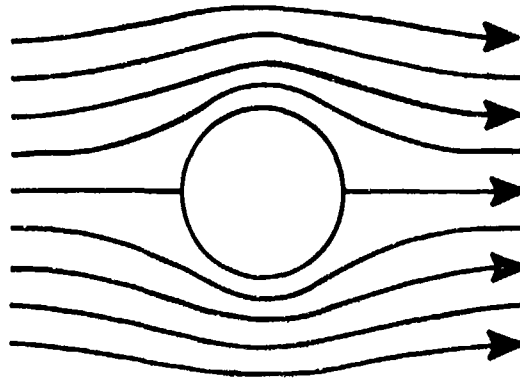


FIGURE 4.6. IDEAL NONVISCIOUS FLOW PAST A CIRCULAR CYLINDER (4.2:33)

Since there is no viscosity, there is no skin friction; therefore, no skin friction drag exists. The flow is also symmetric fore and aft with stagnation points and total pressure recovery on the front and rear of the cylinder. Since the streamlines are symmetric, the pressure distribution fore and aft calculated from the Bernoulli equation is also symmetric; therefore, no pressure drag occurs. Since both skin friction and pressure drag are zero, there is no profile or total drag. Therefore, viscosity must be responsible for both skin friction and pressure drag.

For the symmetric airfoil in an inviscid flow at zero angle of attack shown in Figure 4.7, the results are not quite as obvious. Since there is no viscosity, there is no skin friction drag, but the pressure distribution is not symmetric fore and aft. Nevertheless, the fore and aft components of the pressure force exactly cancel.

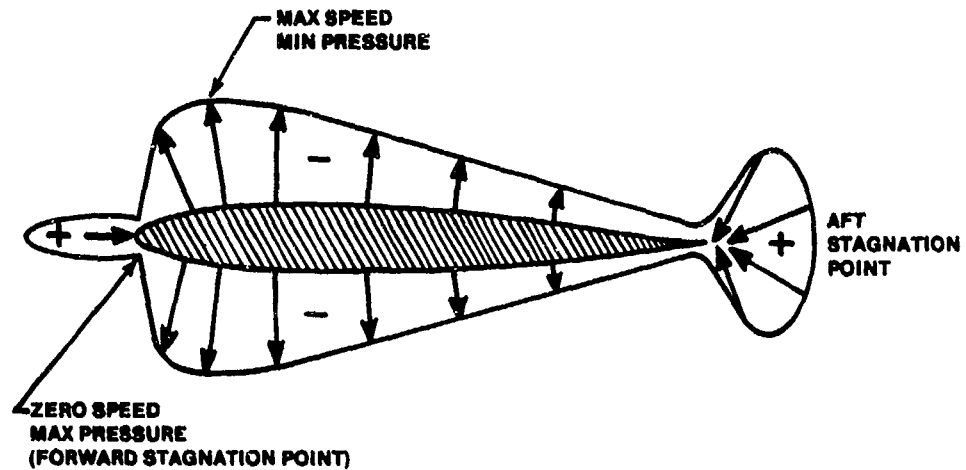


FIGURE 4.7. IDEAL NONVISCIOUS FLOW PRESSURE DISTRIBUTION AROUND A SYMMETRIC WING SECTION AT ZERO ANGLE OF ATTACK

However, nonviscous flow does not occur in the real case. In fact, a flat plate can be used to illustrate the extremes of profile drag. The flat plate perpendicular to the flow in Figure 4.8 shows the case of almost all drag being pressure drag. Therefore, nature and experience are again reconciled, and d'Alembert's paradox is removed by properly accounting for the presence of viscosity (4.3:195).

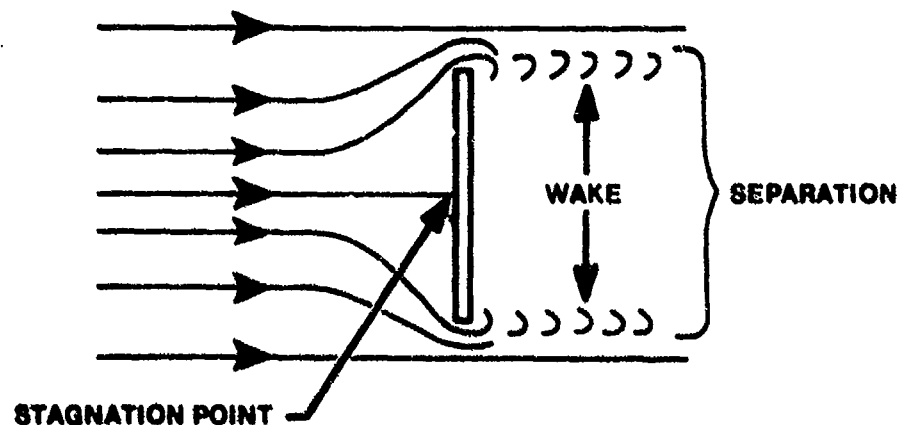


FIGURE 4.8. FLOW PAST A FLAT PLATE PERPENDICULAR TO THE FLOW

The skin friction drag on the two small edges parallel to the flow becomes negligible in comparison to the drag caused by the resulting pressure differential between the front and rear sides of the plate. There is a low pressure region, or wake, behind the plate in which some motion exists in the form of eddies and free vortices. The pressure over the front of the plate is high compared with the lower pressure on the rear of the plate, producing a net retarding force or pressure drag.

The very thin flat plate parallel to the flow shown in Figure 4.9 shows the other extreme in profile drag where almost all drag is skin friction drag. Only a small wake is created, and pressure drag is very small compared to skin friction drag.

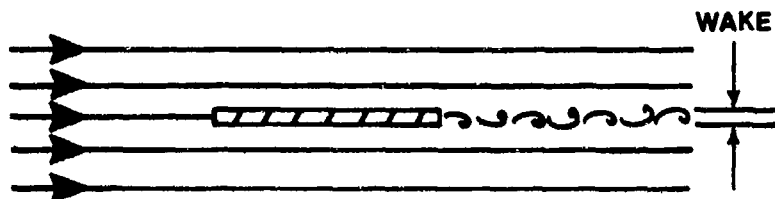


FIGURE 4.9. FLOW PAST A FLAT PLATE PARALLEL TO THE FLOW

Since a flat plate is an extreme case of pressure drag, it has been taken as a standard by which to compare values of profile drag for aerodynamic shapes. Depending on the size and shape of the flat plate and on the Reynolds number at which wind tunnel tests are conducted, values of drag coefficient based on the plate's area have been obtained; 1.28 is the accepted low subsonic value for a large plate in the flight range of Reynolds number. Flat plate drag can be written,

$$D = C_D q S_{\text{plate}} = 1.28 q S_{\text{plate}} \quad (4.4)$$

where S_{plate} is the flat plate's area.

In expressing the drag coefficient of simple nonlifting shapes, it is convenient to base the coefficient on total projected frontal area. Such an area is sometimes referred to as the "proper area" for the particular shape of the body, and the corresponding drag coefficient is defined as the proper drag

coefficient, $C_{D_{\pi}}$. For example, in Equation 4.4, the flat plate's area is also its proper area, and the drag coefficient, $C_{D_{\pi}} = 1.28$, is the proper drag coefficient.

Using this notation, the proper drag coefficient for any nonlifting body can be defined as

$$C_{D_{\pi}} = \frac{D}{qS_{\pi}} \quad (4.5)$$

where S_{π} is the projected frontal area. Now the drags of various aerodynamic shapes can be compared with the drag of a flat plate of the same frontal area. If the ratio $C_{D_{\pi}}/1.28$ is greater than one, the shape is less "efficient" than a flat plate. Figure 4.10 gives the drag coefficients of various aerodynamic shapes and the corresponding value of the ratio $C_{D_{\pi}}/1.28$.

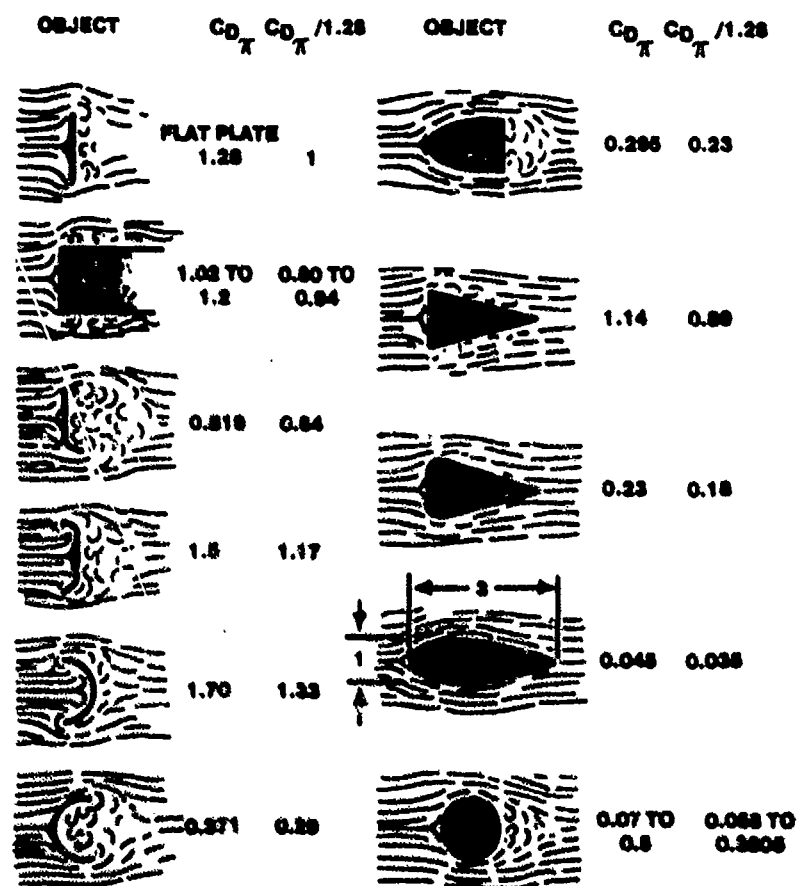


FIGURE 4.10. RELATIVE DRAG OF VARIOUS NONLIFTING AERODYNAMIC SHAPES AT LOW MACH (4.1:194)

Note from Figure 4.10 that a streamlined shape having 3/1 length/diameter ratio gives the lowest value of drag coefficient, namely, 0.045, which is only 3.5% of the drag coefficient of the flat plate.

4.5 INTERFERENCE DRAG

Interference drag is generated when several objects are placed in the same airstream creating eddy currents, turbulence, or restrictions to smooth flow. For example, the air flowing along the fuselage collides with the air flowing over the wing in the area of the wing root. The effects of this collision can be reduced by allowing a smoother merging of the two air currents by installation of a fairing at the fuselage-wing root junction as shown in Figure 4.11. If an external store is hung on the wing of an aircraft and the drag of the aircraft and that of the store are known, the drag actually produced is greater than the sum of the drag of the individual components because of the interference drag created (4.4:39).

Any time two parts of an aircraft are joined or any object is placed on or in close proximity to an aircraft, interference drag is created. In some cases, however, overall drag can actually be reduced by proper streamlining of the flow. An example of this beneficial effect is evidenced in the addition of the conformal tanks on the F-15.

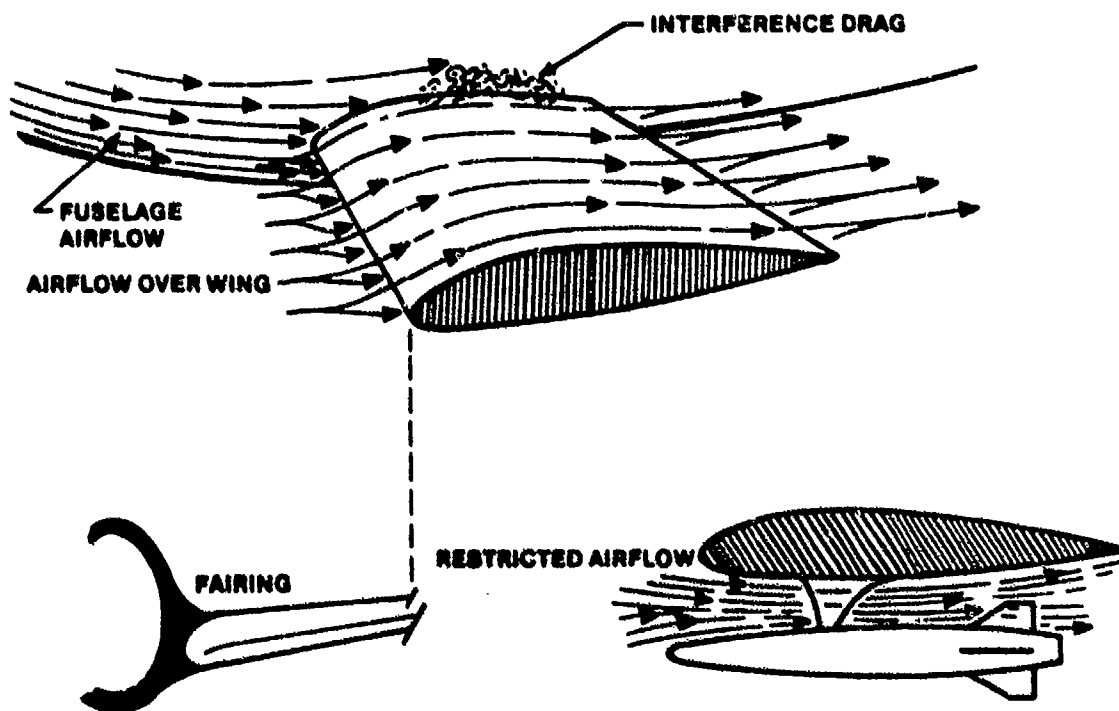


FIGURE 4.11. INTERFERENCE DRAG (4.4:39)

4.6 PARASITE DRAG

Parasite drag is the sum of profile and interference drag. Parasite drag on an aircraft is the drag which is not caused by lift or compressibility effects. Aircraft parasite drag is a constant for a given aircraft velocity, i.e., independent of angle of attack.

The customary method for determining parasite drag is to perform wind tunnel testing. Classically each part of an aircraft (wing, fuselage, empennage, etc.) is individually tested. Then the total parasite drag is the sum of each increment of drag. The drag equation can be written

$$D_p = C_{D_p} qS \quad (4.6)$$

Since an aerodynamic coefficient is completely arbitrary, it may be based on any area. Conventionally, the standard area is the wing area. However, for such external stores as bombs, drop tanks, and missile launchers, the projected frontal area or proper area, defined in Section 4.4, is used.

To determine the increment in drag coefficient that has to be added to an aircraft's drag coefficient due to carrying an external store, the relationship in Equation 4.7 is used.

$$\text{Drag}_{\text{store}} = \Delta \text{Drag}_{\text{aircraft}} \quad (4.7)$$

$$C_{D_\pi} qS_\pi = \Delta C_{D_p} qS \quad (4.8)$$

from which

$$\Delta C_{D_p} = \frac{C_{D_\pi} S_\pi}{S} \quad (4.9)$$

where S is the wing area, S_π is the store's projected frontal area, and C_{D_π} is the store's proper drag coefficient defined in Section 4.4.

4.6.1 Drag Counts

Since it is awkward to speak of increments of drag coefficient based on

wing area, it is customary to use the expression "counts of drag" where one count of drag is a drag coefficient of 0.0001. Thus, a rocket launcher which increased the airplane's parasite drag coefficient by 0.0010 would be said to have ten counts of drag. The term "drag index" is closely related to this. A drag index of ten, for example, means that this configuration has ten counts of drag more than the basic configuration of the airplane. Aircraft flight manuals often use the drag count system in presenting performance data.

4.6.2 Equivalent Flat Plate Area

Instead of indicating the aerodynamic characteristics of a bomb or an aircraft by a parasite drag coefficient, frequently an "equivalent flat plate area" is used. This means that the bomb could be replaced mathematically by a flat plate having the same drag as defined in Equation 4.4.

$$D_p = C_{D_{plate}} q S_{plate} \quad (4.4)$$

where

$$C_{D_{plate}} = 1.28 \text{ (determined from wind tunnel testing).}$$

Therefore

$$C_{D_p} q S = 1.28 q S_{plate} \quad (4.10)$$

or

$$S_{plate} = \frac{C_{D_p} S}{1.28} \quad (4.11)$$

The equivalent flat plate area is a convenient and graphic way of expressing the parasite drag of a body. A drag coefficient of 0.003 has little significance to someone unfamiliar with the normal magnitude of bomb coefficients. An equivalent flat plate area of one square foot has a very definite physical significance. Often, wind tunnel external store testing data are presented in terms of equivalent flat plate area. Sometimes aircraft are compared aerodynamically by computing their equivalent flat plate areas.

4.7 INDUCED DRAG

The portion of the total drag force that is due to the production of lift is defined as induced drag.

When a wing is producing lift, there is a static pressure differential created across the wing with pressure well below atmospheric on most of the top surface and slightly below atmospheric on most of the bottom surface. This pressure differential induces a circulation about the wing as the high pressure air beneath the wing tends to flow into the low pressure area on top of the wing. For the two-dimensional or infinite wing, no tip vortex flow is added to this situation because there are no wingtips. The upwash ahead of the wing is equal to the downwash behind it, so these velocities cancel each other out. The circulation about the wing is called a bound vortex, and because the upwash and downwash velocities are equal and opposite, no induced drag is produced. This situation is illustrated in Figure 4.12.

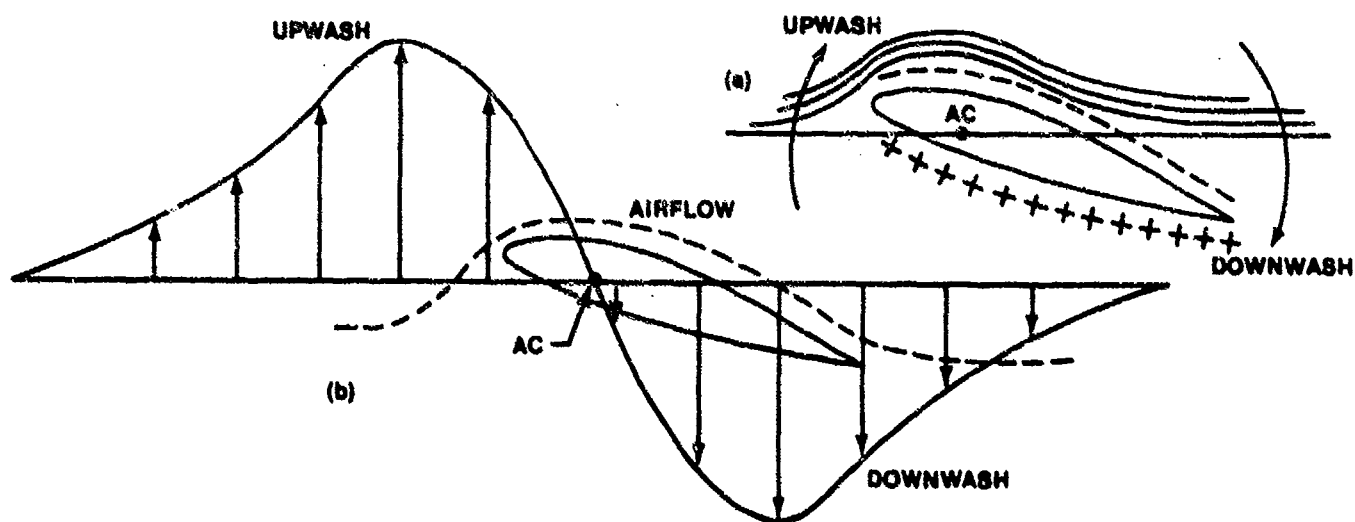


FIGURE 4.12. BOUND VORTEX ON AN INFINITE WING (4.4:41)

Notice that there is no downwash at the aerodynamic center, the point where the aerodynamic force is generated. This is the reason that there is no induced drag in pure two-dimensional flow (4.4:40).

In the three-dimensional finite case, tip vortex flow must be superimposed on the bound vortex. Not only does the air flow over the leading edge and create the circulation of the bound vortex, but it also flows around

and over the wingtips. As the wing moves through the air mass, the air trying to flow around the wingtip causes a vortex behind the wingtip. This wingtip vortex induces a spanwise flow and creates vortices all along the trailing edge of the wing. The trailing edge vortices are strongest at the tips and diminish in intensity progressing toward the center line of the wing as shown in Figure 4.13.

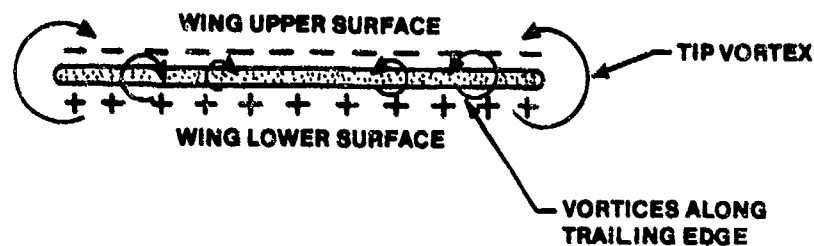


FIGURE 4.13. VORTEX FLOW ON A FINITE WING (4.5:64)

At the center line of the aircraft, there is no trailing edge vortex because the equal and opposite vortices from the left and right sides of the wing cancel each other out. This is also illustrated in Figure 4.13.

This combination of the bound and trailing edge vortices produces vertical velocities as shown in Figure 4.14.

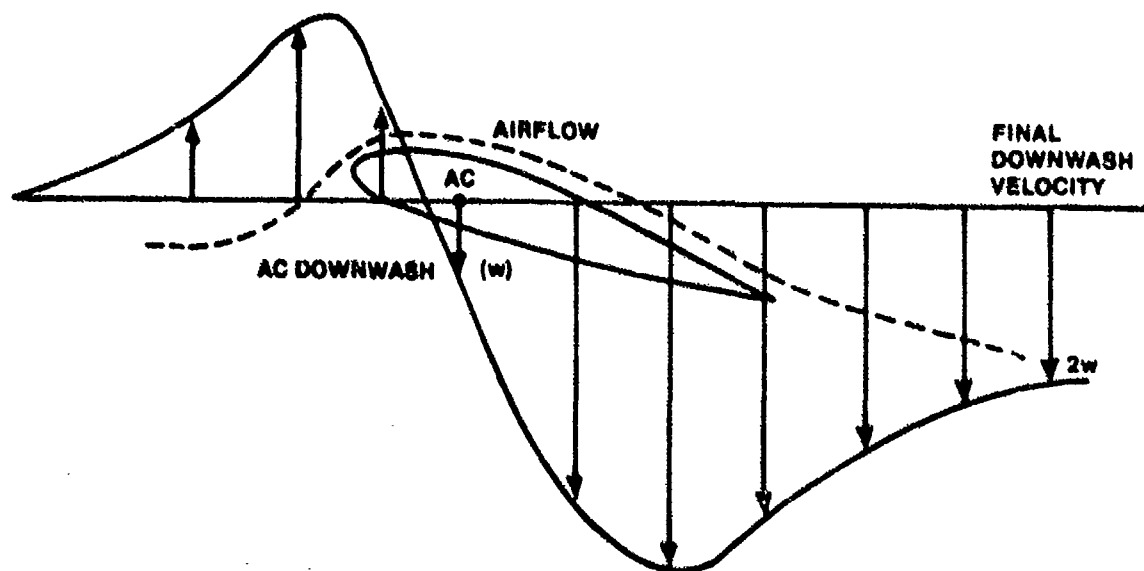


FIGURE 4.14. VERTICAL VELOCITY DUE TO VORTEX FLOW ON A FINITE WING (4.4:42)

The dashed line shows the path of the air mass as it flows over the wing. Notice that for the finite wing, there is a downwash velocity at the aerodynamic center. This downwash velocity vector added to the free stream relative wind vector results in a local relative wind vector that is inclined to the actual flight path. The magnitude of the downwash vector varies from wingtip to wingtip as the intensity of the trailing edge vortices varies.

With the action of tip and bound vortices, a final vertical velocity, w_1 , is imparted to the airstream by the wing producing lift. In Figure 4.15 the flow at the wing aerodynamic center is deflected at an angle $\epsilon/2$ which is evaluated to be,

$$\tan \epsilon/2 = \frac{w}{V_\infty} \quad (4.12)$$

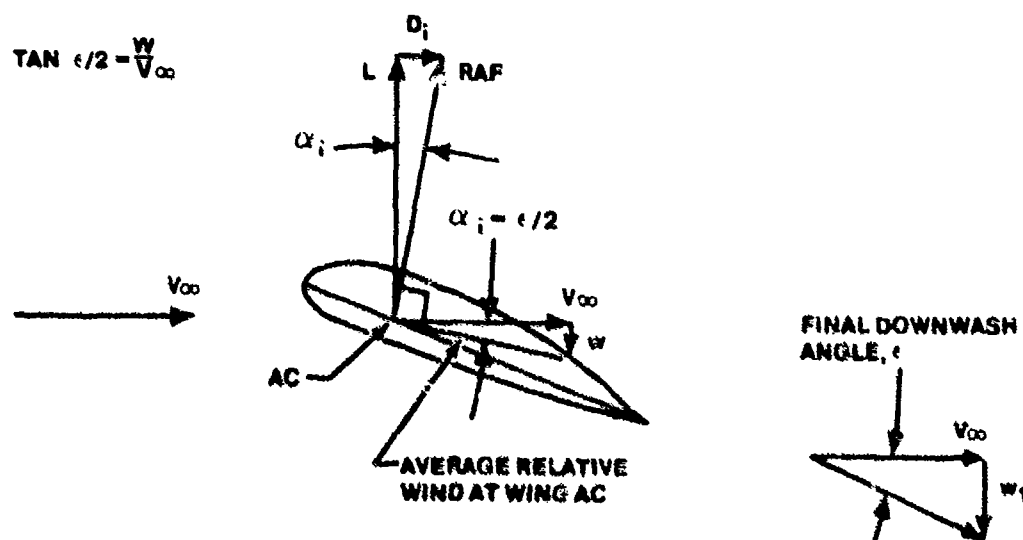


FIGURE 4.15. INDUCED FLOW FIELD

Aerodynamic theory developed by Prandtl shows that $w_1 = 2w$. Or in terms of an "induced" angle of attack, α_i

$$\tan \alpha_i = \frac{w}{V_\infty} \quad (4.13)$$

where $\alpha_i = \epsilon/2$ and is defined as the angle between the free stream relative wind and the average relative wind at the wing aerodynamic center.

The resultant aerodynamic force on a wing acts perpendicular to the local relative wind. For an infinite wing the local flow is the same as the relative wind; however, because of the downwash past a finite wing, the local airflow is inclined downward with respect to the relative wind (being the vector sum of the downwash velocity and relative wind velocity). Thus, the resultant aerodynamic force vector taken perpendicular to the air flow past the wing leans aft with respect to the relative wind and has a component that tends to retard motion. This component, labeled D_i in Figure 4.15, is the induced drag. Equation 4.14 shows that the magnitude of the induced drag depends on the induced angle, α_i . It can be shown from the geometry of the lift and drag on an airfoil in Figure 4.15 that the induced drag is

$$D_i = L\alpha_i \quad (4.14)$$

where α_i is measured in radians and is small (4.1:153).

The problem in calculating the magnitude of induced drag arises from the difficulty in determining the induced angle of attack, α_i , in Equation 4.14.

In summary then, the canting downward of the relative wind from its original direction has two major consequences:

1. The angle of attack of the airfoil section of the wing measured at the aerodynamic center is effectively reduced in comparison to the angle of attack of the wing referenced to the free stream relative wind.
2. Induced drag is developed. There are at least three physical interpretations of induced drag. First, the wingtip vortices alter the flow field about the wing in such a fashion as to change the surface pressure distributions in the direction of increased drag. An alternate explanation is that, because the local relative wind is canted downward, the resultant aerodynamic force vector is tilted back, hence, it contributes a component of force parallel to the free stream relative wind. A third physical explanation of the source of induced drag is that the wingtip vortices contain a certain amount of rotational kinetic energy. This energy has to come from somewhere; in fact, it is supplied by the aircraft propulsion system, where power has to be added to overcome the increment of drag due to induced drag (4.3:180).

The term "induced drag" was coined by Munk in 1918. Induced drag can be considered as the toll levied by nature for the privilege of flying. Since

the function of lift is to overcome weight, induced drag can be correctly described as "drag due-to-lift." Fortunately, the thrust, or power required, to overcome induced drag is not excessive, especially at higher velocities (4.6:110).

4.7.1 Effect of Planform on Induced Drag

The induced angle of attack, α_i , is a minimum if the local downwash velocity, w , at the wing aerodynamic center is uniform across the span. Therefore, as shown by Equation 4.14, a uniform local downwash across the span is desired to minimize induced drag. Prandtl discovered that if the lift distribution over a wing is a semi-ellipse with major axis equal to the wing-span and one-half the minor axis equal to the maximum local lift and located at the midspan, the local downwash is constant along the span. This elliptic lift distribution occurs naturally on an untwisted wing of elliptical planform, like that of the British Spitfire, and is shown in Figure 4.16.

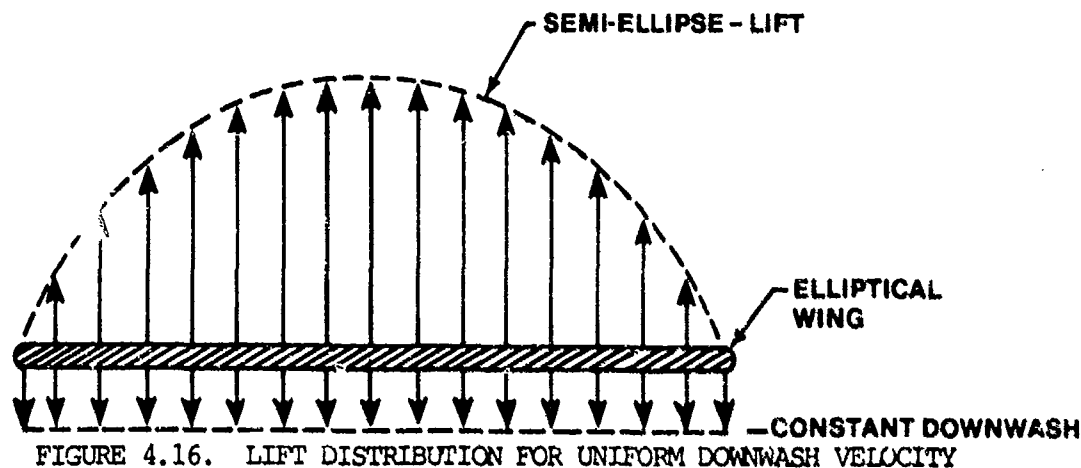


FIGURE 4.16. LIFT DISTRIBUTION FOR UNIFORM DOWNWASH VELOCITY

Only elliptical wings have uniform downwash velocity. Other wing planforms develop downwash distributions which are not constant across the wingspan. The trailing vortex distribution, downwash distribution, sectional lift coefficient distribution, and lift distribution across the wingspan are mutually dependent and are determined by wing planform. Prandtl found that, if the wing has an elliptical planform, where induced angle of attack is

constant across the span, then

$$\alpha_i = \frac{C_L}{\pi AR} \quad (4.15)$$

According to Equation 4.15, the smaller the aspect ratio, AR, the larger the induced angle of attack and thus, the greater the downwash. Substituting Equation 4.15 into Equation 4.14 gives,

$$D_i = L \alpha_i = \left(C_L qS \right) \left(\frac{C_L}{\pi AR} \right) = qS \frac{C_L^2}{\pi AR} \quad (4.16)$$

with $D_i = C_{D_i} qS$, then

$$C_{D_i} = \frac{C_L^2}{\pi AR} \quad (4.17)$$

for a wing with an elliptical planform.

Equation 4.17 can be modified so that an induced drag coefficient can be defined for any given planform by inserting a constant, e , into the denominator as shown in Equation 4.18.

$$C_{D_i} = \frac{C_L^2}{\pi AR e} \quad (4.18)$$

Equation 4.18 is used in the total drag coefficient equation for any wing planform or for an entire aircraft. The constant, e , defined as Oswald's efficiency factor, can be determined for any given aircraft configuration from flight test data. Aircraft efficiency factors generally range from about 0.5 to 1.0, with a value of 1.0 being for an elliptical wing planform without a fuselage.

4.7.2 Effect of Load Factor on Induced Drag

Defining $C_{D_{total}}$ for flight Mach less than M_{crit} as

$$C_{D_{total}} = C_{D_p} + C_{D_i} \quad (4.19)$$

Substituting Equation 4.18 into Equation 4.19 gives

$$C_{D_{total}} = C_{D_p} + \frac{C_L^2}{\pi AR e} \quad (4.20)$$

Multiplying Equation 4.20 by qS , total drag may be expressed as parasite drag plus induced drag as in Equation 4.21.

$$D_{total} = C_{D_p} qS + \left(\frac{C_L^2}{\pi AR e} \right) qS \quad (4.21)$$

Using the definitions of lift coefficient and load factor

$$C_L = \frac{L}{qS}$$

$$n = \frac{L}{W}$$

Equation 4.21 can be written

$$D_{total} = C_{D_p} qS + \left(\frac{nW}{qS} \right)^2 \left(\frac{qS}{\pi AR e} \right) \quad (4.22)$$

Using the definition of aspect ratio

$$AR = b^2/S$$

Equation 4.22 can be written

$$D_{total} = C_{D_p} qS + n^2 \left(\frac{W}{b} \right)^2 \left(\frac{1}{qre} \right) \quad (4.23)$$

The factor W/b in the second term of Equation 4.23 is known as span loading and is an aircraft design parameter. Note for a given weight, induced drag decreases as increasing wingspan squared. For a given span loading, induced

drag increases as load factor squared. There is four times as much induced drag at 2 g's as there is at 1-g. At 4 g's there is 16 times as much induced drag. So it takes lots of thrust to maintain a steady, constant speed 4-g turn because of this large increase in induced drag. This relationship is important in aircraft turning performance.

4.7.3 Reducing Induced Drag

From observation of Equation 4.18, it appears there are two ways to reduce induced drag: increase aspect ratio, or increase aircraft efficiency factor.

$$C_{D_i} = \frac{C_L^2}{\pi AR e} \quad (4.18)$$

Since increasing AR and e have the same effect on induced drag and on the drag polar, ARe is sometimes defined as effective aspect ratio.

Wings with straight leading and trailing edges are much easier to construct than elliptical planform wings, so tapered wings are primarily used on aircraft. Fortunately, the tapered wing with a proper taper ratio has an Oswald's efficiency factor close to 1.0.

There are two common ways of increasing Oswald's efficiency factor of a given tapered wing. One way is to change the airfoil section along the span to provide an elliptical spanwise lift distribution. This may be done by gradually changing a characteristic of a given airfoil along the span such as the thickness ratio or camber. The second way is to twist the wing gradually along the span so that the tip airfoil section angle of attack will be different from the root airfoil section angle of attack.

Another method is to attach endplates, winglets, or tip tanks to the basic wing design. These reduce the intensity of the wingtip vortices which result from the pressure differential between the upper and lower wing surfaces. The result is the same as an increase in aspect ratio. In fact, the efficiency factor of an airfoil with properly located tip tanks can be higher than for the basic wing.

To review, there are five possible ways to obtain a high Oswald's efficiency factor:

1. Design an elliptical planform wing
2. Twist the wing
3. Change airfoil sections along the span
4. Design a tapered wing using methods 2 and 3 above
5. Design a wing with endplates, winglets, or tip tanks

It can be seen from Equation 4.18 that induced drag and the efficiency factor have a noticeable effect on the performance of aircraft flying at low speeds (high C_L).

4.8 WAVE DRAG

Wave drag, often called compressibility or Mach drag, is the drag which results when flow over the surfaces of an aircraft exceeds Mach 1.0. Supersonic flow over aircraft surfaces results in the formation of shock waves, causing a sizeable increase in drag due to the large pressure changes across the shock. Behind the shock wave, the flow field must operate in an adverse pressure gradient due to the large increase in static pressure as the velocity is slowed to a lower supersonic or subsonic value. Recall that the flow is more prone to separate when operating in an adverse pressure gradient. The net drag due to this higher pressure behind a shock wave is the wave drag. The vector resolution of the pressure force perpendicular to the surface illustrated in Figure 4.17 clearly shows a component in the drag direction.

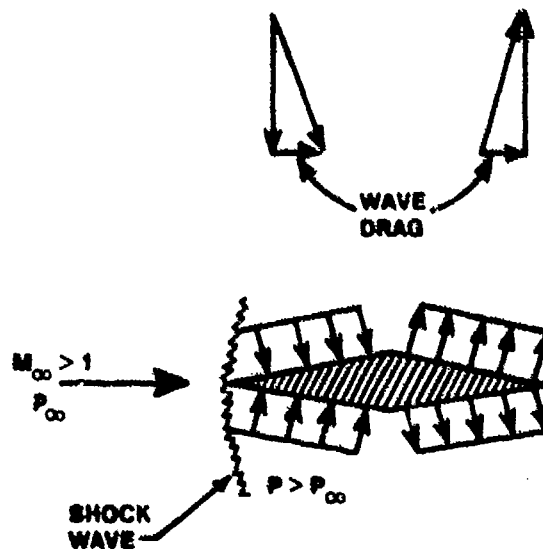


FIGURE 4.17. PRESSURE DISTRIBUTION ON SUPERSONIC SHAPE WITH RESULTANT WAVE DRAG

4.9 MISCELLANEOUS TYPES OF DRAG

The following definitions and explanations are offered for various other terms used to describe types of drag.

4.9.1 Ram Drag

Ram drag is drag due to ram compression in the diffuser of a turbojet or turbofan engine. This term is widely used in propulsion. Net thrust is usually defined as gross thrust minus ram drag.

4.9.2 Cooling Drag

Cooling drag is drag due to energy loss when air is forced past cylinders on an air cooled reciprocating engine. This is a major source of parasite drag on reciprocating propeller driven aircraft. Much flight test time is usually devoted to minimizing cooling drag while providing adequate engine cooling.

4.9.3 Trim Drag

Trim drag is an additional drag force which results from the use of the horizontal tail in trimming the aircraft, i.e., in maintaining longitudinal equilibrium. At high speeds, the tail usually carries a download, which means that the wing must provide additional lift. Therefore, the drag also increases, and the necessary increase in incidence also causes critical Mach to be reduced. This effect is particularly important at high altitude, and if the tail moment arm is short. Tailless aircraft also suffer from high trim drag. One of the advantages of the Canard configuration is that, with the tail in front of the wing instead of behind it, it carries an upload for trim at high speeds. This is equivalent to providing negative trim drag (4.7:292-293).

4.10 TOTAL DRAG

For flight test purposes, it is often not necessary to make such a detailed breakdown of total drag. It is conventional to make the following breakdown: all drag which is not a function of lift is called parasite drag,

and all drag which is a function of lift is called induced drag. If the aircraft velocity is greater than the critical Mach, wave drag accounts for the losses due to shock waves. The total drag may be written as the sum of the major component drags.

$$D_{\text{total}} = D_p + D_i + D_M \quad (4.24)$$

Using the definition of the drag coefficient, Equation 3.4, total drag can be written as

$$C_D = \frac{D}{qS}$$

$$D_{\text{total}} = C_{D_{\text{total}}} qS \quad (4.25)$$

Individual component drags can be written as

$$D_p, \text{ the parasite drag} = C_{D_p} qS \quad (4.6)$$

$$D_i, \text{ the induced drag} = C_{D_i} qS \quad (4.26)$$

$$D_M, \text{ the wave drag} = C_{D_M} qS \quad (4.27)$$

Substitution into Equation 4.24 yields

$$D_{\text{total}} = C_{D_{\text{total}}} qS = C_{D_p} qS + C_{D_i} qS + C_{D_M} qS \quad (4.28)$$

or

$$C_{D_{\text{total}}} = C_{D_p} + C_{D_i} + C_{D_M} \quad (4.29)$$

4.11 SUMMARY OF MAJOR DRAG CATEGORIES

Aerodynamic drag can be broken down into three major categories: parasite drag, induced drag, and Mach or wave drag. There are also four sub-

categories of drag whose relationship to the three major drag categories is shown in Figure 4.18.

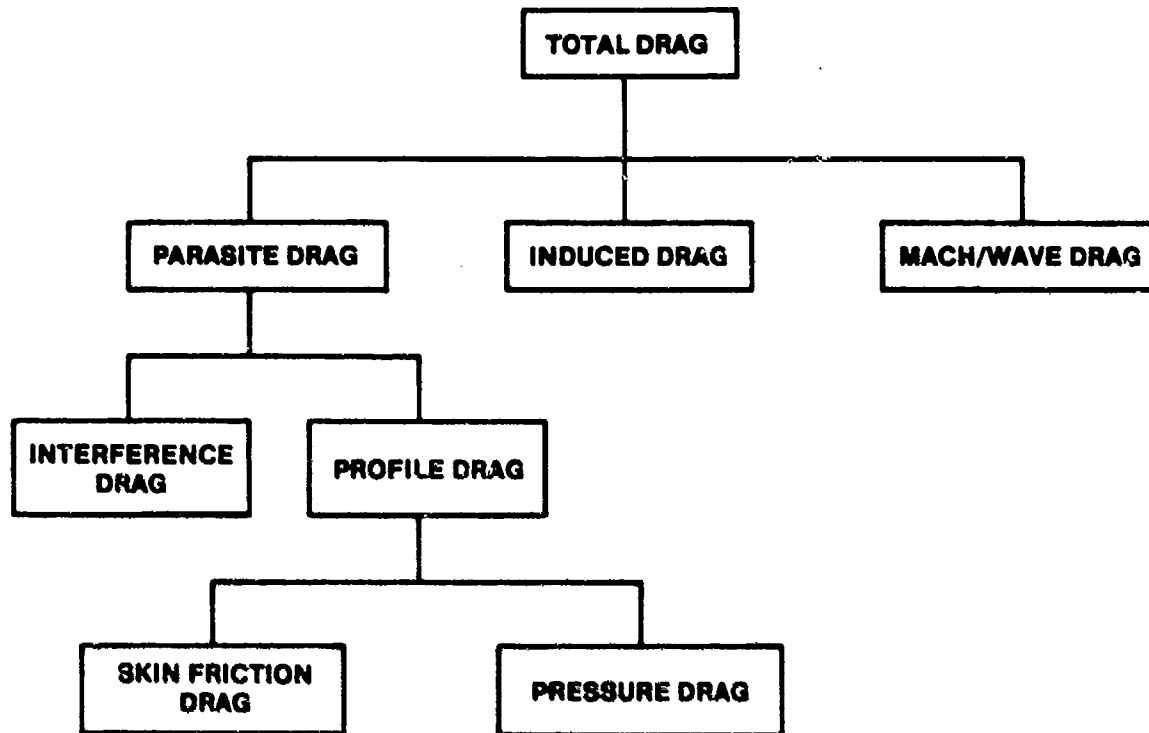


FIGURE 4.18. DRAG CLASSIFICATION

4.12 THE DRAG POLAR

The relationship between lift and drag is normally shown on a plot of C_L versus C_D , which is known as a drag polar. For subsonic flight where $C_{D_M} = 0$,

$$C_{D_{total}} = C_{D_p} + C_{D_i} \quad (4.19)$$

It was already discussed that induced drag is directly related to the generation of lift. Induced drag coefficient was defined as

$$C_{D_i} = \frac{C_L^2}{\pi AR e} \quad (4.18)$$

where e , Oswald's efficiency factor, is a constant for a given configuration. Recall that $C_{D_{total}}$ could then be expressed as

$$C_{D_{total}} = C_{D_p} + \frac{C_L^2}{\pi AR e} \quad (4.20)$$

Experiments have proven that in subsonic flight C_{D_p} is almost a constant.

A general equation for a parabola is

$$y^2 = 4 p (x - a) \quad (4.30)$$

where " p " is a focus and " a " is a constant which represents the intercept on the x axis.

When C_{D_p} , π , AR , and e are all constants, Equation 4.20 can be written

$$C_L^2 = \pi AR e \left(C_{D_{total}} - C_{D_p} \right) \quad (4.31)$$

A direct comparison between Equation 4.30 and 4.31 shows that the relationship between lift and drag coefficients is a parabola which is normally called the drag polar shown in Figure 4.19. This concept was first introduced by Eiffel in about 1890. Eiffel conducted drag experiments by dropping various bodies from the Eiffel Tower and measuring their terminal velocity (4.3:260).

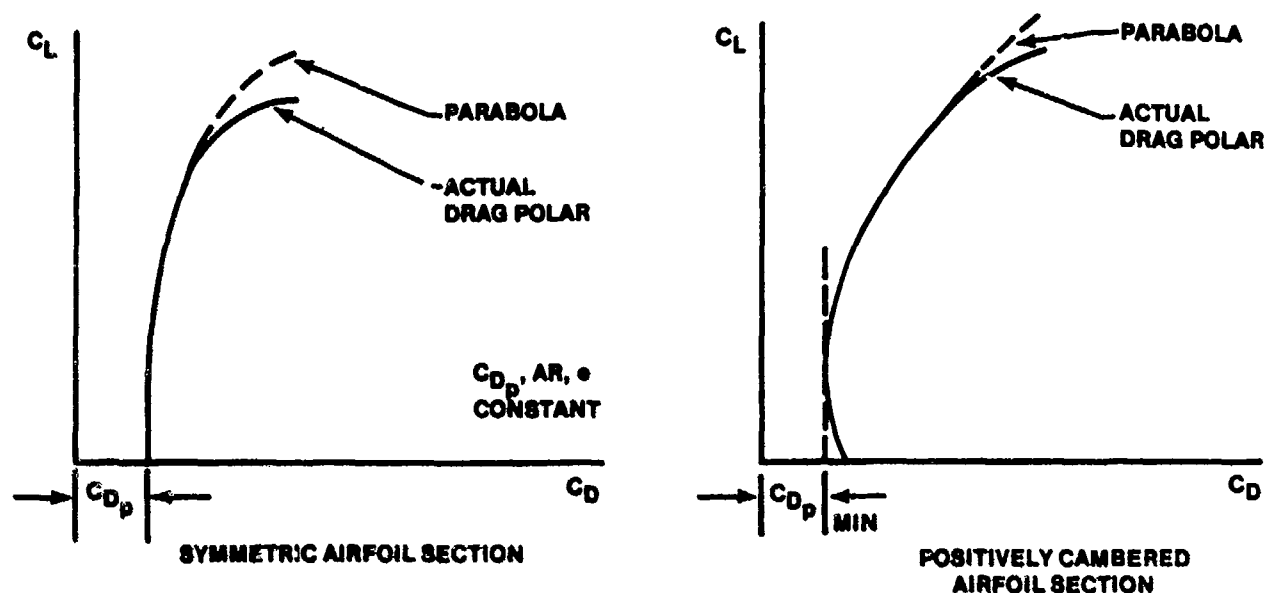


FIGURE 4.19 BASIC DRAG POLAR

Notice that two different representations of the basic drag polar are presented. Recall from airfoil theory that a symmetric airfoil develops no lift at zero angle of attack. Therefore, no induced drag would be produced, and the total drag must be a minimum for $C_L = 0$. However, a positively cambered airfoil can develop lift at zero angle of attack. The minimum drag value is not where C_L is zero, which is usually some negative angle of attack where the airfoil might have some additional pressure drag due to its inclination to the airstream. In fact, the minimum drag on the airfoil may be at some small positive angle of attack where the airfoil is developing lift, but the negative effects of pressure drag due to the wake have decreased significantly.

When the total drag of an aircraft is considered, the minimum drag configuration would normally be where the parasite drag is equal to the induced drag. If the aircraft is producing no lift, then there is no induced drag. The minimum drag would then consist entirely of parasite drag.

Each of the subsequent drag polars illustrating effects of various parameters on the basic drag polar may vary as in Figure 4.19.

4.12.1 Variables Affecting Drag Coefficient

We know from dimensional analysis that

$$C_D = f(M, R_e, \alpha) \quad (2.19A)$$

and that geometrically similar shapes compared at the same Mach, Reynolds number, and angle of attack have the same drag coefficient. The basic drag polar illustrates variation of drag coefficient with angle of attack in the guise of lift coefficient. Variations of Mach and Reynolds number will produce changes in the basic polar. Drag coefficient is also affected by two planform variables, aspect ratio and efficiency factor. The following discussion will illustrate the effects of all these variables on the basic drag polar.

4.12.1.1 Drag Polar Variation with Mach. When the flight velocity is greater than the critical Mach, the drag coefficient increases. Below critical Mach, the low speed polar is unchanged. This effect is shown in Figure 4.20.

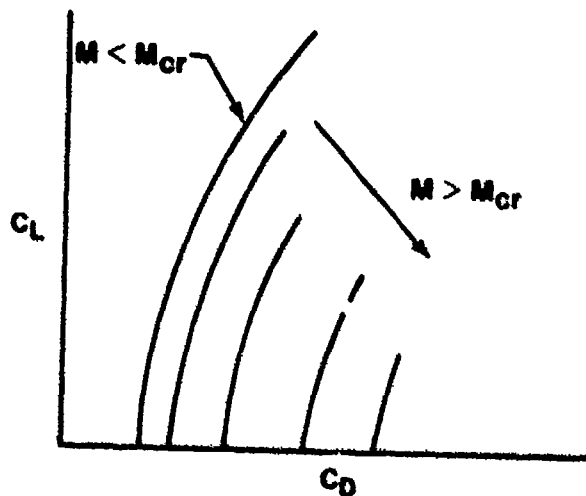


FIGURE 4.20. EFFECT OF MACH ON THE DRAG POLAR

Drag coefficient data are often presented versus Mach at constant values of angle of attack, or more commonly constant lift coefficient as shown in Figure 4.21. In plotting Figure 4.21, parasite drag coefficient and lift coefficient are constant, and Mach drag coefficient is zero until critical Mach is reached. Figure 4.21 shows no increase in C_D until after the critical

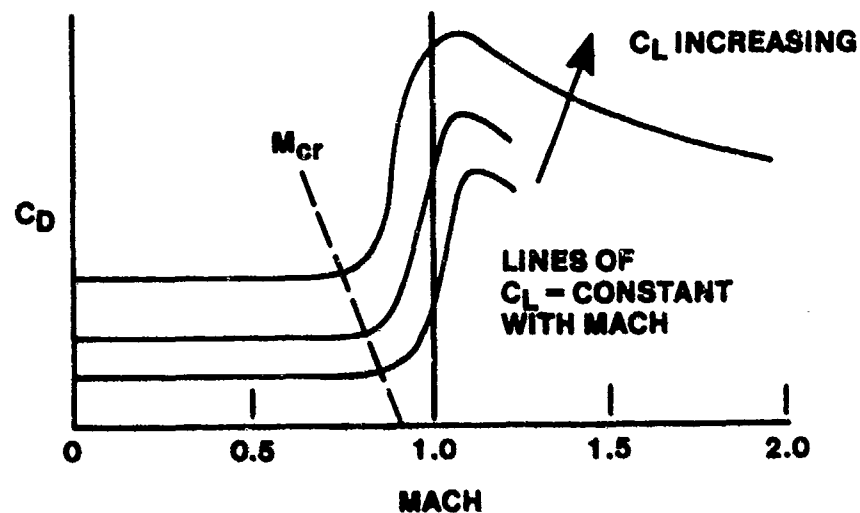


FIGURE 4.21. VARIATION OF DRAG COEFFICIENT WITH MACH AT CONSTANT LIFT COEFFICIENT

Mach is exceeded, then a sudden increase in drag coefficient called drag divergence is experienced. This is caused by the formation of shock waves on the aircraft. The total drag coefficient must now include a term to account for wave drag.

$$C_{D_{total}} = C_{D_p} + \frac{C_L^2}{\pi AR e} + C_{D_M} \quad (4.32)$$

4.12.1.2 Drag Polar Variation with Reynolds Number. The primary result of increasing Reynolds number on the drag polar is to increase the available maximum lift coefficient, as shown in Figure 4.22.

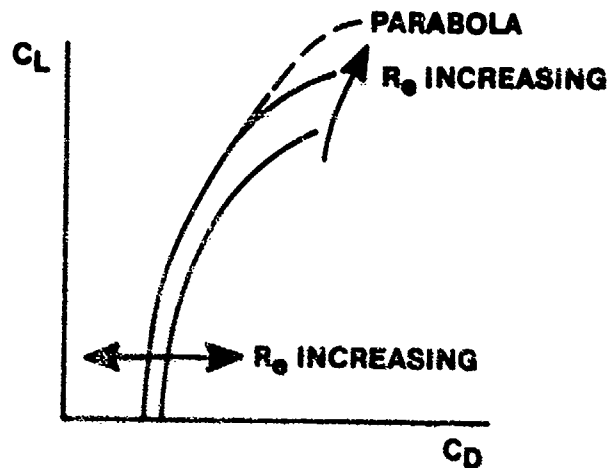


FIGURE 4.22. EFFECT OF REYNOLDS NUMBER ON THE DRAG POLAR

The previous discussion of Reynolds number effects on the lift curve also explains why the maximum C_L occurs at the highest Reynolds number on the drag polar. Increasing Reynolds number delays separation and allows the drag polar curve to remain parabolic to a higher angle of attack (lift coefficient). After separation, the total skin friction drag on the airfoil will decrease; however, pressure drag increases dramatically. Therefore, at a given lift coefficient at high angles of attack, total drag is lower at higher Reynolds number.

Since the Reynolds number of the flow describes how long the boundary layer will remain laminar before transitioning to turbulent flow, skin friction drag at lower angles of attack is also affected by changes in Reynolds number. Depending on the flow situation, the drag polar could show a decrease in C_{D_p} as shown in Figure 4.22, or it could increase.

4.12.1.3 Drag Polar Variation with Oswald's Efficiency Factor. Equation 4.3), which expressed the drag coefficient versus lift coefficient curve as a parabola, can be used to predict changes in the drag polar due to changes in Oswald's efficiency factor.

$$C_L^2 = \pi AR e \left(C_{D_{total}} - C_{D_p} \right) \quad (4.31)$$

Increasing Oswald's efficiency factor, e , in Equation 4.31 increases the "4p" constant term in the general equation of the parabola (Equation 4.30). Mathematically, increasing the value of the "4p" term causes the parabola to "open up," i.e., for any given value of drag coefficient, lift coefficient will be larger. This effect is shown in Figure 4.23.

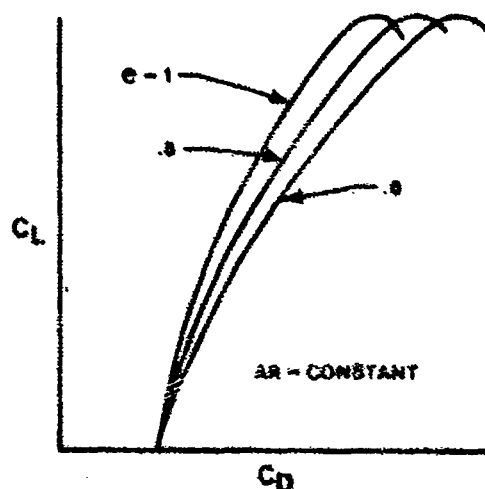


FIGURE 4.23. EFFECT OF OSWALD'S EFFICIENCY FACTOR ON THE DRAG POLAR

4.12.1.4 Drag Polar Variation with Aspect Ratio. Equation 4.31 can also be used to predict changes in the drag polar due to changes in aspect ratio.

$$C_L^2 = \pi AR e \left(C_{D_{total}} - C_{D_p} \right) \quad (4.31)$$

Increasing aspect ratio, AR , in Equation 4.31 again causes the parabola to "open up" and results in larger values of lift coefficient for any given value of drag coefficient as shown in Figure 4.24.

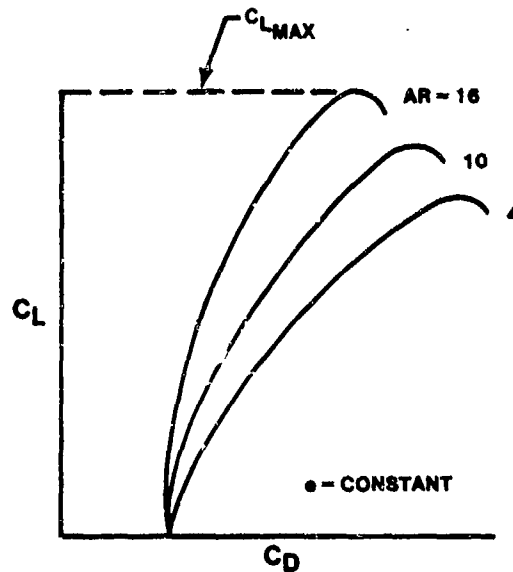


FIGURE 4.24. EFFECT OF ASPECT RATIO ON THE DRAG POLAR

4.12.2 Effect of Flaps on the Drag Polar

It is very difficult to make generalizations about the effect of flaps on the drag polar since flaps have such a wide variety of configurations as shown in Figure 4.25. In general, flaps increase parasite drag coefficient. They are usually installed to increase maximum lift coefficient. As can be seen in Figure 4.25, for some given values of lift coefficient, there are cases where total drag coefficient decreases with flap extension.

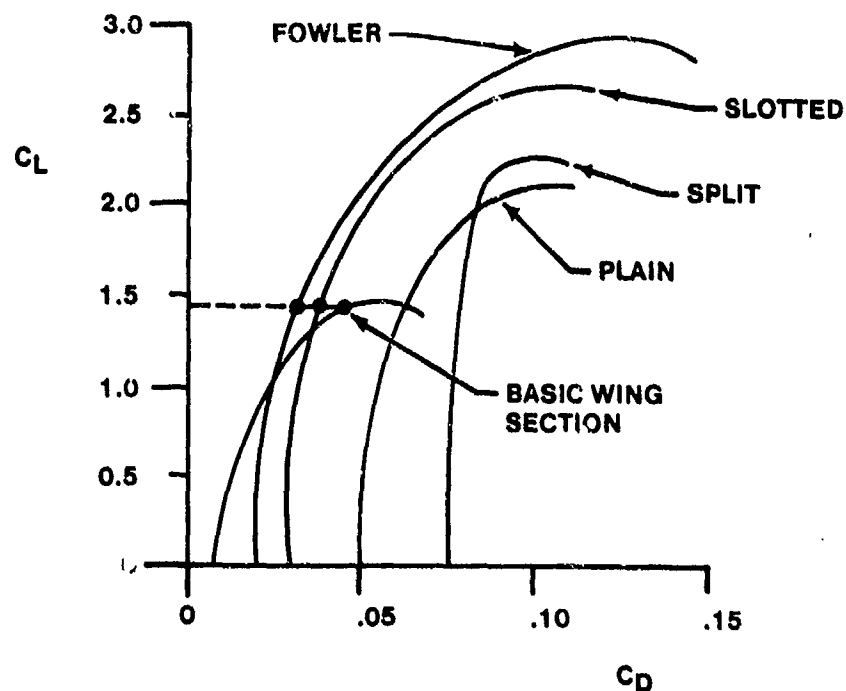


FIGURE 4.25. EFFECT OF FLAPS ON THE DRAG POLAR (4.5:40)

Flaps are normally used in high angle of attack configurations such as takeoff and landing. Figure 4.26 illustrates the effect of flaps on the drag polar during flap extension or retraction. This figure points out that flap management should be exercised with care by the pilot due to large increases in drag during their extension.

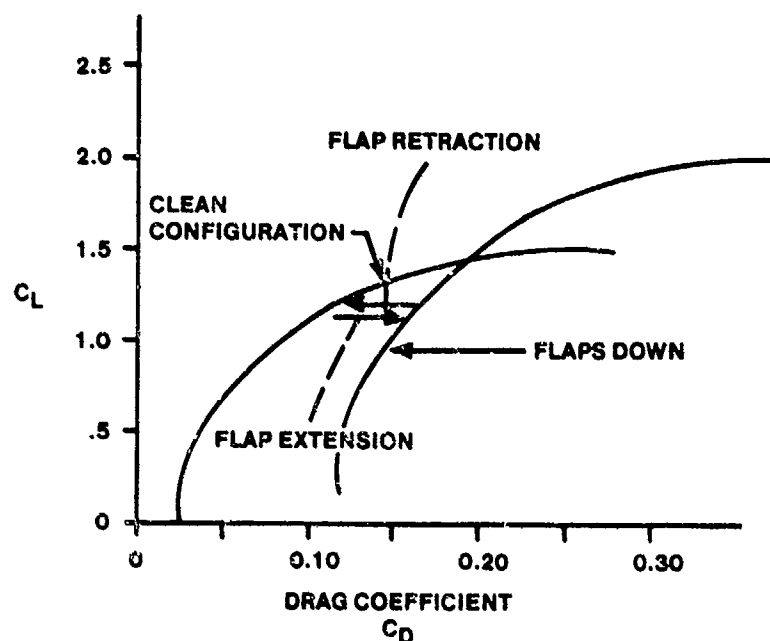


FIGURE 4.26. EFFECT OF FLAP OPERATION ON DRAG POLAR (4.5:44)

4.12.3 Lift Drag Ratio

The lift-drag ratio, L/D , is of importance in flight testing since it directly determines the glide, cruise, and flame-out landing speeds and also affects other areas of performance. The lift-drag ratio can be determined directly from a drag polar since

$$\frac{L}{D} = \frac{C_L q S}{C_D q S} = \frac{C_L}{C_D} \quad (4.33)$$

Therefore, the slope of a line connecting the origin of the C_L versus C_D graph with any point on the polar is the lift-drag ratio as shown in Figure 4.27. The maximum L/D is the point of tangency of this line from the origin with the polar.

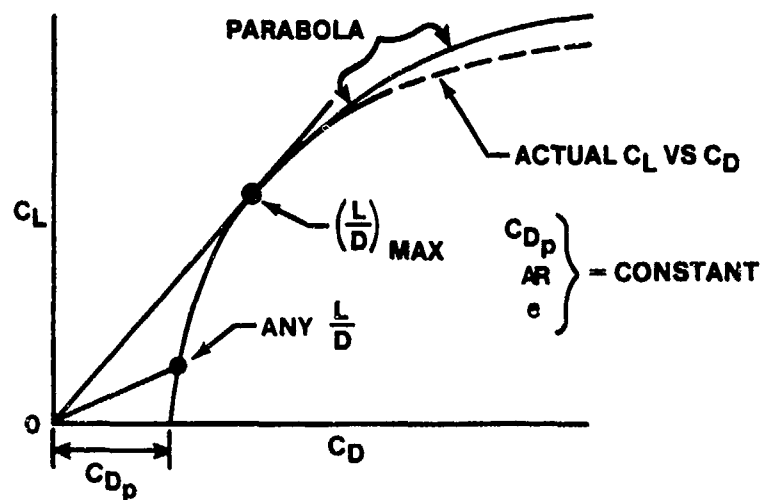


FIGURE 4.27. AIRCRAFT LIFT-DRAG RATIO

Aircraft lift-drag ratios are also quite often plotted versus lift coefficient or angle of attack as shown in Figure 4.28.

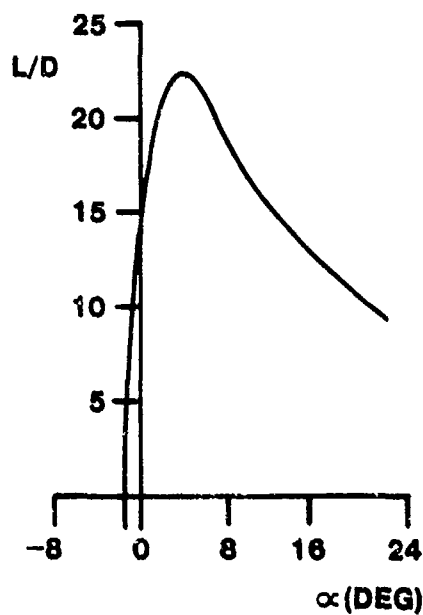


FIGURE 4.28. LIFT-DRAG RATIO FOR A WING OF ASPECT RATIO 6 WITH A NACA 23012 AIRFOIL SECTION (4.1:114)

4.13 FLIGHT TEST DRAG POLAR DETERMINATION

The flight test relationships for determining lift coefficient shown below were derived in Chapter 3.

$$C_L = \frac{nW}{\frac{1}{2} \rho_0 V_e^2 S} = \frac{841.5 nW}{V_e^2 S} \quad (3.24)$$

$$C_L = \frac{nW}{1481 \delta M^2 S} \quad (3.25)$$

By the same reasoning used to obtain Equations 3.24 and 3.25, Equations 4.34 and 4.35 can be derived to express total drag coefficient in terms of equivalent airspeed and Mach.

$$C_{D_{total}} = \frac{D_{total}}{\frac{1}{2} \rho_0 V_e^2 S} = \frac{841.5 D_{total}}{V_e^2 S} \quad (4.34)$$

$$C_{D_{total}} = \frac{D_{total}}{1481 \delta M^2 S} \quad (4.35)$$

If stabilized level flight is assumed, then net thrust is equal to total drag, and Equations 4.34 and 4.35 can be written

$$C_{D_{total}} = \frac{F_n}{\frac{1}{2} \rho_0 V_e^2 S} = \frac{841.5 F_n}{V_e^2 S} \quad (4.36)$$

$$C_{D_{total}} = \frac{F_n}{1481 \delta M^2 S} \quad (4.37)$$

Equations 4.36 and 4.37 are flight test relationships for determining drag coefficient. Equivalent airspeed (or pressure ratio and Mach) are readily obtained from pitot-static measurements. Net thrust can be determined

from in-flight measurements of engine parameters such as engine speed, flight Mach number, ambient temperature, exhaust area, etc.

Since the actual relationship between C_L and C_D does closely approximate a parabola, plotting C_D versus C_L^2 produces a straight line as shown in Figure 4.29.

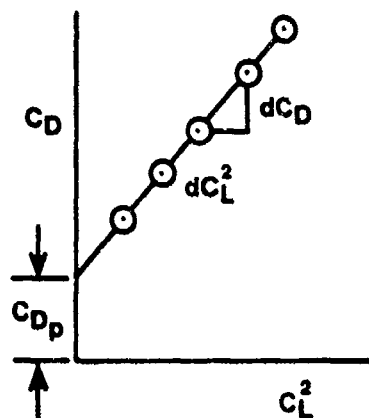


FIGURE 4.29. FLIGHT TEST DRAG POLAR DETERMINATION

A general equation for a straight line is

$$y = mx + b \quad (4.38)$$

where "m" is the slope of the line, dy/dx , and "b" is a constant. A comparison between Equation 4.38 and Equation 4.20 rearranged,

$$y = mx + b \quad (4.38)$$

$$C_{D_{total}} = \frac{1}{\pi AR e} C_L^2 + C_{Dp} \quad (4.20)$$

shows that the slope of the C_D versus C_L^2 curve is

$$\frac{dC_D}{dC_L^2} = \frac{1}{\pi AR e} \quad (4.39)$$

From Equation 4.39 Oswald's efficiency factor, e , can be determined from flight test data by measuring the slope of the C_D versus C_L^2 curve. This curve can also be extrapolated to zero lift coefficient where parasite drag coefficient can be determined as the intercept on the y axis or "b" in Equation 4.38 as shown in Figure 4.28.

4.14 DRAG EFFECTS ON LEVEL FLIGHT PERFORMANCE

The variation of total drag coefficient and total drag with velocity and Mach in stabilized level flight is important for aircraft performance analysis. Equation 4.20 is valid below critical Mach.

$$C_{D_{total}} = C_{D_p} + \frac{C_L^2}{\pi AR e} \quad (4.20)$$

Substituting the flight test relationship, Equation 3.24 into Equation 4.20 gives

$$C_L = \frac{nW}{1/2 \rho_0 V_e^2 S} \quad (3.24)$$

$$C_{D_{total}} = C_{D_p} + \left(\frac{1}{\pi AR e} \right) \left(\frac{nW}{1/2 \rho_0 V_e^2 S} \right)^2 \quad (4.40)$$

In stabilized level flight for a given aircraft configuration and constant weight, Equation 4.40 can be written

$$C_{D_{total}} = C_{D_p} + \frac{K_1}{V_e^4} \quad (4.41)$$

where

$$K_1 = \frac{1}{\pi AR e} \left(\frac{nW}{1/2 \rho_0 S} \right)^2 \quad (4.42)$$

and

$$C_{D_i} = \frac{K_1}{v_e^4} \quad (4.43)$$

Equation 4.41 can be plotted as shown in Figure 4.30 since C_{D_p} and K_1 are constants.

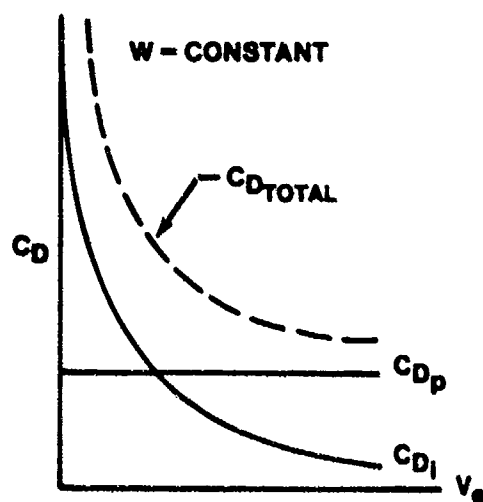


FIGURE 4.30. VARIATION IN DRAG COEFFICIENT WITH VELOCITY FOR STABILIZED LEVEL FLIGHT

If Mach effects are considered, the C_{D_M} has a value other than zero at speeds greater than critical Mach, and drag coefficient versus Mach typically looks like Figure 4.31.

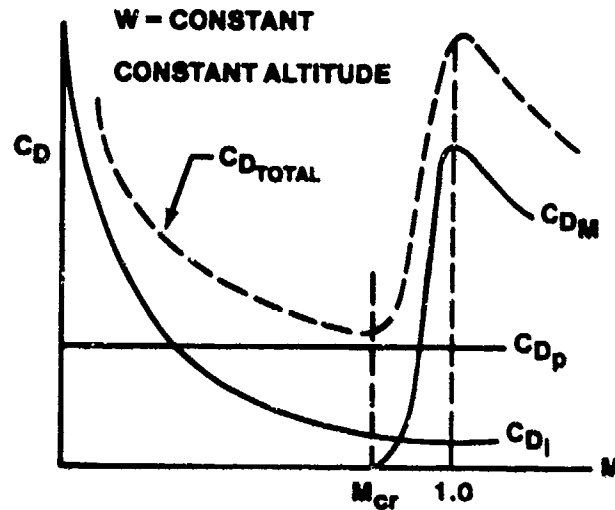


FIGURE 4.31. VARIATION IN DRAG COEFFICIENT WITH MACH FOR STABILIZED LEVEL FLIGHT

To obtain the variation of total drag with velocity and Mach, Equation 4.41 is multiplied by dynamic pressure and wing area.

$$C_{D_{total}} = C_{D_p} + \frac{K_1}{V_e^4} \quad (4.41)$$

$$D_{total} = C_{D_{total}} qS = C_{D_p} qS + \frac{K_1}{V_e^4} qS \quad (4.44)$$

Expressing dynamic pressure in terms of equivalent airspeed, Equation 4.44 can be written

$$D_{total} = C_{D_p} \left(\frac{1}{2} \rho_0 V_e^2 \right) S + \frac{K_1}{V_e^4} \left(\frac{1}{2} \rho_0 V_e^2 \right) S \quad (4.45)$$

which can be simplified to

$$D_{total} = K_2 V_e^2 + \frac{K_3}{V_e^2} \quad (4.46)$$

where

$$K_2 = C_{D_p} \frac{1}{2} \rho_0 S \quad (4.47)$$

and

$$K_3 = K_1 \frac{1}{2} \rho_0 S \quad (4.48)$$

Equation 4.46 can be plotted as shown in Figure 4.32 since K_2 and K_3 are constants.

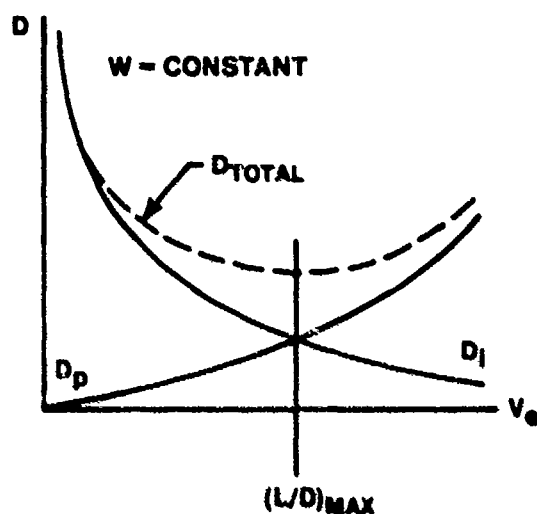


FIGURE 4.32. VARIATION IN TOTAL DRAG WITH VELOCITY FOR STABILIZED LEVEL FLIGHT

Plotting D_{total} for values of V_e less than M_{crit} , we see that the drag decreases to some minimum value and then increases. As airspeed, V_e , increases, the angle of attack required to maintain level flight decreases, i.e., C_L decreases. Therefore, D_i decreases. At the same time the parasite drag increases. The point where the induced drag equals the parasite drag produces minimum drag, and therefore is where L/D is a maximum.

If Mach effects are considered, then a drag rise due to compressibility begins at critical Mach, and drag versus Mach typically looks like Figure 4.33. Note in Figure 4.33 that Mach drag and total drag keep increasing supersonically, which must be the case since increasing values of thrust are required as speed increases supersonically.

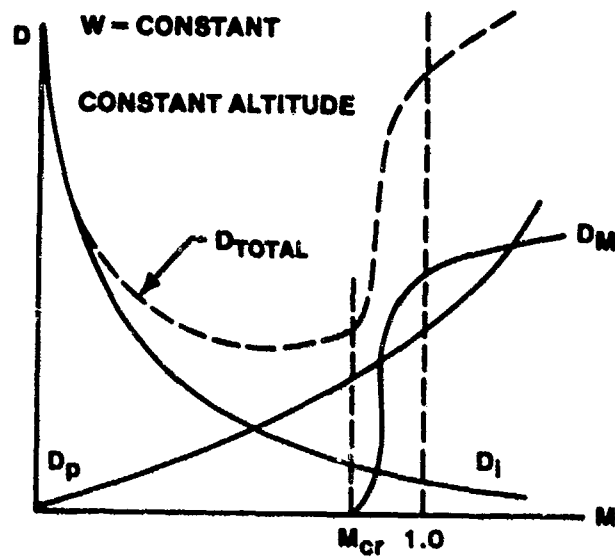


FIGURE 4.33. VARIATION IN TOTAL DRAG WITH MACH FOR STABILIZED LEVEL FLIGHT

An actual drag polar for an early supersonic fighter aircraft is shown in Figure 4.34 along with variations in drag coefficient with Mach for constant values of C_L .

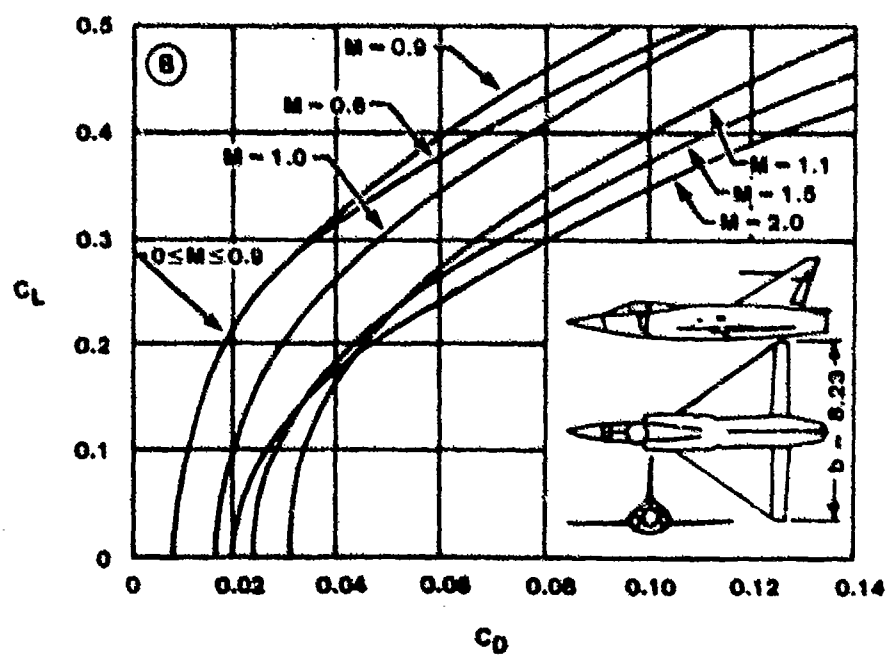
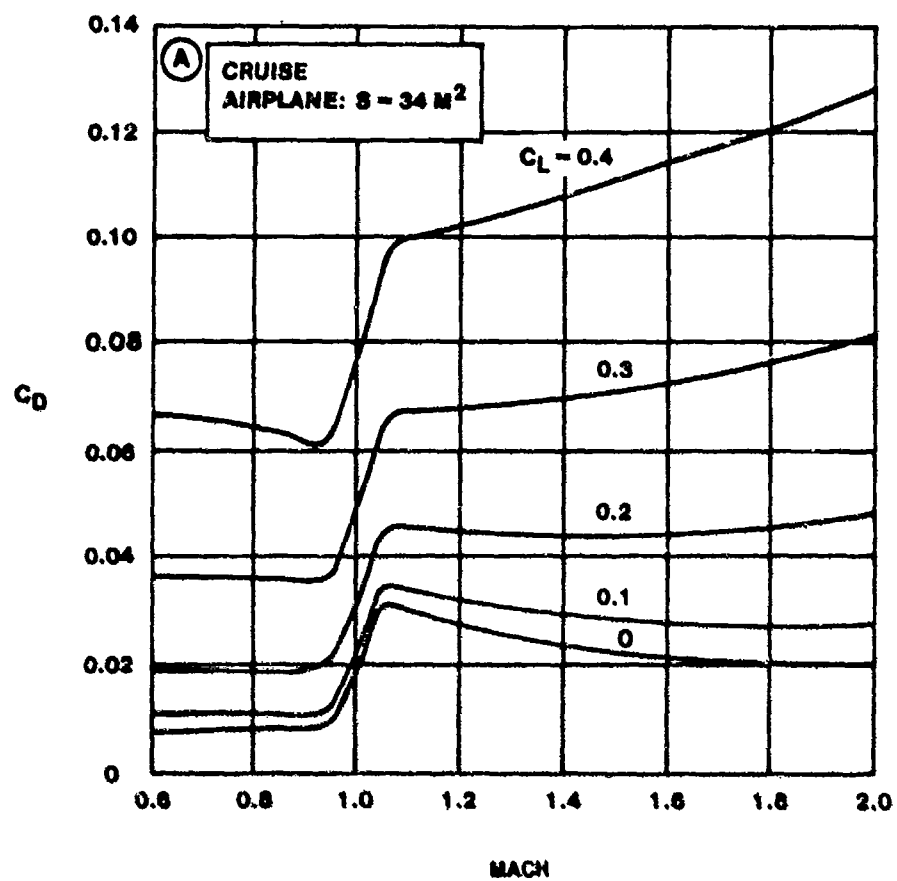


FIGURE 4.34. DRAG CHARACTERISTICS OF AN EARLY SUPERSONIC FIGHTER (4.8:142)

4.15 LAMINAR FLOW AIRFOILS

Since maintaining laminar flow reduces skin friction drag, much effort has been expended in the past and much is going on today to achieve this goal. Laminar flow airfoils are created using one or more of several design techniques.

The first design criterion is that the airfoil be smooth, because rough spots or bumps trigger turbulence and consequently create turbulent flow in the boundary layer. Current efforts are being made to develop "super smooth" surfaces, mainly through the use of composite materials.

Another important factor is the location of the maximum thickness to chord ratio, t/c , of the airfoil with respect to the distance from the leading edge. Locating the maximum thickness further aft, at approximately 40 to 60% chord moves the minimum pressure point farther from the leading edge and creates a long, shallow, negative (favorable) pressure gradient as shown in Figure 4.35.

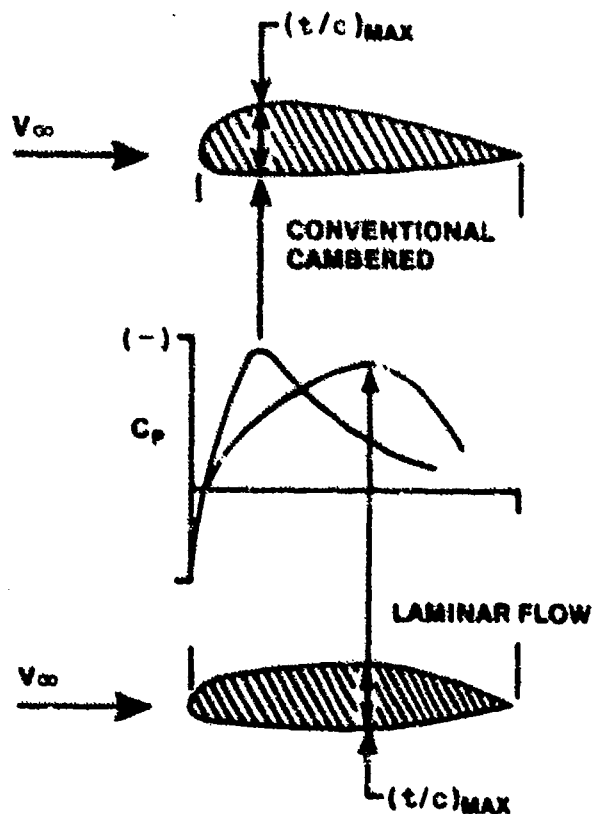


FIGURE 4.35. COMPARISON OF CONVENTIONAL CAMBERED AND LAMINAR WING SECTIONS

This favorable pressure gradient tends to delay boundary layer transition to turbulent flow. The maximum thickness point cannot be located too far aft, or an increase in the total drag due to separation will negate the decrease in skin friction drag. The reason separation is more likely to occur is because of the increased steepness of the adverse pressure gradient aft of the maximum thickness point as shown in Figure 4.35.

Designing an airfoil with a small thickness to chord ratio reduces the local velocity in the boundary layer, which in turn reduces the local Reynolds number. This causes the critical Reynolds number to occur farther aft of the leading edge of the airfoil, which promotes the desired goal of keeping the flow in the boundary layer laminar farther along the surface; however, the airfoil cannot be too thin. It must be thick enough to provide a useable negative pressure gradient which can develop sufficient lift and is large enough to help delay transition.

Another design feature to be considered for a useable laminar airfoil is the shape of the leading edge. Experiments have shown that a parabolic shape is more desirable than sharp or circular leading edges. Because of the relative thinness of laminar flow airfoils, care has to be taken with leading edge radius design to prevent leading edge stall at high angles of attack. Leading edge stall is generally considered disastrous.

A laminar flow airfoil exhibits a decrease in skin friction drag through a rather restricted range of lift coefficients. Usually the airfoil is designed to give the greatest decrease in skin friction drag at low C_L 's, or at high speeds. The drag polar for a laminar flow airfoil with the typical "drag bucket" is compared to the drag polar for a nonlaminar airfoil in Figure 4.36.

By varying the camber of the airfoil, the designer can place the drag bucket around the desired lift coefficient without sacrificing any of the effects of laminarization.

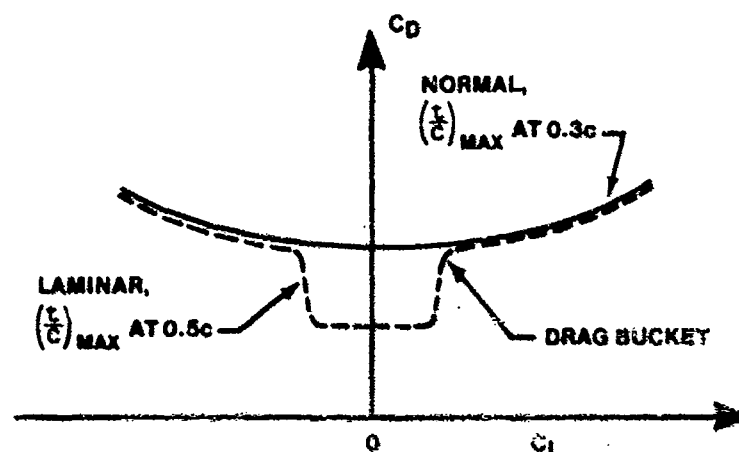


FIGURE 4.36. LAMINAR FLOW WING SECTION DRAG POLAR

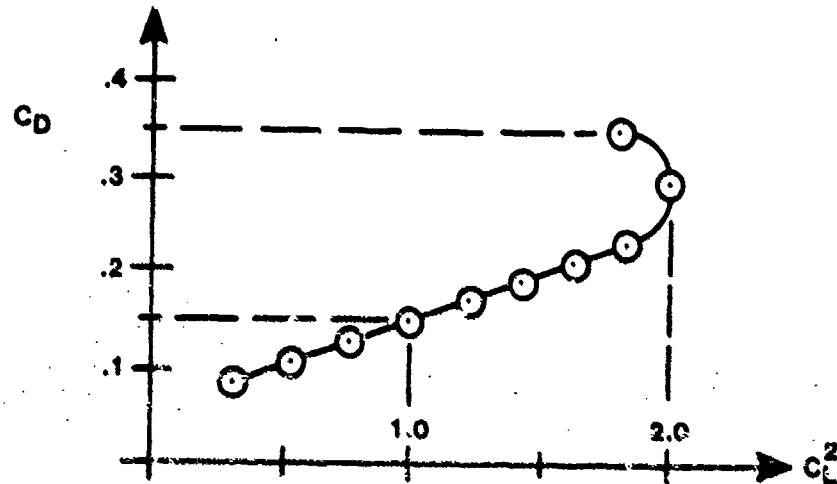
Unfortunately, in spite of very encouraging wind tunnel results which yield laminar flow drag polars, significant drag reduction in-flight has not been realized. Laminar flow cannot be maintained for any significant distance along either a fuselage or a wing surface, and the drag bucket does not appear on drag polars derived from flight test data. Laminar flow airfoils are historically interesting and are widely discussed in the academic literature, but to date results of their use have been disappointing from a practical point of view.

However, if laminar flow could be maintained on just an aircraft wing, the reduction in skin friction drag would be sufficient to greatly increase aircraft range. The idea of using suction to keep a laminar boundary layer attached and stable was tried on the X-21 by Northrop about 1960. Spanwise slots were milled into a jet transport wing, and suction was applied. Although the concept was proven sound, the airplane suffered from the practical difficulties of keeping the highly unstable laminar boundary layer from transitioning to a turbulent layer or separating from the wing. The scheme was finally abandoned, but the concept promises great gains in long range cruise performance if it can be successfully employed. Today, laminar flow control is a high cost, high risk, but potentially high payoff gamble.

Unfortunately, most design methods used to reduce skin friction drag tend to cause early boundary layer separation. This creates pressure drag which is often much larger than the reduction in skin friction drag.

PROBLEMS

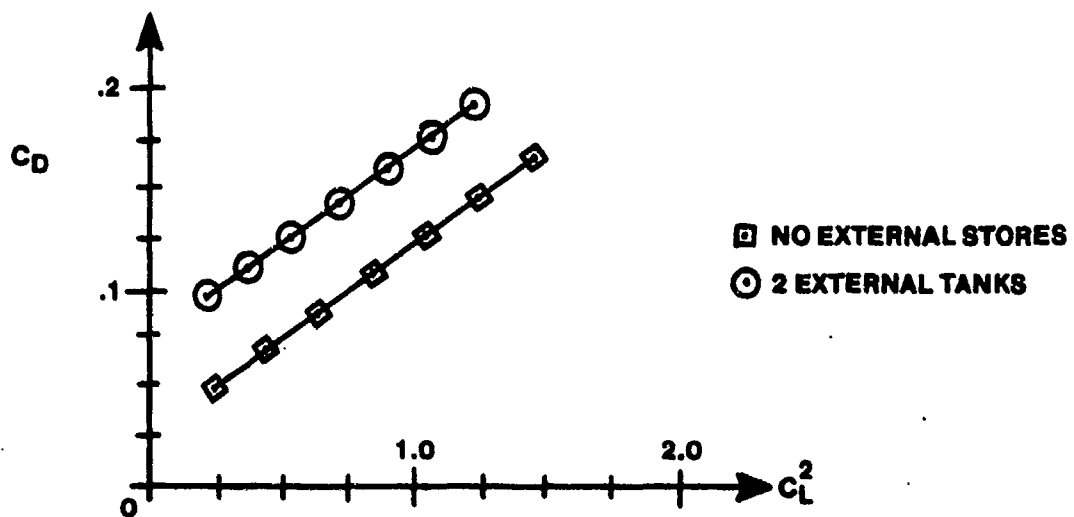
- 4.1 Shown below is the drag polar for the YX-007 in the power approach configuration obtained from flight test. The YX-007 has a wingspan of 40 ft and a wing area of 400 ft². Determine:



- (a) The aircraft's aspect ratio.
- (b) The aircraft's parasite drag coefficient.
- (c) The aircraft's efficiency factor (e).
- (d) The $C_{D_{total}}$ equation for the aircraft as a function of the lift coefficient.
- (e) If the final approach is to be flown at 80% of maximum lift coefficient, what is the final approach equivalent airspeed if aircraft weight = 12,100 lb?
- (f) The final approach L/D ratio if the approach is flown at 80% of maximum lift coefficient.
- (g) The aircraft's equivalent flat plate area in the power approach configuration given that the drag coefficient of a flat plate is 1.28.

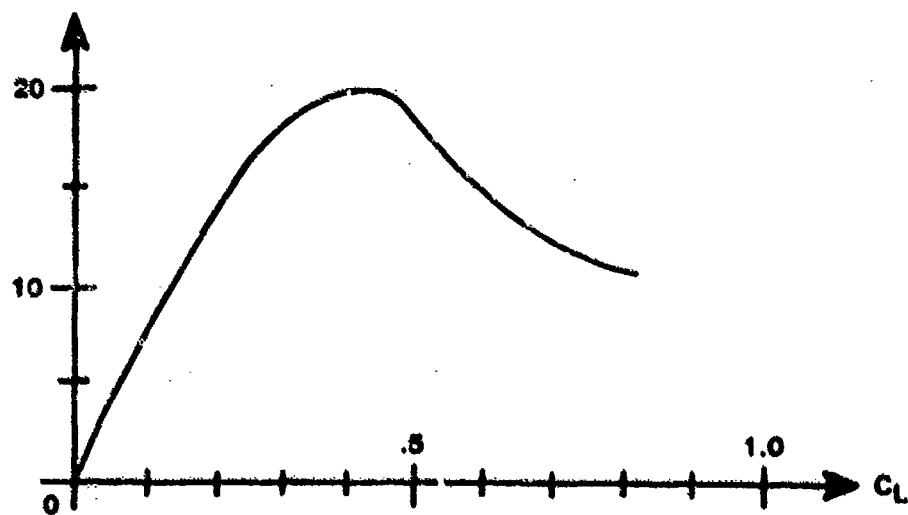
- 4.2 Given the following drag polar, determine:

AIRCRAFT DATA: Wingspan = 60 ft
 Wing Area = 900 ft²
 Cruise Configuration



- Aircraft's parasite drag with 2 external tanks installed.
- The drag count of the 2 external stores.
- The aircraft's maximum L/D with the 2 external stores.

4.3 For the aircraft represented by the plot below, find maximum lift-drag ratio, and parasite drag coefficient.



4.4 On a standard day an aircraft with a wing area of 691 ft^2 and a wingspan of 58.8 ft is in stabilized level flight cruising at an altitude of 38,300 ft and at a true velocity of 400 kts. The aircraft weighed 50,000 lb at takeoff and has since burned 10,000 lb of fuel. The ten engines on the aircraft are producing 300 lb of thrust each.

- (a) What are the aircraft lift and drag coefficients for these flight conditions?
- (b) The same aircraft in preparation for landing has slowed down to an airspeed of 150 ft/sec (V_e) at a gross weight of 18,478 lb in cruise configuration and has stabilized in level flight. Each engine is now producing 166.3 lb of thrust. What are the aircraft lift and drag coefficients for these flight conditions?
- (c) Write the $C_{D_{\text{tot}}}$ equation for the aircraft as a function of lift coefficient.
- (d) Compute induced, parasite, and total drag for the aircraft in Part A.
- (e) Write the total drag equations for the aircraft described as a function of weight and Mach or equivalent velocity. What is the advantage of the equivalent velocity equation?

- 4.5 Two 500 lb bombs with a total drag count of 15 are installed on an A-37. The drag coefficient equation of the A-37 with the bombs installed is given below. The aircraft wing area is 184 ft^2 .

$$C_{D_{\text{TOTAL}}} = 0.0235 + 0.062C_L^2$$

- (a) What is the drag coefficient equation of the A-37 after the bombs are removed?
- (b) If the aspect ratio of the A-37 is 6.2, what is the Oswald efficiency factor with the bombs installed? What is it after they are removed?
- (c) The same bombs are to be installed on a AF-6 whose wing area is 120 ft^2 . The drag coefficient equation of the AF-6 is given below. What is the new drag coefficient equation with the bombs installed?

$$C_{D_{\text{TOTAL}}} = 0.03 + 0.06C_L^2$$

- (d) What was the equivalent flat plate area of the AF-6 before the bombs were installed? What is it after they are installed?

ANSWERS

4.1 (a) $AR = 4.0$

(b) $C_{D_p} = 0.05$

(c) $e = 0.80$

(d) $C_D = .05 + .10 C_L^2$

(e) $V_e = 150 \text{ ft/sec}$

(f) $L/D = 6.35$

(g) $S_{\text{plate}} = 15.63 \text{ ft}^2$

4.2 (a) $C_{D_p} = 0.075$

(b) 500 counts

(c) $L/D/\text{max} = 5.77$

4.3 $L/D/\text{max} = 20$; $C_{D_p} = 0.01$

4.4 (a) 0.40; 0.03 (No Units)

(b) 1.00; 0.09 (No Units)

(d) 1,137 lb; 1,901 lb; = 3,000 lb

4.5 (a) $C_D = .0220 + .062 C_L^2$

(b) 0.828 (No Units)

(d) 2.81 ft^2 ; 3.03 ft^2

BIBLIOGRAPHY

- 4.1 Donnasch, Daniel O., et al., Airplane Aerodynamics, 4th ed. New York: Pitman Publishing Corporation, 1967.
- 4.2 Von Karman, Theodore, Aerodynamics: Selected Topics in the Light of their Historical Development. Ithaca, NY: Cornell University Press, 1954.
- 4.3 Anderson, J.D., Jr., Introduction to Flight; Its Engineering and History. New York: McGraw Hill Book Company, Inc., 1978.
- 4.4 Aerodynamics for Pilots. ATC Pamphlet 51-3, July 1979.
- 4.5 Hurt, H.H., Jr., Aerodynamics for Naval Aviators. NAVWEPS 00-80T-80, Office of the Chief of Naval Operations Aviation Training Division, U.S. Navy, 1960.
- 4.6 Sutton, O.G., The Science of Flight. Baltimore: Penguin Books Inc., 1955.
- 4.7 Clancy, L.J., Aerodynamics. New York: John Wiley and Sons, 1975.
- 4.8 Roskam, Jan, et al., Airplane Aerodynamics and Performance. Ottawa, KS: Roskam Aviation and Engineering, 1980.

CHAPTER 5
PITOT-STATIC FUNDAMENTALS
AND THE
STANDARD ATMOSPHERE

5.1 INTRODUCTION

The propulsive and aerodynamic forces acting upon an airborne vehicle are a function of the temperature, density, pressure, and viscosity of the fluid through which the vehicle is traveling. Because of this, the test engineer needs some means for determining the variation in fluid properties of the atmosphere. From previous measurements, it has been shown that these properties have a daily, seasonal, and geographic dependence and in fact are in a constant state of flux. Solar radiation, water vapor, winds, clouds, large and small scale turbulence, and human activity can cause rapid and significant local variations in the atmosphere. A complete, accurate, and timely description at any one location is presently not possible, but with good weather forecasting some degree of success is possible. The flight test engineer cannot begin to cope with these variances of nature, so a standard atmosphere was constructed to describe the static variation of the fluid properties. With this standard atmosphere, calculations can be made of the standard fluid properties, and when variations from this standard occur, it can be used as a method for calculating or predicting vehicle performance. Because of this dependence on the standard atmosphere for determining vehicle performance, it is necessary to understand how the standard was obtained and how to use it.

5.2 DIVISIONS AND LIMITS OF THE ATMOSPHERE

The atmosphere is divided into four major divisions which are associated with certain physical characteristics. The division closest to the earth's surface is called the troposphere. Its upper limit varies from approximately 28,000 feet and -46°C at the poles to 56,000 feet and -79°C at the equator. These temperatures vary from day to day and with the seasons of the year. This necessitates that a standard be established for comparison purposes. These standards will be discussed in later sections.

In the troposphere, the temperature decreases with height. This phenomenon results from the fact that the lower portion of the atmosphere is almost transparent to most short wave radiation received from the sun. Thus, a large

portion of the sun's radiation is transmitted to and absorbed by the earth's surface. The portion of the atmosphere next to the earth is heated from below by long wave radiation from the earth's surface. This radiation in turn heats the rest of the troposphere mainly by convection, conduction, and re-radiation of the long wave energy. Most turbulence is caused by convection or vertical currents, and practically all weather phenomenon are contained in this division.

The second major division of the atmosphere is the stratosphere. This layer of air extends from the troposphere outward to a distance of approximately 50 miles. However, the designation for this division has lost some popularity in recent years since the original definition of the stratosphere included constant temperature with height. Recent data have shown that the temperature is constant at 216.65°K only between about 7 and 14 miles then increases to approximately 270°K at 30 miles, then decreases to approximately 180°K at 50 miles altitude. Since these temperature variations between 14 and 50 miles destroy one of the basic definitions of the stratosphere, some authors have divided this area into two divisions: Stratosphere, 7 to 14 miles, and Mesosphere from 15 to 50 miles. The boundary between the stratosphere and the troposphere is called the tropopause. In the stratosphere, motion is mainly horizontal, and little turbulence is found.

The third major division is the ionosphere. It extends from approximately 50 miles to 300 miles. Large numbers of free ions are present in this layer, and a number of different electrical phenomenon take place in this portion of the atmosphere. The temperature increases with height to a kinetic temperature of 1500°K at 300 miles. This layer of the atmosphere is becoming more and more important with the development of space vehicles.

The fourth major division is the exosphere. It is the outermost layer of the atmosphere. It starts at 300 miles and is also characterized by a large number of free ions. The molecular temperature increases with height in this area, but the kinetic temperature is practically constant with height. Also, the atmosphere is extremely rare in the outermost layer; the density varies by several orders of magnitude and is dependent upon the activity of the sun and other factors.

Figure 5.1 presents the standard atmosphere temperature lapse versus geopotential altitude. The range of seasonal temperature variation is shown by the double arrow lines.

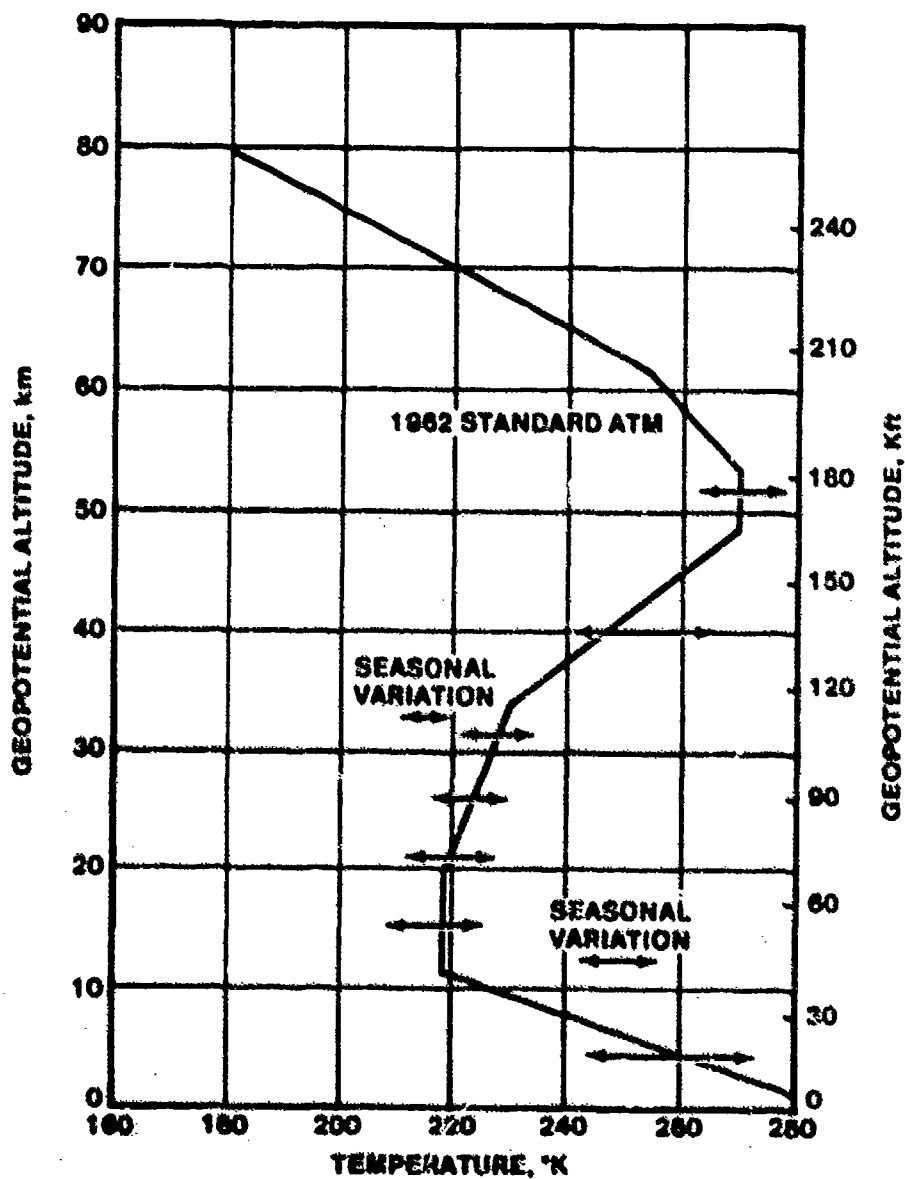


FIGURE 5.1. STANDARD ATMOSPHERE TEMPERATURE LAPSE RATE WITH ALTITUDE. SEASONAL VARIATION IS SHOWN BY THE DOUBLE ARROWS.

5.3 STANDARD ATMOSPHERE

As mentioned previously, the physical characteristics or nature of the atmosphere are not constant but change from day to day with the seasons of the year. Since the performance of an aircraft is a function of the physical characteristics of the air mass through which it flies, it will vary as physical characteristics of the air mass vary. Thus, some standard air mass conditions must be established in order that performance data can have some meaning when used for comparison purposes. As will be shown later, in the case of the altimeter, the setting of a standard will allow for design of an instrument for measuring altitude.

At the present time there are several atmosphere standards which have been established. The most common one in this country is the ARDC 1959 model atmosphere. A more recent one is the U.S. Standard Atmosphere - 1962. The European nations, at least until recently, used the ICAO (International Civil Aviation Organization) standard atmosphere. All of these standard atmospheres were developed to approximate the standard average day conditions at 40° to 45°N latitude.

All three of these standard atmospheres are basically the same up to an altitude of approximately 66,000 feet. Both the 1959 ARDC and the 1962 U.S. Standard Atmosphere are defined to an upper limit of approximately 440 miles, but at higher levels there are some marked differences between the 1959 and 1962 atmospheres. The standard atmosphere used by the Test Pilot School in the performance data reduction programs is the 1962 atmosphere. Appendix B gives the 1962 atmosphere in tabular form to 110,000 ft.

In the U.S. Standard Atmosphere 1962 it is assumed that:

1. The atmosphere is a perfect gas (obeys the equation of state $P/\rho = R^*T/M$ where M = molecular weight).

NOTE: $P/\rho = gRT$ can generally be used for aircraft performance data since molecular weight of air is considered constant up to 55 miles altitude.

2. The air is dry.

3. The standard sea level conditions are $T_{SL} = 15^{\circ}\text{C} = 288.15^{\circ}\text{K}$,
 $P_{SL} = 29.921$ in Hg = 760 mm Hg.
4. The gravitational field decreases with altitude. $g_{SL} = 32.1741$
 ft/sec^2 .
5. Hydrostatic Equilibrium exists:

$$dP_a = -\rho g dh \quad (5.1)$$

This equation is derived by looking at the forces acting on a vertical column of air of unit area. (See Figure 5.2)

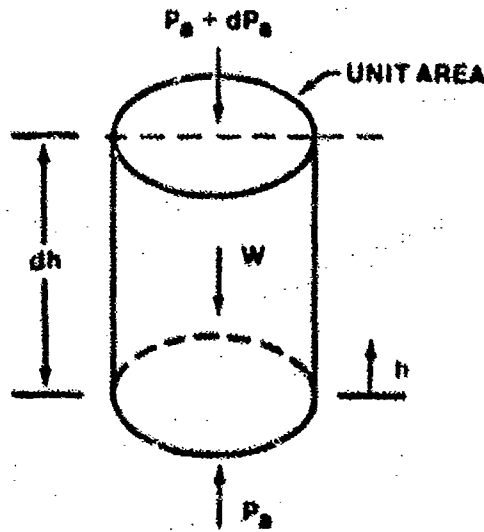


FIGURE 5.2. FORCES ACTING ON A VERTICAL COLUMN OF AIR OF UNIT AREA

6. Vertical displacement is measured in geopotential feet. Geopotential is a measure of the gravitational potential energy of a unit mass at a point relative to mean sea level. It is defined in differential form by the equation

$$G dH = g dh \quad (5.2)$$

where

- h = tapeline altitude; i.e., the actual distance from mean sea level to a point in the atmosphere, feet
 g = acceleration due to gravity at the same point, feet/sec²
 H = geopotential at the point, geopotential feet
 G = a dimensional constant, 32.17405 ft²/sec² - geopotential feet for the above system of units.

Each point in the atmosphere has a definite geopotential as "g" is a function of latitude and altitude. In a physical sense, geopotential is equivalent to the work done in elevating a unit mass from sea level to a tapeline altitude expressed in feet. For most purposes, errors introduced by letting h = H in the troposphere are insignificant. Making this assumption, there is slightly more than a 2% error at 400,000 feet. Appendix B compares tapeline altitude h to geopotential altitude H.

7. Temperature variation with geopotential is expressed as a series of straight line segments: (Figure 5.1)
- (a) The temperature lapse rate (L) in the troposphere (sea level to 36,089 geopotential feet) is 0.00198120°C/geopotential feet.
 - (b) The temperature above 36,089 geopotential feet and below 65,600 geopotential feet is constant -56.50°C.

5.3.1 Equations for the Standard Atmosphere

From the basic assumptions for the standard atmosphere listed above, it is possible to derive the relationships for temperature, pressure, and density as functions of geopotential. Combining Equations 5.1 and 5.2, we can see that

$$dP_a = - \rho G dH \quad (5.3)$$

Now if we eliminate ρ by using the perfect gas law

$$\frac{dP_a}{P_a} = - \frac{G}{R} \frac{dH}{T_a} \quad (5.4)$$

Looking at assumption 7 above, it can be seen that

$$T_a = f_1(H)$$

This means then from equation 5.4 that

$$P_a = f_2(H)$$

From the perfect gas law then we can show that

$$\rho = f_3(H).$$

The equations for our standard atmosphere are derived in Appendix F using Equation 5.4 and our basic assumptions. For geopotentials below 36,089 geopotential feet

$$\theta = \frac{T_a}{T_{aSL}} = (1 - K_1 H) \quad (5.5)$$

$$\zeta = \frac{P_a}{P_{aSL}} = (1 - K_1 H)^{K_2} \quad (5.6)$$

$$\sigma = \frac{\rho}{\rho_{SL}} = (1 - K_1 H)^{K_2-1} \quad (5.7)$$

where

$$K_1 = - \frac{L}{T_{aSL}} = 6.87559 \times 10^{-6} / \text{geopotential feet}$$

$$K_2 = - \frac{G}{RL} = 5.2559$$

For geopotentials above 36,089 geopotential feet and below 82,021 geopotential feet

$$T_a = -56.50^\circ\text{C} = 216.66^\circ\text{K} \quad (5.8)$$

$$\delta = \frac{P_a}{P_{a_{SL}}} = 0.223358e^{-K_3(H-36089)} \quad (5.9)$$

$$\sigma = \frac{\rho}{\rho_{SL}} = 0.29707e^{-K_3(H-36089)} \quad (5.10)$$

where

$$K_3 = \frac{G}{RT_a} = 4.80614 \times 10^{-5} / \text{geopotential feet.}$$

From the above equations, pressure, temperature, and density are tabulated in Appendix B.

5.3.2 The Measurement of Altitude

With the establishment of a set of standards for the atmosphere, there are several different means by which to determine altitude above the ground. This also leads to defining the type of altitude as determined by the means employed. Tapeline altitude, or true altitude, is the actual linear distance above sea level and can be determined by triangulation or radar. In actual practice, this is only important in climb performance tests and for determining the ballistic trajectory of a missile.

Since a set of standards has been established which denotes the standard pressure, temperature, and geopotential, there are now means by which altitude may be determined.

A temperature altitude can be obtained by taking a temperature gauge and modifying it to read in feet for a corresponding temperature as determined from standard tables. Since inversions and nonstandard lapse rate are the rule rather than the exception and temperature changes greatly between day and night, with the seasons of the year, and with latitude, such a technique would yield meaningless results.

If some instrument were available to measure density, the same type of technique could be employed, and density altitude could be determined.

If a highly sensitive accelerometer could be developed to measure the acceleration of gravity in terms of feet, then geopotential altitude could be measured. This device would give the correct reading only when in level-unaccelerated flight.

A fourth technique, a much more practical one, is based on pressure measurement. A pressure gauge is used to sense the ambient pressure. Instead of reading pounds per square inch, or millimeters of mercury, it indicates the corresponding standard altitude for the particular pressure sensed. This altitude is called pressure altitude and is the parameter on which all flight testing is based.

5.3.3 Pressure Variation with Altitude

The fourth technique is the one on which present day altimeters are designed. It should be obvious that the instrument will not give a true reading except when the pressure at altitude is the same as that for a standard day. In most cases, pressure altitude will not agree with the geopotential altitude.

For further understanding of the atmosphere, consider pressure variation with altitude as applied to the operation of the altimeter.

Most present day altimeters are designed to follow Equation 5.6. This equation is used to determine standard variation of pressure with altitude below the tropopause. An example of the variation described by Equation 5.6 is plotted in Figure 5.3.

It is this curve which the altimeter presents as a reading of altitude. If the pressure does not vary exactly as described by this curve, then the altimeter will be in error. A provision is made in the construction of the altimeter in the form of an altimeter setting, whereby the scale reading can be adjusted up or down (the same as moving the curve of Figure 5.3 vertically) so that the altimeter will read true elevation of the ground if the aircraft descends to ground level.

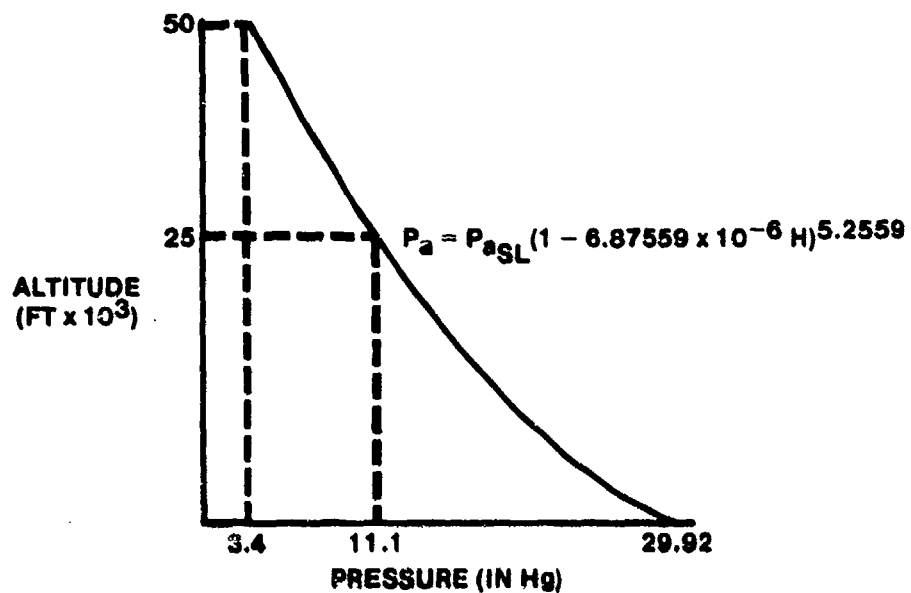


FIGURE 5.3. PRESSURE VARIATION WITH ALTITUDE

Figure 5.3a shows the pressure variation with altitude for a standard day and non-standard days. (Nonstandard day will be referred to as Test day.)

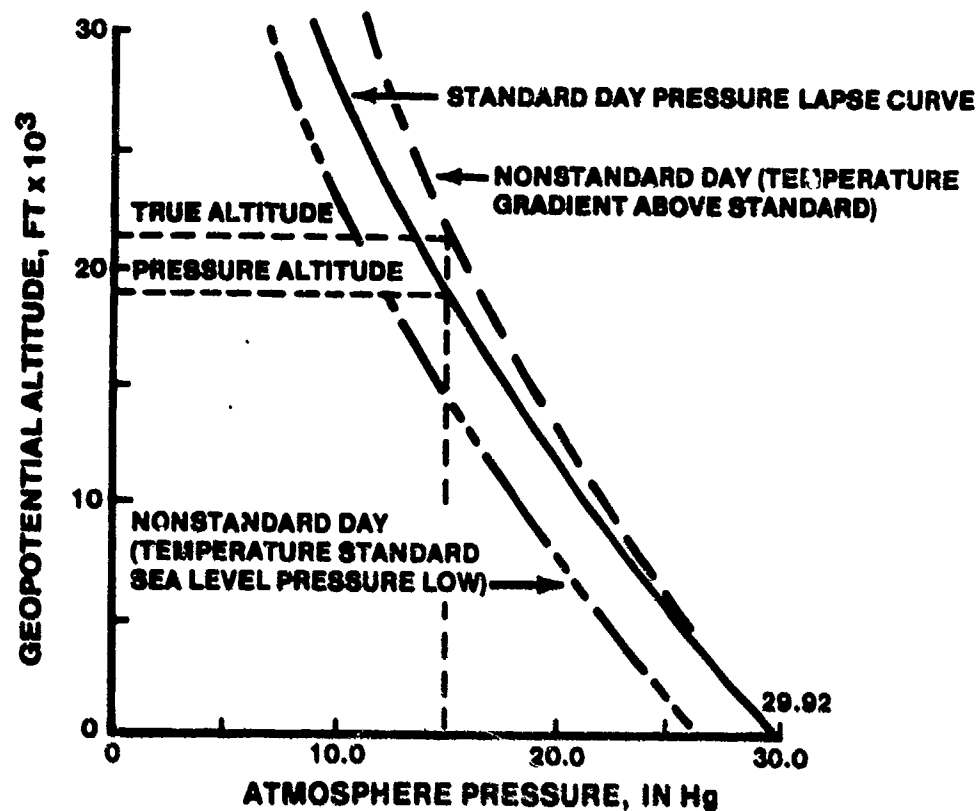


FIGURE 5.3A. STANDARD DAY AND TEST DAY PRESSURE VARIATION WITH ALTITUDE

If an aircraft is flying at some true altitude on a test day, the altimeter will sense the corresponding pressure as shown by the intersection of the dashed lines. However, since the altimeter is built around the standard curve (shown by the solid curve), the instrument will indicate the altitude labeled "pressure altitude."

In order to see how temperature affects the pressure lapse rate, consider Equation 5.4. From this equation, it is apparent that $dh/dp = -f(T)$, which is the slope of the curves in Figures 5.3 and 5.3a.

This means that for a higher temperature, the negative slope of the curve will be greater. Inspecting Figure 5.3a, it is noted that for every constant pressure, the slope of the test day curve is greater than that of the standard day curve. Thus, the temperature for the test day is warmer than that for the standard day. This variance between true altitude and pressure altitude is not as important as it might seem at first. As mentioned previously, true altitude is important only in climb performance tests and for certain ballistic purposes. In a later chapter, climb performance will be discussed, and the technique by which pressure altitude may be corrected to give true altitude will be explained.

The forces acting on an aircraft in flight are directly dependent upon air density. Thus, in theory, density altitude is the independent variable which should be used for aircraft performance comparisons. However, from a practical standpoint, since density is determined by pressure and temperature through the equation of state relationship, pressure altitude is used as the independent variable with test day data corrected for non-standard temperature. This greatly facilitates flight testing since the test pilot can maintain a given pressure altitude regardless of what the test day conditions are. Twenty-thousand feet pressure altitude is the same from one day to the next and from one aircraft to another. The parameter that does vary is temperature. By applying a correction for non-standard temperature to performance data, the data can be presented for any day conditions. Presented in this form, pressure, density, and tapeline altitudes are all equal.

5.4 ALTIMETER THEORY

Most altitude measurements are made with a sensitive absolute pressure gauge, an altimeter, scaled so that a pressure decrease indicates an altitude increase in accordance with the U.S. Standard Atmosphere. If an altimeter setting is 29.92, the altimeter reads pressure altitude or calibrated altitude, H_c , whether in a standard or non-standard atmosphere. An altimeter setting other than 29.92 moves the scale so that the altimeter indicates field elevation when the aircraft touches the ground. In this case, the altimeter indication is being adjusted to show tapeline altitude at that one elevation. In flight testing, the altimeter setting should be 29.92 so that the altimeter

reading is pressure altitude. As shown earlier, pressure altitude is not dependent on temperature. The only parameter which varies the altimeter indication is atmospheric pressure. Therefore, in flight testing, pressure altitude is used as an independent variable.

$$H_C = f(P_a)$$

The altimeter is constructed and calibrated according to the following relationships. These equations are the same ones which define the standard atmosphere.

$$P_a = P_{a_{SL}} (1 - 6.87559 \times 10^{-6} H_C)^{5.2559} \quad (5.6)$$

for $H_C < 36,089$ ft

$$P_a = P_{a_{SL}} \left(0.223358 e^{-4.80614 \times 10^{-5} (H_C - 36,089)} \right) \quad (5.9)$$

for $36,089 < H_C < 82,021$ ft

where

P_a = atmospheric pressure, inches Hg

H_C = pressure altitude, feet

$P_{a_{SL}}$ = 29.92126 in Hg

The heart of the altimeter is an evacuated metal bellows which expands or contracts with changes in outside pressure. The bellows is connected to a series of gears and levers which cause a pointer to move. It is through this network that Equations 5.6 and 5.9 are mechanized. The whole mechanism is placed in an airtight case which is vented to a static source; the indicator reads the pressure supplied to the case. Altimeter construction is shown in Figure 5.4. The distinction between ambient pressure, P_a , and static pressure, P_s , is that P_s is P_a as measured by a pitot-static system.

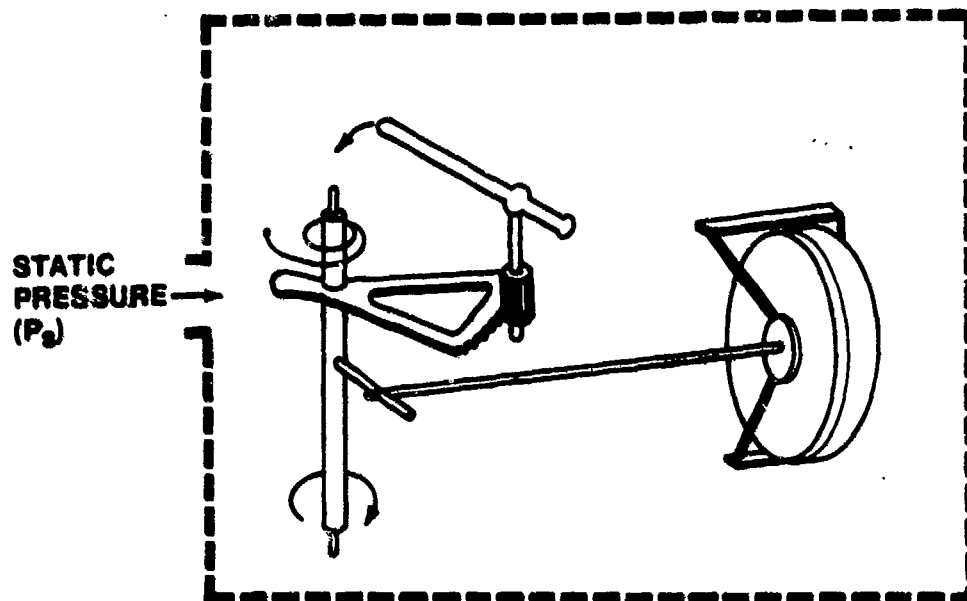


FIGURE 5.4. ALTIMETER SCHEMATIC

5.5 AIRSPED SYSTEM THEORY

Airspeed system theory was first developed with the assumption of incompressible flow. This assumption is only useful for speeds of 250 knots or less at relatively low altitudes. However, since various concepts and nomenclature of incompressible flow are still in use, it is examined here as a step toward the understanding of compressible flow relations.

5.5.1 Incompressible Airspeed Theory:

Airspeed system theory for all types of flow stems from Euler's equation

$$dP + \rho V dV = 0 \quad (5.11)$$

For the incompressible case, density remains constant. Integrating Equation 5.11

$$P + \frac{\rho V^2}{2} = C \quad (5.12)$$

The constant, C , applies to the flow as long as energy is not added to or subtracted from the system.

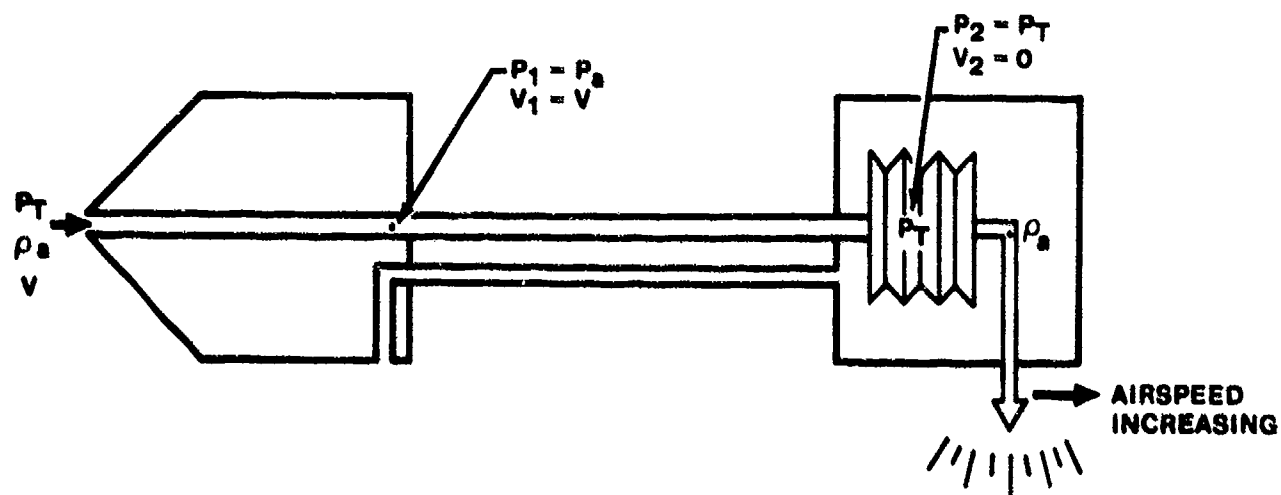


FIGURE 5.5. PITOT-STATIC SCHEMATIC

From Figure 5.5 and Equation 5.12

$$P_1 + \rho_a \frac{V_1^2}{2} = P_2 + \rho_a \frac{V_2^2}{2} \text{ but } V_2 = 0$$

$$P_1 + \rho_a \frac{V_1^2}{2} = P_2$$

Changing subscripts gives

$$P_a + \rho_a \frac{V^2}{2} = P_T$$

Dynamic pressure, q , is defined as

$$\frac{\rho_a}{2} V^2$$

therefore

$$\frac{\rho_a}{2} V^2 = P_T - P_a = q \quad (5.13)$$

True airspeed, in the incompressible case, is

$$V_t = \sqrt{\frac{2}{\rho_a} (P_T - P_a)} = \sqrt{\frac{2q}{\rho_a}} \quad (5.14)$$

It is possible to use a pitot-static system and build an airspeed indicator to conform to this equation. However, there are disadvantages in doing so.

1. Density requires measurement of ambient temperature, which is difficult in flight.
2. The instrument would be complex.

In addition to the simple bellows shown in Figure 5.5, ambient temperature and pressure would have to be measured, converted to density, and used to modify the output of the simple bellows. An instrument of this complexity cannot meet the accuracy requirements of flight testing.

3. Except for navigation, the instrument would not give the pilot information he requires. For example, when landing, the aircraft should be flown at a constant C_L , a fixed amount before stall C_L .

$$\text{LIFT} = \text{WEIGHT} = C_L S \frac{1}{2} \rho_a v_{\text{LAND}}^2$$

$$v_{\text{LAND}} = \sqrt{\frac{2W}{C_L S \rho_a}}$$

Thus, the pilot would have to compute a different landing speed for each condition of weight, pressure altitude, and temperature.

4. Because of its complexity, the instrument would be difficult to calibrate accurately.

Density is the variable which causes the deficiencies in a true airspeed indicator. A solution to the problem is to assume a constant value for density. If ρ_a is replaced by ρ_{SL} in Equation 5.14, the resultant velocity is termed equivalent airspeed, v_e .

$$v_e = \sqrt{\frac{2q}{\rho_{\text{SL}}}} \quad (5.15)$$

Multiply by

$$\sqrt{\frac{\rho_a}{\rho_a}}$$

$$v_e = \sqrt{\frac{\rho_a}{\rho_a} \frac{2q}{\rho_{\text{SL}}}} = \sqrt{\frac{\sigma}{\rho_a} \frac{2q}{\rho_a}} = \sqrt{\sigma} v_t \quad (5.16)$$

It is now possible to build a simple airspeed indicator which measures the quantity $(P_T - P_a)$. Such a system requires only the bellows system shown in Figure 5.5 and has the following advantages:

1. Because of its simplicity, it has a high degree of accuracy.
2. The indicator is easy to calibrate and has only one curve of error, ΔV_{ic} , versus equivalent airspeed, V_e .
3. V_e is a measured quantity of use to the pilot. Using the landing case

$$W = C_L S \frac{1}{2} \rho_a V_{LAND}^2 = C_L S \frac{1}{2} \rho_a \frac{\rho_{SL}}{\rho_a} V_{eLAND}^2$$

$$W = C_L S \frac{1}{2} \rho_{SL} V_{eLAND}^2$$

$$V_{eLAND} = \sqrt{\frac{2W}{C_L S \rho_{SL}}}$$

Thus, in computing either landing or stall speed the pilot need only consider one factor - weight.

4. Since, $V_e = f(P_T - P_a)$, it does not vary with temperature or density. Thus, for a given value of $P_T - P_a$, we have an important relationship:

$$V_{eTEST DAY} = V_{eSTD DAY} \quad (5.17)$$

V_e as derived for the incompressible case was the airspeed used primarily before World War II. However, as aircraft speed and altitude capabilities increased, the error resulting from the assumption that density remains constant became significant. Airspeed indicators for today's aircraft must be built to consider compressibility.

5.5.2 Compressible True Airspeed Theory

Euler's equation is used to develop the equations for compressible flow. Before integrating, several relationships are used to replace the density term.

$$Pv^\gamma = C \quad v = \frac{1}{\rho g} \quad \gamma = \frac{C_p}{C_v} = 1.4 \text{ for air}$$

$$P \left(\frac{1}{\rho g} \right)^\gamma = \frac{P}{(\rho g)^\gamma} = C$$

$$\frac{P}{\rho^\gamma} = C_1$$

or

$$\rho = \left(\frac{P}{C_1} \right)^{1/\gamma} = \frac{P^{1/\gamma}}{C_2}$$

Substituting this term into Equation 5.11 and integrating gives Bernoulli's equation for compressible flow:

$$\frac{v_t^2}{2} + \frac{\gamma}{\gamma-1} \frac{P}{\rho} = C_3 \quad (5.18)$$

Applying this to the pitot-static system in Figure 5.5 gives

$$\frac{v_t^2}{2} + \frac{\gamma}{\gamma-1} \frac{P_a}{\rho_a} = \frac{\gamma}{\gamma-1} \frac{P_T}{\rho_T} \quad (5.19)$$

Since

$$\frac{P}{\rho^\gamma} = \text{CONSTANT}$$

$$\rho_T = \rho_a \left(\frac{P_T}{P_a} \right)^{1/\gamma}$$

Substituted in Equation 5.19

$$\frac{v_t^2}{2} + \frac{\gamma}{\gamma-1} \frac{P_a}{\rho_a} = \frac{\gamma}{\gamma-1} \frac{1}{\rho_a P_T^{1/\gamma}} \frac{P_T}{P_a^{1/\gamma}} \quad (5.20)$$

If the right side of Equation 5.20 is multiplied and divided by $\frac{P}{\rho_a}$ and the relation $\frac{P}{\rho_a^{1/\gamma}} = P \left(\frac{\gamma - 1}{\gamma} \right)$ is used,

$$\frac{V_t^2}{2} + \frac{\gamma}{\gamma - 1} \frac{P_a}{\rho_a} = \frac{\gamma}{\gamma - 1} \frac{P_a}{\rho_a} \left(\frac{P_T}{P_a} \right)^{\frac{\gamma - 1}{\gamma}} \quad (5.21)$$

Add and subtract $\frac{P_a}{P_a}$ to $\frac{P_T}{P_a}$

$$\frac{P_T}{P_a} = \frac{P_T}{P_a} - \frac{P_a}{P_a} + \frac{P_a}{P_a} = \frac{P_T - P_a}{P_a} + 1$$

Equation 5.21 becomes

$$V_t^2 = 2 \frac{\gamma}{\gamma - 1} \frac{P_a}{\rho_a} \left[\left(\frac{P_T - P_a}{P_a} + 1 \right)^{\frac{\gamma - 1}{\gamma}} - 1 \right] \quad (5.22)$$

or

$$V_t = \sqrt{2 \frac{\gamma}{\gamma - 1} \frac{P_a}{\rho_a} \left[\left(\frac{P_T - P_a}{P_a} + 1 \right)^{\frac{\gamma - 1}{\gamma}} - 1 \right]} \quad (5.23)$$

or

$$V_t = \sqrt{2 \frac{\gamma}{\gamma - 1} \frac{P_a}{\rho_a} \left[\left(\frac{q_c}{P_a} + 1 \right)^{\frac{\gamma - 1}{\gamma}} - 1 \right]} \quad (5.24)$$

Equation 5.24 is the compressible true airspeed equation for subsonic airspeeds. A new term was introduced in Equation 5.24, "q compressible," q_c . It is defined as

$$q_c = P_T - P_a \quad (5.25)$$

It is not equal to $\frac{1}{2} \rho V^2$. Under conditions of low altitude and low speed it

approximates the definition of dynamic pressure. The relationship between q_c , "q compressible," and q , "dynamic pressure," is

$$q_c = q \left(1 + \frac{M^2}{4} + \frac{M^4}{40} + \frac{M^6}{1600} + \dots \right) \quad (5.26)$$

This series converges rapidly as Mach becomes small.

5.5.3 Calibrated Airspeed

The compressible flow true airspeed equation (Equation 5.24) has the same disadvantages as the incompressible flow true airspeed case. Additionally, a bellows would have to be added to measure P_a . It should be noted that the simple pitot-static system in Figure 5.5 only measures $P_T - P_a$. In order to modify Equation 5.24 to be useful in measuring only the quantity $(P_T - P_a)$, both ρ_a and P_a are replaced by the constant ρ_{SL} and $P_{a_{SL}}$. The resulting airspeed is defined as calibrated airspeed, V_C .

$$V_C = \sqrt{\frac{2\gamma}{\gamma-1} \frac{P_{a_{SL}}}{\rho_{SL}} \left[\left(\frac{q_c}{P_{a_{SL}}} + 1 \right)^{\frac{\gamma-1}{\gamma}} - 1 \right]} \quad (5.27)$$

Or more simply,

$$V_C = f(P_T - P_a) = f(q_c) \quad (5.28)$$

An instrument designed to follow Equation 5.27 has the following advantages:

1. The indicator is simple in design and construction, accurate, and easy to calibrate.
2. V_C is of direct use to the pilot. The quantity V_C is analogous to V_e in the incompressible case, since at low airspeeds and moderate altitudes $V_e = V_C$. The aircraft stall speed, landing speed, and

handling characteristics are proportional to calibrated airspeed for a given gross weight.

3. Since a temperature or density term is not present in the equation for calibrated airspeed, a given value of $(P_T - P_a)$ has the same significance on all days or

$$V_{C_{TEST}} = V_{C_{STD DAY}} \quad (5.29)$$

Equation 5.27 is limited to subsonic flow. If the flow is supersonic, it must pass through a shock wave in order to slow to stagnation conditions. There is a loss of total pressure when the flow passes through the shock wave. Thus, the indicator does not measure the total pressure of the supersonic flow. The solution for supersonic flight is derived by considering a normal shock compression in front of the total pressure tube and an isentropic compression in the subsonic region aft of the shock. The normal shock assumption is good, since the pitot tube has a small frontal area. Consequently, the radius of the shock in front of the hole may be considered infinite. The resulting equation is known as the Rayleigh Supersonic Pitot Equation. It relates the total pressure behind the shock P_T to the free stream ambient pressure P_a and free stream Mach V/a .

$$\frac{P_T}{P_a} = \left[\frac{\gamma+1}{2} \left(\frac{V}{a} \right)^2 \right]^{\frac{\gamma}{\gamma-1}} \left[\frac{1}{\frac{2\gamma}{\gamma+1} \left(\frac{V}{a} \right)^2 - \frac{\gamma-1}{\gamma+1}} \right]^{\frac{1}{\gamma-1}} \quad (5.30)$$

Equation 5.30 is used to calculate the ratio of dynamic pressure to free stream ambient pressure

$$\frac{P_T - P_a}{P_a} = \frac{q_c}{P_a} = \left[\frac{\gamma+1}{2} \left(\frac{V}{a} \right)^2 \right]^{\frac{\gamma}{\gamma-1}} \left[\frac{1}{\frac{2\gamma}{\gamma+1} \left(\frac{V}{a} \right)^2 - \frac{\gamma-1}{\gamma+1}} \right]^{\frac{1}{\gamma-1}} - 1 \quad (5.31)$$

Equation (5.22) is used to calculate this ratio for subsonic flow.

$$\frac{P_T - P_a}{P_a} = \frac{q_C}{P_a} = \left[\frac{\gamma+1}{2\gamma} \left(\frac{V}{a} \right)^2 + 1 \right]^{\frac{\gamma}{\gamma-1}} - 1 \quad (5.32)$$

If the values of P_a and a for sea level standard conditions are inserted into Equations 5.31 and 5.32, the resulting functions are defined as the calibrated airspeed equations.

$$\frac{q_C}{P_{a_{sl}}} = \left[1 + 0.2 \left(\frac{V_C}{a_{sl}} \right)^2 \right]^{3.5} - 1 \quad (5.33)$$

For $V_C \leq a_{sl}$

$$\frac{q_C}{P_{a_{sl}}} = \frac{166.921 (V_C/a_{sl})^7}{\left[7 (V_C/a_{sl})^2 - 1 \right]^{2.5}} - 1 \quad (5.34)$$

for $V_C \geq a_{SL}$

q_C = differential pressure, in Hg
 $(q_C = P_T - P_a \text{ subsonic and}$
 $q_C = P_T' - P_a \text{ supersonic})$

V_C = calibrated airspeed, kts

a_{SL} = 661.48 kts

$P_{a_{SL}}$ = 29.92126 in Hg

Airspeed indicators are constructed and calibrated according to these equations.

In operation, the airspeed indicator is similar to the altimeter, but instead of being evacuated, the inside of the capsule is connected to the total pressure source, and the case to the static pressure source. The instrument then senses total pressure (P_T') within the capsule and static pressure (P_s) outside it as shown in Figure 5.6.

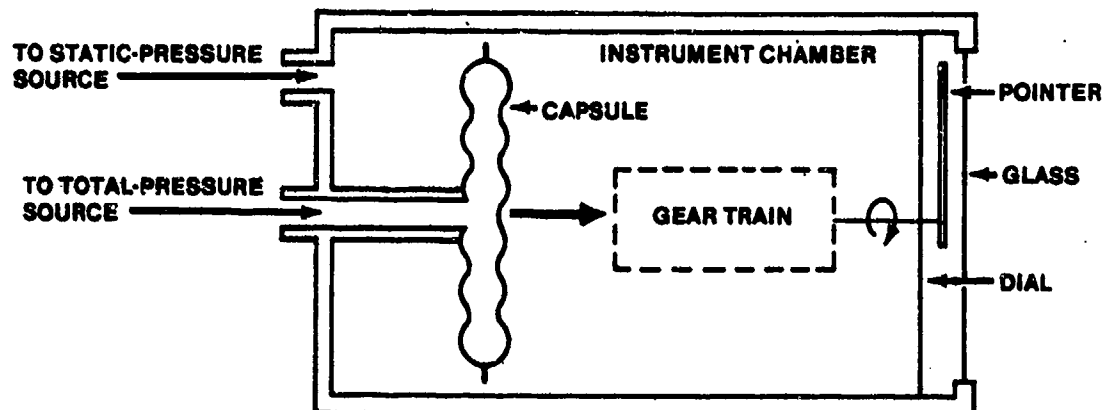


FIGURE 5.6. AIRSPEED INDICATOR SCHEMATIC

5.5.4 Equivalent Airspeed

Equivalent airspeed was derived from incompressible flow theory and has no real meaning for the compressible case. However, it can be an important parameter in analyzing certain performance and stability and control factors as they can be shown to be functions of equivalent airspeed.

The definition of equivalent airspeed when applied to Equation 5.24 is

$$V_e = V_t \sqrt{\sigma}$$

$$V_e = \sqrt{\frac{2\gamma}{\gamma-1} \frac{P_a}{\rho_{SL}} \left[\left(\frac{q_c}{P_a} + 1 \right)^{\frac{\gamma-1}{\gamma}} - 1 \right]} \quad (5.35)$$

5.5.5 Determining V_t from Flight Test Data

From flight test data V_c and H_c can be determined. The method progresses from V_c to V_e to V_t . By definition

$$V_e = V_c - \Delta V_c$$

or

$$\Delta V_C = V_C - V_e \quad (5.36)$$

$$\Delta V_C = f(P_T - P_a, P_a) = f(V_C, H_C) \quad (5.37)$$

Although ΔV_C is termed compressibility correction, it has in fact nothing to do with compressibility effects. This quantity is found in the first chapter of the Performance Section of most flight manuals. ΔV_C can be determined by entering with known values of V_C and H_C , and it is independent of aircraft type.

The next step is to correct V_C to V_t . To do this, the temperature at the test altitude must be known in order to determine the test atmospheric density.

$$V_t = V_e / \sqrt{\sigma} = V_e / \sqrt{\rho_a / \rho_{SL}}$$

To review

$$H_C = f(P_a)$$

$$V_C = f(P_T - P_a)$$

$$\Delta V_C = f(P_T - P_a, P_a) = f(V_C, H_C)$$

$$V_e = f(P_T - P_a, P_a)$$

$$\sigma = \frac{\rho_a}{\rho_{SL}} = f(T_a, P_a)$$

$$V_t = f(P_T - P_a, P_a, \rho_a) = f(P_T - P_a, P_a, T_a)$$

$$V_t = \frac{V_C - \Delta V_C}{\sqrt{\sigma}}$$

5.6 MACHMETER THEORY

Mach, M , is defined as the ratio of the true airspeed to the local atmospheric speed of sound.

$$M = \frac{V_t}{a} = \frac{V_t}{\sqrt{\gamma g R T}}$$

but

$$\frac{P}{\rho} = g R T$$

$$M = \frac{V_t}{\sqrt{\gamma \frac{P}{\rho}}}$$

Substituting this relationship in the equation for V_t (Equation 5.22)

$$\gamma \frac{P_a}{\rho_a} M^2 = \frac{2\gamma}{\gamma-1} \frac{P_a}{\rho_a} \left[\left(\frac{P_T - P_a}{P_a} + 1 \right)^{\frac{\gamma-1}{\gamma}} - 1 \right]$$

or

$$M = \sqrt{\frac{2}{\gamma-1} \left[\left(\frac{P_T - P_a}{P_a} + 1 \right)^{\frac{\gamma-1}{\gamma}} - 1 \right]} \quad (5.38)$$

or

$$\frac{P_T}{P_a} = \left(1 + \frac{\gamma-1}{2} M^2 \right)^{\frac{\gamma}{\gamma-1}}$$

This equation, which relates Mach to the free stream total and ambient pressures, is good for supersonic as well as subsonic flight. It must be remembered, however, that P_T' rather than P_T is measured in supersonic flight. By using the Rayleigh pitot equation and substituting for the constants, Equation 5.31 is used to find Equation 5.40.

$$\frac{q_c}{P_a} = \left(1 + 0.2 M^2\right)^{3.5} - 1 \quad (5.39)$$

for $M < 1$

$$\frac{q_c}{P_a} = \frac{166.921 M^7}{(7M^2 - 1)^{2.5}} - 1 \quad (5.40)$$

for $M > 1$

The Machmeter is essentially a combination altimeter and airspeed indicator designed to solve these equations. An altimeter capsule and an airspeed capsule simultaneously supply signals to a series of gears and levers to produce the Mach indication. A Machmeter schematic is given in Figure 5.7.

Since the construction of the Machmeter requires two bellows, one for q_c and another for P_a , it is complex, difficult to calibrate, and inaccurate. As a result, the Machmeter is not used in flight test work except as a reference instrument.

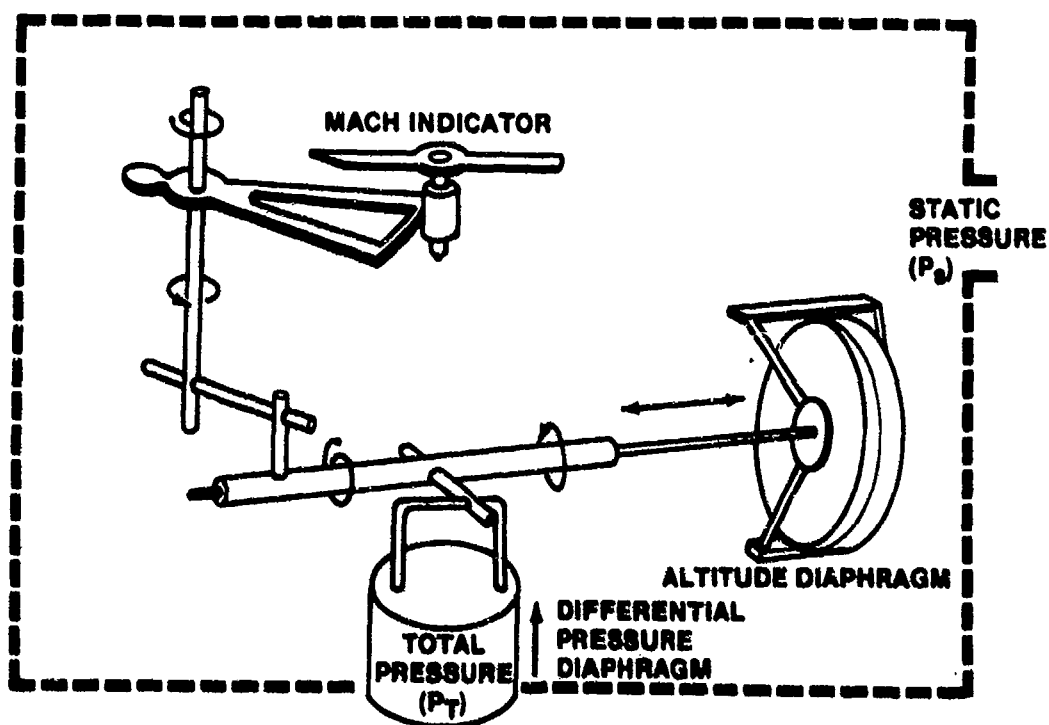


FIGURE 5.7. MACHMETER SCHEMATIC

Of importance in flight test is the fact, obvious from Equations 5.39 and 5.40, that

$$M = f(P_T - P_a, P_a) = f(V_C, H_C)$$

As a result, Mach is independent of temperature, and flying at a given H_C and V_C , the Mach on the test day equals Mach on a standard day.

$$M_{TEST} = M_{STD}$$

Since many aerodynamic effects, particularly in jet engine-airframe performance analysis, are functions of Mach, this fact plays a major role in flight testing.

5.7 INSTRUMENT ERROR THEORY AND CALIBRATION

Several corrections must be applied to the indicated altimeter and airspeed indicator readings (H_i, V_i) before pressure altitude and calibrated airspeed can be determined. The indicated readings must be corrected for instrument error, pressure lag error, and position error, in that order. The instrument error is the subject of this section.

The altimeter and airspeed indicator are sensitive to pressure and pressure differential respectively, but the dials are calibrated to read altitude and airspeed according to Equations 5.5, 5.9, 5.33, and 5.34. It is not possible to perfect an instrument which can represent such nonlinear functions exactly under all flight conditions. As a result, an error exists called instrument error. Instrument error is the result of several factors:

1. Scale error and manufacturing discrepancies. This is primarily due to an imperfect mechanization of the controlling equations.
2. Magnetic Fields. Any change in the relation of metal components changes the associated magnetic fields.
3. Temperature changes.
4. Coulomb and viscous friction. Coulomb friction is simply dry friction as in the meshing of two gears. Viscous friction is involved between a fluid and solid, for instance, a lubricated bearing.
5. Inertia of moving parts.

The calibration of an altimeter and airspeed indicator for instrument error is usually conducted in an instrument laboratory. A known pressure or pressure differential is applied to the instrument to be tested. The instrument error is determined as the difference between this known pressure and the instrument indicated reading.

Data are taken in both directions so that the hysteresis can be determined. Hysteresis literally means "to lag" and is the combination of all the errors in the indicator. Hysteresis is then the difference between the "up" and "down" readings. An instrument with a large hysteresis must be rejected as it is difficult to account for this effect in flight. As can be seen from the major causes of error, an instrument vibrator can be of some assistance in reducing instrument error. Additionally, the instruments are calibrated in a static situation. The hysteresis under a rapidly varying situation must be different, but it is not feasible to calibrate instruments for such conditions.

As an instrument wears, its calibration changes. Therefore, each instrument should be calibrated periodically. The repeatability of the instrument is determined from the instrument calibration history. The repeatability of the instrument must be good for the instrument calibration to be meaningful.

Instrument corrections (ΔH_{ic} , ΔV_{ic}) are determined as the differences between the instrument corrected values (H_{ic} , V_{ic}) and the indicated values (H_i , V_i)

$$\Delta H_{ic} = H_{ic} - H_i \quad (5.41)$$

$$\Delta V_{ic} = V_{ic} - V_i \quad (5.42)$$

Or, to correct the indicated values

$$H_i + \Delta H_{ic} = H_{ic} \quad (5.43)$$

$$V_i + \Delta V_{ic} = V_{ic} \quad (5.44)$$

An example of an instrument error calibration chart is shown in Figure 5.8.

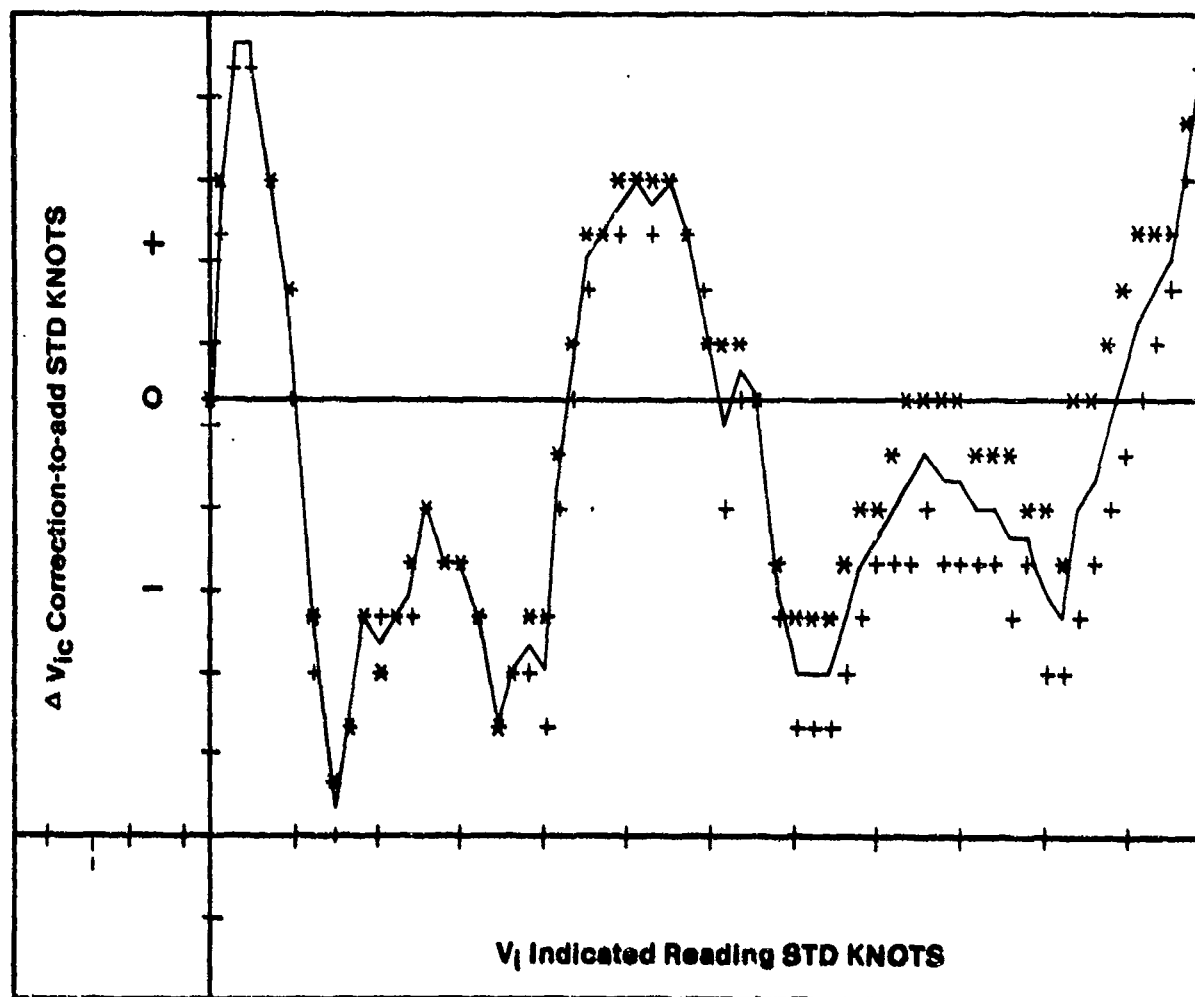


FIGURE 5.8. AIRSPEED INSTRUMENT CALIBRATION

Use of the subscript ic denotes a quantity corrected for instrument error such as V_{ic} or a quantity computed using P_s rather than P_a , such as q_{cic} .

5.7.1 Pressure Lag Error

The altimeter and airspeed indicator are subject to an error called pressure lag error. This error exists only when the aircraft in which the instruments are installed is changing airspeed or altitude. In this case, there is a time lag between the time when the pressure change occurs and when it is indicated on the instrument dial. This effect on the altimeter is obvious. In the airspeed indicator, the lag may cause a reading too large or too small depending on the proportion of the lag in the total and static pressure systems. Converted to feet or knots, this error is often insignificant. However, it may be significant and should be considered in certain maneuvers such as high speed dives and zoom climbs in which the instrument diaphragms must undergo large pressure rates.

Pressure lag is basically a result of:

1. Pressure drop in the tube due to viscous friction.
2. Inertia of the air mass in the tubing.
3. Instrument inertia and viscous and kinetic friction.
4. Finite speed of pressure propagation, or acoustic lag.

A detailed mathematical treatment of the response of such a system would be difficult and is beyond the scope of this text. It has been found that mathematical prediction of the lag constants has not been satisfactory. A ground determination can be made by placing a known varying pressure source to the total and static pressure ports of the pitot-static tube and then correlating this with the indicated values. Airborne determination is possible, but it is complicated and has not normally resulted in satisfactory performance. The altimeter and airspeed indicator lag corrections (Δh_{ic_i} and Δv_{ic_i}) are considered negligible for the majority of flight tests. A good reference for lag error calculations is (5.4: 28 - 47).

5.7.2 Position Error

Determination of the pressure altitude and calibrated airspeed at which an aircraft is operating is dependent upon the measurement of free stream total pressure, P_T , and free stream static pressure, P_a , by the aircraft pitot-static system. Generally, the pressures registered by the pitot-static system differ from free stream pressures as a result of:

1. The existence of other than free stream pressures at the pressure source.
2. Error in the local pressure at the source caused by the pressure sensors.

The resulting error is called position error. In the general case, position error may result from errors at both the static and total pressure sources.

5.7.2.1 Total Pressure Error. As an aircraft moves through the air, a static pressure disturbance is generated in the air, producing a static pressure field around the aircraft. At subsonic speeds, the flow perturbations due to the aircraft static pressure field are very nearly isentropic in nature and hence do not affect the total pressure. Therefore, as long as the total pressure source is not located behind a propeller, in the wing wake, in a boundary layer, or in a region of localized supersonic flow, the total pressure errors due to the position of the total pressure head are usually negligible. Normally, it is possible to locate the total pressure pickup properly and avoid any difficulty.

An aircraft capable of supersonic speeds should be supplied with a noseboom pitot-static system so that the total pressure pickup is located ahead of any shock waves formed by the aircraft. This condition is essential, for it is difficult to correct for total pressure errors which result when oblique shock waves exist ahead of the pickup. The shock wave due to the pickup itself is considered in the calibration equation discussed in the section on CALIBRATED AIRSPEED.

Failure of the total pressure sensor to register the local pressure may result from the shape of the pitot-static head, inclination to the flow angle

of attack, α , or angle of sideslip, β), or a combination of both. Pitot-static tubes have been designed in varied shapes. Some are suitable only for relatively low speeds while others are designed to operate in supersonic flight as well. Therefore, if a proper design is selected and the pitot lips are not damaged, there should be no error in total pressure due to the shape of the probe. Errors in total pressure caused by the angle of incidence of a probe to the relative wind are negligible for most flight conditions. Commonly used probes produce no significant errors at angles of attack or sideslip up to approximately 20° .

From these arguments it can be seen that with proper placement, design, and good leak checks of the pitot probe, total pressure error can be assumed to be zero.

5.7.2.2 Static Pressure Error. The static pressure field surrounding an aircraft in flight is a function of speed and altitude as well as the secondary parameters, angle of attack, Mach, and Reynolds number. Hence, it is seldom possible to find a location for the static pressure source where the free stream pressure is sensed under all flight conditions. Therefore, an error in the measurement of the static pressure due to the position of the static pressure orifice generally exists.

At subsonic speeds, it is often possible to find some position on the fuselage where the static pressure error is small under all flight conditions. Aircraft limited to subsonic speeds are best instrumented by use of a flush static pressure port in such a position. Examples of such positions are shown in Figure 5.9.

On supersonic aircraft a noseboom installation is advantageous for the measurement of static pressure. At supersonic speeds, when the bow wave is located downstream of the static pressure orifices, there is no error due to the aircraft pressure field. Any error which may exist is a result of the probe itself. Available evidence suggests that free stream static pressure is sensed if the static ports are located more than 8 to 10 tube diameters behind the nose of the pitot-static tube and 4 to 6 diameters in front of the shoulder (Figure 5.10).

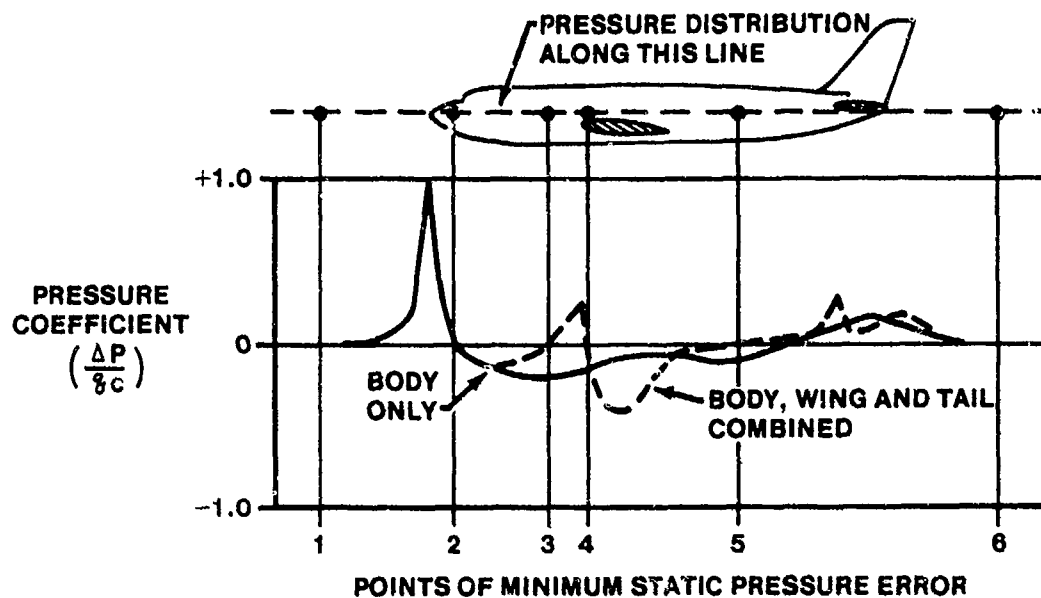


FIGURE 5.9. TYPICAL SUBSONIC STATIC PRESSURE DISTRIBUTION ON AIRCRAFT FUSELAGE. 1 - 6 ARE POINTS OF MINIMUM STATIC PRESSURE ERROR

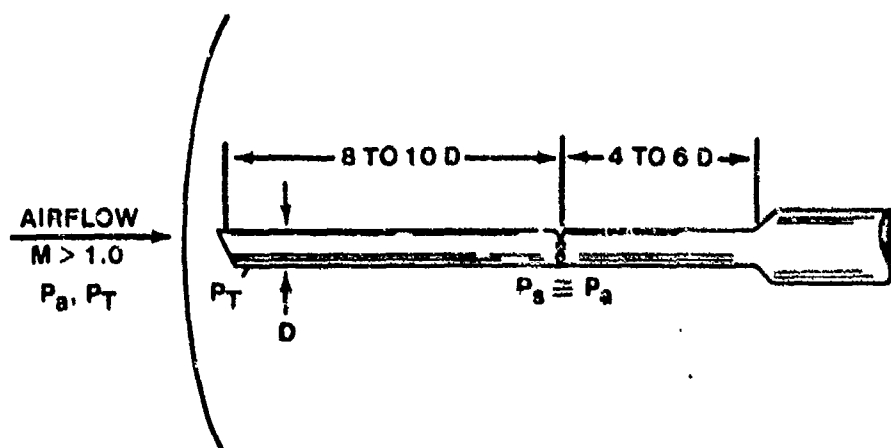


FIGURE 5.10. DETACHED SHOCK WAVE IN FRONT OF PITOT-STATIC PROBE

In addition to the static pressure error introduced by the position of the static pressure orifices in the pressure field of the aircraft, there may be error in the registration of the local static pressure due primarily to inclination of flow. Error due to sideslip is often minimized in the case of the flush mounted static ports by the location of holes on opposite sides of the fuselage manifolded together. In the case of boom installations, circumferential location of the static pressure ports reduces the adverse effect of sideslip and angle of attack.

5.7.2.3 Definition of Position Error. It has been seen that position error is caused at the static pressure source by the pressure field around the aircraft and the pitot-static probe. This development assumes the total pressure source to be free from error. The pressure error at the static source has the symbol ΔP_p and is defined as

$$\Delta P_p = P_s - P_a \quad (5.45)$$

The corrections for this error are termed position error corrections. Airspeed position error correction, ΔV_{pc} , is developed as follows

$$V_c = f(P_T - P_a)$$

$$V_{ic} = f(P_T - P_s)$$

$$\Delta V_{pc} = V_c - V_{ic} = f(\Delta P_p)$$

$$V_c = V_{ic} + \Delta V_{pc} \quad (5.46)$$

Altimeter position error correction, ΔH_{pc} , is

$$H_c = f(P_a)$$

$$H_{ic} = f(P_s)$$

$$\Delta H_{pc} = H_c - H_{ic} = f(\Delta P_p)$$

$$H_c = H_{ic} + \Delta H_{pc} \quad (5.47)$$

Mach position error correction, ΔM_{pc} , is

$$M = f \left(\frac{P_T - P_a}{P_a} \right)$$

$$M_{ic} = f \left(\frac{P_T - P_s}{P_s} \right)$$

$$\Delta M_{pc} = M - M_{ic} = \bar{f}(\Delta P_p)$$

$$M = M_{ic} + \Delta M_{pc} \quad (5.48)$$

The sign convention used results in the position error correction being the same sign as ΔP_p . It can easily be seen that if P_s were greater than P_a , the airspeed indicator would indicate a lower than actual value. Therefore, ΔP_p and ΔV_{pc} would both be positive in order to correct V_{ic} to V_c . This same logic applies to the ΔH_{pc} and ΔM_{pc} .

Since ΔP_p is the source of position error for all three parameters, there must be a mathematical relationship between position error corrections. These relationships have been developed, but it is beyond the scope of this text to present the development or the equations. However, these functions have been placed in graphic form and are contained in the references. Additionally, several rather simple computer programs have been developed to obtain one position error correction from another.

By dimensional analysis, it can be shown that the relation of static pressure (P_s) at any point in a pressure field of an aircraft to the free stream pressure (P_a) depends on Mach (M), angle of attack (α), angle of sideslip (β), Reynolds number (R_e), and Prandtl number (P_r).

$$\frac{P_s}{P_a} = f_1 (M, \alpha, \beta, R_e, P_r)$$

Neglecting heat transfer, P_r is approximately constant; R_e effects are negligible as long as the static source is not located in a thick boundary layer; and it is assumed that sideslip angles are kept small. The relation simplifies to

$$\frac{P_s}{P_a} = f_2 (M, \alpha)$$

With no loss in generality, this equation can be changed to read

$$\frac{\Delta P_p}{q_{cic}} = f_3 (M_{ic}, C_{L_{ic}}) \quad (5.49)$$

because

$$q_{cic} = P_T' - P_s$$

and

$$M_{ic} = f \left(\frac{q_{cic}}{P_s} \right)$$

and

$$C_{L_{ic}} = \frac{2nW}{\gamma P_s M_{ic}^2 S} = \frac{nW}{\delta_{ic}} \frac{1}{M_{ic}^2} \frac{2}{\lambda S P_{a_{SL}}}$$

The term $\Delta P_p / q_{cic}$ is the position error pressure coefficient and is useful in the reduction of position error data. From the definition of $C_{L_{ic}}$,

$$\frac{\Delta P_p}{q_{cic}} = f_4 \left(M_{ic}, \frac{nW}{\delta_{ic}} \right) \quad (5.50)$$

From Equation 5.50 it can be seen that there are three major variables in any particular pitot-static system. These are Mach, weight-load factor combination, and the altitude at which the aircraft is flying. The importance of one of the assumptions must be emphasized. Angle of sideslip was assumed to be small. At large angles of sideslip, an additional variable is introduced.

There are numerous methods of presenting position error data in graphic form. Once the variables in Equation 5.50 have been determined by means of calibration, a chart can be prepared for all weights and all load factors for the given aircraft in a given configuration (Figure 5.11). Other common methods of presenting position error data are ΔV_{pc} versus V_{ic} , ΔH_{pc} versus V_{ic} , and ΔM_{pc} versus M_{ic} .

5.7.2.4 Low Mach Effects. For Mach less than 0.6, the effects of compressibility may be considered negligible. Without introducing serious error, it may be said that the pressure coefficient is a function only of lift coefficient.

Since $C_L = 2nW/\rho_{SL} V_e^2 S$ and in the low Mach range $V_e \approx V_c$, it can be assumed that

$$C_L = \frac{2nW}{\rho_{SL} V_c^2 S}$$

$$C_{L_{ic}} = \frac{2nW}{\rho_{SL} V_c^2 S} \quad (5.51)$$

or

$$\frac{\Delta P_p}{q_{cic}} = f_5 \left(\frac{nW}{V_{ic}^2} \right) \quad (5.52)$$

From Equation 5.52 it can be seen that for low speeds at a constant V_{ic} , the position error is a function of nW or more simply angle of attack. For aircraft with small weight changes, ΔP_p versus V_{ic} generalizes into one curve. This generalization will not apply to such aircraft as the B-52 where large variations in weight occur.

Since ΔP_p is constant for a given V_{ic} , the curve of ΔV_{pc} versus V_{ic} will apply to all altitudes. If weight changes are significant, a family of curves is generated as in Figure 5.12.

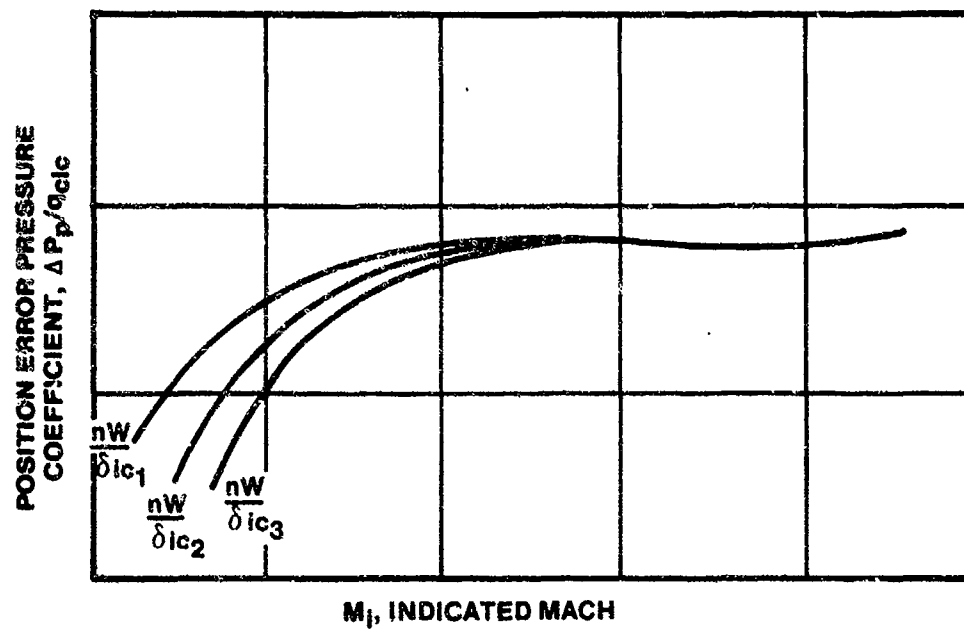


FIGURE 5.11. LOW MACH C_L EFFECTS ON PRESSURE COEFFICIENT

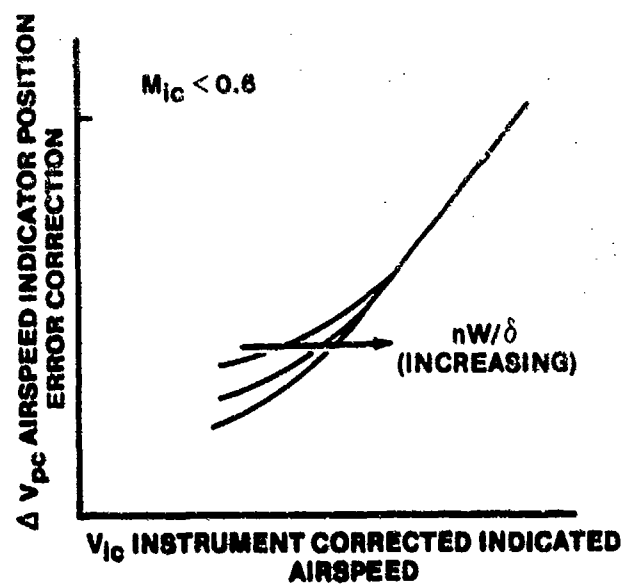


FIGURE 5.12. LOW MACH C_L EFFECTS ON VELOCITY ERROR

If ΔP_p is constant for any given V_{ic} , (assuming no weight effects), then the altitude position error correction, ΔH_{pc} , is a function of altitude. This is because a pressure increment is equivalent to a different tapeline altitude at each pressure level in the atmosphere. This results in a series of curves, one for each pressure altitude as in Figure 5.13.

To discuss Mach at low speeds, C_L is expressed in terms of Mach.

$$C_{L_{ic}} = \frac{nW}{\delta_{ic}} \frac{2}{M_{ic}^2 \gamma SP_{a_{SL}}} \quad (5.53)$$

Thus, at a constant M_{ic} a family of curves for various nW/δ_{ic} values will result.

ΔM_{pc} versus M_{ic} is plotted in Figure 5.14. It merely serves to illustrate that for many pitot-static systems in which ΔV_{pc} versus V_{ic} is a single curve, ΔM_{pc} versus M_{ic} is a series of curves, one for each representative altitude, in the low speed regime.

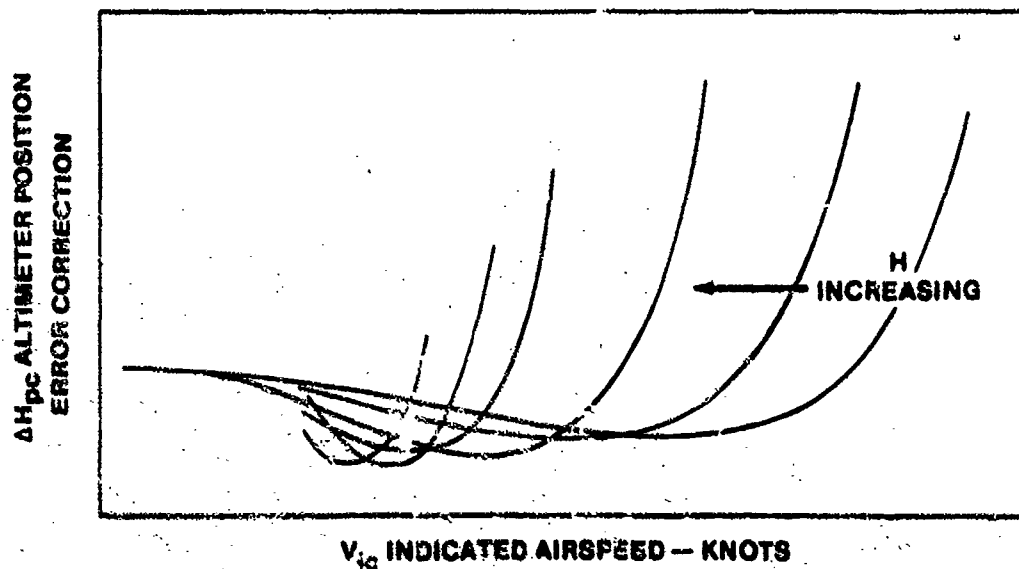


FIGURE 5.13. LOW SPEED ALTITUDE POSITION ERROR CORRECTION

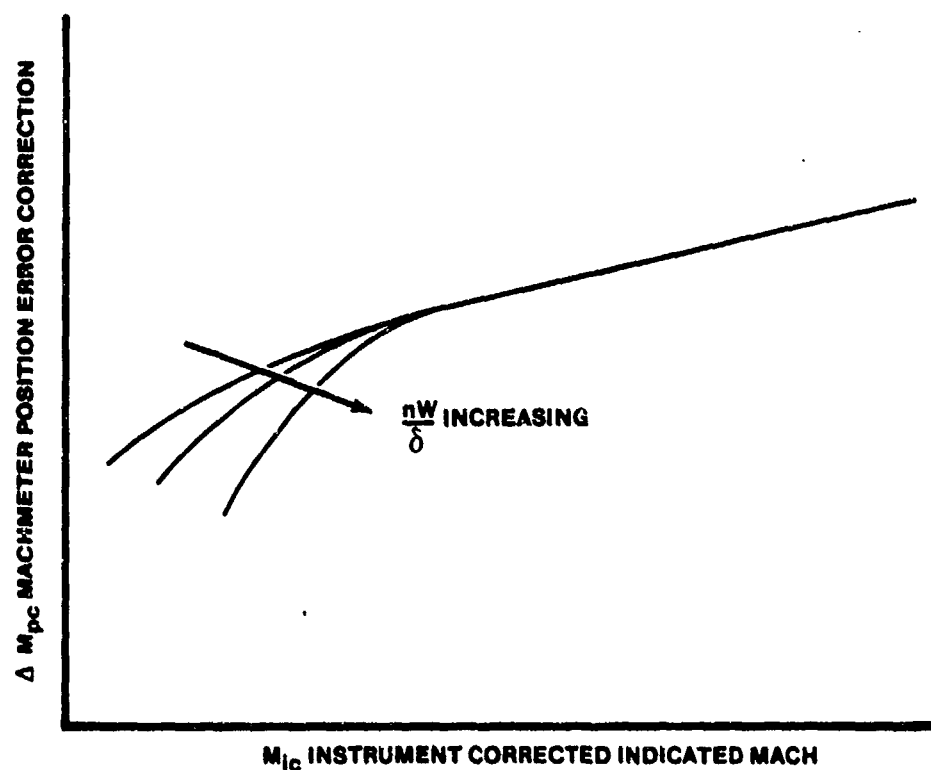


FIGURE 5.14 LOW SPEED MACH POSITION ERROR CORRECTION

5.7.2.5 Medium Subsonic and Transonic Mach Effects. In the Mach range of 0.6 to 1.1, the position error pressure coefficient will in general depend on both M_{ic} and C_L , so Equation 5.50 must be considered

$$\frac{\Delta P}{q_{cic}} = f_4 \left(M_{ic}, \frac{nW}{\delta_{ic}} \right)$$

At high speeds, large changes in airspeed produce relatively small changes in C_L . As a result, the effect of lift coefficient diminishes as airspeed increases. Mach begins to affect the pressure coefficient materially above 0.5. Thus, Mach increasingly tends to become the control-

ling parameter in the high speed regime. The existence of any $C_{L_{ic}}$ effect should be investigated by plotting curves of $\Delta P_p/q_{cic}$ versus M_{ic} for the values of nW/δ_{ic} . The result of a typical noseboom system is shown in Figure 5.15. This curve would be a single line if there were no $C_{L_{ic}}$ effects.

As the aircraft passes critical Mach, shock formation occurs over the various components of the aircraft. As these shock waves approach the static source, the sharp pressure rise which precedes the shock wave will drastically affect the static system. In this region, $\Delta P_p/q_{cic}$ rises rapidly and is strictly a function of Mach (reference Figure 5.15).

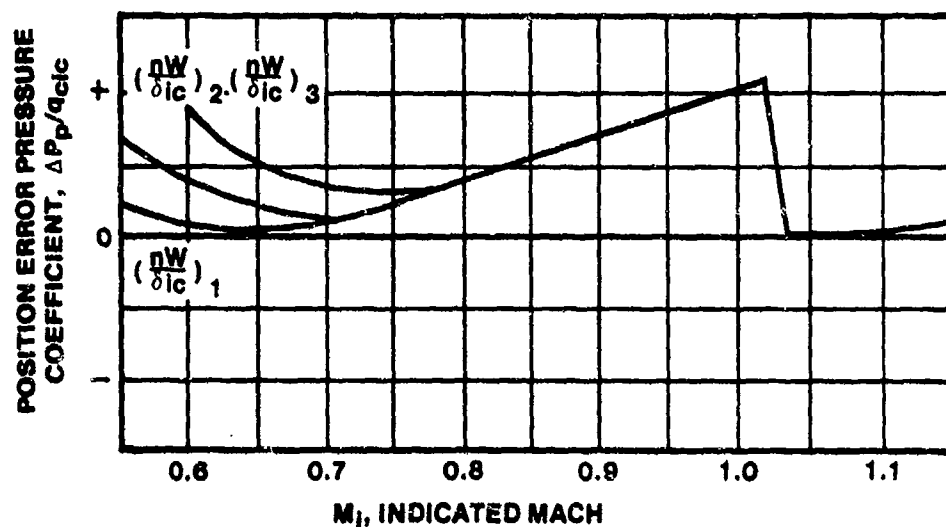


FIGURE 5.15. INDICATED MACH CORRECTED FOR INSTRUMENT ERROR, M_{ic}

Because Mach 1.0 will be a different V_{ic} for each altitude, the airspeed position error correction is in the form of a family of curves with altitude being the variable (reference Figure 5.16).

Using similar logic as in the low speed case, the ΔH_{pc} data is a series of curves. If plotted against M_{ic} , the lines are displaced vertically with increasing altitude. If plotted against V_{ic} , the lines are displaced both horizontally and vertically.

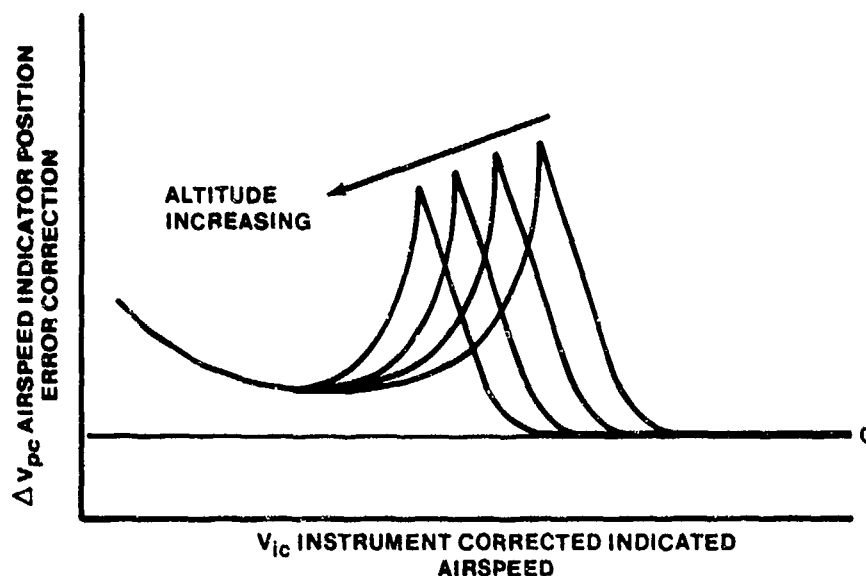


FIGURE 5.16. VELOCITY POSITION ERROR ILLUSTRATING ALTITUDE AND MACH EFFECTS

5.7.2.6 Supersonic Mach Effects. An aircraft capable of supersonic flight should be equipped with a noseboom installation. In this case, the aircraft bow wave passes behind the static pressure ports at a M_{ic} of 1.03 or so. At higher Mach, the effect of lift coefficient on the position error pressure coefficient is zero, as the pressure field of the aircraft is not felt in front of the bow wave. Therefore, any pressure error that does exist is a function of Mach only. In the usual case this error is quite small and may be zero.

5.7.2.7 Extrapolation of Results. The position error pressure coefficient has been shown to depend on both M_{ic} and $C_{L_{ic}}$.

$$\frac{\Delta P_p}{q_{cic}} = f \left(M_{ic}, C_{L_{ic}} \right) \text{ or } f \left(M_{ic}, \frac{nW}{\delta_{ic}} \right)$$

For aircraft with small weight effects and at higher speeds for all aircraft, the effect of lift coefficient variation is negligible. In these cases, a calibration at one altitude can be extrapolated to other altitudes at the same Mach.

$$\frac{\Delta P_p}{q_{cic}} \text{ is a function of Mach only.}$$

The existence of $C_{L_{ic}}$ effects should be investigated by performing tests at two altitudes and plotting the curves of $\Delta P_p/q_{cic}$ vs M_{ic} for values of nw/δ_{ic} . A single line occurs if no weight effects are present. Equation 5.39 can be rearranged to give P_T/P_s as a function of Mach.

$$\frac{P_T}{P_s} = \left(1 + 0.2M_{ic}^2\right)^{3.5} \text{ for } M_{ic} \leq 1.0$$

Differentiating at constant P_T gives

$$\frac{dP_s}{dM_{ic}} = - \frac{1.4 P_s M_{ic}}{(1 + 0.2 M_{ic}^2)}$$

making the approximation

$$dP_s = P_s - P_a = \Delta P_p$$

$$dM_{ic} = M_{ic} - M = \Delta M_p = -\Delta M_{pc}$$

thus

$$\frac{\Delta P_p}{\Delta M_{pc}} = \frac{1.4 P_s M_{ic}}{(1 + 0.2 M_{ic}^2)} \quad (5.54)$$

It has already been shown that ΔH_{pc} is a function of ΔP_p only. Using Equation 5.4 and the approximation that

$$dP_s = P_s - P_a = \Delta P_p$$

$$dH = H_c - H_{ic} = \Delta H_{pc}$$

gives

$$\frac{\Delta P_p}{P_s} = - \frac{G}{R} \frac{\Delta H_{pc}}{T_{as}}$$

Combining this with equation 5.54 results in

$$\frac{\Delta M_{pc}}{\Delta H_{pc}} = \frac{.007438 (1+0.2M_{ic}^2)}{T_{as} M_{ic}}$$

Therefore for $M_{ic1} = M_{ic2}$

$$\frac{\left(\frac{\Delta M_{pc}}{\Delta H_{pc}} \right)_1}{\left(\frac{\Delta M_{pc}}{\Delta H_{pc}} \right)_2} = \frac{T_{as1}}{T_{as2}}$$

or

$$\Delta H_{pc2} = \Delta H_{pc1} \left(\frac{T_{as2}}{T_{as1}} \right)$$

T_{as1} and T_{as2} are the standard air temperatures corresponding to H_{ic1} and H_{ic2} respectively. This equation can be used for ΔH_{pc} errors up to 3000 feet with no loss of accuracy.

5.7.2.8 Presentation of Position Error Correction. As discussed earlier, position error is expected to be most dependent upon Mach, configuration, and perhaps angle of attack or nW/δ_{ic} . The instrument corrected form of Mach M_{ic} and pressure ratio, δ_{ic} , are generally used as the independent variables. The equations use these values because in most data reduction problems the instrument corrected values are known while the calibrated values are unknown. That is, pitot-static measurements are usually made from the point-of-view of the test aircraft. Position error can be evaluated as a function of calibrated values just as well.

Most test pitot-static booms are very insensitive to change in angle of attack or sideslip, in fact angles of 10° or more may have little effect on the static or total pressure readings. Insensitivity to angle of attack simplifies the calibration problem because data taken at one altitude can be extrapolated to other altitudes, and the number of calibration flights can be reduced. The sensitivity to angle of attack should be determined early and is done by comparing measurements made at the same M_{ic} and configuration at a different nW/δ_{ic} . Tests at a different weight W , altitude δ_{ic} or loading n will suffice, but generally a change in altitude is the easiest to perform and will affect nW/δ_{ic} the most. Reynolds number effect may also become significant with large changes in altitude.

Either of two plots may be used for the comparison, $\Delta P_p/q_{cic}$ versus M_{ic} or ΔM_{pc} versus M_{ic} . As shown in Figure 5.17, when there is no sensitivity to angle of attack, the results of tests at different nW/δ_{ic} values converge. Conversely, if the results do not converge, position error cannot be extrapolated except over small changes in altitude, weight, and loading, and separate measurements must be made throughout the operating nW/δ_{ic} range of the aircraft.

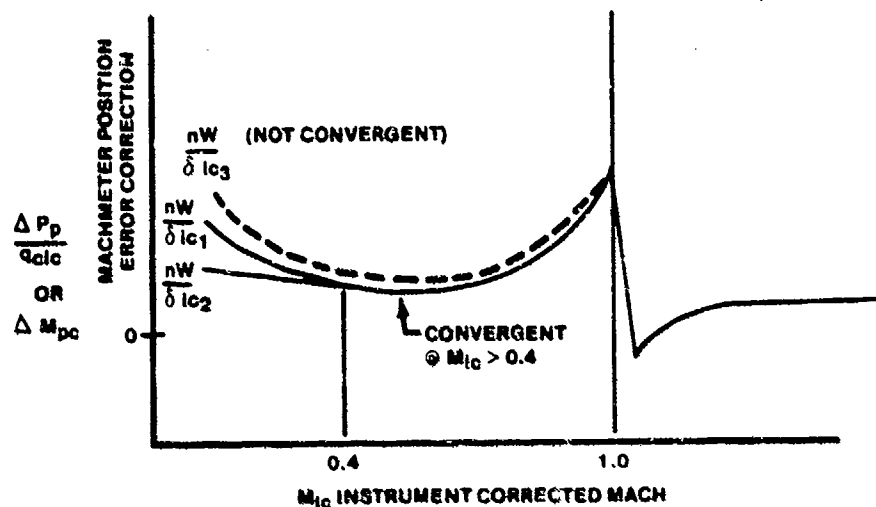


FIGURE 5.17. MACHMETER POSITION ERROR CORRECTION AS A FUNCTION OF INSTRUMENT CORRECTED INDICATED MACH

At low Mach nW/δ_{lc} break offs will usually occur on any pitot-static installation. Since most performance evaluation such as climb, cruise, and descent is done between 0.6 and 0.95 Mach, the break offs are of no consequence. It is quite important, however, to keep the nW/δ_{lc} parameters constant during the low speed points in order to correlate the data on a particular test. All low speed points should be flown at close to the same weight or the altitude should be adjusted.

Position error correction should be presented with data points in the form it was measured. Curves can be fared in, and then the fared values can be used for extrapolation or computation of other forms of position error. Some form of regression may be used to curve-fit the data, but curve values outside the data interval are meaningless. Depending upon the goodness of fit, curve values within the data interval may not be good either. In any case, regression must be used with care, and presentation of data points along with regressed curves adds a measure of confidence.

5.8 PITOT-STATIC SYSTEM TYPES

Many different types of pitot-static systems exist; these are classified primarily by mounting location.

5.8.1 Fuselage Mounted Systems

Due to the curvature of the nose section, a low pressure area is created which tends to become lower with increasing airspeed or decreasing C_L . The static source can be placed where the position error is small for the important phases of flight such as cruise and will remain relatively small for the entire performance envelope if the aircraft operates below the transonic range. This type of system is subject to sideslip errors. By cross manifolding static sources located on opposite sides of the aircraft nose, the error is minimized; however, the error is present and noticeable.

The system is extremely poor for transonic and supersonic operation. Because so many factors can affect the formation of shock waves on the fuselage, the error becomes erratic, nonrepeatable, and assumes gigantic proportions in the high supersonic regime.

5.8.2 Noseboom Systems

The static source lies in a high pressure area forward of the fuselage. The pressure tends to increase further with increasing airspeed up to Mach 1.0. The curves of both ΔM_{pc} versus M_{ic} and ΔV_{pc} versus ΔV_{ic} tend to generalize into a single curve below the critical Mach. Aircraft configuration changes, angles of attack, and sideslip up to approximately 15° do not affect the system. The various position errors, while large at high subsonic speeds, are consistent and repeatable throughout the flight envelope. The position errors drop to zero above Mach 1.0 and remain zero out to Mach number 2.0 to 2.5.

Because of its major advantages, the noseboom system is used on nearly all test aircraft throughout performance and flying qualities testing. It is the only system which can meet the accuracy and repeatability requirements of flight test work.

5.8.3 Wingboom Systems

A wingboom system has basically the same advantages as a noseboom system until shock waves are formed in the transonic area. The shock waves from the fuselage then impinge upon the static sources. This results in erratic and inconsistent errors from that speed into the supersonic range.

5.8.4 Compensated Systems

Pitot-static heads have been designed to create a local low pressure area in the vicinity of the static sources. Such a head can be milled to compensate almost exactly for the general high pressure region existing in the area of a nose mounted test boom. Position error below critical Mach can be brought almost to zero.

However, there are several disadvantages to such a system. In supersonic flight, where free stream conditions exist around the boom, the curved head creates a large built-in error which increases with increasing Mach. Further, the error does not generalize, but tends to exhibit altitude breakoffs at both subsonic and supersonic speeds. For these reasons, the system is normally unsuitable for flight test purposes, and its operational use in Mach 2 aircraft is somewhat suspect.

5.9 FREE AIR TEMPERATURE MEASUREMENT

Knowledge of the air temperature outside an aircraft in flight is essential to true airspeed measurement. Further, accurate temperature measurements are needed for engine control systems, fire control systems, and for accurate bomb release computations.

From the equations derived for flow stagnation conditions

$$\frac{T_T}{T} = 1 + \frac{\gamma - 1}{2} M^2 \quad (5.55)$$

If this equation is expressed in terms of true airspeed,

$$\frac{T_T}{T} = 1 + \frac{\gamma - 1}{2} \frac{V_t^2}{\gamma g R T} \quad (5.56)$$

These temperature relations were derived assuming adiabatic flow or no addition or loss of heat while bringing the flow to stagnation. Isentropic flow is not required. Therefore, Equations 5.55 and 5.56 are valid for supersonic and subsonic flows. If in fact the flow is not perfectly adiabatic, a recovery factor, K_t , is used to modify the kinetic term, and the relations are

$$\frac{T_T}{T} = 1 + \frac{K_t (\gamma - 1)}{2} M^2$$

$$\frac{T_T}{T} = 1 + \frac{K_t (\gamma - 1)}{2} \frac{V_t^2}{\gamma g R T}$$

If the subscripts are changed to show the case of an aircraft and the appropriate constants are used,

$$\frac{T_T}{T_a} = \frac{T_{ic}}{T_a} = 1 + \frac{K_t M^2}{5} \quad (5.57)$$

$$T_T = T_{ic} = T_a + \frac{K_t V_t^2}{7592} \quad (5.58)$$

Where

T_{ic} = indicated temperature corrected for instrument error in $^{\circ}\text{K}$

T_T = total temperature in $^{\circ}\text{K}$

T_a = free stream ambient temperature in $^{\circ}\text{K}$

V_t = true airspeed in knots.

The recovery factor, K_t , is the parameter most often used to indicate how closely the total temperature sensor actually observes the total temperature. The value of K_t varies from 0.7 to 1.0. For test systems a range of 0.95 to 1.0 is more common. There are a number of errors possible in a temperature indicating system. These may, in certain installations, cause the recovery

factor to vary with airspeed, but in the general case the recovery factor is a constant value. The following are the more significant errors:

1. Resistance - Temperature Calibration. In general, it is not possible to build a resistance temperature sensing element which exactly matches the prescribed resistance - temperature curve. A full calibration of each probe must be made, and the correction, ΔT_{ic} , must be applied to the data.
2. Conduction Error. It is difficult to make a clear separation between recovery errors and errors caused by heat flow from the temperature sensing element to the surrounding structure. This error can be reduced by insulating the probe. Performance data lead to the conclusion that this error is small.
3. Radiation Error. When the total temperature being measured is relatively high, heat is radiated from the sensing element, resulting in a reduced indication of temperature. This effect is increased at very high altitude. Radiation error is usually negligible for well-designed sensors when the Mach is less than 3.0 and the altitude below 40,000 feet.
4. Time Constant. The time constant is defined as the time required for a certain percentage of the response to an instantaneous change in temperature to be indicated on the instrument. When the temperature is not changing or is changing at an extremely slow rate, the time constant introduces no error. Practical application of a time constant in flight is extremely difficult because you must know the rate of change of temperature with respect to time. The practical solution is to use steady state testing.

Temperature indicating systems normally use resistance temperature sensing elements in which the electrical resistance of the element varies with temperature. A bridge balance system is used to show this resistance change on an indicator.

There are many probe designs. The guiding aim has been to reduce or eliminate errors due to conduction, radiation, and angles of attack or sideslip. Two examples are shown in Figures 5.18 and 5.19.

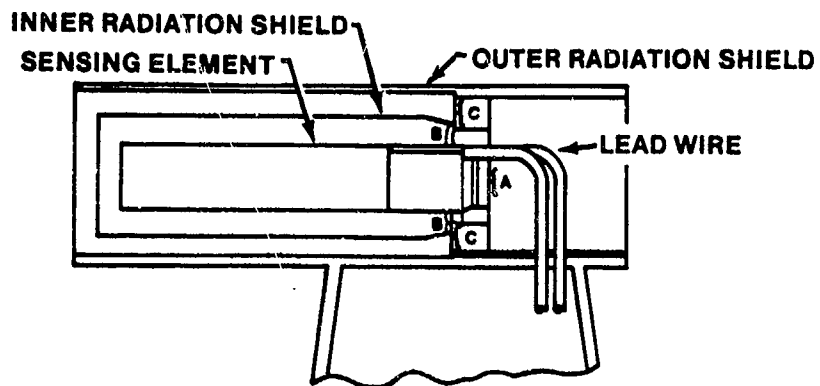


FIGURE 5.18. TOTAL TEMPERATURE SENSOR (NON DE-ICED)

- NOTE:
- A. Indicates the throat area for flow inside the sensing element.
 - B. Indicates the throat area for flow outside the sensing element.
 - C. Indicates the throat area for flow outside the inner shield.

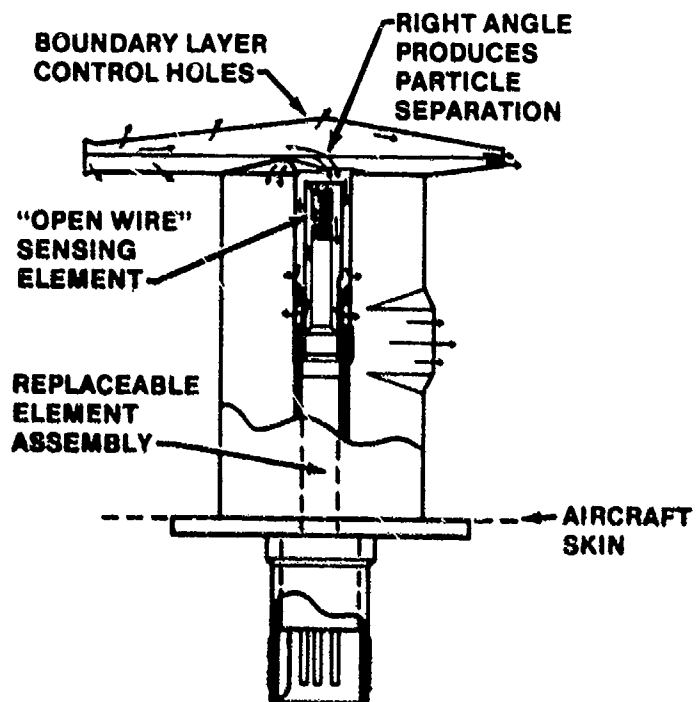


FIGURE 5.19. TOTAL TEMPERATURE SENSOR WITH BOUNDARY LAYER CONTROL

5.9.1 Determination of Temperature Probe Recovery Factor

The temperature recovery system has two errors which must be accounted for, instrument correction, ΔT_{ic} , and temperature recovery factor K_t . Although ΔT_{ic} is called instrument correction, it is more than that. It accounts for many system errors collectively from the indicator to the temperature probe. The ΔT_{ic} correction is obtained under controlled conditions with the entire system operating static, with a known temperature source.

The temperature recovery factor K_t is a measure of how adiabatic the temperature recovery process is (is heat added or lost?). A value of 1.0 for K_t is ideal, but values greater than 1.0 may be observed when heat is added to the sensors by conduction (hot material around the sensor) or radiation (exposure to direct sunlight) and vice versa. The test conditions must be selected to minimize this type of interference.

Normally temperature probe calibration can be done simultaneously with pitot-static calibration. Indicated temperature, instrument correction, aircraft true Mach, and an accurate ambient temperature are the necessary data. The ambient temperature may be obtained from a pacer aircraft, weather balloon, or tower thermometer. Accurate ambient temperature may be particularly difficult to obtain on a tower fly-by test because of steep temperature gradients near the surface and low sun angle early in the morning. Although turbulent air provides mixing and a better sample of ambient temperature to the tower thermometer, it is a poor set of conditions for position error calibration.

The temperature recovery factor at a given Mach may be computed by Equations 5.59 and 5.60.

$$T_{ic} = T_i + \Delta T_{ic} \quad (5.59)$$

$$K_t = \left(\frac{T_{ic}}{T_a} - 1 \right) \frac{5}{M^2} \quad (5.60)$$

The results for subsonic calibrations can be plotted as $(T_{ic}/T_a - 1)$ versus $M^2/5$, and the points should fall on a straight line that goes through zero. The slope of the line is K_t as illustrated in Figure 5.20.

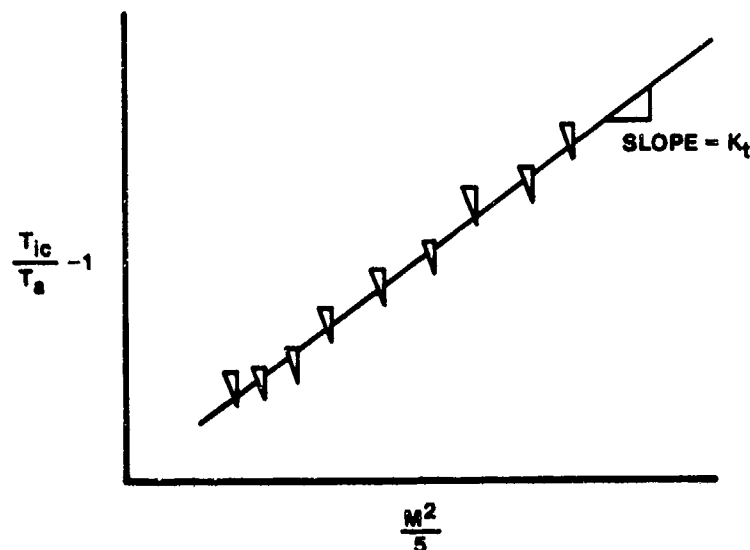


FIGURE 5.20. SUBSONIC TEMPERATURE RECOVERY FACTOR K_t

Temperature recovery factor may be dependent upon Mach at high Mach. A method of presenting the results of tests over a wide range of Mach is shown in Figure 5.21.

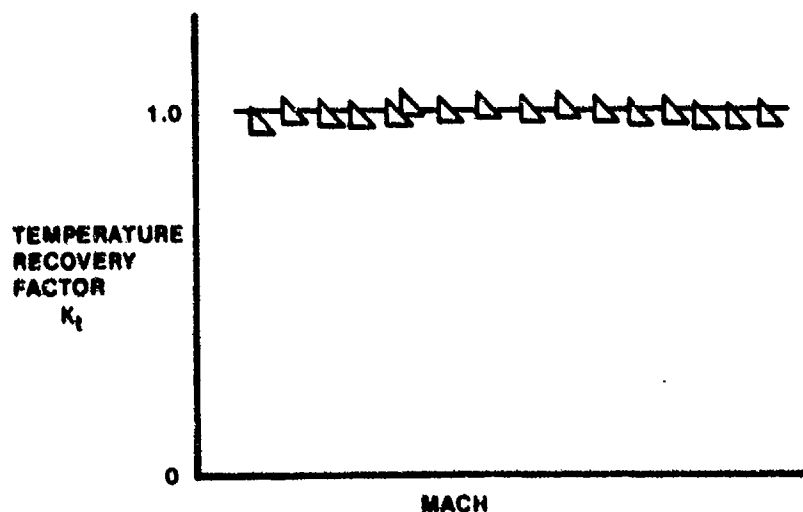


FIGURE 5.21. TEMPERATURE RECOVERY FACTOR VERSUS MACH

5.10 PITOT-STATIC CALIBRATION TESTS

The initial step in any flight test is to measure the pressure and density of the atmosphere and the velocity of the vehicle at the particular time of the test. There are restrictions in the current state-of-the-art as to what can be accurately measured (for example, density cannot be determined from a direct reading instrument), and there are inaccuracies within each measuring system which must be determined and corrected for.

The importance of this phase of flight testing should not be underestimated. Failure to correct properly for pitot-static and temperature errors will render worthless all performance data and most stability and control data as well. For this reason, calibration tests of the pitot-static and temperature systems comprise the first flights in any test program.

The objective of any pitot-static calibration test is to determine position error, usually in the form of altimeter position error correction ΔH_{pc} . The test is designed to produce an accurate calibrated altitude H_c , velocity V_c , or Mach M for the test aircraft. As covered previously, position error is most sensitive to Mach, configuration, and perhaps angle of attack depending upon the type of static source. The test method should be chosen to take advantage of the capability of the instrumentation. Altimeter position error correction ΔH_{pc} is usually evaluated because H_c is fairly easy to determine, and the error can be read more accurately on the altimeter. For example, at 2,300 feet and 400 knots an altimeter position error correction of 100 feet corresponds to approximately two knots of correction in airspeed and a four thousandths correction to Mach. Once position error is determined in one form, the remaining forms may be calculated because the position error coefficient has been determined.

5.10.1 The Tower Fly-by Test

The tower fly-by produces a fairly accurate calibrated altitude, H_c , by triangulation. The aircraft is sighted through a theodolite, as shown in Figure 5.22, and the reading is recorded along with tower pressure altitude on each pass.

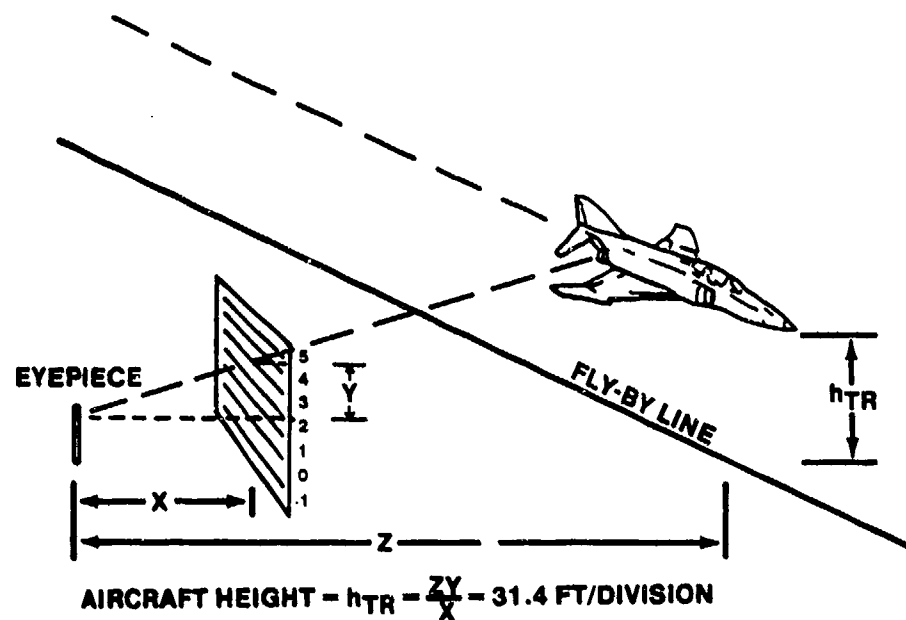


FIGURE 5.22. THE TOWER FLY-BY LINE

The calibrated altitude of the aircraft is the sum of the pressure altitude of the theodolite at the time the point was flown plus the altitude above the theodolite as determined by triangulation.

$$H_{C_{\text{Test Aircraft}}} = H_{C_{\text{Tower}}} + H_{\text{Theodolite Reading}} \quad (5.61)$$

In the Edwards fly-by tower the aircraft is 31.4 feet per theodolite division above the reference line.

Although the tower fly-by method is simple, accurate, and requires no sophisticated equipment, it has some disadvantages. It does not produce an accurate calibrated velocity (V_C), it is limited to subsonic flight, and angle of attack changes due to decreasing gross weight may affect the data. Angle of attack effects are most prevalent at low speeds, and all low speed points

should be flown as close to the same gross weight as possible. Passes should be made at least one wing span above the ground to remain out of ground effect.

5.10.2 The Pacer Test

The pacer calibration is flown in formation with another aircraft whose instrument and position error calibrations are known. The test aircraft may be lead or wing, and the formation is flown with the aircraft level with and abreast of each other so neither aircraft is disturbed by the other's pressure pattern. Half a wing span between aircraft is minimum spacing.

The pacer aircraft provides the test aircraft with calibrated altitude H_c and calibrated airspeed V_c at each test point. This method of calibration takes less flight time and can cover any altitude and airspeed as long as the two aircraft are compatible. Angle of attack effects may be eliminated by flying a range of airspeeds at a constant nw/δ . Normally angle of attack effects within several hundred feet of the test altitude are small enough that calibrations may be done at a constant altitude rather than a constant nw/δ . In any case, the results of the test are usually presented as position error correction for various altitudes rather than the various nw/δ 's in the final report.

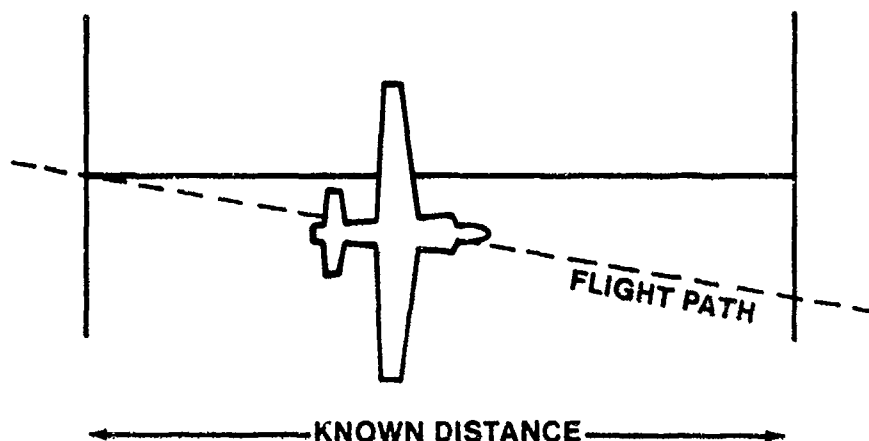
Data cards should be made out the same for both aircraft including H_1 , V_1 , T_1 , fuel, and time. A preflight ground block should be taken to check the instruments and verify the serial numbers for instrument corrections, but the ground block is not needed for data reduction.

5.10.3 The Speed Course

The speed course method produces accurate true airspeed V_T by flying reciprocal headings along a course of known length. The speed course may vary in sophistication from low and slow along a runway or similarly marked course to high and fast when speed is computed by radar or optical tracking. Mach is computed from true airspeed and temperature and compared to instrument corrected Mach M_{ic} to determine Mach position error AM_{pc} .

As shown in Figure 5.23, the course is flown in both directions at the same indicated airspeed with the heading held parallel to the course. The aircraft is allowed to drift with the wind. Time from start to finish is used

to compute speed for each direction, and the speed (not the time) is averaged for true airspeed. The wind is assumed to remain constant for both passes. The data to be recorded for each pass include H_i , V_i , T_i , fuel, and course time. Indicated airspeed is the most important parameter to hold constant, and good results depend heavily on accurate ambient temperature.



NOTE: Edwards speed course is marked in statute miles, not nautical miles.

FIGURE 5.23. SPEED COURSE

5.10.4 Radar Method

The radar method is used for calibrations at airspeeds unsuitable for tower fly-by or pacer techniques (i.e., transonic and supersonic speeds). The procedure requires an accurate radar-theodolite system and a pacer aircraft. If a pacer is unavailable, then the position error of the test aircraft must be known for one value of airspeed at the test altitude. Pitot-static calibration using radar is usually done in conjunction with the pace calibration during TPS missions.

An important aspect of this method is the pressure survey required before the test calibration can be done. To do this, the pace aircraft flies at

constant airspeed and altitude through the air mass to be used by the test aircraft. The radar continuously measures the pacer's tapeline altitude from start to finish of the survey. Since the altimeter position error of the pacer is known, the actual pressure altitude flown is known. The pressure altitude of the test aircraft is then simply the tapeline difference between the test and pace aircraft corrected for non-standard temperature.

$$H_{C_t} = H_{C_{pace}} + \left(H_{R_t} - H_{R_{pace}} \right) \frac{T_{as}}{T_{at}} \quad (5.62)$$

The tracking radar used at the Flight Test Center is accurate to approximately ten feet, but H_R varies with the divergence of the lapse rate from standard day conditions.

As soon as possible after completion of the pressure survey, the test aircraft follows the pacer aircraft through the airmass along the same ground track. A tracking beacon is required in the test aircraft both for accurate radar ranging and to allow ground controllers to provide course corrections when necessary. A typical tracking plot is shown in Figure 5.24.

Because this method is used for transonic and supersonic portions of the calibration test, an accurate time correlation is necessary to properly relate radar data to aircraft instrumentation data.

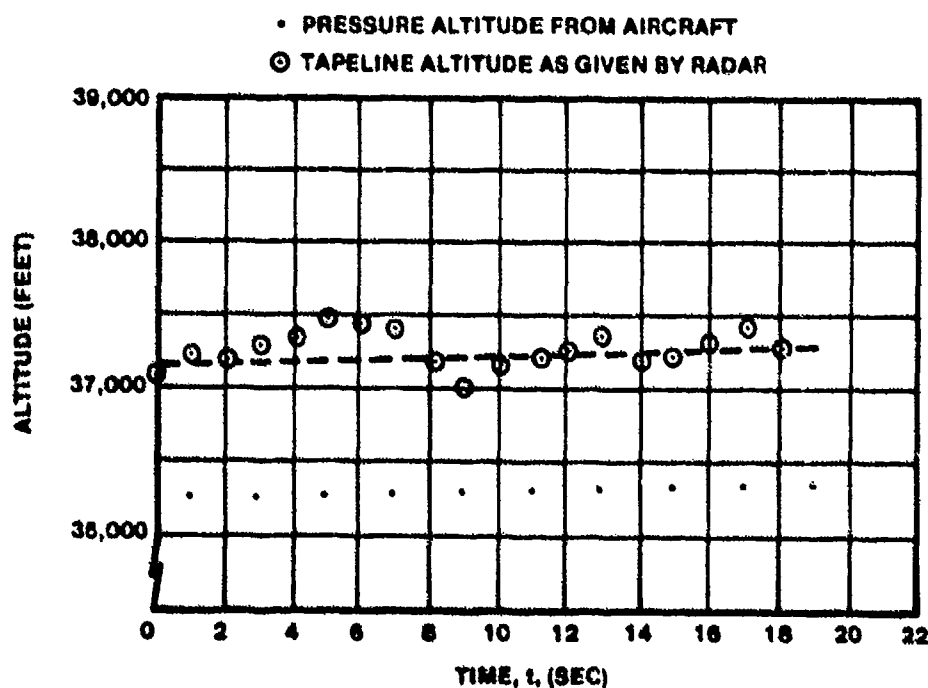


FIGURE 5.24. RADAR TRACKING TIME HISTORY OF PACE PRESSURE SURVEY

5.10.5 Smoke Trail Method

The smoke trail method requires a smoke-laying pacer aircraft. Rather than flight in formation, the pacer lays a smoke trail at the test altitude at a Mach where its position error is well defined. The test aircraft then completes a series of level accelerations and decelerations along the smoke trail where calibrated altitude can be calculated accurately. The method is particularly well suited for testing in the transonic and supersonic range, and large amounts of data can be recorded when photopanel or onboard recorders are used. Figure 5.25 is an illustration of a combined radar/smoke trail method.

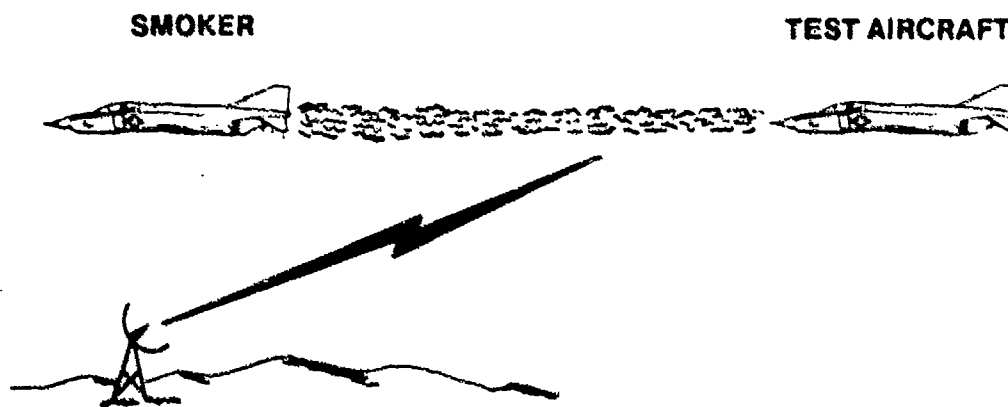


FIGURE 5.25. RADAR/SMOKE TRAIL METHOD

5.10.6 Trailing Bomb Method

The aircraft static pressure P_s is compared directly with the static pressure P_a measured by a static source on a bomb shaped body suspended on a long length of pressure tubing below the aircraft. The trailing bomb, like the aircraft, may have a static source error. This error is usually determined by calibration in a wind tunnel.

The length of tubing required to place the bomb in a region where local static pressure approximates free stream pressure is at least 2x the aircraft wing span. Since the bomb is below the aircraft, the static pressure is higher, but the pressure lapse in the tubing is the same as the free stream atmospheric pressure lapse. Thus if the static source in the bomb is attached to an altimeter next to the aircraft, it will indicate free stream pressure at altimeter level.

Accuracy depends upon the calibration of the bomb and the accuracy of the pressure gauge or altimeter used to read the trailing bomb's static pressure. Stability of the bomb at speeds above .5 Mach must also be considered.

Figure 5.26 illustrates a typical trailing bomb.

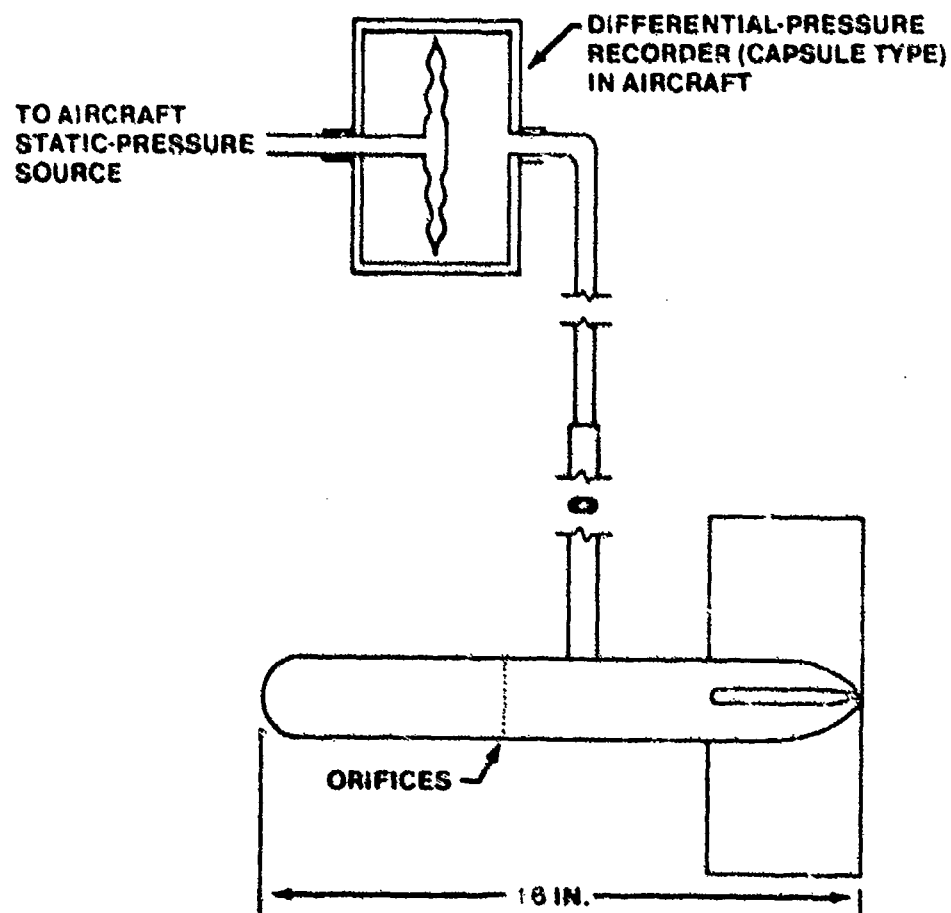


FIGURE 5.26. TYPICAL TRAILING BOMB

5.10.7 Trailing Cone Method

With the trailing cone method, the aircraft's static pressure P_s is compared to the static pressure P_a measured by a static source trailing behind the aircraft. A light weight cone is attached to the tube to stabilize it and keep the pressure tube taut. A schematic of a trailing cone is shown below.

The accuracy depends on the location of the static ports which should be at least six diameters ahead of the cone. The distance behind the aircraft is also important. Due to the uncertainties involved, the trailing cone has been used as a secondary calibration method. The aircraft's pitot-static instruments are calibrated with the trailing cone in place by tower fly-by or pace methods. These results are used to calibrate the cone installation. The cone can be used with good results as a recalibration check of that aircraft's instruments or primary calibration of aircraft of the same model. A typical trailing cone is shown in Figure 5.27.

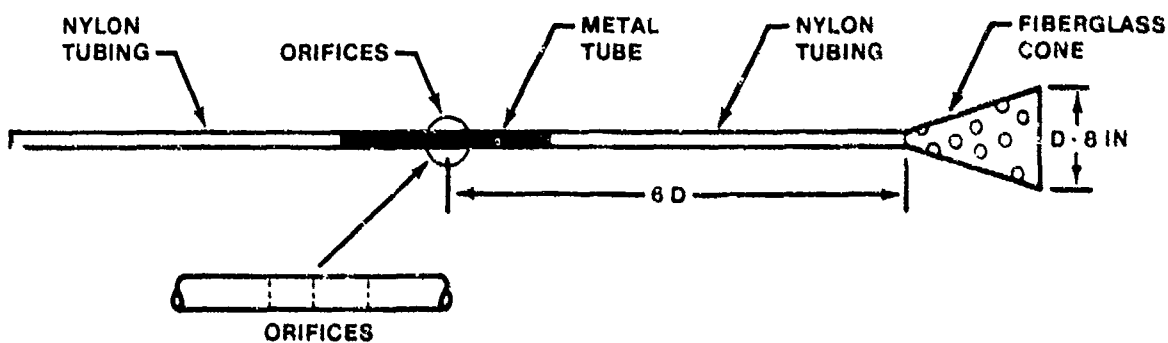


FIGURE 5.27. TYPICAL TRAILING CONE

5.10.8 Data Cards

One particularly important part of planning for any flight test is the in-flight data card. It should be set up to be a maximum help to the crew during the flight and should emphasize the most sensitive flight parameters. For convenience, the data reduction inputs for a computer program should also match the order of test point parameters. Most of the machine-reduced data inputs for performance calibrations are in the following order: H_i , V_i , T_i , fuel, time. An additional parameter such as RPM or fuel flow may be added for some flights. A sample tower fly-by data card is shown in Figure 5.28.

STUDENT FLIGHT RECORD		DATE 5 MAR 75	
NAME OF STUDENT JONES	NAME OF INSTRUCTOR SMITH		
PLANE 205 T-38	TYPE TOWER FLYBY		
WEIGHT CLEAN TO GROSS WT:			
WING AREA 1500	WING SPAN 30	WING LOADING 150	WING AREA 1500
WING AREA 1500	WING SPAN 30	WING LOADING 150	WING AREA 1500
POINT	ALT	H_i	V_i
1			
2			
3			
4			
5			
6			
7			
8			
9			
10			
ALT TIME FUEL PRESSURE ALTITUDE FUEL FLOW RPM FUEL FLOW RPM			

STUDENT FLIGHT RECORD		DATE 5 MAR 75	
NAME OF STUDENT JONES	NAME OF INSTRUCTOR SMITH		
PLANE 205 T-38	TYPE TOWER FLYBY		
WEIGHT TOWER DATA			
WING AREA 1500	WING SPAN 30	WING LOADING 150	WING AREA 1500
WING AREA 1500	WING SPAN 30	WING LOADING 150	WING AREA 1500
POINT	ALT	H_i	V_i
1			
2			
3			
4			
5			
6			
7			
8			
9			
10			
ALT TIME FUEL PRESSURE ALTITUDE FUEL FLOW RPM FUEL FLOW RPM			

FIGURE 5.28. TOWER FLY-BY DATA CARDS

H_i is read first because it is the most critical parameter, and the other parameters are listed in order of decreasing sensitivity. The tower operator's data card should include the tower elevation and the same point numbers and V_{aim} with columns for theodolite reading, time, and perhaps tower pressure altitude. The time entry allows correlation between tower and flight data points while the pressure altitude entry verifies the trend of pressure altitude. Space should also be included on both cards for repeated or

additional data points. Well prepared data cards add to the convenience and execution of the mission and the accuracy of the measurements.

5.10.9 Techniques

There are a few important tips on flying technique during pitot-static calibration flights. During stabilized points, the aircraft should be coordinated, and altitude and angle of attack should be held as steady as possible. Pitch bobbling or sideslip may induce error, so resist making a last-second correction. A slight climb or descent may cause the pilot to read the wrong altitude, particularly if there is any delay in reading the instrument. If altimeter position error is being evaluated, then read the altimeter first. A slight error in the airspeed reading will not have much effect. Make sure all ground blocks and in-flight data are read with 29.92 set in the kollsman window.

PROBLEMS

5.1 This problem is designed to introduce you to the US Standard Atmosphere model, some of the associated constants, and the perfect gas law.

GIVEN:

Density $0.74591102 \text{ kg m}^{-3}$ $1\text{m} = 3.281 \text{ ft}$
Ambient Temperature 1.94°F $1\text{kg} = 2.205 \text{ lb}$

FIND:

1. Ambient temperature $^\circ\text{K}$
2. Density in lbm ft^{-3}
3. Density in slugs ft^{-3}
4. Ambient pressure lbs ft^{-2}
5. Ambient pressure in Hg
6. Are these standard conditions?
7. If so, what altitude?

5.2 This problem is designed to introduce you to the altimeter equation and its various forms.

GIVEN:

$P_a = 10.0 \text{ in Hg}$

FIND:

1. H_c in ft
2. What is standard T_a ($^\circ\text{C}$) for this altitude?

GIVEN:

$H_c = 39,020 \text{ ft}$

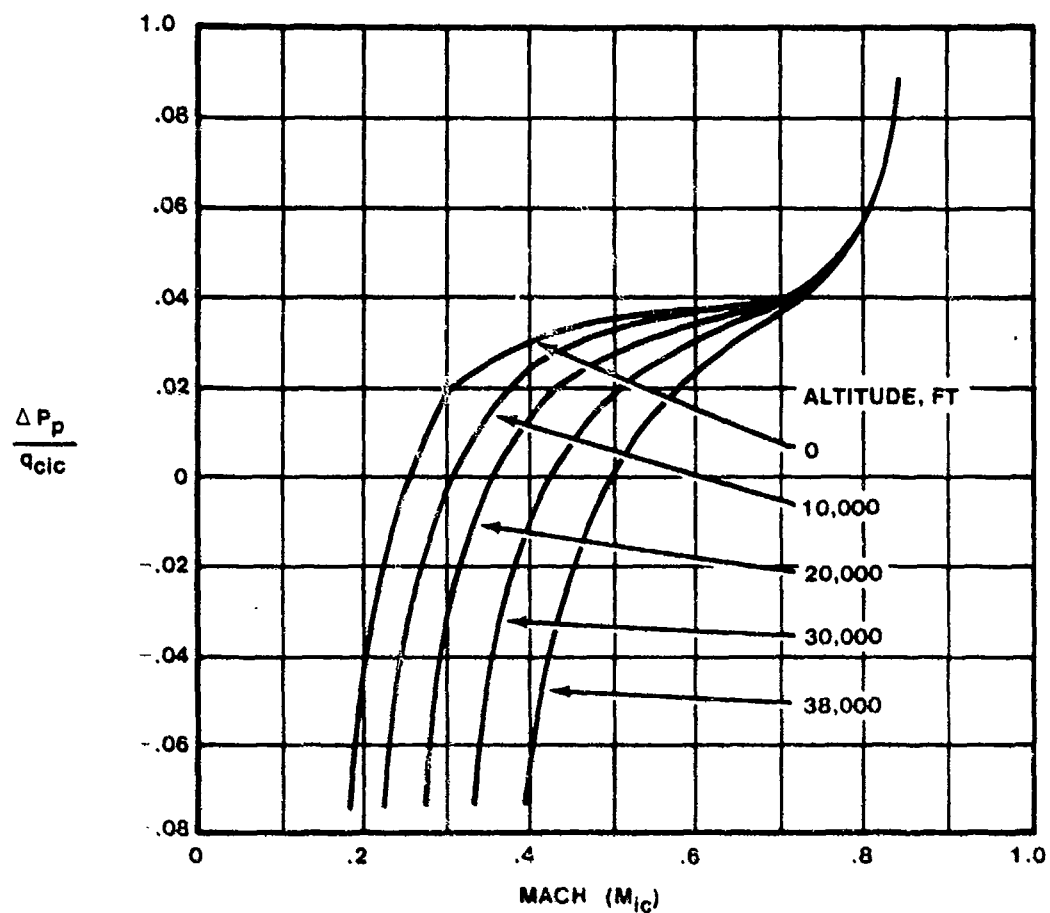
FIND:

3. P_a in Hg and lbf ft^{-2}
 4. $H_c = f(\quad)$. $P_a = f(\quad)$
 5. Does temperature affect the relationship between
 - a. H_c and P_a ?
 - b. h and P_a ?
 6. What does hotter than standard do to the pressure lapse rate?
- 5.3 This is an example in the use of the airspeed equation as it applies to the airspeed indicator, Mach, and equivalent airspeed.
1. Find the correction factor to correct ΔH_c to Δh as a function of G and Temp.
 2. GIVEN:
 $T_a = 220^\circ\text{K}$ $H_c = 43,320 \text{ ft}$ $P_T = 7.0 \text{ in Hg}$
 - a. Find δ and P_a (in Hg)
 - b. Find q_c (in Hg). In words q_c is "_____."
 - c. Find a (in ft/sec and kts). $a = f(\quad)$ or $f(\quad)$.
 - d. Find V_T (in ft/sec and kts). $V_T = f(\quad)$.
 - e. Find V_c (kts). $V_c = f(\quad)$, $q_c = f(\quad)$.
 - f. Find V_e (kts). $V_e = f(\quad)$.
 - g. Find Mach $M = V_T/a$
 3. $V_c = 800 \text{ kts}$. Find q_c (in Hg).

5.4 Given an airplane trimmed in level flight

$$\begin{array}{ll} T_a = 248^\circ\text{K} & V_t = 368 \text{ kts} \\ H_c = 19,950 & T_{ic} = -7.8^\circ\text{C} \end{array}$$

Find a , M , V_e , and K_t (Temperature recovery factor)



Variation of static-pressure error of a wing mounted boom

5.5 Find: ΔH_{pc} , ΔV_{pc} , and ΔM_{pc} for an aircraft at 10,000 ft, M_{ic} 0.5, and standard day.

5.6 Reduce pitot-static tower fly-by data. Refer to instrument corrections listed.

Ground Block Data

Ramp Elevation 2303.4

0700 $H_i = 2210$

$\Delta H_{ic} = -22'$

0830 $H_i = 2270$

$\Delta V_{ic} = 0.2$

Tower Data

Theodolite Elevation = 2305.5

0730 TR = 2.5

$T_a = 22.8^\circ\text{C}$

A/C Data 300 kts = V_{AIM}

$$H_i = 2305 \text{ ft}$$

$$V_i = 302 \text{ kts}$$

Find H_c , H_{ic} , ΔH_{pc} , $\Delta P/P_s$, ΔV_{pc} , ΔM_{pc}

5.7 This problem is an exercise in position error data reduction.

Pacer

Pacer data

$$H_i = 19,950 \qquad \Delta H_{ic} = -30$$

$$V_i = 329 \qquad \Delta V_{ic} = -3$$

Coefficients for pacer position error are 58, -317, 884, 0, 0, 0

FIND: H_c

Test aircraft data

$$H_i = 20,100 \qquad \Delta H_{ic} = -30$$

$$V_i = 326 \qquad \Delta V_{ic} = -1.5$$

Find test H_{ic} , V_{ic} , M_{ic} , and ΔH_{pc}

Find 20,000 H_{ic} , V_{ic} , M_{ic} , and ΔH_{pc}

5.8 This problem is designed to introduce you to the TPS Pitot-Statics Computer Program. After working this problem, you should be able to reduce your tower fly-by, pacer, and radar data. Using the data below determine:

a. ΔH_{pc} vs V_{ic} and M_{ic}

(extrapolate this data to 10,000', 20,000', 30,000', and 40,000')

b. ΔV_{pc} vs V_{ic}

c. ΔM_{pc} vs M_{ic}

d. $\Delta P/q_{cic}$ vs M_{ic}

e. $(T_{ic}/T_a - 1)$ vs $M^2/5$

Tower Fly-by Data

Pilot - J. Goldenarm

Data - Today's Date

Ramp Gross Wt - 12,019#

Data Source - Cockpit

Fuel Source - 3790

A/C - T38 S/N - 63-135

Instrument Serial Numbers - Use current S/N's

Ground Blocks:	TOD	H _i
	08:20	2170
	09:50	2150

Point	H _i	V _i	T _i	Fuel	TOD	TR	T _a (°C)
1	2150	301	34	3200	08:43	2.5	21
2	2170	349	40	2850	08:49	4.5	22
3	2120	404	45	2600	08:54	4.5	23
4	2020	497	60	2300	08:59	5.0	24
5	1860	587	75	1900	09:03	4.5	25

Pacer Data - 20,000' PA

(Test aircraft is same as in Part 2.)

Pace Aircraft - RF-4C S/N 850

Data Source - Cockpit

Instrument Serial Numbers - Use current S/N's

Test and Pace A/C temperature - Indicated

Using the data below:

- Plot ΔH_{pc} vs V_{ic} and compare to extrapolated TFB data from Part 2.
- Plot ΔV_{pc} and $V_c - V_{ic}$ vs V_{ic} and compare.
- Plot ΔM_{pc} vs M_{ic} and compare to 2300' TFB data.
- Plot $(T_{ic}/T_a - 1)$ vs $M^2/5$ for both methods and compute new K factor.

DATA

Points	H_i	V_i	T_i	Fuel	PH_i	PV_i	PT_i
1	19,990	201	-15	2580	20,400	202	-15
2	20,020	246	-10	2400	20,100	248	-10
3	19,860	295	- 5	2380	20,000	297	- 5
4	19,820	348	3	2300	20,070	352	3
5	19,760	396	11	2230	20,090	400	11
6	19,790	444	19	2170	20,050	446	19

Radar Data - 20,000'

(Same test aircraft as in Parts 2 and 3.)

Pacer Data:

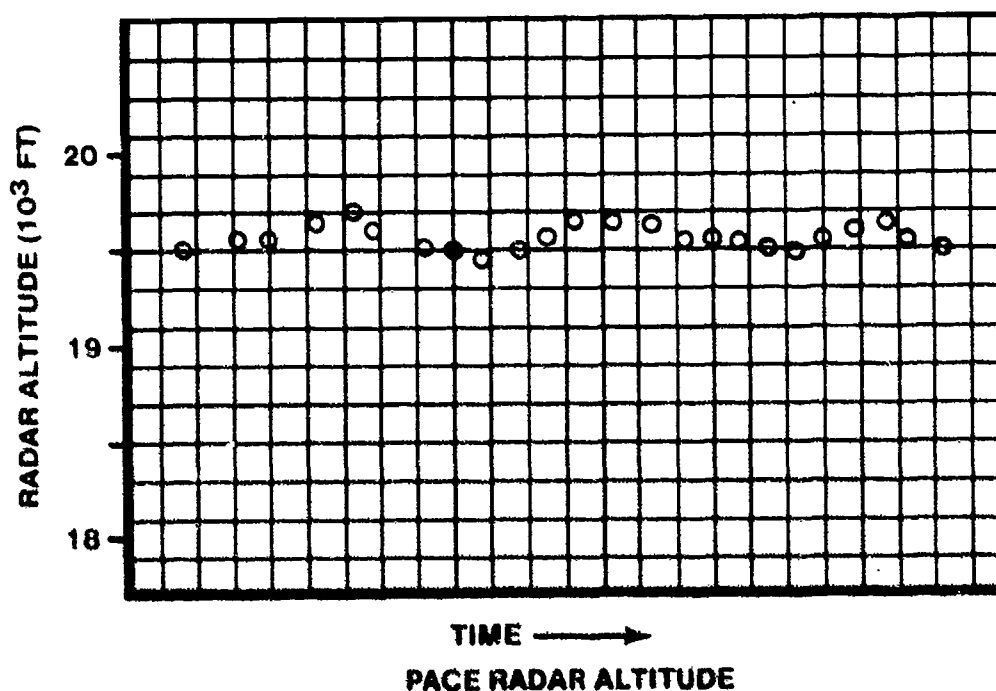
$$\bar{H}_i = 20,000' \quad \bar{V}_i = 300 \quad \bar{T}_{amb} = -4.6^{\circ}\text{C}$$

Test Aircraft Data:

<u>Points</u>	\bar{H}_i	\bar{V}_i	Radar Alt
1	19915	351	19700
2	19770	390	19612
3	19870	440	19822
4	20070	451	20045
5	19740	463	20272
6	20090	471	20288
7	20810	479	20375
8	21490	490	21131
9	21540	511	21328
10	21890	525	21737

From the data determine:

- a. ΔH_{pc} versus M_{ic} and compare to PACE data from Part 3.
- b. $\Delta P_p/q_{cic}$ and plot along with TFB and PACE data to determine MIL SPEC compliance.



5. Redo Part 4a using the Standard value of T_{amb} at 20,000. Note the change in ΔH_{pc} due to (1) nonstandard temperature and (2) climbing 2000' during the Mach run.

ANSWERS TO PITOT-STATIC PROBLEMS

- 5.1 1. $^{\circ}\text{K} = 256.45^{\circ}$
2. $\rho = 0.0465 \text{ lbm/ft}^3$
3. $\rho = 0.001447 \text{ slugs/ft}^3$
4. $P_a = 1146.6 \text{ lb/ft}^2$
5. $P_a = 16.21 \text{ in Hg}$
6. Yes
7. 16,000 ft
- 5.2 1. $H_c = 27,375 \text{ geo. ft}$
2. $T_a = 233.91^{\circ}\text{K} = -39.23^{\circ}\text{C}$
3. $P_a = 5.805 \text{ in Hg} = 410.6 \text{ lb/ft}^2$
- 5.3 1. $\Delta h = \frac{G}{g} \frac{T_a}{T_{a_s}} \Delta H_c$
2a. $\delta = 0.15778, P_a = 4.72 \text{ in Hg}$
b. $q_c = 2.28 \text{ in Hg}$
c. $a = 975.5 \text{ ft/sec} = 577.2 \text{ kts}$
d. $V_T = 753 \text{ ft/sec} = 445.6 \text{ kts}$
e. $V_c = 215.4 \text{ kts}$
f. $V_e = 204.1 \text{ kts}$
g. $M = 0.772$
3. $q_c = 42.94 \text{ in Hg}$
- 5.4 $a = 613.6 \text{ kts}, M = 0.60, V_e = 196.4 \text{ kts}, K_t = 0.972$
- 5.5 $\Delta H_{pc} = 153.6 \text{ ft}, \Delta V_{pc} = 4.24 \text{ kts}, \Delta M_{pc} = 0.0089$

$$5.6 \quad H_c = 2285.3 \text{ ft}, H_{ic} = 2283 \text{ ft}, \Delta H_{pc} = 2.3 \text{ ft}, \Delta P_p/P_s = 8.44 \times 10^{-5},$$

$$\Delta V_{pc} = 0.0776 \text{ kts}, \Delta M_{pc} = 1.326 \times 10^{-4}$$

$$5.7 \quad H_c = 20,155.6 \text{ geo ft.}$$

For test aircraft:

$$H_{ic} = 20,070 \text{ geo ft.}$$

$$V_{ic_t} = 324.5$$

$$M_{ic_t} = 0.7025$$

$$\Delta H_{pc_t} = 85.6$$

For 20,000:

$$\Delta H_{pc_{t20,000}} = 85.7$$

$$H_{ic_{20,000}} = 19914.3$$

$$V_{ic_{20,000}} = 324.9$$

$$M_{ic_{20,000}} = M_{ic_t}$$

BIBLIOGRAPHY

- 5.1 Dommasch, D.O., Sherry, S.S., and Connolly, T.F., Airplane Aerodynamics, New York: Pitman Publishing Corporation, 1967.
- 5.2 Flight Test Manual, Vol. 1, Advisory Group for Aeronautical Research and Development North Atlantic Treaty Organization. Oxford: Pergamon Press, 1962.
- 5.3 Hendrix, Frazier, Godwin, and Durnin, Performance Flight Testing Theory, FTC-TIH-64-2005, Air Force Flight Test Center, December, 1965, UNCLASSIFIED.
- 5.4 Herrington, Shoemaker, Bartlett, and Dunlap, Flight Test Engineering Handbook. FTC-TR-6273, Air Force Flight Test Center, January 1966, UNCLASSIFIED.
- 5.5 Rosemount Engineering Company, Electrical and Temperature Instruments, Bulletin 7637.

CHAPTER 6
SUPERSONIC AERODYNAMICS

6.1 INTRODUCTION

Some of the basic concepts of Aerodynamics and Thermodynamics have previously been covered. These related to determination of the fluid flow around various shapes and the resultant forces acting upon the shapes. Fluids previously studied were assumed to be incompressible. This assumption reduced the number of variables involved and allowed relatively simple solutions to previously complex sets of equations. (This is an everyday activity of the engineer, but care must be taken to make sure the assumptions made to provide an idealized solution to a physical system are still valid if the idealized solution is applied to a different physical system.)

Incompressible flow is a myth. However, for low speed air ($M < 0.3$) the idealized incompressible flow solution was accurate enough. This was the case for aerodynamics up to the late 1930's. But as speed increased, so did the requirements for new idealized solutions to physical systems using different assumptions. In this chapter, the assumption of incompressible flow will be dropped, and the flow field will be considered compressible. Results obtained from the study of compressible fluids will then be applied to transonic and supersonic flow situations.

6.2 TYPES OF IDEAL GASES

A real gas is a compressible, viscous, elastic, nonhomogeneous, and chemically active fluid, and the physical principles governing its behavior are not understood completely enough to permit the exact mathematical formulation of a general flow problem. Even if it were possible, the resulting equations would defy solution. Utilizing reasonable assumptions which can be verified by experiment, specific physical systems can be described by equation, and the necessary properties determined.

The use of three different, idealized fluids has been found acceptable for solving fluid dynamic problems involving subsonic, transonic, and supersonic flows. In each idealized fluid, the fluid is assumed to be homogeneous and non-chemically reacting. The assumption of a homogeneous fluid is acceptable until the mean free path between gas molecules becomes a significant fraction of the size of the object being studied. The assumption

of a non-chemically reacting gas is good up to fairly significant temperatures.

A perfect fluid is one which is incompressible, inelastic, and non-viscous. The perfect fluid assumption gives reasonable results when analyzing flow outside of a boundary layer at less than $M = 0.7$.

An incompressible, inelastic viscous fluid differs from a perfect fluid because of viscosity. This fluid assumption gives reasonable results for flow at less than $M = 0.7$ inside a boundary layer and in wakes behind an object.

A compressible, nonviscous, elastic fluid will be used in this chapter. This fluid assumption provides reasonable results for flow outside of the boundary layer up to hypersonic speeds ($Mach \approx 5.0$). Elasticity is defined as the change in pressure per unit change in specific volume and accounts for the finite propagation of a sound wave.

Analysis of a viscous, compressible fluid is very complex and relies heavily on experimental evidence for confirmation of the theory. Hypersonic flow requires the consideration of a viscous, compressible, nonhomogeneous dissociated, and chemically active fluid. It can be seen that the complexity of this analysis is much greater than subsonic and supersonic flow analysis.

6.3 AERODYNAMIC CONSIDERATION OF COMPRESSIBLE FLOW

Aerodynamics is concerned with the changes in pressure that occur over bodies of various sizes and shapes and the causes and effects of these changes. A large part of early aerodynamic research was based on the assumption of a nonviscous, inelastic, incompressible fluid. The assumption of incompressible, inelastic flow was acceptable at low speeds where a small change in pressure caused virtually no change in the density of the fluid. The assumption of a nonviscous fluid was acceptable as long as the viscous effects were restricted to the vicinity of the surface (in the boundary layer).

With the advent of high speed flight, these assumptions had to be reconsidered. The inelastic flow assumption implies that pressure variations are instantaneously felt everywhere in the fluid. In reality, they are transmitted at a finite speed, the speed of sound.

As the velocity of an aircraft approaches some sizeable fraction of the

speed of sound (one half or more), the results obtained from incompressible flow relations are found to be significantly in error due to the effects of compressibility.

Viscous effects and boundary layers can be omitted from this discussion by studying the flow on an object outside of the boundary layer.

Flow is defined as being compressible when a change in pressure is accompanied by a change in density, and the amount of compressibility depends on the velocity of the fluid flow. All gaseous flow is compressible, and even the so-called incompressible flow experiences some degree of compression. In the incompressible case, the velocity is so low that the change in density is insignificant compared to the change in pressure.

The introduction of a new variable, density, in aerodynamic problems requires the introduction of an equation of state and other thermodynamic relations to describe the changes in pressure, density, and temperature. The study of compressible flow combines the science of fluid mechanics and thermodynamics.

The general solution of a compressible flow problem consists of finding three unknown velocity components and three density and pressure changes with respect to the space coordinates x , y , and z . The mathematical complexity of this solution obscures many of the fundamental concepts of compressible flow which are quite clear when the flow is analyzed in one or two dimensions. In this chapter, fluid flow equations will be developed for one-dimensional flow, and then modification necessary to use the equations for two-dimensional flow will be discussed.

6.4 ONE-DIMENSIONAL FLOW APPROXIMATION

One-dimensional flow generally implies straight line or linear motion; however, it need not be this restrictive. The equations of "one-dimensional" fluid flow can apply to flow through a passage in which the cross-section varies slowly so that components of velocity normal to the primary direction of flow can be considered negligible. For instance, flow in a curved channel can be considered one-dimensional as long as the radius of curvature is large compared to the length of the segment of channel that is under consideration. The channel need not be constant in area as long as the divergence or con-

vergence is small compared with the distance along the channel.

The channel may either be bounded by physical boundaries such as the walls of a pipe or wind tunnel or by streamlines such as those surrounding an airfoil in flight.

The compressible flow equations which relate the flow velocity to the pressure, temperature, and density are obtained from three fundamental conservation principles and the equation of state for the fluid in question.

1. Conservation of Mass
2. Conservation of Momentum
3. Conservation of Energy
4. Equation of State

The assumptions that are made when first developing the compressible flow relations are: the flow is steady, one-dimensional, nonviscous, adiabatic, and the fluid conforms to the equation of state for a perfect gas. As restrictive as these assumptions may seem, they do not seriously limit the validity of the resulting equations.

The one-dimensional assumption can be extended to other than linear motion with certain restrictions, and viscosity can be ignored when flow is examined outside of a boundary layer. The adiabatic assumption can be justified by the fact that the temperature gradients, which are the driving potential for the transfer of heat in a flow, are small, causing the heat transfer, dq , to be small or negligible. The perfect gas assumption is good for air up to moderately high temperatures.

Under these assumptions, the conservation equations and equation of state may be written

Conservation of Mass: (Continuity Equation)

$$\dot{m} = \rho VA = \text{constant} \quad (6.1)$$

Applying the product rule of differentials and dividing by ρVA gives

$$\frac{dp}{\rho} + \frac{dV}{V} + \frac{dA}{A} = 0 \quad (6.2)$$

Conservation of Momentum: (Momentum Equation)

$$dP + \rho V dV = 0 \quad (6.3)$$

Conservation of Energy: (First Law of Thermodynamics)

$$dQ - dw = dE \quad (6.4)$$

Equation of State: (Thermally Perfect Gas)

$$P = \rho R T \quad (6.5)$$

Before deriving the compressible flow equations, the concepts of total properties, speed of sound, Mach, and sound wave propagation must be studied in detail.

The speed of sound is a fundamental parameter in compressible flow theory and is the speed at which small disturbances (sound waves) propagate through a compressible fluid.

Mach is the most important parameter in compressible flow theory, since it compares the speed of sound in a fluid (a significant measure of compressibility effects) and the speed at which the fluid is flowing.

6.5 TOTAL (STAGNATION) PROPERTIES

Temperature, density, and pressure are normally thought of as static properties of a gas. Since we will be dealing entirely with a flowing gas, it becomes convenient to define a new temperature, density, and pressure to include a velocity component. We will find that not only does it simplify calculation, but, under certain conditions, it is more convenient to measure the total values of temperature, density, and pressure than the static values and velocities.

6.5.1 Total Temperature

Consider the restricted steady flow energy equation from Derivation F.4 in Appendix F.

$$h + \frac{V^2}{2} = \text{constant}$$

The kinetic energy term may be combined with enthalpy to form a new term, total enthalpy, h_T

$$h_T \equiv h + \frac{V^2}{2} = \text{constant} \quad (6.6)$$

Consider a calorically perfect gas, then

$$h = C_p T$$

$$h_T = C_p T + \frac{V^2}{2} = C_p \left[T + \frac{V^2}{2C_p} \right] \quad (6.7)$$

$$h_T = C_p T_T \quad (6.8)$$

where $T_T \equiv T + V^2/2C_p$ and is called the Total or Stagnation Temperature. Thus the Total Temperature at a given point in a flow is that temperature that would exist if the flow were slowed down adiabatically to zero velocity. Physically this means in a flowing gas the molecules have superimposed on their random motion the directed motion of the flow. The kinetic energy of the directed motion is the cause of the difference between static and total temperature. If, in some manner, the velocity of the airstream is reduced to zero adiabatically, and in the absence of shaft work, the resulting static temperature of the gas becomes equal to the total temperature of the flowing fluid. This will be true whether the "slowing down" process occurs reversibly or irreversibly. Therefore, a thermometer fixed with respect to the duct will measure total temperature (neglecting heat transfer effects) because it reduces the velocity of a small portion of the stream to zero.

Although the same final temperature T_T is attained whether the slowing down process is reversible or irreversible, the pressure and density finally reached will vary with the degree of irreversibility associated with the slowing down process. For pressure this may be illustrated as follows: in Figure 6-1, imagine the flowing gas at station (1) to be brought to rest adiabatically by means of a duct diverging (dashed lines) to an extremely large area (X) where the flow velocity, in the limit, is zero. If the diverging duct is frictionless, the slowing down process from (1) to (X) is isentropic and is shown as the vertical line from (1) to (2) on the temperature-entropy (T-S) diagram. If the diverging duct is frictional, the slowing down process from (1) to (X) is irreversible but adiabatic (hence, $ds > 0$) and is shown by the line of increasing entropy, (1) to (3), on the T-S diagram.

The final temperature attained at (2) and at (3) is the same; since by the First Law of Thermodynamics written between station (1) and (X) for each of these processes,

$$C_p T_1 + \frac{V^2}{2} = C_p T_2 \quad (\text{frictionless process}) \quad (6.9)$$

$$C_p T_1 + \frac{V^2}{2} = C_p T_3 \quad (\text{frictional process}) \quad (6.10)$$

However $P_b < P_c$.

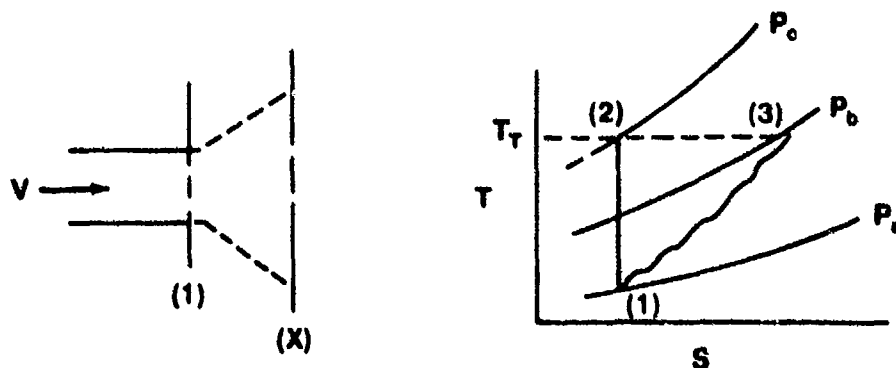


FIGURE 6.1. TOTAL PRESSURE AND DENSITY FOR REVERSIBLE AND IRREVERSIBLE PROCESSES

6.5.2 Total Pressure

The total pressure of a flowing gas is defined as the pressure obtained when the gas is brought to rest isentropically. Thus the pressure corresponding to state (2) on the T-S plot in Figure 6.1 is the total pressure of the gas in state (1), hence $P_{(2)} = P_C = P_T$. The pressure measured by a pitot tube placed in a subsonic flowing gas at any given station corresponds very closely to the total pressure of the gas at that station since the slowing down process preceding the pitot tube is basically isentropic.

6.5.3 Total Density

Total density of a flowing gas is defined similarly to pressure as the density obtained when the gas is brought to rest isentropically.

6.5.4 Mathematical Relationships for Total Properties

By use of the perfect gas law and the equation of state for an isentropic process

$$P\rho^{-\gamma} = \text{constant} \quad (6.11)$$

The following relationships between static and total values of pressure, density, and temperature can be developed

$$\left(\frac{P_T}{P}\right) = \left(\frac{T_T}{T}\right)^{\frac{\gamma}{\gamma-1}} \quad (6.12)$$

$$\frac{\rho_T}{\rho} = \left(\frac{T_T}{T}\right)^{\frac{1}{\gamma-1}} \quad (6.13)$$

Since total properties are constant throughout an isentropic flow and are easily measured, they are useful and convenient tools when evaluating the changes in compressible fluid flow. The subscripts o, t, or T are used to denote total properties. In this text, "T" is used.

6.6 SPEED OF SOUND

The quantity

$$a = \sqrt{\frac{dp}{d\rho}} \quad (6.14)$$

is called the speed of sound or acoustic speed since it is the speed with which sound waves propagate through a fluid. Equation 6.14 is derived for a nonviscous fluid; therefore, it is only valid for small disturbances which do not create any shear forces in the fluid. (Derivation F.1 in Appendix F.)

Sound waves are, by definition, "small"; the criterion being that the velocity gradients in a fluid, dV , due to the pressure disturbances, are so small that they create negligible shear or friction forces, and that

$$a \gg dV$$

It follows that the motion of a sound wave through a fluid is an isentropic phenomenon ($ds = 0$), since it does not disturb the "disorder" of the fluid, i.e., the dp , $d\rho$, and dT in the fluid caused by the passage of a sound wave are very small. In reality, the size of an audible sound wave is so small that the entropy increase near the wave is negligible, and Equation 6.14 is quite accurate for computing the speed of sound wave propagation.

Rewriting Equation 6.14 in terms of a^2 gives a pressure-density relationship for a fluid which may be used to eliminate the pressure term in the momentum equation

$$dp + \rho V dV = 0 \quad (6.3)$$

$$a^2 d\rho + \rho V dV = 0 \quad (6.15)$$

Equation 6.15 is important for later derivation of compressible flow

relations, and the inference of isentropic conditions must be remembered when using it.

If

$$P = P(\rho, s)$$

then

$$dP = \frac{\partial P}{\partial s} ds + \frac{\partial P}{\partial \rho} d\rho$$

and the substitution for $d\rho$ in the momentum equation cannot be made as conveniently. If the flow conditions are isentropic, $ds = 0$, then

$$\frac{dP}{d\rho} = \frac{\partial P}{\partial \rho}$$

and dP can be eliminated from the momentum equation. Since an isentropic process has been assumed, Equation 6.14 should be correctly written as

$$a = \sqrt{\left(\frac{\partial P}{\partial \rho}\right)_s}$$

The speed of sound may be evaluated for a perfect gas from the conservation of energy equation and the equation of state. The relationship between P and ρ evaluated for an isentropic process is

$$\frac{P}{\rho^\gamma} = \text{constant} \quad (6.11)$$

Taking the natural log of this equation and differentiating

$$\ln P - \gamma \ln \rho = \ln c$$

$$\frac{dP}{P} - \gamma \frac{d\rho}{\rho} = 0$$

or

$$\frac{dP}{d\rho} = \gamma \frac{P}{\rho} \quad (6.16)$$

Substituting $\rho = \frac{P}{RT}$ (Equation of State)

$$\frac{dP}{d\rho} = a^2 = \gamma RT$$

or

$$a = \sqrt{\gamma RT} \quad (6.17)$$

Thus the speed of sound is a function of temperature only.

A "cookbook" equation for the speed of sound at a local air temperature is

$$a \text{ [knots]} = 29 \sqrt{T \text{ [}^\circ\text{R]}} \quad (6.18)$$

or

$$a \text{ [ft/sec]} = 49 \sqrt{T \text{ [}^\circ\text{R]}} \quad (6.19a)$$

6.7 MACH

The Mach is defined as the ratio of a flow velocity to a speed of sound.

$$M = \frac{V}{a} \quad (6.19)$$

If the Mach is defined in terms of a local speed of sound, it is called the local Mach. The Mach may be defined in terms of the speed of sound at some given point in the flow, i.e., the ratio of an aircraft velocity to the

speed of sound based on the ambient temperature (as opposed to local temperature). When the local Mach is used, it will be written without a subscript.

For flow in channels, ducts, and nozzles, it is sometimes more convenient to reference the Mach to a specific place in the flow. When this is done, the Mach is written with a subscript or a superscript, i.e.,

$$M_T = \frac{V}{a_T} \quad \text{or} \quad M^* = \frac{V}{a^*}$$

where

a_T is the speed of sound at the stagnation temperature, T_T .

a^* is the speed of sound at local sonic conditions. The concept of the local sonic conditions will be discussed later in this chapter.

Rewriting Equation 6.19 as

$$M^2 = \frac{V^2}{a^2} = \frac{V^2}{\gamma R T}$$

it can be seen that V^2 is a measure of the directed or kinetic energy of the fluid flow and that the temperature term in the denominator is a measure of the internal or random thermal energy of the fluid.

This interpretation points out the two disadvantages of using Mach in flow descriptions:

1. Mach is proportional to the velocity of the flow and also to a temperature.
2. Mach tends toward infinity as the flow velocity increases.

These limitations will become apparent when working with hypersonic fluid flow or at extreme altitudes where the fluid is no longer a continuous medium.

6.8 TWO-DIMENSIONAL PROPAGATION OF SOUND WAVES

Sound waves are a series of alternate compression and rarefaction pressure pulses such as might be caused by a tuning fork. They are propagated or transmitted in all directions in a fluid at a given speed proportional to the temperature of the fluid. If the disturbance which is causing sound waves is motionless in the fluid, these waves appear to radiate out from the disturbance in a series of concentric rings like ripples on a pond as in Figure 6.2a.

If the disturbance is moving in the fluid, the wave pattern is quite different since each wave is emitted from a different point in the fluid. For example, if the disturbance is traveling at some speed which is less than the speed of sound in the fluid, the wave pattern is distorted as shown in Figure 6.2b. In this case, the sound wave outruns the disturbance, forming a series of circles one inside the other, but with different centers.

If the disturbance travels at exactly the speed of sound, the wave front and the disturbance travel together, forming the pattern shown in Figure 6.2c. Each successive wave reinforces the next wave, forming a wave front. This is a sound wave front, which is, by definition, isentropic.

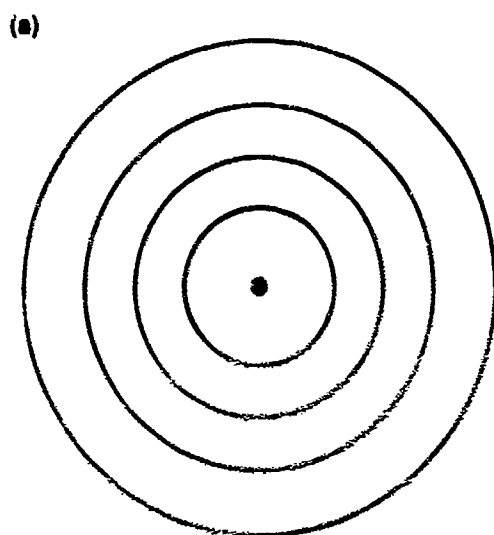
If the disturbance travels at greater than sonic velocity, it outruns the wave patterns which radiate out from the point where they were emitted, forming an oblique wavefront trailing behind the disturbance (Figure 6.2d).

6.8.1 Mach Angles

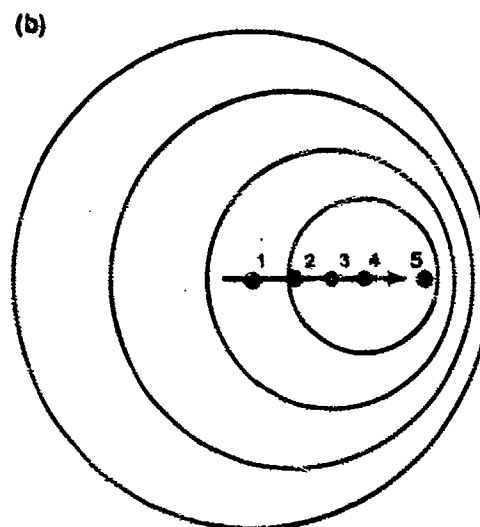
This isentropic wave front (Figure 6.2d) is analogous to the oblique shock wave, and the angle between the wave front and the direction of the disturbance's motion is called the Mach wave angle or Mach angle, μ .

In the paragraph "Oblique Shock Waves," it will be shown that μ is the smallest possible wave angle for any pressure disturbance. It is the angle of a zero strength shock wave (an isentropic shock wave) which is nothing more than a sound wave.

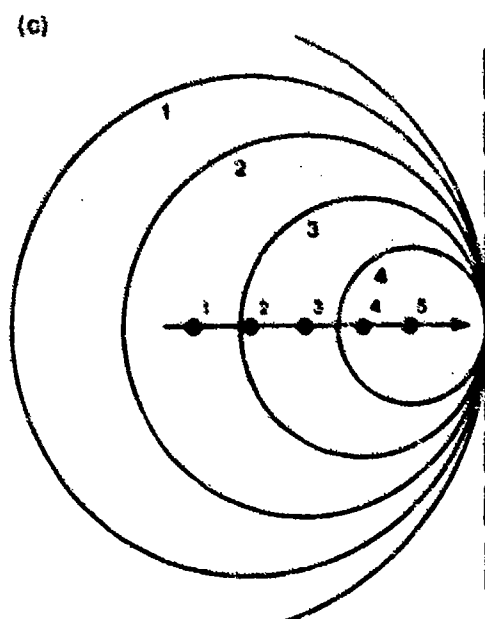
The triangle formed by the Mach angle is called the Mach cone, and from the geometry of the Mach cone it can be seen that



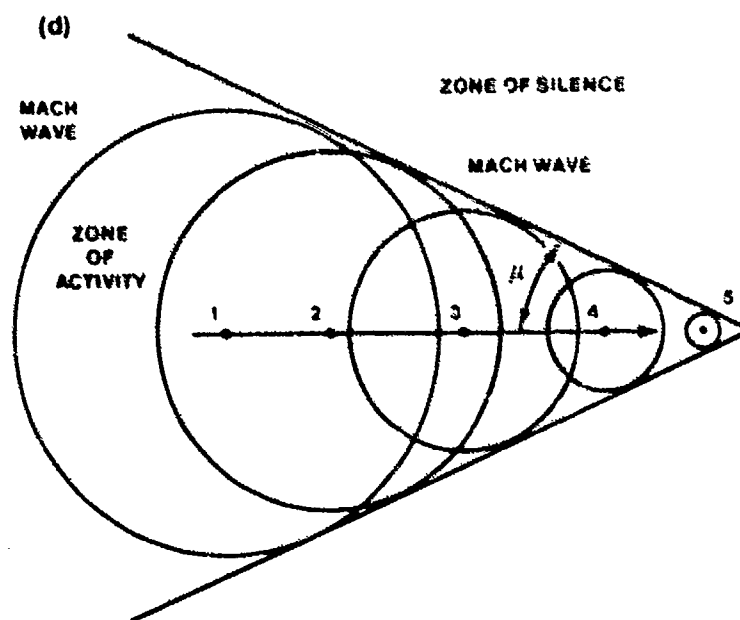
STATIONARY SOURCE



SOURCE MOVING AT
SUBSONIC VELOCITY



SOURCE MOVING AT
SONIC VELOCITY



SOURCE MOVING AT
SUPERSONIC VELOCITY

FIGURE 6.2. SOUND WAVE PROPAGATION
FROM A POINT SOURCE (6.1:160)

$$\sin \mu = \frac{a \, dt}{V \, dt} = \frac{a}{V} = \frac{1}{M}$$

where dt is a given time interval, and

$$\text{Mach Angle} = \mu = \sin^{-1} \frac{1}{M} \quad (6.20)$$

6.8.2 Activity Envelope

The real significance of the propagation of sound waves relative to the speed of the disturbance is the envelope they describe. It can be seen that sound waves or pressure disturbances are not transmitted upstream when the Mach is equal to or greater than one.

The pattern of Figure 6.2d illustrates the three rules of supersonic flow given by Von Karman in 1947 in the Tenth Wright Brothers Lecture. These rules are based on the assumption of small disturbances. They are qualitatively applicable, however, to large disturbances.

- a. The rule of forbidden signals. The effect of pressure changes produced by a body moving at a speed faster than sound cannot reach points ahead of the body.
- b. The zone of activity and zone of silence. All effects produced by a body moving at a supersonic speed are contained within the zone of activity bounded by the Mach cone extending downstream from the body. Conversely, any arbitrary point in a supersonic stream can be affected only by disturbances emanating from source points lying on or within a cone of the vertex angle μ extending upstream from the point considered. The region outside of the zone of activity is called the zone of silence.
- c. The rule of concentrated action. The effects produced by the motion of an object at supersonic speeds are concentrated along the Mach lines. Extrapolating this rule to large disturbances, we can observe its qualitative application in the concentration of effects along a shock wave accompanying a body at supersonic speeds.

6.9 CLASSIFICATION OF SPEED RANGES

It is clear that there are at least two basic speed ranges to be considered: subsonic speeds where the Mach is less than one and supersonic speeds where the Mach is greater than one. When describing the aerodynamics of an aircraft, a range is found extending from high subsonic speeds to low supersonic speeds which is not described by either the subsonic or supersonic flow equations. This is the transonic speed range.

The local flow over an aircraft in transonic flight is part subsonic and part supersonic. The interaction between the two types of flow causes aerodynamic phenomena which have characteristics of neither subsonic nor supersonic flow. These phenomena begin at the critical Mach and continue until the flow on the aircraft is completely supersonic. This range is from about Mach 0.8 to 1.2.

Since the transonic range is difficult (in some cases impossible) to describe mathematically, it will be discussed after more knowledge is gained about supersonic flow.

Extremely low velocities are studied as incompressible flow, and extremely high velocities typify hypersonic flow, which is of current interest to space scientists concerned with orbital and re-entry velocities.

The hypersonic speed range is considered to begin at Mach 5.0, but some hypersonic characteristics appear at speeds as low as Mach 3.5. Hypersonic flow is characterized by high temperatures which cause ionization, gaseous dissociation and recombination, extreme wave angles, boundary layer interaction, and high heat transfer rates.

6.10 ISENTROPIC FLOW

The isentropic flow process was defined as being both adiabatic and reversible. These conditions are very nearly met in one-dimensional, nonviscous, shock-free flow where both the cross-sectional area of the streamtube and the flow direction are constant or change very slowly. The nonviscous assumption is extremely important when flow in a channel is considered, since boundary layer interaction causes irreversible changes in flow properties.

The isentropic flow assumptions, while seemingly quite restrictive, are very useful when evaluating one-dimensional flow conditions existing outside of a boundary layer and between shock waves. Special relationships will be derived later in this chapter for evaluating the changes occurring because of shock waves.

Valuable insight into a great number of real aerodynamic and fluid flow problems can be gained from the ability to predict isentropic changes and changes caused by shock waves in supersonic flow. A few of the isentropic flow equations will be derived from the one-dimensional, conservation equations. Many others can be derived when needed or may be found in most texts on supersonic aerodynamics and fluid dynamics.

Since the stagnation properties P_T , ρ_T , and T_T can be experimentally measured or calculated from energy concepts at any place in an isentropic flow, it is useful to obtain relationships between these stagnation properties and the free stream properties of the flow in terms of Mach, that is,

$$\frac{P_T}{P}, \quad \frac{\rho_T}{\rho}, \quad \frac{T_T}{T} = f(M)$$

Using Equation 6.7 which was developed for adiabatic flow

$$h_T = C_p T + \frac{v^2}{2} \quad (6.7)$$

$$C_p T_T = C_p T + \frac{v^2}{2} \quad (6.21)$$

To write Equation 6.21 in terms of Mach, where $M^2 = v^2/\gamma RT$ divide the equation by $C_p T$

$$\begin{aligned}
\frac{T_T}{T} &= 1 + \frac{V^2}{2C_p T} \\
&= 1 + \left(\frac{V^2}{2C_p T} \right) \left(\frac{RC_v}{RC_v} \right) \\
&= 1 + \left(\frac{R}{2C_v} \right) \left(\frac{V^2}{RT} \right)
\end{aligned}$$

but

$$\frac{R}{C_v} = \gamma - 1 \quad \text{since } R = C_p - C_v \text{ and } \gamma = C_p/C_v$$

therefore,

$$\frac{T_T}{T} = 1 + \frac{\gamma - 1}{2} M^2 \quad (6.22)$$

This is a very important equation relating stagnation temperature to free stream temperature in terms of flow Mach for an adiabatic flow process. Notice that the flow does not have to be isentropic for this equation to be valid. This equation should be recognized as the one used to determine the ambient air temperature, T_a , from flight test data

$$\frac{T_{ic}}{T_a} = 1 + \frac{k_t (\gamma - 1) M^2}{2} \quad (6.23)$$

where k_t is a recovery factor that describes the efficiency of the adiabatic flow process between the ambient air and the temperature probe. The two equations are identical when the recovery factor, k_t , is equal to one, i.e., the probe is perfectly insulated from the ambient air.

To obtain an expression for P_T/P as a function of Mach use Equation 6.12

$$\frac{P_T}{P} = \left(\frac{T_T}{T} \right)^{\frac{\gamma}{\gamma-1}} \quad (6.12)$$

Substituting Equation 6.22 into this equation,

$$\frac{P_T}{P} = \left(1 + \frac{\gamma-1}{2} M^2 \right)^{\frac{\gamma}{\gamma-1}} \quad (6.24)$$

Substituting Equation 6.22 into Equation 6.13,

$$\frac{\rho_T}{\rho} = \left(1 + \frac{\gamma-1}{2} M^2 \right)^{\frac{1}{\gamma-1}} \quad (6.25)$$

It should be noted that it is not necessary for the stagnation properties to actually exist at some point in the flow to write the equations relating them to the free stream pressure, density, and temperature. It is only necessary to assume that the flow at some given point could be slowed isentropically to zero velocity.

It was previously stated that the stagnation properties remained constant throughout an isentropic flow. The proof of this statement begins with the fact that temperature is a direct measure of the internal energy of a flow.

The internal energy of an adiabatic flow is constant since no heat is exchanged with the surroundings. If an adiabatic flow is slowed isentropically to zero velocity, the stagnation temperature measured would be a constant throughout the flow.

If viscous or other irreversible effects were present in the adiabatic flow, the stagnation temperature would still remain constant since no heat is exchanged with the surroundings. The presence of viscous and irreversible effects means that some of the kinetic energy of the flow is converted to thermal energy, but the stagnation temperature of the flow remains constant

for reasons stated.

By integrating the entropy relation, rearranging terms, and evaluating at stagnation conditions

$$s_T = \ln \left[\frac{(T_T)}{P_T} \right]^{\frac{\gamma}{\gamma-1}} + \ln c$$

It can be seen that P_T is constant in isentropic flow, since s_T and T_T are constant. From the equation of state, $P_T = \rho_T R T_T$, it can be seen that ρ_T is also constant in isentropic flow.

Because P_T , ρ_T , and T_T are all constants in isentropic flow, the ratio of free stream conditions at two different stations in the flow may be obtained by taking a ratio of stagnation properties evaluated at the two stations, i.e.,

$$\frac{P_1/P_{T1}}{P_2/P_{T2}} = P_1/P_2$$

Resulting temperature, pressure and density ratios are shown below.

$$\frac{T_1}{T_2} = \frac{1 + \frac{\gamma-1}{2} M_2^2}{1 + \frac{\gamma-1}{2} M_1^2} \quad (6.26)$$

$$\frac{P_1}{P_2} = \left[\frac{1 + \frac{\gamma-1}{2} M_2^2}{1 + \frac{\gamma-1}{2} M_1^2} \right]^{\frac{\gamma}{\gamma-1}} \quad (6.27)$$

$$\frac{\rho_1}{\rho_2} = \left[\frac{1 + \frac{\gamma-1}{2} M_2^2}{1 + \frac{\gamma-1}{2} M_1^2} \right]^{\frac{1}{\gamma-1}} \quad (6.28)$$

Values of P/P_T , ρ/ρ_T , and T/T_T are tabulated versus Mach (at $\gamma = 1.4$ for air) in the appendices of most thermodynamics books. The same quantities are plotted versus Mach in Reference 6.4.

Since Mach is a quantity that may be measured in the flow problem and stagnation properties are constant in isentropic flow, use of these charts and graphs simplifies the work required to calculate P , ρ , and T at a given station in the flow.

6.11 FLOW IN CONVERGENT-DIVERGENT STREAMTUBES

Understanding the characteristics of a compressible fluid flowing through a streamtube is very important in supersonic aerodynamics. If viscous effects are to be neglected in the streamtube, the boundary layer streamline may be used as the streamtube boundary. For this discussion a streamtube is defined as any convergent or divergent section bounded either by physical walls or by streamlines as shown in Figure 6.3. Such a streamtube might be formed by the

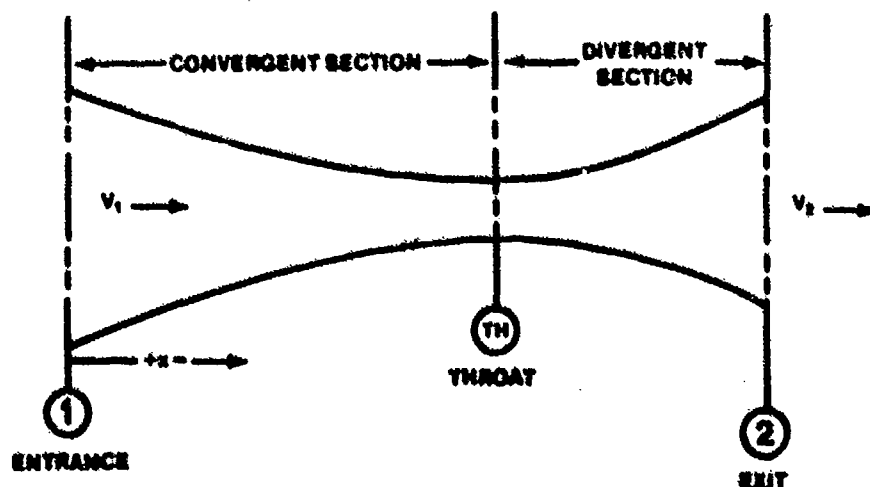


FIGURE 6.3. CONVERGENT DIVERGENT STREAMTUBE

inlet or exhaust duct of a jet aircraft or between converging and diverging streamlines as the air flows over the surface of the aircraft. Also, a supersonic wind tunnel uses convergent-divergent designs to obtain Mach greater than one in the test section.

Compressible flow through a convergent-divergent streamtube is quite different from the classical flow of an incompressible fluid through a venturi. At low velocities, the flow situation is almost identical to the venturi, but at high velocities the change in density causes a complete reversal of the low velocity trends.

Consider steady, nonviscous, compressible, isentropic flow in the streamtube shown in Figure 6.3. In steady flow, the mass entering at Station 1 is equal to the mass leaving at Station 2, and the continuity equation may be used to describe the flow conditions

$$\frac{d\rho}{\rho} + \frac{dV}{V} + \frac{dA}{A} = 0 \quad (6.2)$$

Substituting the definition of the speed of sound into the momentum equation as done in Equation 6.15 yields

$$a^2 d\rho + \rho V dV = 0 \quad (6.15)$$

or

$$\frac{d\rho}{\rho} = -\frac{V dV}{a^2}$$

Multiplying the right side by $\frac{V}{V}$

$$\frac{d\rho}{\rho} = -M^2 \frac{dV}{V} \quad (6.29)$$

and substituting this into the continuity equation above gives

$$-M^2 \frac{dV}{V} + \frac{dV}{V} + \frac{dA}{A} = 0$$

or

$$\frac{dA}{A} = (M^2 - 1) \frac{dV}{V} \quad (6.30)$$

Equation 6.30 describes the flow situation caused by compressible fluid flow in streamtubes. Defining a diverging streamtube as having a positive dA , i.e., an increasing area in the direction of the flow, and a converging streamtube as having a negative dA , the following conclusions can be drawn:

1. When the Mach is less than 1.0, a diverging streamtube causes a decrease in velocity, and a converging streamtube causes an increase in velocity.
2. When the Mach is greater than 1.0, a diverging nozzle causes an increase in velocity, and a converging nozzle causes a decrease in velocity.
3. When the Mach is 1.0, dA must be zero.

Examining Equation 6.29 may give a physical understanding of what happens to subsonic or supersonic, compressible flow in a streamtube.

$$\frac{d\rho}{\rho} = -M^2 \frac{dV}{V} \quad (6.29)$$

It can be seen that for Mach less than 1.0, a small change in velocity results in a proportionately smaller change in density.

For air flowing at Mach of 0.3, 0.9, 1.0, and 2.0, consider the density effects caused by an arbitrary 10% increase in velocity ($dV/V = 10\%$).

At $M = 0.3; \frac{d\rho}{\rho} = -0.9\%$

$M = 0.9; \frac{d\rho}{\rho} = -8.1\%$

$$M = 1.0; \frac{d\rho}{\rho} = -10\%$$

$$M = 2.0; \frac{d\rho}{\rho} = -40\%$$

Notice that for all Mach, an increase in velocity results in a decrease in density. The magnitude of the density change is proportional to the Mach squared; consequently, as the Mach increases, the change in density becomes more pronounced.

It is interesting to note that Equation 6.29 indicates the validity of the incompressible flow assumption. It shows that at low Mach, a change in velocity results in a very small change in density, and as the Mach increases, the assumption becomes poorer, until at Mach 1.0, the change in velocity is of the same magnitude as the change in density.

To complete the picture, an equation must be obtained relating density change to area change as a function of Mach. If in the derivation of Equation 6.30 the value of dV/V had been substituted instead of $d\rho/\rho$, the following relation would have been obtained

$$\frac{dA}{A} = \left(\frac{1}{M^2} - 1 \right) \frac{d\rho}{\rho} \quad (6.31)$$

In the preceding discussion, it was found that for subsonic and supersonic Mach the density always decreased for increased velocity. This leads to the question, what shape is required to produce this decrease in density and increase in velocity? From Equation 6.31 it can be seen that for subsonic speed ($M < 1.0$), a decrease in density (and an increase in velocity) is caused by a converging duct (negative dA). That is, the factor $(1/M^2 - 1)$ is positive for subsonic speeds. Supersonic, this factor is negative; therefore, a diverging duct (positive dA) causes a decrease in density (and a corresponding increase in velocity).

Qualitatively speaking, the decrease in density is a second order effect

and can usually be neglected for flow at low Mach because a reduction in area creates only a proportional increase in velocity. At high subsonic speeds, the reduction in density becomes more significant, but the density still is able to decrease fast enough to allow the velocity to increase as the fluid flows into a converging duct. At supersonic speeds, the density does not decrease fast enough in a converging section; therefore the nozzle must diverge to further reduce the density and allow an increase in velocity.

Only the case of accelerating flow has been considered, but it is obvious that the reverse of the described conditions is also true. That is, a subsonic stream is slowed down by a diverging section, and a supersonic stream is slowed down by a converging section. The general conclusions of the convergent-divergent streamtube problem may be summarized as shown in Figure 6.4.

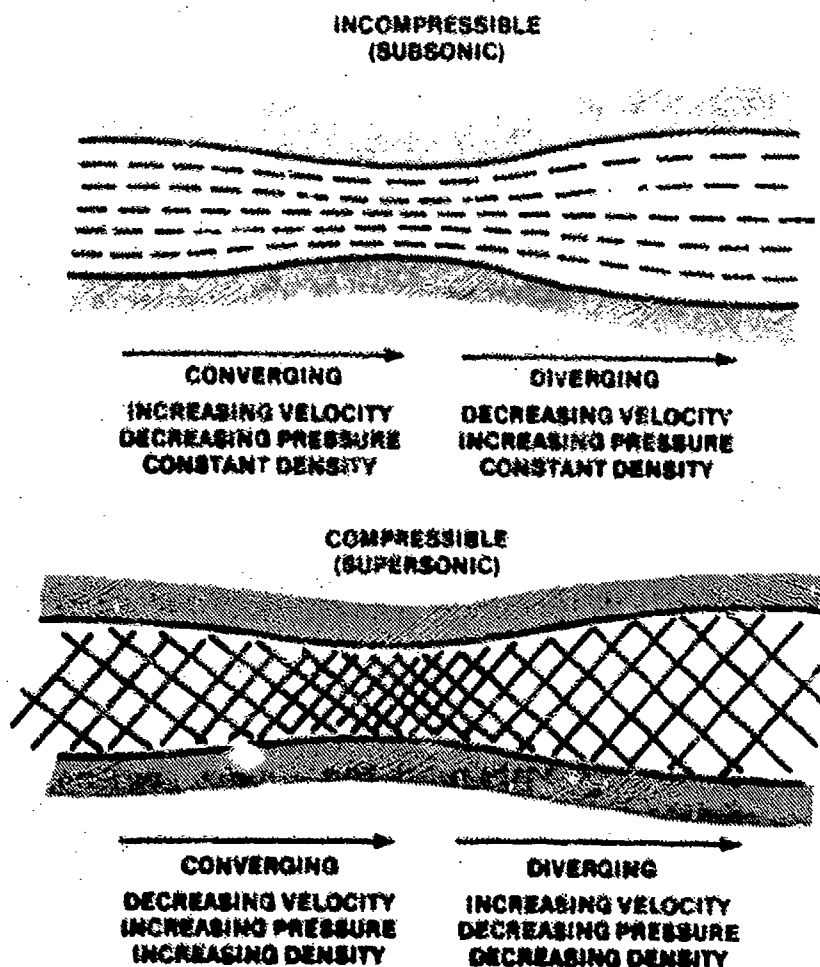


FIGURE 6.4. COMPARISON OF COMPRESSIBLE AND INCOMPRESSIBLE FLOW THROUGH A CLOSED TUBE (6.2:205)

6.11.1 Flow at the Throat

The flow in a convergent-divergent streamtube has been discussed at some length, but now the specific flow characteristics at the throat of the streamtube must be studied.

The minimum cross-sectional area of a convergent-divergent streamtube is called the throat, and at this section, the derivative $dA/dx = 0$, or $dA = 0$. Two conditions can exist at the throat since dA is zero. Either dV and/or $(M^2 - 1)$ must equal zero to satisfy Equation 6.30.

The first condition, $dV = 0$, is characteristic of flow in a subsonic streamtube in which the fluid accelerates to a maximum subsonic speed at the throat and then decelerates again in the divergent section. It is also characteristic of supersonic flow which decelerates in the converging section, reaching a lower supersonic or exactly sonic velocity at the throat and then accelerates again in the divergent section.

The second condition, $(M^2 - 1) = 0$, is characteristic of what is called choked flow. It occurs when $M = 1$ at the throat. This condition exists whenever the flow is accelerated from subsonic to supersonic speeds by a nozzle or when flow is decelerated from supersonic to subsonic speeds by a diffuser. By definition, a nozzle accelerates flow, while a diffuser decelerates flow.

Flow through a streamtube is caused by a pressure differential between the inlet and exit. Increasing the inlet pressure or lowering the exit pressure causes an increase in the flow velocity and the mass flow rate. Since the maximum subsonic velocity occurs at the throat, sonic velocity ($M=1$) is attained first at the throat, and further reduction in exit pressure will not increase the velocity at this point. This may be seen by considering the mechanism which causes a change in the mass flow rate and the flow velocity in the convergent-divergent streamtube (Figure 6.5).

If the exit pressure is exactly equal to the inlet pressure, no flow will occur. There are three values of exit pressure for a given inlet pressure for which isentropic flow exists throughout the nozzle and sonic velocity is attained at the throat. These values are called the first, second, and third critical pressures. Between pressure equilibrium and first critical pressure, the flow will accelerate in the convergent portion of the streamtube and then decelerate through the diverging portion, remaining subsonic throughout. This

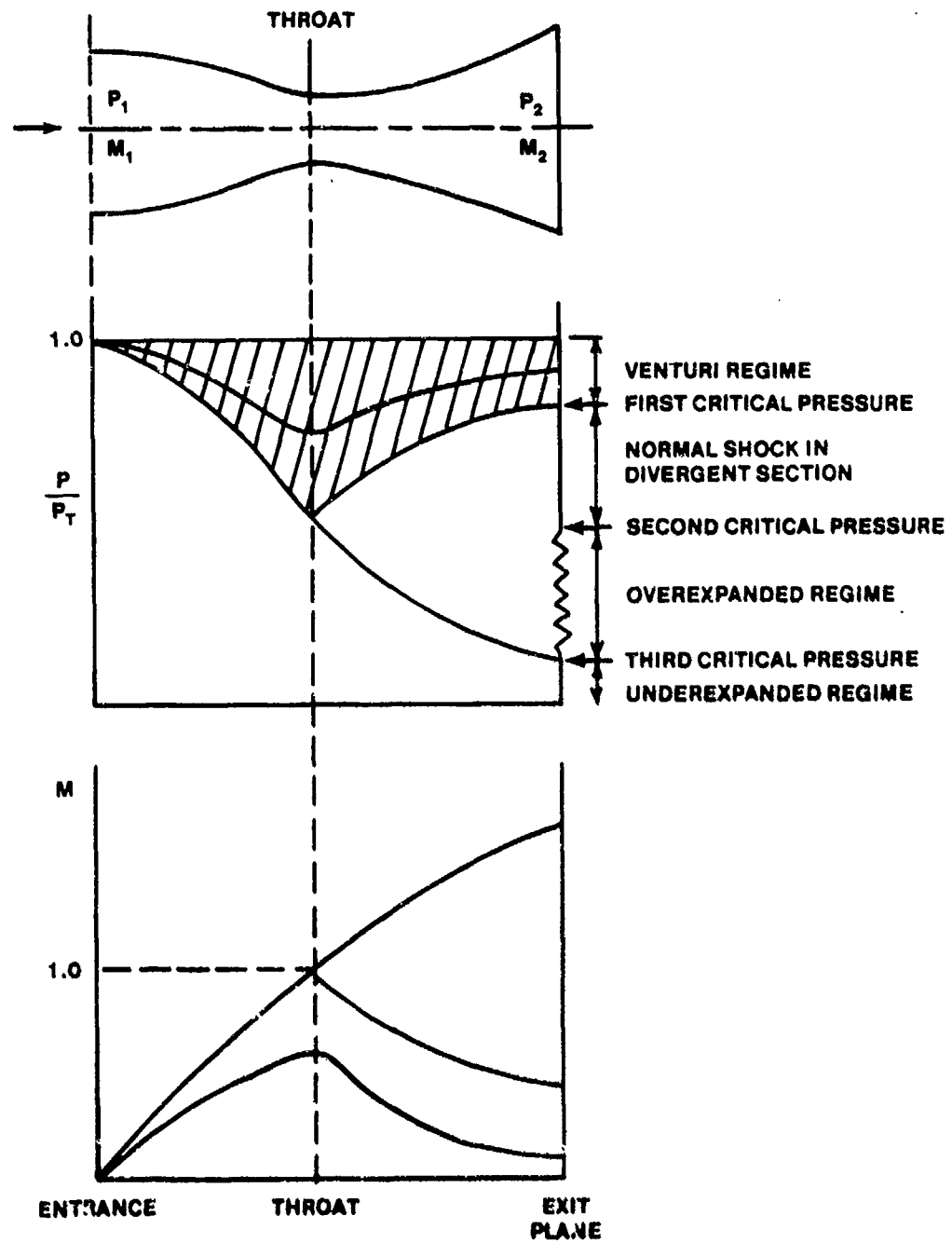


FIGURE 6.5. PRESSURE AND MACH VARIATION
THROUGH A CONVERGING-DIVERGING STREAMTUBE
(6.3:157)

is called the venturi regime. If the pressure is reduced to the first critical pressure at the exit, the flow will accelerate through the convergent portion, reach sonic velocity at the throat, and then decelerate back to a subsonic value. Once sonic conditions have been attained at the throat, further reductions in exit pressure will not affect what happens upstream of the throat. The maximum mass flow rate has been achieved for that inlet pressure, and the streamtube is said to be choked. Further reduction in exit pressure beyond the first critical point will produce a normal shock somewhere in the divergent portion of the streamtube until the second critical pressure is reached. At the second critical pressure, a normal shock stands at the exit plane. Further reduction in exit pressure beyond the second critical value will produce oblique shocks or a combination oblique-normal shock outside the streamtube as shown in Figure 6.6a. This is called the overexpanded condition, indicating that the streamtube is too long, and will occur until reaching the third critical pressure. The third critical value is the only pressure for which no shocks occur anywhere in the streamtube flow field, and supersonic flow is maintained downstream of the throat. This is the on-design condition. Further reduction in pressure below the third critical value is an underexpanded condition, indicating the streamtube is too short, and expansion fans will form outside the streamtube as illustrated in Figure 6.6b.

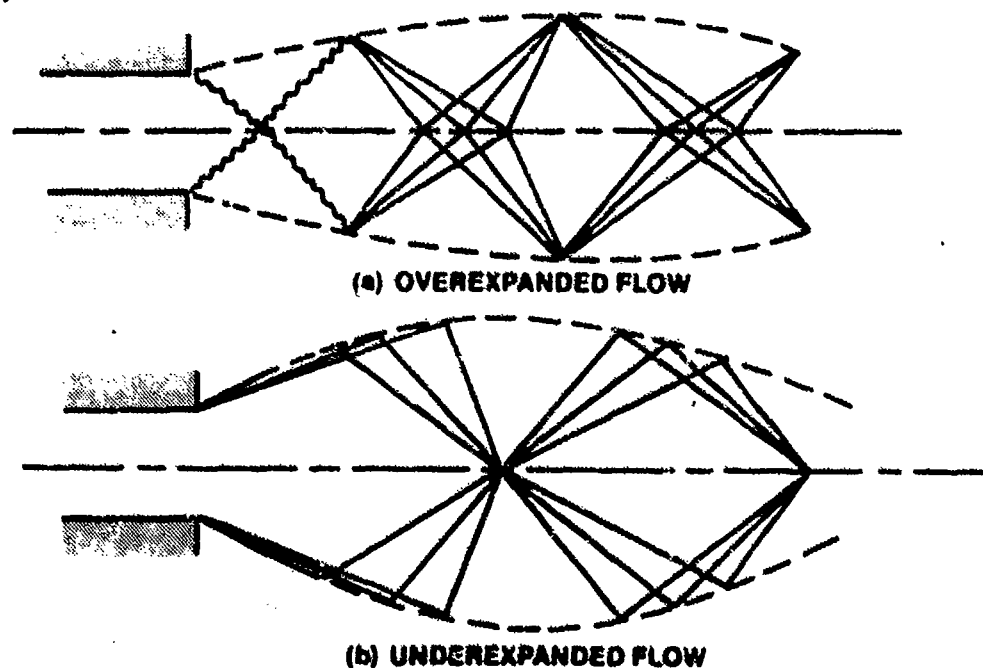


FIGURE 6.6. PRESSURE ADJUSTMENT OUTSIDE
A NOZZLE OR STREAMTUBE (6.3:219, 220)

6.11.2 Mass Flow in a Choked Streamtube

The mass flow rate of a gas ($\dot{m} = \rho VA$) increases with increasing pressure differential between the entrance and exit of a subsonic, converging-diverging streamtube until sonic velocity is attained in the throat. When sonic velocity is reached, it has been shown that the velocity and density at the throat are fixed; consequently the mass flow rate, \dot{m} , is fixed or the streamtube is choked. Sonic velocity is the maximum velocity that can occur in the throat; therefore it fixes the maximum mass flow through the streamtube for given entrance conditions.

This should not be interpreted to mean that a choked streamtube is passing the maximum mass flow for the streamtube; it is passing the maximum mass flow for given entrance conditions. Since the streamtube was assumed isentropic, this is the same as saying a choked streamtube is passing the maximum mass flow for given stagnation conditions.

A choked streamtube makes an excellent metering device for gaseous fluids. By adjusting the stagnation or entrance conditions, the exact mass flow can be measured and calculated. In reality, a well designed metering streamtube passes within 2 - 3% of the mass flow calculated for an isentropic streamtube.

An equation for the mass flow rate through an isentropic streamtube can be derived by substituting appropriate values into $\dot{m} = \rho VA$:

$$\dot{m} = \frac{P_T}{\sqrt{T_T}} A \sqrt{\frac{\gamma}{R}} \frac{M}{\left[1 + \frac{\gamma-1}{2} M^2\right] \left[\frac{\gamma+1}{2(\gamma-1)}\right]} \quad (6.32)$$

If the streamline is choked, $M = 1$ and $A = A_{\text{throat}} = A^*$:

$$\dot{m} = \frac{P_T}{\sqrt{T_T}} A_{\text{throat}} \sqrt{\frac{\gamma}{R}} \left[1 + \frac{\gamma-1}{2}\right] \left[\frac{\gamma+1}{2(\gamma-1)}\right] \quad (6.33)$$

6.11.3 Local Sonic Conditions

When a streamline is choked, specific values for P , ρ , T , A , etc., are determined at the throat. These unique values are designated with a superscript, $*$, and are written P^* , ρ^* , T^* , A^* , etc. The concept of the local sonic area, A^* , where $M = 1$, is similar to the stagnation condition concept. Both refer to flow conditions at some specific Mach, i.e., $M = 1$ for local sonic conditions and $M = 0$ for stagnation conditions.

It is not necessary for the flow to be actually at Mach 1.0 to define the local sonic values. To determine local sonic conditions at some point in a flow, it has to be assumed that the area of the channel could be varied to the value A^* . When this is done, the prevailing conditions at the section with area A^* are local sonic conditions.

For instance, in an isentropic flow, A^* can be imagined at any point, that is, the channel can be reduced in area to that which would reduce a supersonic stream to Mach 1.0 or increase a subsonic stream to Mach 1.0.

Properties at local sonic conditions in an isentropic flow may be conveniently evaluated in terms of stagnation conditions, which are usually known or easily measured. The general procedure is to evaluate the identities

$$p^* = \frac{P_T}{\frac{P_T}{P^*}}, \quad \rho^* = \frac{\rho_T}{\frac{\rho_T}{\rho^*}}, \quad T^* = \frac{T_T}{\frac{T_T}{T^*}}$$

using Equation 6.24

$$\frac{P_T}{P^*} = \left(1 + \frac{\gamma-1}{2} M^2 \right)^{\frac{\gamma}{\gamma-1}} \quad (6.24)$$

and that local sonic conditions are defined where $M = 1$, gives

$$\frac{P_T}{P^*} = \left(1 + \frac{\gamma-1}{2} \right)^{\frac{\gamma}{\gamma-1}}$$

and

$$p^* = \frac{p_T}{\left(1 + \frac{\gamma - 1}{2}\right)^{\frac{\gamma}{\gamma - 1}}} \quad (6.34)$$

The ρ^* and T^* can be easily derived, and for air, $\gamma = 1.4$, the local sonic properties as a function of stagnation properties are

$$p^* = p_T \quad (.528) \quad (6.35)$$

$$\rho^* = \rho_T \quad (.634) \quad (6.36)$$

$$T^* = T_T \quad (.833) \quad (6.37)$$

6.11.4 M^*

The concept of local sonic conditions allows a dimensionless parameter, M^* , to be defined. Mach, M , is a very convenient parameter but has the disadvantages listed in the paragraph, "Mach."

Often it is convenient to work with the parameter M^* , which is the flow velocity V , divided by a^* , the speed of sound at local sonic conditions.

$$M^* = \frac{V}{a^*} \quad (6.38)$$

It should be noted immediately that M^* does not mean Mach at a place where $M = 1$ like all other starred quantities but is defined by Equation 6.38.

Unique relations between M and M^* can be derived for adiabatic flow using the definition of M^* and the energy equation for a perfect gas (refer to Appendix F, Derivation F.5)

$$M^{*2} = \frac{\frac{\gamma+1}{2} M^2}{1 + \frac{\gamma-1}{2} M^2} \quad (6.39)$$

$$M^2 = \frac{\frac{2}{\gamma+1} M^{*2}}{1 - \frac{\gamma-1}{\gamma+1} M^{*2}} \quad (6.40)$$

From these two equations it can be seen that M^* is a simple index of when the flow is subsonic and when the flow is supersonic, i.e.:

when

$$M < 1; \quad M^* < 1$$

$$M > 1; \quad M^* > 1$$

$$M = 1; \quad M^* = 1$$

$$M = 0; \quad M^* = 0$$

$$M = \infty; \quad M^* = \sqrt{\frac{\gamma+1}{\gamma-1}} = \sqrt{6} \quad (\text{for air})$$

Equation 6.39 is tabulated in Reference 6.4, and if M^* is known, then M can be found or vice versa.

6.11.5 Area Ratio

Just as it is convenient to work with dimensionless parameters p/p_T , etc., it is convenient to use a dimensionless area ratio, A/A^* .

Equating Equations 6.32 and 6.33, this parameter is found to be

$$\frac{A}{A^*} = \frac{1}{M} \left[\left(\frac{\gamma+1}{2} \right) \left(1 + \frac{\gamma-1}{2} M^2 \right) \right]^{\frac{\gamma+1}{2(\gamma-1)}} \quad (6.41)$$

and is always greater than one. For a given value of A/A^* , there are always two values of M , one for subsonic flow and the other for supersonic flow.

6.12 NORMAL SHOCK WAVES

Shock waves are observed as a discontinuity between supersonic and subsonic flow. The flow passes from supersonic to subsonic speeds in an extremely short distance which is of the order of magnitude of the mean free path of the molecules in the flow. The kinetic energy of the supersonic, upstream molecules is instantaneously converted to pressure-volume (pv) and thermal energy.

Experimental studies of normal shocks in supersonic wind tunnels show fivefold pressure increases and threefold velocity decreases behind the shock. These changes occur in a distance too small to be measured on a photographic plate, but theoretical calculations and experimental measurements indicate a distance of the order of 10^{-5} inches.

Because changes due to a normal shock occur in such a short distance, the changes are highly irreversible, and a shock wave is not isentropic. Two valid assumptions made when studying normal shocks are that:

1. The flow through a shock is adiabatic.
2. The shock is very thin and has a constant cross-sectional area between the front and rear face.

With these two assumptions and the conservation equations (see "One-Dimensional Flow Approximation"), the changes in flow properties caused by a shock can be derived as functions of M_1 , i.e., P_2/P_1 , ρ_2/ρ_1 , T_2/T_1 , M_2 . These derivations are conceptually simple but involve lengthy mathematical equation juggling which is carried out in most textbooks on compressible flow; therefore only the results of the derivations will be listed (refer to Appendix F, Derivation F.6).

A pictorial representation of a normal shock and the change in flow properties across the shock is shown in Figure 6.7.

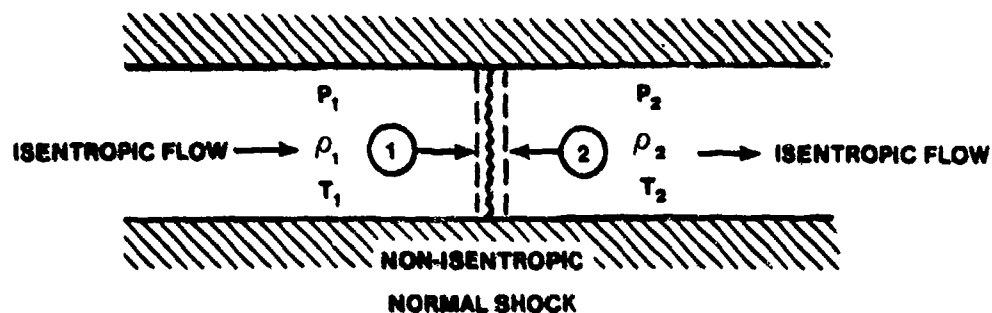


FIGURE 6.7. FLOW PROPERTIES IN THE VICINITY OF A NORMAL SHOCK

6.12.1 Normal Shock Equations

The notation used to describe the flow situation must be established before listing the normal shock equations. For these relations, the following assumptions were made:

1. All property changes occur in a constant area
2. Flow across the shock is adiabatic
3. Flow upstream and downstream of the shock is isentropic

$$\frac{P_2}{P_1} = \frac{1 - \gamma + 2 \gamma M_1^2}{1 + \gamma} \quad (6.42)$$

$$\frac{\rho_2}{\rho_1} = \left(\frac{2 + (\gamma - 1) M_1^2}{(\gamma + 1) M_1^2} \right)^{-1} \quad (6.43)$$

$$\frac{T_2}{T_1} = \left(\frac{1 - \gamma + 2 \gamma M_1^2}{1 + \gamma} \right) \left[\frac{2 + (\gamma - 1) M_1^2}{(1 + \gamma) (M_1^2)} \right] \quad (6.44)$$

$$M_2^2 = \frac{M_1^2 + \frac{2}{\gamma - 1}}{\frac{2\gamma}{\gamma - 1} M_1^2 - 1} \quad (6.45)$$

Values of P_2/P_1 , ρ_2/ρ_1 , T_2/T_1 , and M_2 are tabulated versus Mach, M_1 , (at $\gamma = 1.4$ for air) in the appendices of most thermodynamic books. The same quantities are plotted versus Mach in Reference 6.4.

6.12.2 Normal Shock Summary

A shock wave is an extremely thin discontinuity which forms between supersonic and subsonic flow. The shock wave is an adiabatic process with no stagnation temperature loss across it, but as can be shown by entropy considerations, there is an accompanying stagnation pressure loss.

Supersonic flow always exists upstream of a shock wave, and the upstream stagnation pressure is greater than the downstream stagnation pressure.

General flow properties can be compared and tabulated as

$V_1 > V_2$	$s_1 < s_2$
$T_{T1} = T_{T2}$	$\rho_1 < \rho_2$
$P_{T1} > P_{T2}$	$M_1 > M_2$
$\rho_{T1} > \rho_{T2}$	$a_1 < a_2$
$T_1 < T_2$	$a^*_1 = a^*_2$
$P_1 < P_2$	$M^*_1 > M^*_2$
$A^*_1 < A^*_2$	

6.13 SUPERSONIC PITOT TUBE

The loss in stagnation pressure across a normal shock affects the stagnation pressures sensed by aircraft pitot static systems (Figure 6.8).

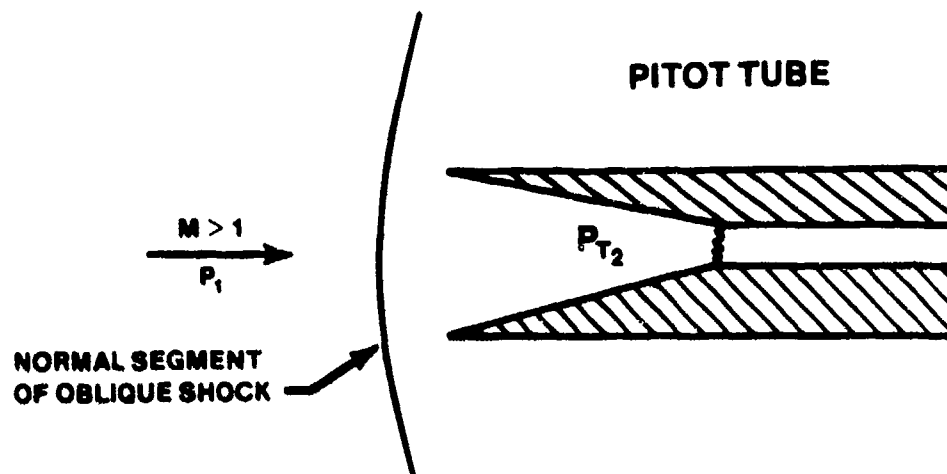


FIGURE 6.8. PITOT TUBE IN SUPERSONIC FLOW

To determine Mach from free stream static pressure and stagnation pressure behind a normal shock standing in front of a pitot tube, the Rayleigh Pitot Relation is often used

$$\frac{P_{T2}}{P_1} = \frac{\left(\frac{\gamma+1}{2} M_1^2 \right)^{\frac{\gamma}{\gamma-1}}}{\left(\frac{2\gamma}{\gamma+1} M_1^2 - \frac{\gamma-1}{\gamma+1} \right)^{\frac{1}{\gamma-1}}} \quad (6.46)$$

By measuring P_1 and P_{T2} , M_1 can be determined, and in many compressible flow textbooks, these values are plotted versus M_1 for $\gamma_{\text{air}} = 1.4$.

When using Equation 6.46, the free stream static pressure must be measured in front of the shock wave. This is a very difficult procedure for an aircraft in supersonic flight. Experiments have proven that if the static

source is approximately ten pitot tube diameters behind the shock wave, the static pressure measured is quite close to free stream static pressure.

On the pitot booms of supersonic aircraft, static pressure measuring holes will be found at varying distances from the end of the boom. The location of these holes usually has been determined experimentally to produce the closest approximation of free stream static pressure in supersonic flight.

6.14 OBLIQUE SHOCK WAVES

In the last paragraph on normal shocks, shock wave theory was presented, and the thermodynamic and kinematic changes that occurred when the flow traversed a normal shock were studied. Next, the changes that occur when flow passes through an oblique shock must be considered.

A normal shock is a special form of a pressure discontinuity in a fluid. In general, the discontinuities observed experimentally are inclined to the free stream velocity and are called oblique shocks.

Oblique shocks occur in supersonic flow because continuous compression waves caused by a concave, curved surface in the flow tend to merge, forming an oblique discontinuity at a finite distance from the surface.

When flow is forced to change direction suddenly at a sharp concave corner, an attached, oblique shock forms at the corner.

Oblique shocks occur in almost all supersonic flow situations of practical interest, but the mere existence of supersonic flow does not imply that there must be shock waves somewhere in the flow.

Developing the relations between the fluid properties on the two sides of an oblique shock is not as formidable a task as it might seem, because many of the normal shock equations with a slight modification apply equally well to oblique shocks.

Suppose a stationary observer sees the flow at Station 1 suddenly decelerate and compress to the conditions at Station 2 because it has traversed a normal shock wave (Figure 6.9).

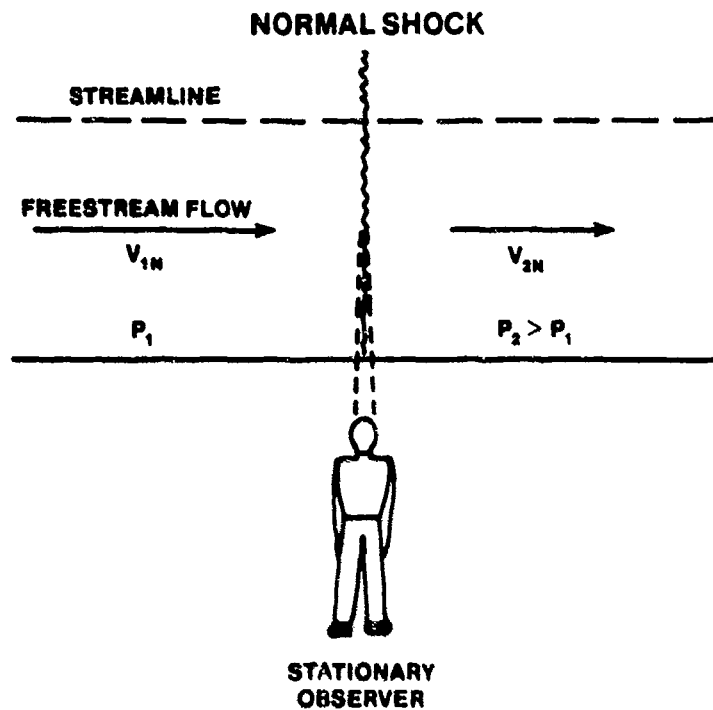


FIGURE 6.9. SHOCK PROCESS AS SEEN BY STATIONARY OBSERVER

Next, imagine that the observer moves along the shock wave in a downward direction with a velocity V_t . The moving observer would see a flow situation in which the shock is inclined to the free stream flow and in which the flow undergoes a sudden change in direction when it crosses the shock (Figure 6.10).

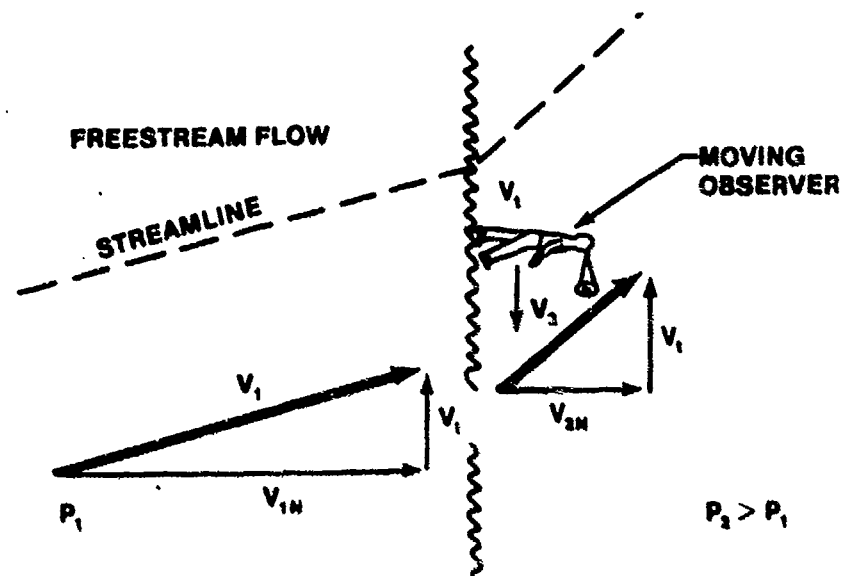


FIGURE 6.10. SHOCK PROCESS AS SEEN BY MOVING OBSERVER

The oblique flow pattern constructed in this manner has equal tangential velocity components, V_t , on both sides of the shock. By placing a solid wall along one of the streamlines in Figure 6.10 and rotating the picture so that incoming velocity, V_1 , is horizontal, the supersonic flow situation in the neighborhood of a concave corner is described (Figure 6.11).

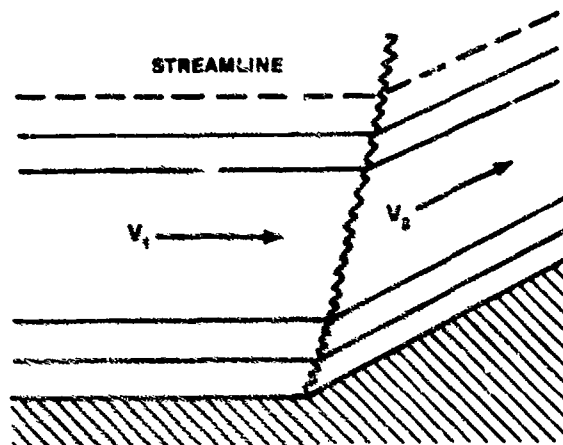


FIGURE 6.11. SUPERSONIC FLOW INTO A CORNER

By imparting a uniform velocity to the flow field along any shock, a straight segment of an oblique shock may be transformed into a normal shock.

To fix this concept, consider the falling rain in Figure 6.12.

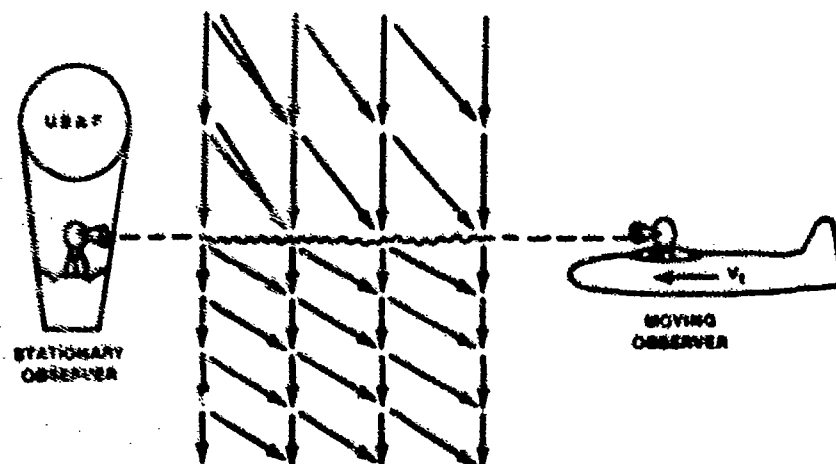


FIGURE 6.12. ANALOGY TO AID UNDERSTANDING OF OBLIQUE SHOCKS

Relative to an observer at rest, the rain is falling vertically. Relative to an observer moving perpendicular to the rainfall, the rain is descending at an angle.

Let the rain be slowed down instantaneously at some altitude. An observer in a balloon at this altitude sees the rain falling vertically and slowing down at this level as shown by the single lines in Figure 6.12. The pilot of an aircraft traveling with a horizontal velocity V_t at this altitude sees the path of the raindrops as though they were being deflected as they pass through this level (double lines in Figure 6.12). The pilot's observation is also correct, for relative to the aircraft the drops are being deflected. Essentially, the velocity of the aircraft has been superimposed upon the changing velocity of the raindrops.

A careful comparison of Figures 6.9 and 6.10 will show that the thermodynamic properties of P , ρ , T , a , and s are unchanged by the motion of the observer. On the other hand, V , M_1 , ρ_{T_1} , and T_{T_1} are altered when the observer's motion V_t is superimposed on the normal shock flow situation.

The magnitude of V_t is arbitrary and depends upon the angle the oblique shock makes with the horizontal streamline in front of the shock and the velocity of the approaching flow. This presents an additional degree of freedom in the oblique shock relations.

An additional degree of freedom means that although only one independent parameter, i.e., approach Mach, M_1 , is required for normal shock relations, two independent parameters are required for oblique shock relations, i.e., M_1 and wave angle, θ .

6.14.1 Oblique Shock Relations

Since a shock appears to be normal or oblique depending upon the relative motion of the observer, the differences between normal and oblique shocks can be explained in geometric terms.

The flow orientation, flow notation, and angle descriptions used when modifying the normal shock equations are shown in Figure 6.13.

The number of degrees the flow must turn due to the concave corner is called the turning angle or wedge angle, δ . The angle the oblique shock makes with the incoming (upstream) streamlines is called the shock wave angle, θ .

Conditions upstream of the oblique shock have the subscript 1, and conditions downstream have the subscript 2.

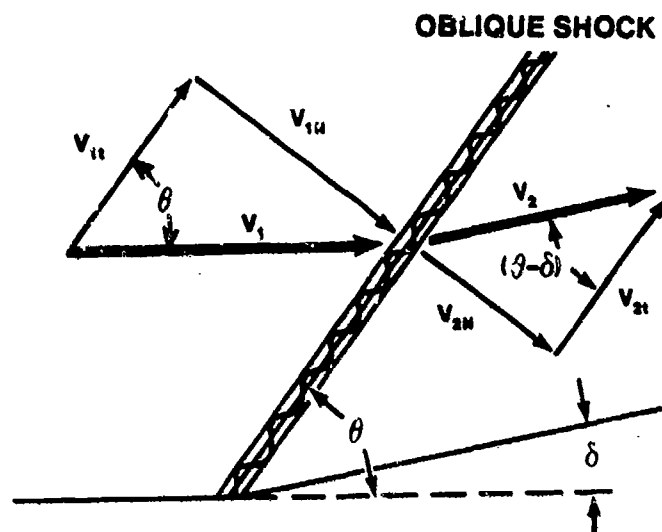


FIGURE 6.13. ANALYSIS OF VELOCITY COMPONENTS ACROSS AN OBLIQUE SHOCK

From this figure, it can be seen that

$$M_{1N} = M_1 \sin \theta \quad (6.47)$$

where

M_{1N} = Flow Mach in front of a normal shock

M_1 = Flow Mach in front of an oblique shock

Consequently, all of the normal shock equations can be modified to apply to oblique shocks by substituting $M_1 \sin \theta$ everywhere M_1 appears. The oblique shock equations are

$$\frac{P_2}{P_1} = \frac{1 - \gamma + 2\gamma M_1^2 \sin^2 \theta}{1 + \gamma} \quad (6.48)$$

$$\frac{\rho_2}{\rho_1} = \left[\frac{2 + (\gamma - 1) M_1^2 \sin^2 \theta}{(\gamma + 1) M_1^2 \sin^2 \theta} \right]^{-1} \quad (6.49)$$

$$\left(\frac{T_2}{T_1} = \frac{2\gamma}{\gamma+1} M_1^2 \sin^2 \theta - \frac{\gamma-1}{\gamma+1} \right) \left(\frac{\gamma-1}{\gamma+1} + \frac{2}{(\gamma+1) M_1^2 \sin^2 \theta} \right) \quad (6.50)$$

$$M_2^2 \sin^2 (\theta - \delta) = \frac{M_1^2 \sin^2 \theta + \frac{2}{\gamma+1}}{\frac{2}{\gamma-1} M_1^2 \sin^2 \theta - 1} \quad (6.51)$$

$$\frac{P_{T_2}}{P_{T_1}} = \left[\frac{1}{\left(\frac{\gamma-1}{\gamma+1} + \frac{2}{(\gamma+1) M_1^2 \sin^2 \theta} \right)^\gamma \left(\frac{2\gamma}{\gamma+1} M_1^2 \sin^2 \theta - \frac{\gamma-1}{\gamma+1} \right)} \right]^{\frac{1}{\gamma-1}}$$

6.14.2 Minimum and Maximum Wave Angles

In the normal shock analysis, it was found that a shock can only occur when the free stream Mach is greater than one. The same is true for oblique shocks; the free stream Mach component normal to the shock must be greater than one.

The minimum wave angle for a given free stream Mach of $M_1 > 1$ can be found from Equation 6.47

$$M_{1N} = M_1 \sin \theta = 1$$

or

$$\theta_{(\text{Min})} = \sin^{-1} \frac{1}{M_1} \quad (6.53)$$

Notice that the minimum oblique shock wave angle, $\theta_{(\text{Min})}$, for the given free stream Mach, M_1 , is the same as the Mach angle, μ , (Equation 6.20) caused by an isentropic pressure disturbance traveling at $M_1 > 1$.

This shows that an oblique shock wave at minimum wave angle to the free stream flow is a zero strength or isentropic shock.

The maximum oblique shock wave angle for a given free stream Mach is 90° . This is the limiting case and is a normal shock.

6.14.3 Relation Between θ and δ

From Figure 6.13

$$\tan \theta = \frac{V_{1N}}{V_{1t}}$$

$$\tan (\theta - \delta) = \frac{V_{2N}}{V_{2t}}$$

Eliminating V_{1t} from these equations, then using the continuity equation, Equation 6.49, and a great amount of algebraic and trigonometric manipulation:

$$\frac{\tan (\theta - \delta)}{\tan \theta} = \frac{(\gamma - 1) M_1^2 \sin^2 \theta + 2}{(\gamma + 1) M_1^2 \sin^2 \theta} \quad (6.54)$$

For a given M_1 , Equation 6.54 is an implicit relation between θ and δ . It may be rewritten to show the dependence of δ explicitly (after much trigonometric manipulation).

$$\tan \delta = 2 \cot \theta \frac{M_1^2 \sin^2 \theta - 1}{M_1^2 (\gamma + \cos 2 \theta) + 2} \quad (6.55)$$

This equation may be solved for various combinations of Mach, M_1 , and wave angle, θ , and plotted as in Figure 6.14.

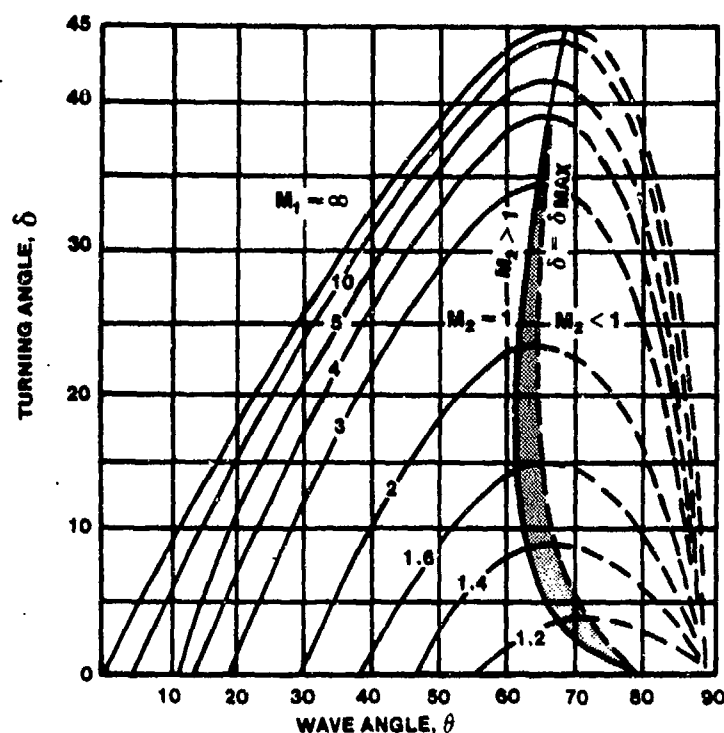


FIGURE 6.14. TURNING ANGLE AS A FUNCTION OF WAVE ANGLE FOR FLOW THROUGH AN OBLIQUE SHOCK

Careful study of this figure will reveal several points of great interest when analyzing the flow through an oblique shock wave.

The existence of a maximum and minimum wave angle is verified by the fact that Equation 6.55 becomes zero at $\theta = \pi/2$ and at $\theta = \sin^{-1} 1/M_1$.

The turning angle, δ , has a maximum value for a given value of M_1 . Turning angles larger than this maximum angle cause the oblique shock to detach from the surface at the concave corner. If δ is less than δ_{\max} , an attached oblique shock will form.

There are two possible oblique shock solutions for a given turning angle, δ , and a given M_1 . The weak shock solution is represented by the solid lines in Figure 6.14, and the strong shock solution by the dotted lines.

The strong shock solution (the oblique shock with the greater wave angle) is characterized by subsonic flow downstream of the shock and by large energy losses in the shock. As a general rule, systems in nature tend to minimize their losses; therefore the weak shock occurs more frequently. However, there is no known mathematical law which predicts the type of shock that will occur for a given free stream Mach and a given turning angle.

The locus of points for which the Mach behind the shock, M_2 , is equal to one is also plotted. It can be seen that the Mach downstream of a weak shock is usually supersonic, but in a small region (cross-hatched) near δ_{\max} for a given free stream Mach, the Mach downstream of a weak shock can be subsonic.

The wave angle, θ , is generally the unknown quantity in analytical work and is conventionally plotted versus M_1 for different turning angles, δ (Figure 6.15).

From this figure, three important points can be noted:

1. There is a minimum allowable flow Mach for a given turning angle, below which the oblique shock will detach from the surface.
2. The wave angle of a weak shock decreases with increased free stream Mach, while the wave angle of a strong shock increases (approaching 90°) with increasing Mach.
3. For a given free stream Mach, the wave angle θ approaches the Mach angle as δ is decreased.

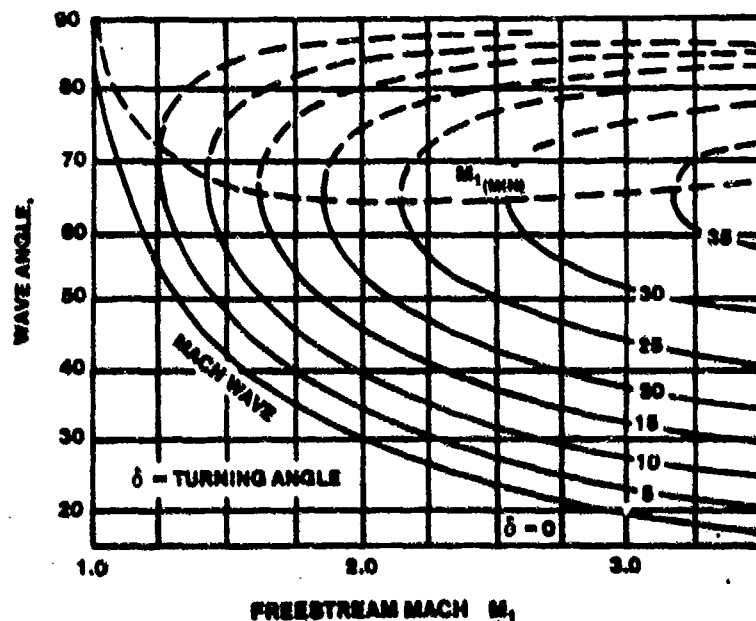


FIGURE 6.15. WAVE ANGLE AS A FUNCTION OF MACH FOR FLOW THROUGH AN OBLIQUE SHOCK

Because of the complexity of the equations for normal and oblique shock waves, it is common practice to use tables or charts of their solutions when solving a compressible flow problem. An excellent set of charts is in Reference 6.4.

6.14.4 Mach Lines

Considering that portion of Figure 6.14 where $M_2 > 1$, a decrease in turning angle δ corresponds to a decrease in wave angle θ . When δ becomes zero, θ reaches the limiting value given by Equation 6.53 which was previously shown to be the Mach angle μ (Equation 6.20).

$$\theta_{\min} = \sin^{-1} \frac{1}{M_1} = \mu \quad (6.53)$$

Analyzing the strength of the oblique shock formed at zero turning angle, with the oblique shock relations, Equations 6.48 through 6.52, it can be seen that the so-called "shock" has zero strength, or that no physical discontinuity in the supersonic flow exists.

For any point in a supersonic flow, there is a characteristic angle associated with the Mach of the flow at that point. This angle is the Mach angle μ . Lines drawn at an inclination of μ at a point in the flow are called Mach lines or sometimes Mach waves.

6.15 ISENTROPIC COMPRESSION

A shock wave compresses supersonic flow by increasing the pressure and density of the fluid in a very short but finite distance. A simple method to compress supersonic flow is to deflect the flow boundary into the flow through an angle, thereby creating an oblique shock wave through which the flow must pass.

By dividing the total boundary deflection into several small segments of $\Delta \delta$, the compression can be visualized as occurring through several successive oblique shocks which divide the flow field near the boundary into segments of uniform flow (Figure 6.16).

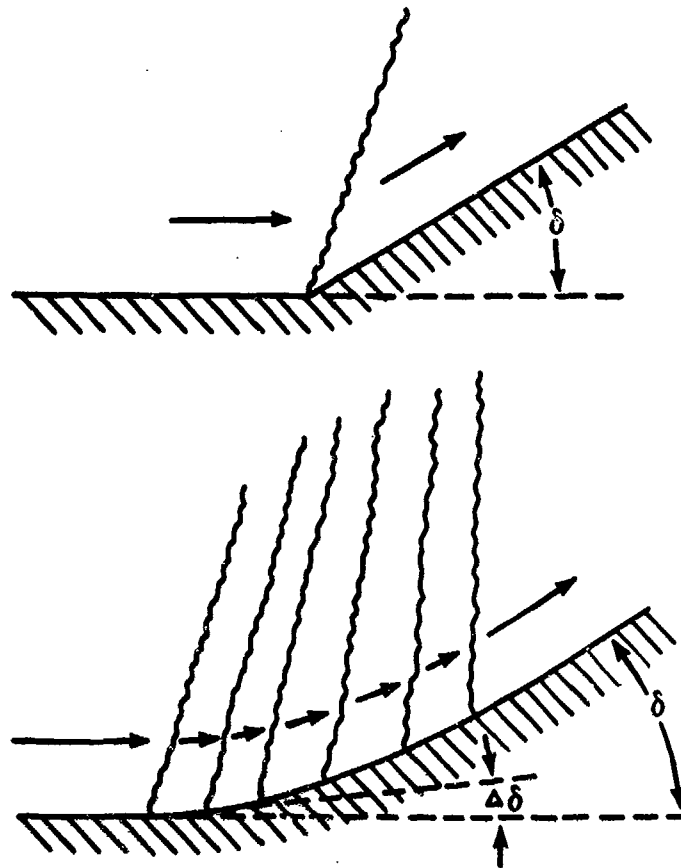


FIGURE 6.16. ISENTROPIC COMPRESSION

In each region between oblique shocks, the supersonic flow is independent of the regions upstream and downstream, making it possible to analyze the flow field region by region.

Using the approximate equation for weak shocks to compare the one shock compression to the multi-shock compression, it can be shown that for each wave

$$\Delta P \approx \Delta \delta$$

$$\Delta S \approx (\Delta \delta)^3$$

If there are n segments being considered in the complete turning angle then

$$\delta = n \Delta \delta$$

and

$$\Delta P_{\text{total}} \approx n \Delta \delta \approx \delta$$

$$\begin{aligned} \Delta S_{\text{total}} &\approx n (\Delta \delta)^3 \approx n \Delta \delta (\Delta \delta)^2 \\ &\approx \delta (\Delta \delta)^2 \end{aligned}$$

Thus, if a large number of weak waves cause the compression, the entropy increase is reduced drastically compared to a one shock compression for the same total turning angle.

By making $\Delta \delta$ smaller and smaller, a smooth turn with $\Delta \delta \rightarrow 0$ is created in the limit, the entropy increase becomes zero, and the compression can be considered isentropic.

This limiting process produces the following results:

1. The oblique shocks approach zero strength and become straight Mach lines.
2. Each region of uniform flow approaches the width of a Mach line; thus on each Mach line the flow inclination and Mach are constant.
3. The flow upstream of each Mach line is not affected by downstream changes in the wall.
4. The approximate equations for changes in properties across weak waves may be written in differential form, i.e., ΔP becomes dP .

The above discussion considers flow near the boundary of the supersonic flow field. Farther away from the wall, due to the convergence of Mach lines, the flow is no longer isentropic, and the Mach lines converge, forming an oblique shock wave.

6.16 ISENTROPIC EXPANSION

When the boundary of a supersonic flow is deflected into the flow, the flow is compressed. If the deflection is abrupt, an oblique shock wave forms

in the corner. If the deflection is smooth, an isentropic analysis of the compression may be performed.

What happens when the boundary is deflected away from the supersonic flow? If a single oblique shock wave formed and the flow expanded through it, this would require that the normal component of velocity after the shock be greater than the normal component of velocity ahead of this shock, i.e., an increase in velocity through the shock (Figure 6.17). This is in direct violation of the second law of thermodynamics because it demands a decrease in entropy (refer to Appendix F, Derivation F.7), even though the equations of motion are satisfied.

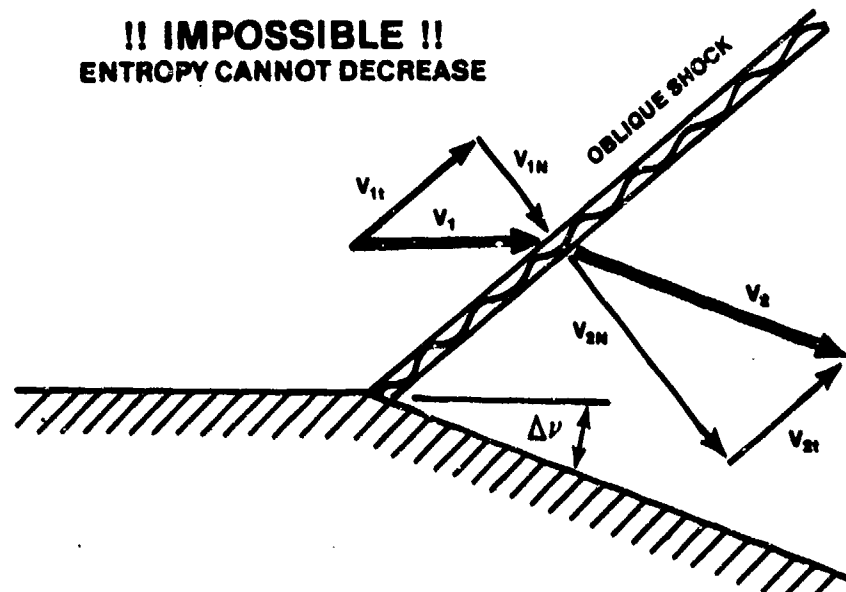


FIGURE 6.17. IMPOSSIBILITY OF SHOCK FORMATION FLOW TURNING AWAY FROM ITSELF

Actually, the same nonlinear effect that makes Mach lines converge in a compression makes the Mach lines diverge in an expansion, and the supersonic expansion is an isentropic phenomenon throughout.

Consider the expansion of supersonic flow caused by the boundary deflection $\Delta\nu$ in Figure 6.18a.

If P_2 is less than P_1 , the disturbances from the lower pressure will be transmitted out into the stream. The pressure P_2 will not be transmitted

upstream since the flow is supersonic, and it will only be felt as far upstream as the Mach line extending out from the corner into the flow.

When the flow passes this Mach line, it will sense the lower pressure and will tend to turn and accelerate because of the pressure differential. Associated with the flow velocity increase is a pressure decrease which changes the flow properties immediately following the Mach line and consequently defines a new Mach line upstream of which the influence of P_2 cannot be felt. Hence, the flow gradually increases velocity and changes direction through an infinite number of these Mach lines, forming a fan shaped array referred to as a "Prandtl-Meyer expansion fan" as shown in Figure 6.18b.

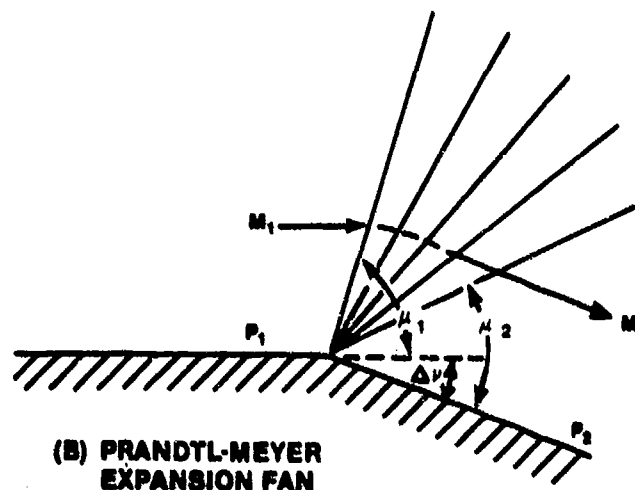
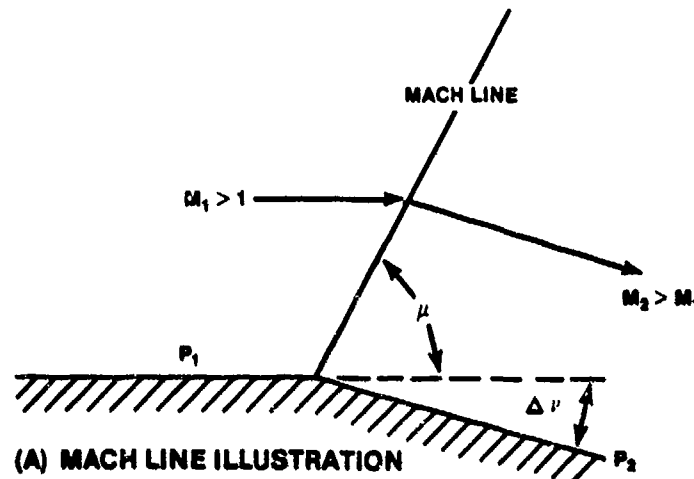


FIGURE 6.18. SUPERSONIC FLOW AROUND A CORNER

As the Mach increases through the first line and the pressure decreases, the approach of subsequent pressure signals is altered slightly by the increased Mach, thus causing the next Mach wave to be more inclined to the free stream. The Mach angle calculated for the last Mach line is that calculated from the final Mach, M_2 , after the turn.

Supersonic expansion occurs not only at abrupt corners but also on smooth surfaces. In this case, the fan is distributed over the entire curve as shown in Figure 6.19.

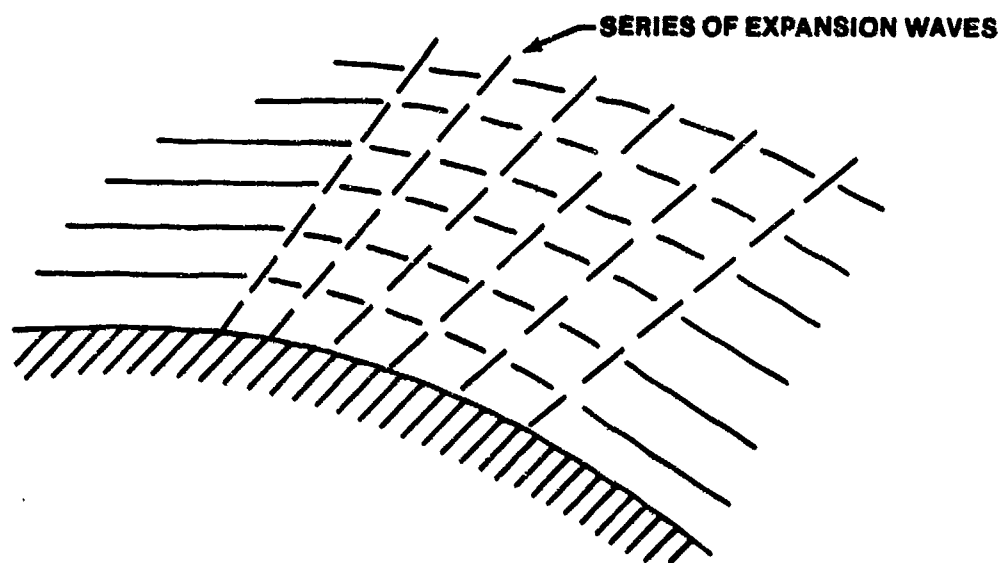


FIGURE 6.19. SUPERSONIC FLOW AROUND A SMOOTH CORNER (6.2:212)

Further insight into the reason for the finite distance required to accelerate the flow around the corner might be gained from a physical interpretation of the acceleration itself. An instantaneous change in velocity and direction around the corner would mean that there was an infinite acceleration for a given mass of fluid. But from Newton's law, $F = ma$, an infinite acceleration requires an infinite force or pressure gradient, and no such source of energy is present; therefore the acceleration cannot be instantaneous.

The equation

$$\frac{\Delta V}{V} = - \frac{\Delta v}{\sqrt{M_1^2 - 1}} \quad (6.56)$$

is an approximate expression relating the velocity change through an isentropic Mach wave to incoming Mach, M_1 , and expansion angle, Δv . Derivation of this equation is tedious and will be omitted. It may be found in many aerodynamic textbooks on supersonic flow.

For small values of Δv and ΔV , Equation 6.56 may be written in differential form

$$-dv = \sqrt{M^2 - 1} \frac{dV}{V}$$

and integrated

$$-v + \text{const} = \int \sqrt{M^2 - 1} \frac{dV}{V} = v(M)$$

To evaluate the integral and thus find an explicit form of $v(M)$, V must be rewritten in terms of M using the following relationships

$$V = a M$$

$$\frac{a_T^2}{a^2} = \frac{\gamma R T_T}{\gamma R T} = \frac{T_T}{T} = 1 + \frac{\gamma - 1}{2} M^2$$

from which

$$\frac{dV}{V} = \frac{dM}{M} + \frac{da}{a} = \frac{dM}{M} \left(\frac{1}{1 + \frac{\gamma-1}{2} M^2} \right)$$

therefore

$$v_{(M)} = \int \frac{\sqrt{M^2 - 1}}{(1 + \frac{\gamma-1}{2} M^2)M} dM$$

This integral may be evaluated between two Mach and is called the Prandtl-Meyer function

$$v_{(M)} = \sqrt{\frac{\gamma+1}{\gamma-1}} \tan^{-1} \sqrt{\frac{\gamma-1}{\gamma+1} (M^2 - 1)} - \tan^{-1} \sqrt{M^2 - 1} \quad (6.57)$$

The constant of integration was chosen such that $v_1 = 0$ when $M_1 = 1.0$. Thus, for every supersonic Mach there is a corresponding angle v which represents the angle through which a flow that is initially at Mach 1.0 must turn to achieve that supersonic Mach.

If M_1 prior to turning is greater than Mach 1.0, the associated v_1 is greater than zero. To find the Mach following a turn through an angle Δv , it is necessary to add Δv to the v_1 corresponding to M_1 and find the final Mach, M_2 , corresponding to v_2 .

In equation form, this may be written

$$v_2 = v_1 + \left| \Delta v \right| \quad (6.58)$$

where Δv is the turning angle shown in Figure 6.18a. Absolute values of Δv are used to avoid any confusion associated with the sign of the turning angle.

Tables for solving two-dimensional isentropic expansion problems may be found in Reference 6.4 and Figure 6.20 outlines the method to be used. Once the Mach after expansion is known, all of the supersonic flow properties may be calculated from isentropic relations.

Consider the problem of $M_1 = 2.0$ flow expanding through an angle of 24° . What is the Mach after the turn? Enter Figure 6.20 with $M_1 = 2.0$ and find $v_1 = 26^\circ$. This is the angle $M_1 = 1$ flow must turn through to reach a value of Mach two. Adding $v_1 = \Delta v$ and reentering the figure at this value of 50° , M_2 can be found to have a value of Mach three.

If the Mach in Equation 6.57 goes to infinity, which corresponds to expanding supersonic flow to zero pressure, the maximum turning angle is obtained

$$\Delta v_{\max} = \frac{\pi}{2} \left(\sqrt{\frac{\gamma+1}{\gamma-1}} - 1 \right) \quad (6.59)$$

Thus a flow that is initially at Mach 1.0 can turn 130.5° . But a stream that is initially at 2.5 Mach can turn only 90° . The higher the initial Mach, the lower the turning capability. Using Equations 6.58 and 6.59, an expression for the turning capability, v_{tc} , of the flow can be obtained.

$$v_{tc} = \Delta v_{\max} - v_1 \quad (6.60)$$

Attention is called to the fact that these are the theoretical angles at which the flow will leave the surface for any initial Mach and that very high deflection angles are indicated at all Mach. In practice, real fluid effects such as boundary layer and viscosity will greatly reduce the angle at which the flow will leave the surface.

Table 6.1 summarizes the characteristics of the three wave forms encountered in supersonic flow.

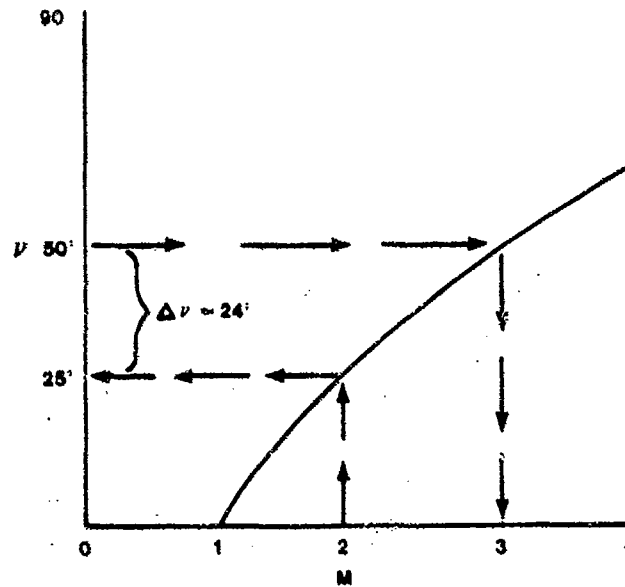


FIGURE 6.20. TURNING ANGLE AS A FUNCTION OF MACH FOR PRANDTL-MEYER FLOW

Type of wave formation	Oblique shock wave	Normal shock wave	Expansion wave.
Flow direction change	"Flow into a corner," turned into preceding flow.	No change	"Flow around a corner," turned away from preceding flow.
Effect on velocity and Mach.	Decreased but still supersonic.	Decreased to subsonic	Increased to higher supersonic.
Effect on static pressure and density.	Increase	Great increase	Decrease.
Effect on energy or total pressure.	Decrease	Great decrease	No change (no shock).

TABLE 6.1. SUPERSONIC WAVE CHARACTERISTICS (6.2:213)

6.17 INTERACTION OF WAVE FORMS

Successive oblique wave forms may interfere with one another. Four cases are possible:

1. Expansion followed by expansion
2. Compression followed by compression
3. Compression followed by expansion
4. Expansion followed by compression

This discussion is limited to two-dimensional analysis.

Case one is most easily analyzed because there are no interference effects. This can be seen with reference to Figure 6.21. The final effect is equivalent to flow over a rounded corner with the same total deflection angle.

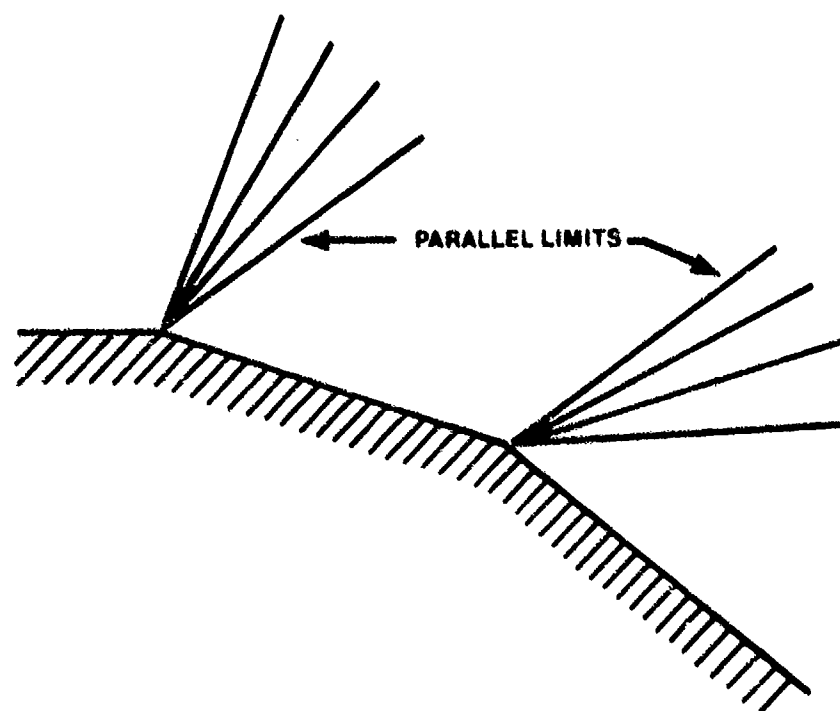


FIGURE 6.21. TWO EXPANSIONS (6.5.132)

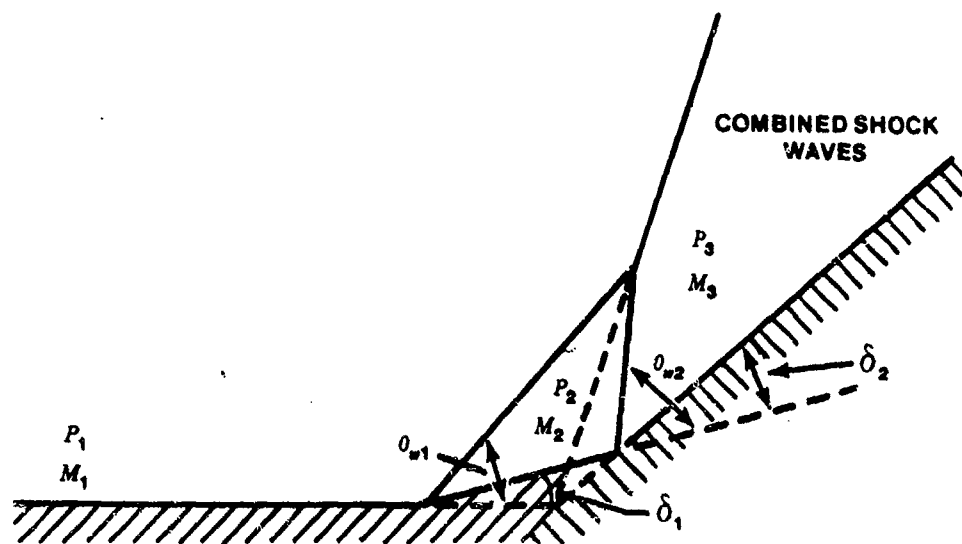


FIGURE 6.22. TWO COMPRESSIONS (6.5.133)

When one oblique shock is followed by another, as in Figure 6.22, interaction must occur and results in a single shock of increased intensity at some distance away from the wall. Recall that the Mach after an oblique shock is always decreased and the flow is bent toward the wave. A second oblique shock generated behind the first with a subsequent second change in flow direction increases the shock wave angle because of the reduction in stream velocity, and the wave will be tilted toward the first oblique shock due to the initial deflection. Therefore, the two shock lines must intersect. The intersection of the two separate waves must form a wave which has the same angle as that applying to a wave formed by a single intersection of the initial and final surfaces. The wave formed by the combination is therefore stronger than either one alone.

If we have an oblique shock followed by an expansion, we must also have an intersection. Because of the nature of expansion waves, the intersection will be a diffuse effect which tends to weaken the shock at points away from the surface. Because the velocity of the wave is dependent upon its intensity, the weakening effect in the regions away from the surface will reduce the propagation velocity and cause the oblique shock wave front to bend as illustrated in Figure 6.23.

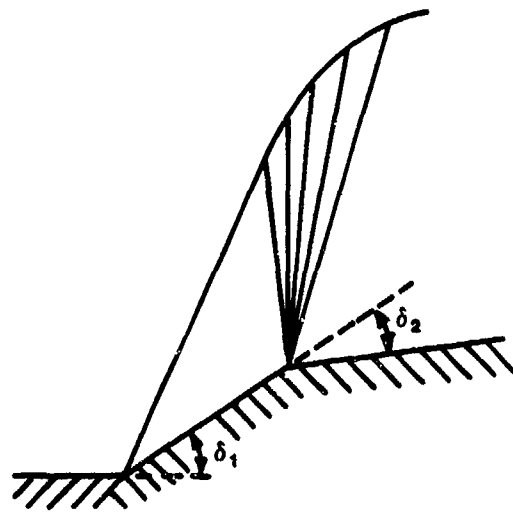


FIGURE 6.23. SHOCK FOLLOWED BY EXPANSION (6.5:134)

The case of expansion followed by compression is very similar to the case just discussed.

Intersection with a weakening of the shock wave must occur. The details of the intersection are different because the intersection occurs on the free stream side of the shock instead of in the reduced velocity region behind the shock. Intersection cannot be avoided because the shock wave stands at a higher angle with respect to the expanded flow lines than do some or all of the local Mach lines at the expansion corner. This case is illustrated in Figure 6.24 (6.5:132-136).

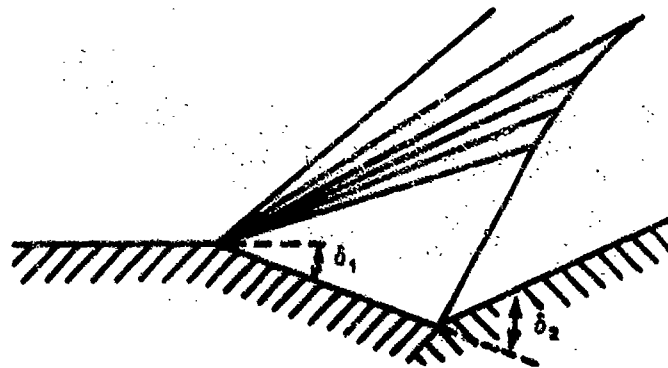


FIGURE 6.24. EXPANSION FOLLOWED BY SHOCK (6.5:135)

6.18 TWO-DIMENSIONAL SUPERSONIC AIRFOILS

In order to appreciate the effect of these various wave forms upon aerodynamic characteristics in supersonic flow, refer to Figure 6.25. Parts a and b show the wave pattern and resulting pressure distribution for a thin flat plate at a positive angle of attack. The airstream moving over the upper surface passes through an expansion wave at the leading edge and an oblique shock at the trailing edge. Therefore, a uniform suction pressure exists over the upper surface. The airstream moving underneath the flat plate passes through an oblique shock wave at the leading edge and an expansion wave at the trailing edge. Therefore, a uniform positive pressure exists on the underside of the section. This pressure distribution produces a net lift and also a drag due to lift. The drag is analagous to induced drag in subsonic flow but is not a function of downwash as is the case in subsonic flow. Remember that pressure disturbances cannot be transmitted ahead of an object in supersonic flow, so the fluid is not aware of the approaching object.

The flat plate, although aerodynamically quite efficient at supersonic speeds, is not structurally satisfactory. It is difficult to give it enough strength to withstand the loads imposed on the airfoil during high speed flight.

Parts c and d of Figure 6.25 show the wave pattern and pressure distribution for a double wedge airfoil at zero lift. The resulting pressure distribution on the surfaces of the double wedge produces no net lift, but the increased pressure on the forward half along with the decreased pressure on the rear half of the section produces wave drag. This wave drag is a result of the components of the pressure forces which are parallel to the free stream direction, and can be a large portion of the total drag at high supersonic speeds.

Parts e and f of Figure 6.25 illustrate the wave pattern and resulting pressure distribution for the double wedge airfoil at a small positive angle of attack. The net pressure distribution produces drag due to lift in addition to the wave drag at zero lift. Parts g and h show the wave pattern and pressure distribution for a circular arc airfoil (also called a bi-convex airfoil) at zero lift. Notice the large wave drag even though no net lift is produced.

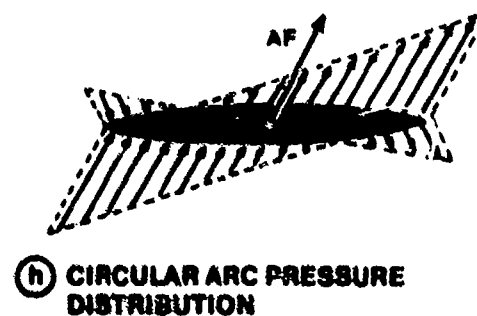
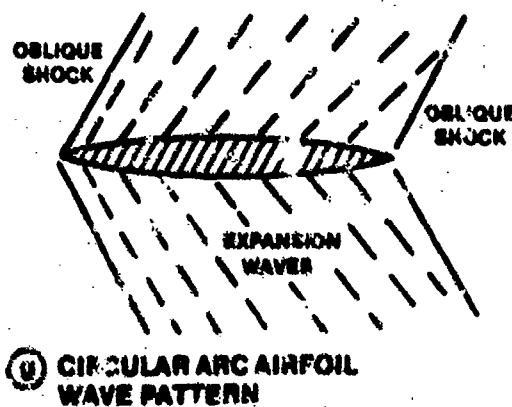
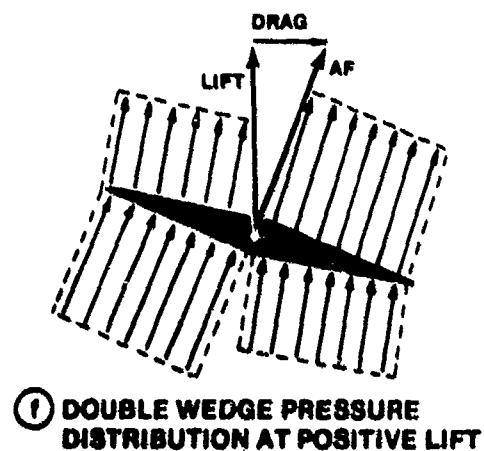
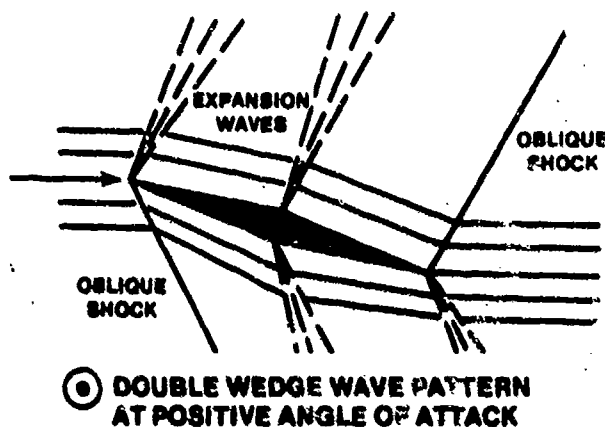
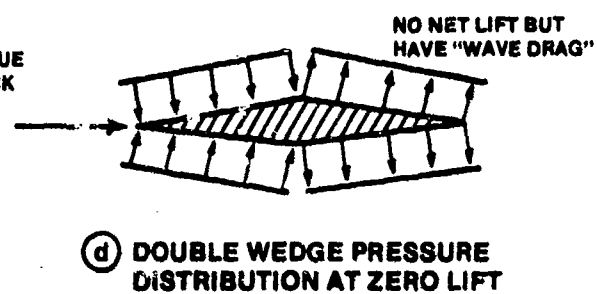
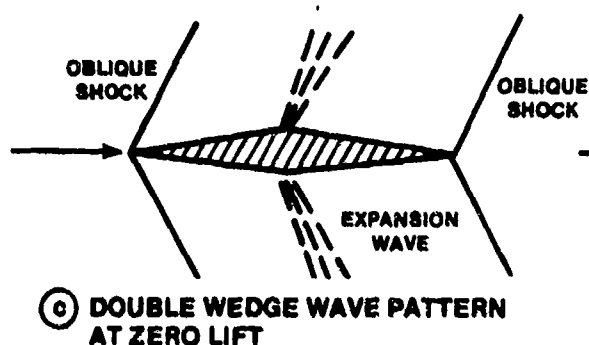
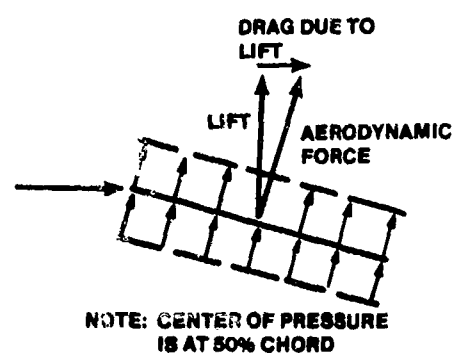
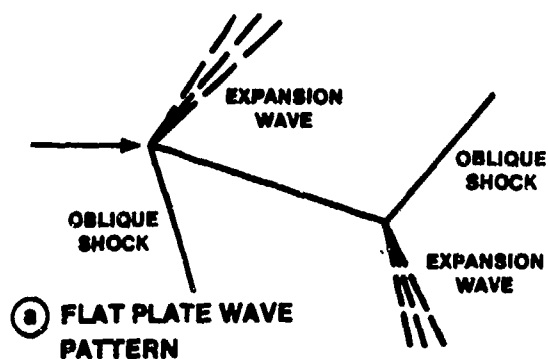


FIGURE 6.25. SUPERSONIC FLOW PATTERN AND DISTRIBUTION OF PRESSURE (6.1:163, 165; 6.2:214)

6.19 PRESSURE COEFFICIENT FOR TWO-DIMENSIONAL SUPERSONIC AIRFOILS AND INFINITE WINGS

The preceding paragraph on the different supersonic waveforms have developed all of the mathematical tools required to compute the lift and drag on a simple two-dimensional supersonic airfoil. Consider the double wedge or diamond airfoil shown in Figure 6.26.

If the flight Mach, M_∞ , remote ambient pressure, P_∞ , angle of attack, α , and the geometry of the wing are known, pressures in areas 2, 3, 5, and 6 can be computed. Oblique shock relationships can be used to determine P_2 and P_5 from P_∞ , and Prandtl-Meyer relations can be used to determine P_3 and P_6 from P_2 and P_5 . Once these pressures are known, lift and drag can be readily determined from geometric relationships.

This problem can be attacked in a more systematic manner by recalling the definition of pressure coefficient

$$C_p = \frac{P - P_\infty}{q_\infty}$$

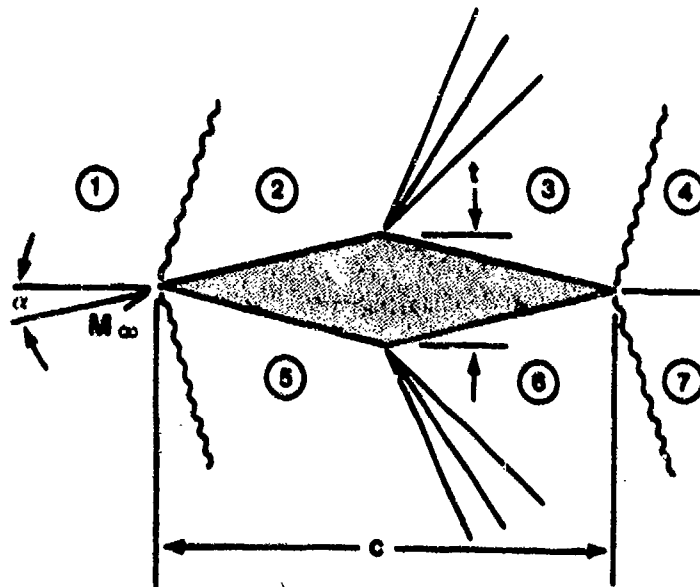


FIGURE 6.26. DOUBLE WEDGE AIRFOIL IN SUPERSONIC FLOW

For an example of the diamond airfoil, the local pressure coefficient can be expressed as

$$\left[C_p \right]_x = \frac{P_x - P_\infty}{q_\infty} \quad (6.61)$$

when $x = 2, 3, 5$, or 6 , depending on the area of the airfoil under consideration.

In terms of remote Mach, M_∞ , Equation 6.61 can be rewritten as

$$\left[C_p \right]_x = \frac{2}{M_\infty^2 \gamma} \left[\frac{P_x}{P_\infty} - 1 \right] \quad (6.62)$$

Given α , the geometry of the airfoil, M_∞ , and $\gamma = 1.4$, C_{p_2} and C_{p_5} can be determined directly from Reference 6.4 and use of Equation 6.61.

The evaluation of Equation 6.62 for C_{p_3} and C_{p_6} can also be easily made. In determining C_{p_3} , for example,

$$P_3/P_\infty = \left[P_2/P_\infty \right] \left[P_{T2}/P_2 \right] \left[P_3/P_{T3} \right] \quad (6.63)$$

All of the ratios on the right side of Equation 6.63 are found in Reference 6.4 tables after M_2 and M_3 are determined. After C_{p_2} , C_{p_3} , C_{p_5} , and C_{p_6} are determined, the forces normal to each surface can be calculated, since

$$F_x = \left[C_p \right]_x q_\infty S$$

when F_x is the force normal to the surface, and again $x = 2, 3, 5$, or 6 , depending upon the area of the airfoil under consideration. Once all the F_x 's are known, they can be resolved into components perpendicular to and parallel with the relative wind to determine lift and drag.

6.20 THIN WING THEORY

Although an exact analytic determination of lift and drag forces acting on even a simple two-dimensional supersonic airfoil is a somewhat lengthy problem (as shown in the paragraph on two-dimensional wings), an approximate determination is readily accomplished.

Probably the most widely accepted of the approximate (or thin wing) supersonic theories is the one due to Ackeret which is either called the linear theory or simply the Ackeret theory. For thin airfoils set at relatively small angles of attack, the Ackeret theory agrees well with experimental data from Mach of about 1.2 to 5.0, and therefore the assumptions made in its development are empirically justified.

A pressure coefficient is developed (Derivation F.8 Appendix F) such that

$$C_p = \frac{\Delta P}{q} = \pm \frac{2\delta}{\sqrt{M^2 - 1}}$$

where the minus sign holds for an expansion and the plus sign holds for a compression.

For the double wedge, Ackeret Theory predicts that

$$C_L = \frac{4\alpha}{\sqrt{M^2 - 1}} \quad (6.64)$$

$$C_D = \frac{4\alpha^2}{\sqrt{M^2 - 1}} + \frac{4}{\sqrt{M^2 - 1}} \left(\frac{t}{c}\right)^2 \quad (6.65)$$

We can write the drag coefficient of the double wedge in the same form we had for subsonic flow,

$$C_{D_{tot}} = C_{D_i} + C_{D_p} \quad (6.66)$$

Comparing the terms in Equation 6.66 with Ackeret theory gives

$$C_{D_p} = \frac{4(t/c)^2}{\sqrt{M^2 - 1}} \quad (6.67)$$

$$C_{D_i} = \frac{4\alpha^2}{\sqrt{M^2 - 1}} \quad (6.68)$$

As in subsonic flow, C_{D_p} is not a function of α . It is often defined as the wave drag coefficient when $\alpha = 0$. This term is due to the profile shape and is similar to the profile (parasite) drag term of a subsonic wing section, although it does not depend on viscosity. C_{D_p} is a function of Mach and the thickness ratio (t/c) defined in Figure 6.26.

The second term, C_{D_i} , can be defined as drag coefficient due to lift and is a direct function of α^2 .

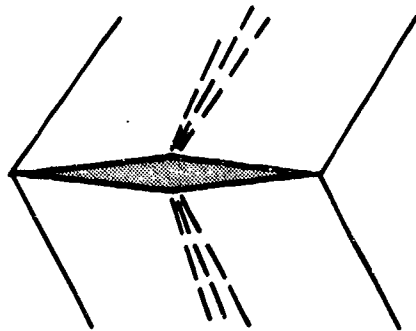
By allowing t to equal zero, Equation 6.65 immediately simplifies to the coefficient of drag equation for a flat plate, Equation 6.69.

$$C_{D_{tot}} = \frac{4\alpha^2}{\sqrt{M^2 - 1}} \quad (6.69)$$

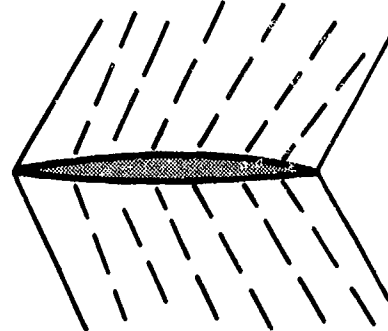
From Ackeret theory the equation for lift coefficient for both the flat plate and for the double wedge turns out to be

$$C_L = \frac{4\alpha}{\sqrt{M^2 - 1}} \quad (6.70)$$

The Ackeret theory presented here may be extended to other airfoil shapes, and in all cases, the form of the equations is similar. Figure 6.27 summarizes the lift and drag coefficient relationships for the double wedge and circular arc airfoils, the two types most commonly used for supersonic flight vehicles.



DOUBLE WEDGE SECTION



CIRCULAR ARC SECTION

WAVE DRAG COEFFICIENT:

$$C_{D_p} = \frac{4 (t/c)^2}{\sqrt{M^2-1}}$$

$$C_{D_p} = \frac{5.33 (t/c)^2}{\sqrt{M^2-1}}$$

LIFT COEFFICIENT:

$$C_L = \frac{4\alpha}{\sqrt{M^2-1}}$$

$$C_L = \frac{4\alpha}{\sqrt{M^2-1}}$$

DRAG DUE TO LIFT:

$$C_{D_i} = \frac{4\alpha^2}{\sqrt{M^2-1}}$$

$$C_{D_i} = \frac{4\alpha^2}{\sqrt{M^2-1}}$$

LIFT CURVE SLOPE:

$$C_{L_\alpha} = \frac{4}{\sqrt{M^2-1}}$$

$$C_{L_\alpha} = \frac{4}{\sqrt{M^2-1}}$$

WHERE

(t/c) = AIRFOIL THICKNESS RATIO

α = ANGLE OF ATTACK (IN RADIANS)

M = MACH

FIGURE 6.27. APPROXIMATE EQUATIONS FOR SUPERSONIC SECTION CHARACTERISTICS (6.2:225)

6.21 SUPERSONIC FLOW IN THREE DIMENSIONS

In supersonic three-dimensional flow we must consider the fact that the stream lines do not turn immediately as they do in the two-dimensional case. Therefore, the shock wave for a typical three-dimensional shape, i.e., a cone, will be weaker for a given velocity. The stream lines approach the object's surface in a rather asymptotic fashion. This is seen from the fact that at all points off the apex of the cone, the section presented to the flow is a hyperbolic section rather than a sharp point. Because of this fact, we have the gradual transition shown in Figure 6.28.

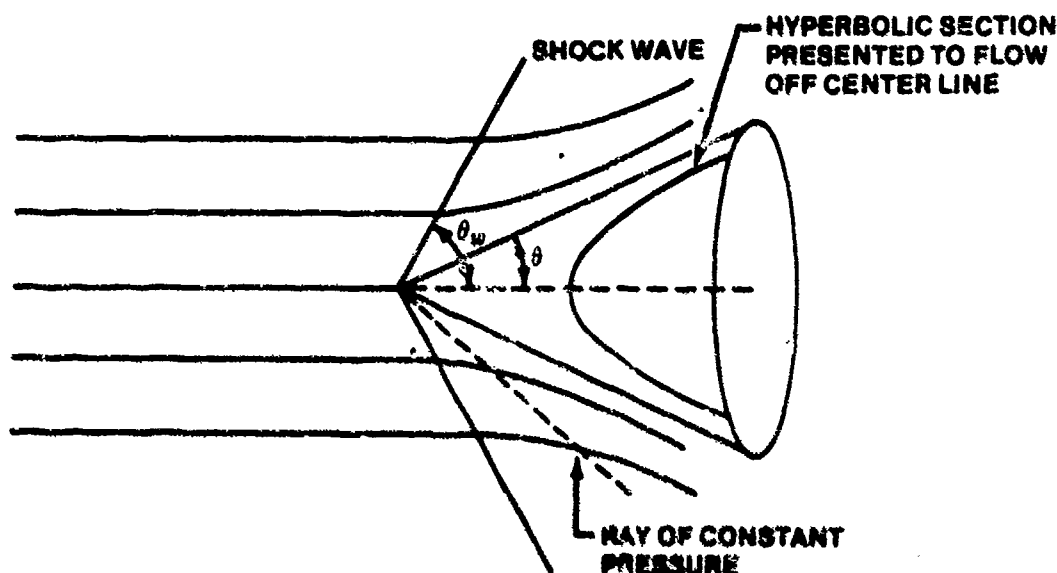


FIGURE 6.28. STREAM LINES ABOUT A CONE (6.5:123)

As would be expected, the pressure, density, temperature, velocity, and Mach all vary between the shock wave and the surface. After increasing through the shock wave, the static pressure and density would continue to increase along a stream line, and the velocity and Mach would therefore continue to decrease. However, the pressure along any ray from the apex of the cone is constant. Since the surface of the cone is essentially the limiting ray from the apex, the surface pressure is constant. Because of the nature of the flow, this pressure is considerably lower than that found at the surface of an infinite wedge of the same apex angle. For a given vertex angle and free stream flow, the pressure change for a cone is

about one-third that for a wedge.

If the cone we have been discussing is suddenly flared out at a new angle, we will have a condition in which the surface is formed by the intersection of two coaxial cones. This situation is illustrated in Figure 6.29.

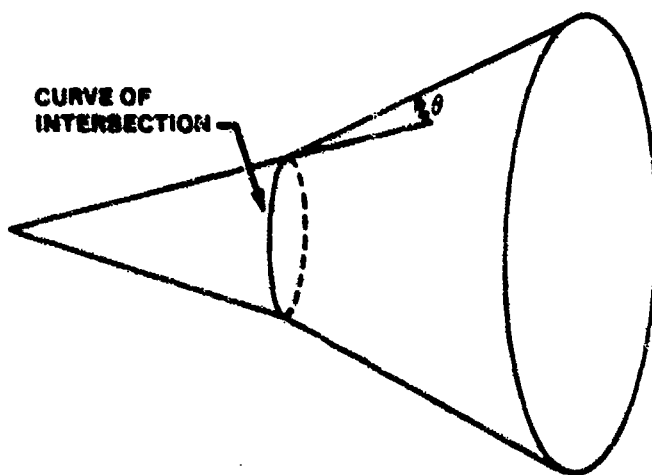


FIGURE 6.29. THE FLARED CONE (6.5:123)

The curve of intersection of the two surfaces is a circle as shown. If this circle is of large radius, we shall have the approximation of two-dimensional flow at the corner as the air is forced to turn through the angle θ . The effect of the rounded shape, however, acts to relieve the severity of the shock and modify the details of the flow. Because of this action, the line of the shock wave will be a curve rather than a straight line. This is illustrated in Figure 6.30.

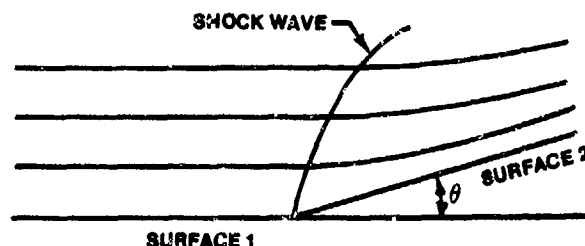


FIGURE 6.30. FLOW IN A ROUND CORNER (6.5:124)

As shown, the stream lines change direction at the shock wave. However, they continue to change gradually to approach the condition of parallel flow as we expect on the surface of a cone. The bending of the shock line is related to the surface curvature (6.5:122-124).

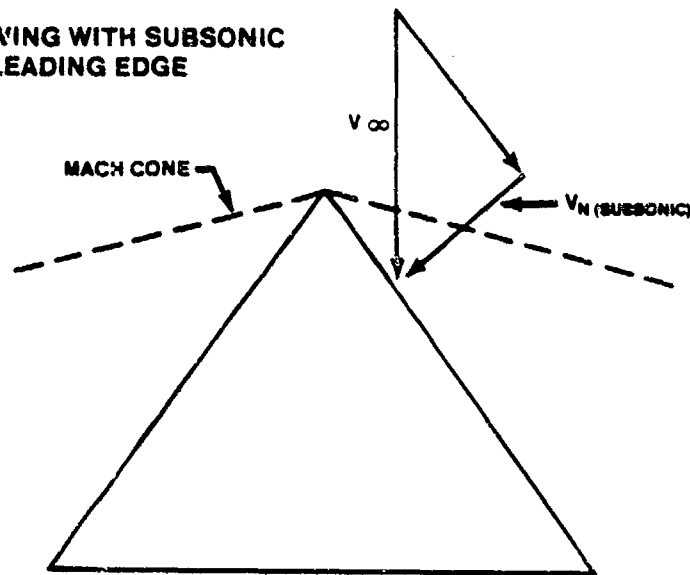
Practical application of the three-dimensional effects discussed above could be applied to the juncture of canopy and nose on an aircraft or to conical plugs found in engine inlets such as those on the SR-71.

6.22 THREE-DIMENSIONAL SUPERSONIC WINGS

To this point we have considered only the infinite wing in two-dimensional flow. If we have a finite planform such as that given in Figure 6.31, we can expect the apex to generate a Mach cone as indicated. This will be true in any practical case of an aircraft in flight because of the nose section ahead of the wing. The nose will generate a cone of disturbance in which at least a portion of the wing will fly. As the velocity of flight, V_∞ , increases, the cone narrows as indicated in Figure 6.31b.

When the leading edge of the wing is behind the Mach cone angle as shown in Figure 6.31a, the normal Mach is subsonic, and no shock wave is created at the leading edge. The pressure distribution and the forces resulting will be equivalent to those found in an airfoil normal to the stream at the corresponding subsonic Mach. In this case, it is advantageous to use a subsonic airfoil section rather than a supersonic section if the wing will always be below the effective Mach of unity.

(A) WING WITH SUBSONIC LEADING EDGE



(B) WING WITH SUPERSONIC LEADING EDGE

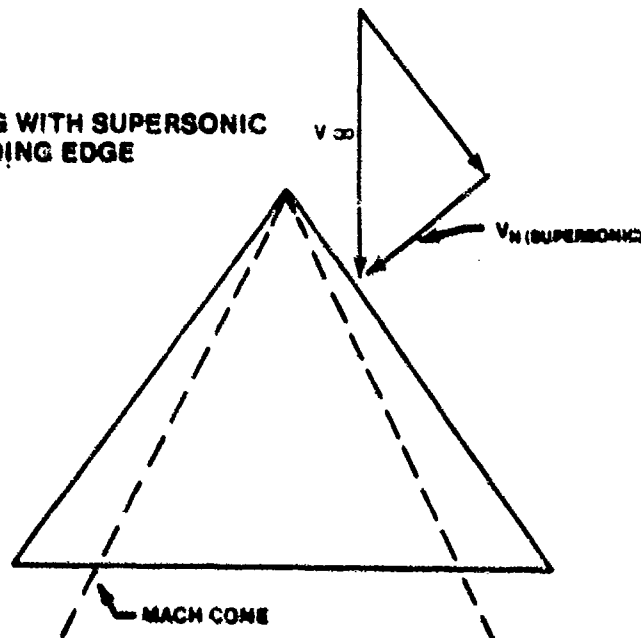


FIGURE 6.31. MACH CONE LIMITS.

If the Mach cone falls behind the leading edge as shown in Figure 6.31b, the effective flow on the wing is supersonic at the leading edge. However, it is quite possible that the effective flow may be supersonic at the leading edge but subsonic at the trailing edge. This would certainly happen behind a shock cone. The pressure distribution is modified by the transition from

supersonic to subsonic flow.

These effects are also involved in the analysis of tip losses. Let us consider a flat plate wing of finite aspect ratio as shown in Figure 6.32.

Since the tip losses are confined to the region within the tip cones, the tips could be cut off at an angle slightly greater than the Mach angle so that none of the wing is contained within the Mach cone. Then there are no induced effects, and the wing acts as in two-dimensional flow, and Equations 6.69 and 6.70 apply.

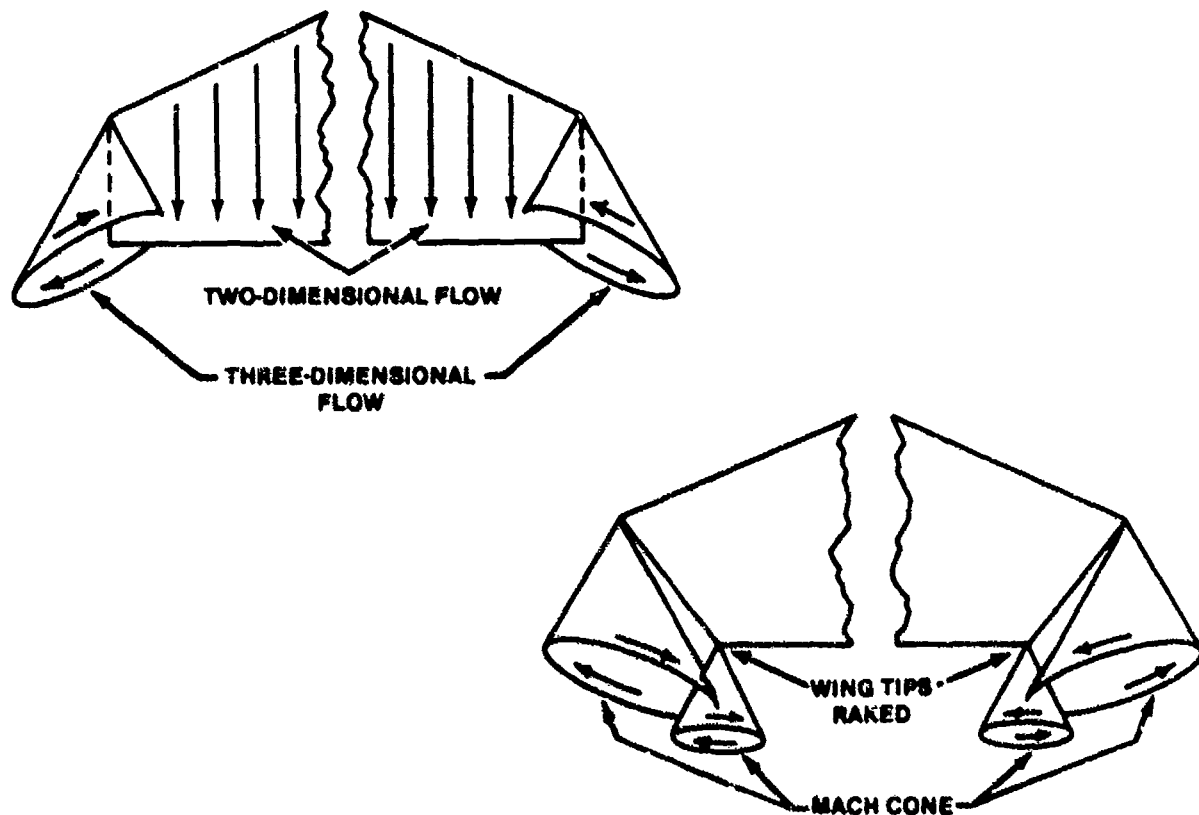


FIGURE 6.32. SUPERSONIC TIP EFFECTS (6.1:166)

6.23 TRANSONIC FLOW REGIME

In the previous paragraphs, the subject of transonic aerodynamics has been judiciously avoided. It can be seen from Ackeret thin wing theory

(Equations 6.67 - 6.70) that lift and drag tend to become infinite in the vicinity of Mach 1.0. A similar result is also found from subsonic theory proposed by Prandtl and Glauert, shown in Figure 6.33.

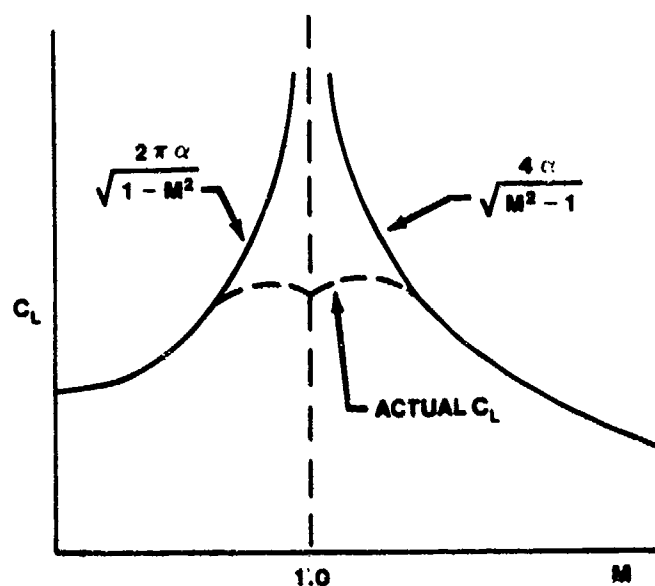


FIGURE 6.33. TRANSONIC LIFT COEFFICIENT CHARACTERISTICS

From this figure comes the concept of the mythical sonic barrier. In the actual case, the lift coefficient follows a trend more like that indicated by the dotted line.

Transonic flow over a body is complicated by the fact that both subsonic and supersonic flows exist simultaneously on the surface of the aircraft. The interaction between these two types of flow plus the viscous effects in the boundary layer create a condition that defies direct mathematical analysis.

Even experimental results in the wind tunnel are difficult to obtain because of the tunnel choking effects caused when a model is placed in the nearly sonic throat of the tunnel. The approach in this chapter will be to extrapolate the concepts of viscous, subsonic flow and nonviscous supersonic

flow into this region of mixed flow conditions resulting in a qualitative look at the transonic speed range.

The transonic speed range begins when sonic flow first occurs over the surface of the vehicle and ends when the flow is supersonic over the entire surface (with the possible exception of a small insignificant subsonic region at the leading edge).

From Bernoulli's theorem, it has been shown that the velocity increases and the pressure decreases as air flows subsonically over the surface of an airfoil. As the Mach of the vehicle is increased, the flow near the thickest portion of the airfoil approaches Mach 1.0 as in Figure 6.34a.

This is the critical Mach of the airfoil and is always less than 1.0. When the vehicle velocity exceeds the critical Mach, regions of subsonic and supersonic flow are created on the airfoil as shown in Figure 6.34, parts b and c.

A shock always exists at the trailing edge of the supersonic region, and as the vehicle velocity is increased above the critical Mach, the supersonic region grows fore and aft of the point of maximum thickness until it reaches the trailing edge and is very nearly attached to the leading edge as in Figure 6.34e.

When the bow shock attaches to the leading edge, the airfoil has left the transonic speed regime and has entered the supersonic regime.

6.23.1 Thickness

As speed increases from subsonic to transonic, thick, unswept, straight-tapered wings show increases in lift-curve slope up to Mach slightly beyond the critical. The slope then drops to a lower value followed by a rise starting near Mach 1.0 to a value almost as high as the value at the critical Mach. This type of behavior is illustrated in Figure 6.33.

Reducing either the aspect ratio, the wing thickness ratio, or both reduces the magnitude of these effects. For very thin wings and for wings of very low aspect ratio, these transonic nonlinearities do not exist, and the C_L -M curve resembles Figure 6.35.

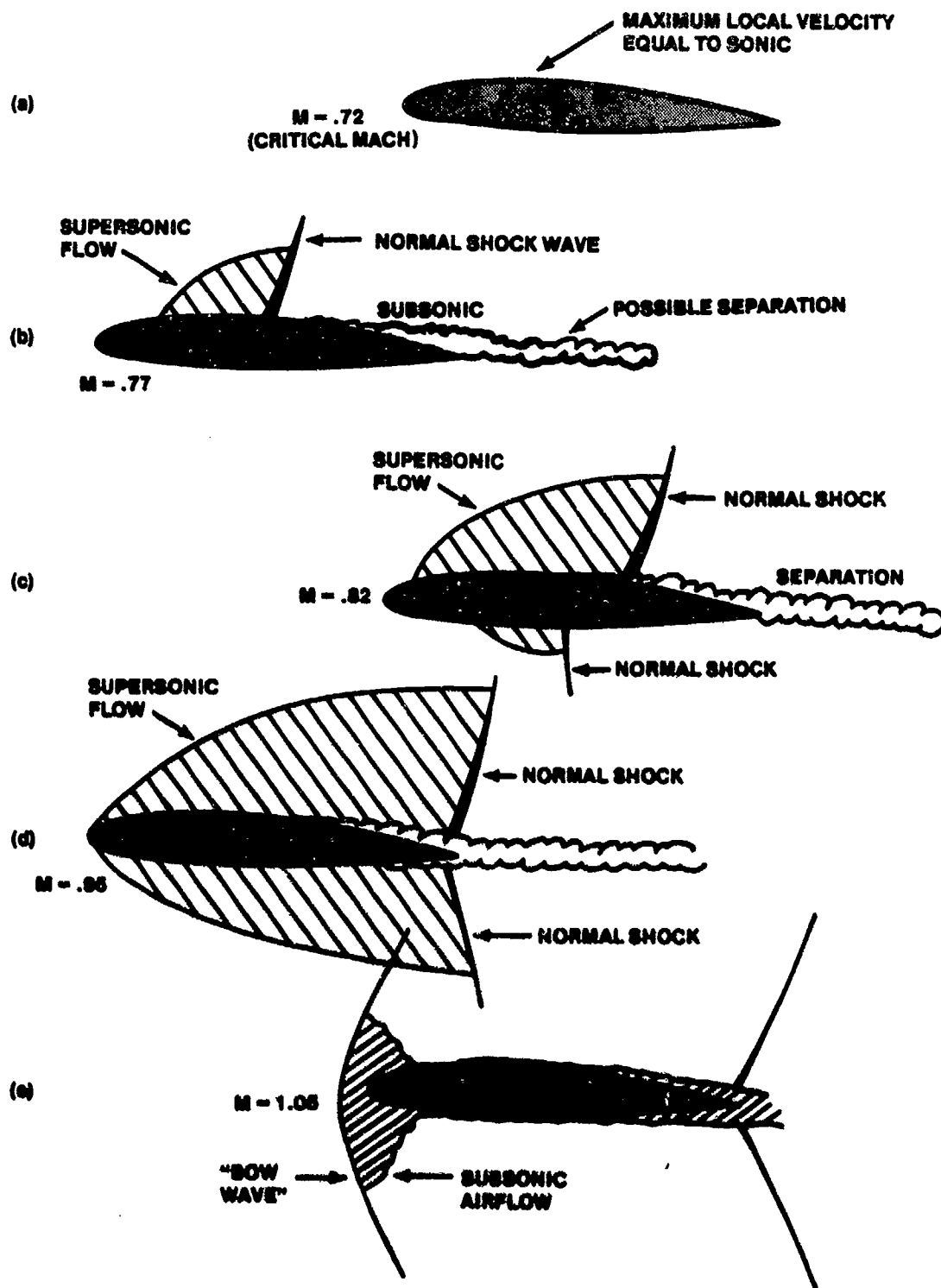


FIGURE 6.34. TRANSONIC FLOW PATTERNS (6.2:216)

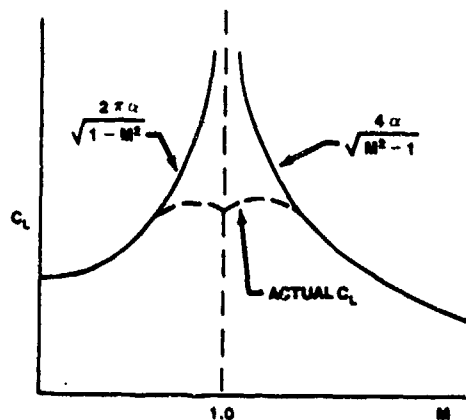


FIGURE 6.35. THIN WING TRANSONIC LIFT COEFFICIENT

Further evidence of the benefits of reducing airfoil thickness for the transonic flight regime is shown in Figure 6.36, where pressure coefficient as a function of critical Mach is shown for various thicknesses of airfoils.

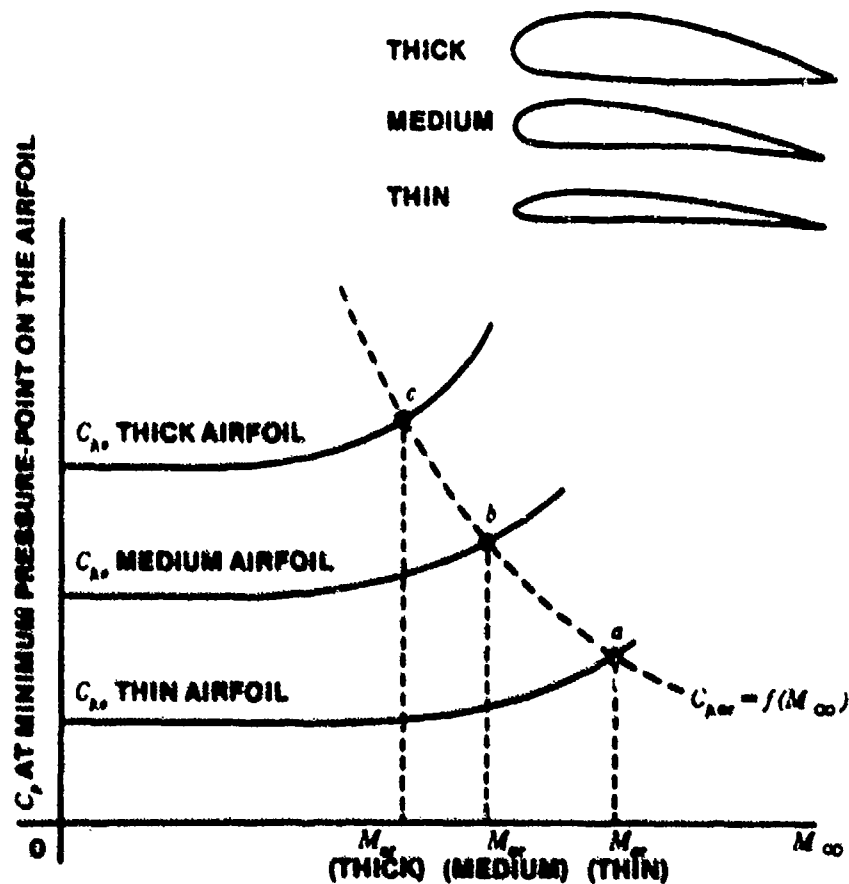


FIGURE 6.36. CRITICAL PRESSURE COEFFICIENT AND CRITICAL MACH FOR AIRFOILS OF DIFFERENT THICKNESSES (6.6:167)

6.23.2 Supercritical Airfoils

Another method which can be utilized to increase critical Mach and delay the transonic drag rise is to use a supercritical airfoil. Such an airfoil is depicted in Figure 6.37. The supercritical airfoil is thicker than the conventional airfoil; this results in greater rigidity and internal volume. At the same time, the recovery shock wave on top of the wing is weaker and is moved much further aft than on conventional airfoils. The supercritical airfoil causes less boundary layer separation, resulting in a delay in the drag rise which occurs on a conventional airfoil section at the critical Mach. The result is that the drag rise associated with passage through critical Mach is delayed.

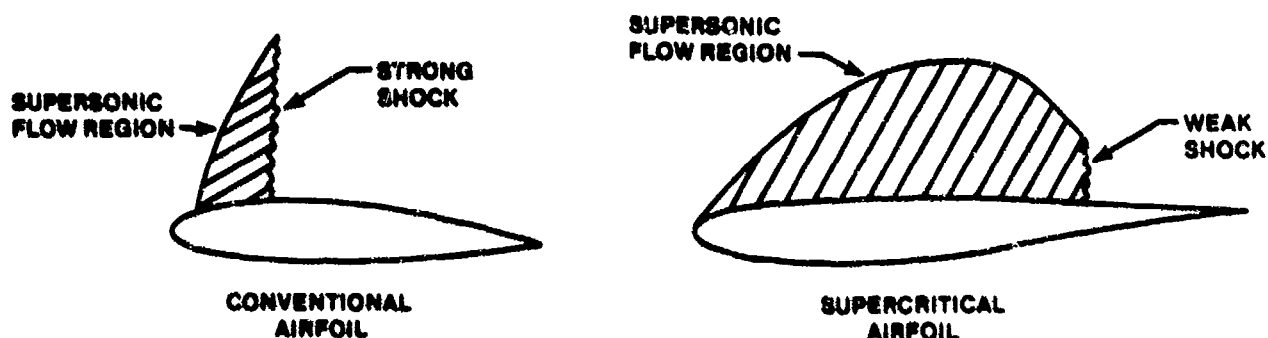


FIGURE 6.37. COMPARISON OF DRAG RISE PHENOMENA AT CRITICAL MACH

6.23.3 Wing Sweep

The final method to be discussed for delaying critical Mach to higher values is wing sweep. To the airstream, the velocity (or Mach) that is important is the component that is perpendicular to the leading edge of the wing. By referring to Figure 6.38a, it is seen that the component of velocity perpendicular to the leading edge of the wing is less than the free stream value by the cosine of the sweep angle Λ . Therefore, the critical Mach is increased, and the transonic drag rise is delayed. Reduction in drag coefficient as a function of Mach for several values of wing sweep is illustrated in Figure 6.38b.

There are, however, some negative aspects of wing sweep. A spanwise flow

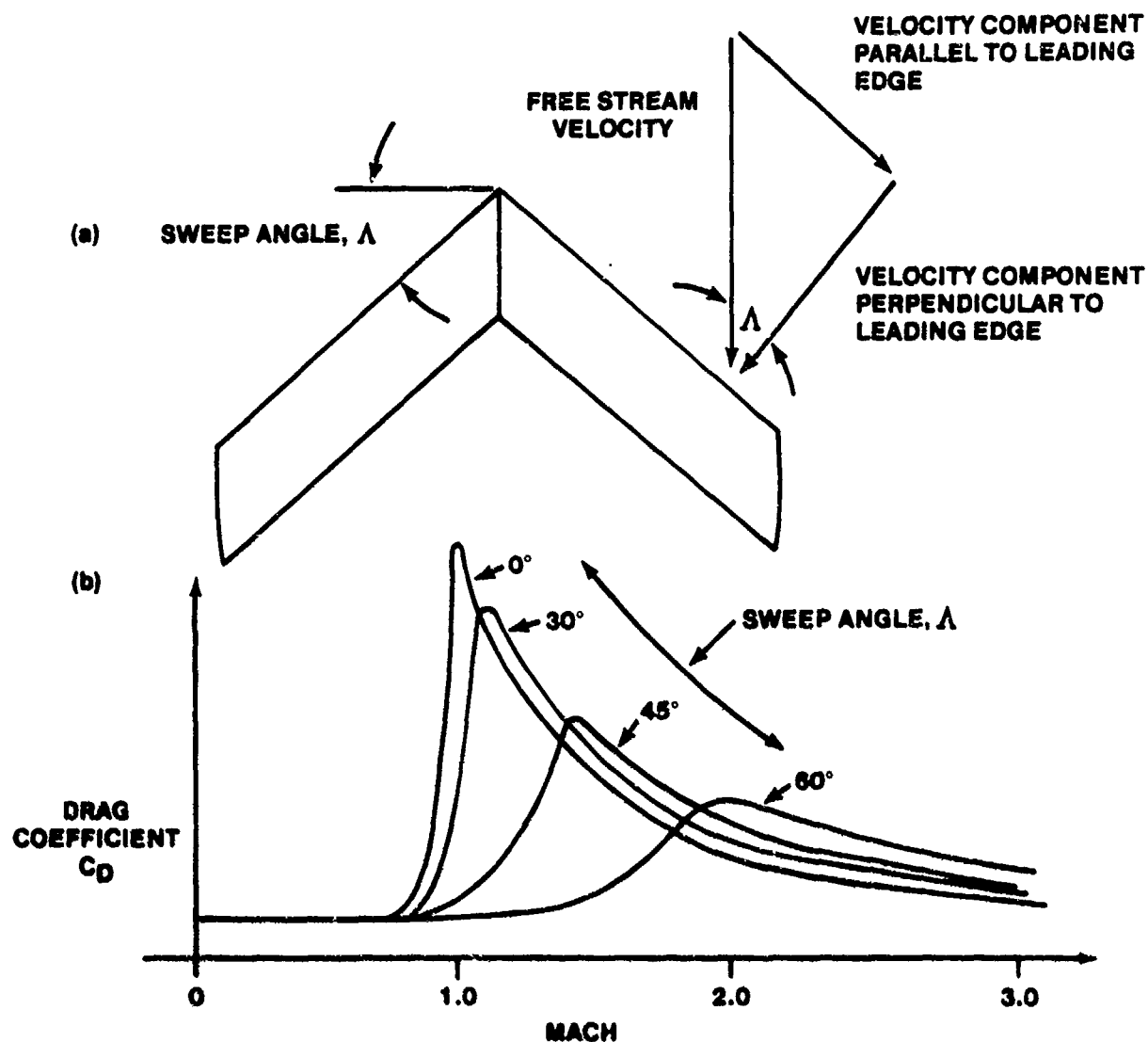


FIGURE 6.38. GENERAL EFFECTS OF SWEEPBACK (6.2:227)

tends to develop from the root toward the tip as depicted in Figure 6.39. This spanwise flow contributes to the strength of wing tip vortices, thereby increasing induced drag at high angles of attack. The swept back wing also tends to separate and stall first at the wing tip. This is, of course, undesirable from a control point of view as ailerons are normally located toward the wing tip. These stall characteristics are also depicted in Figure 6.39. The tendency can be decreased by twisting and/or tapering the wing, but again a penalty arises due to the structural complications caused by bending toward the wing tips; this twists the wing and imposes torsional loading.

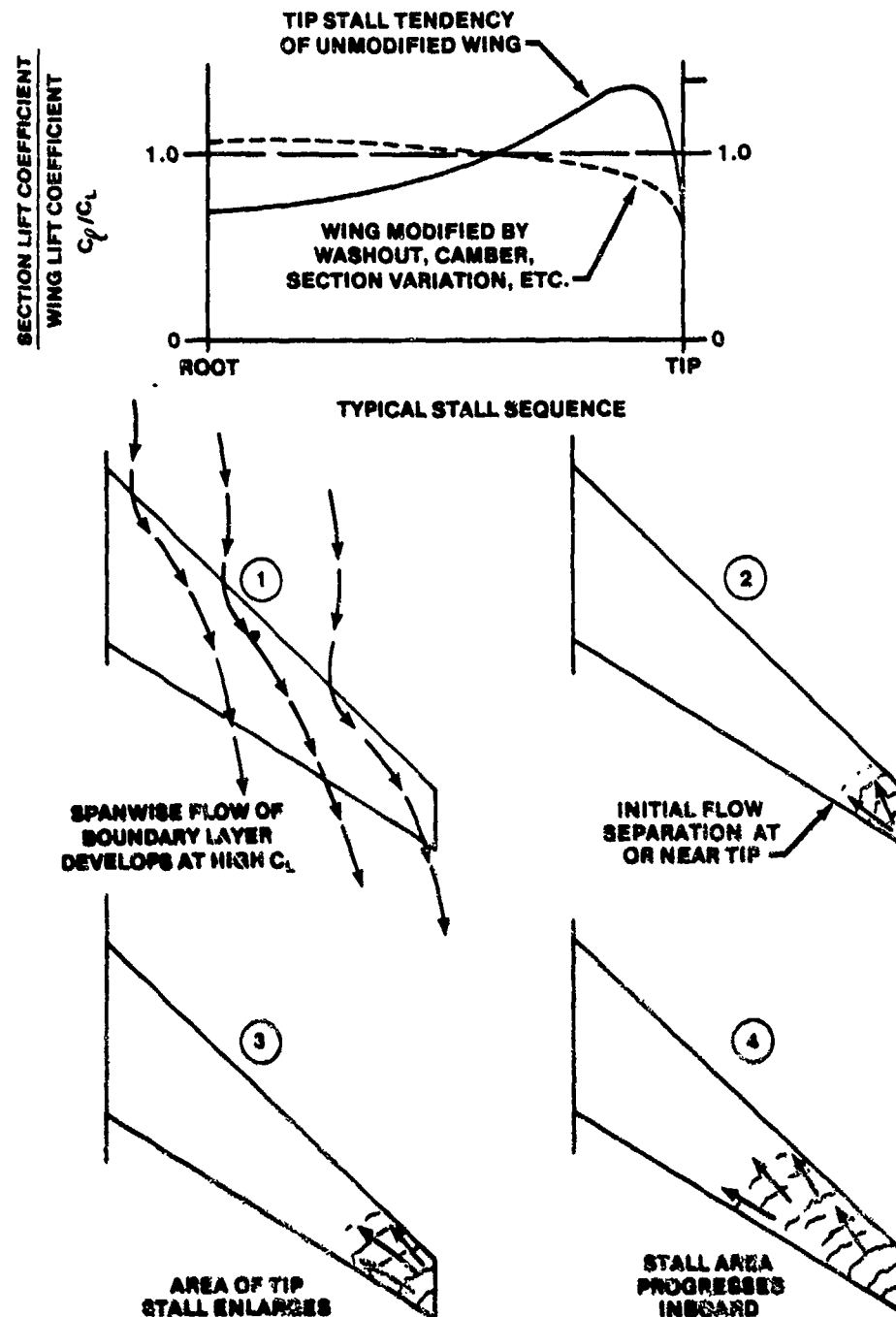


FIGURE 6.39. STALL CHARACTERISTICS OF TAPERED SWEEP WING (6.2:232)

A further disadvantage of wing sweep is illustrated in Figure 6.40. Note that for the same angle of attack, a straight wing is capable of producing a much higher lift coefficient than a swept wing.

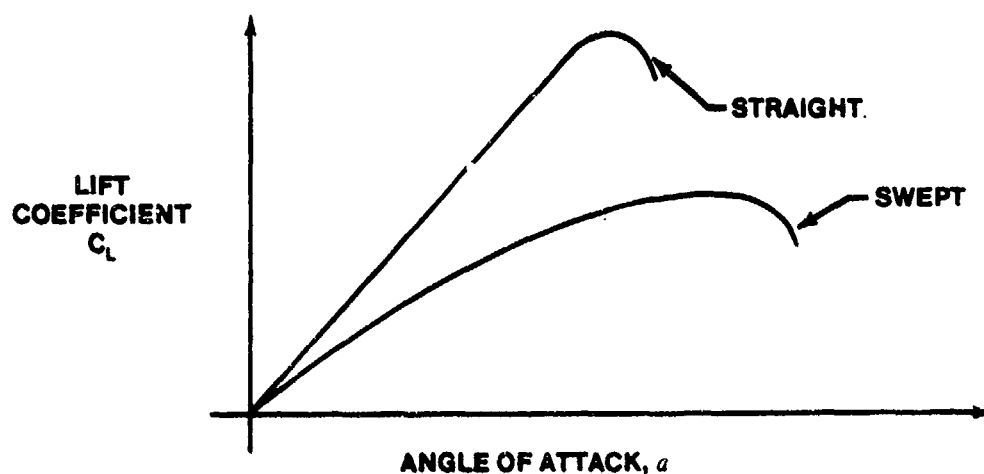


FIGURE 6.40. EFFECT OF SWEEPBACK ON LOW SPEED LIFT CURVE (6.2:228)

Aerodynamically, the effect of wing sweep with regard to delaying critical Mach applies to forward sweep as well as sweep back. The spanwise flow on a forward swept wing, however, is from the tip toward the root and tends to be beneficial. The major reason forward swept wings have not been widely used in the past is because of aeroelastic divergence problems. The present day improvement in composite materials has provided us with a material that has the stiffness needed to combat such problems.

Despite many disadvantages, rearward wing sweep has been for many years the primary method used to delay transonic drag rise. Reference to Figure 5.38b, however, shows that at higher supersonic Mach, a straight wing becomes superior from a drag standpoint.

6.23.4 Fuselage Shape and Area Rule

The onset of shock formation is also accompanied by a very severe drag rise. For an aircraft the best fuselage shape and the best wing fuselage combination that will delay the drag rise and/or tend to limit the severity of

its effect is of major interest.

As a matter of both calculation and testing, it is found that a body of revolution with high fineness ratio (ratio of length to diameter) gives the least drag. The nose section should not be a cone. The best shape for the nose resembles that shown in Figure 6.41.

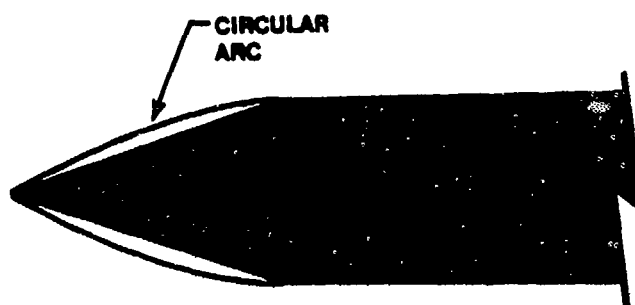


FIGURE 6.41. OPTIMUM NOSE SHAPE

Unfortunately, a true body of revolution is not found in actual vehicles. As an example, the canopy will form a bulge in the fuselage. The wings, when attached, will further modify the shape. However, without the necessity of preserving the exact form of the aircraft, the equivalent effect of wings and canopy can be preserved by making an equivalent body of revolution with the proper bulges located in the appropriate regions. This is shown in Figure 6.42.

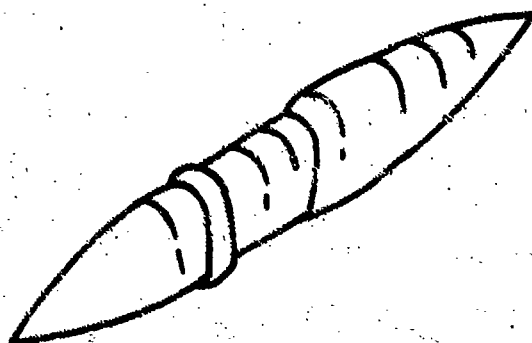


FIGURE 6.42. EQUIVALENT BODY OF REVOLUTION

The abrupt offsets in the surface will cause an increase in drag above that for the ideal body of revolution. To minimize drag it will be necessary to remove material from the region of the bulges. Because the wings must be present, the contour of the fuselage is changed in this region to compensate for them. The same thing can be done in the region of the canopy. In some instances, it may be necessary to introduce bulges in the fuselage behind or ahead of the wing to introduce the equivalent effect of the smooth aerodynamic contour.

A striking example of this effect is the extending of the "cab" of the Boeing 747. Wind tunnel data show that the Mach at which drag rise shows a significant increase is delayed by smoothing the area distribution by fairing the fuselage-cab juncture. The drag effect of the fairing is insignificant until M_{cr} is reached for the unfaired juncture; then the fairing delays the Mach at which waves are generated. As shown in Figure 6.43, the fairing causes an increase in M_{cr} for $0.3 < C_L < 0.5$.

The application of the transonic area rule will delay the drag rise, but in any event shock formation cannot be avoided if the flight Mach is sufficiently increased. The contour of the fuselage that will be effective at Mach 1.0 is not as effective at Mach 1.2. In fact, the conditions which provided an advantage in the transonic region may become a disadvantage at higher Mach. It is generally considered that area rule application is pointless above Mach 1.5. Further illustrations of the effects of area ruling are shown in Figure 6.44.

Transonic flow also produces important changes in the aerodynamic pitching moment characteristics of wing sections. The aerodynamic center of airfoils in subsonic flow is located at about the 25% chord point. As the airfoil is subjected to supersonic flow, the aerodynamic center changes to about the 50% chord point. Thus, the aircraft in transonic flight can experience large changes in longitudinal stability because of the large changes in the position of the aerodynamic center. If an aircraft stabilizes in the transonic region, the aerodynamic center may oscillate between the 25% chord point and the 50% chord point, often at very high frequency; this further aggravates longitudinal stability problems.

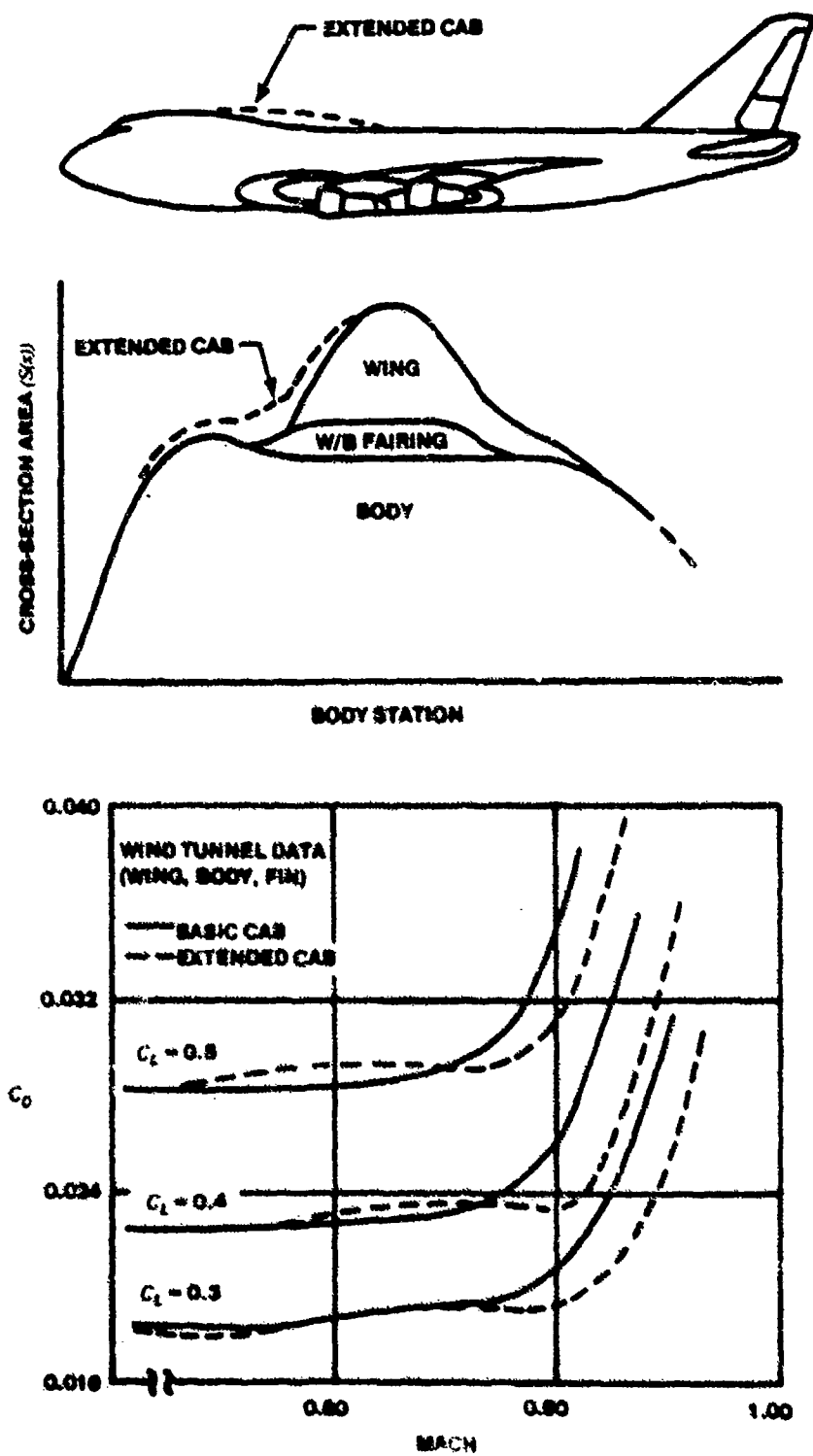


FIGURE 6.43. BENEFITS OF AREA RULE APPLICATION

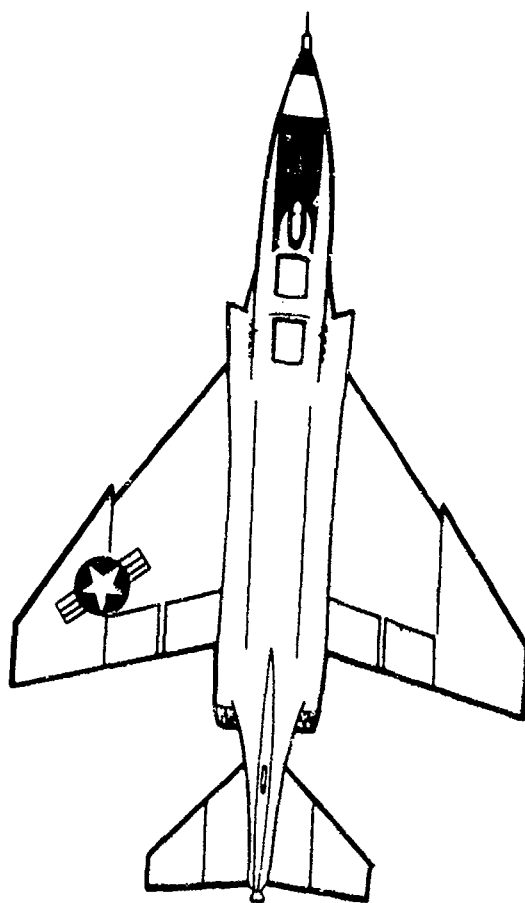


FIGURE 6.44. "COKE BOTTLE" FUSELAGE (6.1:165)

6.23.5 Transonic and Supersonic Control Surfaces

The design of control surfaces for transonic and supersonic flight involves many important considerations. This fact is illustrated by the typical transonic and supersonic flow patterns of Figure 6.45. Trailing edge control surfaces can be affected adversely by the shock waves formed in flight above the critical Mach. If the airflow is separated by the shock wave, the resulting buffet of the control surface can be very objectionable. In addition to the buffet of the surface, the change in the pressure distribution due to separation and the shock wave location can create very large changes in control surface hinge moments. Such large changes in hinge moments create very undesirable control forces and present the need for an "irreversible" control system. An irreversible control system would employ powerful hydraulic or electric actuators to move the surfaces upon control by the pilot, and the airloads developed on the surface could not feed back to the pilot. Of course, suitable control forces would be synthesized by bungees, "q" springs, bobweights, etc.

Transonic and supersonic flight can cause a noticeable reduction in the effectiveness of trailing edge control surfaces. The deflection of a trailing edge control surface at low subsonic speeds alters the pressure distribution on the fixed portion as well as the movable portion of the surface. This is true to the extent that a 1° deflection of a 40% chord elevator produces a lift change very nearly the equivalent of a 1-degree change in stabilizer setting. However, if supersonic flow exists on the surface, a deflection of the trailing edge control surface cannot influence the pressure distribution in the supersonic area ahead of the movable control surface. This is especially true in high supersonic flight where supersonic flow exists over the entire chord and the change in pressure distribution is limited to the area of the control surface. The reduction in effectiveness of the trailing edge control surface at transonic and supersonic speeds necessitates the use of an all movable surface. Application of the all movable control surface to the horizontal tail is most usual since the increase in longitudinal stability in supersonic flight requires a high degree of control effectiveness to achieve required controllability for supersonic maneuvering (6.2:236, 238).

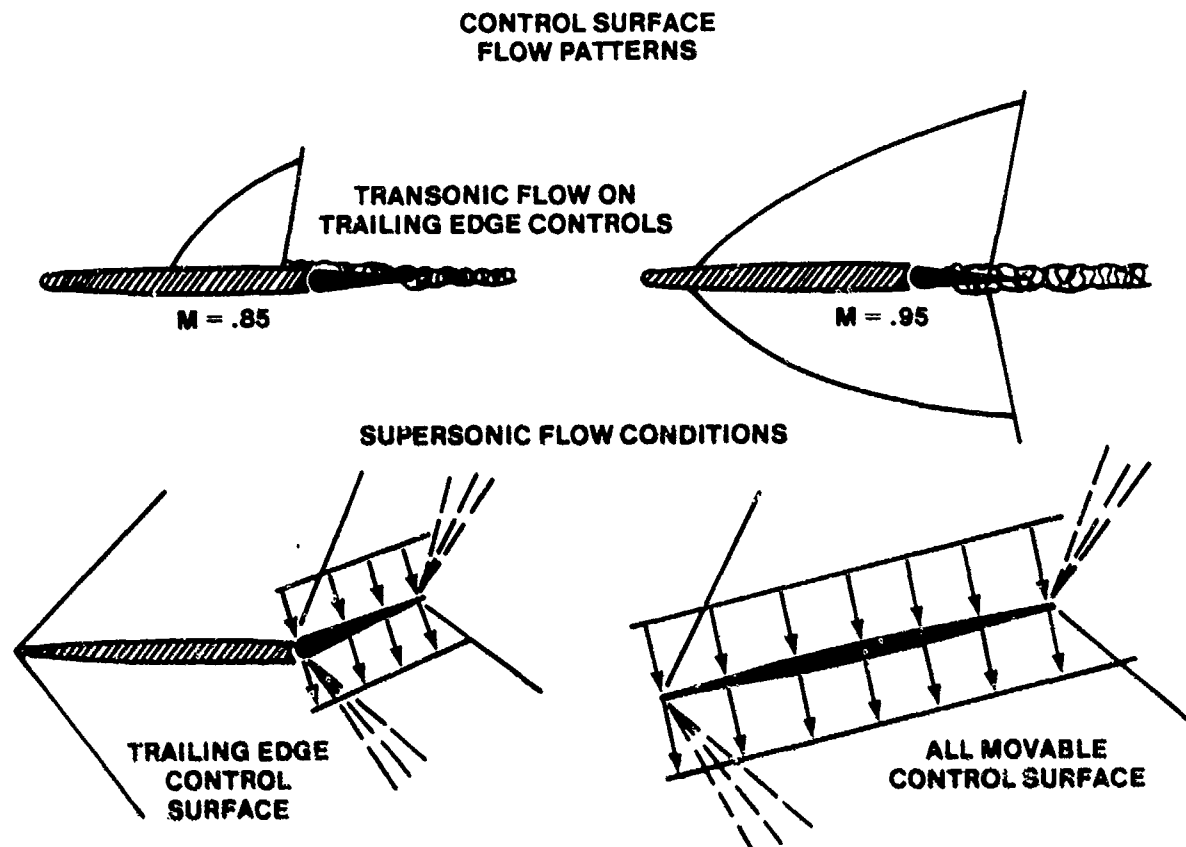


FIGURE 6.45. PLANFORM EFFECTS AND CONTROL SURFACES (6.2:237)

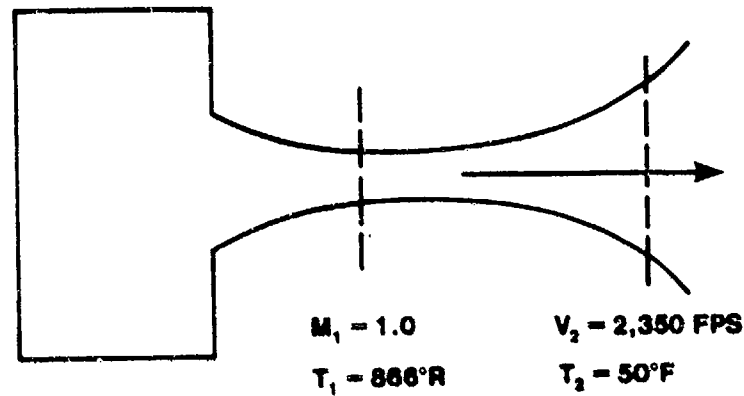
6.24 SUMMARY

In this chapter we have studied the theory of supersonic and transonic flow. Emphasis was placed on the practical application of the theory to realistic two and three dimensional flow problems about aerodynamic shapes. Understanding and application of supersonic theory will be necessary in Chapter 7 on Propulsion.

Present day supersonic aircraft and space shuttle operations necessitate a thorough understanding of this material by the flight test pilot and flight test engineer.

PROBLEMS

- 6.1 Calculate the velocity of sound in air at a temperature of 70°F . Express it in (a) knots, and (b) ft/sec.



- FIND: (c) At station ①, V , in ft/sec.
- (d) At station ②, M_2 .

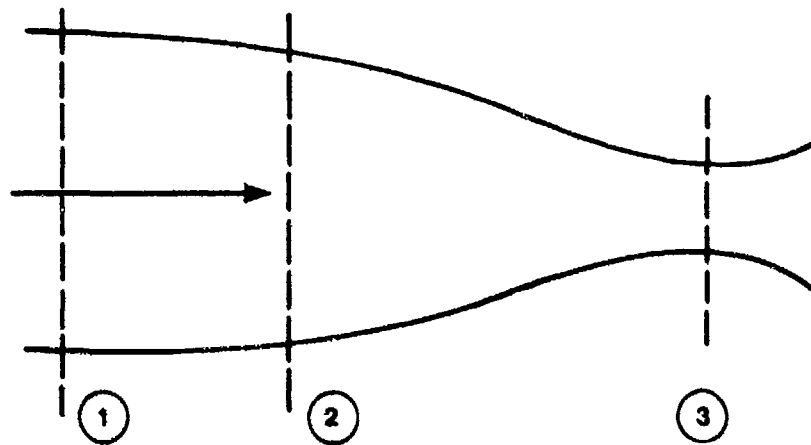
- 6.2 Sketch the Mach cone for $M = 2.0$. Show that

$$\mu = \sin^{-1} \frac{1}{M}$$

- 5.3 $P_0 = 2116 \text{ lb/ft}^2$
 $M_0 = 4.0$
 $T_0 = 165^{\circ}\text{R}$
 $P_T = ?$
 $T_T = ?$

6.4 At point (1) in a nozzle, air flows with a velocity of 500 ft/sec, pressure of 2116 lb/ft², temperature of 40°F, and density of 0.0024 slugs/ft³. Assuming isentropic flow,

- (a) Calculate the quantities listed at point (2) where the area is reduced by 15%.
- (b) Calculate the quantities listed at point (3) where $M = 1.0$.

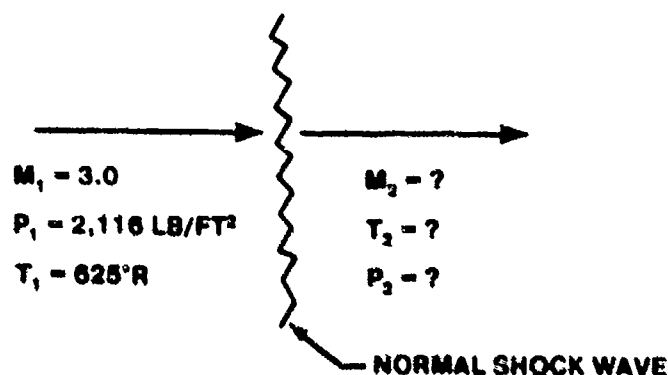


$V_1 = 500 \text{ ft/sec}$	$V_2 =$	$V_3 =$
$P_1 = 2116 \text{ lb/ft}^2$	$P_2 =$	$P_3 =$
$\rho_1 = 0.0024 \text{ slugs/ft}^3$	$\rho_2 =$	$\rho_3 =$
$T_1 = 40^\circ\text{F}$	$T_2 =$	$T_3 =$
$A_1 = A_1$	$A_2 = 0.85A_1$	$A_3 =$
$M_1 =$	$M_2 =$	$M_3 = 1.0$
$P_{T1} =$	$P_{T2} =$	$P_{T3} =$
$T_{T1} =$	$T_{T2} =$	$T_{T3} =$
$\rho_{T1} =$	$\rho_{T2} =$	$\rho_{T3} =$
$M^*_1 =$	$M^*_2 =$	$M^*_3 =$

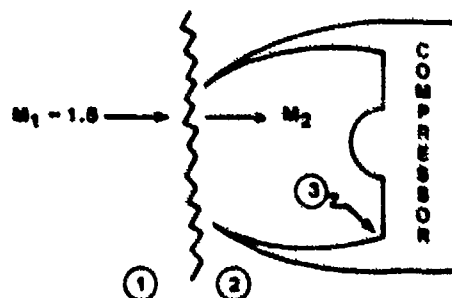
6.5 A surface temperature of 1000°R is recorded for a missile that is flying at an altitude of 50,000 ft in a standard atmosphere. Assume that the conditions on the surface are the same as those at a stagnation point after an isentropic compression. What is the velocity of the missile? What is the pressure at the stagnation point on the missile?

6.6 An intermittent wind tunnel is designed for Mach 4.0 in the test section. The tunnel operates by sucking air from the atmosphere through a duct and into a vacuum tank. The tunnel is at an elevation of 5,000 ft (standard atmosphere). What will be the static temperature, static density, and velocity in the test section assuming an isentropic process?

6.7 Find M_2 , P_2 , T_2 .

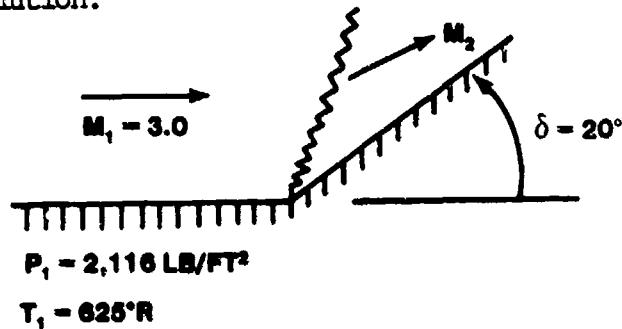


6.8 An intake is a diffuser to slow the flow and recover as much free stream pressure as possible, i.e., to recover all of the total pressure possible while slowing the flow to $M = 0$. The sketch below shows a typical low supersonic inlet (F-100 type).

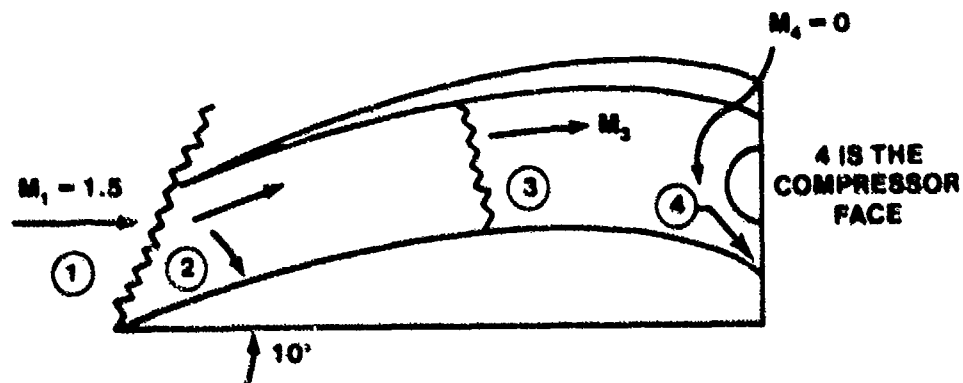


FIND: P_{T_3}/P_{T_1} assuming an isentropic process behind shock from (2) to (3).

- 6.9 FIND M_2 , P_2 , T_2 , and maximum δ possible without detaching shock. Assume a weak shock solution.

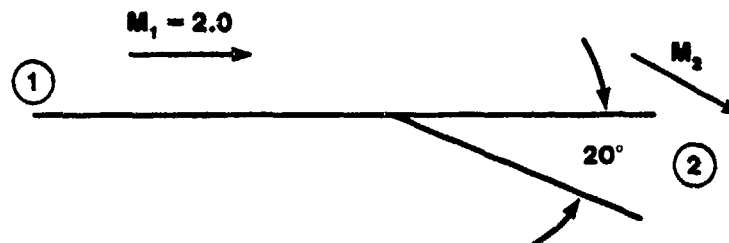


- 6.10 Inlets designed to operate in the high supersonic flight regime (F-104 type inlet) usually utilize multiple shock waves, unlike the F-100 type inlet. Using the tabular information in NACA 1135, you can estimate the improvement in pressure recovery to be expected.



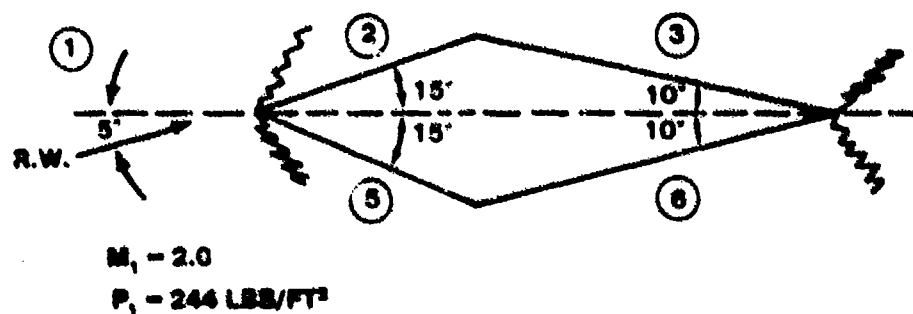
For a weak shock solution from ① to ② find P_{T_4}/P_{T_1} assuming an isentropic process behind shocks from ③ to ④. The second shock is a normal shock. Compare this pressure recovery to that of the F-100 type inlet in Problem 6.8.

6.11



- (a) Assuming a flow Mach of 2.0, what will the Mach be after an expansive deflection of 20° as shown above?
- (b) Find T_2/T_1 and P_2/P_1
- (c) What is the entropy change?
- (d) Draw v_1 and v_2 and find angle of the expansion fan.

6.12 GIVEN: $S_2 = S_5 = 75 \text{ ft}^2$
 $S_3 = S_6 = 125 \text{ ft}^2$
 $t/c = 0.20$



The flow in front of a double wedge airfoil (infinite wing) is inclined at an angle of attack of 5° and has a Mach of 2 (region 1). Weak shock waves are attached at both the leading and trailing edges. Calculate:

(a) The pressure coefficients in regions (2), (3), (5), and (6).

(b) The net drag and net lift using the pressure coefficients found in Part (a).

(c) The drag and lift using thin airfoil theory and compare to the answers derived in Part (b).

ANSWERS

- 6.1 (a) 668 kts
(b) 1128 ft/sec
(c) 1442 ft/sec
(d) 2.12

6.3 321,261 lb/ft²; 693°R

6.4 2709 ft/sec; 6582 lb/ft²

6.5 119°R; 5.68×10^{-5} slug/ft³; 2141 ft/sec

6.6	0.46	638 ft/sec	1021 ft/sec
	2446 lb/ft ²	1933 lb/ft ²	1291 lb/ft ²
	521°R	.00225 slug/ft ³	.00169 slug/ft ³
	.00266 slug/ft ³	487°R	434°R
	0.49	0.59	1.0
		0.62	

6.7 0.4752; 21858 lb/ft²; 1675°R

6.8 0.9298

6.9 2.0; 8096 lb/ft²; 981°R; 34°

6.10 98.6% recovery (93% Problem 6.8)

- 6.11 (a) 2.83
(b) 0.692
0.275
(d) 29.31°

6.12 (a) 0.25; -0.217; 0.66; -0.078
(b) 19,166 lb drag; 30,428 lb lift
(c) lift 26,858 lb; drag 14,655 lb

BIBLIOGRAPHY

- 6.1 Aerodynamic for Pilots, ATC Pamphlet 51-3, July 1979.
- 6.2 Hurt, H.H., Jr., Aerodynamics for Naval Aviators, NAVWEPS 00-80T-80, Office of the Chief of Naval Operations Aviation Training Division, U.S. Navy, 1960.
- 6.3 Zucker, R.D., Fundamentals of Gas Dynamics. Champaign, IL: Matrix Publishers, Inc., 1977.
- 6.4 NACA Report 1135, Equations, Tables, and Charts for Compressible Flow, Ames Research Staff, Ames Aeronautical Laboratory, Moffett Field, CA.
- (6.5 Carroll, R.L., The Aerodynamics of Powered Flight. New York: John Wiley & Sons, 1960.
- 6.6 Anderson, J.D., Jr., Introduction to Flight. New York: McGraw-Hill Inc., 1978.

• U.S. GOVERNMENT PRINTING OFFICE: 1986-583-095/20049

CHAPTER 7

AERO PROPULSION

7.1 INTRODUCTION

→ The steady progress of powered flight has closely followed the development of suitable aircraft powerplants. Unlike the question of the chicken and the egg, there is no doubt as to which was necessary first. Without a lightweight and yet adequately powerful engine, controlled flight of sufficient distance to serve a useful purpose would not be possible. Had it lacked an adequate means of propulsion, the machine conceived by Leonardo da Vinci could not have flown, even if it had been otherwise capable. Although Germany's Dr. N. A. Otto created the four-stroke internal combustion engine in 1876, it was not until twenty years later that Daimler was able to perfect the eight horsepower engine which enabled the Wolfert "Deutschland" to make the first gasoline-powered dirigible flight. Wilbur and Orville Wright had to develop their own engine before they could achieve successful flight at Kitty Hawk in 1903. Later Glenn H. Curtiss met with outstanding success due largely to the engines which he was instrumental in developing. And so it has gone, down through the pages of aviation history; larger and more efficient engines lead to larger, faster, and higher flying aircraft.

7.2 THE FLIGHT SPECTRUM

The pros and cons of powerplant types for aircraft have been hotly debated since the earliest days of powered flight. The reciprocating engine, turboprop, turbofan, turbojet, ramjet, and the rocket each has its limitations as well as uses for which it is best suited.

The reciprocating engine, which has reached its ultimate size and horsepower, has long been with us as the workhorse of low and medium altitudes and airspeeds. The turboprop combines the advantage, inherent in propeller driven aircraft, of short takeoffs with the higher and faster flying capability of the gas turbine engine. The turbojet, with its increased efficiency at high altitudes and airspeeds, is ideal for high-flying, high performance military aircraft and fast, long-range airliners. The turbofan combines the advantages of both the turboprop and turbojet. It offers the high thrust at low airspeeds of the turboprop but without the heavy, complex reduction gearing and propeller, and improved fuel specifics at moderate

airspeeds. On the horizon is yet a further advance, the prop-fan, which further combines turboprop and turbofan technology. A ramjet engine is particularly suited to high altitude and high speed, but it must be carried aloft by some means other than its own thrust to reach a velocity sufficient to allow the engine to start and operate.

Man is a creature who lives miles deep on the bottom of an ocean of air that forms a protective canopy over the surface of the earth. Place him in a vehicle a few miles above the bottom of his ocean, and he cannot survive unless some means are provided to duplicate, approximately, the air temperature and pressure of his normal environment. Above the altitude limitations of the human body, the vehicle must supply pressurized oxygen or air for its passengers and crew. Above the air limitations of the engine which propels it, the vehicle must carry all of its fuel and air (or other means of supporting combustion) with it, as is the case for the rocket.

Aircraft or missiles can be operated in continuous level flight only in a restricted area of the altitude-flight speed spectrum. The minimum speed boundary of this level flight "corridor" is reached when the combined effect of wing lift and centrifugal force is no longer sufficient to support aircraft weight. Transient flight is possible at lower flight speeds by use of a ballistic-type flight path, where altitude is being varied throughout the flight, or by aircraft supported directly by powerplant thrust. Except at very high altitudes, the maximum speed for continuous flight occurs where the increase in aircraft and powerplant structural weight required to overcome the adverse effects of high ram air pressure and temperature becomes excessive. The effects of pressure predominate at low altitudes, whereas the rapid deterioration of the strength of structural materials at high temperatures is the primary factor at high altitudes. Development of better materials and improved construction techniques will tend to raise these maximum speed limits. At very high altitudes, the maximum speed for continuous level flight is limited to the orbiting velocity. Figure 7.1 shows the limits of the so-called continuous level-flight corridor.

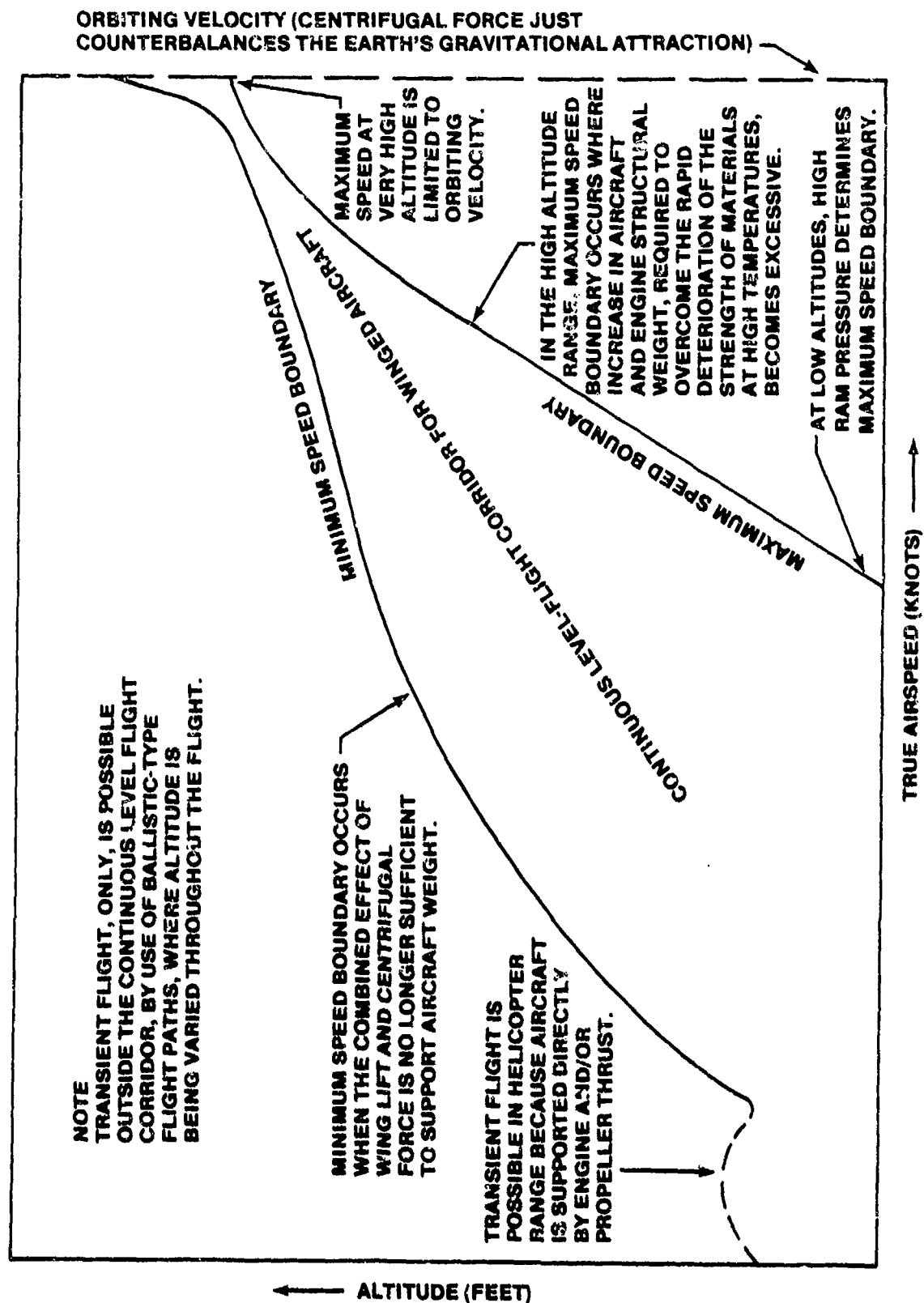


FIGURE 7.1. CONTINUOUS LEVEL FLIGHT CORRIDOR

7.3 PRINCIPLE OF JET PROPULSION

The principle of jet propulsion derives from an application of Newton's laws of motion. When a fluid is accelerated or given a momentum change, a force is required to produce this acceleration in the fluid, and, at the same time, there is an equal and opposite reaction force. This opposite reaction force of the fluid on the engine is called the thrust; therefore, the principle of jet propulsion is based on the reaction principle. A little thought will indicate that all devices or objects that move through fluids must follow this basic propulsion principle. The fish and human swimmer move themselves through the water by this principle, and, in the same manner, birds are able to propel themselves through the air. Even the reciprocating engine with its propeller (which causes a momentum change of air) obeys the same principle of momentum change.

Any fluid can be utilized to achieve the jet propulsion principle; thus, steam, combustion gases, or the hot gases generated by any heating process can be applied to propel a device through a fluid or space. Since many of these devices operate in the air, they change the momentum of the air for their propulsive thrust. These devices are called air-breathing engines because they utilize the air for their working fluid.

7.3.1 The Basic Gas Turbine Engine

The gas turbine is an air-breathing engine. The term, "gas turbine," could be misleading because the word "gas" is so often used for gasoline. The name, however, means exactly what it says: a turbine type of engine which is operated by a gas, differentiated, for instance, from one operated by steam vapor or water. The gas which operates the turbine usually is the product of the combustion which takes place when a suitable fuel is burned with the air passing through the engine. In most gas turbines, the fuel is not gasoline at all, but rather, a low grade distillate such as JP-4 or commercial kerosene.

Both the reciprocating engine and the gas turbine develop power or thrust by burning a combustible mixture of fuel and air. Both convert the energy of the expanding gases into propulsive force. The reciprocating engine does this by changing the energy of combustion into mechanical energy which is used to turn a propeller. Aircraft propulsion is obtained as the propeller imparts a

relatively small amount of acceleration to a large mass of air. The gas turbine, in its basic turbojet configuration, imparts a relatively large amount of acceleration to a smaller mass of air and thus produces thrust or propulsive force directly. Here, the similarity between the two types of engines ceases.

The reciprocating engine is a complicated machine when compared to the gas turbine. If only the basic, mechanically coupled compressor and turbine are considered, the gas turbine has only one major moving part. Air comes in through an opening in the front of the engine and goes out, greatly heated and accelerated, through an opening in the rear. Between the two openings, the engine develops thrust.

Fundamentally, a gas turbine engine may be considered as consisting of five main sections: an inlet, a compressor, a burner, a turbine, and a tailpipe having a jet nozzle. Turbojet versions of gas turbine engines are devices to generate pressures and gases which provide mass and acceleration.

Newton's Second Law states that a change in motion is proportional to the force applied. Expressed as an equation, force equals mass multiplied by acceleration ($F = ma$). Force is the net thrust. Acceleration is a rate of change of velocity; therefore, we can write

$$F = m dv/dt \quad (7.1)$$

The velocity change is between the low velocity of the incoming air, the zero velocity of the fuel, and the high velocity of the outgoing gases, all velocities being relative to that of the engine. Since momentum is defined as mass times velocity, when velocity changes are substituted in the equation in place of acceleration, the idea of momentum changes within the engine being equal to force or thrust can be understood.

Mass, in the case of the turbojet, is the mass of air plus the mass of fuel which pass through the engine. Acceleration of these masses is accomplished in two ways. First, the air mass is compressed, and pressure is built up as the air goes through the compressors with little change in velocity. Secondly, the fuel and part of the air are burned to produce heat. The heated gases expand in the burner section and accelerate through the turbine inlet nozzle at the outlet of the burner section. The turbines

extract power to drive the compressors. This process decelerates the gases but leaves some pressure. The jet nozzle allows the gases to attain their final acceleration and generates the outgoing momentum.

The incoming momentum of the air and the zero momentum of the fuel entering the engine must be subtracted from the outgoing momentum of the gases in order to arrive at the overall change in momentum which represents thrust. The thrust developed by a turbojet engine, then, may be said to result from the unbalanced forces and momentums created within the engine itself. When the static pressure at the jet nozzle or the tailpipe exit exceeds the ambient outside air pressure, an additional amount of thrust is developed at this point. Figure 7.2 graphically represents the manner in which the internal pressures vary throughout the engine. These pressures and the areas on which they work are indicative of the momentum changes within the engine. Since engine pressure is proportional to engine thrust, Figure 7.2 indicates how the overall thrust produced by the engine is developed. The final unbalance of these pressures and areas gives, as a net result, the total thrust which the engine is developing. In practice, this unbalance may be measured or calculated in terms of pressure to enable the pilot to monitor engine thrust.

While turboprop engines function in a similar manner, the chief difference is that the jet thrust produced is held to a minimum. Their relatively large turbines are designed to extract all of the power possible from the expanding gases flowing from the burner section. This power is used to rotate the propeller which, in turn, accelerates a large mass of air to produce thrust to propel the aircraft.

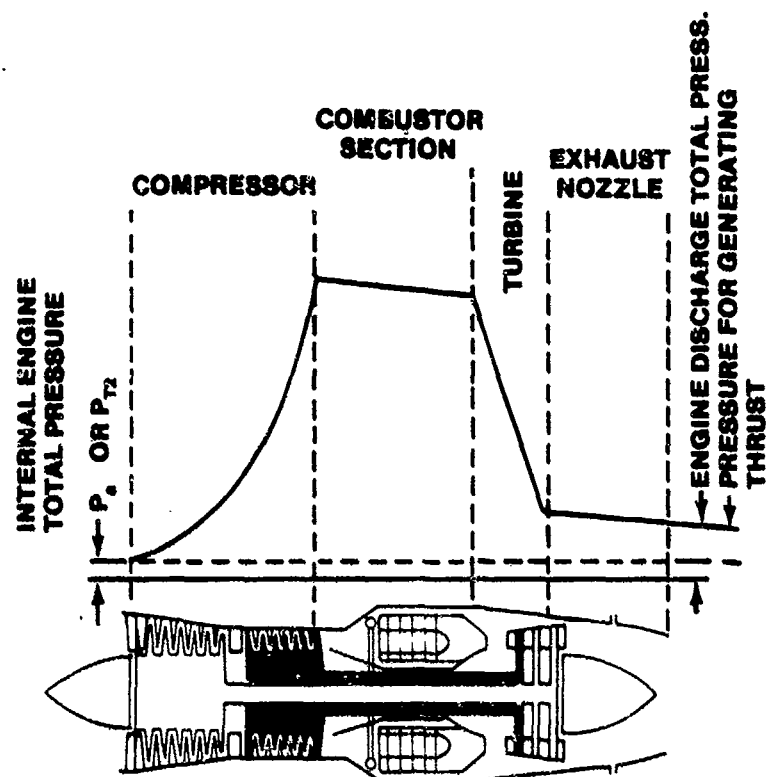


FIGURE 7.2. TYPICAL TURBOJET ENGINE INTERNAL PRESSURE VARIATIONS

7.4 ENGINE CLASSIFICATION

There are five basic air-breathing engines used for aircraft propulsion. These are the ramjet and the four basic gas turbine variants: turbojet, turboprop, turboshaft and turbofan.

7.4.1 The Ramjet Engine

The simplest type of air-breathing engine is the ramjet engine, or, as it is sometimes called, the Athodyd (Aero-THERMO-DYNAMIC-Duct) or Lorin engine (in honor of its original proponent).

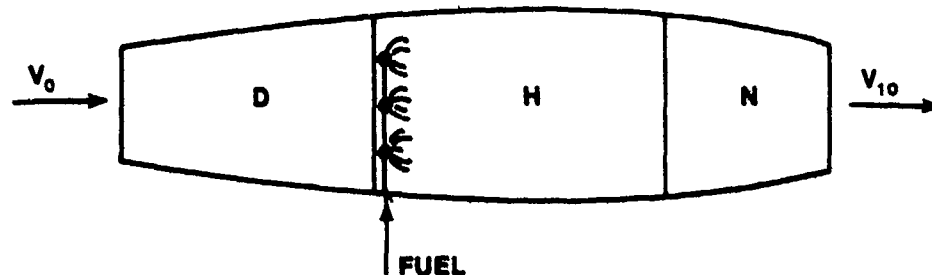


FIGURE 7.3. PRINCIPAL ELEMENTS OF A RAMJET ENGINE

This engine (Figure 7.3) consists of a diffuser, D, a combustion chamber, H, and a discharge nozzle, N. The function of a diffuser is to convert the kinetic energy of the entering air into a pressure rise by decreasing the air velocity. The diffuser delivers the air at a static pressure higher than atmospheric pressure to the combustion chamber, where fuel is mixed with the air and ignited.

The burning causes the specific volume of the air to increase; thus, the air is accelerated in the combustion chamber, where it burns at approximately constant pressure to a high temperature. The air temperature can also be raised by heat transfer from a heater such as a nuclear reactor. In this case, of course, the fuel consumption is effectively zero, since the required energy is derived from the nuclear fission in the reactor. Either way, high temperature and high pressure gases are delivered to the exhaust nozzle to produce an exit velocity greater than the entrance velocity.

Again, the process is one of changing the momentum of the working fluid from a low value at entrance to a high value at exit. The fuel used in this type of engine is usually a liquid hydrocarbon; however, solid fuels can be used to produce a propulsive thrust. Toward the end of World War II, the Germans were experimenting with ramjet engines which operated on coal and oil-cooked wood. It should be noted that the ramjet engine (in its basic form) cannot operate under static conditions, since there will be no pressure rise in the diffuser. Usually, a Mach of at least 0.2 is required for any operation at all, and performance improves as the flight speed is increased.

It is readily apparent why this engine is sometimes called the "flying stovepipe." An ignition system is required to start it. However, once started, the engine is a continuous firing duct in that it burns fuel at a steady rate and takes air in at a steady rate for any given flight velocity.

7.4.2 The Turbojet Engine

The ramjet engine is simple in construction; however, its application is limited, and to date it has not been used extensively. The most common type of air-breathing engine is the turbojet engine illustrated in Figure 7.4.

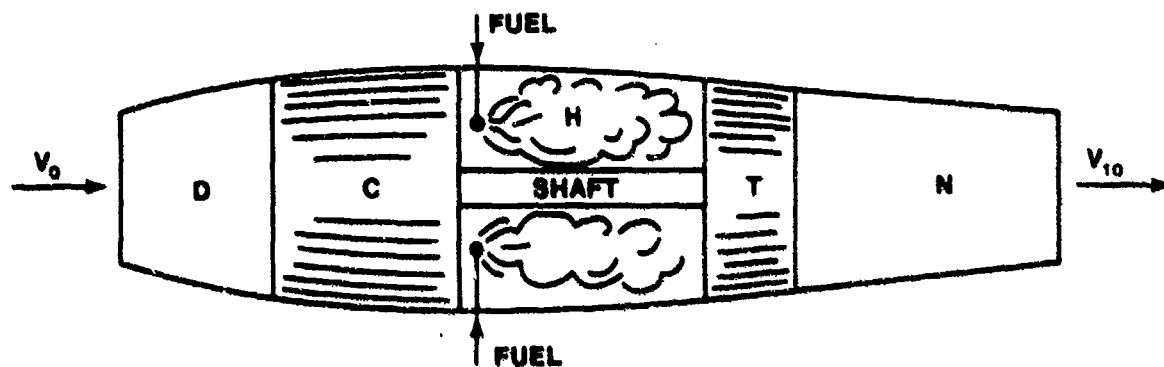


FIGURE 7.4. PRINCIPAL ELEMENTS OF A TURBOJET ENGINE

This engine consists of a diffuser, D, a mechanical compressor, C, a combustion chamber, H, a mechanical turbine, T, and an exhaust nozzle, N. Again, the function of the diffuser is to transform the kinetic energy of the entering air into a static pressure rise. The diffuser delivers its air to the mechanical compressor which further compresses the air and delivers it to the combustion chamber. There, fuel nozzles feed fuel continuously, and continuous combustion takes place at approximately constant pressure. Here also, the air temperature can be raised by heat transfer from a nuclear reactor. The high temperature and high pressure gases then enter the turbine, where they expand to provide driving power for the turbine. The turbine is directly connected to the compressor, and all the power developed by the turbine is absorbed by the compressor and the auxiliary apparatus. The main function of the turbine is to provide power for the mechanical compressor. After the gases leave the turbine, they expand further in the exhaust nozzle and are ejected with a velocity greater than the flight velocity to produce a

thrust for propulsion. It is evident that this engine is not a great deal different from the ramjet engine. Here, a compressor and a turbine are used to provide the additional pressure rise which could not be obtained in a ramjet engine. Since this engine has a mechanical compressor, it is capable of operating under static conditions; however, increases in flight velocity improve its performance because of the benefit of ram pressure achieved by the diffuser. It is again pointed out that the overall pressure ratio of the cycle may be increased to a value greater than that which is possible in a ramjet engine. However, at very high flight speeds (Mach 3 or more), sufficient pressure rises can be obtained from the diffuser alone. Thus, at higher speeds, the ramjet engine may become more attractive than the turbojet engine.

Turbojet engines can be further classified by the type of compressor they employ. The centrifugal compressor works very well in the smaller turbojet and turboprop engines where a high compression ratio is not too essential. This design was standard for early aircraft gas turbines. Large, high performance engines require the greater efficiency and higher compression ratios attainable only with an axial flow type of compressor. Axial flow compressors have the added advantages of being lightweight and having a small frontal area. Either a single compressor (Figure 7.5a), a dual compressor (Figure 7.5b), or a triple-spool may be used. The latter types result in

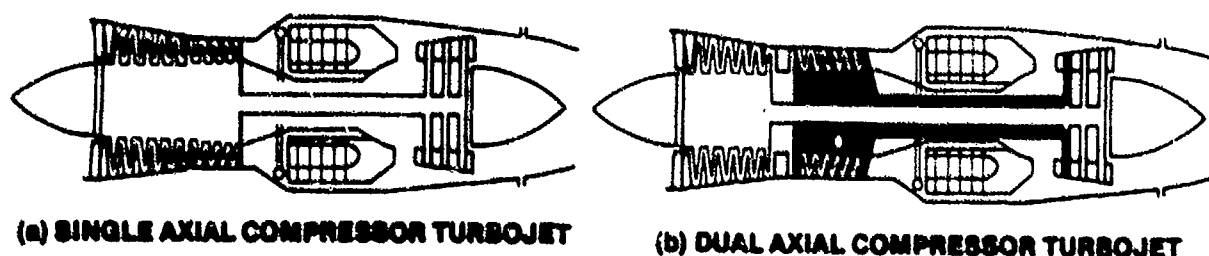


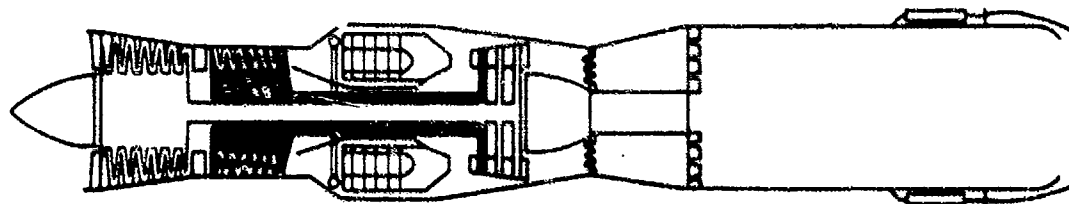
FIGURE 7.5A. SINGLE AXIAL COMPRESSOR TURBOJET

FIGURE 7.5B. DUAL AXIAL COMPRESSOR TURBOJET

higher compressor efficiencies, compression ratios, and thrusts. In dual compressor engines, one turbine or set of turbine wheels drives the high

pressure compressor, and another set drives the low pressure compressor. Both rotor systems operate independently of one another except for airflow. The turbine for the low pressure compressor, the rear turbine, is connected to its compressor by a shaft passing through the hollow center of the high pressure compressor and turbine assembly drive shaft. The dual compressor configuration is often called a dual-rotor, two-spool, or twin-spool engine; the single compressor configuration is likewise called a single-rotor or single-spool engine.

Frequently, a turbojet engine is equipped with an afterburner for increased thrust (Figure 7.6). This increase in thrust can be accomplished regardless of the type of compressor used. Roughly, about 25% of the air



DUAL AXIAL COMPRESSOR TURBOJET WITH AFTERBURNER

FIGURE 7.6. DUAL AXIAL COMPRESSOR TURBOJET WITH AFTERBURNER

entering the compressor and passing through the engine is used for combustion. Only this amount of air is required to attain the maximum temperature that can be tolerated by the metal parts. The balance of the air is needed primarily for cooling purposes. Essentially, an afterburner is simply a huge stovepipe attached to the rear of the engine, through which all of the exhaust gases must pass. Fuel is injected into the forward section of the afterburner and is ignited. Combustion is possible because 75% of the air which originally entered the engine still remains unburned. The result is, in effect, a tremendous blowtorch which increases the total thrust produced by the engine by approximately 50% or more. Although the total fuel consumption increases two to ten times, the net increase in thrust is profitable for takeoff, climb, or acceleration. A turbojet aircraft with an afterburner can often reach a given altitude with the use of less fuel by climbing rapidly in afterburner than by climbing more slowly without the afterburner. The weight and noise of an afterburner, which is used only occasionally, precludes the

device being employed on present day, transport type aircraft; however, afterburners are used to maintain cruise Mach on the SST.

7.4.3 The Turboprop or Turboshaft Engine

In principle, this engine (Figure 7.7) is very similar to the turbojet engine, differing only in that it uses a propeller to provide most of the propulsive thrust.

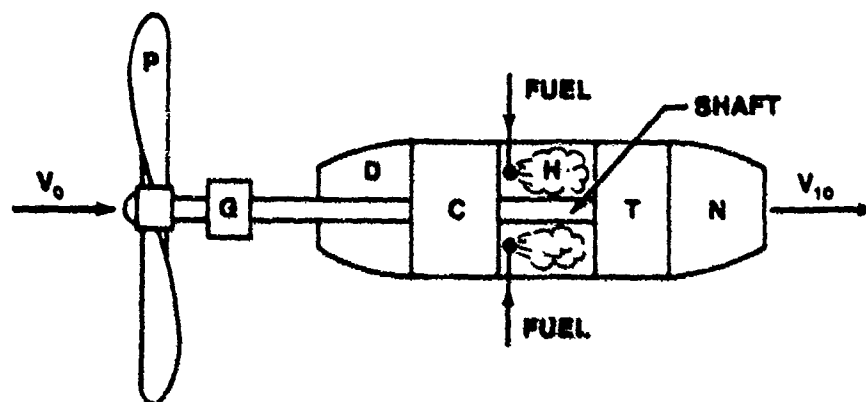
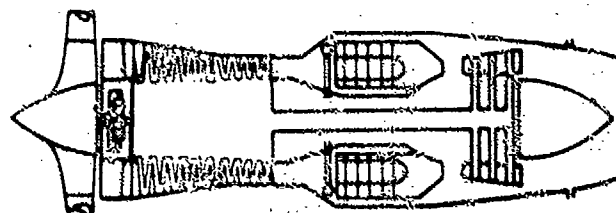


FIGURE 7.7. PRINCIPAL ELEMENTS OF A TURBOPROP ENGINE

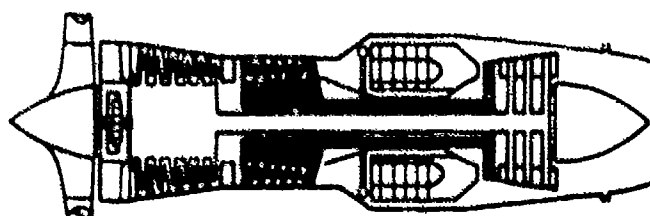
The engine consists of a diffuser, D, a mechanical compressor, C, a combustion chamber, H, a turbine, T, an exhaust nozzle, N, reduction gearing, G, and a propeller, P. The diffuser, mechanical compressor, and combustion chamber function in the same manner as in the turbojet engine. However, in the turboprop engine, the turbine extracts much more power than it does in the turbojet engine because the turbine provides power for both the compressor and the propeller. When all of this energy is extracted from the high temperature gases, there is little energy left for producing jet thrust. Thus, the turboprop engine derives most of its propulsive thrust from the propeller and derives only a small portion (10% to 25% depending on the flight velocity) from the exhaust nozzle. Since the shaft rotation speed of gas turbine engines is very high (approximately 12,000 RPM), reduction gearing must be placed between the turbine shaft and the propeller to enable the propeller to operate efficiently. The turboprop engine is essentially a gas turbine power plant because, as pointed out before, little power is derived from the exhaust nozzle; still, as flight speeds are increased, the ratio of

jet thrust to propeller thrust for maximum thrust tends to become higher. The propulsive thrust is provided by a dual momentum change of the air. First, the propeller increases the air momentum, and second, the overall engine, from diffuser to nozzle, provides an internal momentum increase. The sum of these two thrusts is the total thrust developed by the engine.

The conversion to a turboprop can be accomplished with either a single or multistage centrifugal compressor, a single axial compressor, or a dual axial compressor. In most cases, the propeller reduction drive gearing is connected directly to the compressor drive shaft (Figure 7.8a) or, when a dual axial compressor is used, to the low pressure compressor drive shaft (Figure 7.8b). On still another type, the propeller is driven independently of the compressor



(a) SINGLE AXIAL COMPRESSOR, DIRECT PROPELLER DRIVE TURBOPROP



(b) DUAL AXIAL COMPRESSOR, DIRECT PROPELLER DRIVE TURBOPROP

FIGURE 7.8A. SINGLE AXIAL COMPRESSOR: DIRECT PROPELLER DRIVE TURBOPROP

FIGURE 7.8B. DUAL AXIAL COMPRESSOR: DIRECT PROPELLER DRIVE TURBOPROP

by a free turbine of its own (Figure 7.9). In one version of the free turbine turboprop, both an axial and a centrifugal compressor are used. A single stage turbine, operating by itself, supplies the power to drive both the compressors and the accessories. If a turbine of a gas turbine engine is

connected to a drive shaft which, in addition to the compressor, drives something other than a propeller, the engine is referred to as a shaft turbine or turboshaft engine. Turboshaft engines are most often used to power helicopters.

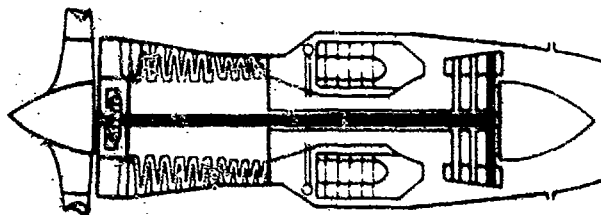


FIGURE 7.9. SINGLE AXIAL COMPRESSOR: FREE TURBINE PROPELLER DRIVE TURBOPROP

7.4.4 The Turbofan Engine

The turbofan engine combines features of both the turbojet and turboprop engines. As a result, it has performance characteristics somewhere between the other two engines. Figure 7.10 schematically illustrates the principal elements of a front fan version of the turbofan engine.

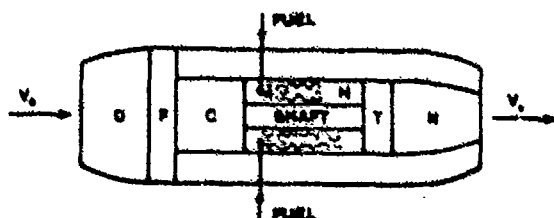


FIGURE 7.10A. PRINCIPAL ELEMENTS OF A TURBOFAN ENGINE (FRONT FAN)

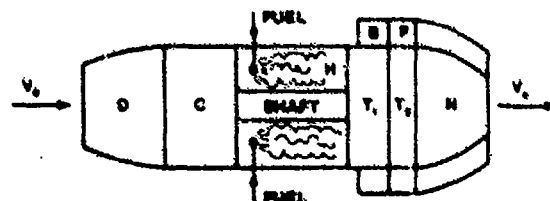


FIGURE 7.10B. PRINCIPAL ELEMENTS OF A TURBOFAN ENGINE (AFT FAN)

The engine consists of a diffuser, D, a front fan, F, a mechanical compressor, C, a combustion chamber, H, a turbine, T, a bypass duct, B, and an exhaust nozzle or nozzles, N. As before, the function of the diffuser is to

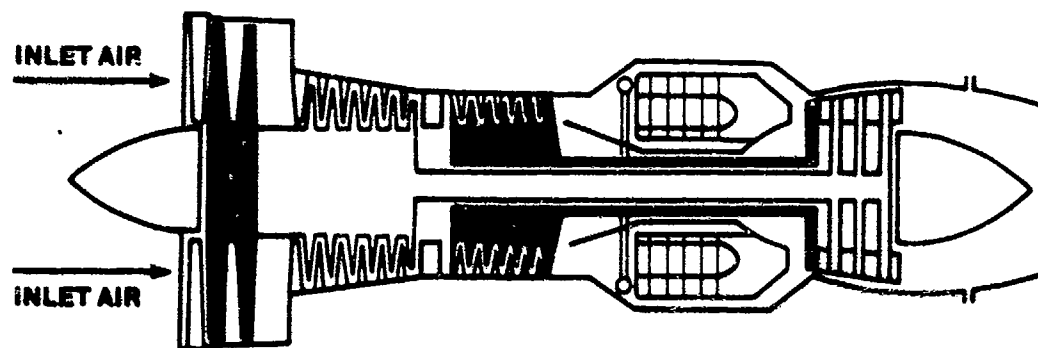
convert the kinetic energy of the entering air into a static pressure rise. The diffuser delivers its air to a fan, which further compresses it a small amount (a pressure ratio of approximately 1.5 to 2.0). The airflow is then split, and a portion enters the bypass duct, while the remainder continues into the mechanical compressor, combustion chamber, and turbine. The ratio of the airflow through the bypass duct to the airflow through the gas generator is defined as the bypass ratio. The turbine, as with the turboprop engine, provides the power for both the fan and the compressor. Unlike the turboprop engine, however, there is still considerable energy available in the gases downstream of the turbine. The exhaust gases are, therefore, further expanded in the exhaust nozzle to a velocity greater than the flight velocity, producing thrust for propulsion. The bypass air is also expanded, either through a common nozzle with the exhaust gases or through a separate nozzle, to a velocity higher than the flight velocity, producing additional thrust for propulsion. The turbofan engine thus derives its propulsive thrust from the high velocity exhausts of both the bypass air and the gas generator gases.

The version of the turbofan engine illustrated in Figure 7.10b differs from the front fan version in that the fan, F , is located aft of the gas generator turbine, T_1 , and is driven by a separate turbine, T_2 . Only bypass air, which can enter a common diffuser, D , or a separate diffuser, B , passes through the fan. However, the propulsive thrust of the engine is still derived from the high velocity exhaust of both the fan and the gas generator.

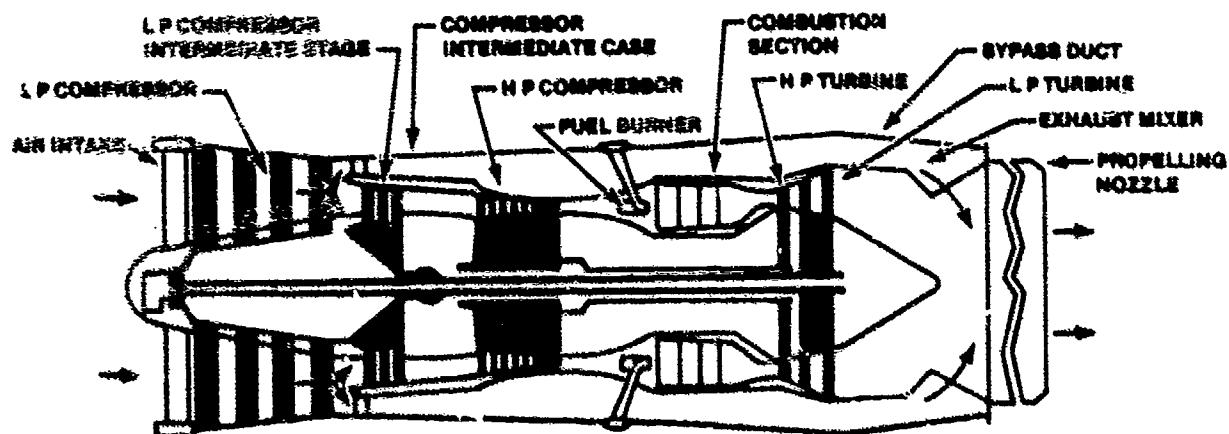
Although these are the two basic configurations of the turbofan engine, many variations are possible. Three different configurations of actual engines are illustrated in Figure 7.11.

As compared to the turbojet and turboprop engines, the turbofan engine derives its thrust from the acceleration of a medium amount of air through a medium velocity increment. The turbojet accelerates a small amount of air through a large velocity increment; the turboprop accelerates a large amount of air (through the propeller) through a small velocity increment.

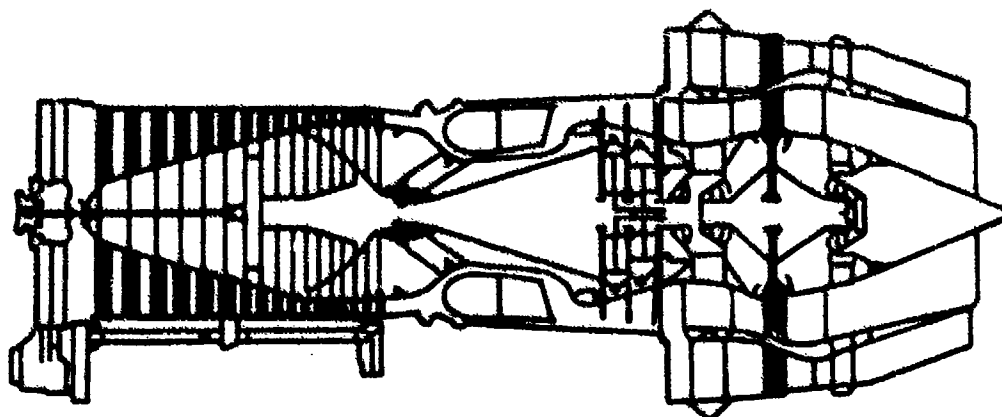
As with the turbojet engine, significant thrust augmentation is also possible with the turbofan engine. Afterburning can be accomplished in either or both of the exhaust streams. In fact, since the bypass stream has no combustion products, very large temperature increases and, hence, exhaust velocity or thrust increases are possible with the turbofan engine.



(a) PRATT & WHITNEY JT3D
FRONT MOUNTED FAN - INDEPENDENT CORE AND BYPASS AIR FLOWS



(b) ROLLS-ROYCE CONWAY R.C.42
FRONT MOUNTED FAN - FAN IS ALSO INITIAL COMPRESSION FOR CORE AIR FLOW



(c) GENERAL ELECTRIC CJ-805-23
AFT MOUNTED FAN - INDEPENDENT CORE AND BYPASS AIR FLOW

FIGURE 7.11. SCHEMATIC DIAGRAMS OF TURBOFAN ENGINES. (A) COURTESY PRATT & WHITNEY AIRCRAFT DIVISION OF UNITED AIRCRAFT CORP. (B) COURTESY ROLLS-ROYCE. (C) COURTESY FLIGHT INTERNATIONAL.

7.5 THRUST

One speaks of horsepower when describing a reciprocating engine or a turboprop. Power is defined as work per unit of time, and work involves a force operating over a distance. Expressed as an equation

$$P = \frac{Fs}{t} \quad (7.2)$$

where: P = Power
F = Force
s = Distance
t = Time

One horsepower is the unit used to describe the equivalent of 33,000 foot-pounds of work performed in one minute, or 550 foot-pounds of work in one second. In a reciprocating engine or turboprop, it is possible to measure distance and time. Torque and RPM are used in computing horsepower. However, these same distance and time elements make the use of the terms "power" and "horsepower" unacceptable for a turbojet engine. When a turbojet engine is static, as in the case of an aircraft parked on the ground or when an engine is mounted in a ground test stand, distance and time are zero because no movement is involved that can be measured against a period of time. Although torque and RPM are produced by the turbine, the horsepower developed is used entirely within the engine itself. According to the definition and equation for power, none is being produced; yet, a forward force is being exerted when the engine is operating. It might be said that thrust is the measurement of the amount that an engine pushes against its attachment points. The propulsive force developed by a turbojet is measured in pounds of thrust.

In order to evaluate various propulsive devices and provide a basis for comparison, we will write an expression which gives a value for thrust. Consider, for example, an air-breathing engine that uses \dot{m}_a slugs/sec or

$$\dot{m}_a = \frac{\dot{w}_a \text{ lb/sec}}{g \text{ ft/sec}^2} \quad (7.3)$$

lb sec/ft of air per second, as shown in Figure 7.12.

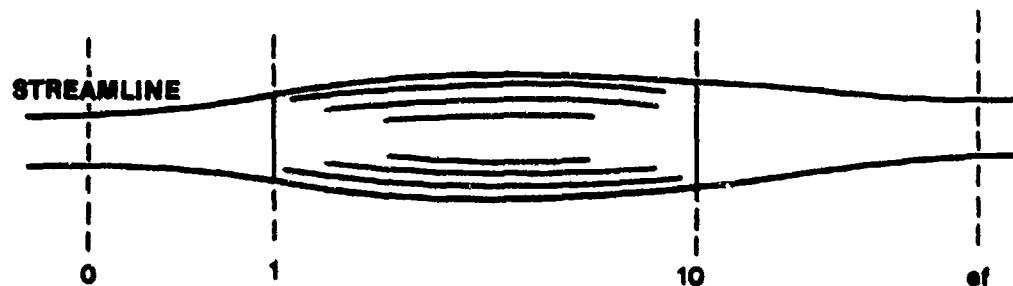


FIGURE 7.12. AIR-BREATHING ENGINE

We consider the air as it flows between the streamlines from entrance to exit as illustrated. All air-breathing engines take in air at approximately flight velocity and atmospheric pressure (in the absence of shock waves), compress it by some means, heat it by combustion, and discharge it through a nozzle so as to increase the momentum of the exit gases. The subscripts in Figure 7.12 have the following meaning: 0 refers to free stream conditions, 1 refers to the engine inlet section, 10 refers to the engine exit section, and ef refers to the section where the pressure of the engine exhaust gases is first equal to the pressure of the surrounding atmosphere.

The thrust of such a device is given by the time rate of momentum change between sections where the pressure is equal (0 and ef). We can write the following expression for the net thrust acting on the engine

$$F = ma = m(dv/dt) = \frac{m}{dt}(v_{ef} - v_0) \quad (7.4)$$

or

$$F = \dot{m}(v_{ef} - v_0) \quad (7.5)$$

To account for the change of mass flow due to the addition of fuel we must write

$$F = \dot{m}_{10}v_{ef} - \dot{m}_a v_0 \quad (7.6)$$

In most air-breathing engines, this addition of fuel is small (about 2%); however, to be analytically correct, we shall consider this factor in our thrust equation. When thrust is evaluated, measurements are usually made at the actual engine exit section and not at Section ef. Therefore, it is desirable to write the first term of Equation 7.6 in terms of conditions at Station 10. The pressure at 10 can be greater or less than the atmospheric pressure, and when this is true, the pressure unbalance will provide an additional force term to the thrust equation. When the thrust equation is written between the free stream condition 0 and the actual engine exit Station 10, it becomes

$$F_{\text{actual}} = \dot{m}_{10} V_{10} + A_{10} (P_{10} - P_0) - \dot{m}_a V_0 \quad (7.7)$$

Equation 7.6 or Equation 7.7 may be used to evaluate the net thrust of a propulsion device, and it has been found from flight measurements that either equation will give satisfactory results. The various terms contained in these equations are given specific names. First, there is the gross thrust, the thrust produced by the nozzle, which is defined as

$$F_{g_{\text{Ideal}}} = \dot{m}_{10} V_{\text{ef}} \quad (7.8)$$

$$F_{g_{\text{Actual}}} = \dot{m}_{10} V_{10} + A_{10} (P_{10} - P_0) \quad (7.8a)$$

Note that these are two forms for the gross thrust. The first is the momentum flux at the effective exit section, and the second is the sum of the momentum flux and the pressure thrust at the exit section. The latter form is the one preferred.

The other term of the thrust equation is called the negative thrust or ram drag. It is defined as

$$F_r = \dot{m}_a V_0 \quad (7.9)$$

This force is a negative one because it represents the equivalent drag of taking on the flight-velocity air. The difference between these two terms (the gross thrust and the ram drag) is called the net thrust because it is the

net force acting on the engine to produce propulsion power. Thus, we can write for net thrust

$$F_n = F_{g_{\text{Actual}}} - F_r = \dot{m}_{10} V_{10} + A_{10} (P_{10} - P_0) - \dot{m}_a V_0 \quad (7.10)$$

or

$$F_n = \dot{m} (V_{10} - V_0) + A_{10} (P_{10} - P_0)$$

neglecting fuel added.

When

$$P_{10} = P_0$$

i.e., for an ideal nozzle

$$F_n = \dot{m} (V_{10} - V_0) \quad (7.11)$$

Sometimes it is more convenient, when evaluating thrust, to express the momentum flux as a function of Mach rather than velocity. This relation was derived from the continuity equation and from the definition of Mach.

$$\dot{m} V = P_\gamma M^2 \quad (7.12)$$

The various forms of the thrust equation are summarized in Table 7.1.

TABLE 7.1
SUMMARY OF THRUST EQUATIONS

Gross Thrust

$$F_g = \dot{m}_{10} V_{10} + A_{10} (P_{10} - P_0)$$

$$F_g = A_{10} \left[P_{10} (\gamma_{10} M_{10}^2 + 1) - P_0 \right]$$

Ram Drag

$$F_r = \dot{m}_a V_0 = A_0 P_0 \gamma_0 M_0^2$$

Net Thrust

$$F_n = F_g - F_r$$

It should be remembered that the net thrust is always the difference between the gross thrust and the ram drag; therefore, it is given by any combination of the various gross thrust and ram drag terms.

When the aircraft and engine are static, net thrust and gross thrust are equal. When the term, "thrust," is used by itself in discussing a gas turbine engine, the reference is usually to net thrust, unless otherwise stated.

Static engine thrust is measured directly in an engine test stand. Stands are usually constructed in such a manner that they float, pushing against a calibrated scale which accurately measures the thrust in pounds. Thrust stands are also available to measure the static thrust exerted by a complete aircraft and engine installation and are often used, although some additional complications are involved. Once an installed engine becomes airborne, direct measurement of thrust is not usually practical. Consequently, compressor RPM and turbine discharge pressure (or engine pressure ratio), that vary with the thrust being developed, are measured and used to indicate the propulsive force which an engine is producing in flight.

7.6 FACTORS AFFECTING THRUST

If a turbojet engine were operated only under static conditions in an air-conditioned room at standard day temperature, there would be no need to

change the quantities used in the foregoing equations for net and gross thrust at any given throttle setting. However, all engines installed in aircraft must operate under varying conditions of airspeed and altitude. These varying conditions will radically affect the temperature and pressure of the air entering the engine, the amount of airflow through the engine, and the jet velocity at the engine exhaust nozzle. This means that, for any given throttle setting, different values must be entered in the thrust equations as the airspeed and/or altitude of the aircraft changes. Although some of these variables are compensated by the engine fuel control, many of the changes that will occur affect the thrust output of the engine directly.

In actual practice, the equation presented previously will seldom be used directly to calculate engine thrust. Nevertheless, an understanding of the effect on the thrust equations of the several variables that will be encountered during normal engine operation will serve to illustrate how the changing conditions at the engine air inlet affect engine performance in flight and on the ground.

7.6.1 Ram Effect

As an aircraft gains speed going down a runway, the outside air is moving past the aircraft with increasing speed. The effect is the same as if the aircraft were stationary in a wind tunnel and air were being blown past the aircraft by means of a fan in the tunnel. The movement of the aircraft relative to the outside air causes air to be rammed into the engine inlet duct. Ram effect increases the airflow to the engine, which, in turn, means more thrust.

Ram effect alone, however, is not all that happens at the engine air inlet as airspeed increases. There are some changes in pressure and velocity which occur inside the air inlet duct because of the shape of the duct itself, as will be explained later. Neglecting these changes for the moment, it has been shown that, as an aircraft gains airspeed, the thrust being produced by the engine decreases for any given throttle setting because V_0 at the engine air inlet is increasing. Yet, because of ram effect, increasing the airspeed also increases the pressure of the airflow into the engine (\dot{m}_a).

What actually takes place, therefore, is the net result of these two different effects, as illustrated in Figure 7.13. In the sketch, the "A"

curve represents the tendency of thrust to drop off as airspeed builds up, due to the increase in free stream velocity, V_0 . The "B" curve represents the thrust generated by the ram effect that increases the airflow, \dot{m}_a , and, consequently, increases the thrust. The "C" curve is the result of combining curves "A" and "B". Notice that the increase in thrust due to ram as the aircraft goes faster and faster, eventually becomes sufficient to make up the loss in thrust caused by the increase in V_0 . Ram will also compensate for some of the loss in thrust due to the reduced pressure at high altitude.

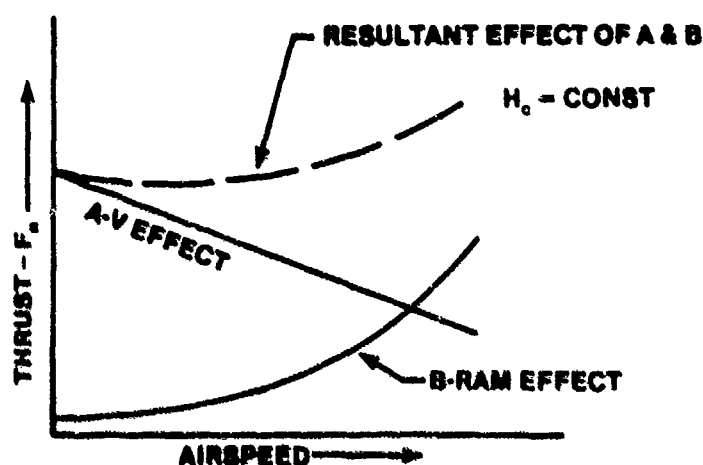


FIGURE 7.13. EFFECT OF RAM PRESSURE ON THRUST

Ram effect is important, particularly in high speed aircraft, because eventually, when the airspeed becomes high enough, the ram effect will produce a significant overall increase in engine thrust. At the subsonic speeds at which aircraft powered by nonafterburning engines usually cruise, ram effect does not greatly affect engine thrust. At supersonic speeds, ram effect can be a major factor in determining how much thrust an engine will produce.

7.6.2 Altitude Effect

The effect of altitude on thrust is really a function of density. As an aircraft gains altitude, the pressure of the outside air decreases, and the temperature of the air will, in general, become colder (Figure 7.14). As the pressure decreases, so does the thrust, but as the temperature decreases, the thrust increases. However, the pressure of the outside air decreases faster than the temperature, so an engine actually produces less thrust as altitude is increased. The temperature becomes constant at about 36,000 feet. But the

ambient pressure continues to drop steadily with increasing altitude. Because of this, thrust will drop off more rapidly above 36,000 feet.

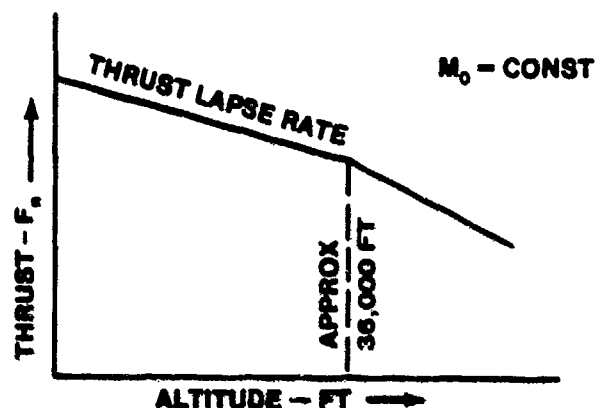


FIGURE 7.14. EFFECT OF ALTITUDE ON THRUST

7.7 SIMPLE CYCLE ANALYSIS

The thermodynamic cycle of the jet engine will be examined in order to obtain an insight into the factors affecting performance. An ideal cycle analysis of the turbojet and turbofan engine will be presented with a number of assumptions that will make the analysis simpler and easier to understand. Although the approach may appear somewhat restrictive, the results will be surprisingly close to those of the actual engine.

7.7.1 Engine Station Designations

Figure 7.15 shows the engine station terminology that will be used throughout this chapter. This designation is normally used for a single-spool (single compressor-single turbine) turbojet engine. The system can be expanded to include dual axial compressors and turbines by adding Station Number 2.5 and 4.5 between the low and high pressure compressor and turbine respectively. Afterburner mechanization is designated by Station Numbers 6 to 9, as required.

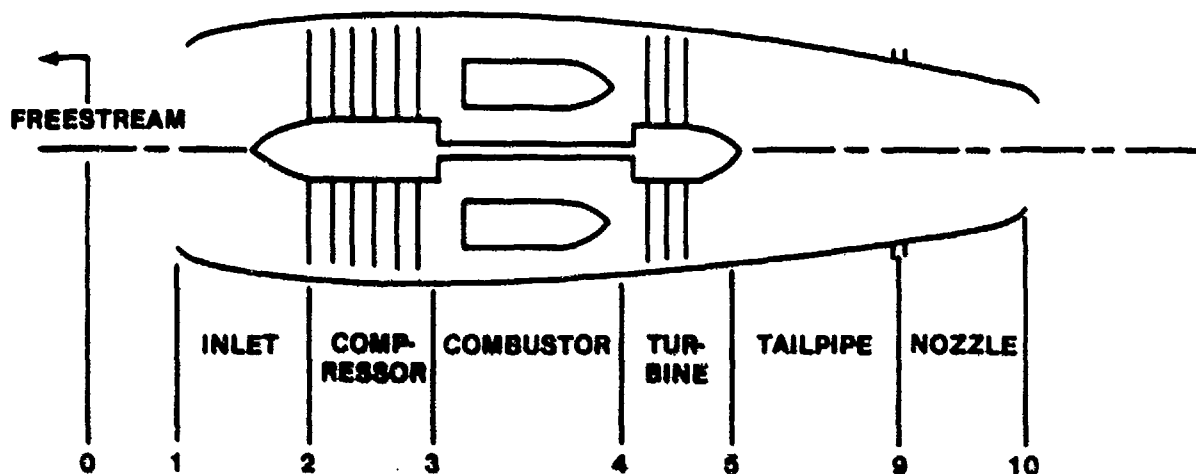


FIGURE 7.15 SINGLE-SPOOL TURBOJET ENGINE STATION DESIGNATIONS

7.7.2 Basic Equations and Processes

The steady flow energy equation, Equation 7.13, will be the primary relationship used throughout the analysis.

$$\Delta Q - \Delta W = \Delta h_T \quad (7.13)$$

where

ΔQ is the heat energy added to the cycle less the heat energy rejected,

ΔW , net work output of the cycle,

Δh_T , net change in total enthalpy.

Enthalpy is a convenient term used in flow analysis because it includes not only the internal energy of the working gas but also the flow and expansion work potential. Total enthalpy is composed of a static term related to

absolute temperature and a kinetic term resulting from the velocity of the gas

$$h_T = h + \frac{v^2}{2gJ} \quad (7.14)$$

$$h = C_p T \quad (7.15)$$

The term $gJ = 25,050 \text{ F-lb/BTU}$ is a conversion factor to keep the equations in standard heat engine units. The specific heat at constant pressure (C_p) is a function of temperature, varying from 0.24 to 0.27 BTU/lb^oR within a typical cycle.

The function of each engine component along with the appropriate form of Equation 7.13 is listed in Table 7.2. All processes in an ideal cycle are reversible, meaning there are no friction losses. In addition, all ideal processes except for combustion are isentropic. Isentropic means that entropy does not change during the process.

Entropy can be defined in several contexts, but in general, most definitions seem to be rather abstract. Although a thorough understanding of entropy is not required to comprehend the thermodynamic cycle, the basic concept is useful in understanding the limits of any heat engine. Entropy is a measure of the relative amount of heat energy that can be converted into mechanical energy, the remaining heat being rejected as lost energy. The Second Law of Thermodynamics gives some insight into the relative amount of energy which can be converted and the efficiency of the process. A process can be isentropic only if there is no heat transfer. Consequently, a combustion process can never be isentropic.

Table 7.2
IDEAL TURBOJET COMPONENT PROCESSES AND EQUATIONS

STATION NUMBER	NAME	PURPOSE	IDEAL PROCESS	IDEAL EQUATION
0	Free Stream			
0 - 1	Aerodynamic Inlet	Accel or Decel Air to Velocity at Inlet Face	Isentropic No Work	$h_{T0} = h_{T1} = h_0 + \frac{V_0^2}{2gJ}$
1	Inlet Face			
1 - 2	Geometric Inlet	Accel or Decel Air to Vel Req'd by Comp	Isentropic No Work	$h_{T1} = h_{T2} = h_{T0}$
2	Comp Ex. 2			
2 - 3	Compressor	Incr Total Pressure Of Airflow Absorb Work of The Turbine	Isentropic With Work	$h_{T2} + W_C = h_{T3}$
3	Comb Face			
3 - 4	Combustor	Incr Total Energy of Flow	Const. Pres Combustion	$h_{T3} + Q_{IN} = h_{T4}$
4	Turb Inlet			
4 - 5	Turbine	Extract Work to Drive Compressor	Isentropic With Work	$h_{T4} = h_{T5} + W_T$
5	Tailpipe Entry			
5 - 9	Tailpipe	Deliver Gas To Nozzle	Isentropic No Work	$h_{T5} = h_{T9}$
9	Noz Entr			
9 - 10	Nozzle Discharge	Incr Kinetic Enrgy of Gas	Isentropic Expansion No Work	$h_{T5} = h_{T10}$ $V_{10} = \sqrt{2gJ(h_{T5} - h_{T10})}$

7.7.3 The Ideal Cycle

A thermodynamic cycle is a series of processes that are repeated in a given order. The working fluid passes through various state changes, returning periodically to the initial state. An ideal cycle is one composed entirely of reversible processes.

The cycle can be constructed with any two independent variables, but a plot of enthalpy versus entropy is most useful. A typical h - s diagram for air is shown in Figure 7.16. Enthalpy and temperature are related by Equation 7.15; however, note that on the diagram the temperature variations of C_p have been included. The lines of constant pressure are given by the equation

$$ds = C_p \ln dT \quad (P = \text{constant}) \quad (7.16)$$

The ideal cycle for a turbojet engine is easily constructed using the equations from Table 7.2. A typical cycle is shown in Figure 7.17. The ideal cycle consists of the following processes in which the working gas is assumed to have negligible velocity at the compressor and turbine inlet and exit:

- 0-1 Air is compressed adiabatically
- 1-2 Air is heated at constant pressure
- 2-3 Gas is expanded isentropically
- 3-0 Gas is cooled at constant pressure within the atmosphere

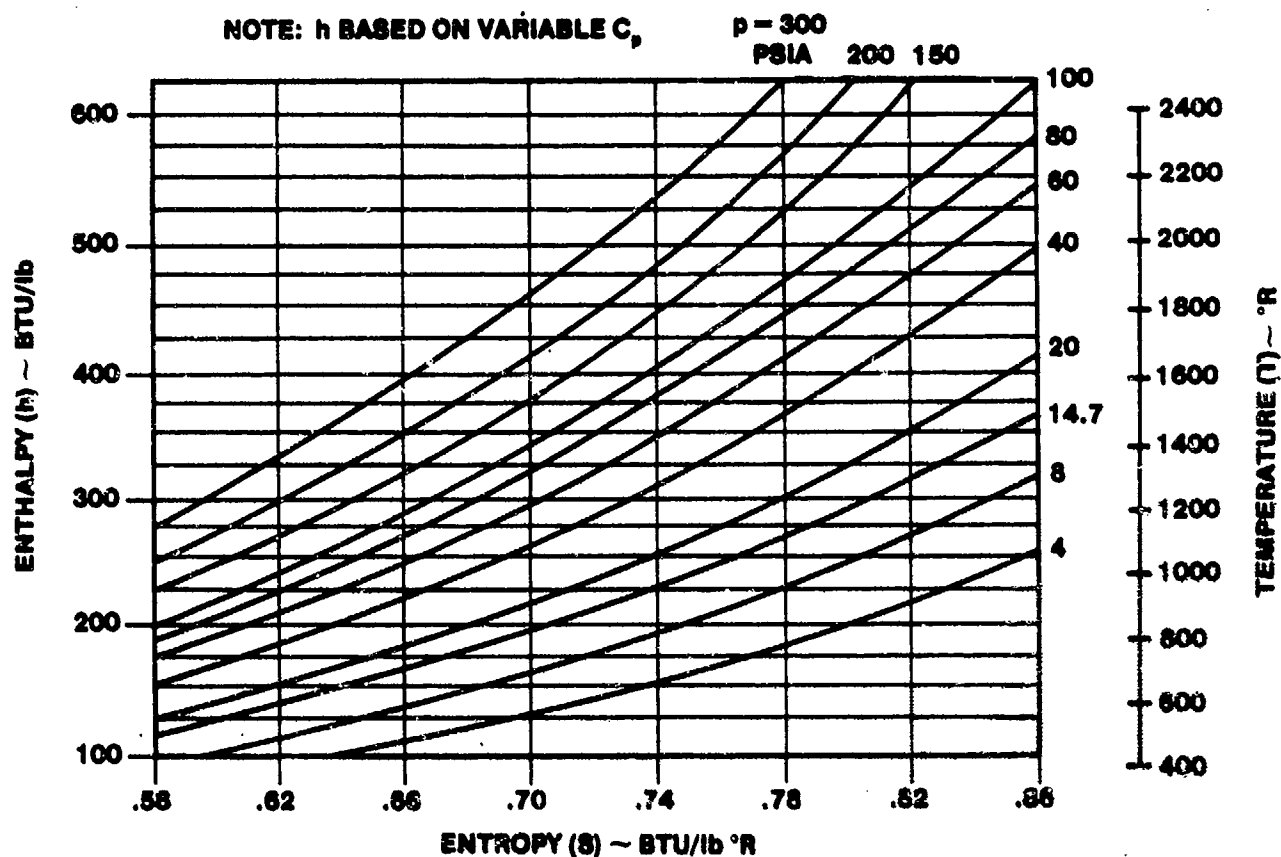


FIGURE 7.16. h - s DIAGRAM FOR AIR

The energy relationships which follow directly from Equation 7.14 are:

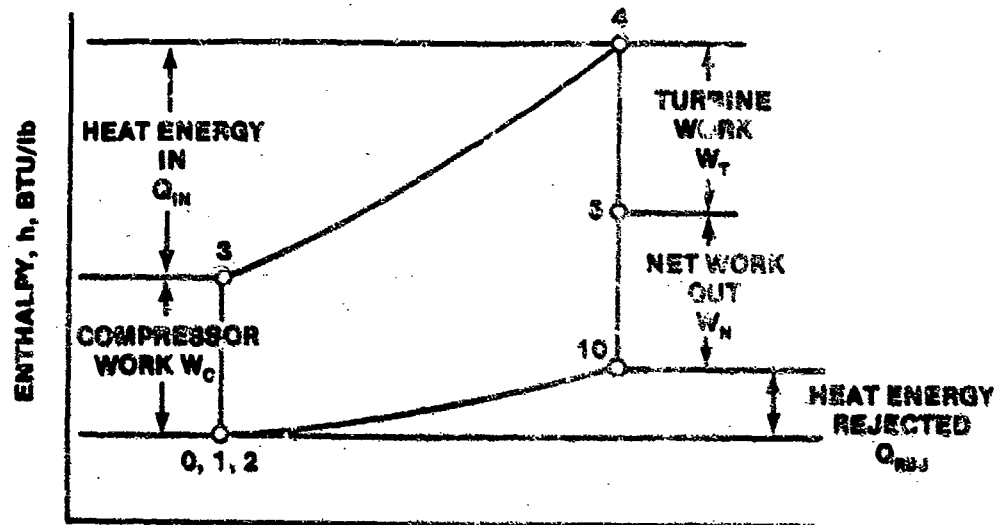
$$\text{Compressor work, } W_C = h_{T3} - h_{T2} = C_p (T_{T3} - T_{T2}) \quad (7.17)$$

$$\text{Turbine work, } W_T = h_{T4} - h_{T5} = C_p (T_{T4} - T_{T5}) \quad (7.18)$$

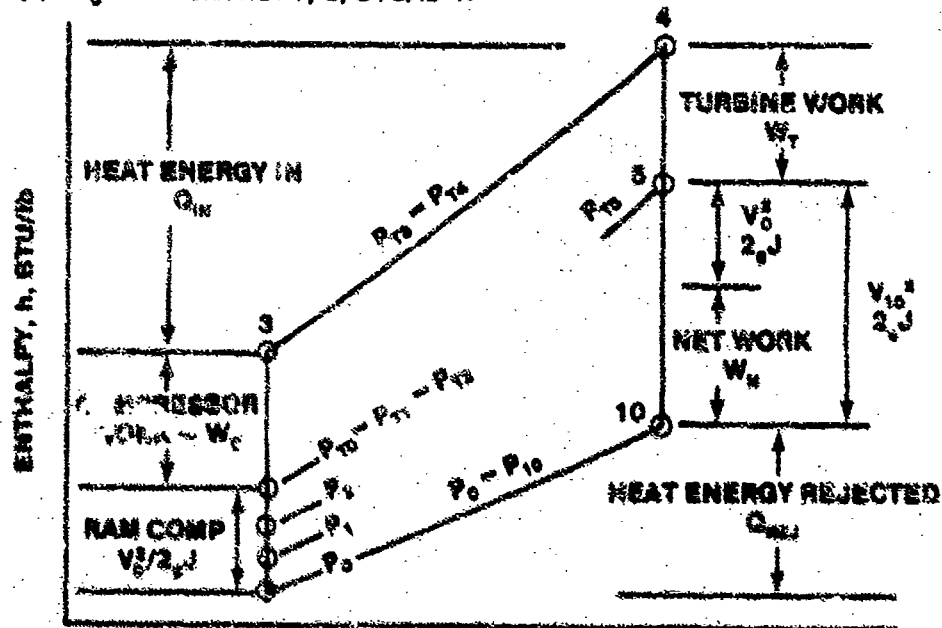
$$\text{Net work out, } W_N = h_{T5} - h_{T0} = C_p (T_{T5} - T_{T0}) \quad (7.19)$$

$$\text{Heat added, } Q_{IN} = h_{T4} - h_{T3} = C_p (T_{T4} - T_{T3}) \quad (7.20)$$

$$\text{Heat rejected, } Q_{REJ} = h_{T0} - h_{T1} = C_p (T_{T0} - T_{T1}) \quad (7.21)$$



(a) $M_0 = 0$ ENTROPY, s , BTU/lb·R



(b) $M_0 > 0$ ENTROPY, s , BTU/lb·R

FIGURE 7.17 TURBOJET ENGINE IDEAL CYCLE

An energy balance of the cycle yields

$$W_c + Q_{IN} = W_t + W_n + Q_{REJ} \quad (7.22)$$

The work done by the turbine is equal to the work required by the compressor in the ideal cycle: $W_c = W_t$. Rearranging Equation (7.22), the net work out is then

$$\begin{aligned}
 W_N &= Q_{IN} - Q_{REJ} \\
 &= (H_{T4} - H_{T3}) - (H_{10} - H_0) \\
 &= C_p (T_{T4} - T_{T3} - T_{10} + T_0) \quad (7.23)
 \end{aligned}$$

7.7.3.1 Note on Temperature Measurements. Equation 7.23 suggests that the output energy of a turbojet engine could be calculated by measuring the turbine inlet temperature ($TIT = T_{T4}$), compressor exit temperature (T_{T3}), nozzle exit temperature (T_{10}), and the ambient free stream temperature (T_0). The net work output could then be easily calculated with a simple calculator. This is in fact done for some engines. However, TIT is very difficult to measure due to temperatures sometimes in excess of $2400^\circ R$.

Another approach follows directly from the ideal relationship $W_C = W_T$. Substituting Equations 7.17 and 7.18

$$C_p (T_{T3} - T_{T2}) = C_p (T_{T4} - T_{T5})$$

Rearranging

$$T_{T4} - T_{T3} = T_{T5} - T_{T2}$$

Substituting into Equation 7.23

$$W_N = C_p (T_{T5} - T_{T2} + T_0 - T_{10}) \quad (7.24)$$

where

T_{T5} = EGT, exhaust gas temperature, and

T_{T2} = CIT, compressor inlet temperature.

Since EGT is considerably lower than TIT , this method is more easily applied in practice and more often used. However, it is not as accurate as the first method because of the assumption $W_C = W_T$.

7.7.4 Thermal Efficiency

Thermal efficiency is a measure of how efficiently heat energy can be converted into net work. By definition,

$$\begin{aligned}
 \eta_{TH} &= \frac{W_N}{Q_{IN}} \\
 &= \frac{C_p (T_{T4} - T_{T3} - T_{10} + T_0)}{C_p (T_{T4} - T_{T3})} \\
 \eta_{TH} &= 1 - \frac{T_{10} - T_0}{T_{T4} - T_{T3}} \quad (7.25)
 \end{aligned}$$

Equation 7.25 is not very transparent in terms of engine design parameters. From the relationship for an ideal gas undergoing an isentropic expansion,

$$\left(\frac{P_1}{P_2} \right)^{\frac{\gamma-1}{\gamma}} = \frac{T_1}{T_2} \quad (7.26)$$

we can write

$$\left(\frac{P_{T3}}{P_0} \right) \left(\frac{P_{10}}{P_{T4}} \right)^{\frac{\gamma-1}{\gamma}} = \left(\frac{T_{T3}}{T_0} \right) \left(\frac{T_{10}}{T_{T4}} \right) \quad (7.27)$$

In the ideal cycle $P_{10} = P_0$ and $P_{T4} = P_{T3}$ so the right side of Equation 7.27 is unity. Hence,

$$\left(\frac{T_{T3}}{T_0} \right) \left(\frac{T_{10}}{T_{T4}} \right) = 1 \quad \text{or} \quad \frac{T_{10}}{T_0} = \frac{T_{T4}}{T_{T3}} \quad (7.28)$$

PROBLEM: Using Equation 7.28,

$$\frac{T_0}{T_{T3}} = \frac{T_{10} - T_0}{T_{T4} - T_{T3}} \quad (7.29)$$

Substituting Equation 7.29 into 7.25

$$\eta_{TH} = 1 - \frac{T_0}{T_{T3}}$$

and applying Equation 7.26 again

$$\eta_{TH} = 1 - \left(\frac{P_0}{P_{T3}} \right)^{\frac{\gamma-1}{\gamma}} \quad (7.30)$$

Note that

$$\frac{P_{T3}}{P_0} = \left(\frac{P_{T3}}{P_{T2}} \right) \left(\frac{P_{T2}}{P_{T0}} \right) \left(\frac{P_{T0}}{P_0} \right)$$

where

$\frac{P_{T3}}{P_{T2}}$ is the compression ratio, CR,

$\frac{P_{T2}}{P_0}$, inlet recovery factor (which is unity in the ideal cycle)

$$\frac{P_{T0}}{P_0} = \left(1 + \frac{\gamma-1}{\gamma} M_0^2 \right)^{-\frac{\gamma-1}{\gamma}}, \quad M_0 \text{ is the free stream Mach}$$

Thus

$$\eta_{TH} = 1 - \left[\left(1 + \frac{\gamma-1}{\gamma} M_0^2 \right) (CR) \right]^{-\frac{\gamma-1}{\gamma}} \quad (7.31)$$

The significance of this equation is that thermal efficiency is now shown to be a function of two design variables: compression ratio and Mach. Efficiency increases with an increase in either parameter. These variations are shown in Figure 7.18 for two different Mach.

Turbine inlet temperature (T_{T4}) also has a small effect on thermal efficiency. Efficiency decreases slightly as TIT is increased, but the effect is smaller than Mach variations. The effects of TIT on thermal efficiency are shown in Figure 7.19.

Thermal efficiency does not tell the entire story because the operating temperatures of the cycle must also be considered. Ambient air temperature (T_0) is fixed by the flight condition. The maximum TIT is also fixed by the metallurgy of the turbine blades. The current state of the art limits TIT to about 3000°R , but higher limits may be permissible with a better technique for cooling the turbine blades.

Fixing T_0 and TIT, a variety of compression ratios are possible with each one yielding a different thermal efficiency. Figure 7.20 shows three cycles. Cycle 0-3-4-0 has a low pressure ratio, a low efficiency, and a low work capacity as denoted by the small enclosed area of the cycle. In the limit (compression ratio = 0), the work capacity and efficiency would be zero. At the other extreme, cycle 0 - 3" - 4" - 0 would have a very high compression ratio and high thermal efficiency, but the work capacity would again be low. In the limit as the compression ratio is increased, the work would be zero, but the efficiency 100%. Obviously, neither of these cycles would be satisfactory in any practical application. These trends are summarized in Table 7.3.

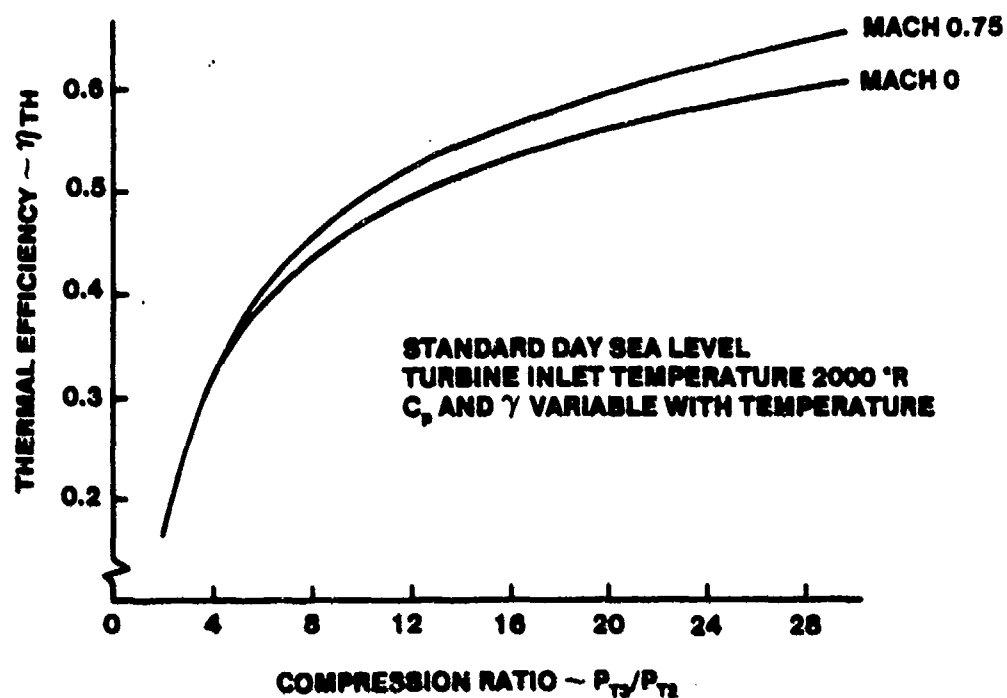


FIGURE 7.18. IDEAL TURBOJET THERMAL EFFICIENCY

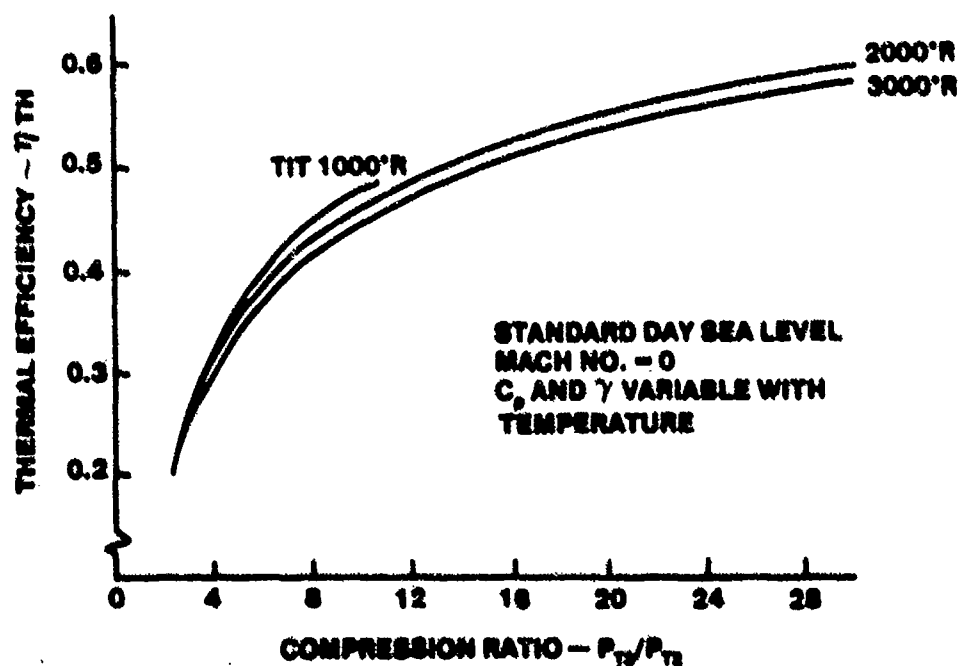


FIGURE 7.19. IDEAL TURBOJET THERMAL EFFICIENCY

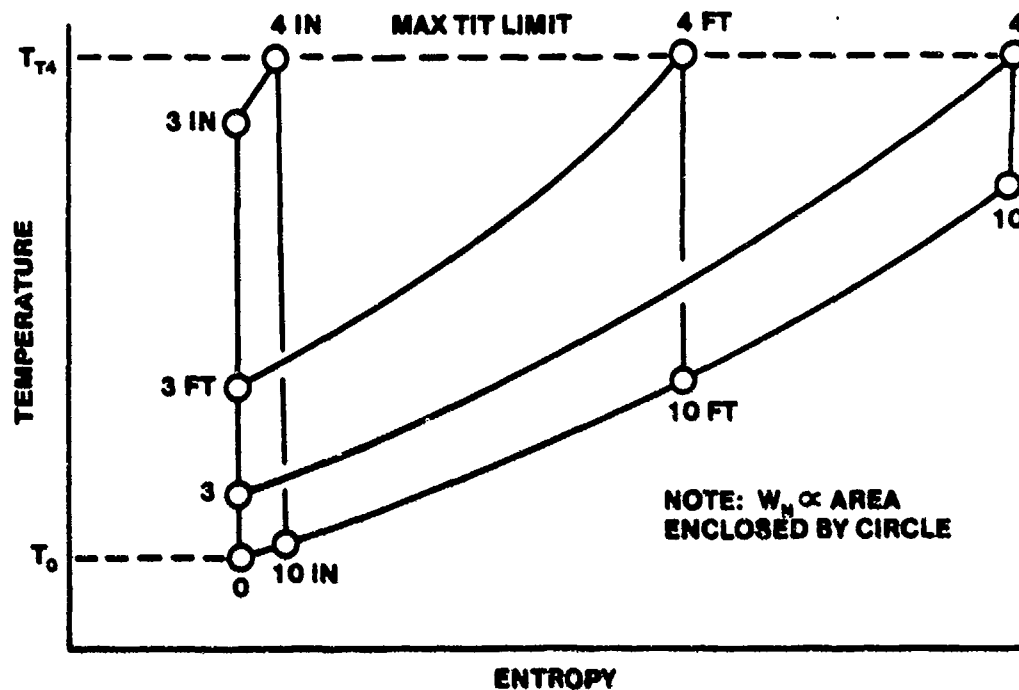


FIGURE 7.20. THERMAL EFFICIENCY VERSUS NET WORK

TABLE 7.3

EFFECTS OF COMPRESSION RATIO ON η_{TH} AND W_N

CYCLE	CR	TH	W_N
0 - 3 - 4 - 0	LOW	LOW	LOW
0 - 3' - 4' - 0	MED	MED	HIGH
0 - 3'' - 4'' - 0	HIGH	HIGH	LOW

What is needed is a compromise compression ratio which will give an adequate work capacity at a reasonable thermal efficiency. The optimum compression ratio is derived in Appendix F for maximum net work.

7.7.5 Ideal Turbojet Performance

We are now ready to determine the ideal cycle for an actual turbojet engine. However, let's slow down a moment and look at the plan of attack.

We would like to determine the net thrust (F_n) and thrust specific fuel consumption (TSFC) of the turbojet engine. The two basic equations are

$$F_n = \frac{\dot{w}_a}{g} (V_{10} - V_0) + A_{10} (P_{10} - P_0) \quad (7.32)$$

$$\text{TSFC} = \frac{\dot{w}_f}{F_n} \quad (7.33)$$

where \dot{w}_a and \dot{w}_f are the air and fuel flow rates respectively. We will then be able to examine trends and tradeoffs as a function of the variables.

The variables can be divided into flight conditions and engine parameters. The significant flight conditions (V_0 , T_0 , and P_0) define the free stream. The engine parameters are compression ratio, turbine inlet temperature, and airflow rate. An actual cycle analysis would also include the individual component efficiencies.

These assumptions will be made:

1. Individual components are 100% efficient
2. $W_T = W_C$ (no auxiliary drives)
3. No bleed air
4. Nozzle perfectly expands gas to ambient pressure
5. Addition of fuel to mass flow rate is negligible

The problem (to determine F_n and TSFC) can be solved analytically or graphically using the h-s diagram. The analytical approach is presented in Appendix F. The remainder of this chapter will be concerned with the graphical approach. The latter approach not only requires less mathematics but also gives a better insight into the actual processes occurring in the engine.

7.7.5.1 Ideal Turbojet Cycle Analysis. In this section we will construct the h-s diagram for a J-79 turbojet and then calculate F_n and TSFC. The specific flight conditions and engine parameters are listed in Table 7.4.

TABLE 7.4

FLIGHT CONDITIONS AND ENGINE PARAMETERS
FOR J-79 TURBOJET ANALYSIS

FLIGHT CONDITIONS			ENGINE PARAMETERS		
V_0	T_0	H_0^*	TIT_{MAX}	CR	\dot{w}_a
230K	40°F	16,000ft	1810°F	13.5	170 lb/sec

*FREE STREAM ALTITUDE

SOLUTION

The problem will be solved in a series of steps. The resulting h-s diagram is shown in Figure 7.21 so that the reader may more easily follow the actual construction.

STEP 1: LOCATE STATION

$$H_0 = 16,000 \text{ ft} \Rightarrow P_0 = 8.0 \text{ PSIA}$$

$$T_0 = 40^\circ\text{F} = 500^\circ\text{R}$$

Enter h-s diagram with P_0 and T_0 ;

read h_0 and s_0 directly

$$h_0 = 120 \text{ BTU/lb}$$

$$s_0 = 0.63 \text{ BTU/lb}^\circ\text{R}$$

STEP 2: LOCATE STATION (1, 2)

$$\begin{aligned} h_{T1} &= h_1 + \frac{V_1^2}{2gJ} = h_{T2} \\ &= h_0 + \frac{V_0^2}{2gJ} \\ &= 120 + \frac{[(1.69)(230)]^2}{50,100} \end{aligned}$$

$$h_{T1} = h_{T2} = 123 \text{ BTU/lb}$$

$$s_1 = s_2 = s_0 = 0.63 \text{ BTU/lb}^\circ\text{R}$$

Read P_{T2} directly from h-s diagram
(interpolate)

$$P_{T2} = 11 \text{ PSIA}$$

NOTES

Only ambient temperature and pressure are required to locate station 0.

From the TPS Performance Manual we find 16,000 ft corresponds to $\delta = 0.5420$. Hence $P_0 = (14.7) \delta$ PSIA.

Always remember to convert $^\circ\text{F}$ to absolute.

$$(^{\circ}\text{R} = ^{\circ}\text{F} + 460^{\circ}).$$

NOTES

The purpose of the inlet is to slow the free stream airflow, thereby converting the kinetic energy of the flow into a pressure rise. This is a consequence of Bernoulli's equation.

In an ideal inlet operating on design, $V_0 = V_1$. Don't forget to convert knots into ft/sec:
(1K = 1.69 ft/sec.)

Since the inlet processes are all isentropic, there can be no loss in total quantities. Hence

$$h_{T0} = h_{T1} = h_{T2}$$

$$s_0 = s_1 = s_2.$$

However, $V_1 = V_2$ as the kinetic and static values may vary.

STEP 3: LOCATE STATION ③

$$P_{T3} = (CR) (P_{T2})$$

$$\text{where } CR = \frac{P_{T3}}{P_{T2}}$$

$$P_{T3} = (13.5) (11) \\ = 150 \text{ PSIA}$$

Read h_{T3} from h-s diagram

$$h_{T3} = 280 \text{ BTU/lb}$$

$$s_3 = 0.63 \text{ BTU/lb}_R$$

NOTES

The compressor increases the total pressure of the airflow. Since the ideal process is isentropic, $s_2 = s_3$.

STEP 4: LOCATE STATION ④

$$P_{T4} = P_{T3} = 150 \text{ PSIA}$$

$$T_{T4} = T_{IT_{MAX}} = 1810^\circ\text{F} = 2270^\circ\text{R}$$

Locate on h-s diagram; read

h & s directly

$$h_{T4} = 565 \text{ BTU/lb}$$

$$s_4 = 0.80 \text{ BTU/lb}_R$$

NOTES

The ideal combustion process occurs at constant pressure.

The exit temperature of the gas is limited to 1810°F which corresponds to MIL POWER.

STEP 5: LOCATE STATION ⑤

From Steps 2 and 3

$$\begin{aligned}W_C &= h_{T3} - h_{T2} \\&= 275 - 123 \\&= 152 \text{ BTU/lb}\end{aligned}$$

Hence,

$$\begin{aligned}W_T &= 152 \text{ BTU/lb} \\h_{T5} &= h_{T4} - W_T \\&= 565 - 152 \\&= 413 \text{ BTU/lb}\end{aligned}$$

$$s_5 = s_4 = 0.80 \text{ BTU/lb}^\circ\text{R}$$

STEP 6: LOCATE STATION ⑩

$$\begin{aligned}P_{10} &= P_0 = 8 \text{ PSIA} \\s_{10} &= s_5 = 0.80 \text{ BTU/lb}^\circ\text{R}\end{aligned}$$

Locate on h-s diagram; read

h_{10} directly

$$\begin{aligned}h_{10} &= 255 \text{ BTU/lb} \\W_N &= h_{T5} - h_{10} \\&= 413 - 255 \\&= 158 \text{ BTU/lb}\end{aligned}$$

NOTES

The turbine, located between Stations 4 and 5 drives the compressor.

The addition of auxiliary drives does not add a significant error in the results if neglected because they require only a small percentage of the energy required by the compressor.

NOTES

Up to this point, the results could apply equally well to a turboprop, turboshaft, or turbofan. In other words, the output energy ($W_N = h_{T5} - h_{10}$) could be used to drive a second turbine or a fan. The turbojet uses a nozzle to convert the static enthalpy at Station 5 into a high velocity gas at Station 10. The ideal nozzle isentropically expands the gas to ambient pressure ($P_{10} = P_0$).

SPECIAL NOTE:

The cycle is closed in the atmosphere as the gas at the nozzle exit cools at ambient pressure to the ambient temperature. The enthalpy, pressure, and temperature at Stations 0 and 10 are static quantities (these are total quantities at all other stations). The total enthalpy at Stations 0 and 10 are

$$h_{T0} = h_{T1} = h_{T2}$$

$$h_{T10} = h_{T5}$$

This shows that the diffuser (inlet) and nozzle perform exactly opposite functions.

STEP 7: CALCULATE EXIT VELOCITY

NOTES

$$\begin{aligned} V_{10} &= \sqrt{2gJ(h_{T5} - h_{10})} \\ &= (50,100)(158) \end{aligned}$$

$$V_{10} = 2814 \text{ ft/sec}$$

$$\text{Since } h_{T10} = h_{T5}$$

and

$$h_{T10} = h_{10} + \frac{V_{10}^2}{2gJ}$$

V_{10} is easily determined.

STEP 8: CALCULATE NET THRUST

NOTES

$$\begin{aligned} F_n &= \frac{\dot{w}_a}{g} (V_{10} - V_0) \\ &= \frac{170}{32.2} (2814 - 389) \end{aligned}$$

$$F_n = 12800 \text{ lb}$$

The fuel contribution has been neglected as it is typically small compared to air flow ($\dot{w}_f < 0.02 \dot{w}_a$).

If the gas at the nozzle is not expanded to the ambient pressure, then Equation 7.10 must be used.

STEP 9: CALCULATE FUEL FLOW RATE

$$\begin{aligned}\dot{w}_f &= 0.195 \dot{w}_a (h_{T4} - h_{T3}) \\ &= 0.195 (170) (565-280) \\ \dot{w}_f &= 9448 \text{ lb/hr}\end{aligned}$$

NOTE

The heat energy input in the cycle (Q_{IN}) is obtained from combustion of hydrocarbons. The average heating value (H.V.) for hydrocarbons is 18,500 BTU/lb fuel. Each pound of air requires a heat input of $Q_{IN} = h_{T4} - h_{T3}$. The total heat input per second is then

$$\dot{w}_a (h_{T4} - h_{T3}).$$

The total heat added is

$$\dot{w}_a (h_{T4} - h_{T3}) = \dot{w}_f \text{ H.V.}$$

Hence

$$\dot{w}_f = \frac{\dot{w}_a}{\text{H.V.}} (h_{T4} - h_{T3})$$

However, fuel flow is normally given in pounds per hour, so the last equation must be multiplied by 3600 sec/hr.

STEP 10: CALCULATE TSFC

NOTE

$$\begin{aligned}\text{TSFC} &= \frac{\dot{w}_f}{F_n} \\ &= \frac{9448}{12800}\end{aligned}$$

$$\text{TSFC} = 0.74 \frac{\text{lb-fuel}}{\text{lb-thrust} \cdot \text{hr}}$$

TSFC is another measure of thermal efficiency and is more commonly given with engine specifications. In this particular example, $\eta_{TH} = 0.54$, which does not convey nearly the information that is contained in TSFC.

This completes the ideal cycle analysis of the turbojet engine. The results were:

$$F_n = 12,800 \text{ lb}$$

$$\text{TSFC} = 0.74 \text{ lb/hr}$$

$$\dot{w}_f = 9448 \text{ lb/hr}$$

Do these values seem reasonable for the J-79?

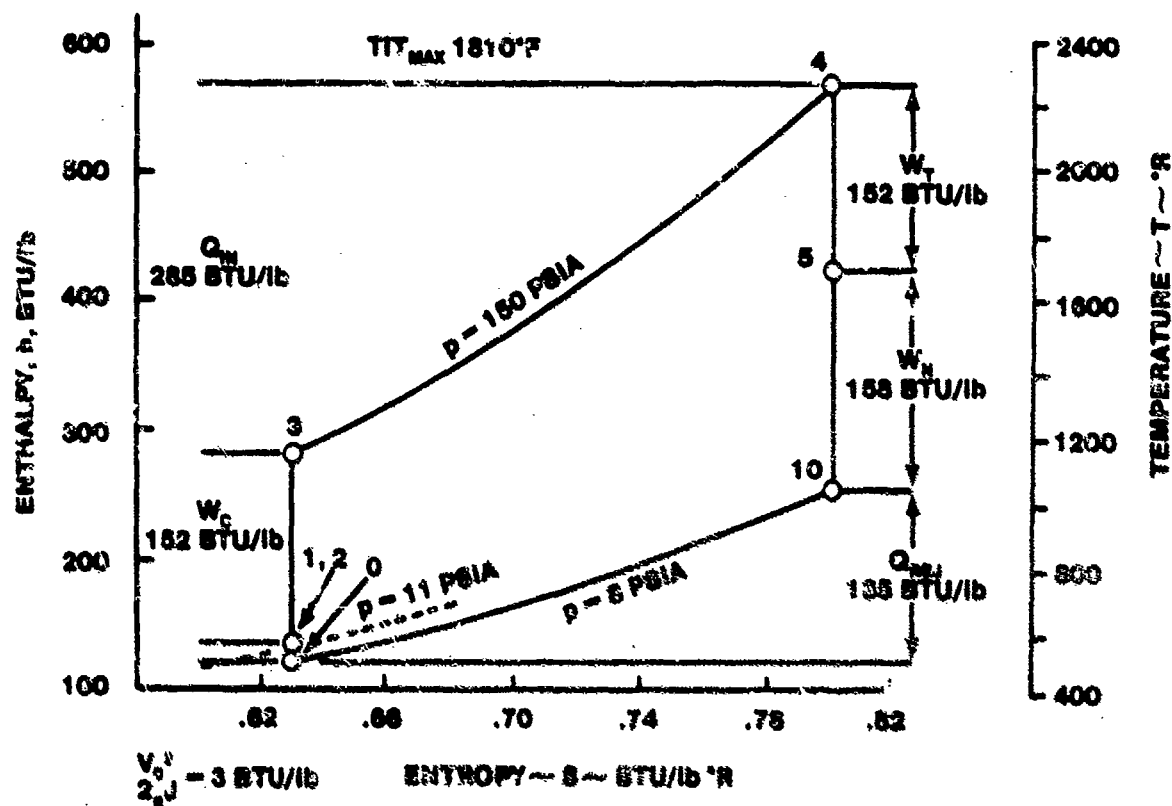


FIGURE 7.21. IDEAL CYCLE FOR THE J-79 TURBOJET (PER LB OF AIR)
 $V_0 = 230$ KTS, $T_0 = 40^\circ$, $h_0 = 16000$ FT

7.7.5.2 Propulsive Efficiency. All jet propulsion devices develop thrust by changing the velocity of the working fluid, and it is desirable to define an efficiency factor which shows how efficiently the process is carried out. This efficiency factor is called the propulsive efficiency, and it is indicative of how efficiently the kinetic energy of the engine is used. It is defined as the ratio of useful thrust power output to the available propulsive energy, which, in turn, is equal to the useful output plus the kinetic energy loss at the exit. That is,

$$\eta_p = \frac{\text{THP output}}{\text{THP output} + \text{KE losses at exit}}$$

$$\eta_p = \frac{F_n V_0}{F_n V_0 = \frac{\Delta KE}{\Delta t}} \quad (7.34)$$

$$\eta_p = \frac{\dot{m}(V_{10} - V_0)V_0}{\dot{m}(V_{10} - V_0)V_0 + \dot{m}\left(\frac{V_{10} - V_0}{2}\right)^2} \quad (7.35)$$

$$\eta_p = \frac{2V_0}{V_{10} + V_0} \quad (7.36)$$

It should be noted that this definition ignores the heat losses which occur at the nozzle exit and considers only the kinetic energy loss at that particular section.

Equation 7.36 applies to the air breathing engine. Note that when flight velocity is zero, there is no useful power; therefore, the propulsive efficiency is zero. Propulsive efficiency is equal to unity when the effective exhaust velocity is equal to the flight velocity. The latter case has no physical meaning because, in this condition, the thrust is zero (no momentum change).

Figure 7.22 illustrates variation of η_p with V_0 for the different air-breathing aircraft engines.

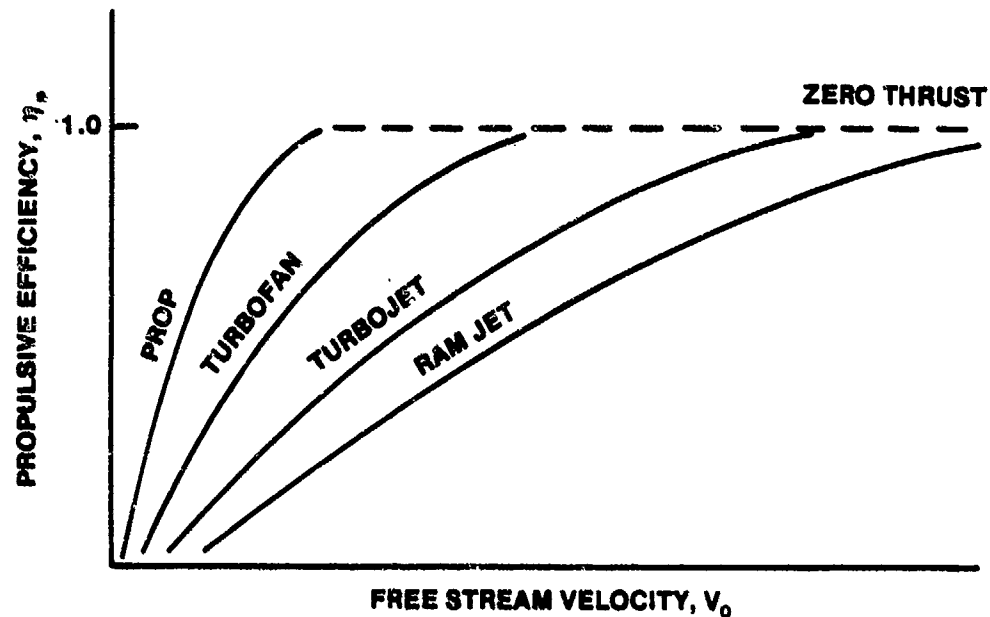


FIGURE 7.22. PROPULSIVE EFFICIENCY OF AIR-BREATHING ENGINES

7.7.5.3 Overall Efficiency. The product of the propulsive and thermal efficiencies yields a further criterion for judging the performance of jet propulsion engines. It is called overall efficiency and is written

$$\eta_0 = \eta_p \eta_{TH} \quad (7.37)$$

7.7.5.4 Ideal Turbojet Trends: Net Thrust. The ideal net thrust per unit mass flow of a turbojet engine is given by

$$F_n / \frac{w_a}{g} = (V_{10} - V_0) \quad (7.38)$$

$$= \sqrt{2gJC_p} \left\{ TIT \left[1 - (Cr f(M))^{-\frac{\gamma-1}{\gamma}} \right] - T_0 \left[(Cr f(M))^{\frac{\gamma-1}{\gamma}} \right] - 1 + V_0^2 \right\} - V_0 \quad (7.39)$$

where

$$f(M) = 1 - \frac{\gamma-1}{2} M_0^2 \quad \& \quad V_0 = M_0 \sqrt{\gamma R T_0}$$

Equation (7.39) is derived in Appendix F. This equation shows that the net thrust per unit mass flow is a function of two design variables (TIT and CR) and two flight parameters (M_0 and T_0). The variations in net thrust per unit mass flow with these parameters are shown in Figures 7.23 and 7.24. The results are summarized in Table 7.5.

TABLE 7.5
SUMMARY OF NET THRUST TRENDS
Ideal Turbojet

VARIABLE INCREASE	$\left(\frac{F_n}{g} \frac{\dot{w}_a}{g} \right)$
TURBINE INLET TEMPERATURE	INCREASE
COMPRESSION RATIO	OPTIMUM
MACH NUMBER - M_0	DECREASE
ALTITUDE - H_0	INCREASE

To fully appreciate the results, it must be understood that the variations tabulated above are valid only when all other variables are held constant. For example, the increase in $\left(\frac{F_n}{g} \frac{\dot{w}_a}{g} \right)$ with altitude does not mean an increase in net thrust. The net thrust actually decreases with increasing altitude because the airflow through the engine decreases.

A particular variable of interest is Mach; the decrease in $\left(\frac{F_n}{g} \frac{\dot{w}_a}{g} \right)$ with increasing M_0 is primarily due to the increase in V_0 , which is the ram drag per unit mass flow. If ram drag is deducted from the net thrust, the gross thrust per unit mass flow would result, which increases with Mach.

One observation worthy of note can be seen by looking at Figures 7.23 and 7.24. The optimum compression ratio (TIT constant) for maximum thrust decreases with increasing Mach number. The limiting case is for $CR = 1$. This engine is called a ramjet.

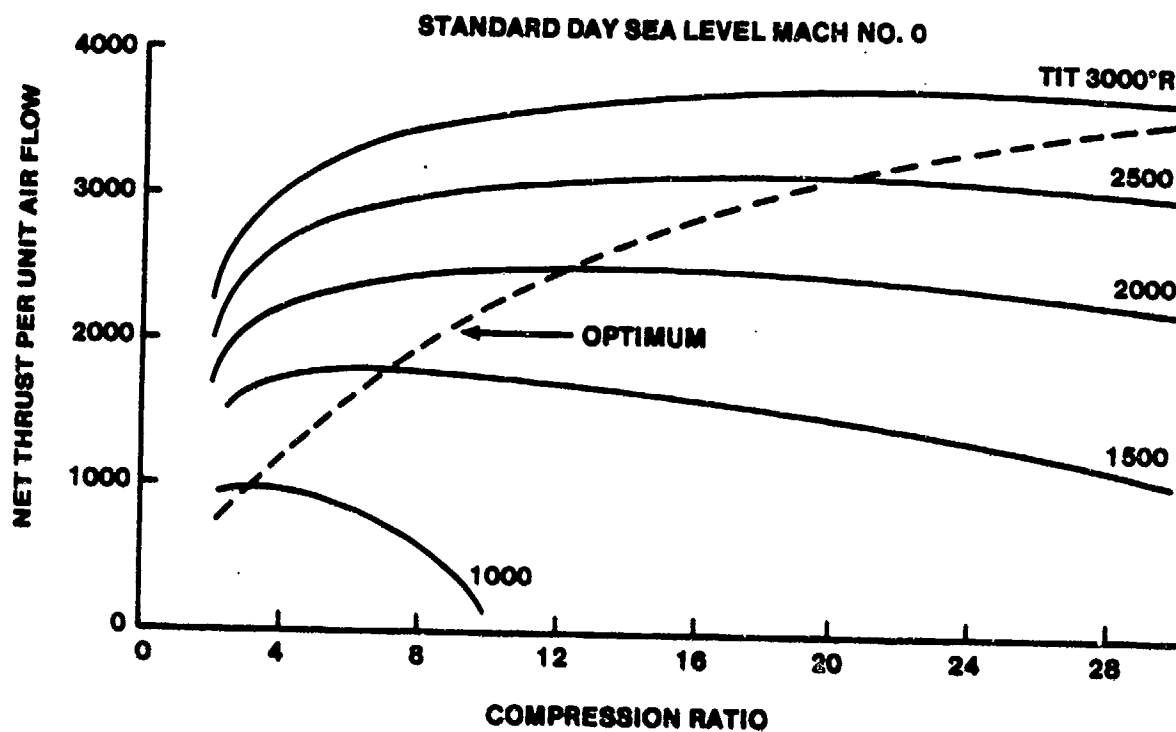


FIGURE 7.23. IDEAL TURBOJET NET THRUST

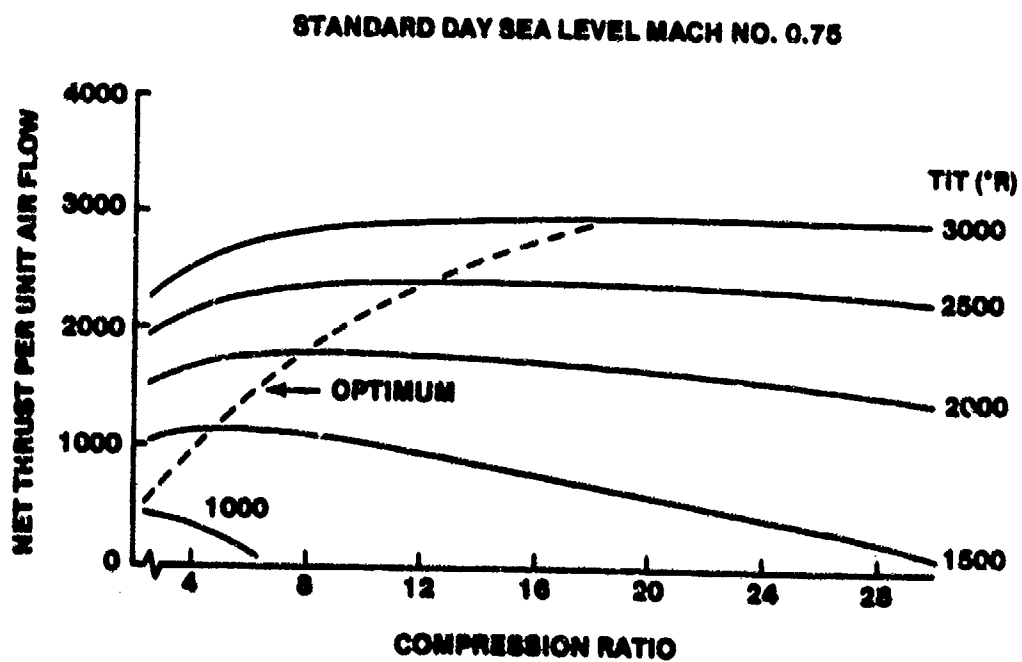


FIGURE 7.24. IDEAL TURBOJET NET THRUST

7.7.5.5 Ideal Turbojet Trends: Thrust Specific Fuel Consumption. The fuel consumption of an engine is usually given in terms of the amount of fuel required to produce a given amount of thrust. It is the key parameter for comparing engines. For example, a particular flight condition for any given aircraft produces a drag which the engine(s) must overcome. If Engine A has better TSFC (lower) than Engine B for the same flight conditions, Engine A will yield better range or require less fuel since both engines must develop the same thrust.

Thrust specific fuel consumption is defined as

$$\begin{aligned} \text{TSFC} &= \frac{\dot{w}_f}{F_n} \quad \frac{\text{lbs fuel}}{\text{lbs thrust hr}} \quad (7.40) \\ &= \frac{w_a (H_{T4} - H_{T3})}{\text{H.V. } F_n} \\ &= \frac{g C_P (T_{T4} - T_{T3})}{\text{H.V. } \left(F_n / \frac{w_a}{g} \right)} \end{aligned}$$

Comparison of Equation 7.41 with 7.39 shows that TSFC is a function of the same variables as net thrust per unit mass flow. Note that the compressor discharge temperature is established by the CR, altitude, and Mach. The effects of these variables are shown in Figure 7.25 and 7.26 and are summarized in Table 7.6.

TABLE 7.6

SUMMARY OF TSFC TRENDS
Ideal Turbojet

VARIABLE INCREASE	TSFC
TURBINE INLET TEMPERATURE	INCREASE
COMPRESSION RATIO	DECREASE
MACH - M_0	INCREASE SLIGHTLY*
ALTITUDE - H_0	DECREASE SLIGHTLY

* This effect is not the inverse of η_{TH} , due to the difference in the $(V_{10} - V_0)$ terms.

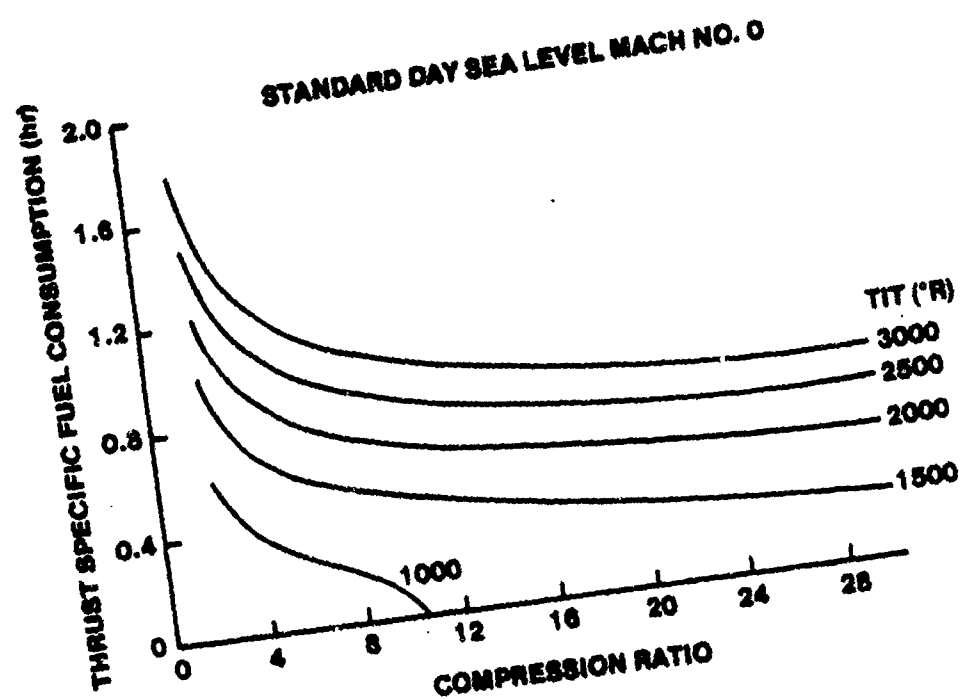


FIGURE 7.25. IDEAL TURBOJET THRUST SPECIFIC FUEL CONSUMPTION

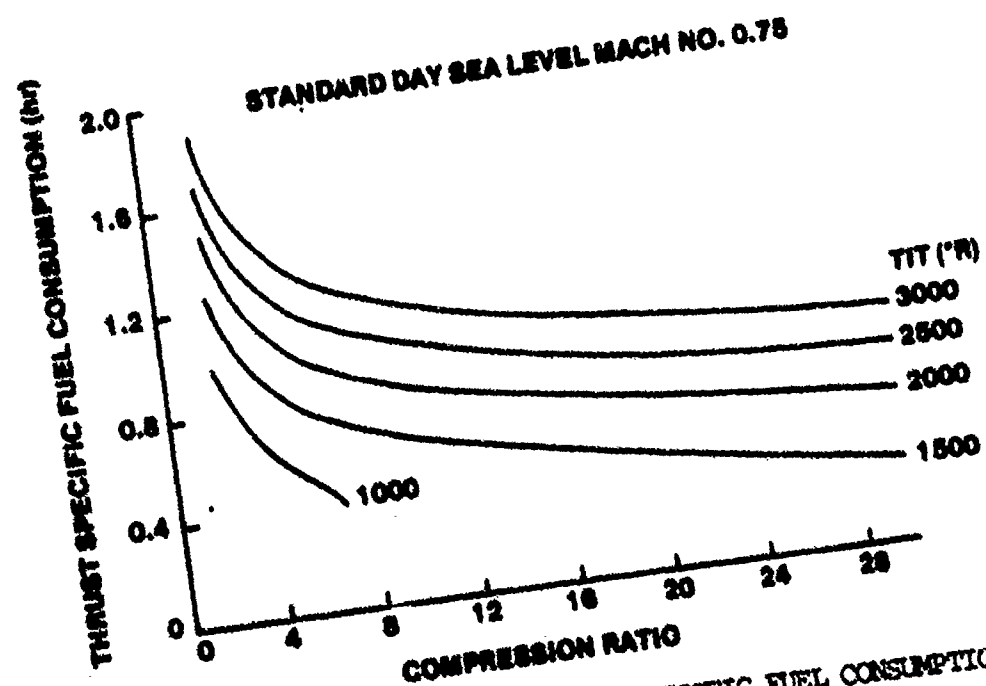


FIGURE 7.26. IDEAL TURBOJET THRUST SPECIFIC FUEL CONSUMPTION

The definition of TSFC can be related to the overall efficiency by converting the jet thrust to jet thrust horsepower. The following expression is obtained:

$$\eta_0 = \frac{V_0}{\text{sfc (H.V.)}} \quad (7.42)$$

where H.V. is the lower heating value of the fuel. Here also, the overall efficiency and sfc are indicative of the same thing. A typical value of sfc for a turbojet engine at sea level static is 0.9 lb per lb-hr. For a turbofan engine a typical sfc for the same condition is 0.7 lb per lb-hr.

Increasing TIT increases both thrust and TSFC (lower efficiency). Also, the optimum compression ratio for optimum thrust is lower than for optimum TSFC. Consequently, the selection of an engine operating point is a compromise. In fact, each design point of every engine component is a compromise within itself. In addition, off-design consideration must also be considered as performance tends to degrade much faster for the off-design condition in some areas. The nozzle is a good example of off-design considerations dictating the operating point.

7.7.6 IDEAL TURBOFAN PERFORMANCE

The turbofan engine has two primary advantages over the turbojet engine: higher net thrust and lower thrust specific fuel consumption. In this section we will demonstrate this by converting the J-79 turbojet engine into a turbofan engine and then calculate F_n and TSFC. Although the results will be optimistic, the overall improvement is considerable. However, the turbofan does have some disadvantages when compared to the turbojet. We will examine the relative merits of each in a subsequent section.

7.7.6.1 Turbofan Operation. The fan stage consists of two primary components: an inlet and a fan compressor. The purpose of the inlet is the same as in the core engine--slow the free stream and thereby convert the kinetic energy of the flow into a pressure rise. In some turbofan configurations, the core and fan stage inlets are identical. The fan compressor increases the total pressure of the bypassed airflow. The ideal

process for both components is obviously isentropic.

Before starting the turbofan cycle analysis we need to discuss the interaction of bypass ratio (β) with fan compression ratio (CR_f). Bypass ratio is defined by

$$\beta = \frac{\dot{w}_a^{\text{duct}}}{\dot{w}_a^c} \quad (7.43)$$

where \dot{w}_a is the air flow rate through the fan duct that doesn't go through the core and \dot{w}_{ac} , the air flow rate through the core engine.

The effect of fan compression ratio and bypass ratio on TSFC is shown in Figure 7.27. The turbine work limit is reached when all of the net energy output of the core engine is used to drive the fan stage (no core engine thrust). The optimum TSFC (and net thrust) is obtained when the core exhaust gas velocity is equal to the bypassed exhaust gas velocity. TSFC improves as the bypass ratio is increased, the limit being a shrouded turboprop engine. However, high bypass engines suffer from lack of performance at higher Mach. Note that the optimum fan compression ratio decreases as bypass ratio increases.

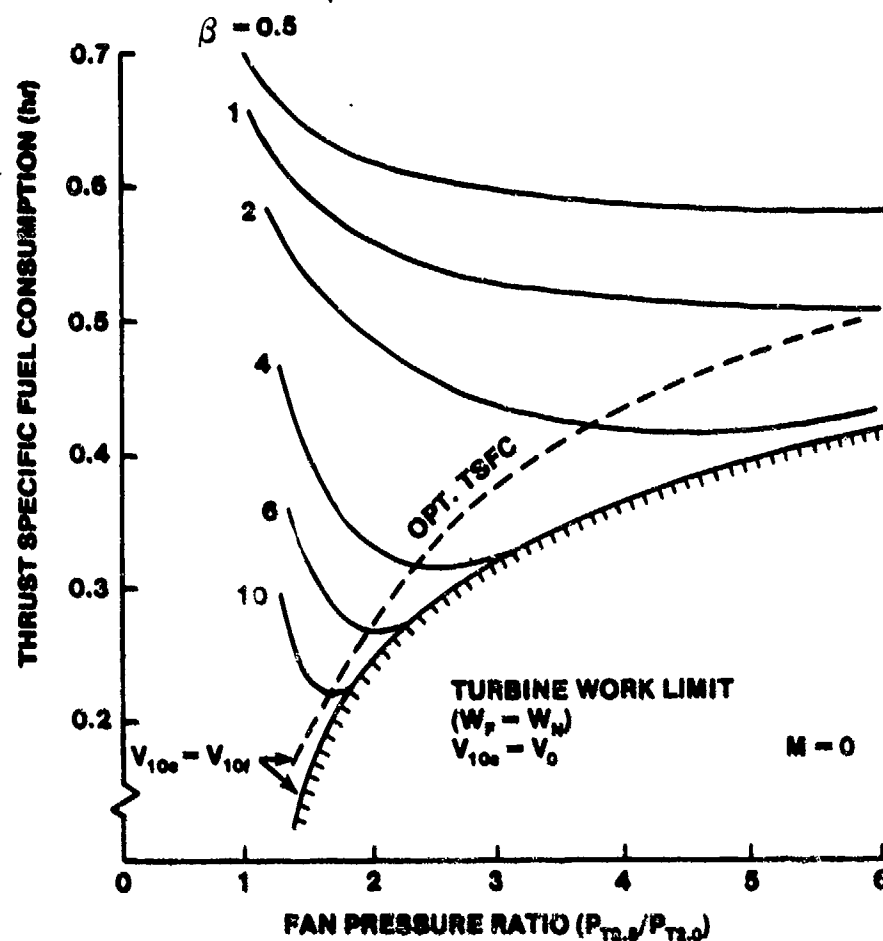


FIGURE 7.27. EFFECTS OF FAN STAGE DESIGN VARIABLES ON TSFC

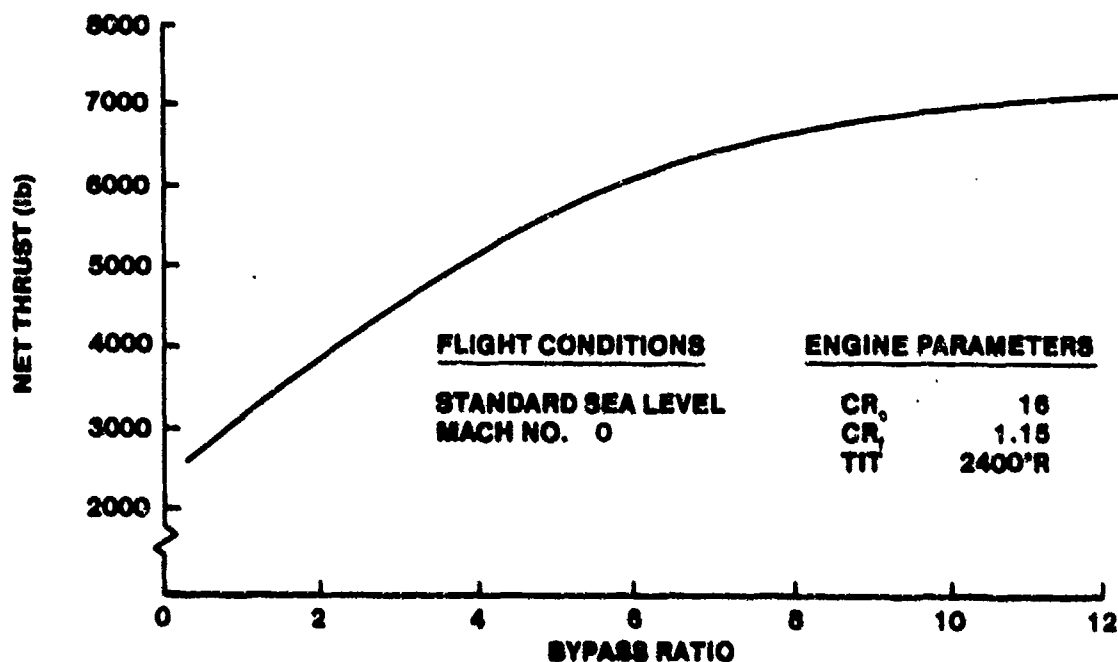
NOTE: EACH BYPASS RATIO HAS AN OPTIMUM FAN COMPRESSION RATIO. THE RATIO OF TSFC OF THE TURBOFAN ENGINE TO THE TURBOJET ENGINE IS

$$\frac{\text{TSFC}_{\text{TF}}}{\text{TSFC}_{\text{TJ}}} = \frac{1}{\sqrt{1 + \beta}}$$

WHERE THE OPTIMUM FAN COMPRESSION RATIO IS USED WITH β . FOR EXAMPLE, A BYPASS RATIO OF TWO WITH THE ASSOCIATED OPTIMUM FAN COMPRESSION RATIO (~ 4) WOULD CUT TSFC IN HALF.

The effect of bypass ratio on net thrust is shown in Figure 7.28. The curve shows that net thrust continues to increase with bypass ratio, but the relative increase becomes smaller for the higher ratios.

Core compression ratio also affects thrust and net TSFC as shown in Figures 7.29 and 7.30. TSFC improves with increasing core compression ratio, whereas there is an optimum core compression ratio required to optimize net thrust. These are the same trends displayed by the core engine.



NOTE:
FOR A SPECIFIC CORE ENGINE AND FAN COMPRESSION RATIO

FIGURE 7.28. NET THRUST IMPROVEMENTS WITH BYPASS RATIO

NOTE: FOR A SPECIFIC CORE ENGINE AND FAN COMPRESSION RATIO

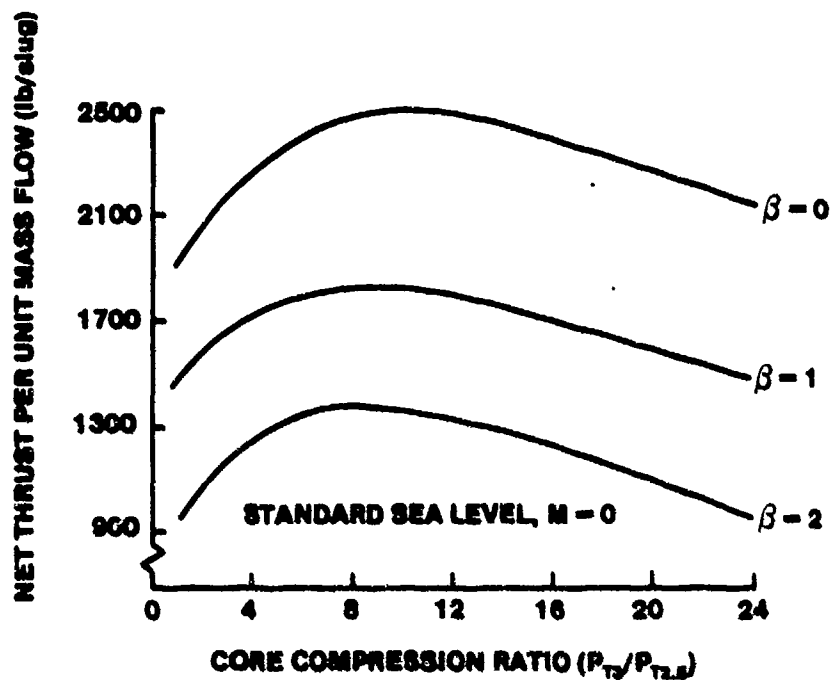


FIGURE 7.29. EFFECT OF CORE COMPRESSION RATIO ON NET THRUST FOR THE TURBOFAN ($TIT = 2400^{\circ}R$ AND $CR_F = 2$)

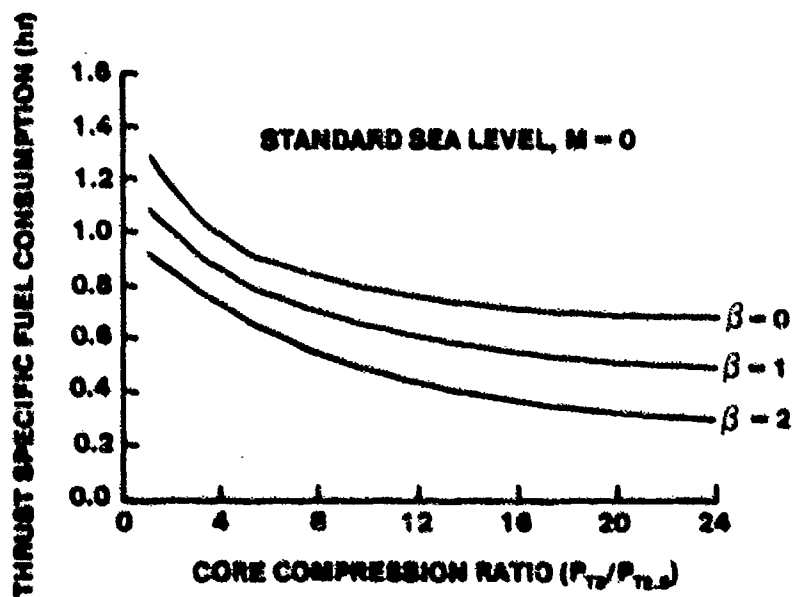


FIGURE 7.30. EFFECT OF CORE COMPRESSION RATIO ON TSFC FOR THE TURBOFAN ($TIT = 2400^{\circ}R$ AND $CR_F = 2$)

7.7.6.2 Variation In TSFC of a Turbofan With Mach. As Mach increases, the optimum (lowest) TSFC occurs at a progressively lower bypass ratio. This trend is shown in Figure 7.31. In addition, TSFC degrades with

increasing Mach. In designing an engine, the propulsion engineer optimizes the performance for the specific mission of the aircraft. For instance, a transport aircraft designed to cruise at Mach 0.8 might have a bypass ratio and fan compression ratio of two.

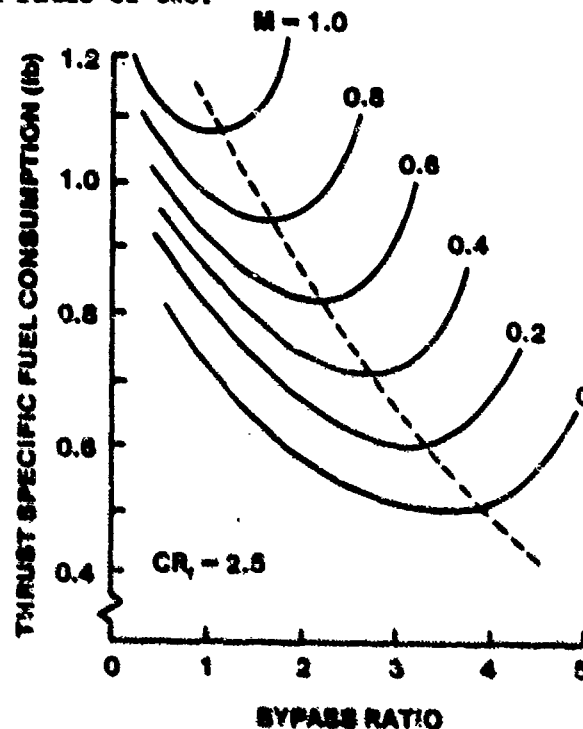


FIGURE 7.31. MACH EFFECTS FOR AN ACTUAL TURBOFAN ENGINE

A fighter type aircraft presents a more complex problem since the overall mission is divided into several phases, each requiring a different Mach/altitude combination. Two solutions are possible: (1) compromise engine, and (2) a variable cycle engine. Current production engines compromise overall performance while attempting to retain adequate performance in the most crucial phases of the mission.

7.7.6.3 The Variable Cycle Engine. The variable cycle engine is basically a variable bypass engine. The amount of bypass air is varied over a wide range and programmed so that the engine has the optimum bypass ratio for every flight speed. It also has the potential for substantially reducing installation losses in both the inlet and the nozzle.

Engine technology required to implement variable cycle engines includes (1) variable-pitch, variable-camber fans (similar in basic principle to the variable-pitch propeller but more complex), (2) variable-area turbine inlet nozzles, (3) variable-area convergent-divergent (C-D) exhaust nozzles, and (4) a propulsion control system capable of integrating all the variable-area components with a fuel control.

7.7.6.4 Ideal Turbofan Cycle Analysis. In this section we will construct the h-s diagram for a turbofan engine using the J-79 turbojet as the core. We will then calculate F_n and TSFC and compare these with our original values for the core engine. The specific flight conditions and core engine parameter will be the same as in Table 7.4. We will arbitrarily pick a bypass ratio of two and a fan compression ratio of three. The flight conditions and engine parameters are summarized in Table 7.7.

TABLE 7.7

FLIGHT CONDITIONS AND ENGINE PARAMETERS
FOR CONVERTED J-79 TURBOFAN ANALYSIS

FLIGHT CONDITIONS			CORE ENGINE			FAN ENGINE	
V_0	T_0	H_0	TIT_{MAX}	CR_C	\dot{w}_{ac}	ρ	CR_f
230K	40°F	16,000F	1810°F	13.5	170 lb/sec	2	3

The subscript "c" refers to core engine parameters, and "f," fan engine parameters.

SOLUTION

The solution to the problem is identical to the ideal turbojet engine analysis up to Step 7. The net energy output of the cycle was found to be 158 BTU/lb. Part of this energy will now be used to drive the fan, while the remainder will be expanded in the core engine nozzle to produce the core thrust. Continuing the analysis from Step 6 of the turbojet engine, we must next construct the h - s diagram for the fan section.

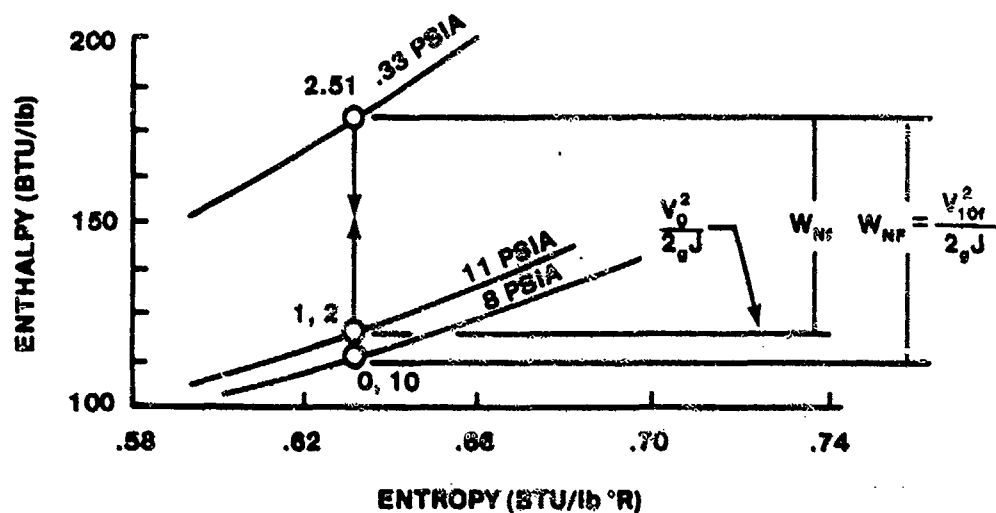


FIGURE 7.32. h-s DIAGRAM FOR THE FAN STAGE

STEP 7A: LOCATE FAN STATION ①

NOTES

Locate on h-s DIAGRAM

This step is identical with Step 1 for the turbojet because the free stream is identical.

$$P_0 = 8 \text{ PSIA}$$

$$T_0 = 500^\circ\text{R}$$

Read h and s directly

$$h_0 = 120 \text{ BTU/lb}$$

$$s_0 = 0.63 \text{ BTU/lb}^\circ\text{R}$$

STEP 8A: LOCATE FAN STATION ②

NOTES

$$h_{TIF} = h_{T2f} = h_0 + \frac{V_0^2}{2gJ}$$

$$= 120 + \frac{(1.69)(230)^2}{50,100}$$

$$= 123 \text{ BTU/lb}$$

Again this step is identical with Step 2 for the turbojet analysis because the fan and core inlets see the same free stream velocity.

$$s_1 = s_2 = s_0 = 0.63 \text{ BTU/lb}^\circ\text{R}$$

$$P_{T2} = 11 \text{ PSIA}$$

STEP 9A: LOCATE FAN STATION (3)

NOTES

$$P_{T2.5} = (CR_f) (P_{T2f})$$

This is the first step which differs.

$$\text{where } CR_f = \frac{P_{T3f}}{P_{T2f}}$$

$$P_{T2.5} = (3) (11)$$

$$= 33 \text{ PSIA}$$

Read h directly

$$h_{T2.5} = 175 \text{ BTU/lb}$$

$$s_{2.5} = s_{2f} = s_{1f} = s_{0f}$$

STEP 10A: LOCATE FAN STATION (10)

NOTES

$$P_{10f} = P_{0f} = 8 \text{ PSIA}$$

$$h_{10f} = h_0 = 120 \text{ BTU/lb}$$

$$s_{10f} = s_0$$

The high pressure gas is now expanded to the ambient pressure without any additional processing. The ideal fan section is isentropic; hence, the entropy does not change throughout the cycle.

STEP 11A: CALCULATE FAN EXIT VELOCITY

NOTES

$$V_{10f} = \sqrt{2gJ(h_{T3t} - h_{10f})}$$

$$= (50,100) (175-120)$$

$$V_{10f} = 1660 \text{ fps}$$

A duct burning fan would add heat energy at this point instead of expanding the flow. The analysis would then follow the turbojet cycle, but there would not be a turbine to drive.

STEP 12A: CALCULATE WORK THE CORE ENGINE
MUST SUPPLY TO DRIVE THE FAN

$$W_F = \dot{S}W_f = \dot{S}(h_{T3f} - h_{T2f})$$

$$= 2 (175 - 123)$$

$$W_F = 104 \text{ BTU/lb}_{\text{core}}$$

NOTES

This step is straightforward but requires some thought. The fan acts on an airflow equal to $\dot{S}\dot{W}_{ac}$.

Each pound of this air requires an amount of work equal to W_f . The total work required by the fan is thus $\dot{S}\dot{W}_{ac}W_f$. The core

engine supplies an amount of work equal to W_F per pound of core

airflow. The total work supplied by the core engine is then $\dot{S}\dot{W}_{ac}W_F$.

Since this must be equal to the work required by the fan,

$$\dot{S}\dot{W}_{ac}W_F = \dot{S}\dot{W}_{ac}W_f$$

$$\therefore W_F = \dot{S}W_f$$

STEP 13A: LOCATE STATION 5 OF CORE
ENGINE ON CORE h-s DIAGRAM

$$H_{T4.5} = H_{t4} - W_C$$

$$H_{T4.5} = 413$$

$$H_{T5} = H_{T4.5} - W_F$$

$$= 413 - 104$$

$$H_{T5} = 309 \text{ BTU/lb}$$

NOTES

The turbine which drives the core compressor is located between Stations 4.0 and 4.5. The turbine which drives the fan is located between Stations 4.5 and 5.0. Generally, the rotor speed of the core turbine is higher than the fan turbine. Why? (Think about blade tip Mach effects versus diameter.)

STEP 14A: CALCULATE CORE GAS EXIT VELOCITY

$$V_{10c} = \sqrt{2gJ (h_{T5} - h_{10})}$$

$$= \sqrt{(50,100) (309-255)}$$

$$V_{10c} = 1645 \text{ fps}$$

STEP 15A: CALCULATE F_n

$$F_n = \frac{\dot{w}_{ac}}{g} [(V_{10c} - V_0) + \beta (V_{10f} - V_0)]$$

$$= \frac{170}{32.2} [(1645-389) + 2(1660-389)]$$

$$F_n = 20,039 \text{ lb}$$

STEP 16A: CALCULATE TSFC

$$TSFC = \frac{\dot{w}_f}{F_n}$$

$$= \frac{9448}{20,039}$$

$$TSFC = 0.47$$

NOTES

The two exit velocities, V_{10f} and V_{10c} , are almost identical. This means TSFC and F_n are nearly optimized for the particular β chosen.

NOTES

Actually we have just combined the two thrust equations

$$F_{nc} = \frac{\dot{w}_{ac}}{g} (V_{10c} - V_0)$$

$$F_{nf} = \frac{\beta \dot{w}_{ac}}{g} (V_{10f} - V_0)$$

where

$$F_n = F_{nc} + F_{nf}$$

NOTES

Here lies the beauty of the turbofan. We have increased the net thrust at absolutely no penalty in fuel. No additional fuel is required because the bypass air is not heated. Who says you can't get something for nothing?!

7.7.7 Comparison of the Cycle Turbojet and Turbofan Ideal Cycle

ANALYSIS

The ideal cycle analysis results for the J-79 turbojet and J-79 turbofan are shown in Table 7.8.

TABLE 7.8

COMPARISON OF RESULTS

	J-79 TURBOJET	J-79 TURBOFAN	IMPROVEMENT
F_n (lbs)	12800	20,039	57%
TSFC $\left(\frac{\text{lbs-fuel}}{\text{lbs-thrust-hr}} \right)$	0.74	0.47	36%

You may ask, "If this much improvement can be made by just adding a fan stage, then why hasn't it been done?" It was . . . the CJ805-23A turbofan with $F_n = 16,000$ lb and TSFC - 0.53. But there are more problems associated with reconfiguring an old core engine (J-79 is 1956 vintage) than starting from scratch, which permits use of the latest technology in compressor and turbine design. When a turbojet aircraft is refitted with a turbofan, inlet compatibility becomes a serious problem. The inlet was designed for an airflow rate of w_a . The turbofan requires an airflow rate of $(\beta + 1) w_{ac}$. Since the inlet cannot be redesigned without major aircraft modifications in the case of fighter type aircraft, the retrofit is not generally practical. However, a retrofit would be practical for transport type aircraft that use engine pods.

7.7.8 Comparison of Turbojet and Turbofan Engines

The relative merits and disadvantages of the turbofan engine are summarized in Table 7.9.

TABLE 7.9

CHARACTERISTICS OF THE TURBOFAN ENGINE

CHARACTERISTIC	SIGNIFICANCE
ADVANTAGES OF TURBOFAN OVER TURBOJET	
Bypass air is not heated	Lower TSFC
Accelerates larger air mass at a lower velocity	Yields higher propulsive efficiency
More thrust at lower airspeed	Shorter takeoff roll <u>or</u> higher gross weight potential
Lower average exhaust velocity	Lower engine noise
DISADVANTAGES OF TURBOFAN OVER TURBOJET	
Addition of fan	More mechanical complexity <u>and</u> bigger FOD potential
Larger mass flow rate	Relight harder in flight
Fan tip losses	Lower airspeed limit

In summary, the turbofan engine is more efficient in producing thrust for a given amount of fuel. The gas generator (compressor-combustor-turbine) produces a specified energy output. The energy can be used in many ways, but the ultimate purpose is to produce thrust. The nozzle is a means of converting a high pressure flow into a high velocity thrust. However, nozzles are not as efficient as propellers at low flight velocities as the propeller is a momentum transfer device. These trends are shown in Figure 7.33. Note that the turboprop engine is the most efficient at low velocities.

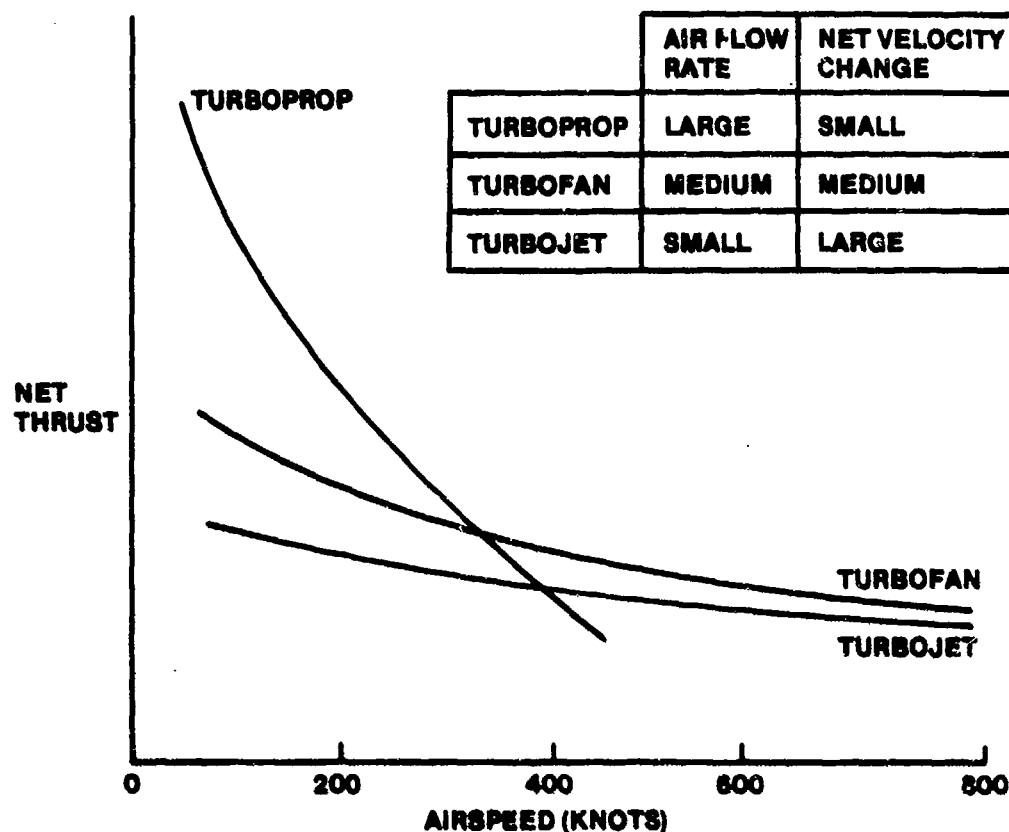


FIGURE 7.33. COMPARISON OF NET THRUST VERSUS AIRSPEED FOR THE TURBOPROP, TURBOFAN, AND TURBOJET ENGINE

In most present day applications, the overall characteristics of the turbofan engine are superior to the turbojet. The biggest advantage of the turbofan, of course, is significantly more net thrust output at a lower TSFC. However, in some applications such as Mach 2 to 3 cruise, the turbojet is still employed. Sometimes the relative merits of each are about the same. The F-16 uses a turbofan engine while the YF-17 used two turbojet engines even though both aircraft were designed for identical missions!

7.8 ENGINE COMPONENTS

The physical features, functions, and performance of the major components included in the various types of gas turbine engines will be discussed in the order of their location, front to rear, on the engine.

7.8.1 Air Inlet Duct

The engine inlet and the inlet ducting serve the function of a diffuser and furnish a relatively distortion-free, high-energy supply of air, in the required quantity, to the face of the compressor. A uniform and steady airflow is necessary to avoid compressor stall and excessive internal engine temperatures at the turbine. The high energy enables the engine to produce an optimum amount of thrust. Normally, the air inlet duct is considered an airframe part, and not a part of the engine. However, the duct itself is so important to engine performance that it must be considered in any discussion of the complete engine.

A gas turbine engine consumes six to ten times as much air per hour as a reciprocating engine of equivalent size. The air entrance passage is correspondingly larger. Furthermore, it is more critical than a reciprocating-engine air scoop in determining engine and aircraft performance, especially at high airspeeds. Inefficiencies of the duct result in successively magnified losses through other components of the engine. The inlet duct, or diffuser, has two engine functions and one aircraft function. First, it must be able to recover as much of the total pressure of the free airstream as possible and deliver this pressure to the front of the engine with a minimum loss of pressure or differential. This recovery is known as "ram recovery" or, sometimes, as "total pressure recovery." Secondly, the duct must uniformly deliver air to the compressor inlet with as little turbulence and pressure variation as possible. As far as the aircraft is concerned, the duct must hold the drag effect it creates to a minimum.

Pressure drop or differential is caused by the friction of the air along the sides of the duct and by the bends in the duct system. Smooth flow depends upon keeping the amount of turbulence as the air enters the duct to a minimum. The duct must have a sufficiently straight section to ensure smooth, even airflow within. The choice of configuration of the entrance to the duct is dictated by the location of the engine within the aircraft and the airspeed, altitude, and attitude at which the aircraft is designed to operate. A detailed discussion of the diffuser will help in understanding how the above design requirements can be met.

7.8.2 Diffuser

In the aeronautical sense of the word, a diffuser is a device which reduces the velocity and increases the static pressure of a fluid, such as a gas or air passing through a gas turbine engine. A diffuser operates on the principle of physics stated by Bernoulli's theorem which says that at any point in a fluid stream tube, the sum of the pressure energy, the potential energy, and the kinetic energy is a constant; that is, if one of the energy factors in a gas flow changes, one or both of the other variables must also change in order that the total energy may remain constant. Specifically, if velocity decreases, the pressure increases.

The primary purpose of the jet propulsion engine diffuser is to increase the static pressure of the free stream fluid. This function is accomplished by converting the available kinetic energy of the free stream air into a pressure rise. The basic function of a diffuser is exactly the same as the function of a mechanical compressor; thus, anything that can be done to improve the diffuser performance will benefit an engine's overall performance in the same way as an improvement in mechanical compressor design will benefit the overall engine performance. Since modern jet propulsion engines are operated, for the most part, at subsonic flight velocities, consider first the subsonic diffuser.

7.8.2.1 Subsonic Diffuser. Figure 7.34 illustrates schematically a subsonic diffuser with a simple inlet that is operating in an airstream of velocity V_0 .

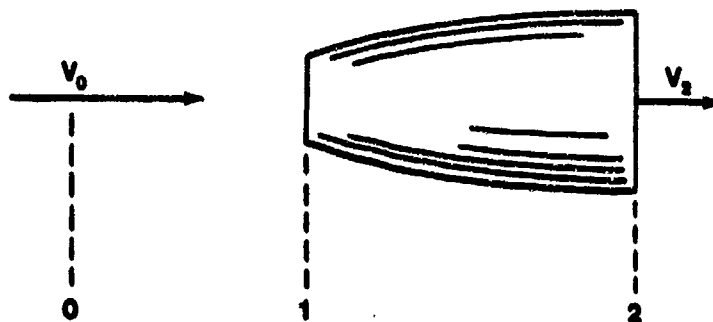


FIGURE 7.34. SUBSONIC DIFFUSER

Since the diffuser is designed to transform kinetic energy into a pressure rise, it is necessary to evaluate the total energy in the free stream

and express it in terms of the total pressure that might be available for an ideal diffuser. The total-to-static temperature ratio can be expressed in terms of the flight Mach, as was done before and then the isentropic pressure-temperature relation can be applied to give the following expression for total-to-static pressure ratio

$$\frac{T_{T0}}{T_0} = 1 + \frac{\gamma-1}{2} M_0^2 \quad (7.44)$$

$$\frac{P_{T0}}{P_0} = \left[1 + \frac{\gamma-1}{2} M_0^2 \right]^{\frac{\gamma}{\gamma-1}} \quad (7.45)$$

The total pressure in Equation 7.45 is the maximum available pressure energy that can be derived from the free stream Mach, M_0 . It is the job of the diffuser to slow down the fluid so as to increase the static pressure at Station 2; however, it is still necessary to try to achieve high static pressures at the diffuser exit, and if we have an ideal diffuser, the total pressure at the diffuser exit will be equal to the total pressure in the free stream. This obviously cannot be achieved in practice because every diffuser has certain losses, primarily due to the friction that exists between the fluid and the diffuser walls. Figure 7.35 illustrates the diffuser process on a T-s plane and shows the relative pressure rise accomplished by an ideal and an actual diffuser.

In Figure 7.35, the free stream condition corresponds to Point 0. An ideal diffuser will accomplish isentropic compression to Point 2'. The actual diffuser, which has losses and therefore causes an increase in entropy, will follow a curved path from 0 to 2. The total temperature for the ideal and actual diffuser will, of course, be the same because we are assuming an adiabatic flow process (See Equation 7.44). From this diagram it is readily apparent that the total pressure in the ideal process is greater than the total pressure for the actual process, and the total energy and temperature in both processes are exactly the same for the adiabatic assumption. In the actual process, some of the available pressure energy goes into friction, which appears as heat, bringing the total temperature back to the value achieved by isentropic compression.

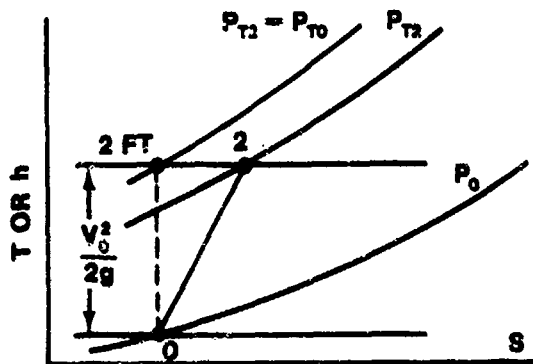


FIGURE 7.35. DIFFUSER PROCESS ON A T-s PLANE

The losses in the diffuser are usually accounted for by an efficiency factor. In these notes the total pressure recovery factor is defined as

$$\eta_r = \frac{P_{T2}}{P_{T0}} = \frac{P_{T2}}{P_T} \frac{P_0}{P_0} \quad (7.46)$$

where P_{T0} is the ideal free stream total pressure. This equation can be expressed in terms of a flight Mach by the use of Equation 7.45 to give

$$\frac{P_{T2}}{P_0} = \eta_r \left[1 + \frac{\gamma - 1}{2} M_0^2 \right]^{\frac{\gamma}{\gamma - 1}} \quad (7.47)$$

Figure 7.36 presents graphically the solution of Equations 7.44 and 7.47, allowing direct determination of the pressure and temperature ratios across a diffuser for a given η_r and Mach.

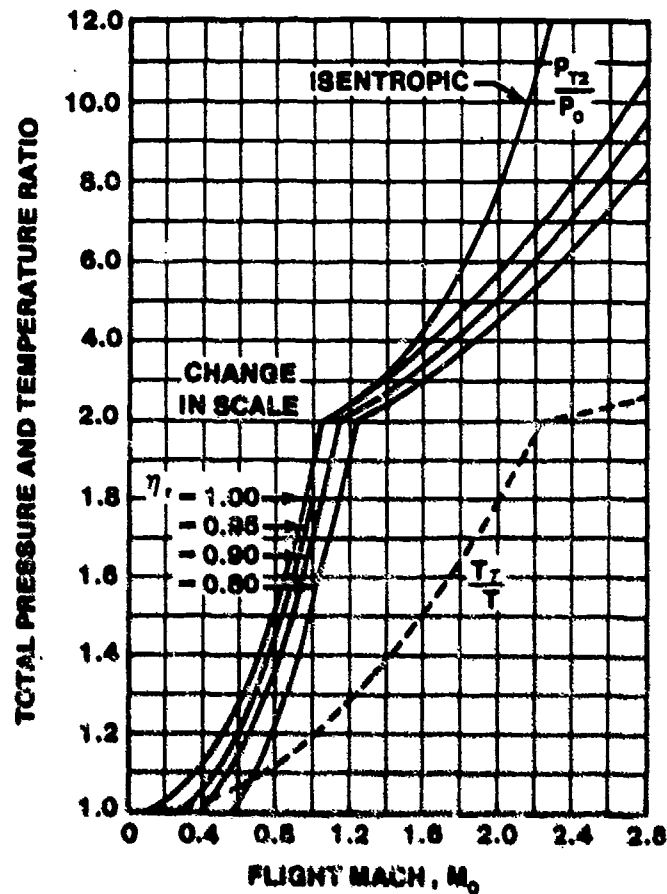


FIGURE 7.36. VARIATION OF TOTAL PRESSURE RATIO AND TOTAL TEMPERATURE RATIO FOR VARIOUS VALUES OF DIFFUSER RECOVERY FACTORS ASSUMING A NORMAL SHOCK FOR MACH GREATER THAN ONE.

For subsonic diffusers, consider only Mach less than one. It is readily apparent that the maximum pressure rise occurs when $\eta_p = 1$. Note that one curve applies to the total temperature ratio across a diffuser. This relationship is true because the total temperature, which is representative of total energy, is independent of the amount of friction in a process. Figure 7.36 is very useful for finding the total pressure at a diffuser exit when the flight Mach and diffuser ram recovery factor are known.

Example

A turbojet engine is operated at a flight Mach of 0.6 at standard sea level conditions. If the diffuser ram recovery factor is 0.90, what is the total pressure and temperature at the diffuser exit?

Solution

From Figure 7.36 for $\eta_r = 0.90$, read

$$\frac{P_T}{P} = 1.148 \quad \text{and} \quad \frac{T_T}{T} = 1.072$$

Thus $P_{T2} = 1.148 \times 14.7 = 16.9 \text{ PSIA}$

and $T_{T2} = 1.072 \times 520 = 557^\circ\text{R}$

7.8.2.2 Subsonic Duct Losses. The fundamental causes of pressure losses in subsonic duct components are skin friction and flow separation. Skin friction is present in all flows and is the primary contributor to pressure losses in straight, constant area ducts. Flow separation losses can be much larger, however, and major effort in subsonic duct design is directed to minimizing such losses. Flow separation tends to occur when forces arise in the stream which oppose the direction of flow (adverse pressure gradient). The pressure rise in a diffuser due to the flow deceleration causes an adverse pressure gradient. Bends in the duct also produce forces that tend to separate the flow from the inner surface of the bend. The total pressure recovery for a subsonic duct is determined by analyzing the duct for each of these areas of pressure loss.

7.8.2.3 Supersonic Diffusers. Jet propulsion devices designed to operate at supersonic Mach present an even more complex problem for the inlet designer. At these high flight speeds the available total pressure is higher, but the drag associated with the diffuser can become prohibitive. Couple these two factors with the necessity to operate well down into the subsonic flight regime for landing and it becomes difficult to fulfill the design objectives of high total pressure recovery and minimal ram drag over such a

wide range of flight conditions. One method of classifying these complex diffusers is by geometry. The two basic geometric shapes are: two-dimensional and three-dimensional. Figure 7.37 shows two types of two-dimensional inlets.

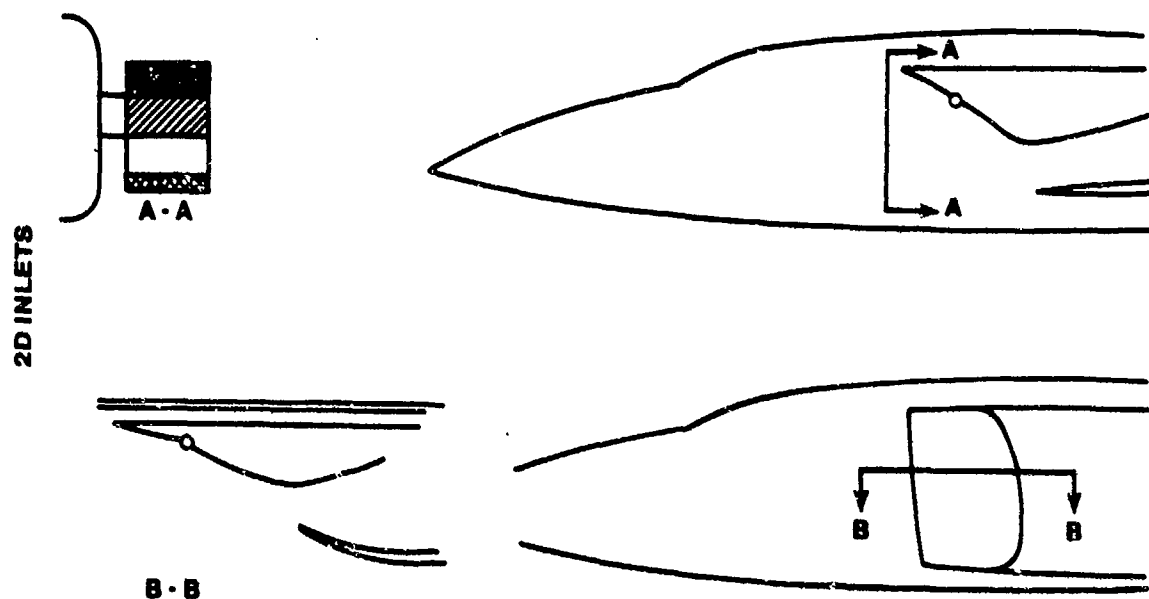


FIGURE 7.37. TWO-DIMENSIONAL INLETS

The axisymmetrical inlet of the Lightning, illustrated in Figure 7.38, is typical of the three-dimensional supersonic inlet.

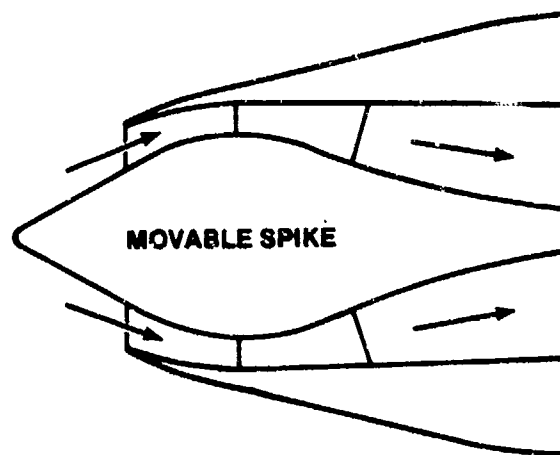


FIGURE 7.38. AXISYMMETRIC INLET

Another, and perhaps more useful, means of classifying supersonic inlets is according to how the compression takes place. Basically, there are three types of inlets under this scheme of classification: (1) normal shock inlets, (2) internal compression inlets, and (3) external compression inlets. However, mixed compression inlets, that combine internal and external compression, appear to be the most attractive design for most supersonic applications of the future.

7.8.2.3.1 Normal Shock Inlets. The normal shock inlet is very similar to the subsonic diffuser of Paragraph 7.8.2.1. The chief differences are that it operates in a supersonic flow region and the lips are usually somewhat sharper than those of a subsonic inlet. But it is simply a diverging duct, as shown in Figure 7.39 operating in supersonic conditions. In this figure, there are two distinct effects of compression: (1) the static pressure rise across the normal shock, and (2) the diffusion process which follows the normal shock.

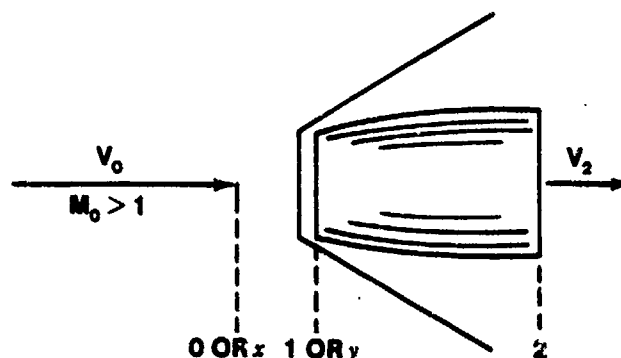


FIGURE 7.39. SUBSONIC DIFFUSER OPERATING IN A SUPERSONIC STREAM.

It can be shown that the Mach after a normal shock, M_y , is always subsonic; therefore, the process from y to 2 is merely a duplication of the subsonic diffuser which has already been discussed. The pressure ratio across the normal shock can be found in any normal shock tables.

For supersonic flow in a simple diffuser, the curve for $\eta_r = 1$ is the maximum possible pressure ratio that can be achieved with a normal shock at a diffuser entrance and isentropic compression inside the diffuser after the normal shock.

Even if $\eta_r = 1$, however, the total pressure loss through the normal shock becomes prohibitive for $M_0 > 1.5$. Figure 7.40 illustrates the total pressure recovery through a normal shock (with $\eta_r = 1$) as a percentage of the total pressure recovery expressed by Equation 7.45. At $M_0 = 1.5$, the total pressure recovery is 93%, whereas the total pressure recovery is 72% at $M_0 = 2$. Because of this loss in total pressure recovery, the normal shock diffuser is not used for aircraft designed to fly in excess of $M_0 = 1.5$.

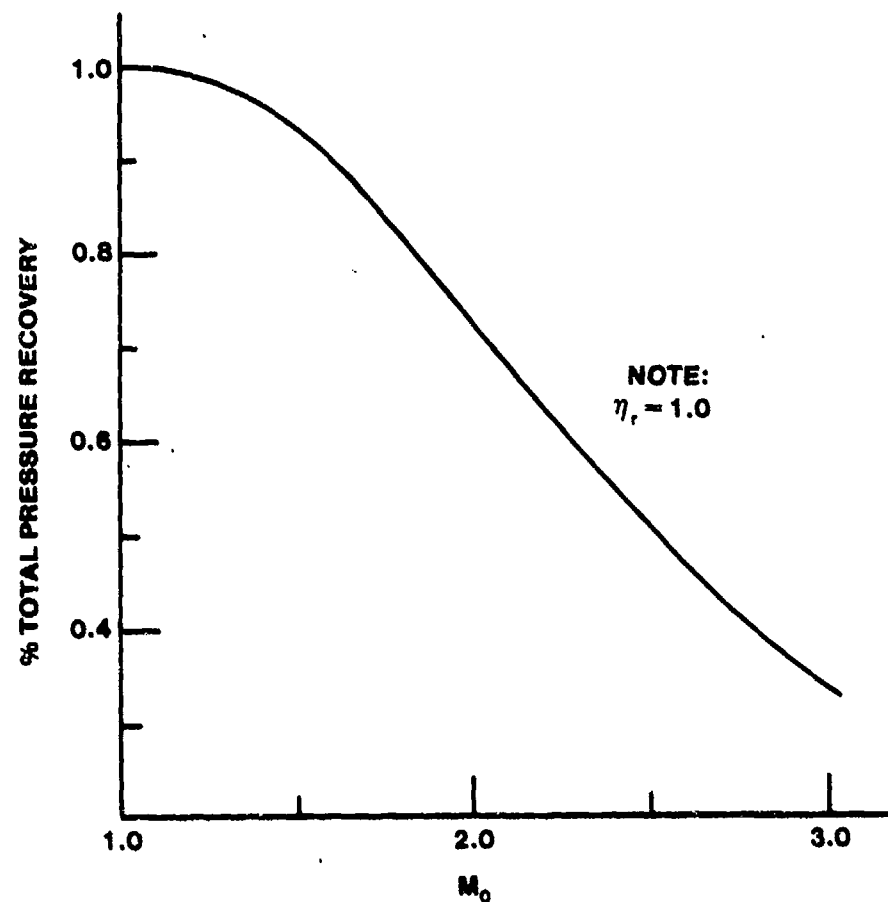


FIGURE 7.40. TOTAL PRESSURE LOSS IN NORMAL SHOCK INLET

The performance of the normal shock inlet deteriorates rapidly when operated at off-design conditions. If more air is required by the engine than the inlet is delivering, the flow adjustment must take place within the inlet, since pressure signals cannot move upstream of the normal shock wave. The normal shock wave is "swallowed" as shown in Figure 7.41 to make this flow adjustment.

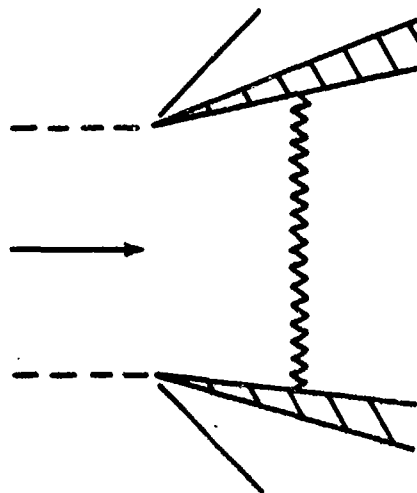


FIGURE 7.41. NORMAL SHOCK INLET WITH SWALLOWED SHOCK

In this case, though, the flow is accelerated in the diverging duct, and the total pressure recovery is reduced because of the stronger shock wave. On the other hand, if the engine requires less air than the inlet is delivering, the flow adjustment is made by a repositioning of the shock forward of the inlet lip as shown in Figure 7.42. The total pressure recovery remains high, but air is compressed by the shock wave and spilled around the inlet. This spillage causes additional drag and therefore degrades the overall engine-inlet performance. These disadvantages, along with other less important ones, force the inlet designer to look for alternatives to the normal shock inlet.

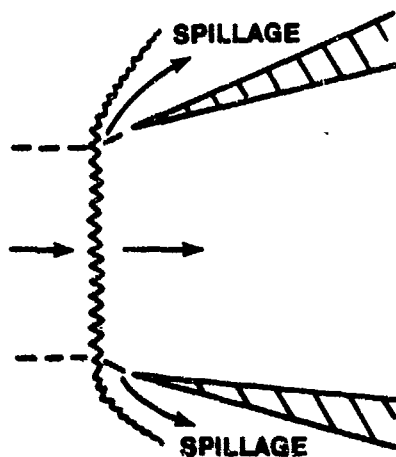


FIGURE 7.42. NORMAL SHOCK INLET WITH
EXPULSED SHOCK

7.8.2.3.2 Internal Compression Inlets. Figure 7.43 shows three ways inlet designers have approached the problem. In this section, the internal contraction or internal compression inlet will be discussed. This type of diffuser is in essence a reversed supersonic nozzle. The convergent section up to the throat slows the supersonic flow to sonic velocity (ideally) and then further slows the flow in the diverging section. Theoretically, this type of inlet would provide very high total pressure recovery when operating at its design Mach because the compression would occur without shock waves. At off-design conditions, even this idealized inlet would suffer serious losses. If the free stream Mach is greater than design Mach, for example, a strong shock wave could develop in the divergent section downstream of the throat, giving high total pressure losses. Conversely, a strong shock wave could develop in the converging section upstream of the throat. This shock wave could easily be expelled, resulting in high ram drag.

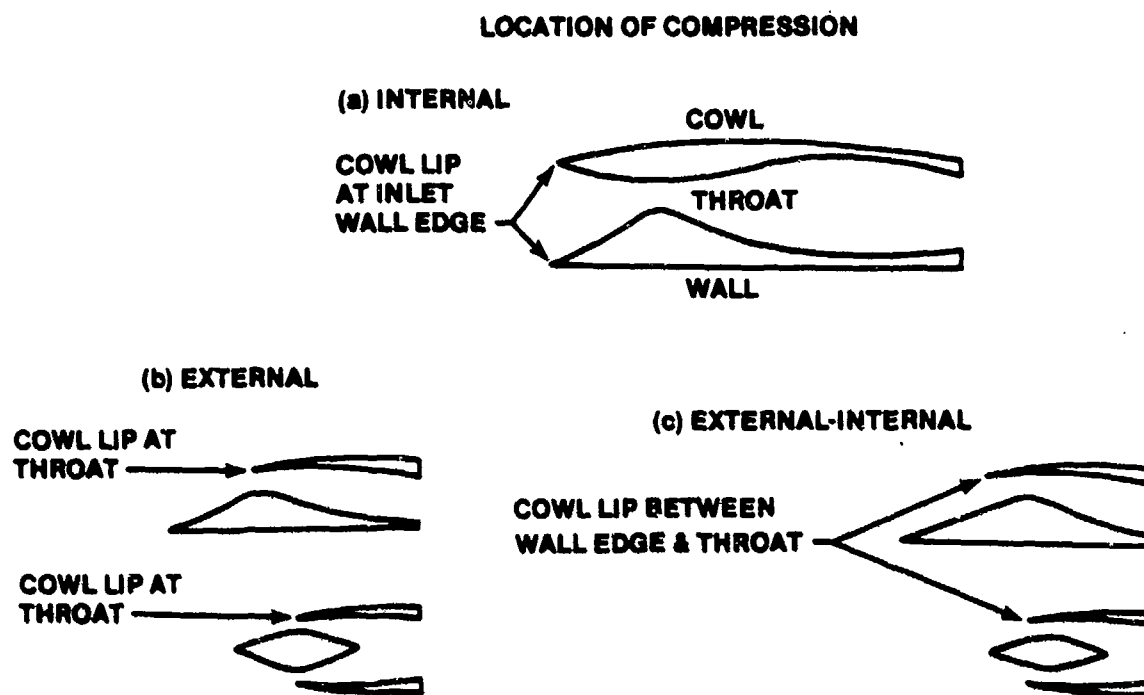


FIGURE 7.43. TYPES OF SUPERSONIC INLETS (REFERENCE)

From a practical viewpoint, the internal compression inlet has several other disadvantages. The boundary layer in such an inlet is very difficult to predict since an adverse pressure gradient exists along the length of the duct. The boundary layer thickness alters the flow area and directly affects performance of the inlet. Another problem is "starting" such an inlet. If the inlet is accelerated from subsonic speeds (as in an aircraft), the converging section will accelerate the flow. Choked flow will exist with a normal shock ahead of the throat until the design Mach is reached or exceeded, when the normal shock will be swallowed and thus disappear. The losses through this normal shock are not acceptable for an aircraft, generally, and could even prevent the vehicle from reaching the design Mach. Figure 7.44 shows one answer to the starting problem - variable geometry.

DESIGN ELEMENTS OF SUPERSONIC INLETS
INLET CROSS-SECTION

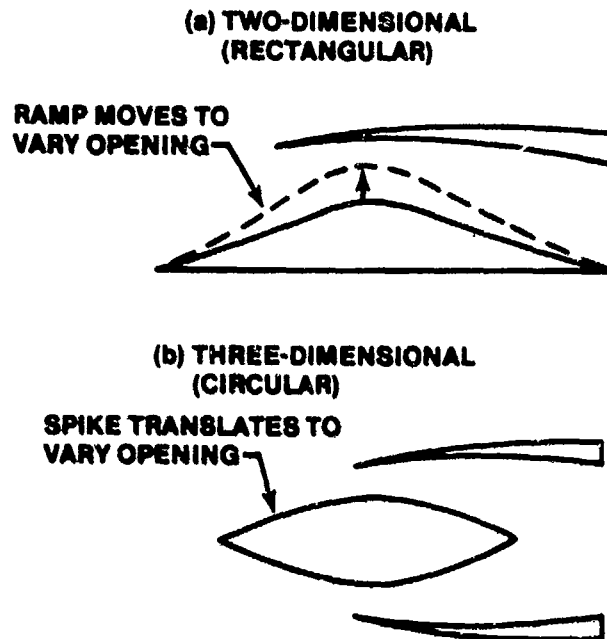


FIGURE 7.44. TWO CONCEPTS ILLUSTRATING
VARIABLE GEOMETRY

At flight velocities lower than the design Mach, the throat is enlarged for less flow restriction. As Mach is increased, the throat area is decreased, thereby allowing the inlet to function shock-free over a range of Mach.

7.8.2.3.3 External Compression Inlets. The problems of the internal compression inlet are such that a better solution was sought. Such aircraft as the F8U, the F-104, and the B-58 use an inlet similar to those labelled "external compression" in Figure 7.43b. At the design operating conditions, the oblique shock wave generated by the leading edge of the compression surface (Figure 7.45) should intersect the cowl lip. The flow is slowed due to passing through the oblique shock wave and the turning of the flow to parallel the compression surface. At the cowl lip (where minimum area also occurs), a normal shock wave slows the flow to a subsonic Mach, after which it is slowed still further in the duct delivery to the compressor face.

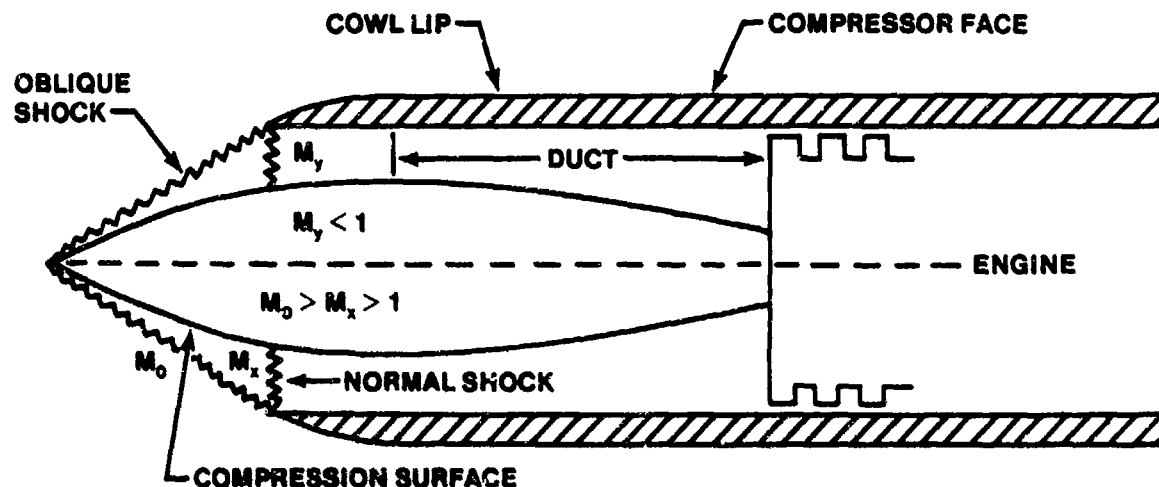


FIGURE 7.45. EXTERNAL COMPRESSION INLET
AT DESIGN CONDITIONS

A shock wave system utilizing two shock waves, one oblique and one normal, recovers significantly more total pressure than the single normal shock for free stream Mach greater than 1.5. Further, such an inlet avoids the starting problem since the normal wave is forward of the cowl lip for $M_0 \leq M_{DES}$. However, this type of inlet also suffers a deterioration in performance at off-design flight conditions. Furthermore, the total pressure recovery can be increased still further by increasing the number of oblique shocks.

7.8.2.3.4 Mixed Compression Inlets. Typical examples of two-shock, three-shock, and multiple shock compression schemes are shown in Figure 7.46. The inlets utilizing a pattern of three or more shocks are frequently called mixed compression or external-internal contraction inlets. (See Figure 7.43c). These inlets capitalize on the better total pressure recovery ratios available with oblique shock waves. Figure 7.47 graphically illustrates the improvement in total pressure recovery from mixed compression inlets.

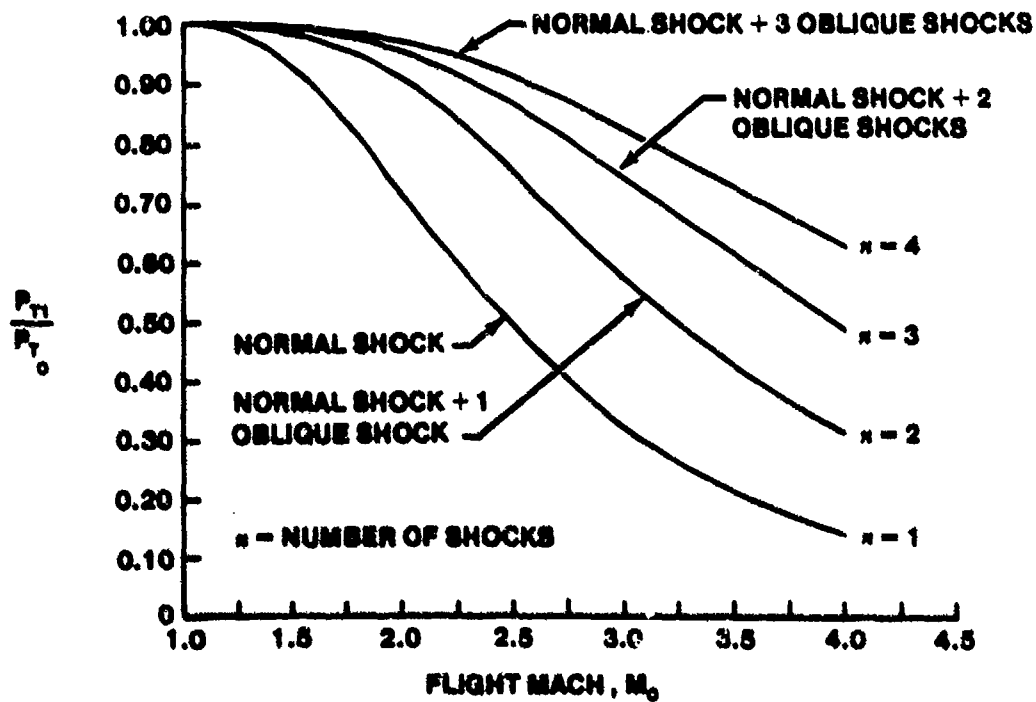
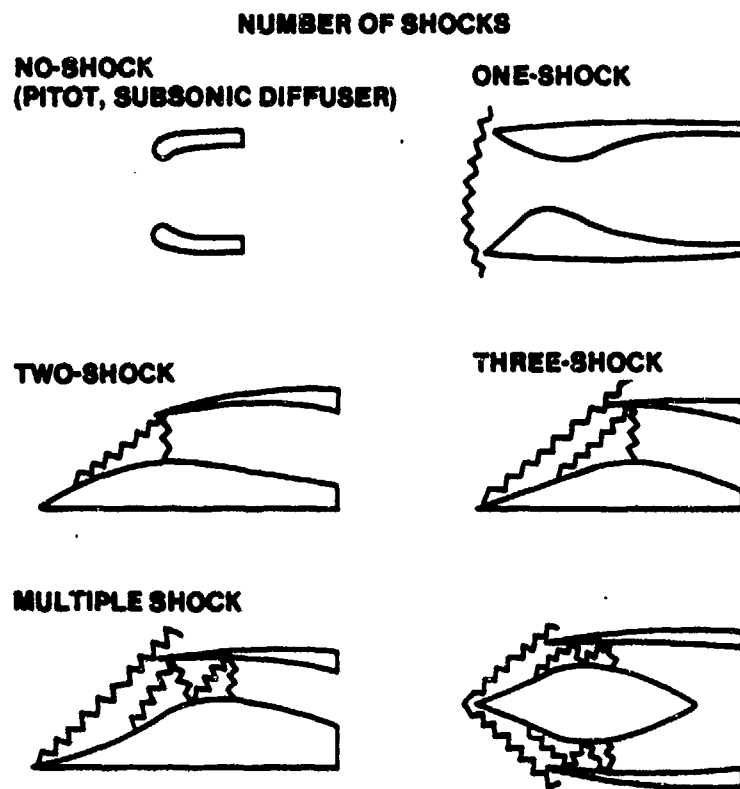


FIGURE 7.47. EFFECT OF NUMBER OF SHOCKS ON TOTAL PRESSURE RECOVERY

However, mixed compression inlets are susceptible to starting difficulties and may expell the normal shock (or "unstart") if the inlet is operated too far from the design conditions. Consequently, variable geometry is frequently used with mixed compression inlets. Mixed compression inlets can also be susceptible to inlet buzz or other forms of instability.

7.8.2.4 Mass Flow. The criterion of diffuser performance discussed thus far has dealt solely with the ram recovery factor. This factor is important, but does not, in itself, dictate the overall performance of a diffuser. In addition to having a high ram recovery, a good diffuser must have air-handling characteristics which are matched with the engine, as well as low drag and good flow stability. For example, if a given installation had an η_r value of 0.95 for the air which it handled but supplied only 80% of the air required by the engine, it would not be a good diffuser. The importance of the airflow matching characteristics can be shown from the area considerations of Figure 7.48 which is a sketch of a typical subsonic diffuser and a typical ramp-type supersonic diffuser.

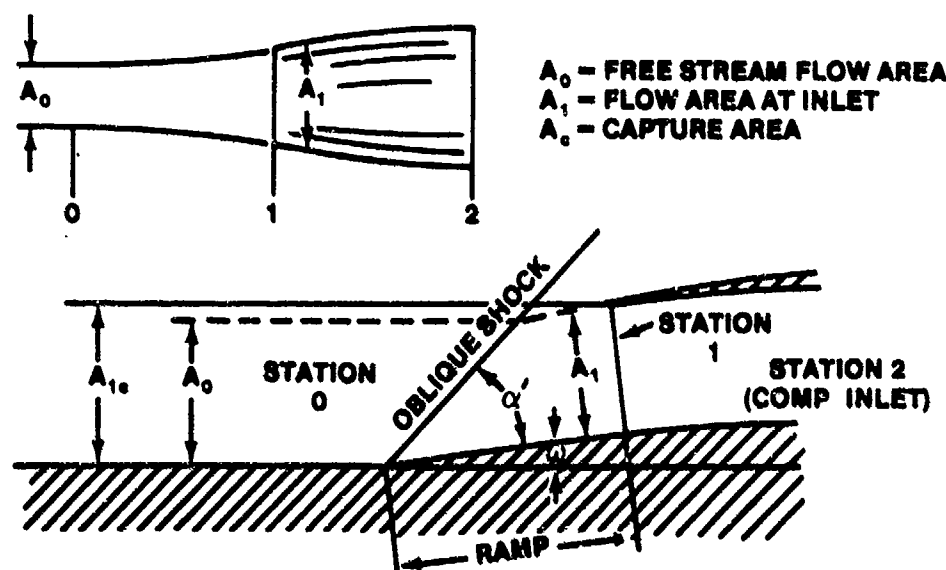


FIGURE 7.48 TYPICAL SUBSONIC AND SUPERSONIC DIFFUSERS

If an inlet were designed for $M_0 = M_2$, there would be no requirement for A_0 to be different than A_2 . However, most of the time the subsonic inlet will be operating with M_0 greater than M_2 . M_2 is a function of compressor rpm and

inlet geometry, and the compressor will usually demand airflow at .3 to .4 Mach. By use of the Area Ratio relation found in shock tables, Equation 7.48, which was derived in Supersonic Aero, one is able to relate inlet Mach to inlet areas.

$$\frac{A_X}{A_Y} = f(M_Y/M_X) \quad (7.48)$$

For a typical fixed geometry, subsonic diffuser operating on design at $M_0 = 0.8$ and $M_2 = 0.3$, the inlet would be like that shown in Figure 7.49.

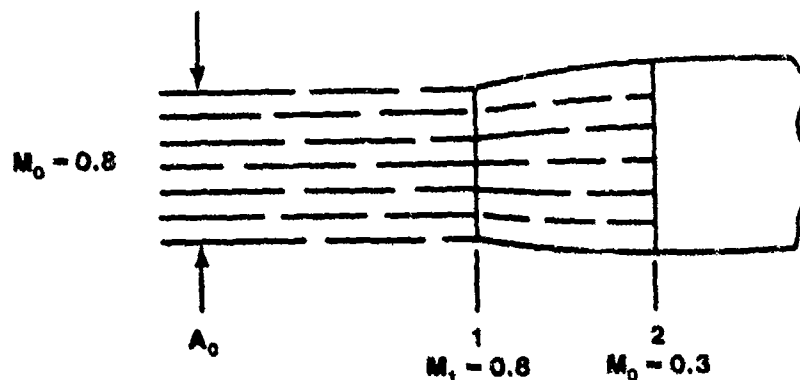


FIGURE 7.49. SUBSONIC DIFFUSER OPERATING ON DESIGN

For the given design conditions, $A_0 = A_1$ and $A_2/A_1 = 1.961$.

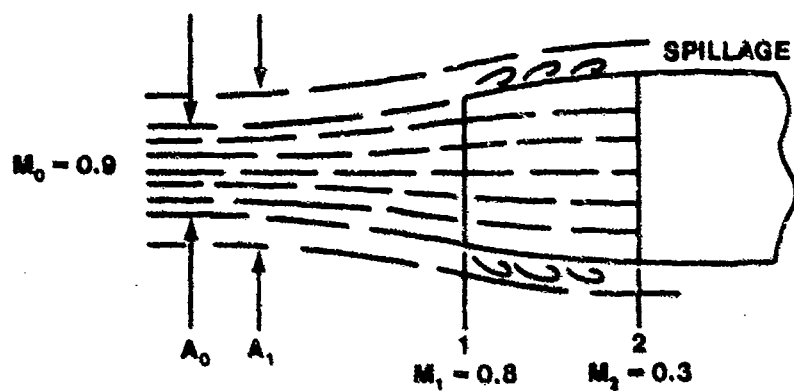
Once the area ratio of a subsonic inlet is determined for a specific design condition, the inlet contours are usually fixed, and there will exist numerous flight/engine conditions during which the inlet is operating "off-design." These off-design conditions, $A_1/A_0 \neq 1$, may affect the aircraft and/or engine performance.

For the fixed geometry subsonic inlet, the engine RPM will dictate the Mach that will exist at both compressor face and inlet entrance as long as $M_0 < 1.0$. For an inlet operating at a flight Mach greater than design, $A_1 > A_0$, spillage will occur and the drag increase. This off-design condition is shown in Figure 7.50a. The spillage and external flow separation will seldom affect engine operation but will adversely affect aircraft performance due to the increased drag.

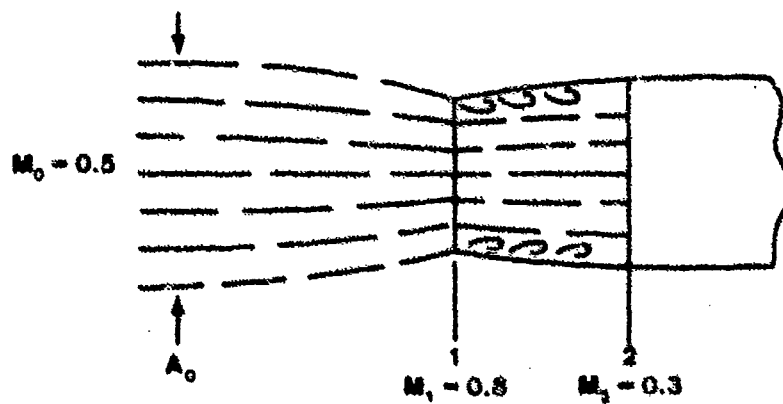
If the inlet is operating off-design with the flight Mach less than design, Figure 7.50b, the engine will have to "suck in" the air. This may result in internal flow separation and can result in flow distortion at the compressor face and low pressure recovery. Distortion can cause compressor stall. The internal flow separation may become critical during the takeoff phase when the aircraft is rotated. One solution for this off design condition, Figure 7.50c, is the installation of auxiliary inlet doors, "sucker doors," near the inlet entrance to effectively increase A_1 . The doors may be mechanically actuated but are usually opened automatically by the static pressure imbalance.

For a given set of operating flight conditions, the airflow requirements are fixed by the pumping characteristics of the engine, Figure 7.51. For the subsonic diffuser, if A_1 is too small to handle the air, the engine must "suck in" the lacking amount of air, resulting in a decreased ram recovery. If A_1 is too large, the diffuser will supply more air than the engine can use, resulting in excess drag because the excess air must be bypassed around the engine or "spilled" back out of the inlet. Too much air or too little air is detrimental to diffuser performance.

a. OFF DESIGN OPERATION $M_0 > M_c$ DESIGN



b. OFF DESIGN OPERATION $M_0 < M_c$ DESIGN



c. BLOW-IN DOOR OPERATION $M_0 < M_c$ DESIGN

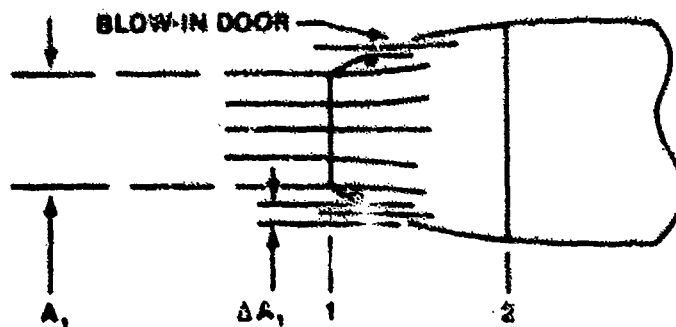


FIGURE 7.50

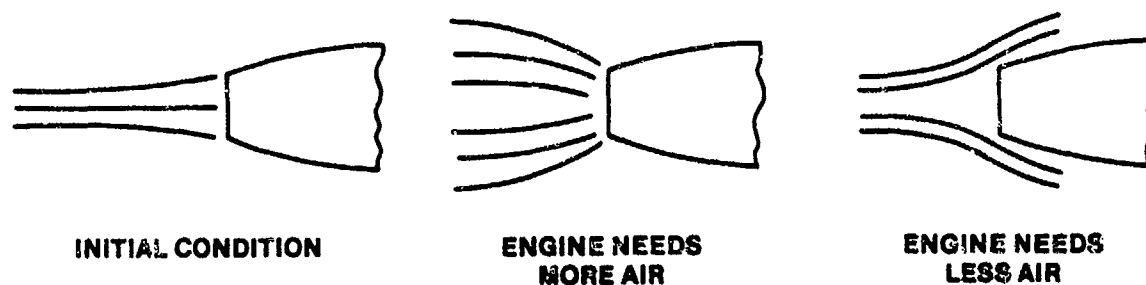


FIGURE 7.51. SUBSONIC DIFFUSER WITH SEVERAL DEMANDS FOR INLET AIR

In supersonic flow, when oblique shocks are formed, the condition is more serious because the "pressure signals" from the engine, which are sent to advise the free stream to give more or less air, cannot get to the free stream, or even to the inlet section, since supersonic velocities exist within the inlet. Consider an operating condition as shown in Figure 7.52.

Let us examine qualitatively what happens to the inlet flow characteristics when the engine demands a change in mass flow rate. If the engine demands more air than shown in the stabilized condition of Figure 7.52, it will decrease the pressure behind the normal shock and actually make that portion of the diffuser behind the normal shock act as an expanding supersonic nozzle. More shocks will occur with a consequent loss of total and static pressure. If the engine demands less air, the pressure behind the normal

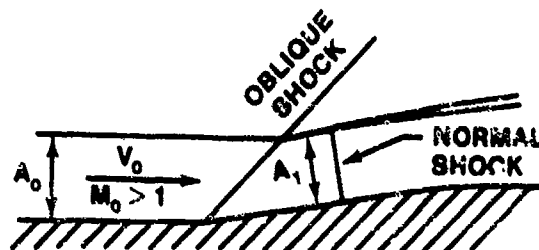


FIGURE 7.52. SUPERSONIC RAMP-TYPE DIFFUSER

shock will increase and become greater than the normal shock can support for the given M_1 . Therefore, the normal shock will move forward ahead of the inlet. The problem with the inlet operating under this condition is the attendant spillage and the possibility of distortion and inlet flow unsteadiness (buzz). This results because a portion of the air entering the engine has gone through an oblique shock, and a portion through a normal shock. This produces a shear layer (distortion) as shown in Figure 7.53.

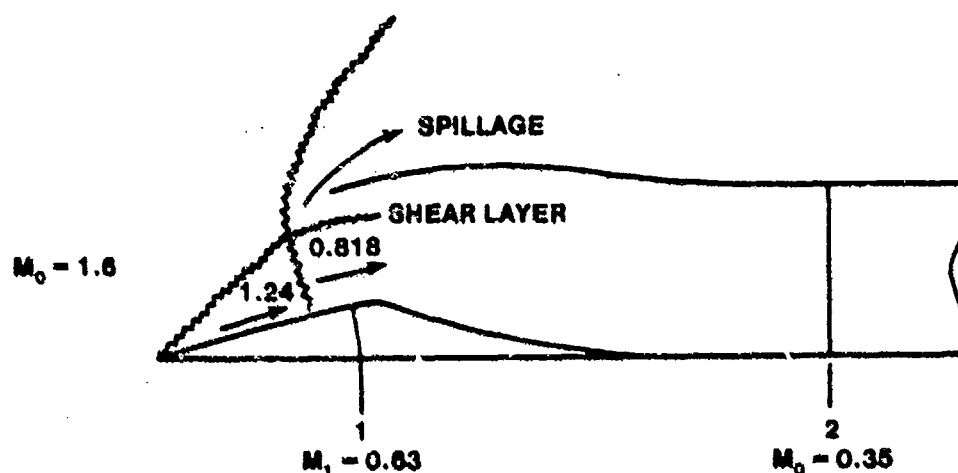


FIGURE 7.53. MULTIPLE SHOCK INLET - OFF-DESIGN

Because of the significant increase in drag due to spillage and adverse engine and inlet operation due to the distortion, the shock should be attached to the inlet lip or slightly swallowed to provide efficient and stable inlet and engine operation. The normal shock can be moved to the inlet lip by one or a combination of means. If bleed doors are opened downstream of the inlet entrance but prior to the compressor, the total airflow through A_1 will increase. The bleed doors have to be scheduled as a function of both free stream and compressor Mach to maintain ideal operating conditions. Another means used to attach the shock is to increase M_1 by decreasing A_1 in order to match the area to subsonic Mach after the normal shock. This could be accomplished by increasing the ramp angle, decreasing A_1 as shown by the dashed line on Figure 7.54. Caution must be exercised when increasing the ramp angle such that the oblique shock does not detach. If this occurs, a

second ramp angle may be added to decrease A_1 . The inlet area could also be decreased by deflecting the external lip inboard. For optimum inlet performance, the oblique shocks should intersect the lip to reduce spillage.

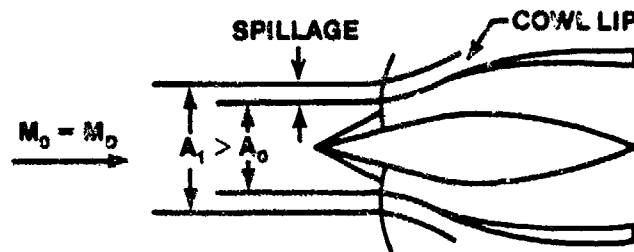
From the previous discussion, it becomes clear that any off-design operation produces problems. The ultimate goal would be to have a fully variable inlet such that all flight/engine conditions are on-design. The variable geometry inlets described attempt to achieve this goal but may result in other problems. Each configuration must be weighed, comparing the gains of increased thrust, reduced drag, and stable inlet/engine operation to the penalties of cost, complexity, weight, and reliability.



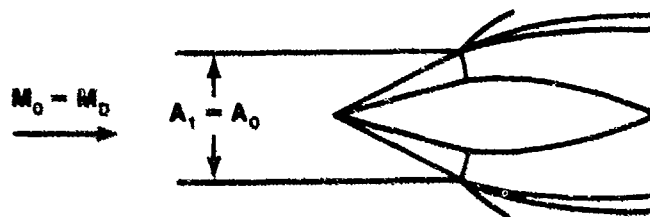
FIGURE 7.54. ADJUSTING INLET AREA WITH VARIABLE RAMP

7.8.2.5 Modes of Supersonic Diffuser Operation. It has been pointed out that the performance of a supersonic diffuser is as much a function of the mode of operation as it is of other factors; therefore, it is appropriate to examine some typical supersonic inlet operating modes. The three basic modes of operation frequently referred to are subcritical operation, critical operation, and supercritical operation. These three types of operation are shown for a conical inlet in Figure 7.55.

(a) SUBCRITICAL OPERATION, $\dot{m}_1 / \dot{m} < 1$, $M_{cowl} < 1$



(b) CRITICAL OPERATION, $\dot{m}_1 / \dot{m} = 1$, $M_{cowl} = 1$



(c) SUPERCRITICAL OPERATION, $\dot{m}_1 / \dot{m} = 1$, $M_{cowl} > 1$

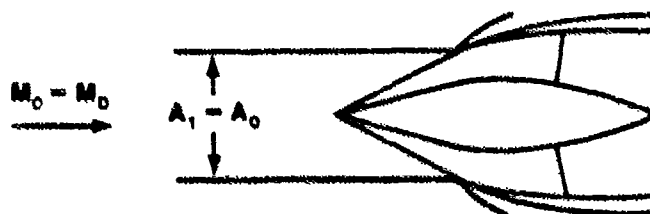


FIGURE 7.55. A CONICAL INLET AT ZERO ANGLE OF ATTACK AND DESIGN MACH SHOWING THREE MODES OF OPERATION

All three inlets are operated at the design Mach which means that the conical shock or conical shock extended will intersect the cowl lip. Figure 7.55a illustrates subcritical operation where the normal shock is external and subsonic velocities exist at the cowl. For this condition spillage exists, and the inlet is not swallowing air at maximum capacity. Pressure recovery is low since some of the air goes through a single, near normal shock. Inlet drag is high because of the intense shock. Operation is generally unstable and conducive to a condition called "buzz" (normal shock moves in and out of the inlet at relatively high frequencies). In general, subcritical operation is unsatisfactory and should be avoided. As the flow resistance downstream of the diffuser is increased, the mass flow can be reduced to its limit value of

zero at which point no flow exists. When, for the same design Mach, the downstream flow resistance is decreased, perhaps by increasing the RPM and pumping action of turbojet engine compressor, the mass flow will increase and the normal shock will move downstream. At one unique condition, it will be located at the cowl lip, Figure 7.55b. This condition illustrates critical operation. As the normal shock moves downstream from its location in Figure 7.55a to that in Figure 7.55b, the ram recovery also increases because more of the shock through which the entering air passes becomes oblique. For critical operation, both maximum mass flow and ram recovery are attained for the design Mach; thus, this condition represents the optimum performance condition. It has the disadvantage, however, of being marginally unstable in actual applications because small changes in angles of attack, yaw, or boundary layer separation can induce the critical mode of operation across the threshold into the subcritical regime. Consequently, for actual operation it is usually better to operate the inlet in a more stable condition, the supercritical regime shown in Figure 7.55c. For this case, the mass flow is maximum, but the recovery factor is reduced slightly because of the more intense normal shock which occurs downstream of the throat section. As with subcritical operation, there are various degrees of supercritical operation, the better operation in this regime being where the normal shock is far enough downstream from the throat to produce stable operation but not excessively far downstream to lower the ram recovery factor to unacceptable values.

The three modes of inlet operation discussed above can and do occur for other than design Mach operation. In accelerating to the design Mach, for example, the conical shock will lie outside the cowl lip, and, depending on the mass flow required by the engine for a given Mach, operation can be either subcritical or supercritical.

7.8.2.6 Other Supersonic Diffuser Performance Parameters. As mentioned previously, the design of induction systems for aircraft involves a number of compromises in order to obtain the optimum arrangement. Usually the compromises are directed toward maximizing the thrust minus drag and minimizing the weight of the aircraft insofar as the induction system influences it. In addition to the factors already mentioned (ram pressure

recovery, additive drag, and inlet engine airflow matching), there are a number of other inlet parameters which also influence this optimization. Included are the following: (1) the effect of boundary layer; (2) inlet flow stability; (3) inlet flow distortion; and (4) the static and low speed losses of the sharp lips which are required for low drag at high speed.

The boundary layer influences the performance of a supersonic inlet in several ways. These include friction losses, the displacement effect of the boundary layer on the compression field, and shock-boundary layer interaction. Friction losses are similar to the losses in subsonic diffusers. For inlets located adjacent to the fuselage, the boundary layer buildup on the fuselage presents a potential additional loss in that the low energy air of the fuselage may be inducted, significantly reducing the diffuser pressure recovery. For this reason, it is normal practice to move the inlet from the fuselage and to provide a boundary layer removal duct which prevents the low energy air from entering the main induction system. Even though this increases the frontal area of the aircraft and the total aircraft drag, the improvement in inlet recovery more than balances the extra drag. Figure 7.56 shows the improvement in total pressure recovery with increasing depth of the boundary layer removal diverter for a double conical side fuselage inlet.

From Figure 7.56, it may be seen that increasing the depth of the boundary removal diverter increases the inlet pressure recovery to the point that the depth of the diverter equals the boundary layer thickness. Converting the relation in Figure 7.56 into thrust minus drag shows that the overall aircraft performance also increases to $h/\delta = 1$.

Probably the greatest effect of the boundary layer on supersonic diffusers is in the area of shock-boundary layer interaction. Both the shock wave and the boundary layer can be significantly modified by this interaction, depending upon the strength of the shock and the boundary layer type (laminar or turbulent).

In extreme cases, the interaction can result in a separation of the boundary layer. Obviously, such extremes should be avoided in supersonic inlets when high pressure recovery is desired. Two methods can be used to control the interaction and prevent separation. The first is to bleed off the boundary layer. A boundary layer removal duct similar to that shown in Figure 7.56 can thus serve two purposes: to prevent low energy air from entering the

inlet and to minimize shock boundary layer interaction. Where shocks occur internally, the boundary layer can be bled off through flush scoops. Where such boundary layer removal is not possible, separation can still be prevented by maintaining the strength of the intersecting shock below the critical value.

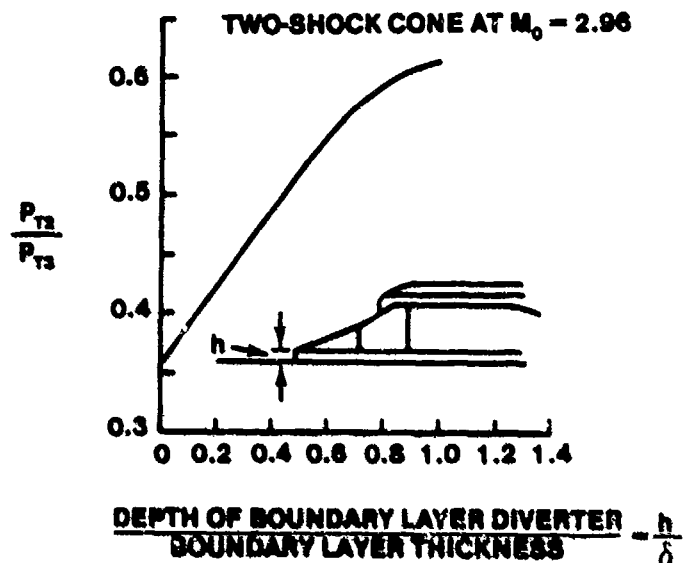


FIGURE 7.56 EFFECT OF BOUNDARY LAYER REMOVAL DEPTH ON TOTAL PRESSURE RECOVERY OF FUSELAGE SIDE INLET

Supersonic diffuser flow stability is another important inlet parameter. Flow instability, often called inlet buzz, is a very complex phenomenon associated with the subcritical region of inlet operation. Buzz manifests itself as large and often violent flow pulsations or fluctuations which can occur randomly or regularly. There are a number of apparent causes of the instability, but no final explanation has yet been developed. Inlets which are at all prone to buzz are normally operated supercritically even at the expense of pressure recovery in order to avoid any possibility of encountering the buzz phenomenon.

Another important inlet parameter is the flow uniformity at the exit of the diffuser (at the engine inlet). Nonuniform flows at this station can significantly affect the engine performance and hence the aircraft. Such nonuniformity or distortion causes a significant reduction in compressor stall

margin, decreases the internal performance of the engine, and increases the vibratory stresses on the compressor blades. Although distortion can be either radial or circumferential, the latter appears to be the more important with respect to compressor stall margin reduction.

There are a number of ways in which flow distortion can be minimized with respect to diffuser design. These include minimizing bends in the duct, low diffusion angles, and adequate boundary layer removal. Aircraft attitudes, such as very high angles of attack or yaw, will also tend to increase the distortion. Probably the best way of reducing the distortion, regardless of other effects, is to incorporate as long a straight cylindrical section as possible ahead of the engine.

In the interests of low drag at high Mach, the lips of supersonic inlets must be as thin and sharp as possible. For low speed or static operation, however, high lip angles of attack occur and flow separation often occurs on the inside of the lips, resulting in high pressure losses. These losses can be appreciable for a choked inlet (21% statically). Additional losses will occur in the diffuser downstream of the inlet.

7.8.3 Compressors

The combustion of fuel and air at normal barometric pressure will not produce sufficient energy to enable enough power to be extracted from the expanding gases to produce useful work at reasonable efficiencies. The compressor provides increased air pressure as is needed to increase the efficiency of the combustion cycle.

Finding a satisfactory manner in which to accomplish this necessary compression phase of the gas turbine cycle constituted the main stumbling block during the early years of turbojet engine development. Great Britain's Sir Frank Whittle and Germany's Hans Von Ohain solved the problem by using a compressor of the centrifugal type. This form of compressor is still being used successfully in many of the smaller gas turbine engines today. However, the engine efficiency levels with single-stage centrifugal compressors are somewhat better, but still do not compare with those of axial flow compressors. A compression ratio of 8 to 1 is about the maximum capability of

single-stage centrifugal compressors. Axial compressors were first introduced by Dr. Anselm Franz, an Austrian working for Germany in 1939. With multiple stages, axial compressors produce much higher pressure ratios. A high efficiency dual axial compressor, for instance, can attain a ratio of 23 to 1, or better. Axial compressors have the added advantages of being more compact and presenting a relatively small frontal area, which are important features in a high speed aircraft engine. Therefore, most large fan and turbojet engines employ this type of compressor.

7.8.3.1 General Thermodynamic Energy Analysis. Before examining details of specific compressors, consider a general energy analysis of the compression process. Figure 7.57 depicts a mechanical compressor which takes in its fluid at Section 2, does work on it, and delivers the fluid at a higher pressure level at Section 3.

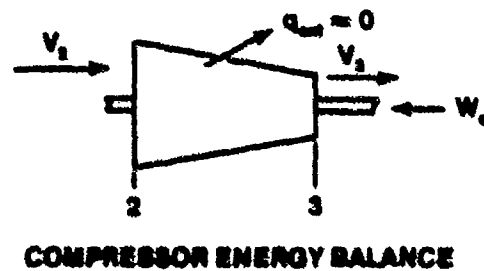


FIGURE 7.57. COMPRESSOR ENERGY BALANCE

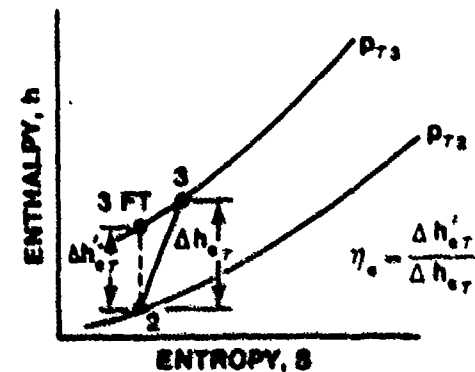


FIGURE 7.58. IDEAL AND ACTUAL ADIABATIC COMPRESSION PROCESSES

An energy balance on this machine considers the various energy terms which are applicable between entrance and exit. The general energy equation, when written between these sections, is as follows

$$z_2 + \frac{V_2^2}{2g} + h_2 - q_{\text{ext}} + W_c = z_3 + \frac{V_3^2}{2g} + h_3 \quad (7.49)$$

Since in most compressors the difference in potential energy is negligible and the amount of heat gained or lost from the machine is very small in comparison to the amount of work which is delivered to the machine, a logical assumption is that the process is without change in potential energy, and that it is adiabatic; thus

$$\Delta z = q_{\text{ext}} = 0 \quad (7.50)$$

By these assumptions, the work required by a compressor can be written

$$W_c = \frac{V_3^2 - V_2^2}{2g} + h_3 - h_2 \quad (7.51)$$

Note: V_3 will usually be less than V_2 in practice.

It is usually more convenient to consider the total enthalpy at exit and entrance in order that one need not measure the velocity at these sections. When Equation 7.51 is written in terms of total conditions, it takes the following form:

$$W_c = h_{T_3} - h_{T_2} = \Delta h_c \quad (7.52)$$

For constant specific heats, Equation 7.46 can also be written as

$$W_c = C_p (T_{T_3} - T_{T_2}) = C_p \Delta T_c \quad (7.53)$$

Equations 7.52 and 7.53 merely state that the work required by the compressor is equal to the total energy delivered to the fluid.

The energy absorbed by the fluid is reflected in a change of velocity, temperature, and pressure, and since the function of a compressor is primarily to increase the pressure of its fluid, all efforts are made to make the major

portion of the energy transfer reflect as a change in pressure. Since pressure increase is the function of a compressor, it is desirable to establish an efficiency factor that is based on the pressure ratio of the machine. Figure 7.58 shows two adiabatic compression processes on an h-s diagram between Pressures P_{T_2} and P_{T_3} .

For the assumption of the adiabatic flow process, we can state that there are in general two types of compression between Pressures 2 and 3 namely, the isentropic process and the general adiabatic process with friction. Since the pressure lines diverge with increasing entropy on an h-s diagram, it is readily apparent that the most efficient adiabatic process of compression is an isentropic path which is depicted as Line 2-3'. The adiabatic process with friction involves an increase in entropy and is shown as Line 2-3. The amount of compression work for either process is given by Equation 7.52, and the amount of work is equal to the actual enthalpy change of the fluid. An actual machine requires more work (because of frictional losses) to accomplish the same pressure rise than an ideal machine. The ratio of enthalpy change of an ideal adiabatic process to the enthalpy change of an actual adiabatic process is defined as the compressor adiabatic efficiency; thus, we can write

$$\eta_c = \frac{\Delta h'_{c_t}}{\Delta h_{c_t}} \quad (7.54)$$

It should be noted that this efficiency is a comparison between an ideal machine operating between the same total pressure limits.

Another useful form in which the compressor work can be expressed is as the shaft horsepower absorbed by the compressor.

$$HP_c = \frac{\Delta h_{c_t} \dot{W}}{550J} \quad (7.55)$$

7.8.3.2 Centrifugal Compressors. The centrifugal compressor was the type utilized in our first turbojet-powered airplane, and it has long had other applications. Its early engineering uses lay in pumping water and other

liquids. Turbo-supercharged aircraft engines utilize a centrifugal compressor as the supercharger; many of the earlier turbojet engines and even some current ones use the centrifugal compressor. The more important advantages of the centrifugal compressor are that it produces a large pressure ratio for a single stage of compression, and it is easily manufactured.

Centrifugal compressors operate by taking in outside air near their hub and rotating it by means of an impeller. The impeller, which is usually an aluminum alloy forging, guides the air toward the outer circumference of the compressor, building up the velocity of the air by means of the high rotational speed of the impeller. The compressor consists of three main parts; an impeller, a diffuser and a compressor manifold (Figure 7.59). Air leaves the impeller at high speed and flows through the diffuser, which converts high-velocity kinetic energy to a low-velocity, high-pressure energy. The diffuser also serves to straighten the airflow and to turn the air so that it may be picked up by the compressor manifold which acts as a collector ring. The diffuser blades direct the flow of air into the manifold at an angle designed to retain a maximum of the energy imparted by the impeller. They also deliver air to the manifold at a velocity and pressure which will be satisfactory for use in the burner section of the engine.

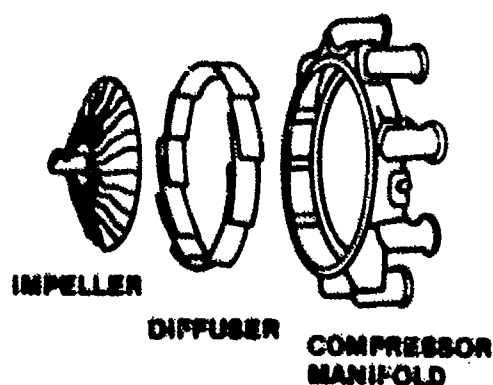


FIGURE 7.59. COMPONENTS OF A CENTRIFUGAL COMPRESSOR

The compressor shown in Figure 7.59 is known as a single-face or single-entry compressor. A variation of this is the double-face or double-entry compressor in which the impeller is constructed as shown in

Figure 7.60. The double-face compressor can handle the same amount of airflow and has a smaller diameter than a single-face compressor. This advantage is

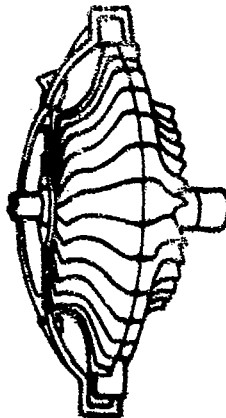


FIGURE 7.60. DOUBLE-ENTRY COMPRESSOR IMPELLER

partially offset by the complications involved in delivering air from the engine inlet duct to the rear face of the impeller. Double-entry centrifugal compressors must have a plenum chamber to enable the incoming air to be collected and fed to the rear impeller. Plenum chambers are, in essence, air chambers in which the compressor-inlet air is brought to low velocity after having passed through the inlet duct of the aircraft. This air is brought in at ambient pressure plus ram pressure. The pressure in the plenum chamber is, therefore, greater than that of the outside atmosphere. The plenum chamber is actually a diffuser that acts as a tool which the rear impeller is able to receive its air supply.

Multistage centrifugal compressors consist of two or more single compressors mounted in tandem on the same shaft (Figure 7.61). The air compressed by the first stage is passed on to the second stage at its point of entry near the hub. This stage further compresses the air before passing it on to still another stage, if there is one. In compressors of this type, the greatest difficulty is encountered in turning the air as it is passed from one stage to the next.

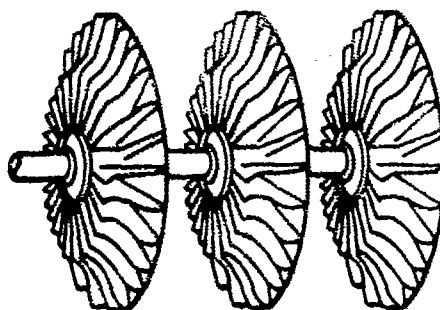


FIGURE 7.61. MULTISTAGE CENTRIFUGAL COMPRESSOR

7.8.3.3 Axial Flow Compressors. During the early development of turbojet engines, it was realized that the centrifugal flow compressors would impose certain performance limitations upon the high-thrust engines of the future. Consequently, the axial flow compressor development program was initiated early in turbojet engine history. This is borne out by the fact that the first all American turbojet engine was the 19A engine, an axial flow compressor engine designed and constructed by Westinghouse. As mentioned previously, the pressure ratios attainable in centrifugal flow compressors is about 8:1 (unless multistaging is employed, resulting in multiple air turning problems) at an efficiency of about 70 to 85%. The axial flow compressor, however, can achieve a much higher pressure ratio at a high level of efficiency; thus, where high pressure ratios are required, it is this type of compressor that must be used. Perhaps the greatest advantage of the axial flow compressor is its high thrust per unit frontal area.

In today's engines, the average axial flow type attains a static thrust per unit area of about 1500 lb/ft^2 , which is about four times the amount of the average centrifugal flow type engine developing about 400 lb/ft^2 . These two characteristics of the axial flow compressor - high pressure ratios at good efficiency and high thrust per unit frontal area - indicate the realm of its best application in high-thrust engines for high-speed aircraft. Briefly, the axial flow compressor provides large air-handling abilities with a small frontal area, a straight-through flow system, and high pressure ratios with

relatively high efficiencies. Its chief disadvantage is its complexity and cost. Hundreds of blades are needed to achieve the pressure ratios required by turbojet engines. Figure 7.62 shows the stator and rotor blades of a typical axial flow type compressor.

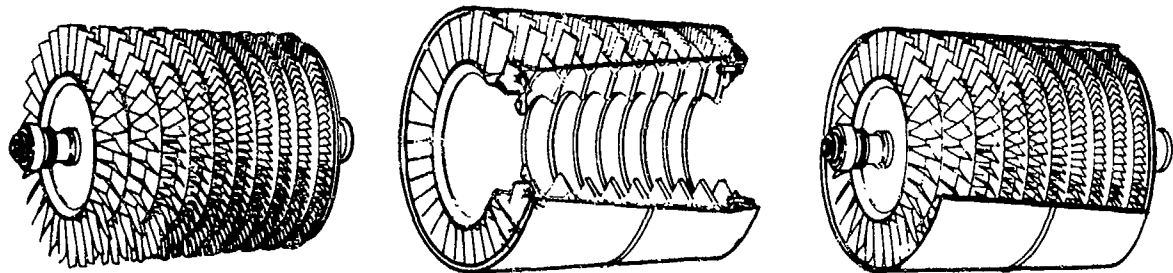


FIGURE 7.62. COMPONENTS AND ASSEMBLY OF AXIAL FLOW COMPRESSOR

The complexity can be visualized from Figure 7.62. In general, each row of rotor and stator blades is a different size and design. Compressor blades are usually made of steel, magnesium alloy, aluminum alloy, or titanium, and it is not uncommon for one compressor to have some steel blades and some alloy blades. The rotor blades must be secured properly to the rotor disk to withstand the stresses imposed by high rotational speeds.

7.8.3.4 Principle of Operation and Basic Terms. The basic principle of operation of the axial flow compressor is the same as that of the centrifugal compressor, namely, imparting kinetic energy to the air by means of the rotating blades, and thence converting the kinetic energy to a pressure rise. Referring to Figure 7.63, the air enters axially from the left and into the inlet guide vanes where it is turned through a certain angle to impinge on the first row of rotating blades with the proper angle of attack. The rotating vanes add kinetic energy to the air and increase the pressure slightly, then discharge it with the proper angle to the first row of stator blades where the pressure is further increased by diffusion. The air is then directed to the

second row of rotating blades, and the process is repeated through the remaining stages of the compressor. A compressor stage consists of a row of rotating blades followed by a row of stator blades. Most compressors have one to three rows of "straightener" or "diffuser" blades installed after the last stage to straighten and slow the air prior to its entry into the combustion chamber. If the purpose of these latter stator vanes is to provide additional air turbulence (as is sometimes necessary to alleviate combustion problems), they are called "mixer" blades.

The pressure ratio accomplished per stage of compression for subsonic stages is very modest when compared to one stage of a centrifugal compressor. For a typical axial flow compressor, the average pressure ratio per stage is about 1.20. Modern technology demonstrations have produced stage pressure ratios of 1.4. The over-all pressure ratio of an n stage compressor can be calculated by the relationship

$$\text{SPR}^n = \text{TPR} \quad (7.56)$$

where

SPR = stage pressure ratio

n = number of stages

TPR = total compressor pressure ratio

For a 10-stage compressor with an average SPR of 1.14, $1.14^{10} = 3.7$. The Allison /Rolls Royce TF-41 engine used in the A-7D and A7E has SPR's up to 1.36 in the low pressure compressor (Reference 2). These relatively low stage pressure ratios are the reason for the large number of stages to achieve an overall pressure ratio up to 21 (as in the TF-41).

7.8.3.5 Velocity Vector Analysis. The velocity vectors entering the compressor and through the first stage of the compressor are defined in Table 7.10. (See also Figure 7.64).

TABLE 7.10
Axial Flow Compressor Velocities

Symbol	Definition
$c_o = c_a$	absolute velocity of air entering the inlet guide vanes
c_1	absolute velocity of air leaving the inlet guide vanes
u_1	absolute linear velocity of a point on Rotor Stage 1 ($u_1 = 2\pi r_1 N/60$)
w_1	velocity of air entering the rotor, <u>relative to Rotor Stage 1</u>
c_2	absolute velocity of air leaving Rotor Stage 1
u_2	absolute linear velocity of a point on Rotor Stage 1 ($u_2 = 2\pi r_2 N/60$)
w_2	velocity of air leaving the rotor, <u>relative to Rotor Stage 1</u>
c_3	absolute velocity of air leaving Stator Stage 1
u_3	absolute linear velocity of a point on Rotor Stage 2
w_3	velocity of air entering Rotor Stage 2, <u>relative to Rotor Stage 2</u>

Figure 7.64 is a schematic diagram of the inlet guide-vanes and two stages of compressor blades that shows the air flow path through these blades, the velocity diagrams for each row of blades, and the static and total pressure variation of the air as it passes through the blades. This figure provides a vivid illustration of the principle of operation of an axial flow compressor.

The inlet guide vanes direct the air to give a proper angle of attack for the first row of rotating blades. During this process, the absolute air velocity, c , increases and the static pressure decreases. The first row of rotating blades imparts kinetic energy to the air proportional to $(w_1^2 - w_2^2 + c_2^2 - c_1^2)$, which brings about a total pressure increase proportional to the same term and a static pressure increase proportional to $(w_1^2 - w_2^2)$.

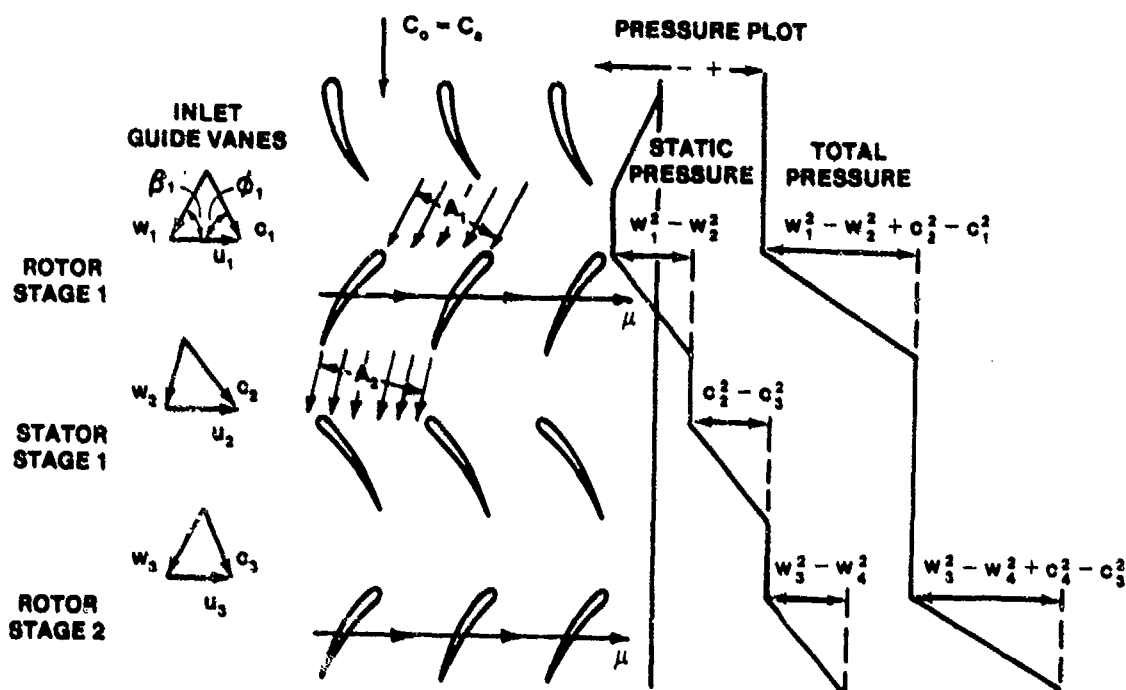


FIGURE 7.64. SCHEMATIC DIAGRAM OF COMPRESSOR BLADING EFFECTS

The air velocity relative to the rotating blades decreases ($w_2 < w_1$) because the flow area increases ($A_2 > A_1$). The stator blades of the first stage decrease the absolute air velocity ($c_3 < c_2$) to bring about a static pressure rise and turn the air to achieve the proper angle of attack for the second stage of rotating blades. Table 7.11 shows the pertinent variation that occurs in a typical axial flow compressor stage.

TABLE 7.11
VARIATION ACROSS A TYPICAL AXIAL FLOW COMPRESSOR STAGE

	<u>Absolute Velocity c</u>	<u>Relative Velocity w</u>	<u>Flow Width</u>	<u>Static Pressure P</u>	<u>Total Pressure P_T</u>
Rotor	increases	decreases	increases	increases	increases
Stator	decreases	increases	increases	increases	about constant

Normally, the temperature change caused by diffusion alone, is not significant. The temperature rise which causes the air to get hotter and hotter as it continues through the compressor is the result of the work being done on the air by the compressor rotors.

Because the airflow process in an axial compressor is diffusion, i.e., an adverse pressure gradient exists; it is very unstable. High efficiencies can be maintained only at very small rates of diffusion. When compared with a turbine, quite a number of compressor stages are necessary in order to keep the diffusion rate small through each individual stage. Also, the permissible turning angles of the blades are considerably smaller than those which can be used in turbines. These are the reasons why an axial compressor has such a small pressure ratio per stage and must have many more stages than does the turbine which drives it.

7.8.3.6 Dual Axial Compressors. A single axial compressor might theoretically be built to consist of as many stages as would be necessary to produce any required compression ratio. If such were the case, at low off-design speeds the rearmost stages of the compressor would operate inefficiently, and the foremost stages would be overloaded. Such a condition would produce "compressor stall". This condition can be corrected by bleeding interstage compressor air overboard or varying the airflow and pressure ratio of the stages by use of variable vanes during part-throttle operation. Excessive air bleeding, however, is wasteful. Greater flexibility for part-throttle conditions and for starting can be attained more efficiently by splitting the compressor into two mechanically independent rotor systems. Each is driven by its own separate turbine, at its own best speed (Figure 7.65). The high pressure compressor has shorter blades than the low pressure compressor, and is lighter in weight. Since the work of compression by the high pressure compressor heats the air within the compressor to higher

temperatures than occur within the low pressure compressor, higher tip speeds are possible before the blade tips attain their limiting Mach, because the speed of sound increases as the air temperature increases. Hence, the high pressure compressor can run at a higher speed than the low pressure compressor.

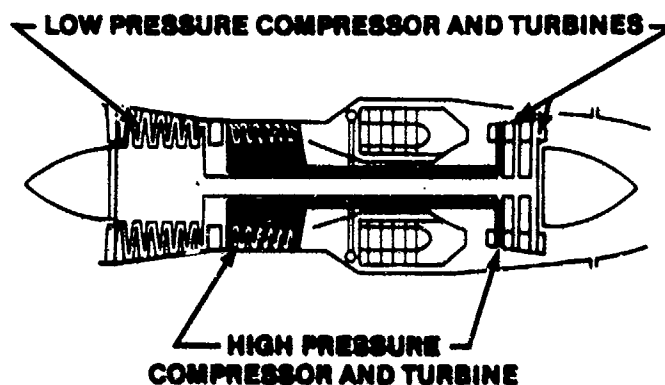


FIGURE 7.65. DUAL AXIAL COMPRESSOR
OR TWIN-SPOOL SYSTEM

When dual, or, as sometimes called, split or twin-spool, compressors are used, high compression ratios can be attained with minimum total compressor weight and frontal area. Usually when dual compressors are used, the high pressure compressor rotor is the rotor to which the engine starter drive is connected. Only the lighter part of the compressor is cranked, which considerably reduces the torque required to start the engine. The size and weight of the starting system may therefore be appreciably less. The speeds of the two rotors are matched for best efficiency and stall margin.

7.8.3.7 Compressor Performance Charts. Compressor performance charts map the various regions of operation of the compressor. Their use gives a quick visual presentation of operational characteristics that could not be matched by scores of equations or tables.

From the dimensional analysis techniques discussed in Chapter 2, several dimensionless ratios used to analyze engine compressor performance can be derived. These ratios are listed in Table 7.12.

TABLE 7.12

COMPRESSOR DIMENSIONLESS PERFORMANCE RATIOS

Actual Value	Corrected Value
Thrust F_n	F_n/δ
Fuel Flow \dot{w}_f	$\frac{\dot{w}_f}{\delta \sqrt{\theta}}$
Air Flow \dot{w}_a	$\frac{\dot{w}_a \sqrt{\theta}}{\delta}$
RPM's n	$\frac{N}{\sqrt{\theta}}$

Figure 7.66 shows a typical compressor performance chart, which presents pressure ratio plotted against the corrected weight-flow rate for various corrected RPM's.

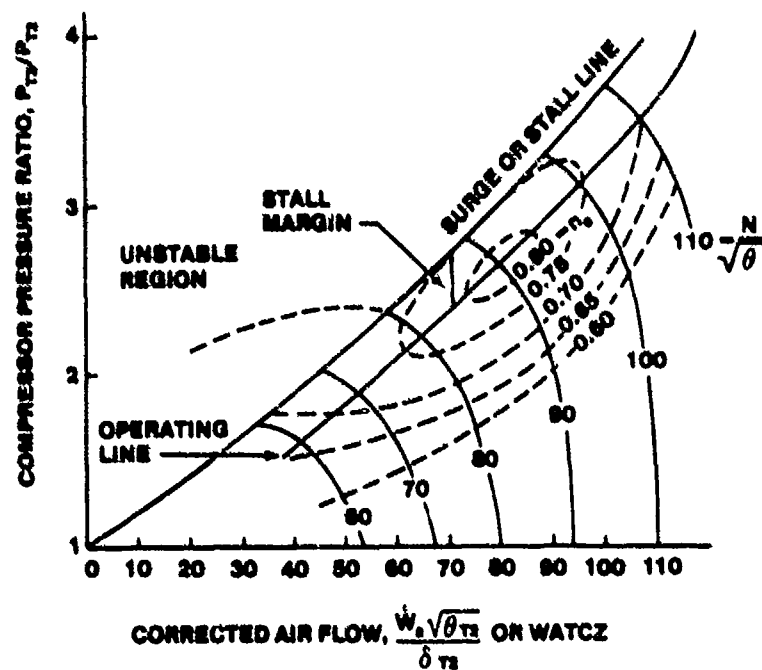


FIGURE 7.66. TYPICAL COMPRESSOR PERFORMANCE CHART

Note that all RPM operating lines reach the limiting surge, or stall, line. Operation to the left of this line is unstable. Thus, the slope of the RPM line in a stable region must always be negative. A positive slope indicates unstable operation; therefore, do not operate to the left of the surge line. One dotted line in Figure 7.66 shows the RPM line as it appears in unstable operation.

Normally, a cross plot of compressor adiabatic efficiency is also made on the performance chart as illustrated in Figure 7.66. These various efficiencies show that at one optimum design flow rate, RPM, and pressure ratio, maximum efficiency is achieved. This point is properly called the design point. It should be noted, therefore, that a compressor should be operated as much as possible near the design point in order to maintain reasonable values of efficiency. For example, if the RPM is decreased from the design condition, the efficiency drops off. Furthermore, if the pressure of the system is decreased or increased, the efficiency also drops off.

The compressor performance chart can be used to explain many turbojet engine operating characteristics. In Figure 7.66 the curve labeled "Operating Line" is that line on which the compressor operates when installed in a given fixed geometry engine. This line corresponds to the flow resistance of a given assembly of combustion chamber, turbine, tailpipe, and exhaust nozzle. Any change of these components would produce a new operating line. If the exhaust nozzle area were reduced, flow resistance would be added and the operating line would move upward nearer the surge line.

Compressor Stall Margin is defined as the difference between the compressor pressure ratio at the stall line and the CPR at the operating line divided by the CPR at the operating line for a constant value of WATCZ.

Mathematically

$$SM = \frac{CPR_{STALL} - CPR_{op}}{CPR_{op}} \quad \left| \begin{array}{l} (7.57) \\ WATCZ \text{ CONST} \end{array} \right.$$

7.8.3.8 Compressor Stall. It is a characteristic common to gas turbine compressors of all types to stall under certain operating conditions. Some call this surge. Others endeavor to differentiate between stall and surge, but usually the two terms may be considered synonymous and may be treated as

one and the same thing. Compressor stall occurs in many different forms and under many different conditions. Stall is neither easy to describe nor to understand, particularly because the stall characteristics of no two engine designs will be the same. In general, stall results when the compressor attempts to supply pressure ratios higher than its capability.

In its milder form, compressor stall can be recognized by the condition known as "chugging" which is occasionally encountered during ground engine operation at low thrust. In flight, under severe conditions of "slam" acceleration, or when slipping or skidding during evasive action, or when flying in very turbulent air, stall may become sufficiently pronounced to cause loud bangs and engine vibration. In most cases, this condition is of short duration and will either correct itself or can be corrected by retarding the throttle to IDLE and advancing it again, slowly.

If a physical occurrence took place which greatly increased the blade angle of attack, the blade would stall. For example, if the air flow rate were reduced, the blade angle of attack would increase, and stall might occur. This same phenomenon can occur during rapid rotor acceleration if the fuel scheduling to the combustor is improper. If the fuel flow rate during acceleration is too high, the high temperature and pressure resulting in the combustor will produce excessive back pressure, causing an increase in blade angle of attack, which if great enough, will produce stall. Compressor stall due to engine acceleration and afterburner initiation are the most common types of stall. Another type compressor stall is "rotating stall." This type of stall is characterized by the stall region progressing from one blade to the adjacent blade, and the resulting stall cell rotates in the direction of the rotor at .4 - .5 rotor speed. The flow separation on the stalled blade causes the angle of attack to increase on the adjacent blade. This stalls it, causing stall on the next blade, and so on.

During rotating stall, although the pressure ratio and flow rate of the engine system may be in equilibrium, the compressor and turbine torques are not equal. The turbine torque has fallen off because the turbine pressure ratio and flow rate are at lower values, and it generates less torque. The compressor torque is reduced, but not as much as the turbine due to large energy dissipation in the compressor. The compressor torque will usually exceed the turbine torque significantly, and the rotor will tend to decelerate.

The occurrence of rotating stall also causes combustor gas temperature to rise rapidly because the airflow rate drops quickly and the fuel-to-air ratio in the combustor is increased. The danger of rotating stall operation in a gas turbine engine is that the combustor gas temperature will exceed allowable limits for the turbine and/or that the rotor speed will fall below the self-sustaining level. Generally, it will then be necessary to shut down the engine and allow it to cool somewhat before restarting. All but the very minor degrees of compressor stall are to be avoided by both design and operation.

There are a number of other factors that tend to induce compressor stalls — high altitude operation, with its consequent reduction in compressor inlet Reynolds number, causes a slight reduction in the compressor stall pressure ratio. The pressure gradients which may exist over the "face" (entering section) of the compressor may reduce the stall margin by decreasing the stall line sufficiently to cause stall. These pressure distortions can result from poor inlet duct design, inadequate removal of inlet duct boundary layer, operation of aircraft at high angles of attack or side slip, expulsion of gun and rocket gases into the inlets, and so on. Most of these items can be controlled by good airframe design.

There are many degrees of compressor stall. It may range from one or several blades of single stage to complete flow breakdown, and the flow will momentarily reverse to cause a loss of combustor flame. Flameouts can occur even in less severe cases.

7.8.3.9 Methods of Increasing Stall Margin. Current engines employ several techniques for either lowering the operating line or increasing the stall line for increased stall margin.

Paragraph 7.8.3.6 discusses the use of compressor bleed and variable compressor vanes as techniques for improving stall margin at the lower rotor speeds. New engines also vary the fan operating line based on the level of distortion the inlet is generating and/or if a throttle transient is being requested. These techniques for maximizing either performance or stall margin, depending on current conditions, are becoming more viable with the use of digital flight and propulsion control systems.

7.8.4 Combustion Chambers

The combustion chamber of an air-breathing gas turbine jet propulsion engine is required to deliver large amounts of heat energy to the airstream and direct it with proper temperature level and temperature profile to the turbine. A good combustion chamber must provide complete burning of the fuel with a minimum of pressure loss, operate without accumulating deposits, ignite the fuel easily, and give reliable service over an extended period of time. The above requirements must be met over the complete range of jet engine operation - engine RPM, flight speed, and altitude.

In order to meet these requirements, the combustion chambers of turbojet and turboprop engines have evolved into two basic types: (1) the can or tubular type and (2) the annular type.

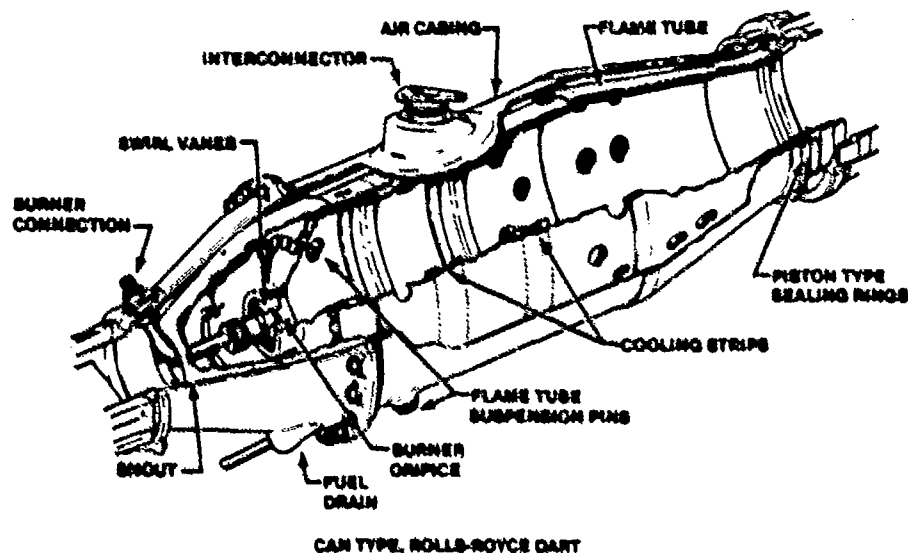


FIGURE 7.67. THE CAN OR TUBULAR-TYPE COMBUSTION CHAMBER

Both types contain the same basic elements: an outer casing or shell, a perforated inner liner or flame tube, a primary combustion zone, a liquid fuel-injection system, and provisions for initial ignition. Figures 7.67 and 7.68 respectively, present a typical can or tubular-type combustion chamber and typical annular combustion chamber.

The can-type combustor illustrated in Figure 7.68 is one of several (7-14) such units that make up the overall combustion chamber for a given

engine. These individual "cans" are interconnected by means of tubes located between the cans in order to provide uniform combustion characteristics in each tube and to allow flame travel between "cans" for ignition since, in the normal installation, only two cans will be equipped with spark plugs or igniters. The cans are located around the main rotor shaft and are connected to the compressor and turbine sections. The annular type combustion chamber illustrated in Figure 7.68 similarly has only two igniters. The relative merits of the two types of burners are about equal.

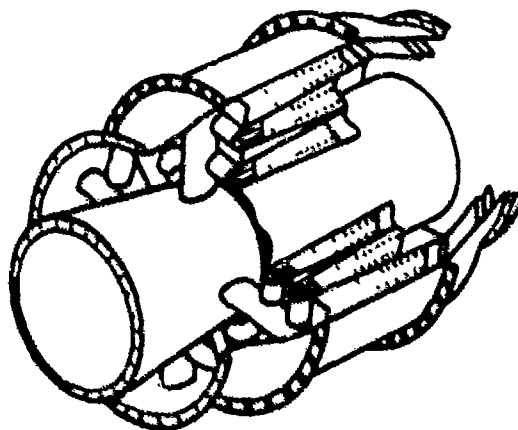


FIGURE 7.68. TYPICAL ANNULAR COMBUSTION CHAMBER

7.8.4.1 Combustor Operation. Combustion chamber design is dictated mainly by the general characteristics found in any type of combustion process. The requirements deriving from these characteristics are basic, whether considering combustion in a fireplace or in a turbojet engine. They are: (1) proper mixture ratio, (2) temperature of reactants, (3) turbulence for good mixing, and (4) time for burning. In addition, for aircraft turbine engines, the combustion process should be accomplished with a minimum possible pressure loss.

The first requirement in any combustion process is mixture ratio because fuel-air ratios have lean and rich limits of inflammability beyond which burning is impossible. For heat engines, these limits in terms of fuel-air ratio are about 0.04 for the lean limit, and about 0.15 for the rich limit.

For most hydrocarbon liquid fuels, the stoichiometric fuel-air ratio is about 0.066. Thus, it is apparent that any combustion chamber must maintain a mixture ratio which is within allowable limits if burning is to occur at all, and within much more stringent limits if good burning is to occur. In gas turbine engines, operation with overall mixture ratios which even approach the stoichiometric value are not feasible, because such mixture ratios produce exhaust gas temperatures of about 4000°R , well in excess of the maximum allowable turbine blade inlet temperature. In order to reduce the temperature of the gases leaving the combustion chamber to an allowable value, it is necessary to operate the combustion chambers with a large quantity of excess air to provide adequate cooling. The large amount of excess air required reduces the overall fuel-air ratio to a value which is generally below 0.02. This fuel-air ratio is, of course, too lean for burning; hence, the burner design must provide a method of bypassing about 60 to 75% of the air around the actual combustion zone. The bypassed air is known as secondary air because it does not enter into the combustion process, whereas the remainder of the air, that which actually takes part in the combustion process, is known as primary air. The amount of primary air is dictated by the fuel-air ratio in the actual combustion zone, or primary zone, of about 0.08. Figure 7.69 presents a schematic diagram of the cross section of a typical burner.

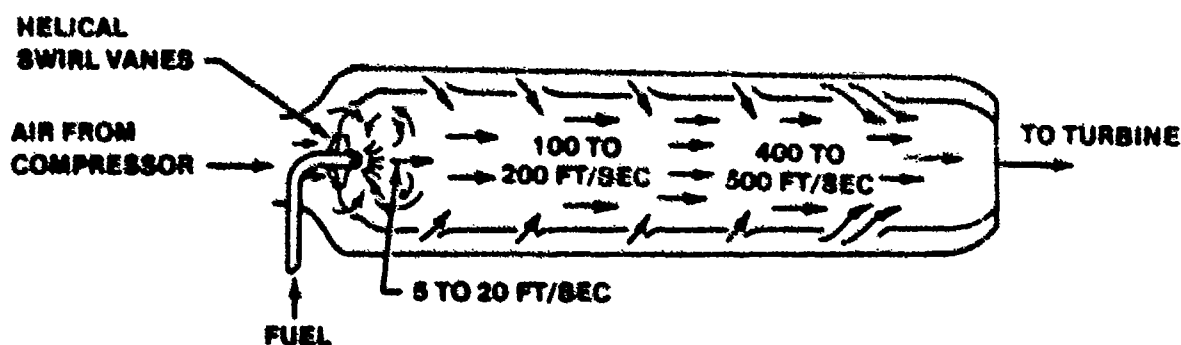


FIGURE 7.69. SCHEMATIC DIAGRAM OF BURNER CROSS SECTION

This diagram shows the flow path of the primary and secondary air. The secondary air is progressively mixed with the combustion gases as they flow within the inner liner in order to cool the overall mixture to its proper

temperature where it enters the turbine section, and to provide a film of cool air to protect the inner liner. It is evident that the combustion chamber design is largely dictated by the mixture ratio requirements, and the proportioning of the primary and secondary airflows must be properly maintained during the whole process. This mixing of the secondary air must also be accomplished to provide the proper temperature profile to the turbine.

After proper mixture ratio is attained, combustion will not be maintained unless the three T's of combustion - temperature, turbulence, and time - are also present. The temperature of the reactants must be above the ignition temperature. For initial combustion, this temperature is usually provided by means of electrical energy in the form of a spark. Normally, two spark igniters are located in the combustion chamber to initiate combustion by providing localized regions where the reactant temperature will be considerably above the ignition temperature. After ignition occurs and burning begins, reactants are kept at a high temperature by the heat released from the burning fuel, and the spark energy is no longer required.

Sufficient turbulence must be created and maintained for combustion to be complete, because each fuel molecule requires an exact number of oxygen molecules before complete combustion can occur. Adequate turbulence insures that each fuel molecule will intimately mix with the air and find its proper number of oxygen molecules. Since turbulence is accompanied by a fluid pressure drop, it is essential that only enough turbulence be created to achieve proper mixing, otherwise excess pressure drop will occur with a consequent reduction in overall engine thrust.

Sufficient time must be allocated for the fuel to burn if the combustion process is to be complete. If the air flow velocities are greater than the flame speeds, approximately 60-100 ft/sec, the flame will be blown down the combustion chamber and out of the engine, causing flameout.

7.8.4.2 Combustion Process and Efficiency. The ideal combustion process occurs at constant pressure with complete release of the fuel heating value. In an actual combustion process, the total pressure drops slightly due to friction and the momentum pressure drop due to heat addition (static pressure drops because of friction as well as gas acceleration), and the combustion is not complete because some of the fuel molecules are not burned.

As shown in Figure 7.70, the ideal process occurs at the constant total pressure P_{T3} from the burner inlet Section 3 to the burner outlet Section 4'. The actual process occurs from Sections 3 to 4, which, compared to the ideal process, represents a loss in total pressure (about 5% in modern combustors) and a loss in end temperature because of incomplete combustion. Figure 7.70 shows the combustor process for the maximum full throttle position where T_{T4} is equal to the maximum allowable turbine inlet temperature. Operation at less than full throttle will produce T_{T4} values, which are less than that shown on the figure.

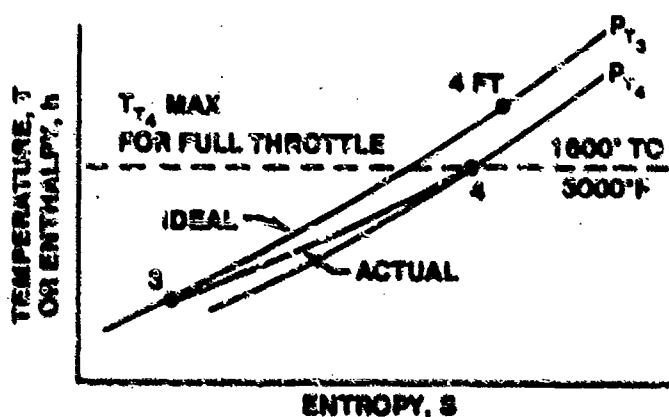


FIGURE 7.70. IDEAL AND ACTUAL COMBUSTION PROCESS ON h-s PLANE

The combustion chamber efficiency is defined as the ratio of the actual heat released to that which ideally could be released from a given quantity of fuel, or

$$\eta_b = \frac{h_{T4} - h_{T3}}{h_{T4'} - h_{T3}} \quad (7.58)$$

For constant specific heat this becomes

$$\eta_b = \frac{T_{T_4} - T_{T_3}}{T_{T_4}^i - T_{T_3}^i} \quad (7.59)$$

In most turbojet and turbofan engine operations, combustor efficiencies vary between 98% and 100%.

7.8.4.3 Fuel Control Units. The amount of fuel supplied to the combustion chamber must be closely controlled and adjusted for different engine operating conditions; altitude, temperature, engine RPM, and forward flight speed. This job is performed by the fuel control unit. In basic fuel control units, the unit senses throttle position, engine RPM, engine air inlet pressure, and engine air inlet temperature.

Many aircraft turbine engines have a much more complicated fuel control system than the basic unit. These are the variable geometry engines, those equipped with variable area exhaust nozzles, variable angle inlet guide vanes, or variable angle compressor stator vanes. On engines of this type, the fuel control unit, in addition to sensing these variables, must also sense turbine outlet temperature and control the exhaust nozzle area or inlet guide vane area.

7.8.4.3.1 Digital Electronic Engine Control. The Digital Electronic Engine Control (DEEC) is a much more advanced system than the current generation of ordinary fuel control systems. Although it is a completely electronic system, a hydro-mechanical Back-Up Control (BUC) may be selected either by the pilot or automatically by the DEEC if the need arises.

The primary engine variables that are sensed and controlled by the DEEC are illustrated in Figure 7.71.

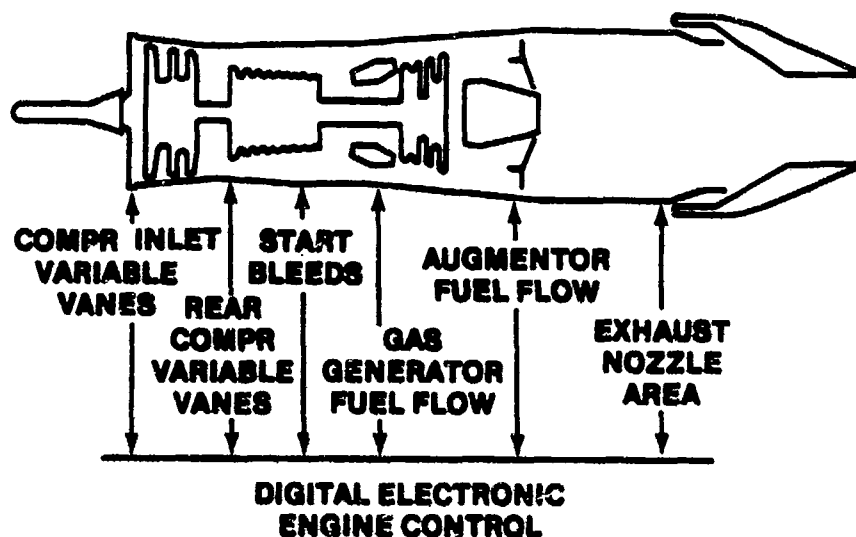


FIGURE 7.71. DEEC VARIABLES

Sequencing and control of these variables allows the DEEC to provide:

- 1) Reliable engine starts (including airstarts)
- 2) Safe throttle transients without stall, overtemperature or blowout
- 3) Consistent idle thrust
- 4) Stable intermediate thrust without exceeding speed or temperature limits
- 5) Smooth augmentor transients without blowout or stall
- 6) Backup control capability
- 7) No required engine trim

Pilot workload is considerably reduced with incorporation of DEEC.

7.8.5 Gas Turbines

The primary purpose of the gas turbine in a turbojet or turbofan engine is to extract mechanical energy from the hot gases delivered to it by the combustion chamber and to supply shaft power to drive the compressor. The

turbine must also supply power to the auxiliary equipment, such as fuel pumps, oil pumps, and electrical generators. In turboprop and turboshaft engines, the turbine must also supply power to drive the propeller or helicopter rotor. Typically, three-fourths of all the energy available for the products of combustion is necessary to drive the compressor. If the engine is a turboprop or turboshaft, the turbine is designed to extract all the energy possible from the gases passing through the engine. So efficient is the turbine, in this case, that in a turboprop aircraft the propeller provides approximately 90% of the propulsive force, leaving but 10% to be supplied by jet thrust.

The axial flow turbine is comprised of two main elements: a turbine wheel, or rotor, and a set of stationary vanes (Figure 7.72).

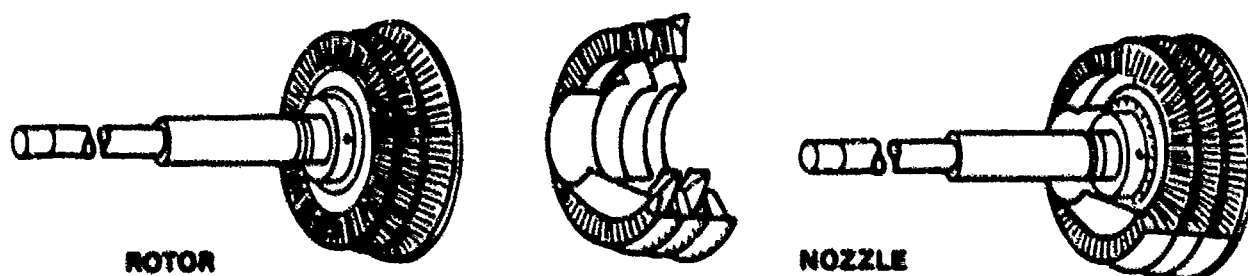


FIGURE 7.72. TURBINE ELEMENTS

The stationary section consists of a plane of contoured vanes, concentric with the axis of the turbine, and set at an angle to form a series of small nozzles which discharge the turbine gases onto the blades of the turbine wheel. For this reason, the stationary vane assembly is usually referred to as the turbine nozzle, and the vanes, themselves, are called nozzle guide vanes. Aerodynamic design of turbine blades is less critical than compressor blades because they operate in a regime of favorable pressure gradient rather than an adverse pressure gradient. Turbine-nozzle area is a critical part of turbine

design because it establishes the engine (compressor operating line). The jets of escaping gases which are formed by the nozzle discharge are directed against the rotating turbine blades in a direction which enables the kinetic energy of the gases to be transformed into mechanical energy which is generated by the rotating turbine wheel.

Turbines may be either single or multiple-stage. When the turbine has more than one stage, stationary vanes are inserted between each rotor wheel and the rotor wheel downstream, as well as at the entrance and exit of the turbine unit. Each set of stationary vanes forms a nozzle vane assembly for the turbine wheel that follows. The exit set of vanes serves to straighten the gas flow before passage through the jet nozzle.

7.8.5.1 Turbine Design Considerations. Turbines are subjected to both high rotor speeds and high temperatures. High rotor speeds result in high centrifugal forces, and because of high temperatures, turbines must operate close to temperature limits which, if exceeded, will lower the strength of the construction materials used in them. Turbine blades with continued use undergo distortion of the blade, which is known as "creep." Creep means that the blade stretches or elongates. This condition is cumulative, the rate of creep being determined by the load imposed on the turbine and the strength of the blade, which is determined by the temperature within the turbine.

From Figure 7.73 it may be seen that the highest stress plus fatigue considerations near the blade root require a lower temperature to maximize the blade material strength.

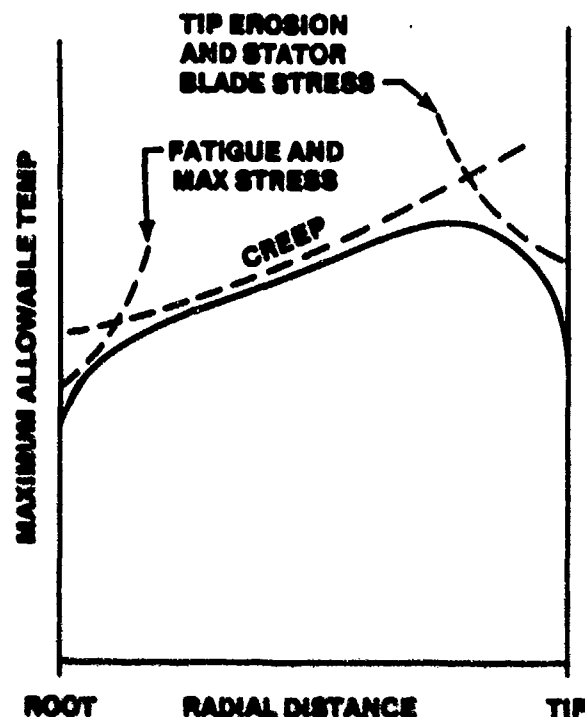


FIGURE 7.73. TURBINE INLET BLADE TEMPERATURE PROFILE LIMITATIONS

Creep is the dominant factor in the middle of the blade. Higher temperatures are allowable further out because of the lower stresses. Near the blade tip, erosion or stator blade stresses again reduce the temperature level. With these limits established, the combustion chamber design objective is to match the desired gas temperature profile as closely as possible.

The turbine wheel is a dynamically balanced unit consisting of steel alloy blades, or buckets, as they are sometimes called, attached to a rotating disc. The base of the blade is usually of a so-called "fir tree" design to enable it to be firmly attached to the disc and still allow room for expansion. In some turbines, the rotating blades are open at their outer perimeter. In others, the blade is shrouded at the tip, as shown in Figure 7.74. The shrouded blades form a band around the perimeter of the turbine wheel, which serves to reduce blade vibrations. The weight of the shrouded tips is offset because the shrouds permit thinner, more efficient blade sections than are otherwise possible because of vibration limitations. Also, by acting in the same manner as aircraft wingtip fences, the shrouds improve the air flow characteristics

and increase the efficiency of the turbine. The shrouds also serve to cut down gas leakage around the tips of the turbine blades.

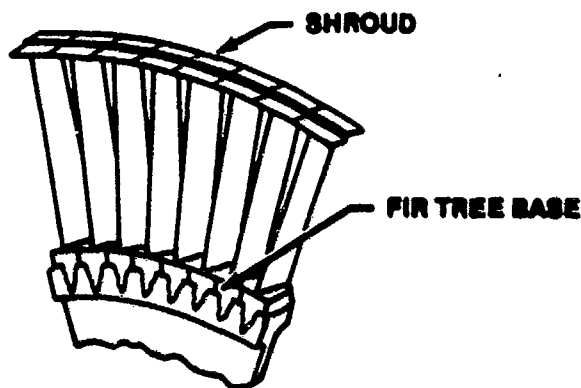
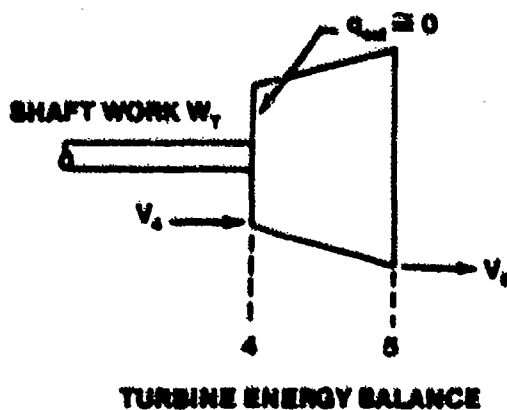


FIGURE 7.74. SHROUDED TURBINE-ROTOR BLADES

7.8.5.2 General Thermodynamic Analysis. Figure 7.75 depicts the energy balance of a gas turbine. It receives high-temperature, high-pressure gas at Section 4, extracts energy from it in the form of shaft work, and discharges the gas at a lower level of pressure and temperature.



TURBINE ENERGY BALANCE

FIGURE 7.75. TURBINE ENERGY BALANCE

The energy equation for this machine, when written for no change in potential energy and an adiabatic process, is

$$\frac{V_4^2}{2g} + h_4 = W_T + \frac{V_5^2}{2g} + h_5 \quad (7.60)$$

Solving Equation 7.60 for the turbine work and expressing the gas energy content at Sections 4 and 5 in terms of total conditions gives

$$W_T = h_{T_4} - h_{T_5} = C_p(T_{T_4} - T_{T_5}) \quad (7.61)$$

Total conditions are used in preference to the sum of static enthalpy and kinetic energy, because it is far easier to measure and evaluate two total enthalpies than it is to measure two static enthalpies and two velocities. Equation 7.61 merely states that the turbine work is equal to the change in energy content of the gases passing through the turbine.

Figure 7.76 shows the actual and ideal turbine process on an h-s diagram.

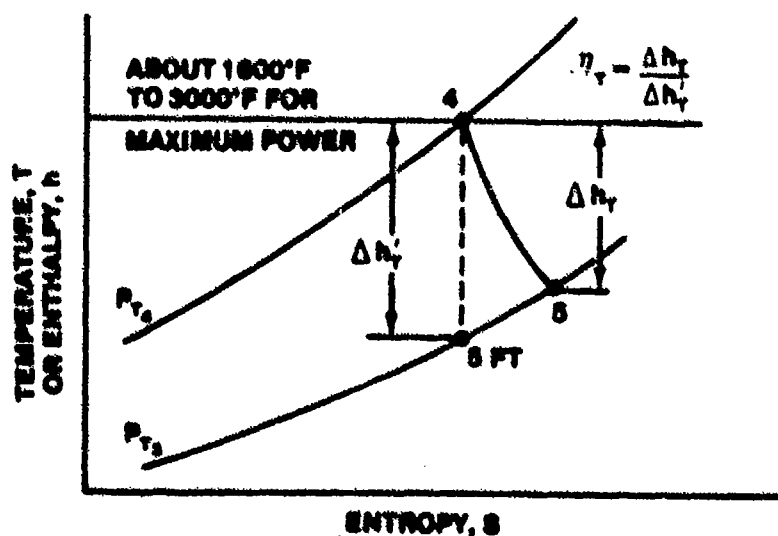


FIGURE 7.76. IDEAL AND ACTUAL ADIABATIC TURBINE EXPANSION PROCESS

Note that the ideal and actual processes for the turbine are defined in the same manner as they were for the compressor, namely, between the same two total pressure lines. For the assumption of an adiabatic flow process between pressures P_{T_4} and P_{T_5} , we can have either the ideal isentropic process 4-5' or a general adiabatic process with friction 4-5. It is evident that for an adiabatic process between two pressure lines, maximum turbine work will occur along a constant entropy path; therefore, great effort is expended to minimize the friction in turbines. The turbine adiabatic efficiency is defined as

$$\eta_T = \frac{h_{T_4} - h_{T_5}}{h_{T_4} - h_{T_5}'} = \frac{\Delta h_T}{\Delta h_T'} \quad (7.62)$$

The work produced per pound of fluid can be expressed in terms of the ideal path 4-5' as

$$W_T = \eta_T \Delta h_{T'} = \eta_T C_p (T_{T_4} - T_{T_5}') \quad (7.63)$$

Since, by definition, the total pressure at points 5 and 5' are equal, the turbine work can be expressed in terms of pressure ratio and inlet temperature as

$$W_T = \eta_T C_p T_{T_4} \left[1 - \left(\frac{P_{T_5}}{P_{T_4}} \right)^{\frac{\gamma-1}{\gamma}} \right] \quad (7.64)$$

Considering Equation 7.64, the important factors which affect turbine work, namely, turbine efficiency η_T , turbine inlet temperature T_{T_4} , and turbine pressure ratio P_{T_4}/P_{T_5} may be seen. An increase in any of these three factors will allow the turbine to develop more work per pound of fluid. Only

small gains can be expected to accrue from improvements of turbine efficiency, since present efficiencies are up near the peak of development, 85% to 93%. Because of gas friction over the many turbine blades and the leakage losses over the blade tips, turbines inherently have about 10% overall loss. However, the prospect of operating turbines at higher inlet temperatures is indeed an attractive one to achieve more work per pound of fluid because, as shown in Equation 7.64, the turbine work is directly proportional to the absolute temperature of the entering gases.

$$\text{Turbine Shaft Horsepower} = \frac{\dot{w} h_T}{550J} \quad (7.65)$$

7.8.5.3 Velocity Vector Analysis. Recalling the definitions of the velocity vectors c , w and u from the compressor section, Figure 7.77 illustrates the velocity, static pressure, and total pressure changes through a two-stage turbine.

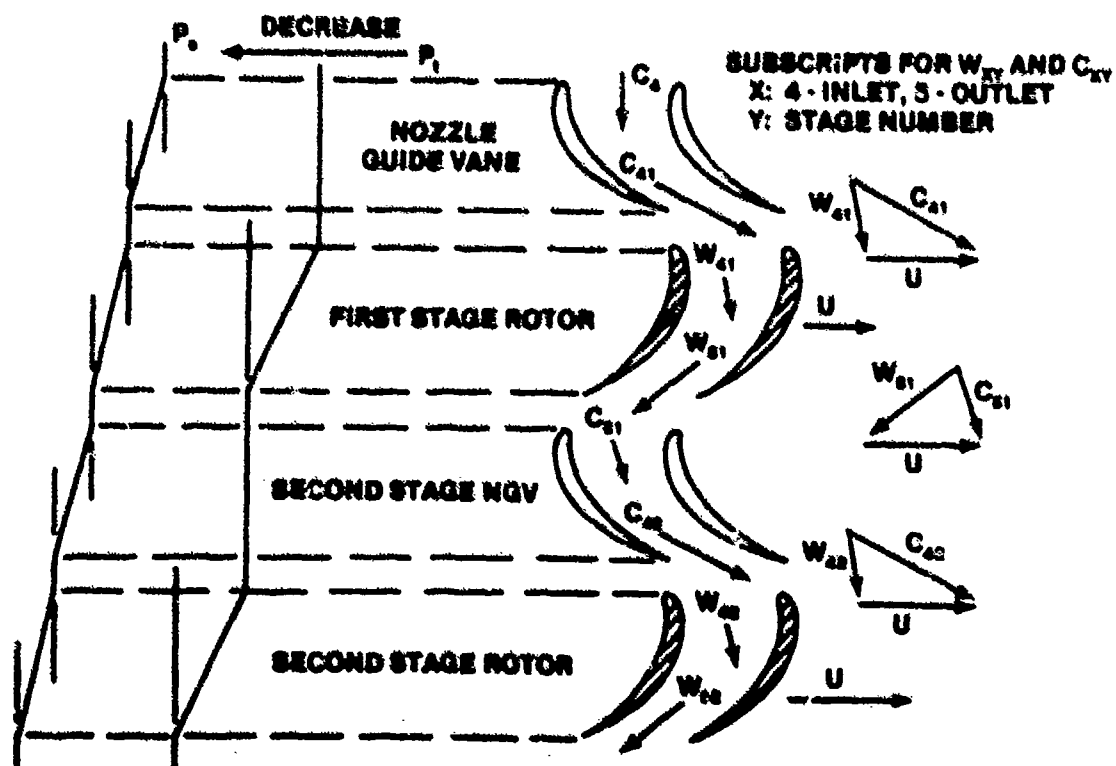


FIGURE 7.77. TURBINE ENERGY TRANSFER

7.8.5.4 Improvement of Turbine Inlet Temperature. The most attractive method of increasing thrust and turbine work per pound is to increase the turbine inlet temperature. Increases in turbine inlet temperature are directly tied to the need for better materials in construction of turbine blades and efficient methods of cooling them.

7.8.5.4.1 Materials Considerations. Much work has been done in recent years toward improving the high-temperature strength characteristics of metals and alloys. From this effort has come a series of cobalt and nickel-based alloys that offer significant high temperature strength improvements over iron-based alloys. Newer, more exotic materials hold still greater promise. Improved metallurgical techniques have allowed blades made of materials which have been directionally solidified, subjected to rapid solidification rates, or even constructed of a single crystal to be manufactured. Gains due to these metallurgical techniques are illustrated in Figure 7.78.

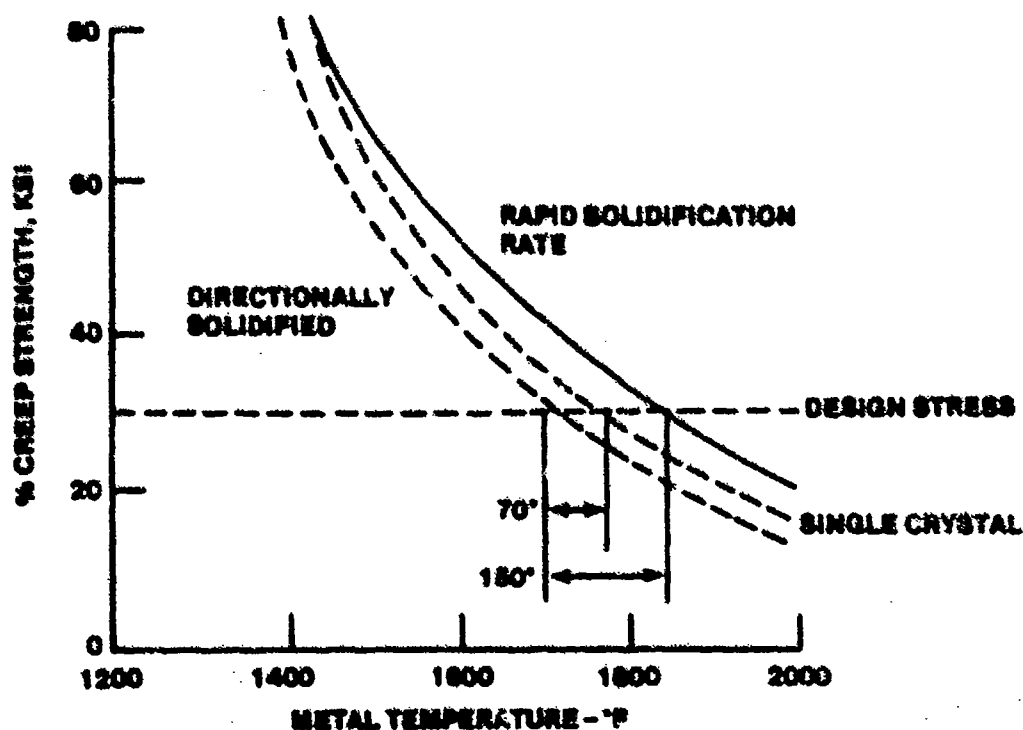


FIGURE 7.78. IMPROVEMENT IN TURBINE BLADE TEMPERATURE LIMITS DUE TO IMPROVED METALLURGICAL TECHNIQUES

Some manufacturers are presently investigating the use of ceramic materials for use in turbine blades. While these blades hold a significant advantage over metal blades with regard to their ability to withstand high temperatures, problems associated with stresses due to centrifugal loads associated with high rotation rates open new avenues of difficulties to overcome.

7.8.5.4.2 Turbine Blade Cooling. Turbine blades can be cooled by several different methods, but basically, each method uses a cooling fluid that passes through the blade so as to keep the blade metal within safe operating limits. The fact that air-cooled blades can produce appreciable power gains makes utilization of compressor bleed air appear to be the best overall system for blade cooling. The criteria for achieving good cooling effectiveness come directly from the principles of heat transfer of a fluid in a closed duct. To attain high heat transfer rates in such a system, it is necessary to meet two basic requirements, namely, (1) flow the cooling fluid with a high Reynolds number, and (2) provide a large surface area for the heat flow path. With these points in mind, it is obvious why a finned blade is many times better than an open hollow blade. The open hollow blade does very little cooling, because a boundary layer which acts as an excellent insulator to heat transfer forms over the inner surface of the blade. The insertion of fins or tubes in the blade causes the cooling air to pass over greater surface area with high turbulence or a rubbing action, which produces a turbulent boundary layer that readily passes heat.

Another disadvantage of the open hollow blade is its structural limitation. Without fins or supporting members, the open hollow blade vibrates readily, and with large magnitude at its resonant frequency to produce a "breathing action" with consequent fatigue failure.

There are three general methods employed for blade cooling. These are the convection, impingement, and film cooling methods. A fourth method called transpiration cooling may be found in the literature, but the differences between film cooling and transpiration cooling are difficult to distinguish. The three methods discussed here are illustrated in Figure 7.79.

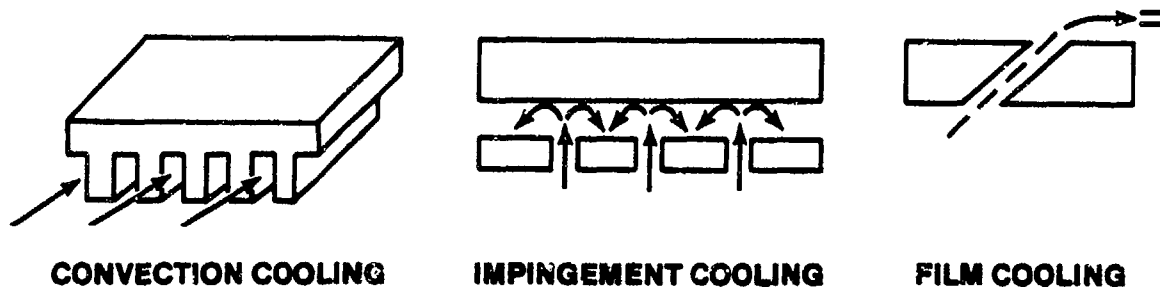


FIGURE 7.79. GENERAL TURBINE BLADE COOLING METHODS

Convection cooling is the simplest and was the first turbine blade cooling method used. With the convection cooling method, the coolant air flows outward from the base of the turbine blade to the end through internal passages within the blade. The effectiveness of convection cooling is limited by the size of the internal passages within the blade and the restriction on the quantity of cooling air available.

Impingement cooling is a form of convection cooling, but instead of the air flowing radially through one or more sections of the blade, the air is turned normal to the radial direction and passed through a series of holes so that it impinges on the inside of the blade at the area where cooling is desired. Impingement cooling is a very effective method in local areas and is easily adapted to stator blades. This method is usually employed at the leading edge of the blade where the highest temperatures are expected because of impingement of hot gases, but may be employed in any desired area.

Film cooling involves the injection of a secondary fluid, usually air, into the boundary layer of the primary fluid (hot gas). Injection of too much air into the boundary layer can defeat the purpose of increasing turbine inlet temperature. Film cooling is more effective than either convection cooling or impingement cooling. The air used for film cooling must be under high pressure because it is quickly dissipated by downstream mixing of the film air with mainstream hot gases.

The effectiveness of the three cooling methods is compared in Figure 7.80.

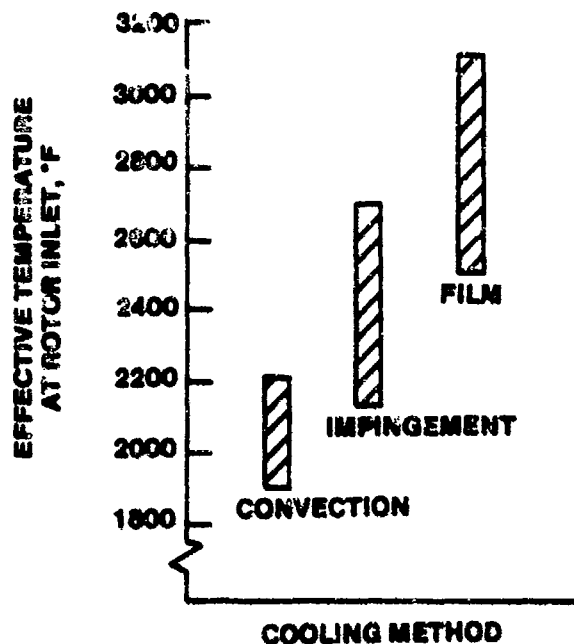


FIGURE 7.80. RELATIVE EFFECTIVENESS OF TURBINE BLADE COOLING METHODS

Like any other system which presents advantages to engine performance, there are also disadvantages incurred by cooling turbine blades. A cursory examination of the turbine blade-cooling problem leads one to think that the solution is relatively simple, that is, merely pass some compressor bleed air through hollow turbine blades, and the job is done. A more detailed study of the subject, however, will show that the overall turbine blade cooling problem is very complex. The basic problems of heat transfer in a duct are made more difficult and more complicated because the cooling air within the blades is accelerated by centrifugal forces while it absorbs large quantities of heat and the tendency for internal gas choking is present. At a given turbine inlet temperature, an engine with cooled blades suffers a definite performance loss relative to one with uncooled blades because the coolant air bled from the compressor does not take part in the combustion process, nor can it develop power in the turbine. It also requires pumping work to force it through the cooling system. Perhaps the greatest disadvantage of turbine blade cooling is cost due to complexity in fabrication. It has already been pointed out that the simple, open, hollow blades do not cool well enough; the

ones with fins, inserts, and bundles of tubes, are difficult to manufacture but do provide adequate cooling. These complex cooled blades must be manufactured properly. In addition to providing adequate cooling, they must withstand the high stresses imposed on them by centrifugal loads. The turbine rotor required for cooled blades is also difficult to manufacture. In addition to the fabrication problems, a rotor supplying cooling air is further complicated by the air-sealing problem at the section where the coolant is brought into the rotor hub.

Some advantages and disadvantages of turbine blade cooling have been discussed, and in spite of the many complexities added to the engine by a blade cooling system, the performance attractiveness is still great, especially for turboprop engines, turbojet engines for high Mach flight, and high bypass ratio turbofan engines.

Historical and expected gains in turbine inlet temperature from combined materials improvement and cooling effectiveness are shown in Figure 7.81.

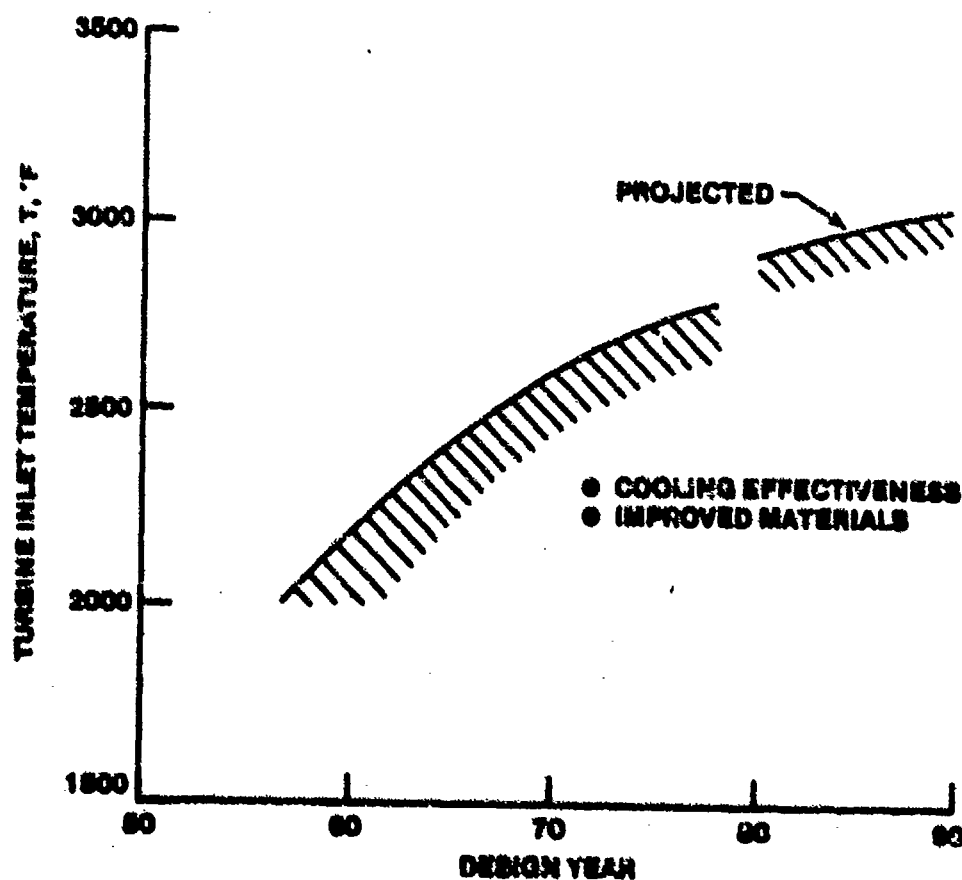


FIGURE 7.81. CHRONOLOGICAL IMPROVEMENT IN TURBINE INLET TEMPERATURE AS A FUNCTION OF TURBINE BLADE COOLING

7.8.5.5 Engine Internal Temperature Control. In the event of a malfunction or under extreme flight conditions, regulation of engine internal temperatures can be marginal or even above the desired limits. Overtemperatures can't be treated lightly. Just because the turbine does not melt away, there is no reason to assume that the engine cannot be or has not been damaged. Several momentarily high overtemperatures will have as profound an effect on the engine as a single prolonged one of a lesser degree. Excessive internal temperatures aggravate such conditions as creep, deformation of sheet metal parts, and drooping. Operating the engine within the specified limits of temperature, RPM, and turbine discharge pressure or engine pressure ratio should become an instinctive technique to the turbojet, turbofan, and turboprop pilot. Modern digital electronic controls will automatically eliminate overtemperatures without pilot attention.

7.8.6 Exhaust Duct/Nozzle

The term, "exhaust duct," applies to the engine exhaust pipe or tailpipe connecting the turbine outlet and the jet nozzle of a nonafterburning engine. Although an afterburner might also be considered a type of exhaust duct, afterburning is a subject in itself and is dealt with subsequently.

If the engine exhaust gases could be discharged directly to the outside air in an exact axial direction at the turbine exit, an exhaust duct would not be necessary. This, however, is not practical. The largest total thrust can be obtained from the engine if the gases are discharged from the aircraft at the velocity obtained when nozzle exhaust static pressure is equal to ambient pressure. This was discussed in Chapter Six. An exhaust duct is therefore added, both to collect and straighten the gas flow as it comes from the turbine, and to increase the velocity of the gases before they are discharged from the exhaust nozzle at the rear of the duct. Increasing the velocity of the gases increases their momentum and increases the thrust produced.

7.8.6.1 Convergent Exhaust Nozzle. The velocity of the gases within a convergent exhaust duct (Figure 7.82) are held to Mach 1 or less. These nozzles are used on subsonic aircraft where small performance penalties are incurred due to non-optimum expansion, but the weight and cost of a divergent nozzle is not cost effective.

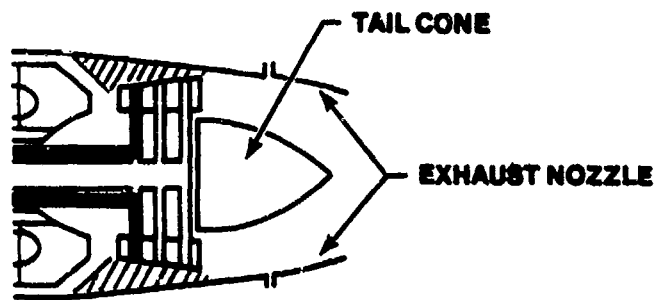


FIGURE 7.82. CONVENTIONAL CONVERGENT EXHAUST DUCT

7.8.6.2 Convergent - Divergent Exhaust Nozzle. Whenever the pressure ratio across an exhaust nozzle is high enough to produce gas velocities greater than Mach 1, more thrust can be gained by using a convergent-divergent type of nozzle (Figure 7.83). The advantage of a convergent-divergent nozzle is greatest at high Mach because it allows maximum thrust to be obtained.

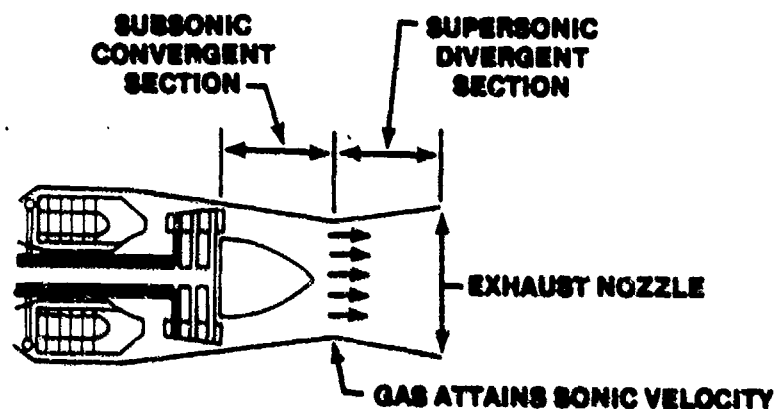


FIGURE 7.83 CONVERGENT-DIVERGENT EXHAUST DUCT (NOZZLE)

In the discussion on thrust, it was pointed out that all of the pressure generated within an engine cannot be converted to velocity.

7.8.6.3 Variable Area Nozzles. In order to obtain optimum performance, the pressure at the nozzle exhaust plane must match the ambient pressure. Recall that for a fixed area ratio, only one pressure ratio will give optimum performance. Therefore, in order to ensure a continuous pressure match over the entire flight spectrum, some method of varying the area ratio must be employed. This can be accomplished by varying either the nozzle throat area or the exit plane area.

For an engine with an afterburner, the governing flow parameter which is a constant for choked flow is

$$\dot{w} \frac{\sqrt{T_{T_8}}}{P_{T_8} A^*}$$

Looking at this relationship, we can analyze the changes that occur when the afterburner is ignited at supersonic speeds. First, mass flow rate (\dot{w}) is almost constant, increasing only by the fuel added to the afterburner which is a small fraction of the total mass flow. On the other hand, T_{T_8} goes up dramatically when the afterburner is lit. Since P_{T_8} changes little in the afterburner nozzle, A^* must increase to keep the flow parameter a constant. Thus for supersonic flight, A_e/A^* must be variable to maintain optimum pressure balance for peak performance.

7.8.6.4 Two-Dimensional Nozzles. Research is presently being conducted on the use of two-dimensional exhaust nozzles. Tests have shown that there is no degradation in thrust with a 2-d nozzle from that of the axisymmetric nozzle for a given engine.

An added benefit with a 2-d nozzle is the capability for thrust vectoring. Thrust vectoring capability would be beneficial in helping to control glidepath angle during approaches. Vectored thrust might also be useful during spin recoveries.

Thrust reverses are more easily incorporated in a 2-d system than an axisymmetric one. The 2-d nozzle system can be installed with aerodynamically clean contours and may have a more efficient cooling system than its axisymmetric counterpart.

7.8.6.5. Jet Nozzle Velocity. At the higher throttle settings and airspeeds encountered during normal aircraft operation, the nozzle throat will probably be "choked" most of the time, which means that the gases passing through the convergent section of the nozzle will be at or near the speed of sound. When the nozzle is choked, the only variation in the exit velocity of the gases will be due to changes in the engine exhaust gas temperature. Whenever the nozzle is not choked, varied atmospheric conditions will cause some change in jet nozzle velocity. As can be seen by the thrust equations, changes in the exhaust gas or nozzle velocity (V_{10}) will affect thrust.

7.8.6.6 Nozzle Efficiency. Since losses are present in an actual nozzle flow process, it is desirable to examine nozzle flow with friction. Let us

consider a nozzle which operates between a pressure at inlet, P_{T_5} , and a lower pressure at exit, P_{10} . Figure 7.84 illustrates such a nozzle with its expansion process on a T-s or h-s plane.

As pointed out previously, the function of the nozzle is to transform the high pressure-temperature energy (enthalpy) of the gases at this entrance position (Point 5) into kinetic energy. This is done by decreasing the pressure and temperature of the gases in the nozzle. Referring to Figure 7.84, it is evident that the maximum amount of transformation will result with an isentropic process between the pressures at entrance and exit. Such a process is illustrated as the Path 5-10. Now, when nozzle flow is accompanied with friction, an increase in entropy results, and the path is curved as illustrated by Line 5-10'. It is noted that the actual enthalpy change is somewhat less than the enthalpy change for an isentropic process. The difference in the enthalpy change between the actual process and ideal process is due to friction.

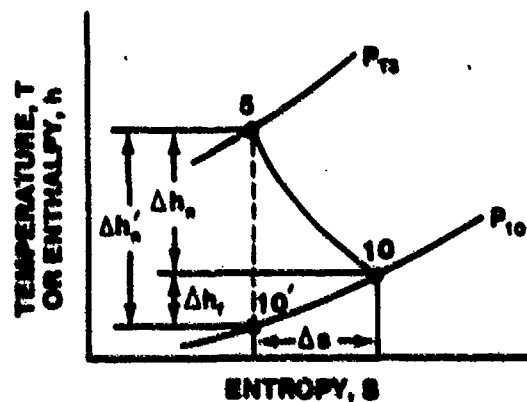


FIGURE 7.84. COMPARISON OF IDEAL AND ACTUAL NOZZLE EXPANSION ON A T-s OR h-s PLANE

Since an actual nozzle does not have as great an enthalpy drop as an ideal nozzle, the relative merits of the ideal nozzle and the actual nozzle can be compared using the ratio of the two enthalpy drops between the same pressure limits. This ratio is defined as the nozzle adiabatic efficiency and is

$$\eta_n = \frac{h_{T_5} - h_{10}}{h_{T_5} - h_{10}'} = \frac{\Delta h_n}{\Delta h_n'} = \frac{C_p(T_{T_5} - T_{10})}{C_p(T_{T_5} - T_{10}')} \quad (7.66)$$

The value of η_n for a good nozzle should be somewhere in the range of .9 to .96.

7.8.7 Thrust Augmentation

To achieve better takeoff performance, higher rates of climb, and increased performance at altitude during combat maneuvers, there has always been a demand for increasing the thrust output of aircraft powerplants for short intervals of time. In addition, a recent desire for sustained operation at supersonic speeds requires a significant increase in the thrust/frontal area output of aircraft engines. Two basic methods of providing thrust augmentation for turbojet and turbofan engines will be discussed: (1) afterburning or tailpipe burning (by far the most popular current type of thrust augmentation); and (2) water injection (either at the compressor inlet or in the combustion chamber). Each method provides a substantial thrust increase over the normal engine thrust but also requires a considerable increase in liquid consumption. Because each method produces overall engine efficiencies which are less than that of the normal engine, thrust augmentation devices should normally be operated for only short time intervals. The exception to this is for sustained supersonic operation where the only method of achieving the condition is with thrust augmentation. Each method of augmentation also makes the basic engine more complex -- additional controls are required, engine geometry is changed, and special liquids with suitable lines and controls are required. Despite these disadvantages, the requirements for thrust augmentation have provided sufficient stimulus for much development effort. This effort, which continues, has resulted in reliabilities for the thrust augmentation system essentially equivalent to the basic engine.

7.8.7.1 The Afterburner. Turbine temperature limits the basic engine fuel/air ratio to about 0.025. As a result, the gases which are exhausted from the turbine section are primarily air; thus, if a suitable burner is installed between the turbine and exhaust nozzle, a considerable amount of fuel can be burned in this section to produce temperatures entering the nozzle as high as 3500°F. The increased temperature greatly augments the exhaust gas velocity and hence provides a thrust increase.

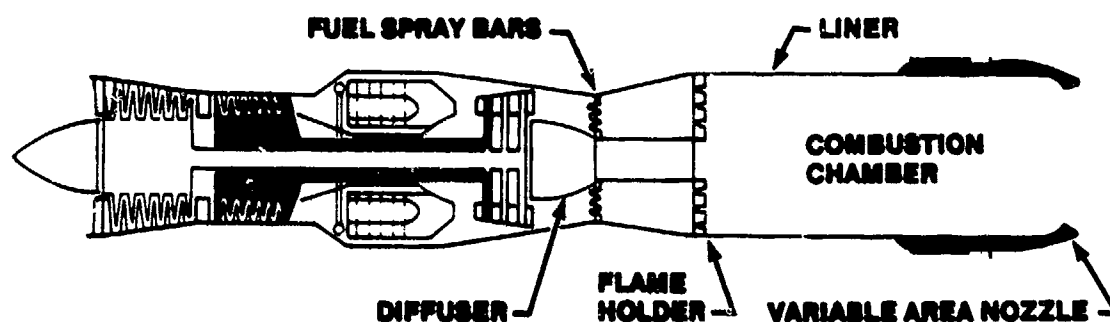


FIGURE 7.85. TYPICAL AFTERBURNING TURBOJET

Figure 7.85 shows a typical afterburning turbojet engine. The figure identifies the various afterburning components and reveals that the afterburner meets the basic requirements of the normal combustion chamber. First, the air discharging from the turbine must be slowed down to a low velocity so that combustion can be stabilized. To decrease the air velocity adequately, a diffuser section known as the turbine discharge diffuser, is placed between the turbine and the burner section (note the gradual area increase between the afterburner wall and the tail cone downstream of the turbine). Fuel is injected through a spray nozzle system which produces a mist that will thoroughly mix with the air.

Provisions must also be made for igniting the fuel-air mixture. Ignition is accomplished either by spark igniters which function in the same manner as in the normal burner or by the so-called "hot streak" method. The latter scheme requires that a small-diameter, high-velocity fuel stream be squirted from the main combustion chamber through the turbine blades into the afterburner. This small fuel stream, literally a hot streak, is ignited in the main burner and its flame volume increases progressively as it flows into the afterburner where it ignites the fuel-air mixture. The turbine blades are not overheated by the hot streak because of its relatively low energy content, and since a portion of the fuel vaporizes in the fuel stream, some cooling is provided; furthermore, the hot streak is operated only briefly.

To maintain a flame after ignition is accomplished, the afterburner requires the equivalent of the primary combustion zone in the normal burner. This is accomplished by a series of so-called "flame holders", which are usually V-shaped gutters mounted concentrically about the longitudinal axis of the burner.

To allow time and space for good combustion, the afterburner must contain a volume which is considerably larger than the normal combustion chamber. This extra volume requirement is necessary, because the after-burner consumes up to three times as much fuel as the normal burner. In general, when an afterburner is added to an engine, the overall engine length is about doubled. External cooling can be accomplished by producing airflow between the afterburner and aircraft structure. Insulating blankets may also be wrapped around the outer shell to provide an additional restriction to heat flow.

7.8.7.1.1 Afterburner Performance. It was mentioned that it is necessary to increase the nozzle area when the afterburner is operating. It is desirable to examine the reasons for the necessity of increasing the nozzle exit area. Assume that an afterburner engine is initially operated nonafterburning with full-throttle conditions (military thrust) so that the nozzle flow is choked. When the afterburner is turned on, each pound of air passing through the afterburner grows in volume by a factor of about two because of the increase in temperature. Therefore, in order not to reduce the mass flow rate through the nozzle, the nozzle must be opened to compensate for the increased gas volume.

A good afterburner installation is one which produces no uncalled for changes in the operating conditions of the basic engine components when the afterburner is turned on and off; that is, the basic engine should not be able to feel the difference between afterburner and nonafterburner operation.

Figure 7.86 shows the cycle diagram of a turbojet engine equipped with afterburner on the h - s plane. The process lines up to the turbine section are the same as for a basic engine. The afterburner process 5-6 is ideally a constant pressure process, but the internal drag losses and momentum pressure loss produce a total pressure drop such that P_{T_6} is about 5% less than P_{T_5} . It is apparent that more thrust can be realized per pound of air by examining

the relative magnitude of the enthalpy drops across the normal nozzle 5-ef (see dotted line) and across the afterburner nozzle 6-ef.

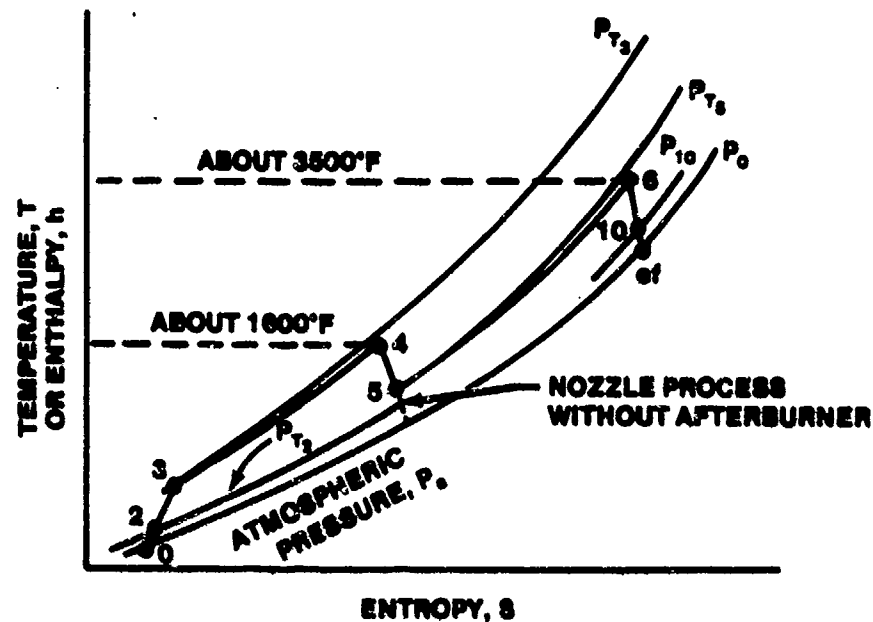


FIGURE 7.86. h-s DIAGRAM OF A TURBOJET ENGINE WITH AFTERBURNER

Afterburner performance is normally expressed in terms of the ratio of augmented thrust (thrust available with afterburner on) to military thrust without afterburner. Expressing this ratio in terms of gross thrust

$$\frac{(F_G)_a}{F_G} = \left(\frac{(w_{10})_a}{w_{10}} \right) \left(\frac{(V_{10})_a}{V_{10}} \right) \quad (7.67)$$

where subscript a refers to the augmented condition.

Table 7.13 summarizes the characteristics of some current U.S. and British afterburning turbojet engines.

TABLE 7.13

CHARACTERISTICS OF SOME CURRENT U.S. AND BRITISH
AFTERBURNING TURBOJET ENGINES

Engine Designation	Manufac- turer	Afterburner			Weight (lb)	Diameter (in.)	Length (in.)
		Afterburner Takeoff Thrust (lb)	On Takeoff sfc (lb/hr/lb)	Off Takeoff Thrust (lb)			
J85-GE-5	G.E.	3850	2.20	2500	538	20	104
J79-GE-8	G.E.	17000	2.00	12000	3630	32	208
J57-P-20	P. & W.	18000	2.35	10700	4750	40.5	267
J75-P-19W	P. & W.	26500	2.20	16100	5960	43	259
J58-P-2	P. & W.	32000	—	25500	7000+	45	—
YJ93-GE-3	G.E.	30000	—	—	5800+	52.5	237
Olympus 201R	B.S.	24000	—	17000	4550	42	354
Orpheus 12SR	B.S.	8170	1.62	6740	1560	32	181
Gyron Jr.	D.H.	14000	1.80	10000	3100	32	191
Avon (300)	R.R.	16600	2.0	12500	3800	42	256

*G.E. - General Electric; P. & W. - Pratt & Whitney; B.S. - Bristol-Siddeley; D.H. - DeHavilland; R.R. - Rolls-Royce.

7.8.7.1.2 Afterburner Screech Liners. Afterburners are occasionally subject to a type of combustion instability known as "screech". Screech is a condition of periodic, violent pressure fluctuations in the afterburner duct, resulting from cyclic vibration due to unsteady release of combustion energy. Cyclic vibration is a pressure variation of high frequency, 400 - 600Hz, and intensity, which can sometimes attain destructive proportions. Screech is characterized by intense noise. When screech occurs, heat transfer rates and temperatures of the afterburner parts increase greatly. Moderate to severe screech can cause rapid deterioration or failure of the flameholders or the afterburner duct. Screech is controlled by placing so-called "screech liners" in the duct. These are inner steel sleeves which are literally perforated by thousands and thousands of small holes. The special design of the sleeves tends to absorb the periodic, combustion-energy fluctuations, and to prevent random pressure fluctuations from developing into cyclic vibrations of large amplitude.

7.8.7.1.3 Rumble. With the introduction of the mixed-flow augmentor in turbofan engines, a type of low frequency instability known as rumble or chugging became a serious problem. Rumble is a periodic afterburning combustion instability (pressure oscillations fed by the combustion process) usually occurring at high fuel-air ratios at flight Mach and altitude when low duct inlet air temperatures and pressure exist. This instability usually leads to afterburner blowout and/or fan surge and engine stall. The frequency of oscillation usually lies between 30 and 200 Hz.

Even subtle changes in flameholder designs have altered the rumble characteristics of a turbofan engine. With some experience at hand, the design engineer has successfully produced "fixes" for unstable conditions. Redistribution of the fuel-to-air mixture ratio has worked, and deriching the fan duct has lessened rumble problems in the past.

As a result of analytical and experimental efforts, the following major conclusions have been reached:

Rumble was identified as a system problem in which the airflow dynamics couple with the combustion process.

Experimental rig tests identified fuel distribution as a rumble contributor.

The most significant driver of rumble is the falloff in combustion efficiency as fuel-air ratio is increased.

The variations of augmentor efficiency caused by pressure, velocity, and temperature were identified as minor rumble drivers.

7.8.7.2 Water Injection. The sensitivity of gas turbine engines to compressor inlet temperature results in appreciable loss of thrust available for takeoff on a hot day. It is frequently necessary, therefore, to provide some means of thrust augmentation for non-afterburning engines during takeoff on warm or hot days. Ten to thirty percent additional thrust (power) can be gained by injecting water into the engine, either at the compressor air inlet or the combustor inlet.

When water is added, thrust or power augmentation is obtained principally by cooling the air entering the engine by means of vaporization of the water introduced into the airstream. Cooling the air has the effect of reducing the compressor inlet temperature. The reduction in temperature increases the air

density and the mass airflow. More and cooler air to the combustors permits more fuel to be burned before limiting turbine inlet temperatures are reached, which, in turn, means more thrust.

7.8.7.3 Summary of Thrust Augmentation Devices. Table 7.14 presents a summary of the augmented thrust ratios and specific liquid consumptions obtainable from typical turbojet engines. Remarks are included in the table to summarize the application and limitations of the various thrust augmentation devices.

TABLE 7.14

SUMMARY OF PERFORMANCE DATA OF TYPICAL
THRUST AUGMENTATION DEVICES

Method	Thrust Ratio and Liquid Con- sumption	Sea Level		35,000 Feet		Remarks
		M=0	M=2.0	M=0	M=2.0	
Afterburner	F_{n_a} / F_n	1.5	3.0	1.5	2.5	Limited by stoichiometric mixture or thermal choking.
	slc	2.4	2.4	2.0	2.2	In service use on an extensive basis.
Water in- jection at compressor inlet	F_{n_a} / F_n	1.4	2.6	1.2	2.0	Requires separated liquid. Limited by air saturation at compressor outlet. In service use on limited basis, primarily for thrust restoration at take-off.
	slc	3.2	9.0	2.4	6.0	
Water in- jection into combustor	F_{n_a} / F_n	1.3	2.4			Not practical on engines operating near stall line.
	slc	8.0	15.0			Limited by compressor stall. In service use on limited basis.

7.9 OVERALL ENGINE ANALYSIS

The individual components of gas turbine engines have been discussed in detail. To summarize, it might be beneficial to examine the variation of gas properties throughout the overall engine. Figure 7.87 is a sketch of a typical axial flow turbojet engine showing the variation of T , T_T , P , P_T , V , and thrust force through each engine component.

The figure applies to an in-flight condition where the diffuser develops a positive pressure rise. Thrust force variation is shown below the engine - positive slopes indicate that forward thrust forces act on the engine, and conversely, negative slopes indicate rearward thrust forces. For example, the axial flow compressor receives a forward thrust force which increases in magnitude as the flow progresses through the stages. The unbalanced engine force, labeled F_n , is the net force that is delivered to the airframe for propulsion.

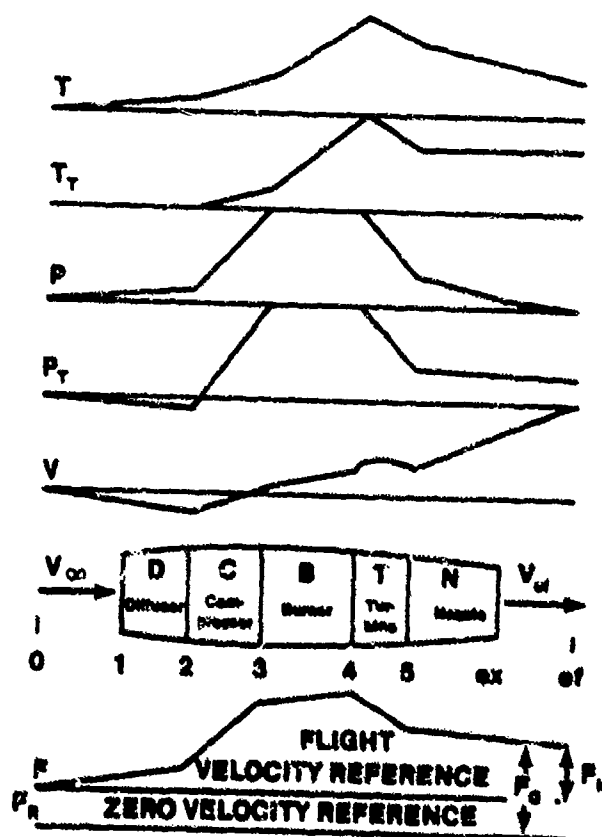


FIGURE 7.87. VARIATION OF GAS PROPERTIES THROUGH A TURBOJET ENGINE DURING FLIGHT

Figure 7.88 shows an enthalpy-entropy diagram for a real engine with reasonable irreversible effects and typical temperatures, for a compressor pressure ratio of ten. Afterburning and non-afterburning processes are shown, with the exhaust pressure equal to ambient pressure in both cases.

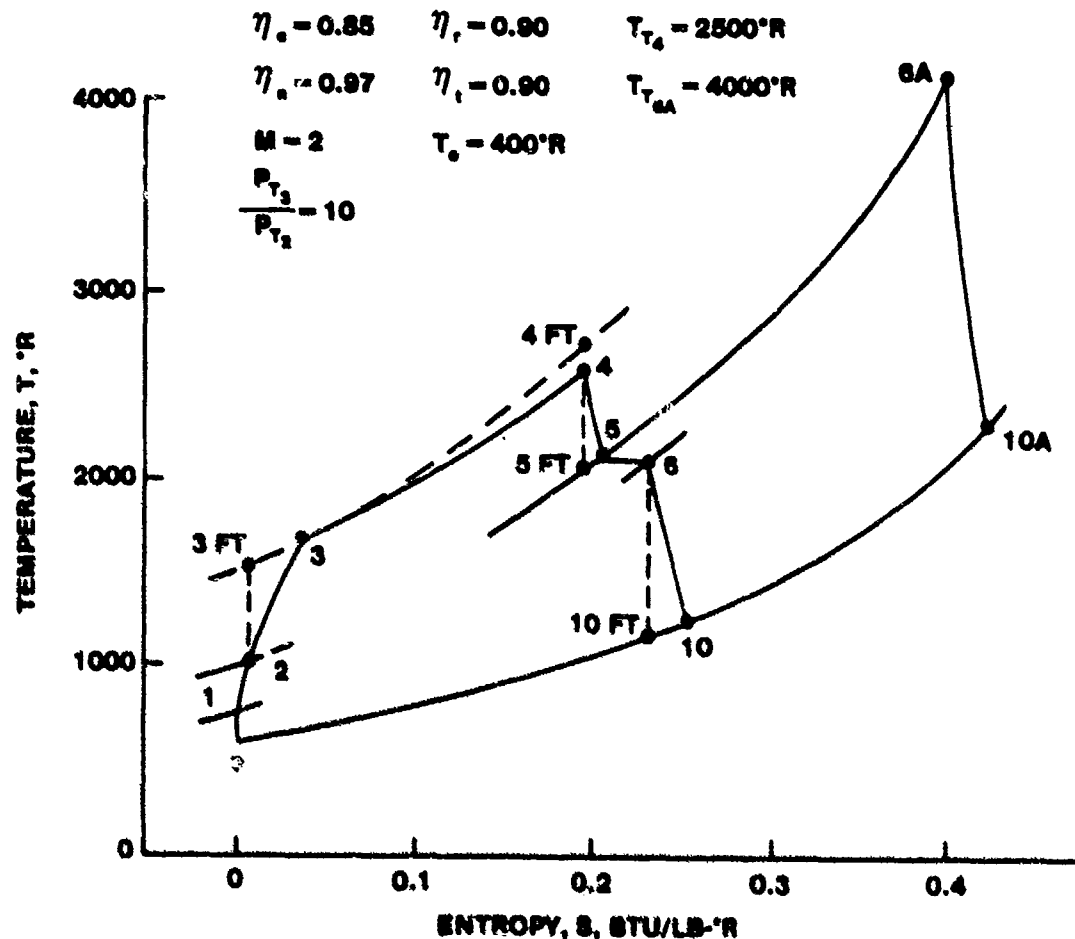


FIGURE 7.88. T-s DIAGRAM FOR TYPICAL TURBOJET ENGINES

The process begins with atmospheric air at h_0 , P_0 . By virtue of the relative (flight) velocity between the air and the engine, this air has a stagnation enthalpy h_{T_0} , higher than h_0 . Further, since no work or heat transfer occurs between 1 and 2, the stagnation enthalpy is constant through Station 2. The air is externally decelerated from 0 to 1. For all practical purposes this external deceleration is an isentropic process (unless an

external shock occurs), hence State 1 is on an isentrope with State 0 and $P_{T_1} = P_{T_0}$. From 1 to 2 the air is further decelerated, accompanied by an increase in entropy though frictional effects. Note that this results in a decrease in stagnation pressure. From 2 to 3 the air is compressed, again with an increase of entropy due to irreversibilities in the compression process. State 3' is defined as that state which would exist if the air could be compressed isentropically to the actual outlet stagnation pressure. State 3 is the actual outlet stagnation state.

From Station 3 to Station 4, some fuel is mixed with the air and combustion occurs. Strictly speaking, the fluid composition changes between these stations, and a continuous path between them should not be shown. However, since the fluid characteristics do not change markedly, there is no difficulty in showing the two substances on different portions of the same diagram. The stagnation pressure at 4 must be less than at 3 because of fluid friction, and also because of the drop in stagnation pressure due to heat addition at finite velocity. As we shall see later, it is advantageous to make T_{T_4} as high as material limitations will allow.

From 4 to 5, the fluid expands through the turbine, providing shaft power equal to the shaft power input to the compressor (plus any mechanical losses or accessory power). Since no work or heat transfer occurs downstream of Station 5, the stagnation enthalpy remains constant throughout the rest of the machine. State 6 depends on the geometry involved, but P_{T_6} must be less than P_{T_5} . The exhaust pressure P_{10} generally equals the atmospheric pressure P_0 , but it may be different if the exhaust flow is supersonic. If the afterburner is operative, the fluid is raised in temperature to State 6A, after which it expands in the nozzle to State 10A.

Again it can be seen that the exhaust kinetic energy is the relatively small difference between the total available enthalpy drop from State 4 and the compressor work input. For a given compressor-pressure ratio, irreversibilities increase the compressor power requirement while at the same time increasing the necessary turbine pressure drop. Both effects decrease the exhaust kinetic energy, so that overall performance may be expected to be very sensitive to compressor and turbine performance.

7.9.1 Effect of Humidity on Engine Performance

Humidity affects turbojet and turboprop engine performance because the mixture of water vapor and air has gas properties which differ slightly from those of dry air. The primary reason for this difference is the fact that water vapor is lighter than air. This is evident from their relative molecular weights: $H_2O = 18$, and air = 29.0. However, even at 100% relative humidity, the effect on engine performance is only about 1%. Many Flight Manuals give the method for correcting for humidity in those cases where extreme accuracy is desired.

7.9.2 Thrust Horsepower

Thrust horsepower is defined as the rate of doing work. Therefore thrust horsepower can be expressed as

$$THP = F_n V_0 \quad (7.68)$$

The units of the above equation are ft lb/sec. Care must be taken to convert horsepower units depending on the units in which velocity is given for a particular calculation.

For the propulsion of aircraft, thrust horsepower is used to overcome drag. When the maximum thrust horsepower is equal to the power required for steady level flight, the maximum velocity for a particular engine-aircraft combination is achieved.

7.9.3 Specific Impulse

Specific impulse is another term for measuring fuel and thrust efficiency. It is generally used for rockets, but occasionally used for turbine engines. Specific impulse is defined as the ratio of thrust to fuel consumed, i.e., $I_s = F_n / \dot{w}_f$, and is the reciprocal of thrust specific fuel consumption. High pressure cryogenic rocketry provides I_s in excess of 400 sec. The \dot{w}_f for a rocket includes both fuel and oxidizer since there is no compressor. For comparison, a jet engine with a tsfc of 0.5 would have an $I_s = 1/0.5 \text{ hr} = 2 \times 3600 \text{ sec/hr} = 7200 \text{ sec}$. or 18 times better than a rocket. Therefore, vehicles operating in the atmosphere for any flight duration should obviously use the air for an oxidizer.

7.10 ENGINE OPERATIONAL CHARACTERISTICS

The foregoing sections have described the features of the three basic, gas turbine engine types: the turbojet, the turboprop and the turbofan. Particular attention has been given to the turbojet because this is the most common configuration. Less has been said about the operational characteristics of the other two engine types or the particular use to which each is best suited. Like engines of all types, each of the three engine configurations has limitations and advantages.

7.10.1 Advantages and Disadvantages of the Turbojet

Because the efficiency of the straight turbojet is sustained at high altitude and high airspeed, engines of this type are ideal for high-flying, high-speed aircraft that operate over a sufficient range to make the climb to their best operating altitude worthwhile. Exceptionally high thrust at low airspeed is not a turbojet characteristic. Hence, aircraft powered with these engines require a relatively long takeoff roll or a low wing loading. Turbojet thrust specific fuel consumption (TSFC) is higher than that of a turboprop or turbofan; this disadvantage decreasing as the altitude and airspeed increase. In addition to their high-speed capabilities and the very high altitudes at which they can operate, axial compressor turbojet engines present a relatively small frontal area. The smaller diameter of the frontal area of a turbojet, however, does not necessarily mean less drag in flight, because the large frontal area created by a propeller or fan does not produce a proportionally high parasitic drag when turboprop or turbofan engines are operating. Nevertheless, the small diameter does mean that turbojet engine-nacelle ground clearance is less of a problem to the aircraft designer than in some aircraft, particularly when it is necessary that an engine be mounted in a pod beneath a wing.

7.10.2 Turboprop Characteristics

A turboprop engine has some fundamental characteristics which make it quite different from a turbojet from the standpoint of the pilot.

A turboprop engine combines the advantages of a turbojet engine with the propulsive efficiency of a propeller. The turbojet engine derives its thrust

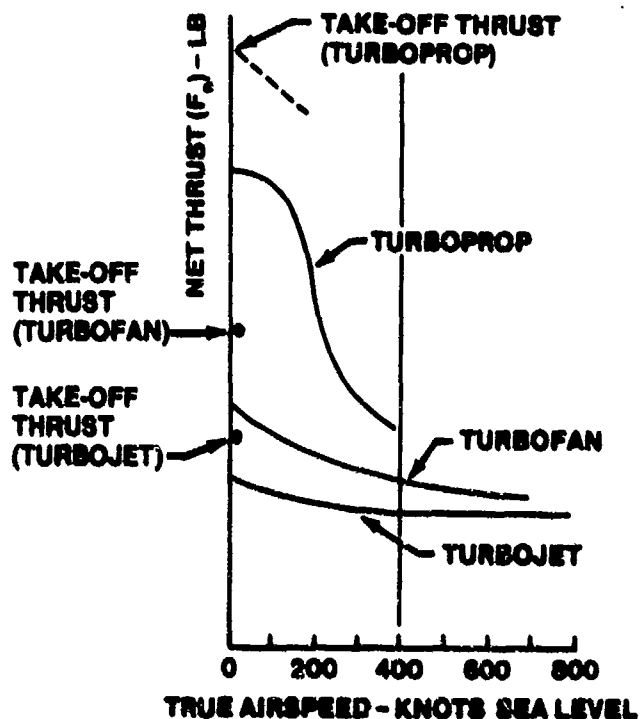
by a rapid acceleration of a relatively small mass of air. The turboprop develops propulsive force by imparting less acceleration to a relatively small mass of air. The turbine of a turbojet engine extracts only the necessary shaft horsepower to drive the compressor and the accessories. The turbine of a turboprop is designed to absorb large amounts of energy from the expanding combustion gases in order to provide not only the power required to satisfy the compressor and other components of the engine, but to deliver the maximum torque possible to a propeller shaft, as well. Propulsion is produced through the combined action of a propeller at the front and the thrust produced by the unbalanced forces created with the engine that result in the discharge of high-velocity gases through a nozzle at the rear. The propeller of a typical turboprop engine is responsible for roughly 90% of the total thrust under sea level, static conditions on a standard day. This percentage varies with airspeed, exhaust-nozzle area and, to a lesser extent, temperature, barometric pressure and the power rating of the engine. The power supplied to the propeller is measured as shaft horsepower (shp), to which must be added the effect of jet thrust when the total power output or equivalent shaft horsepower (eshp) of a turboprop engine is calculated.

Although some turboprop engines employ a compressor of the centrifugal type, larger, high-performance models almost invariably require the greater efficiency and higher compression ratios attainable only with an axial flow compressor. The compressor may be either of a single or dual rotor design; the latter having both a low pressure compressor and a high pressure compressor. When a single compressor is used, the propeller reduction and drive gear is usually connected directly to the compressor shaft, and, when a dual, or so-called split, compressor is used, it is connected to the low pressure rotor. Sometimes, the propeller is driven independently of the compressor by a free turbine of its own.

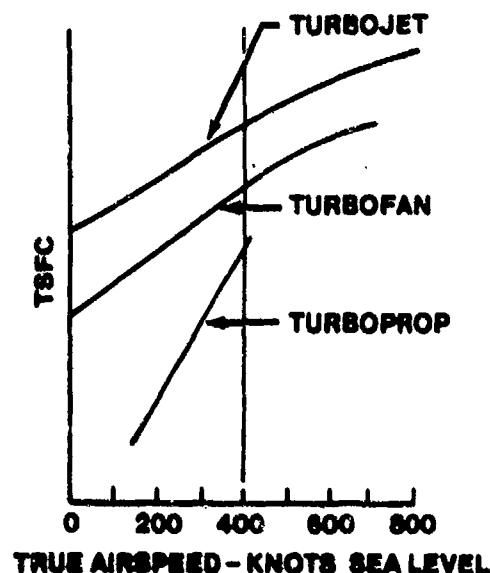
In spite of the fact that it is more complicated and heavier than a turbojet engine of equivalent power, the turboprop will deliver more thrust up to moderately high subsonic speeds (Figure 7.89a). This advantage decreases as airspeed increases. In normal cruising speed ranges, the propulsive efficiency of a turboprop remains more or less constant, whereas the propulsive efficiency of a turbojet increases rapidly as airspeed increases. The spectacular performance of the turboprop during takeoff and climb is the

result of the ability of the propeller to accelerate a large mass of air at relatively low flight speed.

If it is assumed that the fuel flow of a turbojet and a turboprop of approximately the same size will be substantially the same under similar conditions, it follows that the one delivering the most thrust will have the lower TSFC. Because of its propeller, this will be the turboprop version of a basic gas generator. The TSFC for a turbofan version of the same gas generator will fall between the TSFC for the turboprop and the TSFC for a turbojet (Figure 7.89b).



7.89a. COMPARATIVE NET THRUST AT SEA LEVEL



7.89b. COMPARATIVE THRUST SPECIFIC FUEL CONSUMPTION

The turboprop attains its most economical operation at a somewhat lower airspeed than a turbojet of equivalent power. Usable power at a high efficiency is produced only when the engine is operating within a narrow range of high RPM. The efficiency of a vane-type compressor, whether centrifugal or axial, is dependent upon high RPM. Progressively larger amounts of turboprop power are obtained by increasing the propeller blade angle and fuel flow rather than by increasing RPM.

Figure 7.90, portraying typical turboprop performance as it relates to throttle setting, gives an indication of what to expect when this type of engine is operated. The curves, as presented, are more or less representative of the characteristics of a Pratt & Whitney Aircraft PT2 or T34 turboprop engine. The curves will change somewhat when different fuel controls are used. Typical curves for other turboprop engines (the RPM curve, in particular) will not be the same, although they, in all probability, will reflect the same general engine characteristics.

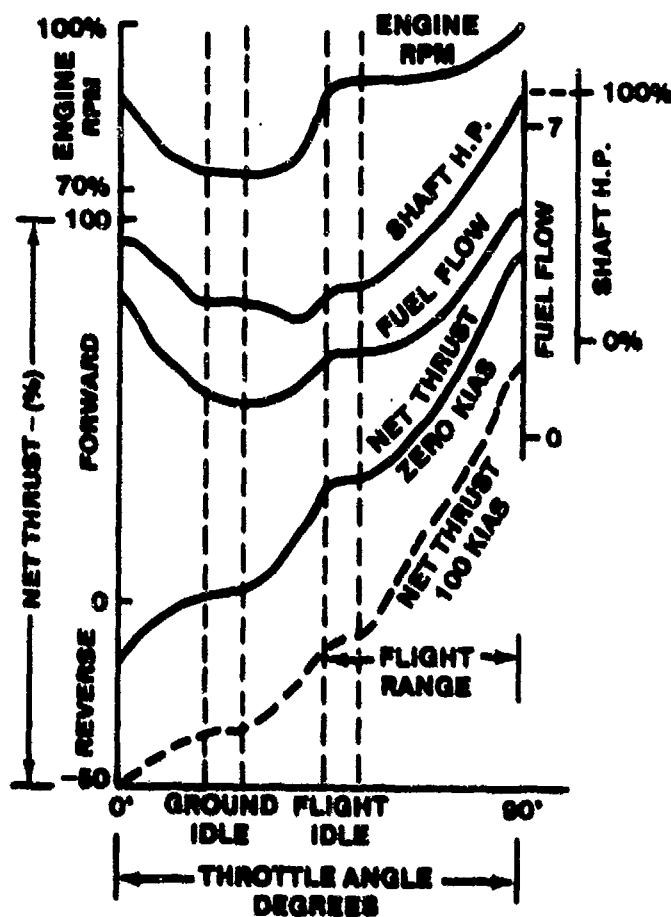


FIGURE 7.90. TYPICAL P & WA PT2 OR T34 TURBOPROP PERFORMANCE

7.10.2.1 The Turboprop Propeller. The propeller of a turboprop engine retains most of the essential features common to those employed on large piston engine installations. Both hydromechanical and electrically controlled propellers are in current use. From an operational standpoint, the differences between the two types are minor.

The fuel control operates in conjunction with a propeller governor in a turboprop engine. The propeller and engine RPM are mechanically governed in the flight operating range. In the Beta or ground operating range, propeller pitch varies with throttle position. Propeller blade angles from full feather to full reverse pitch may be obtained throughout the entire range of operating RPM. Because of the high RPM of a gas turbine engine, a reduction gear arrangement, is usually used.

The blades of a turboprop propeller must have very rapid pitch-changing characteristics. The narrow RPM operating range of the engine requires that the propeller blades change angle at a much more rapid rate than is required in the case of the reciprocating engine. The blades of a turboprop propeller must change from about 5° to 45° in only 10% of the RPM range (Figure 7.91). Translated into flight-operating-technique, this means that the turboprop engine is very sensitive to throttle movement.

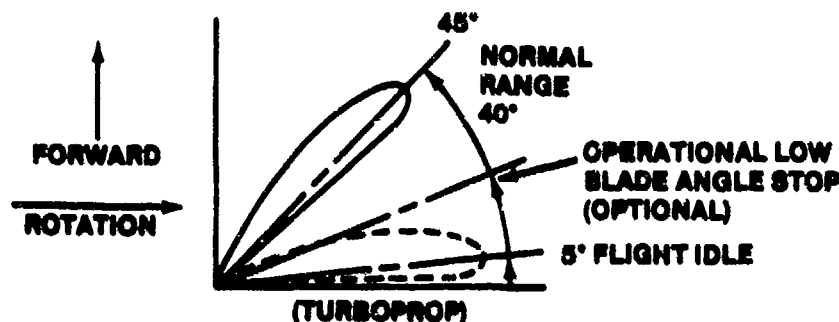


FIGURE 7.91. PROPELLER BLADE ANGLE VARIATION

The turboprop propeller blade angle at Flight Idle is small (approximately 20°) during a glide at minimum power. The turboprop aircraft, consequently, can have high aerodynamic drag, provided that the fuel control and propeller governor are adjusted to provide this characteristic during glide and approach. High drag will result in a rapid rate of descent.

7.10.3 The Turbofan Engine

In principle, the turbofan version of an aircraft gas turbine is the same as the turboprop, the geared propeller being replaced by a duct-enclosed fan driven at engine speed. One fundamental, operational difference between the

turbofan and the turboprop is that the airflow through the fan of the turbofan is controlled by design so that the air velocity relative to the fan blades is unaffected by the airspeed of the aircraft. This eliminates the loss in operational efficiency at high airspeeds, which limits the airspeed capability of a turboprop engine. Also, the total airflow through the fan is much less than that through the propeller of a turboprop.

Because of its greater inlet-area, the fan draws in considerably more air than the compressor of the turbojet. However, a great deal of this air, after being compressed by the fan, is released through the fan exit ducts, completely bypassing the burner and turbine sections. This bypass air is ducted outside the basic engine because the air has already been accelerated by the fan and has therefore served its purpose of providing additional thrust; the same kind of additional thrust that would be gained from air passing through the propeller of a turboprop or reciprocating engine.

One might ask, "Why not use a conventional propeller instead of a fan?" There are two reasons. First, the engine and propeller combination in a propeller-driven aircraft commences to lose efficiency rather rapidly at airspeeds above 400 knots at cruising altitude, while turbofan engines produce thrust efficiently at the airspeeds flown by present-day commercial aircraft (Figure 7.89a). Secondly, the complexity and weight of the propeller reduction gearing and the intricate propeller governing feature of a turboprop are completely eliminated in a turbofan. The turbofan is therefore not only lighter than a turboprop, but, of even more importance, the turbofan can never be plagued by any of the malfunctions to which the propeller and its associated systems in a turboprop are sometimes susceptible. Here, then, lie the main advantages of a turbofan over a turboprop version of the same gas generator.

Ducting the fan exhaust overboard instead of through the combustion chamber enables a turbofan engine to obtain low specific fuel consumption. From the time that the air enters a turbojet engine until the burned gases leave the combustion chamber, temperatures are progressively rising. First, the compressor works on the air, raising its temperature, and then the combustion process adds energy in great quantities. To do all this, of course, takes energy which must come from the fuel burned. If the fan exhaust were passed all the way through the engine, its temperature would be greatly

increased, only later to be wasted as heat energy thrown out the engine exhaust nozzle. Not having to heat the air that passes only through the fan serves to add to the efficiency of a turbofan engine.

Like the turboprop, a turbofan accelerates a relatively large mass of air to a relatively low velocity. When large air masses are accelerated at reduced velocity, the propulsive efficiency of an engine is vastly improved. Therefore, a turbofan engine operates more efficiently and thus operates at a lower TSFC than a turbojet engine of similar size (Figure 7.92).

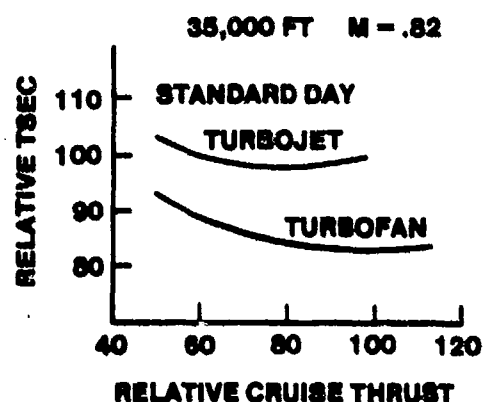


FIGURE 7.92. RELATIVE PERFORMANCE AT MAXIMUM CRUISE

A fan engine accelerates much larger quantities of air than a turbojet. This enables the turbofan to produce more thrust than a turbojet at low airspeeds, such as during climb (Figure 7.93), or even when an aircraft is standing still on the ground. This thrust increase for a turbofan in comparison to a similar basic turbojet varies as m_{TF}/m_{TJ} where m_{TF} is the mass flow rate through the turbofan engine and m_{TJ} is the mass flow rate through the basic turbojet (Reference 7.1). For this reason, an aircraft powered by turbofan engines will have more available thrust for takeoff (Figure 7.94) and therefore will not need as much distance for takeoff as will the same aircraft powered by turbojets of the same approximate size. By the same virtue, the aircraft with the turbofans can take off at a much higher gross weight than can the aircraft powered by turbojets. This feature,

combined with the much higher speed characteristics of the turbofan when compared with a turboprop, makes the engine a very attractive powerplant for passenger and cargo type aircraft, whether short or long range.

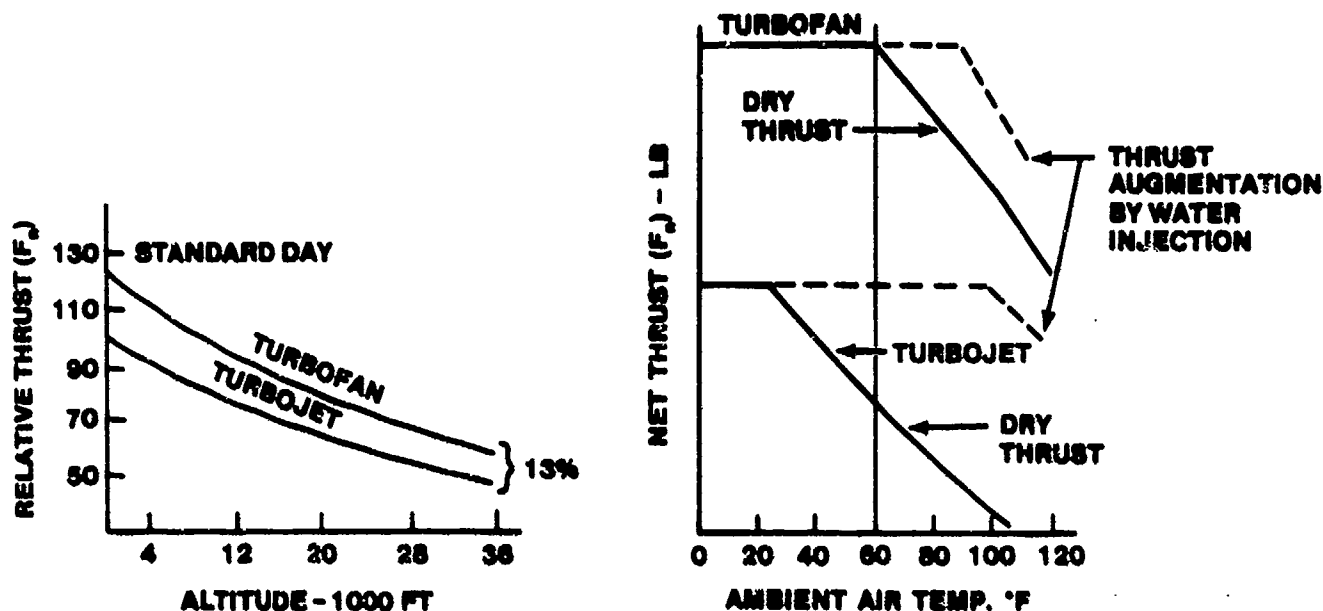


FIGURE 7.93 RELATIVE MAXIMUM-CONTINUOUS-THRUST COMPARISON DURING CLIMB

FIGURE 7.94 SEA LEVEL STATIC TAKEOFF THRUST

Still another advantage of the turbofan is a lower engine noise level. This is because the velocity of the gases as they leave the engine tailpipe is lower than that for a turbojet engine of comparable size. The decrease in velocity is due to the fact that a turbofan engine has an additional turbine stage which extracts power from the exhaust gases to drive the fan. Less velocity results in less noise.

7.11 PROPELLER THEORY

A propeller is a device which absorbs the horsepower from the engine and generates a thrust which propels the aircraft. The propeller can be considered as a device which accelerates the air passing by it, thereby generating thrust by the rate of change of momentum, or as a rotating wing that generates a lift which is a thrust.

It is obvious from Figure 7.95 that aircraft operating at vehicle speeds less than 300 knots will be using propellers as the most efficient means of propulsion.

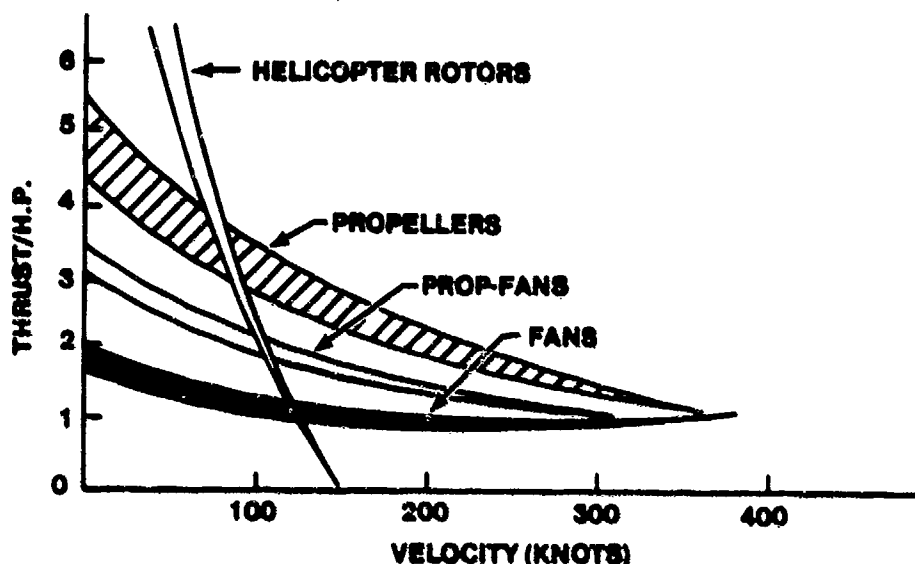


FIGURE 7.95. THRUST PER HORSEPOWER VERSUS VEHICLE SPEED

The efficiency of the various types of propulsion systems depends primarily on the disk loading of the system, which essentially means that a propulsive system is most efficient when it accelerates a large mass of air through a small velocity increment. As the mass of air decreases and the velocity increment increases, the overall efficiency decreases as is obvious from the curves in Figure 7.95. The reason that the rotor, which is very efficient at low speeds, peaks out at approximately 150 knots airspeed is because of retreating blade stall and advancing tip compressibility problems. Low disc loaded propellers of large diameter, and therefore high tip velocities, have high speed limitations due to tip Mach compressibility problems. Not only are propellers much more efficient than jets at low air speeds, but with proper design and low tip speeds, they can be much quieter.

Regardless of the type of propulsive method, the thrust is produced as a consequence of Newton's Second Law:

$$\text{Force} = \text{Mass (acceleration)} = m \frac{dv}{dt}$$

)

1



where p = Atmospheric pressure
 p' = Pressure just ahead of the actuator disc
 ρ = Density
 V = Free stream velocity
 v = Velocity increment at the actuator disc
 v_1 = Velocity increment in the wake

The change in pressure across the disc must be equal to the change in total pressure.

The thrust acting on the disc is $T = A\Delta p$

where A = Disc area

$$T = A\rho \left(V + \frac{v_1}{2} \right) v_1 \quad (7.69)$$

Newton's Second Law also applies

$$T = ma = m \frac{dv}{dt}$$

The mass per unit time = $Q = A (V + v)$

and $dv = v_1$

$$T = m \frac{dv}{dt} = A\rho (V + v) v_1 \quad (7.70)$$

Equating 7.69 and 7.70

$$A\rho \left(V + \frac{v_1}{2} \right) v_1 = A\rho (V + v) v_1$$

$$\text{or} \quad v_1 = 2v \quad (7.71)$$

which states that the change in velocity at the exit of the control volume is exactly twice the increase in velocity at the actuator disc. Substituting Equation 7.71 into Equation 7.70 yields

$$\text{Thrust } (T) = 2\rho A (V + v) v$$

The ideal or theoretical efficiency is defined as the ratio of the power output of the actuator disc to the power input.

$$\eta = \frac{TV}{T(V+v)} = \frac{V}{V+v} \quad (7.72)$$

Another useful expression will result if the wake velocity V_w is substituted for $V+v$.

$$\eta = \frac{2}{1 + \frac{w}{V}} = \frac{V}{V+u} \quad (7.73)$$

where

$$V_w = V + 2v$$

This ideal efficiency cannot be obtained in practice due to the initial assumption; however, the momentum theory can give a simple iteration on propeller operation. The actual design of a propeller or rotor requires a much more detailed analysis than the simplified momentum theory, one of the big shortcomings being that the actual shape of the propeller is not defined.

7.11.2 Blade Element Theory

The momentum theory is useful in determining theoretical maximum efficiencies but tells nothing about blade geometry and the effects of a finite number of blades with profile drag characteristics. Therefore, the blade element theory was developed; it gives more realistic results in the prediction of propeller and rotor operating characteristics. The blade element theory consists of determining the force acting on an element of the propeller blade, then integrating over the entire blade to obtain thrust and torque characteristics. The primary assumptions in the blade element theory are that uniform inflow exists, the flow is irrotational, and the blade is twisted such that each element of the blade is operating at its maximum L/D angle of attack.

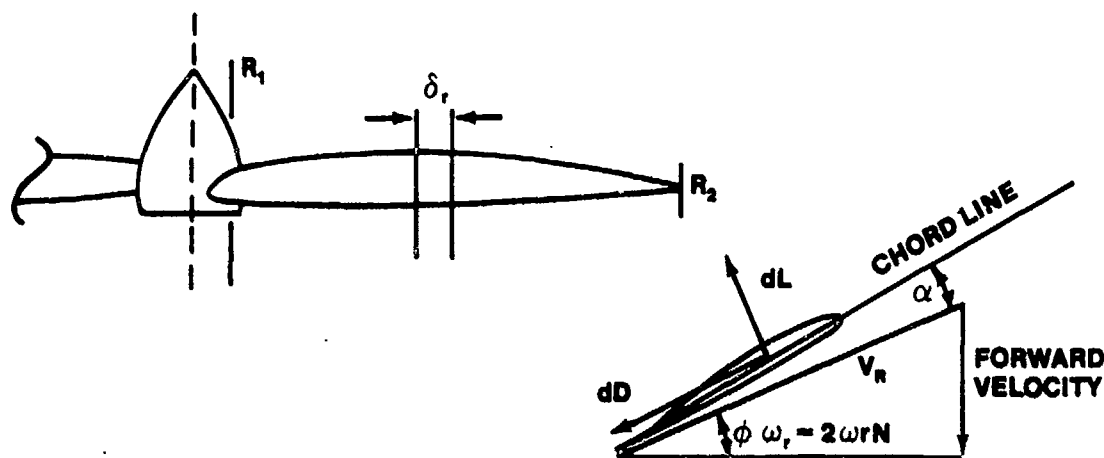


FIGURE 7.97. PROPELLER BLADE ELEMENT THEORY

The resultant velocity (V_r) that each blade element sees is the geometric sum of the aircraft forward velocity (V) and the local tangential velocity of the element (ωr) where ω = angular velocity in rad/sec and r is the radius of the element from the center of rotation (Figure 7.97).

$$V_r = \sqrt{V^2 + (\omega r)^2} \quad (7.74)$$

The blade element lift = $dL = 1/2 \rho V_r^2 (C \delta r) C_L$

where c is the average chord and C_L average lift coefficient

and the blade element drag = $dD = 1/2 V_r^2 (C \delta r) C_D$

where C_D is the average drag coefficient.

Note that the blade element lift and drag are perpendicular and parallel to the relative local free stream respectively and to convert to a thrust and a torque requires summing the component of lift and drag perpendicular and in the plane of rotation of the propeller.

The thrust component = $dT = dL \cos \phi - dD \sin \phi$

Therefore by substituting and integrating, the total thrust (T) can be determined

$$\text{Thrust (T)} = N \int_{R1}^{R2} \frac{1}{2} \rho V_R^2 (C_L \cos \phi - C_D \sin \phi) dr \quad (7.75)$$

Similarly, the total torque required to drive the propeller at the angular velocity necessary to develop the torque (Q) is

$$\text{Torque (Q)} = N \int_{R1}^{R2} \frac{1}{2} \rho V_R^2 cr (C_L \sin \phi + C_D \cos \phi) dr \quad (7.76)$$

The above blade element theory gives results with the accuracy compromised by the basic assumption of irrotational, uniform inflow and optimized twist distribution.

7.11.3 Vortex Theory

The vortex theory using the technique of finite wings computes the induced flow velocities at each radial station rather than assuming uniform inflow. More exact theories have been developed by Goldstein and Theodorsen which account for tip loss, nonuniform blade twist distribution, and interference losses. The computer time required to perform the above vortex theory computations is extensive in comparison to the relatively small increase in predicted propeller performance accuracy.

Figure 7.98 gives a comparison between the calculated and the actual thrust distribution on a propeller blade. It can be seen that the difference primarily occurs on the inner one-third of the blade where it is difficult to achieve the necessary blade twist distribution to generate lift. Figure 7.98 shows that only the outer two-thirds of a propeller blade generates thrust and the inner one-third is there to provide attachment to the shaft. Designers try to minimize the drag of the inner one-third to prevent reverse flow, improve engine cooling, and reduce the torque required. Due to the fact that propellers often operate in proximity to engine nacelles and other parts of the airframe, etc., as well as problems with simple accurate prediction methods, light aircraft propeller manufacturers operate from past experience, NACA propeller charts, and black art.

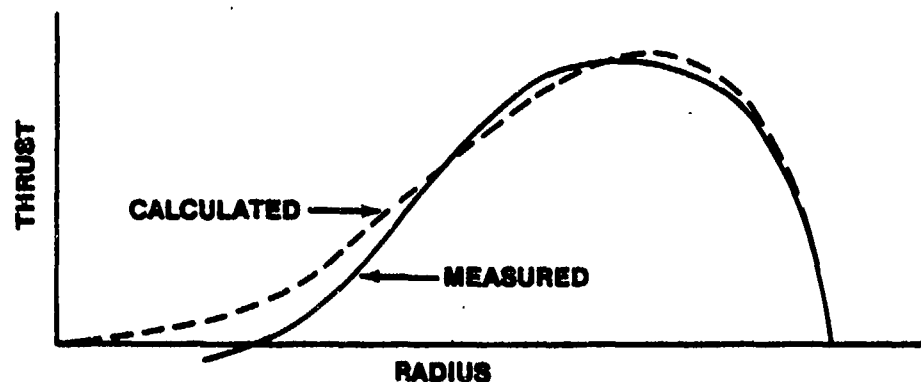


FIGURE 7.98. COMPARISON OF CALCULATED AND MEASURED THRUST DISTRIBUTION ON A PROPELLER BLADE

The above thrust distribution is good for one combination of free stream velocity and propeller RPM and assumes that each blade element is twisted to achieve its optimum L/D ratio. It is obvious that if either the RPM or free stream velocity changes, the propeller advance ratio, (J), where

$$J = \frac{V}{N D} = \frac{\text{Free Stream Velocity}}{(\text{RPM}) (\text{Diameter})} = \text{Advance Ratio}, \quad (7.77)$$

changes. Therefore, for a propeller with a fixed pitch, the thrust to torque ratio will be non-optimum, and the propeller efficiency will decrease. Similarly if a propeller is designed for a certain advance ratio and horsepower, increasing the horsepower driving the propeller will require either increasing the propeller RPM, which may cause tip compressibility problems, or increasing the blade pitch angle to absorb the horsepower. Increasing the blade pitch angle means that each blade element is not at the optimum L/D angle of attack and the propeller efficiency will decrease.

Another method of absorbing more horsepower with a propeller is to increase the propeller diameter. Besides running into tip compressibility problems, the diameter is limited by ground and airframe clearance problems. Increasing the number of blades increases the problem of hub design, enlarges the hub diameter, and creates large aerodynamic interference problems between

blades. Five blades seem to be the maximum operationally feasible number. Counter-rotating propellers are capable of absorbing large amounts of horsepower at reasonable diameters as there is more blade area. An additional benefit from the use of counter-rotating propellers is the lack of rotating slip stream and the lack of an out of balance torque on the aircraft. To have an equal amount of horsepower absorbed by both counter-rotating propellers, the rear propeller must be set at a slightly finer blade angle (approximately $1-1/2^\circ$) to allow for the slip stream of the front propeller. The disadvantages of counter-rotating propellers are weight, complexity and cost, and their non-availability for general aviation use.

7.11.4 Propeller Performance

To obtain an understanding of the factors that influence propeller performance, the laws of similitude will be applied, i.e., since a propeller is a rotating airfoil, the laws of airfoils will be applied:

Airfoils: Force = (Dynamic Pressure) (Area) (Coefficient of Lift)

(At constant angle) $(1/2 \rho_0 V_e^2)$ (S) (C_L)

Propellers: Force = (Dynamic Pressure) (Area) (Coefficient of Thrust)

$(1/2 \rho (ND)^2)$ $(D)^2$ (C_T)

(thrust)

where

D = Reference Length

D^2 = Reference Area

ND = Reference Velocity

Note that all of the constants have been dropped in the above referenced dimensions.

Therefore propeller thrust (T) = $\rho (ND)^2 D^2 C_T$

$$T = \rho N^2 D^4 C_T \quad (7.78)$$

The factor 1/2 is included in the thrust coefficient C_T and is not carried around as it is in airfoil aerodynamics. From the above equation it

is clear that the thrust generated by the propeller is a very powerful function of propeller diameter.

Similarly, propeller torque is a thrust multiplied by an additional reference length D .

$$\text{Propeller torque (Q)} = \rho N^2 D^4 C_Q (D) = \rho N^2 D^5 C_Q \quad (7.79)$$

where C_Q is the propeller torque coefficient

Propeller power is the propeller torque multiplied by the angular velocity, which is a linear function of the RPM (N).

$$\text{Propeller power (P)} = \rho N^3 D^5 C_P \quad (7.80)$$

where C_P is the propeller power coefficient

The coefficients C_T , C_Q , and C_P are functions of angle, Reynolds number, Mach and propeller planform shape, similar to the airfoil coefficients C_L and $C_D = f(\omega, R_e, M, \text{Shape})$.

The resultant inflow velocity is a function of both the aircraft forward velocity and the local angular velocity of the propeller, Figure 7.99.

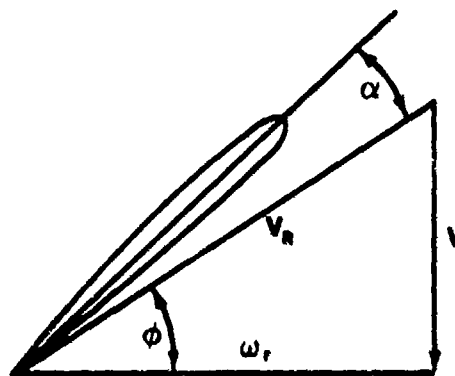


FIGURE 7.99. REPRESENTATIVE ANGLE FOR PROPELLERS

The propeller advance ratio (J) can be considered a representative angle for a propeller in a manner similar to the angle of attack (α) being used for airfoils.

$$\begin{aligned}
 \text{The propeller efficiency } (\eta) &= \frac{\text{Power Output}}{\text{Power Input}} \\
 &= \frac{(\text{Thrust}) (\text{Velocity})}{(\text{Torque}) (\text{Angular Velocity})} \\
 &= \frac{1}{2\pi} \frac{T}{Q} \frac{V}{N}
 \end{aligned}$$

and since $T = \rho N^2 D^4 C_T$ and $Q = \rho N^2 D^5 C_Q$ then,

$$\text{Propeller Efficiency} = \frac{C_T}{C_Q} \frac{V}{N D} = \frac{C_T}{C_Q} J \quad (7.81)$$

This indicates that the propeller efficiency is a function of thrust to torque ratio and propeller advance ratio which is similar to the efficiency of airfoils, i.e., the lift to drag ratio.

7.11.5 Propeller Wind Tunnel Testing

Wind tunnel testing of propellers is generally performed in special large test section wind tunnels that have reinforced test section enclosures and are equipped with large, variable speed and variable power electric motors capable of driving most propellers. The propeller thrust, torque, and power requirements are generally direct measurements from strain gauge instrumentation. The final data are plotted in the form shown in Figure 7.100.

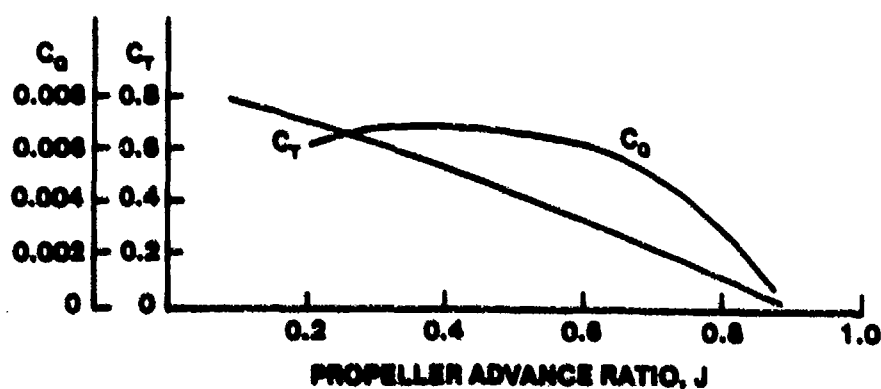


FIGURE 7.100. TYPICAL PROPELLER WIND TUNNEL RESULTS

The data presented in Figure 7.100 are not in the most useful form for aircraft designers, and often the propeller data are presented as shown in

Figure 7.101. The propeller efficiency curve is used by the aircraft designers to ensure that the condition of the local free stream at the propeller or compressor in conjunction with the propulsive RPM are sufficient to achieve the peak efficiency. The three states of the propeller are also shown in Figure 7.101: the propulsive state in which the propeller absorbs power and delivers a thrust, the brake state in which the propeller absorbs power and delivers a drag, and the windmill state where the propeller absorbs power and delivers power from the free stream and produces a drag. Many propellers, especially those in turbo propeller installations, are placarded against extended operation in the windmill state because of propeller governor, bearing oil pressure, and bearing stress problems.

The data shown in Figure 7.101 apply to the propeller at one fixed blade setting, which is the blade angle of the propeller with respect to the plane of rotation. A fixed pitch propeller has the characteristic curves presented in Figure 7.101, and peak efficiency occurs only at one advance ratio. Therefore, most fixed pitch propellers are designed for use in optimum conditions such as cruise or climb, and non-optimum conditions are accepted in other flight regimes. The ground adjustable propeller used between 1925 and 1940 was the first attempt at using one propeller and having the capability of adjusting the pitch on the ground only for the most used flight conditions. The two pitch position propeller controllable in flight is a simple two position propeller in which one position is used for takeoff and climb and the other position for the cruise flight conditions. The controllable pitch propeller, similar to the early electrically operated propellers, had an infinite number of pitch settings between mechanical stops, that could be selected by the pilot for most efficient operation in every flight regime. To efficiently operate the controllable pitch propeller, the pilot must be given sufficient data by the airframe and propeller manufacturer regarding power settings, forward speed, and engine RPM.

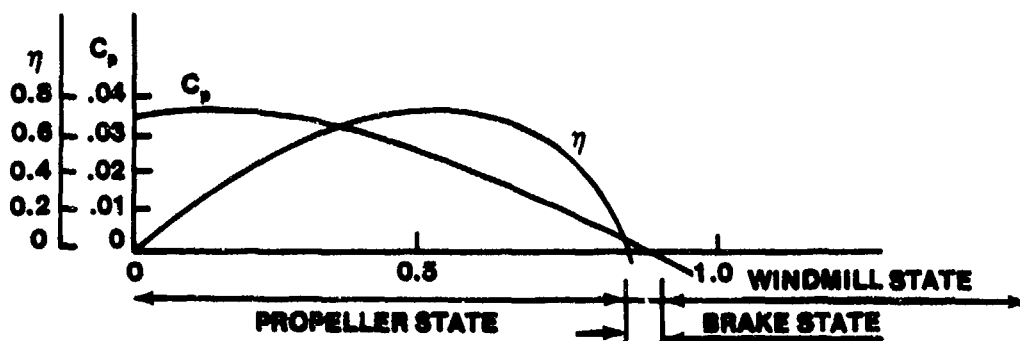


FIGURE 7.101. PROPELLER POWER COEFFICIENT AND PROPELLER EFFICIENCY CURVES

The constant speed propeller operates under the principle that the pilot sets the desired RPM on the propeller governor and uses the throttle to command the power output of the engine. Once the power is sufficient to drive the propeller to the set RPM, additional power is absorbed by the propeller at the preset RPM by changing its pitch angle automatically. The use of a variable pitch or constant speed propeller modifies the propeller efficiency curves to those shown in Figure 7.102.

Obviously, from Figure 7.102, near peak efficiency is attainable on these variable pitch propellers throughout most operating conditions encountered in flight. A comparison of the characteristics of various types of propellers is shown in Figure 7.103 for a particular engine and airframe configuration. The variable pitch and constant speed propellers deliver the most thrust throughout the complete speed range of the aircraft, and the selection of a fixed pitch propeller depends on the aircraft's mission such as cruise efficiency or glidertowing.

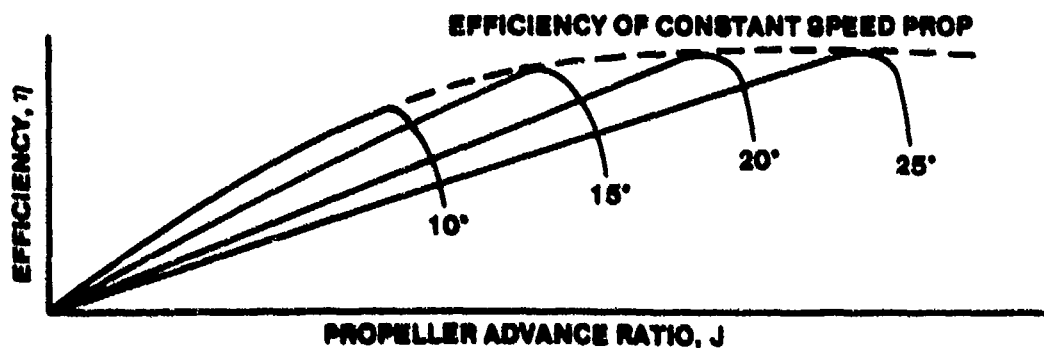


FIGURE 7.102. PROPELLER EFFICIENCY AND VARIABLE PITCH PROPELLERS

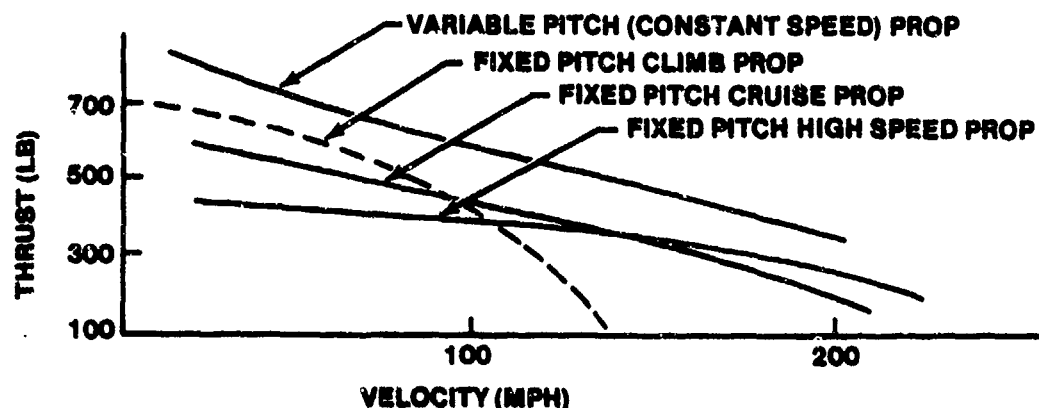


FIGURE 7.103. PROPELLER CHARACTERISTICS OF VARIOUS TYPES OF PROPELLERS

7.11.6 The Effects of Blade Geometry on Propeller Characteristics

7.11.6.1 Blade Width. The propeller power coefficient increases with blade width; however, the propeller efficiency drops off with an increase in blade width. Both effects are due largely to increased slipstream velocity with the wider blades.

7.11.6.2 Number of Blades. The number of blades affects the solidity ratio of the propeller disc where the solidity ratio,

$$\sigma = \frac{Bb}{\pi r} \quad (7.82)$$

B = Number of blades

b = Blade width

r = Length of blade

The factor Bb is very important in propeller work, and it has been found that a two-bladed propeller should have the same thrust, torque, and efficiency as a propeller having four blades, each half as wide, i.e., constant solidity. This is not completely true, due to an increase in interference drag, scale effects, and tip losses. However, an increase in the number of blades ensures a smoother operation.

7.11.6.3 Blade Thickness. Blade thickness has little effect on propeller performance except in power requirements. Wooden propellers tend to be thicker due to structural requirements whereas aluminum blades can be thinner.

Metal blades tend to be 4% to 7% more efficient than the equivalent wooden blades. Thinner metal blades would have a higher critical tip Mach.

7.11.6.4 Blade Section. The airfoil sections of propellers are often made with a flat lower surface to facilitate measurement of the twist distribution. Therefore, the shape of the profile is fairly well limited by the thickness ratio. With these factors fixed, any reasonably good airfoil section will give very nearly the same propeller characteristics as the best possible section. Promising results are being predicted for super critical airfoil sections in which relatively high lift to drag ratios can be achieved with a thick blade. The thick sections of the super critical blade look promising for hollow, blade type construction; this would be a big weight savings.

7.11.6.5 Planform. The effect of planform on propeller performance is not great. The difference between a constant section planform and a tapered section is less than 1% efficiency. The tapered blades are advantageous from strength considerations.

Sweep back and rake of the blades have appreciable effects on the aerodynamic characteristics of a propeller; they affect the twist of the blades while operating and, therefore, the pitch. The blades on wooden propellers are often swept back in order to obtain smooth running qualities and to eliminate flutter.

7.11.6.6 Blade Tips. The geometry of the blade tips is very similar to the effect of wingtip geometry on wing characteristics and is difficult to measure in flight test because of the very small increments of thrust or drag involved. Due to the high centrifugal loads imposed on propeller tips, very little work has been performed on the effect of the geometry on propeller performance. Recently, the 'Q' tip propeller has been advanced by the propeller manufacturers as a method of improving propeller efficiency and decreasing propeller noise. Since the blade tip is bent backward (similar to a wingtip being bent downward) opposite to the current growth of winglets on aircraft, the performance improvements are questionable, and measurements have shown no perceptible noise decrease over regular propellers on the same aircraft.

7.11.7 Shrouded Propellers

Shrouded or ducted propellers have been used on tug boat propulsive systems since the early 1900's to increase the static thrust of the propeller at very low vehicle forward velocities. The use of the shrouded propeller for aircraft propulsion has been slow to catch on with the light aircraft manufacturers in the United States. However, a number of shrouded propeller military research vehicles were test flown in the mid 1960's with encouraging results, and a shrouded propeller is used on the German Fan Trainer.

A shrouded propeller, shown in Figure 7.104, consists of an airfoil sectional circular shroud around a propeller with the shroud cambered on the inside and the propeller located near the minimum diameter point in the shroud. The inherent circulation of the cambered shroud induces a velocity increment at the propeller plane. This increase in circulation produced by the thrust of the propeller promotes a low pressure region close to the leading edge of the shroud, which, when integrated circumferentially, results in a thrust perpendicular to the plane of the shroud and in the same direction as the thrust of the propeller. This thrust increment, together with the increased efficiency of the propeller blades due to the end plating effect of the shroud, gives a considerable increase in thrust over the open propeller at both static and slow forward velocities.

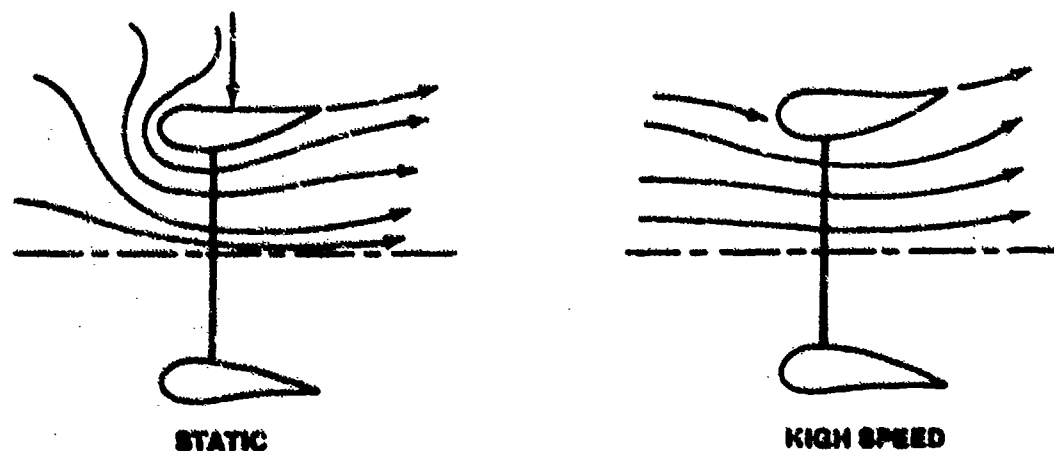


FIGURE 7.104. SKETCHES OF A SHROUDED PROPELLER

The thrust increase due to the presence of the shroud decreases with forward velocity. As the forward velocity increases, the front stagnation point on the shroud moves to the front of the shroud, thereby reducing the shroud circulation. Also, since the shroud has a parasitic drag which increases as the square of the forward velocity, it is obvious that there is some break even velocity where the thrust increment of the shroud equals the drag increment of the shroud (Figure 7.105).

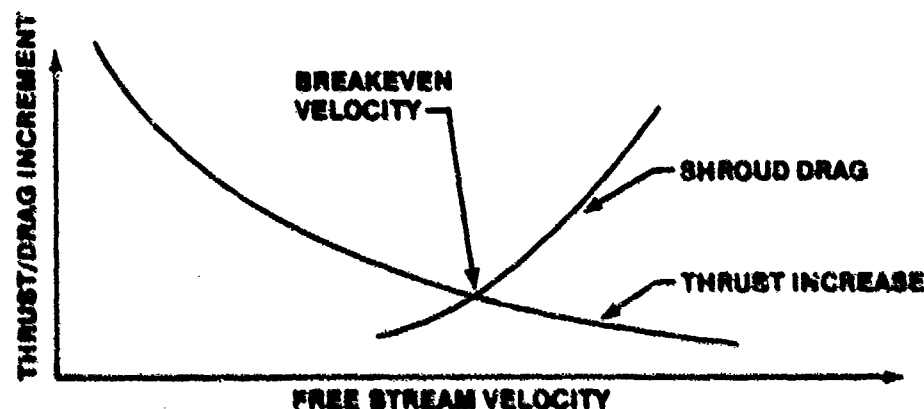


FIGURE 7.105. THRUST AND DRAG INCREMENTS OF A SHROUD WITH FORWARD VELOCITY

The shrouded propeller, which is a combination of a propeller and a shroud, must be designed as a unit because the propeller and shroud are mutually interacting.

The general problem is to determine the flow field around a ring airfoil of known camber and thickness distribution inside of which exists a pressure discontinuity normal to the axis of symmetry and which is in the presence of a uniform free stream of arbitrary direction and magnitude. From the details of the flow field, the aerodynamic forces, moments, and overall efficiency can be calculated by integrating pressures over the various surfaces. Some of the methods of solving the above problem are briefly outlined as follows.

7.11.7.1 Method of Singularities. Using this method, the shroud airfoil camber line is replaced by a distribution of vortices which produce the desired circulation equal to that of the shroud. Also, the effect of duct profile thickness and of centerbodies could be included by the use of additional distributed singularities. The mathematical expressions for

determining the velocities induced throughout an inviscid, ideal, incompressible fluid due to an arbitrary distribution of potential vortices are well known and can be used in solving for the flow field. Helmbold, in advancing his method, assumed that the mathematical form of the shroud vorticity distribution had a number of unspecified coefficients for each term and that he had to satisfy the boundary condition at a number of points on the shroud equal to the number of unknown coefficients. Using this approach, Helmbold calculated the performance of a family of shrouds having assumed parabolic camber lines. These solutions of assumed vorticity distributions represent rather special cases and are not generally applicable unless a small chord-diameter ratio is used.

The mathematical difficulties encountered in the method of singularities make it very unpopular with designers; therefore, they use either the momentum methods or some modified method of their own.

7.11.7.2 Momentum Methods. The total thrust and power relationships of ducted propeller are quickly found by the application of Newton's Second Law to axial flow in front of and behind the duct. For example, the thrust can be expressed as a product of the mass flow per unit time through the duct and the change in velocity from infinity ahead to infinity behind the duct. This method is simple; however, certain assumptions must be made. The flow must be irrotational either by counterrotating propellers or by straightening vanes. Also, it generally is assumed that the jet area at infinity downstream equals the exit area of the duct. This overcomes the necessity of resorting to the method of singularities of linking the wake area and the wake velocity with the shroud design. However, assuming that the duct exit area is equal to the wake area implies that the velocity distribution in the wake is constant and also that the static pressure at the shroud exit is equal to ambient pressure. In other words, using this theory, the entire character of the wake is assumed.

Another wake area assumption suggested by Weinig and developed by Trefftz is that the final wake area is related to the cross-sectional area and diffuser angle at the trailing edge of the duct, i.e.,

$$\frac{S_{\text{Final}}}{S_{\text{Exit}}} = \frac{1}{1 - 0.453} \quad (7.83)$$

where θ is the angle of inclination of the inside surface of the duct trailing edge with respect to the duct axis. The above equation, of course, is restricted to small values of θ unless some means of boundary layer control is applied to prevent flow separation.

7.11.7.3 Other Methods. These methods are generally approximate methods that either place emphasis on the propeller, by using a blade element theory and modifying the blade element theory to take into account some of the influence of the shroud, or the emphasis is placed on the shroud, which usually consists of an approximation to the method of singularities. For example, the shroud may be represented approximately by a single vortex ring.

An electrical analogue to the method of singularities for three-dimensional potential flow problems has been applied to the ducted propeller problem by Malavard. The boundary conditions are satisfied by the application of appropriate electrical potentials at the shroud and at the wake boundary, which is assumed to be of constant diameter.

In summary, it can be said that the mathematics are at our disposal for solving the problem of ducted propellers, provided that either the shroud camber line or the shroud vorticity distribution is specified. However, the mathematics are involved and complicated, and in practical applications where the inflow to the ducted propeller is not uniform, i.e., a ducted propeller at the rear of a fuselage, approximate methods using the momentum theory developed by Kuchmann and Weber are generally sufficiently accurate. Once the shroud shape is determined and the velocity distribution through the disc calculated, the required propeller twist can be determined using existing propeller design techniques.

7.11.8 Shrouded Fans

The multi-bladed shrouded fan, driven by any type of engine including reciprocating, rotary or gas turbine engines, closely approximates the high bypass ratio turbofan in operational concept. High bypass ratio turbofans are much quieter than turbojets and therefore more environmentally acceptable. Shrouded propellers tend to be much quieter than open propellers, primarily due to the shroud end plating of the propeller blades and the fact that shrouded fans and propellers direct their noise output forward and rearward, thereby having low sideline acoustic signatures. The 1980 noise standards for

general aviation aircraft in the United States and particularly in European countries have increased the possibility of using shrouded propellers on light aircraft for normal operational use. In 1978, Dowty of England installed and flight tested two shrouded fans on an Islander aircraft with an impressive reduction in propeller noise.

Design and trade-off studies of shrouded fans and propellers have been made by numerous companies, and a typical comparison is shown in Table 7.15, together with a drawing of the shrouded propeller/Q Fan. (Figure 7.106.)

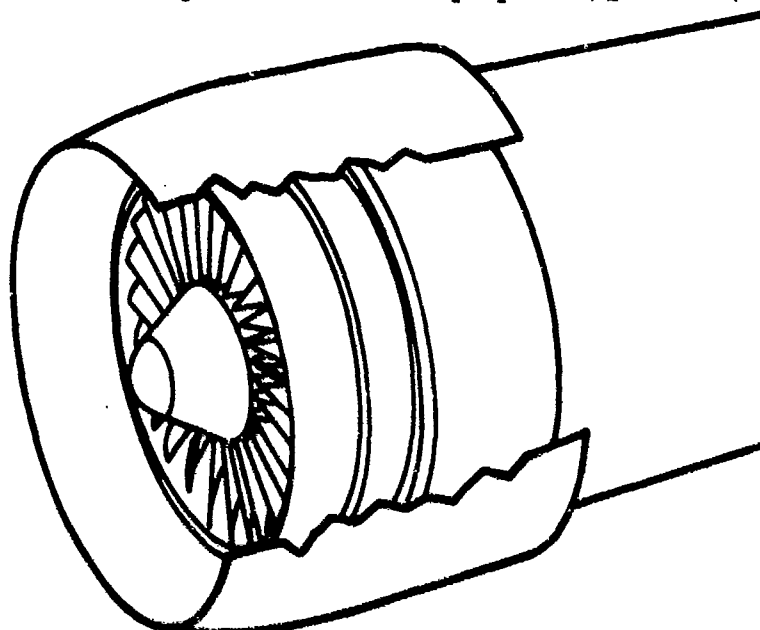


FIGURE 7.106. SHROUDED PROPELLER/Q FAN

TABLE 7.15

COMPARISON OF PROPELLER AND Q FAN CHARACTERISTICS

Propulsor Characteristics	Propeller	Q Fan
Diameter (Ft.)	6.5	3.0
Number of Blades	3	9
Tip Speed/RPM	915/2700	640/4060
Thrust at 66 Kts./M = .33	880/316	880/329
Weight (lbs.)	77	175
Noise Level (dB)	99.5	83.5

When both the propeller and the shrouded fan are designed for the same climb and cruise performance characteristics, the noise level of the fan is a fraction of the noise level of the propeller, but the weight penalty of the shroud is approximately 100 lbs. This weight penalty may be offset in the fan by elimination of a gear box so that high speed engines such as rotary engines can be used to drive the fan directly.

7.11.9 F.A.A. Certification Requirements

The F.A.A. airworthiness standard for propellers, F.A.R. Part 35, requires that a whirl test be performed to demonstrate that the propeller can withstand 200% of the maximum centrifugal force encountered in normal operations. Vibration tests must be performed on metal propellers, and an endurance test of 10 hours at maximum RPM and maximum certified diameter must be performed. The endurance test can also be accomplished with 50 hours of flight time consisting of 5 hours at 100% RPM and 45 hours at 90% RPM for fixed pitch propellers. Variable pitch propellers require 100 hours at maximum RPM and power on the engine for which they are to be certified. Functional tests of manually controllable, constant speed, feathering, and reversible systems must also be performed for a number of cycles without malfunctions.

The F.A.A. Part 23 requirements essentially deal with installation of the propeller(s) on the airframe, calling out ground clearance, water clearance, propeller tip, and structural clearances.

7.11.10 Ground Testing

Most of the ground testing of propellers is performed to demonstrate the structural, vibrational, and endurance requirements for certification on a particular engine. However, performance ground testing can often be very rewarding if the necessary facilities are available. Static thrust measurements as a function of power input will give an insight into the maximum power that can efficiently be absorbed by a particular installation as shown in Figure 7.107.

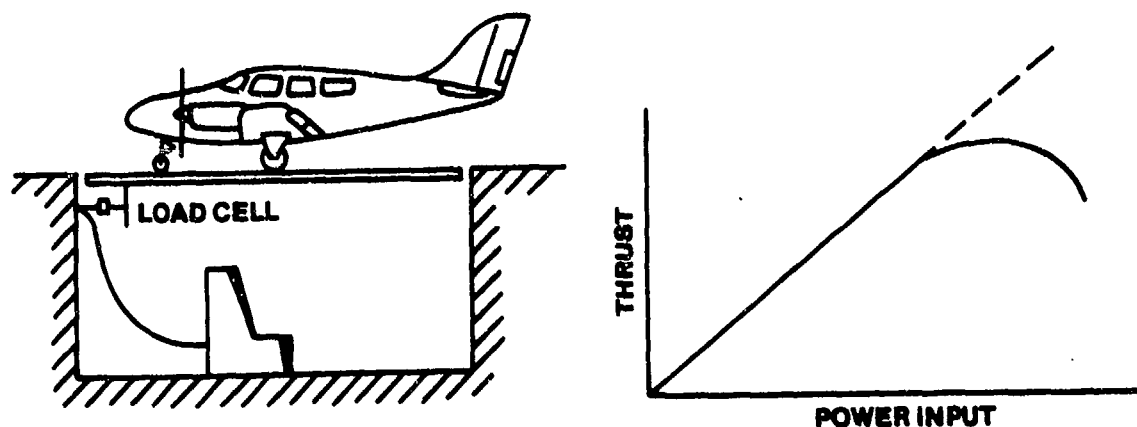


FIGURE 7.107. STATIC THRUST MEASUREMENTS
OF ENGINE PROPELLER COMBINATIONS

7.11.11 Flight Testing

Most propeller flight test hours are spent on endurance flying and ensuring that the engine-propeller combination is vibration free and the fatigue life of the blade is acceptable. The blades are strain gauged and the signals fed through slip rings on the shafts to recording equipment in the aircraft. Flight tests to determine propeller efficiency can be performed, but they require either a strain gauged propeller shaft that can measure shaft torque and propeller thrust or a special thrust and torque load cell mounted between the engine and the propeller.

$$\text{Propeller Efficiency} = \frac{(\text{Thrust}) (\text{Forward Velocity})}{(\text{Torque}) (\text{Angular Velocity})}$$

The incremental drag method of measuring the propeller efficiency in flight is based on the assumption that the propeller efficiency does not change significantly with small incremental power changes where the propeller advance ratio is maintained constant. Instrumentation required is a small drag device such as a training cone connected to the aircraft by a load cell capable of directly measuring the drag of the trailing cone. The flight test technique is to obtain power-velocity data of the cruise configuration aircraft at a constant altitude and engine rpm and then return and attach the

load cell and trailing cone and repeat the cruise tests at the same RPM and altitude. The data analysis is as follows:

Cruise Configuration Aircraft

$$\eta_p \text{ (B.H.P.)} = \frac{(\text{Drag}) (\text{Velocity})}{550} = \frac{D.V.}{550} \quad (7.84)$$

Aircraft with Cone

$$\eta_p \text{ (B.H.P. + B.H.P.)} = \frac{(\text{Drag} + \Delta \text{ Drag}) (\text{Velocity})}{550} = \frac{(D + \Delta D) (V)}{550} \quad (7.85)$$

The unknown in the two equations above are propeller efficiency, (η) and aircraft drag (D). The solutions are:

$$\text{Propeller Efficiency } (\eta_p) = \frac{(\text{Velocity}) (\Delta \text{ Drag})}{(550) (\Delta \text{ B.H.P.})} \quad (7.86)$$

$$\text{Aircraft Drag (D)} = \frac{(\text{B.H.P.}) (\Delta \text{ Drag})}{(\Delta \text{ B.H.P.})} \quad (7.87)$$

The problems with the incremental drag method are that the technique consists of measuring small differences between large numbers. The drag device must be large enough to be able to measure differences in horsepower required, yet not large enough to violate the basic assumption that the propeller efficiency will not change with small increases in power absorbed. A comparison of theoretical predictions with propeller test results is shown in Figure 7.108.

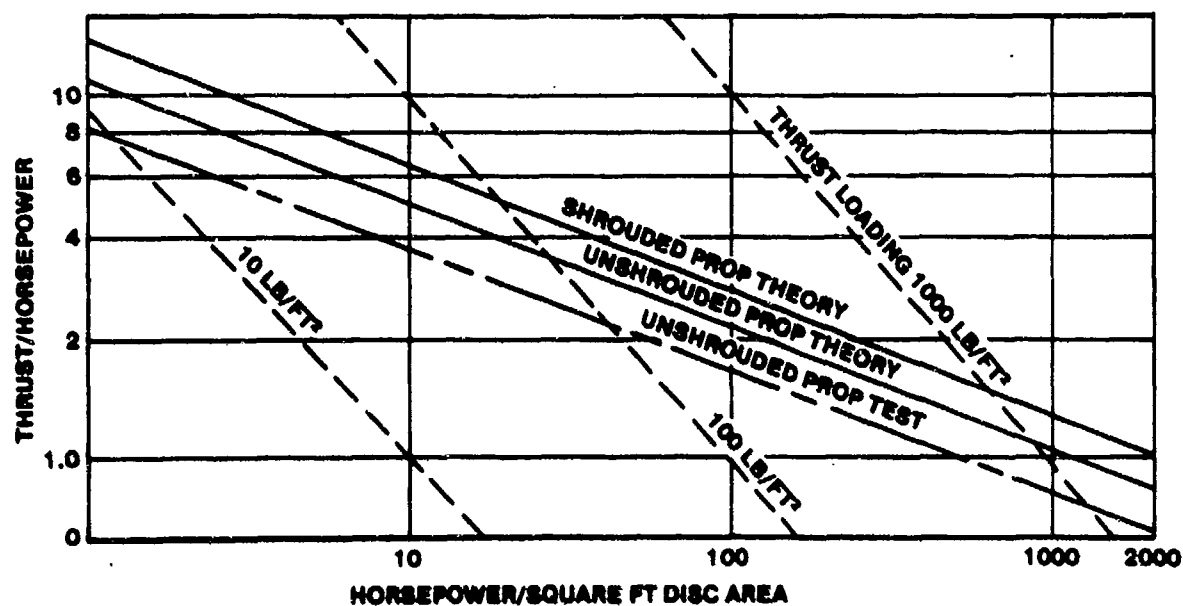


FIGURE 7.108 DUCTED PROPULSOR PERFORMANCE

7.11.12 Advanced Design Propellers

The previous paragraphs on propeller theory, FAA certification, and ground and flight testing all apply to so-called conventional propellers. During the last few years, due to the constant quest for higher and higher fuel efficiency, much research has been done concerning a whole new generation of advanced concept propeller designs. Most of this work has been conducted at the NASA Lewis facility in Cleveland, Ohio. Figure 7.109 is a typical example of what this new generation of propellers looks like.

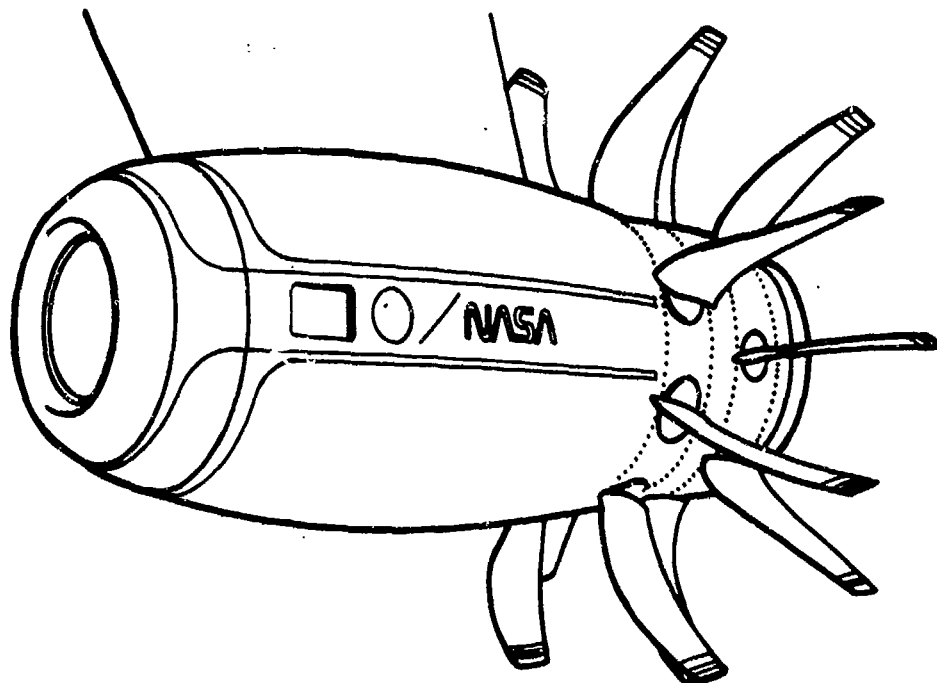


FIGURE 7.109. GENERAL ELECTRIC/NASA UNDUCTED FAN (UDF) DEMONSTRATOR ENGINE

These advanced propeller designs are intended for use with a turbine power plant rather than a reciprocating engine because of the much greater thrust to weight ratio of gas-turbines.

An advance design propeller would have very thin and highly swept blades to minimize both compressibility losses and propeller noise during high speed cruise. An area-ruled spinner and an integrated nacelle shape would also be used to minimize compressibility losses in the propeller-blade hub region. Propeller diameter would be kept to a minimum by using 8 to 10 blades with a high propeller power loading. These blades would be constructed using modern propeller blade fabrication techniques. The advanced propeller must be powered by a large, modern turboshaft engine and gearbox.

The basic reason for the attractiveness of this advanced turboprop concept is its potential for high propulsive efficiency in the Mach 0.7 to Mach 0.8 speed range. Older model turboprops had relatively thick, unswept propeller blades and experienced rapid increases in compressibility losses above Mach 0.6. Current high-bypass-ratio turbofans exhibit their highest

propulsive efficiency (about 65%) at cruise speeds somewhere above Mach 0.8. The advanced turboprop concept is estimated to be about 20% more efficient than high-bypass-ratio turbofans at Mach 0.8. At lower cruise speeds, the efficiency advantage of the advanced turboprop is even larger. This high propulsive efficiency of the advanced turboprop makes it an attractive powerplant for many aircraft applications.

7.12 PROPULSION SYSTEM TESTING

Propulsion system flight testing remains the only true test of the marriage between an engine and an airframe. Although extensive test cell/wind tunnel testing of engines at sea level, altitude, and various Mach is accomplished prior to flight qualification, the almost infinite number of variables to which an actual flying installation is exposed can not yet be duplicated on the ground. As engines become more complex, even more variables are introduced such that ground test programs also become extremely complex. Duplication of high angles of attack, high positive or negative load factors, and high yaw angles cannot be adequately duplicated in a test cell. Efforts are continually underway to design programs and ground test facilities to reduce the risk and cost of developing an engine. The final proof of any propulsion design requires testing the installation in the environment for which it was designed, i.e., flight test.

7.12.1 Propulsion Flight Test Categories

Propulsion flight test activity may fall into three categories: (1) flight test of a new engine, (2) flight test of components of an existing engine (Component Improvement Program, CIP), and (3) flight test of an existing engine with a new fuel. Typically, when a new engine is developed, the engine manufacturer performs the bulk of ground testing under the supervision of the Propulsion System Program Office (SPO). This ground testing starts at the factory and eventually progresses to "wind tunnel tests" simulating in-flight conditions. After the engine has been exposed to the aircraft flight envelope in the wind tunnel, it is ready for flight test.

The types of flight tests performed in a propulsion program fall into two basic categories: (1) tests to extract engine aerodynamic performance, and

(2) tests to evaluate systems operation. Since aircraft performance is directly linked to engine thrust, aircraft performance testing and engine performance testing are inseparable. Therefore, the same performance maneuvers are flown for engine and airframe performance data. These maneuvers consist of the classical performance tests such as cruise performance, level accelerations, turn performance, and climb and descent performance.

To evaluate the engine operation from the systems aspect, the following types of tests are typically made:

1. Installed ground tests
2. Throttle transients
3. Transfers to backup control
4. Climbs and descents
5. Airstarts
6. Engine handling/response (i.e., formation, air refueling)
7. Fuel/oil temperature exposure
8. Gas ingestion
9. Ice ingestion

7.12.2 Installed Ground Tests

Installed ground tests are initially performed to ensure compatibility between engine and airframe systems operation. Prior to installation in the aircraft, all aircraft unique systems operations such as bleed air and power extraction are simulated. Installed ground tests serve as a final check of engine/aircraft interface prior to first flight. Additionally, instrumentation parameters are exercised as much as possible to ensure proper operation. All possible engine functions are exercised during these tests, such as starting, throttle transients, transfer to backup control, etc.

Typically, these tests are performed with the instrumentation system fully operational and data is telemetered to a ground station for real time monitoring of critical parameters.

7.12.2.1 Ground Starting. Ground starting of operational engines is usually a routine event. However, many problems can arise during initial test and evaluation of new engines or old engines in new airframes. Numerous starting mechanisms [air, gas generators, turboshaft starters (jet fuel starter), cross bleed systems, etc.] can all have their own peculiar problems. Compressor spin-up rate, fuel scheduling, starter cut-out speed, ignition systems, and

ambient atmospheric conditions can all take their toll in hung starts, hot starts, no-lights, and starter failures. Unless specific problems arise, ground engine starting evaluations are confined to monitoring engine parameters during numerous starts in varying conditions.

7.12.3 Throttle Transients

The ability of the engine to follow pilot-commanded changes via the power lever (throttle) is essential to successful mission completion. Rapid engine acceleration and deceleration are required without any adverse effects such as turbine temperature overshoots or undershoots, compressor over or under-speed conditions, compressor stalls, or flameouts. The purpose of throttle transients is to (1) evaluate stall free operations throughout the flight envelope under worst case conditions, (2) evaluate engine acceleration/deceleration requirements and afterburner light requirements, and (3) evaluate back-up control operation.

The two basic types of transients used in flight tests are BODIES and SNAPS.

A BODIE is a transient that exposes the engine to operation nearest the compressor stall line. It is usually performed in dry power (non-afterburner) conditions, and involves a rapid throttle movement from military power to idle and a reversal back to military power prior to the engine RPM reading its steady state idle RPM.

A SNAP transient is a rapid throttle movement (approximately one second or less full travel time) from one end of the throttle range to another. These transients are performed under steady state flight conditions (Mach/altitude) at one g and under "maneuvering" conditions such as maximum angle of attack (α), maximum sideslip (β), and maximum α and β simultaneously. Typical throttle transients are shown in Figure 7.110.

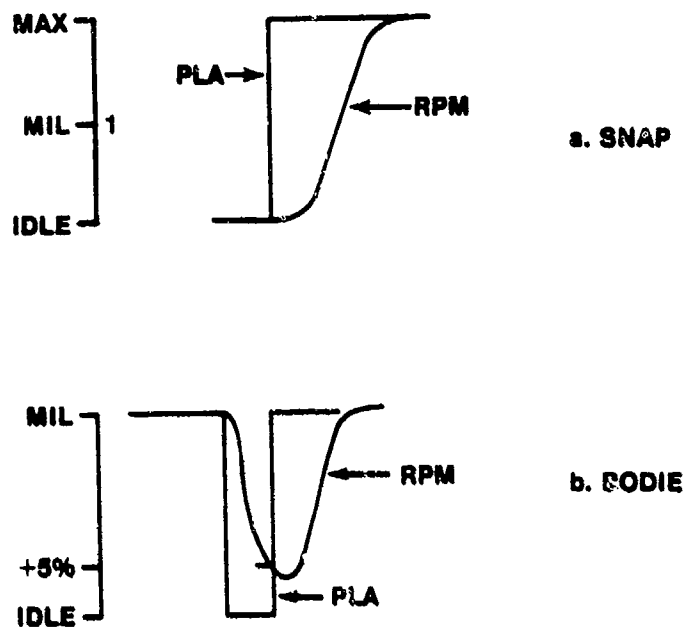


FIGURE 7.110. TYPICAL THROTTLE TRANSIENTS

Of utmost importance during engine testing is the use of the "buildup approach" when performing throttle transients, especially on single engine aircraft. Normally, transients should start at some agreed upon "heart of the envelope" flight condition and build up to critical parts of the envelope. A typical buildup approach is shown in Figure 7.111.

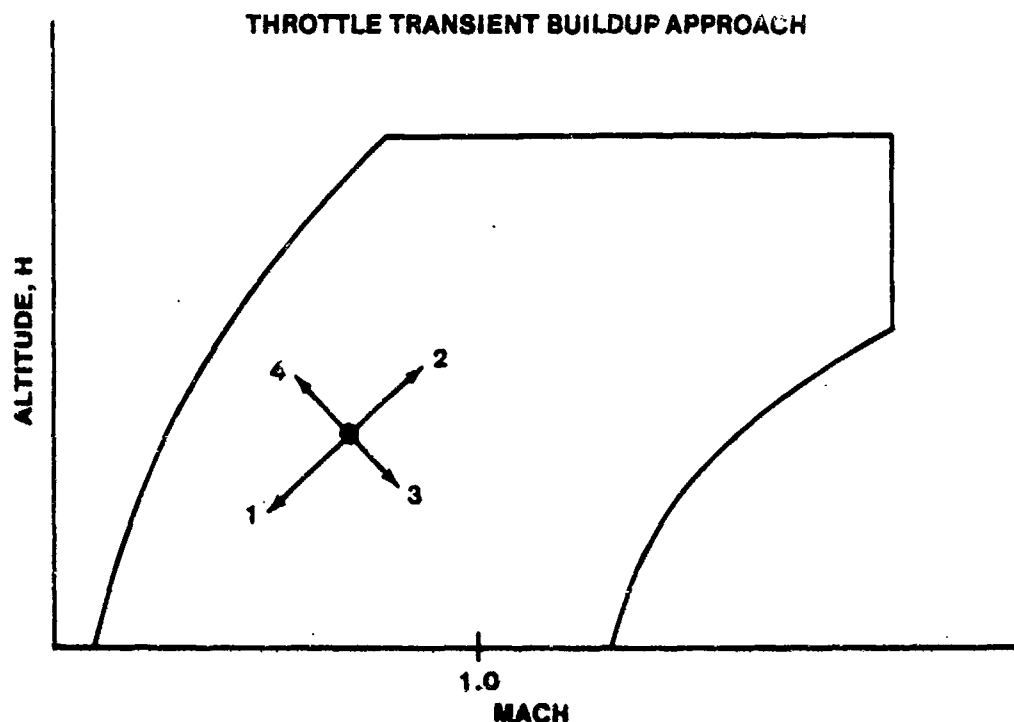


FIGURE 7.111. THROTTLE TRANSIENT BUILDUP APPROACH

Several problems frequently occur during these tests, especially on early development models of engines. Off-idle stalls, that is, compressor stalls that occur as functions of compressor map stall/accelerating lines, fuel flow scheduling, compressor inlet guide vane scheduling, bleed valve scheduling, or inlet air flow distortion. Stalls of this nature are usually mild and self-clearing with throttle retardation.

Sub-idle conditions or hung stall conditions below normal idle speed can occur, usually at high altitude, upon rapid throttle retardation. Fuel control scheduling is usually the culprit in these cases. In one airplane, a "floor" was added to the fuel control schedule so the burner pressure could not decrease below that required to maintain compressor speed.

Afterburner ignition and flameout are almost always problem areas on new engines. Afterburner design is based as much on "cut and try" processes as it is on theoretical design analysis. Because of this, much wind-tunnel and flight testing is required. A new engine development program may encompass many hundreds of afterburner tests using many combinations and ignition schemes. Variable exit-area nozzles are typically problem areas because of their hostile environment and complicated operating demands, especially when attached to a fan engine. Fan stalls due to duct pressure waves traveling

forward in the fan duct caused by improper scheduling or operation of the nozzle are common occurrences in development engines.

Evaluation of transport type engine response is typically less demanding than it is on a fighter type aircraft, simply because of the difference in mission. Throttle transients on these types of engines are more closely related to electrical generator load and bleed air extractions. Because of the lack of an afterburner, testing is usually simpler. The advent of in-flight use of engine thrust reversers such as installed on STOL type transports may complicate this picture.

7.12.4 Climbs and Descents

Since ambient temperature and pressure change with altitude, these two parameters are incorporated in some manner in virtually all turbine engine fuel controls. In order to evaluate the adequacy of these controls with respect to accuracy, lag times, repeatability, drift, and the like, climbs and descents are performed at various rates of altitude change and at various engine power settings. The throttles are normally "locked" in a fixed position so that any changes detected are a function of the engine controls only and not pilot input. These maneuvers are usually combined with performance evaluations in the interest of conserving flight time.

7.12.5 Airstarts

A flight test program to determine the airstart characteristics of an engine will be a critical portion of any engine test program. The purpose of in-flight testing of engine airstarts is two-fold. First, the airstart envelope must be determined and second, emergency procedures for airstarts must be developed.

In general, there are three types of airstarts: windmilling, spooldown, and assisted airstarts.

A windmilling airstart is one in which the ram air due to aircraft velocity is used to maintain compressor speed sufficient for an airstart. Most turbojet engines will windmill at 10 - 15% RPM at minimum flight speed which is enough to begin an airstart. Turbofans, however, seldom windmill satisfactorily and, if allowed to cage (engine rotation stops), may require over 400 kts to regain rotation.

Spooldown airstarts are done by initiating the airstart as the RPM decreases after shutdown. These can be time critical as beginning the airstart at too high an RPM frequently results in a hot start requiring shutdown and beginning at too low an RPM may not prevent the engine from caging.

An assisted airstart is one where either crossbleed from a good engine or a smaller starter motor is used to motor the compressor during main engine start. Engine starters are more common on modern turbofan engines and allow lower airspeed starts.

Airstart testing is normally done very early in an engine test program. Because of the critical nature of engine tests, especially in single-engine aircraft, the heart of the predicted airstart envelope should be verified within the first few flights. Optimizing pilot procedures, expanding the airstart envelope, and demonstrating back-up fuel control airstarts can be delayed to later phases of the test.

Typical airstart characteristics for a turbofan engine are shown in Figures 7.112 through 7.114.

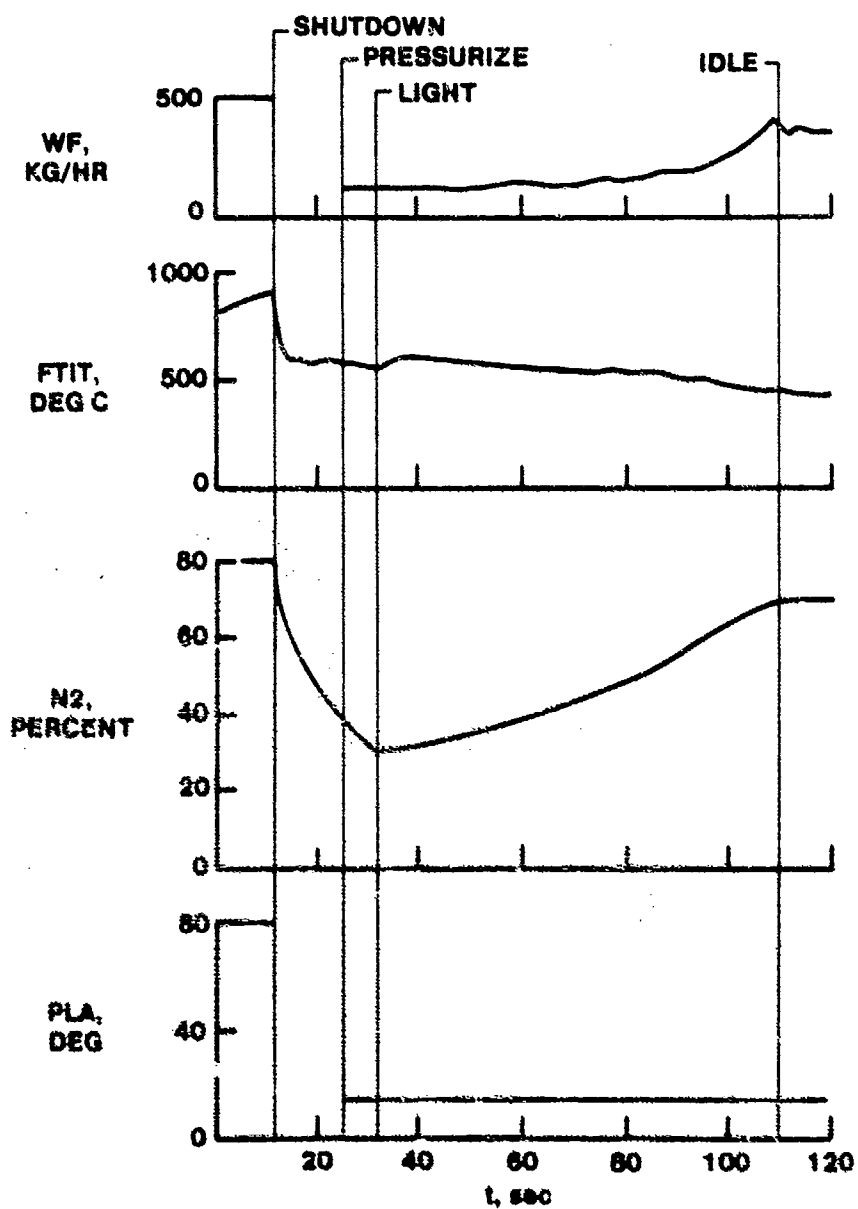


FIGURE 7.112. 40 PERCENT SPOOLDOWN AIRSTART, $V = 200\text{KTS}$

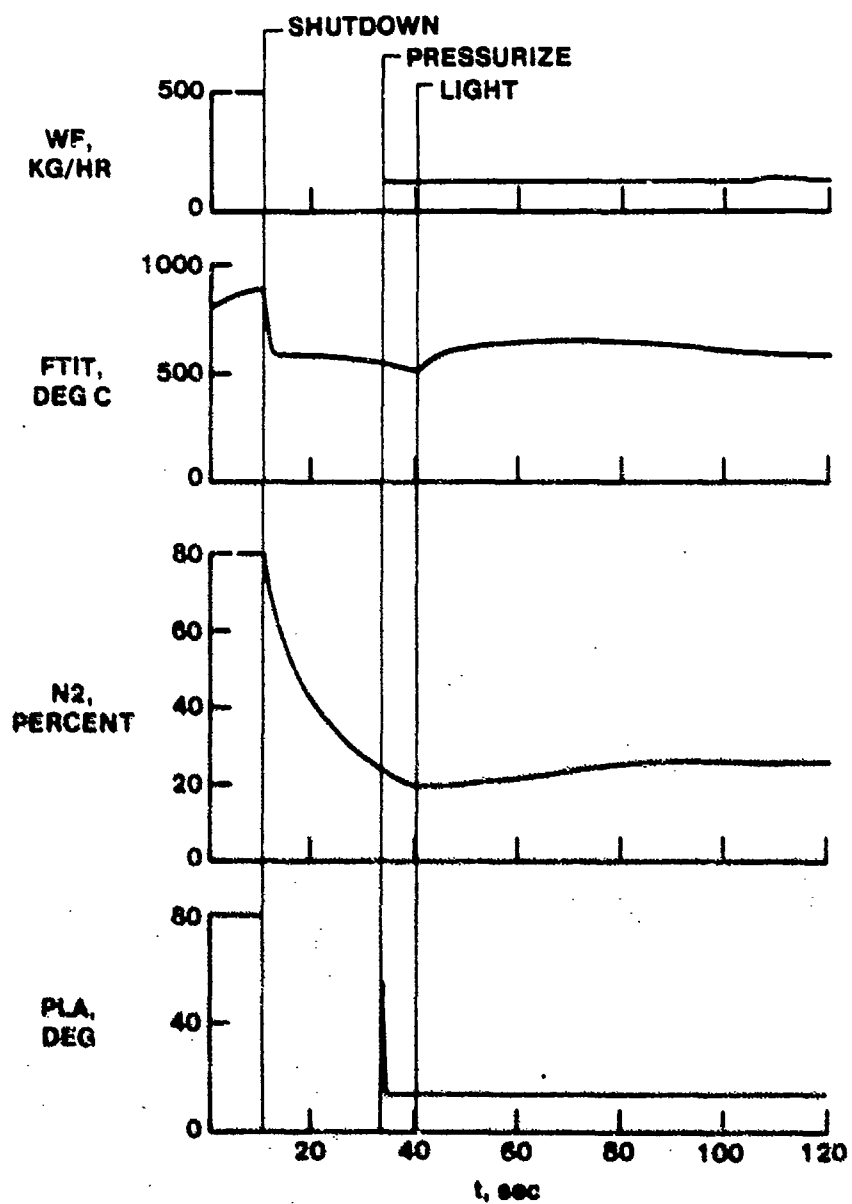


FIGURE 7.113. 25 PERCENT SPOOLDOWN - HUNG START

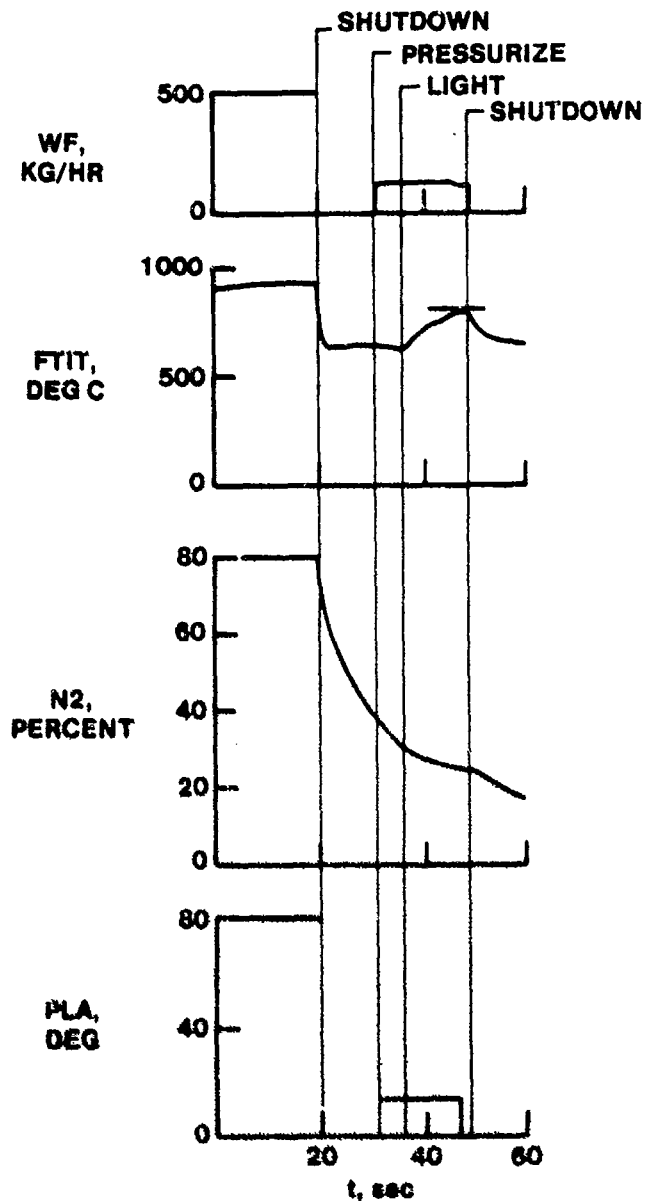


FIGURE 7.114. 40 PERCENT SPOOLDOWN - HOT START

7.12.6 Engine Handling and Response

Engine handling and response will be evaluated to some degree on every flight. Pilots should report on the ease or difficulty encountered in doing all engine related tasks. However, certain tasks should be planned to investigate specifically how the thrust response affects pilot workload. Two of the best ways are to perform close formation tasks and air refueling. If

there is an appreciable delay in thrust response these tasks should show the severity of the problem

7.12.7 Gas Ingestion

On fighter or ground support type aircraft, gas generated from firing of guns, cannons, and forward firing missiles can be ingested into engine inlets. This is a function of the physical relationship of the engine inlets to the source of the gas. Severe engine compressor stalls and complete engine flameouts have been experienced due to ingestion of hot, noncombustible, gun or rocket exhaust gases. The systems test programs consist of initially firing guns and rockets at high altitude at various representative delivery conditions of airspeed, angle of attack, sideslip, etc. Once the system is clear of any problems in this flight regime, air-to-air and air-to-ground firings are performed in the normal operational mode. Engine inlet rakes and engine instrumentation monitoring inlet temperature, compressor discharge pressure, and exhaust gas temperature, and chase photography are used to verify the presence or absence of foreign gas ingestion.

PROBLEMS

- 7.1 Calculate gross thrust, net thrust, and TSFC for the following engine

$$\dot{M}_{10} = \dot{M}_0 = \frac{\dot{w}_0}{g} = \frac{434.7 \text{ lb/sec}}{32.2 \text{ ft/sec}^2} = 7.76 \frac{\text{lb sec}}{\text{ft}}$$

$$V_0 = 2805 \text{ ft/sec} \quad P_{10} = P_A = 15 \text{ lb/in}^2$$

$$V_{10} = 3922 \text{ ft/sec} \quad A_{10} = 6.0 \text{ ft}^2$$

$$\dot{w}_{\text{FUEL}} = 15 \frac{\text{lb}}{\text{sec}}$$

- 7.2 Construct a typical h-s diagram for an ideal ramjet. What is required to allow a ramjet to function compared to a turbojet?
- 7.3 If an "ideal" compressor has a pressure ratio of 8.0 and an inlet temperature of 100°F , what would be the value of T_{T_3} ?
- 7.4 What T_{T_3} should be used to get maximum net work for an "ideal" engine designed to run in the isotherm region at $M_0 = 3.0$ if T_{T_4} is limited to 3000°R ?
- 7.5 At what compressor pressure ratio would the engine of Problem 7.4 operate?
- 7.6 If $\text{EPR } (P_{T10}/P_{T2}) = 3.0$, $T_{s10} = 2000^\circ\text{R}$ and $\text{WAT2C} = 250 \text{ lb/sec}$, what is ideal net thrust at $M_0 = 1.0$, sea level? Assume standard day conditions with 5007D ram recovery (refer to pgs. 68-84 of M/H/B).
- 7.7 An F-100 fan flows 200 lb/sec airflow at sea level standard day when the rotor speed is 9000 RPM. If we fly to 40,000 ft, $M_0 = .8$, maintain the same corrected flow and rotor speed, at what airflow and rotor speed (\dot{w}_a and N_1) will the engine be operating?

- 7.8 Sketch a subsonic inlet operating below design Mach. What is the potential result?
- 7.9 Sketch a subsonic inlet at a Mach above design. What is the major penalty?
- 7.10 Explain how total pressure is increased in a compressor.
- 7.11 List the advantages of an axial flow compressor over a centrifugal compressor.
- 7.12 A fan is operating at S.L.S. ($M_0 = 0$, Alt = 0). Its pressure ratio ($P_{T_{2.5}}/P_{T_2}$) is 3.0, and its discharge total temperature is 272.0°F . What is the fan's efficiency?
- 7.13 Sketch the fan's operation (Prob. 7.12) on an h-s diagram.
- 7.14 If the fan from Problem 7.12 had WATC2 = 250 lb/sec, how much horsepower does the rotor shaft have to deliver to the fan?
- 7.15 Discuss the 3 T's of combustion.
- 7.16 If the compressor from Problem 7.12 is powered by a turbine with $T_{T4} = 2000^\circ\text{R}$ and $P_{T4} = 30 \text{ lb/in}^2$, what would T_{T5} be assuming turbine efficiency of 100%?
- Assume $C_p = 0.28$ and $\delta = 1.33$
- 7.17 List three methods of air cooling turbine blades and vanes.
- 7.18 What is P_{T_5} for Problem 7.16?
- 7.19 List 3 types of nozzles and explain good and bad points of each.

7.20 What nozzle would you expect on

- a) a subsonic transport
 - b) a STOL fighter
 - c) a supersonic interceptor
- and why?

ANSWERS

7.1 $F_g = 52,947 \text{ lb}$
 $F_n = 37,868 \text{ lb}$
 $\text{TSFC} = 1.43$

7.3 $T_{T3} = 556^{\circ}\text{F}$

7.4 $T_{T3} = 1082^{\circ}\text{F}$

7.5 $P_{T3}/P_{T2} = 1.0$

7.6 $F_n = 37,868 \text{ lb}$

7.7 $w_a = 61.2 \text{ lb/sec}$

$N_1 = 8290 \text{ RPM}$

7.12 908

7.14 18,080 HP

7.16 $T_{T5} = 1817^{\circ}\text{R}$

7.18 $P_{T5} = 20.4 \text{ lb/in}^2$

BIBLIOGRAPHY

- 7.1 Heiser, W.H., "Modern Turbine Aerodynamics," unpublished lecture notes for University of Tennessee Space Institute short course, December, 1969.
- 7.2 Henderson, R.E., "Improvement of Turbo Engine Components," unpublished lecture notes for University of Tennessee Space Institute short course, December 1969.
- 7.3 Hesse, W.J., Jet Propulsion. New York: Pittman Publishing Corporation, 1958.
- 7.4 "Inlets for Supersonic Aircraft," Space/Aeronautics, May 1967, pp. 90-100.
- 7.5 Mallett, W.E., "An Explanation of the Performance Characteristics of Turbojet Engines and Their Components," TPT 1-58, Naval Air Test Center, Patuxent River, Maryland, February, 1958.
- 7.6 "Principles of Propulsion," Department of Aeronautics, United States Air Force Academy, n.d.
- 7.7 Tipton, D.L., "Supersonic Compressor Loss Calculations," unpublished lecture notes for University of Tennessee Space Institute short course, December 1969.

CHAPTER 8
TAKEOFF AND LANDING PERFORMANCE

8.1 INTRODUCTION

A very important part of the testing of any aircraft is the takeoff, landing, and operation in close proximity to the ground. Takeoff and landing are greatly dependent upon pilot judgement and technique and, therefore, are subject to considerable variation for any given aircraft and set of conditions. Because of this largely unpredictable variable, the pilot, it is neither possible nor practical to make exact prediction or correction of takeoff and landing performance. It is only possible to estimate the approximate capabilities of an aircraft within rather broad limits. For this reason, takeoff and landing performance will be considered from a rather general point of view taking into account only the major variables and making some assumptions concerning the lesser variables.

The major purposes of these types of tests include development and/or verification of pilot techniques appropriate for the test aircraft, formulation of performance estimates for inclusion in the flight manual, and verification of compliance, or lack of compliance, with contractual specifications. In addition to normal takeoffs and landings, a complete series of tests will include refused takeoffs (high speed aborts), crosswind operations, wet/icy runway tests, barrier tests, and engine out operations.

This chapter will not cover the specifics of such parameters as refusal speeds, minimum control speeds, or critical runway lengths, since these will be covered in detail during the "engine out" phase of instruction.

8.2 TAKEOFF THEORY

8.2.1 Method of Development

The mechanics of the takeoff can conveniently be examined in two phases, the air phase and the ground phase. The air phase is normally considered to be that portion of flight from leaving the ground until reaching a measured altitude above ground level of 50 feet. In a few rare cases, it may be possible to stabilize at a constant climb speed before reaching 50 feet, in which case the air phase of operation must be broken into a transition phase and a steady state climb phase. For most high performance aircraft, the transition to a steady climb speed will not be completed before reaching 50

feet, even for a maximum climb angle takeoff. The ground phase begins at brake release and terminates when the aircraft first becomes airborne.

In this chapter, equations will be developed that can be used to study the effects of the various factors which influence takeoff performance. The assumptions required to achieve workable equations make the equations unusable for prediction of takeoff performance but do not make them invalid for analysis and correction.

8.2.2 Forces (Ground Phase)

In addition to the usual forces of lift, weight, thrust, and drag, an aircraft on takeoff roll is affected by an additional "resistance" force which includes wheel bearing friction, brake drag, tire deformation, energy absorbed by the wheels as they increase rotation speed, etc. This force will become smaller as the weight on the wheels is reduced and can be mathematically expressed as $\mu (W-L)$. Typical values of μ , the "coefficient of resistance" range between .02 and .05 for a dry concrete runway. The forces acting on the aircraft during the ground roll are illustrated in Figure 8.1.

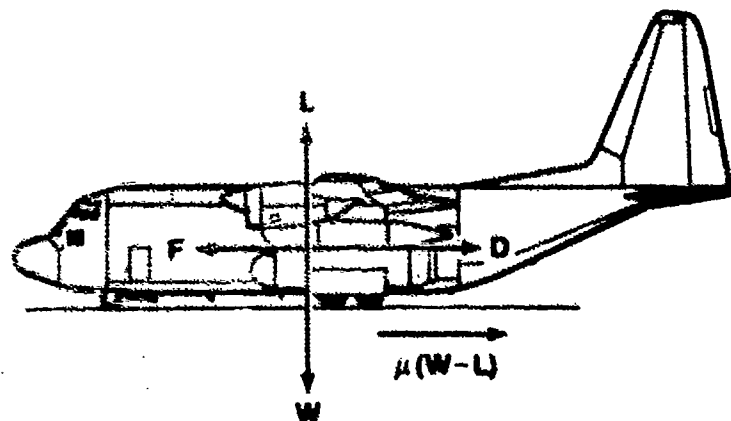


FIGURE 8.1. TAKEOFF ROLL FORCES

Note that this depiction of forces includes the assumption that engine thrust is parallel to the runway. For aircraft with engines mounted at an angle, the horizontal component of thrust is not reduced significantly until the angle becomes quite large. The vertical component of thrust from inclined engines reduces the effective weight of the aircraft. The mass of the aircraft, however, must be computed using the actual weight.

8.2.3 Ground Roll Equation

Setting the work done equal to the change in energy, we can write

$$\int_0^{S_g} [F-D-\mu(W-L)] ds = 1/2 W/g (V_{TO}^2 - 0) \quad (8.1)$$

where S_g is the total ground distance and V_{TO} is the ground speed at liftoff. None of the terms under the integral are constant during the roll, and an exact evaluation is virtually impossible. If, however, we make the assumption that the entire quantity remains constant at some average value, the integration is simple and the expression becomes

$$[F-D-\mu(W-L)]_{avg} S_g = 1/2 W/g V_{TO}^2 \quad (8.2)$$

or

$$S_g = \frac{W V_{TO}^2}{2g [F-D-\mu(W-L)]_{avg}} \quad (8.3)$$

At first glance, this assumption appears gross but further examination of the individual forces shows it to be reasonable. Engine thrust can be expected to decrease slightly as speed increases. A jet engine may enter ram recovery prior to liftoff and realize an increase in thrust over that at lower speed. Propeller thrust will decrease throughout the takeoff roll. Aerodynamic lift and drag increase during the roll in direct proportion to the square of the airspeed. If the aircraft attitude is changed considerably at rotation, both lift and drag will increase sharply. The coefficient of resistance, μ , and the aircraft gross weight remain nearly constant. These variations in forces for a turbojet aircraft are shown graphically in Figure 8.2.

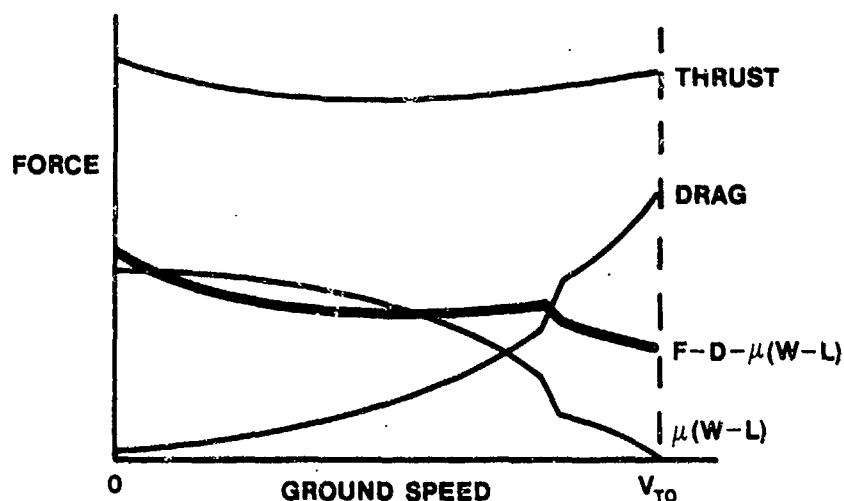


FIGURE 8.2. VARIATION OF FORCES DURING TAKEOFF GROUND ROLL

For a propeller aircraft, the thrust curve will show a greater decrease, while the shape of the drag and wheel force curves will not change. In general, the excess thrust (the vector sum of all three forces) at liftoff will be about 80% of its initial value for a jet aircraft and 40% for a propeller aircraft. In either case, test data show that use of the actual excess thrust at $0.75 V_{TO}$ as the average value in Equation 8.3 gives reasonable results.

8.2.4 Shortening the Ground Roll

Equation 8.3 shows that ground roll can be shortened very effectively by lifting off at a lower speed, since the distance increases with the square of the takeoff speed. Looking at the problem from the standpoint of minimizing the ground roll, the aircraft should be lifted off at $C_{L_{max}}$. However, the aerodynamic drag created by this technique may reduce the excess thrust to an unacceptable level. In extreme cases, rotation to $C_{L_{max}}$ may reduce excess thrust to zero or negative values, a definitely unacceptable situation. If sufficient thrust is available to overcome the drag penalty, high lift devices such as slats and flaps can provide a higher available lift coefficient.

A second approach to decreasing S_g is through increasing the thrust

available, F , either by operating the engine above its maximum rated power, such as by water injection, or by use of an auxiliary engine such as JATO (Jet Assisted Take Off), RATO (Rocket Assisted Take Off), etc. Thrust augmentation is of maximum value if it can be used throughout the takeoff roll. If it is limited to a time shorter than that required for takeoff, then it is of interest to find whether the augmentation should be used early or late in the ground roll.

Since the energy gained equals the work done, limited augmentation is most efficient if used where the work done is a maximum. If the augmentation provides an increase in thrust, ΔF , for a fixed period of time, Δt , during which distance, ΔS , is traveled, then $\Delta S = V \Delta t$ and the work done will be

$$\text{work done} = \Delta F \times \Delta S = \Delta F \times V \Delta t \quad (8.4)$$

Both ΔF and Δt are fixed by the limitations of the augmenting engine. The pilot can obtain maximum gain by making V as large as possible. For minimum ground roll, therefore, limited thrust augmentation should be fired late, such that it will burn out or reach its time limit just as the aircraft becomes airborne.

Excess thrust during the takeoff roll is also dependent on aircraft angle of attack through both the drag term itself and the inclusion of lift in the wheel force term. We can determine the best angle of attack to maximize excess thrust by finding the optimum value of C_L .

$$F_{\text{ex}} = F - D - \mu (W - L) \quad (8.5)$$

Recall that

$$D = C_D qS$$

$$L = C_L qS$$

$$C_D = C_{D_p} + \frac{C_L^2}{\pi AR e}$$

Substituting into Equation 8.5

$$F_{ex} = F - \left(C_{D_p} + \frac{C_L^2}{\pi AR e} \right) qS - \mu (W - C_L qS) \quad (8.6)$$

Differentiating with respect to C_L

$$\frac{\partial F_{ex}}{\partial C_L} = - \frac{2C_L}{\pi AR e} qS + \mu qS \quad (8.7)$$

Setting the right side of Equation 8.7 equal to zero, the velocity term (q) drops out and the value of C_L for maximum excess thrust is constant at

$$C_{L_{opt}} = \frac{\mu \pi AR e}{2} \quad (8.8)$$

This lift coefficient is quite small for most aircraft and obviously results in extremely long takeoff distance if held throughout the roll. The optimum technique would be to establish the angle of attack which corresponds to $C_{L_{opt}}$ in Equation 8.8, maintain that until the speed permits liftoff at the maximum practical C_L available, and then rotate the aircraft to the liftoff attitude.

It should be pointed out that this technique is very seldom used. The inherent danger of overrotating, lack of elevator power, crosswind effects, and possible aircraft stability problems usually override any gain achieved. However, most aircraft are configured so that in the taxi attitude, the wing is near the optimum angle of attack for minimizing the total resistance throughout the takeoff roll.

8.2.5 Air Phase Equation

The equation for ground distance covered between liftoff and 50 feet altitude is obtained in a similar manner to the ground roll equation, except that the wheel force no longer exists. However, a potential energy term must be included:

$$\int_0^{S_a} (F-D) \, dS = \frac{W}{2g} \left[V_{50}^2 - V_{TO}^2 \right] + 50W \quad (8.9)$$

where S_a is the air phase distance and V_{50} is the ground speed at 50 feet. If we make the same assumption concerning excess thrust,

$$S_a = \frac{W \left[\frac{(V_{50}^2 - V_{TO}^2)}{2g} + 50 \right]}{(F-D)_{avg}} \quad (8.10)$$

Air distance for a given weight would obviously be minimum for a constant speed climb at maximum excess thrust. Maximum excess thrust occurs at the speed for minimum drag (max L/D). Most aircraft, however, lift off at an airspeed much slower than that for max L/D. In most cases, the gain due to an increase in excess thrust realized by accelerating prior to the initial climb is more than offset by the increase in distance due to the large kinetic energy change required. The number of variables involved, particularly if time limited thrust augmentation is included, makes definition of a single "best" technique impossible.

8.3 LANDING THEORY

8.3.1 Ground Distance Equation

The forces acting on an aircraft on landing roll can be depicted similarly to those shown in Figure 8.1 for takeoff. Low power settings and the increase in μ , the coefficient of resistance, due to brake application result in excess thrust less than zero. The equation for landing ground roll is also quite similar to the takeoff equation.

$$\int_0^{S_g} [F-D-\mu(W-L)] \, dS = W/2g (0-V_{TD}^2) \quad (8.11)$$

Where V_{TD} is the ground speed at touchdown. The required integration is accomplished using the same assumption. Equation 8.11 becomes

$$S_g = - \frac{W V_{TD}^2}{2g [F-D-\mu (W-L)]_{avg}} \quad (8.12)$$

8.3.2 Shortening the Landing Roll

Touchdown speed is obviously one of the most important determinants of distance required to stop. In addition to weight and speed at touchdown, landing roll can be influenced by all the factors in the excess thrust term. Thrust should be reduced to the minimum practical, and reverse thrust, if available, should be employed as soon as possible after touchdown. The logic for early application of reverse thrust is the same as for thrust augmentation on takeoff. Additional drag, whether from increased angle of attack or deployment of a drag chute, is most effective in the initial part of the landing roll for two reasons. Not only is a given force most effective at high speed, the force itself is greater due to its dependence on V^2 . Runway surface condition, as well as the mechanical design of the brakes themselves, can cause the value of μ to vary over a considerable range.

Our assumption of constant excess thrust is not unreasonable as long as the attitude of the aircraft remains relatively constant. It gets a bit shaky, however, if nose high aerodynamic braking is followed by maximum effort wheel braking. This technique is, for some aircraft, the recommended procedure for minimum landing roll. The question arises as to the most advantageous point to transition from one braking mode to the other. The relative magnitudes of the forces involved are shown in Figure 8.3. Note that μ_2 , with brakes applied, is much greater than μ_1 , which is the same as takeoff resistance. For minimum stopping distance, aerodynamic braking should be employed only as long as it provides a greater decelerating force than maximum wheel braking. An equation can be developed for the appropriate speed at which to make the transition using Equation 8.6 evaluated for both conditions. Unfortunately, the form of the resulting expression does not permit generalization of results.

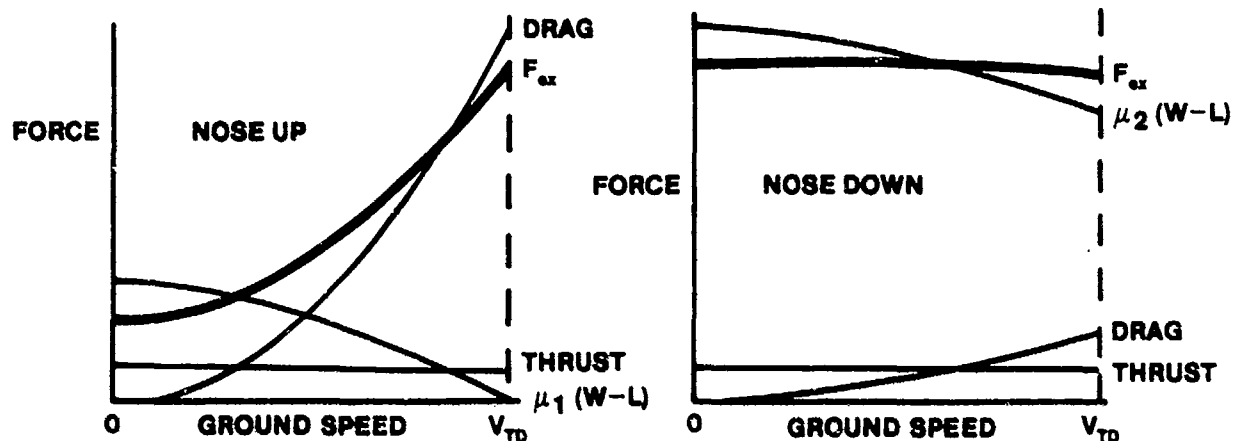


FIGURE 8.3. VARIATION OF FORCES DURING LANDING ROLLOUT

8.3.3 Air Distance Equation

The landing air distance equation is developed in exactly the same manner as the takeoff equation.

$$S_a = \frac{W \left[\frac{(V_{TD}^2 - V_{50}^2)}{2g} - 50 \right]}{(F-D)_{avg}} \quad (8.13)$$

Rearranging signs for consistent form,

$$S_a = \frac{-W \left[\frac{(V_{50}^2 - V_{TD}^2)}{2g} + 50 \right]}{(F-D)_{avg}} \quad (8.14)$$

Examination of Equation 8.14 shows that air distance is minimized if touch-down speed is maintained throughout the final descent (no flare!) and a high drag/low thrust configuration (steep glide path) is used. The structural integrity of the aircraft becomes the limiting factor.

8.4 CORRECTIONS TO STANDARD CONDITIONS

Now that a set of equations are available, we can use them to determine the effects of nonstandard conditions on actual takeoff performance. Remember, the equations were developed for this purpose, and cannot be used to predict exact performance.

8.4.1 Wind

The wind correction is normally the first to be applied. The velocity in Equation 8.3 is ground speed at liftoff, since this defines the energy level required. The aircraft, however, flies according to its airspeed which can be considerably different from ground speed in significant winds. Since ground speed and true airspeed are equal in a no wind situation, the ground speed required with wind is

$$V_{TO_w} = V_{TO} - V_w \quad (8.15)$$

where V_w is positive for a headwind, and includes only the component of wind velocity parallel to the runway. From Equations 8.3 and 8.5

$$S_{g_w} = \frac{W V_{TO_w}^2}{2g F_{ex_{avg_w}}} \quad (8.16)$$

where the subscript w indicates parameters in the wind environment. Substituting Equation 8.15 into Equation 8.3

$$S_g = \frac{W (V_{TO_w} + V_w)^2}{2g F_{ex_{avg}}} \quad (8.17)$$

Dividing Equation 8.17 by Equation 8.16

$$\frac{S_g}{S_{g_w}} = \frac{F_{ex_w}}{F_{ex_{avg}}} \frac{(V_{TO_w} + V_w)^2}{V_{TO_w}^2} \quad (8.18)$$

$$S_g = S_{g_w} \frac{F_{ex_{avg_w}}}{F_{ex_{avg}}} \left(1 + \frac{V_w}{V_{TO_w}}\right)^2 \quad (8.19)$$

The difference in excess thrust due to wind is difficult to determine, but has a significant effect on takeoff roll. An empirical relationship has been developed which works well for steady winds less than 10 knots. This relationship provides the following equation for correction of wind effect:

$$S_g = S_{g_w} \left(1 + \frac{V_w}{V_{TO_w}}\right)^{1.85} \quad (8.20)$$

Equation 8.20 does not account for gusts, which might have considerable effect if occurring near liftoff speed. For this and other reasons it is often required that winds be kept below 5 knots before takeoff data will be accepted.

For the air phase an exact determination of wind velocity is even more difficult. The correction, however, is quite simple, based on the fact that change in distance caused by wind is $\Delta S = V_w t$.

$$S_a = S_{a_s} + \Delta S \quad (8.21)$$

8.4.2 Runway Slope

If we define runway slope angle θ as positive downhill, we can obtain a correction equation by adding a potential energy term to Equation 8.2 (subscript sl indicates sloping runway parameters).

$$F_{\text{ex avg}} S_{g_{sl}} = \frac{1}{2} \frac{W}{g} V_{TO}^2 - W S_{g_{sl}} \sin \theta \quad (8.22)$$

$$S_{g_{sl}} = \frac{W V_{TO}^2}{2g (F_{\text{ex avg}} + W \sin \theta)} \quad (8.23)$$

Solving Equations 8.3 and 8.23 for $F_{\text{ex avg}}$ and equating the results

$$\frac{W V_{TO}^2}{2g S_g} = \frac{W V_{TO}^2}{2g S_{g_{sl}}} - W \sin \theta \quad (8.24)$$

Solving for S_g ,

$$S_g = \frac{S_{g_{sl}}}{1 - \frac{S_{g_{sl}}}{V_{TO}^2} \sin \theta} \quad (8.25)$$

The relationship is such that a fairly large slope is required before data will be significantly affected. Low thrust-to-weight aircraft with relatively low takeoff speeds (trash haulers) will be affected more than high thrust-to-weight, high wing loaded (fighter) aircraft.

8.4.3 Thrust, Weight, and Density

Atmospheric conditions will affect the thrust available from the engines as well as changing the true airspeed required to fly a given weight at the standard lift coefficient. As the weight changes, the airspeed required to fly at that C_L will also change. The analysis of these effects results in extremely complex expressions, and sophisticated computer operations are required for their evaluation.

Empirical relationships have been developed which provide reasonably accurate results. For jet aircraft, the expressions are (subscripts s and t refer to standard day and test day parameters, respectively):

$$\frac{S_{g_s}}{S_{g_t}} = \left(\frac{W_s}{W_t} \right)^{2.3} \left(\frac{\sigma_t}{\sigma_s} \right) \left(\frac{F_{n_t}}{F_{n_s}} \right)^{1.3} \quad (8.26)$$

$$\frac{S_{a_s}}{S_{a_t}} = \left(\frac{W_s}{W_t} \right)^{2.3} \left(\frac{\sigma_t}{\sigma_s} \right)^{0.7} \left(\frac{F_{n_t}}{F_{n_s}} \right)^{1.6} \quad (8.27)$$

The accuracy of these equations depends very heavily on the determination of net engine thrust, F_n . Equations developed from thrust stand data are normally used.

For turboprop aircraft with constant speed props, the correction equations are

$$\frac{S_{g_s}}{S_{g_t}} = \left(\frac{W_s}{W_t} \right)^{2.6} \left(\frac{\sigma_t}{\sigma_s} \right)^{1.9} \left(\frac{N_t}{N_s} \right)^{0.7} \left(\frac{P_{a_t}}{P_{a_s}} \right)^{0.5} \quad (8.28)$$

$$\frac{S_{a_s}}{S_{a_t}} = \left(\frac{W_s}{W_t} \right)^{2.6} \left(\frac{\sigma_t}{\sigma_s} \right)^{1.9} \left(\frac{N_t}{N_s} \right)^{0.8} \left(\frac{P_{a_t}}{P_{a_s}} \right)^{0.6} \quad (8.29)$$

where N is propeller rpm.

8.4.4 Pilot Technique

Individual pilot technique is probably the factor causing the greatest variation in takeoff data. Unfortunately, it cannot be quantified and mathematical corrections are impossible. Some of the factors which can significantly affect takeoff performance are:

1. Speed and sequence of brake release and power application.
2. The use of nose wheel steering, differential braking or rudder deflection for directional control.
3. The number and amplitude of directional control inputs used.
4. Aileron and elevator position during acceleration.
5. Airspeed at rotation.
6. Pitch rate during rotation.
7. Angle of attack at liftoff.

8.4.5 Landing Data Corrections

The corrections of landing data to standard day are basically identical to the methods used in takeoff. The wind correction equations and runway slope correction are identical to takeoff performance. The equation for thrust, weight, and density will be the same if reverse thrust is used, but may be simplified if idle thrust is used by setting $F_{n_t} = F_{n_s}$.

Then

$$S_{g_s} = S_{g_t} \left(\frac{W_s}{W_t} \right)^2 \left(\frac{\sigma_t}{\sigma_s} \right) \quad (8.30)$$

$$S_{a_s} = S_{a_t} \left(\frac{W_s}{W_t} \right) \left(2 + \frac{h_v}{h_v + 50} \right) \left(\frac{\sigma_t}{\sigma_s} \right) \frac{h_v}{h_v + 50} \quad (8.31)$$

where h_v is the kinetic energy change during the air phase

$$h_v = \frac{v_{50}^2 - v_{TD}^2}{2g} \quad (8.32)$$

Experience has shown the weight correction to be valid only over a very small range. In order to obtain data over a wide range of gross weights, a large number of tests must be conducted at carefully controlled weight near preselected standard weights.

Pilot technique is even more important in landing data than in takeoff data. Data scatter will result from variations in:

1. Power handling during approach, flare, and touchdown
2. Altitude of flare initiation
3. Rate of rotation in flare
4. Length of hold-off time
5. Touchdown speed
6. Rapidity of initiation of braking (aerodynamic and/or wheel)
7. Use of drag chute and/or reverse thrust
8. Brake pedal pressure

8.5 FLIGHT TEST

Takeoff and landing tests are important portions of the flight test program for any aircraft. Generally, during the course of a flight test program, all takeoffs and landings will be recorded for data purposes whenever weather and other factors permit; in addition, a number of test missions may be devoted entirely to takeoffs in various configurations, refused takeoffs, and landings in various configurations, all done at various gross weights.

More than any other tests, takeoffs and landings are affected by factors which cannot be accurately measured and properly compensated for. It is only possible to estimate the capabilities of the airplane within rather broad limits, relying on a statistical average of as many takeoff and landing maneuvers as possible to cancel residual errors.

Dedicated takeoff and landing tests are typically delayed during the development flight test phase of a new aircraft. This is mainly due to the fact that these tests take a fair amount of support and time to perform. Except for basic initial data taking and safety considerations, the delay is

due to higher priority of other airframe and systems tests. A minimum amount of initial tests in the takeoff and landing phase are performed to clear the aircraft envelope and "spot check" estimated performance. The bulk of the more hazardous takeoff and landing tests are performed downstream of the initial development flight test phase when more opportune test resources and airframes are available. It is the responsibility of the program manager to ensure that adequate flight test data is available in this area prior to critical phases of aircraft development such as operational deployment.

8.5.1 High Speed Taxi Tests

Since the takeoff precedes the landing of an aircraft, it is logical that takeoff tests precede landing tests. However, because the possibility of a refused takeoff is always present, high speed taxi tests are normally conducted prior to actual takeoff or landing tests because certain parameters must be determined which are important to both.

The parameters normally determined from high speed taxi tests are thrust transients, drag, and rolling coefficient of friction. Tests must be conducted on surfaces of different composition and under wet and dry conditions. Aircraft should also be tested at several gross weights and in all configurations within the aircraft's mission capability.

Some braking tests would also be conducted as part of the high speed taxi tests. However, full braking effectiveness can only be evaluated during refused takeoff or actual landing tests.

8.5.2 Takeoff Tests

In a takeoff performance test, ground roll distance and air distance to clear a 50 foot obstacle must be determined. Effort must be made to determine optimum rotation speeds for different gross weights and aircraft configurations. Runway composition and condition must again be considered.

In the event of an unplanned refused takeoff, knowledge of the parameters determined during high speed taxi tests is very beneficial.

Planned refused takeoff tests must be conducted to determine stopping distances and braking capability with the aircraft in the three point attitude. The controllability of the aircraft and operation of the antiskid system (if installed) must be assessed.

8.5.3 Landing Tests

A typical landing test is broken down into several phases. The importance of the parameters determined during the high speed taxi tests cannot be overemphasized.

The initial phase of a landing test would be to determine the air distance from 50 feet above the ground to touchdown. Methods of determining this distance are contained in Reference 8.3. Other than determination of the air distance, the particulars of this phase of the test are more pertinent to handling qualities of the aircraft during landing approach.

Once the aircraft has touched down, stopping distance and brake effectiveness must be evaluated. Stopping distance is, once again, a function of the type of surface and condition of the surface.

Braking effectiveness is a function of brake energy, temperature, and aircraft weight. Weight variation up to the maximum energy capability of the brake system should be explored, keeping a careful record of degradation of braking effectiveness due to temperature increase. Brake wear must also be recorded to determine intervals at which brake system components must be replaced to prevent hazardous landings.

The effects of aerodynamic braking and other methods of reducing ground roll distance, i.e., thrust reversing and drag chute, should also be determined. If the aircraft is equipped with an arresting hook, tests must be made to ensure that the aircraft can withstand the structural loads during an arrestment and still be stopped safely and effectively.

One last area that has a definite effect on landing characteristics is crosswind. Once again the airborne phase of this particular test is more pertinent to flying qualities testing. The ground handling characteristics of the aircraft during takeoff and landing rollout and taxiing must be evaluated to determine the effects of crosswinds up to the maximum crosswind component acceptable for the aircraft.

8.5.4 Safety

The importance of safety during conduct of all high speed taxi, takeoff, and landing tests cannot be overemphasized. These tests are all classified as hazardous. The danger of losing control of the aircraft is ever present. During braking tests, elevated temperatures may cause overheating of the brake

system or even fire. Therefore, safety must be considered during the initial test planning, and proper safeguards should be ensured throughout the test program.

8.5.5. Data Recording Methods

Data recording during takeoff and landing tests is divided into two categories:

1. External Data - Ground roll, distance to 50-foot height, ground speed and acceleration, runway temperature, ambient pressure, and runway wind conditions.
2. Internal Data - Power parameters, V_i , H_i , T_i , EGT, etc. The most desirable method of recording internal data is by use of on board instrumentation; however, limited hand recorded data can be taken.

External data is usually recorded by a phototeodolite which yields distance, velocity (ground speed), and acceleration as shown in Figure 8.4.

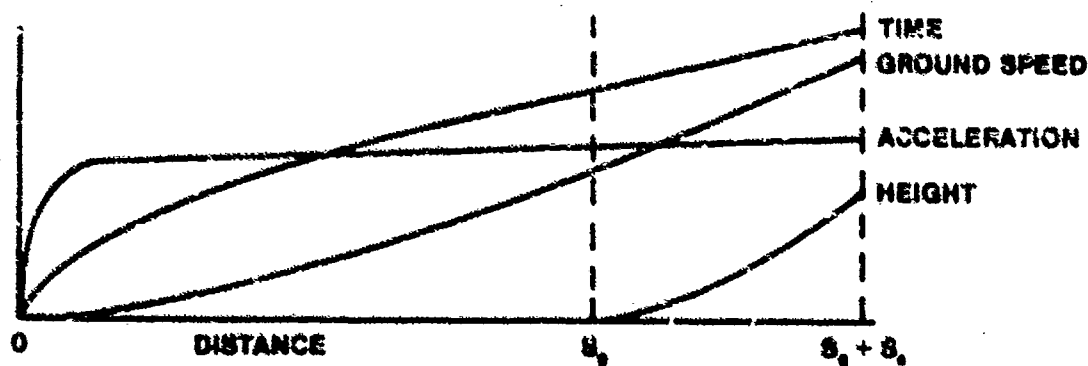


FIGURE 8.4. TAKEOFF DATA

The theodolite data will normally be in the form of printed digital readouts which can be used to develop plots similar to those in Figure 8.4.

If a phototheodolite is not available, the pilot can estimate ground roll and total distance to a 50-foot height. Distance can be estimated by reference to runway markers and edge lights. (The lights at Edwards AFB are 200 feet apart). If takeoff roll is started abeam a light, ground distance can usually be judged within \pm one light. Air distance determination by pilot estimate is at best a rough approximation and probably almost useless. Not only is it difficult to determine distance down the runway, it is virtually impossible to accurately judge 50 feet altitude.

Temperature, ambient pressure, and wind velocity and direction should be monitored continuously at the runway. This information may be supplied as part of the technical support data; however, the pilot should record the same information as a cross-check and back up. The pilot should always attempt to estimate takeoff performance by reference to runway markers even with theodolite coverage to provide an additional means of correlation and cross-check.

8.5.6 Standardization Technique

The large amount of data scatter introduced by pilot technique was discussed in Sections 8.4.4 and 8.4.5. Although this scatter can never be eliminated, it can be minimized by as much standardization of technique as possible among members of the test team. Items which can be standardized include:

1. Throttle setting prior to brake release
2. Throttle technique at/immediately after brake release
3. Control position during acceleration
4. Airspeed at rotation
5. Rate of rotation
6. Aircraft attitude at liftoff
7. Gear and flap retraction points

These are by no means the only items to be considered. The degree of standardization available and the effect on data scatter will vary considerably between different aircraft types.

8.5.7 Summary

Takeoff and landing tests are an important part of the performance testing of any aircraft. The large number of variables involved, especially the strong influence of individual pilot technique, results in a vast amount of data scatter and a very low degree of repeatability. A large number of data points are required to accurately predict the actual capabilities of the aircraft.

PROBLEMS

8.1 Certain simplifying assumptions may be made to the takeoff problem with very little loss of accuracy. Consider the following aircraft during takeoff roll:

$$T/W = 0.80$$

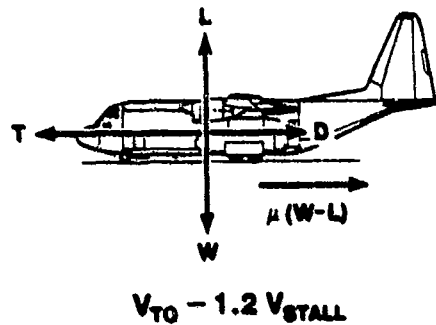
$$C_D = 0.02 + .2 C_L^2$$

$$C_L = 0.1$$

$$\mu = 0.04$$

$$W = 40,000 \text{ lbs}$$

$$S = 550 \text{ ft}^2$$



- a. Assuming that the acceleration is constant over the takeoff ground run, show that

$$S_G = 1/2 \frac{V_{TO}^2}{a} \text{ where } a = \frac{dV}{dt}$$

- b. Using $\Sigma F = ma$, derive an expression for the average acceleration during the ground run.
- c. Using the data given above at sea level, calculate a value for each term in the equation for acceleration. Assume $V_{ave} = 100 \text{ KTAS}$.
- d. Observe the quantities found in Part c: which of these can be eliminated from the equation with only a small loss in accuracy?

- e. Show that a good 1st order approximation for takeoff ground run may be expressed as

$$S_G = \frac{1.44}{g \rho C_{L_{\max}}} \left(\frac{W}{S} \right) \left(\frac{W}{T} \right)$$

- f. Using the approximation of Part e: answer the following questions. Assume all other conditions remain the same.

1. Calculate the ratio of takeoff distances for an aircraft at a gross weight of 55,000 lbs to one of 35,500 lbs.
2. Calculate the ratio of takeoff distances for an aircraft at sea level to one at 6,000 ft. Use standard day conditions. Do not neglect the change in thrust.
3. Calculate the ratio of takeoff distances for an aircraft in a cruise configuration $\left(C_{L_{\max}} = 0.9 \right)$ to one with takeoff flaps $\left(C_{L_{\max}} = 1.6 \right)$.
4. Calculate the ratio of takeoff distances for a day when the temperature is 20°F to a day when it is 90°F . The atmospheric pressure in both cases is sea level standard day. The effect of temperature change upon the thrust output of the engine is not easily determined. Use the assumption that there is approximately a 25% decrease in thrust for a 70° temperature increase.

ANSWERS TO PROBLEMS

8.1 d. All but thrust

f1. 2.47

f2. .67

f3. 1.78

BIBLIOGRAPHY

- 8.1 Lush, K.J., Standardization of Takeoff Performance Measurements for Airplanes, USAF Technical Note R-12, AFFTC, 1952.
- 8.2 FTC-TIH-70-1001, Performance, USAF Test Pilot School, 1973.
- 8.3 Herrington, R.M., et al., Flight Test Engineering Handbook, AF Technical Report No. 6273, Revised January 1966.

CHAPTER 9
ENERGY CONCEPTS

9.1 INTRODUCTION

To evaluate modern aircraft and aircraft systems requires an understanding of how aerodynamic performance can be optimized. Performance specifications today go well beyond point design specifications and depend heavily on optimization to fit specific tactical requirements whether the vehicle is designed as an interceptor, an air supremacy fighter, a strategic airlifter, a strategic bomber, or for any other operational role. The goal is to demand a performance efficiency covering the entire flight envelope that will meet the operational need with the best overall combination of armament, engine, and airframe. The F-14 and F-15 were the first generation of fighter aircraft to be designed and evaluated within this approach. Newer fighter designs like the F-16, the F-18, the Tornado, and the Mirage 2000 have been conceived with full cognizance of the need for optimized performance. At least since the mid 1960's, fighter performance has been driven by fuel prices and shortages. Service airlift commands and the airlines have shown renewed interest in optimized performance for C-141's, L-1011's, and other transport aircraft. New systems, based on optimization that are closely akin to the energy state approximation, have been proposed and put into service on these aircraft. All in all, interest in performance optimization of this type seems to be increasing. Hence, the test engineer and test pilot must have a working knowledge of the energy approximation and the concepts associated with performance optimization.

9.1.1 Aircraft Performance Models

The almost universally accepted mathematical model for aircraft performance is a point-mass model; that is, we need only consider the forces acting on the center of gravity of the airplane. But even this simple set of governing equations can be manipulated under a wide range of assumptions. Bryson, Desai, and Hoffman (10.1:481ff) have conveniently catalogued several of these approximations from an optimal control perspective. For our convenience, we will lump these models into three categories:

1. Steady state approximation
2. Energy state approximation

3. Higher order optimal control approximations

In this chapter, we will consider only the first two of these models, with by far the heaviest emphasis on the energy state approximation.

9.1.2 Need for Nonsteady State Models

The classical approach to aircraft performance problems is a "static" or steady state one. For this approximation, either true airspeed or altitude (or both) must be held constant. Therefore, the model is inadequate for analyzing climb profiles, for example, of supersonic aircraft. Both true airspeed and altitude change rapidly for such airplanes. Obviously, the steady state approximation cannot cope satisfactorily with vehicles like the Space Shuttle Orbiter which never achieves steady state flight.

At the other end of the sophistication spectrum, we do not require test engineers and test pilots to have a complete working knowledge of the calculus of variations and optimal control theory. Hence, higher order models will be considered only cursorily, usually for comparison purposes.

9.2 STEADY STATE CLIMBS AND DESCENTS

Climbs and descents at constant true airspeed ($dV/dt = 0$) are a subset of problems associated with performance optimization. They could be called "static" performance problems and, as such, are useful as first order tools of analysis. For our purposes, they also serve as an introduction to the energy state approximation.

9.2.1 Forces Acting on an Aircraft in Flight

The forces acting on an aircraft in flight are conventionally resolved perpendicular and parallel to the direction of flight, as shown in Figure 9.1.

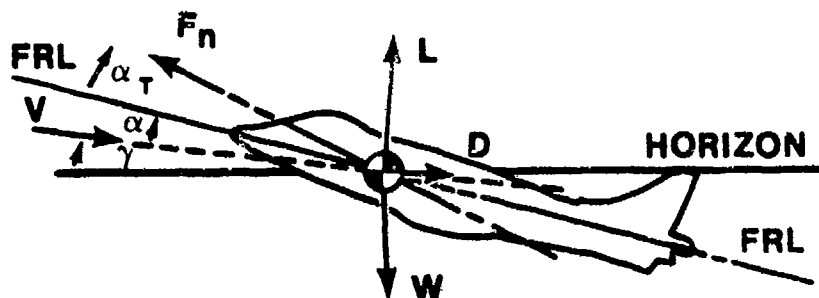


FIGURE 9.1. FORCES ACTING ON AN AIRCRAFT IN FLIGHT

Perpendicular to the flight path

$$L - W \cos \gamma + F_n \sin (\alpha + \alpha_T) = m a_z$$

Parallel to the flight path

$$F_n \cos (\alpha + \alpha_T) - D - W \sin \gamma = m a_x$$

With the following relatively minor simplifying assumptions

$$\alpha = 0 \text{ and } \alpha_T = 0$$

$$a_z = 0 \text{ and } a_x = \frac{dv}{dt}$$

these equations take on simpler, more recognizable forms.

$$L - W \cos \gamma = 0 \quad (9.1)$$

$$F_n - D - W \sin \gamma = \frac{W}{g} \frac{dv}{dt} \quad (9.2)$$

For purposes of examining how to maximize γ , true airspeed is held constant. At a constant true airspeed, $dv/dt = 0$. With this restriction, Equation 9.2 becomes

$$F_n - D = W \sin \gamma$$

which gives a useful expression for γ

$$\gamma = \sin^{-1} \left[\frac{F_n - D}{W} \right] \quad (9.3)$$

or

$$V \sin \gamma = \left[\frac{F_n - D}{W} \right] V$$

But $V \sin \gamma$ is simply the rate of climb or rate of descent, as Figure 9.2 illustrates.

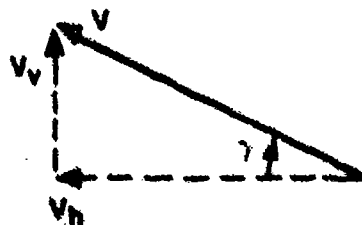


FIGURE 9.2. RATE OF CLIMB

$$V_v = \frac{dh}{dt} = V \sin \gamma = \frac{(F_n - D)}{W} V \quad (9.4)$$

This expression clearly shows that if net thrust is greater than drag, dh/dt is positive; that is, $F_n > D$ produces a climb. Conversely, $F_n < D$ produces a descent and dh/dt is negative. Gliding flight is the special case when $F_n = 0$. This simple expression also allows the careful student to deduce the

effects of altitude, weight, wind, and velocity on angle of climb performance and rate of climb performance.

9.2.2 Angle of Climb Performance

As Equation 9.3 clearly shows, the flight path (or climb) angle γ depends on "specific excess thrust": $(F_n - D)/W$. As an aircraft with an air breathing powerplant climbs, the propulsive thrust decreases. Drag remains essentially constant. Thus, there is an absolute ceiling where $F_n = D$ and $\gamma = 0$. In other words, increasing altitude decreases specific excess thrust and the climb angle.

The effect of increasing weight on angle of climb is also obvious from Equation 9.3. Increasing weight directly reduces the climb angle because of the reciprocal relationship.

A steady wind actually has no effect on angle of climb. However, the prime reason for optimizing angle of climb (or descent) is to gain obstacle clearance during either the takeoff or landing phases of flight. The maximum climb angle must give the most altitude gained for horizontal distance covered. Winds do affect this horizontal distance and give apparent changes in γ as depicted in Figure 9.3. Not surprisingly, the obvious point is to always land and takeoff into a headwind if obstacle clearance is a concern.

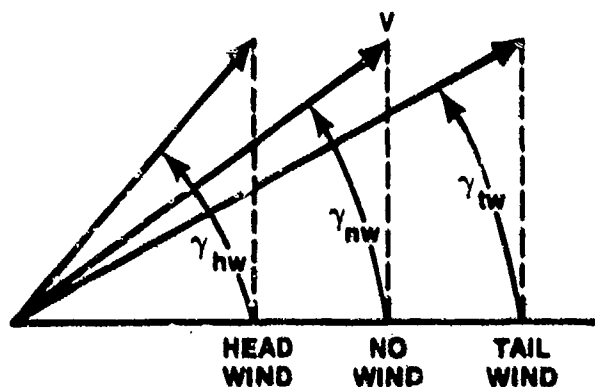


FIGURE 9.3. WIND EFFECT ON CLIMB ANGLE

Thrust curves show that excess thrust, $F_n - D$ is a function of airspeed. Figure 9.4 illustrates this point for the T-38. Whatever the type of propulsion — jet, turboprop, or reciprocating engine—the aircraft must be flown at the velocity where maximum excess thrust occurs to achieve the maximum climb angle.

Typically, the net thrust available from a pure turbojet varies little with airspeed at a given altitude. The J-85 operated at military thrust in the T-38, as shown in Figure 9.4, illustrates this characteristic well. Therefore, a jet aircraft, lacking any form of thrust augmentation, usually climbs at the velocity for minimum drag (or minimum thrust required) to achieve the maximum angle of climb. This classical result leads to the sometimes overemphasized notion that γ_{\max} occurs at $V_{L/D_{\max}}$.

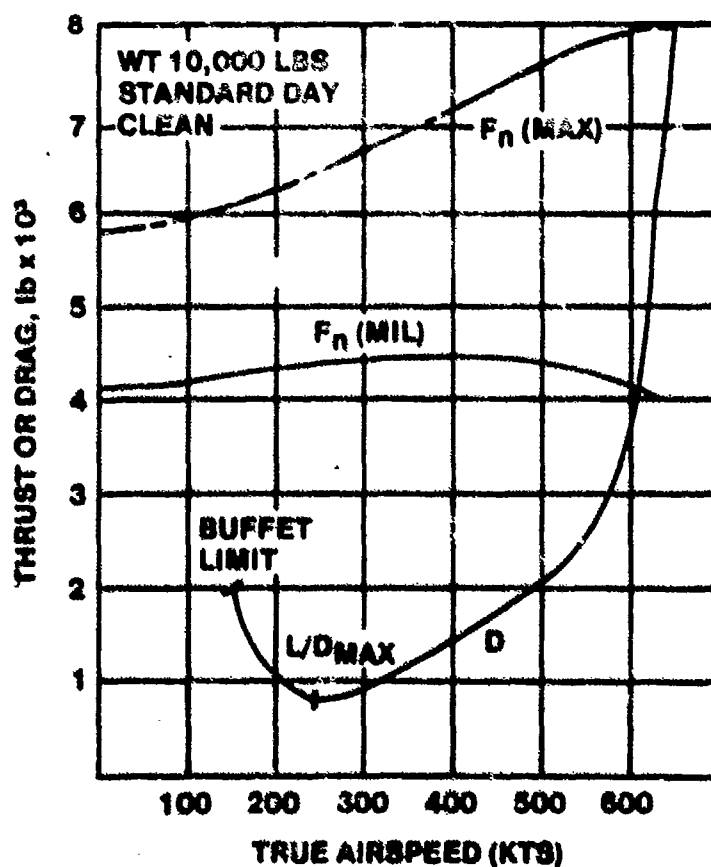


FIGURE 9.4. T-38 THRUST AND DRAG

This generalization is based on too many assumptions to be absolutely accurate. Any variation in thrust available with airspeed obviously affects the optimum velocity for maximum climb angle. Careful examination of Figure 9.4 reveals that in the T-38 any true airspeed between 240 and 270 knots results in approximately the same specific excess thrust, hence about the same γ . Any large variation in thrust available with airspeed, as is illustrated in the maximum afterburner curve for the T-38, clearly destroys the idea that γ_{\max} always occurs at $V_{L/D_{\max}}$.

The point is that precise determination of maximum angle of climb performance depends on specific excess thrust, which in turn requires knowledge of both airframe drag characteristics and propulsive system characteristics. The rule of thumb that a jet aircraft should climb at $V_{L/D_{\max}}$ for obstacle

clearance can be grossly in error for turbofans, turboprops, or any form of thrust augmentation. Propeller driven aircraft must account for propeller efficiencies and has its own peculiar thrust available curve. But, whether specific excess thrust is measured directly or calculated from independent estimates of thrust, drag, and weight, this parameter determines angle of climb performance.

9.2.3 Rate of Climb Performance

Referring again to Equation 9.4, rate of climb, dh/dt , depends upon "specific excess power." The terminology is analogous to specific excess thrust, which was defined as the difference between net thrust available and drag (or thrust required). Excess power is similarly defined as the difference between the power available to do work in a unit of time and the work done by drag per unit of time.

$$F_n V = \text{power available}$$

$$DV = \text{power dissipated by drag (or power required)}$$

$$\frac{dh}{dt} = \frac{(F_n - D) V}{W} = \frac{F_n V - DV}{W} = \frac{P_A - P_R}{W} \quad (9.5)$$

Altitude has an effect on rate of climb similar to its effect upon angle of climb. Rate of climb at the absolute ceiling goes to zero because $F_n = D$ and, obviously, excess power is nil. In military specifications, there are two other performance ceilings defined by rate of climb performance. The service ceiling and combat ceiling are respectively the altitudes where 100 ft/min and 500 ft/min rates of climb can be maintained.

Weight affects rate of climb directly and in the same manner as it does climb angle. Increasing weight with no change in excess power reduces rate of climb.

Wind affects rate of climb negligibly unless gradient and direction changes are large within the air mass.

True airspeed strongly affects rate of climb performance since thrust and drag are functions of velocity themselves, and further specific excess power explicitly depends upon true airspeed according to Equation 9.4. Figure 9.5 illustrates the typical power available and power required for a turbojet and propeller aircraft. The propeller driven aircraft obtains maximum rate of climb at a true airspeed close to the velocity for maximum L/D. For jet aircraft, maximum rate of climb occurs at some higher true airspeed. Figure 9.6 compares the power required and power available (both at military and maximum power) for the T-38. This chart, based on Figure 9.4, supports the validity of the idealized estimates of Figure 9.5. Whatever the shape of the actual measured curves, maximum specific excess power produces maximum rate of climb in a constant airspeed climb.

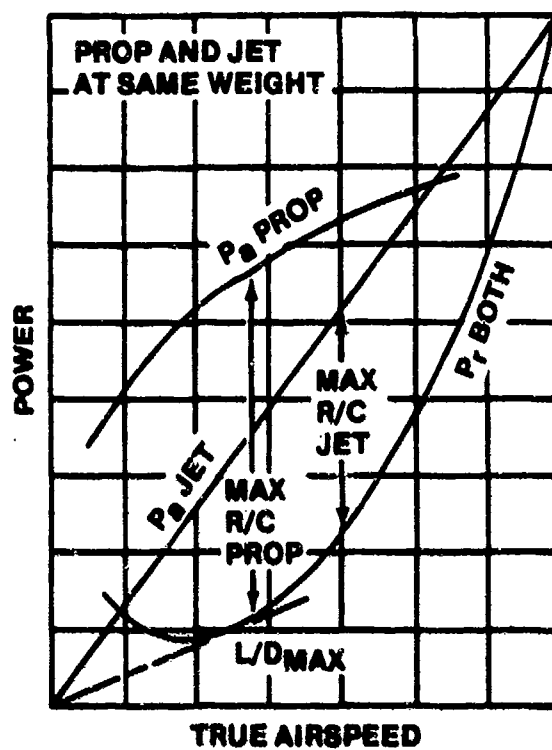


FIGURE 9.5. TYPICAL RATE OF CLIMB PERFORMANCE

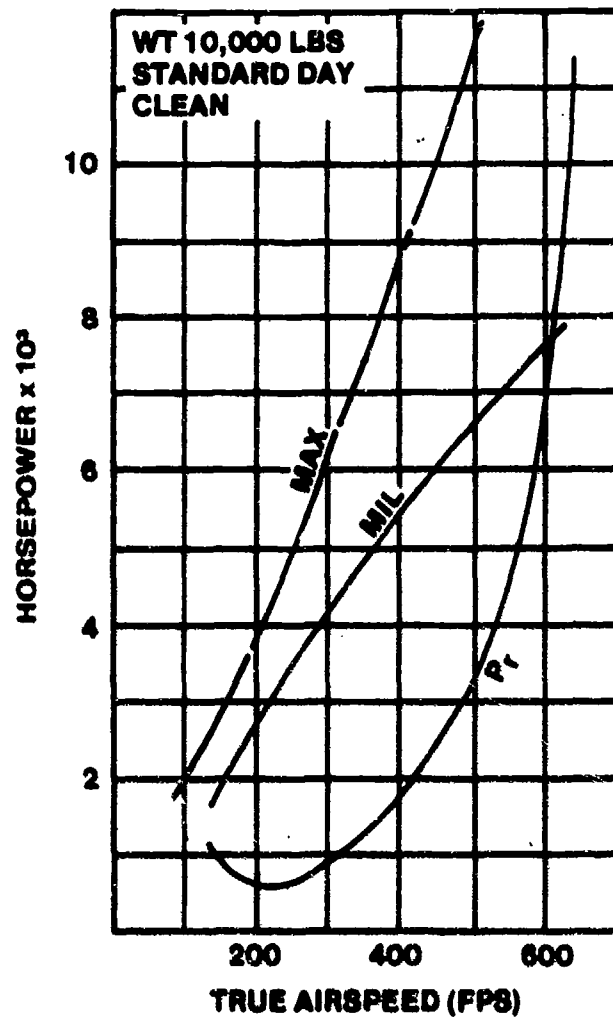


FIGURE 9.6. T-38 RATE OF CLIMB PERFORMANCE

9.2.4 Time to Climb Determination

The climb performance parameter of most interest to the operational pilot is usually time required to climb to a given altitude. Rates of climb discussed so far are instantaneous values. At each altitude, there is one velocity which yields maximum rate of climb. That value of maximum rate of climb pertains only to that discrete altitude. Continuous variations in rate of climb suggest a summation through integration (see Figure 9.7).

$$dt = \frac{dh}{\frac{dh}{dt}}, \text{ where } \frac{dh}{dt} = f(h)$$

or

$$\int_0^t dt = t = \int_0^h \frac{dh}{dh/dt} \quad (9.6)$$

However, dh/dt is usually not available as an analytical function of altitude; hence, Equation 9.6 can rarely be integrated, except with graphical or numerical techniques.

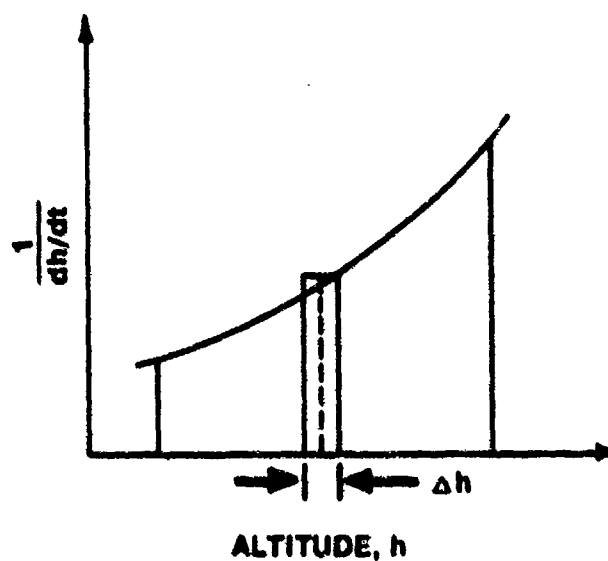


FIGURE 9.7. TIME TO CLIMB

9.2.5 Gliding Performance

Gliding flight ($F_n = 0$) offers a simple application of Equations 9.3 and 9.4. This special case also leads to results that further illuminate the usefulness and importance of the velocity for maximum L/D . Attacking the angle of descent (negative angle of climb) problem first, the ratio of the horizontal distance covered to altitude lost defines γ . As can be seen from Figure 9.8,

$$L = W \cos \gamma$$

$$D = W \sin \gamma$$

or

$$\boxed{\frac{L}{D} = \cot \gamma} \quad (9.7)$$

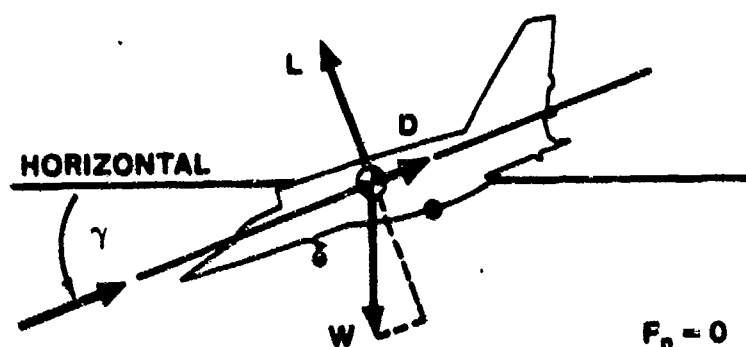


FIGURE 9.8. FORCES ACTING IN A GLIDE

Equation 9.7 expresses the fact that when $|\gamma|$ is a minimum, $|\cot \gamma|$ is a maximum. In other words, when L/D is maximum, the maximum horizontal distance is achieved for a given altitude loss. The trigonometric relations show that the ratio of horizontal distance travelled to vertical distance (or horizontal velocity to vertical velocity for a constant true airspeed descent) is equal to L/D . Hence, L/D_{\max} gives the "best" glide ratio and is frequently called the glide ratio.

To minimize the rate of descent in a glide, Equation 9.4 is specialized with $F_n = 0$.

$$\frac{dh}{dt} = - \frac{DV}{W} \quad (9.8)$$

Once again, dh/dt is a function of "power" dissipated and is not a simple function of drag. If one assumes a parabolic drag polar, it can be shown that the velocity for minimum rate of descent is about 25% less than the true airspeed for minimum glide angle. This result (which will be demonstrated in homework and class discussion) means that the pilot who tries to stretch his glide by minimizing sink rate is actually reducing the horizontal distance covered (range) for a given loss in altitude.

Two identical sailplanes operating at different gross weights will have identical glide ratios, since they will have the same L/D ratio. Figure 9.9 illustrates two sets of equilibrium conditions. Note that $L_2 > L_1$ to support

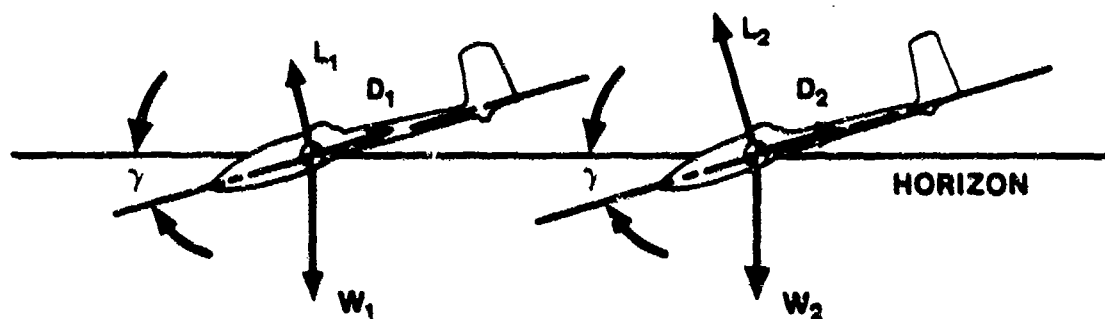


FIGURE 9.9. EFFECT OF WEIGHT ON GLIDE RATIO

the increased weight. But to obtain $(L/D)_{\max}$, the pilot holds the same angle of attack. Thus, to maintain the force equilibrium, he must increase speed to increase L_1 to L_2 . As the heavier sailplane flies faster, it also generates more drag. Hence, the heavier aircraft flies faster, arriving sooner and descending faster, but covers the same distance. This principle is the driving influence behind jettisonable water ballast for competition sailplanes, when one of the goals is to cover a given closed course distance in minimum time.

9.2.6 Polar Diagrams

Polar diagrams are graphical means of summarizing aircraft steady state performance. Three conditions are assumed for any one diagram.

1. Aircraft weight is constant
2. Altitude is constant
3. Throttle setting is constant

A change in any one of these constants calls for a new diagram to describe the new steady state. Figure 9.10 is a typical polar diagram for military thrust in a jet aircraft.

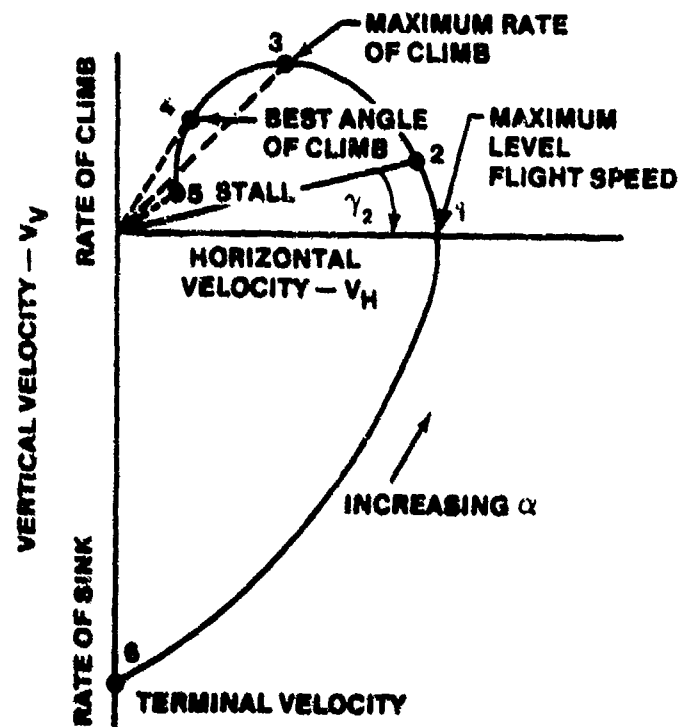


FIGURE 9.10. MILITARY THRUST POLAR DIAGRAM

This plot represents all the combinations of vertical and horizontal velocities that the airplane can attain in unaccelerated flight at a given altitude, throttle setting, and weight.

Point 1, for example, represents the maximum attainable level flight speed with these conditions. Point 2 represents a steady state climb at the flight path angle (γ_2) indicated. A line drawn from the origin to any point on the diagram represents vectorially the true airspeed for that flight condition. The angle of climb for any steady state pair of velocity components is the angle between the true "airspeed vector" and the horizontal velocity component (x-axis). Point 3, the maximum value for rate of climb, obviously provides a lower climb angle than Point 4. The fact that $V_{\max R/C}$ is greater than $V_{\gamma \max}$ is driven home, if one notes the magnitudes of the true airspeed vectors for Points 3 and 4. It is graphically clear that from a diagram like this, one can obtain γ_{\max} and the $V_{\gamma \max}$ by simply drawing a line from the origin tangent to the curve. Point 5 depicts the stalling speed. This example represents an aircraft that is capable of climbing at military thrust when it stalls. Point 6 represents the vertical velocity the airplane could attain if it were diving with $\gamma = 90^\circ$ at military thrust. This speed, termed the terminal velocity, is often of academic interest only because many aircraft would break up before it could be attained. This point highlights the fact that polar diagrams show only aerodynamic (thrust and drag) information; structural limitations, control limitations, and other non-aerodynamic constraints are not usually noted. Finally, the polar diagram can also have angle of attack annotations. At Point 5, the angle of attack is α_g ; at Point 4, α is that for L/D_{\max} ; and at Point 6, α is the angle of attack for zero lift. Hence, α increases as one travels in a counterclockwise direction around the polar.

Since weight, altitude, and power setting are constant, a family of curves is necessary to describe the effect of these variables. However, since each of these variables affects performance in a similar way, qualitatively any one of these changes can be represented by shifting the curve itself up or down. The power-off polar diagram, Figure 9.11, shows the differences in

airspeed for (1) minimum glide angle, (2) minimum rate of descent, and (3) minimum speed. The fallacy of trying to "stretch the glide" by flying slower is graphically portrayed, since γ_{\max} occurs at Point 1, where the true airspeed vector is tangent to the polar.

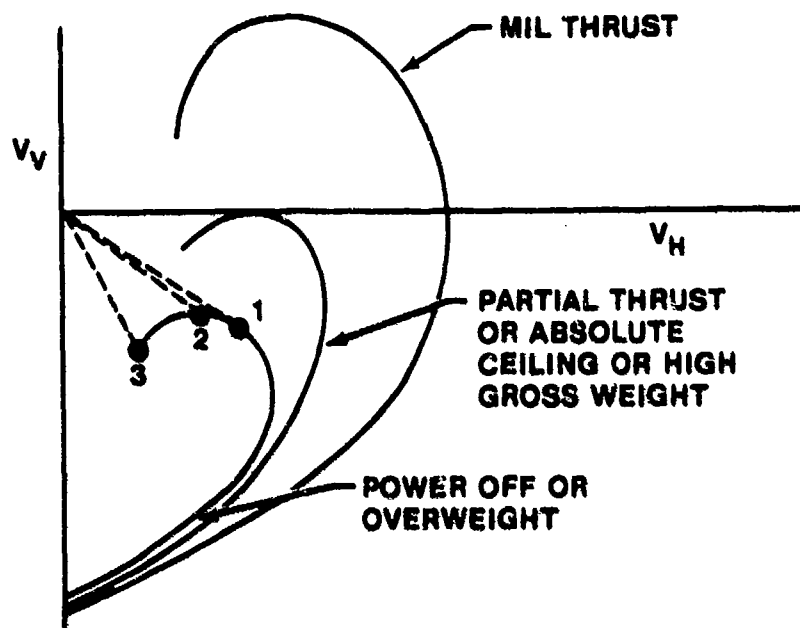


FIGURE 9.11. FAMILY OF POLAR DIAGRAMS

In summary, polar diagrams are handy for visualizing some of the basic concepts of steady state climb and descent performance. Important parameters, like γ_{\max} , $V_{\gamma_{\max}}$, V_{\max} r/c, are graphically portrayed. However, because of the constraints used in their construction and the consequent necessity to examine families of curves, polar diagrams are little used by operators. Soaring buffs do use them in constructing "speed-to-fly" charts that specify optimum transit speeds between thermal activity. Apart from such uses where the variables are limited by the nature of the vehicle, polar diagrams are largely useful only as a teaching tool.

9.3 BASIC ENERGY STATE CONCEPTS

A more general approach to aircraft performance was formulated by Rutowski in the early 1950's. His analysis is based on "the balance that must exist between the potential and kinetic energy exchange of the aircraft, the energy dissipated against the drag, and the energy derived from the fuel" (9.2:187). The definitions and explanations which follow are based on and generally parallel Rutowski's original development, though portions have been altered to clarify and amplify the concepts.

9.3.1 Assumptions

There are usually four basic assumptions made for elementary energy state analyses:

1. Configuration is fixed
2. Weight is constant
3. Load factor is constant
4. Thrust level is fixed

The underlying reason for each of these assumptions is to reduce the complexity of the mathematical problem. In fact, as we will see, these assumptions allow us to define an energy state with only two variables--altitude and true airspeed. However, we will also see that these assumptions can be relaxed for specific purposes. Weight and load factor will specifically be considered as parameters, for example, later on.

In addition to these four basic assumptions, we will be rather cavalier in this introductory course with the interchange between different forms of energy. As a first order approximation, we will assume that airspeed and altitude can be exchanged instantaneously with no energy dissipation. Such processes are, of course, idealized ones and would exceed angle of attack and load factor limitations if you attempted such maneuvers. But to add such constraints complicates the energy state approximation and obscures too many concepts for our purposes.

9.3.2 Energy Definitions

The total energy of an aircraft is comprised of kinetic energy in the form of airspeed and potential energy in the form of altitude.

$$\begin{aligned} E &= PE + KE \\ &= Wh + \frac{W V^2}{2g} \end{aligned} \quad (9.9)$$

An aircraft in a climb is increasing potential energy either by the expenditure of chemical energy (by the powerplant) or by decreasing kinetic energy (trading airspeed for altitude). Descents are also a change in potential energy which may or may not be accompanied by a change in kinetic energy. Constant true airspeed descents, for example, involve a decrease in potential energy (and therefore total energy) due to the work done by drag forces.

9.3.3 Specific Energy

In analyzing climbs and accelerations for aircraft having different weights at the same altitude-airspeed combinations, energy per pound of aircraft weight or "specific energy" is more convenient than total energy. Equation 9.9 can be rearranged and E_s defined as specific energy.

$$E_s = \frac{E}{W} = h + \frac{V^2}{2g} \quad (9.10)$$

Occasionally, E_s is called "energy height" since it has units of length only. Physically, this terminology suggests that "energy height" is the altitude the aircraft would attain if all its kinetic energy could be converted with no loss to potential energy. Alternatively, if all the altitude were converted to kinetic energy, the corresponding true airspeed is the maximum speed attainable with a given specific energy level.

9.3.4 Specific Excess Power

Perhaps the most important parameter in the energy methodology is obtained by differentiating Equation 9.10 with respect to time.

$$\frac{dE_s}{dt} = \frac{dh}{dt} + \frac{V}{g} \frac{dV}{dt} \quad (9.11)$$

It is not necessary to assume dh/dt and dV/dt are zero as was done for steady state performance analysis. However, from Equation 9.2

$$F_n - D - W \sin \gamma = \frac{W}{g} \frac{dV}{dt}$$

Dividing through by W/V and transposing

$$\frac{(F_n - D) V}{W} = V \sin \gamma + \frac{V}{g} \frac{dV}{dt}$$

But $V \sin \gamma = dh/dt$, therefore

$$\frac{dE_s}{dt} = \frac{(F_n - D) V}{W} \quad (9.12)$$

The term on the right side of Equation 9.12 is excess thrust multiplied by velocity and normalized for weight. Since thrust times velocity is power, dE_s/dt may be defined as specific excess power. We will define a new symbol for this term, P_s :

$$P_s = \frac{dE_s}{dt}$$

P_s characterizes the engine-airframe capability to change energy levels at a given airspeed, altitude, and power setting.

9.4 THEORETICAL BASIS FOR ENERGY OPTIMIZATIONS

Having defined terms and introduced the energy approach by reviewing steady state performance considerations, a theoretical foundation for applying energy techniques must be laid. The idea of applying powerful mathematical tools like the calculus of variations to aircraft performance was suggested by Graham (9.2:190) in Rutowski's original paper. Theoreticians are still adding to our store of knowledge in applying these tools. Test personnel need to be introduced to the basic variational principles so they can apply energy concepts to flight test problems and understand how flight test data provide operational users with information to develop optimized tactical profiles. However, the flight test team normally does not require a complete working knowledge of variational techniques. This section introduces only the most elementary ideas from the calculus of variations, but these simple notions are key to appreciating the power of the energy approximation.

9.4.1 Maxima and Minima

The calculus of variations is a branch of mathematics concerned with determining maxima and minima of expressions involving carefully specified unknown functions. Said another way, the calculus of variations provides a way to mathematically select optimized functions (or paths) from a set of functions (functional). Techniques of the calculus of variations are analogous to procedures used in the differential calculus to determine maximum and minimum values of a function. For example, if $y = y(x)$ is a continuously differentiable function over the interval (a, b) , a necessary condition for the existence of a maximum at x_0 (with $a < x_0 < b$) is that $dy/dx = 0$. A sufficient condition that y be a maximum is that $d^2y/dx^2 < 0$ at x_0 as shown in Figure 9.12.

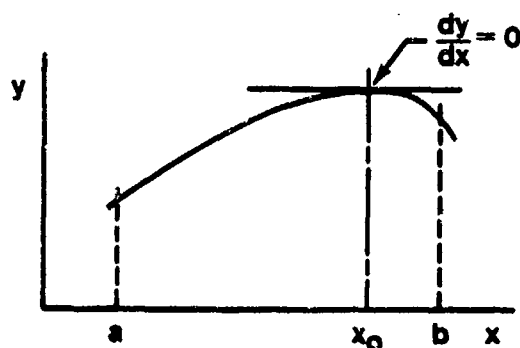


FIGURE 9.12. MAXIMUM VALUE OF A FUNCTION

Taking the next step up in complexity, assume that $z = z(x, y)$ is a continuous function of two independent variables throughout a region R . Then, the necessary conditions that z possess a relative maximum or minimum at an interior point (x_0, y_0) are: $\partial z / \partial x = 0$ and $\partial z / \partial y = 0$ simultaneously at (x_0, y_0) . Said another way,

$$dz = \frac{\partial z}{\partial x} dx + \frac{\partial z}{\partial y} dy = 0$$

at (x_0, y_0) , for arbitrary values of dx and dy , is a necessary condition for a relative maximum or minimum. It can be shown that the sufficient conditions for a relative maximum at (x_0, y_0) (9.3:193) are:

$$\frac{\partial^2 z}{\partial x^2} < 0 \quad \text{and} \quad \frac{\partial^2 z}{\partial x^2} \frac{\partial^2 z}{\partial y^2} - \left(\frac{\partial^2 z}{\partial x \partial y} \right)^2 > 0$$

further, $z(x_0, y_0)$ is a relative minimum only if

$$\frac{\partial^2 z}{\partial x^2} > 0 \quad \text{and} \quad \frac{\partial^2 z}{\partial x^2} \frac{\partial^2 z}{\partial y^2} - \left(\frac{\partial^2 z}{\partial x \partial y} \right)^2 > 0$$

Conditions for relative maxima or minima can also be shown for functions of n variables.

Simply maximizing a function, however, does not satisfy the demands of any physical problems. Generally, the interest lies in selecting a function of several dependent variables from a set of possible functions. Said another way, in most physical problems like the aircraft performance optimization problem, one must select an optimized path from a set of several varied paths. This set of possible solutions or paths is called a functional. Selecting the optimal path (or paths) from a functional requires a mathematical tool like the calculus of variations.

9.4.2 Basic Problems of the Calculus of Variations

The basic concern of the calculus of variations is to determine a function such that a certain definite integral involving that function and certain of its derivatives takes on a maximum or minimum value. If x is the independent variable, $y = y(x)$, and $F = F(x, y, dy/dx)$, the task is one of finding an extreme value (maximum or minimum) for the integral

$$I = \int_{x_1}^{x_2} F(x, y, y') \, dx \quad (9.13)$$

It can be shown that

$$\frac{d}{dx} \frac{\partial F}{\partial y'} - \frac{\partial F}{\partial y} = 0 \quad (9.14)$$

The common form of the Euler equation expresses the necessary condition for $y(x)$ to maximize or minimize the integral given by Equation 9.13.

This elementary development of the simplest case of the variational calculus (single independent variable, one dependent variable, and the first derivative of the dependent variable) can be generalized to n dependent variables and one independent variable. The necessary conditions that

$$I = \int_{x_1}^{x_2} F \, dx,$$

where $F = F(x; y_1, y_2, y_3, \dots, y_n; y_1', y_2', y_3', \dots, y_n')$,
have an extreme value are that

$$\frac{d}{dx} \frac{\partial F}{\partial y_r'} - \frac{\partial F}{\partial y_r} = 0 \quad \text{for } r = 1, 2, 3, \dots, n \quad (9.15)$$

9.4.3 Application of the Euler Equations

The mathematical results of the previous paragraph can be applied to the specific energy relationship of Equation 9.11. The corresponding variables, functions, and functional are shown in Table 9.1.

Table 9.1

MATHEMATICAL CORRESPONDENCE	
Equation 9.15	Equation 9.11
F	$p_s \left(\text{i.e. } \frac{dE_s}{dt} \right)$
x	t
y_1	h
y_2	v
y_1'	\dot{h}
y_2'	\dot{v}

Note that time is now the independent variable. Substituting into Equation 9.15 gives:

$$\frac{d}{dt} \left(\frac{\partial P_s}{\partial \dot{h}} \right) - \frac{\partial P_s}{\partial h} = 0$$

$$\frac{d}{dt} \left(\frac{\partial P_s}{\partial \dot{V}} \right) - \frac{\partial P_s}{\partial V} = 0$$

But,

$$P_s = \frac{(F_n - D)}{W} V = P_s(h, V)$$

since

$$F_n = F_n(h, V) \text{ and } D = D(h, V)$$

which implies

$$\frac{\partial P_s}{\partial \dot{h}} = 0 \text{ and } \frac{\partial P_s}{\partial \dot{V}} = 0$$

Thus, the necessary conditions for existence of extreme values of specific energy over any path between t_1 and t_2 are:

$$\frac{\partial P_s}{\partial V} = 0$$

$$\frac{\partial P_s}{\partial h} = 0$$

(9.16)

This brief excursion into mathematics provides the theoretical underpinning for practical means of maximizing the rate of transfer between specific energy levels. Remember that this mathematical technique applies to any integrand for an integral to be optimized that can be written in the form of Equation 9.13.

9.5 GRAPHICAL TOOLS FOR ENERGY APPROXIMATION

Solutions to even the basic calculus of variations problem outlined in the preceding paragraph are best left to optimal control specialists. However, a number of simple graphical approximations and tools provide useful

information to designers and operational tacticians. Since the most reliable raw data to construct these graphical tools come from flight tests, it is imperative that the test pilot and test engineer have a working knowledge of them.

9.5.1 Specific Energy Overlay

Having specified h and V as dependent variables, it is customary to utilize standard linearly scaled rectangular coordinates to depict energy states in terms of these two variables. However, since the energy approximation requires consideration of events that take place at levels of constant energy, a constant E_s grid is commonly overlaid on the h, V axes. Figure 9.13 shows such an overlay.

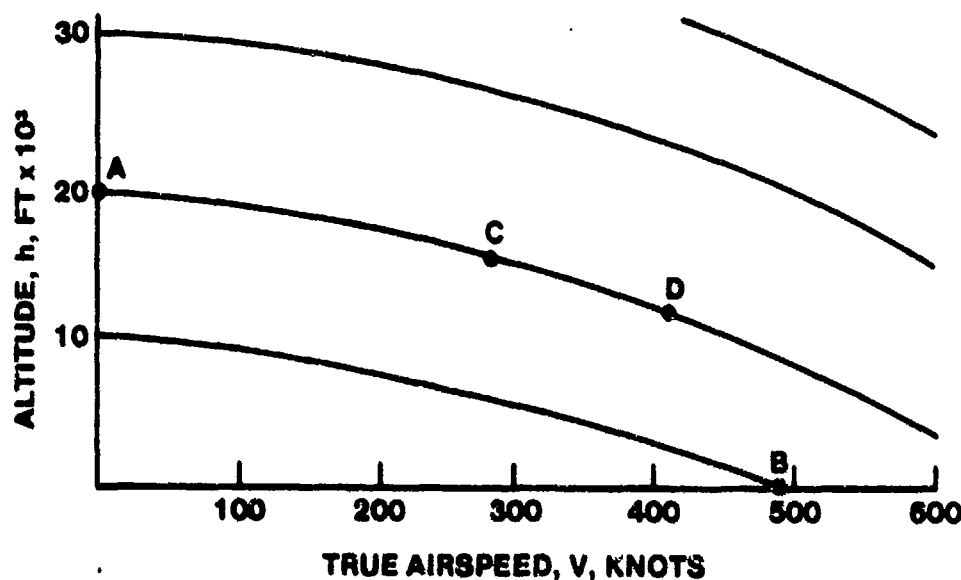


FIGURE 9.13. SPECIFIC ENERGY OVERLAY

As Equation 9.10 suggests, these lines of constant E_s are parabolic segments, with the altitude intercept (Point A) representing a body having only potential energy ($V = 0$). Point B, on the other hand, represents a body having only kinetic energy ($h = 0$).

One of the limitations (or perhaps fallacies) of the energy approach is also apparent from Figure 9.13. Note that time (the independent variable) does not appear on the specific energy grid. In his original formulation, Rutowski assumed that an exchange of potential energy for kinetic along a constant energy path could be made instantaneously. Anyone who has ever tried to trade airspeed for altitude recognizes this approximation as rather crude; such maneuvers quickly exceed the assumptions of small α and negligible normal acceleration. Much of the work done to build on Rutowski's concept has been aimed at optimal solutions relaxing this impracticality (9.4:93 and 9.5:315). This simplification means that an aircraft could ideally zoom or dive between points C and D or any other points along a constant E_s contour in zero time.

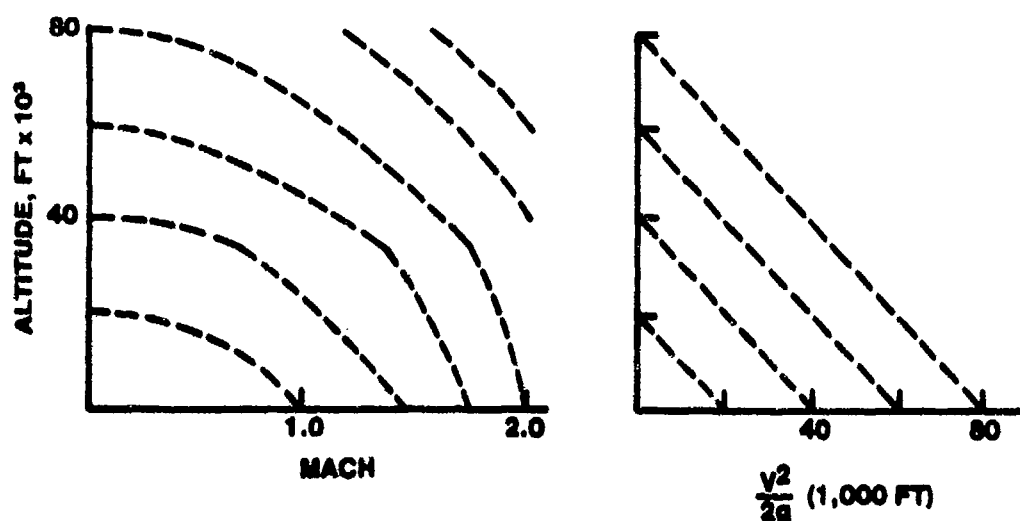


FIGURE 9.14. ALTERNATIVE SPECIFIC ENERGY OVERLAYS

In addition to the basic representation of E_s on h, V diagrams, there are several alternative ways to display the same information. Two such alternatives are shown in Figure 9.14. The h, M plot is a common substitution of dependent variables (M for V) for supersonic aircraft in operationally oriented literature. Notice the "knee" in the E grid lines when they are plotted on the h, M axes. It will be left as an exercise for the reader to show why this discontinuity in slope arises.

Sometimes, plotting specific potential energy versus specific kinetic energy ($V^2/2g$) is useful in graphically obtaining the points of tangency (a procedure to be elaborated upon later). The form of the overlay should be suited to the user's purpose; in any case, the information is essentially the same. These overlays of constant E_s allow one to choose paths of constant E_s or paths of known change in E_s .

9.5.2 Specific Excess Power Plots

The specific excess power plot is the basic graphical tool used to display total performance capability of an aircraft with the energy approach. Values of P_s are determined for the entire envelope, and then points of equal P_s are connected to form the contours of constant P_s as shown in Figure 9.15. Ways to determine these values for P_s from flight test will be discussed later in this chapter.

The $P_s = 0$ contour has special significance. For points outside this dividing line, the aircraft has negative specific excess power. From Equation 9.4,

$$\begin{aligned} \frac{(F_n - D)}{W} V &= V \sin \gamma + \frac{V}{g} \frac{dV}{dt} \\ &= \frac{dh}{dt} + \frac{V}{g} \frac{dV}{dt} \end{aligned}$$

Thus, Equation 9.11, which defined P_s , becomes:

$$P_s = \frac{(F_n - D)}{W} V = \frac{P_a - P_r}{W} \quad (9.17)$$

where P_a = power available

P_r = power required

Hence, the $P_s = 0$ contour represents the locus of states for which $F_n = D$, since the difference of these two variables is the only term in Equation 9.17 that can force P_s to 0 with the aircraft in flight. At any point along the $P_s = 0$ contour, the aircraft has no capability to increase its specific energy, so long as throttle setting, load factor, weight, or configuration do not change. It will, therefore, stabilize in steady state level flight on a $P_s = 0$ contour (state A in Figure 9.15, for example). Values of P_s inside this contour are positive, and if the aircraft were at state B, it could either climb, accelerate, or both at the same energy state. This aircraft could, for example, climb to an altitude of about 47,000 feet while reducing its kinetic energy to give $M = 0.8$. In fact, the pilot could zoom all the way to state C (if he did not stall) with the same energy level. However, he would have a negative P_s at C and could not stabilize there. Point D also represents the subsonic maximum h stabilized point. If there is a slight reduction in speed and the pilot increases angle of attack in an attempt to maintain altitude, the aircraft will lose specific energy and stabilize at some lower altitude point on the $P_s = 0$ curve. This portion of the $P_s = 0$ curve is akin to the classical "back side" of the power curve. This process can occur repetitively until the aircraft reaches stall speed (point E in Figure 9.15). Of course, this chain of events can be broken if the pilot reduces angle of attack (and thus, drag) and exchanges potential energy for kinetic energy. In other words, P_s contours, and the $P_s = 0$ contour in particular, are direct measures of an aircraft's capacity for climb, acceleration, and stabilized flight.

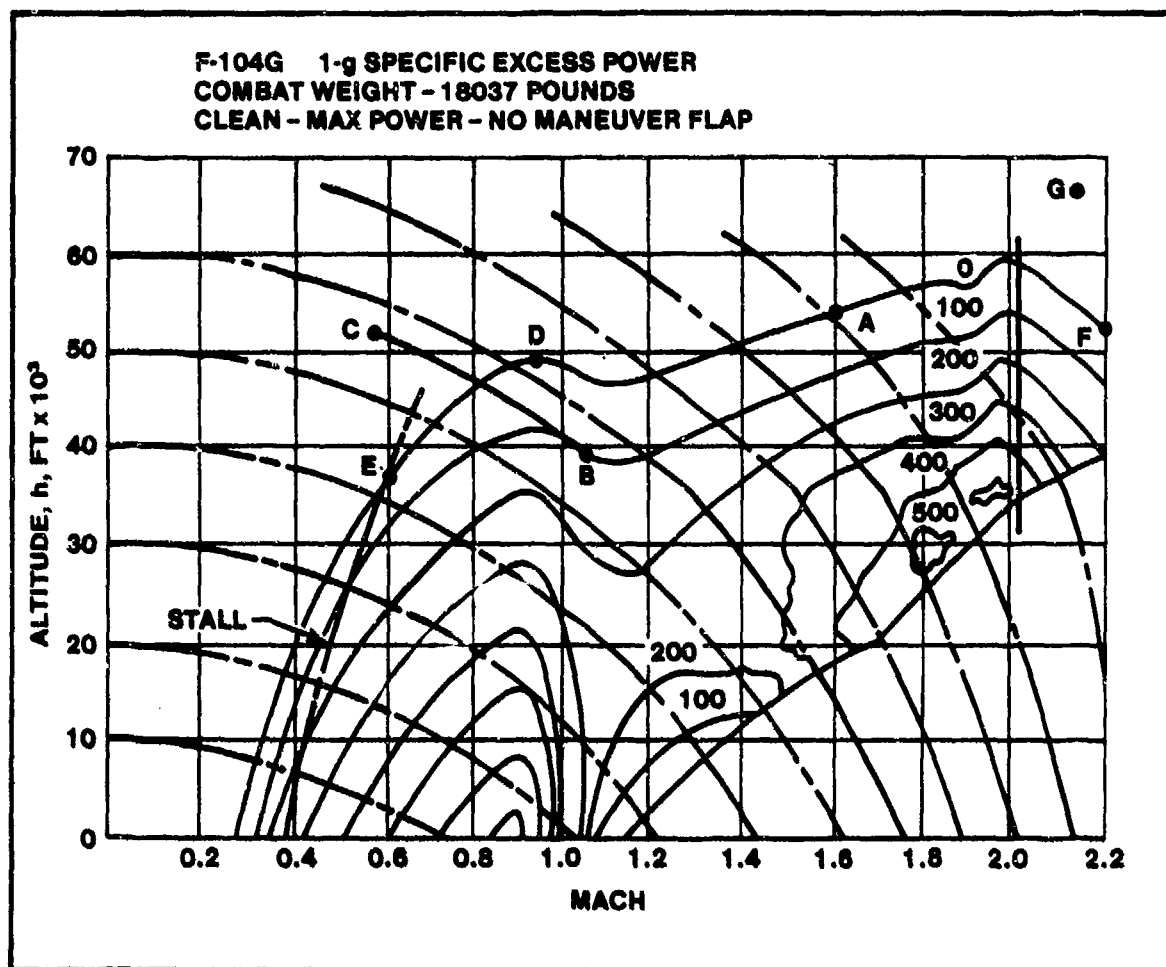


FIGURE 9.15. F-104g 1g SPECIFIC EXCESS POWER

It must be emphasized that each P_s contour plot is valid for only one configuration, one load factor, one weight, and one power setting. They are also valid for one set of atmospheric conditions, usually standard day. Increasing drag, increasing load factor, or reducing thrust all have the effect of shrinking the $P_s = 0$ contour as shown in Figure 9.16. Notice that this shrinking is not a proportional shrinkage; the $P_s = 0$ contours also change shape (distort) as these factors change.

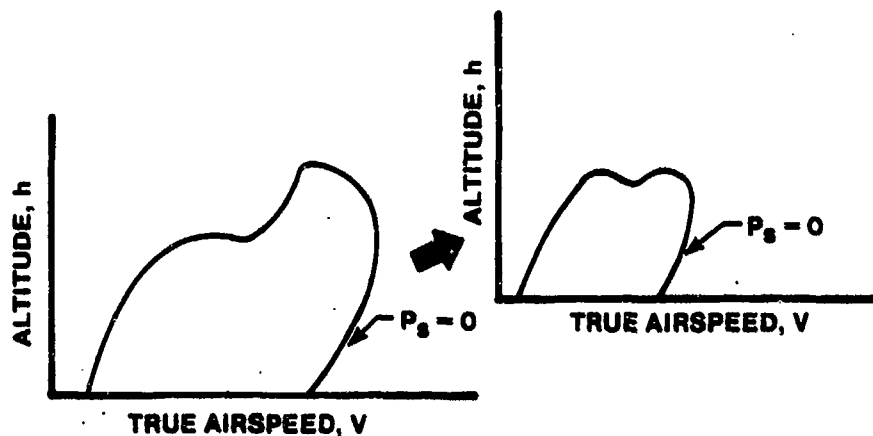


FIGURE 9.16. EFFECT OF INCREASING DRAG, INCREASING LOAD FACTOR, OR REDUCING THRUST

To round out this introduction to P_s plots, note that the maximum energy level attainable is about 123,000 feet, state F in Figure 9.15. Theoretically, this point is the state from which an ideal zoom to maximum altitude or an ideal dive to maximum speed should begin. However, the aircraft simply cannot reach the energy level represented by point G in Figure 9.15. But there are other factors which may further constrain aircraft performance. The $P_s = 0$ contour recognizes no aircraft limitations -- aerodynamic, structural, or controllability; it considers only what the engine/airframe combination is capable of producing in terms of potential and kinetic energy. Figure 9.17 illustrates how dynamic pressure loads, inlet temperature limits, fuel control performance, external store considerations, loss of control, and other factors can modify the usable P_s envelope.

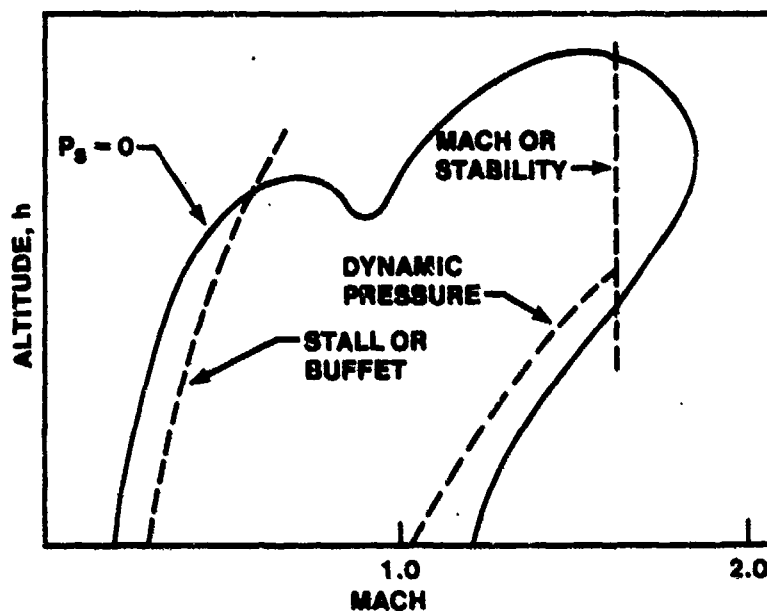


FIGURE 9.17. POSSIBLE AIRCRAFT LIMITS

9.6 TIME OPTIMAL CLIMBS

9.6.1 Graphical Approximations to Rutowski Conditions

Having now laid the theoretical groundwork (which is too complex, as usual) and developed the graphical tools (that are usable), one can now marry the two to obtain optimized performance. Rutowski proposed a very easy to use graphical means of obtaining climb schedules from P_s plots (9.2:190,191). He reasoned that one obtains maximum unaccelerated rate of climb under the mathematical conditions expressed by Equation 9.16.

Perhaps we can illustrate the method starting with subsonic aircraft and its P_s contours as shown in Figure 9.18, using two different types of E_s grid overlays. Holding altitude constant, we graphically satisfy the partial differential equation

$$\left. \frac{\partial P_s}{\partial V} \right|_{h = \text{constant}} = 0$$

by picking the true airspeed where the P_s contour is tangent to a line of constant altitude; that is, the peak of the P_s contour. This peak is labeled A in Figure 9.18. The climb schedule associated with such points for each P_s contour plotted is usually termed the maximum rate of climb schedule. The term is not wholly descriptive since, though the schedule minimizes the time to reach a given altitude, it is not necessarily unique.

9.6.2 Minimum Time to Energy Level Profiles

In a similar vein, Rutowski suggested that Equation 9.16 could be satisfied graphically by choosing a point where the P_s contours were tangent to lines of constant E_s . The climb schedule generated along this so-called Rutowski path represents minimum time to achieve a given energy state. This profile is labeled "optimum energy" in Figure 9.18.

To help locate these points of tangency, it is sometimes useful to plot P_s contours as a function of specific potential energy (h) and specific kinetic energy ($V^2/2g$). Depending on the shape of the redefined P_s contours, the points of tangency may be easier to choose with these straight line E_s contours. Of course, it is then necessary to compute the climb schedule (obtaining V from $V^2/2g$), rather than reading it directly.

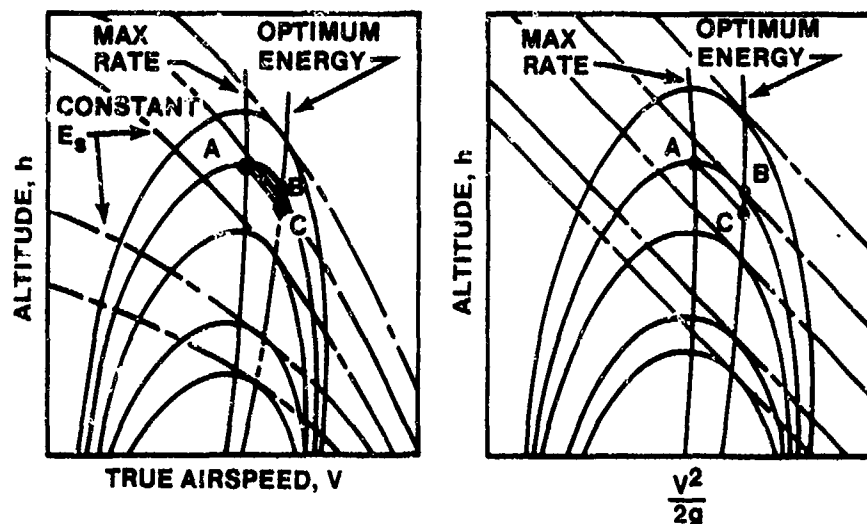


FIGURE 9.18. SUBSONIC CLIMB PATHS

9.6.3 Subsonic to Supersonic Transitions

No matter what kind of plot is used, Rutowski suggested climbing along the optimum energy path to C, which would put the aircraft at a specific energy level equal to that at A. However, the aircraft's potential energy would be lower with kinetic energy making up the difference. Upon reaching C (in less time than that required to follow the maximum rate of climb path to A), Rutowski assumed the aircraft would transition in zero time with no loss in energy along an ideal zoom to A. It becomes immediately obvious why these transitions are of such interest to Rutowski's successors in performance optimization; the potential gains predicted by the energy approximation can be completely negated by the real process of exchanging kinetic and potential energies. In fact, for subsonic aircraft, the difference in the two climb paths is usually within measurement error for flight test purposes.

However, for a supersonic aircraft, the energy approximation becomes much more meaningful. Figure 9.19 illustrates a typical climb schedule for a supersonic aircraft. The path essentially consists of four segments to reach energy state E in minimum time. Segment AB represents a constant altitude

acceleration from $V = 0$ to climb speed at state B. The subsonic climb segment follows a path similar to the one illustrated in Figure 9.18 approximately to the tropopause (state C). As a rule of thumb, this subsonic climb is usually a nearly constant Mach schedule. An ideal pushover or dive is then carried out at constant E_s from C to D. Finally, the supersonic climb segment from state D to E is normally very close to a constant calibrated airspeed climb. Notice that this path is an idealized Rutowski path except for the takeoff and acceleration to climb speed and the ideal (zero time) dive between states C and D. Segments BC and DE fit Rutowski's conditions by passing through points on P_s contours that are tangent to lines of constant E_s .

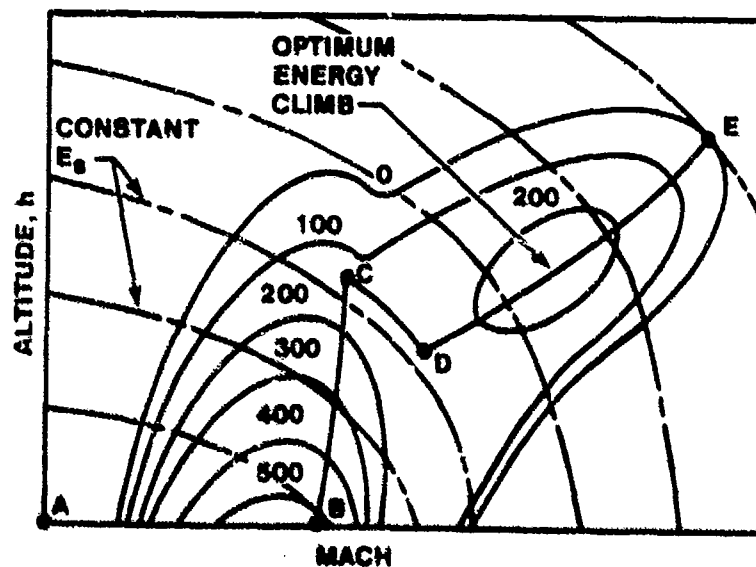


FIGURE 9.19. SUPERSONIC CLIMB PATH

Of course, there is a question of when and how to transition from the subsonic segment to the supersonic segment. The P_s contours near $M = 1$ are poorly defined, and there is not complete agreement on when to start the pushover. Most analysts suggest flying toward the most expeditious path toward the highest P_s contour available without decreasing E_s . Such an assumption implies that one should climb subsonically until intercepting an E_s

level tangent to two P_s contours of equal value -- one in a subsonic region and the other in the supersonic region. Path CD in Figure 9.19 illustrates a typical transition following this reasoning. However, Figure 9.20 (9.6:17) illustrates rather well how difficult the choice of transition paths becomes when P_s contours become irregular in the transonic region. The ideal climb path for the F-104G resulted in a time to 35,000 feet and $M = 2.0$ of about 194 seconds. This time compares to a time of 251 seconds for a subsonic climb at maximum rate to 35,000 feet followed by a level acceleration to $M = 2.0$ at constant altitude (9.6:18), a gain of 23% in time to intercept.

However, before the rosy glow gets too bright, how about the story with real transitions as opposed to ideal zooms and dives? Figure 9.20 shows a more realistic climb path with the "corners rounded off"--meaning that abrupt discontinuities in angle of attack and attitude were avoided in the actual climb. For one supersonic airplane, the ideal minimum time path to $h = 65,000$ feet and $M = 1$ took 277 seconds with zero time for dives and zooms. Using a more complete mathematical model, Bryson and Desai estimated 40 seconds for the dive and 60 seconds for the zoom for a total time of 377 seconds to the desired energy state. However, by treating V , h , γ , and W as variables and controlling them with angle of attack, the same aircraft was estimated to require 332 seconds to reach $h = 65,000$ feet and $M = 1$ (9.1:483).

F-104G 1-g SPECIFIC EXCESS POWER
COMBAT WEIGHT - 18037 POUNDS
CLEAN - MAX POWER - NO MANEUVER FLAP

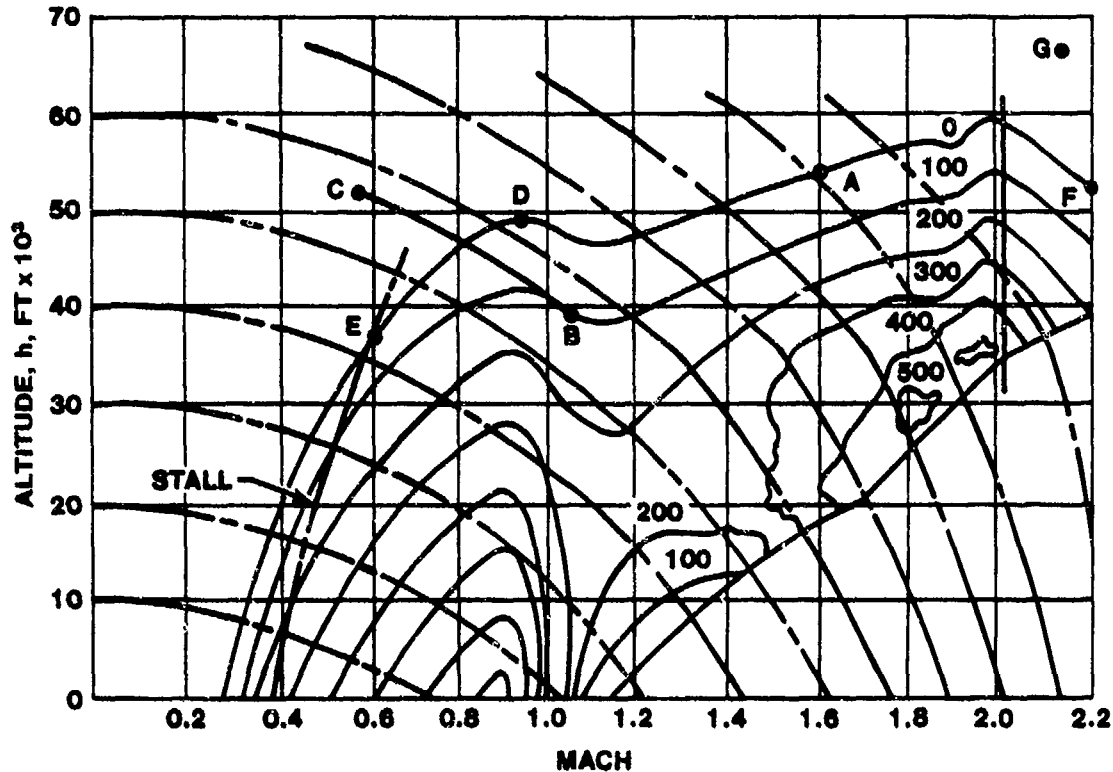


FIGURE 9.20. F-104G MINIMUM TIME TO ENERGY LEVEL CLIMB PATH

9.7 FUEL OPTIMAL CLIMBS

The energy approximation can be used to treat a number of performance optimizations other than minimum time to climb. For example, if it is desired to expend minimum fuel to achieve a given energy level, the mathematical formulation of this optimization proposed by Rutowski (9.2:192) is identical to the minimum time problem with appropriate variable changes. The objective is to increase total mechanical energy while conserving internal energy (fuel) for future use.

9.7.1 Fuel Efficiency

To achieve the stated goal ("expend minimum fuel to achieve a given energy level"), we must define a measure of fuel efficiency that can be

quantified. These words suggest looking at how much total energy is added to our mechanical system (the aircraft) per pound of fuel burned. In symbols, our measure of merit is

$$\Delta E_s / \Delta w_f$$

where Δw_f is the weight of fuel burned. In the limit

$$\lim_{\Delta t \rightarrow 0} \frac{\Delta E_s}{\Delta w_f} = \frac{\Delta E_s / \Delta t}{\Delta w_f / \Delta t} = \frac{dE_s / dt}{dw_f / dt} = \frac{P_s}{\dot{w}_f}$$

Usually, fuel flow rate can be treated as a function of h and v , just as thrust and drag were in Equation 9.17. The integral to be maximized in this case is

$$E_s = \int_{w_1}^{w_2} \frac{dE_s}{dw} dw$$

Since $dE_s = P_s dt$

and

$$dw = -\dot{w}_f dt$$

$$\frac{dE_s}{dw} = - \frac{P_s}{\dot{w}_f}$$

the integral to be maximized can be written as

$$E_s = \int_{w_1}^{w_2} \frac{dP_s}{\dot{w}_f} dw \quad (9.20)$$

Clearly, Equation 9.18 is of the same form as Equation 9.13, and if $P_s = P_s(h, V)$ and $\dot{w}_f = \dot{w}_f(h, V)$ the Euler equations are:

$$\frac{\partial P_s / \dot{w}_f}{\partial h} = 0$$

$$\frac{\partial P_s / \dot{w}_f}{\partial V} = 0$$

As before, both these partial derivatives are evaluated at constant E_s in the graphical approach to minimizing fuel used to reach higher energy levels. These conditions are satisfied at those points in the h - V plane where the E_s lines are tangent to the $1-g P_s / \dot{w}_f$ contours, as shown in Figure 9.21. This path is the locus of points where the maximum energy per pound of fuel burned is instantaneously attained at a given specific energy level. These kinds of paths, while mathematically and qualitatively similar to minimum time paths, consistently lie above the minimum time paths on an h - V diagram--as will be illustrated shortly.

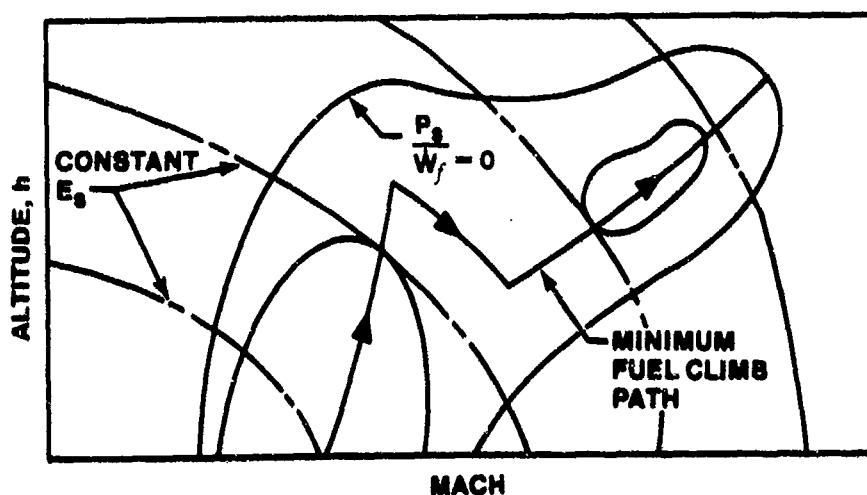


FIGURE 9.21. MINIMUM FUEL TO ENERGY LEVEL CLIMB PATH

9.7.2 Maneuver Energy

P_s/\dot{w}_f contours are a measure of efficiency since they depict the specific energy gained per pound of fuel expended. However, it is more common to use maneuver energy (formerly called energy maneuverability efficiency) which is defined as the amount of energy gained for the internal energy expended. Maneuver energy, then, can be expressed as

$$E_m = \frac{P_s^*}{\dot{w}_f} w_{f_a}$$

where P_s^* is the average P_s over the fuel weight interval and w_{f_a} is the fuel available. Notice that w_{f_a} will vary with mission profile and required fuel reserve, as well as the fuel required to reach a given energy state. Hence, we can define w_{f_a} arbitrarily, making the maneuver energy plot independent of the path taken to reach a given energy state, or we can base w_{f_a} upon the fuel consumed in reaching a given energy state. In the latter case, the E_m plot is dependent on the path used to reach the energy level.

9.7.3 Path Independent Maneuver Energy Diagrams

A path independent maneuver energy diagram is one in which all computations of P_s are based on a constant fuel weight, usually 50% of total fuel weight. For this case

$$E_m = \frac{P_s}{\dot{w}_f} w_{f_c}$$

and P_s is not tied to weight interval, but is simply taken from a constant weight energy rate diagram. Such a diagram is path independent because the amount of fuel available at each energy state is not affected by the path

taken to arrive at the state. Figure 9.22 illustrates such a path independent maneuver energy plot.

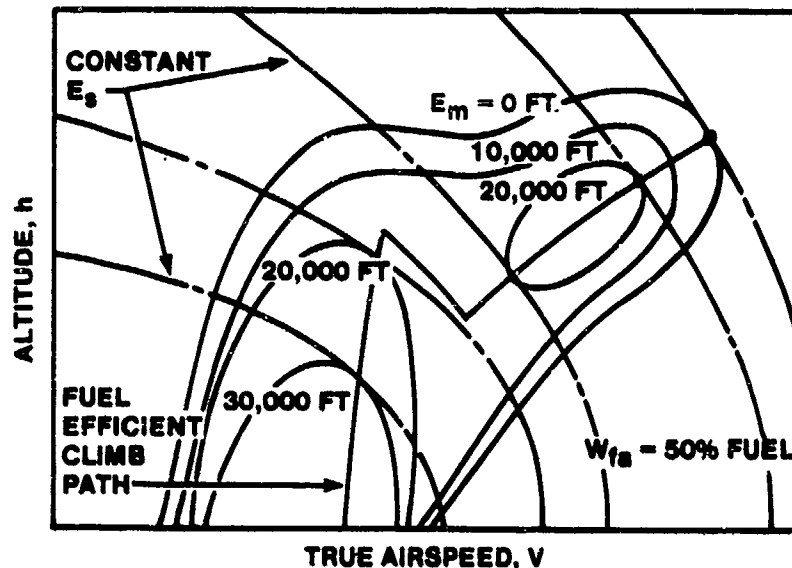


FIGURE 9.22. PATH INDEPENDENT MANEUVER ENERGY PLOT

9.7.4 Path Dependent Maneuver Energy Diagram

The second type of maneuver energy diagram looks very much like the path independent plot. The difference between the two lies in recomputation of fuel weight for each interval of time. For the second class of diagrams, it is assumed that a minimum fuel path has been flown from some reference energy level to the energy state under consideration. This assumption leaves the diagram heavily dependent on the path previously flown to reach each energy state. The function $(P_g^*/\dot{w}_f)w_{fa}$ varies with the path in two ways. First, available fuel weight w_{fa} is obtained by subtracting required fuel reserves and the fuel used in reaching the present energy state along a minimum fuel path from total usable fuel. Second, P_g^* is the average P_g^* value over a given, usually small, aircraft weight increment. Constructing such a path dependent maneuver energy diagram is more complex than constructing a path independent one. Further, as we shall emphasize later, one of the main values of such

diagrams is comparison between two aircraft. More often than not, constructing the path dependent maneuver energy diagram is not worth the extra effort.

9.7.5 Maneuver Energy and Persistency

From a tactical viewpoint, maneuver energy levels and P_s provide a measure of the time available to engage the enemy. Observe that

$$\Delta t = \frac{w_f a}{w_f}$$

can be used to compare competing designs in terms of combat time available. Clearly, if the maneuver energy level is known and P_s is known at any altitude and velocity, we have a measure of persistency of the design, that is, how long it can fight under the prescribed conditions.

9.7.6 Comparison of Fuel Optimal and Time Optimal Paths

Figures 9.21 and 9.22 illustrate paths similar in appearance to the time optimal paths of Figures 9.19 and 9.20. How do they compare for the same airplane? Figure 9.23 (9.7:118, 124) answers this question specifically for a clean F-105D at maximum power and is representative of the general case. Typically, as these data show, the fuel optimal path lies above but roughly parallels the time optimal path. Note that to reach the desired state ($h = 45,000$ feet and $M = 1.85$) requires an ideal climb, an ideal dive, and an ideal zoom in the time optimal case. Hence, for this example at least, the fuel optimal path is closer to achievable reality than the time optimal path.

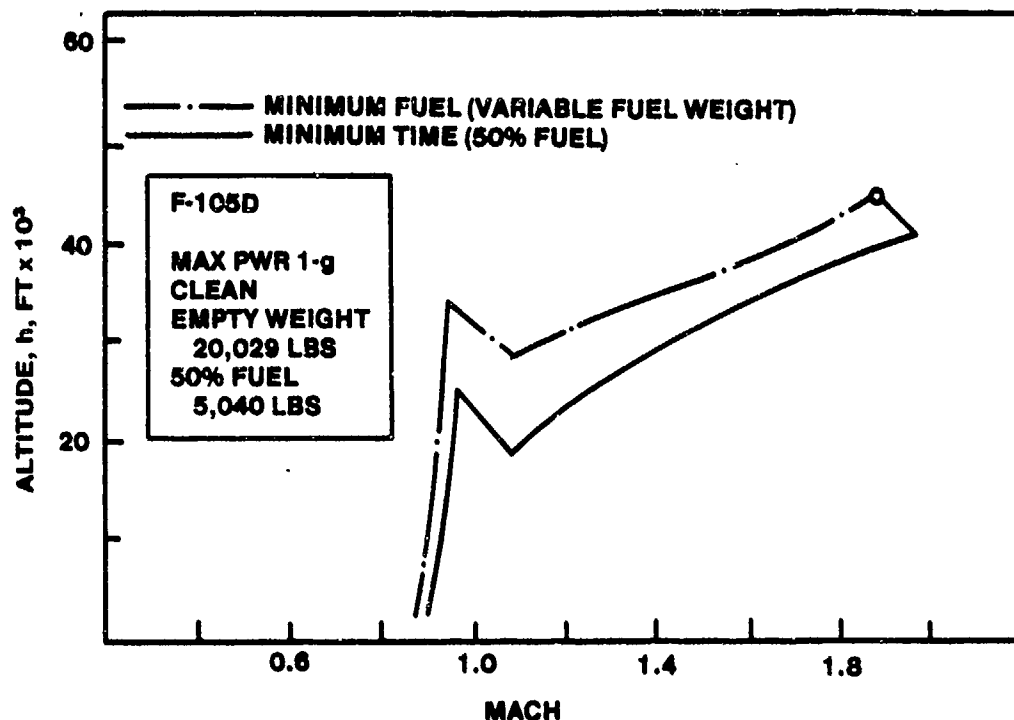


FIGURE 9.23. COMPARISON OF TIME OPTIMAL AND FUEL OPTIMAL PATHS (9.7:118,124)

9.8 MANEUVERABILITY

Though we have defined and discussed maneuver energy, maneuverability in the sense of three-dimensional trajectories has not been discussed. (Remember, maneuver energy is a measure of efficiency—fuel efficiency to be precise.) Now we need to re-examine the optimization problem with a view to extending the problem to include turning maneuvers. Indeed, several authors have used names like "extended energy management" (9.5:314) or "energy turns" (9.8:575). What we must do first is describe turning maneuvers and acknowledge at least two different types of maneuverability—both of which are related to turning maneuvers.

9.8.1 Instantaneous Maneuverability

The rate and radius of turn can be instantaneously expressed as

$$R = \frac{V^2}{gn_r} \quad (9.19)$$

$$\omega = \frac{gn_r}{V} \quad (9.20)$$

where

R = radius of turn

V = true airspeed

n_r = radial load factor

ω = rate of turn

The most common way to present such instantaneous data to the pilot is a V-n diagram illustrated in Figure 9.24. Notice that altitude strongly affects the V-n envelope.

The purpose of such a diagram is to provide a pilot with useful information on the maximum instantaneous turning capability of the aircraft. Corner velocity is defined as the indicated airspeed at which design structural limits and aerodynamic limits coincide. When considering only instantaneous turning capabilities, minimum radius and maximum rate of turn occur at the aircraft's corner velocity. Corner velocity is located on the V-n Diagram at the point of intersection of the horizontal structural limit (upper line) and the aerodynamic buffet or stall line (curved line on the upper left). Of course, the V-n Diagram also shows other limits, like the maximum true airspeed or Mach limit depicted by the right hand vertical line. Overall, the V-n Diagram provides maximum available instantaneous turning performance in terms of available load factor. But it has a very serious limitation: V-n Diagrams give no information at all with regard to loss of energy during turning maneuvers. This limitation leads us to the need for information on sustained maneuverability.

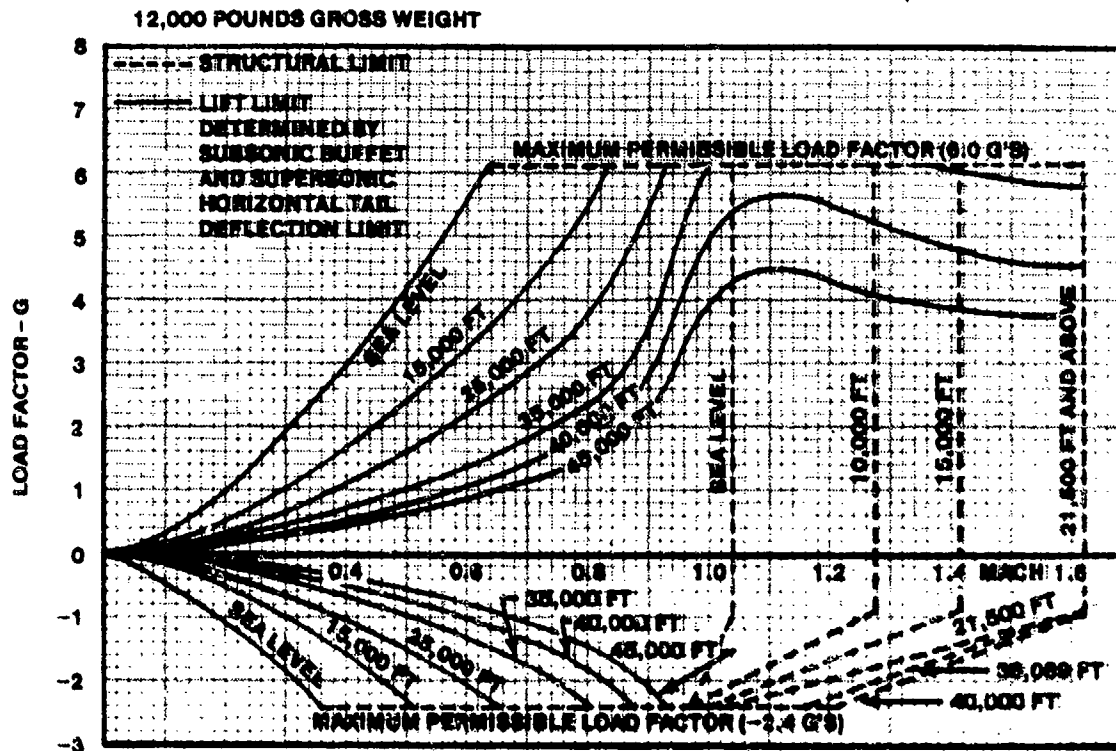


FIGURE 9.24. T-38 V-n DIAGRAM

9.8.2 Sustained Maneuverability

As noted in the previous paragraph, maneuverability is related to change in heading (turning). However, maneuverability is not characterized solely by the capacity to make directional changes. A maneuvering aircraft must also remain within its maximum airspeed and altitude limits; that is, maneuvering must be conducted within maximum energy levels attainable and minimum energy levels usually associated with controllability limits. Moreover, in an air-to-air battle, a maneuverability advantage belongs to the pilot who can attack and counterattack while retaining a relative energy advantage. Hence, the rate of change of energy, P_s , becomes a key player in sustaining the capacity to maneuver. To gain energy more rapidly than an adversary and thus gain offensive maneuvering advantage, a combatant must first have an aircraft capable of achieving a higher positive P_s and then must follow a profile of energy states that exploits this advantage. Conversely, if a defender has the capacity to lose energy faster than his attacker, he may choose to temporarily use this capability to force his opponent to overshoot. The essential point for this discussion is that sustained maneuverability suggests there is a

tradeoff between P_g and turn performance in the air-to-air chess game. To understand this interchange better, we must first understand how load factor (a convenient measure of turning performance) affects P_g contours.

9.8.3 Effect of Load Factor on P_g Contours

So far, all energy rate diagrams have been presented as 1-g contours. Changing the load factor obviously changes drag and the excess thrust term in P_g . This change is by no means a linear change with increasing load factors; after all, induced drag is certainly not linear with load factor. Hence, P_g contours invariably shrink with increasing positive load factor, which suggests that maximum P_g versus load factor for most aircraft occurs near zero load factor (minimum induced drag). Figure 9.25 graphically portrays the changes in the $P_g = 0$ envelope for the F-5E as load factor increases. Notice that the 3-g and 5-g envelopes characteristically shrink and distort in comparison to the 1-g $P_g = 0$ envelope. As expected, applying load factor is a very expedient way to decrease energy rapidly. Though the contours are not shown in Figure 9.25, an energy decay of over 2,000 ft/sec is achievable at 42,000 feet and $M = 1.2$ in the F-5E. Clearly, this energy state is well within the F-5E's 1-g $P_g = 0$ envelope.

As Equations 9.19 and 9.20 explicitly show, both turn rate and turn radius are related to radial acceleration. Thus, radial acceleration can be taken as the measure of merit for turning performance. For the practicing tactician, who really sees aircraft load factor on the g-meter, this measure of maneuverability also depends on orientation with respect to the earth's gravitational pull as shown in Figure 9.26. In other words, the acceleration of gravity can be used to "tighten up" (decrease the instantaneous radius and increase the rate of a turn) by maneuvering in the vertical plane. Needless to say, this vertical maneuvering advantage is very useful. However, for our theoretical purposes, this illustration serves only to show that our equations deal with radial acceleration, not actual accelerometer readings.

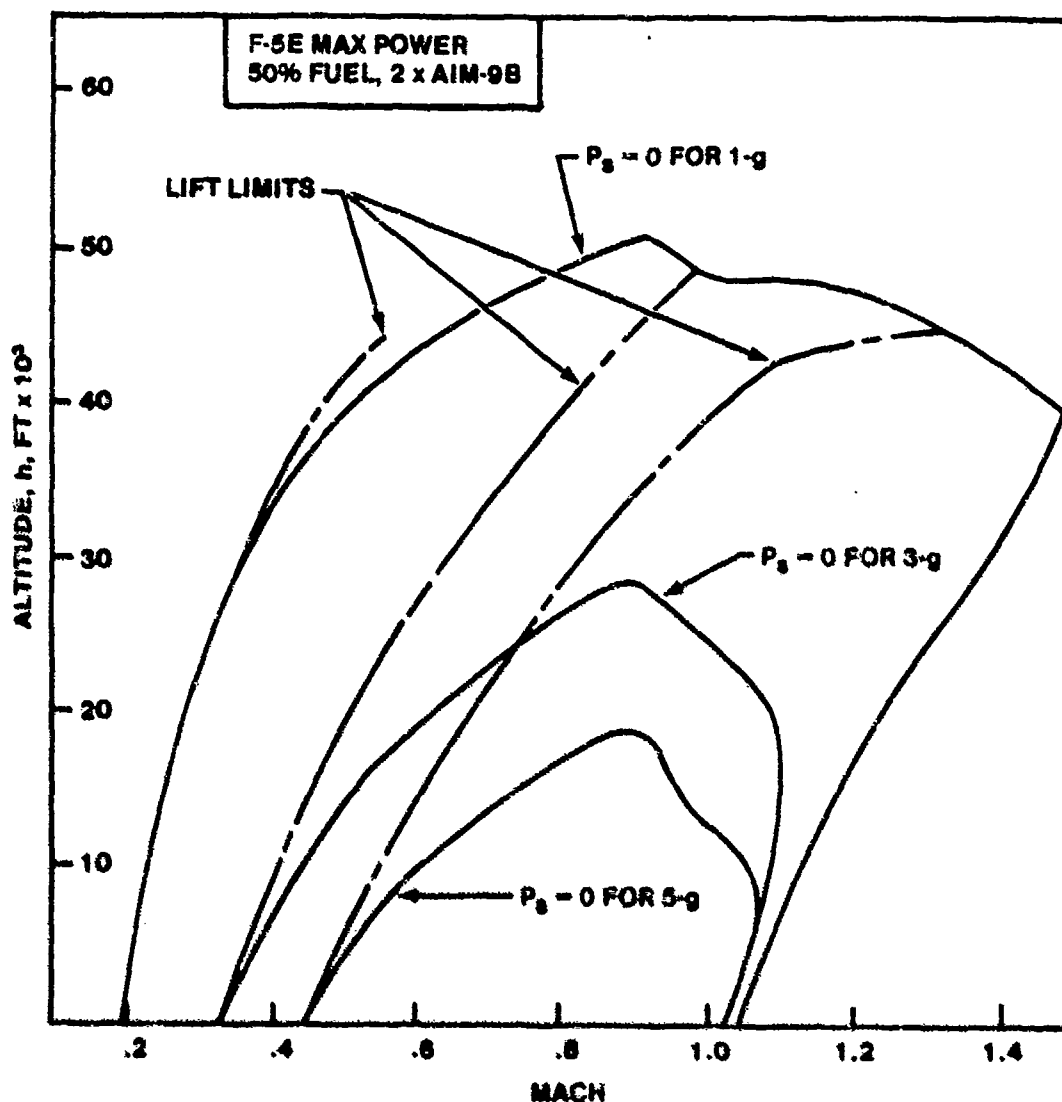


FIGURE 9.25. EFFECT OF LOAD FACTOR ON P_s CONTOURS

Thus, turn rate, turn radius, and radial acceleration are very important parameters, along with P_s , in comparing relative performance of maneuvering aircraft. Such comparisons, derived from the energy approximation, are of extreme interest to designers, operators, and test personnel.

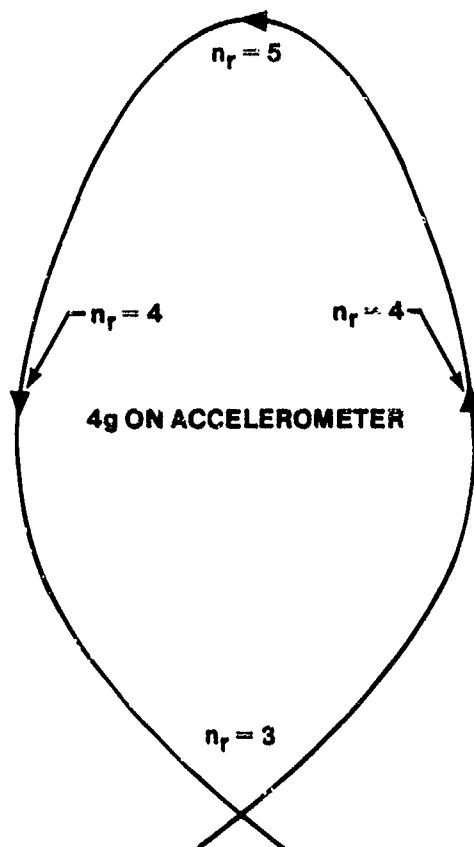


FIGURE 9.26. ILLUSTRATION OF RADIAL ACCELERATION FOR A VERTICAL MANEUVER

9.9 COMPARISON TECHNIQUES AND TOOLS

There are many ways to compare competing aircraft with tools based on the energy approximation. In this section, we will consider only a few of them. The central purpose is to expose the prospective test pilot and test engineer to enough formats and different kinds of plots so that he or she will be prepared to critically analyze any set of data, no matter what the presentation looks like.

9.9.1 P_s Overlays

Perhaps the simplest comparison tool is the specific excess power overlay chart. P_s envelopes for two or more aircraft can simply be plotted on the

same chart as suggested in Figure 9.27. Aircraft A in this case is clearly superior to Aircraft B throughout the $P_s = 0$ envelope. For every energy state, A enjoys a positive P_s greater than does B. Such a chart as this can very graphically portray areas of superiority and inferiority for any pair of aircraft. But simple overlays can become very confusing if the two aircraft do not have quite similar $P_s = 0$ envelopes. Extrapolation is necessary to quantify the difference in P_s at any energy state.

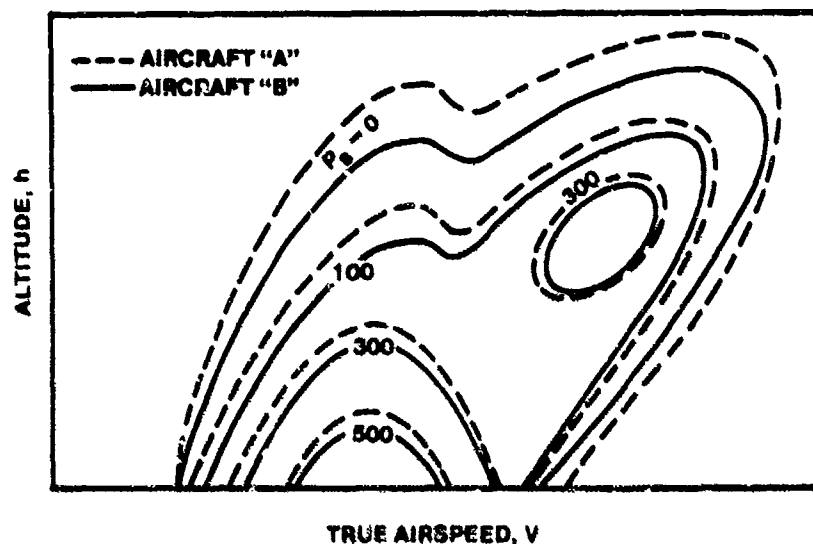


FIGURE 9.27. TYPICAL P_s OVERLAY

9.9.2 Differential P_s Charts

The next logical step if one is comparing two aircraft is to form the difference

$$\Delta P_s = P_{s_A} - P_{s_B}$$

at every point in the envelope (or even outside the envelope). Figure 9.28 is a sketch of how this difference function might look if plotted in the h - V space. Such charts clearly identify those areas where one aircraft can sustain an energy state while the other cannot--the so called "exclusive"

regions. Exclusive, in this context, means that P_s for the opponent is negative. In Figure 9.28, for example, Aircraft B would lose energy if operated in the shaded region. It is in this sense that Aircraft A owns this energy space, for A can either gain or sustain energy here.

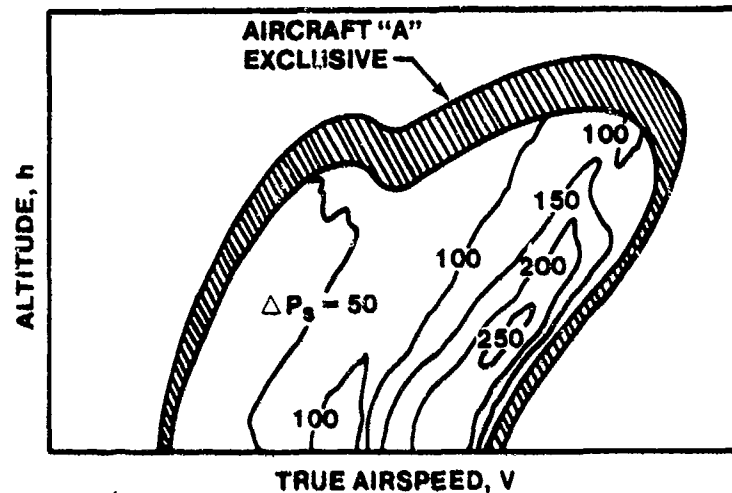


FIGURE 9.28. DIFFERENTIAL P_s CONTOURS

Differential P_s contours also quantify areas inside the $P_s = 0$ envelope where the relative energy rates still favor A, but in this comparison plot, the superiority of A is quantified. Quantifying the relative superiority produces a very graphic depiction of where in the energy space Aircraft A should attempt to engage Aircraft B.

Figure 9.29 shows a more likely set of ΔP_s contours; that is, there are areas where both aircraft have exclusive regions. Aircraft B, in this case, can gain or sustain P_s in the horizontally crosshatched areas. Much of the region where Aircraft B is exclusive lies at higher energy levels than Aircraft A is capable of reaching. In these areas, Aircraft A is incapable of even transient operations. In other areas of the B-exclusive region, Aircraft A could transiently operate at negative P_s , but could not sustain the flight conditions. In the B-exclusive region, ΔP_s contours are not shown for reasons of clarity, but if they were, all values would be negative.

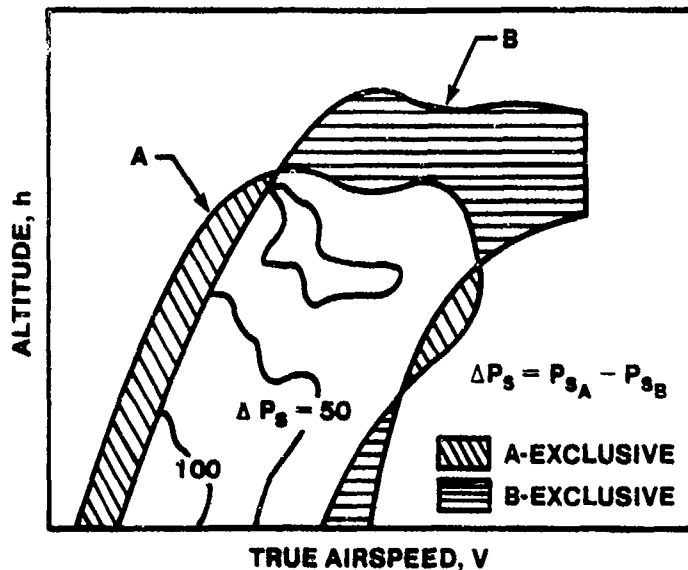


FIGURE 9.29. TYPICAL OVERLAY OF P_s CONTOUR

9.9.3 P_s Versus Turn Rate

There is little standardization in presentation of energy data in the Air Force, and much less so between aerospace contractors. Hence, in the next three paragraphs, we will examine three other ways of looking at this kind of information. It is all based on the principles previously presented, but as test pilots and test engineers, you will be expected to analyze data from any source, whatever the format, and compare the results to specifications or competing designs.

One such data format is the P_s versus turn rate chart illustrated in Figure 9.30. Such a chart relates energy data from several energy rate diagrams for various radial accelerations through Equation 9.20. In this sense, the chart is a cross plot of these P_s diagrams for a given altitude and airspeed. The maximum turn rate that can be sustained by the aircraft is easily obtained by noting the point where $P_s = 0$. Of course, Equation 9.20 would also give the maximum radial acceleration (load factor for a level turn) that can be sustained without losing energy. Figure 9.30 also shows that the

maximum instantaneous turn occurs at maximum lift or where maximum radial acceleration ($V = \text{constant}$) occurs. Finally, of course, the turn rate starts to decrease as angle of attack is increased beyond that for maximum lift. Indeed, for some aircraft, maximum lift and maximum angle of attack occur very close together.

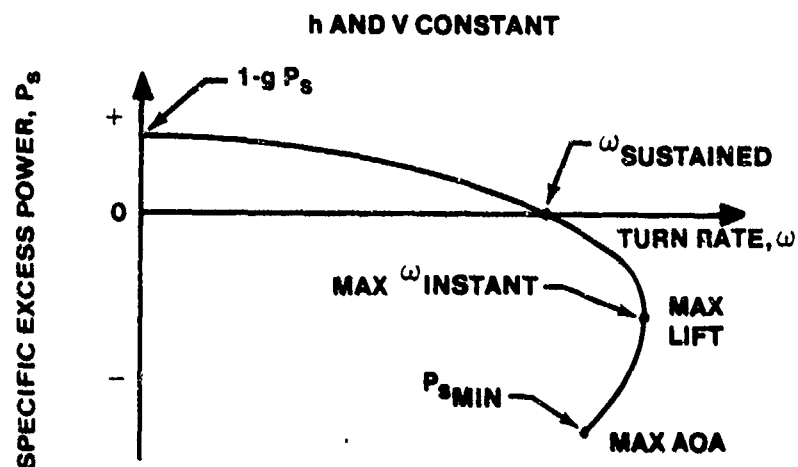


FIGURE 9.30. P_s VERSUS TURN RATE

Clearly, we can use these kinds of plots to compare aircraft, as suggested by Figure 9.31. Each of the increments in performance on these plots represents tactical usage. The difference in $1-g P_s$ represents a difference in climb or acceleration capability. It could, for example, be used to separate from an adversary. The difference in sustained turn rate capability suggests that one of the aircraft could maneuver to obtain a gun firing position. The instantaneous turn rate difference indicates an ability to force an overshoot as a defensive maneuver. A measure of ability to slow down rapidly is $\Delta P_{s_{\min}}$, a capacity that can also be used to defensive advantage. Clearly, then, such charts are useful in developing new designs as well as indicating tactical options for operating against potential adversaries.

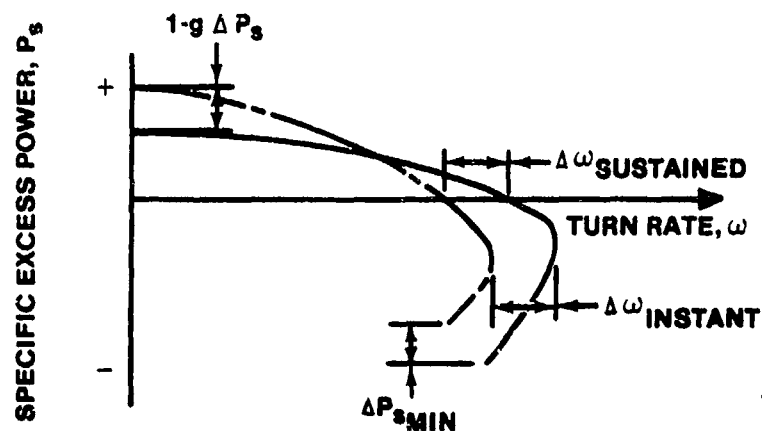


FIGURE 9.31. COMPARISON OF TURNING PERFORMANCE - SPECIFIED ALTITUDE AND AIRSPEED

As noted on Figure 9.30, the simple charts depicting P_s versus turn rate are good for only one altitude and one airspeed. Obviously, a large number of them would be required to define the complete performance envelope of an aircraft. Figure 9.32 (9.9:5) is an attempt to consolidate several such $P_s - \omega$ charts. Note that it still shows only one Mach.

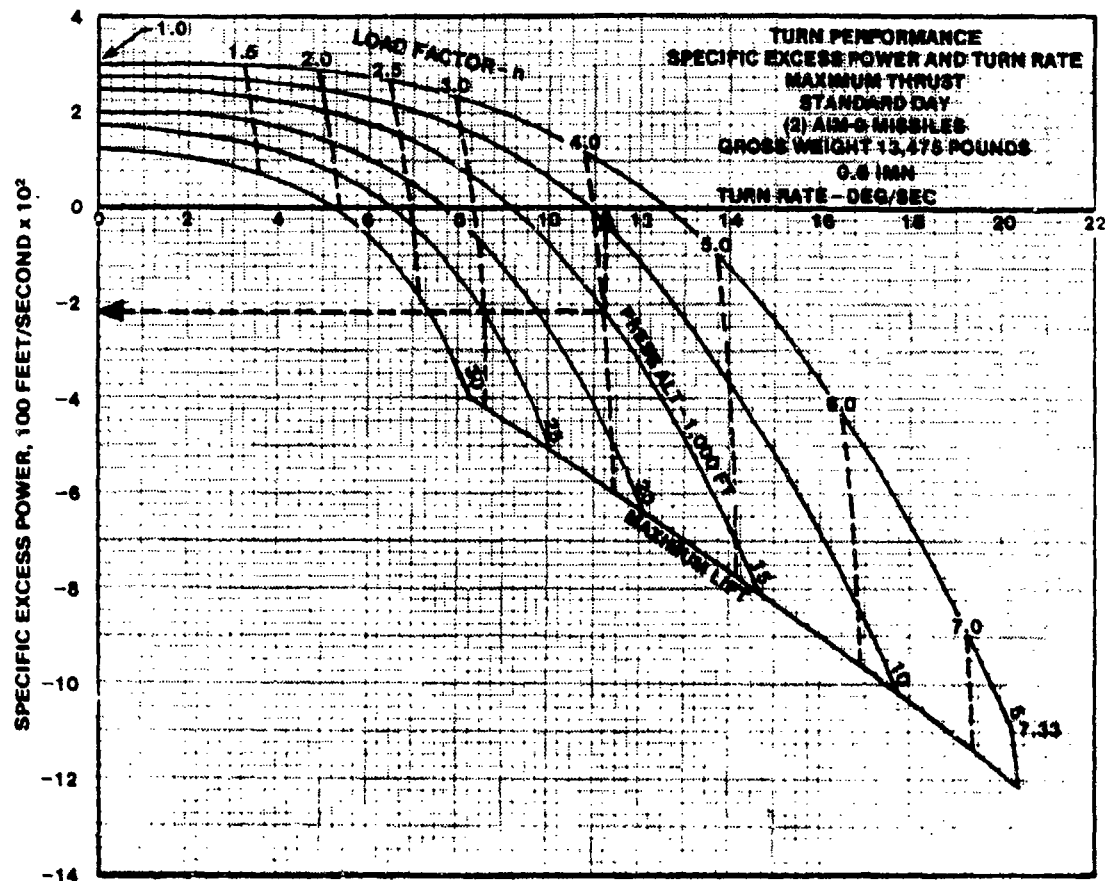


FIGURE 9.32. P_s VERSUS TURN RATE
(CONSTANT MACH, s VARIOUS ALTITUDES)

9.9.4 P_s Versus True Airspeed/Mach

Instead of holding both state variables (h and V) constant, one could map P_s across the true airspeed envelope. Alternatively, of course, for a stated altitude, one might plot P_s against Mach. This sort of chart, with an overlay of level turn load factors, is especially useful to show the rate at which energy can be gained or lost as a result of "pulling g." Figure 9.33 is a typical plot of this type. Notice that it is valid only for the specified altitude.

If one enters the diagram by selecting a Mach and then moving vertically to a desired load factor, the available energy rate in a level turn at this load factor is found by moving horizontally to the left P_s scale. Obviously, if P_s is positive, that power can be used to climb or accelerate along the flight path, or one could choose to turn tighter by increasing the

load factor. Conversely, if P_s is negative, the aircraft must either descend, lose Mach, reduce the load factor, or accept some combination of these energy losing possibilities.

For example, if the aircraft of Figure 9.33 has established 0.8 Mach at 15,000 feet, it can sustain 6 g in a level turn. Enter with $M = 0.8$, proceed vertically to 6-g contour and read $P_s \approx 0$ by moving horizontally left from point 1. If the pilot relaxes to 3 g, he then has the option of initially climbing at 840 ft/sec (point 2) or increasing Mach, all at 3-g.

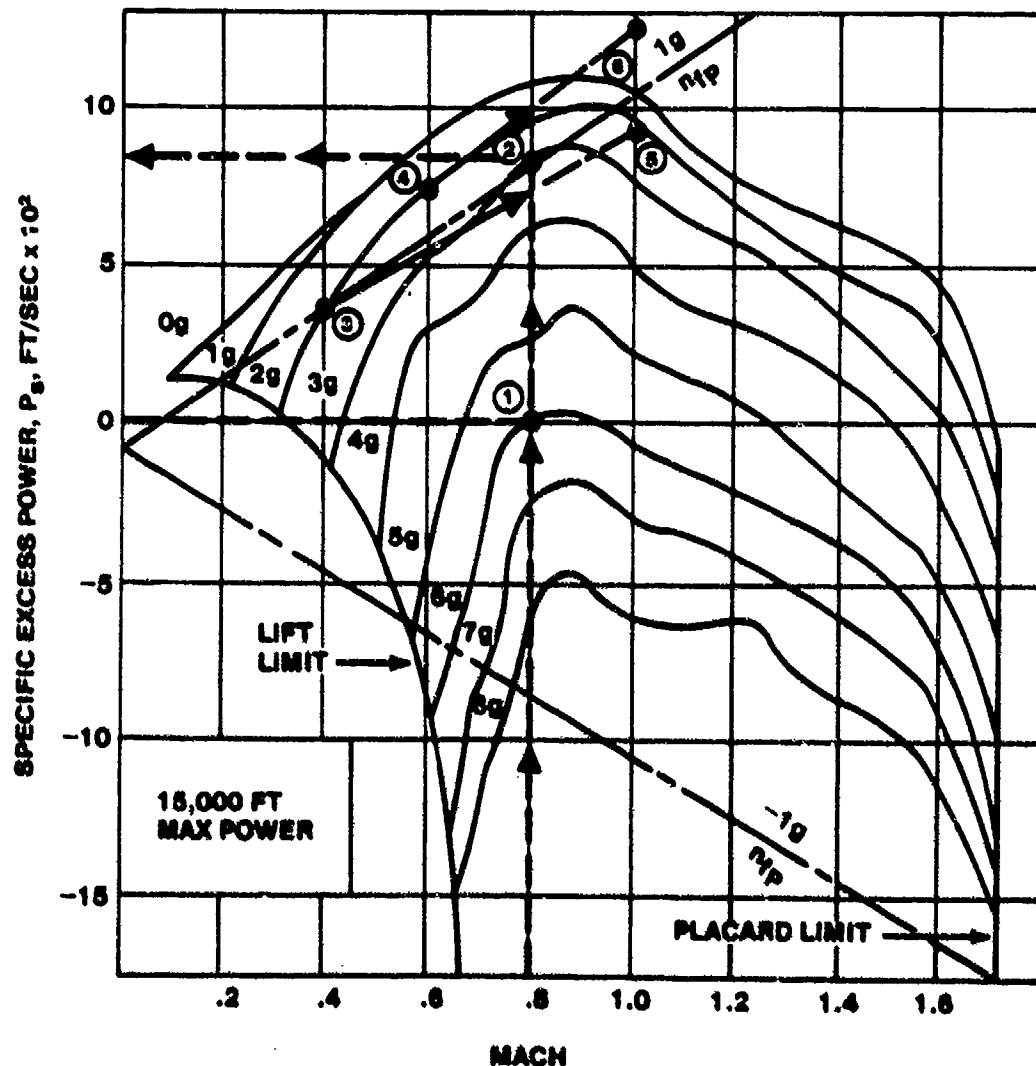


FIGURE 9.33. P_s VS MACH AT SPECIFIED G LOADS, SPECIFIED ALTITUDE

The diagonal reference lines on Figure 9.33 also provide useful information to the tactical planner. They provide a reference indicating the rate at which the aircraft gains or loses airspeed and suggest a way to estimate the time needed to change airspeed by a given amount for a specified load factor. Notice that acceleration along the flight path can be defined in g by

$$n_{FP} = \frac{a_{FP}}{g}$$

But since acceleration along the flight path is also given by Newton's Second Law, $F = ma$:

$$F = F_N - D = \frac{W}{g} a_{FP}$$

$$n_{FP} = \frac{F_n - D}{W}$$

Recalling that

$$P_s = \frac{(F_n - D)V}{W}$$

$$n_{FP} = \frac{P_s}{V} \quad (9.21)$$

From this expression, it is a relatively simple matter to obtain the initial rate of acceleration along the flight path for any Mach and load factor at the specified altitude. For example, to accelerate from 0.4 to 0.6 M while in a 2-g level turn, the initial flight path acceleration (point 3) would be about 0.90-g and the final acceleration would be about 1.18-g (point 4). These flight path accelerations can be obtained graphically as shown by constructing a straight line through $P_s = 0$ and points in question (3 and 4). Extending these lines to points 5 and 6 and recalling that at 15,000 feet,

$M = 1$, $V = 1058$ ft/sec in lieu of figuring TAS in ft/sec (at points 4 and 6), the initial flight path acceleration is

$$n_{FP_i} = \frac{950}{1058} = 0.90$$

with 950 ft/sec the P_s at point 5. Similarly from point 6, the final flight path acceleration is

$$n_{FP_f} = \frac{1250}{1058} = 1.18$$

Since $a_{FP} = \Delta V / \Delta t$ if the time interval is small, we can crudely estimate that the average acceleration is

$$n_{FP_{avg}} = \frac{n_{FP_i} + n_{FP_f}}{2} = \frac{0.90 + 1.18}{2} = 1.04 = \frac{a_{FP_{avg}}}{g}$$

or

$$a_{FP_{avg}} = 1.04 \times 32.2 = 33.5 \text{ ft/sec}^2$$

So

$$\Delta t = \frac{\Delta V}{a_{FP_{avg}}}$$

$$\Delta t = \frac{(0.6 - 0.4) (1058)}{33.5} = 6.32 \text{ sec}$$

Clearly, this approximation improves as the increment of time decreases, and as the averaging process becomes more accurate, the procedure becomes a numerical integration that is relatively simple for computers of today.

This simple illustration indicates the power of the energy approximation to provide useful tools to designer and tactician alike. The test team must be clearly aware of such uses and strive for accuracy in collection, reduction, and presentation of such data.

9.9.5 Rate-Radius Diagrams

Another common method of depicting turning performance is to plot rate of turn versus radius of turn for a level turn at a given altitude. Figure 9.34 illustrates such a plot. In the simple rate-radius diagram, only one overlay is shown, that is, P_g contours for the aircraft in question. Recalling the parameters used to calculate ω and R from Equations 9.19 and 9.20, it would have been quite a simple matter to overlay additional information on the chart. For example, calibrated airspeed and load factor are often plotted on rate-radius diagrams. Obviously, one could also overlay different aircraft rate-radius diagrams for comparison purposes.

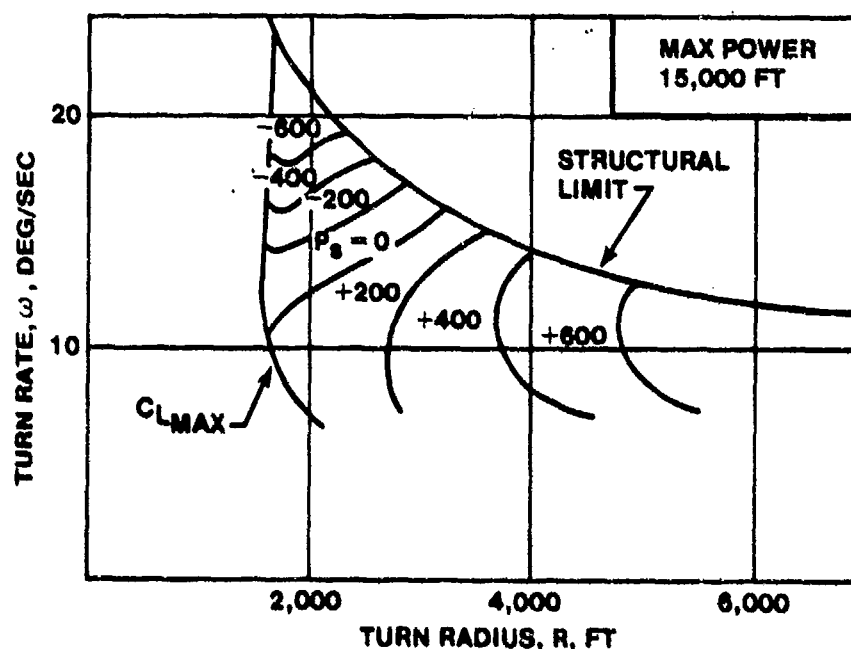
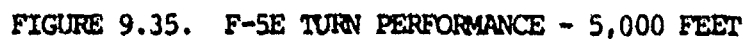


FIGURE 9.34. RATE OF TURN VS RADIUS OF TURN

Figures 9.35, 9.36, and 9.37 (9.9:4,5) represent a slight variation on the rate-radius chart, but present essentially the same information. This

P.S.



9.10 PROFILE OPTIMIZATION

Application of energy analysis to bomber/cargo and airline application follows the same basic principles, but is usually more concerned with cost functionals having to do with range, endurance, and operating constraints (Air Traffic Control restrictions or local fuel costs, for example) than with P_s or parameters derived from P_s considerations. Of course, fighter operators have the same concerns when faced with ferry flights, combat air patrol, or similar missions. Usually, it is best to break up the profiles into climb, cruise, and descent segments. Thus, the optimization becomes a composite problem. Furthermore, the functional to be optimized in each segment frequently is more complex than just minimum time or minimum fuel. Finally, since each segment may be optimized with either different cost functionals and/or different constraints, great care must be used in piecing together each segment. In this section, we will look only at the descent segment and the appropriate way to piece together total profiles. The optimization climb profiles have already been adequately covered in this chapter, and cruise performance is covered in Chapter 11 of this textbook.

9.10.1 Maximum Range Climb

Though shutting all engines down to minimize fuel consumed in the descent is hardly a practical operational procedure, it is useful to understand the optimization of maximum range glides in constructing total profiles. Horizontal range rate is given by

$$\frac{dR}{dt} = V$$

$$\frac{dE_s}{dt} = \frac{V(F_n - D)}{W} = \frac{dR}{dt} \frac{(F_n - D)}{W}$$

Then, if $F_n = 0$ for gliding flight

$$\frac{dE_s}{dR} = -\frac{D}{W}$$

$$R = \int_{E_{s1}}^{E_{s2}} -\frac{W}{D} dE_s \quad (9.22)$$

Thus, to maximize range in a power-off glide, fly at minimum drag. If drag contours are plotted on an h-V diagram, with an E_s contour overlay, the results are typified by Figure 9.38. The graphical approximation to Rutowski's conditions once again give maximum conditions where the integrand (in this case, Drag) contours are tangent to the lines of constant E . Connecting these points of tangency results in the maximum range glide. Also, as with earlier ideal optimizations, if initial conditions are off this maximum range glide profile, constant energy dives or zooms are the most energy efficient way to reach this optimum profile.

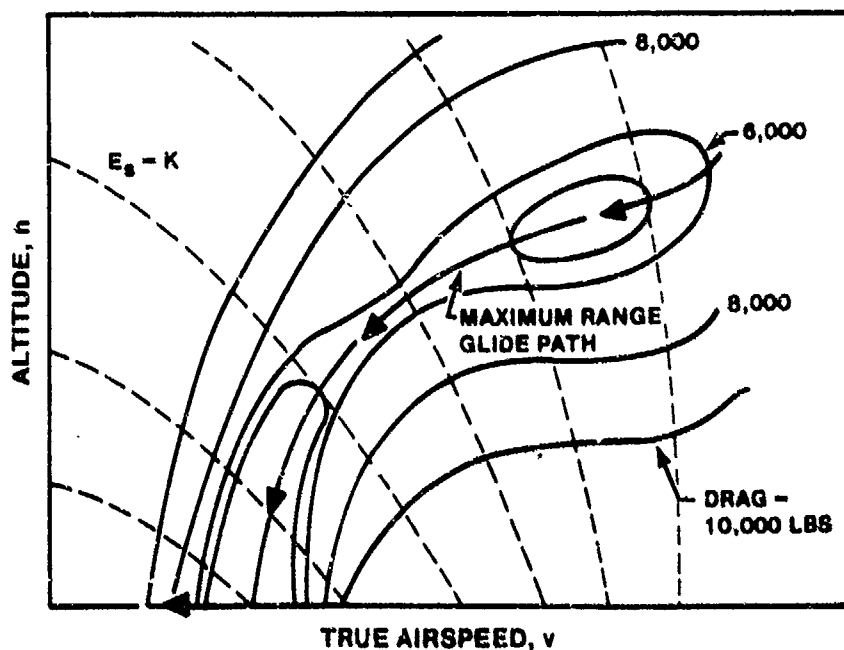


FIGURE 9.38. MAXIMUM RANGE GLIDE PATH

9.10.2 Maximum Range for Given Fuel

Having examined the optimization for unpowered flight, which comes close to maximum range for descents with minimum power, we now turn to the problem of maximum range for both powered flight and a descent. The first approximation could include a cruise segment, but for our purposes such an intermediate segment is not imperative. But we must consider both a climb segment and a descent segment and then decide how to piece the two together.

9.10.3 Maximum Range at Fixed Throttle

For a given amount of fuel, maximum range at a fixed throttle setting amounts to maximizing V/\dot{w}_f as the following development indicates.

$$\frac{dR}{dt} = V, \quad R = \int_{t_1}^{t_2} V dt$$

since $\dot{w}_f = \frac{dw_f}{dt}$

$$R = \int_{w_{f1}}^{w_{f2}} \frac{V}{\dot{w}_f} dw_f \quad (9.23)$$

Though it may not be intuitively obvious, V/\dot{w}_f is a function that maximizes at maximum altitude for any value of E_s . However, remember that we are looking not for a maximum value of V/\dot{w}_f , but an optimal path which gives maximum range. (This description clearly illustrates the difference between a functional and a function.) This optimal path, which is maximum range for a given amount of fuel at a fixed throttle setting or minimum fuel for a given range at fixed throttle, starts close to the minimum fuel for a given energy level as Figure 9.39 illustrates. After gaining some energy, the path departs

from this initial trajectory to maximize V/\dot{w}_f at higher altitudes. There is no convenient graphical solution to this optimization problem. Notice also that the path typically tracks well outside the steady state P_s boundary. This unconstrained optimization would thus not be practical if a cruise segment were planned; nor does this kind of optimization consider a gliding descent after the given fuel is expended. So let's consider the case for total range, including the glide.

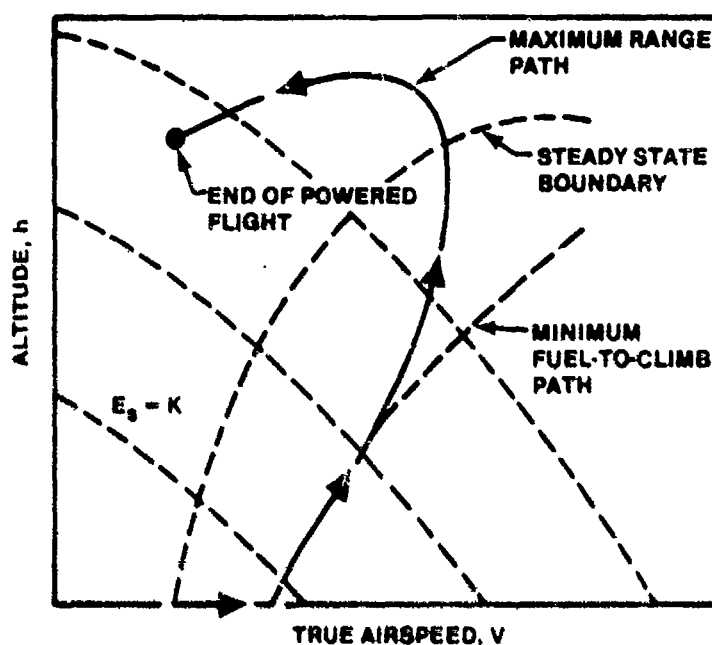


FIGURE 9.39. MAXIMUM RANGE FOR A GIVEN FUEL AT FIXED THROTTLE

9.10.4 Maximum Range Profile

The total range for a fixed throttle climb followed by a power-off descent is given by

$$R = \int_{w_{f1}}^{w_{f2}} \frac{V \dot{w}_f}{\dot{w}_f} + \int_{E_{s1}}^{E_{s2}} - \frac{W}{D} dE_s \quad (9.24)$$

In this case, a critical factor in the optimization is the energy state for starting the descent. Remember that when only the maximum range achievable in the powered climb was considered, gaining altitude to reduce fuel flow was the driving consideration. Now that we wish to consider total range of both a climb and descent segment, we must concern ourselves with the energy state at the end of the climb in order to give ourselves reasonable starting conditions for the descent segment. Figure 9.40 graphically shows this optimization.

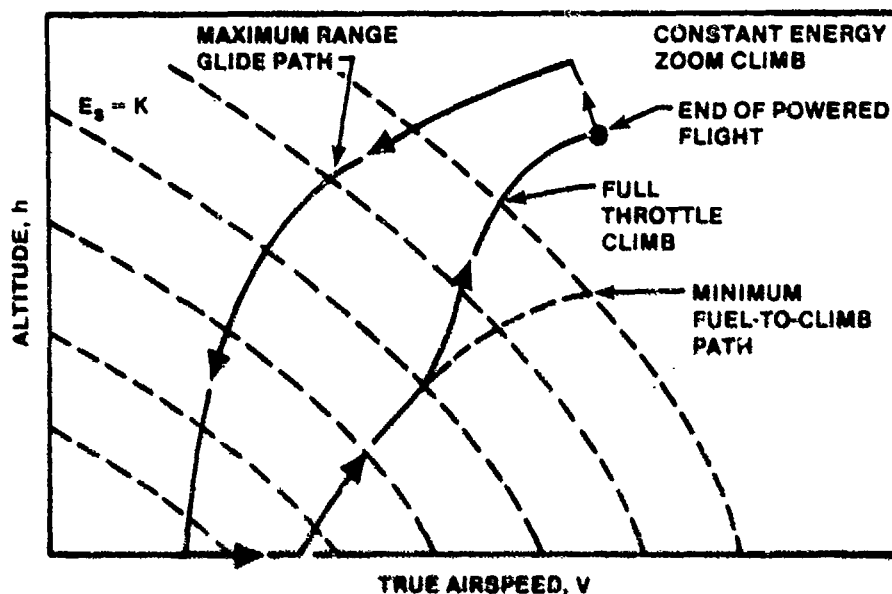


FIGURE 9.40. MAXIMUM RANGE FOR A GIVEN FUEL WITH GLIDE

Figure 9.41, which compares these two profiles, clearly shows the difference that energy state at the end of the powered climb makes in total range. A maximum range glide has been added to the path shown in Figure 9.39 to clearly show that maximum total range is obtained when the climb ends at a higher kinetic energy.

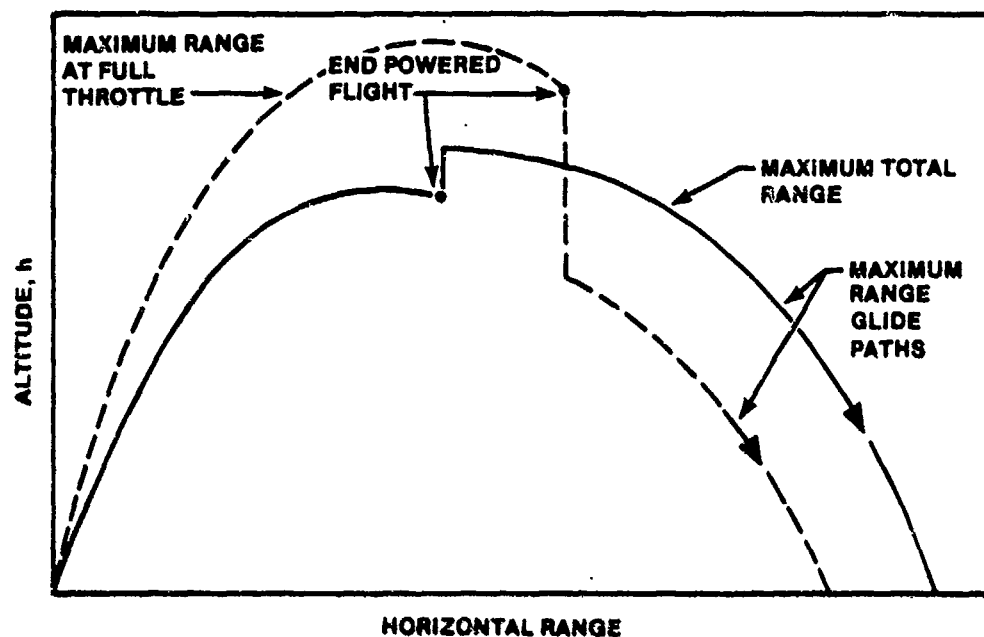


FIGURE 9.41. COMPARISON OF MAXIMUM RANGE PROFILES FOR A GIVEN FUEL

These range profiles are more theoretical than practical. They are discussed in this text only to highlight the optimization approaches to using these principles.

9.11 OPERATIONAL APPLICATIONS TO TRANSPORT OPERATIONS

Both the military and the airlines became increasingly interested in more energy efficient operations when fuel costs soared in the 1970's. For the Air Force, cargo/bomber/tanker aircraft accounted for over 60% of fuel used, and the C-141, C-5, C-130, and KC-135 accounted for over 40% of it in 1973 (9.10:9). Consequently, there have been a variety of proposals to implement energy management principles at varying levels of sophistication. Everything from flight plans computed with these near optimal techniques to fully automated systems have been suggested, tested, and in a few instances, installed.

One computer study of C-141A operations compared two near optimal

profiles to conventional profiles (9.10:78-84) for stage lengths up to 500 nm. These profiles exhibit the characteristics suggested in the preceding paragraphs and illustrated in Figures 9.40 and 9.41. Two types of optimizations for a 200 nm stage were compared to the conventional profile consisting of a constant 250 KIAS climb from 2,000 feet to 10,000 feet, a 280 KIAS climb to 23,000 feet, cruise for approximately 65 nm at 80% throttle, a 300 KIAS descent to 10,000 feet with throttles at idle, and a 250 KIAS, throttles idle descent from 10,000 feet to 2,000 feet. Optimization 1 utilized a normal rating thrust (NRT) climb at a constant 279 KIAS to a range of about 100 nm, followed immediately by an idle thrust descent at near maximum L/D. Optimization 2 produced the best results with a profile also utilizing throttle manipulation as well as constant Mach climb. Figure 9.42 shows each of these profiles.

The fuel consumption for these three different profiles is shown in Table 9.2. Both optimized trajectories employ idle descents at speeds near the speed for maximum L/D. These descents produce considerable fuel savings even though they take more time. The mechanics of flying Optimization 1 are quite simple, and the results in terms of fuel consumption are quite comparable to those for Optimization 2, which would require some form of throttle schedule or auto-throttle mechanization.

Table 9.2

FUEL CONSUMPTION FOR 200 NM PROFILES

<u>Profile</u>	<u>Fuel Used (lbs)</u>	<u>Percent Over Optimization 2</u>
Optimization 2	7420	---
Optimization 1	7515	1.3
Conventional	8347	12.5
		(9.10:81)

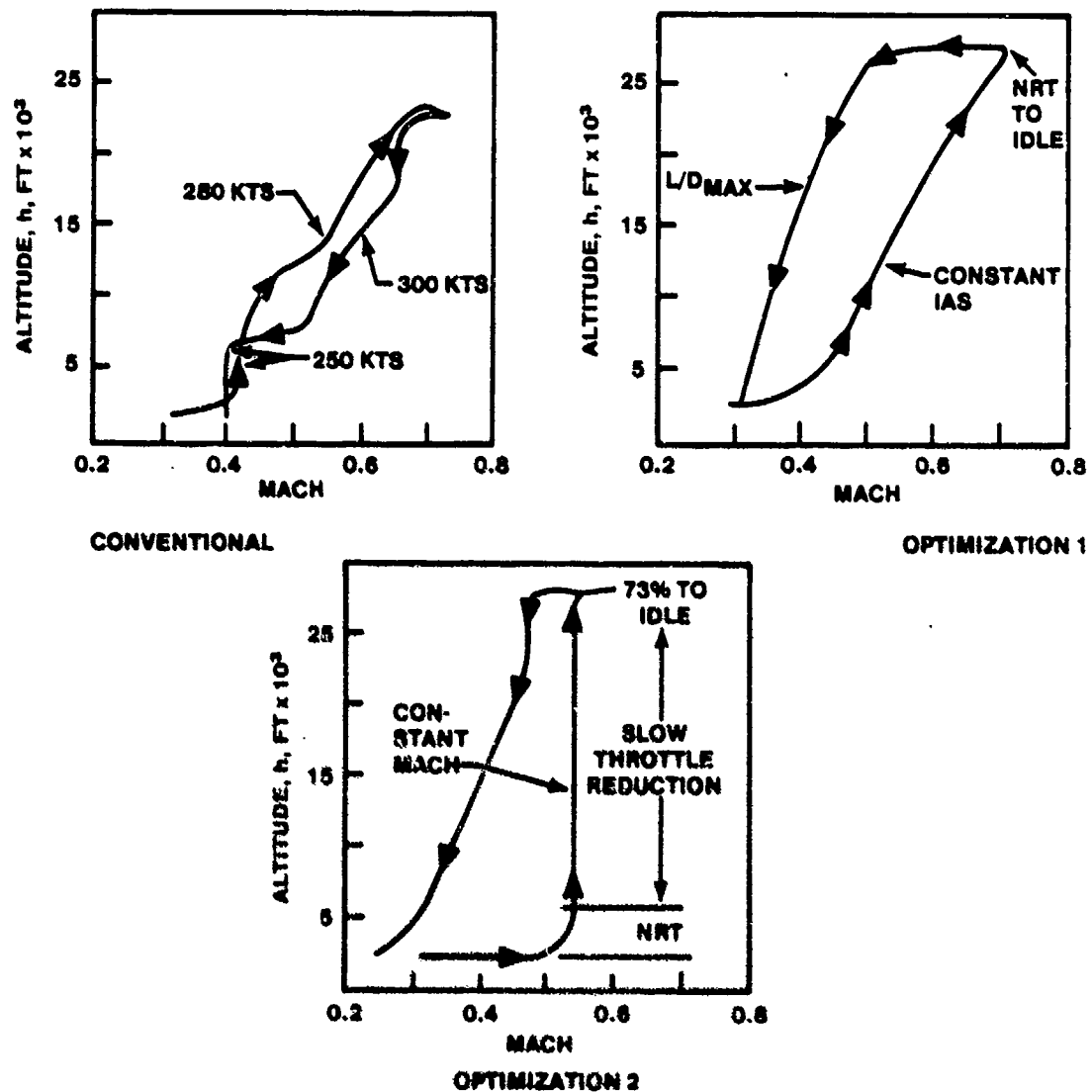


FIGURE 9.42. PROFILES FOR 200 NM RANGE (9.10:82)

For medium and long range profiles, the driving factor becomes the cruise conditions selected. However, if one chooses both altitude and Mach for maximum range and follows the climb and descent schedules suggested for Optimization 1, a constant altitude cruise segment gives results fairly close to those for Optimization 2. (This optimization provides the minimum fuel

usage of the three profiles discussed.) Optimization 1, with either a constant altitude cruise segment or a cruise-climb, provides fuel usage within 1.5% of Optimization 2 (9.10:88,89, and 92).

Notice so far we have considered fuel as the optimizing variable. But fuel consumption alone is by no means the only cost, and, of course, commercial operators like airlines are certainly driven by the profit motive. Costs, like personnel, frequency of overhaul, and life expectancy of equipment, can all be related to flying hours. Hence, profiles optimized for minimum fuel consumption may not be minimum cost. Needless to say, as fuel costs increase, minimum fuel profiles tend to be minimum cost profiles.

All sorts of performance oriented systems, from hand held calculators up through systems coupled through autopilots and autothrottles, are now in use. Such systems have been in service for some time and are now standard commercial equipment. Such systems include both minimum fuel and minimum cost options and claim a 3% to 9% saving in fuel (9.11:124). Clearly, the principles of energy management are important for all types of aircraft in making design tradeoffs, in developing tactics and operational procedures, and in laying out test programs.

9.12 DATA COLLECTION FOR ENERGY METHODS

9.12.1 Measurement Techniques

One of the strengths of the energy methods is the variety of means available for data collection. Pitot-static data, if accurately calibrated and correlated with time, can give the basic information. Of course, for real time profile management displays or feedback information for automatic flight path control, one must have corrected air data as well as acceleration sensors of considerable precision and sensitivity. Evaluation of such systems requires careful planning on the part of the flight test engineer, with careful note taken of the range, precision, and dynamic response of the required flight test instrumentation.

9.12.1.1 Pressure Methods. Sometimes called airspeed/altitude (A/A) methods, the collection (and correction) of pitot-static data has been rather completely discussed in Chapter 5 of this textbook. Since these data are available in one form or another on any military aircraft and since they have

been collected and used from the very beginning of flight, pressure data must be considered one of the most readily available and reliable sources of data. The required aircraft system for data collection, however, is not always suitable as flight test quality data. Sensitive instruments and panel vibrators, for example, are often needed to provide usable airspeed/altitude information. Further, time correlation through photographic means or in some other fashion is essential to obtain rate information. Further, some form of numerical differentiation, which is an inherently inaccurate process, must be carried out to get accelerations and rates of climb or descent.

9.12.1.2 Position Measurements. There are a number of ways to directly measure position in space, and they can be used to obtain energy state and energy rate. Radar tracking (RT) is a very common method, and it has been in use for a number of years. While it requires a moderate amount of data reduction including transformations for both rates and positions as well as wind corrections, it is a relatively costly and not very accurate technique. Compounding these drawbacks is the relatively low availability of flight test quality radar data except on highly instrumented ranges.

9.12.1.3 Optical Tracking (OT). OT is also a means of obtaining usable position information. No on board transponders or computing devices are necessary. It is less available than radar and is located only at a few sites. Such devices are limited by weather conditions and are generally used for shorter ranges. It is fairly accurate, better than radar, but not comparable to laser devices.

9.12.1.4 Laser Tracking (LT). LT are now coming into wider usage but are not completely reliable so far. The promise of better tracking accuracy is clearly present, but more experience is needed to prove their utility. There are some mobile systems for close-in work to help alleviate the scarcity of such devices. Laser tracking also needs very little on board equipment to provide good results.

9.12.1.5 Acceleration Measurements. There are at least two very accurate devices for measuring performance on board the aircraft. Changes in energy states are readily available from the flight path accelerometer (FPA) and/or inertial navigation systems (INS). Both have been and are being used successfully to collect energy data. Both techniques are very accurate and seem to be quite reliable, but the installation and calibration of the sensors

is a special problem. The FPA, for example, must be calibrated for boom bending at various air loads and load factors. Further, at some point in the data reduction process, correction to the data must be made accounting for the relative position of the accelerometers and the aircraft center of gravity, especially when significant angular rates and accelerations are involved. (That is, nearly all the time!) Any inertial measurement scheme, like those using the INS that may be installed, requires similar corrections. At least these techniques measure accelerations and rates directly, and numerical integrations produce position (potential energy) data instead of numerically differentiating to arrive at rates and accelerations.

9.12.2 Relative Merits

From the preceding discussion, it should be clear that no single means of taking energy data is superior for all aircraft and all time. The choice of measurement is one of the many engineering judgments based on the intended use of the data, the available equipment on the test article, the cost of the instrumentation, the need for reliability, availability, and the time and money available for data processing. Table 9.3 is an approximate rank ordering of the techniques discussed under five possible headings. This matrix should not be used blindly; instead, develop your own with rankings based on your system, your test objectives, and your constraints. Then, keep updating it as priorities change.

Table 9.3

RANK ORDERING OF MEASUREMENT TECHNIQUES (1 is most desirable)

<u>Rank</u>	<u>Accuracy</u>	<u>Reliability or Availability</u>	<u>Data Processing</u>	<u>Cost</u>
1	FPA	A/A	FPA	A/A
2	INS	FPA	INS	OT
3	LT	RT	RT	FPA
4	OT	INS	OT	LT
5	RT	OT	LT	RT
6	A/A	LT	A/A	INS

9.13 CLIMB AND DESCENT TESTS

The tests that are associated with the determination of the climb performance of an aircraft will now be explained. The climb performance is determined from an airspeed schedule, and the first order of business is to determine that schedule. Lower performance aircraft can use the sawtooth climb method for climb speed determination. The level acceleration method is more suitable for high performance aircraft.

Once the climb speed schedule has been determined, the actual climb performance of the aircraft is obtained by running check climbs to altitude. In general, the same procedure is used for both reciprocating engine and jet aircraft. The factor which complicates climb performance determination is the fact that all data must be corrected to standard day conditions. Test day performance is easily obtained but has no meaning if used to compare two aircraft flown on two different days. It is therefore necessary that sufficient data be recorded and proper techniques employed to reduce the results to standard day conditions.

The most important factor is nonstandard temperature, from a performance standpoint. Other corrections such as those for nonstandard weight, vertical wind gradient effects, and climb path acceleration are normally of lesser importance.

Since large lag errors occur in the measurement of the free air temperature, the temperature as obtained from a weather station may be satisfactory and is sometimes more accurate than that obtained from the aircraft instrument when insufficient time has been allowed for stabilization.

9.13.1 Sawtooth Climb Test

The sawtooth climb test is one method of obtaining the airspeed schedule for maximum rate of climb. Its name is derived from the barograph trace resulting from a series of short, timed climbs through the same pressure altitude band. This test provides little or no useful information on climb performance. It merely establishes the best airspeed at which to climb.

Essentially, this test employs a trial and error method. A series of timed climbs is made at different speeds from a point below the test altitude to a point above it. Speeds are chosen to bracket the expected best climb

speed of the aircraft.

Climbs are performed at the same power setting and aircraft configuration as will be used in the check climb. The altitude increment should be chosen such that the aircraft will traverse it in about one minute. Smaller time increments will introduce excessive scatter in the data.

The aircraft is first trimmed in the climb configuration while still well below the nominal altitude. Power is applied and final trim adjustments are made before reaching the lower limit of the altitude band being measured.

The exact time of entering and leaving the altitude band is recorded by stopwatch or instrumentation system.

Upon emerging from the altitude increment, data are recorded, and a 180° descending turn is initialized to bring the aircraft below the altitude band for another run. As many points as possible should be flown at each altitude. In addition, a full power unaccelerated minimum speed point and a maximum speed point should be obtained at the test altitude in order to complete the curve. These latter two points should be flown at the beginning of the test so that weight corrections will be minimized.

An effort should be made to confine the flights to the bounds of a limited geographical area since the primary concern is the shape of the curve obtained rather than the magnitude. If the aircraft remains in this area, the effects of lifting and atmospheric conditions should be minimized.

For each altitude, a standard data card should be prepared with the aim indicated airspeed (aim V_i) included for each point. Provision should be made for recording in flight actual V_i , Δ time, fuel counts, and either outside air temperature or time of day.

On the back of the data card, a running plot of observed time to climb versus V_i should be kept, and before leaving the test altitude, it should be examined for points that might need repeating.

9.13.2 Level Flight Acceleration Test

With the advent of high performance aircraft, the performance envelope has greatly expanded, and additional areas of investigation have become important. Higher wing loadings require higher wing speeds, and the acceleration from brake release to climb speed assumes greater importance. Supersonic capabilities result in a wide differential between best climb speed

and maximum level flight speed, and the level acceleration performance at altitude becomes important. For most supersonic aircraft, a supersonic climb speed schedule is of interest in addition to the familiar subsonic schedule.

The level flight acceleration test serves two purposes. It makes available acceleration time and fuel consumption data in level flight, and it may be used for determining climb speed schedules both subsonically and supersonically.

9.13.2.1 Method. Level flight accelerations from near minimum to near maximum airspeeds are normally flown at a variety of altitudes. As in the sawtooth climb test, power settings and aircraft configurations are those which will later be used in the check climb. Since a number of simultaneous readings are required and since data points are only a few seconds apart, recording must be mechanical, usually by a Data Acquisition System (DAS). Values of indicated airspeed and time are the primary parameters. Fuel flow and free air temperature data are recorded, and indicated altitude is included so that errors caused by climb or descent may be corrected.

9.13.2.2 Preflight Preparation. A data card should be drawn up, and entries should be recorded in order that correlation between runs, power settings, time of day, etc., may be facilitated. Required entries include:

1. RUN NUMBER
2. ALTITUDE
3. POWER SETTING (MIL OR MAX)
4. RPM
5. TIME OF DAY (TOO)
6. COUNTER NUMBER (START AND FINISH)
7. FUEL (START AND FINISH)

Any other desired parameters not included on the DAS may be recorded as necessary.

The pilot should make himself familiar with altitude position error corrections of the aircraft so that he can plan for a slight indicated rate of climb or descent which will result in a nearly level flight path.

9.13.2.3 Uses. The level flight acceleration is the method used to obtain climb schedules for high performance aircraft chiefly because:

1. It is relatively easy to obtain good data at values of P_s where climb rates would be too high for accurate sawtooth climbs. In fact, the data accuracy improves at higher values of P_s .
2. Flying time required is much less than for the sawtooth climb. Usually one-half the time or less will cover the same speed and altitude range.
3. Wind gradient errors are smaller.
4. Acceleration data is obtained in conjunction with climb speed data.
5. Supersonic climb speed schedules can be found by this method.

9.13.2.4 Limitations. Limitations in the method exist in that:

1. At low climb rates, the peaks of the curves are poorly defined. This limits the usefulness of the method for low performance aircraft and for any aircraft as it approaches its service ceiling.
2. Data reduction processes are tedious if a hand reduction method is used. Computer data reduction programs reduce the time considerably, although loading the raw data can still be tedious.
3. Unless some form of mechanical recording device is available, data cannot be collected rapidly and accurately enough to be of value.
4. Because scatter is always fairly high, a single level acceleration is not reliable. From two to ten or more runs at any altitude are required to properly define the curve.

9.13.3 Check Climb Test for Jet Aircraft

The check climb test is flown to evaluate the standard day climb performance of an aircraft in a specific configuration. The three main areas of investigation are:

1. TIME TO CLIMB
2. DISTANCE TRAVELED
3. FUEL USED

In addition, data may be obtained on various engine parameters such as engine speed, exhaust gas temperature, engine pressure ratio, gross thrust,

etc. These are useful to the analyst but are secondary to the three main parameters.

The general method is to climb the aircraft to just below the maximum ceiling while maintaining precisely a predetermined climb schedule. This schedule may be a best climb schedule as obtained by flight test, a schedule recommended by the manufacturer, or some other schedule for which climb performance is of interest. Care should be taken to specify on each climb performance chart the schedule flown.

Data should be recorded at approximately equal increments of altitude and should include time, speed, fuel used, temperature, and any other desired parameters. For most jet aircraft, a mechanical recording means will be necessary to obtain simultaneous reading of the many parameters of interest.

9.13.3.1 Preflight Preparation. The data card serves a double purpose; it provides the pilot with a list of aim speeds for each altitude and is used to record pertinent data facts. The first portion of the data card is used to record fuel used to start and taxi, and fuel and time required to accelerate from brake release to climb schedule. A sample layout is illustrated in Figure 9.43.

Aim speeds should be adjusted for instrument error and position error of both the airspeed indicator and altimeter. If the anticipated rate of climb is low, airspeeds would be presented every 1,000 or 2,000 feet with speeds to 1/2 knot. If the rate of climb is high, every 5,000 feet is sufficient with speeds to the nearest knot. It may be advisable to decrease the interval to every 2,500 feet or 2,000 feet as the rate of climb decreases with altitude.

Perhaps the most difficult step in obtaining good check climb data is finding an area of satisfactory meteorological conditions. An area of smooth air, light winds, and stable temperature gradients from ground level to the aircraft's maximum ceiling is desirable. A survey balloon should be sent up before the flight for wind and temperature data and an area chosen where the climb can be performed at 90° to the average wind direction.

Since aircraft gross weight and fuel density are extremely important, arrangements should be made, if possible, to weigh the aircraft fully fueled immediately prior to takeoff. In any case, fuel samples from the tanks should be taken to obtain fuel temperature and density.

RUNWAY _____ PRESSURE _____
 TEMPERATURE _____ ALTITUDE _____ WIND _____

TAXI AND TAKEOFF				
DATA POINT	TIME	FUEL COUNTS	DAS TIME	
ENGINE START				
BRAKE RELEASE				
INTERCEPTING CLIMB SCHEDULE				

CHECK CLIMB				
H _i	V _i	EVENT NO.	TIME OF DAY	OTHER DESIRED ITEM
4 000	370			
6 000	352			
8 000	354			
10 000	347			
ETC.	ETC.			

FIGURE 9.43. SAMPLE DATA CARD

9.13.3.2 Flight Techniques. Data on fuel used and time for taxi, takeoff, and acceleration to climb schedule should be taken whenever conditions permit. Upon reaching climb speed, it is usually advisable to discontinue recording data and start afresh with the check climb entry.

Two basic methods for entering a check climb are available. In either case, the first step is to establish the aircraft in level flight as low as possible, consistent with safety, and on the climb heading. If a DAS is being used to record data, it should be on and running before entering the climb. If the instrumentation system is a type that can't be run continuously such as a photopanel, take readings every 500 feet (every 1,000 feet is adequate for training purposes).

If the rate of climb is high, the best entry is usually achieved by first stabilizing in level flight with partial power at some speed below the

scheduled climb speed. The aircraft should be trimmed for hands-off flight. When all preparations are complete and the data recorder is running, power should be applied, and as the climb speed is approached, the aircraft should be rotated to intercept and maintain the climb schedule. If rotation is begun too early, the aircraft may climb several thousand feet before intercepting the desired schedule. On the other hand, if rotation is begun too late, the rate of rotation will be rapid, and it will be difficult to avoid overshooting the desired pitch attitude.

If the rate of climb is fairly low, a better entry can sometimes be achieved by stabilizing on the aim speed 1,000 feet below entry altitude. When preparations are complete and the aircraft is trimmed, the power should be advanced smoothly, and the aircraft should be simultaneously rotated to maintain airspeed. As the desired power setting is reached, the rotation should be stopped, at which time the aircraft will be approximately established on the climb schedule.

During the climb, the aircraft should be constantly trimmed for hands-off flight. The climb schedule should be maintained to within one-half knot where possible, taking care to keep a steady bleed rate. A rapid crosscheck between external horizon and the airspeed indicator is required. If the pitch attitude is very steep, it may be necessary to substitute the aircraft attitude indicator for the external horizon during initial portions of the climb.

During climbs, wind gradient effects will appear as sudden airspeed changes. If these affect the climb speed schedule, corrective action is to make a small, but immediate, attitude correction. If the aircraft does not respond at once, another correction should be applied. The pilot should also be prepared to take instant corrective action as the wind gradient effect dies away, resulting in a climb speed error in the opposite direction.

At high altitudes, the problem of maintaining a precise speed schedule becomes difficult. A slight rate of change of indicated airspeed implies a much larger rate of change of kinetic energy. Therefore, any undesirable trend is difficult to stop with relatively ineffective aerodynamic controls. The best way to cope with this problem is to avoid it by a rapid crosscheck, precise control, and constant attention to trim. If corrections do become necessary, care should be taken to avoid reversing the motion of the airspeed

indicator because of the resulting hysteresis problem.

Upon completion of the climb, data recording should be shut off to conserve tape, and pertinent items such as time of day recorded.

9.13.4 Reciprocating Engine Check Climb Test

The primary purposes of the check climb test for reciprocating engine powered aircraft are identical with those of the jet check climb. Minor items on which data are obtained at each altitude include available manifold pressure and brake horsepower.

Preflight preparation and in-flight techniques parallel closely those described in the jet check climb. An additional complication at lower altitude arises from the necessity of maintaining a predetermined manifold pressure with the throttle. A satisfactory method is to set the manifold pressure to approximately 0.5 inches Hg above the desired, then readjust every 1,000 feet until critical altitude is reached.

If hand recording is to be used, data should be recorded every 1,000 feet, if possible. The following items should be recorded:

Actual V_i	Carburetor Air Temperature
RPM	Free Air Temperature
Manifold Pressure	Fuel Counter
Time	

The same precautions used to obtain accurate fuel consumption and gross weight data for jet aircraft would be observed.

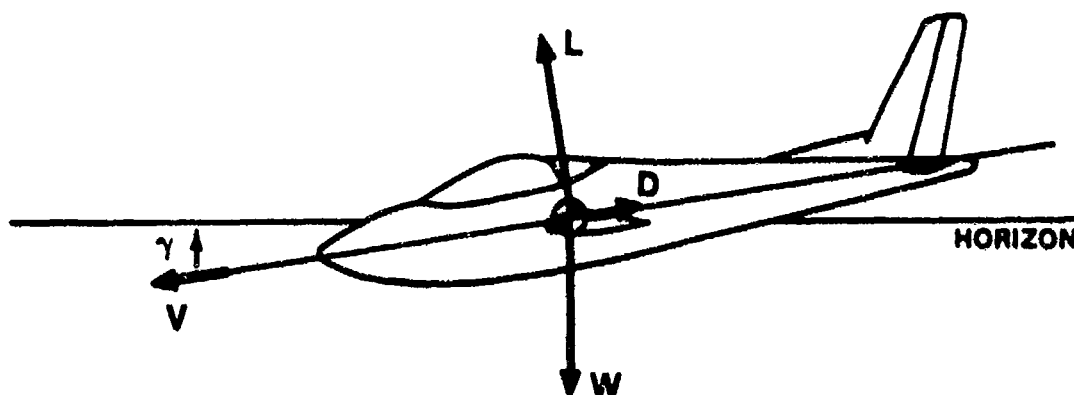
9.14 SUMMARY

In this chapter, the subject of performance optimization has been introduced. A point-mass model was accepted, and the fundamental (classical) performance equations were developed. Certain limitations in this steady state formulation led us to consider at length the energy state approximation. The purpose has been to expose you as a flight test engineer and a test pilot to the underlying notions of performance optimization without going through

the tedium of numerical calculations. The understanding you have gained is merely a beginning; you are by no means optimization experts. But, hopefully, some of the mystery has been removed. Remember Rutowski!

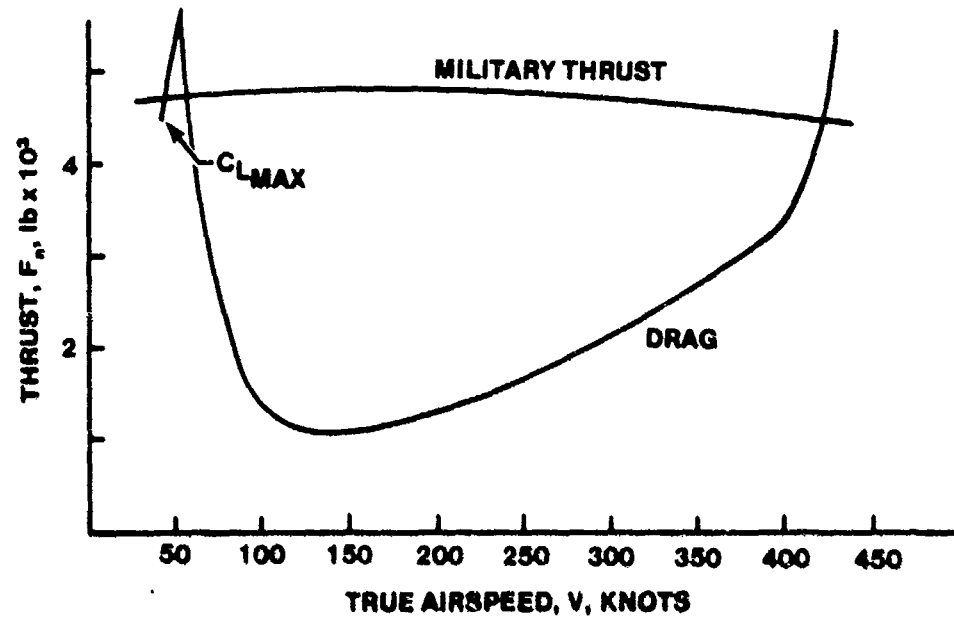
PROBLEMS

- 9.1 What are the four basic assumptions used in the development of the energy approximation? Briefly explain how each of these assumptions simplifies the mathematical formulation.
- 9.2A Assuming steady state conditions hold, derive an expression for a sailplane rate of descent, starting with the following free-body diagram.



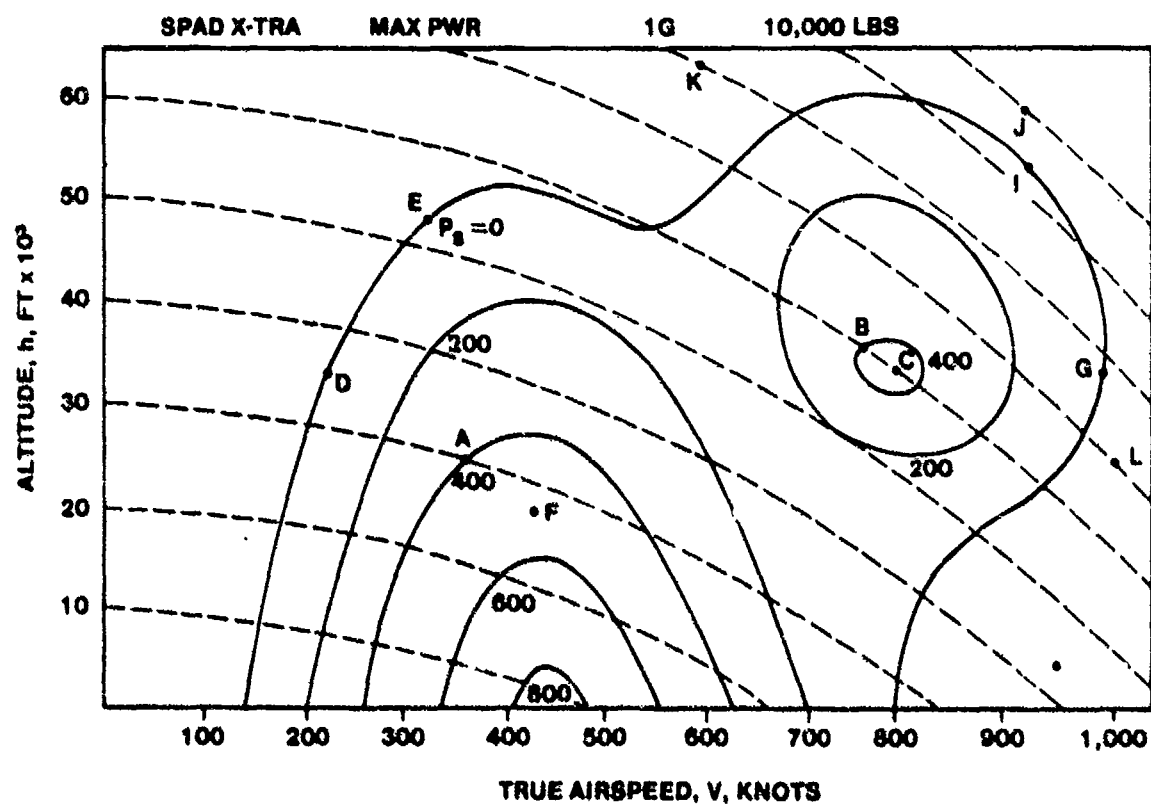
- 9.2B A Schweizer 2-32 sailplane weighing 1020 lb is flown at 55 mph. At this speed, its rate of descent is measured at 150 ft/min. What is the drag of the sailplane?
- 9.3 An F-15C weighs 45,000 lb, with the F-100 engine producing 25,000 lb of thrust from each engine at 10,000 ft. At 400 KTAS, drag is 12,000 lb.
- At this speed and altitude, what is the maximum rate of climb if true airspeed is held constant?
 - What is the initial acceleration, holding altitude constant?

- 9.4 A proposed replacement for the T-38 is a nonafterburning turbojet, having the estimated thrust and drag curves shown below.



- a. At approximately what velocity does L/D_{\max} occur?
 - b. At what velocity will maximum climb angle occur?
 - c. Outline how you might graphically determine the speed for maximum instantaneous rate of climb.
- 9.5 Write an expression for each of the following energy relationships. Give the physical meaning for each term in the expressions in your own words.
- a. Specific energy
 - b. Rate of change of specific energy
 - c. Relate specific energy to specific excess thrust.
- 9.6 Use the energy plot and data on the following page. Assume constant gross weight.
- a. Sketch the maximum rate of climb schedule to 50,000 ft (subsonic only).

- b. Sketch the minimum time path schedule from takeoff to Point K.
- c. What is the maximum altitude at which the "SPAD X-TRA" can maintain an unaccelerated rate of climb of 12,000 ft/min?



d. Can the "X-TRA" stabilize at the following points?

(1-g conditions - max thrust)

A

C

D

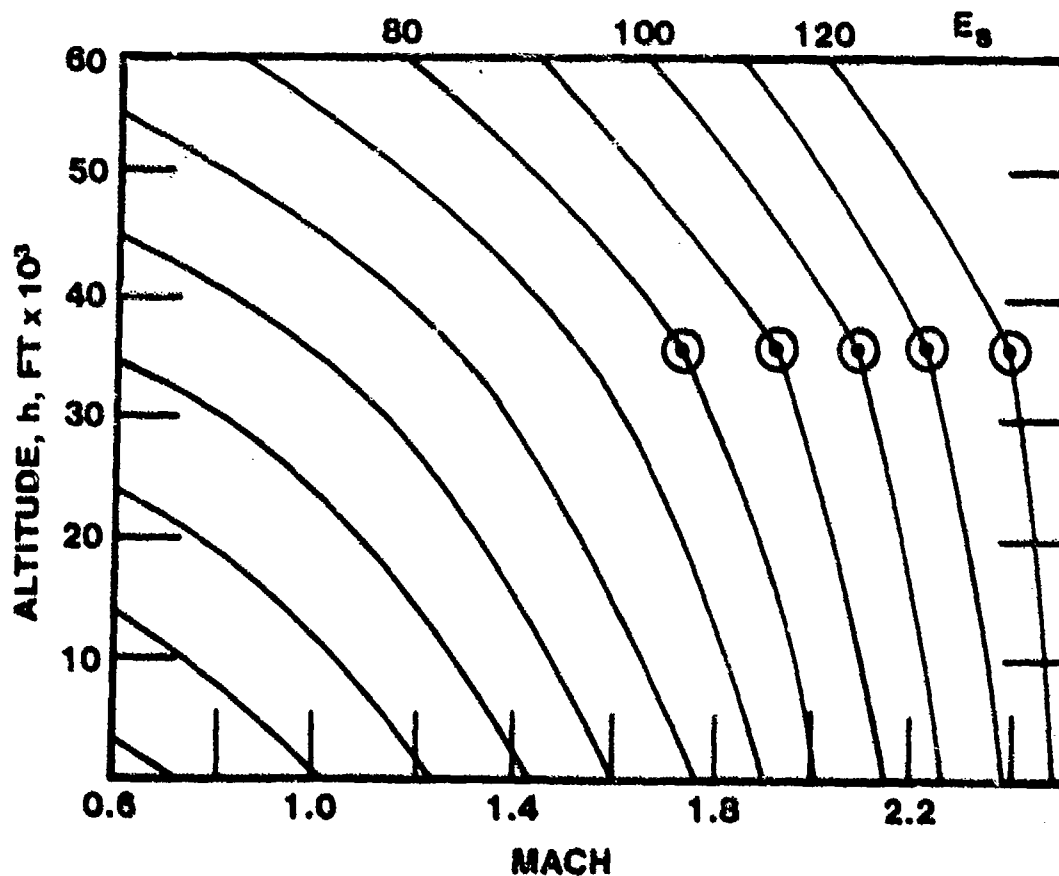
I

e. Can the "X-TRA" reach Point L?

f. Can the "X-TRA" reach Point J?

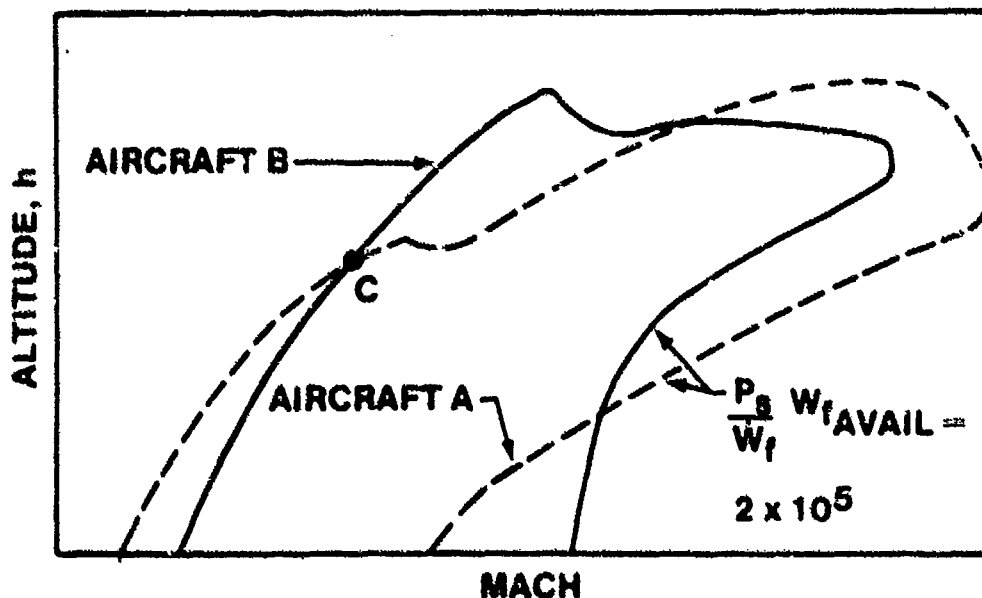
g. What is the total specific energy at Point A?

9.7 Energy diagrams using H and M usually have a "knee" (discontinuous slope) as shown in the accompanying sketch. Should this be shown? Why?



- 9.8 a. Is it true that minimum fuel paths to an energy level normally make the transonic transition to the supersonic portion at a lower altitude than minimum time paths to the same energy level?
- b. Name the units of P_s , and P_s/\dot{W}_f , and maneuver energy (E_M).
- c. What is the difference between path-dependent and path-independent E_M diagrams?
- 9.9 The following two aircraft (A & B) arrive at Point C with 50% internal fuel:

	Aircraft "A"	Aircraft "B"
Empty Weight	20,000 lb	18,000 lb
Max Internal Fuel	10,000 lb	6,000 lb
Max Power Fuel Flow	30,000 lb/hr	20,000 lb/hr

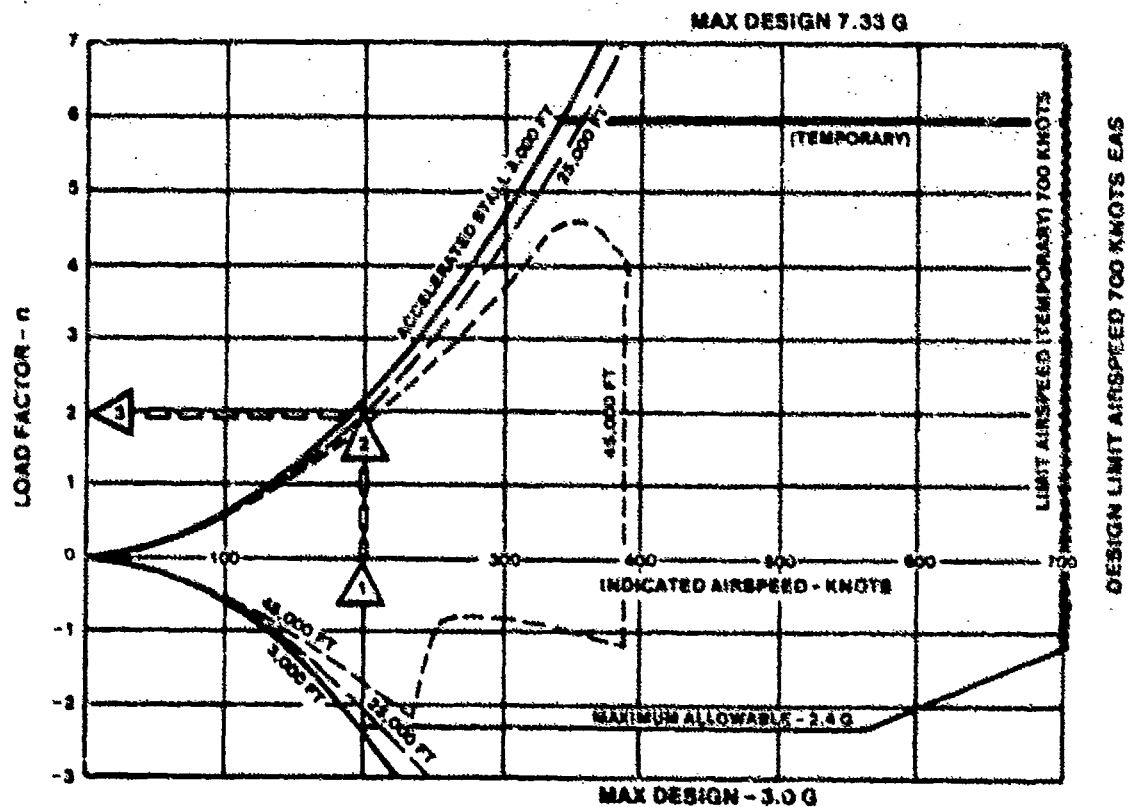


- a. Which aircraft has the highest specific excess power (P_s) at Point C? (Justify your answer).
- b. Which aircraft has the most excess thrust at Point C? (Justify your answer).

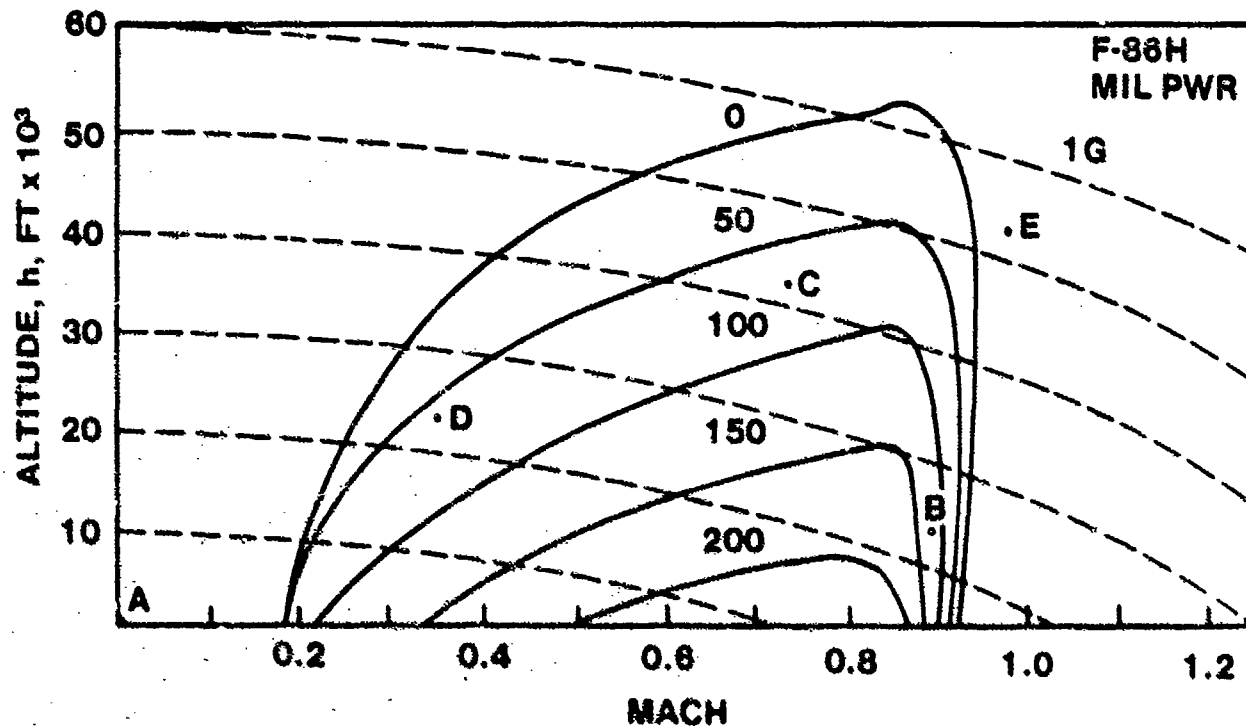
9.10 What factors usually determine the boundaries for a V-n or V-g diagram?
What is the major limitation of such a diagram?

OPERATING FLIGHT LIMITS

EXTERNAL LOAD: NONE
COMBAT CONDITION (GROSS WEIGHT
28,700 LBS)

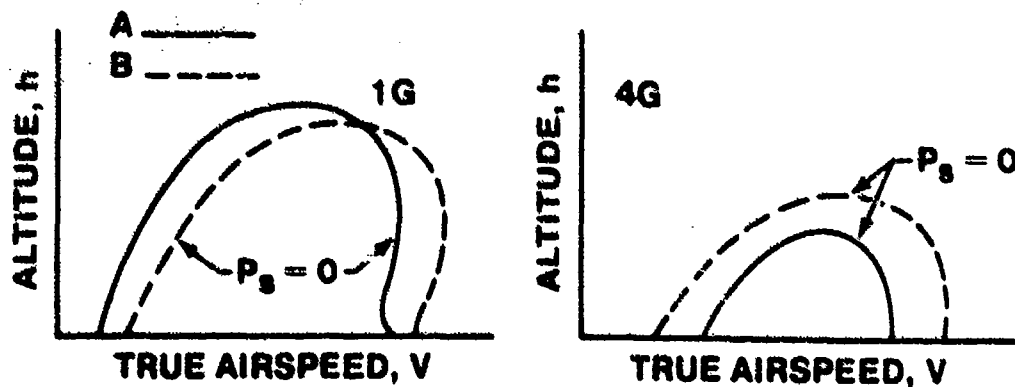


9.11 The following energy plot was obtained for a subsonic aircraft:



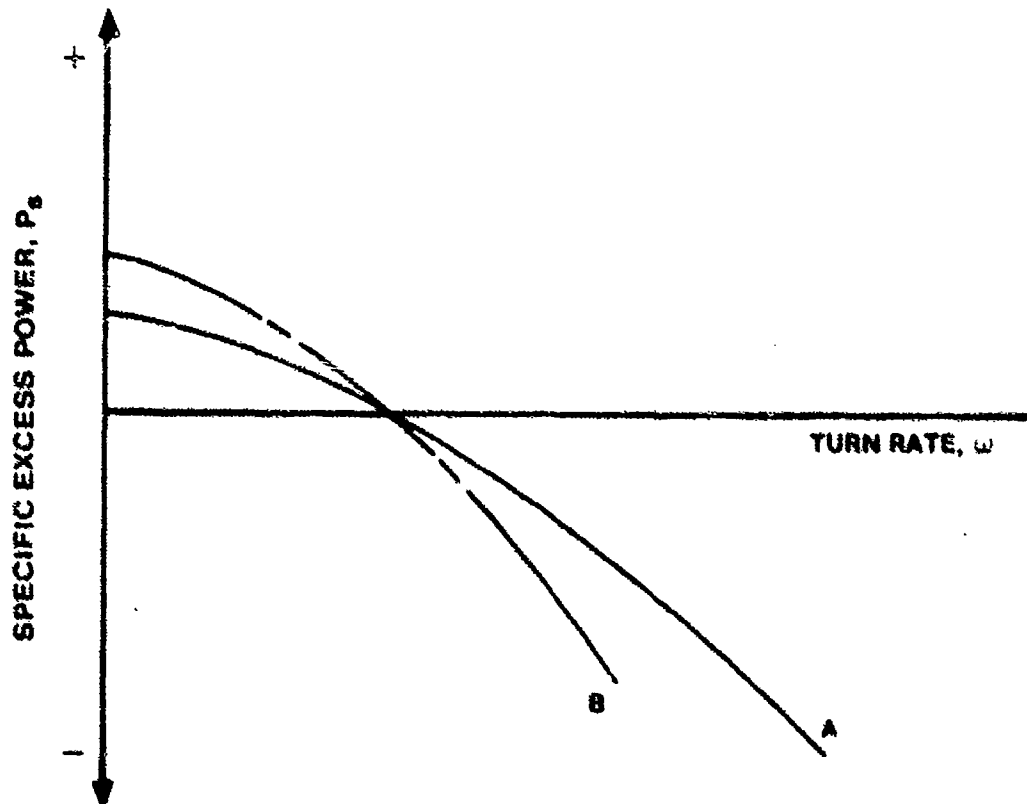
- Sketch theoretical minimum time optimum energy flight path from Point A to 30,000 ft.
- Sketch theoretical minimum time optimum energy path from B to C.
- Can the aircraft stabilize at Point D?
- Can the aircraft reach Point E?

9.12



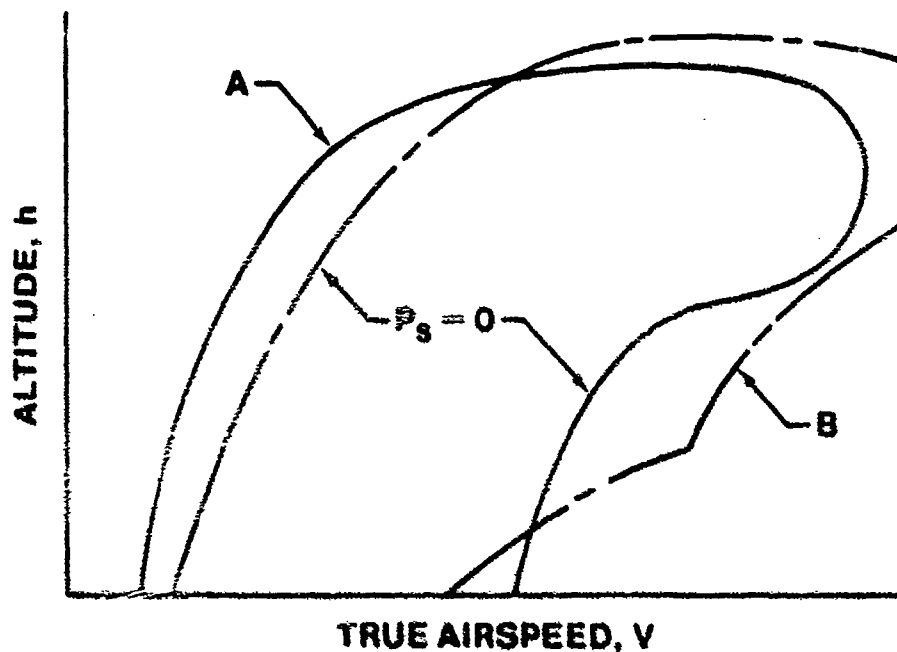
Which aircraft probably has the highest wing loading/lowest aspect ratio?
Briefly explain your answer.

9.13 The following figure depicts maneuvering (climb and turn) capabilities of two aircraft (A & B) at a particular altitude and airspeed.

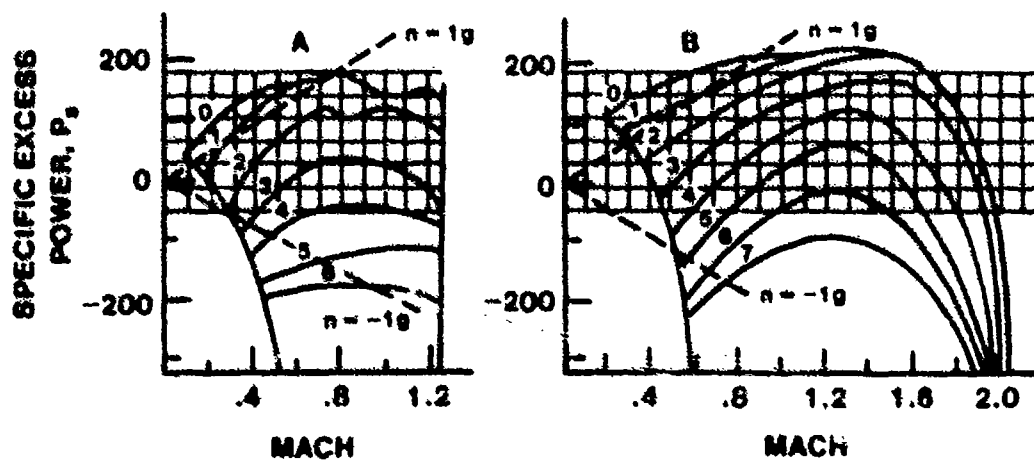


- Which aircraft has the greatest instantaneous climb potential?
- Which aircraft has the greatest sustained maneuver capability?
- Which aircraft has the greatest instantaneous turn capability?
- Suggest one feature that could be designed into your aircraft to increase its maneuvering capabilities (ω relative to P_s).

- 9.14 Using the 1-g P_s diagrams for the two aircraft shown below, mark those areas where Aircraft A is superior and where Aircraft B is superior -- superiority being defined for this problem as an edge in energy rate.



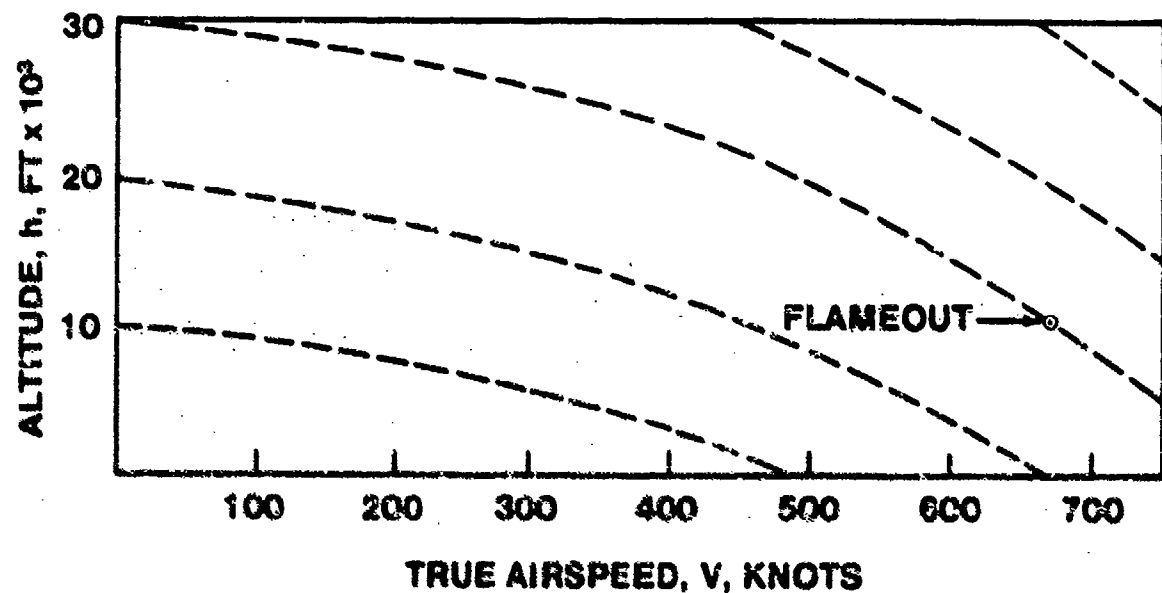
- 9.15 Using the P_s - Mach Charts given below, answer the following questions comparing the two aircraft represented.



- At $M = 0.8$ and 3-gs, what options does the pilot of Aircraft A have? The pilot of Aircraft B?
- Which aircraft will dissipate energy faster in a 5g lift limited turn? How much faster?

9.16 Major Sack set up for a low level bomb run in his XB-13. At 10,000 ft/672 KTAS all engines flamed-out.

- What is the theoretical maximum altitude he could zoom to assuming no losses and no aerodynamic limits?
- Sketch this ideal zoom on the H-V Plot below.
- Sketch a real world zoom for this zero thrust bomber on the same plot.



- Is it true that the variable of most interest in performance evaluations is specific energy (E_s)?
- List two reasons we have non-steady state testing (dynamic performance flight testing).
- The F-5 Program utilized a flight path accelerometer (FPA) for performance data acquisition. What are two other methods mentioned in class or notes used to obtain performance data?
- Name two sources of possible errors in data gathering using a FPA. There are more than two.

9.18 The P_s/\dot{w}_f contours for Aircraft A are shown on the next page.

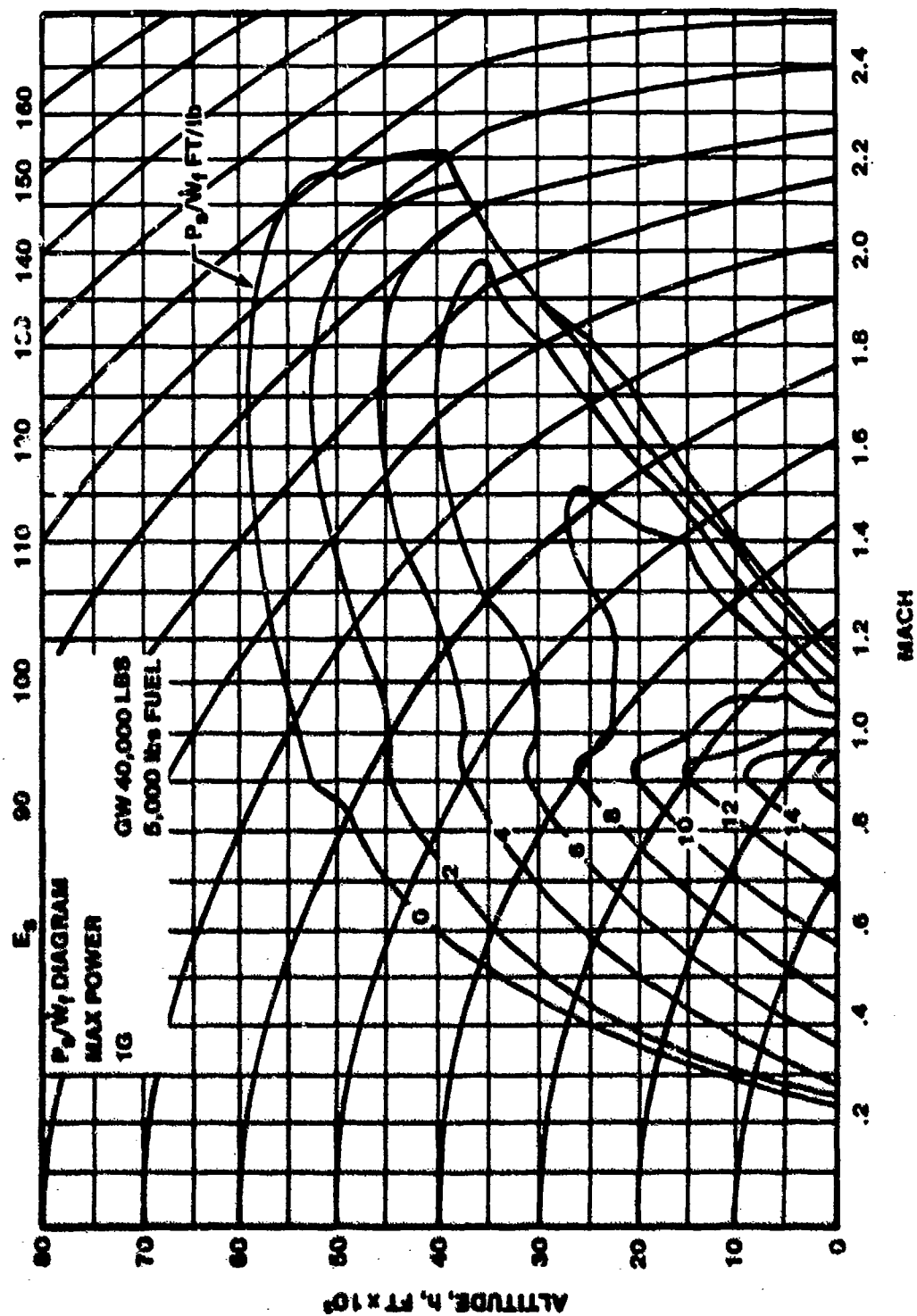
- a. Determine the Maneuver Energy for the aircraft at 15,000 ft/1.0 MACH/max thrust with 5,000 lb of fuel available.
- b. If the fuel flow (\dot{w}_f) at this point is 18,000 lb/hr, determine the maximum longitudinal acceleration potential in Gs, (n_x).
- c. Aircraft A engages Aircraft B with the following characteristics at the same point:

$$P_s = 1,000 \text{ ft/sec}$$

$$\dot{w}_f = 24,000 \text{ lb/hr}$$

$$w_{F_A} = 8,000 \text{ lb}$$

Which has the greatest Maneuver Energy, A or B?



9.19 The time rate of change of specific energy is equal to the specific excess power, which is often represented by the symbol P_s . P_s represents how rapidly an airplane is gaining or losing energy height. We have

$$\frac{(F_n - D)V}{W} = P_s = \frac{dh}{dt} + \frac{V}{g} \frac{dV}{dt} = \frac{dE_s}{dt}$$

- a. What does each term represent?
- b. If thrust, drag, velocity, and weight are known, then P_s can be evaluated. Once P_s is known (at a given altitude, weight, load factor, throttle setting, and configuration), then the airplane's capability to climb and/or accelerate is known for that flight condition.
 1. Estimate P_s for a T-38 with $n = 2$, $M = 0.5$ at sea level in the cruise configuration at maximum thrust, given that

$$(T/W)_{\max} = 0.676, W = 10,000 \text{ lb}, C_D = .0152 + 0.126 C_L^2$$

- c. If an airplane can be flight tested and Mach, velocity, time, and altitude are recorded, then rate-of-climb and acceleration can be computed at a known flight condition (altitude, Mach, load factor, throttle setting, weight, and configuration). Thus, P_s can be evaluated by flight testing. Two methods are frequently used: (1) the constant velocity climb, (2) the constant altitude acceleration.
 1. Estimate P_s and find the Mach for which it is valid, given that a T-38 (with $n = 2$, max thrust, $W = 10,000 \text{ lb}$, at sea level, in the cruise configuration) does a level turn while accelerating from 548 ft/sec to 568 ft/sec in 1.18 sec.
 2. Estimate P_s for a T-38 at $n = 1$, $W = 10,000 \text{ lb}$, $M = 0.85$, altitude = 30,000 ft, in the cruise configuration if the airplane does a constant velocity climb from 29,000 ft to 31,000 ft in 11.4 sec.

9.20 Once P_s values are known for differing airplanes (for example, adversaries in combat), then their performance capabilities may be compared. From the data given, compare the airplanes' performance capabilities.

- a. Both airplanes at $M = 0.80$, sea level, $n = 1$, max thrust, cruise configuration, combat weight.
 1. F-16: $P_s = 1,030$ ft/sec
 2. Mig 21: P_s (estimated) = 670 ft/sec
- b. Both airplanes at $M = 1.2$, 30,000 ft, $n = 5$, max thrust, cruise configuration, combat weight.
 1. F-16: P_s (estimated) = - 100 ft/sec
 2. Mig 21: P_s (estimated) = - 400 ft/sec
- c. When comparing airplanes in combat, what other factors (besides P_s) should be considered?

ANSWERS

9.2b. $D = 31.6 \text{ lb}$

9.3a. $R/C_{\max} = 34,228 \text{ ft/min}$

b. $dV/dt = 0.84 \text{ g}$

9.4a. 135 kts

b. 135 kts

9.6c. $40,000 \text{ ft subsonic; } 50,000 \text{ ft supersonic}$

g. 30 M ft

9.15b. 25 ft/sec

9.16a. $30,000 \text{ ft}$

9.18a. $50,000 \text{ ft}$

b. 0.047 g

9.19b. $P_s = 279 \text{ ft/sec}$

9.19c. 1. $P_s = 294 \text{ ft/sec}$

2. $P_s = 175 \text{ ft/sec}$

BIBLIOGRAPHY

- 9.1 Bryson, A.E. Jr., Desai, M.K., and Hoffman, W.C., "Energy-State Approximation in Performance Optimization of Supersonic Aircraft," Journal of Aircraft, Vol. 6, No. 6, November-December 1969, pp. 481-488.
- 9.2 Rutowski, E.S., "Energy Approach to the General Aircraft Performance Problem," Journal of the Aeronautical Sciences, Vol. 21, No. 3, March 1954, pp. 187-195.
- 9.3 Hildebrand, F.B., Methods of Applied Mathematics, Englewood Cliffs, NJ: Prentice-Hall, Inc., 1965.
- 9.4 Kelley, H.J., and Edelbaum, T.N., "Energy Climbs, Energy Turns, and Asymptotic Expansion," Journal of Aircraft, Vol. 7, No. 1, January-February 1970, pp. 93-95.
- 9.5 Calise, A.J., "Extended Energy Management Methods for Flight Performance Optimization," AIAA Journal, Vol. 15, No. 3, March 1977, pp. 314-321.
- 9.6 Reaves, G.L., "The Energy Maneuverability Concept and Recommended Air Combat Tactics for the F-104," The SURE Project, Lecture 6, Lockheed Report CA/ME 2383, July 1967.
- 9.7 Chase, W.V., "Energy Maneuverability; USAF and USN Aircraft in Clean Configuration," APGC-TR-66-4, Vol. II (Part A), Air Force Armament Laboratory, Eglin AFB, FL, December 1966, (SECRET).
- 9.8 Kelley, H.J., and Lefton, L., "Supersonic Aircraft Energy Turns," Automatica, Vol. 8, 1972, pp. 575-580.
- 9.9 Weir, T.J., "Fundamentals of Air Combat Maneuvering," F-5 Technical Digest, Vol. 2, No. 5, May 1975, pp. 3-6.
- 9.10 Stengel, R.F., and Marcus, F.J., "Energy Management Techniques for Fuel Conservation in Military Transport Aircraft," AFFDL-TR-75-156, Air Force Flight Dynamics Laboratory, Wright-Patterson AFB, OH 45433, February 1976.
- 9.11 Moor, D.A., "Development of the L-1011 Flight Management System", SETP Technical Review, Vol. 14, No. 2, The Society of Experimental Test Pilots, Lancaster, CA, 27-30 September 1978.

CHAPTER 10
TURN PERFORMANCE

10.1 INTRODUCTION

Turn performance is of primary importance for fighter type aircraft where parameters such as turn rate, turn radius, and sustained g capability are used to assess combat capability. Large multiengine cargo and trainer type aircraft are more concerned with instantaneous g capability to define the lift and structural limits of the aircraft. These limits are established in what is commonly known as the V-g or V-n diagram.

10.2 THE V-n DIAGRAM

Instantaneous maneuver capability is defined with the use of the V-n diagram. A typical V-n diagram is shown in Figure 10.1.

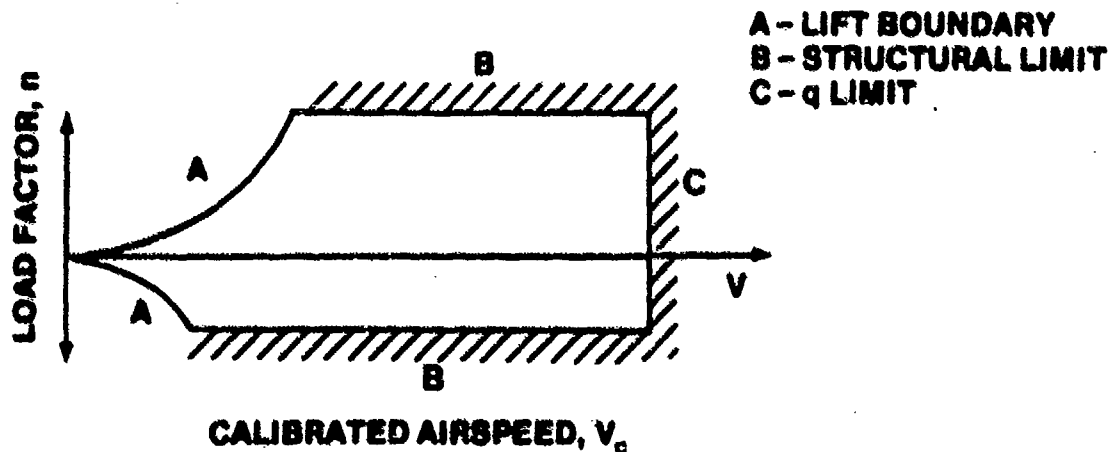


FIGURE 10.1. V-n DIAGRAM

Although a V-n diagram is published for most aircraft, the information contained in it does not include the aircraft thrust capability which is necessary to determine sustained maneuverability.

The aircraft limitations shown on the V-n diagram are:

1. The lift boundary limitation
2. The structural limitation
3. The q limitation

10.2.1 Lift Boundary Limitation

The lift limitation on turning performance refers to that portion of the flight envelope in which the aircraft is limited in angle of attack because of aerodynamic stall, pitch up, or other controllability factors. This is depicted by Curves A in Figure 10.1, the upper curve being in the positive g environment and the lower curve for values of negative g . Every point along the lift boundary curve, the position of which is a function of gross weight, altitude, and aircraft configuration, represents a condition of $C_{L_{\max}}$ or angle of attack limit. It is important to note that for each configuration, $C_{L_{\max}}$ occurs at a particular α_{\max} , independent of load factor; i.e., an aircraft stalls at the same angle of attack and C_L in accelerated flight, $n > 1$, as it does in unaccelerated flight, $n = 1$.

This area of operation is investigated through a test called the "lift boundary" investigation. Since this is primarily a problem in aircraft controllability, it is investigated in the Flying Qualities portion of the course.

All aircraft can be flown to the lift boundary limitation in level flight in the low speed portion of the flight envelope. By combined diving and turning maneuvers, this limitation may be explored through a large portion of the airspeed range.

10.2.2 Structural Limitations

Structural limitation is normally due to the aircraft limit load factor, which is defined as the load factor where permanent structural deformation may take place or to the ultimate load factor, which is defined as the load factor where structural failure may occur. Normally, the ultimate load factor is equal to approximately 1.5 times the limit load factor and is a property of the materials from which the aircraft is constructed. Limit load factors are indicated by Curves B in Figure 10.1.

It will become evident that all aircraft, regardless of design or weight, will achieve the same rate and radius of turn when maintaining the same velocity and load factor. Thus, when the limit load factor is reached in flight, tests can be discontinued, and the rate and radius of turn can be calculated for that portion of the airspeed range in which limit load factor

can be maintained.

Even among high performance aircraft, there is only a small portion of the flight envelope in which limit load factor can be maintained in level flight, although it can be achieved in maneuvers such as dives and pullouts through a much larger portion of the envelope.

10.2.3 q Limitation

q limitation is simply the maximum dynamic pressure the aircraft can withstand or the maximum flight velocity. The q limitation is shown by Curve C in Figure 10.1.

10.3 PILOT LIMITATIONS

Another limitation which must be considered is the physiological limitations of the human pilot. Although physiological limits have nothing to do with the V-n diagram directly, g limits on the human body can be thought of in the same terms as g limits upon the aircraft.

If the pilot can withstand greater g-loads than the aircraft, he must always be aware not to exceed the aircraft limitations. If the aircraft can withstand greater g-loads than the pilot, the pilot must always be alert to the possibility of gray-out or black-out when pushing the aircraft to the boundaries of the flight envelope. Naturally, this physical limitation will vary with the individual pilot.

10.4 THRUST LIMITATIONS

The thrust limitation on turning performance is the primary area of investigation in the performance phase of flight testing. In stabilized level flight, thrust and drag considerations will be the limiting factors through a large portion of the flight envelope. For combat flying, this is the limitation on sustained turning ability without loss of energy ($P_g = 0$). For aircraft which are not expected to engage in combat, this phase of testing is of much less importance and is generally omitted.

10.5 SUSTAINED TURN PERFORMANCE

Sustained turn performance is very useful in establishing a fighter type aircraft's capability for air-to-air combat. Once determined, this information can be used to compare an aircraft to possible adversaries. Unlike the V-n diagram, sustained turning performance analysis includes the thrust capability of the aircraft. This performance is defined at the point where thrust equals drag in a level turn at a specified power setting (usually MIL or MAX power). We see then that aircraft sustained turning performance may be lift limited, structurally limited, or thrust limited depending on the aerodynamic design, structural strength or thrust capability.

10.6 FORCES IN A TURN

In a stabilized level turn, it can be seen from Figure 10.2 that the lift must be significantly increased over that required for level flight.

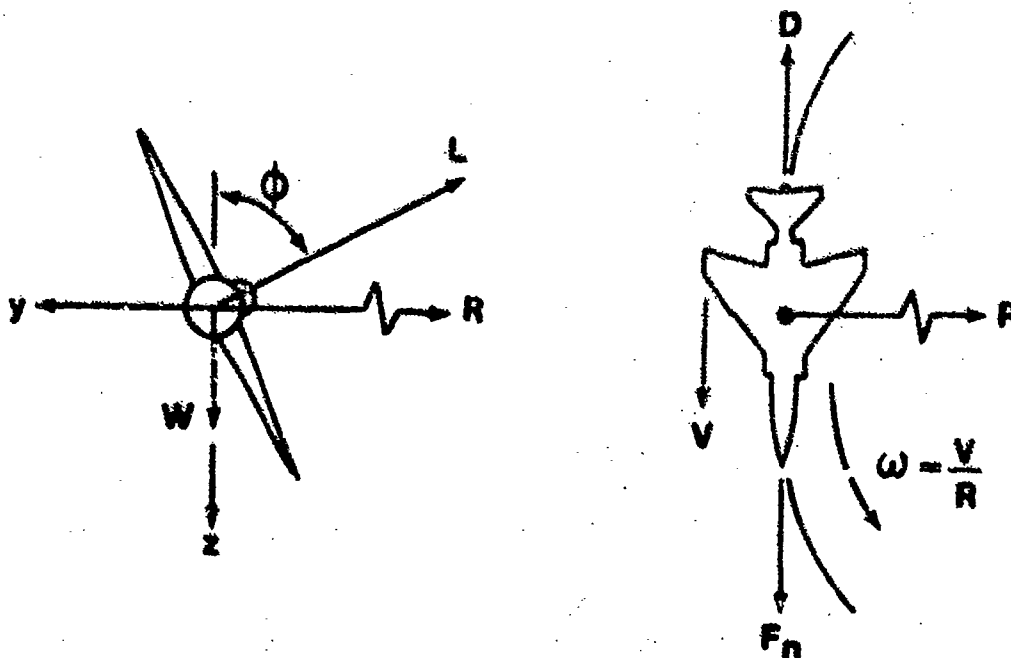


FIGURE 10.2. FORCES IN A TURN

The greater the bank angle, the greater the increase in lift required. Naturally, an increase in lift produces an increase in induced drag. The increase in induced drag requires an increase in thrust to maintain the aircraft in a constant airspeed, constant altitude turn. The vertical component of lift is still required to offset the aircraft weight, and the horizontal component of lift is the force which is offset by the centrifugal force in the turn. The aircraft experiences a centripetal acceleration toward the center of the turn.

To analyze mathematically the forces acting on the aircraft in Figure 10.2, we will consider an aircraft of weight (W) in a stabilized level turn of radius (R) with bank angle (ϕ).

Since airspeed is constant, thrust equals drag, and forces in the X-Z plane are balanced. The aircraft centripetal acceleration is given by V^2/R .

Summation of the vertical forces yields

$$\begin{aligned}\Sigma F_z &= -L \cos \phi + W = 0 \\ L \cos \phi &= W\end{aligned}\tag{10.1}$$

from which

$$\frac{L}{W} = \frac{1}{\cos \phi}$$

But

$$n = \frac{L}{W}$$

Therefore,

$$\boxed{n = \frac{1}{\cos \phi}}\tag{10.2}$$

Note that n is dependent only on the bank angle and is independent of aircraft type or configuration.

Summation of the horizontal forces yields

$$\begin{aligned}\Sigma F_y &= m a_y \\ L \sin \phi &= m a_y\end{aligned}$$

but the centripetal acceleration is

$$a_y = \frac{v^2}{R} \quad (10.3)$$

Therefore

$$L \sin \phi = \frac{W}{g} \frac{v^2}{R} \quad (10.4)$$

From the trigonometric identity $\cos^2 \phi + \sin^2 \phi = 1$, we can say that

$$L^2 = (L \cos \phi)^2 + (L \sin \phi)^2$$

using

$$L = nW \quad \text{or} \quad L^2 = n^2 W^2$$

$$L \cos \phi = W \quad \text{or} \quad (L \cos \phi)^2 = W^2$$

$$L \sin \phi = \frac{W}{g} \frac{v^2}{R} \quad \text{or} \quad (L \sin \phi)^2 = \left(\frac{W}{g} \frac{v^2}{R} \right)^2$$

and substituting

$$n^2 W^2 = W^2 + \left(\frac{W}{g} \frac{v^2}{R} \right)^2$$

dividing through by W^2 yields

$$n^2 = 1 + \left(\frac{v^2}{gR} \right)^2$$

or

$$n^2 = 1 + \frac{v^4}{g^2 R^2}$$

from which

$$R^2 = \frac{v^4}{g^2 (n^2 - 1)}$$

and

$$R = \frac{V^2}{g \sqrt{n^2 - 1}} \quad (10.5)$$

which is the radius of turn and is seen to be a function of velocity and load factor. Minimum turn radius will be a function of the sustained g capability of the aircraft and the velocity.

Recall that ω , the turn rate, is given by $\omega = V/R$.

Substitution of Equation 10.5 into this relationship yields

$$\omega = \frac{V}{V^2 / g \sqrt{n^2 - 1}}$$

or

$$\omega = \frac{g \sqrt{n^2 - 1}}{V} \quad (10.6)$$

Equation 10.6 tells us that turn rate is also a function of load factor and velocity.

Solving Equation 10.6 for n yields

$$n = \sqrt{\left(\frac{\omega V}{g}\right)^2 + 1} \quad (10.7)$$

Equation 10.7 is a very important relationship used in turn flight testing because turn rate can be measured directly.

10.7 TURNING PERFORMANCE CHARTS

Combining the relationships for turn rate and turn radius yields a chart such as Figure 10.3 which is good for a single altitude, but independent of aircraft type.

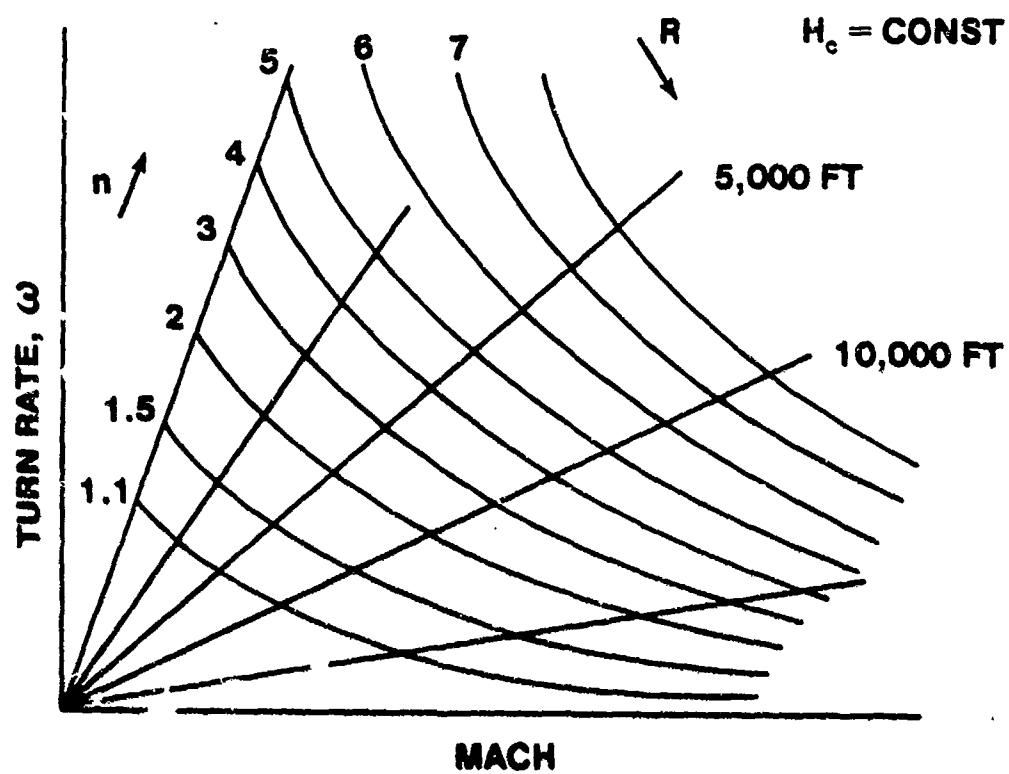


FIGURE 10.3. TURN RATE - TURN RADIUS RELATIONSHIPS

Overlaying a $P_g = 0$ curve for a particular aircraft onto Figure 10.3 will yield three Mach numbers of interest as illustrated in Figure 10.4.

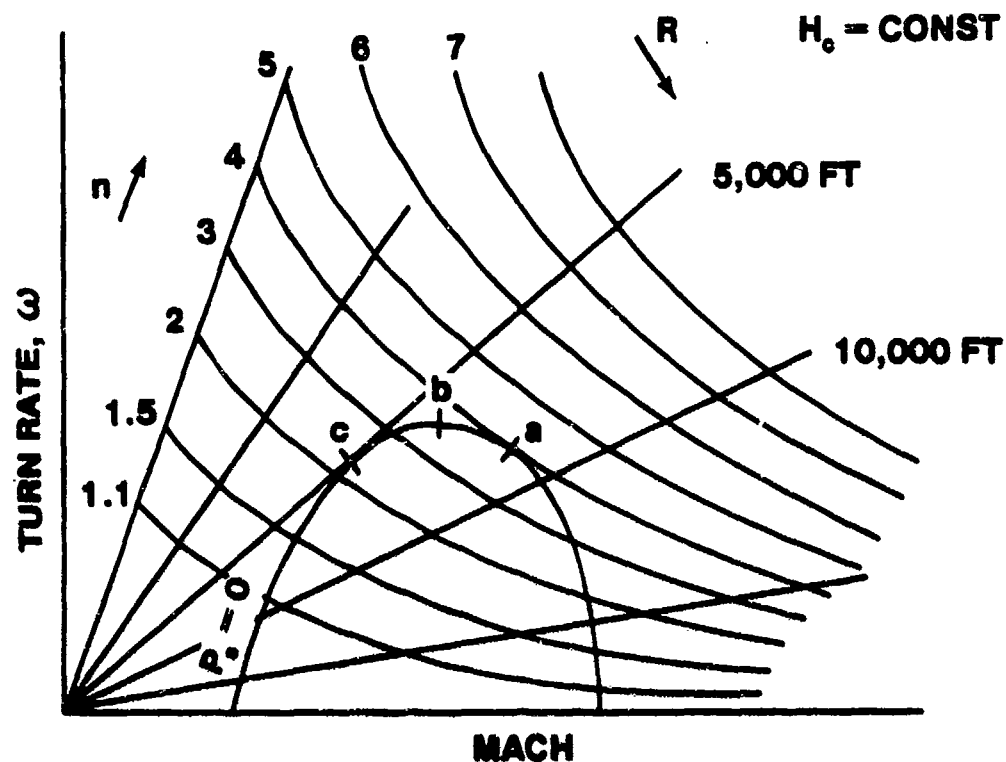


FIGURE 10.4. TURN RATE/RADIUS P_g OVERLAY

The point where the $P_g = 0$ curve is tangent to a constant load factor line (Point a in Figure 10.4) yields the Mach for maximum sustained g for that configuration. The peak of the $P_g = 0$ curve (Point b in Figure 10.4) yields the Mach for maximum turn rate, and the point where the $P_g = 0$ curve is tangent to a value of constant turn radius (Point c in Figure 10.4) is the Mach for minimum turn radius. For all cases

$$M_{n_{\max}} > M_{\omega_{\max}} > M_{R_{\min}}$$

Graphs of this type are published for fighter aircraft to define their sustained turn capabilities and are normally classified.

The turning capability where thrust equals drag ($P_s = 0$) may be better visualized by analyzing Figure 10.5.

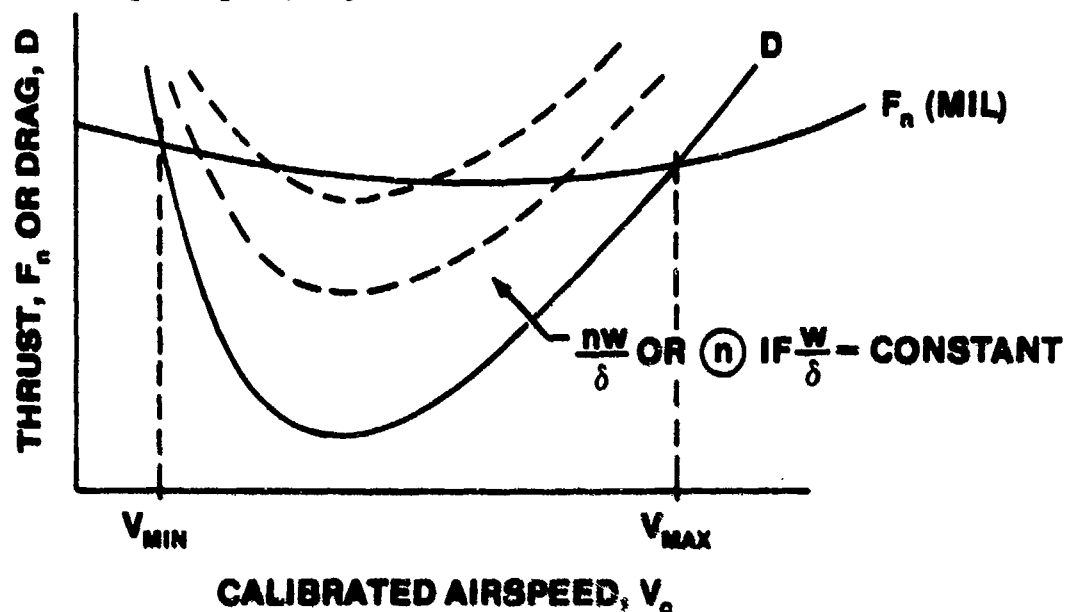


FIGURE 10.5. FACTORS AFFECTING TURNING PERFORMANCE

Note that for a given weight and altitude there are two stable points for each value of load factor, n .

Figure 10.5 implies that a graph of n as a function of M for a sustained turn ($F_n = D$) would look like Figure 10.6.

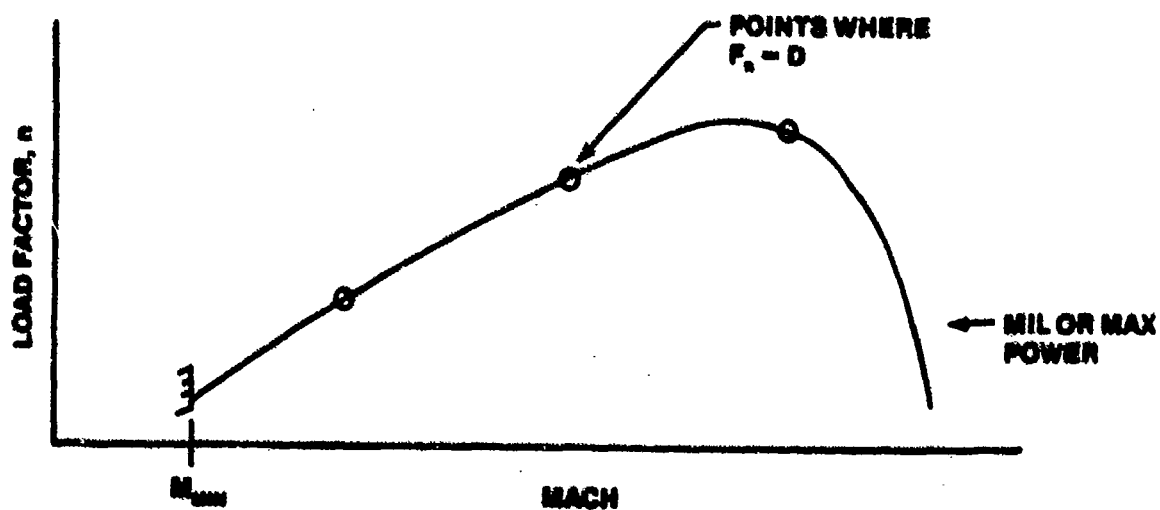


FIGURE 10.6. LOAD FACTOR VS MACH FOR A SUSTAINED TURN

Once n is known, ω and R can be calculated. Typical results are shown in Figure 10.7.

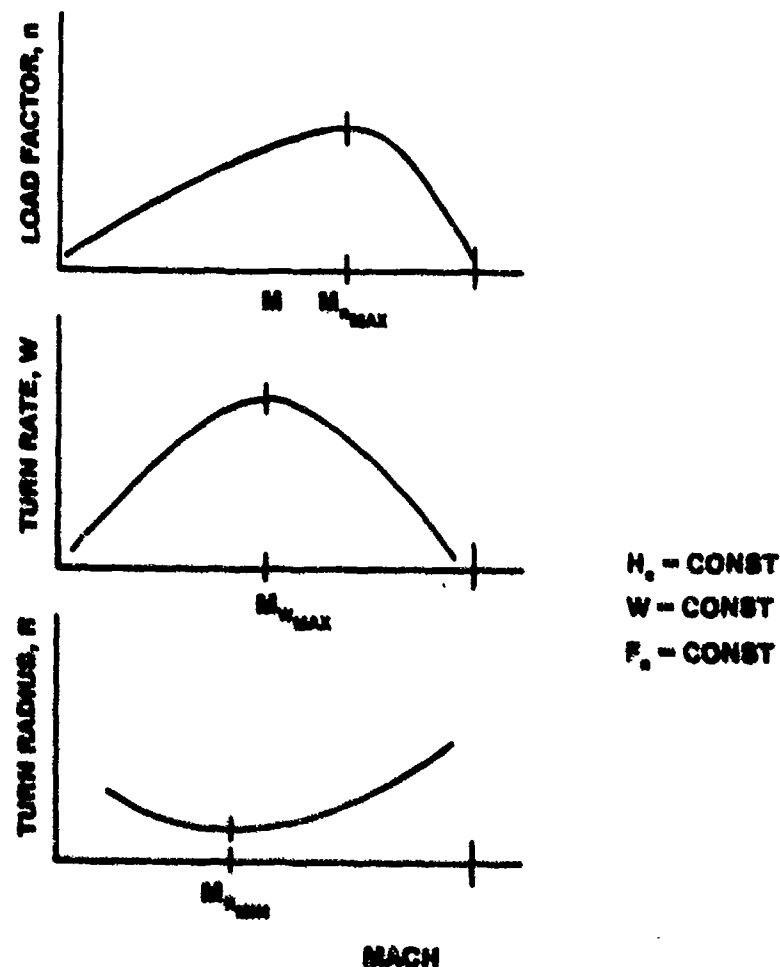


FIGURE 10.7. SUSTAINED TURN PERFORMANCE RESULTS

These curves are normally presented in technical performance reports to more accurately define an aircraft's turning performance. Charts of the type presented in Figure 10.5 are more useful to operational analysts to study combat performance.

10.8 THRUST AND DRAG ANALYSIS IN A TURN

For a sustained turn, thrust equals drag. Thrust is normally fixed at either military or maximum power, but does vary according to the relationship

$$\frac{F_n}{\epsilon} = f(M, N/\sqrt{\theta})$$

As was previously stated, the drag increase in a sustained turn is strictly induced drag due to the increase in lift required to sustain level flight. Therefore, we can write

$$\Delta D = \Delta D_p + \Delta D_i$$

but

$$\Delta D_p = 0$$

and

$$\Delta D_i = \Delta C_{D_i} qS$$

also

$$\Delta C_{D_i} = \frac{(\Delta C_L)^2}{\pi AR e}$$

or

$$\Delta C_{D_i} = K (\Delta C_L)^2$$

where

$$K = \frac{1}{\pi AR e}$$

For a given weight

$$\frac{\Delta L}{W} = \Delta n = \frac{\Delta C_L qS}{W}$$

Therefore

$$\Delta C_L = \frac{\Delta n W}{qS}$$

Recalling that

$$\Delta D_1 = \Delta C_{D_1} qS$$

and that

$$\Delta C_{D_1} = K(\Delta C_L)^2$$

$$\Delta C_{D_1} = K \left(\frac{\Delta nW}{qS} \right)^2$$

$$\Delta D_1 = K \left(\frac{\Delta nW}{qS} \right)^2 qS$$

or

$$\Delta D_1 = \frac{K}{S} \frac{(\Delta nW)^2}{q}$$

But q can be written

$$q = 1481 \delta M^2$$

Therefore

$$\Delta D_1 = \frac{K}{1481 S} \frac{1}{\delta} \left(\frac{\Delta nW}{M} \right)^2$$

or

$$\Delta D_1 = \frac{K_1}{\delta} \left(\frac{\Delta nW}{M} \right)^2$$

where

$$K_1 = \frac{K}{1481 S}$$

Dividing both sides of this equation by δ yields

$$\boxed{\frac{\Delta D_1}{\delta} = K_1 \left(\frac{\Delta nW}{\delta M} \right)^2}$$

(10.8)

Equation 10.8 is helpful in analyzing the independent variables that control induced drag in a sustained level turn and contains parameters which can be measured directly in flight tests.

10.9 TURNING PERFORMANCE TESTS

Turning performance of an aircraft is usually obtained by one of two general methods. These two methods are:

1. Stabilized turn method
2. Level acceleration method

10.9.1 Stabilized Turn Method

The stabilized turn test is usually performed at several different altitudes with a series of turns flown at each altitude. If airspeed and altitude are constant during the maneuver, then $P_g = 0$. The stabilized turn test is good for hand-held data acquisition and is usually performed to spot check values that have been determined from the level acceleration test.

Three techniques are used to obtain the stabilized turn data, as illustrated in Figure 10.8.

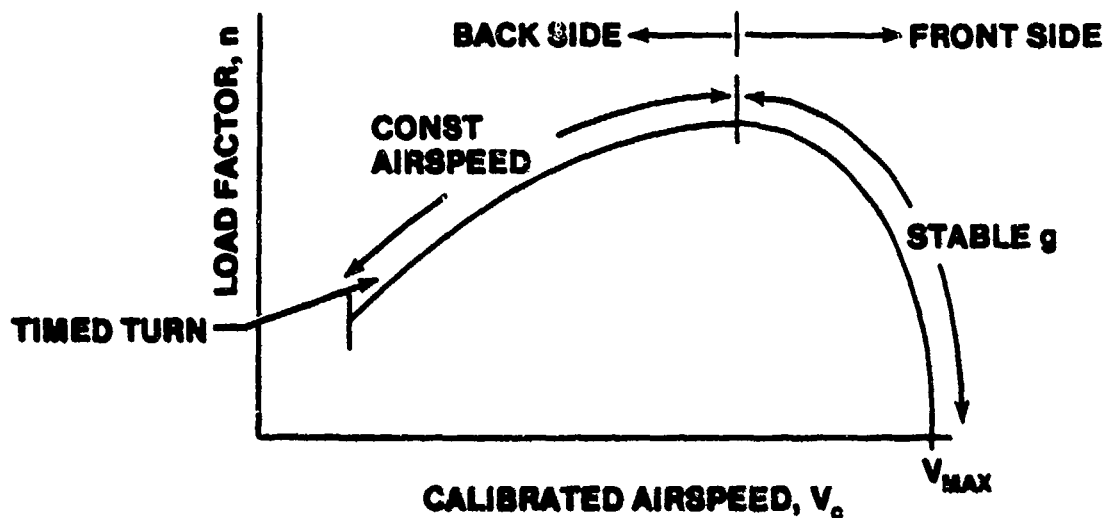


FIGURE 10.8. STABILIZED TURN TEST METHOD

The general method of performing the stabilized turning performance test is to fly the test aircraft in a level turn at either MIL or MAX power at constant airspeed, altitude, and load factor. The aircraft instrumentation accuracy, data reduction capability, and the test aircraft itself will determine the most important parameter for the test pilot to maintain constant. If the aircraft load factor can be measured accurately, then this is the parameter that should be held constant.

10.9.1.1 Stable g Method. The stable g method is flown by holding an aim load factor for approximately ten seconds. Load factor (n) and velocity should be recorded. Knowing n and V allows computation of rate of turn (ω) and radius of turn (R).

10.9.1.2 Constant Airspeed Method. The constant airspeed method is flown by holding an aim airspeed and recording the resulting load factor. Normally, conditions need only be held constant for approximately ten seconds at the higher load factors and through 360° of turn at the lower load factors ($n < 2$).

10.9.1.3 Timed Turn Method. The timed turn method is normally used at low airspeeds and for $n < 2$. It is also used if a coarse or inaccurate method of

measuring load factor is available. For a timed turn maneuver, the bank angle (ϕ) or the velocity is held constant, and the turn is maintained through 360° (2π radians) from which

$$\omega = \frac{2\pi}{\Delta t} \quad (10.9)$$

Since ω is known, n and R can be calculated.

10.9.2 Level Acceleration Method

Generally speaking, the level acceleration test is the best data source for turn performance. This method is most commonly used if the aircraft has a good instrumentation system. An additional benefit from the level acceleration test is the fact that level acceleration and turn performance can be determined concurrently. The method is, however, dependent on good thrust curves and good drag polars being available.

The determination of turning performance through a level acceleration test first requires calculation of energy height from the relationship

$$E_s = H + \frac{V^2}{2g} \quad (10.10)$$

Differentiating E_s with respect to time yields

$$\dot{E}_s = \frac{dE_s}{dt} = \frac{dH}{dt} + \frac{V}{g} \frac{dV}{dt} \quad (10.11)$$

which you will recall is the definition of specific excess power, P_s .

Since the level acceleration is performed at a constant altitude

$$\frac{dH}{dt} = 0$$

The aircraft is accelerating. Therefore,

$$F_{ex} = F_n - D = ma_x$$

but

$$a_x = \frac{dV}{dt} = \frac{\dot{E}_s g}{V}$$

from Equation 10.11. Therefore,

$$\begin{aligned} F_{ex} &= \frac{W}{g} a_x \\ &= \frac{W}{g} \frac{\dot{E}_s g}{V} \end{aligned}$$

or

$$F_{ex} = \frac{W}{V} \dot{E}_s \quad (10.12)$$

Computers are normally utilized to determine \dot{E}_s . However, if a computerized data reduction system is not available, \dot{E}_s can be determined graphically. E_s and V can be plotted as functions of time for the duration of the level acceleration test run as shown in Figure 10.9.

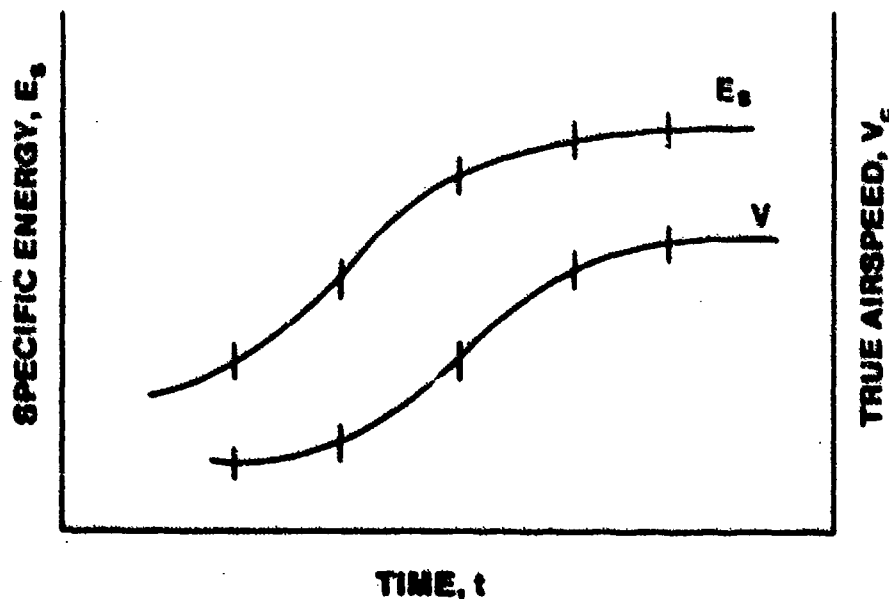


FIGURE 10.9. GRAPHICAL DETERMINATION OF \dot{E}_s

For each Δt , the slope of the curve $\Delta E_s / \Delta t$ or E_s can be determined. Similarly, $\Delta V / \Delta t = \dot{V} = a_x$. Excess thrust for a given velocity is then readily determined from

$$F_{ex_v} = \frac{\dot{W}_{E_s} \text{ at } t = \text{constant}}{V \text{ at } t = \text{constant}}$$

and can be normalized by dividing by the pressure ratio, δ .

Since the test must be performed at several altitudes, F_{ex} / δ must be plotted as a function of Mach for each altitude as shown in Figure 10.10.

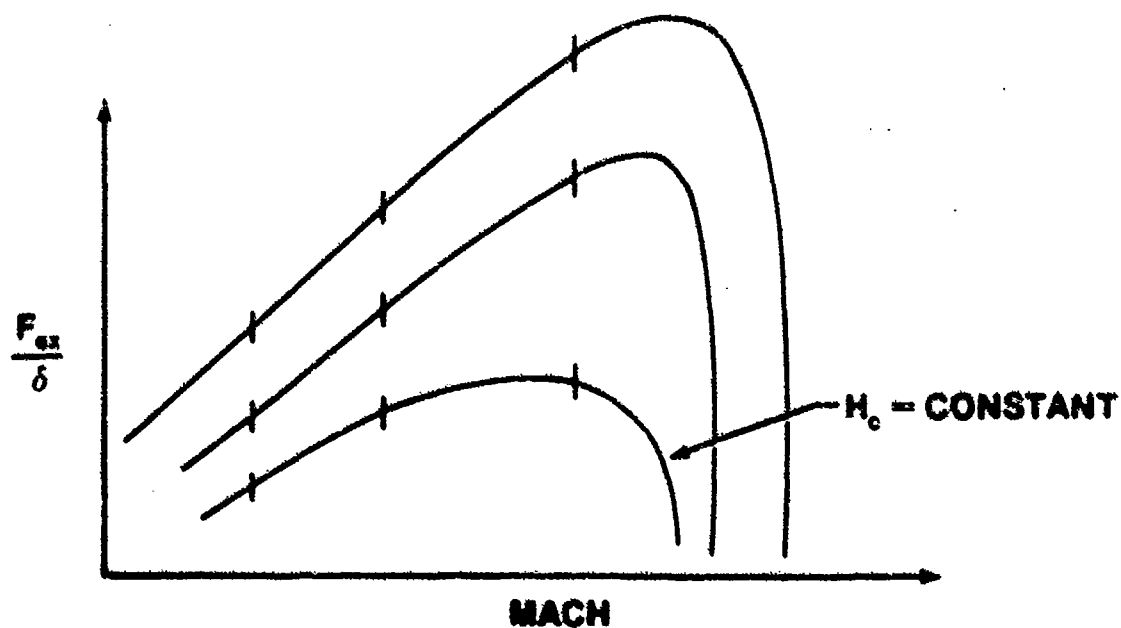


FIGURE 10.10. NORMALIZED EXCESS THRUST VS MACH

From Figure 10.10 and Equation 10.8, F_{ex} / A can be plotted as a function of $(nW / \dot{W})^2$ at a given Mach and at $n = 1$ as shown in Figure 10.11.

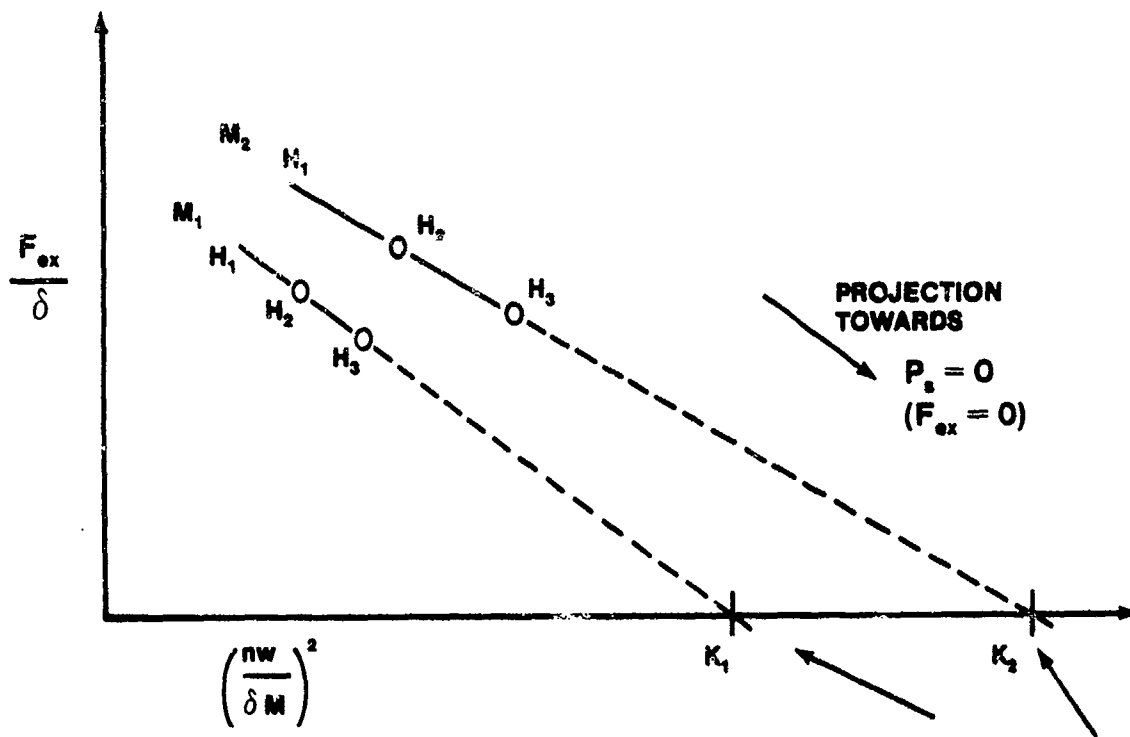


FIGURE 10.11. EXCESS THRUST EXTRAPOLATION

Lines of constant Mach should appear in Figure 10.11 as straight lines and can be extrapolated to zero thrust. The point at which zero excess thrust is reached is the point of maximum sustained load factor in a turn ($P_s = 0$). Load factor can be calculated once the value of K is known.

$$K_1 = \left(\frac{n_1 W}{\delta M_1} \right)^2 \quad (10.13)$$

for each gross weight and each altitude. The sustained load factor calculated can then be plotted as a function of Mach as shown in Figure 10.12.

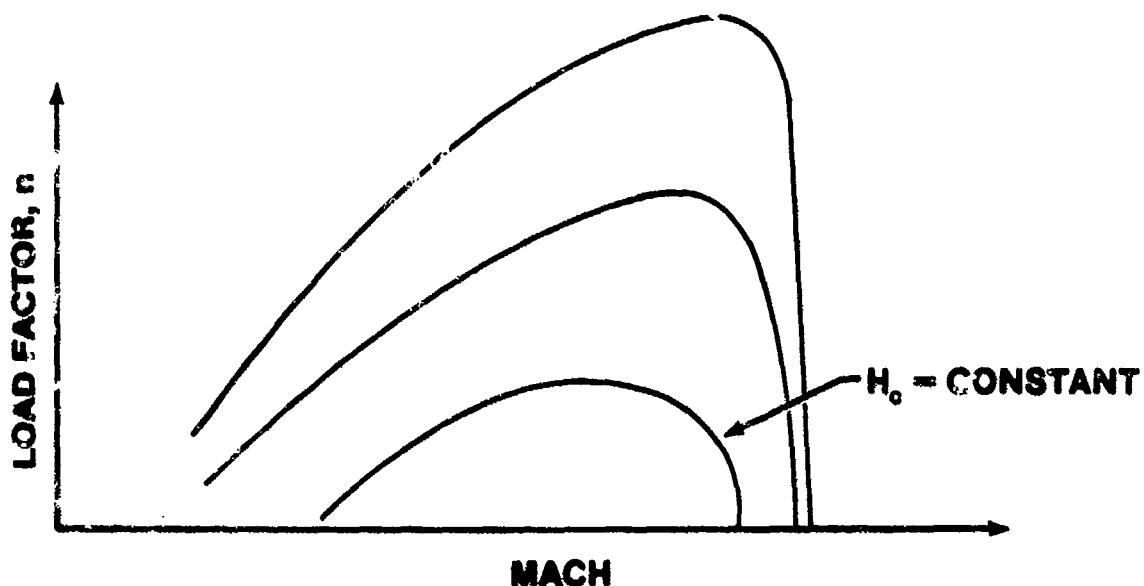


FIGURE 10.12. SUSTAINED g VS MACH

Turn rate (ω) and turn radius (R) can be obtained from Equations 10.5 and 10.6.

Two limitations of the level acceleration method are:

1. The thrust component due to angle of attack is not accounted for.
2. Engine lag characteristics during acceleration are unaccounted for.

The net result of these limitations is that the values for sustained load factor will be slightly lower using the level acceleration method than the stabilized turn method.

PROBLEMS

10.1 a. Generate a set of force equations to evaluate level turn performance.

b. Generate a general equation for vertical turn radius and a general equation for turn rate. Sketch a constant velocity, constant "g" loop.

10.2 Find the load factor, bank angle, and turn radius for an aircraft in a level turn at a true airspeed of 120 kts and a turn rate of 3 deg/s.

10.3 a. Show that for vertical turns (e.g., pullout and loop) the turn radius at any point in the turn is given by:

$$R = \frac{v^2}{g (n - \cos \theta)}$$

where θ is an angle measured from the upward vertical direction to the lift vector.

b. Discuss, in terms of load factor and speed, how a pilot can fly a "perfect" loop; that is, a vertical 360° turn of constant radius.

c. For an airplane flying at 150 m/s, which is capable of "pulling" 7.33 g's, find the radius of turn at:

1. The bottom of a pullout.
2. The top of a loop.

10.4 The quickest, tightest turn occurs at the combination of low speed and high load factor called the maneuver point. At the maneuver point:

$$n = n_{\max} \quad \text{and} \quad v = v_s = \sqrt{\frac{2 n_{\max} W}{\rho C_{L_{\max}} S}}$$

by using the following data for a T-38 at sea level:

$$\begin{aligned} n_{\max} &= 7.33 & C_D &= 0.015 + 0.220 C_L^2 \\ C_{L_{\max}} & \text{(based on buffet limit)} = 0.65 & W/S &= 2500 \text{ N/m}^2 \end{aligned}$$

- Calculate V at the maneuver point.
- Find the (instantaneous) minimum radius of turn.
- Find the (instantaneous) maximum rate of turn.
- Find the ratio L/D in a turn at the maneuver point.

10.5 The following information is provided for a non-afterburning fighter at sea level, static, standard day conditions. Answer the questions below.

$$\begin{aligned} n_{\max} &= 7.33 & T/W &= 0.40 \\ K &= 0.12 & W/S &= 60 \text{ lbf/ft}^2 \\ C_{L_{\max}} &= 1.12 & C_{D_0} &= .015 \end{aligned}$$

- Calculate the corner velocity.
- Find the minimum instantaneous radius of turn for a level turn.
- Find the maximum instantaneous rate of turn for a level turn.
- What is the aircraft's L/D in this corner velocity turn?
- Does this aircraft have sufficient thrust to sustain this turn at corner velocity? (Assume α small.)
- Calculate the maximum load factor that the aircraft can sustain and the velocity at which this occurs for minimum sustained turn radius.
- Find the minimum sustained radius of turn and velocity at which this occurs.
- Find the maximum sustained rate of turn and velocity at which it occurs.

10.6 For an aircraft in level turning flight, derive the equations of motion accounting for variation of thrust with angle of attack. From these equations, develop an expression for C_L .

ANSWERS

- 10.3 c. 1.) $R = 362 \text{ m}$
2.) $R = 275 \text{ m}$

- 10.4 a. $V = 215 \text{ m/s}$
b. $R = 640 \text{ m}$
c. $\omega = .334 \text{ rad/sec}$
d. $L/D = 6.02$

- 10.5 a. 574 ft/sec
b. $1,409 \text{ ft}$
c. $.41 \text{ rad/sec}$
d. 6.77
e. No
f. $n = 2.71$; $V = 349 \text{ ft/sec}$
g. $R_{\min} = 1,502 \text{ ft}$; $V = 349 \text{ ft/sec}$
h. $\omega = .232 \text{ rad/sec}$; $V = 349 \text{ ft/sec}$

CHAPTER 11
CRUISE PERFORMANCE THEORY

11.1 CRUISE PERFORMANCE THEORY

This chapter examines the theory and flight tests required to determine cruise data presented in aircraft flight manuals. Aircraft performance is dependent upon the combination of airplane aerodynamics and engine characteristics. Basic aerodynamic and engine theory applied to flight testing are covered. Aerodynamic forces acting on the aircraft, i.e., lift and drag, and engine parameters are presented as functions of easily measured parameters. Engine and aerodynamic functions are then combined to complete the analysis. The end result provides a method by which engine and airplane performance characteristics may be determined with minimum flight testing. The data obtained from the flight tests are used to determine cruise data (nautical air miles per pound, endurance, range, etc.) presented in the flight manual.

Only those aircraft and engine characteristics which pertain to level, unaccelerated flight will be investigated. By definition, the aircraft is in level, unaccelerated flight when the sum of the forces acting upon it equal zero. Therefore, the lift force (L) is equal to the aircraft weight (W), and the net thrust (F_n) is equal to the aircraft drag (D) (Figure 11.1).

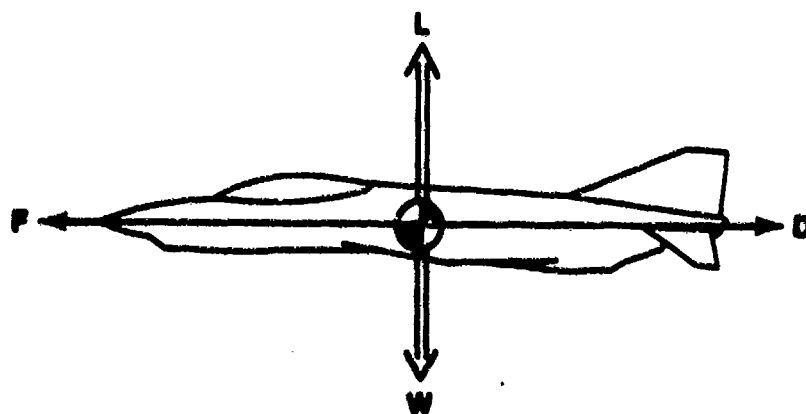


FIGURE 11.1. STEADY STATE FLIGHT

11.2 LIFT AND DRAG FUNCTIONAL RELATIONSHIPS

Functional relationships are used to combine the aircraft's aerodynamic characteristics with the engine's performance. The equations of lift and drag are used to develop these functional relationships. These (in conjunction with flight test data and engine thrust curves) are used to plot drag polars.

From aerodynamic theory lift can be written as

$$L = \frac{\rho_a v^2 S C_L}{2} \quad (11.1)$$

In steady state flight, lift equals weight, therefore

$$L = W = \frac{\rho_a v^2 S C_L}{2} \quad (11.2)$$

From aerodynamic theory

$$M = \frac{v}{a}$$

Therefore

$$v^2 = M^2 a^2 \quad (11.3)$$

Using the Perfect Gas law

$$(P_a = g \rho_a RT)$$

we know

$$\frac{P_a}{\rho_a} = g RT \quad (11.4)$$

Substituting Equation 11.4 into the definition of speed of sound

we obtain

$$a = \sqrt{g RT} = \sqrt{\frac{P_a}{\rho_a}} \quad (11.5)$$

or

$$a^2 = \gamma \frac{P_a}{\rho_a} \quad (11.6)$$

Now Equation 11.3 becomes

$$V^2 = M^2 a^2 = M^2 \gamma \frac{P_a}{\rho_a} \quad (11.7)$$

Substituting this result into Equation 11.2 we obtain

$$W = \frac{\rho_a V^2 S C_L}{2} = \frac{\rho_a S C_L}{2} \left(M^2 \gamma \frac{P_a}{\rho_a} \right)$$
$$W = \frac{S C_L M^2 \gamma P_a}{2} \quad (11.8)$$

Multiplying Equation 11.8 by P_0/P_0 , we obtain

$$W = \frac{S C_L M^2 \gamma P_a P_0}{2 P_0} \quad (11.9)$$

From aerodynamics $\delta = P_a/P_0$; therefore, Equation 11.9 becomes

$$W = \frac{S C_L M^2 \gamma \delta P_0}{2} \quad (11.10)$$

Solving Equation 11.10 for the lift coefficient

$$C_L = \frac{2W}{\gamma \delta P_0 M^2 S} = \frac{2 \left(\frac{W}{\delta} \right)}{\gamma P_0 M^2 S}$$

For a given aircraft and standard sea level conditions, γ , P_0 , and S are constants.

Therefore

$$C_L = \frac{\left(\frac{W}{\delta}\right)}{1481 M^2 S} \quad (11.11)$$

This shows that

$$C_L = f\left(\frac{W}{\delta}, M\right) \quad (11.12)$$

Stabilized points can be flown at different values of W/δ and M to determine lift coefficients.

From aerodynamic theory drag can be written as

$$D = \frac{\rho_a V^2 S C_D}{2} \quad (11.13)$$

By analyzing this equation as we did the lift equation, we obtain

$$C_D = \frac{\frac{D}{\delta}}{1481 M^2 S} \quad (11.14)$$

From the level flight assumption, thrust equals drag.

Therefore

$$\frac{D}{\delta} = \frac{F_n}{\delta} \quad (11.15)$$

and

$$C_D = \frac{F_n / \delta}{1481 M^2 S} \quad (11.16)$$

Equation 11.16 coupled with engine thrust curves and flight test data from stable points, is used to compute drag coefficients. The coefficients of lift and drag from Equations 11.11 and 11.16 are plotted to construct the drag polar as shown in Figure 11.2. This drag polar represents the aerodynamic characteristics of an aircraft and is extensively used to develop performance data presented in a flight manual.

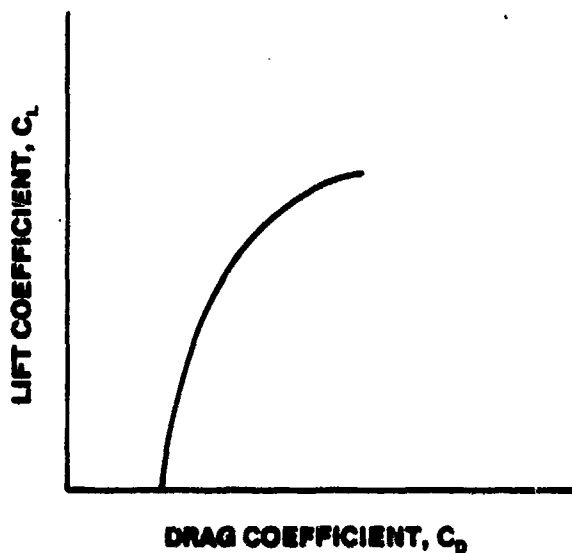


FIGURE 11.2. DRAG POLAR

Equation 11.14 can be rewritten

$$\frac{D}{\delta} = f(C_D, M) \quad (11.17)$$

The total drag coefficient (C_D) is the sum of the parasite (C_{D_p}), induced (C_{D_i}), and Mach (C_{D_M}) drag coefficients. Mach drag will not be considered. Therefore,

$$C_D = C_{D_p} + C_{D_i} \quad (11.18)$$

The parasite drag coefficient is constant for a given aircraft configuration. The induced drag coefficient was defined in aerodynamic theory as

$$C_{D_i} = \frac{C_L^2}{\pi AR e} \quad (11.19)$$

For a given aircraft, AR and e are constants. Therefore

$$C_{D_i} = f(C_L) \quad (11.20)$$

and,

$$C_D = C_{D_p} + C_{D_i} = f(C_L) \quad (11.21)$$

Substituting $C_L = f\left(\frac{W}{\delta}, M\right)$ from Equation 11.12 into Equation 11.21

$$C_D = f\left(\frac{W}{\delta}, M\right) \quad (11.22)$$

From Equations 11.16 and 11.22

$$\frac{D}{\delta} = \frac{F_n}{\delta} = f\left(\frac{W}{\delta}, M\right) \quad (11.23)$$

11.3 ENGINE PARAMETER FUNCTIONAL RELATIONSHIPS

Relationships for engine parameters can be developed using the Buckingham π technique of dimensional analysis.

From an analysis of the variables which affect thrust, we can write

$$F_n = f(V, T, P, N, D, \mu, \eta_I, \eta_C, \eta_B, \eta_t, \eta_n)$$

Since the component efficiencies are primarily functions of V, T, P, N , and D , and μ is primarily a function of T and P , we can simplify the above equation and express thrust as a function of its prime variables

$$F_n = f(V, T, P, N, D)$$

Since this relationship consists of six variables, and since we have three fundamental units, Buckingham's π theorem states that we can express these variables in terms of three dimensionless numbers.

We are primarily interested in two of these possible dimensionless numbers, i.e., the corrected thrust parameter and the corrected fuel flow parameter, although both are related to $N/\sqrt{\theta}$, the corrected RPM parameter. The functional relationship for the corrected thrust parameter is

$$\frac{F_n}{\delta} = f\left(\frac{N}{\sqrt{\theta}}, M\right) \quad (11.24)$$

This functional relationship states that the corrected thrust parameter (F_n/δ) is a function of the Mach and the corrected RPM parameter ($N/\sqrt{\theta}$).

Similarly, the functional relationship for the corrected fuel flow is

$$\frac{\dot{W}_f}{\delta \sqrt{\theta}} = f \left(\frac{N}{\sqrt{\theta}}, M \right) \quad (11.25)$$

11.4 ENGINE THRUST CURVES

Accurate thrust data can be obtained by flight testing an aircraft and measuring the thrust at various airspeeds, altitudes, and temperatures. This thrust data is desirable, but aircraft engines frequently are not adequately instrumented to provide all the engine parameters necessary to obtain thrust. The ground static test is a cheaper and more frequently used method to obtain thrust data. Figure 11.3 is a plot of net thrust versus Mach for an engine at 100% RPM.

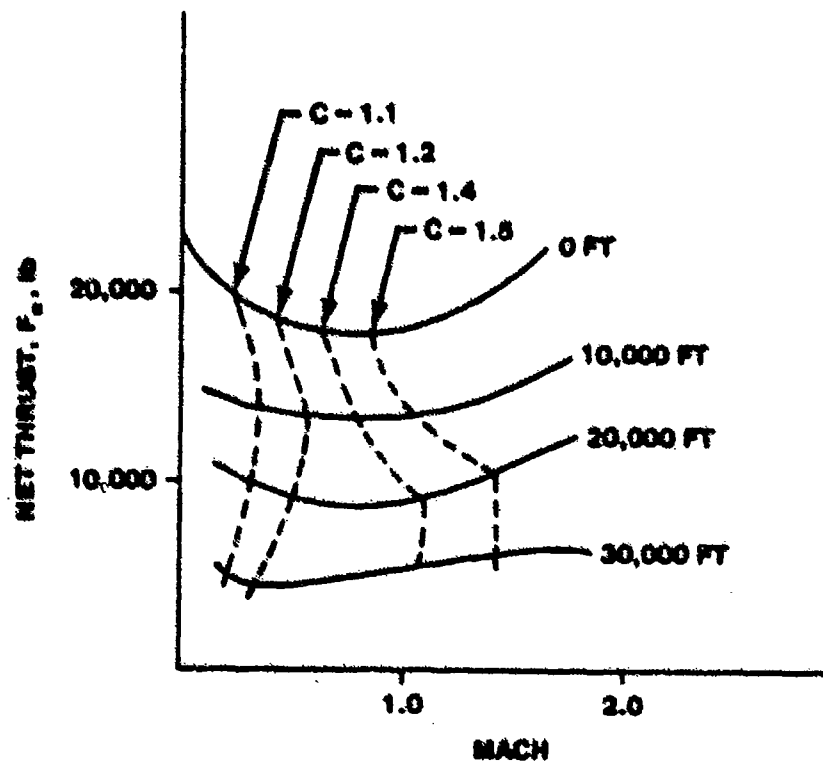


FIGURE 11.3. ENGINE THRUST CURVE, 100% RPM

The dotted lines represent specific fuel consumption (C); the solid lines represent altitude. Figure 11.4 is a plot of net thrust versus Mach for the same engine at 95% RPM.

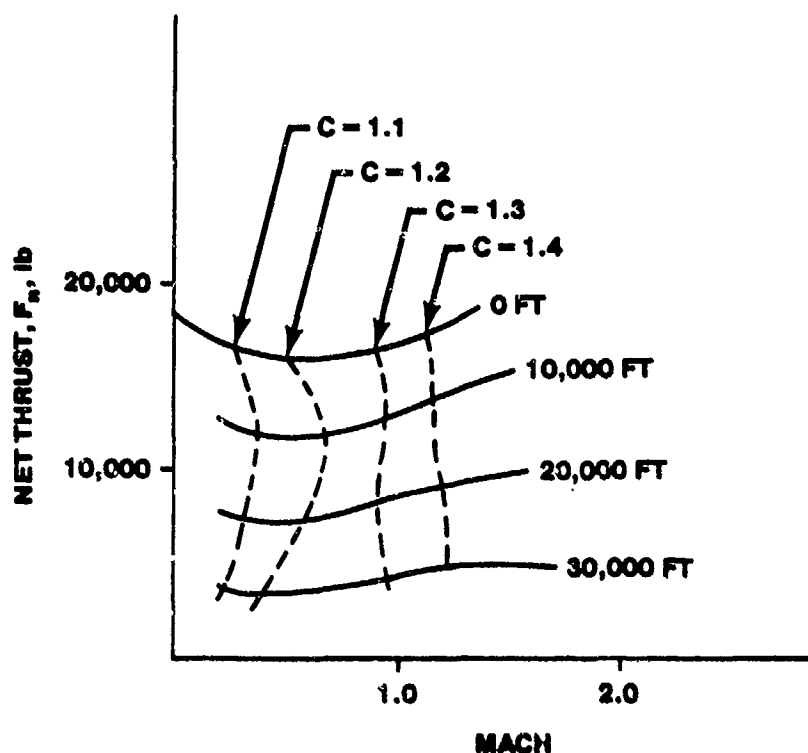


FIGURE 11.4. ENGINE THRUST CURVE, 95% RPM

Note the thrust variations between the 100% and 95% RPM plots. Many plots similar to Figure 11.3 and 11.4 are necessary to completely describe the thrust characteristics of the engine throughout the Mach and altitude range required. Data can be crossplotted to obtain Figure 11.5, which is a plot of engine thrust at all altitudes and Mach.

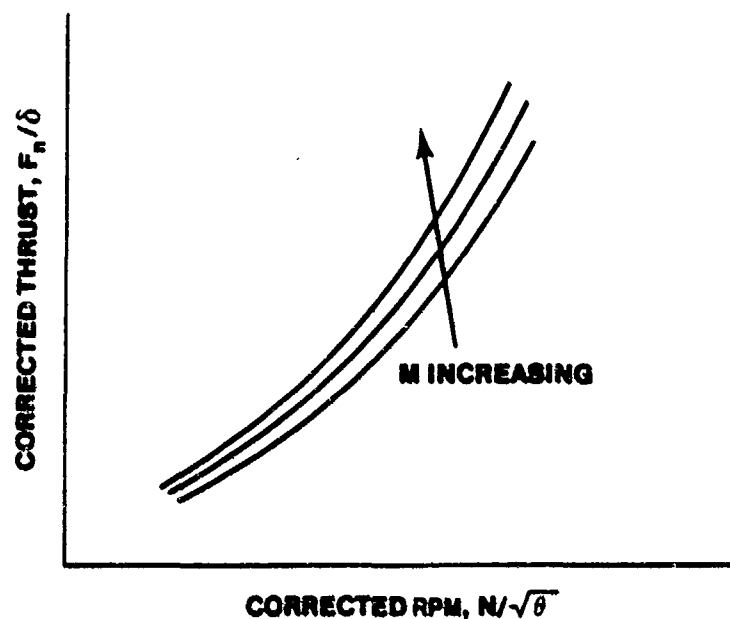


FIGURE 11.5. ENGINE THRUST CURVE

Note that these data are presented in the form of the functional relationship developed earlier

$$\frac{F_n}{\delta} = f\left(\frac{N}{\sqrt{\theta}}, M\right) \quad (11.24)$$

The engine manufacturer normally supplies this thrust curve, presented as the engine-airframe thrust deck.

11.5 ENGINE-AIRPLANE FUNCTIONAL COMBINATIONS

In previous paragraphs the following aircraft and engine performance relationships were shown.

$$\frac{D}{\delta} = f\left(\frac{W}{\delta}, M\right) \quad (11.23)$$

$$\frac{F_n}{\delta} = f\left(\frac{N}{\sqrt{\theta}}, M\right) \quad (11.24)$$

$$\frac{\dot{W}_F}{S \sqrt{\theta}} = f\left(\frac{N}{\sqrt{\theta}}, M\right) \quad (11.25)$$

In this paragraph these relationships will be combined. The thrust curves in conjunction with the drag polar are used to determine all the aircraft's performance characteristics.

In steady flight, thrust equals drag. Therefore Equation 11.24 can be written

$$\frac{D}{\delta} = f\left(\frac{N}{\sqrt{\theta}}, M\right)$$

Substituting this result for D/δ into Equation 11.23, we obtain

$$f\left(\frac{N}{\sqrt{\theta}}, M\right) = f\left(\frac{W}{\delta}, M\right)$$

A further reduction produces

$$M = f\left(\frac{W}{\delta}, \frac{N}{\sqrt{\theta}}\right) \quad (11.26)$$

This functional relationship is extremely important and leads directly to a manner in which we can flight test an aircraft to obtain performance data used in the flight manual. It is the basis for the "Speed Power Flight Test."

Flight test personnel have learned from experience that the easiest and the most accurate method to solve this functional relationship is to fly a constant W/δ and vary M and $N/\sqrt{\theta}$. The test pilot preplans what pressure altitude (δ) he should fly for each fuel weight in order to maintain a constant W/δ . While flying a constant W/δ profile and stabilizing at various Mach, the test pilot records airspeed (V_1), RPM (N), temperature (T_1), altitude (H_1), fuel quantity at start of time interval, fuel quantity at end of time interval, and the time interval. Data obtained in this flight test can be plotted in many different forms. Flight test data obtained from speed power tests is directly used to plot the functional relationship given in Equation 11.23 as shown in Figure 11.6

$$\frac{F_N}{\delta} = f\left(\frac{W}{\delta}, M\right)$$

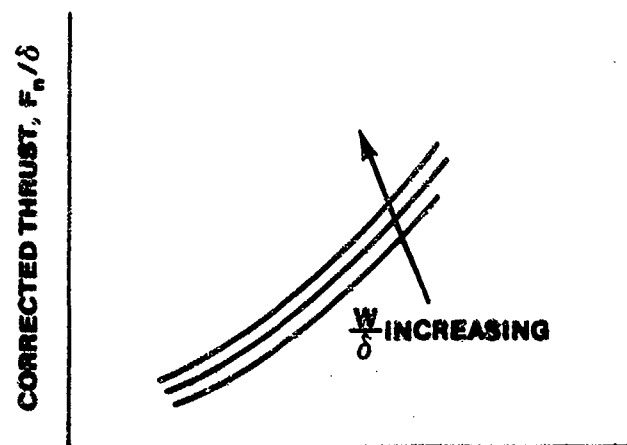


FIGURE 11.6. CORRECTED THRUST

Substituting $M = f\left(\frac{W}{\delta}, \frac{N}{\sqrt{\theta}}\right)$ into Equation 11.25 we obtain

$$\frac{\dot{w}_f}{\delta \sqrt{\theta}} = f\left(\frac{N}{\sqrt{\theta}}, \frac{W}{\delta}\right) \quad (11.27)$$

Flight test data obtained from speed power tests are directly used to plot this functional relationship as shown in Figure 11.7. Parts (a) and (b) of Figure 11.7 are for different engines/airframe combinations; thus they are considerably different.

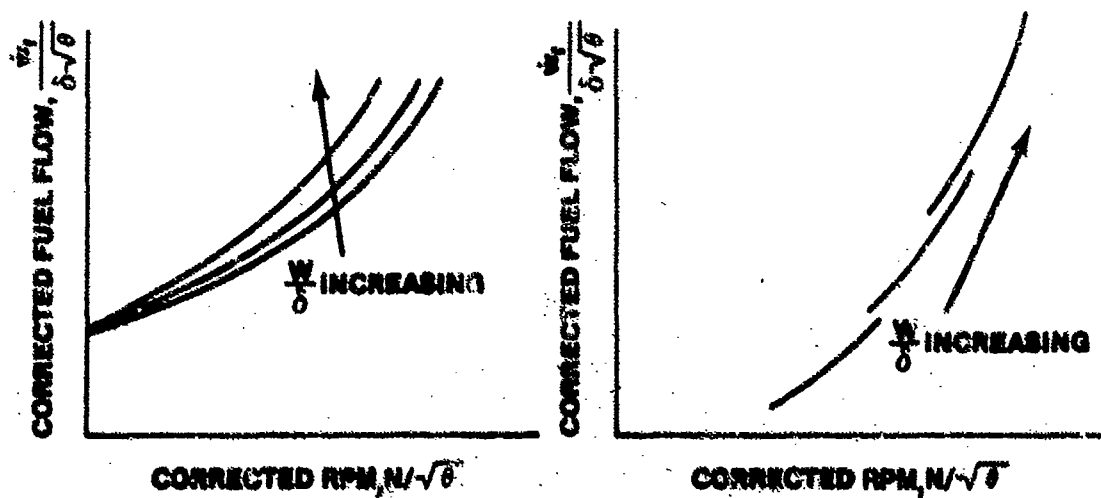


FIGURE 11.7. CORRECTED FUEL FLOW

11.6 ENDURANCE, JET AIRCRAFT

Endurance (E) is defined as as

$$E = \int dt \quad (11.28)$$

Fuel flow (\dot{w}_f) can be defined as the time rate of change of aircraft gross weight

$$\dot{w}_f = - \frac{dW}{dt} \frac{lb}{hr} \quad (11.29)$$

The negative sign indicates the gross weight decreases with time.

Turbojet specific fuel consumption (C) is defined as

$$C = \frac{\dot{w}_f}{F_n}$$

Therefore

$$\dot{w}_f = CF_n \quad (11.30)$$

Substituting Equation 11.29 into Equation 11.30 for \dot{w}_f

$$- \frac{dW}{dt} = CF_n$$

and

$$dt = - \frac{dW}{CF_n} \quad (11.31)$$

Substituting Equation 11.31 into Equation 11.28 for dt yields

$$E = - \int \frac{dW}{CF_n}$$

Multiplying by $\frac{W}{W}$

$$E = - \int \frac{dW}{CF_n} \frac{W}{W}$$

Integrating from an initial gross weight (W_i) to a final gross weight (W_f)

$$E = - \int_{W_i}^{W_f} \frac{dW}{CF_n} \frac{W}{W} \quad 11.12$$

Reversing the limits of integration to change the sign yields

$$E = \int_{W_f}^{W_i} \frac{dW}{C_F} \frac{W}{W}$$

In stabilized level flight $F_n = D$ and $L = W$. Therefore

$$E = \int_{W_f}^{W_i} \frac{dW}{C_D} \left(\frac{W}{W} \right) = \int_{W_f}^{W_i} \frac{1}{C} \left(\frac{L}{D} \right) \frac{dW}{W}$$

Assuming $\frac{L}{D}$ and specific fuel consumption are constant

$$E = \left(\frac{1}{C} \right) \left(\frac{L}{D} \right) \ln \frac{W_i}{W_f} = \left(\frac{1}{C} \right) \left(\frac{C_L}{C_D} \right) \ln \frac{W_i}{W_f} \quad (11.32)$$

Equation 11.32 illustrates that in order to obtain maximum endurance at a particular altitude, the jet powered aircraft must fly at a speed where C_L/C_D is maximum. The drag coefficient equation must be examined to determine where this speed occurs.

$$C_D = C_{D_p} + \frac{C_L^2}{\pi AR e} \quad (11.18)$$

Replacing $\frac{1}{\pi AR e}$ by the constant K

$$C_D = C_{D_p} + K C_L^2$$

Dividing both sides of the equation by C_L yields

$$\frac{C_D}{C_L} = \frac{C_{D_p} + K C_L^2}{C_L}$$

Differentiating with respect to C_L and equating the result to zero

$$\frac{d \left(\frac{C_{D_p} + K C_L^2}{C_L} \right)}{d C_L} = \frac{2K C_L^2 - (C_{D_p} + K C_L^2)}{C_L^2}$$

$$2K C_L^2 - C_{D_p} - K C_L^2 = 0$$

$$K C_L^2 = C_{D_p}$$

$$C_{D_i} = C_{D_p} \quad (11.33)$$

The second derivative of C_D/C_L with respect to C_L is positive; therefore, C_D/C_L is a minimum when $C_{D_i} = C_{D_p}$. Therefore C_L/C_D maximum occurs where induced drag equal parasite drag. From Equations 11.32 and 11.33 is apparent that maximum endurance can be obtained by flying at a speed where C_L/C_D or L/D is maximum. This is shown in Figure 11.8.

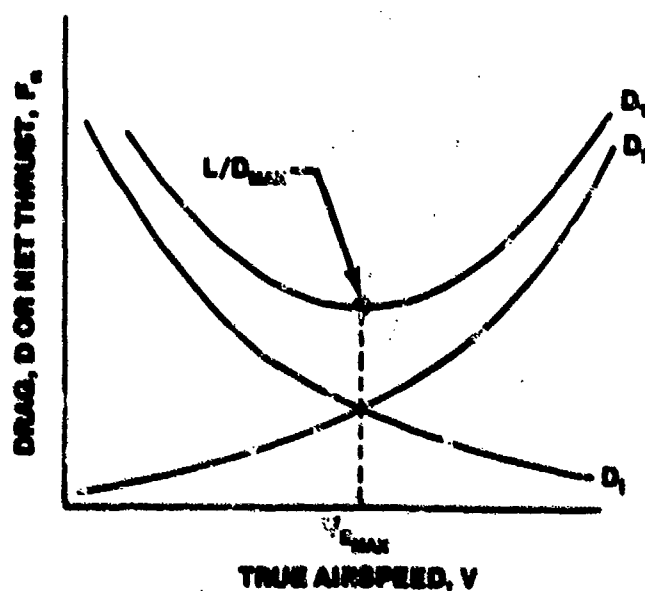


FIGURE 11.8. THRUST REQUIRED

Equation 11.32 may indicate that a jet powered aircraft could loiter equally well at all altitudes, provided the engine and intake duct efficiency did not change with altitude and C remained constant.

In practice, this is not a true statement, because specific fuel consumption is dependent on thrust developed, internal component efficiencies, free air temperature, true airspeed, and ambient air pressure and may change appreciably with increased altitude. Because higher engine speeds are required to maintain a true airspeed commensurate with the minimum drag point and engine efficiency improves with an increase in RPM, endurance should increase with an increase in altitude.

11.7 RANGE, JET AIRCRAFT

Range is defined as

$$R = \int dS = \int V dt \quad (11.34)$$

Substituting Equation 11.31 for dt into Equation 11.34

$$dt = \frac{dW}{CF_n} \quad (11.31)$$

$$R = - \int V \frac{dW}{CF_n}$$

Multiply by $\frac{W}{W}$

$$R = - \int V \frac{dW}{W} \frac{W}{CF_n}$$

For steady state $L = W$, $F_n = D$

$$R = - \int V \frac{1}{C} \frac{L}{D} \frac{dW}{W}$$

If we integrate from final to initial

$$R = \int_{W_f}^{W_i} \frac{1}{C} V \frac{L}{D} \frac{dW}{W} \quad (11.35)$$

This is the general range equation. In order to maximize range from Equation 11.35, we must maximize VL/D , minimize specific fuel consumption, and have a large fuel fraction W_i/W_f .

From aerodynamic theory

$$L = C_L \frac{\rho_a V^2}{2} S$$

or

$$V = \sqrt{\frac{2L}{\rho_a C_L S}}$$

For steady state flight, $L = W$

$$V = \sqrt{\frac{2W}{\rho_a C_L S}}$$

Substituting this result for V into Equation 11.35,

$$\begin{aligned} R &= \int_{W_f}^{W_i} \left(\frac{2W}{\rho_a C_L S} \right)^{1/2} \frac{1}{C} \frac{L}{D} \frac{dW}{W} \\ &= \int_{W_f}^{W_i} \left(\frac{2W}{\rho_a C_L S} \right)^{1/2} \frac{1}{C} \frac{C_L}{C_D} \frac{dW}{W} \\ &= \int_{W_f}^{W_i} \left(\frac{2}{\rho_a S} \right)^{1/2} \frac{1}{C} \left(\frac{C_L}{C_D} \right)^{1/2} \frac{dW}{W^{1/2}} \end{aligned}$$

Assuming a constant altitude, angle of attack profile, and constant specific fuel consumption,

$$R = \left(\frac{2}{\rho_a S} \right)^{1/2} \frac{1}{C} \frac{C_L^{1/2}}{C_D} \int_{W_f}^{W_i} W^{-1/2} dW$$

so,

$$R = 2 \left(\frac{2}{\rho_a S} \right)^{1/2} \frac{1}{C} \frac{C_L^{1/2}}{C_D} \left[\sqrt{W_i} - \sqrt{W_f} \right] \quad (11.36)$$

Examination of this equation gives the following conclusions for maximum range:

1. The aircraft should be flown at a speed where $C_L^{1/2}/C_D$ is maximum.
2. Increasing altitude (decreasing ρ_a) will increase the range. (This is limited to the optimum cruise altitude.)

The point where $C_L^{1/2}/C_D$ is a maximum should be examined. The drag coefficient is

$$C_D = C_{D_P} + KC_L^2$$

$$\frac{C_L^{1/2}}{C_D} = \frac{C_L^{1/2}}{C_{D_P} + KC_L^2}$$

Differentiating with respect to C_L and equating the result to zero:

$$\frac{d}{dC_L} \left(\frac{C_L^{1/2}}{C_{D_P} + KC_L^2} \right) = \frac{(C_{D_P} + KC_L^2)^{-1/2} C_L^{-1/2} - C_L^{1/2} (2KC_L)}{(C_{D_P} + KC_L^2)^2} = 0$$

$$(C_{D_P} + KC_L^2)^{-1/2} C_L^{-1/2} - 2KC_L^{3/2} = 0$$

$$\frac{1}{2} \frac{C_{D_P}}{C_L^{1/2}} + \frac{1}{2} KC_L^{3/2} - 2KC_L^{3/2} = 0$$

$$\frac{1}{2} \frac{C_{D_P}}{C_L^{1/2}} - \frac{2}{3} K C_L^{3/2} = 0$$

$$\frac{1}{2} \frac{C_{D_P}}{C_L^{1/2}} = \frac{2}{3} K C_L^{3/2}$$

$$C_{D_P} = 3K C_L^2$$

$$C_{D_P} = 3C_{D_i} \quad (11.37)$$

The second derivative of $C_L^{1/2}/C_D$ with respect to C_L is negative. Therefore $C_L^{1/2}/C_D$ is maximum when $C_{D_P} = 3C_{D_i}$.

Cruise flight for maximum range conditions should be conducted so that the maximum number of miles can be flown with the minimum amount of fuel. Specific range (SR) is defined as

$$SR \equiv \frac{dR}{dW} \quad (11.38)$$

Multiplying by $\frac{dt}{dt}$

$$SR = \frac{dR}{dW} \frac{dt}{dt} = \frac{dR/dt}{dW/dt} = \frac{V}{w_f} \text{ (NAMPP)} \quad (11.39)$$

Where NAMPP is defined as nautical air miles per pound.

Figure 11.9 is a classic drag (thrust required) curve with the vertical axis labeled fuel flow as opposed to thrust required.

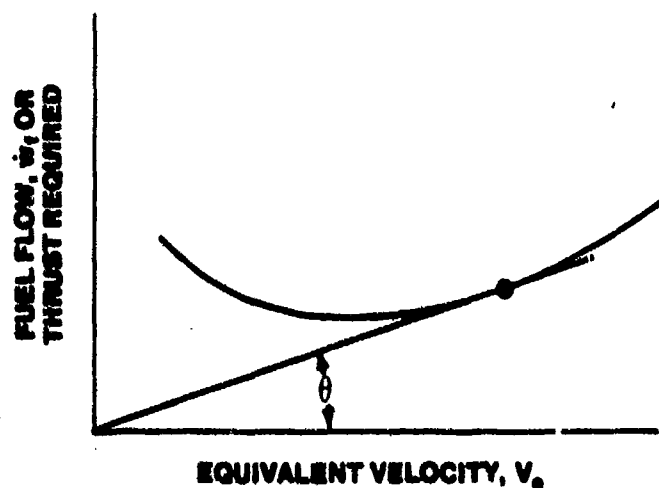


FIGURE 11.9 FUEL FLOW

Since a level flight drag curve is the only place an aircraft operates under cruise conditions, it is apparent that to maximize specific range (SR), the aircraft must be flown at the tangent point of a line from the origin to the drag curve. At this point

$$\begin{aligned}\tan \theta &= \frac{F_{nR}}{V} = \frac{D}{V} \\ &= \frac{1}{2} \rho_0 V_e C_D S\end{aligned}\tag{11.40}$$

Substituting

$$\begin{aligned}V_e &= \left(\frac{2W}{\rho_0 C_L S} \right)^{1/2} \\ \tan \theta &= \left(\frac{\rho_0 W}{2S} \right)^{1/2} \left(\frac{C_D}{C_L^{1/2}} \right) \\ \tan \theta &= K \frac{C_D}{C_L^{1/2}}\end{aligned}\tag{11.41}$$

Flying at this tangent point, minimum θ , results in maximizing specific range (SR), and $C_L^{1/2}/C_D$.

11.8 THE CRUISE CLIMB

It is well known that the specific range of a jet airplane increases with increasing altitude. The reason for this may be seen from an examination of Equation 11.36, which shows that range varies inversely as the square root of the density, so that as long as C , the specific fuel consumption, does not increase markedly, a continuous gain of range is experienced as altitude is gained.

Actually, up to the stratosphere, C tends to decrease for most engines, so that greater gains in range are obtained than would be found if C were assumed constant. Moreover, at low altitudes, inefficient part throttle operation further increases the obtainable C , producing an additional

decrease in range. At high altitudes (above 35,000 to 40,000 ft) C starts to increase so that present test data reveal a "leveling off" in data range for stratospheric conditions. As airplanes fly higher, this leveling off should result in an optimum best range altitude for any given gross weight, above which altitude, decreases in range will be encountered.

Because increases in altitude result in increases in specific range, it may be reasoned that a gradual climb should increase overall range, provided that the climb were made at close to the optimum aerodynamic speed for best range and close to the engine throttle setting for best thrust specific fuel consumption. This thinking leads at once to the concept of the cruise climb.

The cruise climb amounts first to setting the airplane to fly at the optimum range Mach at a given value of W/δ . Then, as fuel is used up and W decreases, allow a gradual climb so that the ratio of W/δ is kept constant as the Mach is also held constant. This amounts to flight at the optimum Mach for the selected W/δ value.

Flight test has established that the cruise climb procedure results in improved range performance over that obtained by flight at constant altitude (varying W/δ and M). A plot of maximum specific range in nautical miles per lb of fuel as a function of gross weight and W/δ is shown in Figure 11.10.

In practice, the cruise climb is accomplished by starting out at some value of W/δ , and establishing the optimum Mach for that W/δ . Given a schedule of weight versus altitude presented in some convenient form, the pilot then climbs the airplane so as to maintain a constant W/δ and M as the gross weight decreases. This means that he flies from Point (1) to (2) of Figure 11.10 with the net range being given by the shaded area of the figure.

In this same figure, flight at constant altitude is illustrated by the dashed line between (1) and (3), with the increase in range of the cruise climb shown as the area bounded by the Lines 1-2, 2-3, 3-1.

We have assumed that the fuel consumption data obtained in level flight will be adequate to describe conditions in the cruise climb even though the cruise climb does not represent level flight conditions. Experiments have demonstrated that this assumption is satisfactory, at least for present day airplanes, for the simple reason that the climb rates are quite small and produce negligible errors. Accordingly, cruise climb fuel consumption

characteristics may legitimately be computed on the basis of data obtained during level flight runs.

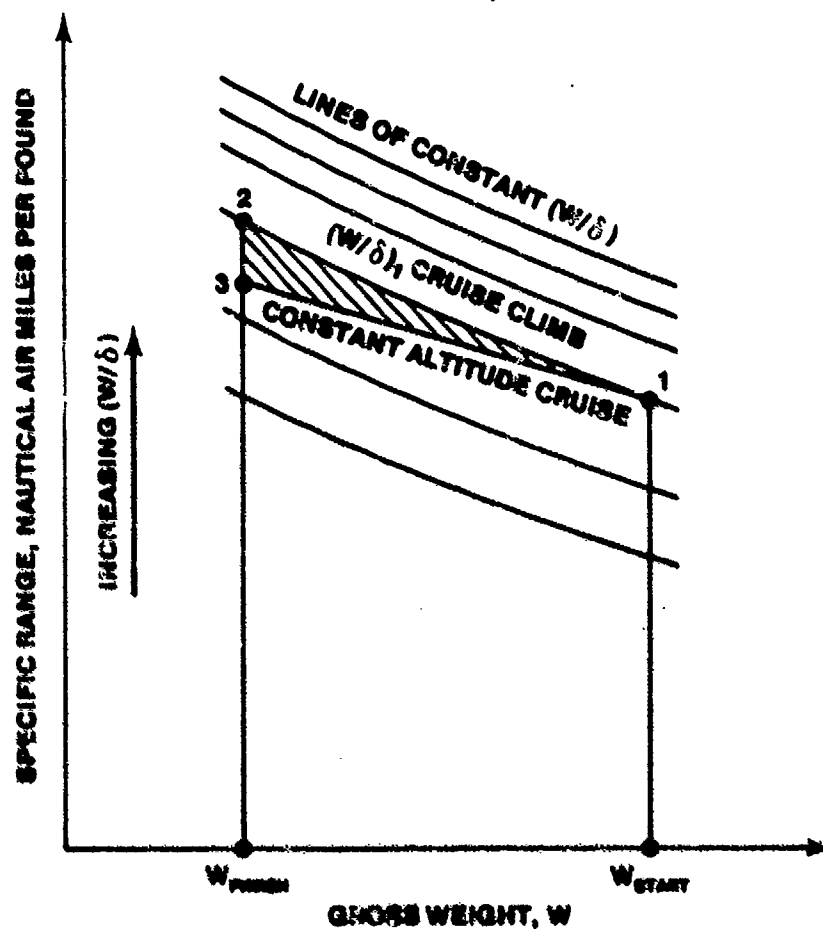


FIGURE 11.10. COMPARISON OF CRUISE CLIMB AND CONSTANT ALTITUDE FLIGHT

The maximum range profile is developed from specific range data obtained on speed power test flights. To develop the maximum range profile, an additional parameter needs to be defined.

Range factor is defined as

$$RF = (SR) (W) \quad (11.42)$$

Recalling that

$$R = \int V dt \quad (11.34)$$

$$SR = \frac{V}{\dot{W}_f} \quad (11.39)$$

$$\dot{W}_f = - \frac{dW}{dt} \quad (11.29)$$

then

$$R = - \int SR dW$$

Multiplying by $\frac{W}{W}$ yields

$$R = - \int (SR) (W) \frac{dW}{W}$$

and therefore,

$$R = - \int RF \frac{dW}{W} \quad (11.43)$$

For a constant Mach, constant W/δ cruise climb, if range factor can be proven to be constant, it will be easy to integrate the range equation. The following analysis is offered for proof of this factor.

$$M = f \left(\frac{W}{\delta}, \frac{N}{\sqrt{\theta}} \right) \quad (11.26)$$

Therefore,

$$\frac{N}{\sqrt{\theta}} = f \left(\frac{W}{\delta}, M \right)$$

The maximum range profile is flown at a constant W/δ and M . Therefore $N\sqrt{\theta}$ is constant. As previously discussed,

$$\frac{\dot{W}_f}{\delta \sqrt{\theta}} = f \left(\frac{N}{\sqrt{\theta}}, \frac{W}{\delta} \right) \quad (11.27)$$

For a constant $N/\sqrt{\theta}$ and W/δ , $\dot{w}_f/(\delta\sqrt{\theta})$ is constant.

$$\frac{\dot{w}_f}{\delta\sqrt{\theta}} = K_1 \quad (11.44)$$

Mach is defined $M = \frac{V}{a}$, therefore

$$\begin{aligned} M &= \frac{V}{\sqrt{\gamma g R T}} \\ M &= \frac{V}{\sqrt{\gamma g R T}} \frac{\sqrt{T_0}}{\sqrt{T_0}} \\ M &= \frac{1}{\sqrt{\gamma g R T_0}} \left(\frac{V}{\sqrt{\theta}} \right) \\ M &= K_2 \frac{V}{\sqrt{\theta}} \end{aligned}$$

Since Mach is constant

$$V = K_3 \sqrt{\theta} \quad (11.45)$$

Specific range is

$$SR = \frac{V}{\dot{w}_f} \quad (11.39)$$

Substituting Equation 11.44 and 11.45 for V and \dot{w}_f yields

$$\begin{aligned} SR &= \frac{K_3 \sqrt{\theta}}{K_1 \delta \sqrt{\theta}} \\ SR &= \frac{K_4}{\delta} \end{aligned} \quad (11.46)$$

Substituting Equation 11.46 into the range factor definition yields

$$RF = \frac{K_4 W}{\delta}$$

$$RF = K_4 \frac{W}{\delta}$$

Since W/δ is constant, range factor is constant and Equation 11.43 becomes

$$R = - \int RF \frac{dW}{W} = - RF \frac{dW}{W}$$

Integrating from initial gross weight (W_i) to final gross weight (W_f),

$$R = - RF \int_{W_i}^{W_f} \frac{dW}{W}$$

Or

$$R = RF \int_{W_f}^{W_i} \frac{dW}{W}$$

$$R = RF \ln \frac{W_i}{W_f} \quad (11.47)$$

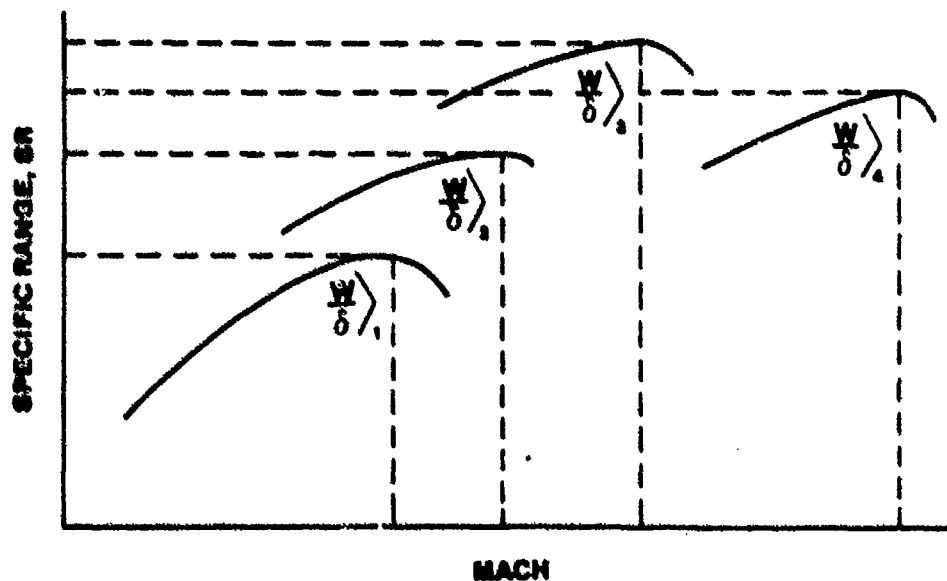


FIGURE 11.11 SPECIFIC RANGE

From the speed power test data the range factor for each maximum specific range is computed using

$$RF_i = SR_i W_i$$

where W_i is the standard weight used to compute the particular W/δ . These data are plotted versus W/δ as shown in Figure 11.12. Mach for each corresponding maximum specific range are also plotted.

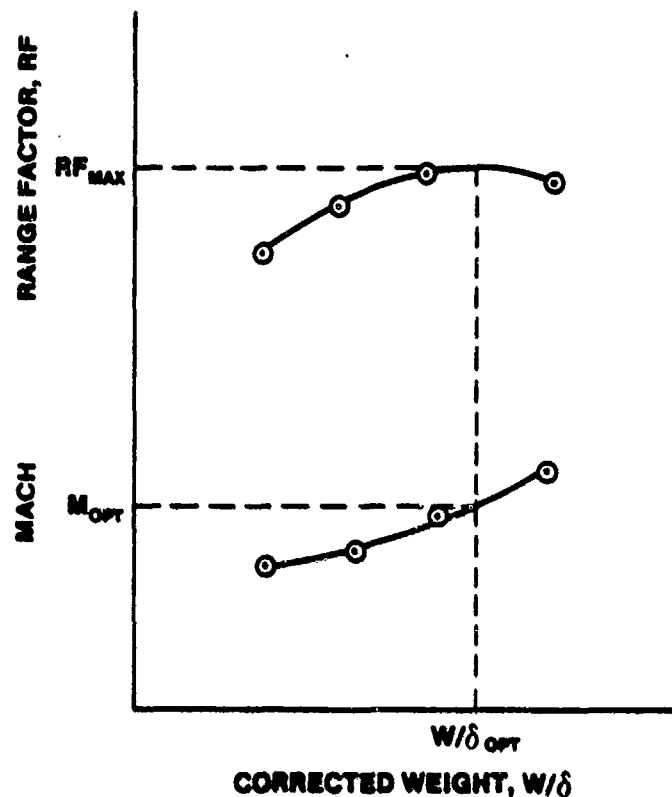


FIGURE 11.12. DETERMINATION OF OPTIMUM MACH FOR ANY GIVEN RANGE FACTOR

The maximum range of the aircraft is obtained by flying a constant Mach, constant W/δ cruise climb at the optimum W/δ and associated Mach from Figure 11.12.

It is important to understand that Figure 11.12 is good for all altitudes, gross weights and associated W/δ 's. However, the range factor curve may have gross weight breakouts if the ratio of fuel weight to maximum gross weight is extremely large. The maximum range for any given W/δ can only be attained by flying the Mach associated with the maximum specific range for the W/δ as shown in Figure 11.12.

11.9 DRAG POLAR DETERMINATION

Another important outcome of the speed power flight test is the determination of the aircraft's drag polar. Recalling that

$$C_L = \frac{W/\delta}{1481M^2S}$$

and

$$C_D = \frac{D/\delta}{1481M^2S} = \frac{F_n/\delta}{1481M^2S}$$

Knowing the test W/δ and M , C_L can be calculated.

From the functional relationship

$$\frac{N}{\sqrt{\theta}} = f\left(M, \frac{W}{\delta}\right)$$

$N/\sqrt{\theta}$ can be determined.

Using $N/\sqrt{\theta}$ and the functional relationship

$$\frac{F_n}{\delta} = f\left(\frac{N}{\sqrt{\theta}}, M\right)$$

C_D can be calculated.

The aircraft drag polar can be determined by plotting C_L as a function of C_D from the speed power flight test data.

In summary, cruise performance of a jet aircraft is determined by using the speed power flight test method. The data can be analyzed to determine maximum specific range and endurance fuel flow and associated airspeeds (Mach). Further analysis results in determination of the optimum W/δ and Mach to fly to obtain the maximum range of the aircraft.

11.10 VARIABLE GEOMETRY AND DUAL ROTOR ENGINES

Previous sections of this chapter were restricted to constant geometry, single rotor engines. In this section some of the complications encountered with variable geometry and dual rotor engines are analyzed. In defining the performance characteristics of a variable geometry engine, it is advantageous to directly measure thrust. If thrust is directly measured, then this functional relationship is still valid.

$$\frac{F_n}{\delta} = f \left(M, \frac{W}{\delta} \right) \quad (11.23)$$

This relationship combined with the constant geometry engine analysis gives

$$M = f \left(\frac{W}{\delta}, \frac{N}{\sqrt{\theta}} \right) \quad (11.26)$$

If thrust parameter is not used, then the following complex equations must be used:

For variable geometry

$$M = f \left(\frac{W}{\delta}, \frac{N}{\sqrt{\theta}}, \Delta \right) \quad (11.48)$$

For dual rotor

$$M = f \left(\frac{W}{\delta}, \frac{N_1}{\sqrt{\theta}}, \frac{N_2}{\sqrt{\theta}} \right) \quad (11.49)$$

where Δ is the ratio of the variable area to some reference area; N_1 , N_2 are the two rotor speeds of a dual rotor engine. Engine speeds in a dual rotor engine are physically more difficult to measure and are less directly a function of thrust output. However, engine pressure ratio (EPR), is a direct measure of the thrust output of the engine. EPR is defined

$$EPR = \frac{P_{T_{10}}}{P_{T_2}} \quad (11.50)$$

$P_{T_{10}}$ is the total pressure at the exhaust nozzle outlet. P_{T_2} is the total pressure at the compressor face. When the EPR is used, it replaces the $N/\sqrt{\theta}$ term used throughout this chapter.

11.11 PROPELLER-DRIVEN AIRCRAFT CRUISE THEORY

The cruise performance of a propeller-driven aircraft can be obtained with the engine horsepower curves and steady state aircraft flight test data. The data reduction equations and constant altitude flight test technique will be briefly discussed in this section.

Up to this point, only drag and thrust have been considered, but in the case of the propeller-driven aircraft, it is more convenient to consider the aircraft requirements in terms of power. Power is defined as the time rate of doing work.

$$\text{Power} = \frac{\text{work}}{\text{time}} = \frac{Fd}{t}$$

Since distance (d) divided by time (t) is true airspeed (V), power may be expressed

$$\text{Power} = FV$$

Horsepower (HP) is the unit of power most commonly used and is defined

$$\text{HP} = 33,000 \frac{\text{ft-lb}}{\text{min}} = 550 \frac{\text{ft-lb}}{\text{sec}}$$

When the velocity is expressed in ft/sec, horsepower is expressed

$$\text{HP} = \frac{F V}{550}$$

Assuming steady state flight ($F_n = D$), HP must be expressed as thrust horsepower required (THP_r).

$$\text{THP}_r = \frac{DV}{550} \quad (11.51)$$

The drag equation may be written

$$D = C_{D_P} \frac{\rho_a V^2 S}{2} + \frac{2 L^2}{\rho_a V^2 S \pi AR e} \quad (11.52)$$

Substituting Equation 11.52 into Equation 11.51,

$$\frac{DV}{550} = C_{D_P} \frac{\rho_a V^3 S}{1100} + \frac{L^2}{275 \rho_a V S \pi AR e}$$

For steady state flight $L = W$,

$$THP_r = \frac{C_{D_P} \rho_a V^3 S}{1100} + \frac{W^2}{275 \rho_a V S \pi AR e}$$

Substituting,

$$V = \frac{V_e}{\sqrt{\sigma}}$$

$$THP_r = \frac{C_{D_P} \rho_a V_e^3 S}{1100 \sigma^{3/2}} + \frac{W^2 \sqrt{\sigma}}{275 \rho_a V_e S \pi AR e}$$

Multiplying by $\frac{\rho_0}{\rho_0}$

$$THP_r = \frac{C_{D_P} \rho_a \rho_0 V_e^3 S}{1100 \sigma^{3/2} \rho_0} + \frac{W^2 \rho_0 \sqrt{\sigma}}{275 \rho_a \rho_0 V_e S \pi AR e}$$

$$THP_r = \frac{C_{D_P} \rho_0 V_e^3 S}{1100 \sqrt{\sigma}} + \frac{W^2}{275 \sqrt{\sigma} \rho_0 V_e S \pi AR e}$$

$$\sqrt{\sigma} THP_r = \frac{C_{D_P} \rho_0 V_e^3 S}{1100} + \frac{W^2}{275 \rho_0 V_e S \pi AR e}$$

Dividing both sides of the equation by $W^{3/2}$,

$$\frac{\sqrt{\sigma} THP_r}{W^{3/2}} = \frac{C_{D_P} \rho_0 V_e^3 S}{1100 W^{3/2}} + \frac{W^{1/2}}{275 \rho_0 V_e S \pi AR e} \quad (11.53)$$

The W in Equation 11.53 is the test weight (W_t). Eliminating weight as a variable by multiplying both sides of Equation 11.53 by $W_s^{3/2}$ (the standard weight),

$$\frac{\sqrt{\sigma} \text{THP}_r}{\left(\frac{W_t}{W_s}\right)^{3/2}} = \frac{C_{Dp} \rho_0 S}{1100} \left[\frac{V_e}{\left(\frac{W_t}{W_s}\right)^{1/2}} \right]^3 + \frac{W_s^2}{275 \rho_0 \left[\frac{V_e}{\left(\frac{W_t}{W_s}\right)^{1/2}} \right] S \pi A R e} \quad (11.54)$$

Let

$$K_1 = \frac{C_{Dp} \rho_0 S}{1100}$$

$$K_2 = \frac{1}{275 \rho_0 S \pi A R e}$$

Substituting these constants into Equation 11.54,

$$\frac{\sqrt{\sigma} \text{THP}_r}{\left(\frac{W_t}{W_s}\right)^{3/2}} = K_1 \left[\frac{V_e}{\left(\frac{W_t}{W_s}\right)^{1/2}} \right]^3 + \frac{K_2 W_s^2}{\left[\frac{V_e}{\left(\frac{W_t}{W_s}\right)^{1/2}} \right]} \quad (11.55)$$

To simplify Equation 11.55, substitute

$$P_{iw} = \frac{\sqrt{\sigma} \text{THP}_r}{\left(\frac{W_t}{W_s}\right)^{3/2}}$$

$$V_{iw} = \left[\frac{V_e}{\left(\frac{W_t}{W_s} \right)^{1/2}} \right]$$

Where P_{iw} is power required, corrected to a standard weight, and V_{iw} is equivalent airspeed corrected to a standard weight.

Now Equation 11.55 becomes

$$P_{iw} = K_1 (V_{iw})^3 + \frac{K_2 W_s^2}{V_{iw}} \quad (11.56)$$

Figure 11.13 is a plot of the power required for level flight of a propeller driven aircraft at all altitudes, temperatures, and weights. This data can be obtained from level flight test data in conjunction with engine horsepower data.

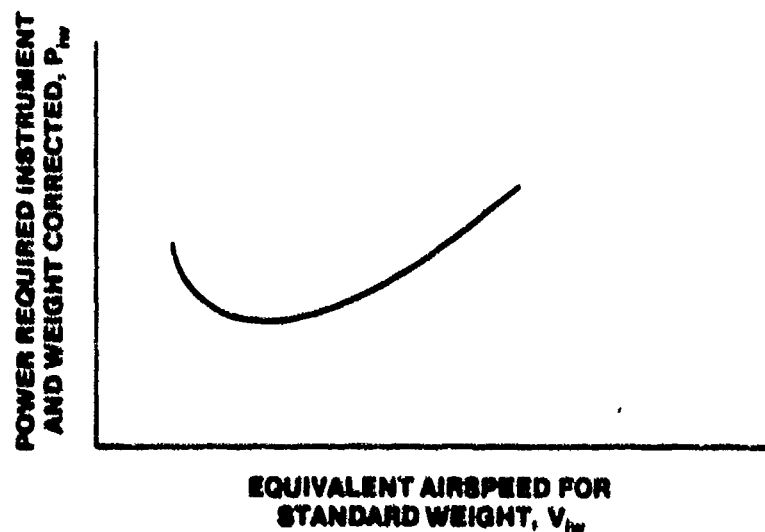


FIGURE 11.13 POWER REQUIRED FOR LEVEL FLIGHT

Figure 11.14 is a typical plot of propeller engine horsepower data. The Continental 0-470-M engine data are presented in this figure.

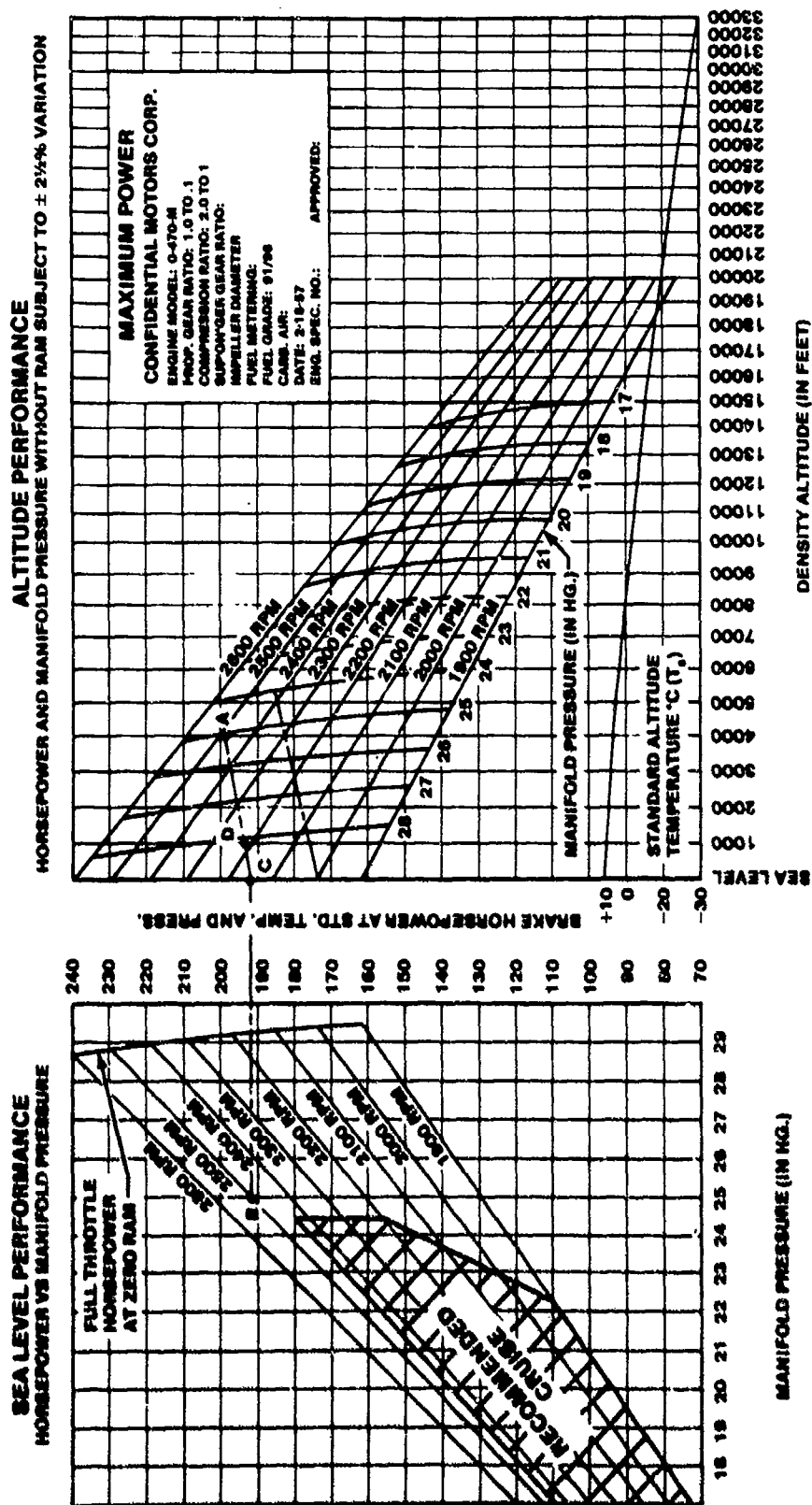


FIGURE 11.14 ENGINE HORSEPOWER CURVE

The constant altitude flight test technique is used to determine cruise data for the propeller-driven aircraft. Steady state points are flown at different airspeeds throughout the flight envelope. Airspeed (V_i), temperature (T_i), altitude (H_i), manifold pressure, RPM, and fuel weight are recorded at each stabilized point. BHP is calculated from Figure 11.14 with the manifold pressure and RPM recorded from each stable point. Propeller efficiency (η_p) is defined

$$\eta_p = \frac{THP}{BHP}$$

The propeller efficiency is obtained from wind tunnel data. Propeller efficiencies normally vary from .50 at stall airspeed to .75 at cruising airspeed. P_{iw} is calculated with the wind tunnel propeller efficiency, the BHP from the engine horsepower chart, test altitude (H_i), test weight (W_t), and the standard weight (W_s).

$$P_{iw} = \frac{\sqrt{\sigma} BHP \eta_p}{\left(\frac{W_t}{W_s}\right)^{3/2}} \quad (11.57)$$

Equivalent airspeed (V_e) is calculated with V_i , H_i , and T_i . V_{iw} is calculated using.

$$V_{iw} = \left[\frac{e}{\left(\frac{W_t}{W_s}\right)^{1/2}} \right] \quad (11.58)$$

Data are obtained at different airspeeds throughout the flight envelope. Data scatter is reduced by plotting $(P_{iw}) (V_{iw})$ versus $(V_{iw})^4$ as in Figure 11.15. A straight line can be drawn through the data points.

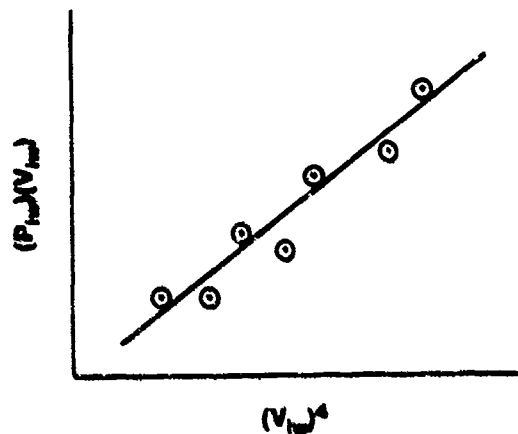


FIGURE 11.15 LINEARIZED POWER REQUIRED

Points are crossplotted from Figure 11.15 to obtain Figure 11.16 (the BHP required for level flight).

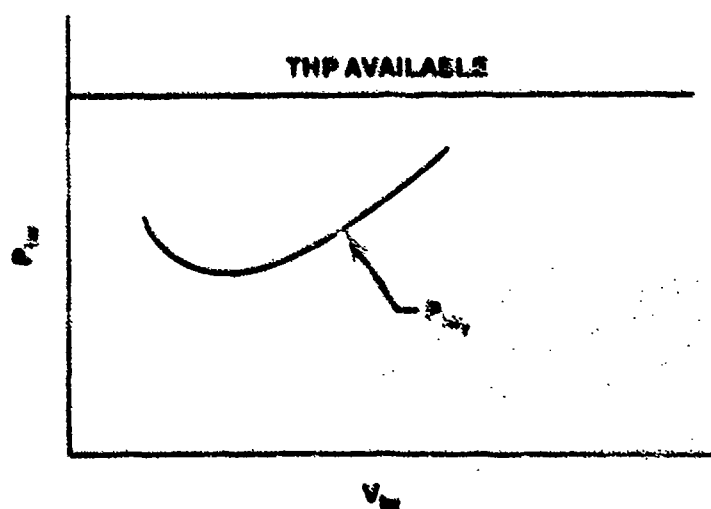


FIGURE 11.16 POWER REQUIRED FOR LEVEL FLIGHT

A drag polar can also be constructed from level flight cruise data.

From Equation 11.51

$$D = \frac{(\text{THP}_r) (550)}{V}$$

From Equation 11.57

$$\text{THP}_r = \frac{P_{iw} \left(\frac{W_t}{W_s} \right)^{3/2}}{\sqrt{\sigma}}$$

Therefore

$$D = \frac{P_{iw} \left(\frac{W_t}{W_s} \right)^{3/2} 550}{V \sqrt{\sigma}}$$

$$D = \frac{P_{iw} \left(\frac{W_t}{W_s} \right)^{3/2} 550}{V_e}$$

(11.59)

From aerodynamics

$$D = \frac{1}{2} \rho_0 V_e^2 S C_D$$

or

$$C_D = \frac{2D}{\rho_0 V_e^2 S}$$

Substituting Equation 11.59 for D

$$C_D = \frac{1100 P_{iw} \left(\frac{W_t}{W_s} \right)^{3/2}}{\rho_0 V_e^3 S} \quad (11.60)$$

From Equation 11.58

$$\left(\frac{W_t}{W_s} \right)^{1/2} = \frac{V_e}{V_{iw}}$$

Or

$$\left(\frac{W_t}{W_s} \right)^{3/2} = \frac{V_e^3}{V_{iw}^3}$$

Substituting this result into Equation 11.60

$$C_D = \frac{1100 P_{iw}}{\rho_0 S V_{iw}^3} \quad (11.61)$$

From aerodynamics

$$C_L = \frac{2L}{\rho_0 V_e^2 S}$$

For a steady state flight $L = W$, or

$$C_L = \frac{2W}{\rho_0 V_e^2 S} = \frac{2 W_t}{\rho_0 V_e^2 S} \quad (11.62)$$

From Equation 11.58

$$W_t = \frac{V_e^2 W_s}{V_{iw}^2}$$

Substituting this result into Equation 11.62

$$C_L = \frac{2 W_s}{\rho_0 S v_{iw}^2} \quad (11.63)$$

Using Equation 11.61 for C_D and Equation 11.63 for C_L , we can plot a drag polar from level flight cruise data (Figure 11.2).

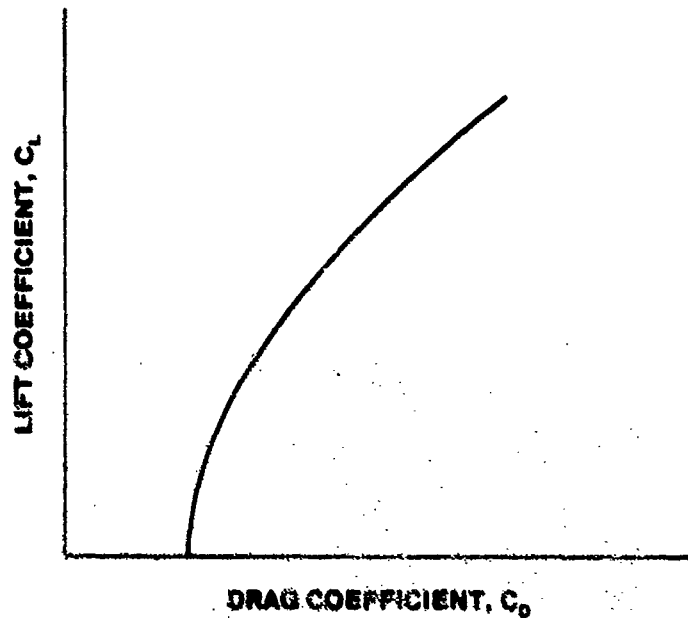


FIGURE 11.2. DRAG POLAR

11.12 PROPELLER-DRIVEN AIRCRAFT ENDURANCE AND RANGE

The computation of both maximum endurance and maximum range airspeeds for a propeller driven aircraft can be simplified if the brake specific fuel consumption (C) and the propeller efficiency (η_p) are assumed constant.

The change of aircraft gross weight due to fuel with time is

$$\frac{dW}{dt} = - C (\text{BHP}) \quad (11.64)$$

where

$$C = \frac{\text{lb}}{\text{BHP} \cdot \text{hr.}}$$

Therefore, the units for dW/dt are lb/hr.

11.12.1 Range

Recalling that range is defined as

$$R = \int ds = \int V dt \quad (11.34)$$

Rearranging Equation 11.64

$$dt = - \frac{dW}{(\text{BHP}) C}$$

Substituting this result into the range equation

$$R = - \int \frac{V dW}{(\text{BHP}) C}$$

$$\text{Substituting for BHP, } \text{BHP} = \frac{\text{THP}}{\eta_p} = \frac{DV}{550 \eta_p}$$

$$R = - \int \frac{\eta_p 550 V dW}{DV C}$$

$$R = - \int \frac{\eta_p 550 dW}{DV C}$$

$$R = \int_{W_f}^{W_i} \frac{\eta_p 550 dW}{D C}$$

$$R = \frac{\eta_p 550}{C} \int_{W_f}^{W_i} \frac{dW}{D}$$

Multiplying by $\frac{W}{W}$

$$R = \frac{\eta_p 550}{C} \int_{W_f}^{W_i} \frac{W dW}{DW}$$

For steady state flight $L = W$, or

$$R = \frac{\eta_p 550}{C} \int_{W_f}^{W_i} \frac{C_L}{C_D} \frac{dW}{W}$$

Assuming a constant angle of attack,

$$R = \frac{\eta_p 550}{C} \left(\frac{C_L}{C_D} \right) \int_{W_f}^{W_i} \frac{dW}{W} \quad (11.65)$$

$$R = \frac{\eta_p 550}{C} \left(\frac{C_L}{C_D} \right) \ln \frac{W_i}{W_f} \quad (11.66)$$

Equation 11.66 indicates maximum range requires

1. η_p/C be a maximum.
2. Fly at C_L/C_D maximum.

Note that the altitude does not appear in the range equation for a reciprocating engine. However, C will decrease with an increase in altitude.

C_L/C_D maximum occurs when parasite drag equals induced drag. This occurs at the tangent to the P_{iw} versus V_{iw} curve as depicted in Figure 11.15. Therefore, the airspeed for maximum range is available from level flight performance data discussed in the range section. Figure 11.15 also illustrates the airspeed for maximum endurance (minimum P_{iw} point).

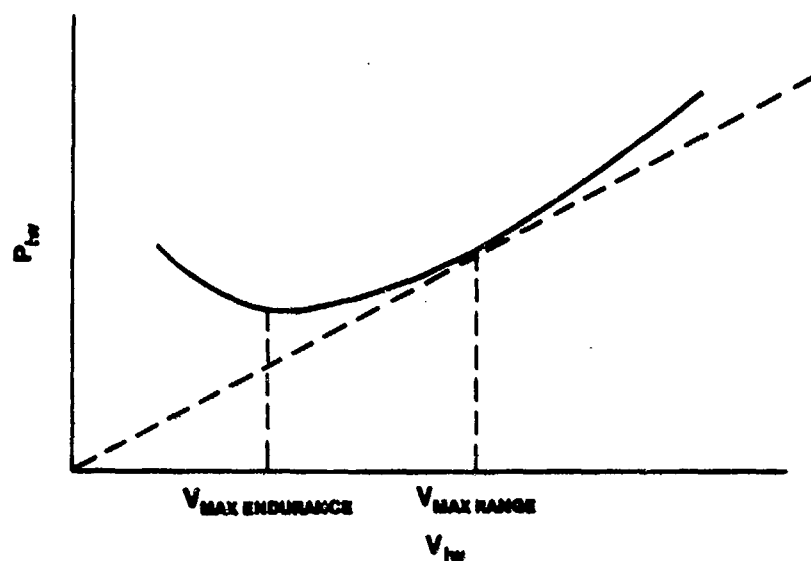


FIGURE 11.17 DETERMINATION OF MAXIMUM ENDURANCE AND MAXIMUM RANGE AIRSPEEDS

11.12.2 Endurance

For maximum endurance an aircraft should fly at an airspeed to minimize dW/dt . Assuming specific fuel consumption is constant, this airspeed occurs at minimum BHP. Assuming propeller efficiency is constant, the airspeed for maximum endurance occurs where P_{iw} is minimum on Figure 11.12. Therefore, flight test results (P_{iw} versus V_{iw}) provide the maximum endurance airspeed.

Endurance is defined:

$$E = - \int dt = - \int \frac{dW}{(BHP) C}$$

Recalling that $BHP = \frac{DV}{550 \eta_p}$,

$$E = - \int \frac{\eta_p 550 dW}{DVC}$$

Since $D = \frac{W}{L/D}$,

$$E = - \int \frac{\eta_p 550}{VC} \left(\frac{L}{D} \right) \frac{dW}{W}$$

Velocity can be expressed as $V = \left[\frac{2W}{C_L \rho S} \right]^{1/2}$

$$E = - \int_{W_f}^{W_i} \frac{\eta_p 550}{C} \left(\frac{L}{D} \right) \left(\frac{C_L \rho S}{2W} \right)^{1/2} \frac{dW}{W} \left(\frac{C_L \rho S}{2W} \right)^{1/2}$$

$$E = - \frac{\eta_p 550}{C} \frac{C_L^{3/2}}{C_D} \sqrt{\frac{\rho S}{2}} \int_{W_f}^{W_i} \frac{dW}{W^{3/2}}$$

$$E = - \frac{\eta_p 550}{C} \frac{C_L^{3/2}}{C_D} \sqrt{\frac{\rho S}{2}} \left[\frac{1}{\sqrt{W_f}} - \frac{1}{\sqrt{W_i}} \right] \quad (11.67)$$

Equation 11.67 shows that maximum endurance should be achieved by flying at high altitude at a speed where $C_L^{3/2}/C_D$ is maximized. The velocity for maximum endurance shown in Figure 11.15 occurs where induced drag equals three times parasite drag.

In conclusion, we fly stable points in a propeller driven aircraft to obtain a power required for level flight curve and drag polar. The maximum endurance and maximum range airspeeds are obtained from the power required for level flight curve.

11.13 CRUISE PERFORMANCE TESTING

The speed power flight test is a common method used to obtain the cruise performance of an aircraft. This method allows determination of both maximum endurance and maximum range airspeeds and considerably reduces the number of flight test sorties required.

The speed power flight test involves gathering fuel flow data at various altitudes, gross weights, and airspeeds that sufficiently define the operating envelop of the aircraft. These data are generally presented as shown in Figure 11.18.

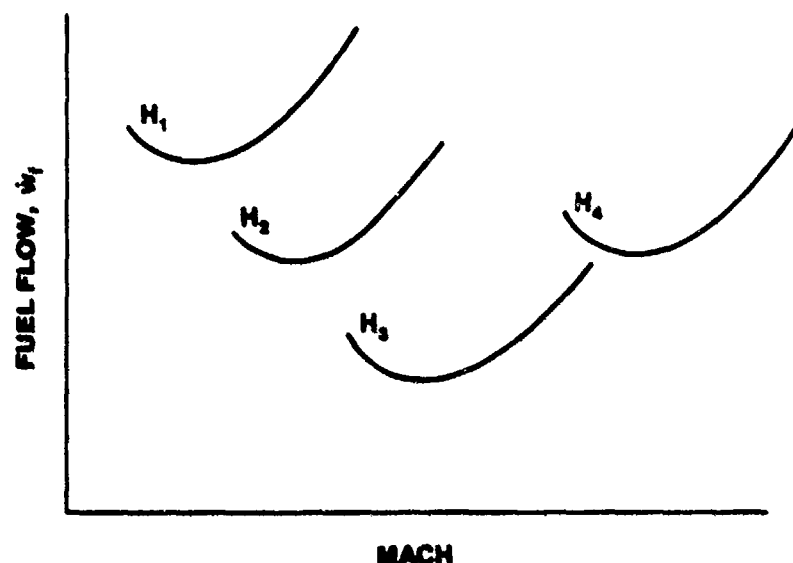


FIGURE 11.18 STANDARD FUEL FLOW

Each of the curves depicted in Figure 11.16 represents one altitude and one gross weight and therefore one W/δ . It is important to note that these curves do not represent all altitude and gross weight combinations that result in the particular W/δ of the curve, but are restricted to one altitude and one gross weight. As an example, an aircraft weighing 100,000 lb at an altitude of 18,000 ft has the same W/δ as a 200,000 lb aircraft at sea level. However, it should be obvious that the fuel flow at 18,000 ft will be much less than that at sea level, resulting in a different fuel flow versus Mach curve. When the specific range is multiplied by the aircraft's weight, however, the range factor will be the same in both cases.

Since it is not realistic to consider taking data at only one altitude and one gross weight due to fuel consumption, the data must be collected within a reasonable tolerance and then standardized to the altitude and gross weight of interest. As a rule, if the W/δ of the test is held within $\pm 2\%$ of the standard W/δ and the altitude is within ± 2000 ft of the standard altitude, this functional relationship will hold true.

Recalling Equation 11.27 from the dimensional analysis of the fuel flow parameter, we have

$$\frac{\dot{w}_f}{\delta \sqrt{\theta}} = f \left(\frac{N}{\sqrt{\theta}}, \frac{W}{\delta} \right) = f \left(\frac{N}{\sqrt{\theta}}, M \right)$$

With the data from the speed power flight test, this functional relationship can be determined and plotted as shown in Figure 11.19.

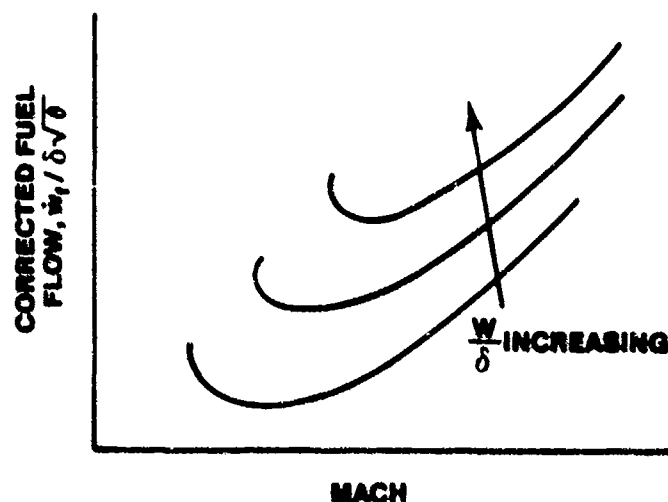


FIGURE 11.19 CORRECTED FUEL FLOW

This functional relationship states that for a given corrected RPM, $N/\sqrt{\theta}$, and corrected weight, W/δ , there is only one corrected fuel flow $\dot{w}_f / \delta \sqrt{\theta}$. If W/δ is held constant during the flight test, then

$$\left(\frac{\dot{w}_f}{\delta \sqrt{\theta}} \right)_{\text{test}} = \left(\frac{\dot{w}_f}{\delta \sqrt{\theta}} \right)_{\text{standard}}$$

for a given $N/\sqrt{\theta}$ and therefore

$$\left(\frac{\dot{w}_f}{\delta \sqrt{\theta}} \right)_s = \left(\frac{\dot{w}_f}{\delta \sqrt{\theta}} \right)_t \left(\delta \sqrt{\theta} \right)_s$$

Since

$$M = f \left(\frac{N}{\sqrt{\theta}}, \frac{W}{\delta} \right) \text{ for the}$$

measured $N/\sqrt{\theta}$ and W/δ , then $M_t = M_s$.

This is the method by which the standard fuel flow versus Mach graph is obtained.

From the $\dot{w}_f/\delta \sqrt{\theta}$ versus Mach plot, the maximum endurance airspeed can be determined for any given W/δ by picking the point of minimum fuel flow. However, this particular plot does not readily indicate the altitude effects and whether climbing will increase endurance (decrease fuel flow). However, maximum endurance is the point of minimum fuel flow, and the effect of climbing is evident from Figure 11.18, the fuel flow versus Mach plot.

Recalling the definition of specific range,

$$SR = \frac{V}{\dot{w}_f}$$

the maximum specific range for a given corrected weight, W/δ , can be calculated from the fuel flow versus Mach plot. It is the point of tangency of a line drawn from the origin as shown in Figure 11.20.

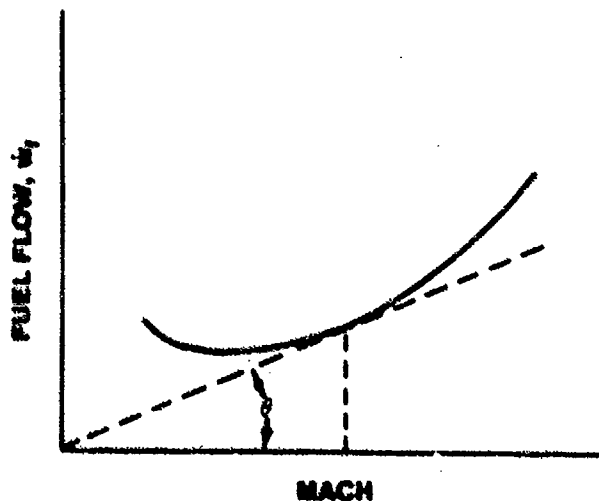


FIGURE 11.20 FUEL FLOW

From Figure 11.20,

$$\tan \theta = \frac{\dot{w}_f}{N} = \frac{\dot{w}_f}{V} = \frac{1}{SR}$$

From this equation it can be seen that maximum specific range occurs at the minimum angle, θ .

Specific range can be plotted from the fuel flow versus Mach data. A typical set of curves is shown in Figure 11.21.

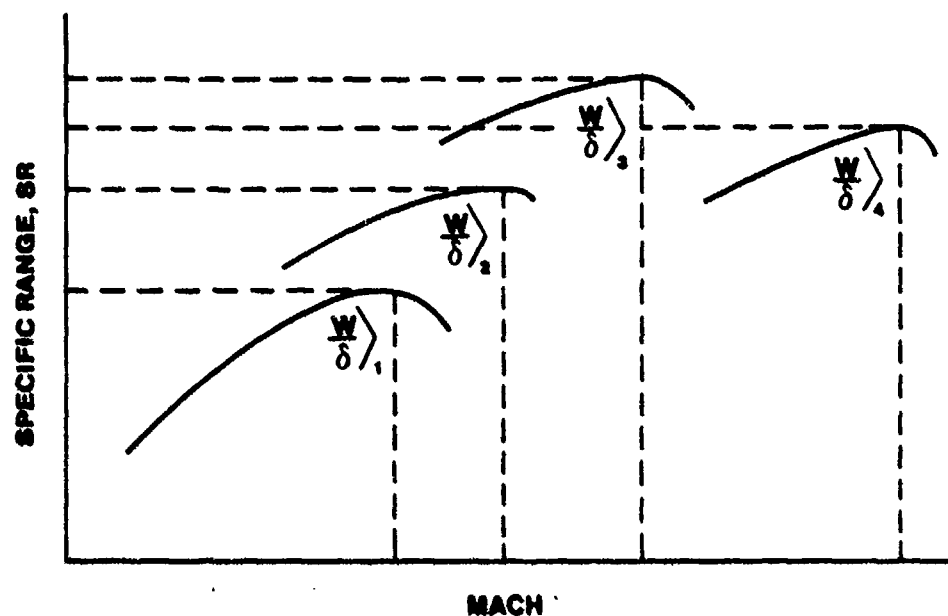


FIGURE 11.21 SPECIFIC RANGE

The same information obtained from the fuel flow versus Mach curves can also be obtained from the specific range versus Mach curves.

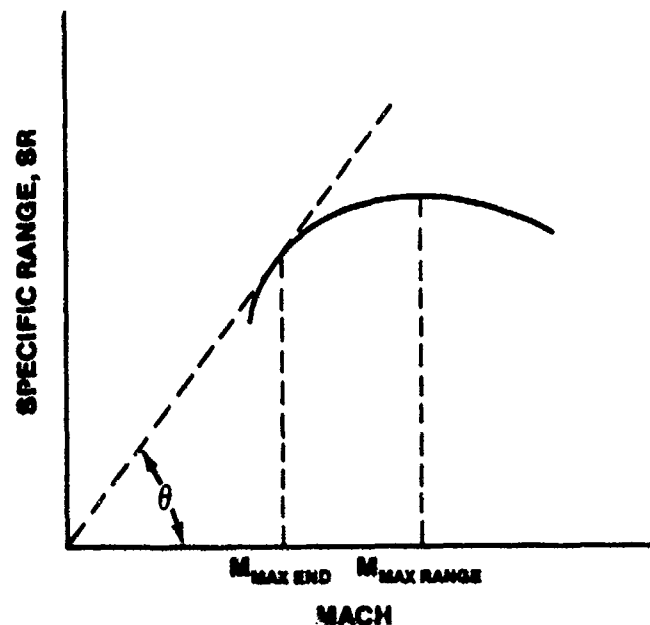


FIGURE 11.22 SPECIFIC RANGE, ONE ALTITUDE

Referring to Figure 11.22, it can be seen that maximum specific range occurs at the peak of the curve. Maximum endurance occurs at the tangency point of a line drawn from the origin.

$$\tan \theta = \frac{SR}{M} = \frac{V/\dot{w}_f}{M} = \frac{V/\dot{w}_f}{V} = \frac{1}{\dot{w}_f}$$

From this relationship it can be seen that minimum fuel flow occurs at the maximum value of θ .

Taking the peaks of the curves, (the points of maximum specific range) and multiplying by the specific weight, the range factor (RF) versus W/δ curve can be generated. This curve is good for all altitudes and all gross weights.

$$RF = (SR) (W) = \frac{1}{C} V \left(\frac{L}{D} \right)$$

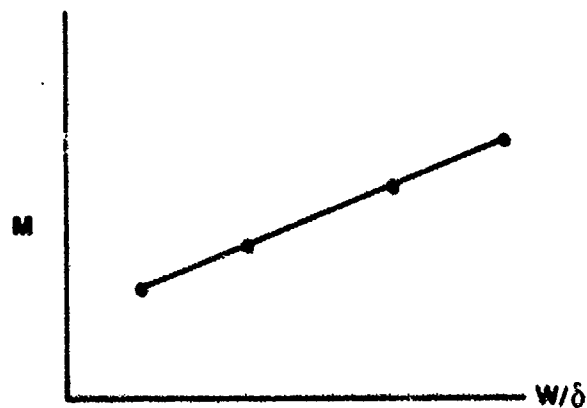
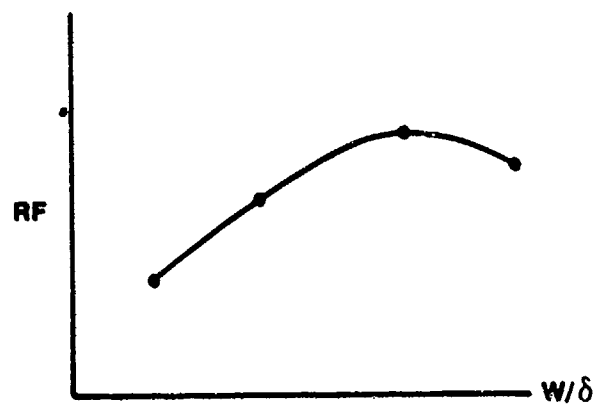


FIGURE 11.23. RANGE FACTOR, ALL ALTITUDES AND WEIGHTS

PROBLEMS

11.1 Define and write symbols for:

Weight-pressure parameter (ratio)

Specific range

Corrected thrust parameter

Corrected fuel flow parameter

Corrected drag parameter

Range factor

Specific fuel consumption (turbojet)

Corrected engine speed parameter

11.2 The design lift coefficient of the T-38A for cruise is 0.28. If design optimum cruise Mach is 0.88 and the aircraft wing area is 170 ft², estimate the optimum cruise weight-pressure ratio.

11.3 For the T-38A design cruise condition in Problem 11.2, the T-38A parasite drag coefficient is 0.15, the aircraft efficiency factor is 0.79, and the aspect ratio is 3.75. What is the initial corrected thrust parameter F_n/δ required for cruise? How does corrected thrust parameter change during cruise climb?

HINT:

$$\frac{D}{\delta} = 1481 C_{D_p} S M^2 + \frac{n^2}{1481 S \pi AR \epsilon} \left(\frac{W}{\delta} \right)^2 \frac{1}{M^2}$$

11.4 During a speed power test point at 360 kts, the fuel flow was 1090 lb/hr. What is the specific range for this aircraft?

11.5 An aircraft in-flight is attaining a specific range of 0.33 NAMPP at a gross weight of 14,000 lb. What is its range factor?

11.6 How far will the aircraft in Problem 11.5 cruise on 4,000 lb of fuel at the same range factor if its end cruise gross weight is 10,000 lb? How is this accomplished?

11.7 An aircraft was flown on a constant W/6 profile of 60,000 lb. The aircraft standard weight was 17,820 lb. On one speed-power point stabilized at 30,300 ft, the fuel flow was measured to be 2,000 lb/hr at 96% RPM. The ambient temperature while stabilized was measured to be 225.75°K. What is the standard fuel flow and RPM?

HINT: Use Appendix A, Performance Handbook, FTC-TIH-79-1, for atmospheric data.

11.8 Show that straight lines through the origin of a plot of SR versus true airspeed represent lines of constant fuel flow.

11.9 Given the following equations:

$$E_1 = \frac{1}{C} \left(\frac{C_L}{C_D} \right) \ln \frac{W_i}{W_f} \quad E_6 = \left(\frac{\dot{W}_f}{\delta \sqrt{\theta}} \right)_t$$

$$E_2 = C_{D_p} + \frac{C_L^2}{\pi AR e}$$

$$E_3 = RF \ln \frac{W_i}{W_f} \quad E_7 = F \left(\frac{N}{\sqrt{\theta}}, M \right)$$

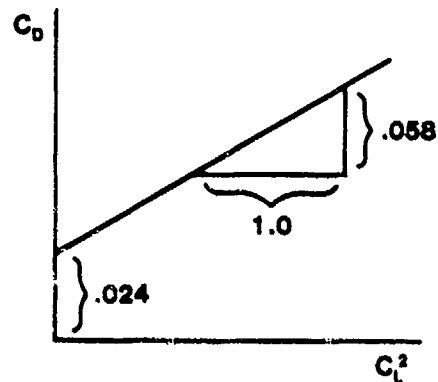
$$E_4 = 2 \left(\frac{2}{\rho S} \right)^{1/2} \left(\frac{C_L^{1/2}}{C_D} \right) \left(\frac{1}{C} \right) \left[\sqrt{W_i} - \sqrt{W_f} \right]$$

$$E_5 = \left(\frac{N}{\sqrt{\theta}} \right)_t$$

Answer the following questions:

- A. Equation _____ is the general range equation, turbojet or propeller.
- B. Equation _____ is an endurance equation developed from aerodynamic analysis for turbojet aircraft.
- C. Equation _____ is equal to standard day corrected RPM parameter.
- D. Equation _____ is the drag polar equation.
- E. Equation _____ is used to calculate range available from a given fuel load at a given range factor.
- F. Equation _____ is used to determine an aircraft's thrust deck.
- G. Equation _____ is a range equation developed from aerodynamic analysis for turbojet aircraft.
- H. Equation _____ is used for determining standard day corrected fuel flow parameter.
- I. Equation _____ is used for determining standard day range factor from flight test range mission data.

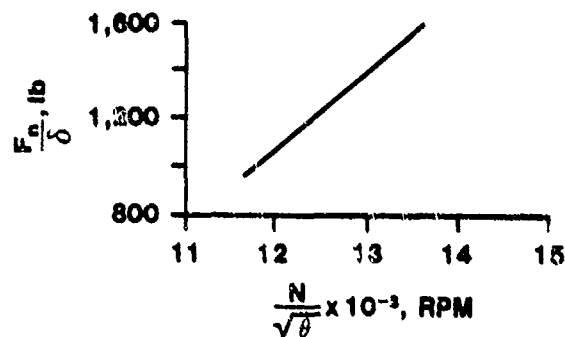
- 11.10 A. The manufacturer's estimated drag polar of a YAT-37D aircraft is presented below. The aircraft reference wing area is 184 ft². Using the equation developed in class for corrected drag parameter (repeated below), estimate D/δ for a speed power point flown at W/δ of 16,168 lb (weight is 6,000 lb, altitude is 25,000 ft) stabilized at Mach 0.4.



$$\frac{D}{\delta} = 1481 C_{Dp} S M^2 + \frac{n^2}{1481 S \pi A R e} \left(\frac{W}{\delta} \right)^2 \frac{1}{M^2}$$

- 11.10 B. At the same speed power point described in Problem 4A, the ambient temperature was determined to be 233 deg K and engine RPM, N , was measured as 11,700 RPM. Using the manufacturer's furnished chart below, what is the engine corrected thrust parameter? Does this agree well with the results of Problem 4A?

**YAT-37D
MANUFACTURER'S ENGINE THRUST CURVE
TWO J85/J2 ENGINES CRUISE**



- 11.11 The following questions apply to the YAT-37D with the drag polar and aircraft data given in Problem 4A.

- A. Estimate the aircraft's L/D_{\max} . What is the significance of this point?
- B. If the aircraft weighs 6,000 lb, what equivalent velocity should be flown to obtain maximum L/D ?
- C. Estimate the aircraft's maximum value of $C_L^{1/2}/C_D$. What would this value be used for?
- D. If the aircraft weighs 6,000 lb, what equivalent velocity should be flown to obtain maximum $C_L^{1/2}/C_D$? What is the significance of this velocity?
- E. What is the maximum range L/D for constant altitude cruise?

11.12 The following problem is based on data from the T-38A Category II Performance Test, FTC-TDR-63-27, Nov 63, AFFTC, Edwards AFB, CA.

- A. The contractor initially estimates that maximum range will result from a constant 0.88 Mach cruise at a constant W/δ of 54,000 lb. Since you have three speed power missions available to determine optimum cruise, you elect to fly the three missions whose results are tabulated below:

W_s (lb)	Altitude (H_c) ft	Maximum SR	Mach for Max. SR
10,094	36,000	0.357	0.87
9,990	40,000	0.380	0.88
9,805	45,500	0.388	0.89

Does the speed power data verify the contractor's prediction?

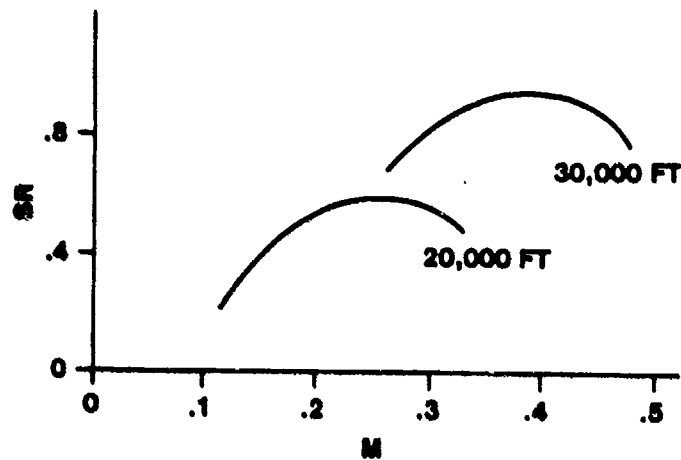
- B. The contractor revises his estimate and now predicts that maximum range will result from a constant 0.88 Mach cruise

at W/δ of 58,000 lb. You elect to fly a ferry range mission at these cruise conditions. During the climb nearing cruise altitude, you notice you have burned 1,006 lb of fuel. You estimate that it will take 60 lb to stabilize at your initial start cruise altitude. Using the weight and fuel data given below, at what altitude should you begin cruise?

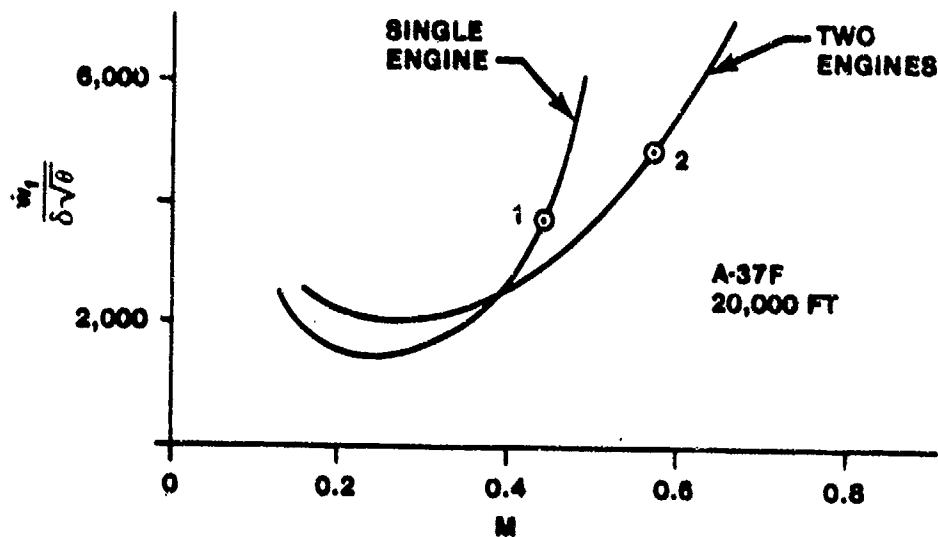
Gross weight at engine start	12,330 lb
Total fuel	3,650 lb
MIL-C-5011A fuel reserve	805 lb

- C. After flying your constant W/δ profile for one hour and twelve minutes, you have to terminate cruise because of an emergency with a fuel reading of 980 lb. Data reduction shows that the cruise climb was flown at a constant T_a of -76°F , and at a constant 0.88 Mach. If the aircraft traveled 75 nm in the climb to cruise altitude, what was the total test range?
- D. What was the test day range factor?
- E. What was the standard day range factor?
- F. Estimate what the total range of the test mission would have been if the emergency had not occurred and you could have continued cruise to your MIL-C-5011A fuel reserve.
- G. Does the test day range factor verify your speed power data?
- H. If you had one more speed power mission to fly to verify maximum cruise range, what test conditions would you pick?

- 11.13 Given the flight test data below, which of the two altitudes would you choose for max endurance holding? Why? (Assume you're already at the selected altitude when you establish max endurance; i.e., ignore fuel required to climb/descend to holding altitude).



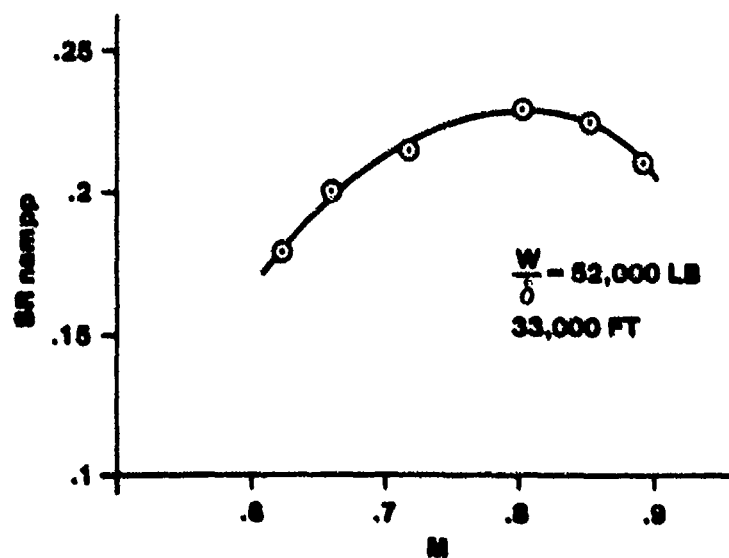
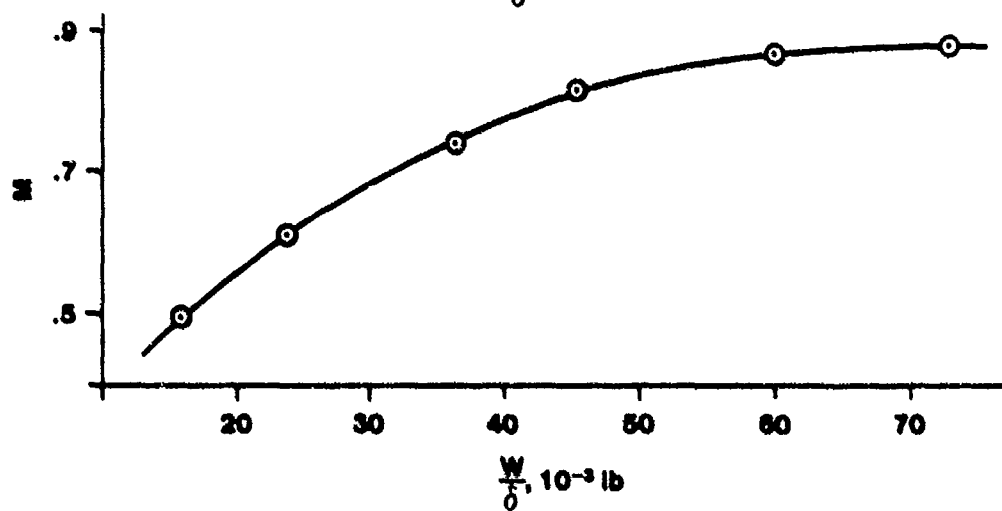
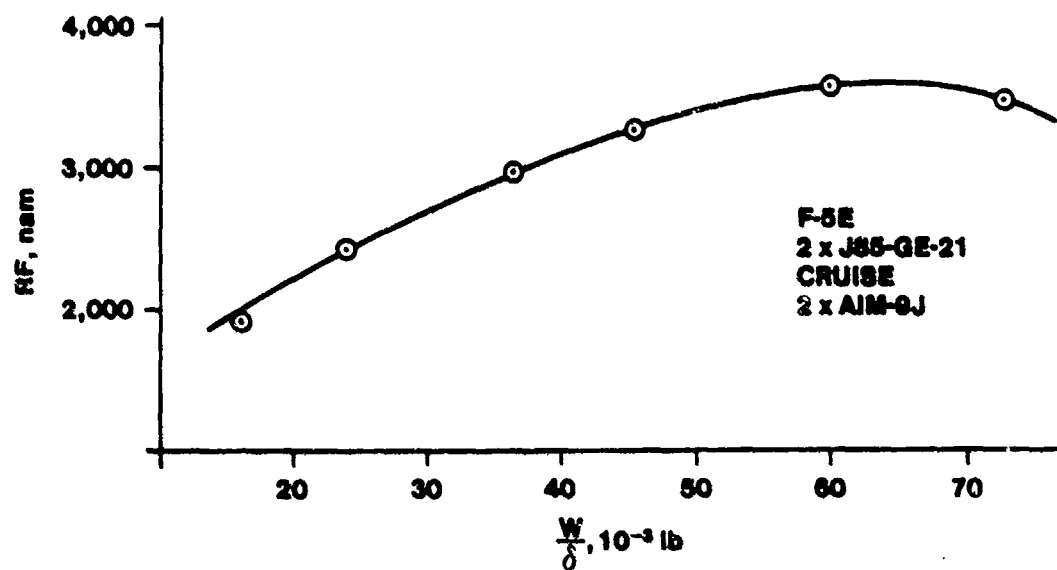
- 11.14 Given the flight test data below, does Point 1 or Point 2 give the best range? Explain.



11.15 (a) The contractor has provided the plots in Figure 1 of range factor and cruise Mach versus weight-pressure ratio based on his initial flight test data. You have just flown the speed power mission plotted in Figure 2. Does your data agree with the contractor's? Explain briefly.

(b) Using the contractor data in Part A and the fuel and weight data below, estimate the maximum cruise distance available.

Gross weight at engine start	15,745
Gross weight at start cruise	14,618
Total usable fuel	4,375
MIL-C-5011A fuel reserve	952



(c) Based on the contractor data in Parts A & B, what altitude and Mach would you plan to stabilize at to start cruise for maximum range?

(d) You were held at the end of the runway for 20 minutes and did not start cruise until 2820 lb remaining. You also landed at your alternate, terminating your cruise climb 45 min after level off with 1400 lb. Given a constant temperature of -58°F , what was the standard day range factor?

(e) Do your results confirm the contractor's estimates? Explain briefly.

(f) You are carrying an AIM-9J with a special lens limited to .8 Mach. Assuming a start cruise weight of 14,781 lb, at what altitude should you plan to level off for best range?

11.16 Given the test data below, plot the aircraft drag polar.

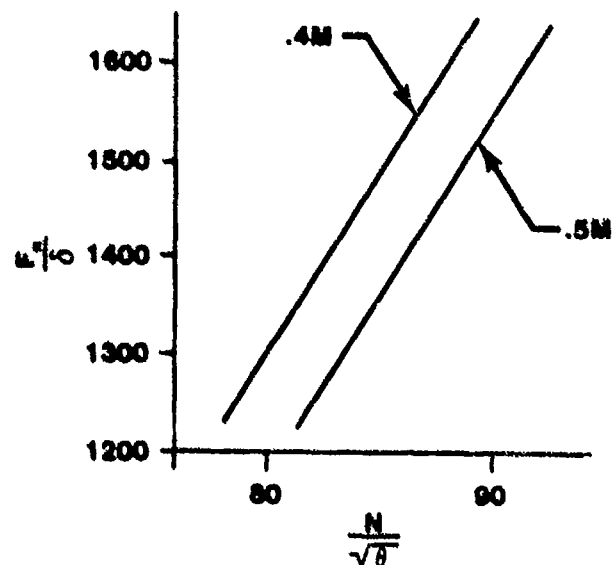
$$\frac{W}{S} = 20,000$$

$$AR = 18.0$$

$$S = 175$$

$$\text{At } M = 0.4, N/\sqrt{\theta} = 80$$

$$\text{At } M = 0.5, N/\sqrt{\theta} = 90$$



ANSWERS

11.2 54,590

11.3 30,880

11.4 .33

11.5 4620

11.6 1550 mi

11.7 $w_{fs} = 1815$

$N_s = 87\%$

11.10 A. 1,394 lb

B. 1,400 lb

11.11 A. 13.4

B. 207 ft/sec

C. 19

D. 272 ft/sec

E. 11.6

11.12 B. 39,000 ft

C. 675 nam

D. 3,909

F. 747 nam

CHAPTER 12
DATA REDUCTION AND CORRECTIONS
TO STANDARD DAY

12.1 INTRODUCTION

An ancient report, from the early days of flying, discussing the crash of a "Jenny" shortly after takeoff on a hot summer day, concluded that the primary cause was "there was no lift in the air that day." The determination of the effects of nonstandard atmospheric conditions on aircraft performance has come a long way since then. These determinations are particularly important in flight test, since performance specifications must be written for some set of "standard" conditions, and flight tests are not usually conducted on "standard" days. Modern computer data reduction capabilities have greatly reduced the manual labor required for performance calculations. On the other hand, they tend to hide assumptions and factors which can turn out to be extremely important in performance testing.

This section examines how test day performance data may be reduced or related to performance under standard conditions. Emphasis is placed on the relationship between data reduction and available instrumentation. The techniques are those used in the TPS performance data reduction programs, which are similar to those used in AFFTC flight test programs.

12.2 STANDARD CONDITIONS

The procuring activity, usually the system program office (SPC), normally determines which conditions will be considered standard for performance specification compliance. Some of the parameters which must be considered are discussed below.

12.2.1 Atmospheric Conditions

These include the variation of ambient temperature and static pressure with altitude. Depending on the aircraft mission, a standard, Arctic standard, tropical standard, or some combination will be specified. Standard day conditions are discussed in Chapter 5. The TPS data reduction programs use the 1962 U.S. Standard Atmosphere.

12.2.2 Weight

A standard weight must be specified since weight affects the angle of attack, drag, and acceleration characteristics for a given set of flight conditions. This depends on the aircraft mission and several standard weights will normally be specified for various portions of the mission profile. To determine standard weight for any aircraft:

- a. The average maximum gross weight for the aircraft is found in the Flight Manual or from manufacturer's data.
- b. The average fuel used during engine start and ground maneuvering is subtracted from the maximum gross weight to determine the standard weight for takeoff data reduction.
- c. The aircraft weight at level off at a particular altitude is the standard weight for level accels, sawtooth climbs and check climbs.
 1. Compute the sea level standard weight by subtracting the fuel required to accelerate to climb speed from the takeoff standard weight.
 2. Subtract the fuel required to climb to different altitudes from the standard weight at sea level. This gives a standard weight at each altitude.
- d. Determine the MIL-C-5011A fuel reserve. This weight is added to the aircraft empty weight and used as a standard weight for descent performance. (e.g. 5% of initial fuel + 20 minutes at sea level at maximum endurance.)
- e. The standard weights for performance tests such as turns, W/S planning, or ferry range missions can be determined by averaging the results from c and d.

12.2.3 Center of Gravity (CG)

The CG position determines the elevator (or slab) position required to maintain a given set of flight conditions. This directly affects parasite drag and can have a large effect on performance. (The TPS programs do not correct for CG position.)

12.2.4 Wind

No-wind conditions are specified in most cases. Wind and wind shear influence climb and descent performance. (The TPS programs do not correct for wind.)

12.2.5 Configuration

Standard configurations must be defined and tested. In TPS performance testing, only the cruise (clean) and speed-brake out (for penetration descents) configurations are specified.

12.2.6 Schedules and Techniques

Climb, descent, cruise, and acceleration schedules must be specified for specific performance determinations. Off-schedule tests may be corrected to standard schedules but the TPS programs do not include these corrections.

12.2.7 Other Considerations

Other factors may be specified depending on the aircraft. These can include the number of operating engines, trim position, and several other factors. Specific requirements must be stated for each flight condition and desired performance parameter.

12.3 PITOT-STATIC DATA REDUCTION

Altitude and airspeed are the two variables that are of primary concern throughout performance and flying qualities testing. Unfortunately, the measurement of these variables by the aircraft's pitot-static system is complicated by the errors discussed in Chapter 5.

12.3.1 Tower Fly-by Data Reduction

Position error is found from tower fly-by data using the following:

1. Find the test aircraft H_C .
 - a. Plot pressure altitude versus time as shown in Figure 12.1 from the preflight and postflight ground blocks. This is called the ground block method. Ramp H_C is the pressure altitude read on the altimeter corrected for instrument error.

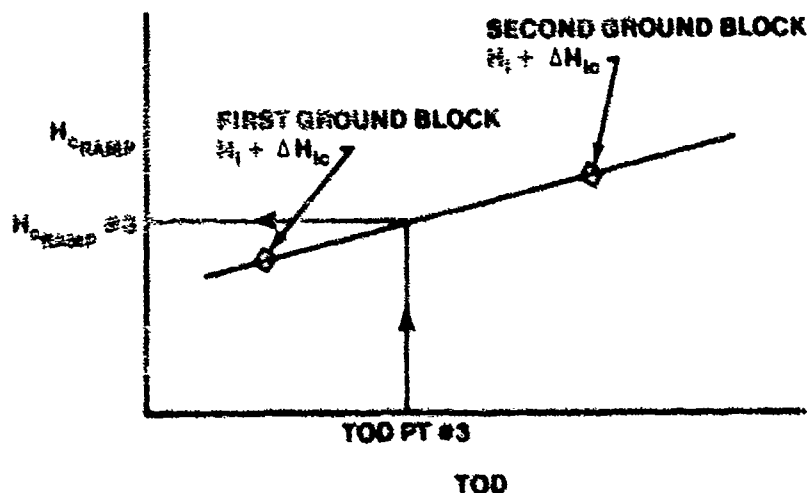


FIGURE 12.1. GROUND BLOCK PRESSURE ALTITUDE PLOT

$$H_{C \text{ Ramp}} = H_{1 \text{ Ramp}} + \Delta H_{IC} \quad (12.1)$$

This plot provides ramp H_C for anytime during the flight.

- b. Find theodolite H_C by adding the difference in elevation between the ramp and the theodolite.

$$H_{C \text{ Theodolite}} = H_{C \text{ Ramp}} + \left(\text{Elevation}_{\text{Theodolite}} - \text{Elevation}_{\text{Ramp}} \right) \frac{T_{as}}{T_a} \quad (12.2)$$

An alternate method to obtain $H_{C \text{ Theodolite}}$ is to read it directly in a theodolite tower with a sensitive pressure instrument at the tower zero gridline.

- c. Find the test aircraft H_C by adding theodolite reading, TR, and correcting for nonstandard temperature.

$$H_{C_{\text{Test Aircraft}}} = H_{C_{\text{Theodolite}}} + \frac{T_{as}}{T_a} \text{ TR } 31.4 \quad (12.3)$$

where 31.4 is the geometric conversion factor for the Edwards Tower - Theodolite System.

2. Find instrument-corrected altitude H_{ic} , velocity V_{ic} , static pressure ratio $P_s/P_{a_{sl}}$, differential pressure ratio $q_{cic}/P_{a_{sl}}$, and instrument-corrected Mach M_{ic} .

a. $H_{ic_t} = H_i + \Delta H_{ic} \quad (12.4)$

b. $V_{ic_t} = V_i + \Delta V_{ic} \quad (12.5)$

- c. Use the low altitude altimeter equation for:
t SL

$$P_{s_t}/P_{a_{sl}} = \delta_{ic_t} = \left[1 - 6.87559 \times 10^{-6} H_{ic_t} \right]^{5.2559} \quad (12.6)$$

- d. Use the subsonic calibrated airspeed equation for:

$$q_{cic_t}/P_{a_{sl}} = \left[1 + 0.2 \left(\frac{V_{ic_t}}{a_{sl}} \right)^2 \right]^{3.5} - 1 \quad (12.7)$$

e. Use the Mach equation for:

$$M_{ic} = \sqrt{5 \left[\left(\frac{q_{cic_t}}{p_{s_t}} + 1 \right)^{2/7} - 1 \right]} \quad (12.8)$$

where

$$\frac{q_{cic_t}}{p_{s_t}} = \frac{\frac{q_{cic_t}}{p_{a_{sl}}}}{\delta_{ic_t}} \quad (12.9)$$

3. Standardize ΔH_{pc} and V_{ic} . Altimeter position error and instrument corrected velocity are standardized to 2,300 feet for the tower fly-by test at Edwards.

- a. Find ΔH_{pc_t} . The necessary information is available to compute altimeter position error correction ΔH_{pc} at the test H_{ic} and M_{ic} . The test points were taken in steady state conditions when lag correction is zero so the test altimeter position error correction is computed according to

$$\Delta H_{pc_t} = H_{c_t} - H_{ic_t} \quad (12.10)$$

This is one form of position error for the test conditions H_{ic} , M_{ic} , and gross weight.

- b. Correct ΔH_{pc_t} to $\Delta H_{pc_{2300}}$ (12.11)

The altimeter position error must be standardized to one altitude. Each data point was taken at a different instrument corrected altitude, H_{ic} , and must be corrected to a common H_{ic} for comparison. When altitude changes are small or angle of attack effects are not significant the following correction can be made:

$$\Delta H_{pc_{2300}} = \Delta H_{pc_t} \frac{\theta_{s_{2300}}}{\theta_{s_t}} \quad (12.12)$$

where θ_{s_t} is the standard temperature ratio evaluated at the H_{ic} of the test aircraft.

$$\theta_{s_t} = 1 - 6.87559 \times 10^{-6} H_{ic_t} \quad (12.13)$$

- c. Correct V_{ic_t} to $V_{ic_{2300}}$. Altimeter position error is assumed to be a function of M_{ic} and H_{ic} rather than V_{ic} and H_{ic} so a corrected V_{ic} is computed assuming the data point was flown at an H_{ic} of 2,300 feet and the test M_{ic} . From Equation 12.8, the differential pressure ratio for the standard altitude of 2,300 feet is the same as that for the test altitude.

$$\frac{q_{cic_{2300}}}{P_{s_{2300}}} = \frac{q_{cic_t}}{P_{s_t}} \quad (12.14)$$

From

$$\frac{q_{cic_{2300}}}{P_{a_{sl}}} = \left(\frac{q_{cic_t}}{P_{s_t}} \right) \delta_{2300} \quad (12.14)$$

$V_{ic_{2300}}$ can be computed using the calibrated airspeed equation.

$$V_{ic_{2300}} = a_{sl} \sqrt{5 \left[\left(\frac{q_{cic_{2300}}}{P_{a_{sl}}} + 1 \right)^{2/7} \right] - 1} \quad (12.16)$$

4. The parameter nW/δ_{ic} is necessary to evaluate the angle of attack effect. First, determine the most representative gross weight. The gross weight and speed determine what angle of attack is required for flight at a given Mach during a level steady state test point. The gross weight during the low speed test points is most representative because of the relatively high angle of attack.

$$nW/\delta_{2300} = \frac{\text{Average Low Speed Gross Weight}}{\delta_{2300}} \quad (12.17)$$

The ratio W/δ cannot be held constant for a tower fly-by test so all low speed points should be flown at nearly the same gross weight. During pacer missions, W/δ may be held constant by increasing altitude as the gross weight decreases to eliminate the angle of attack effect entirely.

Sideslip angle may also affect position error. If sideslip angle effects are suspected, data points should be repeated with known variations in sideslip angle.

5. Calculate the other forms of position error, position error pressure ratio $\Delta P_p/P_s$, airspeed position error correction ΔV_{pc} , Mach position error correction ΔM_{pc} , and position error pressure coefficient, $\Delta P_p/q_{cic}$.

$$a. \quad \Delta P_p/P_s = \frac{3.61382 \times 10^{-5}}{\theta_{st}} \Delta H_{pc} \quad (12.18)$$

where θ_{st} is the standard atmospheric temperature ratio

$$\theta_{st} = 1 - 6.87559 \times 10^{-6} H_{ic} \quad (12.19)$$

Position error pressure ratio is the difference between static and ambient pressure to ambient pressure

$$\frac{\Delta P_p}{P_s} = 1 - \frac{\delta}{\delta_{ic}} \quad (12.20)$$

and is a convenient form of position error for determining ΔV_{pc} and ΔM_{pc} .

$$b. \quad \Delta V_{pc} = \frac{a_{sl}^2 \delta_{ic}}{1.4 V_{ic} \left[1 + 0.2 \left(\frac{V_{ic}}{a_{sl}} \right)^2 \right]^{2.5}} \frac{\Delta P_p}{P_s} \quad (12.21)$$

This conversion is good for $V_{ic} \leq 661.48$ knots.

$$c. \quad \Delta M_{pc} = \frac{(1 + 0.2 M_{ic}^2)}{1.4 M_{ic}} \frac{\Delta P_P}{P_S} \quad (12.22)$$

This conversion is good for $M_{ic} \leq 1.0$.

$$d. \quad \frac{\Delta P_P}{q_{cic}} = \frac{\Delta P_P/P_S}{q_{cic}/P_S} \quad (12.23)$$

This position error pressure coefficient should be plotted as a function of M_{ic} .

12.3.2 Pacer Data Reduction

With the exception of finding H_c and V_c , the data reduction is the same as for tower fly-by.

1. Find pacer aircraft H_c and V_c

$$H_{c_p} = H_{i_p} + \Delta H_{ic_p} + \Delta H_{pc_p} \quad (12.24)$$

$$V_{c_p} = V_{i_p} + \Delta V_{ic_p} + \Delta V_{pc_p} \quad (12.25)$$

Equations are available that represent position error for the pacer aircraft.

2. Find the test aircraft H_{ic_t} and V_{ic_t} as in the tower fly-by data reduction.
3. Determine altimeter position error ΔH_{pc} and airspeed position error ΔV_{pc} .

- a. Assume $H_{c_{\text{test aircraft}}} = H_{c_{\text{pacer aircraft}}}$ and $V_{c_{\text{test aircraft}}} = V_{c_{\text{pacer aircraft}}}$ since aircraft were level and co-speed.

- b. Find ΔH_{pc_t} and correct it to the desired test altitude as in tower fly-by data reduction.

$$c. \quad \Delta V_{pc_t} = V_c - V_{ic_t} \quad (12.26)$$

This yields airspeed position error ΔV_{pc} independently from the altitude method and provides a comparison to see if total pressure P_T is fully recovered.

d. Find ΔH_{pc_t} from the ΔV_{pc_t} using Equations 12.18 and 12.21.

e. Correct ΔH_{pc_t} determined from ΔV_{pc_t} to the desired test altitude and compare the results.

12.3.3 Radar Data Reduction

1. Select data point acquired from on-board instrumentation and correct for instrument error, if necessary.

$$H_{ic} = H_i + \Delta H_{ic} \quad (12.27)$$

2. Determine

$$H_{c_{pace}} = H_{i_p} + \Delta H_{ic_p} + \Delta H_{pc_p} \quad (12.28)$$

3. Change tapeline difference to pressure altitude difference through the temperature correction

$$\Delta H_c = \Delta h \frac{T_{a_s}}{T_{a_t}} \quad (12.29)$$

where $\Delta h = H_{R_{test}} - H_{R_{pace}}$ and H_R represent radar measured altitude.

4. Determine test pressure altitude and position error and standardize to the test altitude

$$\Delta H_{pc_t} = H_{c_t} - H_{ic} \quad (12.30)$$

5. Calculate velocity position error from ΔH_{pc} as in the tower fly-by method.

12.3.4 Speed Course Data Reduction

1. Find the average true airspeed V_T .

$$V_T = 1800 \left(\frac{D}{t_1} + \frac{D}{t_2} \right) \quad (12.31)$$

where D is the course length in nautical miles and t_1 and t_2 are the course times in seconds.

2. Ambient temperature: $T_a = (T_i + \Delta T_{ic} + 273.16) - \frac{K_t V_T^2}{7592}$ (12.32)

where K_t is the temperature recovery factor.

3. $M = \frac{V_T}{38.967 \sqrt{T_a}}$ (12.33)

$$4. \quad H_{ic_t} = H_i + \Delta H_{ic}$$

$$V_{ic_t} = V_i + \Delta V_{ic}$$

$$5. \quad a. \quad \frac{q_{cic_t}}{p_{asl}} = \left[1 + 0.2 \left(\frac{V_{cic_t}}{a_{sl}} \right)^2 \right]^{3.5} - 1 \quad (12.34)$$

$$b. \quad \delta_{ic_t} = \left[1 - 6.87559 \times 10^{-6} H_{ic_t} \right]^{5.2559} \quad (12.35)$$

$$c. \quad M_{ic} = \sqrt{5 \left[\left(\frac{q_{cic_t}}{p_{st}} + 1 \right)^{2/7} - 1 \right]} \quad (12.36)$$

where

$$\frac{q_{cic_t}}{p_{s_t}} = \frac{\frac{q_{cic_t}}{p_{a_{sl}}}}{\delta_{ic_t}} \quad (12.37)$$

6. $\Delta M_{pc} = M - M_{ic}$

Mach position error correction does not need to be standardized.

It always remains constant over small altitude changes and remains constant over large altitude changes if angle of attack effects are not significant.

7. Find position error pressure ratio $\Delta p/p_s$, altitude position error correction ΔH_{pc} , and airspeed position error correction ΔV_{pc} as in Section 5.7.2.3.

$$\frac{\Delta p}{p_s} = 1.4 \left[\frac{M_{ic} + \frac{\Delta M_{pc}}{2}}{1 + 0.2 M_{ic} + \frac{\Delta M_{pc}}{2}} \right] \Delta M_{pc} \quad (12.38)$$

8. Correct V_{ic_t} to $V_{ic_{2300}}$

Standardize V_{ic} to the instrument correct airspeed that would have been computed if the test Mach had been flown at the standard test altitude.

12.4 TAKEOFF DATA REDUCTION

Takeoff data will be recorded on all missions during the performance phase. The purpose is to determine the ground roll at the instant of lift-off and to correct this data for nonstandard conditions. While cinetheodolite data is the most accurate, the resources required prohibit its acquisition on all missions. Most data must come from pilot estimates. To improve the quality of this pilot estimated data, there are certain steps that should be taken.

1. Obtain current pressure altitude and temperature from ATIS or ground control just before takeoff; also record fuel used or remaining.
2. Record the wind speed and direction given by the tower with takeoff clearance.
3. Align the aircraft with a runway light for run-up. Consider selecting the appropriate light so predicted liftoff will be abeam a runway marker; e.g., with a predicted 2600 feet roll, line up three lights before a runway marker and expect to be airborne after passing two additional runway markers.
4. Assign one crewmember primary responsibility for obtaining takeoff airspeed, the other crewmember for distance, but attempt to verify each other's readings.
5. Take off using the test team's standardized procedures as specified in the test plan.

Reduction of takeoff data to standard conditions is not difficult but becomes rather tedious when accomplished manually due to the large number of data points required. By using Equations 12.41, 12.42 and 12.43 as a basis to correct for wind, slope, thrust, weight, and density, the test day data can be corrected for nonstandard conditions.

The use of these equations requires test day ground roll, ground speed, headwind, runway slope, aircraft test and standard weight, test and standard day air density and thrust. To determine these, collect the following data:

1. Takeoff speed (kts, V_{jc} for pilot data, V_{GS} for Cinetheodolite)
2. Ground roll distance, S_{gt} (ft)
3. Fuel remaining (lbs)
4. Runway temperature ($^{\circ}\text{C}$)
5. Pressure altitude (ft)
6. Wind speed, V_w (kts)
7. Wind direction, X_w (deg magnetic)
8. Runway heading, X_r (deg magnetic)
9. Runway slope angle, θ (deg)

Ground speed at liftoff is obtained directly from Cinetheodolite data. For pilot estimated data, indicated airspeed at liftoff must be used along with pressure and temperature to calculate true airspeed. Subtracting headwind yields the ground speed.

- a. Calculate headwind

$$V_{w_h} = V_w \cos (X_w - X_T) \quad (12.39)$$

- b. Calculate true airspeed and ground speed. For cinetheodolite data, ground speed is measured and true airspeed is calculated.

$$V_T = V_{GS} + V_{w_h} \quad (12.40)$$

For crew observed data, true airspeed, V_T , is obtained using pitot-static equations. Ground speed is calculated by subtracting the test day headwind.

$$V_{GS} = V_T - V_{w_h} \quad (12.40a)$$

- c. Correct ground roll for wind

$$S_{g_{cw}} = S_{g_t} \left(\frac{V_T}{V_{GS}} \right)^{1.85} \quad (12.41)$$

- d. Correct ground roll for slope

$$S_{g_{cs}} = \frac{S_{g_{cw}}}{1 - \frac{2g S_{g_{cw}} \sin \theta}{V_{GS}^2}} \quad (12.42)$$

- e. Standardize ground roll to sea level standard day for the test day true airspeed by applying thrust, weight, and air density, corrections.

$$S_{g_s} = S_{g_{cs}} \left(\frac{W_s}{W_t} \right)^{2.3} \left(\sigma_t \right) \left(\frac{F_{n_t}}{F_{n_s}} \right)^{1.3} \quad (12.43)$$

The terms F_{n_t} and F_{n_s} represent the test day and standard day net thrust respectively. These values are calculated from the model furnished by the manufacturer in the engine thrust deck. For example, Appendix D contains simplified thrust curves for the A-37B, T-38A and RF-4C aircraft. Knowledge of θ , δ , and M is sufficient to determine net thrust from these curves.

The weight and air density corrections to ground roll include not only their effect on acceleration, but also their effect on correct takeoff speed. A similar correction must be applied to the takeoff speed.

- f. Standardize takeoff speed for weight and air density.

$$V_{T_s} = V_T \left[\left(\frac{W_s}{W_t} \right) \sigma_T \right]^{1/2} \quad (12.44)$$

Standardized ground roll should be plotted as a function of standardized takeoff speed as shown in Figure 12.2.

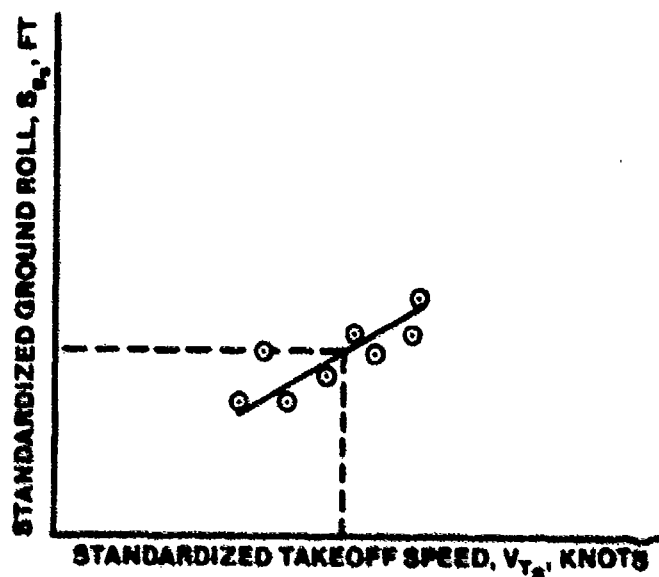


FIGURE 12.2. GROUND-ROLL TAKEOFF DISTANCE

There will be significant scatter in the data points since it is difficult to determine liftoff point and the corresponding ground-roll. Use of cinetheodolite data greatly improves the data, although most data will still be crew estimated. Since some data will represent higher than nominal takeoff speeds or late readings, and some will represent lower than nominal speeds or early readings, a curve through the data should be roughly parabolic. This corresponds to the curve one would obtain during a ground acceleration test. By plotting the final portion of the takeoff acceleration obtained from cinetheodolite missions, the shape of the curve can be obtained. This will assist in drawing a curve through the large number of data points. The sea level standard day takeoff distance is then read from the curve at the accepted takeoff speed.

12.5 ENERGY METHOD DATA REDUCTIONS

Energy characteristics are of paramount importance to the effectiveness of fighter aircraft. Specific excess power P_s , as a function of Mach, and altitude H , graphically display an aircraft's ability to climb, accelerate and turn.

12.5.1 Excess Thrust

Every performance parameter, except fuel flow, is a direct function of excess thrust

$$F_{\text{ex}} = F_n - D \quad (12.45)$$

where F_n = net thrust (along the flight path) and D = total drag

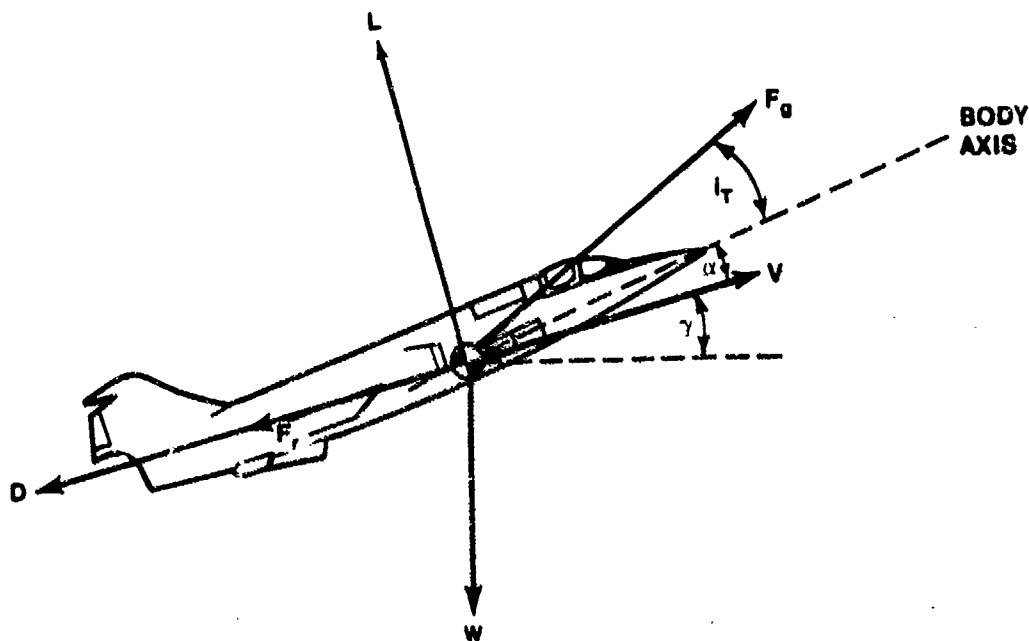


FIGURE 12.3. FORCE DIAGRAM

F_g = Gross thrust

F_r = Ram drag

i_T = Thrust incidence angle

α = Angle of attack

γ = Flight path angle

D = Drag

L = Lift

W = Weight

V = True airspeed

Summing Forces along the flight path (velocity vector)

$$\Sigma F_x = F_g \cos (i_T + \alpha) - F_r - D - W \sin \gamma = \frac{W}{g} \dot{V}$$

Defining

$$F_n = F_g \cos (i_T + \alpha) - F_r$$

$$a_x = \dot{V} + g \sin \gamma$$

Then

$$F_n - D = F_{ex} = \frac{W}{g} a_x \quad (12.46)$$

Similarly, perpendicular to the flight path,

$$\Sigma F_z = L + F_g \sin (i_T + \alpha) - W \cos \gamma = \frac{W}{g} V \dot{\gamma}$$

Defining normal acceleration,

$$a_z = V \dot{\gamma} + g \cos \gamma$$

Then

$$L + F_g \sin (i_T + \alpha) = \frac{W}{g} a_z \quad (12.47)$$

Note that Equations 12.46 and 12.47 make no assumptions concerning steady or non-steady flight. These equations are the basis for the in-flight measurement of F_{ex} by the use of flight path accelerometers or inertial systems.

Specific excess power is

$$P_s = \frac{F_{ex} V}{W} = \dot{H} + V \frac{\dot{V}}{g} \quad (12.48)$$

where \dot{H} is the true (tapeline) altitude rate of change, and V is the inertial velocity. This equation is fundamental to data reduction for many of the flight test methods, e.g.

Level, unaccelerated flight: $F_{ex} = 0$

Constant airspeed climbs/descents: $\dot{H} = F_{ex} V/W$

Climb potential from level accels: $\dot{H} = \frac{F_{ex} V}{W} - V \frac{\dot{V}}{g}$

Any performance parameter can be determined by knowing F_{ex} for an arbitrary set of flight conditions. This is the parameter that is most easily corrected to determine standard day performance. Therefore, F_{ex} is the basic performance parameter which must be determined from flight test.

12.5.2 Determination of F_{ex}

Classically, Equation 12.48 determined excess thrust from flight test data. By recording pitot-static data (H_1 and V_1) during a controlled maneuver, test day F_{ex} may be calculated directly. This method is inexpensive, reliable, but subject to many errors: instrument lag and hysteresis, the results of imprecise flying, and the need for precise temperature measurement. Additionally, time measurement must be very precise since rates must be calculated from difference equations, i.e.

$$\dot{V} = \frac{\Delta V}{\Delta t}, \quad \dot{H} = \frac{\Delta H}{\Delta t}$$

Another approach is the use of flight path accelerometers or inertial systems to measure a_x and a_z directly. These systems are accurate and do not require precise flying, but they are expensive and require precise measurement of angle of attack (to determine direction of the flight path). Upwash, vibrations, and nose boom bending can cause large errors.

Finally, H and V may be determined by radar or cinetheodolite tracking. The accuracy of this method depends on equipment accuracy, range, and atmospheric conditions (winds, pressure levels, etc.)

The first (pitot-statics) method is the most widely used and is used at the TPS.

12.5.3 Correction to Standard Conditions

There are several approaches to data reduction. They are similar in that they correct the flight test data for nonstandard conditions, essentially predicting the performance of the aircraft flown on a standard day at the standard altitude and at the standard weight. They differ primarily in the sequence and method in which the corrections are applied. One method is to apply corrections in a "one-at-a-time" sequence. This step-by-step method clearly delineates the assumptions and approximations used to reduce the data, but must be modified for each type of test to be analyzed. An example of this method is presented below for both climb and descent performance.

A more general approach is the method of standardizing excess thrust. This method used in the Test Pilot School's data reduction system, is described following the step-by-step method.

12.5.4 Climb Performance Data Reduction Using Step-By-Step Method

12.5.4.1 General. Once a climb speed schedule has been obtained, using any of the methods discussed in Chapter 9, the flight test program will call for a series of climbs to be performed to determine the following:

Rate of climb (or time to climb)

Fuel used during the climb

Distance traveled in climb

In order to permit meaningful comparison between flight test data performed under varying conditions, it is necessary to correct all values to some standard condition. Normally, all climb performance data are reduced to ICAO standard day conditions for comparison and presentation.

The fuel used and the distance traveled during the climb are, to a large degree, dependent upon the rate of climb. Therefore, the major emphasis is devoted to adjustments of the rate of climb.

Seven corrections are required in our analysis. Four are associated with temperature variables, one corrects for wind, and two result from nonstandard weight differences. The corrections are listed below in the order in which they are generally applied to climb data:

<u>Correction</u>	<u>Cause</u>
1. Tapeline altitude	Nonstandard temperature
2. True speed	Nonstandard temperature
3. Thrust	Nonstandard temperature
4. Wind	Wind <u>gradient</u>
5. Acceleration	Nonstandard temperature <u>lapse rate</u>
6. Inertia	Nonstandard weight
7. Induced drag	Nonstandard weight

In the following analysis the numerical rate of climb subscripts will maintain their identity from beginning to end. Subscript "t" will refer to test day uncorrected climb conditions. Subscript "1" will refer to values corrected for tapeline altitudes only. Each succeeding subscript will refer to values adjusted for all preceding corrections. The subscript "s" will refer to standard day data with corrections applied.

12.5.4.2 Tapeline Altitudes. With the aircraft altimeter set to 29.92" Hg, accurate values of H_c , and therefore of P_a , are available from climb data. But a given change in P_a on a test day does not represent the change in true, or "tapeline," altitude that it would represent on a standard day, since the change of pressure with altitude is not a linear function. Figure 12.4 illustrates the pressure versus altitude relationship for a standard day and for a hotter than standard day.

Let us assume that during a climb on a hotter than standard day our altimeter sensed a change of pressure of ΔP . Since the altimeter is constructed on a standard pressure lapse rate, this ΔP will register a change of altitude of ΔH_1 on the instrument. However, we are actually on the nonstandard pressure curve and our actual change of altitude would be ΔH_2 . As shown in Figure 12.4, this actual altitude, or true altitude change, is greater than registered by the altimeter. The additional energy for this increased altitude must be provided by the engine, and a correction is required to determine the standard day rate of climb.

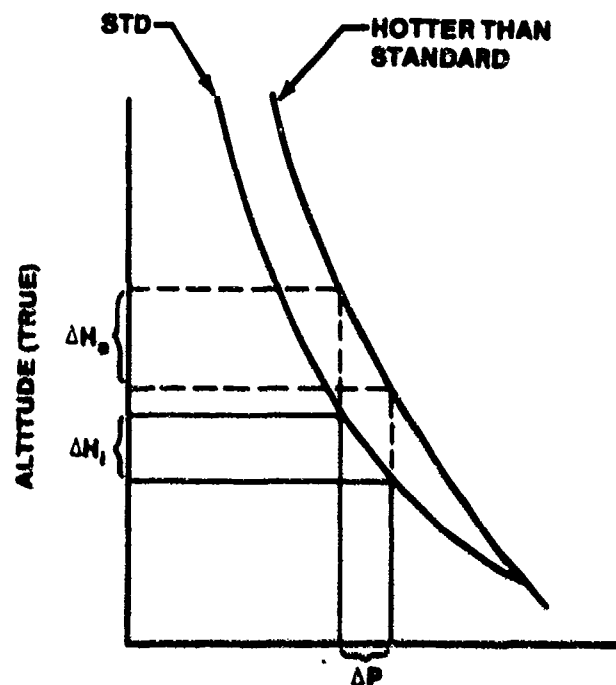


FIGURE 12.4. PRESSURE (ALTIMETER READING)

Since we fly pressure altitudes,

$$P_t = P_s \text{ (as sensed by altimeter)}$$

$$P_t = \rho_t gRT_t \quad P_s = \rho_s gRT_s$$

Therefore

$$\rho_t gRT_t = \rho_s gRT_s$$

or

$$\frac{\rho_s}{\rho_t} = \frac{T_t}{T_s}$$

Recall from Chapter 5 that

$$\frac{dH}{dP} = -\frac{1}{\rho g}$$

Then, for small changes,

$$\Delta H = -\frac{\Delta P}{\rho g}$$

For a given ΔP (as sensed by the altimeter)

$$\text{Indicated or apparent } \Delta H_i = -\frac{\Delta P}{\rho_s g}$$

$$\text{Actual } \Delta H_a = -\frac{\Delta P}{\rho_t g}$$

Now dividing ΔH_a by ΔH_i

$$\frac{\Delta H_a}{\Delta H_i} = \frac{\rho_s}{\rho_t} \text{ or } \Delta H_a = \Delta H_i \frac{\rho_s}{\rho_t}$$

Since

$$\frac{\rho_s}{\rho_t} = \frac{T_t}{T_s}$$

and dividing by Δt

$$\frac{\Delta H_a}{\Delta t} = \frac{\Delta H_i}{\Delta t} \frac{T_t}{T_s}$$

where $\Delta H_i/\Delta t$ is the apparent rate of climb (R/C_t) and $\Delta H_a/\Delta t$ is the actual rate of climb (R/C)

This can be written as

$$R/C_1 = R/C_t \frac{T_t}{T_s} \quad (12.49)$$

This is called the tapeline altitude correction. This correction is always applied to climb data. Temperatures are absolute and are taken at the midpoint of the altitude band under consideration.

12.5.4.3 True Speed and Thrust Correction. The nonstandard temperature effects on true speed and thrust are so closely related that they cannot be easily separated. A change in temperature will produce a change in thrust and in true speed, V , and the change in V will, in turn, produce a secondary change in thrust of a jet engine or in thrust horsepower of a piston engine or turboprop. Ultimately, the thrust correction must be based upon known thrust data, which is obtained from manufacturer's thrust stand data for the particular engine. For simplicity, the two effects (true speed and thrust) will be analyzed simultaneously and separated into the two causes after analysis. The analysis is based upon two premises:

- 1) Thrust horsepower available (THP_a) changes with true velocity and with thrust.
- 2) Thrust horsepower required (THP_r) or drag, changes with true velocity, but not with thrust. The only effect of temperature on drag is assumed to be through the change in V .

Assuming an unaccelerated climb and recalling the energy relationships

$$R/C = \frac{(F_n - D) V}{W}$$

$$R/C = \frac{F_n V - DV}{W}$$

$$F_n V = THP_a \text{ and } DV = THP_r$$

Then

$$\frac{THP_{a_s}}{THP_{a_t}} = \frac{F_{n_s} V_s}{F_{n_t} V_t}$$

Since $M_t = M_s$ and $V = M \sqrt{\gamma g R T} = K M \sqrt{T}$

$$THP_{a_s} = THP_{a_t} \left(\frac{F_{n_s}}{F_{n_t}} \sqrt{\frac{T_s}{T_t}} \right) \quad (12.50)$$

Similarly

$$THP_{r_s} = THP_{r_t} \left(\frac{D_s}{D_t} \sqrt{\frac{T_s}{T_t}} \right) \quad (12.51)$$

From aerodynamic theory, drag is given by

$$D = 1481 \delta M^2 S C_D$$

Assuming test and standard day C_D are equal (while this is not true, this correction will be made in step 7), and since $M_s = M_t$, then

$$\frac{D_s}{D_t} = \frac{\delta_s}{\delta_t} \quad (12.52)$$

Then

$$R/C_3 = \frac{THP_{a_s} - THP_{r_s}}{W} = \left[\frac{F_{n_s}}{F_{n_t}} \sqrt{\frac{T_s}{T_t}} THP_{a_t} - \frac{\delta_s}{\delta_t} \sqrt{\frac{T_s}{T_t}} THP_{r_t} \right] \frac{1}{W} \quad (12.53)$$

$$= \frac{\delta_s}{\delta_t} \sqrt{\frac{T_s}{T_t}} \left[\left(\frac{F_{n_s}}{\delta_s} \right) THP_{a_t} - THP_{r_t} \right] \frac{1}{W} \quad (12.54)$$

Let

$$\frac{F_{n_s}}{\delta_s} = \frac{F_{n_t}}{\delta_t} + \Delta \frac{F_n}{\delta}$$

Then

$$\frac{\left(\frac{F_{n_s}}{\delta_s}\right)}{\left(\frac{F_{n_t}}{\delta_t}\right)} = \frac{\left(\frac{F_{n_t}}{\delta_t}\right) + \left(\Delta \frac{F_n}{\delta}\right)}{\left(\frac{F_{n_t}}{\delta_t}\right)} = 1 + \frac{\left(\Delta \frac{F_n}{\delta}\right)}{\left(\frac{F_{n_t}}{\delta_t}\right)} \quad (12.55)$$

$$\begin{aligned} R/C_3 &= \frac{\delta_s}{\delta_t} \sqrt{\frac{T_s}{T_t}} \left[\left(1 + \frac{\left(\Delta \frac{F_n}{\delta}\right)}{\left(\frac{F_{n_t}}{\delta_t}\right)} \right) THP_{a_t} - THP_{r_t} \right] \frac{1}{W} \\ &= \frac{\delta_s}{\delta_t} \sqrt{\frac{T_s}{T_t}} \left[THP_{a_t} - THP_{r_t} \right] \frac{1}{W} + \frac{\delta_s}{\delta_t} \sqrt{\frac{T_s}{T_t}} \frac{THP_{a_t}}{W} \frac{\left(\Delta \frac{F_n}{\delta}\right)}{\left(\frac{F_{n_t}}{\delta_t}\right)} \\ &= \frac{\delta_s}{\delta_t} \sqrt{\frac{T_s}{T_t}} R/C_1 + \frac{\delta_s}{\delta_t} \sqrt{\frac{T_s}{T_t}} \frac{THP_{a_t}}{W} \frac{\left(\Delta \frac{F_n}{\delta}\right)}{\left(\frac{F_{n_t}}{\delta_t}\right)} \quad (12.56) \end{aligned}$$

For convenience, the second term of Equation 12.56 is designated $\Delta R/C_1$ and the equation becomes

$$R/C_3 = \frac{\delta_s}{\delta_t} \sqrt{\frac{T_s}{T_t}} R/C_1 + \Delta R/C_1 \quad (12.57)$$

Equation 12.57 is now the total correction for tapeline altitude, true speed, and thrust.

12.5.4.4 $\Delta R/C_1$ Determination. Values of $\Delta F_n/\delta$ must come from thrust data, and are often presented in chart form. For jet aircraft, a common approach is to organize the charts so that a plot will be entered with Mach, engine speed, N_t , and test day temperature, T_t , to get the generalized thrust parameter, $(F_n/\delta)_t$.

The same chart is entered at N_s and T_s to get a standard day thrust parameter, $(F_n/\delta)_s$

Then

$$\left(\Delta \frac{F_n}{\delta} \right) = \left(\frac{F_n}{\delta} \right)_s - \left(\frac{F_n}{\delta} \right)_t$$

Note that five variables, temperature, RPM, altitude, speed, and weight, go into the determination of the thrust effect $\Delta R/C_1$. If thrust stand data is available in the correct form at each speed, altitude, and temperature flown, then a simpler form of the $\Delta R/C_1$ equation can be used.

Substituting

$$\begin{aligned} \sqrt{\frac{T_s}{T_t}} &= \frac{V_s}{V_t} \text{ and } THP_a = F_n V \\ \Delta R/C_1 &= \frac{\delta_s}{\delta_t} \frac{V_s}{V_t} \frac{F_{n_t} V_t}{W} \frac{\left(\Delta \frac{F_n}{\delta} \right)}{\left(\frac{F_{n_t}}{\delta_t} \right)} \\ \Delta R/C_1 &= \frac{V_s \delta_s}{W} \left(\Delta \frac{F_n}{\delta} \right) \end{aligned} \quad (12.58)$$

$\Delta R/C_1$ is usually a large correction and is always applied to nonstandard climb data.

12.5.4.5 Wind Correction. A wind of constant velocity will not affect the rate of climb of an aircraft regardless of its magnitude or direction. However, it is normal to experience some wind gradient in a climb even under

the best of conditions. A wind gradient affects the climb performance in two ways. First, if an aircraft is climbing into an increasing headwind (called a positive gradient), its inertia will carry it along at essentially a constant inertial speed. But the increased headwind velocity will register on the pitot-static instruments as an increase in airspeed. The pilot will correct the airspeed by raising the nose of the aircraft, and the rate of climb will increase.

Secondly, if the wind direction changes, the relative wind vector is rotated and the effect on the pitot-static instruments is similar to a wind gradient. Since the mechanics of calculating this effect are quite detailed, and because the effect is usually much less than the gradient effect, it will not be considered during this discussion.

The term V_w will be used to denote the total resultant headwind/tailwind component. The wind gradient with altitude is equal to dV_w/dH . For purpose of analysis, dV_w/dH may be treated as a sudden acceleration equal in magnitude to the change in wind velocity. From the energy equations

$$\frac{(F_n - D) V}{W} = \frac{dH}{dt} + \frac{V}{g} \frac{dV}{dt}$$

Assuming an unaccelerated standard day climb

$$R/C_s = R/C_t + \frac{V}{g} \frac{dV}{dt}$$

Expanding dV/dt into $dV/dH \cdot dH/dt$

$$\begin{aligned} R/C_s &= R/C_t + \frac{V}{g} \frac{dV}{dH} \frac{dH}{dt} \\ &= R/C_t + \frac{V}{g} \frac{dV}{dH} R/C_t \end{aligned} \quad (12.60)$$

The quantity dV/dH is produced by, and is equal in magnitude to, the vertical wind gradient, dV_w/dH , but has the opposite sign. This is due to the difference in sign conventions between wind velocities and aircraft velocities. If we maintain the convention of a headwind being positive, the equation becomes

$$R/C_s = R/C_t - \frac{V}{g} \frac{dv_w}{dH} R/C_t \quad (12.61)$$

Recalling that we make corrections in the proper order and that we must always use test R/C corrected for all previous nonstandard conditions, the equation becomes

$$R/C_4 = R/C_3 - \frac{V}{g} \frac{dv_w}{dH} R/C_3 \quad (12.62)$$

where R/C_3 is the test rate of climb corrected for tapeline altitude, true speed, and thrust, and R/C_4 includes the wind correction.

As for most corrections, the wind correction is less valid if the error is large. Attempts are made to minimize the error by flying 90° to the wind direction, by flying in light winds, and by flying successive climbs in opposite directions when possible. This last procedure also serves as a check on the magnitude of wind error, since the vertical displacement of the R/C curve will be a direct measure of the wind gradient (Figure 12.5).

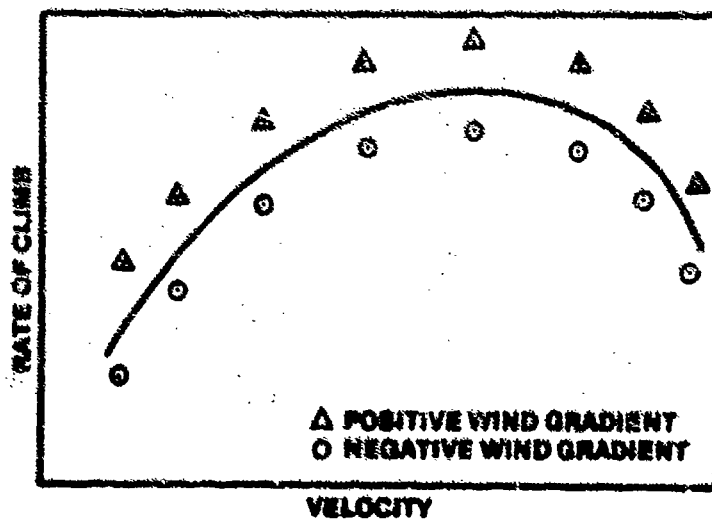


FIGURE 12.5. WIND GRADIENT EFFECT ON RATE OF CLIMB

Since winds are generally not constant in speed or direction during climbs, there will normally remain some residual error. The valid application of the wind correction equation requires that this wind gradient be known accurately. This requirement seriously limits the effective use of this correction. The release of a weather balloon at the time the climb is being performed will give fair, but far from perfect wind data. Normally, the correction equation is not used. Instead, the most widely used technique is to perform a number of climbs in different directions (90° to the wind, if possible) on different days, plot all data points on a single chart and draw an average line through them, and ignore the residual wind error altogether. It is hoped that the error will thus be averaged to a negligible value.

12.5.4.6 Acceleration Error. The first three corrections that were made adjusted the rate of climb for a nonstandard temperature. Compensation was made for a nonstandard true velocity due to nonstandard temperature. Under most actual atmospheric conditions, there will exist not only a temperature difference from standard, but a change in this temperature difference with altitude or a nonstandard temperature lapse rate. This comparison is illustrated in Figure 12.6.

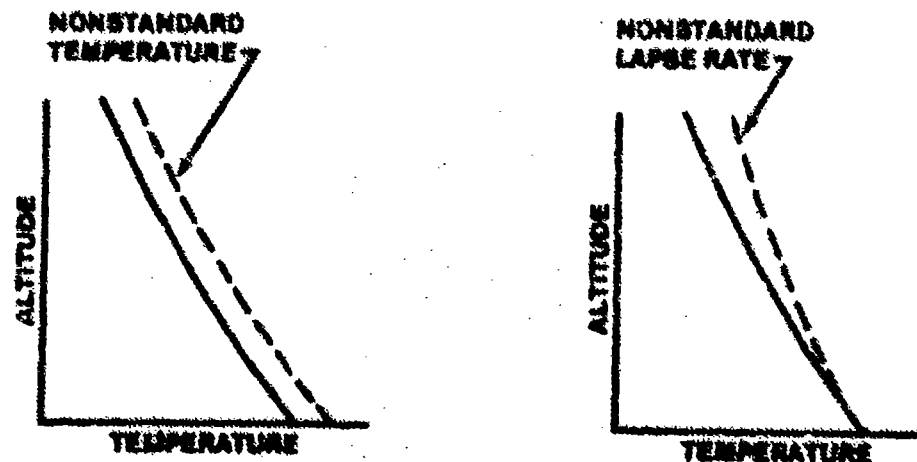


FIGURE 12.6.

Since true velocity changes with temperature (for a constant indicated velocity), this nonstandard temperature gradient will introduce a nonstandard acceleration for which a correction to the rate of climb must be applied.

Considering a climb during which data are taken at altitudes H_1 and H_2 , let $\Delta H = H_2 - H_1$, and $\Delta V = V_2 - V_1$, where V_1 is taken at H_1 and V_2 at H_2 . To correct this climb to zero acceleration it is only necessary to apply Equation 12.60

$$R/C_s = R/C_t + \frac{V}{g} \frac{dV}{dH} R/C_t$$

where dV/dH is obtained from test day data and is equal to $\Delta V/\Delta H$. However, this will produce the corrected rate of climb only if the desired standard day climb schedule is a constant V (zero acceleration) schedule. Most climb schedules are not constant V schedules, and a slightly different correction equation is required. If the test day acceleration between altitudes H_1 and H_2 is not equal to the desired standard day acceleration, the equation must be modified to

$$R/C_s = R/C_t + \left(\frac{V_t}{g} \frac{\Delta V_t}{\Delta H} - \frac{V_s}{g} \frac{\Delta V_s}{\Delta H} \right) R/C_t \quad (12.63)$$

assuming that $V_t \approx V_s$, then

$$R/C_s \approx R/C_t - \frac{V_t}{g \Delta H} (\Delta V_s - \Delta V_t) R/C_t$$

adjusting this to the usual form

$$R/C_5 \approx R/C_4 - \frac{V_t}{g \Delta H} (\Delta V_s - \Delta V_t) R/C_4 \quad (12.64)$$

where R/C_4 is corrected for tapeline altitude, true speed, thrust, and wind.

The acceleration correction is always applied to climb data and should be applied in incremental altitude bands.

12.5.4.7 Weight Corrections. "Standard weight" is determined by the test force and may be any weight so designated. The standard weight parameter, at any given altitude, should normally be the weight at level off following a

standard day takeoff and climb to that altitude. The standard weight often involves an average of many test weights and may be adjusted, if necessary, as the test program progresses.

Nonstandard weight of an aircraft affects its climb performance in two ways. First, an aircraft which is heavier than normal requires more energy from the engine to increase its altitude a given ΔH , since potential energy increase equals $W\Delta H$. Second, a heavier aircraft must have a higher wing loading to maintain equilibrium; therefore, at a given speed it must fly at a higher angle of attack and will generate more induced drag. This extra drag must also be overcome by the engine.

For purposes of this analysis it will be assumed that the total excess thrust $(F_n - D)$ is expended in generating rate of climb. While this is not strictly true in all cases, the portion of energy spent on acceleration will have little effect on the analysis.

From energy concepts

$$R/C = \frac{(F_n - D)}{W} V = \frac{F_n V - DV}{W}$$

Differentiating this expression with respect to weight

$$\frac{d(R/C)}{dW} = - \frac{(F_n - D) V}{W^2} - \frac{V}{W} \frac{dD}{dW}$$

The assumption was made that the small change in angle of attack due to weight will not affect the thrust (i.e. $dF_n/dW = 0$). Then, evaluating these terms at the test condition

$$\frac{d(R/C)}{dW} = - \left(\frac{R/C_t}{W_t} + \frac{V_t}{W_t} \frac{dD}{dW} \right)$$

Multiplying by dW , and using the weight changes $\Delta W = W_s - W_t$ for dW , $\Delta D = D_s - D_t$ for dD , and $\Delta R/C = R/C_s - R/C_t$ for $d(R/C)$

$$\Delta R/C_{\text{weight}} = - \left(R/C_t \frac{\Delta W}{W_t} + \frac{V_t}{W_t} \Delta D \right) \quad (12.65)$$

The first term in the parentheses in the above equation is the effect of increased potential energy required for heavier aircraft, and is called the "inertia effect". The inertia correction by convention is called $\Delta R/C_2$ and is given by

$$\Delta R/C_2 = R/C_t \frac{(W_t - W_s)}{W_t} \quad (12.66)$$

$$\Delta R/C_2 = R/C_5 \frac{(W_t - W_s)}{W_t} \quad (12.67)$$

where R/C_5 incorporates all previous corrections.

The "induced drag" portion of the weight correction is derived from an equation for induced drag in terms of known aircraft parameters as follows:

$$D_i = \frac{K(nW)^2 \cos^2 \gamma}{b^2 e M^2 \delta} \quad (12.68)$$

when K is a dimensional constant.

The change in induced drag caused by weight is then

$$\Delta D_i = \frac{K \cos^2 \gamma}{b^2 M^2 e \delta_t} (W_s^2 - W_t^2) \quad (12.69)$$

12.5.4.8 Summary. Using the above information, the total standard day correction for climb performance may be summarized as

$$R/C_1 = (R/C_t) \frac{T_t}{T_s}$$

$$\Delta R/C_1 = \frac{V_s \delta_s}{W_t} \left(\frac{F_{n_s}}{\delta_s} - \frac{F_{n_t}}{\delta_t} \right)$$

$$R/C_3 = R/C_1 \frac{\delta_s}{\delta_t} \sqrt{\frac{T_s}{T_t}} + \Delta R/C_1$$

$$R/C_4 = R/C_3 - \frac{V_t}{g} \frac{dV_w}{dH} R/C_3$$

$$R/C_5 = R/C_4 - \frac{V_t}{g} \left(\frac{\Delta V_s}{\Delta H} - \frac{\Delta V_t}{\Delta H} \right) R/C_4$$

$$\Delta R/C_{\text{weight}} = R/C_5 \frac{(W_t - W_s)}{W_t} + \frac{V_t}{W_t} \frac{K \cos^2 \gamma}{b^2 M^2 e \delta_t} (W_t^2 - W_s^2)$$

$$R/C_S = R/C_5 + \Delta R/C_{\text{weight}}$$

Applying the corrections in this order should result in the larger corrections being applied first to minimize errors. This may not always occur, particularly if the test weight varies considerably from standard. But in most cases, climb tests are made directly from takeoff and weight corrections can be kept small.

12.5.5 Descent Performance Data Reduction Using Step-By-Step Method

Descent performance can be analyzed in exactly the same manner as climb performance, and the same equations apply. Obviously, a negative rate of climb will result, which can be considered as a rate of descent if desired. Corrections to descent performance are not always as valid as those to climb performance, however.

12.5.5.1 Thrust Correction. Thrust data is usually complete for engines operating at military or maximum power. At idle power, however, data is not complete, and the engine trim is often less reliable. Since the thrust is usually relatively small at idle, it is often a good procedure to simply consider it zero and apply no thrust correction. Of course, an increase in thrust will decrease the rate of descent.

12.5.5.2 Weight Correction. In a descent, the induced drag portion of the weight correction will remain as in the climb. The inertia portion is different in a descent since the forward component of force acting on the aircraft is primarily a component of weight.

A change in weight will result in a change in induced drag but also in the component opposing drag. If the speed is held constant the result may be an increase or a decrease in rate of descent depending upon whether the glide speed is above or below that for best L/D ratio. If the best L/D is maintained, the induced drag will remain constant, and the glide angle will also remain very nearly constant, but the rate of descent will increase.

In flight test operations descents can usually be made at or near the desired standard descent weight, and the weight ambiguity can usually be neglected.

12.5.6 Standardization of Excess Thrust.

While the step-by-step method clearly delineates each assumption and approximation to correct climb performance data to standard day conditions, it is extremely laborious and must be modified for each type of test. A simpler, and more general technique is to standardize the excess thrust to standard day conditions. This allows each energy test (level accel, sawtooth climb, check climb, descent, and turns) to be analyzed using a similar approach.

The first step is to calculate the test day excess thrust using the expression

$$F_{ex_t} = \frac{W_t}{V_t} \left(\dot{H}_t + \frac{V_t \dot{V}_t}{g} \right) \quad (12.70)$$

where V_t is the average true airspeed on the test day, \dot{V}_t is its rate of change at the instant under investigation, and \dot{H}_t is the rate of change of the aircraft's tapeline altitude. This can be obtained from calibrated altitude, using the same tapeline altitude correction derived in the step by step approach, that is

$$\dot{H}_t = \dot{H}_c \left(\frac{T_t}{T_s} \right) \quad (12.71)$$

The second step is to estimate, or predict, what the excess thrust would have been on a standard day by using the relationship

$$F_{ex_s} = F_{ex_t} + \Delta I_n - \Delta D \quad (12.72)$$

The terms ΔF_n and ΔD represent the predicted change in the net thrust and drag, respectively, between the test day and standard day.

$$\Delta F_n = F_{n_s} - F_{n_t} \quad (12.73)$$

$$\Delta D = D_s - D_t$$

As with the step-by-step method, the change in the net thrust is calculated by using engine thrust data provided by the manufacturer. Test day and standard day drag are calculated by using the relationship

$$D = 1481 \delta M^2 SC_D$$

where δ and M are measured in the flight test and C_D can be calculated from C_L , using the aircraft's drag polar. The aircraft lift coefficient, C_L , is calculated from the relationship

$$C_L = \frac{nW}{1481 \delta M^2 S}$$

where n and W are measured quantities.

At first glance the need for both the engine thrust data and the aircraft's drag polar to perform the data reduction appears to be a ridiculous requirement. Given thrust and drag, the performance characteristics being tested could be calculated. So why bother with the test? The answer lies in how this data is used. While test day net thrust and drag are calculated from the thrust data and drag polar, respectively, they are not used in an absolute sense. They are used only to obtain correction terms. That is, test day net thrust is not used by itself but only in conjunction with standard day net thrust to calculate the delta change. As a result, small errors in the thrust data have little effect on the accuracy of the data reduction, provided standard day and test conditions are nearly identical. This is because bias error will be present in both and should cancel. This is in contrast to the accuracy requirement for predicting aircraft performance from thrust data and drag polar, without any test data. In this case, errors in either will translate directly into errors in predicted excess thrust and therefore

aircraft performance. In summary, while data reduction requires thrust curves and a drag polar, these data can be slightly in error (i.e. estimated data) without significantly affecting the quality of the flight test data reduction.

The third, and final step, is to use the predicted excess thrust to calculate the other quantities of interest. For example, standard day specific excess power can be calculated from

$$P_{s_s} = \frac{F_{ex_s} V_s}{W_s} \quad (12.75)$$

and standard day climb performance can be calculated from

$$\dot{H}_s = \frac{F_{ex_s} V_s}{W_s} - \frac{V_s \dot{V}_s}{g} \quad (12.76)$$

where \dot{V}_s represents the rate of change of true airspeed associated with the desired climb schedule.

12.5.7 Level Acceleration and Sawtooth Climb Data Reduction

The level acceleration and sawtooth climb tests are used to gather data to determine P_s and to predict sustained turn capability. From a data reduction point of view the two techniques are similar, only differing in the magnitude of the altitude rate versus airspeed rate terms. A time history of the following parameters is the required input to the data reduction.

Altitude, H_i (ft)

Indicated Airspeed, V_i (ft/sec)

Engine RPM, N (RPM)

Outside Air Temperature, T_a ($^{\circ}$ K)

Aircraft Weight, W_t (lbs)

In addition, the altitude at which the data are to be standardized, as well as the corresponding aircraft's standard weight, W_s (lb) are required. The following calculations should then be performed.

- a. Use pitot-static relationships to calculate

$$H_{c1}, V_{T1}, T_{a1}, M_1$$

$$H_{c2}, V_{T2}, T_{a2}, M_2$$

where the subscripts 1 and 2 refer to two adjacent data points, e.g. two different speeds for level acceleration tests or two altitudes for a sawtooth climb.

- b. Calculate test day average values

$$H_c = \frac{H_{c1} + H_{c2}}{2}$$

$$M = \frac{M_1 + M_2}{2}$$

$$T_t = \frac{T_{a1} + T_{a2}}{2}$$

$$W_t = \frac{W_{t1} + W_{t2}}{2}$$

$$N = \frac{N_1 + N_2}{2}$$

- c. Use pitot-static relationships to calculate the following test and standard day parameters.

$$V_{Tt}, \delta_t, \theta_t \text{ calculated from } H_c, M, T_t$$

$$V_{Ts}, \delta_s, \theta_s \text{ from } M \text{ and standard altitude}$$

d. Calculate rates

$$\dot{H}_C \approx \frac{H_{C2} - H_{C1}}{\Delta t} \quad (12.78)$$

$$\dot{V}_{T_t} \approx \frac{V_{T2} - V_{T1}}{\Delta t} \quad (12.79)$$

where Δt is the recorded time difference between data points 1 and 2.

e. Calculate test day parameters

$$F_{ex_t} = W_t \left[\frac{\dot{V}_{T_t}}{g} + \frac{\dot{H}_C}{V_{T_t}} \frac{T_t}{T_s} \right]$$

where T_s is the standard day ambient temperature at the test altitude^s

$$\gamma_t = \sin^{-1} \left[\frac{\dot{H}_C}{V_{T_t}} \frac{T_t}{T_s} \right] \quad (12.80)$$

$$C_{L_t} = \frac{W_t \cos \gamma_t}{1481 M^2 S \delta_t}$$

C_{D_t} : From drag curve using C_{L_t} and M

$$D_t = (1481 M^2 S \delta_t) C_{D_t}$$

F_{n_t} : From thrust curve using M , N , θ_t , and δ_t

f. Calculate standard day parameters

$$C_{L_s} = \frac{W_s}{1481 M^2 S \delta_s}$$

C_{D_s} : From drag curve using C_{L_s} and M

$$D_s = 1481 M^2 S \delta_s C_{D_s} \quad (12.81)$$

F_{n_s} : From thrust curve using M, N, θ_s , and δ_s

$$\Delta D = D_s - D_t$$

$$\Delta F_n = F_{n_s} - F_{n_t}$$

$$F_{ex_s} = F_{ex_t} + \Delta F_n - \Delta D$$

- g. Calculate standard day specific excess power, P_s

$$P_{s_s} = F_{ex_s} \frac{V_{T_s}}{W_s} \quad (12.82)$$

- h. Predict the aircraft's sustained turn capability by assuming that lift can be increased until the increased drag balances the calculated standard day excess thrust.

$$C_{D_{lim_s}} = C_{D_s} + \frac{F_{ex_s}}{1481 M^2 S \delta_s}$$

$C_{L_{lim_s}}$: From drag curve using $C_{D_{lim_s}}$ and M

$$n_{lim_s} = \frac{C_{L_{lim_s}}}{C_{L_s}}$$

The standard day specific excess power, P_{ss} , should then be plotted versus Mach for a specific standard altitude and power setting. A family of these curves, for various altitudes, is shown in Figure 12.7:

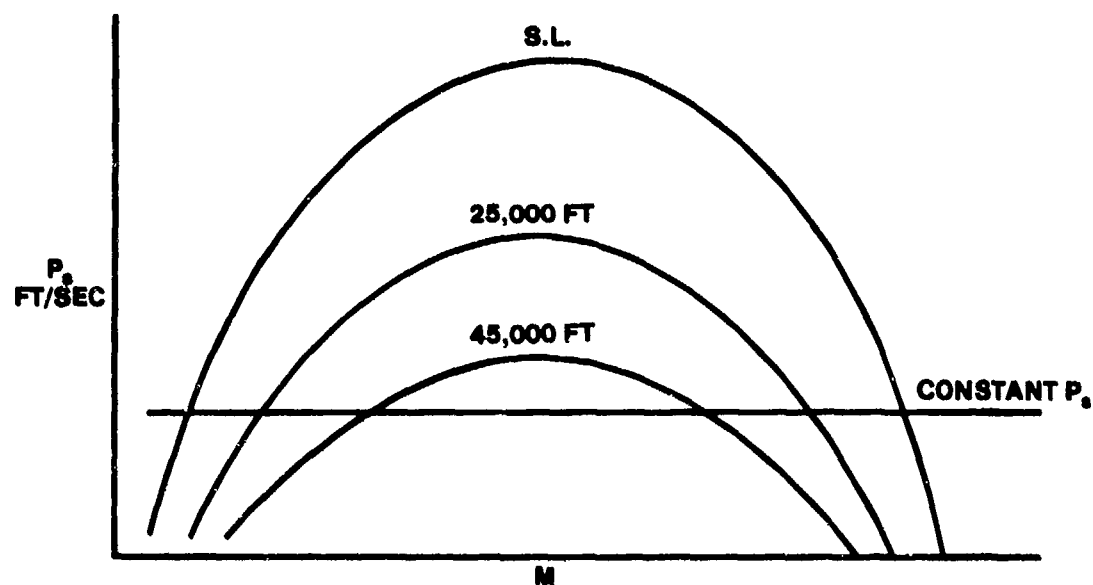


FIGURE 12.7. P_s VERSUS M FROM LEVEL ACCEL

The contour plot of constant P_s as a function of altitude and Mach (Figure 12.8) can now be generated. By drawing lines at constant P_s and reading off the Mach corresponding to each altitude, the following crossplot is produced.

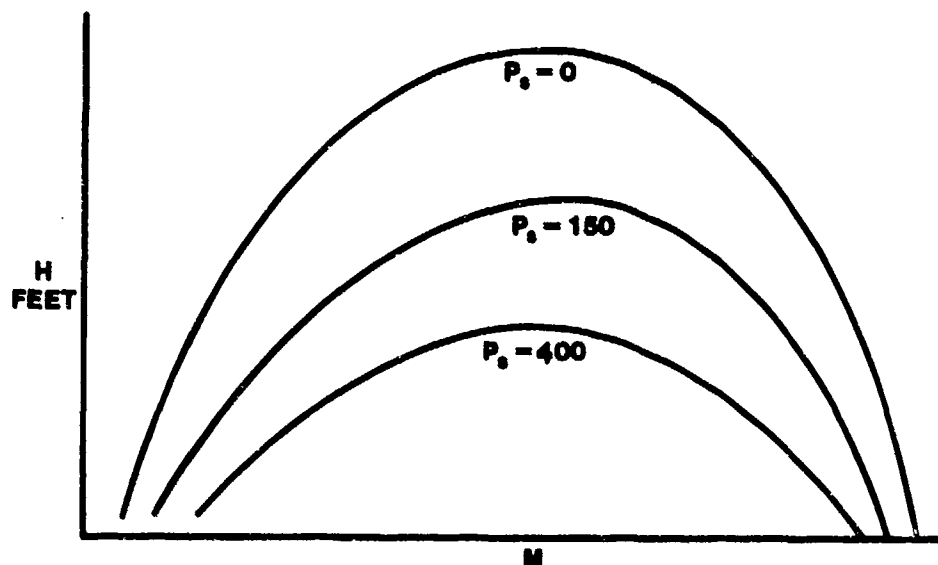


FIGURE 12.8. P_s VERSUS H AND M FROM LEVEL ACCEL

On this chart, the climb schedule for maximum rate of climb can be found by a line joining the peaks of the curves. Lines of constant specific energy may also be drawn and the points where these are tangent to the lines of constant P_s will define the optimum energy climb schedule (Figure 12.9).

In practice, it is easier and almost as accurate to obtain an approximation of the optimum energy climb schedule. This is done by selecting an altitude one percent below the peak of any P_s curve and finding a point at this altitude on the high speed side. Joining these points will give a climb schedule which, for the subsonic case, will usually agree with the optimum energy climb within the accuracy of data obtained. A supersonic climb schedule may also be found from this plot, although approximate methods may not be effective.

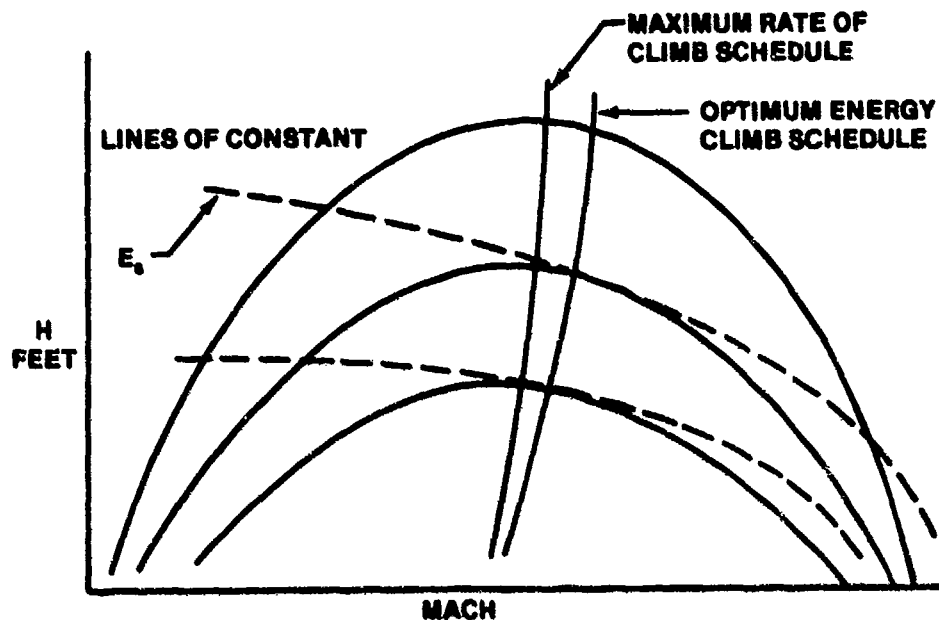


FIGURE 12.9. CLIMB SCHEDULES FROM LEVEL ACCEL DATA

The maximum sustainable load factor, n_{lim_g} , predicted from level acceleration data should be plotted versus Mach for a specific altitude and power setting. This data should be compared with the data generated during the turn performance test to assure agreement. But since the standard weight for level acceleration tests is frequently different than that for turn performance, care should be taken to use a common standard weight when comparing these two methods.

12.5.8 Check Climb Data Reduction

A series of check climbs are flown to verify and refine the optimum climb schedule predicted by the level acceleration tests. It is important that the pilot accurately fly the prescribed schedule since the data reduction technique described below uses the test day climb schedule in the standard day calculations. To analyze check climb data, a time history of the following parameters should be recorded:

Altitude, H_i (ft)

Indicated Airspeed, V_i (ft/sec)

Engine RPM, N (RPM)

Outside Air Temperature, T_a ($^{\circ}$ K)

Aircraft Weight, W_t (lbs)

The standard weight, W_{s_0} (lbs) at the initial altitude of the check climb is required.

Check climb data is analyzed by breaking the climb into a series of small altitude bands, with the previous list of parameters recorded at the bottom and the top of each band. Pairs of data points are analyzed to predict the standard day rate of climb, time to climb, fuel used, distance traveled, and aircraft weight for that data band. The cumulative standard day time, fuel, distance, and weight are then calculated by summing the time, fuel used, and distance for each of the individual data bands.

- a. For the "n+1" data band, use pitot-static relationships to calculate:

$$H_{C_1}, V_{T_1}, T_{a_1}, M_1$$

$$H_{C_2}, V_{T_2}, T_{a_2}, M_2$$

where the subscripts 1 and 2 refer to the bottom and top data points, respectively, of the data interval. The data reduction technique calculates the standard day rate of climb, based upon this test data, for an altitude and Mach that is the average of the test day values.

- b. Calculate test day average values:

$$H_C = \frac{H_{C_1} + H_{C_2}}{2} \quad (12.77)$$

$$M = \frac{M_1 + M_2}{2}$$

$$T_t = \frac{T_{a1} + T_{a2}}{2}$$

$$W_t = \frac{W_{t1} + W_{t2}}{2}$$

$$N = \frac{N_1 + N_2}{2}$$

- c. Use pitot-static relationships to calculate the following test and standard day parameters:

$$V_{T_t}, \delta_t, \theta_t \text{ calculated from } H_c, M, T_t$$

$V_{T_s}, \delta_s, \theta_s$ calculated from M and the standard altitude. For check climb data, the standard altitude is assumed to be the same as the test day pressure altitude, and therefore:

$$\delta_s = \delta_t \text{ (hereafter referred to as simply } \delta)$$

- d. Calculate rates

$$\dot{H}_c = \frac{H_{c2} - H_{c1}}{\Delta t_t} \quad (12.78)$$

$$\dot{V}_{T_t} = \frac{V_{T2} - V_{T1}}{\Delta t_t} \quad (12.79)$$

$$\dot{W}_t = \frac{W_{t2} - W_{t1}}{\Delta t_t} \quad (12.83)$$

where Δt_t is the recorded time difference between data points 1 and 2.

e. Calculate test day parameters

$$\dot{H} = \dot{H}_c \frac{T_t}{T_s}$$

where T_s is the standard day ambient temperature at the test altitude.

$$F_{ex_t} = W_t \left[\frac{\dot{V}_{T_t}}{g} + \frac{\dot{H}}{V_{T_t}} \right]$$

$$\gamma_t = \sin^{-1} \left(\frac{\dot{H}}{V_{T_t}} \right) \quad (12.80)$$

$$C_{L_t} = \frac{W_t \cos \gamma_t}{1481 M^2 S \delta}$$

C_{D_t} : From drag curve using C_{L_t} and M

$$D_t = 1481 M^2 S \delta C_{D_t}$$

F_{n_t} : From thrust curve using M , N , θ_t , and δ

f. Calculate standard day parameters:

F_{n_s} : From thrust curve using M , N , θ_s , and δ

$$\dot{W}_s = \dot{W}_t + \Delta \dot{W}$$

where $\Delta \dot{W}$ is the difference in the engine fuel flow between the test day and the standard day. This can be calculated by using manufacturer's charts of the engine characteristics. If the engine is a single spool jet engine, the fuel flow should be described by the following functional relationship, as described in Chapter 7.

Corrected fuel flow = function of Mach and
corrected RPM

$$\frac{\dot{W}}{\delta \sqrt{\theta}} = f(M, N/\sqrt{\theta})$$

If fuel flow is of this form, then ΔW can be calculated from M , N , δ (since $\delta_s = \delta_t$), θ_s , and θ_t .

Since rate of climb depends upon the aircraft standard weight, and standard weight depends upon time to climb, an iterative approach is necessary to complete the check climb data reduction. Certain variables must be initialized and are then updated each iteration through the loop.

$$\gamma = \gamma_t$$

$$\Delta t = \Delta t_t$$

$$W = W_{s_n} - \dot{W}_s \frac{\Delta t}{2}$$

The subscript "n" on W_s refers to the aircraft standard weight at the top of the previous or "nth" data interval. This is found by subtracting the fuel used during each of the first "n" data intervals from the aircraft standard weight at the start of the climb, W_{s_0} . For example, if the data being analyzed represents the sixth data pair, the average weight for this interval would initially be estimated to be the standard weight found at the top of the fifth data interval, less the initial estimate of the fuel used during half the sixth interval.

Start of iterative loop

$$C_L = \frac{W \cos \gamma}{1481 M^2 S \delta}$$

C_D : From drag curve using C_L and M

$$D = 1481 M^2 S \delta C_D$$

$$\Delta F_n = F_{n_s} - F_{n_t}$$

$$\Delta D = D - D_t \quad (12.85)$$

$$F_{ex} = F_{ex_t} + \Delta F_n - \Delta D$$

$$\dot{H} = V_{T_s} \frac{F_{ex}}{W} - \frac{\Delta V_{T_s}}{g \Delta t}$$

where ΔV_{T_s} is the desired climb schedule, assumed to be the same as the schedule flown on the test day. Therefore

$$\Delta V_{T_s} = V_{T_{s_2}} - V_{T_{s_1}}$$

where $V_{T_{s_1}}$ and $V_{T_{s_2}}$ are calculated using M_1 , M_2 and the standard day temperature at H_{C_1} and H_{C_2} .

$$\gamma = \sin^{-1} \left(\frac{\dot{H}}{V_{T_s}} \right)$$

$$\Delta t = \frac{H_{C_2} - H_{C_1}}{\dot{H}}$$

$$W = W_{s_r} + \dot{W}_s \frac{\Delta t}{2}$$

Check for convergence by comparing the rate of climb, \dot{H} , calculated on two successive passes through the above calculation. If the rate of climb has not converged, the calculation beginning with the evaluation of C_L should be

repeated, but now using the updated values for γ , W , and Δt . The following calculations should be performed after convergence has been achieved.

$$C_{L_s} = \frac{W \cos \gamma}{1481 M^2 S \delta}$$

C_{D_s} : From drag curve using C_{L_s} and M

$$D_s = 1481 M^2 S \delta C_{D_s}$$

$$\Delta F_n = F_{n_s} - F_{n_t}$$

$$\Delta D = D_s - D_t \quad (12.86)$$

$$F_{ex_s} = F_{ex_t} + \Delta F - \Delta D$$

$$H_s = \frac{V_{T_s} F_{ex_s}}{W} - \frac{\Delta V_{T_s}}{g \Delta t}$$

$$\Delta t_s = \frac{H_{c_2} - H_{c_1}}{\dot{H}_s}$$

$$W_s = W_{s_n} + \dot{W}_s \frac{\Delta t_s}{2}$$

$$P_{s_s} = F_{ex_s} \cdot \frac{V_{T_s}}{W_s}$$

- g. Calculate cumulative horizontal distance traveled, time to climb, fuel used, and aircraft weight at the altitude corresponding to the top of the data interval, that is H_{c_2} .

$$\text{Dist}_{n+1} = \text{Dist}_n + V_{T_s} \Delta t_s$$

$$\text{Time}_{n+1} = \text{Time}_n + \Delta t_s$$

$$\text{Fuel Used}_{n+1} = \text{Fuel used}_n + \dot{W}_s \Delta t_s \quad (12.87)$$

$$W_{s_{n+1}} = W_{s_n} - \dot{W}_s \Delta t_s$$

The quantities Dist_0 , Time_0 , and Fuel Used_0 represent the distance, time, and fuel used at the start of the climb. They can be initialized at zero or to other values to account for the distance, time, and fuel used during the takeoff, acceleration to climb speed, and the climb to the initial data altitude. Since they do not enter into the data reduction calculations, the only effect of these initial values is to shift the curves. The standard weight at the initial altitude, W_{s_0} , is an important factor in the data reduction and will change the shape and magnitude of the rate of climb.

After all the data intervals have been analyzed and cumulative values of distance, time, fuel, and weight have been generated, a series of plots can be made as shown in Figure 12.10. The dotted segments represent extrapolated values to sea level. Additional plots of fuel flow and airspeed or Mach could be shown in a similar fashion.

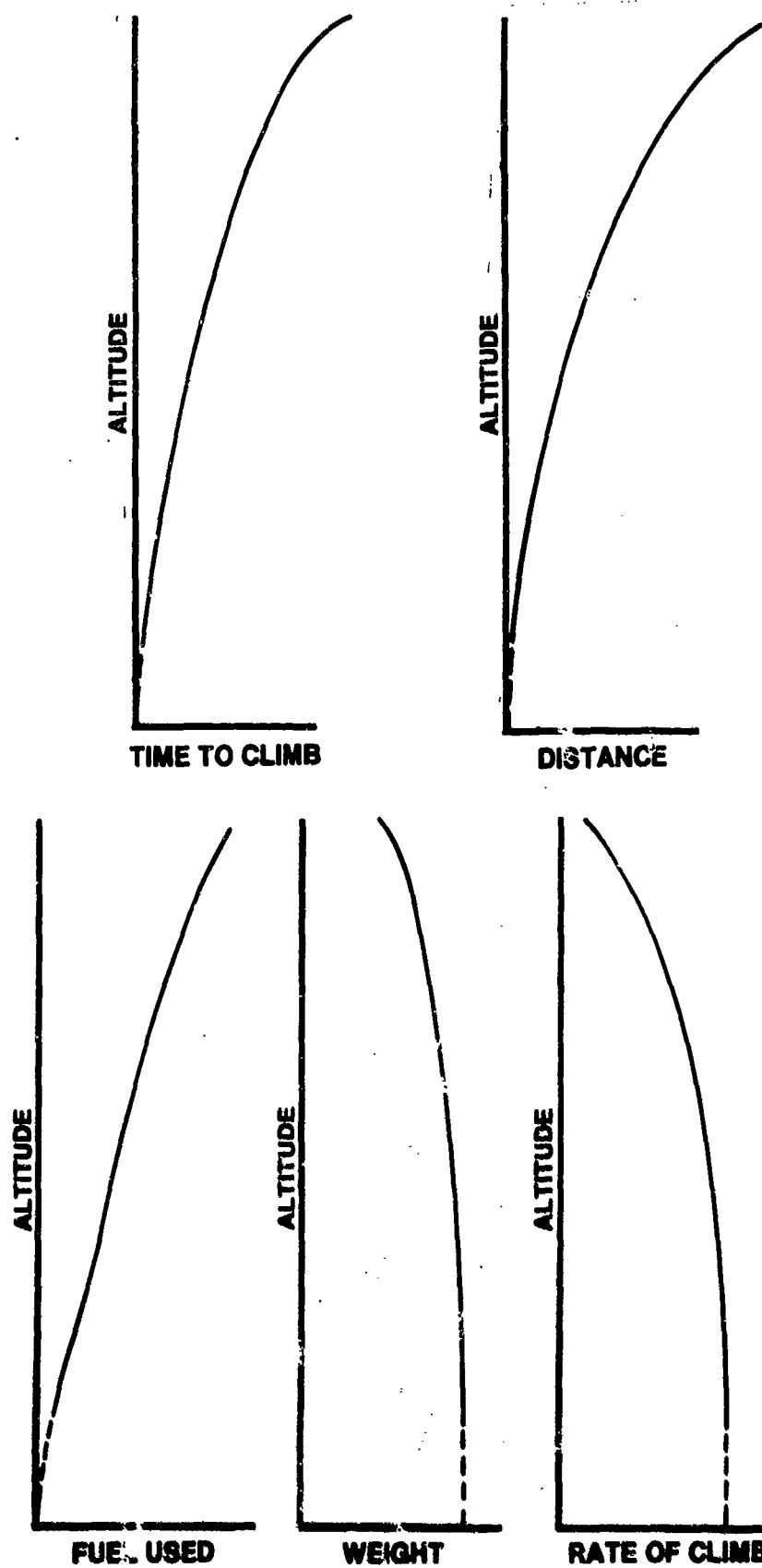


FIGURE 12.10. CLIMB PERFORMANCE SUMMARY

12.5.9 Turn Performance Data Reduction

The turn test is performed to determine an aircraft's sustained turn capability, and associated turn rate and turn radius, as a function of Mach and altitude at a specific power setting. The following data should be recorded during a stable turn.

Normal acceleration, n_t (g's) or time to complete a 360° turn, Δt (sec)

Indicated Altitude, H_i (ft)

Indicated Airspeed, V_i (ft/sec)

Outside Air Temperature, T_a ($^\circ\text{K}$)

Engine RPM, N (RPM)

Aircraft Weight, W_t (lbs)

The altitude at which the data is to be standardized and the corresponding standard weight, W_s , are also required.

- a. Use pitot-static relationships to calculate

$H_c, M, V_{T_t}, \delta_t, \theta_t$ from H_i, V_i , and T_a

$V_{T_s}, \delta_s, \theta_s$ from M and standard altitude

- b. If timed turn, calculate aircraft normal acceleration (load factor).

$$n_t = \sqrt{\left(\frac{2\pi}{\Delta t} \frac{V_{T_t}}{g}\right)^2 + 1} \quad (12.88)$$

- c. Calculate test day parameters

$$C_{L_t} = \frac{n_t W_t}{1481 M^2 S \delta_t}$$

$$C_{D_t} : \text{From drag curve using } C_{L_t} \text{ and } M \quad (12.89)$$

$$F_{n_t} : \text{From thrust curve using } M, N, \theta_t, \delta_t$$

d. Calculate standard day parameters

$$F_{n_s} : \text{From thrust curve using } M, N, \theta_s, \delta_s$$

Predict the aircraft's standard day sustained turn capability by assuming the test day lift can be increased (or decreased) until the increased (or decreased) drag balances the calculated net thrust change between the test and standard day.

$$C_{D_{lim_s}} = C_{D_t} \frac{\delta_t}{\delta_s} + \frac{F_{n_s} - F_{n_t}}{1481 M^2 S \delta_s}$$

$$C_{L_{lim_s}} : \text{From drag curve using } C_{D_{lim_s}} \text{ and } M$$

$$n_s = \frac{1481 M^2 S \delta_s C_{L_{lim_s}}}{W_s} \quad (12.90)$$

$$R_s = \frac{V_{T_s}^2}{g \sqrt{n_s^2 - 1}} \quad \text{for } n_s \geq 1$$

$$\omega_s = \frac{V_{T_s}}{R_s}$$

The standard day normal acceleration or load factor, n_s (g's), turn radius, R_s (ft), and turn rate, ω_s (rad/sec) should be plotted as a function of Mach, M , for the specific standard altitude and power setting.

12.6 CRUISE PERFORMANCE DATA REDUCTION

The importance of cruise performance should not be understated. Accurate determination of the endurance and range, as well as the corresponding optimum airspeed/altitude profile, is critical in the development and testing of new aircraft. The weight-pressure ratio (W/δ) data collection and reduction technique for cruise performance is described in this section. This method is normally used for turbojet aircraft cruise tests while a constant altitude method is normally used to determine cruise data for a reciprocating engine aircraft. Both are based upon the stable speed-power flight test technique described in Chapter 11. By recording fuel flow data for a sufficiently long stable point at numerous airspeed, altitude, and weight combinations, an estimate of the range and endurance of the aircraft can be obtained. In addition, assuming an accurate model of the thrust characteristics of the engines exist, or can be measured, the speed power flight test technique can be used to estimate the aircraft's drag polar. Finally, ferry range missions can be flown to confirm and refine the range estimates obtained from the speed-power tests.

Test techniques pertaining to the constant W/δ speed-power test are written primarily for the single spool compressor, constant geometry engine. However, they apply equally well to twin spool compressor, variable geometry engines. The data reduction outline, on the other hand, applies only to fixed geometry engines. The power parameters used in the outline are engine speed for single spool compressor engines or the engine pressure ratio, $P_{T_{10}}/P_{T_2}$.

The outlines described here should be modified for more complex engines. Because of the variety of configurations that exist, it is not practical, nor possible, to describe methods for correcting engine data to standard conditions which are suitable for all types. Frequently, it is not immediately evident as to which dimensional analysis methods are applicable. The characteristics of each of the more complex engines should be studied so that methods may be modified for the individual case. Engine manufacturer's charts are a good source of data when making this analysis.

12.6.1 Speed-Power Test, Constant W/δ Method

The constant W/δ method is used to determine the standard day level flight performance of the turbojet aircraft. It is based upon the following mathematical relationships, as were described in Chapter 11.

$$\frac{D}{\delta} = f_1 \left(\frac{W}{\delta}, M \right) \quad (12.91)$$

From Buckingham π analysis for jet engines (single spool),

$$\frac{F_n}{\delta} = f_2 \left(\frac{N}{\sqrt{\theta}}, M \right) \quad (12.92)$$

Then, since $D = F_n$

$$f_1 \left(\frac{W}{\delta}, M \right) = f_2 \left(\frac{N}{\sqrt{\theta}}, M \right)$$

$$M = f_3 \left(\frac{W}{\delta}, \frac{N}{\sqrt{\theta}} \right)$$

or

$$\frac{N}{\sqrt{\theta}} = f_4 \left(\frac{W}{\delta}, M \right) \quad (12.93)$$

The test program covers the range of airspeeds for specific values of $N/\sqrt{\theta}$ and W/δ , and presents the relationship between these parameters and Mach. This gives the relationship between true airspeed, engine speed, and altitude at standard weight and temperature.

In general, the test consists of stabilizing at different airspeeds and power settings while maintaining a constant W/δ . There may be some difficulty in obtaining good data near and below the speed for minimum drag, i.e. the backside of the power curve. While this data will be for speeds below that for maximum endurance, the data is still important. It will be this low speed data that generates the down-turn in the specific range plot (and up-turn in the fuel flow) and therefore defines the peak of the curves. To improve the quality of the data, it is acceptable to allow a slight descent or climb (about 100 ft/min) to maintain airspeed. This method usually gives more reliable data because hysteresis or elastic lag effects in the altimeter are almost eliminated.

For the best results the W/δ should be maintained as close as possible to the desired value, however $\pm 2\%$ is usually satisfactory.

12.6.1.1 Preflight Preparation. In order to fly at a constant W/δ certain preflight preparations must be made. The pilot must have charts relating fuel counter to altimeter reading for a constant W/δ . Consider both altitude position error and instrument error when preparing a suitable flight data card. This test is well suited to hand record data.

The following data are required before the necessary charts and tables are prepared:

- (1) The empty weight of the aircraft
- (2) Fuel density and fuel loading
- (3) Altimeter calibrations relevant to altitude and airspeed of the test
- (4) Airspeed calibrations (Position and instrument errors)

The following procedures may be used to obtain the charts required to perform the test:

- (1) Determine the standard pressure altitude (H_{cs}) at which the test is to be flown and obtain the corresponding δ from standard atmospheric tables
- (2) Determine the standard weight (W_s) corresponding to this altitude
- (3) Calculate $(W/\delta)_s$
- (4) Obtain the values for the following table:

<u>Altitude</u>	<u>Pressure Ratio</u>	<u>Weight for Standard W/δ</u>
$H_{C_S} + 2000'$	δ_1	W_1
$H_{C_S} + 1000'$	δ_2	W_2
H_{C_S}	δ_S	W_S
$H_{C_S} - 1000'$	δ_3	W_3
$H_{C_S} - 2000'$	δ_4	W_4

Example:

$$W_1 = (W/\delta)_S \times \delta_1$$

- (5) Construct a plot of H_C versus weight (Figure 12.11). Given a weight, this plot can be used to determine altitude to fly to achieve the desired W/δ .

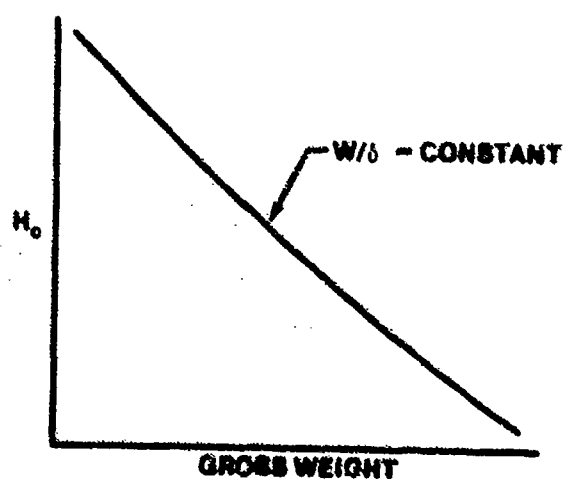


FIGURE 12.11. H_C AS A FUNCTION OF GROSS WEIGHT

- (6) Convert gross weight into fuel used during the mission in gallons. Plot H_c versus fuel used as shown in Figure 12.12. The dashed lines shown are the $\pm 2\%$ W/δ variation that is permitted. If fuel temperature changes throughout the flight, use an average value for determining fuel density.

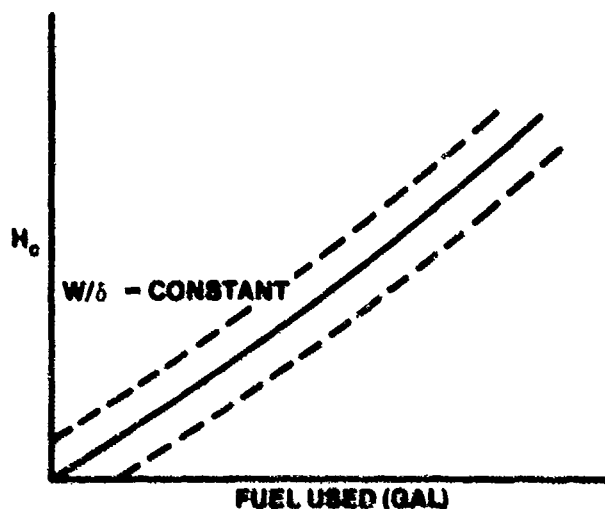


FIGURE 12.12. H_c AS A FUNCTION OF FUEL USED

Figure 12.12 yields the correct altitude to fly at any value of fuel used for a given W/δ .

Note that a plot of fuel counter (F/C) reading versus gross weight is a straight line and is dependent upon the basic weight of the aircraft. If the basic weight of the aircraft changes or the test is flown in another aircraft, this curve (F/C reading versus gross weight) can be easily changed.

- (7) Since the values read from the above chart are "altitudes to fly," curves of ΔH_{pc} versus V_{ic} and ΔH_{ic} versus H_i should be used. Give particular attention to the sign (sense) of this correction because the above procedure necessitates going from calibrated values to indicated values.

- (8) Below is a suggested data card to be used by the pilot, showing typical entries:

AIM V_i KTS	ACTUAL V_i KTS	ALT FT	F/C START GAL'S USED	F/C END GAL'S USED	T SEC	T_i °C	N_i %	\dot{w}_f lb/hr
v_{max}	456.5	18540	290.1	295.7	1:06.2	20.0	99.9	2000
410	411.0	18810	320.2	331.1	1:14.5	16.5	96.4	1900
370	368.5	19060	352.8	359.3	1:25.3	12.0	93.7	1800

12.6.1.2 In-flight Techniques. The following is a recommended procedure for performing the speed-power test using the constant W/δ method so that flight time may be used efficiently:

- (1) Before engine start the pilot should assure himself of the correct fuel loading and that the fuel counters are set correctly.
- (2) When approaching within 2000 to 3000 feet of the test altitude, read the fuel counters and extrapolate to account for the 3-5 minutes it will take to stabilize on condition. Obtain an "altitude to fly" for the first data point based upon this fuel counter estimate.
- (3) Using the aim airspeed from the flight data card, enter the AH versus V_i curve and determine the correction to apply to H_c . Using the allowed fuel, establish a stable point at the aim airspeed and corrected altitude.
- (4) Record the fuel counter reading and start the stop watch when the aircraft is stabilized within 2 percent of the desired W/δ . Fly the aircraft at the required altitude for a minimum of one minute, then record the fuel counter reading and other data. Ideally, the fuel counter reading for the correct W/δ would occur midway through the timed period. For low fuel rates a longer stable point may be required. This is especially true for an instrumentation system with a fuel flow resolution of 0.1 gallons or more, such as used at the TPS. In this case, a minimum two minute stable point is required to obtain accurate estimates of fuel flow.

The pilot should be absolutely certain that the aircraft is stabilized before recording data. If the airspeed changes more than + 2 knots using the front side technique or the vertical velocity exceeds + 100 ft/min using the back side technique, the point should be repeated.

- (5) Obtain enough stabilized points to completely define the fuel flow versus velocity curve at the particular W/δ tested. By plotting fuel flow versus velocity during the mission, the pilot can be assured he has taken a sufficient number of points.
- (6) The pilot can expedite stabilizing the aircraft by proper trimming, pitch control by outside reference, and recording data in an organized sequence. The aircraft should be trimmed for hands-off flight when stabilized. Altitude control on the front side points and airspeed control on back side point can be controlled precisely by the attitude method. It will be found that the majority of the data may be recorded while waiting for the aircraft to stabilize.

12.6.1.3 W/ δ Data Reduction. Pairs of data points, representing the start and stop of each stable point, should be recorded for use in the data reduction equations listed below. The following parameters should be recorded.

Altitude, H_i (ft)

Indicated Airspeed, V_i (ft/sec)

Engine RPM, N (RPM)

or

Engine Pressure Ratio, $P_{T_{10}}/P_{T_2}$ (EPR)

Outside Air Temperature, T_a ($^{\circ}$ K)

Aircraft Weight, W_t (lb)

Time, t (sec)

The standard altitude, H_{c_s} (ft), and corresponding standard weight, W_s (lbs) are also required.

The following steps should then be performed

- a) Use pitot-static relationships to calculate:

$$H_{c_1}, M_1, T_{a_1}$$

$$H_{c2}, M_2, T_{a2}$$

where the subscripts 1 and 2 refer to the start and stop times respectively.

- b) Calculate test day average values:

$$H_c = \frac{H_{c1} + H_{c2}}{2}$$

$$M = \frac{M_1 + M_2}{2}$$

$$T_t = \frac{T_{a1} + T_{a2}}{2}$$

$$W_t = \frac{W_{t1} + W_{t2}}{2}$$

$$N = \frac{N_{t1} + N_{t2}}{2}$$

- (c) Use pitot-static relationships to calculate the following test and standard day parameters.

V_c, δ_t, θ_t calculated from $H_c, M,$ and T_t

δ_s, θ_s calculated from H_{cs}

- (d) Calculate average fuel flow rate:

$$\dot{W}_{f_t} = \frac{W_{t1} - W_{t2}}{\Delta t}$$

where Δt is the duration of the stable point.

- (e) Calculate range performance parameters.

The following equations predict the range performance on a standard day. As with all data reduction, it is necessary to determine which parameters are invariant between test and standard day conditions. As stated in Chapter 11, aircraft performance is fully described by two independent variables, Mach, and weight to pressure ratio, W/δ . Corrected fuel flow, $\dot{W}_f/\delta\sqrt{\theta}$, corrected RPM, $N/\sqrt{\theta}$, and range factor, $V_t W/\dot{W}_f$, are each a function of only these two variables and therefore are invariant between test and standard day. This means, for example, the corrected fuel flow measured on the test day will be precisely the same value as would have been measured on a standard day at the same Mach and W/δ . This is true even if the test day weight is different than the standard weight, provided the test day altitude is such that it corresponds to the same value of W/δ . On the other hand, other parameters such as fuel flow, \dot{W}_f , and specific range, SR, are a function of more than two variables, in particular M, W/δ , and altitude. They are therefore not invariant between test and standard day. This fact is shown below in the plot of SR versus Mach.

The following parameters should be calculated:

- (1) Compare test and standard day weight to pressure ratio

$$\% \text{ Error} = \frac{W_t/\delta_t - W_s/\delta_s}{W_s/\delta_s} \times 100 \quad (12.94)$$

If the % Error is greater than 2%, then this data point should be ignored since no equations are given to correct for W/δ errors.

- (2) Calculate standard day specific range

$$\dot{W}_{f_s} = \dot{W}_{f_t} \frac{\delta_s \sqrt{\theta_s}}{\delta_t \sqrt{\theta_t}} \quad (12.95)$$

$$SR_s = \frac{Ma_0 \sqrt{\theta_s}}{\dot{W}_{f_s}} \quad (12.96)$$

where a_0 is the standard day speed of sound at sea level. A set of specific ranges, SR_s , for various Mach, at one desired weight to pressure ratio, W/δ_s , should be plotted as shown in Figure 12.13. Because specific range is a function of more than two variables, it

is valid only for the Mach, weight-pressure ratio, and standard altitude for which it has been calculated. This is indicated on the plot shown below, where H_1 is the standard altitude corresponding to the desired W/δ .

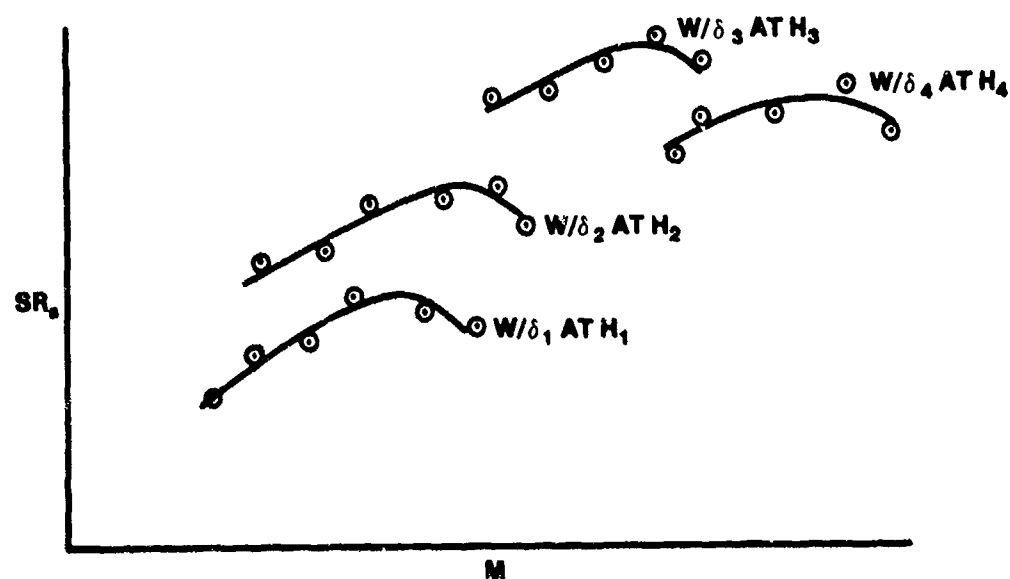


FIGURE 12.13. SPECIFIC RANGE VERSUS MACH FOR VARIOUS WEIGHT-PRESSURE RATIOS

The data plotted above can now be used to determine the optimum Mach and weight to pressure ratio for maximum range. The range factor, RF, given by

$$RF = (W_s) SR_s \quad (12.97)$$

should be calculated for each of the four points (or as many as there are W/δ curves) representing the maximum of each specific range curve. The standard weight, W_s , in this equation corresponds to each standard altitude. For example, for the curve corresponding to W/δ_2 at H_2 , the standard weight is given by

$$W_{s_2} = \left(\frac{W}{\delta} \right)_2 \delta_2 \text{ where } \delta_2 \text{ is found from } H_2 \quad (12.98)$$

These four range factors, as well as the corresponding Mach, should be plotted versus W/δ as shown in Figure 12.14.

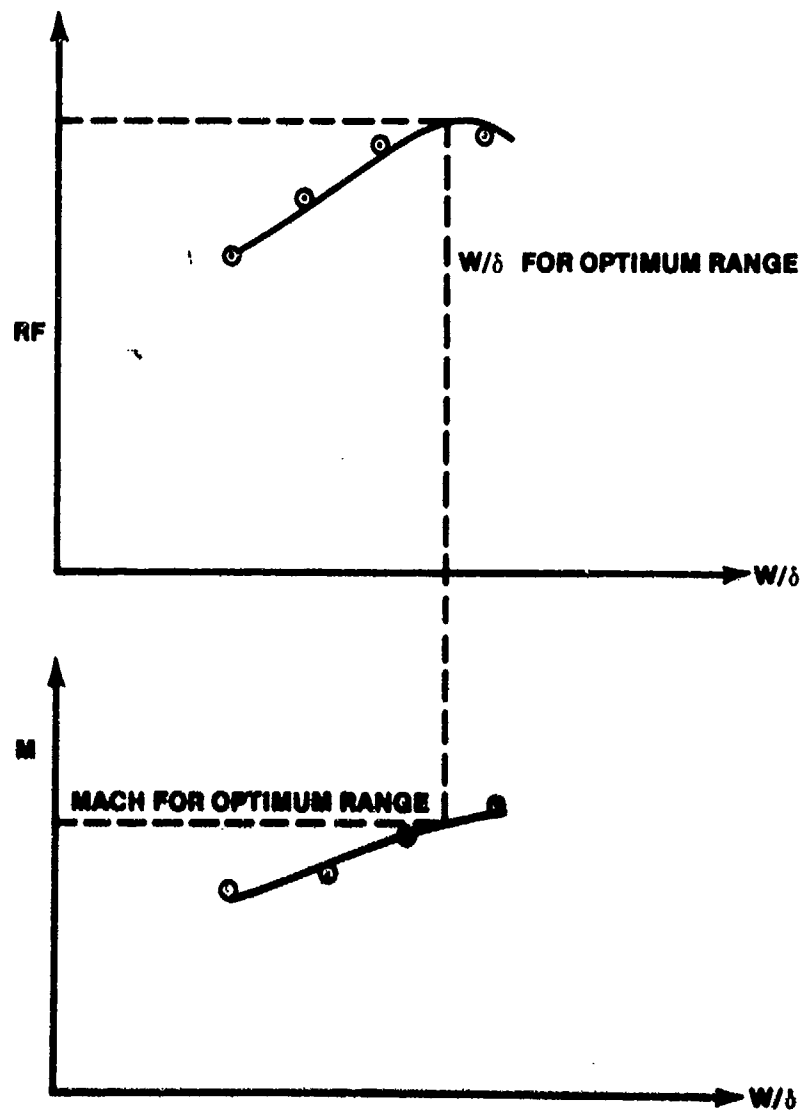


FIGURE 12.14. RANGE FACTOR AND MACH VERSUS WEIGHT-PRESSURE RATIO

The range factor corresponding to the optimum Mach and weight to pressure ratio can now be determined. From theory, the range for this optimum range factor can be calculated from

$$R = RF \ln \frac{W_i}{W_f} \quad (12.99)$$

where W_i is the aircraft weight at the start of the cruise and W_f is the weight at the end of the cruise. An aircraft's maximum ferry range can be calculated by using the maximum weight for W_i , and the minimum weight for W_f . Maximum W_i should take into account the fuel used for ground operations, takeoff, acceleration to climb speed, and climb to the altitude for the start of the cruise climb. Minimum W_f is found using MIL-C-5011A fuel reserve. The distance traveled during the climb and descent should be added to the range during the cruise climb to determine the total ferry range.

12.6.1.4 Drag Polar Determination. The aircraft's drag polar can be predicted from the speed-power test, provided an accurate model of the thrust characteristics of the engine exists or can be measured. The calculations necessary to plot the drag polar are listed below.

- a) Calculate test day lift coefficient and drag coefficient

$$C_{L_t} = \frac{W_t}{1481 M^2 S \delta_t}$$

$$F_{n_t} = \text{From thrust curve using } M, N, \theta_t \text{ and } \delta_t$$

Since the aircraft is unaccelerating during the speed-power test, thrust equals drag.

$$D_t = F_{n_t}$$

Test day drag coefficient is calculated from

$$C_{D_t} = \frac{D_t}{1481 M^2 S \delta_t}$$

The drag polar can be plotted as shown in Figure 12.15. Since the drag polar is a function of Mach, only those points of equal Mach can be connected with a curve. However, for all practical purposes, the drag polar is independent of Mach below $M = 0.75$. Hopefully enough data will be below this Mach to permit an accurate curve of the subsonic drag polar and the corresponding Oswald efficiency factor "e" to be generated. Test points at higher Mach can be used to estimate the effect of Mach on the parasitic drag.

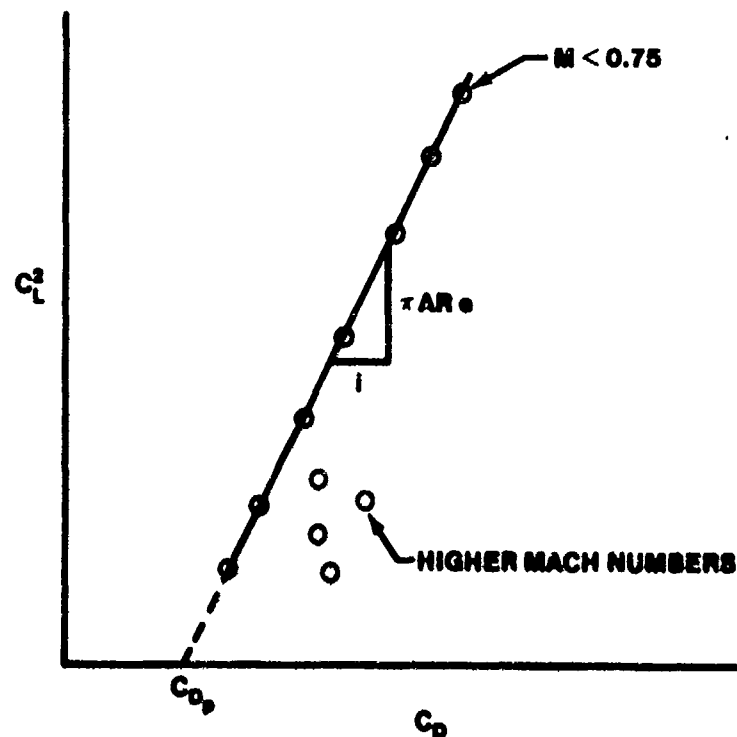


FIGURE 12.15. DRAG POLAR

12.6.2 Range Cruise Control Test

The range cruise control test (Ferry Range Mission) is used to verify and refine the estimates of the range performance generated during the W/δ tests. Specifically, it should be used to check the optimum W/δ and the total ferry range. Usually a series of flights will be flown at W/δ above and below the

predicted optimum W/δ . The standard day range from each of these can be used to determine the actual optimum W/δ and compared with the data predicted by W/δ testing.

Planning of the time or distance flown during the cruise portion of the test is outlined below:

	Fuel Used	Fuel Remaining
1. Prior to Eng Start		
2. Engine Start + Taxi		
3. Takeoff and Accelerate to Climb Schedule		
4. Climb		
5. Cruise		
6. Fuel Reserve		

Estimated fuel used for engine start, taxi, takeoff, and acceleration to climb schedule is obtained from manufacturer's charts. Fuel used in the climb is obtained from the check climb test. Fuel reserve is determined by reference to MIL-C-5011A. The total of these fuel increments subtracted from the total fuel available gives the amount of fuel available for the cruise portion of the test.

The following is a suggested flight data card to be used by the pilot:

Pilot _____ A/C No. _____ Date _____

$W/\delta =$ _____

Data Point	Time	F/C	V_i	H_i	T_i	RPM	\dot{W}_f
------------	------	-----	-------	-------	-------	-----	-------------

Prior Eng Start

Start

Taxi

T. O.

Start of Climb

End of Climb

Start Cruise

The pilot should plan the fuel used during the climb as a function of the W/δ profile. When on the cruise schedule, the crew should record data often enough to obtain at least 10 points.

A fuel counter versus altitude chart for the desired W/δ can be prepared as is outlined in the preflight section of the speed-power at constant W/δ test.

12.6.2.1 Inflight Techniques. A recommended procedure for performing the range cruise control test is:

- (1) Prior to engine start, check that the correct amount of fuel is onboard and that the fuel counter is set correctly.
- (2) Record data at each point planned, i.e., engine start, taxi, takeoff, start of climb and end of climb.
- (3) Upon reaching the altitude that corresponds to the fuel counter reading for the desired W/δ , set up the cruise climb at the desired Mach.
- (4) Increase altitude as the fuel counter is decreased to maintain a constant W/δ by performing a shallow climb. An alternate method is to hold a constant altitude and stair-step the aircraft in increments of 100 to 200 feet. Cruise should begin in the stratosphere and the Mach and RPM should remain constant (using a constant velocity for the Mach is preferred due to the accuracy of the instruments). If cruise should begin below the tropopause, a slight decrease in RPM will be required initially. Equation 12.93

shows that for a given W/δ and Mach a constant $N/\sqrt{\theta}$ is required and therefore engine RPM is decreased as T_a decreases to hold $N/\sqrt{\theta}$ constant.

Throttle movements should be held to a minimum. If turns are required, they should be very shallow.

12.6.2.2 Ferry Range Data Reduction. Record the following parameters throughout the ferry range test. Collect sufficient data points to minimize the effect of errors in reading the data.

Altitude, H_i (ft)

Indicated Airspeed, V_i (ft/sec)

Outside Air Temperature, T_a ($^{\circ}$ K)

Aircraft Weight, W_t (lb)

Time, t (sec)

The data reduction outline presented below also requires the standard day initial cruise weight, W_{s_i} (lb), and the final cruise weight, W_{s_f} (lb). Pitot-static relationships should be used to calculate the aircraft's true airspeed, V_T (ft/sec) and Mach. The test day W/δ for each set of data points should also be calculated to ensure the test pilot flew the planned Mach and W/δ . The test day total range (air miles) is found by numerically integrating the true airspeed with respect to time. That is

$$R_t = \sum_{j=1}^n V_j \Delta t_j \quad (12.100)$$

where Δt_j represents each of the "n" time intervals between data points and V_j is the average true airspeed during that time interval. The test day average range factor, RF_t , is found from

$$RF_t = \frac{t}{\ln\left(\frac{W_i}{W_f}\right)} \quad (12.99)$$

where W_i and W_f are the test day initial and final cruise weights respectively. Standard day cruise range is then predicted using

$$R_s = RF_t \ln \left(\frac{W_{s_i}}{W_{s_f}} \right) \quad (12.101)$$

The total range capability of the aircraft can now be evaluated. Total range is equal to the sum of nautical air miles traveled during climb plus nautical air miles traveled during cruise. Range credit is not allowed for takeoff and acceleration to climb speed. Distance traveled during the climb is obtained from the check climb test and distance traveled during cruise is computed by using the range factor just determined in Equation 12.101 where W_{s_i} is the standard weight at the start of cruise (end of climb) using fuel allowances for ground time and acceleration of climb speed and fuel for climb from the check climb test. W_{s_f} is the standard weight at the MIL-C-5011A fuel reserve requirements. Figure 12.16 shows typical format for ferry range data.

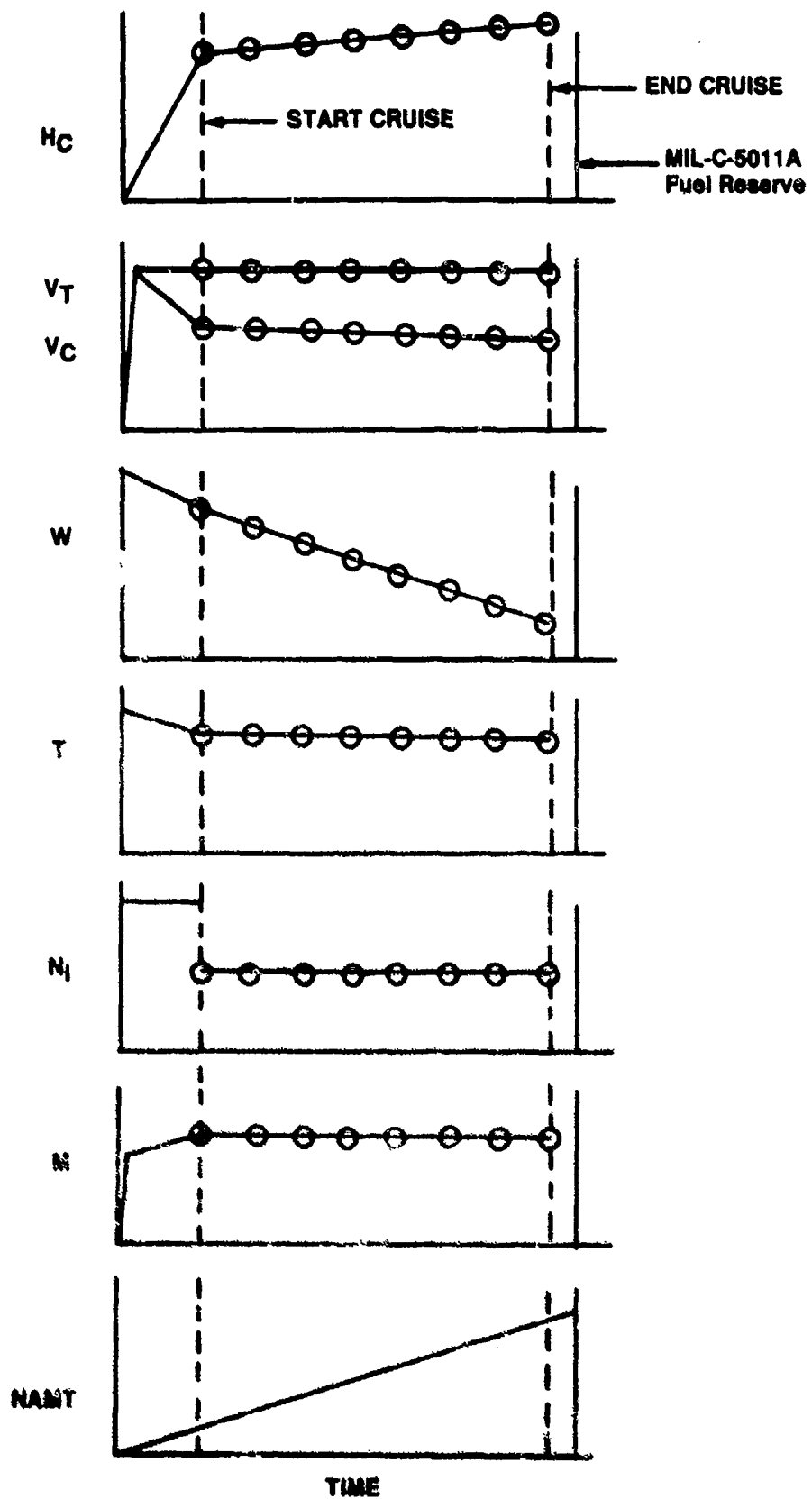


FIGURE 12.16. FERRY RANGE

CHAPTER 13
DATA ANALYSIS

Table of Contents

<u>Section</u>	<u>Page</u>
13.1 Introduction to Data Analysis	13.1
13.1.1 Types of Errors	13.1
13.1.2 Types of Data	13.1
13.1.3 Abbreviations and Symbols	13.3
13.2 Elementary Probability	13.3
13.2.1 Classical Probability	13.4
13.2.2 Experimental Probability	13.5
13.2.3 Probability Axioms	13.5
13.2.4 Probability Examples	13.6
13.3 Populations and Samples	13.8
13.3.1 Definitions	13.8
13.3.2 Assumptions	13.8
13.3.3 Measures of Central Tendency	13.9
13.3.4 Dispersion	13.10
13.3.5 Notation	13.11
13.3.6 Example	13.12
13.4 Probability Distributions	13.13
13.4.1 Discrete Probability Distributions	13.14
13.4.2 Continuous Probability Distributions	13.15
13.4.3 Cumulative Probability Distributions	13.17
13.4.4 Special Probability Distributions	13.17
13.4.4.1 The Binomial Distribution	13.18
13.4.4.2 The Normal Distribution	13.18
13.4.4.3 The Student's t Distribution	13.23
13.4.4.4 The Chi-Squared Distribution	13.25
13.5 Confidence Limits	13.27
13.5.1 Central Limit Theorem	13.27
13.5.2 Confidence Interval for Mean	13.18
13.5.3 Confidence Interval for Mean for Small Samples	13.30
13.5.4 Confidence Interval for Variance	13.31
13.6 Hypothesis Testing	13.34
13.6.1 Null and Alternate Hypotheses	13.35
13.6.2 Types of Errors	13.35
13.6.3 One-Tailed vs Two-Tailed Tests	13.36
13.6.4 Tests on Means	13.37
13.6.5 Tests on Variances	13.39
13.6.6 Summary	13.40

13.7	Nonparametric Tests	13.42
13.7.1	Parametric vs Nonparametric Tests	13.42
13.7.2	Rank Sum Test	13.42
13.7.3	Sign Test	13.44
13.7.4	Signed Rank Test	13.46
13.8	Sample Size	13.48
13.8.1	Accuracy Driven	13.48
13.8.2	General Approach	13.49
13.8.3	Tradeoffs	13.51
13.8.4	Nonparametric Tests	13.52
13.9	Error Analysis	13.53
13.9.1	Significant Figures	13.53
13.9.2	Error Propagation	13.54
13.9.3	Standard Deviation of a Calculated Value	13.55
13.10	Data Presentation	13.57
13.10.1	Scale Choice	13.57
13.10.2	Curve Fitting	13.58
13.10.3	Method of Least Squares	13.59
13.10.4	Data Rejection	13.61
Problem Set 1	13.63
Problem Set 2	13.64
Problem Set 3	13.65
Problem Set 4	13.66
Problem Set 5	13.67
Problem Set 6	13.68
References	13.69
Appendix 1	Areas under the Standard Normal Curve from ϕ to z . . .	A-13.1
Appendix 2	Percentile Values for Student's t Distribution	A-13.2
Appendix 3	Percentile Values for the Chi-Squared Distribution . . .	A-13.3
Appendix 4	Table of Critical Values for U	A-13.4
Appendix 5	Table of Binomial Probabilities.	A-13.5
Appendix 6	Table of Critical Values for the Signed Rank Test . . .	A-13.6

13.1 GENERAL INTRODUCTION

Flight testing consists almost entirely of experimental observations from which we record numbers: time to climb, fuel flow, short period frequency, Cooper-Harper ratings, INS drift rate, to name a few. All experimental observations have inaccuracies. Understanding the extent of these errors and developing methods to reduce their magnitude to an acceptable level is the subject of this course.

13.1.1 Type of Errors

In discussing the errors in our experimental observations, we need to make a distinction between two very different kinds of errors: systemic errors and random errors.

Systemic errors are repeatable errors caused by some flaw in our measuring system. For example, if we measure lengths with a ruler that has the first inch broken off, our data will all have a one inch systemic error. The instrument corrections we apply to indicated airspeed and altitude to obtain calibrated airspeed and altitude is an example of compensating for a known systemic error.

Random errors are not repeatable. If we make multiple observations of the same parameter with the same equipment under the same conditions, we will still have small variations in the results. These variations are caused by unobserved changes in the experimental situation. They can result from small errors in the judgment of the observer, such as in interpolating between the marks of the smallest scale division of an instrument. Other error sources could be unpredictable variations in temperature, voltage, or friction. Because these errors are not repeatable, they can never be eliminated. Empirically, however, it has been found that such random errors are frequently distributed according to a simple law. Therefore, it is possible to use statistical methods to deal with these random errors.

13.1.2 Types of Data

All data are not of the same type. When we use a scale of one to ten to rate the handling qualities of an aircraft, these data cannot be mathematically treated in the same way that we treat miss distance data on the bombing

range. In fact there are four different types of data: nominal, ordinal, interval, and ratio data.

Nominal data are numerical in name only. If we record spin susceptibility as 1, 2, 3, or 4 (depending on whether the aircraft is highly susceptible, susceptible, resistant, or highly resistant to spinning), we cannot treat these data with any of the normal arithmetic processes. For instance, we cannot say that $3 > 1$ or that $3 - 1 = 2$ or that $4 \div 2 = 2$. With nominal data, none of these arithmetic operations are applicable.

Ordinal data contains information about rank order only. If we rank order different aircraft by their maximum speed, then the resulting data can be compared to say that for example, $3 > 1$ meaning aircraft three is faster than aircraft one. We cannot, however, say that $3 - 2 = 1$, or that $4 \div 2 = 2$. Ordinal data can only be used to set up inequalities between the data.

Interval data contains both the rank order information of ordinal data, plus difference information. For example, temperature data has rank and difference information. If it is 30°F , 45°F , and 60°F at different times, the successive differences in temperature are the same, that is 15°F . In both cases, the same amount of heat had to be added to raise the temperature by 15°F . We cannot say, however, that the end temperature of 60° is twice as hot as 30° even though $60^{\circ} \div 30^{\circ} = 2$. The reason is that our zero point is arbitrary. Zero degrees Fahrenheit does not mean the absence of temperature. Thus, interval data has relative and difference information, but not ratio information.

Ratio data contains the information necessary to perform all the basic mathematic operations on the data. Most of our data falls into this category. Airspeed, fuel flow, range, etc, data all can be compared relatively, subtracted, and divided. We can legitimately say that a 1000 NM range in an F-4 is 4 times as great as a 250 NM range in an A-37.

This distinction between nominal, ordinal, interval, and ratio data is important. The type of data we have in a particular case may dictate the use of certain statistical techniques. But, before we can develop and use these statistical methods, we must first establish a common base of understanding of elementary probability.

13.1.3 Abbreviations and Symbols The following unique symbols will be used in this text:

H_0	null hypothesis
H_1	alternate hypothesis
n	number of samples
$P(A)$	probability of event A
s	sample standard deviation
U	rank sum statistic
W	sign rank statistic
\bar{x}	sample mean
\tilde{x}	sample median
\hat{x}	sample mode
z	standard normal deviate
α	probability of type I error
β	probability of type II error
γ	efficiency of nonparametric test
δ	difference in means
μ	population mean
ν	degrees of freedom
σ	population standard deviation

13.2 ELEMENTARY PROBABILITY

A quantitative analysis of the random errors of measurement in flight testing (or any other experiment) must rely on probability theory. Probability theory is a mathematical structure which has evolved for the purpose of providing a model for chance happenings. The probability of an event is taken to mean the likelihood of that event happening. Mathematically, the probability of event A occurring is the fraction of the total times that we expect A to occur, or

$$P(A) = \frac{n_a}{N}$$

Where: $P(A)$ is the probability of A occurring.

n_a is the number of times we expect A to occur.

N is the total number of attempts or trials.

From this definition, it can be seen that $P(A)$ will lie between zero and one since the least that n_A can be is zero (A never happens), and the most it can be is N (A always happens).

In order to determine this fraction, n_A/N , we can approach the problem in two distinctly different ways. We can use our foreknowledge and make assumptions to predict the probability (classical or 'a priori' probability) or we can conduct experiments to determine the probability (experimental or 'a posteriori' probability).

13.2.1 Classical Probability

The study of classical probability began hundreds of years ago when games of chance became fashionable. There was much interest in questions about how frequently a certain type of card would be drawn or that a die would fall in a certain way. For example, it is almost obvious that if an ideal die (six sided) is honestly cast, there are six possible outcomes and the chance of getting a particular face number is one out of six; i.e., the probability is 0.16667.

The underlying conditions for simple evaluations such as this one are that:

1. every single trial must lead to one of a finite number of known possible outcomes, and
2. each possible outcome must be equally likely.

If we satisfy these two conditions, then the probability of event A is just

$$P(A) = \frac{n_A}{N}$$

where now: n_A is the number of ways A can happen.

N is the total number of possible outcomes.

For example, what is the probability of getting no heads when we toss two fair coins? The possible outcomes are:

(H,H) (H,T) (T,H) (T,T)

Thus, $N = 4$ (that is four distinct, equally likely results) and $n_A = 1$ (only the result T,T has no heads).

Therefore, $P(\text{no heads}) = \frac{1}{4} = .25$

This approach to determining probabilities is instructive, but, in general, it is not applicable to experimental situations where the number of

possible events is usually infinite and each possible outcome is not equally likely. Thus, we turn to experimental ('a posteriori') probability.

13.2.2 Experimental Probability

By definition, experimental probability is

$$P(A) = \lim_{N \rightarrow \infty} \frac{n_{A_{\text{obs}}}}{N_{\text{obs}}}$$

where now: $n_{A_{\text{obs}}}$ is the number of times we observe A.

N_{obs} is the number of trials

For example, suppose we wish to check the classical result that the probability of getting a head when tossing a coin is $1/2$. We toss the coin a large number of times and keep a record of the results. A typical graph of the results of such an experiment is shown in Figure 1. We will never, of course, reach an infinite number of trials, but our confidence in the probability of getting a heads will increase as the number of trials increases. As can be seen in Figure 1, the fraction of observed heads fluctuates dramatically when N is small, but as N increases, the probability steadies down to an apparently equilibrium value.

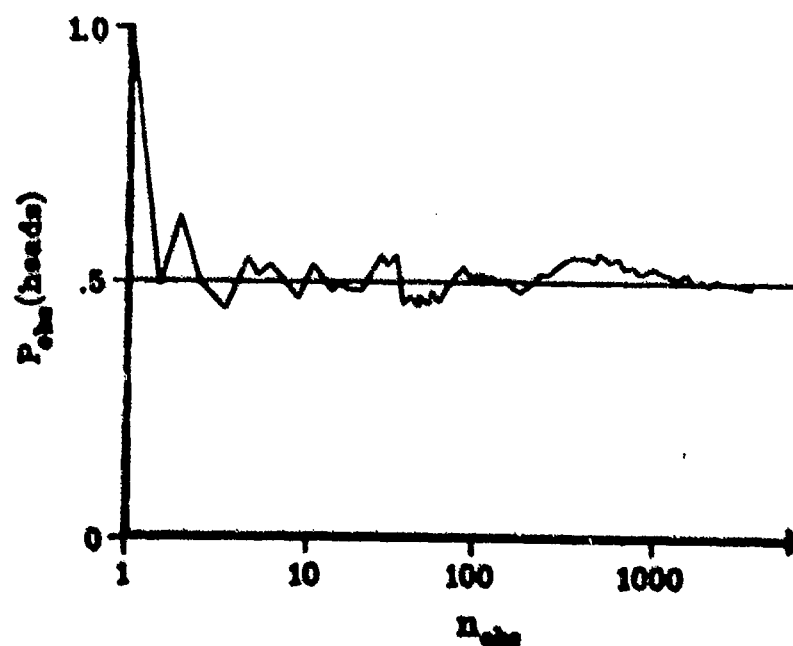


Figure 1. Experimental Probability

13.2.3 Probability Axioms

Probability theory can be used to describe the relationships between multiple events. Several axioms are presented. First, if the probability of A occurring is $P(A)$, then the probability of A not occurring, $P(\bar{A})$, is just:

$$P(\bar{A}) = 1 - P(A)$$

This is easy to accept without a rigorous proof since the probability of something occurring has to be one.

The remaining axioms presented below for multiple outcomes assume that each outcome is independent (A occurring does not subsequently affect the probability of A or B occurring) and mutually exclusive (only one can occur in a single trial). The two remaining axioms are:

$$P(A \text{ or } B) = P(A) + P(B)$$

$$P(A \text{ and } B) = P(A) \times P(B)$$

These axioms are also easily justified (as opposed to proven) by looking at classical probability. If we take the example of tossing a coin, then

$$P(H) = .5 \quad P(T) = .5$$

and

$$P(H \text{ or } T) = .5 + .5$$

which makes sense, because the probability of the coin coming up either heads or tails has to be one (excluding the chance of landing on edge).

Also, from the example of getting two tails in section 13.2.1.

$$P(T \text{ and } T) = P(T) \times P(T) = .5 \times .5 = .25$$

which is the same answer we got by examining all of the possible outcomes.

13.2.4 Probability Examples

Problem: Based on historical data, suppose we determine that 95% of the time an F-4 will make a successful approach and barrier engagement. If we

have a flight of four that must use the barrier due to icy runway conditions, what is the probability that at least one aircraft will miss the barrier?

Solution: The probability that at least one will miss is the complement of the probability that all will successfully engage. That is

$$P(1 \text{ or more miss}) = 1 - P(\text{all engage})$$

The probability that all four engage is

$$\begin{aligned} P(\text{all engage}) &= P(1\text{st engages}) \times P(2\text{nd engages}) \times P(\dots) \\ &= P(\text{single engagement})^4 \end{aligned}$$

Finally, since $P(\text{engage}) = .95$,

$$P(1 \text{ or more miss}) = 1 - (.95)^4 = 1 - .81 = \underline{.19}$$

Or roughly speaking, about one out of five times, a flight of four F-4s would have at least one barrier miss.

Problem: What is the probability of getting craps (total of 2, 3, or 12) on a single roll of a pair of dice?

Solution: Since getting 2, 3 or 12 are independent, mutually exclusive events, we can use the following:

$$P(2, 3, \text{ or } 12) = P(2) + P(3) + P(12)$$

To get individual probabilities, first note that there are 36 possible outcomes (6^2) with two dice, each having six sides. In order to get a total of 2 or 12, there is only one way the dice can come up: 1 and 1 or 6 and 6, respectively. For a total of 3, the dice can come up two ways 1 and 2 or 2 and 1. Therefore, since $P(A) = \frac{n_A}{N}$, we have:

$$P(2) = \frac{1}{36}$$

$$P(3) = \frac{2}{36}$$

$$P(12) = \frac{1}{36}$$

and finally

$$P(2, 3, \text{ or } 12) = \frac{1}{36} + \frac{2}{36} + \frac{1}{36} = \frac{1}{9}$$

Thus, about 11% of the time that you roll the dice, you will crap out.

13.3 POPULATIONS AND SAMPLES

13.3.1 Definition

Thus far in our discussion, we have made no distinction between populations and samples. The difference is an important one in the study of statistics. The definitions follow.

A data population is all conceivable possible observations of a certain phenomena. Thus, many populations are infinite. For example, the population of the totals of two dice are all possible (infinite) outcomes of rolling two dice. Another example, the population of weapon deliveries from an aircraft is all the possible drops it could make in its lifetime. A more limited population would be the scores of your class on the final exam. This population would have only 24 or 25 possible observations, not infinity.

A data sample is any subset of a given population. Thus the results of 1000 rolls of two dice constitute a sample of all possible results. The scores from 100 F-4 sorties could be another example. The scores of 5 of your classmates would be a sample of the results of the whole class.

13.3.2 Assumptions

Constructing a population (what should be included as possibilities, what should be excluded?) or selecting a sample from a population must be done with care if we are later to apply statistical analysis techniques. The assumptions we normally impose on samples are that the data be homogeneous, independent, and random.

A homogeneous sample has data from one population only. If, for example, we allow bomb scores from an F-4C (iron sight) and an F-16C (predictive heads-up display) to be included in a single sample, the results would not be very meaningful.

An independent sample is one where the selection of one data point does not affect the likelihood of subsequent data points. For example, after dropping a bomb thirty feet long on the first pass, the probability that the next drop will miss by the same distance (or any other distance) is unaffected (independent). An example where the subsequent probabilities are affected is sampling from a finite population without replacement. For example, the

probability of drawing a heart from a deck of cards changes if you sample and discard. The sample would remain independent if you replaced the card after each draw.

A random sample is one where there is an equal probability of selecting any member of the population. An example of a nonrandom sample would be using a single F-16 with a boresight error causing a bias in downrange miss distance to produce samples intended to be representative of all F-16 weapon deliveries.

13.3.3 Measures of Central Tendency

Given a homogeneous, independent, random sample, we now turn to methods to describe the contents of that sample. Suppose, for instance, we wish to be very accurate in measuring a hard steel rod with a micrometer. The population of measurements is all of the possible measurements that could be made with the micrometer. If we take a sample of ten measurements, we will probably get several different answers. The unpredictable variations could come from any of several different sources: we may tighten the micrometer more sometimes than others, there may be small dust particles sometimes, we may make small errors in estimating tenths of the smallest scale division, and so forth. Even so, we would expect to get a better answer by measuring many times rather than just once.

But what should we do with the multiple measurements, some of which are different? The most obvious procedure would be to average them. When we average the contents of a sample, we call the result the arithmetic mean, usually denoted by \bar{x} :

$$\bar{x} = \frac{1}{N} \sum_{i=1}^N x_i$$

The mean is the most common measure of central tendency, but not the only one. If we had taken 10 measurements and 8 of them were the same, we might feel justified in stating that this most common answer is the correct one and that the other 2 different answers were due to some unseen error. Using the most common sample is called taking the mode. The mode (usually denoted \hat{x}) is the most frequent sample value. In some samples, there may be more than one mode.

A third measure of central tendency is the median. The median (usually denoted \tilde{x}) value is the middle value. If we rank order the sample elements, then for an odd number of elements the median is just the middle value. For an even number of elements, we define the median as the arithmetic average of the two middle values.

Of the three different measures of central tendency (mean, mode, and median), the mean or arithmetic average is most commonly used.

13.3.4 Dispersion

Given that we usually use the mean, \bar{x} , as the single measure of central tendency of a sample, is that enough to adequately characterize the contents of a given sample? The answer is no. Using the mean by itself can be very misleading. For instance, consider the following two samples:

Sample 1: 99.9, 100, 100.1

Sample 2: 0.1, 100, 199.1

As can be seen, the mean (and median in this case) is the same for both samples yet there is a significant difference between these two samples. The difference is in the variation of sample elements from the mean, or dispersion. Thus, we now need some measure of the dispersion within a sample.

To obtain a measure of dispersion, first define the deviation, d_i , as the difference between the i th element of the sample and the sample mean:

$$d_i = x_i - \bar{x}$$

The first inclination may be to average these deviations, but the result is not illuminating since:

$$\begin{aligned}\bar{d}_1 &= \frac{1}{N} \sum_{i=1}^N d_i = \frac{1}{N} \sum_{i=1}^N (x_i - \bar{x}) \\ &= \frac{1}{N} \sum_{i=1}^N x_i - \bar{x} \\ &= \bar{x} - \bar{x} = 0\end{aligned}$$

Because of the definition of the mean, the deviations above the mean will always exactly cancel the deviations below the mean. This result may lead you to conclude that we should average the absolute values of the individual deviations. Doing so produces what is referred to as the mean deviation:

$$\text{mean deviation} = \frac{1}{N} \sum_{i=1}^N |x_i - \bar{x}|$$

This quantity is sometimes used as a measure of dispersion, but for reasons that will become apparent later on, a more common measure of dispersion is the standard deviation, which is defined next.

In defining the standard deviation, we eliminate the negative individual deviations by squaring each term, rather than by taking the absolute values. We then average the squares and finally take the positive square root of the results. Thus, the standard deviation (denoted by σ) is the root-mean-square deviation:

$$\sigma = \sqrt{\frac{1}{N} \sum_{i=1}^N (d_i)^2}$$

The square of the standard deviation, σ^2 , is called the variance.

13.3.5 Notation

Normally, we use Greek letters to denote statistics (such as mean and variance) for populations and we use Roman letters for statistics of samples. Therefore, we will use:

μ and σ^2 for population mean and variance

\bar{x} and s^2 for sample mean and variance

There is one other difference between population and sample statistics. The sample standard deviation is defined slightly differently than the population standard deviation:

$$s = \sqrt{\frac{1}{N-1} \sum_{i=1}^N (x_i - \bar{x})^2}$$

The difference is that the sum of the squares is divided by $N - 1$ for the sample rather than by just N as for the population standard deviation. The

effect is to make the sample standard deviation slightly larger than it would have been and the difference decreases as the sample gets larger.

13.3.6 Example

Problem: Given the following 10 observations find the sample mean, median, mode, and standard deviation: (3, 4, 6, 6, 6, 8, 9, 10, 12, 15)

Solution:

$$\begin{aligned}\bar{x} &= \frac{1}{10} (3 + 4 + 6 + 6 + 6 + 8 + 9 + 10 + 12 + 15) \\ &= 7.9\end{aligned}$$

$$\hat{x} = 6 \text{ (Most Frequent)}$$

$$\tilde{x} = \frac{1}{2} (6 + 8) = 7 \text{ (average of two middle values)}$$

$$\begin{aligned}s &= \sqrt{\frac{1}{9} (4.9^2 + 3.9^2 + 1.9^2 + 1.9^2 + 1.9^2 + .1^2 + 1.1^2 + 2.1^2 + 4.1^2 + 7.1^2)} \\ &= 3.695\end{aligned}$$

13.4 PROBABILITY DISTRIBUTIONS

Now that we have covered elementary probability concepts and introduced the idea of population and samples, we turn to probability distributions. Application of statistical methods requires an understanding of the characteristics of the data obtained. Probability distributions, either empirical or theoretical can give us these required characteristics. Most statistical methods are based on theoretical distributions which approximate the actual distributions.

13.4.1 Discrete Probability Distributions

To introduce the idea of a probability distribution, let's go back to the example of tossing two coins in Section 13.2.1. We can calculate from classical probability the probability of getting 0, 1, or 2 heads. Tabulating this as $f(n)$, where n is the number of heads:

n	$f(n)$
0	.25
1	.50
2	.25

Table 1. Probability of getting n heads
in two tosses of a fair coin.

Another method of presenting this data would be graphically by means of a bar graph, as shown in Figure 2.

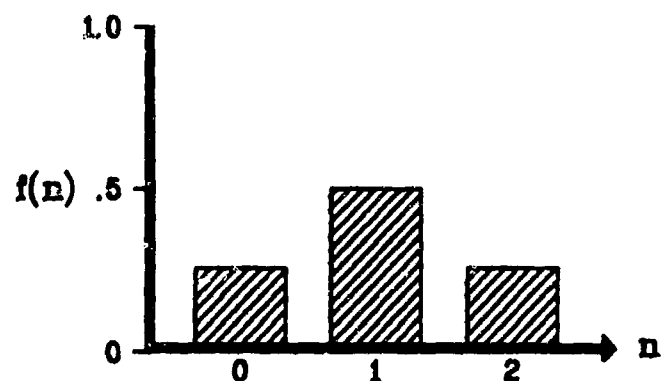


Figure 2. Probability of getting n heads in two tosses of a fair coin.

Thus, $f(n)$ is called the probability distribution of n . The above example is a theoretical calculation. More frequently, we are concerned with empirical distributions. For example, suppose we collect a sample of data on T-38 landings as shown in Table 2.

Touchdown Distance from Aim Point	Frequency in Distance Interval	Relative Frequency
0 - 100 ft	2	.05
101 - 200 ft	10	.25
201 - 300 ft	18	.43
301 - 400 ft	8	.20
401 - 500 ft	3	.07

Table 2. Touchdown data.

Plotting the data in a histogram as in Figure 3 will give us a graphical representation of this empirical probability distribution.

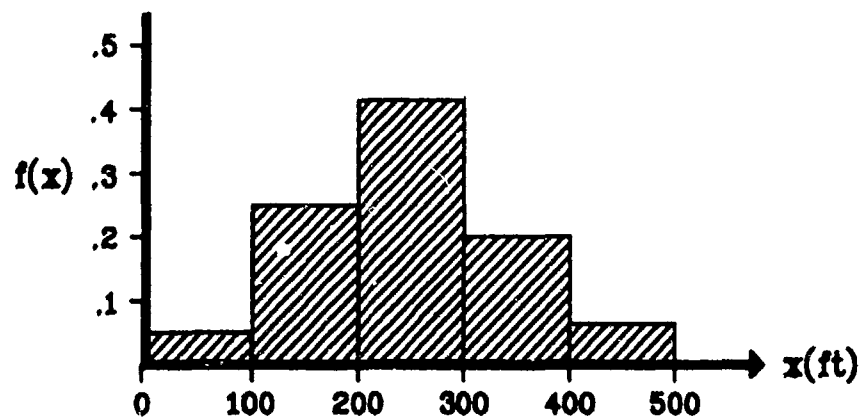


Figure 3. Probability distribution of touchdown miss distance

13.4.2 Continuous Probability Distribution

If we acquire more data on T-38 landings and reduce the size of the intervals, we could draw a new histogram. In the limit as we acquire more and more data, and reduce the interval size to smaller and smaller values, the histogram approaches a smooth curve, as shown in Figure 4.

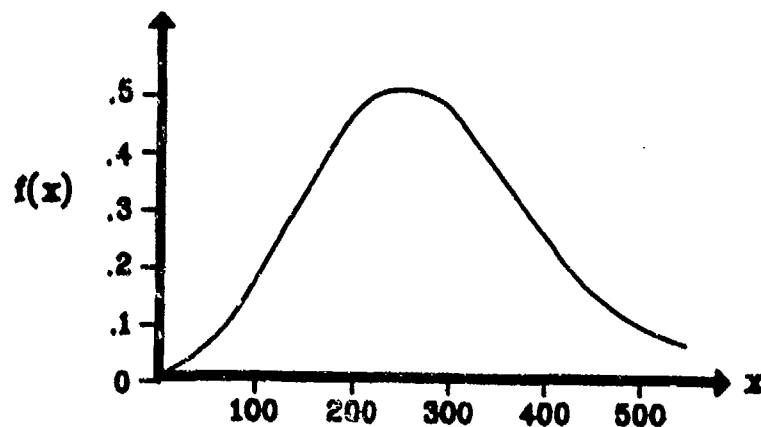


Figure 4. Continuous probability distribution of of touchdown miss distance.

This smooth, continuous probability distribution cannot be interpreted in the same way as the discrete distribution. In Figure 3, the height of the bar above the interval is the probability that x will have a value within that interval. In Figure 4, the height of the curve above a point is not the probability of x having that point value. Since there are an infinite number of points (i.e., a continuous curve) the probability of x having a single specific value is zero. We can, however, talk about the probability of x being between two points, a and b . Then, the interpretation of the continuous probability distribution is as follows:

$$P(a \leq x \leq b) = \int_a^b f(x) dx$$

That is, the probability that x falls between a and b is the area under the probability distribution curve between $x = a$ and $x = b$, as shown in Figure 5.

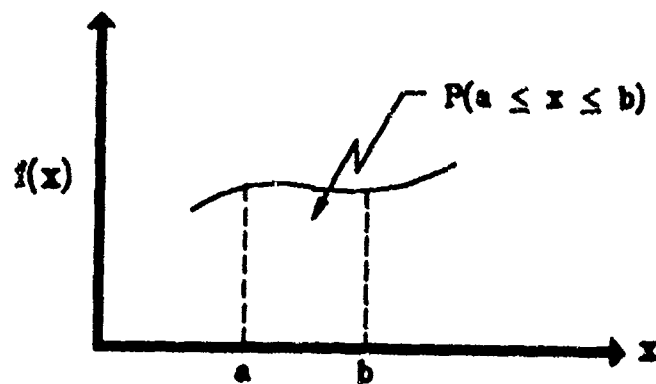


Figure 5. Probability vs. the area under a continuous probability distribution.

From this, we can see that $f(x)$ must always be greater than or equal to zero. Negative areas would be meaningless. Also, since the maximum probability is one, we have:

$$\int_{-\infty}^{\infty} f(x) dx = 1$$

13.4.3 Cumulative Probability Distribution

For some applications, displaying the probability distribution as a cumulative function is the most useful method. A cumulative probability distribution gives the probability that a random variable x is equal to or less than a given value, a . In mathematical terms:

$$F(x) = P(x \leq a) = \int_{-\infty}^a f(x)dx$$

For example, the relative probability of T-38 miss distances from Figure 4 could be displayed in a cumulative distribution as in Figure 6.

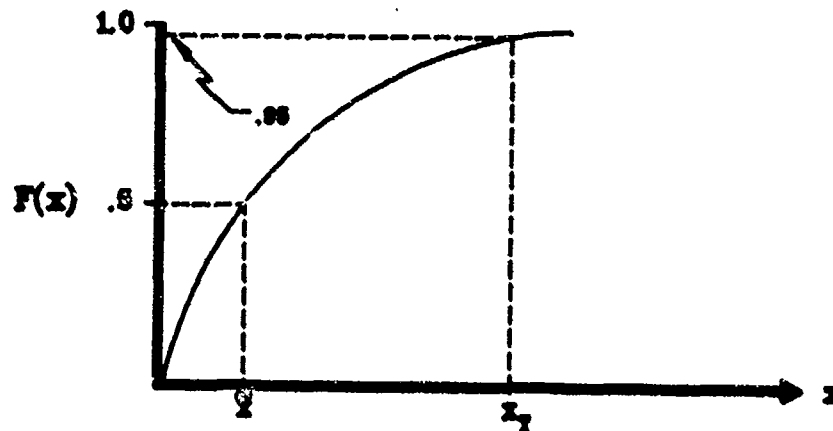


Figure 6. Cumulative probability distribution

From this type of display, the median, \bar{x} , can be directly read. Also, we can see that 95% of the time we expect the miss distance to be below some value, x_T .

13.4.4 Special Probability Distributions

There are numerous theoretically derived probability distributions used in analyzing data. In this course, we will limit our scope to only four distributions: binomial, normal, student's t , and χ^2 . Each is briefly introduced below.

13.4.4.1 The Binomial Distribution

The first special probability distribution that we will examine is a discrete probability distribution, the binomial distribution. The binomial distribution is a theoretically derived distribution of probabilities for trials in which there are two possible results, usually called success and failure. This can be applied to a large number of problems if success and failure are defined beforehand, for example:

1. Toss of a coin - heads (success) or tails (failure).
2. Roll of two dice - total of 7 (success) or other than 7 (failure).
3. Qualitative evaluation of a flight control modification - better (success) or worse (failure).

To determine the probability of getting exactly n successes in N trials given the probability of a single success is the problem. Let p represent the probability of a single success. First, the limiting cases are very simple. If $n = N$, then the probability is just p^N . If $n = 0$ (all failures), then the probability is simply $(1 - p)^N$, or, if we let $1 - p = q$, then q^N .

The in between probabilities are not as simple. If we have n successes and $N - n$ failures, we might be tempted to say the $p^n q^{N-n}$ is the probability, but there are multiple combinations of n objects possible in N events. Luckily, mathematicians have quantified how many combinations are possible and the probability of exactly n successes in N trials is:

$$f(n) = \frac{N!}{n!(N-n)!} p^n q^{N-n}$$

where $x! = x(x-1)(x-2) \dots (3)(2)(1)$

An example may help illustrate. If two different flight control systems are really equally desirable, then the probability of 6 out of 8 pilots preferring system A over system B can be found using the binomial distribution. If A and B are truly equally good, the probability of a pilot picking A over B is equal to $\frac{1}{2}$ ($p = q = .5$). The probability of 6 out of 8 picking A is

$$f(6) = \frac{8!}{6!2!} (.5)^6 (.5)^2 = .109$$

Thus, if you assumed that A and B were equally good, then there is only an 11% chance of getting the test results you observed, implying that your initial assumption may be in error. In a similar way, the probabilities for all possible results can be graphed as shown in Figure 7.

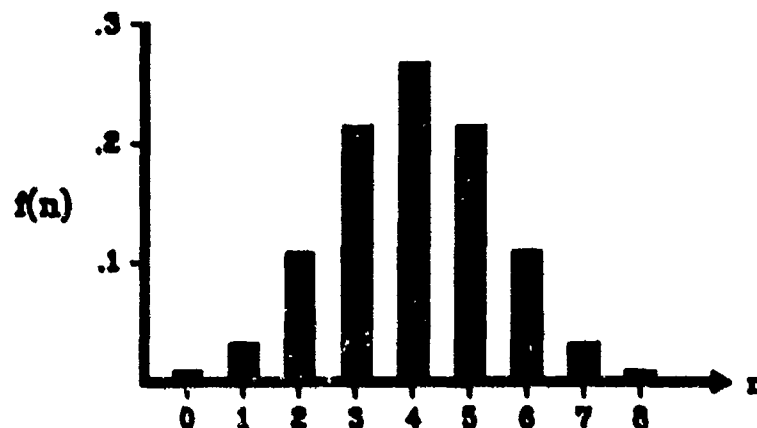


Figure 7. Probability that n of 8 pilots will prefer system A if $p=q=0.5$

13.4.4.2 The Normal Distribution

The normal distribution is the single most important distribution in data analysis. The theoretical basis for the normal distribution lies in the binomial distribution. If we consider any deviation from the mean as the result of a large number of elemental errors, all of equal magnitude and each equally likely to be positive or negative, we can derive the following:

$$f(x) = \frac{1}{\sqrt{2\pi} \sigma} e^{-(x-\mu)^2/2\sigma^2}$$

Thus, the normal distribution is a continuous probability distribution, valid from $-\infty < x < \infty$. Its graphical representation is shown in Figure 8.

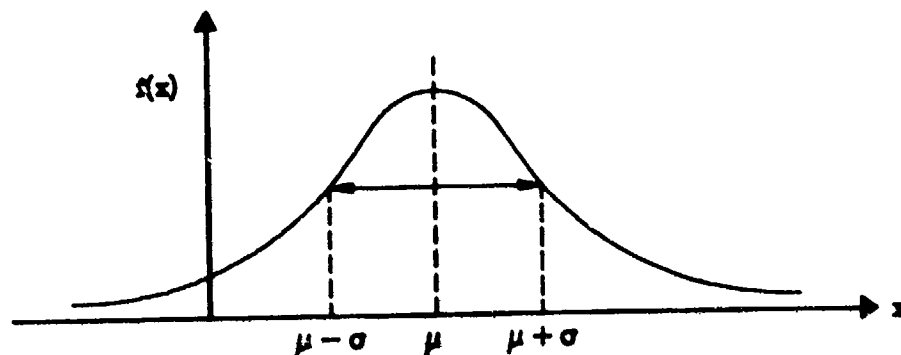


Figure 8. Normal Probability Distribution.

From this figure, it can be seen that $f(x)$ is symmetric about $x = \mu$, that $x = \mu$ yields the maximum value of $f(x)$. Also, $x = \mu \pm \sigma$ are the two points of inflection on the curve of $f(x)$.

Notwithstanding the mathematical derivation of the normal distribution from a binomial distribution, the most compelling justification for its use and study is the fact that many sets of experimental observations have been shown to obey it. Accordingly, the distribution has been studied extensively.

Recalling that for a continuous probability distribution, the probability that x lies between a and b is defined by the integral of $f(x)$ between a and b , we come to a major drawback of the normal distribution. For example, what is the probability of getting $x < a$ if x is normally distributed? Just

$$P(X < A) = \int_{-\infty}^a \frac{1}{\sqrt{2\pi} \sigma} e^{-(x-\mu)^2/2\sigma^2} dx$$

which cannot be solved in closed form. Numerical techniques are required. Tables could be used except different tables would be needed for each combination of μ and σ . The problem is overcome by making a substitution of variables in $f(x)$ by letting

$$z = \frac{x - \mu}{\sigma}$$

then

$$f(z) = \frac{1}{\sqrt{2\pi}} e^{-z^2/2}$$

Tables are abundant for $f(z)$ which is, in effect, the normal distribution with a mean of zero and a standard deviation of one. To use these standardized normal tables, we must simply change our variable x to z as shown above. Values for $f(z)$ are tabulated in the appendix.

A graph of the standard normal distribution curve, with approximate percentages under the curve is given in Figure 9.

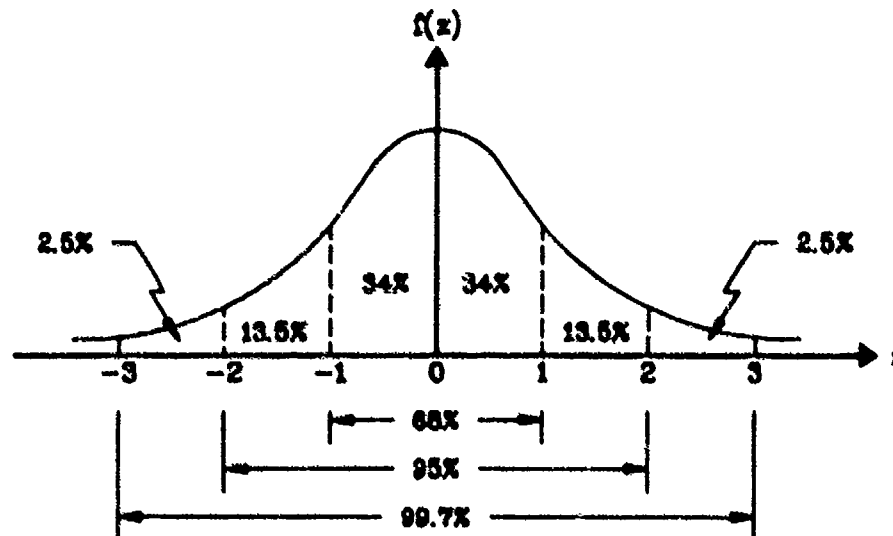


Figure 9. Standardized Normal Distribution

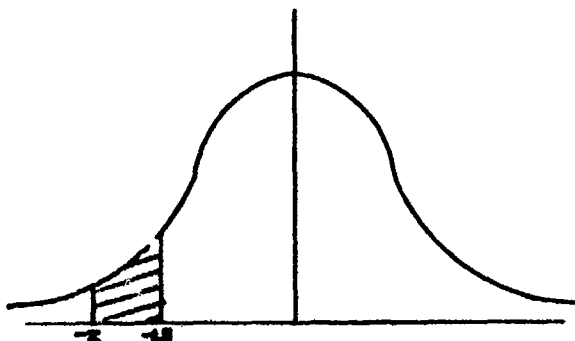
The following three examples may help illustrate the meaning of the normal distribution and the uses of the standardized tables:

NORMAL DISTRIBUTION EXAMPLES

1. Find the area between $z = .81$ and $z = 1.94$. Using the normal distribution table in the appendix, proceed down the column marked z until entry 1.9 is reached, then right to the column marked 4. The result, .4738, is the area between 0 and 1.94.

Similarly, .2910 is the area from 0 to .81. If we subtract these two values (area between $z = 0$ and $z = 1.94$) - (area between $z = 0$ and $z = .81$), $.4738 - .2910 = .1828 = P(.81 \leq z \leq 1.94)$.

2. Find the value of z such that the area between -1.5 and z is $.0217$.
(Assume z is negative but the left of -1.5 .)



$$\begin{aligned} \text{Area between } z \text{ and } -1.5 &= (\text{area between } z \text{ and } 0) \\ &\quad - (\text{area between } -1.5 \text{ and } 0) \end{aligned}$$

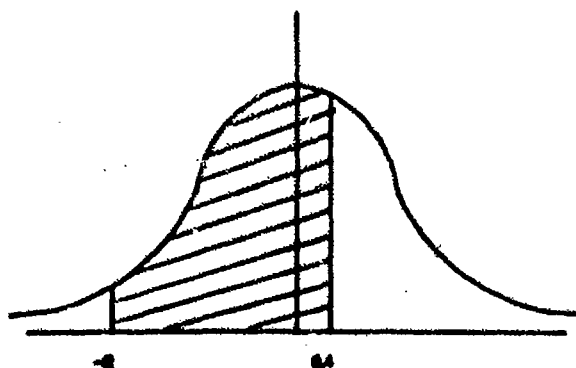
$$\begin{aligned} .0217 &= (\text{area between } z \text{ and } 0) \\ &\quad - .4332 \end{aligned}$$

$$\therefore z = -1.694$$

3. The mean fuel used for a given profile flown 40 times was 8000 lbs, and the standard deviation was 500 lbs. Assuming the data is normally distributed, find the probability of the next sortie using between 7000 and 8200 pounds.

$$7000 \text{ lbs in standard units} = \frac{x - \mu}{\sigma} = \frac{7000 - 8000}{500} = -2$$

$$8200 \text{ lbs in standard units} = \frac{8200 - 8000}{500} = .4$$



$$\begin{aligned} P(-2 \leq z \leq .4) &= (\text{area between } z = -2 \text{ and } z = 0) + \\ &\quad (\text{area between } z = 0 \text{ and } z = .4) \end{aligned}$$

$$= .4772 + .1554 = \underline{.6326}$$

13.4.4.3 The Student's t Distribution

In order to use the standard normal distribution, we must know the population mean and standard deviation. In practical applications, we frequently do not know these values and instead must use the sample mean and standard deviation. The difference between the sample mean and true mean of a population was investigated first by W. S. Gossett. He developed a theoretical distribution for the statistic

$$t = \frac{\bar{x} - \mu}{s/\sqrt{n}}$$

where t is used as a measure of the difference between the sample mean and the true mean. As can be seen, the value of t is also influenced by how much dispersion we have in our sample and by the size of that sample.

For each possible value of n , we can plot a probability distribution of t . The distribution looks very similar to the standard normal distribution, especially for large values of n . In fact, it can be shown mathematically that as $n \rightarrow \infty$, the t distribution approaches the normal distribution. Figure 10 compares t distributions for different values of n .

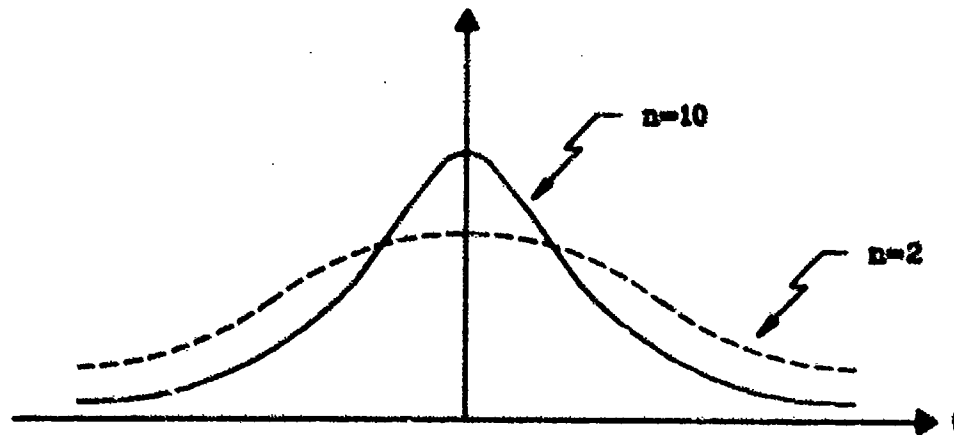


Figure 10. Change in t -distribution with sample size.

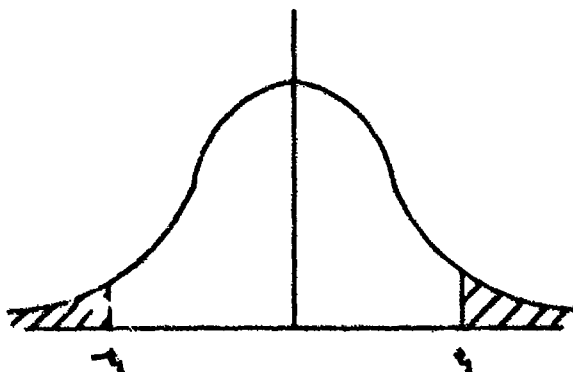
Because of this change in t with sample size, different t distributions must be tabulated for each value of n . Typically, as in the appendix, different critical values of $f(t)$ are tabulated for different values of n up to

about $n = 30$, beyond which one could use the standard normal distribution with $\bar{x} = \mu$ and $s = \sigma$ with very little error. It should be noted that most tables use degrees of freedom, v , instead of n , where

$$v = n - 1$$

The theoretical reasons for this change are of little consequence to us here.

t - DISTRIBUTION EXAMPLES



1. Find the t_1 for which the total shaded area on the right = .05, if we assume 9 degrees of freedom.

If the area on the right of $t_1 = .05$, then the area to the left is $(1 - .05) = .95$ and t_1 represents the 95th percentile, $t_{.95}$. Referring to the t - distribution table in the appendix proceed down the column headed v until reaching 9. Then proceed right to column headed $t_{.95}$. The result 1.83 is the required value of t .

2. Find the t_1 for which the total shaded area = .05, assuming 9 degrees of freedom. (Two Tailed)

If the total shaded area is .05, then the shaded area on the right is .025 by symmetry. Thus, the area to the left of t_1 is $(1 - .025) = .975$ and t_1 is $t_{.975}$. From the appendix, we find

2.26 as the required value of t .

13.4.4.4 The Chi-Squared Distribution

Just as the sample mean differs from the population mean, we expect the sample standard deviation to differ from the true population value. The difference is distributed according to the Chi-squared distribution of the statistic

$$\chi^2 = \frac{(n-1)s^2}{\sigma^2}$$

which is a measure of the dispersion of experimental s values around the population value, σ , caused by taking only limited sample sizes. A sketch of the Chi-square probability distribution is shown in Figure 11.

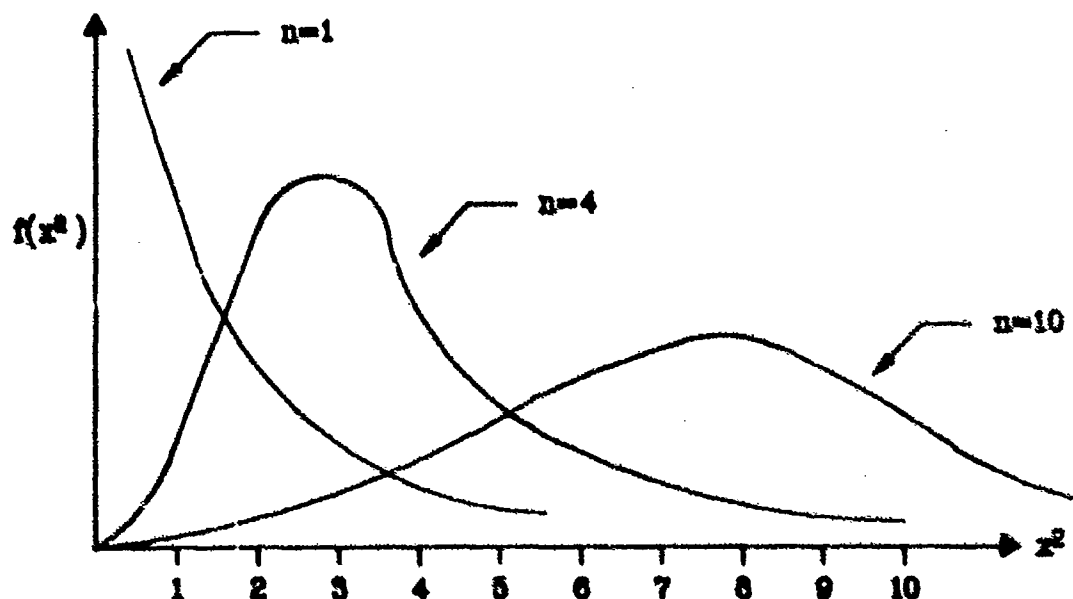
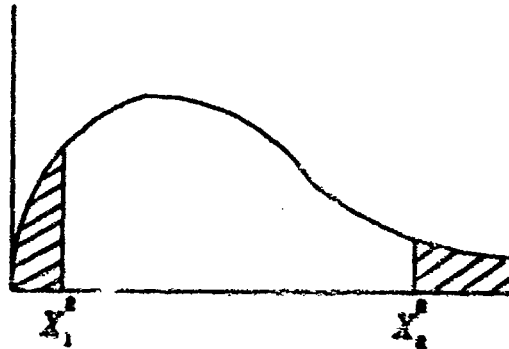


Figure 11. Change in χ^2 distribution with sample size.

As with the t distribution, the χ^2 distribution changes with sample size and therefore critical values of χ^2 are normally tabulated (as in the appendix) for various degrees of freedom ($n - 1$).

CHI-SQUARE DISTRIBUTION EXAMPLES



1. Find the value of x_1^2 for which the shaded area on the right = .05 assuming 5 degrees of freedom.

If the shaded area on the right is .05, then the total area to the left of x_1^2 is $(1 - .05) = .95$ and x_1^2 represents the 95th percentile, $x_{.95}^2$. Referring to the χ^2 distribution table in the appendix, proceed down the v column until entry 5 is reached. Then proceed right to the column headed $x_{.95}^2$. The result, 11.1 is the required value of x_1^2 .

2. Find x_1^2 and x_2^2 for which the total shaded area = .05, assuming 5 degrees of freedom.

Since the distribution is not symmetric, there are many values for which the total shaded area = .05. It is customary, unless otherwise specified, to choose the two areas equal. In this example, then, each area = .025.

If the shaded area on the right is .025, the area to the left of x_1^2 is $(1 - .025) = .975$ and x_1^2 is the 97.5th percentile, $x_{.975}^2$ which from the appendix is 12.8.

Similarly, if the shaded area on the left is .025, the area to the left of x_2^2 is 0.025, and x_2^2 represents the 2.5th percentile, $x_{.025}^2$ which equals .831.

3. Find the median value of χ^2 corresponding to 28 degrees of freedom.

Using the table in the appendix, we find in the column headed $x_{.50}^2$ (since the median is the 50th percentile), the value is 27.3 corresponding to $v = 28$.

13.5 CONFIDENCE LIMITS

In practical situations, we normally take a sample of a large population such as takeoff distance or bomb miss distance, and we use the mean of our multiple observations as a point estimate of the true population mean. We often report this sample mean as though it were the true answer. We must realize, however, that any subsequent single observation can be expected to differ from our sample mean and that the true population mean may differ from our sample mean. If we design the test correctly (standardize the method and conditions) and take sufficient samples (to be discussed in a later section), we will have confidence that our answer is sufficiently accurate. There exist quantitative methods for determining how far away our answer is likely to be from the true answer (a confidence interval). These methods are the subject of this section.

13.5.1 Central Limit Theorem

The central limit theorem is required to establish confidence limits on both the population mean and standard deviation. The central limit theorem can be stated as follows:

Given a population with mean, μ , and variance, σ^2 , then the distribution of successive sample means, from samples of n observations, approaches a normal distribution with mean, μ , and variance σ^2/n .

In simpler terms, if we start with a general population A , where the mean is μ_A and the variance is σ_A^2 , and take multiple samples each of size n , then the resulting sample means will also have some distribution with a mean and variance ($\mu_{\bar{x}}$, $\sigma_{\bar{x}}^2$). Regardless of the original distribution of A , the distribution of the means will be approximately normal (it gets better as n is increased). Also, the mean of the means will be the same as the mean of A , and, finally, the variance of the means is the variance of A divided by n . This is depicted in Figure 12.

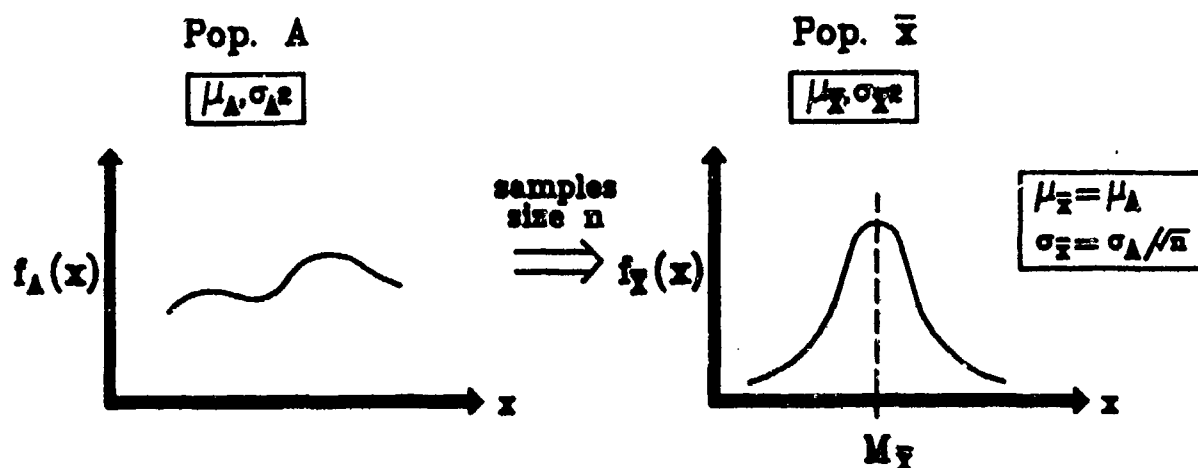


Figure 12. Central Limit Theorem.

Although proof of the central limit theorem is beyond our scope here, a cursory inspection shows that it passes the common sense test. If our sample size is very small (say 1), then for many samples, the distribution of our means is identical to the original and $\mu_{\bar{X}} = \mu_A$ and $\sigma_{\bar{X}} = \sigma_A$. At the other extreme, if n is infinite (exhaustive) then we always get the true population mean and variance. Accordingly, $\mu_{\bar{X}} = \mu_A$ and $\sigma_{\bar{X}} = 0$.

We now turn to using the central limit theorem to establish confidence intervals.

13.5.2 Confidence Interval for the Mean

If we take a sample of size n , we now know that the distribution of the means of multiple samples would be approximately normally distributed, as shown in Figure 13.

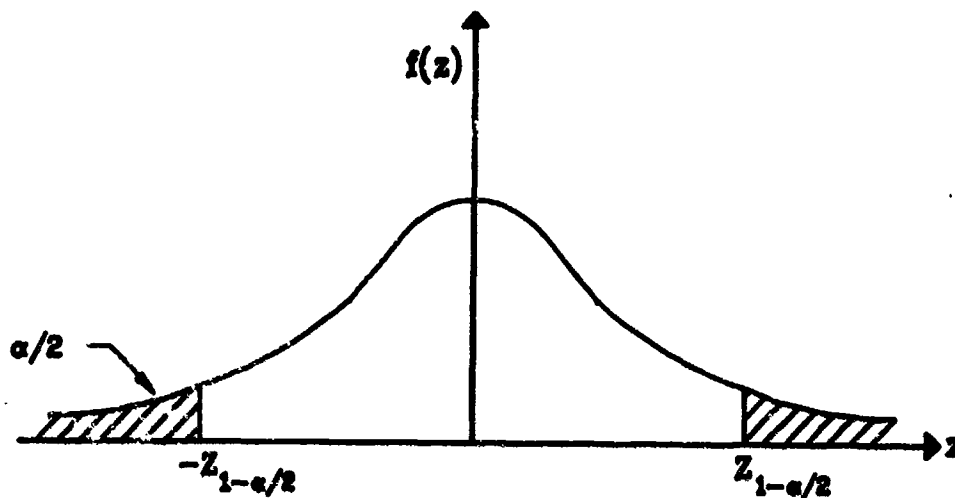


Figure 13. Establishing confidence limits on the mean.

From the definition of a normal probability distribution, we can say that a sample z will be between $-z_{1-\alpha/2}$ and $z_{1-\alpha/2}$ with probability $1 - \alpha$, or

$$P(-z_{1-\alpha/2} < z < z_{1-\alpha/2}) = 1 - \alpha$$

If our z comes from one of the sample means,

$$z = \frac{\bar{x} - \mu_{\bar{x}}}{\sigma_{\bar{x}}}$$

or, using the central limit theorem

$$z = \frac{\bar{x} - \mu}{\sigma/\sqrt{n}}$$

thus

$$P(-z_{1-\alpha/2} < \frac{\bar{x} - \mu}{\sigma/\sqrt{n}} < z_{1-\alpha/2}) = 1 - \alpha$$

or

$$P(\bar{x} - z_{1-\alpha/2} \frac{\sigma}{\sqrt{n}} < \mu < \bar{x} + z_{1-\alpha/2} \frac{\sigma}{\sqrt{n}}) = 1 - \alpha$$

That is, $(1 - \alpha)$ 100% of the time, the true population mean, μ , will be within $\pm z_{1-\alpha/2} \frac{\sigma}{\sqrt{n}}$ of the sample mean. The range of values is the interval and $(1 - \alpha)$ is the confidence level.

As an example, suppose we wanted to know the 95% and 99% confidence intervals for the maximum thrust of new F-100 engines given that a sample of 50 engines produced a mean max thrust of 22,700 lbs with a sample standard deviation $s = 500$ lbs.

1. At 95%, $\alpha = .05$ and $z_{1-\alpha/2} = 1.96$.

$$\mu = \bar{x} \pm z_{1-\alpha/2} \frac{\sigma}{\sqrt{n}}$$

Therefore

$$= 22,700 \pm 1.96 \frac{500}{\sqrt{50}}$$

or

$$22,561 < \mu < 22,839$$

2. At 99%, $\alpha = .01$ and $z_{1-\alpha/2} = 2.58$.

Thus

$$\mu = 22,700 \pm 2.58 \frac{500}{\sqrt{50}}$$

or

$$22,518 < \mu < 22,882$$

The above example points out two important considerations. As you might have anticipated, as the requirement for certainty increases (95 + 99%), the interval widens. Given that the normal probability is continuous from $-\infty$ to $+\infty$, if we require that we be 100% certain that the true μ falls within our interval, the confidence interval becomes meaningless: $-\infty < \mu < +\infty$.

The second important point is that to construct the interval we had to use s as an estimate of σ . This is, in fact, a legitimate estimate if $n \geq 30$. For smaller sample sizes, we cannot make this assumption and must resort to the method described in the next section.

13.5.3 Confidence Interval for Mean for Small Samples

When the sample size is less than 30 and the population variance is unknown (the typical case in flight testing), we must substitute t (defined earlier) for z :

$$(\bar{x} - t_{v, 1-\alpha/2} \frac{s}{\sqrt{n}}) < \mu < (\bar{x} + t_{v, 1-\alpha/2} \frac{s}{\sqrt{n}})$$

As an example, suppose our earlier data on F-100 engines was based on a sample of only 5 engines. Then at the 95% confidence level:

$$\alpha/2 = .025 \text{ and } v = 4, \text{ thus } t_{4, 0.975} = 2.78$$

and

$$\begin{aligned} \mu &= \bar{x} \pm t_{v, 1-\alpha/2} \frac{s}{\sqrt{n}} \\ &= 22,700 \pm 2.78 \frac{500}{\sqrt{5}} \end{aligned}$$

or

$$22,078 < \mu < 23,321$$

And as you should have expected, the interval at the same confidence level had to increase to accommodate the smaller sample size.

13.5.4 Confidence Interval for Variance

In a manner similar to that of confidence intervals for the mean, we can establish a confidence interval for the variance based on the previously defined statistic χ^2 :

$$\chi^2 = \frac{(n-1)s^2}{\sigma^2}$$

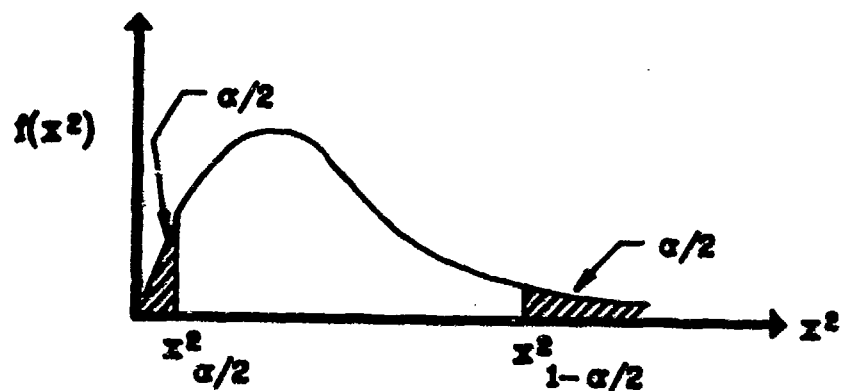


Figure 14. Establishing confidence limits on variance.

From Figure 14, we can see that the probability of our sample statistic χ^2 falling between $\chi^2_{\alpha/2}$ and $\chi^2_{1-\alpha/2}$ is just $1-\alpha$.

$$P(\chi^2_{\alpha/2} < \frac{(n-1)s^2}{\sigma^2} < \chi^2_{1-\alpha/2}) = 1 - \alpha$$

Thus, with $(1-\alpha)$ 100% confidence,

$$\chi^2_{\alpha/2} < \frac{(n-1)s^2}{\sigma^2} < \chi^2_{1-\alpha/2}$$

or

$$\frac{(n-1)s^2}{\chi^2_{1-\alpha/2}} < \sigma^2 < \frac{(n-1)s^2}{\chi^2_{\alpha/2}}$$

For example, if we take a sample of size 6 and find that the sample standard deviation is 2, we can specify with 95% probability between what limits the true population variance lies. In this case, we have:

$$\alpha/2 = .025, 1-\alpha/2 = 0.975, v = 5, s = 2$$

thus

$$\frac{(6-1)2^2}{\chi^2_{5,.975}} < \sigma^2 < \frac{(6-1)2^2}{\chi^2_{5,.025}}$$

where

$$\chi^2_{5,.975} = 12.8, \chi^2_{5,.025} = .831$$

thus

$$\frac{5(4)}{12.8} < \sigma^2 < \frac{5(4)}{.831}$$

or

$$1.56 < \sigma^2 < 24.1$$

The large band is due to the small sample size. If the sample variance were the same for a larger sample (say $n = 18$), then the confidence interval would be smaller; for instance

$$\frac{17(4)}{30.2} < \sigma^2 < \frac{17(4)}{7.56}$$

$$2.25 < \sigma^2 < 8.99$$

13.6 HYPOTHESIS TESTING

Closely tied to the idea of confidence intervals is perhaps the most important part of statistical analysis: hypothesis testing. A statistical hypothesis is a statement, which may or may not be true, concerning one or more populations. Instead of using our sample data to make a point or interval estimate of some population parameter, we first hypothesize that a population parameter is such and such, and then use sample data to determine the reasonableness of our hypothesis. The truth or falsity of a statistical hypothesis is never known with absolute certainty unless we examine the entire population. This is certainly the case in nearly all flight tests. A simple example may illustrate the concept.

Suppose we assume (hypothesize) that a given coin is fair, that is, the probability of heads is .5. To determine if our assumption is correct we toss the coin 100 times. If the results are 48 heads, we may conclude that it is reasonable to say the coin is fair. If, on the other hand, we get only 35 heads, it may be more reasonable to conclude that the coin is not fair.

The subject of this section is how to draw the line in cases like this.

13.6.1 Null and Alternate Hypotheses

It should be emphasized at the outset that the acceptance of a statistical hypothesis is a result of insufficient evidence to reject it and does not necessarily mean that it is true. Because of the fact, we must be careful in setting up our hypothesis since in the absence of data, we will be forced to accept our original hypothesis. Usually, we select this hypothesis with the sole objective of rejecting (or nullifying) it. Hence, it is called the null hypothesis, denoted H_0 . The null hypothesis is usually formulated so that in the case of insufficient data, we return to the status quo or safe decision. Examples of null hypothesis are:

1. The defendant is innocent (not a statistical hypothesis, but a good illustration).
2. The lock-on range of a new RADAR is no better than that of the present RADAR.
3. The MTBF of a new part is no better than that of the existing part.

Since we are attempting to negate our null hypothesis, we should have established an alternate hypothesis, denoted H_1 to reflect what we want to prove and let H_0 then be the negation of H_1 .

EXAMPLES:

- | | | | |
|-----------|-----------------|--------|--------------------|
| 1. $H_0:$ | $\mu = 15$ | $H_1:$ | $\mu \neq 15$ |
| 2. $H_0:$ | $p \geq .9$ | $H_1:$ | $p < .9$ |
| 3. $H_0:$ | $\mu_1 = \mu_2$ | $H_1:$ | $\mu_1 \neq \mu_2$ |

13.6.2 Types of Errors

Regardless of how carefully we set up a test, there is always the chance that we will come to the wrong conclusion. In our earlier example of tossing a coin assumed to be fair, the result of 35 heads out of 100 times could be simply due to chance variation of a fair coin (the probability of this occurring is small, .0026, but not zero). If we reject the null hypothesis when in fact it is true, this is called a Type I error, and the probability of doing so is denoted α , called the level of significance.

A different error results if we accept the null hypothesis when it is false. This is a Type II error, and its probability is denoted by β . For example, if in the coin experiment, we concluded it was a fair coin based on a result of 48 heads out of 100, the coin may really have a probability of heads of .4 and the 48 result was due to chance variation (in this case $\beta = .10$).

These two different errors are summarized in Table 3. Generally, because of the fail-safe wording of the null hypothesis, we desire to have α , the probability of rejecting H_0 when it is true, very small, usually .05 (occasionally .01). The smaller α is, however, the larger β becomes. Generally, β is larger than α since this is a more acceptable error (a large β implies we stay with the status quo, H_0 , more frequently than we should). The only way to reduce both α and β is to take more data. If we do exhaustive sampling, α and β go to zero.

if	and H_0 is	
	True	False
Accept H_0	O.K.	Type II
Reject H_0	Type I	O.K.

Table 3. Errors in Hypothesis Testing

13.6.3 One Tailed vs Two Tailed Tests

During some tests, we are interested in extreme values in either direction. Burn times on rocket motors might be an example. Too long or too short of a burn time may have dire consequences for system performance. For tests of this sort, we would form hypothesis of the form:

$$H_0: \mu = \mu_0 \text{ and } H_1: \mu \neq \mu_0$$

In these cases, we should reject H_0 whenever our sample produced results that were either too high or too low. Thus, our level of significance, α , would be divided into two equal regions as shown in Figure 15b.

In most flight test examples, however, we are concerned with extremes in one direction only. For example, we hypothesize that the aircraft meets the contractual specification for takeoff distance. The only significant alternative hypothesis is that the actual takeoff distance is longer than the specification. For tests of this sort, we would form hypothesis of this form:

$$H_0: \mu \leq \mu_0 \text{ and } H_1: \mu > \mu_0$$

or

$$H_0: \mu \geq \mu_0 \text{ and } H_1: \mu < \mu_0$$

In these cases, we would reject H_0 only when our sample produced results that were extreme in one direction. Thus, our level of significance, α , would be in one tail of the curve only as shown in Figure 15a.

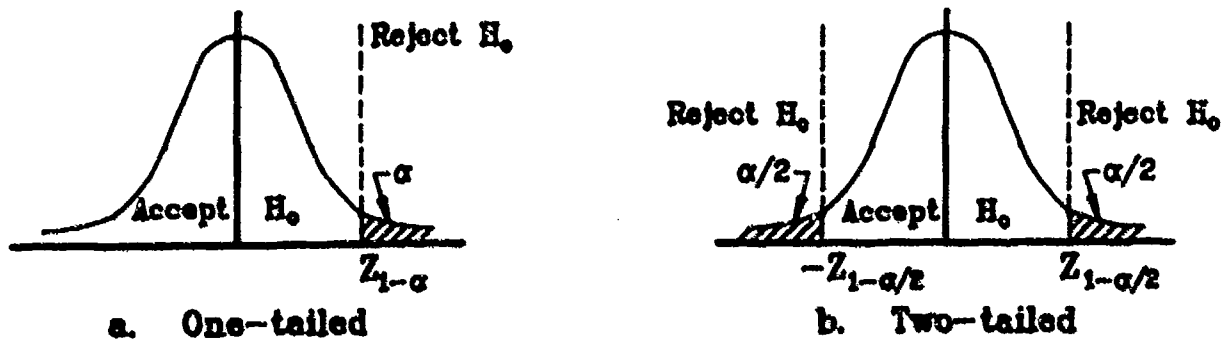


Figure 15. One-tailed vs. two-tailed tests.

13.6.4 Tests on Means

The first step in hypothesis testing is to formulate the null and alternate hypothesis. Second, choose the level of significance (α) and define the areas of acceptance and rejection. Third, collect data and compare the results to what was expected. Fourth, accept or reject the null hypothesis. For tests on means, we will use the same statistic we used in constructing confidence intervals:

1. For $n > 30$ or σ known, use $z = \frac{\bar{x} - \mu_0}{\sigma/\sqrt{n}}$
2. For $n < 30$ and σ unknown, use $t = \frac{\bar{x} - \mu_0}{s/\sqrt{n}}$

The following two examples should illustrate the method:

EXAMPLE 1: Two tailed test on mean, σ known. During early testing of the F-19 bombing system, it was determined that the cross range errors for 30° dive bomb passes were normally distributed with a mean error of 20 feet and a standard deviation of 3 feet. After a flight control modification to reduce adverse high AOA flying qualities, it was found that the mean cross range error for nine bomb runs was 22 feet. Has the mean changed at the .05 level of significance?

Step one: Form null and alternate hypothesis:

$$H_0: \mu = 20 \text{ (status quo)}$$

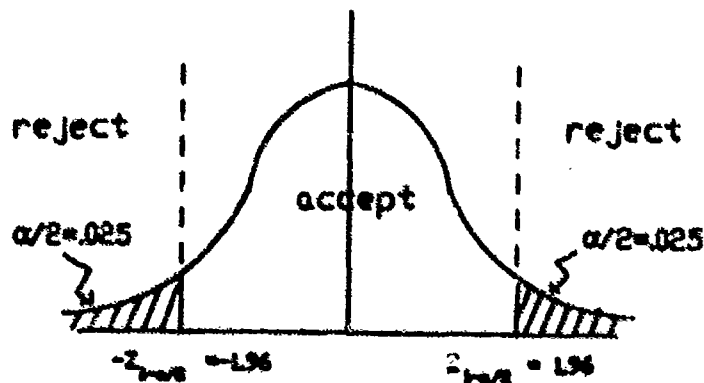
$$H_1: \mu \neq 20$$

Step two: $\alpha = .05$ (given) and this will be divided into two tails, high and low, since extreme values in either direction would indicate that μ has changed.

Step three: Since s was not given, we will assume that σ has not changed significantly from the unmodified system. This is not an obvious truth, but its use here illustrates the criteria for using the z statistic. In any case, our data gives:

$$z = \frac{\bar{x} - \mu_0}{\sigma/\sqrt{n}} = \frac{22 - 20}{3/\sqrt{9}} = 2$$

Compare this to the areas of rejection/acceptance below



Step four: Because $z > z_{1-\alpha/2}$ ($2 > 1.96$), we must reject the null hypothesis and conclude that (with 95% confidence) the mean cross range bombing error has changed due to the flight control modification.

EXAMPLE 2: One tailed test on mean, small sample, σ unknown. Suppose we fly nine sea level to 20,000 ft PA check climbs to verify a contract specification which states that the fuel used in this climb shall not be greater than 1500 pounds. We find that our sample of nine climbs used an average of 1600 pounds with a sample standard deviation of 200 pounds.

Step one: Form null and alternate hypothesis:

$$H_0: \mu \leq 1500 \text{ (innocent until proven guilty)}$$

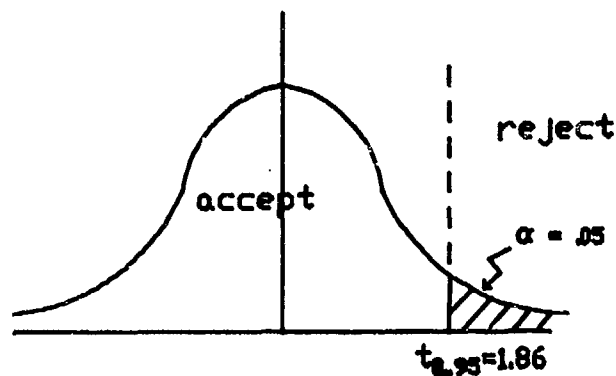
$$H_1: \mu > 1500$$

Step two: Choose $\alpha = .05$. An α of .01 is usually reserved for safety of flight questions. At other times, it may be specified in the contract. This is a one tailed test.

Step three: Since we have less than 30 data points and σ is unknown, use the data to calculate the t statistic:

$$t = \frac{\bar{x} - \mu_0}{s/\sqrt{n}} = \frac{1600 - 1500}{200/\sqrt{9}} = 1.5$$

Comparing this to the areas of acceptance/rejection below:



Step four: Because $t < t_{\alpha, 1-\alpha}$ ($1.5 < 1.867$) we must accept the null hypothesis and accept the contractor's claim that he has met the specification. Another way of saying it is that we don't have the data at 95% confidence to prove that the contractor has failed to meet the specification.

13.6.5 Tests on Variance

The four steps for testing hypotheses on means described in the previous section are still valid here. The only difference in the two procedures is the use here of the chi-squared statistic instead of the z or t statistic:

$$\chi^2 = \frac{(n-1)s^2}{\sigma^2}$$

For example, in a bombing system, the mean should be close to zero. Thus, the goodness of a system can best be measured by the dispersion of the system. Generally, the circular error probable is used as a measure of dispersion. We could, however, use the standard deviation.

Suppose the F-19 contract specification states that the standard deviation of miss distances for a particular computed delivery mode shall not

exceed 10 meters at the 90% confidence level. In ten test runs, we get a standard deviation of 12 meters. Can we fine the contractor?

Step one: Form null and alternate hypotheses:

$$H_0: \sigma \leq 10$$

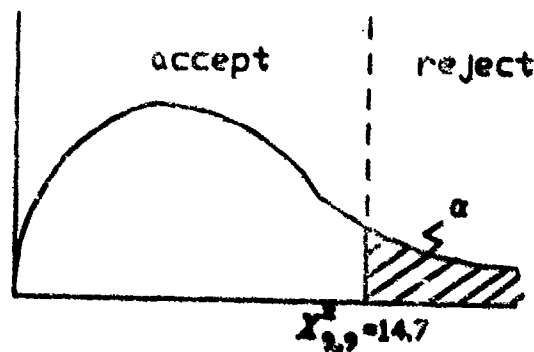
$$H_1: \sigma > 10$$

Step two: An α of .10 is specified. Since smaller σ 's are good, our test is a one tailed test. Only extreme large σ 's will result in nullifying H_0 .

Step three: Using our data, we calculate χ^2 :

$$\chi^2 = \frac{(n-1)s^2}{\sigma^2} = \frac{9 \times 144}{100} = 13$$

Comparing this to $\chi^2_{v, 1-\alpha}$:



Step four: Because $\chi^2 < \chi^2_{9, .9}$ ($13 < 14.7$) we do not have adequate data to conclude that the contractor has failed the specification. Accept H_0 .

13.6.6 Summary

At times, it can be a little confusing, especially with tests on variances, as to when to reject or accept the null hypotheses. Drawing figures with areas of acceptance and rejection, as has been done in the above examples, can help eliminate the uncertainty. As an aid, the critical regions delineated in Table 4 can also be used to define areas of acceptance and rejection.

H_0	Statistics	H_1	Critical Region
$\mu = \mu_0$	$z = \frac{\bar{x} - \mu_0}{\sigma/\sqrt{n}}$ <p>$(n \geq 30 \text{ or } \sigma \text{ known})$</p>	$\mu < \mu_0$ $\mu > \mu_0$ $\mu \neq \mu_0$	$z < -z_{1-\alpha}$ $z > z_{1-\alpha}$ $z < -z_{1-\alpha}/2, z > z_{1-\alpha}/2$
$\mu = \mu_0$	$t = \frac{\bar{x} - \mu_0}{s/\sqrt{n}}$ <p>$(n < 30 \text{ and } \sigma \text{ unknown})$</p>	$\mu < \mu_0$ $\mu > \mu_0$ $\mu \neq \mu_0$	$t < -t_{1-\alpha}$ $t > t_{1-\alpha}$ $t < -t_{1-\alpha}/2, t > t_{1-\alpha}/2$
$\sigma^2 = \sigma_0^2$	$\chi^2 = \frac{(n-1)s^2}{\sigma_0^2}$	$\sigma^2 < \sigma_0^2$ $\sigma^2 > \sigma_0^2$ $\sigma^2 \neq \sigma_0^2$	$\chi^2 < \chi_{\alpha}^2$ $\chi^2 > \chi_{1-\alpha}^2$ $\chi^2 < \chi_{\alpha/2}^2, \chi^2 > \chi_{1-\alpha/2}^2$

Table 4. Test Criteria for Means and Variances

13.7 NONPARAMETRIC TESTS

The preceding section describes tests for populations that have normal or approximately normal distributions. Most phenomena are in fact normal. Some, however, are more accurately described by other distributions, such as the Raleigh, Cauchy, Log Normal, etc. The method of testing hypotheses described is still applicable, but the test statistic and the shape of the probability distribution would change. Tabulated values of these distributions are not always readily available. More frequently, determining the correct distribution type may be difficult. This section describes tests for populations whose distributions are not known to be normal.

13.7.1 Parametric vs Nonparametric Tests

Nonparametric tests make no assumption concerning the shape of the population distribution. These types of tests are less powerful than the tests described in the previous section when they are used on normally distributed data. That is, they require larger sample sizes to give us the same information from the test. Because of this, the preferred procedure would be to use various tests (called goodness of fit tests) to determine the population distribution and then to use the appropriate parametric test. Failing this, a nonparametric test could be used.

Three nonparametric tests that can be useful in flight testing will be presented here: rank sum test, sign test, and signed rank test. The underlying basis for each of these tests is the binomial probability distribution described earlier. Essentially, each test starts out assuming that two populations are equivalent ($f_1(x) = f_2(x)$ and thus $\mu_1 = \mu_2$) and calculates statistics from two samples. Based on these test statistics, you can determine the probability of your observations, assuming identical populations. Given that probability, we can decide if our original assumption was correct.

13.7.2 The Rank Sum Test

The rank sum test is also known as the U test, the Wilcoxon test, and the Mann-Whitney test in various references. This test, along with the other two nonparametric tests described in this section, can be used to test the null hypothesis that two different samples come from identical populations.

The method consists of the following steps:

1. Rank order all of the data from the two samples, noting whether each data point came from sample one or two.
2. Assign rank values to each point, one to the lowest, two to the next, etc. In the event that two or more data points have the same value, give each an average rank. For instance, if the 7th and 8th points are the same, give both a rank of 7.5.
3. Compute the sum of the ranks of each sample (R_1 , R_2).
4. Calculate the following U statistic where n_1 and n_2 are sample sizes:

$$U_1 = n_1 n_2 + \frac{n_1(n_1 + 1)}{2} - R_1$$

$$U_2 = n_1 n_2 + \frac{n_2(n_2 + 1)}{2} - R_2$$

Note: $U_1 + U_2 = n_1 n_2$ can be used as a math check.

5. Compare the smaller U to the critical values of U listed in the appendix for $\alpha = .10$ or $\alpha = .05$.
6. If $U < \text{critical value}$, reject H_0 : $\mu_1 = \mu_2$.

While the procedure may not appear to be very intuitive, its basis is in the binomial distribution. That is, if two samples are taken from identical populations, what is the probability of getting them in a particular rank order?

As an example, consider the following. The detection ranges of two radars under controlled conditions were tested with the following results:

System 1: 9, 10, 11, 14, 15, 16, 20

System 2: 4, 5, 5, 6, 7, 8, 12, 13, 17

Is there a difference between the two systems at 90% confidence?

Using the steps described above:

1. Rank order all scores.
2. Assign Rank values.

Score	4,	5,	5,	6,	7,	8,	9,	10,	11,	12,	13,	14,	15,	16,	17,	20
System	2,	2,	2,	2,	2,	2,	1,	1,	1,	2,	2,	1,	1,	1,	2,	1
Rank	1,	2.5,	2.5,	4,	5,	6,	7,	8,	9,	10,	11,	12,	13,	14,	15,	16

3. Compute R_1 , R_2 .

$$R_1 = 7 + 8 + 9 + 12 + 13 + 14 + 16 = 79$$

$$R_2 = 1 + 2.5 + 2.5 + 4 + 5 + 6 + 10 + 11 + 15 = 57$$

4. Calculate U_1 , U_2 .

$$U_1 = n_1 n_2 + \frac{n_1(n_1+1)}{2} - R_1 = 7 \times 9 + \frac{7(8)}{2} - 79 = 12$$

$$U_2 = n_1 n_2 + \frac{n_2(n_2+1)}{2} - R_2 = 7 \times 9 + \frac{9(10)}{2} - 57 = 51$$

5. Compare the smaller U (12 in this case) with critical values

$$\text{for } \alpha = .10, n_1 = 7, n_2 = 9, U_{cr} = 15$$

6. Since $U < U_{cr}$, we can reject the null hypothesis that the two radars have the same performance with 90% confidence.

13.7.3 The Sign Test

The sign test is an even simpler nonparametric test which has the advantage that it can be applied to nominal data. All that is required is paired observations of two samples with a "better than" evaluation. For example, this test can be used when each of a group of pilots evaluates two systems and identifies which he prefers.

Like the rank sum test, the null hypothesis is that the two samples came from the same population and therefore the chance of preferring System A over B is just the same as preferring B over A (i.e., .5). Therefore, here we can use the binomial distribution directly. If System A is preferred x times in N tests, the probability of this happening is:

$$f(x) = \frac{N!}{x!(N-x)!} p^x q^{N-x} = \frac{N!}{x!(N-x)!} (.5)^N$$

(Note that values for $f(x)$ are tabulated in the appendix.)

But this is a point probability in our discrete distribution, and we need the entire tail. See Figure 16.

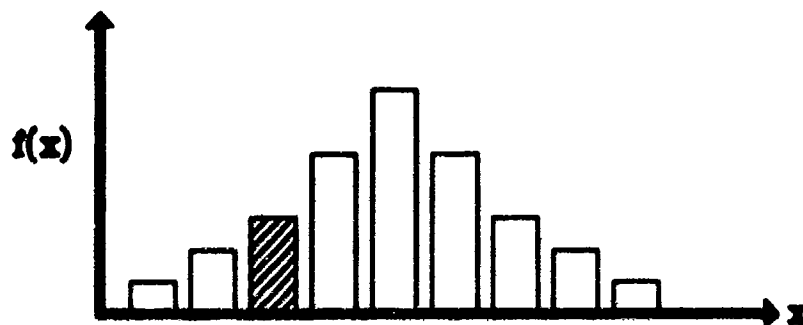


Figure 16. Point probability (shaded area) on a binomial distribution.

Thus, if you need to test a single tailed hypothesis, then sum the probabilities from the end up to the sample data result:

$$P(0 \leq n \leq x) = \sum_{i=0}^x \frac{N!}{i!(N-i)!} (0.5)^N$$

If the probability of getting a value in the tail(s) of concern is less than your chosen level of significance, then you should reject the null hypothesis that there is no difference between the systems.

For example, suppose 10 pilots evaluate the power approach handling qualities of the F-19 with two different control laws and 7 prefer System B, 2 prefer System A, and 1 has no preference. Should we switch production lines to System B? The cost is high, but if we wait to do more testing the cost will be prohibitive.

The null hypothesis is that System A and B are equally desirable. The no preference is discarded with that null hypothesis. Choose a level of significance of .05 since safety of flight is not a concern. We must now

calculate the probability of getting 0, 1, or 2 pilots to choose system A if there really were no difference. If this probability is less than our level of significance, then we will reject H_0 and conclude that B is better than A.

$$P(0 \text{ prefer A}) = \frac{9!}{0!(9)!} (.5)^9 = .002$$

$$P(1 \text{ prefers A}) = \frac{9!}{1!(8)!} (.5)^9 = .018$$

$$P(2 \text{ prefers A}) = \frac{9!}{2!(7)!} (.5)^9 = .070$$

Total	<u>.090</u>
-------	-------------

Thus, we can only be 91% sure that B is really better than A. Not enough (at 95% significance) to justify the added expense of System A. That is, accept H_0 : no significant difference between A and B.

For sample sizes of 15 or larger, we can use the normal approximation to the binomial distribution with very little error. In this case,

$$z = \frac{x - np}{\sqrt{npq}}$$

As a comparison, checking the approximation for our last example with $n = 9$, $p = .5$, $q = .5$, and with $x = 2.5$ (discrete function so a continuous approximation should start 1/2 unit higher), we get

$$z = \frac{2.5 - 9/2}{\sqrt{9/4}} = -1.33$$

From the tables in the appendix, this corresponds to single tail probability of 90.8%, only 1% off our more exact calculation. While not this accurate for all combinations of x and n , when $n \geq 15$, any difference can be neglected.

13.7.4 The Signed Rank Test

The signed rank test combines elements of both the sign test and the rank sum test. Thus, the underlying assumptions are the same. System A is no better or worse than System B. Although the sign test was very simple, if we have some indication of how much better System B is than System A, then use of

the sign test alone would ignore perhaps crucial data. The signed rank test incorporates this data.

The method is as follows:

1. First, rank the differences between paired observations by absolute magnitude. Ignore cases where a pair of observations is identical (i.e., no preference). Also, if there is a tie in rank order, assign an average rank to each tie.
2. Next, sum the positive and negative ranks (W_+ , W_-). The test statistic is the smaller W .
3. Compare W with critical values in the table in the appendix for the appropriate level of significance.
4. Reject H_0 if $W < W_{cr}$.

As an example, suppose our previous 10 pilots who evaluated the F-19 flight control system gave systems A and B the following Cooper-Harper ratings (1 best, 10 worst):

<u>Pilot</u>	<u>System A</u>	<u>System B</u>	<u>Difference</u>
1	3	1	2
2	5	2	3
3	3	4	-1
4	4	3	1
5	3	3	0
6	4	2	2
7	4	1	3
8	2	1	1
9	3	1	2
10	1	2	-1

Ranking the differences by absolute magnitude, ignoring the zero difference gives:

Rank	2.5	2.5	2.5	2.5	6	6	6	8.5	8.5
Difference	-1	1	1	-1	2	2	2	3	3

where now

$$W_+ = 2.5 + 2.5 + 6 + 6 + 6 + 8.5 + 8.5 = 40.0$$

$$W_- = 2.5 + 2.5 = 5.0$$

Using $\alpha = .05$, W_{cr} from the tables in the appendix is 8 (use one tailed criteria since B is obviously not worse than A). Since $W < W_{cr}$ ($5 < 8$), we can now reject H_0 and conclude that System B is better than System A with 95% confidence.

13.8 SAMPLE SIZE

All of the tests presented so far assume the data has all been collected before analysis began. Because collecting data in flight testing can be very costly in terms of money and time (there are always more things to be tested than resources allow), a scientific method to determine how many data points are needed to get statistically significant results would be very useful. We do not want our results obscured by the random variations experienced during the test. On the other hand, excessive sample sizes would give us little additional information at the expense of delaying a lower priority (but required) test.

Presented below are two approaches for determining sample size: accuracy driven and a general approach for establishing a significant difference between means.

13.8.1 Accuracy Driven

If we are required to determine a population statistic (say the mean takeoff distance) within some accuracy (say 10%), then we can use the concept of a confidence interval to determine the number of samples we need to take. The confidence interval for the mean (σ known) is:

$$(\bar{x} - z_{1-\alpha/2} \frac{\sigma}{\sqrt{n}}) \leq \mu \leq (\bar{x} + z_{1-\alpha/2} \frac{\sigma}{\sqrt{n}})$$

or

$$|\mu - \bar{x}| \leq z_{1-\alpha/2} \frac{\sigma}{\sqrt{n}}$$

or

$$n \leq \left| \frac{z_{1-\alpha/2} \sigma}{|\bar{x} - \mu|} \right|^2$$

but $|\bar{x} - \mu|$ is the error in measuring μ . Thus, we can write

$$n \leq \left| \frac{z_{1-\alpha/2} \sigma}{E} \right|^2$$

For example, suppose a review of similar aircraft takeoff data shows that historically the standard deviation is about 20% of the mean. Then if the SPO wants us to determine takeoff distance to within 10% with 95% confidence, we can determine the number of times to schedule a takeoff test:

$$z_{.975} = 1.96, \quad \sigma = .2\mu, \quad E = \pm .1\mu$$

so

$$n \leq \left| \frac{(1.96)(.2\mu)}{(.1\mu)} \right|^2 = 15.4$$

Therefore, 16 sorties should be adequate to achieve the accuracy required by the SPC. As the test is in progress, we should continually check to see if our assumption concerning the standard deviation remains reasonable (tests of hypotheses on variance).

13.8.2 General Approach

Another frequent problem in flight testing is to determine if a system meets a specification (does $\mu = \mu_0$?) or comparing two systems to see if there is a difference (does $\mu_1 = \mu_2$?). Determining the required sample size is a lot more complex than when the criteria is simply accuracy.

Suppose we sample two different populations with means μ_1 and μ_2 . As we take paired samples, we calculate the differences between them, δ . If we took a large number of samples, the resulting δ 's would have some mean and distribution. If there really were no difference between the two populations, then the mean would be zero as shown in Figure 17. If the means were different, then the mean would be some value δ_1 as shown in Figure 18.

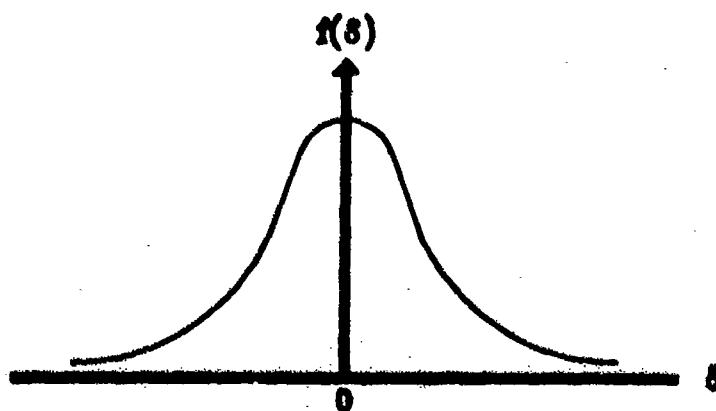


Figure 17. Distribution of $x_1 - x_2 = \delta$ when $\mu_1 = \mu_2$.

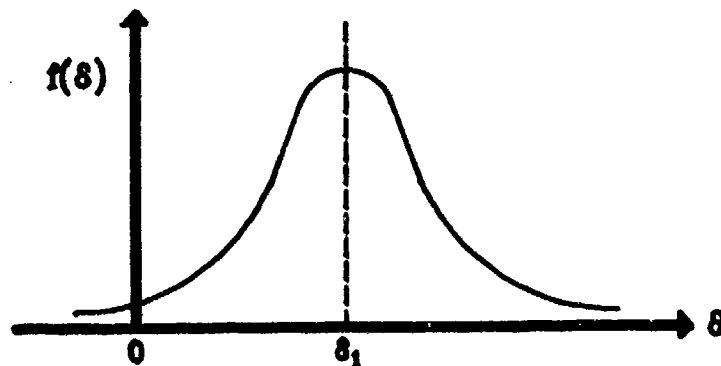


Figure 18. Distribution of $x_1 - x_2 = \delta$ when $\mu_1 - \mu_2 = \delta_1$.

Combining these two alternatives in Figure 19, we can see that the two curves cross at some value $\delta = x_c$. A test result that gave a mean of differences above x_c would lead us to conclude that populations one and two differed in their means with level of significance of α . On the other hand, a value less than x_c would lead us to believe there was not a difference when in fact there was (with probability β as shown). The relationship between α and β can be seen graphically in Figure 19. If we move x_c to the right, we reduce α but increase β . Conversely, minimizing β by moving x_c left results in an increase in α . The only way to decrease α and β at the same time is to increase the sample size.

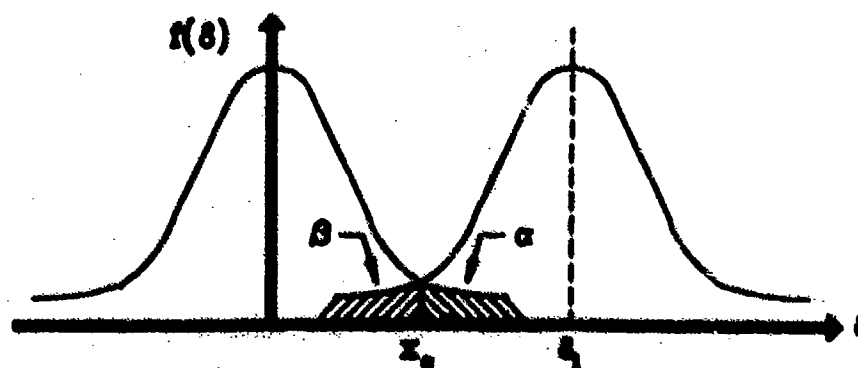


Figure 19. Probability of type I and II errors for comparing means.

Recalling from the central limit theorem that $\sigma_{\bar{x}} = \sigma_x/\sqrt{n}$, we can see that α and β are direct functions of the number of samples taken and the value of δ_1 . The relationship between these variables is:

$$n = \frac{(z_{1-\alpha} + z_{1-\beta})^2 (\sigma_1^2 + \sigma_2^2)}{\delta_1^2}$$

The way to use this relationship is as follows:

1. Specify α . Normally, .10, .05, or .01.
2. Specify β . Usually larger than α , typically set at .10 or .20.
3. Specify δ_1 . This is the least difference between μ_1 and μ_2 considered operationally significant.
4. Calculate σ_1 and σ_2 . Initially, this will come from historical examples or be simply a guess.) As the test continues, it can be refined. Note that if μ_2 is a specification, then $\sigma_2 = 0$.

For example, how many tests are required to determine if the contractor met the specification for a weapon delivery accuracy of 5 mils? Assume a normal error distribution with a standard deviation of 3 mils (from previous tests).

1. Set $\alpha = .05$
2. Set $\beta = .10$
3. Let $\delta_1 = 1$ mil (operationally significant)
4. $\sigma_1 = 3$ mils and $\sigma_2 = 0$ (specification)

Now, we can calculate n :

$$n = \frac{(z_{.95} + z_{.90})^2 (3^2 + 0^2)}{1^2} = (1.645 + 1.28)^2 \cdot 9 = 77$$

Thus, 77 data points are required. Practically speaking, this may be an unacceptable answer, requiring that something in a, b, or c above be changed. Tradeoffs are the subject of the next section.

13.8.3 Tradeoffs

As can be seen from the example above, we cannot always live with our answers. In calculating n , there were many choices, some for which the consequences were not obvious. How significant is it if we change β from .10 to .20, or if we change δ_1 from 1.0 to 1.5? One good way to approach

these choices is to plot the required n for various changes in α , β , and δ_1 . Then engineering judgment can be used where discretion is available. Figure 20 is one such example.

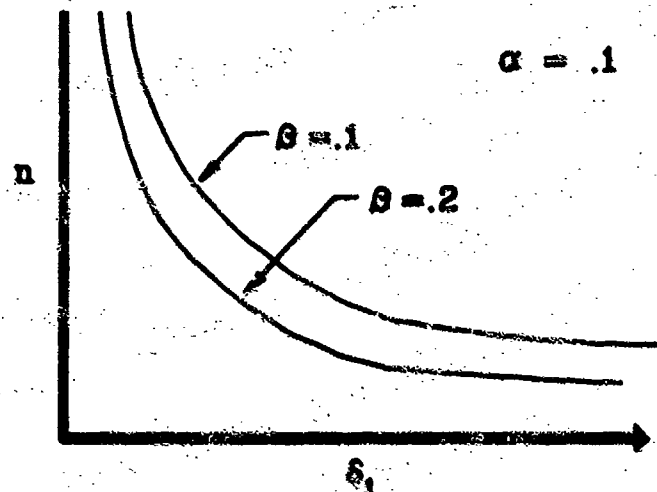


Figure 20. Typical variation of sample size, n , with minimum significant difference, δ_1 .

13.8.4 Nonparametric Tests

The required sample size for nonparametric tests cannot be determined with accuracy. In practice, however, it has been found that the signed rank test is about 90% as efficient as a test on means using the z statistic. Therefore, you could calculate n as described earlier and divide by .9.

For example, how many pilots do we need to evaluate new power approach control laws in the F-19? We want to be 90% certain that there is a significant improvement (defined here as 1 Cooper-Harper rating).

1. $\alpha = .10$
2. $\beta = .20$ (arbitrary)
3. $\delta_1 = 1$
4. σ_1, σ_2 (review of similar tests show $\sigma = 1$)

Thus,

$$n = \frac{1}{.9} \frac{(z_{.9} + z_{.8})^2 (1^2 + 1^2)}{1^2}$$

$$= \frac{1}{.9} (1.33 + .84)^2 2 = 9.99$$

Or 10 evaluation pilots should be planned.

13.9 ERROR ANALYSIS

Thus far in the course, we have only been concerned with the statistics of directly measured values. Often, however, measured values are used to compute some parameter of interest. For example, fuel used is usually obtained from fuel flow rate times time ($\dot{m} \times t$), and specific range is velocity divided by fuel flow (v/\dot{m}).

In this section, rules for determining the precision of the computed results are presented. Specifically, we will discuss significant figures, error propagation, and standard deviation of calculated values.

13.9.1 Significant Figures

The precision of an experimental result is implied by the way in which the result is written. To indicate the precision, we write a number with as many digits as are significant. The number of significant figures is defined as follows:

1. The leftmost nonzero digit is the most significant digit.
2. If there is no decimal point, the rightmost nonzero digit is the least significant digit.
3. If there is a decimal point, the rightmost digit is the least significant digit, even if it is zero.
4. All digits between the least and most significant digits are counted as significant digits.

For example, the following numbers each have four significant digits: 1234, 123,400; 123.4; 1001; 1000.; 10.10; 0.0001010; 100.0.

Although there are no uniform rules for deciding the exact number of digits to use when quoting measured values, the number of significant figures should be approximately one more than that dictated by the experimental precision (i.e., small scale division). For example, if we measure an event using a watch with tenth of a second divisions, we should not record a reading with more than two decimal places (10.24 seconds for instance). When computing a value, the following general rules apply:

1. In addition and subtraction, retain in the more accurate numbers one more decimal digit than is contained in the least accurate number ($1.0 + 3.55 + 4.50 + 1.20 = 1.0 + 3.55 + 4.50 + 1.2 = 10.25$).

2. In all other computations, retain from the beginning one more significant figure in the more accurate numbers than is contained in the least accurate number, then round off the final result to the same number of significant figures as are in the least accurate number ($4.521/2.0 = 4.52/2.0 = 2.26 = \underline{2.3}$).

When insignificant digits are dropped from a number, the last digit retained should be rounded off for the best accuracy. To round off a number to a smaller number of significant digits than are specified originally, truncate the number to the desired number of significant digits and treat the excess digits as a decimal fraction. Then

1. If the fraction is greater than $\frac{1}{2}$, increment the least significant digit.
2. If the fraction is less than $\frac{1}{2}$, do not increment.
3. If the fraction equals $\frac{1}{2}$, increment the least significant digit only if it is odd.

FOR EXAMPLE: $2.53 = 2.5$; $2.56 = 2.6$; $2.55 = 2.6$; $2.45 = 2.4$

13.9.2 Error Propagation

It should be obvious that the precision of a computed value is dependent on the precision of each directly measured value. In order to show that relationship, consider determining the volume of a right cylinder by measuring the radius and height:

$$V = \pi r^2 h$$

Given that there is some error in each measurement, call them Δr and Δh , producing some error in V , call it ΔV , then

$$V + \Delta V = \pi(r + \Delta r)^2 (h + \Delta h)$$

If the errors in r and h are small, then we can drop products of Δ 's after expanding the above equation, as those products will be insignificant in comparison. This gives the following:

$$\Delta V = \pi(r^2 \Delta h + 2rh \Delta r)$$

or

$$\Delta V = \Delta h(\pi r^2) + \Delta r(2\pi rh)$$

This grouping of the terms reminds one of partial derivatives. Specifically, it is the same as:

$$\Delta V \approx \Delta h \left(\frac{\partial V}{\partial h} \right) + \Delta r \left(\frac{\partial V}{\partial r} \right)$$

In general, it can be shown that for a function Q, where

$$Q = f(a, b, c, \dots)$$

that the error in Q from errors in each independent variable (a, b, c...) is:

$$\Delta Q = \frac{\partial Q}{\partial a} \Delta a + \frac{\partial Q}{\partial b} \Delta b + \frac{\partial Q}{\partial c} \Delta c + \dots$$

13.9.3 Standard Deviation

As we have seen throughout this course, we can't specify the errors in our measurements with certainty. Thus, in the place of the Δ 's in the last section, a more useable equation would specify the error in the calculated parameter in terms of the standard deviation of each measured value.

From the definition of variance:

$$\sigma_Q^2 = \frac{1}{N} \sum_{i=1}^N (\Delta Q_i)^2$$

Using the earlier approximation for ΔQ ,

$$\sigma_Q^2 = \frac{1}{N} \sum_{i=1}^N \left(\frac{\partial Q}{\partial a} \Delta a_i + \frac{\partial Q}{\partial b} \Delta b_i + \dots \right)^2$$

Again, dropping cross products as insignificant, we can write

$$\sigma_Q^2 = \frac{1}{N} \sum_{i=1}^N \left| \left(\frac{\partial Q}{\partial a} \right)^2 (\Delta a_i)^2 + \left(\frac{\partial Q}{\partial b} \right)^2 (\Delta b_i)^2 + \dots \right|$$

Since the partial derivatives are common to each summation, they may be taken out:

$$\sigma_Q^2 = \left(\frac{\partial Q}{\partial a} \right)^2 \frac{1}{N} \sum_{i=1}^N (\Delta a_i)^2 + \left(\frac{\partial Q}{\partial b} \right)^2 \frac{1}{N} \sum_{i=1}^N (\Delta b_i)^2 + \dots$$

where now the term following each partial derivation should be recognized as the definition of variance:

$$\sigma_Q^2 = \left(\frac{\partial Q}{\partial a} \right)^2 \sigma_a^2 + \left(\frac{\partial Q}{\partial b} \right)^2 \sigma_b^2 + \dots$$

As an example, consider the problem of calculating lift coefficient from the following flight test relationship:

$$C_L = \frac{841.5 \text{ nW}}{V_e^2 S}$$

Assume that the error in S is insignificant in comparison to other errors. What is the standard deviation of C_L for 1% standard deviation in each of n, W, and V_e ?

First, write

$$\sigma_{C_L}^2 = \left(\frac{\partial C_L}{\partial n}\right)^2 \sigma_n^2 + \left(\frac{\partial C_L}{\partial W}\right)^2 \sigma_W^2 + \left(\frac{\partial C_L}{\partial V_e}\right)^2 \sigma_{V_e}^2$$

or

$$\sigma_{C_L}^2 = \left(\frac{841.5W}{V_e^2 S}\right)^2 (0.01n)^2 + \left(\frac{841.5n}{V_e^2 S}\right)^2 (0.01W)^2 + \left(-2 \frac{841.5nW}{V_e^3 S}\right)^2 (0.01V_e)^2$$

or

$$\sigma_{C_L}^2 = (0.01)^2 C_L^2 + (0.01)^2 C_L^2 + (0.02)^2 C_L^2$$

giving

$$\sigma_{C_L} = 0.024 C_L$$

Thus, a 1% error in each term results in a 2.4% error in the final result.

13.10 DATA PRESENTATION

This section deals with the display of test data to allow quick analysis, to facilitate comparisons, and to permit easy reference to data. Further, by graphically plotting one variable versus another, we may see a correlation (or perhaps as important, a lack of correlation where we expected one) between the two variables. Data smoothing, extrapolation into regions not tested, and interpolation between measured points are all procedures most easily done with a graphical analysis. Thus, good data plots can be an effective testing tool.

13.10.1 Coordinate Scales

A poor choice of scales for the coordinates, more than any other single factor, will make an otherwise acceptable graph unsatisfactory as a tool. Such being the case, the need for suitability rules is evident. Although none can be given to fit all cases, where the maximum revelation of content of data plotted or the maximum of ease and comfort in the use of the plot as a tool are concerned, certain general rules may be stated. Granted the best selection of graph paper, experience has shown it generally desirable to choose the coordinate scales in accordance with the following rules.

- Rule 1 The scale for the independent variable should be measured along the so called x-axis.
- Rule 2 The scales should be so chosen that the coordinates of any point on the plot may be determined quickly and easily.
- Rule 3 The scales should be numbered so that the resultant curve is as extensive as the sheet permits, provided the uncertainties of measurement are not made thereby to correspond to more than one of the smallest divisions.
- Rule 4 Other things being equal, the variables should be manipulated to give a resultant curve which approaches as nearly as practical a straight line.

Sometimes when the data fit a certain type of equation, a straight line graph can be obtained by plotting the measured variables on other than regular rectangular graphpaper more simply than by manipulating the variables. For instance, the coordinates $X = \log x$ and $Y = \log y$ are convenient for plotting curves of the form $y^r = ax^n$. Similarly, semilogarithmic paper is especially

useful for the graphical analysis of data that are theoretically related by an equation involving the appearance of one of the variates in the exponent, of the general form $y = Aa^{Bx}$. The coordinates $y = \log_b y$ and $X = x$ plot a straight line.

13.10.2 Qualitative Curve Fitting

For this discussion, we assume there are sufficient points to justify drawing a smooth continuous curve to represent the actual variation of the related variables under consideration in the regions between the plotted points. Proficiency in judging the most likely course of a smooth curve through a set of plotted points requires practice. There are several basic principles, however, which help us in this task.

1. Acquire background on similar type data. A priori estimates of what our test results are likely to look like are usually available. Such information as approximate magnitudes and trends are of primary importance in giving us a hint as to what our plot is likely to look like. The source of these estimates can be obtained from classic theory, contractual specifications, military specifications, Dash-1's, etc.
2. The curve which is fitted to the data should be first order, or at most, a second order polynomial. The only time this principle would not be followed is if you knew that the expected wave form is of higher order, such as the dynamic free response of an aircraft.
3. The curve should be smooth, with few inflections.
4. The curve should pass as close as reasonably possible to all of the plotted points.
5. The curve need not pass through a single point, much less through either of the end points. Very often, they are end points because of limits in the accuracy of the instrument or of the method used. In such cases, less weight should be given to them than to the other points of the plot.
6. The curve should usually, but not always, contain no inexplicable discontinuities, cusps, or other peculiarities.
7. When taken in moderate sized groups, about one-half of the plotted points of each group should fall on one side of the curve and the other half on the other side.

Using these guidelines and good engineering judgment can produce excellent results. On occasion, however, the latitude allowed here may be

enough to span the gap between success and failure. In these cases, a mathematical best fit can be used to reduce arguments over how to fit the curve through that data. The method of least squares is one accepted way of defining a mathematical best fit.

13.10.3 Method of Least Squares

To obtain a definition of best fit, consider Figure 21 in which the data points are $(x_1, y_1), \dots, (x_n, y_n)$. For a given value of x , say x_1 , there will be a difference between the value y_1 and the corresponding value as determined from the curve C . We denote this difference by d_1 , which may be positive, negative or zero. Similarly, corresponding to the values x_1, \dots, x_n we obtain the deviations d_1, \dots, d_n .

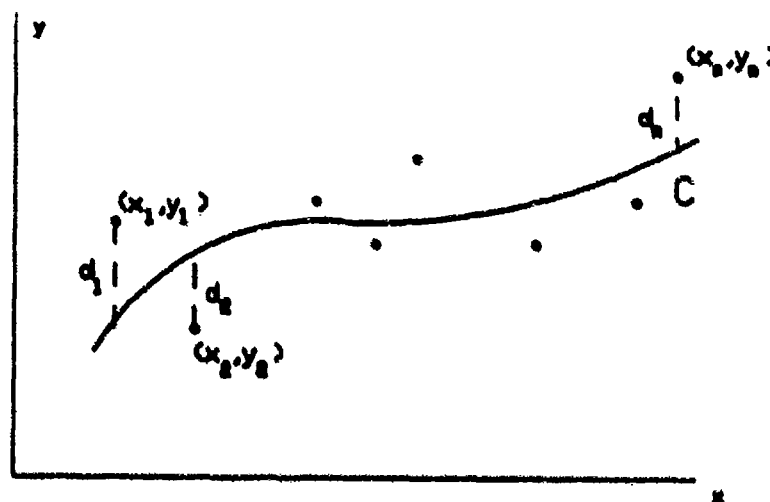


Figure 21. Curve Fitting

A measure of the "goodness of the fit" of the curve C to the set of data is provided by the quantity $d_1^2 + d_2^2 + \dots + d_n^2$. If this is small, the fit is good, if it is large, the fit is bad. We therefore make the following

DEFINITION Of all curves approximating a given set of data points, the curve having the property that

$$d_1^2 + d_2^2 + \dots + d_n^2 = \text{a minimum}$$

is the best fitting curve.

A curve having this property is said to fit the data in the least squares sense and is called a least squares curve. Thus, a line having this property is called a least squares line, a parabola with this property is called a least squares parabola, etc.

For a straight line, for example, the least squares curve can be found as follows. The equation for the line is

$$y = a + bx$$

where a and b must be determined from the available data. For each data point, the deviation defined above is

$$d_i = a + bx_i - y_i$$

and the sum of the squares is

$$\sum_{i=1}^N d_i^2 = \sum_{i=1}^N (a + bx_i - y_i)^2$$

To find the minimum sum of the squares, differentiate this expression with respect to both a and b and set the result equal to zero:

$$\frac{\partial}{\partial a} \left(\sum_{i=1}^N d_i^2 \right) = \sum_{i=1}^N 2(a + bx_i - y_i) = 0$$

$$\frac{\partial}{\partial b} \left(\sum_{i=1}^N d_i^2 \right) = \sum_{i=1}^N 2x_i(a + bx_i - y_i) = 0$$

This gives the following two simultaneous equations with two unknowns, a and b .

$$\sum_{i=1}^N y_i = an + b \sum_{i=1}^N x_i$$

$$\sum_{i=1}^N x_i y_i = a \sum_{i=1}^N x_i + b \sum_{i=1}^N x_i^2$$

For example, if we have the following data:

$$(x,y) = (1,1), (3,2), (4,4), (6,4), (8,5), (9,7), (11,8), \text{ and } (14,9)$$

Then

$$\begin{aligned}\Sigma y &= 40 \\ \Sigma x &= 56 \\ \Sigma xy &= 364 \\ \Sigma x^2 &= 524 \\ n &= 8\end{aligned}$$

Therefore:

$$\begin{aligned}40 &= 8a + 56b \\ 364 &= 56a + 524b\end{aligned}$$

Solving simultaneously, $a = 6/11 = .545$ and $b = 7/11 = .636$. Thus, the least squares line is $y = .545 + .626x$.

Similarly, the least squares parabola which fits a set of sample points is given by

$$y = a + bx + cx^2$$

where a , b , c are determined from the normal equations

$$\begin{aligned}\Sigma y &= na + b \Sigma x + c \Sigma x^2 \\ \Sigma xy &= a \Sigma x + b \Sigma x^2 + c \Sigma x^3 \\ \Sigma x^2 y &= a \Sigma x^2 + b \Sigma x^3 + c \Sigma x^4\end{aligned}$$

While the advantages of the method of least squares are pretty obvious, it does have some disadvantages. Most importantly, all points are given equal weight. Typically in flight testing, the end points are more suspect than middle points. Also, use of the method removes engineering judgment. One approach to the advantages and disadvantages is to use the method first then use engineering judgment to decide if the resulting curve should be used or modified.

13.10.4 Data Rejection

Before concluding, a few remarks are in order about one of the most difficult problems of data analysis: the question of mistakes in the data and the rejection of data.

When the measurement of a quantity is repeated several times, it often happens that one or more of the values differs from the others by relatively large amounts. There is no problem when these anomalous measurements can be directly traced to some systematic disturbance or fluctuation in the controlled conditions of the test. In this case, the values can be corrected for the effects or the data may be rejected. More difficult is the case where no cause for the anomalous values can be ascertained. The analyst

is often tempted to discard the anomalous values anyway on the ground that some error in reading the instruments must have occurred. This temptation must be resisted strongly.

The first point to be made is that seemingly large fluctuations are possible, as we have seen in our discussion of distribution error. Thus, it is very often true that the seemingly anomalous values are perfectly acceptable. If the normal probability law indicates that the fluctuation is reasonable, obviously nothing is to be done and the data are certainly to be retained without change.

Now, let us suppose that the deviation we are investigating has a very small chance of occurring. That is, we have computed the chance of obtaining one of our N values with a deviation from the mean as large as was observed, and the probability is calculated to be less than $1/N$. Because of random fluctuations in a series of N measurements, we may reasonably expect very much less. It is a matter of preference at what point one chooses to cut this; a widely used standard is Chauvenet's criterion, which states that if the probability of the value deviating from the mean by the observed amount is $1/2N$ or less, the data should be rejected.

For example, if we make 10 observations, then according to Chauvenet's criteria we should disregard any data if its deviation from the mean has a probability of occurrence less than $1/20$. If the data is normally distributed, then this occurs when $|z| > 1.96$.

A distinct danger in applying Chauvenet's or any other criterion for the rejection of data without determinate cause is that important effects may be "swept under the rug." We should rather adopt the view that Chauvenet's criterion should be used to flag suspicious situations. When the deviation observed is larger than one can reasonably expect, this should serve as a stimulus to find out what happened. If it appears that nothing happened, then the data should generally be left as is unless the analyst uses his judgment and experience to determine that it is more likely that the undetected systematic fluctuation occurred than that the effect is real. We cannot stress too strongly that judgment is involved here. The blind use of Chauvenet's criterion is a guarantee of never finding anything that was unanticipated at the beginning.

PROBLEM SET NUMBER 1

1. Your data group has been asked to verify the takeoff performance in the T-38. Your group decides to do 10 takeoffs all on the same day in the same aircraft without refueling between takeoffs. All 5 pilots want to fly, so it is decided to let each pilot do 2 takeoffs. Are your data:
 - a. homogeneous?
 - b. independent?
 - c. random?

2. Two cards are drawn from a single deck. Find the probability that they are both aces if the first card is:
 - a. replaced
 - b. not replaced

3. Given the following random, independent 360° aileron roll data:

<u>Test Point</u>	<u>Time to 360°</u>
1	3.5 seconds
2	4.0 seconds
3	3.8 seconds
4	4.2 seconds
5	3.7 seconds

Find:

- a. Sample Mean
- b. Sample Median
- c. Sample Standard Deviation

PROBLEM SET NUMBER 2

1. The AFFTC has just completed a 100 sortie test to determine the stall speed of the F-19. The standardized data were normally distributed with a mean of 125 knots and a standard deviation of 2 knots. What is the probability of a random operational pilot stalling the aircraft at 130 knots or greater?
2. Suppose four random operational pilots stall the F-19 in problem one. Ninety-nine percent of the time, their average stall speed will be less than what value? Assume $S = \sigma$.
3. Ninety-nine percent of the time, the standard deviation of the stall speed for the four pilots in problem two will be less than what value?

PROBLEM SET NUMBER 3

1. Ten MIL power takeoff rolls were measured by your data group. The standardized data have a mean of 2700 ft and a standard deviation of 200 ft. What are the 95% confidence limits for the actual value?

2. Rocket motors have burn times of 3 sec (μ_0) when produced. A sample of 9 motors which were stored for 5 years had an average burn time of 3.1 sec and a standard deviation of .1 sec. At the 95% confidence level, has the burn time changed?

3. The specification for engine thrust on the F-120 is 28,000 lbs. You test 11 engines and find that the mean is 27,500 with a standard deviation of 350 lbs. Did the contractor meet the specification at the 90% level of significance?

PROBLEM SET NUMBER 4

1. We want to know if the logic in a new RADAR tape has increased detection range. We need to be 90% certain before we give the SPO the green light. Given the following data, decide. Do not assume normally distributed data.

Detection Range

Before: 4, 5, 5, 6, 7, 8, 12, 13, 17

After: 9, 10, 11, 14, 15, 16, 20

2. The YF-19 has vertical tape instruments. Before going into production, the SPO Director polls the test pilots and finds that 10 prefer round dials, 2 have no preference, and 5 want to keep the tapes. You want to be 95% sure before approving an ECP. What should you do?

3. Ten WSOs have rated the Stealth bomber's two proposed offensive systems stations on a scale of one (best) to five (worst). The results are:

WSO	1	2	3	4	5	6	7	8	9	10
System A	2	1	3	1	2	4	2	3	4	2
System B	3	2	3	3	2	2	4	2	5	3

System A costs 50% more than System B. You want to be 95% confident that System A is significantly better than B. Should we buy System A?

PROBLEM SET NUMBER 5

1. How many samples do we need to determine the mean at the 95% confidence level if we want the error to be:
 - a. less than $.1 \sigma$?
 - b. less than $.2 \sigma$?
 - c. less than σ ?

2. A new RADAR component is being tested to determine its effect on detection range. From previous tests, the standard deviation of such tests is about 1.5 NM. How many test points must we fly with both the old and new component if we want to detect a mean difference of 1 NM at 95% confidence while guarding against the false positive with probability 90%.

PROBLEM SET NUMBER 6

1. To what fractional accuracy (%) can we specify the volume of a sphere ($V = \frac{4}{3}\pi r^3$) if we can measure the radius to within 1%?

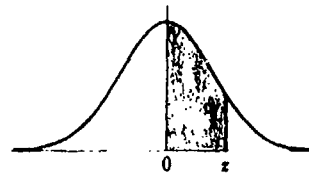
2. Use the method of least squares to find the best straight line to fit the following data:

X	2	7	9	1	5	12
Y	13	21	23	14	15	21

References

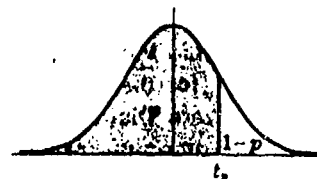
- Bethea, R. M. et. al., Statistical Methods for Engineers and Scitentists, Marcel Delher, Inc., NY, 1975.
- Young, H. D., Statistical Treatment of Experimental Data, McGraw-Hill Book Co, New York, NY, 1962.
- Freund, J. E., Modern Elementary Statistics (6th Edition), Printice-Hall, Inc., NJ, 1984.
- Choi, Sang C., Introductorty Applied Statistics in Science, Prentice-Hall, Inc., NJ, 1978.
- Walpole, R. E. and Myers, R. H., Probability and Statistics for Engineers and Scientists, Macmillan Co., NY, 1972.
- Iman, R. L. and Conover, W. J., A Modern Approach to Statistics, John Wiley & Sons, Inc., NY, 1983.

Areas
under the
Standard
Normal Curve
from 0 to z



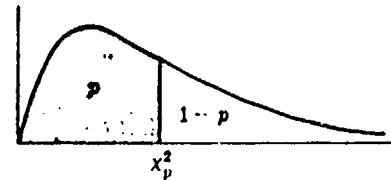
z	0	1	2	3	4	5	6	7	8	9
0.0	.0000	.0040	.0080	.0120	.0160	.0199	.0239	.0279	.0319	.0359
0.1	.0398	.0438	.0478	.0517	.0557	.0596	.0636	.0675	.0714	.0754
0.2	.0793	.0832	.0871	.0910	.0948	.0987	.1026	.1064	.1103	.1141
0.3	.1179	.1217	.1255	.1293	.1331	.1368	.1406	.1443	.1480	.1517
0.4	.1554	.1591	.1628	.1664	.1700	.1736	.1772	.1808	.1844	.1879
0.5	.1915	.1950	.1985	.2019	.2054	.2088	.2123	.2157	.2190	.2224
0.6	.2258	.2291	.2324	.2357	.2389	.2422	.2454	.2486	.2518	.2549
0.7	.2580	.2612	.2642	.2673	.2704	.2734	.2764	.2794	.2823	.2852
0.8	.2881	.2910	.2939	.2967	.2996	.3023	.3051	.3078	.3106	.3133
0.9	.3159	.3186	.3212	.3238	.3264	.3289	.3315	.3340	.3365	.3389
1.0	.3413	.3438	.3461	.3485	.3508	.3531	.3554	.3577	.3599	.3621
1.1	.3643	.3665	.3686	.3708	.3729	.3749	.3770	.3790	.3810	.3830
1.2	.3849	.3869	.3888	.3907	.3925	.3944	.3962	.3980	.3997	.4015
1.3	.4032	.4049	.4066	.4082	.4099	.4115	.4131	.4147	.4162	.4177
1.4	.4192	.4207	.4222	.4236	.4251	.4265	.4279	.4292	.4306	.4319
1.5	.4332	.4345	.4357	.4370	.4382	.4394	.4406	.4418	.4429	.4441
1.6	.4452	.4463	.4474	.4484	.4495	.4505	.4515	.4525	.4535	.4545
1.7	.4554	.4564	.4573	.4582	.4591	.4599	.4608	.4616	.4625	.4633
1.8	.4641	.4649	.4656	.4664	.4671	.4678	.4686	.4693	.4699	.4706
1.9	.4713	.4719	.4726	.4732	.4738	.4744	.4750	.4756	.4761	.4767
2.0	.4772	.4778	.4783	.4788	.4793	.4798	.4803	.4808	.4812	.4817
2.1	.4821	.4826	.4830	.4834	.4838	.4842	.4846	.4850	.4854	.4857
2.2	.4861	.4864	.4868	.4871	.4875	.4878	.4881	.4884	.4887	.4890
2.3	.4893	.4896	.4898	.4901	.4904	.4906	.4909	.4911	.4913	.4916
2.4	.4918	.4920	.4922	.4925	.4927	.4929	.4931	.4932	.4934	.4936
2.5	.4938	.4940	.4941	.4943	.4945	.4946	.4948	.4949	.4951	.4952
2.6	.4953	.4955	.4956	.4957	.4959	.4960	.4961	.4962	.4963	.4964
2.7	.4965	.4966	.4967	.4968	.4969	.4970	.4971	.4972	.4973	.4974
2.8	.4974	.4975	.4976	.4977	.4977	.4978	.4979	.4979	.4980	.4981
2.9	.4981	.4982	.4982	.4983	.4984	.4984	.4985	.4985	.4986	.4986
3.0	.4987	.4987	.4987	.4988	.4988	.4989	.4989	.4989	.4990	.4990
3.1	.4990	.4991	.4991	.4991	.4992	.4992	.4992	.4992	.4993	.4993
3.2	.4993	.4993	.4994	.4994	.4994	.4994	.4994	.4995	.4995	.4995
3.3	.4995	.4995	.4995	.4996	.4996	.4996	.4996	.4996	.4996	.4997
3.4	.4997	.4997	.4997	.4997	.4997	.4997	.4997	.4997	.4997	.4998
3.5	.4998	.4998	.4998	.4998	.4998	.4998	.4998	.4998	.4998	.4998
3.6	.4998	.4998	.4999	.4999	.4999	.4999	.4999	.4999	.4999	.4999
3.7	.4999	.4999	.4999	.4999	.4999	.4999	.4999	.4999	.4999	.4999
3.8	.4999	.4999	.4999	.4999	.4999	.4999	.4999	.4999	.4999	.4999
3.9	.5000	.5000	.5000	.5000	.5000	.5000	.5000	.5000	.5000	.5000

Percentile Values (t_p)
for
Student's t Distribution
with ν Degrees of Freedom



ν	$t_{.35}$	$t_{.30}$	$t_{.20}$	$t_{.15}$	$t_{.10}$	$t_{.05}$	$t_{.025}$	$t_{.01}$	$t_{.005}$
1	.158	.325	.727	1.000	1.376	3.08	6.31	12.71	63.66
2	.142	.289	.617	.816	1.061	1.89	2.92	4.30	9.92
3	.137	.277	.584	.765	.978	1.64	2.35	3.18	5.84
4	.134	.271	.569	.741	.941	1.53	2.13	2.78	4.60
5	.132	.267	.559	.727	.920	1.48	2.02	2.57	4.03
6	.131	.265	.553	.718	.906	1.44	1.94	2.45	3.71
7	.130	.263	.549	.711	.896	1.42	1.90	2.36	3.50
8	.130	.262	.546	.706	.889	1.40	1.86	2.31	3.36
9	.129	.261	.543	.703	.883	1.38	1.83	2.26	3.25
10	.129	.260	.542	.700	.879	1.37	1.81	2.23	3.17
11	.129	.260	.540	.697	.876	1.36	1.80	2.20	3.11
12	.128	.259	.539	.695	.873	1.36	1.78	2.18	3.06
13	.128	.259	.538	.694	.870	1.35	1.77	2.16	3.01
14	.128	.258	.537	.692	.868	1.34	1.76	2.14	2.98
15	.128	.258	.536	.691	.866	1.34	1.75	2.13	2.95
16	.128	.258	.535	.690	.865	1.34	1.75	2.12	2.92
17	.128	.257	.534	.689	.863	1.33	1.74	2.11	2.90
18	.127	.257	.534	.688	.862	1.33	1.73	2.10	2.88
19	.127	.257	.533	.688	.861	1.33	1.73	2.09	2.86
20	.127	.257	.533	.687	.860	1.32	1.72	2.09	2.84
21	.127	.257	.532	.686	.859	1.32	1.72	2.08	2.83
22	.127	.256	.532	.686	.858	1.32	1.72	2.07	2.82
23	.127	.256	.532	.685	.858	1.32	1.71	2.07	2.81
24	.127	.256	.531	.685	.857	1.32	1.71	2.06	2.80
25	.127	.256	.531	.684	.856	1.32	1.71	2.06	2.79
26	.127	.256	.531	.684	.856	1.32	1.71	2.06	2.78
27	.127	.256	.531	.684	.855	1.31	1.70	2.05	2.77
28	.127	.256	.530	.683	.855	1.31	1.70	2.05	2.76
29	.127	.256	.530	.683	.854	1.31	1.70	2.04	2.76
30	.127	.256	.530	.683	.854	1.31	1.70	2.04	2.75
40	.126	.255	.529	.681	.851	1.30	1.68	2.02	2.70
60	.126	.254	.527	.679	.848	1.30	1.67	2.00	2.66
120	.126	.254	.526	.677	.845	1.29	1.66	1.98	2.62
∞	.126	.253	.524	.674	.842	1.28	1.645	1.96	2.58

Percentile Values (χ_p^2)
for the
Chi-Square Distribution
with ν Degrees of Freedom



ν	$\chi^2_{.995}$	$\chi^2_{.99}$	$\chi^2_{.975}$	$\chi^2_{.95}$	$\chi^2_{.90}$	$\chi^2_{.85}$	$\chi^2_{.80}$	$\chi^2_{.75}$	$\chi^2_{.70}$	$\chi^2_{.65}$	$\chi^2_{.60}$	$\chi^2_{.55}$	$\chi^2_{.50}$	$\chi^2_{.45}$	$\chi^2_{.40}$	$\chi^2_{.35}$	$\chi^2_{.30}$	$\chi^2_{.25}$	$\chi^2_{.20}$	$\chi^2_{.15}$	$\chi^2_{.10}$	$\chi^2_{.05}$	$\chi^2_{.025}$	$\chi^2_{.01}$	$\chi^2_{.005}$	
1	.0000	.0002	.0010	.0039	.0158	.102	.455	1.32	2.71	3.84	5.02	6.63	7.88	10.8	13.8	16.3	18.5	20.5	22.5	24.3	26.1	27.9	29.6	31.3	32.9	34.5
2	.0100	.0201	.0506	.103	.211	.375	1.39	2.77	4.61	5.99	7.38	9.21	10.6	13.8	16.3	18.5	20.5	22.5	24.3	26.1	27.9	29.6	31.3	32.9	34.5	36.1
3	.0717	.115	.216	.352	.584	1.21	2.37	4.11	6.25	7.81	9.35	11.3	12.8	14.9	16.7	18.5	20.5	22.5	24.3	26.1	27.9	29.6	31.3	32.9	34.5	36.1
4	.207	.297	.484	.711	1.06	1.92	3.36	5.39	7.78	9.49	11.1	12.8	15.1	16.7	18.5	20.5	22.5	24.3	26.1	27.9	29.6	31.3	32.9	34.5	36.1	37.7
5	.412	.554	.851	1.15	1.61	2.67	4.35	6.63	9.24	11.1	12.8	15.1	16.7	18.5	20.5	22.5	24.3	26.1	27.9	29.6	31.3	32.9	34.5	36.1	37.7	39.3
6	.876	.872	1.24	1.64	2.20	3.45	5.35	7.84	10.6	12.6	14.4	16.8	18.5	20.3	24.3	26.1	27.9	29.6	31.3	32.9	34.5	36.1	37.7	39.3	40.8	42.3
7	.989	1.24	1.69	2.17	2.83	4.25	6.35	9.04	12.0	14.1	16.0	18.5	20.3	24.3	26.1	27.9	29.6	31.3	32.9	34.5	36.1	37.7	39.3	40.8	42.3	43.8
8	1.34	1.65	2.18	2.73	3.49	5.07	7.34	10.2	13.4	15.5	17.5	20.1	22.0	26.1	27.9	29.6	31.3	32.9	34.5	36.1	37.7	39.3	40.8	42.3	43.8	45.3
9	1.73	2.09	2.70	3.33	4.17	5.90	8.34	11.4	14.7	16.9	19.0	21.7	23.6	27.9	29.6	31.3	32.9	34.5	36.1	37.7	39.3	40.8	42.3	43.8	45.3	46.8
10	2.16	2.56	3.25	3.94	4.87	6.74	9.34	12.5	16.0	18.3	20.5	23.2	25.2	29.6	31.3	32.9	34.5	36.1	37.7	39.3	40.8	42.3	43.8	45.3	46.8	48.3
11	2.60	3.05	3.82	4.57	5.58	7.58	10.3	13.7	17.3	19.7	21.9	24.7	26.8	31.3	32.9	34.5	36.1	37.7	39.3	40.8	42.3	43.8	45.3	46.8	48.3	49.7
12	3.07	3.57	4.40	5.23	6.30	8.44	11.3	14.8	18.5	21.0	23.3	26.2	28.3	32.9	34.5	36.1	37.7	39.3	40.8	42.3	43.8	45.3	46.8	48.3	49.7	51.2
13	3.57	4.11	5.01	5.89	7.04	9.30	12.3	16.0	19.8	22.4	24.7	27.7	29.8	34.5	36.1	37.7	39.3	40.8	42.3	43.8	45.3	46.8	48.3	49.7	51.2	52.6
14	4.07	4.66	5.63	6.57	7.79	10.2	13.3	17.1	21.1	23.7	26.1	29.1	31.3	36.1	37.7	39.3	40.8	42.3	43.8	45.3	46.8	48.3	49.7	51.2	52.6	54.1
15	4.60	5.23	6.26	7.26	8.55	11.0	14.3	18.2	22.3	25.0	27.5	30.6	32.8	37.7	39.3	40.8	42.3	43.8	45.3	46.8	48.3	49.7	51.2	52.6	54.1	55.5
16	5.14	5.81	6.91	7.96	9.31	11.9	15.3	19.4	23.5	26.3	28.8	32.0	34.3	39.3	40.8	42.3	43.8	45.3	46.8	48.3	49.7	51.2	52.6	54.1	55.5	56.9
17	5.70	6.41	7.56	8.67	10.1	12.8	16.3	20.5	24.8	27.6	30.2	33.4	35.7	40.8	42.3	43.8	45.3	46.8	48.3	49.7	51.2	52.6	54.1	55.5	56.9	58.3
18	6.26	7.01	8.23	9.39	10.9	13.7	17.3	21.6	26.0	28.9	31.5	34.8	37.2	42.3	43.8	45.3	46.8	48.3	49.7	51.2	52.6	54.1	55.5	56.9	58.3	59.7
19	6.84	7.63	8.91	10.1	11.7	14.6	18.3	22.7	27.2	30.1	32.9	36.2	38.6	43.8	45.3	46.8	48.3	49.7	51.2	52.6	54.1	55.5	56.9	58.3	59.7	61.1
20	7.43	8.26	9.59	10.9	12.4	15.5	19.3	23.8	28.4	31.4	34.2	37.6	40.0	45.3	46.8	48.3	49.7	51.2	52.6	54.1	55.5	56.9	58.3	59.7	61.1	62.5
21	8.03	8.90	10.3	11.6	13.2	16.3	20.3	24.9	29.6	32.7	35.5	38.9	41.4	46.8	48.3	49.7	51.2	52.6	54.1	55.5	56.9	58.3	59.7	61.1	62.5	63.9
22	8.64	9.54	11.0	12.3	14.0	17.2	21.3	26.0	30.8	33.9	36.8	40.3	42.8	48.3	49.7	51.2	52.6	54.1	55.5	56.9	58.3	59.7	61.1	62.5	63.9	65.3
23	9.26	10.2	11.7	13.1	14.8	18.1	22.3	27.1	32.0	35.2	38.1	41.6	44.2	49.7	51.2	52.6	54.1	55.5	56.9	58.3	59.7	61.1	62.5	63.9	65.3	66.7
24	9.89	10.9	12.4	13.8	15.7	19.0	23.3	28.2	33.2	36.4	39.4	43.0	45.6	51.2	52.6	54.1	55.5	56.9	58.3	59.7	61.1	62.5	63.9	65.3	66.7	68.1
25	10.5	11.5	13.1	14.6	16.5	19.9	24.3	29.3	34.4	37.7	40.6	44.3	46.9	52.6	54.1	55.5	56.9	58.3	59.7	61.1	62.5	63.9	65.3	66.7	68.1	69.5
26	11.2	12.2	13.8	15.4	17.3	20.8	25.3	30.4	35.6	38.9	41.9	45.6	48.3	54.1	55.5	56.9	58.3	59.7	61.1	62.5	63.9	65.3	66.7	68.1	69.5	70.9
27	11.8	12.9	14.6	16.2	18.1	21.7	26.3	31.5	36.7	40.1	43.2	47.0	49.6	55.5	56.9	58.3	59.7	61.1	62.5	63.9	65.3	66.7	68.1	69.5	70.9	72.3
28	12.5	13.6	15.3	16.9	18.9	22.7	27.3	32.6	37.9	41.3	44.6	48.3	51.0	56.9	58.3	59.7	61.1	62.5	63.9	65.3	66.7	68.1	69.5	70.9	72.3	73.7
29	13.1	14.3	16.0	17.7	19.8	23.6	28.3	33.7	39.1	42.6	45.7	49.6	52.3	58.3	59.7	61.1	62.5	63.9	65.3	66.7	68.1	69.5	70.9	72.3	73.7	75.1
30	13.8	15.0	16.8	18.5	20.6	24.5	29.3	34.8	40.3	43.9	47.0	50.9	53.7	59.7	61.1	62.5	63.9	65.3	66.7	68.1	69.5	70.9	72.3	73.7	75.1	76.5
40	20.7	22.2	24.4	26.5	29.1	33.7	39.3	45.6	51.8	55.8	59.3	63.7	66.8	73.4	75.1	76.5	77.9	79.3	80.7	82.1	83.5	84.9	86.3	87.7	89.1	90.5
50	28.0	29.7	32.4	34.8	37.7	42.9	49.3	56.3	63.2	67.5	71.4	76.2	79.5	86.7	88.3	89.7	91.1	92.5	93.9	95.3	96.7	98.1	99.5	100.9	102.3	103.7
60	35.5	37.5	40.5	43.2	46.5	52.8	59.3	67.0	74.4	79.1	83.3	88.4	92.0	99.6	101.2	102.6	104.0	105.4	106.8	108.2	109.6	111.0	112.4	113.8	115.2	116.6
70	43.8	45.9	48.9	51.7	55.2	61.7	69.3	77.6	85.5	90.5	95.0	100	104	112	113.8	115.2	116.6	118.0	119.4	120.8	122.2	123.6	125.0	126.4	127.8	129.2
80	51.2	53.5	57.2	60.4	64.2	71.1	79.8	88.1	96.6	102	107	112	116	125	126.4	127.8	129.2	130.6	132.0	133.4	134.8	136.2	137.6	139.0	140.4	141.8
90	59.2	61.8	65.6	69.1	73.2	80.6	89.3	98.6	108	113	118	124	128	137	138.4	139.8	141.2	142.6	144.0	145.4	146.8	148.2	149.6	151.0	152.4	153.8
100	67.8	70.1	74.2	77.9	82.4	90.1	99.8	109	118	124	130	136	140	149	150.4	151.8	153.2	154.6	156.0	157.4	158.8	160.2	161.6	163.0	164.4	165.8

$\alpha = .05$

$n_1 \backslash n_2$	9	10	11	12	13	14	15	16	17	18	19	20
1												
2	0	0	0	1	1	1	1	1	2	2	2	2
3	2	3	3	4	4	5	5	6	6	7	7	8
4	4	5	6	7	8	9	10	11	11	12	13	13
5	7	8	9	11	12	13	14	15	17	18	19	20
6	10	11	13	14	16	17	19	21	22	24	25	27
7	12	14	16	18	20	22	24	26	28	30	32	34
8	15	17	19	22	24	26	29	31	34	36	38	41
9	17	20	23	26	28	31	34	37	39	42	45	48
10	20	23	26	29	33	36	39	42	45	48	52	55
11	23	26	30	33	37	40	44	47	51	55	58	62
12	26	29	33	37	41	45	49	53	57	61	65	69
13	28	33	37	41	45	50	54	59	63	67	72	76
14	31	36	40	45	50	55	59	64	67	74	76	83
15	34	39	44	49	54	59	64	70	75	80	85	90
16	37	42	47	53	59	64	70	75	81	86	92	98
17	39	45	51	57	63	67	75	81	87	93	99	105
18	42	48	55	61	67	74	80	86	93	99	106	112
19	45	52	58	65	72	78	85	92	99	106	113	119
20	48	55	62	69	76	83	90	98	105	112	119	127

$\alpha = .10$

$n_1 \backslash n_2$	9	10	11	12	13	14	15	16	17	18	19	20
1											0	0
2	1	1	1	2	2	2	3	3	3	4	4	4
3	3	4	5	5	6	7	7	8	9	9	10	11
4	6	7	8	9	10	11	12	14	15	16	17	18
5	9	11	12	13	15	16	18	19	20	22	23	25
6	12	14	16	17	19	21	23	25	26	28	30	32
7	15	17	19	21	24	26	28	30	33	35	37	39
8	18	20	23	26	28	31	33	36	39	41	44	47
9	21	24	27	30	33	36	39	42	45	48	51	54
10	24	27	31	34	37	41	44	48	51	55	58	62
11	27	31	34	38	42	46	50	54	57	61	65	69
12	30	34	38	42	47	51	55	60	64	68	72	77
13	33	37	42	47	51	56	61	65	70	75	80	84
14	36	41	46	51	56	61	66	71	77	82	87	92
15	39	44	50	55	61	66	72	77	83	88	94	100
16	42	48	54	60	65	71	77	83	89	95	101	107
17	45	51	57	64	70	77	83	89	96	102	109	115
18	48	55	61	68	75	82	88	95	102	109	116	123
19	51	58	65	72	80	87	94	101	109	116	123	130
20	54	62	69	77	84	92	100	107	115	123	130	138

Table of Critical Values of J in the Mann-Whitney Test

x n	0	1	2	3	4	5	6	7	8	9	10	11	12	13
2	.250	.500	.250											
3	.125	.375	.375	.125										
4	.062	.250	.375	.250	.062									
5	.031	.156	.312	.312	.156	.031								
6	.016	.094	.234	.312	.234	.094	.016							
7	.008	.055	.164	.273	.273	.164	.055	.008						
8	.004	.031	.109	.219	.273	.219	.109	.031	.004					
9	.002	.018	.070	.164	.246	.246	.164	.070	.018	.002				
10	.001	.010	.044	.117	.205	.246	.205	.117	.044	.010	.001			
11		.005	.027	.081	.161	.226	.226	.161	.081	.027	.005			
12		.003	.016	.054	.121	.193	.226	.193	.121	.054	.016	.003		
13		.002	.010	.035	.087	.157	.209	.209	.157	.087	.035	.010	.002	
14		.001	.006	.022	.061	.122	.183	.209	.183	.122	.061	.022	.006	.001

Table of Binomial Probabilities for $P = q = .5$

Two-Tailed Alternative			One-Tailed Alternative		
n	$\alpha = .05$	$\alpha = .01$	n	$\alpha = .05$	$\alpha = .01$
4			4		
5			5	1	
6	1		6	2	
7	2		7	4	0
8	4	0	8	6	2
9	6	2	9	8	3
10	8	3	10	11	5
11	11	5	11	14	7
12	14	7	12	17	10
13	17	10	13	21	13
14	21	13	14	26	16
15	25	16	15	30	20
16	30	19	16	36	24
17	35	23	17	41	28
18	40	28	18	47	33
19	46	32	19	54	38
20	52	37	20	60	43
21	59	43	21	68	49
22	66	49	22	75	56
23	73	55	23	83	62
24	81	61	24	92	69
25	90	68	25	101	77

Table of Critical Values for Signed Rank Test

APPENDIX A

SYMBOLS, TERMS, AND ABBREVIATIONS

SYMBOLS, TERMS, AND ABBREVIATIONS

<u>ARABIC</u> <u>Symbol or Term</u>	<u>Definition</u>	<u>Units</u>
a	Acceleration	ft/sec ²
a	Lift curve slope	per deg or per rad
a	Speed of sound	ft/sec, mi/hr, kts
ac	Aerodynamic center	
A	Area	ft ² , m ²
AR	Aspect ratio	
b	Wingspan	ft, m
	Blade Width	ft, m
B	Number of blades	
BHP	Brake horsepower	
B.L.	Base line	
c	Absolute velocity	
c	Chord	ft, m
C	Compression	
C	Specific fuel consumption	lb/hr
°C	Degrees centigrade	deg

SYMBOLS, TERMS, AND ABBREVIATIONS

<u>ARABIC Symbol or Term</u>	<u>Definition</u>	<u>Units</u>
C_r	Root chord	ft, m
C_t	Tip chord	ft, m
C_p	Specific heat at constant pressure	btu/lb $^{\circ}R$
C_v	Specific heat at constant volume	btu/lb $^{\circ}R$
C_d	Section drag coefficient	
C_f	Skin friction coefficient	
C_l	Section lift coefficient	
C_m	Section moment coefficient	
C_F	Force coefficient	
C_D	Aircraft drag coefficient	
C_L	Aircraft lift coefficient	
$C_{L_{ic}}$	Indicated lift coefficient	
C_M	Aircraft moment coefficient	
C_p	Pressure coefficient	

SYMBOLS, TERMS, AND ABBREVIATIONS

ARABIC <u>Symbol or Term</u>	<u>Definition</u>	<u>Units</u>
C_P	Propeller power coefficient	
C_Q	Propeller torque coefficient	
C_T	Propeller thrust coefficient	
cg	Center of gravity	
cp	Center of pressure	
CR	Compression ratio	
CPR	Compressor Pressure ratio	
d	Differential	
D	Diameter	ft
D	Drag	lb
D	Diffuser	
d/dt	Time rate of change	
dC_L/da	Lift curve slope	per deg or per rad
e	Oswald's efficiency factor	
E	Shear modulus	

SYMBOLS, TERMS, AND ABBREVIATIONS

<u>ARABIC Symbol or Term</u>	<u>Definition</u>	<u>Units</u>
E	Endurance	hr
E	Total energy	ft lbs
E_m	Maneuver energy	ft lbs
E_s	Specific energy	ft
EGT	Exhaust gas temperature	deg
f	Function of	
f	Equivalent flat plate area	ft ²
F	Force	lb
F	Fan	
F	Resultant aerodynamic force	lb
$^{\circ}F$	Degrees Fahrenheit	deg
F_g	Gross thrust	lb
F_n	Net thrust	lb
F_{ex}	Excess thrust	lb
F.R.L	Fuselage reference line	

SYMBOLS, TERMS, AND ABBREVIATIONS

<u>ARABIC Symbol or Term</u>	<u>Definition</u>	<u>Units</u>
F.S.	Fuselage station	
g	Acceleration due to gravity	ft/sec ²
G	Gravitational constant	32.17405 ft ² /sec ² geo- potential ft
h	Enthalpy	btu/lb
h	Tapeline altitude	ft
h_v	Kinetic energy	
H	Total head pressure	lb/in ²
H	Combustor	
H	Altitude, general	ft
H	Geopotential at a point	geopotential ft
H_c	Pressure altitude	ft
H_i	Indicated altitude	ft

SYMBOLS, TERMS, AND ABBREVIATIONS

ARABIC Symbol or Term	Definition	Units
H_{ic}	Indicated altitude corrected for instrument error, $H_{ic} + \Delta H_{ic}$	ft
ΔH_{ic}	Altimeter instrument correction	ft
H_{ic_l}	Indicated altitude corrected for instrument and lag errors, $H_i + \Delta H_{ic} + \Delta H_{ic_l}$	ft
ΔH_{ic_l}	Altimeter lag correction	ft
ΔH_p	Altimeter position error corresponding to ΔP_p	ft
ΔH_{pc}	Altimeter position error correction	ft
HP	Horsepower	hp
H.V.	Heating value of hydrocarbon fuel	btu/lb
I_s	Specific impulse	sec
J	Propeller advance ratio	
K_n	A constant	
K_t	Temperature probe recovery factor	
$^{\circ}K$	Degrees Kelvin	deg

SYMBOLS, TERMS, AND ABBREVIATIONS

<u>ARABIC Symbol or Term</u>	<u>Definition</u>	<u>Units</u>
KE	Kinetic Energy	
l	Characteristic length	ft
ln	Natural logarithm	
L	Lift	lb
L	Length, dimensional analysis	
L	Standard lapse rate -1.98 °C/1000 ft	deg/ft
m	Slope of a line at a point	
m	Mass	slug
mac	Mean aerodynamic chord	
M	Mass, dimensional analysis	
M	Mach, flight or free stream	
M_i	Indicated Mach	
M_{ic}	Indicated Mach corrected for instrument error, $M_i + \Delta M_{ic}$	
ΔM_{ic}	Machmeter instrument correction	
ΔM_p	Machmeter position error corresponding to P_p	

SYMBOLS, TERMS, AND ABBREVIATIONS

<u>ARABIC Symbol or Term</u>	<u>Definition</u>	<u>Units</u>
ΔM_{pc}	Machmeter position error correction	
M	Moment	ft lb
MAC	Mean aerodynamic chord	
n	Load factor	
n	Number of stages	
N	Nozzle	
N	Revolutions per minute	
NACA	National Advisory Committee for Aeronautics	
NASA	National Aeronautics and Space Administration	
N_{pr}	Prandtl number	
P	Power	hp, ft lb/sec
p	Pressure, general	lb/in ²
p	The applied pressure at a point at a time, t	in Hg
P_a	Atmospheric pressure corresponding to H_c	in Hg

SYMBOLS, TERMS, AND ABBREVIATIONS

ARABIC Symbol or Term	Definition	Units
$P_{a_{sl}}$	Atmospheric pressure at standard sea level	2116.22 lb/ft ² 29.92126 in Hg
P_i	The indicated pressure at a point at a time, t	in Hg
ΔP_p	Static pressure error or position error	in Hg
P_s	Pressure corresponding to H_{ic}	in Hg
P_s	Specific Excess power	
P_t or P_T	Free stream total pressure	in Hg, lb/in ²
P'_t	Total pressure at total pressure source	in Hg
PE	Potential energy	ft lb
q	Dynamic pressure, $\rho V_T^2/2$	in Hg
q_c	Differential pressure, $P'_t - P_a$	in Hg
q_{cic}	Differential pressure corresponding to V_{ic} , $P'_t - P_s$	in Hg
Q	Heat or heat energy	btu
Q	Torque	in lb

SYMBOLS, TERMS, AND ABBREVIATIONS

ARABIC <u>Symbol or Term</u>	<u>Definition</u>	<u>Units</u>
r	Blade length	in, ft
R	Radius of turn	
R	Range	
R	Gas constant for dry air	ft ² /sec ² °R
°R	Degrees Rankine	deg
R _e	Radius of the earth	ft
R _e	Reynolds Number	
RF	Range factor	
ROC	Required operational capability	
ROC	Rate of climb	
RW	Relative wind	
s	Specific Entropy	btu/lb
s	Distance	ft
S	Total wing or planform area	ft ²
S _a	Air distance	ft

SYMBOLS, TERMS, AND ABBREVIATIONS

<u>ARABIC Symbol or Term</u>	<u>Definition</u>	<u>Units</u>
S_g	Ground roll distance	ft
SM	Stall margin	
SR	Specific range	nam
SFC	Specific fuel consumption	
SPR	Stage pressure ratio	
t	Thickness	in, ft
t	Time	sec
t_a	Atmospheric temperature	$^{\circ}\text{C}$
t_{as}	Standard day atmospheric temperature corresponding to H_c	$^{\circ}\text{C}$
t_{asl}	Standard sea level atmospheric temperature	15°C
t_{at}	Test day atmospheric temperature	$^{\circ}\text{C}$
t_i	Indicated temperature	$^{\circ}\text{C}$
t_{ic}	Indicated temperature corrected for instrument error, $t_i + \Delta t_{ic}$	$^{\circ}\text{C}$
Δt_{ic}	Air temperature instrument correction	$^{\circ}\text{C}$

SYMBOLS, TERMS, AND ABBREVIATIONS

<u>ARABIC Symbol or Term</u>	<u>Definition</u>	<u>Units</u>
T	Temperature	deg
T	Time, dimensional analysis	
T	Turbine	
T	Propeller thrust	lb
T_a	Atmospheric temperature	$^{\circ}\text{K}$
T_{as}	Standard day atmospheric temperature corresponding to H_c	$^{\circ}\text{K}$
T_{asl}	Standard sea level atmospheric temperature	288.16°K
T_{at}	Test day atmospheric temperature	$^{\circ}\text{K}$
T_i	Indicated temperature	$^{\circ}\text{K}$
T_{ic}	Indicated temperature corrected for instrument error, $T_i + \Delta T_{ic}$	$^{\circ}\text{K}$
ΔT_{ic}	Air temperature instrument correction	$^{\circ}\text{K}$
T_t	Total temperature	$^{\circ}\text{K}$
T_T	Total temperature (general)	deg

SYMBOLS, TERMS, AND ABBREVIATIONS

<u>ARABIC Symbol or Term</u>	<u>Definition</u>	<u>Units</u>
TE	Total energy	
THP	Thrust horsepower	
TIT	Turbine inlet temperature	deg
TPR	Total pressure ratio	
TSFC	Thrust specific fuel consumption	lb/hr
u	Linear velocity	ft/sec
V	Velocity or true airspeed	
V_c	Calibrated airspeed, $V_i + \Delta V_{ic} + \Delta V_{pc}$	kts
V_e	Equivalent airspeed, $V_c + \Delta V_c$ or $V\sqrt{\sigma}$	kts
V_i	Indicated airspeed	kts
V_{ic}	Indicated airspeed corrected for instrument error, $V_i + \Delta V_{ic}$	kts
ΔV_{ic}	Airspeed indicator instrument correction	kts
V_{ic_i}	Indicated airspeed corrected for instrument and lag errors, $V_i + \Delta V_{ic} + \Delta V_{ic}$	kts

SYMBOLS, TERMS, AND ABBREVIATIONS

<u>ARABIC Symbol or Term</u>	<u>Definition</u>	<u>Units</u>
ΔV_{ic_l}	Airspeed indicator lag corrections	kts
ΔV_p	Airspeed indicator position error corresponding to ΔP_p	kts
ΔV_{pc}	Airspeed indicator position error correction	kts
ΔV_c	Compressibility correction	kts
V_s	Standard day true airspeed	kts
V_t	Test day true airspeed	kts
w	Relative velocity	ft/sec
w or W	Work	ft/lb
w	Downwash velocity	ft/sec
W	Aircraft gross weight	lb
\dot{w}_a	Airflow rate	lb/hr or lb/sec
\dot{w}_f	Fuel flow rate	lb/hr or lb/sec
W.L.	Water line	
X	Distance	ft
z	Energy reference height	ft
-	Proportional to	

SYMBOLS, TERMS, AND ABBREVIATIONS

<u>Symbol or Term</u>	<u>Definition</u>	<u>Units</u>
α	Angle of attack	deg, rad
β	Angle of sideslip	deg
β	Bypass ratio	
γ	Ratio of specific heats	
γ	Flight path angle	deg
δ	Pressure ratio , $P_a/P_{a_{sl}}$	
δ_{ic}	$P_s/P_{a_{sl}}$	
δ_L	Laminar boundary layer thickness	
δ_T	Turbulent boundary layer thickness	
δ	Wedge angle or turning angle	
Δ	Change in any quantity	
ϵ	Axial strain	
ϵ	Downwash angle	deg, rad
η	Efficiency	
η_o	Overall efficiency	
η_p	Propulsive efficiency	

SYMBOLS, TERMS, AND ABBREVIATIONS

<u>Symbol or Term</u>	<u>Definition</u>	<u>Units</u>
η_{th}	Thermal efficiency	
θ	Temperature ratio, $T_a/T_{a_{sl}}$	
θ_s	$T_{as}/T_{a_{sl}}$	
θ_t	$T_{at}/T_{a_{sl}}$	
θ	Shock wave angle	
λ	Lag constant	sec
$\lambda_{H_{ic}}$	Lag constant corresponding to H_{ic}	sec
λ_s	Static pressure lag constant	sec
λ_{sl}	Lag constant at standard sea level	sec
$\lambda_{s_{sl}}$	Static pressure lag constant at standard sea level	sec
λ_t	Total pressure lag constant	sec
$\lambda_{t_{sl}}$	Total pressure lag constant at standard sea level	sec
λ	Taper ratio	
λ	Sweep angle	deg

SYMBOLS, TERMS, AND ABBREVIATIONS

<u>Symbol or Term</u>	<u>Definition</u>	<u>Units</u>
μ	Coefficient of absolute viscosity	lb sec/ft ²
μ	Viscosity at temperature T_a	lb sec/ft ²
$\mu_{H_{ic}}$	Viscosity corresponding to H_{ic}	lb sec/ft ²
μ_{sl}	Viscosity at standard sea level	3.7452×10^{-7} lb sec/ft ²
μ	Mach angle	deg
μ	Coefficient of friction	
ν	Kinematic viscosity	ft sec
ν	Turning angle	deg
π	3.14159 ...	
π	Buckingham π	
ρ	Air density	slug/ft ³
ρ_a	Standard day air density corresponding to H_c	slug/ft ³
ρ_{sl}	Air density at standard sea level	.0023769 slug/ft ³
ρ_t	Test day air density	slug/ft ³
σ	Density ratio, ρ_a/ρ_{sl}	
σ_s	ρ_s/ρ_{sl}	

SYMBOLS, TERMS, AND ABBREVIATIONS

<u>Symbol or Term</u>	<u>Definition</u>	<u>Units</u>
σ_t	ρ_t/ρ_{sl}	
σ	Axial stress	lb/in ²
σ	Solidity ratio	
τ	Acoustic lag	sec
τ	Shear stress	lb/in ²
ϕ	Bank angle	deg
ω	Rate of turn	deg/sec or rad/sec

SUBSCRIPTS

<u>Symbol or Term</u>	<u>Definition</u>
a	Ambient
a	Available
cr	Critical
e	Equivalent
ex	Excess
f	Final
i	Induced
i	Initial
iw	Corrected to a standard weight
L	Laminar
M	Wave
N	Normal (perpendicular)
o	Stagnation or total
p	Parasite

SUBSCRIPTS

<u>Symbol or Term</u>	<u>Definition</u>
P	Pressure
r	Required
r	Root
s	Static
s	Standard day
sl	Sea level
t	Tangential
t	Test day
T	Total
TD	Touchdown
TO	Takeoff
X	Conditions upstream of shock wave
Y	Conditions downstream of shock wave
OL	Zero lift
1,2,3, etc.	Specific condition or station

SUBSCRIPTS

Symbol or Term

Definition

∞

Free stream condition

SUPERSCRIPT

Symbol or Term

Definition

*

Choked condition

APPENDIX B
U.S STANDARD ATMOSPHERE, 1962

APPENDIX B
U.S. STANDARD ATMOSPHERE, 1962
Altitude, Temperature, Pressure, and Density

ADOPTED PRIMARY CONSTANTS

Symbol	Units
p_0	2116.22 lbf ft ⁻²
ρ_0	0.076474 lb ft ⁻³
T_0	15_C; 59.0_F
G_0	32.1741 ft sec ⁻²
R^*	1545.31 lbf _R ⁻¹ lb-mol ⁻¹
Z	Tapeline Altitude ft
H	Geopotential Altitude ft

GEOPOTENTIAL ALTITUDE, ENGLISH UNITS

ALTITUDE		TEMPERATURE			PRESSURE			DENSITY	
H, FT	Z, FT	T, °R	t, °F	t, °C	P, mB	P, IN. HG	$\frac{P}{P_0}$	ρ , LB FT ⁻³	$\frac{\rho}{\rho_0}$
-1000	-1000	522.338	62.566	16.981	1.08641 + 3	3.10186 + 1	1.00007 + 0	7.8737 - 2	1.0000 + 0
-900	-900	521.880	62.310	16.783	1.04684	3.00073	1.00000	7.8600	1.0000
-800	-800	521.523	61.853	16.585	1.04389	3.07986	1.00005	7.8261	1.0000
-700	-700	521.166	61.400	16.387	1.00014	3.00000	1.00000	7.8003	1.0000
-600	-600	520.810	61.140	16.189	1.00041	3.06757	1.00187	7.7826	1.0177
-500	-500	520.453	60.783	15.991	1.00100	3.04000	1.01000	7.7600	1.0147
-400	-400	520.096	60.426	15.792	1.00700	3.00563	1.01454	7.7373	1.0118
-300	-300	519.740	60.070	15.594	1.00436	3.00471	1.01000	7.7146	1.0088
-200	-200	519.383	59.713	15.396	1.00000	3.01381	1.00725	7.6923	1.0059
-100	-100	519.027	59.357	15.198	1.01000	3.00000	1.00500	7.6698	1.0029
0	0	518.670	59.000	15.000	1.01325 + 3	3.00013 + 1	1.00000 + 0	7.6474 - 2	1.0000 + 0
100	100	518.313	58.643	14.802	1.00000	2.98133	0.99391 - 1	7.6251	0.9708 - 1
200	200	517.957	58.287	14.604	1.00000	2.97000	0.98793	7.6028	0.9416
300	300	517.600	57.930	14.406	1.00031	2.95803	0.98204	7.5805	0.9125
400	400	517.244	57.574	14.208	0.99999 + 2	2.94613	0.97629	7.5583	0.8835
500	500	516.887	57.217	14.010	0.99975	2.93446	0.97063	7.5362	0.8545
600	600	516.530	56.860	13.811	0.99172	2.92282	0.96507	7.5141	0.8256
700	700	516.174	56.504	13.613	0.97980	2.91121	0.95951	7.4920	0.7966
800	800	515.817	56.147	13.415	0.96400	2.90000	0.95400	7.4700	0.7680
900	900	515.460	55.790	13.217	0.94736	2.88900	0.94850	7.4480	0.7393
1000	1000	515.104	55.434	13.019	0.93185 + 2	2.87800 + 1	0.94307 - 1	7.4261 - 2	0.7106 - 1
1100	1100	514.747	55.077	12.821	0.91745	2.86700	0.93803	7.4043	0.6821
1200	1200	514.391	54.721	12.623	0.90315	2.85603	0.93300	7.3825	0.6535
1300	1300	514.034	54.364	12.424	0.88900	2.84500	0.92800	7.3607	0.6251
1400	1400	513.677	54.007	12.226	0.87500	2.83400	0.92300	7.3390	0.5967
1500	1500	513.321	53.651	12.028	0.86117	2.82300	0.91800	7.3174	0.5684
1600	1600	512.964	53.294	11.830	0.84749	2.81200	0.91300	7.2957	0.5401
1700	1700	512.608	52.938	11.632	0.83391	2.80100	0.90800	7.2742	0.5119
1800	1800	512.251	52.581	11.434	0.82045	2.79000	0.90300	7.2527	0.4838
1900	1900	511.894	52.224	11.236	0.80700	2.77900	0.89800	7.2312	0.4557
2000	2000	511.538	51.868	11.038	0.79360 + 2	2.76800 + 1	0.89300 - 1	7.2098 - 2	0.4277 - 1
2100	2100	511.181	51.511	10.840	0.78020	2.75700	0.88800	7.1884	0.3996
2200	2200	510.824	51.154	10.641	0.76680	2.74600	0.88300	7.1671	0.3719
2300	2300	510.468	50.798	10.443	0.75340	2.73500	0.87800	7.1458	0.3441
2400	2400	510.111	50.441	10.245	0.74000	2.72400	0.87300	7.1246	0.3164
2500	2500	509.755	50.085	10.047	0.72660	2.71300	0.86800	7.1034	0.2887
2600	2600	509.398	49.728	9.849	0.71320	2.70200	0.86300	7.0823	0.2610
2700	2700	509.041	49.371	9.651	0.70000	2.69100	0.85800	7.0612	0.2335
2800	2800	508.685	49.015	9.453	0.68680	2.68000	0.85300	7.0400	0.2060
2900	2900	508.328	48.658	9.255	0.67360	2.66900	0.84800	7.0189	0.1785
3000	3000	507.972	48.302	9.057	0.66040 + 2	2.65800 + 1	0.84300 - 1	6.9978 - 2	0.1512 - 1
3100	3100	507.615	47.945	8.859	0.64720	2.64700	0.83800	6.9767	0.1239
3200	3200	507.259	47.589	8.661	0.63400	2.63600	0.83300	6.9557	0.0966
3300	3300	506.902	47.232	8.463	0.62080	2.62500	0.82800	6.9347	0.0694
3400	3400	506.546	46.875	8.265	0.60760	2.61400	0.82300	6.9137	0.0423
3500	3500	506.189	46.518	8.067	0.59440	2.60300	0.81800	6.8927	0.0152
3600	3600	505.833	46.162	7.869	0.58120	2.59200	0.81300	6.8717	0.0080
3700	3700	505.476	45.805	7.671	0.56800	2.58100	0.80800	6.8507	0.0013
3800	3800	505.120	45.449	7.473	0.55480	2.57000	0.80300	6.8297	0.0000
3900	3900	504.763	45.092	7.275	0.54160	2.55900	0.79800	6.8087	0.0000
4000	4000	504.407	44.736	7.077	0.52840 + 2	2.54800 + 1	0.79300 - 1	6.7878 - 2	0.0000 - 1
4100	4100	504.050	44.379	6.879	0.51520	2.53700	0.78800	6.7668	0.0000
4200	4200	503.694	44.023	6.681	0.50200	2.52600	0.78300	6.7458	0.0000
4300	4300	503.338	43.666	6.483	0.48880	2.51500	0.77800	6.7248	0.0000
4400	4400	502.981	43.310	6.285	0.47560	2.50400	0.77300	6.7038	0.0000
4500	4500	502.625	42.954	6.087	0.46240	2.49300	0.76800	6.6828	0.0000
4600	4600	502.268	42.598	5.889	0.44920	2.48200	0.76300	6.6618	0.0000
4700	4700	501.912	42.242	5.691	0.43600	2.47100	0.75800	6.6408	0.0000
4800	4800	501.555	41.885	5.493	0.42280	2.46000	0.75300	6.6198	0.0000
4900	4900	501.200	41.529	5.295	0.40960	2.44900	0.74800	6.5988	0.0000
5000	5000	500.843	41.172	5.097	0.39640 + 2	2.43800 + 1	0.74300 - 1	6.5778 - 2	0.0000 - 1
5100	5100	500.487	40.816	4.899	0.38320	2.42700	0.73800	6.5568	0.0000
5200	5200	500.130	40.460	4.701	0.37000	2.41600	0.73300	6.5358	0.0000
5300	5300	499.774	40.104	4.503	0.35680	2.40500	0.72800	6.5148	0.0000
5400	5400	499.417	39.748	4.305	0.34360	2.39400	0.72300	6.4938	0.0000
5500	5500	499.061	39.392	4.107	0.33040	2.38300	0.71800	6.4728	0.0000
5600	5600	498.704	39.036	3.909	0.31720	2.37200	0.71300	6.4518	0.0000
5700	5700	498.348	38.680	3.711	0.30400	2.36100	0.70800	6.4308	0.0000
5800	5800	497.991	38.324	3.513	0.29080	2.35000	0.70300	6.4098	0.0000
5900	5900	497.635	37.968	3.315	0.27760 + 2	2.33900 + 1	0.69800 - 1	6.3888 - 2	0.0000 - 1
6000	6000	497.278	37.612	3.117	0.26440	2.32800	0.69300	6.3678	0.0000
6100	6100	496.922	37.256	2.919	0.25120	2.31700	0.68800	6.3468	0.0000
6200	6200	496.565	36.900	2.721	0.23800	2.30600	0.68300	6.3258	0.0000
6300	6300	496.209	36.544	2.523	0.22480	2.29500	0.67800	6.3048	0.0000
6400	6400	495.852	36.188	2.325	0.21160	2.28400	0.67300	6.2838	0.0000
6500	6500	495.496	35.832	2.127	0.19840	2.27300	0.66800	6.2628	0.0000
6600	6600	495.139	35.476	1.929	0.18520	2.26200	0.66300	6.2418	0.0000
6700	6700	494.783	35.120	1.731	0.17200	2.25100	0.65800	6.2208	0.0000
6800	6800	494.426	34.764	1.533	0.15880	2.24000	0.65300	6.1998	0.0000
6900	6900	494.070	34.408	1.335	0.14560	2.22900	0.64800	6.1788	0.0000
7000	7000	493.713	34.052	1.137	0.13240	2.21800	0.64300	6.1578	0.0000
7100	7100	493.357	33.696	0.939	0.11920 + 2	2.20700 + 1	0.63800 - 1	6.1368 - 2	0.0000 - 1
7200	7200	493.000	33.340	0.741	0.10600	2.19600	0.63300	6.1158	0.0000
7300	7300	492.644	32.984	0.543	0.09280	2.18500	0.62800	6.0948	0.0000
7400	7400	492.287	32.628	0.345	0.07960	2.17400	0.62300	6.0738	0.0000
7500	7500	491.931	32.272	0.147	0.06640	2.16300	0.61800	6.0528	0.0000
7600	7600	491.574	31.916	0.000	0.05320	2.15200	0.61300	6.0318	0.0000
7700	7700	491.218	31.560	0.000	0.04000	2.14100	0.60800	6.0108	0.0000
7800	7800	490.861	31.204	0.000	0.02680	2.13000	0.60300	5.9898	0.0000
7900	7900	490.505	30.848	0.000	0.01360	2.11900	0.59800	5.9688	0.0000
8000	8000	490.148	30.492	0.000	0.00040	2.10800	0.59300	5.9478	0.0000

140

GEOPOTENTIAL ALTITUDE, ENGLISH UNITS

ALTITUDE		TEMPERATURE			PRESSURE			DENSITY	
H, FT	Z, FT	T, °R	t, °F	t, °C	P, mB	P, IN. HG	$\frac{P}{P_0}$	ρ , LB FT ⁻³	$\frac{\rho}{\rho_0}$
7000	7002	481.707	34.037	1.132	7.61863 + 2	2.30881 + 1	7.71629 - 1	6.1883 - 2	8.1064 - 1
7100	7102	483.350	33.880	0.933	7.70880	2.30886	7.68704	6.1883	8.0816
7200	7202	485.994	33.324	0.735	7.79895	2.30133	7.65788	6.1813	8.0567
7300	7302	488.637	32.967	0.537	7.79895	2.29384	7.62871	6.1743	8.0318
7400	7403	488.280	32.610	0.339	7.79895	2.27397	7.59953	6.1235	8.0072
7500	7503	491.924	32.254	0.141	7.87125	2.26632	7.57034	6.1048	7.9826
7600	7603	491.567	31.897	-0.057	7.84387	2.25670	7.54314	6.0856	7.9580
7700	7703	491.211	31.541	-0.255	7.81280	2.24611	7.51342	6.0670	7.9334
7800	7803	488.854	31.184	-0.453	7.78397	2.23364	7.48480	6.0483	7.9088
7900	7903	488.497	30.827	-0.651	7.75604	2.22161	7.45486	6.0296	7.8842
8000	8003	489.141	30.471	-0.849	7.72863 + 2	2.20950 + 1	7.42781 - 1	6.0110 - 2	7.8596 - 1
8100	8103	489.784	30.114	-1.046	7.69770	2.21401	7.39945	5.9924	7.8350
8200	8203	489.427	29.757	-1.244	7.66885	2.20855	7.37118	5.9738	7.8104
8300	8303	489.071	29.401	-1.442	7.64000	2.19712	7.34350	5.9552	7.7858
8400	8403	488.714	29.044	-1.640	7.61182	2.18671	7.31480	5.9366	7.7612
8500	8503	488.358	28.688	-1.838	7.58344	2.17533	7.28608	5.9180	7.7366
8600	8604	488.001	28.331	-2.036	7.55434	2.17197	7.25696	5.8994	7.7120
8700	8704	487.644	27.974	-2.234	7.52484	2.16364	7.22713	5.8808	7.6874
8800	8804	487.288	27.618	-2.432	7.49500	2.15534	7.19733	5.8622	7.6628
8900	8904	486.931	27.261	-2.630	7.46570	2.14706	7.17571	5.8435	7.6382
9000	9004	486.575	26.905	-2.828	7.43686 + 2	2.13851 + 1	7.14813 - 1	5.8249 - 2	7.6136 - 1
9100	9104	486.218	26.548	-3.026	7.40770	2.12980	7.12064	5.8063	7.5890
9200	9204	485.861	26.191	-3.224	7.37772	2.12233	7.09243	5.7878	7.5644
9300	9304	485.505	25.835	-3.422	7.34844	2.11421	7.06391	5.7692	7.5398
9400	9404	485.148	25.478	-3.620	7.31884	2.10606	7.03488	5.7506	7.5152
9500	9504	484.791	25.121	-3.818	7.28943	2.09794	7.01152	5.7320	7.4906
9600	9604	484.435	24.765	-4.016	7.25970	2.08984	6.98446	5.7134	7.4660
9700	9704	484.078	24.408	-4.214	7.22984	2.08177	6.95748	5.6948	7.4414
9800	9804	483.722	24.052	-4.412	7.19984	2.07372	6.93004	5.6762	7.4168
9900	9904	483.366	23.695	-4.610	7.16984	2.06560	6.90277	5.6576	7.3922
10000	10006	483.009	23.338	-4.808	7.13984 + 2	2.05770 + 1	6.87704 - 1	5.6390 - 2	7.3676 - 1
10100	10106	482.652	22.982	-5.006	7.10984	2.04972	6.85040	5.6204	7.3430
10200	10206	482.296	22.625	-5.204	7.07984	2.04176	6.82383	5.6018	7.3184
10300	10306	481.939	22.269	-5.402	7.04984	2.03380	6.79736	5.5832	7.2938
10400	10406	481.582	21.912	-5.600	7.01984	2.02584	6.77084	5.5646	7.2692
10500	10506	481.225	21.555	-5.798	6.98984	2.01788	6.74446	5.5460	7.2446
10600	10606	480.868	21.198	-5.996	6.95984	2.00992	6.71804	5.5274	7.2200
10700	10706	480.511	20.842	-6.194	6.92984	2.00196	6.69166	5.5088	7.1954
10800	10806	480.154	20.485	-6.392	6.89984	1.99400	6.66524	5.4902	7.1708
10900	10906	479.797	20.128	-6.590	6.86984	1.98604	6.63883	5.4716	7.1462
11000	11006	479.440	19.772	-6.788	6.83984 + 2	1.97808 + 1	6.61233 - 1	5.4530 - 2	7.1216 - 1
11100	11106	479.083	19.415	-6.986	6.80984	1.97012	6.58583	5.4344	7.0970
11200	11206	478.726	19.058	-7.184	6.77984	1.96216	6.55936	5.4158	7.0724
11300	11306	478.369	18.702	-7.382	6.74984	1.95420	6.53288	5.3972	7.0478
11400	11406	478.012	18.345	-7.580	6.71984	1.94624	6.50640	5.3786	7.0232
11500	11506	477.655	17.988	-7.778	6.68984	1.93828	6.47992	5.3600	7.0000
11600	11606	477.298	17.632	-7.976	6.65984	1.93032	6.45344	5.3414	6.9754
11700	11706	476.941	17.275	-8.174	6.62984	1.92236	6.42696	5.3228	6.9508
11800	11806	476.584	16.918	-8.372	6.59984	1.91440	6.40048	5.3042	6.9262
11900	11906	476.227	16.562	-8.570	6.56984	1.90644	6.37400	5.2856	6.9016
12000	12006	475.870	16.205	-8.768	6.53984 + 2	1.89848 + 1	6.34752 - 1	5.2670 - 2	6.8770 - 1
12100	12106	475.513	15.848	-8.966	6.50984	1.89052	6.32104	5.2484	6.8524
12200	12206	475.156	15.492	-9.164	6.47984	1.88256	6.29456	5.2298	6.8278
12300	12306	474.799	15.135	-9.362	6.44984	1.87460	6.26808	5.2112	6.8032
12400	12406	474.442	14.778	-9.560	6.41984	1.86664	6.24160	5.1926	6.7786
12500	12506	474.085	14.422	-9.758	6.38984	1.85868	6.21512	5.1740	6.7540
12600	12606	473.728	14.065	-9.956	6.35984	1.85072	6.18864	5.1554	6.7294
12700	12706	473.371	13.708	-10.154	6.32984	1.84276	6.16216	5.1368	6.7048
12800	12806	473.014	13.352	-10.352	6.29984	1.83480	6.13568	5.1182	6.6802
12900	12906	472.657	12.995	-10.550	6.26984 + 2	1.82684 + 1	6.10920 - 1	5.0996 - 2	6.6556 - 1
13000	13006	472.300	12.638	-10.748	6.23984	1.81888	6.08272	5.0810	6.6310
13100	13106	471.943	12.282	-10.946	6.20984	1.81092	6.05624	5.0624	6.6064
13200	13206	471.586	11.925	-11.144	6.17984	1.80296	6.02976	5.0438	6.5818
13300	13306	471.229	11.568	-11.342	6.14984	1.79500	6.00328	5.0252	6.5572
13400	13406	470.872	11.212	-11.540	6.11984	1.78704	5.97680	5.0066	6.5326
13500	13506	470.515	10.855	-11.738	6.08984	1.77908	5.95032	4.9880	6.5080
13600	13606	470.158	10.498	-11.936	6.05984	1.77112	5.92384	4.9694	6.4834
13700	13706	469.801	10.142	-12.134	6.02984	1.76316	5.89736	4.9508	6.4588
13800	13806	469.444	9.785	-12.332	6.00000	1.75520	5.87088	4.9322	6.4342
13900	13906	469.087	9.428	-12.530	5.96984 + 2	1.74724 + 1	5.84440 - 1	4.9136 - 2	6.4096 - 1
14000	14006	468.730	9.072	-12.728	5.93984	1.73928	5.81792	4.8950	6.3850
14100	14106	468.373	8.715	-12.926	5.90984	1.73132	5.79144	4.8764	6.3604
14200	14206	468.016	8.358	-13.124	5.87984	1.72336	5.76496	4.8578	6.3358
14300	14306	467.659	7.999	-13.322	5.84984	1.71540	5.73848	4.8392	6.3112
14400	14406	467.302	7.642	-13.520	5.81984	1.70744	5.71200	4.8206	6.2866
14500	14506	466.945	7.285	-13.718	5.78984	1.69948	5.68552	4.8020	6.2620
14600	14606	466.588	6.928	-13.916	5.75984	1.69152	5.65904	4.7834	6.2374
14700	14706	466.231	6.571	-14.114	5.72984	1.68356	5.63256	4.7648	6.2128
14800	14806	465.874	6.214	-14.312	5.69984	1.67560	5.60608	4.7462	6.1882
14900	14906	465.517	5.857	-14.510	5.66984 + 2	1.66764 + 1	5.57960 - 1	4.7276 - 2	6.1636 - 1
15000	15006	465.160	5.500	-14.708	5.63984	1.65968	5.55312	4.7090	6.1390

GEOPOTENTIAL ALTITUDE, ENGLISH UNITS

ALTITUDE		TEMPERATURE			PRESSURE			DENSITY	
H, FT	Z, FT	T, °R	t, °F	t, °C	P, mB	P, IN. HG	$\frac{P}{P_0}$	ρ , LB FT ⁻³	$\frac{\rho}{\rho_0}$
15000	15011	486.170	5.500	-14.710	5.71619 + 2	1.00000 + 1	5.66342 - 1	4.8130 - 2	0.2004 - 1
15100	15111	484.821	5.151	-14.810	5.69610	1.00179	5.62071	4.7964	0.2719
15200	15211	484.464	4.794	-14.914	5.67236	1.00358	5.54800	4.7807	0.2514
15300	15311	484.108	4.438	-15.012	5.64461	1.00537	5.47583	4.7651	0.2310
15400	15411	483.751	4.081	-15.110	5.61286	1.00716	5.40365	4.7500	0.2107
15500	15512	483.395	3.725	-15.208	5.57711	1.00895	5.33148	4.7348	0.1904
15600	15612	483.038	3.368	-15.307	5.54136	1.01074	5.25931	4.7195	0.1701
15700	15712	482.681	3.011	-15.405	5.50161	1.01253	5.18714	4.7043	0.1498
15800	15812	482.325	2.655	-15.503	5.45786	1.01432	5.11497	4.6891	0.1295
15900	15912	481.968	2.298	-15.601	5.41011	1.01611	5.04280	4.6739	0.1092
16000	16012	481.611	1.941	-15.699	5.36036	1.01790	4.97063	4.6587	0.0889
16100	16112	481.255	1.585	-15.797	5.30861	1.01969	4.89846	4.6435	0.0686
16200	16213	480.898	1.228	-15.895	5.25486	1.02148	4.82629	4.6283	0.0483
16300	16313	480.542	0.872	-15.993	5.19911	1.02327	4.75412	4.6131	0.0280
16400	16413	480.185	0.515	-16.091	5.14136	1.02506	4.68195	4.5979	0.0077
16500	16513	479.828	0.158	-16.189	5.08161	1.02685	4.60978	4.5827	0.0000
16600	16613	479.472	-0.190	-16.287	5.01986	1.02864	4.53761	4.5675	0.0000
16700	16713	479.115	-0.546	-16.385	4.95611	1.03043	4.46544	4.5523	0.0000
16800	16814	478.759	-0.911	-16.483	4.89036	1.03222	4.39327	4.5371	0.0000
16900	16914	478.402	-1.286	-16.581	4.82261	1.03401	4.32110	4.5219	0.0000
17000	17014	478.045	-1.661	-16.679	4.75286	1.03580	4.24893	4.5067	0.0000
17100	17114	477.688	-2.036	-16.777	4.68111	1.03759	4.17676	4.4915	0.0000
17200	17214	477.332	-2.411	-16.875	4.60736	1.03938	4.10459	4.4763	0.0000
17300	17314	476.975	-2.786	-16.973	4.53161	1.04117	4.03242	4.4611	0.0000
17400	17415	476.618	-3.161	-17.071	4.45386	1.04296	3.96025	4.4459	0.0000
17500	17515	476.262	-3.536	-17.169	4.37411	1.04475	3.88808	4.4307	0.0000
17600	17615	475.905	-3.911	-17.267	4.29236	1.04654	3.81591	4.4155	0.0000
17700	17715	475.548	-4.286	-17.365	4.20861	1.04833	3.74374	4.4003	0.0000
17800	17815	475.192	-4.661	-17.463	4.12286	1.05012	3.67157	4.3851	0.0000
17900	17915	474.835	-5.036	-17.561	4.03511	1.05191	3.60000	4.3699	0.0000
18000	18016	474.478	-5.411	-17.659	3.94536	1.05370	3.52883	4.3547	0.0000
18100	18116	474.122	-5.786	-17.757	3.85361	1.05549	3.45866	4.3395	0.0000
18200	18216	473.765	-6.161	-17.855	3.75986	1.05728	3.38849	4.3243	0.0000
18300	18316	473.408	-6.536	-17.953	3.66411	1.05907	3.31832	4.3091	0.0000
18400	18416	473.052	-6.911	-18.051	3.56636	1.06086	3.24815	4.2939	0.0000
18500	18516	472.695	-7.286	-18.149	3.46661	1.06265	3.17798	4.2787	0.0000
18600	18616	472.338	-7.661	-18.247	3.36486	1.06444	3.10781	4.2635	0.0000
18700	18717	471.982	-8.036	-18.345	3.26111	1.06623	3.03764	4.2483	0.0000
18800	18817	471.625	-8.411	-18.443	3.15536	1.06802	2.96747	4.2331	0.0000
18900	18917	471.268	-8.786	-18.541	3.04761	1.06981	2.89730	4.2179	0.0000
19000	19017	470.912	-9.161	-18.639	2.93786	1.07160	2.82713	4.2027	0.0000
19100	19117	470.555	-9.536	-18.737	2.82611	1.07339	2.75696	4.1875	0.0000
19200	19217	470.198	-9.911	-18.835	2.71236	1.07518	2.68679	4.1723	0.0000
19300	19317	469.842	-10.286	-18.933	2.59661	1.07697	2.61662	4.1571	0.0000
19400	19417	469.485	-10.661	-19.031	2.47886	1.07876	2.54645	4.1419	0.0000
19500	19517	469.128	-11.036	-19.129	2.35911	1.08055	2.47628	4.1267	0.0000
19600	19617	468.772	-11.411	-19.227	2.23736	1.08234	2.40611	4.1115	0.0000
19700	19717	468.415	-11.786	-19.325	2.11361	1.08413	2.33594	4.0963	0.0000
19800	19817	468.058	-12.161	-19.423	1.98786	1.08592	2.26577	4.0811	0.0000
19900	19917	467.702	-12.536	-19.521	1.86011	1.08771	2.19560	4.0659	0.0000
20000	20017	467.345	-12.911	-19.619	1.73036	1.08950	2.12543	4.0507	0.0000
20100	20117	466.988	-13.286	-19.717	1.59861	1.09129	2.05526	4.0355	0.0000
20200	20217	466.632	-13.661	-19.815	1.46486	1.09308	1.98509	4.0203	0.0000
20300	20317	466.275	-14.036	-19.913	1.32911	1.09487	1.91492	4.0051	0.0000
20400	20417	465.918	-14.411	-20.011	1.19136	1.09666	1.84475	3.9899	0.0000
20500	20517	465.562	-14.786	-20.109	1.05161	1.09845	1.77458	3.9747	0.0000
20600	20617	465.205	-15.161	-20.207	0.90986	1.09999	1.70441	3.9595	0.0000
20700	20717	464.848	-15.536	-20.305	0.76611	1.10148	1.63424	3.9443	0.0000
20800	20817	464.492	-15.911	-20.403	0.62036	1.10297	1.56407	3.9291	0.0000
20900	20917	464.135	-16.286	-20.501	0.47261	1.10446	1.49390	3.9139	0.0000
21000	21017	463.778	-16.661	-20.599	0.32286	1.10595	1.42373	3.8987	0.0000
21100	21117	463.422	-17.036	-20.697	0.17111	1.10744	1.35356	3.8835	0.0000
21200	21217	463.065	-17.411	-20.795	0.01736	1.10893	1.28339	3.8683	0.0000
21300	21317	462.708	-17.786	-20.893	-0.13639	1.11042	1.21322	3.8531	0.0000
21400	21417	462.352	-18.161	-20.991	-0.28814	1.11191	1.14305	3.8379	0.0000
21500	21517	461.995	-18.536	-21.089	-0.43789	1.11340	1.07288	3.8227	0.0000
21600	21617	461.638	-18.911	-21.187	-0.58564	1.11489	1.00271	3.8075	0.0000
21700	21717	461.282	-19.286	-21.285	-0.73139	1.11638	0.93254	3.7923	0.0000
21800	21817	460.925	-19.661	-21.383	-0.87514	1.11787	0.86237	3.7771	0.0000
21900	21917	460.568	-20.036	-21.481	-1.01689	1.11936	0.79220	3.7619	0.0000
22000	22017	460.212	-20.411	-21.579	-1.15664	1.12085	0.72203	3.7467	0.0000
22100	22117	459.855	-20.786	-21.677	-1.29439	1.12234	0.65186	3.7315	0.0000
22200	22217	459.498	-21.161	-21.775	-1.43014	1.12383	0.58169	3.7163	0.0000
22300	22317	459.142	-21.536	-21.873	-1.56389	1.12532	0.51152	3.7011	0.0000
22400	22417	458.785	-21.911	-21.971	-1.69564	1.12681	0.44135	3.6859	0.0000
22500	22517	458.428	-22.286	-22.069	-1.82539	1.12830	0.37118	3.6707	0.0000
22600	22617	458.072	-22.661	-22.167	-1.95314	1.12979	0.30101	3.6555	0.0000
22700	22717	457.715	-23.036	-22.265	-2.07889	1.13128	0.23084	3.6403	0.0000
22800	22817	457.358	-23.411	-22.363	-2.20264	1.13277	0.16067	3.6251	0.0000
22900	22917	456.992	-23.786	-22.461	-2.32439	1.13426	0.09050	3.6099	0.0000
23000	23017	456.635	-24.161	-22.559	-2.44414	1.13575	0.02033	3.5947	0.0000
23100	23117	456.278	-24.536	-22.657	-2.56189	1.13724	-0.04984	3.5795	0.0000
23200	23217	455.922	-24.911	-22.755	-2.67764	1.13873	-0.11967	3.5643	0.0000
23300	23317	455.565	-25.286	-22.853	-2.79139	1.14022	-0.18950	3.5491	0.0000
23400	23417	455.208	-25.661	-22.951	-2.90314	1.14171	-0.25933	3.5339	0.0000
23500	23517	454.852	-26.036	-23.049	-3.01289	1.14320	-0.32916	3.5187	0.0000
23600	23617	454.495	-26.411	-23.147	-3.12064	1.14469	-0.39899	3.5035	0.0000
23700	23717	454.138	-26.786	-23.245	-3.22639	1.14618	-0.46882	3.4883	0.0000
23800	23817	453.782	-27.161	-23.343	-3.33014	1.14767	-0.53865	3.4731	0.0000
23900	23917	453.425	-27.536	-23.441	-3.43189	1.14916	-0.60848	3.4579	0.0000
24000	24017	453.068	-27.911	-23.539	-3.53164	1.15065	-0.67831	3.4427	0.0000
24100	24117	452.712	-28.286	-23.637	-3.62939	1.15214	-0.74814	3.4275	0.0000
24200	24217	452.355	-28.661	-23.735	-3.72514	1.15363	-0.81797	3.4123	0.0000
24300	24317	451.998	-29.036	-23.833	-3.81889	1.15512	-0.88780	3.3971	0.0000
24400	24417	451.642	-29.411	-23.931	-3.91064	1.15661	-0.95763	3.3819	0.0000
24500	24517	451.285	-29.786	-24.029	-4.00039	1.15810	-1.02746	3.3667	0.0000
24600	24617	450.928	-30.161	-24.127	-4.08814	1.15959	-1.09729	3.3515	0.0000
24700	24717	450.572	-30.536	-24.225	-4.17389	1.16108	-1.16712	3.3363	0.0000
24800	24817	450.215	-30.911	-24.323	-4.25764	1.16257	-1.23695	3.3211	0.0000
24900	24917	449.858	-31.286	-24.421	-4.33939	1.16406	-1.30678	3.3059	0.0000
25000	25017	449.502	-31.661	-24.519	-4.41914	1.16555	-1.37661	3.2907	0.0000

GEOPOTENTIAL ALTITUDE, ENGLISH UNITS

ALTITUDE		TEMPERATURE			PRESSURE			DENSITY	
H, FT	Z, FT	T, °R	t, °F	t, °C	P, mb	P, IN. HG	$\frac{P}{P_0}$	ρ , LB FT ⁻³	$\frac{\rho}{\rho_0}$
23000	23000	436.446	-23.022	-30.568	4.10000 + 2	1.31075 + 1	4.04645 - 1	3.6758 - 2	4.8000 - 1
23100	23100	436.282	-23.378	-30.768	4.08240	1.30866	4.03911	3.6830	4.7899
23200	23200	436.036	-23.735	-30.964	4.06480	1.30659	4.03183	3.6903	4.7792
23300	23300	435.578	-24.092	-31.162	4.04754	1.30454	3.99461	3.6376	4.7506
23400	23400	435.222	-24.448	-31.360	4.03015	1.30250	3.97745	3.6240	4.7401
23500	23500	434.865	-24.805	-31.558	4.01282	1.30046	3.96035	3.6123	4.7298
23600	23600	434.508	-25.161	-31.756	3.99546	1.29843	3.94331	3.5997	4.7191
23700	23700	434.152	-25.518	-31.954	3.97836	1.29641	3.92633	3.5872	4.7087
23800	23800	433.795	-25.875	-32.153	3.96121	1.29439	3.90941	3.5746	4.6983
23900	23900	433.438	-26.231	-32.351	3.94412	1.29237	3.89255	3.5622	4.6880
24000	24000	433.082	-26.588	-32.549	3.92710 + 2	1.29035 + 1	3.87574 - 1	3.5497 - 2	4.6777 - 1
24100	24100	432.726	-26.944	-32.747	3.91015	1.28833	3.85890	3.5373	4.6674
24200	24200	432.369	-27.301	-32.945	3.89328	1.28631	3.84201	3.5249	4.6571
24300	24300	432.012	-27.658	-33.143	3.87637	1.28429	3.82508	3.5125	4.6468
24400	24400	431.656	-28.014	-33.341	3.85948	1.28227	3.80812	3.5001	4.6365
24500	24500	431.299	-28.371	-33.539	3.84260	1.28025	3.79119	3.4877	4.6262
24600	24600	430.942	-28.728	-33.737	3.82573	1.27823	3.77425	3.4753	4.6159
24700	24700	430.586	-29.084	-33.935	3.80887	1.27621	3.75730	3.4629	4.6056
24800	24800	430.229	-29.441	-34.133	3.79202	1.27419	3.74034	3.4505	4.5953
24900	24900	429.873	-29.797	-34.332	3.77518	1.27217	3.72339	3.4381	4.5850
25000	25000	429.516	-30.154	-34.530	3.75835 + 2	1.27015 + 1	3.70642 - 1	3.4257 - 2	4.5747 - 1
25100	25100	429.159	-30.511	-34.728	3.74151	1.26813	3.68947	3.4133	4.5644
25200	25200	428.803	-30.867	-34.926	3.72467	1.26611	3.67254	3.4009	4.5541
25300	25300	428.446	-31.224	-35.124	3.70782	1.26409	3.65560	3.3885	4.5438
25400	25400	428.090	-31.580	-35.322	3.69098	1.26207	3.63866	3.3761	4.5335
25500	25500	427.733	-31.937	-35.520	3.67414	1.26005	3.62172	3.3637	4.5232
25600	25600	427.376	-32.294	-35.718	3.65730	1.25803	3.60478	3.3513	4.5129
25700	25700	427.020	-32.650	-35.917	3.64046	1.25601	3.58784	3.3389	4.5026
25800	25800	426.663	-33.007	-36.115	3.62362	1.25399	3.57090	3.3265	4.4923
25900	25900	426.306	-33.364	-36.313	3.60678	1.25197	3.55396	3.3141	4.4820
26000	26000	425.950	-33.720	-36.511	3.58994 + 2	1.24995 + 1	3.53701 - 1	3.3017 - 2	4.4717 - 1
26100	26100	425.593	-34.077	-36.709	3.57310	1.24793	3.52007	3.2893	4.4614
26200	26200	425.236	-34.433	-36.907	3.55626	1.24591	3.50313	3.2769	4.4511
26300	26300	424.880	-34.790	-37.105	3.53942	1.24389	3.48619	3.2645	4.4408
26400	26400	424.523	-35.147	-37.303	3.52258	1.24187	3.46925	3.2521	4.4305
26500	26500	424.167	-35.503	-37.501	3.50574	1.23985	3.45231	3.2397	4.4202
26600	26600	423.810	-35.860	-37.699	3.48890	1.23783	3.43537	3.2273	4.4099
26700	26700	423.454	-36.216	-37.897	3.47206	1.23581	3.41843	3.2149	4.3996
26800	26800	423.097	-36.573	-38.095	3.45522	1.23379	3.40149	3.2025	4.3893
26900	26900	422.740	-36.930	-38.293	3.43838	1.23177	3.38455	3.1901	4.3790
27000	27000	422.384	-37.286	-38.491	3.42154 + 2	1.22975 + 1	3.36761 - 1	3.1777 - 2	4.3687 - 1
27100	27100	422.027	-37.643	-38.689	3.40470	1.22773	3.35067	3.1653	4.3584
27200	27200	421.670	-38.000	-38.887	3.38786	1.22571	3.33373	3.1529	4.3481
27300	27300	421.313	-38.356	-39.085	3.37102	1.22369	3.31679	3.1405	4.3378
27400	27400	420.956	-38.713	-39.283	3.35418	1.22167	3.29985	3.1281	4.3275
27500	27500	420.600	-39.069	-39.481	3.33734	1.21965	3.28291	3.1157	4.3172
27600	27600	420.243	-39.426	-39.679	3.32050	1.21763	3.26597	3.1033	4.3069
27700	27700	419.887	-39.783	-39.877	3.30366	1.21561	3.24903	3.0909	4.2966
27800	27800	419.530	-40.140	-40.075	3.28682	1.21359	3.23209	3.0785	4.2863
27900	27900	419.174	-40.496	-40.273	3.27000	1.21157	3.21515	3.0661	4.2760
28000	28000	418.818	-40.853	-40.471	3.25318 + 2	1.20955 + 1	3.19821 - 1	3.0537 - 2	4.2657 - 1
28100	28100	418.461	-41.210	-40.669	3.23636	1.20753	3.18127	3.0413	4.2554
28200	28200	418.104	-41.567	-40.867	3.21954	1.20551	3.16433	3.0289	4.2451
28300	28300	417.748	-41.924	-41.065	3.20272	1.20349	3.14739	3.0165	4.2348
28400	28400	417.391	-42.281	-41.263	3.18590	1.20147	3.13045	3.0041	4.2245
28500	28500	417.034	-42.638	-41.461	3.16908	1.19945	3.11351	2.9917	4.2142
28600	28600	416.678	-42.995	-41.659	3.15226	1.19743	3.09657	2.9793	4.2039
28700	28700	416.321	-43.352	-41.857	3.13544	1.19541	3.07963	2.9669	4.1936
28800	28800	415.965	-43.709	-42.055	3.11862	1.19339	3.06269	2.9545	4.1833
28900	28900	415.608	-44.066	-42.253	3.10180	1.19137	3.04575	2.9421	4.1730
29000	29000	415.252	-44.423	-42.451	3.08500	1.18935	3.02881	2.9297	4.1627
29100	29100	414.895	-44.780	-42.649	3.06820	1.18733	3.01187	2.9173	4.1524
29200	29200	414.538	-45.137	-42.847	3.05140	1.18531	2.99493	2.9049	4.1421
29300	29300	414.181	-45.494	-43.045	3.03460	1.18329	2.97799	2.8925	4.1318
29400	29400	413.824	-45.851	-43.243	3.01780	1.18127	2.96105	2.8801	4.1215
29500	29500	413.467	-46.208	-43.441	3.00100	1.17925	2.94411	2.8677	4.1112
29600	29600	413.110	-46.565	-43.639	2.98420	1.17723	2.92717	2.8553	4.1009
29700	29700	412.753	-46.922	-43.837	2.96740	1.17521	2.91023	2.8429	4.0906
29800	29800	412.396	-47.279	-44.035	2.95060	1.17319	2.89329	2.8305	4.0803
29900	29900	412.039	-47.636	-44.233	2.93380	1.17117	2.87635	2.8181	4.0700
30000	30000	411.682	-47.993	-44.431	2.91700	1.16915	2.85941	2.8057	4.0597
30100	30100	411.325	-48.350	-44.629	2.90020	1.16713	2.84247	2.7933	4.0494
30200	30200	410.968	-48.707	-44.827	2.88340	1.16511	2.82553	2.7809	4.0391
30300	30300	410.611	-49.064	-45.025	2.86660	1.16309	2.80859	2.7685	4.0288
30400	30400	410.254	-49.421	-45.223	2.84980	1.16107	2.79165	2.7561	4.0185
30500	30500	409.897	-49.778	-45.421	2.83300	1.15905	2.77471	2.7437	4.0082
30600	30600	409.540	-50.135	-45.619	2.81620	1.15703	2.75777	2.7313	4.0000
30700	30700	409.183	-50.492	-45.817	2.79940	1.15501	2.74083	2.7189	3.9917
30800	30800	408.826	-50.849	-46.015	2.78260	1.15299	2.72389	2.7065	3.9834
30900	30900	408.469	-51.206	-46.213	2.76580	1.15097	2.70695	2.6941	3.9751
31000	31000	408.112	-51.563	-46.411	2.74900	1.14895	2.69001	2.6817	3.9668
31100	31100	407.755	-51.920	-46.609	2.73220	1.14693	2.67307	2.6693	3.9585
31200	31200	407.398	-52.277	-46.807	2.71540	1.14491	2.65613	2.6569	3.9502
31300	31300	407.041	-52.634	-47.005	2.69860	1.14289	2.63919	2.6445	3.9419
31400	31400	406.684	-52.991	-47.203	2.68180	1.14087	2.62225	2.6321	3.9336
31500	31500	406.327	-53.348	-47.401	2.66500	1.13885	2.60531	2.6197	3.9253
31600	31600	405.970	-53.705	-47.599	2.64820	1.13683	2.58837	2.6073	3.9170
31700	31700	405.613	-54.062	-47.797	2.63140	1.13481	2.57143	2.5949	3.9087
31800	31800	405.256	-54.419	-47.995	2.61460	1.13279	2.55449	2.5825	3.9004
31900	31900	404.899	-54.776	-48.193	2.59780	1.13077	2.53755	2.5701	3.8921
32000	32000	404.542	-55.133	-48.391	2.58100	1.12875	2.52061	2.5577	3.8838
32100	32100	404.185	-55.490	-48.589	2.56420	1.12673	2.50367	2.5453	3.8755
32200	32200	403.828	-55.847	-48.787	2.54740	1.12471	2.48673	2.5329	3.8672
32300	32300	403.471	-56.204	-48.985	2.53060	1.12269	2.46979	2.5205	3.8589
32400	32400	403.114	-56.561	-49.183	2.51380	1.12067	2.45285	2.5081	3.8506
32500	32500	402.757	-56.918	-49.381	2.49700	1.11865	2.43591	2.4957	3.8423
32600	32600	402.400	-57.275	-49.579	2.48020	1.11663	2.41897	2.4833	3.8340
32700	32700	402.043	-57.632	-49.777	2.46340	1.11461	2.40203	2.4709	3.8257
32800	32800	401.686	-57.989	-49.975	2.44660	1.11259	2.38509	2.4585	3.8174
32900	32900	401.329	-58.346	-50.173	2.42980	1.11057	2.36815	2.4461	3.8091
33000	33000	400.972	-58.703	-50.371	2.41300	1.10855	2.35121	2.4337	3.8008
33100	33100	400.615	-59.060	-50.569	2.39620	1.10653	2.33427	2.4213	3.7925
33200	33200	400.258	-						

GEOPOTENTIAL ALTITUDE, ENGLISH UNITS

ALTITUDE		TEMPERATURE			PRESSURE			DENSITY	
H, FT	Z, FT	T, °R	t, °F	t, °C	P, mB	P, IN. HG	$\frac{P}{P_0}$	ρ , LB FT ⁻³	$\frac{\rho}{\rho_0}$
31000	31046	408.119	-51.551	-46.417	2.07446 + 2	8.48629 + 0	2.83097	2.7571 - 2	1.0053
31100	31146	407.762	-51.908	-46.815	2.06129	8.44838	2.82387	2.7490	1.0019
31200	31247	407.406	-52.264	-47.213	2.04816	8.41061	2.81691	2.7407	0.9985
31300	31347	407.049	-52.621	-47.612	2.03508	8.37199	2.79901	2.7326	0.9951
31400	31447	406.693	-52.977	-48.010	2.02205	8.33351	2.78515	2.7244	0.9917
31500	31548	406.336	-53.334	-48.408	2.00907	8.29517	2.77233	2.7164	0.9883
31600	31648	405.979	-53.691	-48.806	2.79613	8.25686	2.75957	2.7081	0.9849
31700	31749	405.623	-54.047	-49.204	2.78325	8.21863	2.74685	2.7001	0.9815
31800	31849	405.266	-54.404	-49.602	2.77041	8.18102	2.73418	2.6920	0.9781
31900	31949	404.909	-54.761	-49.999	2.75762	8.14326	2.72156	2.6840	0.9747
32000	32049	404.553	-55.117	-48.398	2.74486 + 2	8.10563 + 0	2.70899 - 1	2.6761 - 2	1.0000
32100	32149	404.198	-55.474	-48.797	2.73219	8.06815	2.69646	2.6681	0.9966
32200	32250	403.840	-55.830	-49.195	2.71954	8.03081	2.68398	2.6602	0.9932
32300	32350	403.483	-56.187	-49.593	2.70694	7.99360	2.67155	2.6523	0.9898
32400	32450	403.126	-56.544	-49.991	2.69439	7.95654	2.65916	2.6444	0.9864
32500	32551	402.770	-56.900	-50.389	2.68189	7.91961	2.64682	2.6365	0.9830
32600	32651	402.413	-57.257	-50.787	2.66943	7.88283	2.63452	2.6286	0.9796
32700	32751	402.057	-57.613	-51.185	2.65698	7.84618	2.62228	2.6207	0.9762
32800	32852	401.700	-57.970	-51.583	2.64456	7.80967	2.61008	2.6127	0.9728
32900	32952	401.343	-58.327	-51.981	2.63234	7.77330	2.59792	2.6048	0.9694
33000	33052	400.987	-58.683	-52.380	2.62007 + 2	7.73707 + 0	2.58581 - 1	2.5978 - 2	1.0000
33100	33153	400.630	-59.040	-52.778	2.60786	7.70097	2.57375	2.5899	0.9966
33200	33253	400.273	-59.397	-53.176	2.59567	7.66501	2.56173	2.5820	0.9932
33300	33353	399.917	-59.753	-53.574	2.58354	7.62919	2.54975	2.5741	0.9898
33400	33454	399.560	-60.110	-53.972	2.57146	7.59350	2.53783	2.5662	0.9864
33500	33554	399.204	-60.466	-54.370	2.55941	7.55794	2.52594	2.5583	0.9830
33600	33654	398.847	-60.823	-54.768	2.54742	7.52253	2.51411	2.5504	0.9796
33700	33755	398.490	-61.180	-55.166	2.53547	7.48734	2.50232	2.5425	0.9762
33800	33855	398.134	-61.536	-55.564	2.52357	7.45230	2.49057	2.5346	0.9728
33900	33955	397.777	-61.893	-55.962	2.51171	7.41738	2.47887	2.5267	0.9694
34000	34056	397.421	-62.249	-56.361	2.49989 + 2	7.38219 + 0	2.46721 - 1	2.5188 - 2	1.0000
34100	34156	397.064	-62.606	-56.759	2.48813	7.34714	2.45559	2.5109	0.9966
34200	34256	396.707	-62.963	-57.157	2.47641	7.31230	2.44402	2.5030	0.9932
34300	34357	396.351	-63.319	-57.555	2.46473	7.27763	2.43250	2.4951	0.9898
34400	34457	395.994	-63.676	-57.953	2.45310	7.24319	2.42103	2.4872	0.9864
34500	34557	395.637	-64.033	-58.351	2.44151	7.20897	2.40961	2.4793	0.9830
34600	34658	395.281	-64.389	-58.749	2.43000	7.17496	2.39821	2.4714	0.9796
34700	34758	394.924	-64.746	-59.147	2.41848	7.14117	2.38684	2.4635	0.9762
34800	34858	394.568	-65.102	-59.545	2.40701	7.10759	2.37553	2.4556	0.9728
34900	34959	394.211	-65.459	-59.943	2.39560	7.07419	2.36427	2.4477	0.9694
35000	35060	393.854	-65.816	-60.342	2.38423 + 2	7.04099 + 0	2.35306 - 1	2.4398 - 2	1.0000
35100	35160	393.497	-66.173	-60.740	2.37292	7.00798	2.34193	2.4319	0.9966
35200	35260	393.140	-66.530	-61.138	2.36165	6.97512	2.33084	2.4240	0.9932
35300	35361	392.783	-66.887	-61.536	2.35043	6.94240	2.31983	2.4161	0.9898
35400	35461	392.426	-67.244	-61.934	2.33926	6.90981	2.30887	2.4082	0.9864
35500	35562	392.069	-67.601	-62.332	2.32813	6.87736	2.29796	2.4003	0.9830
35600	35662	391.712	-67.958	-62.730	2.31705	6.84504	2.28709	2.3924	0.9796
35700	35763	391.355	-68.315	-63.128	2.30602	6.81284	2.27627	2.3845	0.9762
35800	35863	390.998	-68.672	-63.526	2.29504	6.78076	2.26549	2.3766	0.9728
35900	35964	390.641	-69.029	-63.924	2.28411	6.74880	2.25475	2.3687	0.9694
36000	36064	390.284	-69.386	-64.322	2.27323	6.71695	2.24405	2.3608	0.9660
36100	36165	389.927	-69.743	-64.720	2.26240	6.68521	2.23339	2.3529	0.9626
36200	36265	389.570	-70.100	-65.118	2.25162	6.65358	2.22277	2.3450	0.9592
36300	36366	389.213	-70.457	-65.516	2.24089	6.62206	2.21219	2.3371	0.9558
36400	36466	388.856	-70.814	-65.914	2.23021	6.59064	2.20165	2.3292	0.9524
36500	36567	388.499	-71.171	-66.312	2.21958	6.55932	2.19115	2.3213	0.9490
36600	36667	388.142	-71.528	-66.710	2.20900	6.52810	2.18069	2.3134	0.9456
36700	36768	387.785	-71.885	-67.108	2.19847	6.49698	2.17027	2.3055	0.9422
36800	36868	387.428	-72.242	-67.506	2.18800	6.46596	2.15989	2.2976	0.9388
36900	36969	387.071	-72.599	-67.904	2.17757	6.43504	2.14955	2.2897	0.9354
37000	37069	386.714	-72.956	-68.302	2.16719	6.40422	2.13925	2.2818	0.9320
37100	37170	386.357	-73.313	-68.700	2.15686	6.37350	2.12899	2.2739	0.9286
37200	37270	385.999	-73.670	-69.098	2.14658	6.34288	2.11877	2.2660	0.9252
37300	37371	385.642	-74.027	-69.496	2.13635	6.31236	2.10859	2.2581	0.9218
37400	37471	385.285	-74.384	-69.894	2.12617	6.28194	2.09845	2.2502	0.9184
37500	37572	384.928	-74.741	-70.292	2.11604	6.25162	2.08835	2.2423	0.9150
37600	37672	384.571	-75.098	-70.690	2.10596	6.22140	2.07829	2.2344	0.9116
37700	37773	384.214	-75.455	-71.088	2.09593	6.19128	2.06827	2.2265	0.9082
37800	37873	383.857	-75.812	-71.486	2.08595	6.16126	2.05829	2.2186	0.9048
37900	37974	383.499	-76.169	-71.884	2.07602	6.13134	2.04835	2.2107	0.9014
38000	38074	383.142	-76.526	-72.282	2.06614	6.10152	2.03845	2.2028	0.8980
38100	38175	382.785	-76.883	-72.680	2.05631	6.07180	2.02859	2.1949	0.8946
38200	38275	382.428	-77.240	-73.078	2.04653	6.04218	2.01877	2.1870	0.8912
38300	38376	382.071	-77.597	-73.476	2.03680	6.01266	2.00899	2.1791	0.8878
38400	38476	381.714	-77.954	-73.874	2.02712	5.98324	1.99925	2.1712	0.8844
38500	38577	381.357	-78.311	-74.272	2.01749	5.95392	1.98955	2.1633	0.8810
38600	38677	380.999	-78.668	-74.670	2.00791	5.92470	1.97989	2.1554	0.8776
38700	38778	380.642	-79.025	-75.068	1.99838	5.89558	1.97027	2.1475	0.8742
38800	38878	380.285	-79.382	-75.466	1.98890	5.86656	1.96069	2.1396	0.8708
38900	38979	379.928	-79.739	-75.864	1.97947	5.83764	1.95115	2.1317	0.8674
39000	39079	379.571	-80.096	-76.262	1.97009	5.80882	1.94165	2.1238	0.8640
39100	39180	379.214	-80.453	-76.660	1.96076	5.78010	1.93219	2.1159	0.8606
39200	39280	378.857	-80.810	-77.058	1.95148	5.75148	1.92277	2.1080	0.8572
39300	39381	378.499	-81.167	-77.456	1.94225	5.72296	1.91339	2.0999	0.8538
39400	39481	378.142	-81.524	-77.854	1.93307	5.69454	1.90405	2.0919	0.8504
39500	39582	377.785	-81.881	-78.252	1.92394	5.66622	1.89475	2.0839	0.8470
39600	39682	377.428	-82.238	-78.650	1.91486	5.63800	1.88549	2.0759	0.8436
39700	39783	377.071	-82.595	-79.048	1.90583	5.60988	1.87627	2.0679	0.8402
39800	39883	376.714	-82.952	-79.446	1.89685	5.58186	1.86709	2.0599	0.8368
39900	39984	376.357	-83.309	-79.844	1.88792	5.55394	1.85795	2.0519	0.8334
40000	40084	375.999	-83.666	-80.242	1.87904	5.52612	1.84885	2.0439	0.8300
40100	40185	375.642	-84.023	-80.640	1.87021	5.49840	1.83979	2.0359	0.8266
40200	40285	375.285	-84.380	-81.038	1.86143	5.47078	1.83077	2.0279	0.8232
40300	40386	374.928	-84.737	-81.436	1.85270	5.44326	1.82179	2.0199	0.8198
40400	40486	374.571	-85.094	-81.834	1.84402	5.41584	1.81285	2.0119	0.8164
40500	40587	374.214	-85.451	-82.232	1.83539	5.38852	1.80395	2.0039	0.8130
40600	40687	373.857	-85.808	-82.630	1.82681	5.36130	1.79509	1.9959	0.8096
40700	40788	373.499	-86.165	-83.028	1.81828	5.33418	1.78627	1.9879	0.8062
40800	40888	373.142	-86.522	-83.426	1.80980	5.30716	1.77749	1.9799	0.8028
40900	40989	372.785	-86.879	-83.824	1.80137	5.28024	1.76875	1.9719	0.7994
41000	41089	372.428	-87.236	-84.222	1.79299	5.25342	1.75999	1.9639	0.7960
41100	41190	372.071	-87.593	-84.620	1.78466	5.22670	1.75127	1.9559	0.7926
41200	41290	371.714	-87.950	-85.018	1.77638	5.199			

GEOPOTENTIAL ALTITUDE, ENGLISH UNITS

ALTITUDE		TEMPERATURE			PRESSURE			DENSITY	
H, FT	Z, FT	T, °R	t, °F	t, °C	P, mB	P, IN. HG	$\frac{P}{P_0}$	ρ , LB FT ⁻³	$\frac{\rho}{\rho_0}$
43000	43000	389.970	-89.700	-68.800	1.02387 + 2	4.79430 + 0	1.00000 - 1	1.00000 - 2	2.1511 - 1
43000	43000	389.970	-89.700	-68.800	1.00000	4.74000	1.58701	1.6142	2.1106
43000	43001	389.970	-89.700	-68.800	1.00000	4.70310	1.57102	1.59007	2.0908
43000	43001	389.970	-89.700	-68.800	1.07741	4.68310	1.55679	1.56330	2.0708
43000	43002	389.970	-89.700	-68.800	1.06028	4.61384	1.54189	1.55003	2.0508
44000	44003	389.970	-89.700	-68.800	1.04730	4.50941	1.52714	1.53635	2.0311
44000	44204	389.970	-89.700	-68.800	1.53287	4.52509	1.51263	1.53364	2.0117
44000	44405	389.970	-89.700	-68.800	1.51781	4.48340	1.49808	1.5237	1.9925
44000	44606	389.970	-89.700	-68.800	1.50329	4.43081	1.48373	1.5091	1.9734
44000	44807	389.970	-89.700	-68.800	1.48901	4.39704	1.46964	1.4947	1.9545
45000	45007	389.970	-89.700	-68.800	1.47476 + 2	4.35400 + 0	1.45548 - 1	1.4804 - 2	1.9358 - 1
45000	45208	389.970	-89.700	-68.800	1.46068	4.31332	1.44156	1.4662	1.9173
45000	45409	389.970	-89.700	-68.800	1.44680	4.27276	1.42776	1.4522	1.8990
45000	45710	389.970	-89.700	-68.800	1.43304	4.23118	1.41411	1.4383	1.8808
45000	45911	389.970	-89.700	-68.800	1.41914	4.19070	1.40068	1.4246	1.8628
45000	46112	389.970	-89.700	-68.800	1.40586	4.15081	1.38718	1.4110	1.8450
45000	46313	389.970	-89.700	-68.800	1.39211	4.11091	1.37391	1.3974	1.8273
45000	46514	389.970	-89.700	-68.800	1.37879	4.07150	1.36076	1.3841	1.8099
45000	46715	389.970	-89.700	-68.800	1.36589	4.03263	1.34775	1.3708	1.7925
45000	46916	389.970	-89.700	-68.800	1.35354	3.99428	1.33485	1.3577	1.7754
47000	47118	389.970	-89.700	-68.800	1.33980 + 2	3.95584 + 0	1.32208 - 1	1.3447 - 2	1.7584 - 1
47000	47319	389.970	-89.700	-68.800	1.32679	3.91800	1.30844	1.3319	1.7418
47000	47520	389.970	-89.700	-68.800	1.31409	3.88081	1.29491	1.3191	1.7249
47000	47721	389.970	-89.700	-68.800	1.30152	3.84439	1.28240	1.3066	1.7084
47000	47922	389.970	-89.700	-68.800	1.28907	3.80862	1.27021	1.2940	1.6921
47000	48123	389.970	-89.700	-68.800	1.27674	3.77354	1.25844	1.2816	1.6759
47000	48324	389.970	-89.700	-68.800	1.26452	3.73914	1.24709	1.2694	1.6599
47000	48525	389.970	-89.700	-68.800	1.25243	3.70541	1.23608	1.2572	1.6440
47000	48726	389.970	-89.700	-68.800	1.24054	3.67233	1.22542	1.2454	1.6282
47000	48927	389.970	-89.700	-68.800	1.22886	3.63989	1.21501	1.2343	1.6127
49000	49115	389.970	-89.700	-68.800	1.21642 + 2	3.60720 + 0	1.20491 - 1	1.2245 - 2	1.5977 - 1
49000	49316	389.970	-89.700	-68.800	1.20418	3.57520	1.19504	1.2148	1.5829
49000	49517	389.970	-89.700	-68.800	1.19208	3.54380	1.18539	1.2053	1.5682
49000	49718	389.970	-89.700	-68.800	1.18012	3.51291	1.17594	1.1959	1.5538
49000	49919	389.970	-89.700	-68.800	1.16830	3.48254	1.16669	1.1866	1.5395
49000	50120	389.970	-89.700	-68.800	1.15662	3.45269	1.15764	1.1774	1.5254
49000	50321	389.970	-89.700	-68.800	1.14508	3.42336	1.14879	1.1684	1.5114
49000	50522	389.970	-89.700	-68.800	1.13368	3.39456	1.13994	1.1594	1.4975
49000	50723	389.970	-89.700	-68.800	1.12242	3.36629	1.13129	1.1504	1.4837
49000	50924	389.970	-89.700	-68.800	1.11130	3.33854	1.12284	1.1416	1.4699
51000	51126	389.970	-89.700	-68.800	1.10042 + 2	3.31130 + 0	1.11468 - 1	1.1332 - 2	1.4562 - 1
51000	51327	389.970	-89.700	-68.800	1.08967	3.28457	1.10641	1.1249	1.4427
51000	51528	389.970	-89.700	-68.800	1.07908	3.25836	1.09830	1.1168	1.4293
51000	51729	389.970	-89.700	-68.800	1.06864	3.23266	1.09034	1.1088	1.4160
51000	51930	389.970	-89.700	-68.800	1.05835	3.20747	1.08254	1.1009	1.4028
51000	52131	389.970	-89.700	-68.800	1.04820	3.18269	1.07489	1.0931	1.3897
51000	52332	389.970	-89.700	-68.800	1.03819	3.15832	1.06739	1.0854	1.3767
51000	52533	389.970	-89.700	-68.800	1.02832	3.13436	1.05994	1.0778	1.3638
51000	52734	389.970	-89.700	-68.800	1.01858	3.11080	1.05254	1.0702	1.3510
51000	52935	389.970	-89.700	-68.800	1.00896	3.08764	1.04519	1.0627	1.3383
53000	53136	389.970	-89.700	-68.800	1.00048 + 2	3.06488 + 0	1.03789 - 1	1.0553 - 2	1.3257 - 1
53000	53337	389.970	-89.700	-68.800	0.99214	3.04252	1.03064	1.0479	1.3132
53000	53538	389.970	-89.700	-68.800	0.98394	3.02056	1.02344	1.0405	1.3008
53000	53739	389.970	-89.700	-68.800	0.97587	3.00000	1.01629	1.0331	1.2885
53000	53940	389.970	-89.700	-68.800	0.96792	2.97984	1.00919	1.0257	1.2762
53000	54141	389.970	-89.700	-68.800	0.96008	2.96000	1.00214	1.0183	1.2640
53000	54342	389.970	-89.700	-68.800	0.95236	2.94044	0.99514	1.0109	1.2518
53000	54543	389.970	-89.700	-68.800	0.94476	2.92118	0.98819	1.0035	1.2397
53000	54744	389.970	-89.700	-68.800	0.93728	2.90222	0.98129	0.9961	1.2276
53000	54945	389.970	-89.700	-68.800	0.92992	2.88356	0.97444	0.9887	1.2156
55000	55146	389.970	-89.700	-68.800	0.92268 + 2	2.86520 + 0	0.96764 - 1	0.9813 - 2	1.2037 - 1
55000	55347	389.970	-89.700	-68.800	0.91556	2.84724	0.96089	0.9739	1.1918
55000	55548	389.970	-89.700	-68.800	0.90856	2.82958	0.95419	0.9665	1.1799
55000	55749	389.970	-89.700	-68.800	0.90168	2.81222	0.94754	0.9591	1.1681
55000	55950	389.970	-89.700	-68.800	0.89492	2.79516	0.94094	0.9517	1.1563
55000	56151	389.970	-89.700	-68.800	0.88828	2.77840	0.93439	0.9443	1.1445
55000	56352	389.970	-89.700	-68.800	0.88176	2.76194	0.92789	0.9369	1.1327
55000	56553	389.970	-89.700	-68.800	0.87536	2.74578	0.92144	0.9295	1.1210
55000	56754	389.970	-89.700	-68.800	0.86908	2.72992	0.91504	0.9221	1.1093
55000	56955	389.970	-89.700	-68.800	0.86292	2.71436	0.90869	0.9147	1.0976
57000	57156	389.970	-89.700	-68.800	0.85688 + 2	2.69900 + 0	0.90239 - 1	0.9073 - 2	1.0860 - 1
57000	57357	389.970	-89.700	-68.800	0.85096	2.68384	0.89609	0.8999	1.0744
57000	57558	389.970	-89.700	-68.800	0.84516	2.66898	0.88984	0.8935	1.0628
57000	57759	389.970	-89.700	-68.800	0.83948	2.65442	0.88364	0.8871	1.0513
57000	57960	389.970	-89.700	-68.800	0.83392	2.64016	0.87749	0.8807	1.0398
57000	58161	389.970	-89.700	-68.800	0.82848	2.62620	0.87139	0.8743	1.0283
57000	58362	389.970	-89.700	-68.800	0.82316	2.61254	0.86534	0.8679	1.0168
57000	58563	389.970	-89.700	-68.800	0.81796	2.59918	0.85934	0.8615	1.0053
57000	58764	389.970	-89.700	-68.800	0.81288	2.58612	0.85339	0.8551	0.9938
59000	59165	389.970	-89.700	-68.800	0.80792 + 2	2.57326 + 0	0.84749 - 1	0.8487 - 2	0.9824 - 1
59000	59366	389.970	-89.700	-68.800	0.80308	2.56060	0.84164	0.8423	0.9710
59000	59567	389.970	-89.700	-68.800	0.79836	2.54814	0.83584	0.8359	0.9596
59000	59768	389.970	-89.700	-68.800	0.79376	2.53588	0.83009	0.8295	0.9482
59000	59969	389.970	-89.700	-68.800	0.78928	2.52382	0.82439	0.8234	0.9368
59000	60170	389.970	-89.700	-68.800	0.78492	2.51196	0.81874	0.8174	0.9254
59000	60371	389.970	-89.700	-68.800	0.78068	2.50030	0.81314	0.8114	0.9140
59000	60572	389.970	-89.700	-68.800	0.77656	2.48884	0.80759	0.8054	0.9026
59000	60773	389.970	-89.700	-68.800	0.77256	2.47758	0.80209	0.8000	0.8912
59000	60974	389.970	-89.700	-68.800	0.76868	2.46652	0.79664	0.7941	0.8798
59000	61175	389.970	-89.700	-68.800	0.76492	2.45566	0.79124	0.7883	0.8684
61000	61176	389.970	-89.700	-68.800	0.76128 + 2	2.44490 + 0	0.78589 - 1	0.7824 - 2	0.8570 - 1
61000	61377	389.970	-89.700	-68.800	0.75776	2.43434	0.78059	0.7766	0.8456
61000	61578	389.970	-89.700	-68.800	0.75436	2.42398	0.77534	0.7709	0.8342
61000	61779	389.970	-89.700	-68.800	0.75108	2.41382	0.77014	0.7653	0.8228
61000	61980	389.970	-89.700	-68.800	0.74792	2.40386	0.76499	0.7599	0.8114
61000	62181	389.970	-89.700	-68.800	0.74488	2.39400	0.75989	0.7544	0.8000
61000	62382	389.970	-89.700	-68.800	0.74196	2.38434	0.75484	0.7489	0.7886
61000	62583	389.970	-89.700	-68.800	0.73916	2.37488	0.74984	0.7435	0.7772
61000	62784	389.970	-89.700	-68.800	0.73648	2.36562	0.74489	0.7379	0.7658
61000	62985	389.970	-89.700	-68.800	0.73392	2.35656	0.73999	0.7324	0.7544
63000	63186	389.970	-89.700	-68.800	0.73148 + 2	2.34760 + 0	0.73514 - 1	0.7311 - 2	0.7430 - 1
63000	63387	389.970	-89.700	-68.800	0.72916	2			

GEOPOTENTIAL ALTITUDE, ENGLISH UNITS

ALTITUDE		TEMPERATURE			PRESSURE		DENSITY		
H, FT	Z, FT	T, °R	t, °F	t, °C	P, mb	P, IN. HG	$\frac{P}{P_0}$	ρ , LB FT ⁻³	$\frac{\rho}{\rho_0}$
8000	50187	389.970	-61.700	-54.500	7.63473 + 1	2.22206 + 0	7.42633 - 2	7.6636 - 3	0.9772 - 2
8000	50200	389.970	-61.700	-54.500	7.63754	2.20079	7.38430	7.68113	0.97827
8000	50210	389.970	-61.700	-54.500	7.64035	2.17974	7.34242	7.69871	0.97931
8000	50220	389.970	-61.700	-54.500	7.64316	2.15869	7.30053	7.71632	0.98034
8000	50230	389.970	-61.700	-54.500	7.64597	2.13764	7.25864	7.73393	0.98138
8000	50240	389.970	-61.700	-54.500	7.64878	2.11659	7.21675	7.75154	0.98241
8000	50250	389.970	-61.700	-54.500	7.65159	2.09554	7.17486	7.76915	0.98345
8000	50260	389.970	-61.700	-54.500	7.65440	2.07449	7.13297	7.78676	0.98448
8000	50270	389.970	-61.700	-54.500	7.65721	2.05344	7.09108	7.80437	0.98552
8000	50280	389.970	-61.700	-54.500	7.66002	2.03239	7.04919	7.82198	0.98655
8000	50290	389.970	-61.700	-54.500	7.66283	2.01134	7.00730	7.83959	0.98759
8000	50300	389.970	-61.700	-54.500	7.66564	1.99029	6.96541	7.85720	0.98862
8000	50310	389.970	-61.700	-54.500	7.66845	1.96924	6.92352	7.87481	0.98966
8000	50320	389.970	-61.700	-54.500	7.67126	1.94819	6.88163	7.89242	0.99069
8000	50330	389.970	-61.700	-54.500	7.67407	1.92714	6.83974	7.91003	0.99173
8000	50340	389.970	-61.700	-54.500	7.67688	1.90609	6.79785	7.92764	0.99276
8000	50350	389.970	-61.700	-54.500	7.67969	1.88504	6.75596	7.94525	0.99380
8000	50360	389.970	-61.700	-54.500	7.68250	1.86399	6.71407	7.96286	0.99483
8000	50370	389.970	-61.700	-54.500	7.68531	1.84294	6.67218	7.98047	0.99587
8000	50380	389.970	-61.700	-54.500	7.68812	1.82189	6.63029	7.99808	0.99690
8000	50390	389.970	-61.700	-54.500	7.69093	1.80084	6.58840	8.01569	0.99794
8000	50400	389.970	-61.700	-54.500	7.69374	1.77979	6.54651	8.03330	0.99897
8000	50410	389.970	-61.700	-54.500	7.69655	1.75874	6.50462	8.05091	0.99999
8000	50420	389.970	-61.700	-54.500	7.69936	1.73769	6.46273	8.06852	1.00103
8000	50430	389.970	-61.700	-54.500	7.70217	1.71664	6.42084	8.08613	1.00206
8000	50440	389.970	-61.700	-54.500	7.70498	1.69559	6.37895	8.10374	1.00309
8000	50450	389.970	-61.700	-54.500	7.70779	1.67454	6.33706	8.12135	1.00413
8000	50460	389.970	-61.700	-54.500	7.71060	1.65349	6.29517	8.13896	1.00516
8000	50470	389.970	-61.700	-54.500	7.71341	1.63244	6.25328	8.15657	1.00620
8000	50480	389.970	-61.700	-54.500	7.71622	1.61139	6.21139	8.17418	1.00723
8000	50490	389.970	-61.700	-54.500	7.71903	1.59034	6.16950	8.19179	1.00827
8000	50500	389.970	-61.700	-54.500	7.72184	1.56929	6.12761	8.20940	1.00930
8000	50510	389.970	-61.700	-54.500	7.72465	1.54824	6.08572	8.22701	1.01034

GEOPOTENTIAL ALTITUDE, ENGLISH UNITS

ALTITUDE		TEMPERATURE			PRESSURE			DENSITY	
H, FT	Z, FT	T, °R	t, °F	t, °C	P, mB	F, IN. HG	$\frac{P}{P_0}$	ρ , LB FT ⁻³	$\frac{\rho}{\rho_0}$
75000	75271	705.118	-44.583	-53.646	3.49779 + 1	1.03280 + 0	3.44308 - 2	3.4004 - 3	4.8318 - 2
75300	75472	704.226	-44.442	-53.579	3.48476	1.03214	3.41948	3.4318	4.6976
75600	75974	703.537	-44.333	-53.518	3.43206	1.01349	3.39718	3.3904	4.4439
76000	76475	703.447	-44.223	-53.487	3.38087	1.00000	3.36438	3.3804	4.0977
76300	76977	703.557	-44.113	-53.398	3.32780	0.94483 - 1	3.32387	3.3327	4.3680
76600	77478	703.667	-44.003	-53.338	3.27694	0.88974	3.28232	3.3004	4.3157
76900	77979	703.778	-43.894	-53.274	3.22439	0.83597	3.24118	3.2684	4.3738
77200	78481	703.888	-43.784	-53.213	3.17226	0.78358	3.20044	3.2367	4.2534
77500	78982	703.998	-43.674	-53.152	3.12046	0.73247	3.16020	3.2053	4.1913
77800	79484	704.108	-43.564	-53.091	3.06899	0.68261	3.12046	3.1742	4.1507
78100	79985	704.218	-43.455	-53.030	3.01781	0.63399	3.08121	3.1434	4.1105 - 2
78400	80487	704.328	-43.345	-52.969	2.96692	0.58668	3.04246	3.1126	4.0706
78700	80988	704.438	-43.235	-52.908	2.91623	0.54067	3.00371	3.0818	4.0312
79000	81490	704.548	-43.126	-52.848	2.86574	0.49596	2.96521	3.0510	3.9922
79300	81991	704.658	-43.016	-52.787	2.81545	0.45255	2.92693	3.0204	3.9535
79600	82493	704.768	-42.906	-52.726	2.76536	0.41044	2.88884	2.9900	3.9152
79900	82994	704.878	-42.796	-52.665	2.71547	0.36963	2.85094	2.9602	3.8774
80200	83496	704.988	-42.686	-52.604	2.66578	0.33012	2.81327	2.9308	3.8399
80500	83997	705.098	-42.576	-52.543	2.61639	0.29191	2.77591	2.9018	3.8027
80800	84499	705.208	-42.466	-52.482	2.56723	0.25500	2.73884	2.8730	3.7658
81100	84999	705.318	-42.357	-52.421	2.51829	0.21939	2.70206	2.8444	3.7292
81400	85499	705.428	-42.247	-52.360	2.46957	0.18508	2.66557	2.8160	3.6929
81700	85999	705.538	-42.137	-52.299	2.42107	0.15207	2.62937	2.7878	3.6568
82000	86499	705.648	-42.027	-52.238	2.37279	0.12026	2.59346	2.7598	3.6209
82300	86999	705.758	-41.917	-52.177	2.32473	0.08965	2.55784	2.7320	3.5852
82600	87499	705.868	-41.807	-52.116	2.27689	0.06024	2.52251	2.7044	3.5497
82900	87999	705.978	-41.697	-52.055	2.22927	0.03203	2.48746	2.6770	3.5144
83200	88499	706.088	-41.587	-51.994	2.18187	0.00502	2.45269	2.6498	3.4792
83500	88999	706.198	-41.477	-51.933	2.13469	0.00000	2.41820	2.6228	3.4442
83800	89499	706.308	-41.367	-51.872	2.08773		2.38399	2.5959	3.4093
84100	89999	706.418	-41.257	-51.811	2.04100		2.35006	2.5692	3.3745
84400	90499	706.528	-41.147	-51.750	1.99448		2.31641	2.5426	3.3398
84700	90999	706.638	-41.037	-51.689	1.94817		2.28304	2.5162	3.3052
85000	91499	706.748	-40.927	-51.628	1.90207		2.24994	2.4899	3.2707
85300	91999	706.858	-40.817	-51.567	1.85618		2.21711	2.4637	3.2363
85600	92499	706.968	-40.707	-51.506	1.81050		2.18455	2.4376	3.2020
85900	92999	707.078	-40.597	-51.445	1.76503		2.15226	2.4116	3.1678
86200	93499	707.188	-40.487	-51.384	1.71977		2.12024	2.3857	3.1337
86500	93999	707.298	-40.377	-51.323	1.67472		2.08849	2.3598	3.1000
86800	94499	707.408	-40.267	-51.262	1.62988		2.05699	2.3340	3.0664
87100	94999	707.518	-40.157	-51.201	1.58525		2.02574	2.3083	3.0329
87400	95499	707.628	-40.047	-51.140	1.54083		1.99474	2.2827	3.0000
87700	95999	707.738	-39.937	-51.079	1.49662		1.96399	2.2572	2.9672
88000	96499	707.848	-39.827	-51.018	1.45262		1.93349	2.2318	2.9345
88300	96999	707.958	-39.717	-50.957	1.40883		1.90324	2.2065	2.9019
88600	97499	708.068	-39.607	-50.896	1.36525		1.87324	2.1813	2.8694
88900	97999	708.178	-39.497	-50.835	1.32188		1.84349	2.1562	2.8370
89200	98499	708.288	-39.387	-50.774	1.27872		1.81389	2.1312	2.8047
89500	98999	708.398	-39.277	-50.713	1.23577		1.78444	2.1063	2.7725
89800	99499	708.508	-39.167	-50.652	1.19303		1.75514	2.0815	2.7404
90100	99999	708.618	-39.057	-50.591	1.15049		1.72600	2.0568	2.7084
90400		708.728	-38.947	-50.530	1.10816		1.69701	2.0322	2.6765
90700		708.838	-38.837	-50.469	1.06603		1.66817	2.0077	2.6446
91000		708.948	-38.727	-50.408	1.02411		1.63948	1.9833	2.6128
91300		709.058	-38.617	-50.347	0.98239		1.61094	1.9590	2.5810
91600		709.168	-38.507	-50.286	0.94087		1.58255	1.9348	2.5493
91900		709.278	-38.397	-50.225	0.89955		1.55431	1.9107	2.5177
92200		709.388	-38.287	-50.164	0.85843		1.52622	1.8867	2.4862
92500		709.498	-38.177	-50.103	0.81751		1.49828	1.8628	2.4548
92800		709.608	-38.067	-50.042	0.77679		1.47049	1.8390	2.4234
93100		709.718	-37.957	-49.981	0.73627		1.44285	1.8153	2.3921
93400		709.828	-37.847	-49.920	0.69595		1.41536	1.7917	2.3608
93700		709.938	-37.737	-49.859	0.65583		1.38801	1.7682	2.3295
94000		710.048	-37.627	-49.798	0.61591		1.36080	1.7448	2.2982
94300		710.158	-37.517	-49.737	0.57619		1.33373	1.7215	2.2670
94600		710.268	-37.407	-49.676	0.53667		1.30680	1.6983	2.2358
94900		710.378	-37.297	-49.615	0.49735		1.28001	1.6751	2.2046
95200		710.488	-37.187	-49.554	0.45823		1.25336	1.6520	2.1734
95500		710.598	-37.077	-49.493	0.41931		1.22685	1.6290	2.1422
95800		710.708	-36.967	-49.432	0.38059		1.20048	1.6061	2.1110
96100		710.818	-36.857	-49.371	0.34207		1.17425	1.5833	2.0800
96400		710.928	-36.747	-49.310	0.30375		1.14816	1.5605	2.0490
96700		711.038	-36.637	-49.249	0.26563		1.12221	1.5378	2.0180
97000		711.148	-36.527	-49.188	0.22771		1.09640	1.5151	2.0000
97300		711.258	-36.417	-49.127	0.19000		1.07072	1.4925	1.9777
97600		711.368	-36.307	-49.066	0.15250		1.04517	1.4700	1.9554
97900		711.478	-36.197	-49.005	0.11520		1.01975	1.4475	1.9331
98200		711.588	-36.087	-48.944	0.07810		0.99446	1.4251	1.9108
98500		711.698	-35.977	-48.883	0.04120		0.96929	1.4027	1.8885
98800		711.808	-35.867	-48.822	0.00450		0.94424	1.3804	1.8662
99100		711.918	-35.757	-48.761	0.00000		0.91931	1.3581	1.8439
99400		712.028	-35.647	-48.700			0.89450	1.3358	1.8216
99700		712.138	-35.537	-48.639			0.86980	1.3135	1.7993
100000		712.248	-35.427	-48.578			0.84521	1.2912	1.7770

GEOPOTENTIAL ALTITUDE, ENGLISH UNITS

ALTITUDE		TEMPERATURE			PRESSURE			DENSITY	
H, FT	Z, FT	T, °R	t, °F	t, °C	P, mB	P, IN. HG	$\frac{P}{P_0}$	ρ , LB FT ⁻³	$\frac{\rho}{\rho_0}$
91000	91399	403.896	-55.774	-48.763	1.85110 + 1	4.87570 - 1	1.62961 - 2	1.6003 - 3	2.0926 - 2
91200	91601	404.006	-55.664	-48.702	1.83586	4.83066	1.61446	1.5851	2.0727
91400	91802	404.116	-55.554	-48.641	1.82074	4.78606	1.59965	1.5700	2.0530
91600	92004	404.225	-55.445	-48.580	1.80578	4.74187	1.58478	1.5551	2.0336
91800	92206	404.335	-55.335	-48.519	1.79086	4.69816	1.57015	1.5403	2.0142
92000	92408	404.445	-55.225	-48.458	1.77628	4.65475	1.55567	1.5257	1.9950
92200	92609	404.555	-55.115	-48.397	1.76174	4.61182	1.54132	1.5112	1.9761
92400	92811	404.664	-55.006	-48.336	1.54734	4.56928	1.52710	1.4969	1.9573
92600	93013	404.774	-54.896	-48.275	1.53307	4.52716	1.51302	1.4827	1.9388
92800	93215	404.884	-54.786	-48.215	1.51894	4.48543	1.49908	1.4686	1.9204
93000	93417	404.994	-54.676	-48.154	1.50494 + 1	4.44410 - 1	1.48526 - 2	1.4547 - 3	1.9022 - 2
93200	93618	405.103	-54.567	-48.093	1.49108	4.40216	1.47158	1.4409	1.8841
93400	93820	405.213	-54.457	-48.032	1.47735	4.36061	1.45803	1.4272	1.8663
93600	94022	405.323	-54.347	-47.971	1.46375	4.32244	1.44460	1.4137	1.8486
93800	94224	405.432	-54.238	-47.910	1.45027	4.28265	1.43131	1.4003	1.8311
94000	94426	405.542	-54.128	-47.849	1.43683	4.24234	1.41814	1.3870	1.8137
94200	94627	405.652	-54.018	-47.788	1.42371	4.20241	1.40509	1.3739	1.7966
94400	94829	405.762	-53.908	-47.727	1.41061	4.16254	1.39217	1.3609	1.7796
94600	95031	405.871	-53.799	-47.666	1.39764	4.12274	1.37937	1.3480	1.7627
94800	95233	405.981	-53.689	-47.605	1.38479	4.08300	1.36669	1.3353	1.7460
95000	95435	406.091	-53.579	-47.544	1.37207 + 1	4.05172 - 1	1.35413 - 2	1.3226 - 3	1.7296 - 2
95200	95637	406.201	-53.469	-47.483	1.35946	4.01449	1.34169	1.3101	1.7132
95400	95838	406.310	-53.360	-47.422	1.34698	3.97762	1.32936	1.2976	1.6970
95600	96040	406.420	-53.250	-47.361	1.33461	3.94110	1.31716	1.2855	1.6809
95800	96242	406.530	-53.140	-47.300	1.32236	3.90492	1.30506	1.2733	1.6651
96000	96444	406.639	-53.031	-47.239	1.31022	3.86908	1.29309	1.2613	1.6493
96200	96646	406.749	-52.921	-47.178	1.29820	3.83358	1.28122	1.2494	1.6338
96400	96848	406.859	-52.811	-47.117	1.28629	3.79842	1.26947	1.2376	1.6183
96600	97050	406.969	-52.701	-47.056	1.27450	3.76358	1.25783	1.2259	1.6031
96800	97251	407.078	-52.592	-46.995	1.26281	3.72908	1.24630	1.2144	1.5879
97000	97453	407.188	-52.482	-46.934	1.25124 + 1	3.69490 - 1	1.23488 - 2	1.2029 - 3	1.5730 - 2
97200	97655	407.298	-52.372	-46.873	1.23977	3.66106	1.22356	1.1916	1.5581
97400	97857	407.408	-52.262	-46.812	1.22842	3.62751	1.21235	1.1803	1.5434
97600	98059	407.517	-52.153	-46.752	1.21717	3.59429	1.20125	1.1692	1.5289
97800	98261	407.627	-52.043	-46.691	1.20602	3.56136	1.19025	1.1582	1.5145
98000	98463	407.737	-51.933	-46.630	1.19496	3.52879	1.17936	1.1473	1.5002
98200	98665	407.846	-51.824	-46.569	1.18406	3.49650	1.16857	1.1365	1.4861
98400	98867	407.956	-51.714	-46.508	1.17322	3.46451	1.15788	1.1258	1.4721
98600	99068	408.066	-51.604	-46.447	1.16249	3.43283	1.14729	1.1152	1.4583
98800	99270	408.176	-51.494	-46.386	1.15186	3.40144	1.13680	1.1047	1.4445
99000	99472	408.285	-51.385	-46.325	1.14133 + 1	3.37035 - 1	1.12641 - 2	1.0943 - 3	1.4309 - 2
99200	99674	408.395	-51.275	-46.264	1.13090	3.33965	1.11611	1.0840	1.4175
99400	99876	408.505	-51.165	-46.203	1.12057	3.30904	1.10592	1.0738	1.4042
99600	100078	408.615	-51.055	-46.142	1.11034	3.27862	1.09582	1.0637	1.3910
99800	100280	408.724	-50.946	-46.081	1.10020	3.24838	1.08581	1.0537	1.3779
100000	100482	408.834	-50.836	-46.020	1.09015	3.21822	1.07590	1.0438	1.3649
100200	100684	408.944	-50.726	-45.959	1.08020	3.18824	1.06608	1.0340	1.3521
100400	100886	409.053	-50.617	-45.898	1.07035	3.15874	1.05635	1.0243	1.3394
100600	101088	409.163	-50.507	-45.837	1.06059	3.12919	1.04672	1.0147	1.3269
100800	101290	409.273	-50.397	-45.776	1.05092	3.10062	1.03717	1.0052	1.3144
101000	101492	409.383	-50.287	-45.715	1.04133 + 1	3.07208 - 1	1.02772 - 2	9.9575 - 4	1.3021 - 2
101200	101694	409.492	-50.178	-45.654	1.03184	3.04370	1.01835	9.8641	1.2899
101400	101896	409.602	-50.068	-45.593	1.02244	3.01527	1.00907	9.7716	1.2778
101600	102097	409.712	-49.958	-45.532	1.01313	2.98717	9.98681 - 3	9.6800	1.2658
101800	102299	409.822	-49.848	-45.471	1.00390	2.95943	9.90178	9.5893	1.2539
102000	102501	409.931	-49.739	-45.410	9.94763 + 0	2.93754	9.81755	9.4996	1.2422
102200	102703	410.041	-49.629	-45.349	9.92509	2.91080	9.72819	9.4105	1.2306
102400	102905	410.151	-49.519	-45.288	9.90241	2.88431	9.63968	9.3224	1.2190
102600	103107	410.260	-49.410	-45.228	9.87955	2.85807	9.55199	9.2351	1.2076
102800	103309	410.370	-49.300	-45.167	9.85663	2.83208	9.46511	9.1483	1.1963
103000	103511	410.480	-49.190	-45.106	9.83333 + 0	2.80633 - 1	0.37908 - 3	9.0630 - 4	1.1851 - 2
103200	103713	410.590	-49.080	-45.045	9.81005	2.78082	9.38380	8.9783	1.1740
103400	103915	410.699	-48.971	-44.984	9.78684	2.75555	9.30365	8.8943	1.1630
103600	104117	410.809	-48.861	-44.923	9.76366	2.73053	9.22569	8.8111	1.1522
103800	104319	410.919	-48.751	-44.862	9.74052	2.70573	9.14880	8.7288	1.1414
104000	104521	411.029	-48.641	-44.801	9.71743	2.68115	9.07297	8.6472	1.1307
104200	104723	411.138	-48.532	-44.740	9.69439	2.65681	8.99735	8.5664	1.1202
104400	104925	411.248	-48.422	-44.679	9.67155	2.63270	8.92207	8.4864	1.1097
104600	105127	411.358	-48.312	-44.618	9.64877	2.60882	8.84716	8.4072	1.0993
104800	105329	411.467	-48.203	-44.557	9.62594	2.58516	8.77286	8.3287	1.0891
105000	105531	411.576	-48.093	-44.496	9.60316 + 0	2.56171 - 1	8.69851 - 3	8.2507 - 4	1.0789 - 2
105200	105733	411.686	-47.982	-44.435	9.58044	2.53844	8.62465	8.1661	1.0687
105400	105935	411.795	-47.872	-44.374	9.55772	2.51537	8.55097	8.0824	1.0586
105600	106137	411.905	-47.762	-44.313	9.53500	2.49250	8.47747	8.0000	1.0486
105800	106339	412.014	-47.652	-44.252	9.51228	2.46982	8.40416	7.9176	1.0387
106000	106541	412.124	-47.542	-44.191	9.48956	2.44734	8.33104	7.8352	1.0288
106200	106743	412.233	-47.432	-44.130	9.46684	2.42505	8.25811	7.7528	1.0189
106400	106945	412.343	-47.322	-44.069	9.44412	2.40296	8.18537	7.6704	1.0091
106600	107147	412.452	-47.212	-44.008	9.42140	2.38106	8.11282	7.5880	0.9993
106800	107349	412.562	-47.102	-43.947	9.39868	2.35934	8.04047	7.5056	0.9895
107000	107551	412.671	-46.992	-43.886	9.37596	2.33781	7.96831	7.4232	0.9797
107200	107753	412.781	-46.882	-43.825	9.35324	2.31647	7.89634	7.3408	0.9699
107400	107955	412.890	-46.772	-43.764	9.33052	2.29531	7.82457	7.2584	0.9601
107600	108157	413.000	-46.662	-43.703	9.30780	2.27434	7.75290	7.1760	0.9503
107800	108359	413.109	-46.552	-43.642	9.28508	2.25356	7.68143	7.0936	0.9405
108000	108561	413.219	-46.442	-43.581	9.26236	2.23297	7.61016	7.0112	0.9307
108200	108763	413.328	-46.332	-43.520	9.23964	2.21257	7.53909	6.9288	0.9209
108400	108965	413.438	-46.222	-43.459	9.21692	2.19236	7.46831	6.8464	0.9111
108600	109167	413.547	-46.112	-43.398	9.19420	2.17234	7.39772	6.7640	0.9013
108800	109369	413.657	-46.002	-43.337	9.17148	2.15252	7.32734	6.6816	0.8915
109000	109571	413.766	-45.892	-43.276	9.14876	2.13289	7.25716	6.5992	0.8817
109200	109773	413.876	-45.782	-43.215	9.12604	2.11346	7.18718	6.5168	0.8719
109400	109975	413.985	-45.672	-43.154	9.10332	2.09422	7.11739	6.4344	0.8621
109600	110177	414.095	-45.562	-43.093	9.08060	2.07517	7.04770	6.3520	0.8523

APPENDIX C-1
PITOT-STATIC POSITION ERROR RELATIONS

APPENDIX C-1

PITOT-STATIC POSITION ERROR RELATIONS

<u>PAGE NUMBER</u>	<u>TITLE</u>
C-1-1 - C-1-4	$\Delta V_{PC}, \Delta H_{PC} \text{ vs } \Delta P_P$
C-1-5 - C-1-8	$-\Delta V_{PC}, -\Delta H_{PC} \text{ vs } -\Delta P_P$
C-1-9 - C-1-12	$\Delta M_{PC}, \Delta H_{PC} \text{ vs } \Delta P_P/P_S$
C-1-13 - C-1-16	$-\Delta M_{PC}, -\Delta H_{PC} \text{ vs } -\Delta P_P/P_S$
C-1-17 - C-1-19	$\Delta V_{PC} \text{ vs } \Delta V_{IC} \text{ at } \Delta P_P/Q_{CIC} = \text{Const}$
C-1-20	$\Delta M_{PC} \text{ vs } \Delta P_P/Q_{CIC}$
C-1-21	$-\Delta M_{PC} \text{ vs } -\Delta P_P/Q_{CIC}$

APRIL 1967

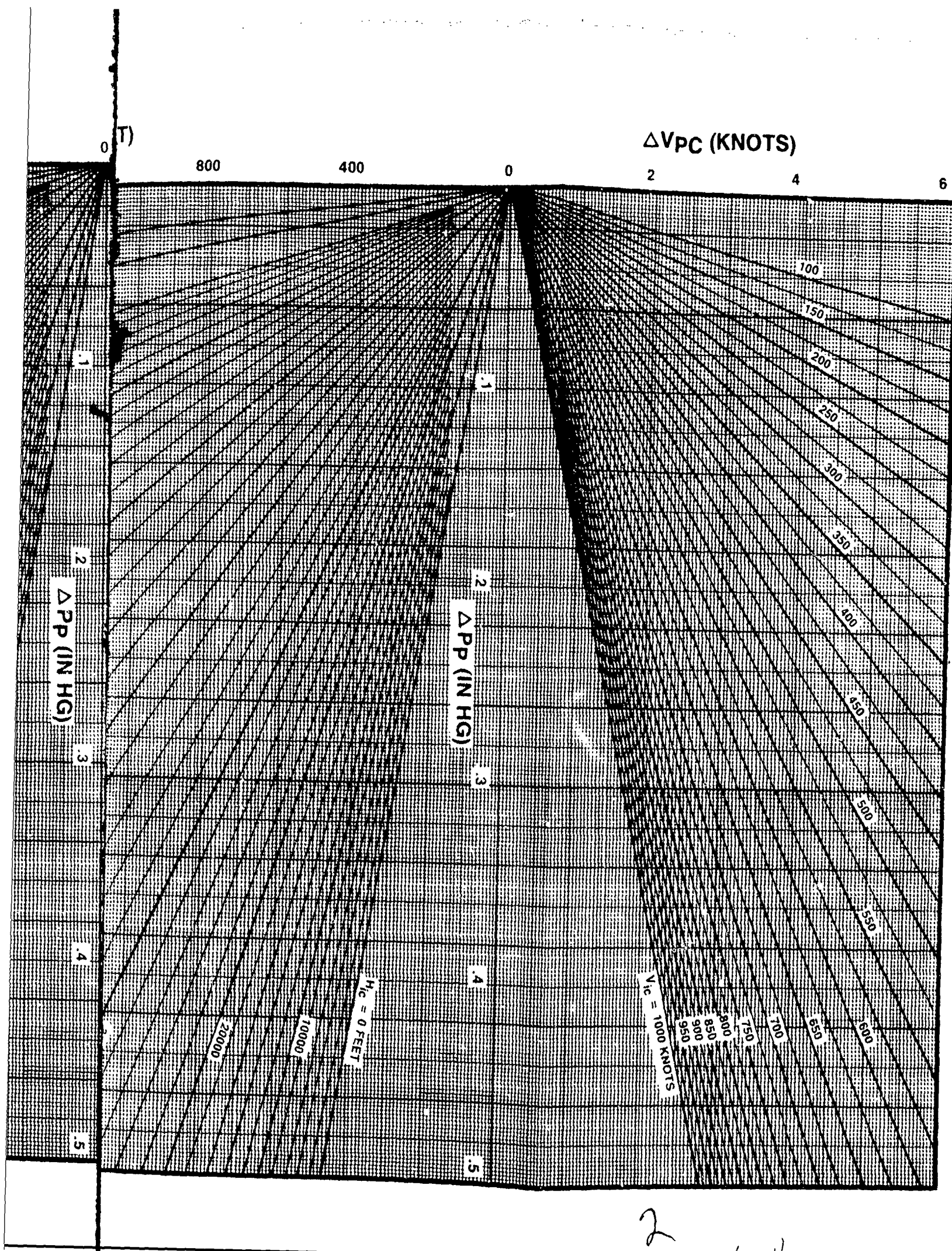
ΔH_{PC} (FEET)

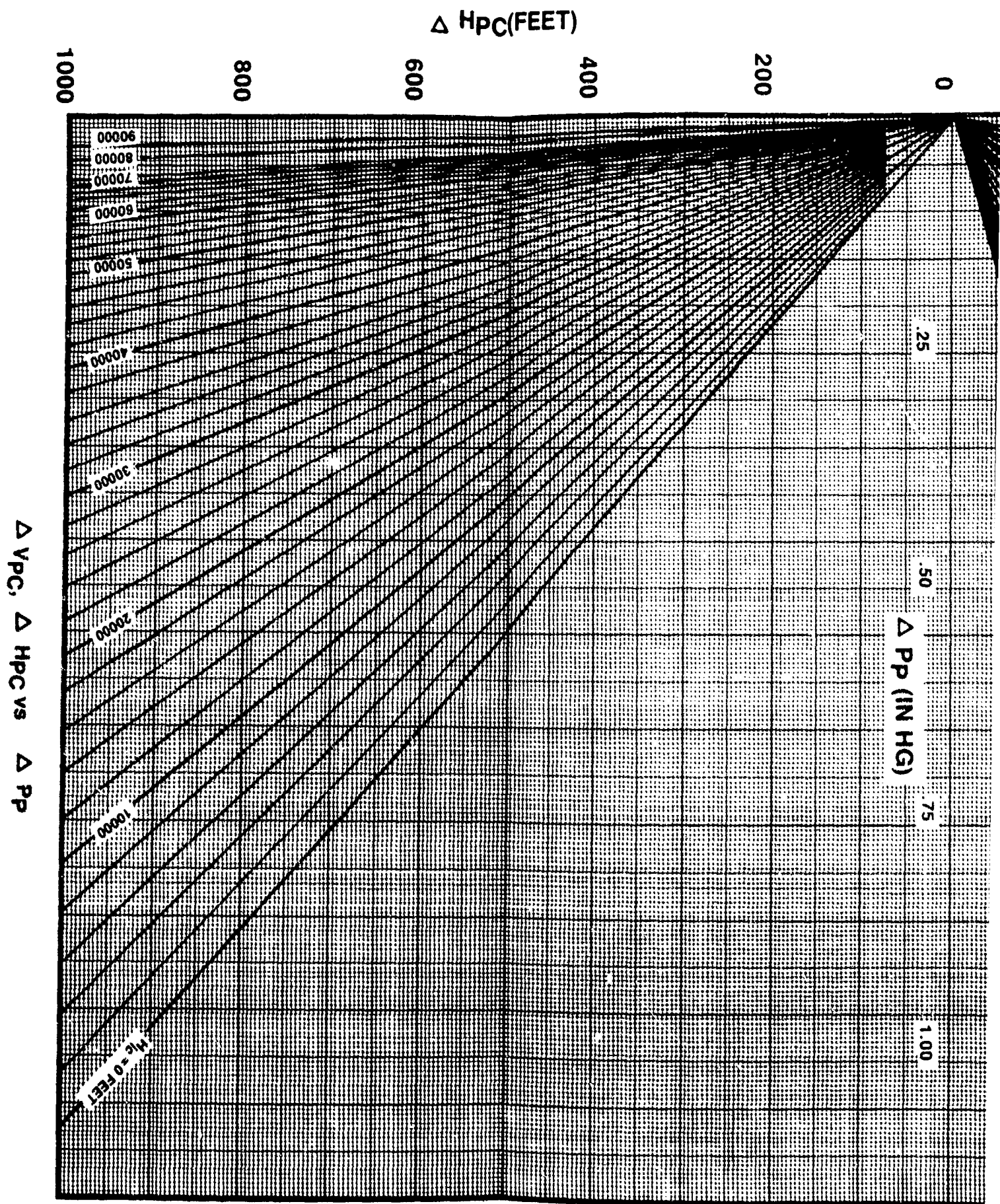
2400 2000 1600 1200 800 400

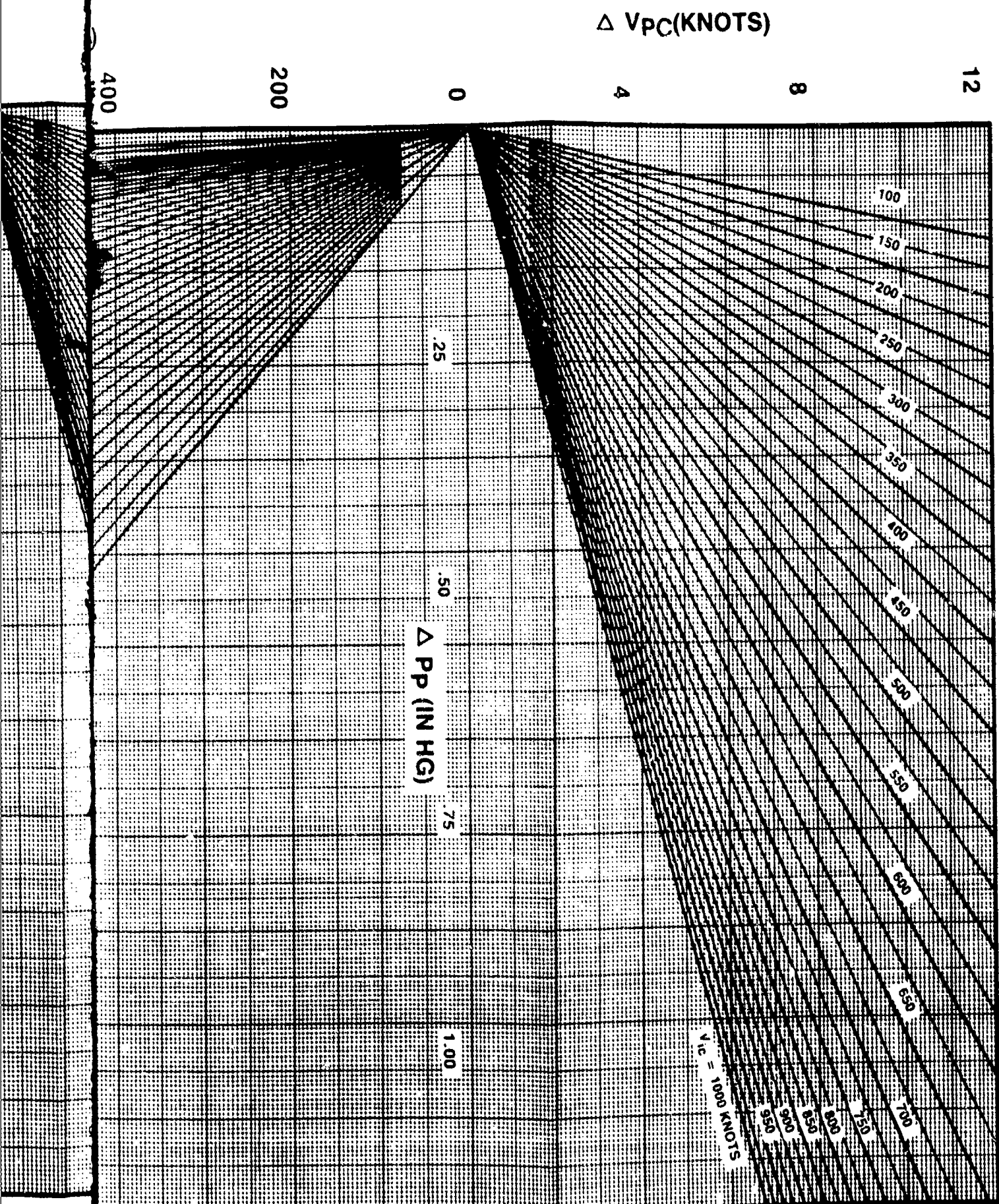
ΔV_{PC} , ΔH_{PC} VS ΔP_p

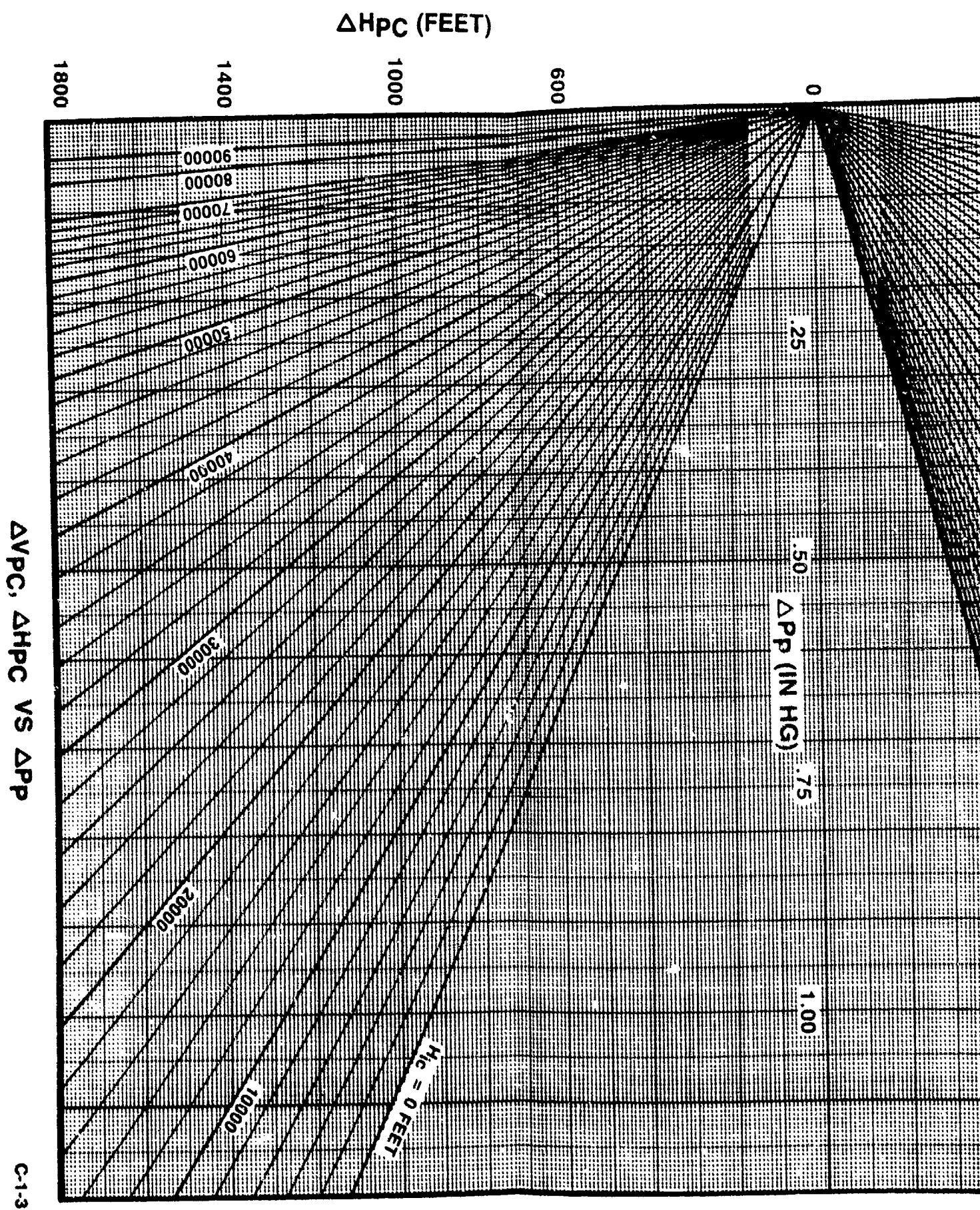


C-1-1

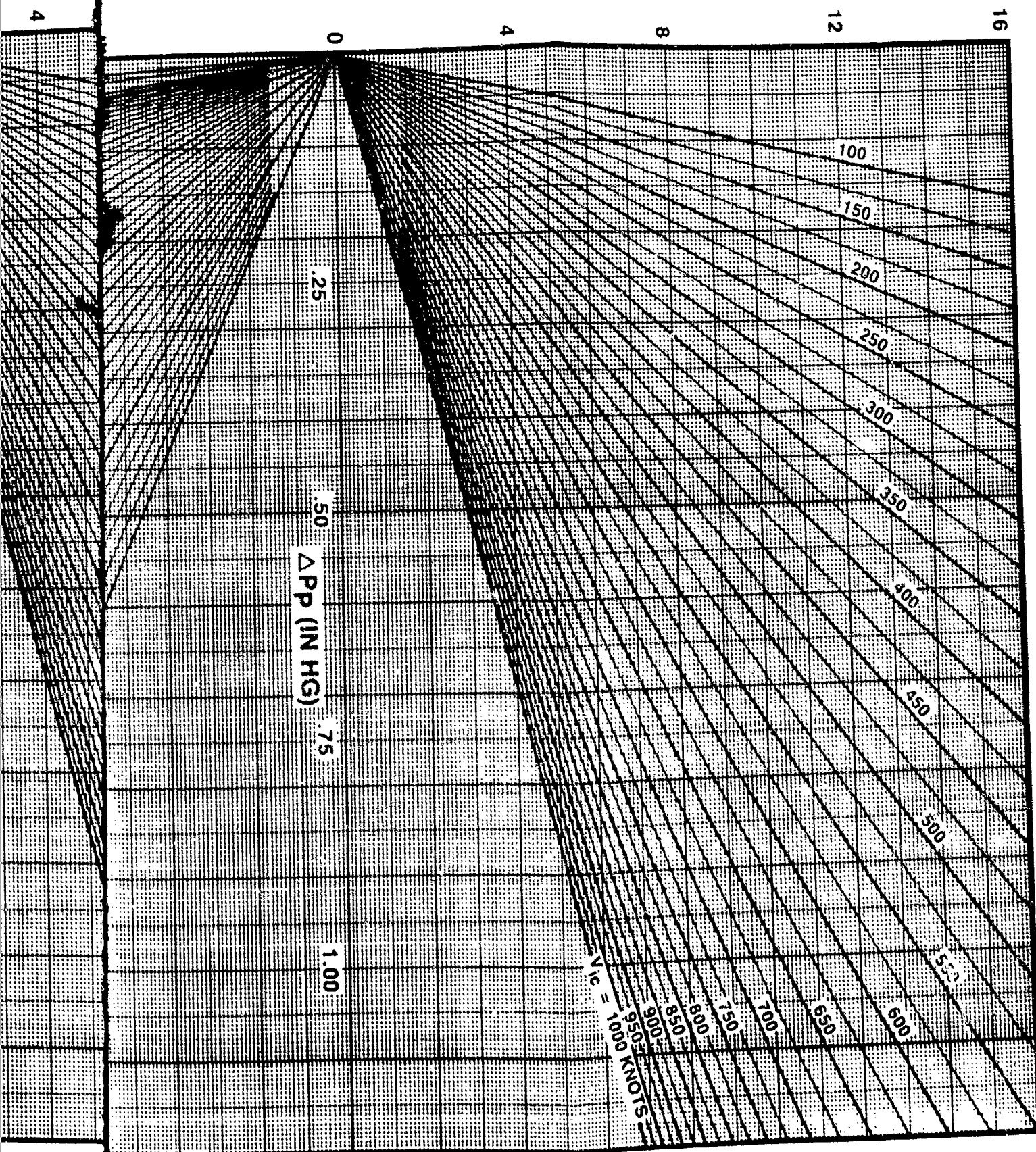


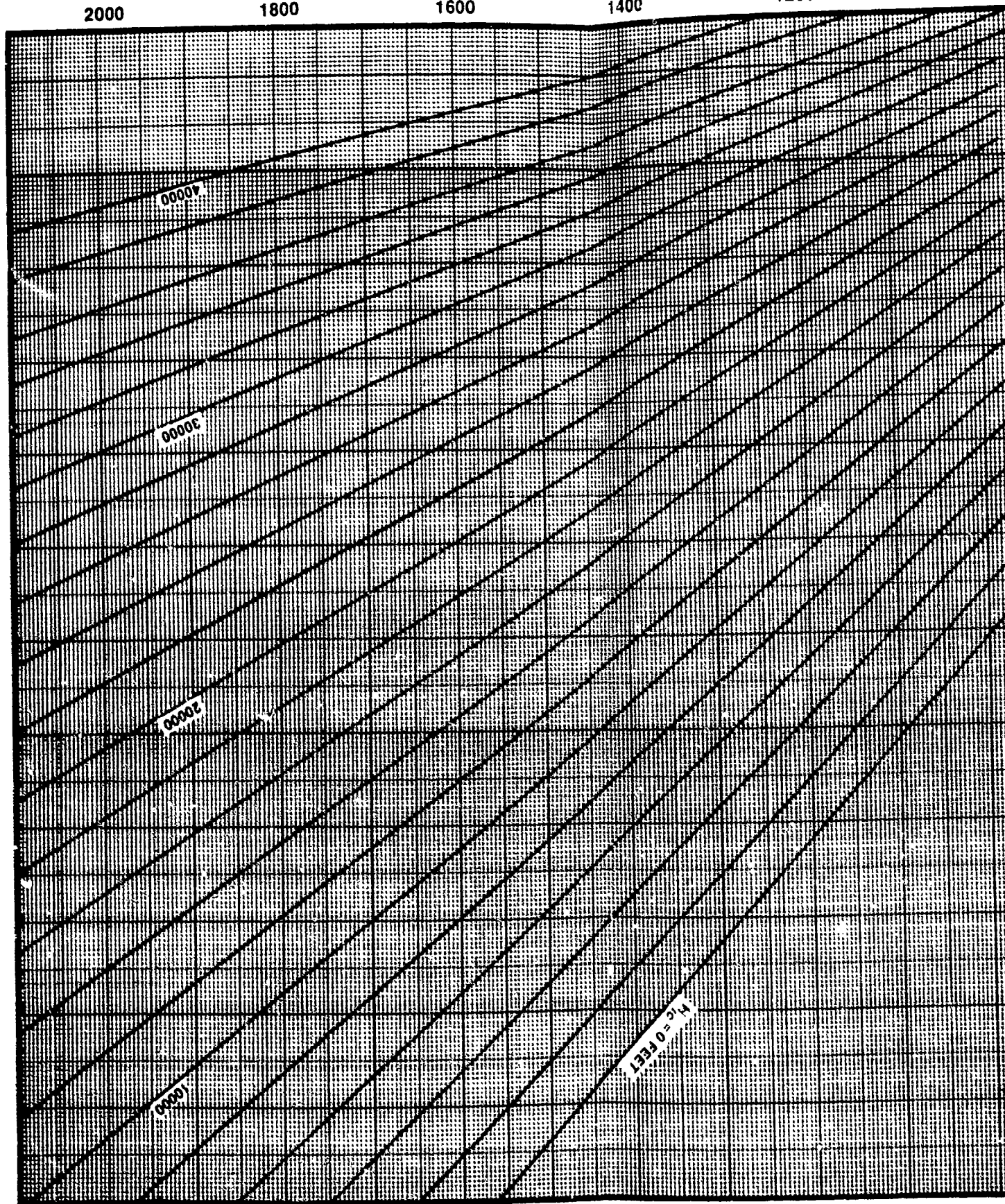






ΔV_{PC} (KNOTS)





ΔV_{PC} (KNOTS)

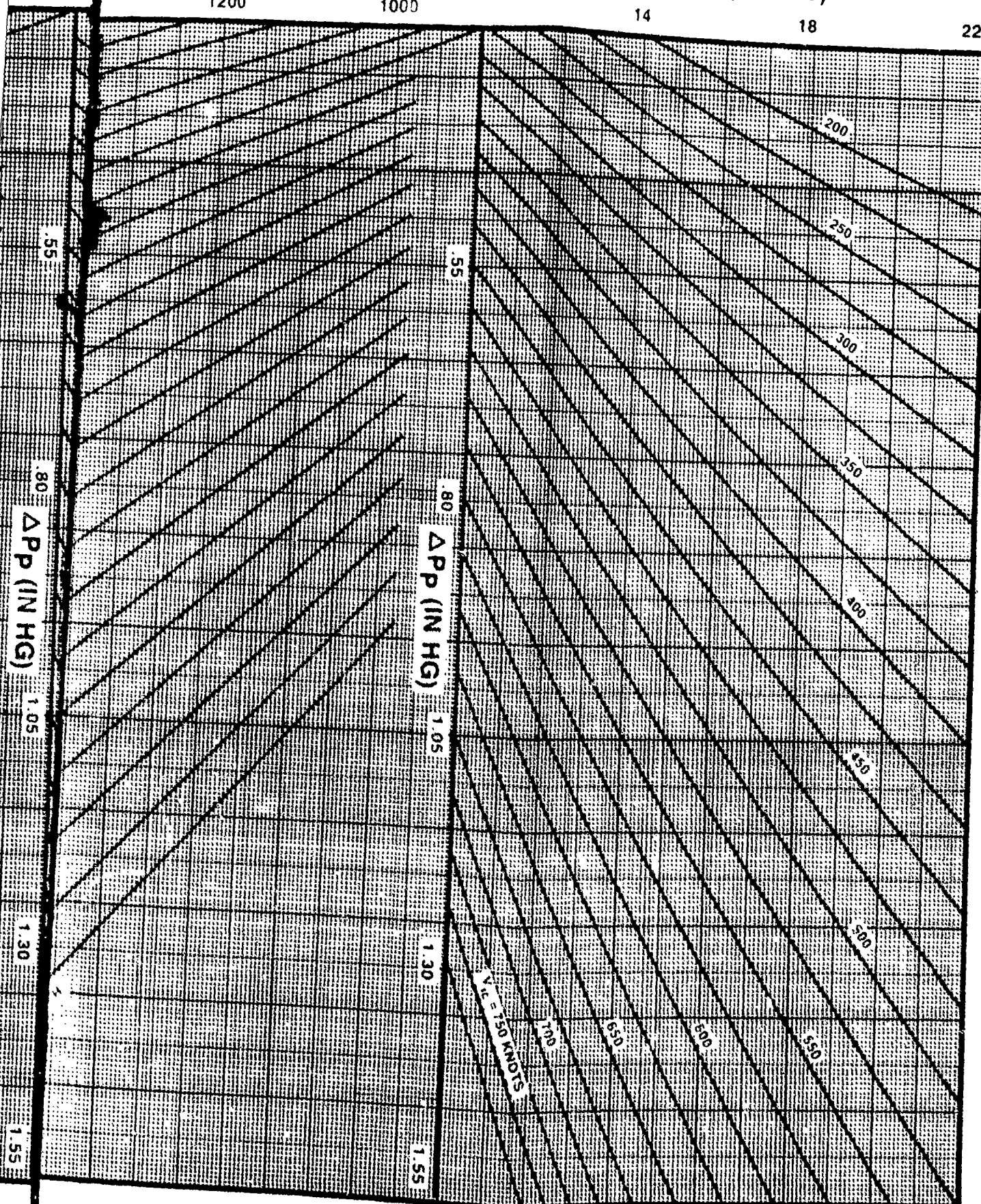
1200

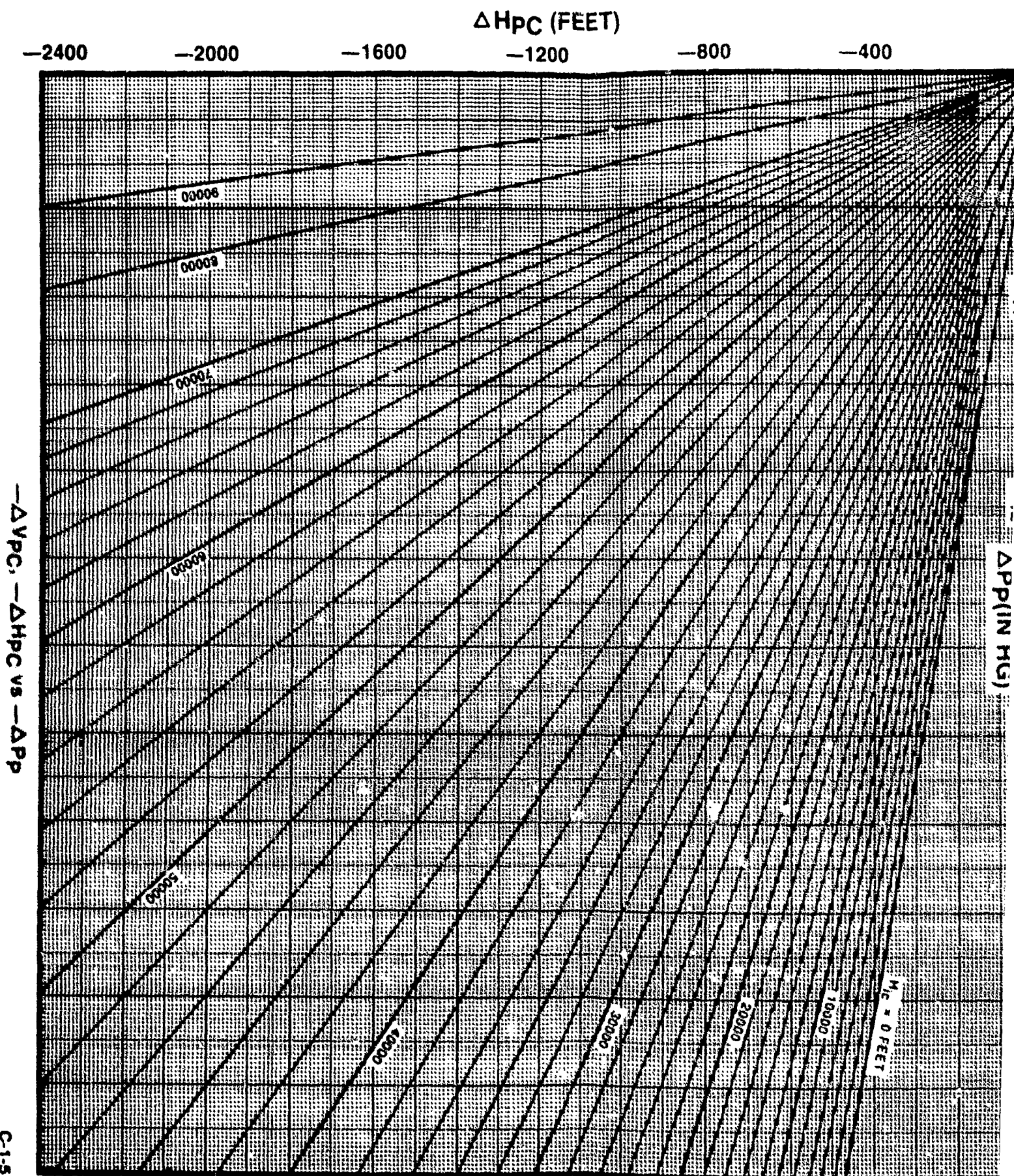
1000

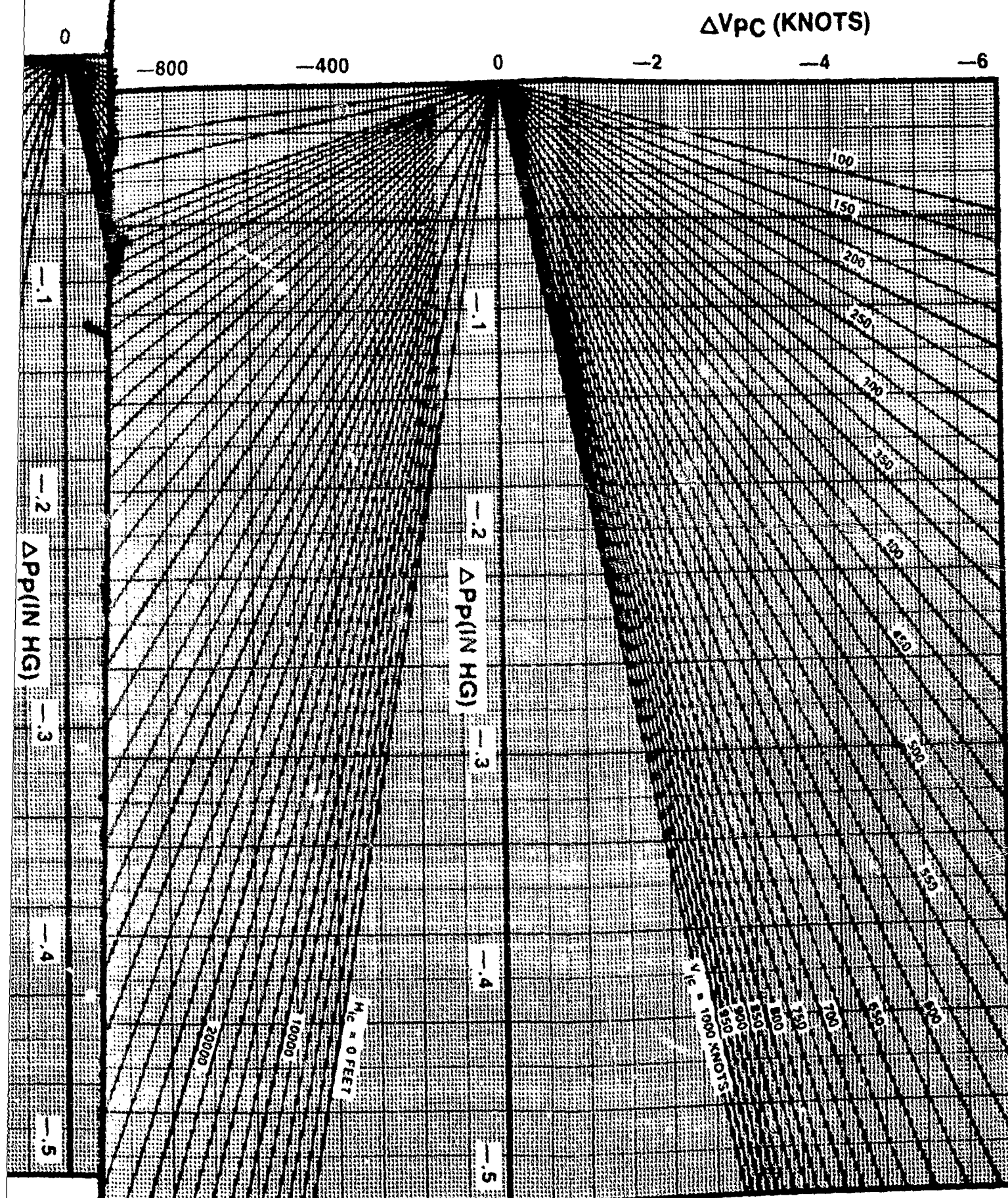
14

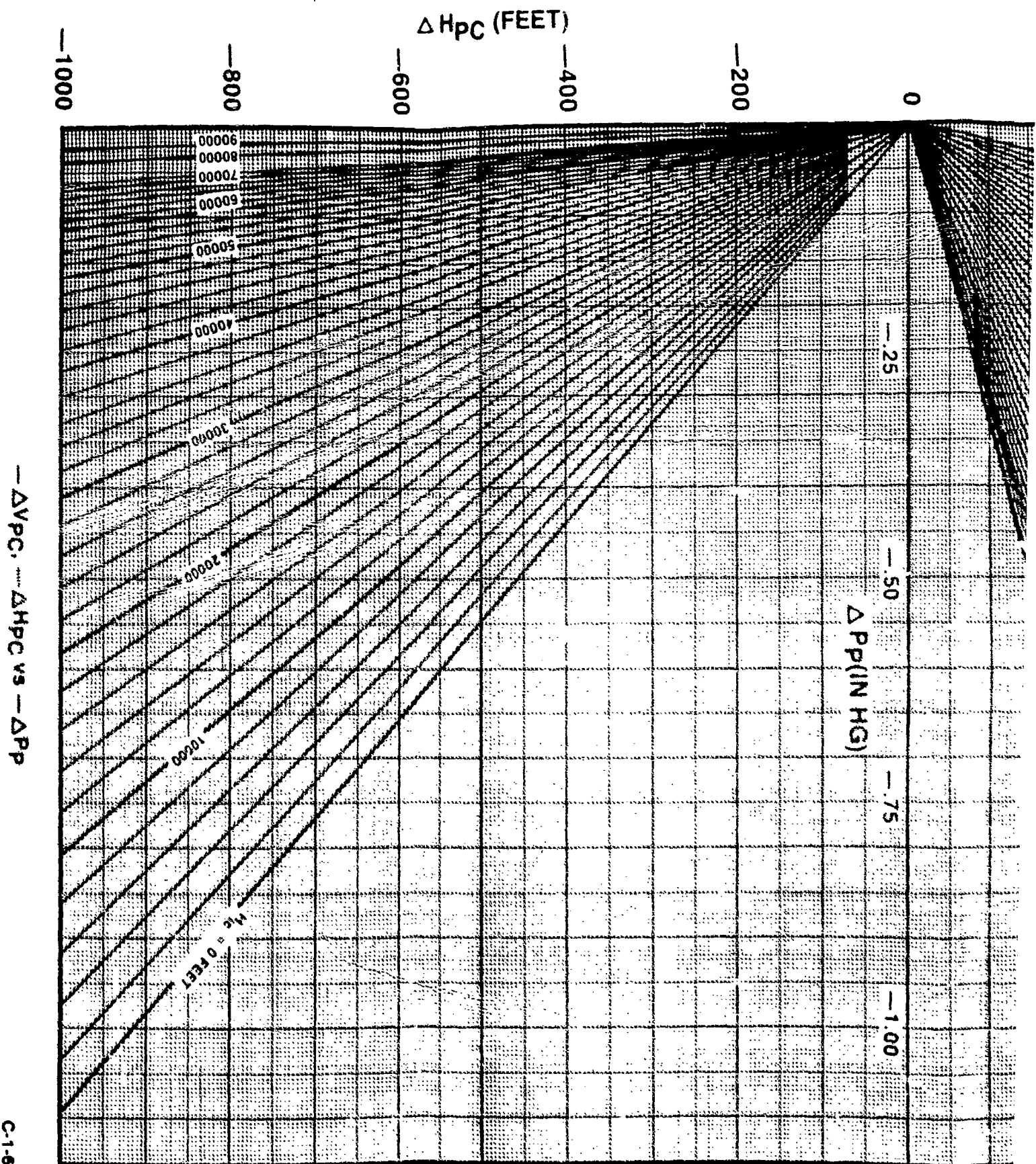
18

22









C (FEET)

—400

—200

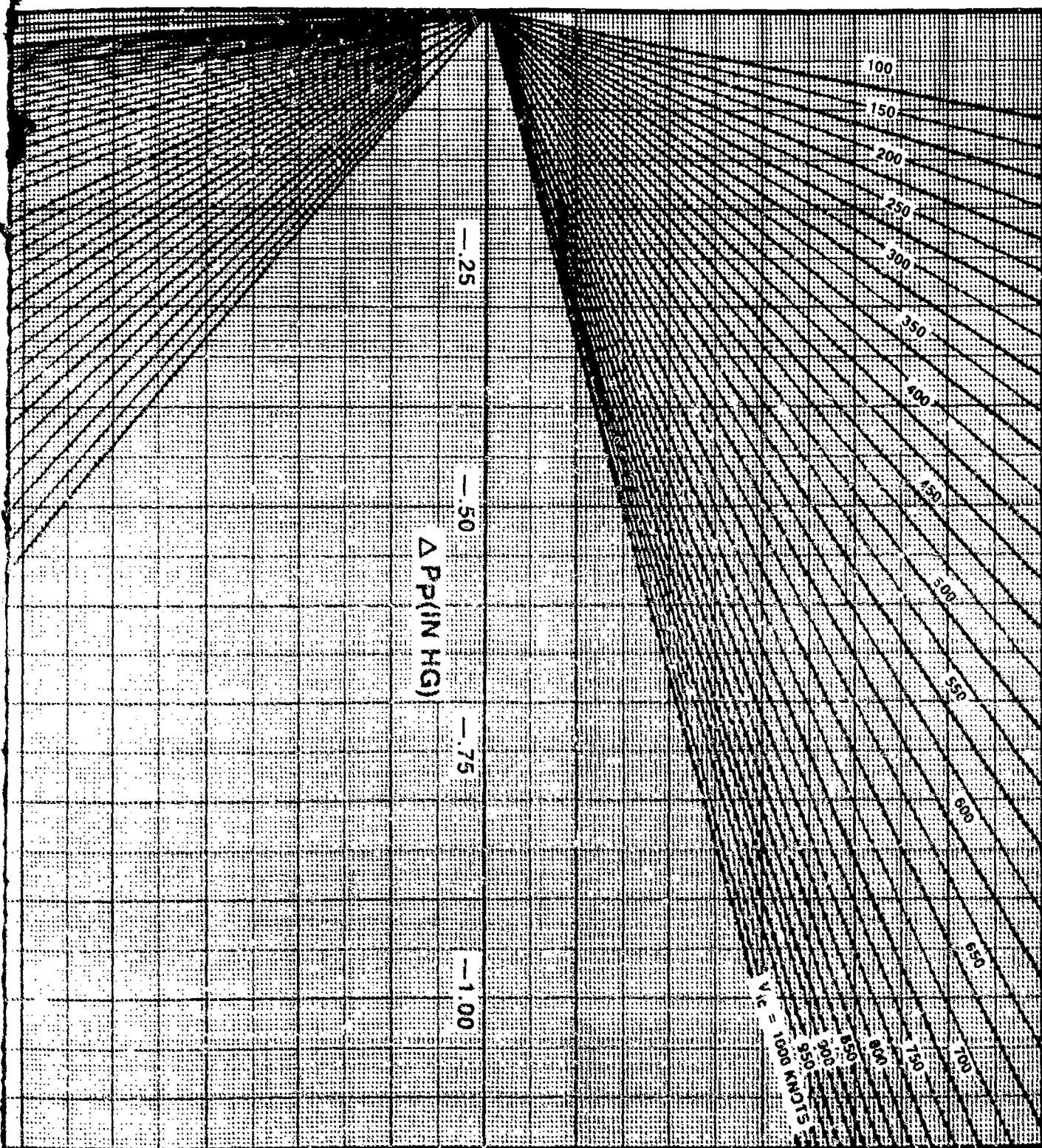
0

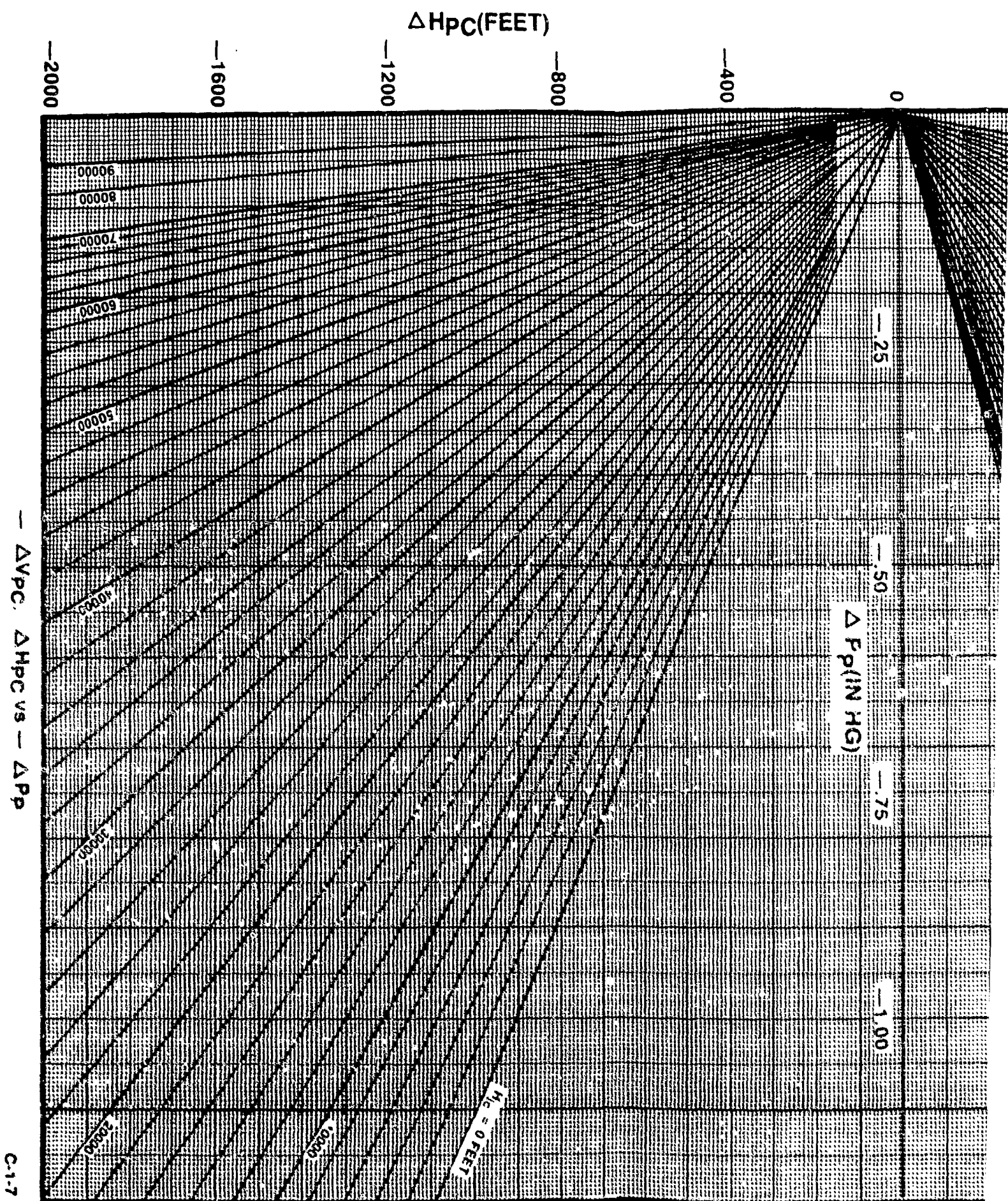
ΔV_{PC} (KNOTS)

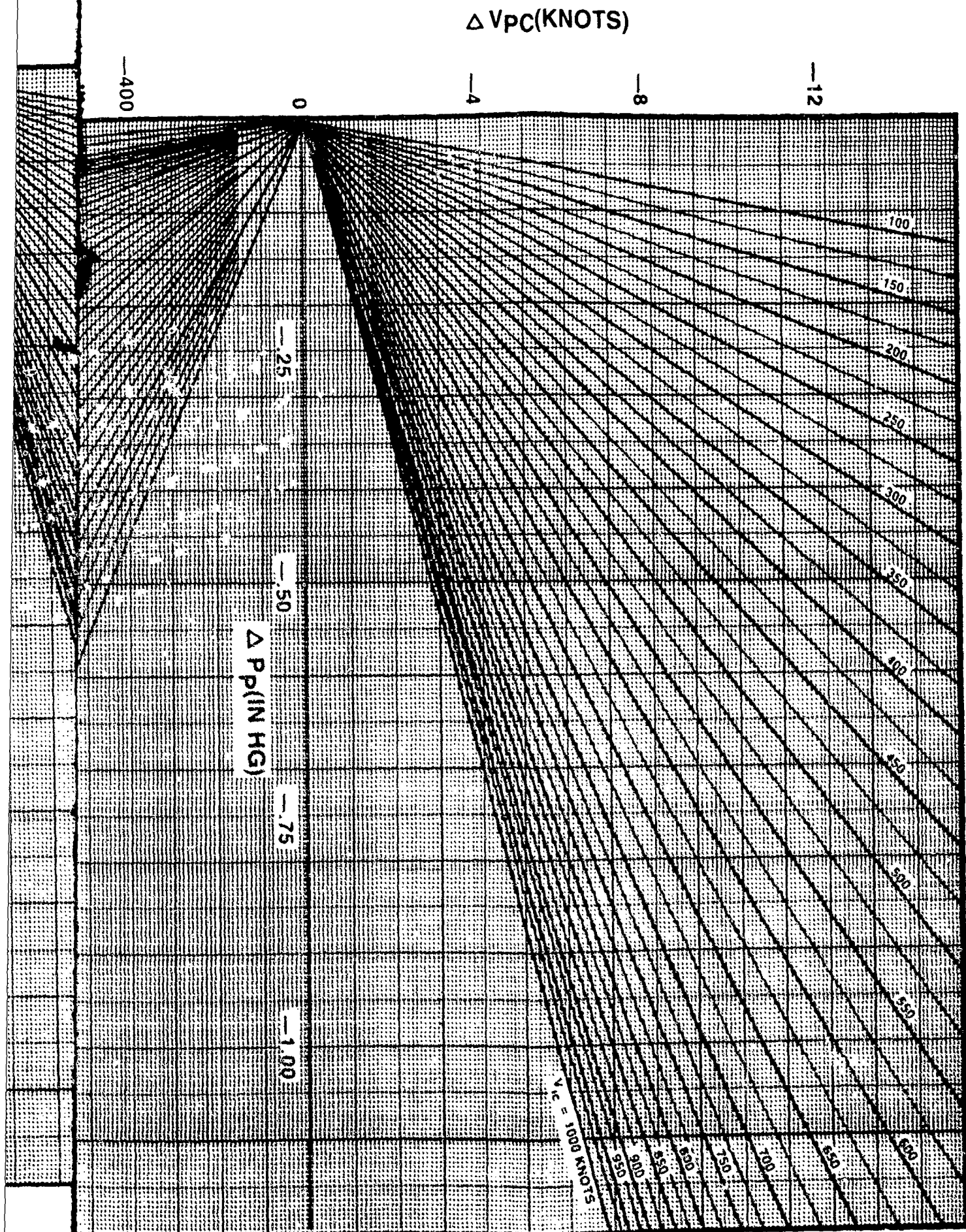
—4

—8

—12





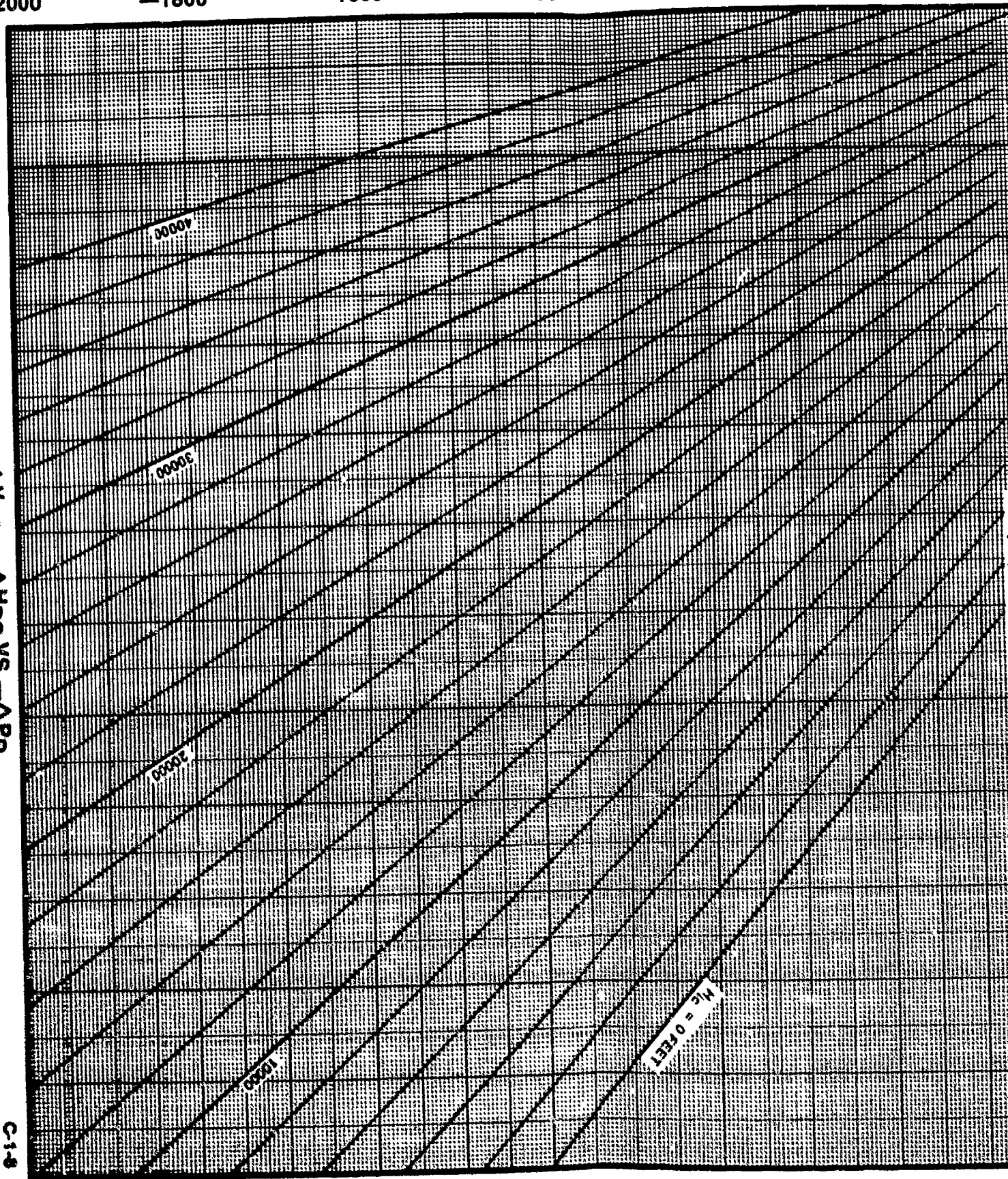


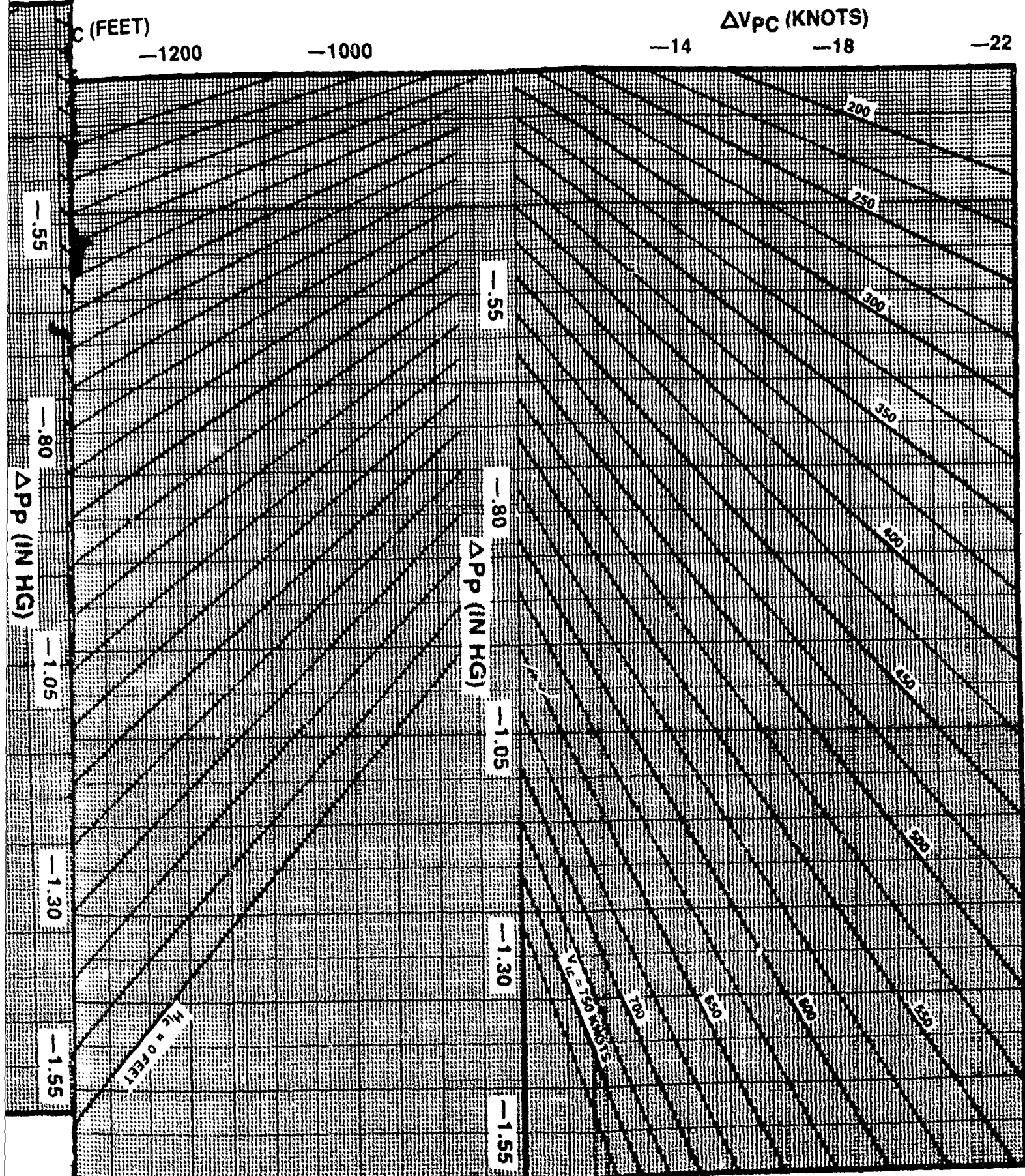
ΔH_{PC} (FEET)

—2000 —1800 —1600 —1400 —1200 —1000

— ΔV_{PC} , — ΔH_{PC} VS — ΔP_P

C-1-8





Δ Mpc (MACH)

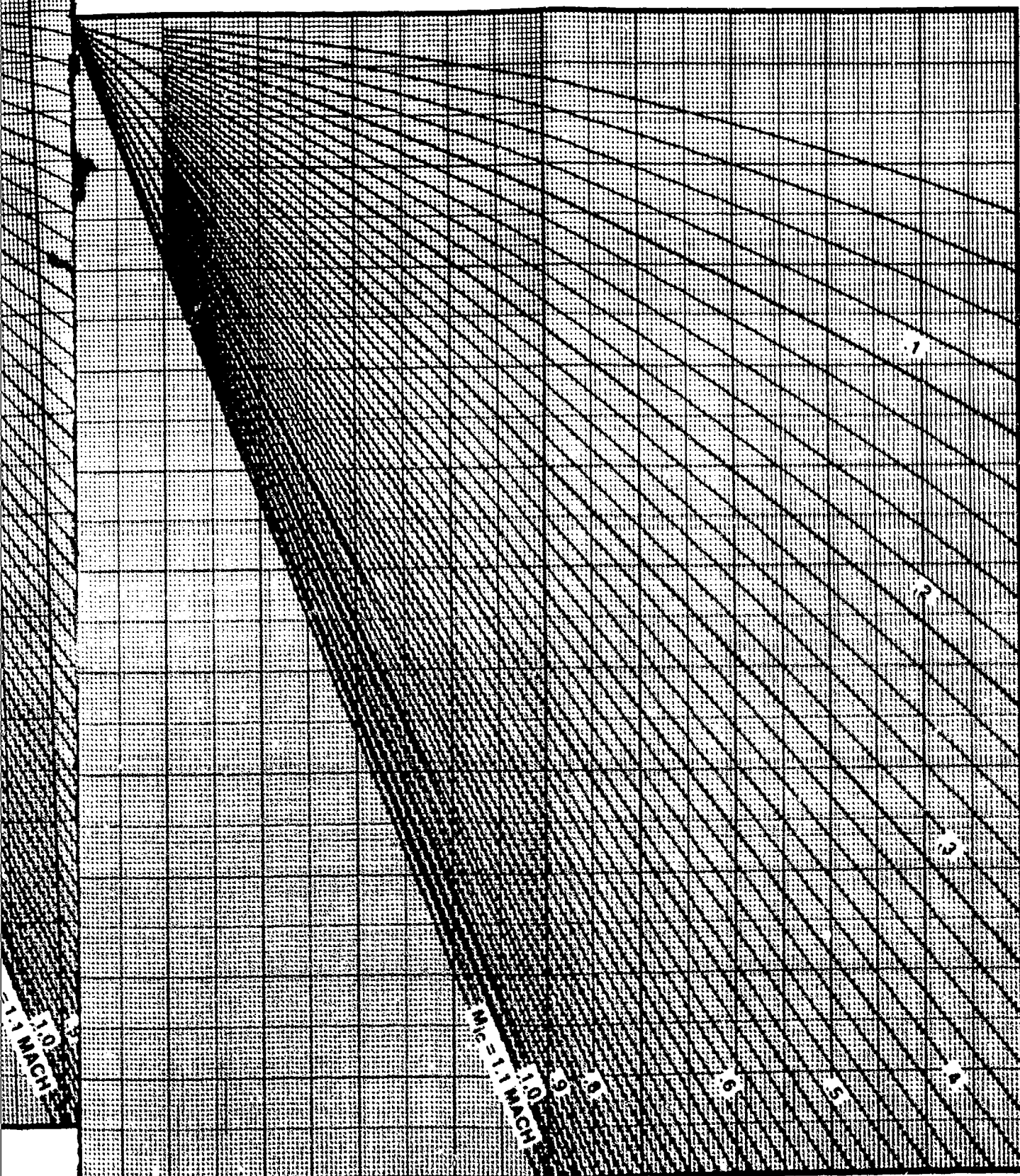
.02

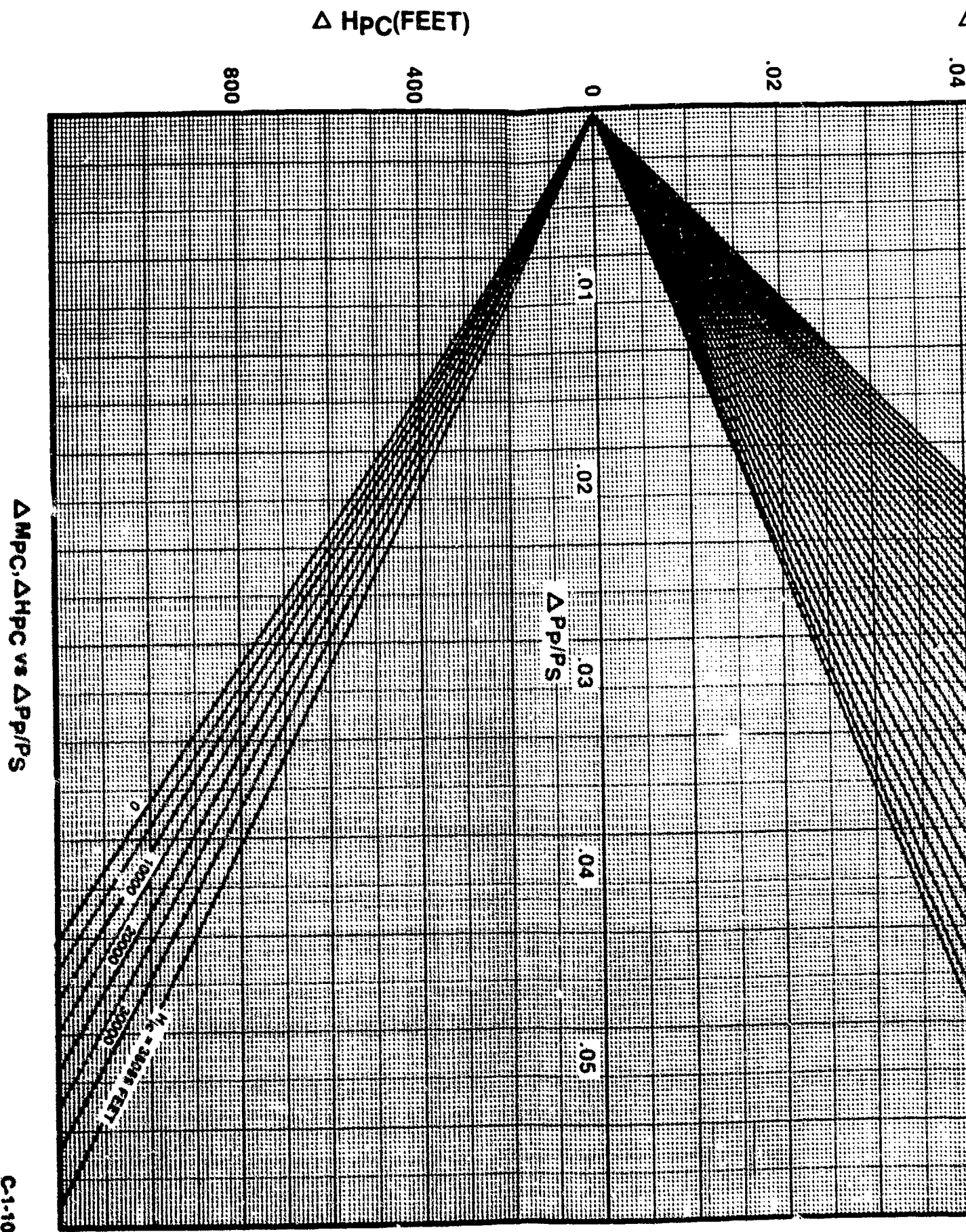
.04

90.

80.

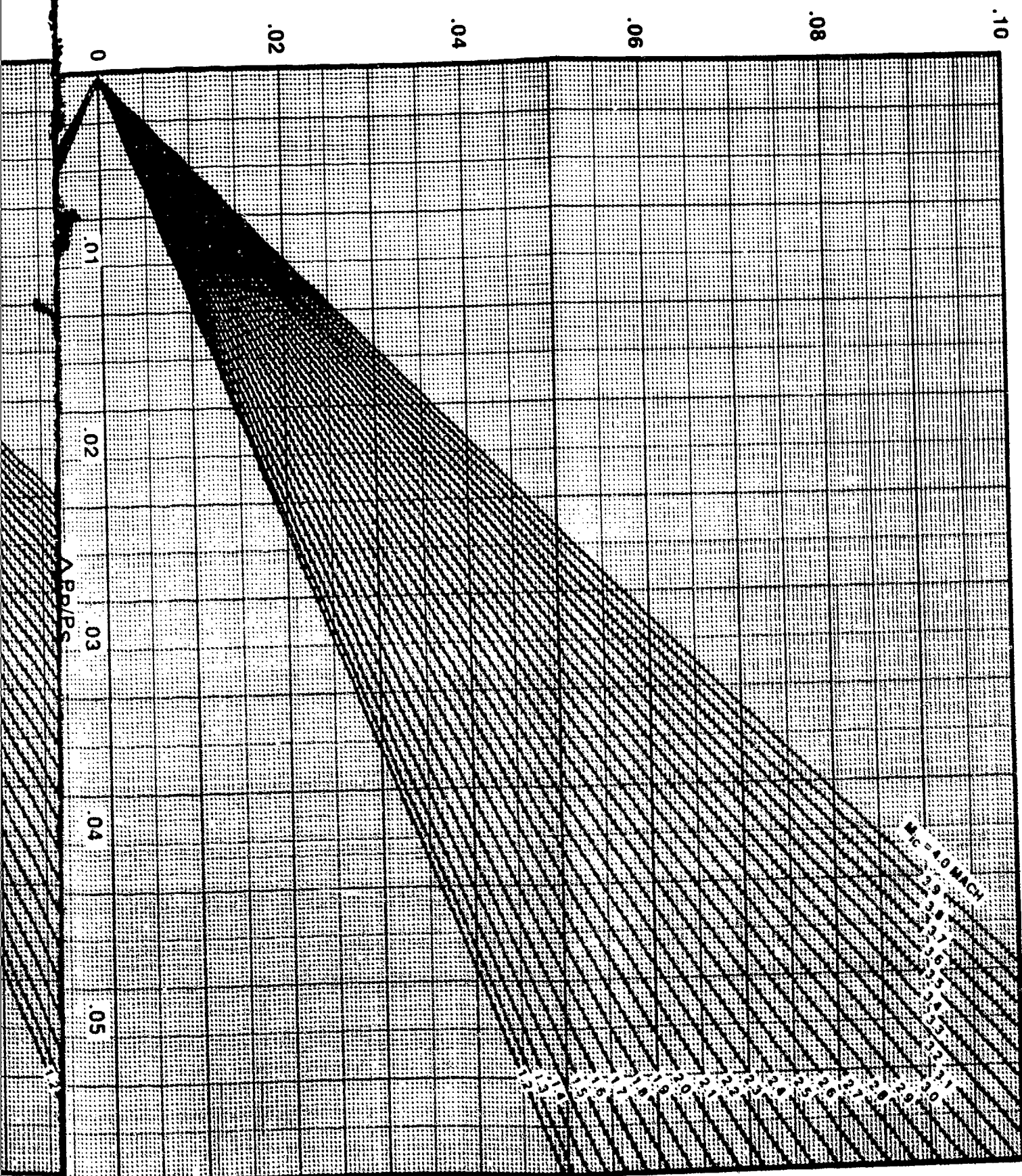
10.



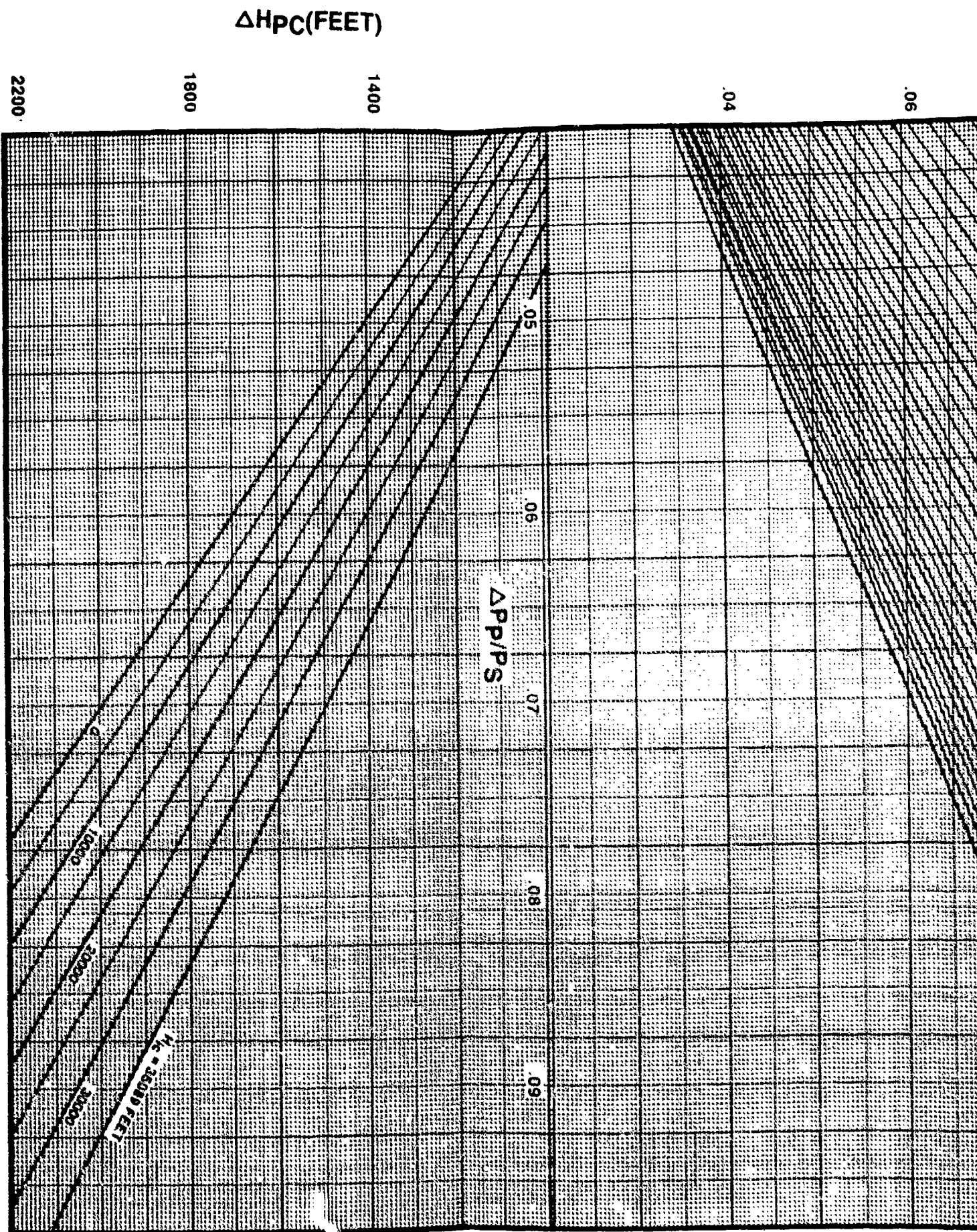


ΔM_P

$\Delta M_{PC} \text{ (MACH)}$



$\Delta M_{PC}, \Delta H_{PC}$ vs $\Delta P/P_S$



$\Delta M_{PC}(\text{MACH})$

.04

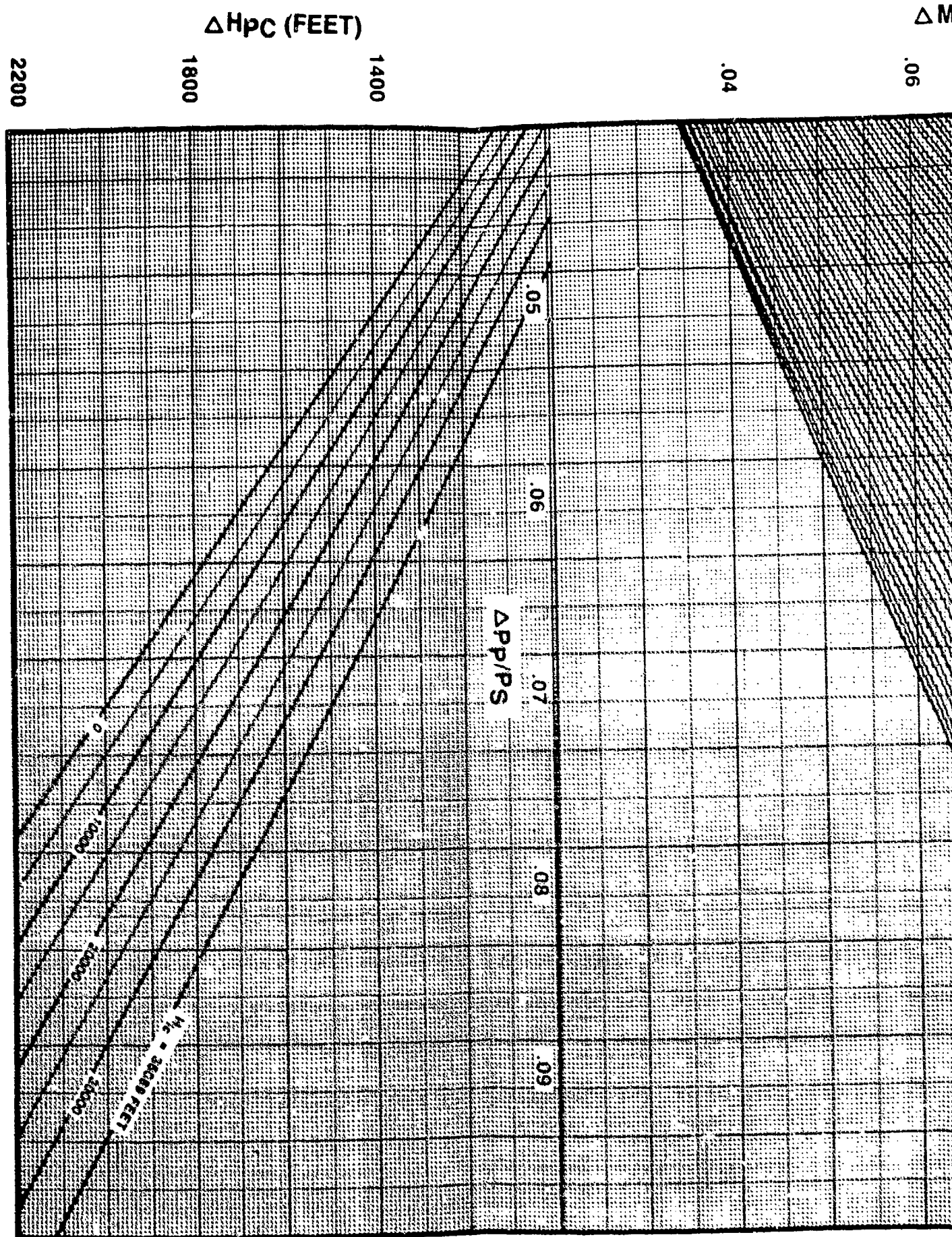
.06

.08

.10

.12

$M_{PC}(\text{MACH})$



— ΔM_{PC} , — ΔH_{PC} vs — $\Delta P/P_S$

ΔM_{PC} (MACH)

.06

.08

.10

.12

$M_{\infty} = 4.0$ MACH

1.88

1.65

1.41

1.28

1.05

1.00

1.28

1.26

1.24

1.22

1.20

1.18

1.16

1.14

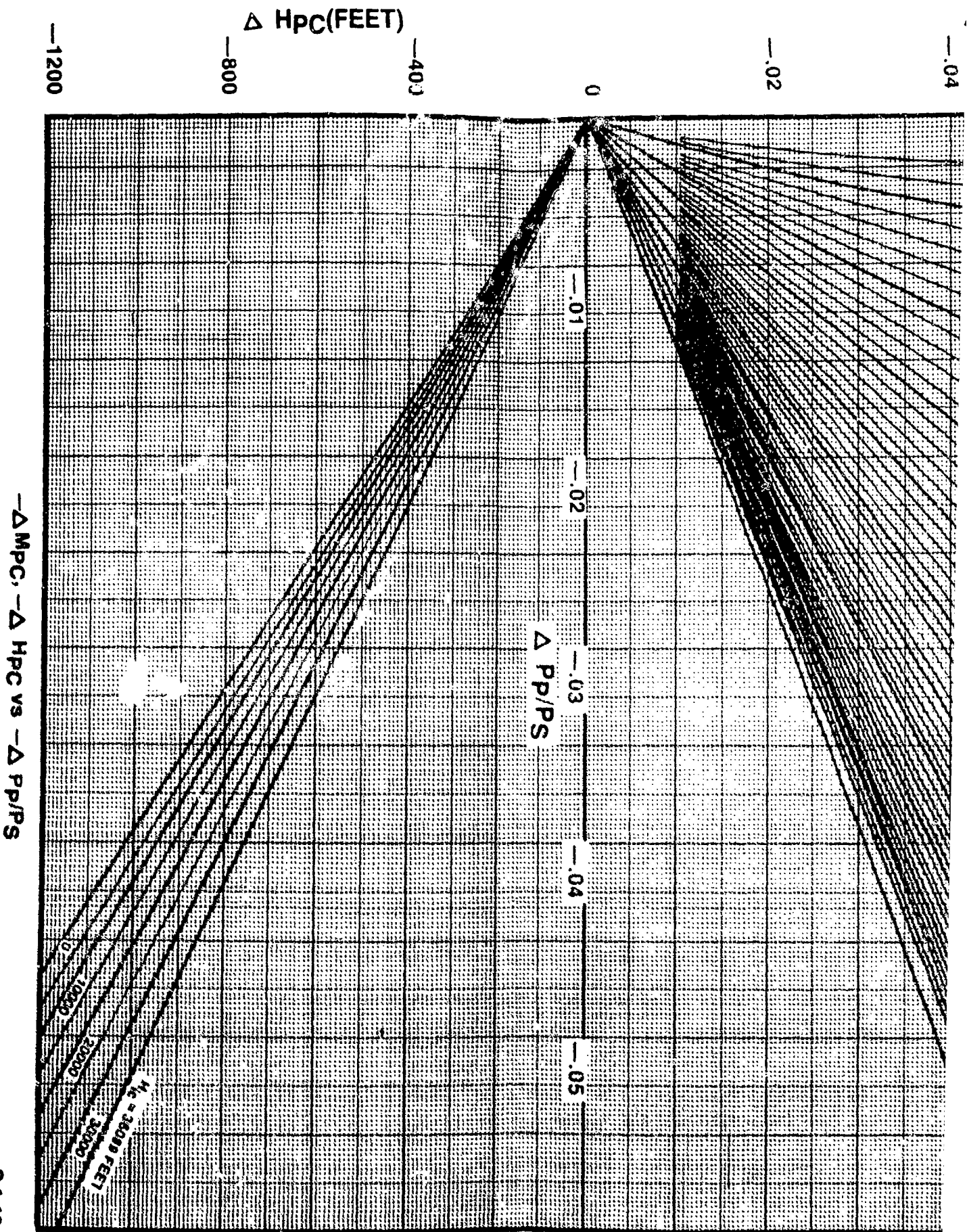
1.12

1.10

1.08

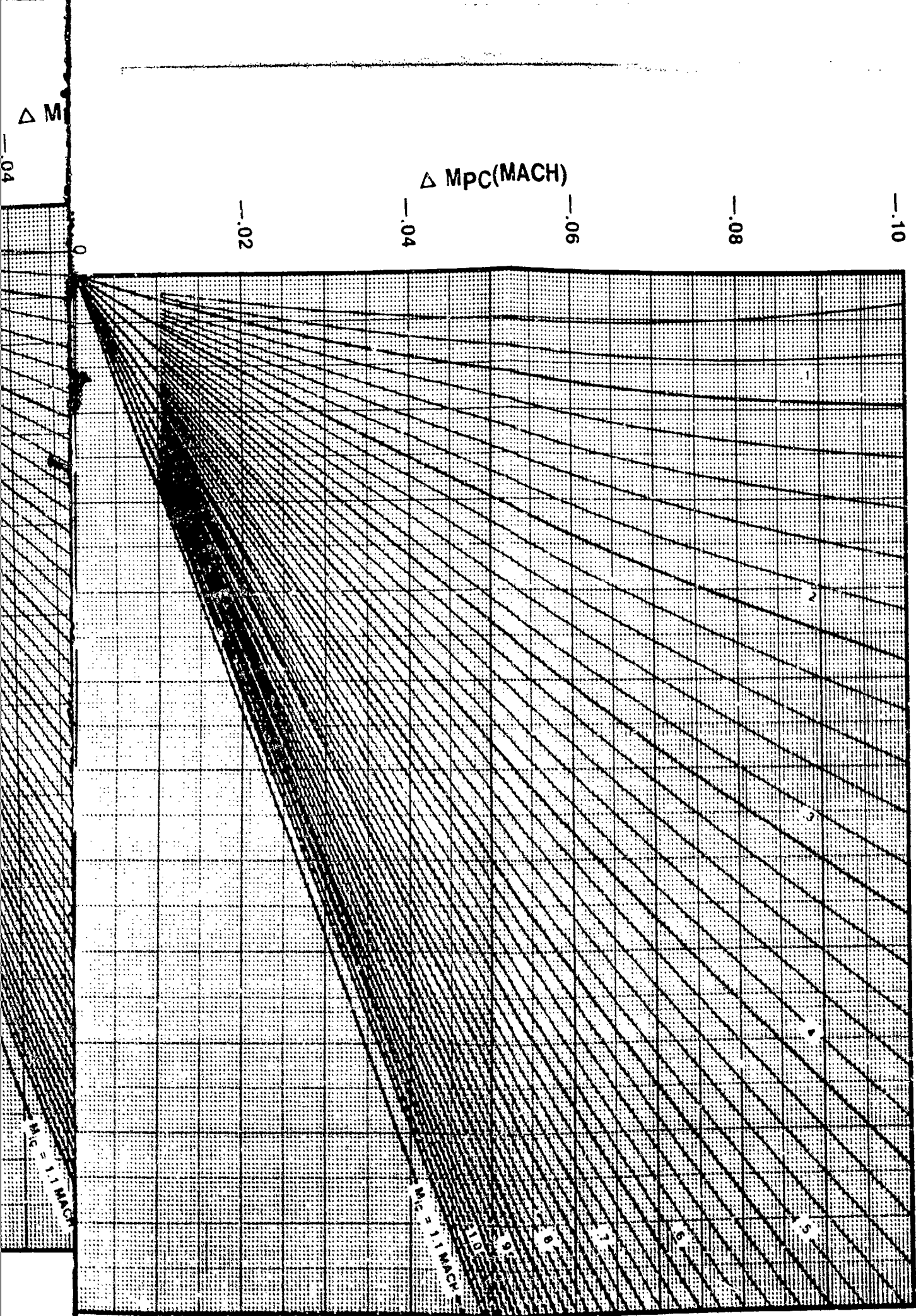
1.06

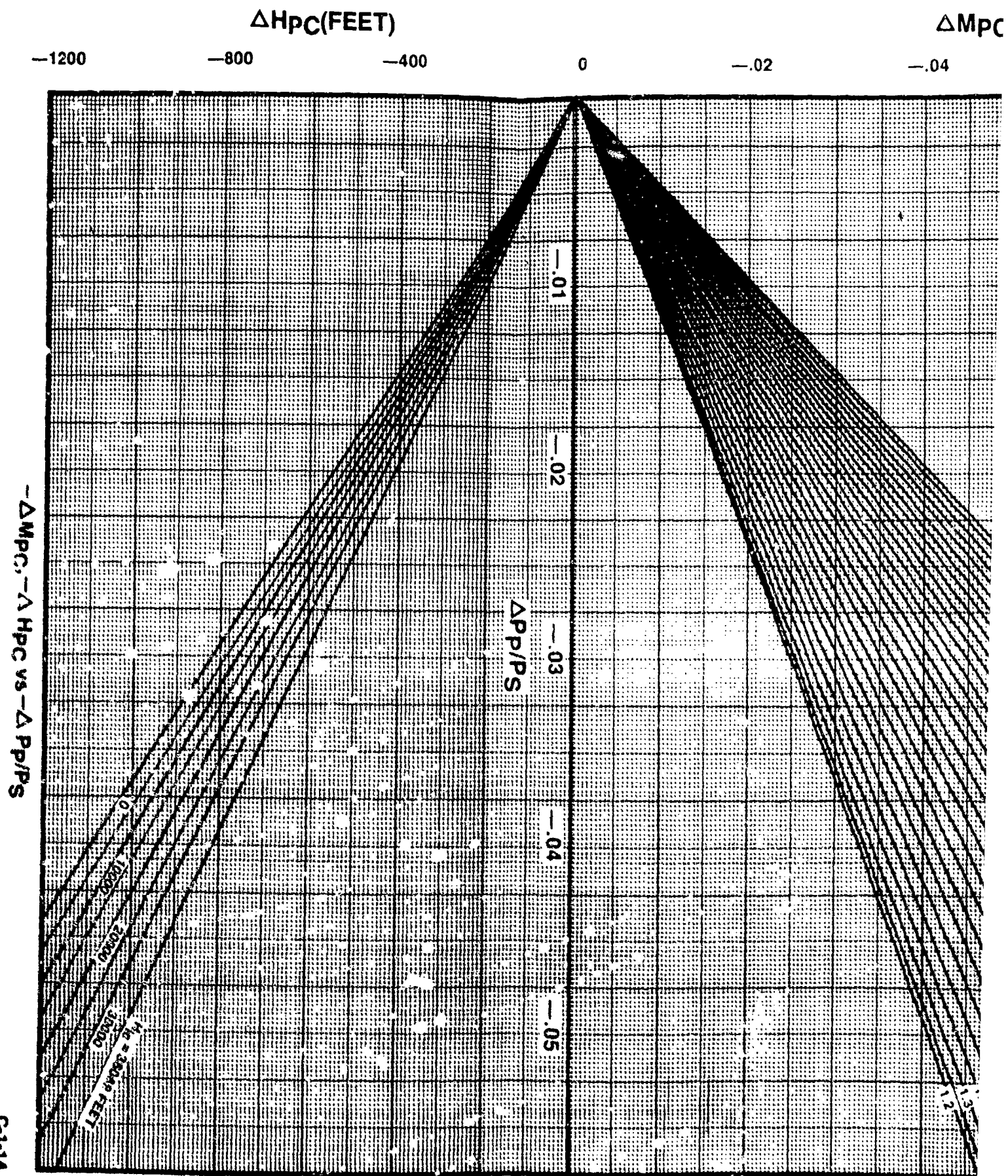
2



— ΔM_{PC} , — ΔH_{PC} vs — $\Delta PP/PS$

C-1-13





C-1-14

C(MA

$\Delta M_{PC}(\text{MACH})$

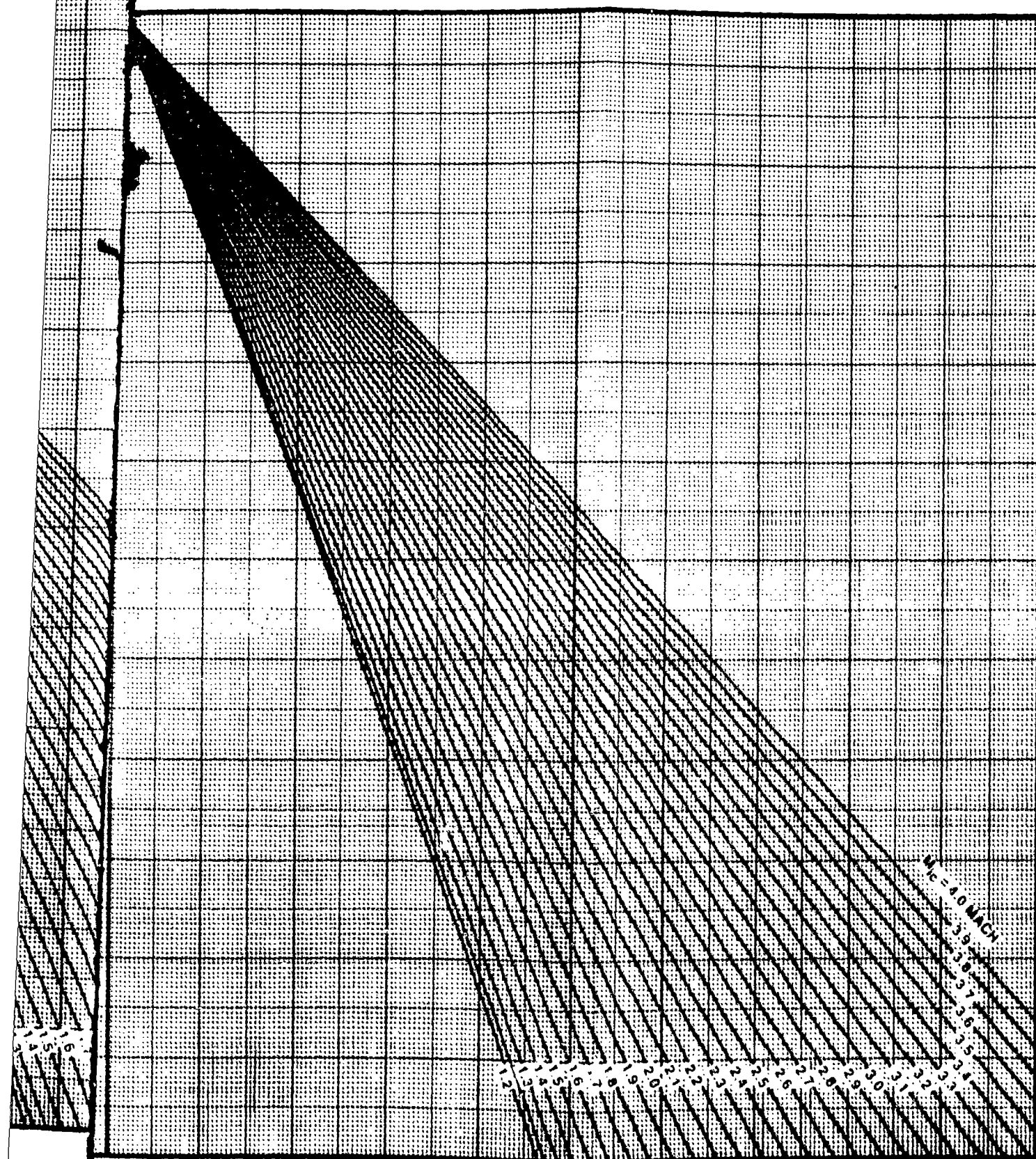
-.02

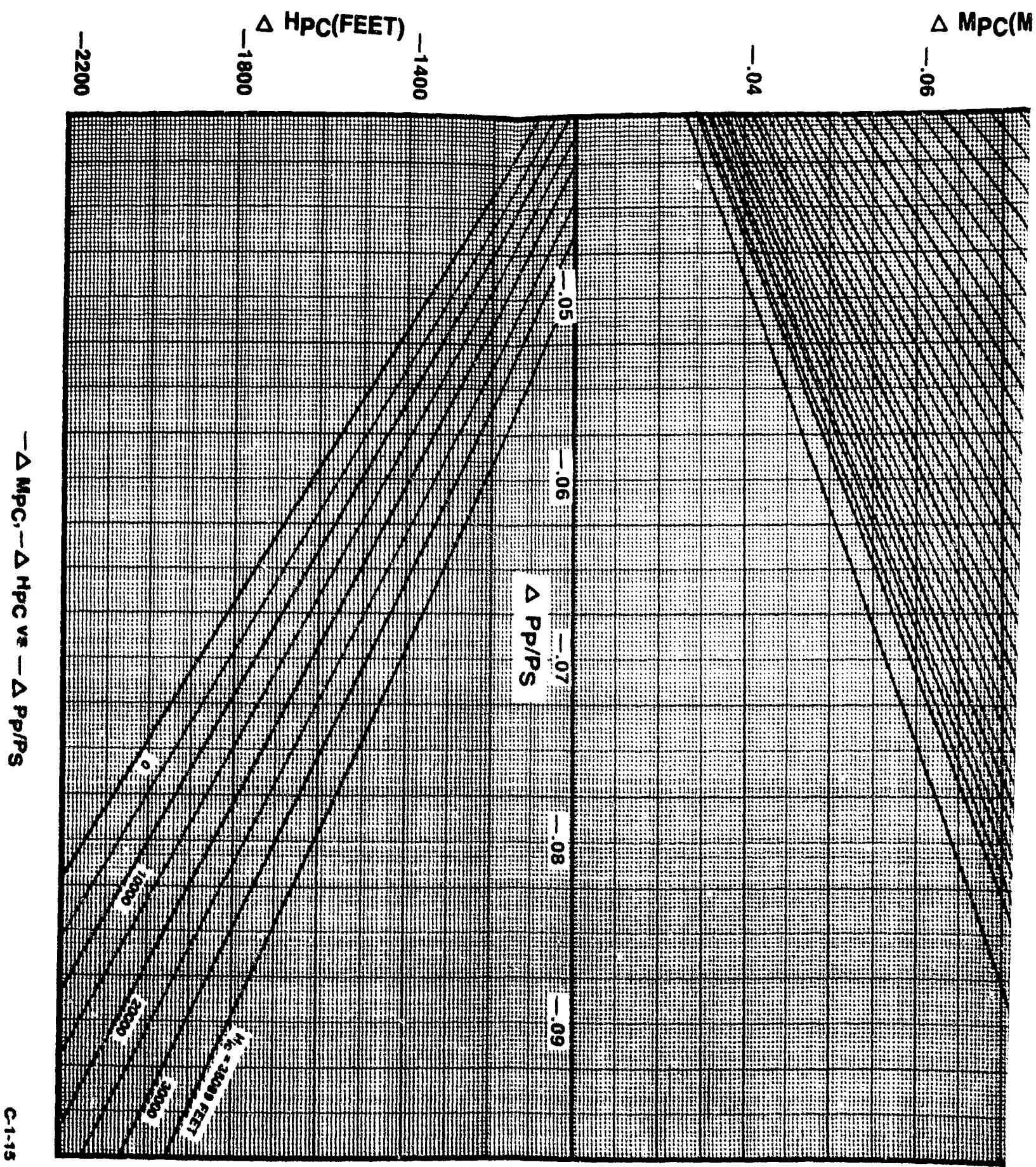
-.04

-.06

-.08

-.10





— ΔMPC , — ΔHPC vs — $\Delta PPI/PS$

(MACH

$\Delta M_{PC}(MACH)$

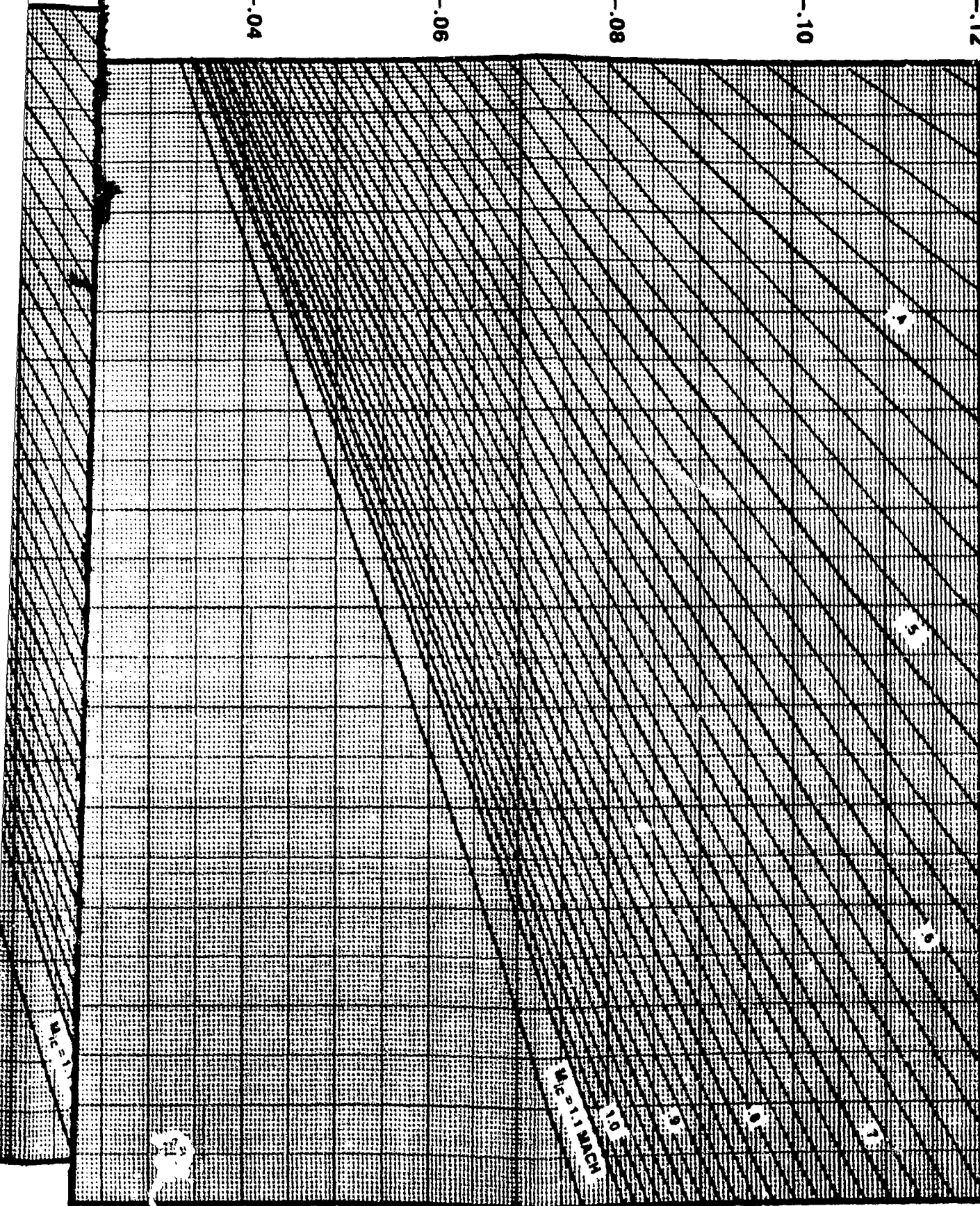
-.04

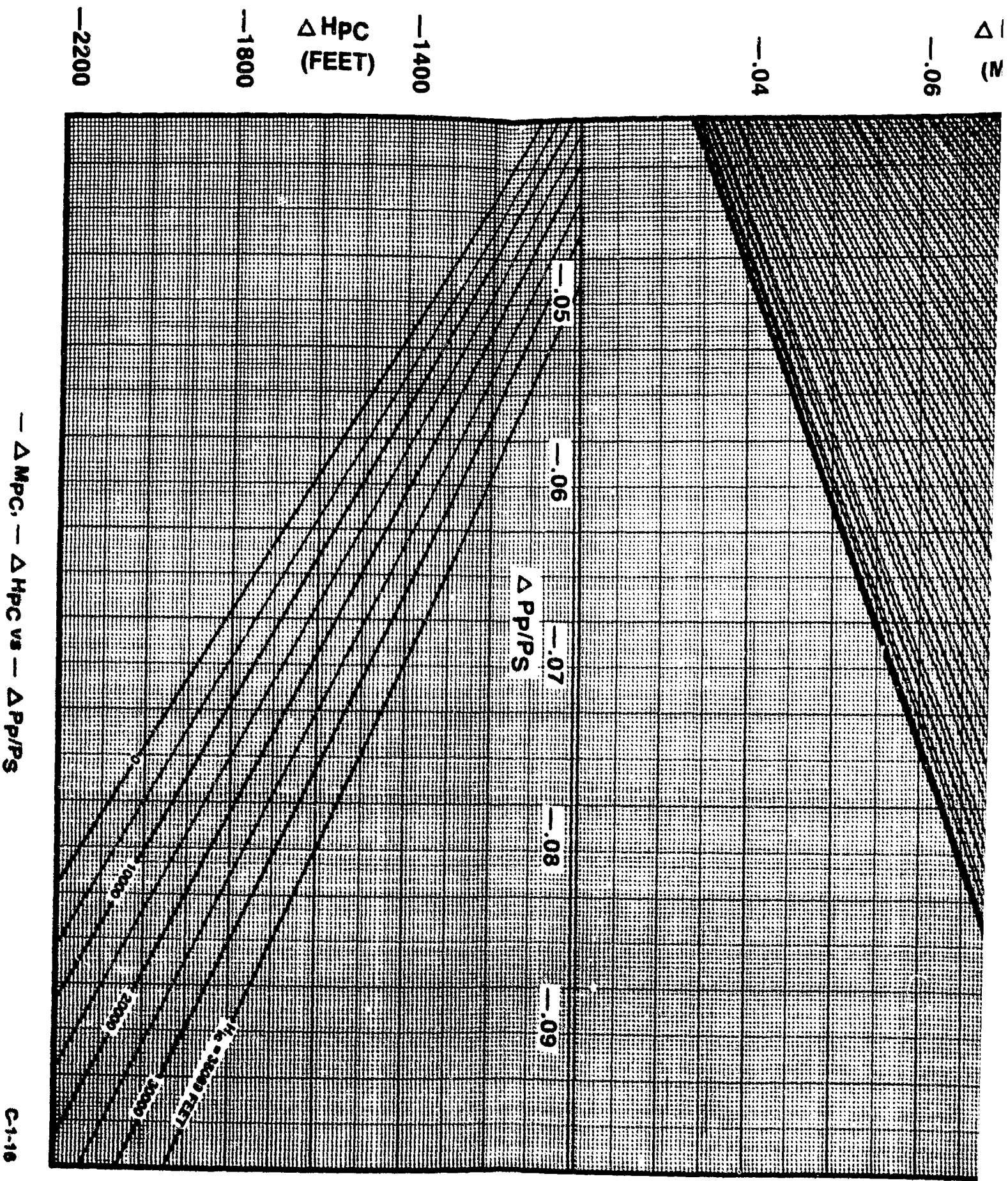
-.06

-.08

-.10

-.12





C-1-16

MPC
MACH

Δ MPC
(MACH)

-.04

-.06

-.08

-.10

-.12

$M_c = 4.0$ MACH

0.8

0.6

0.4

0.2

0.0

0.2

0.4

0.6

0.8

1.0

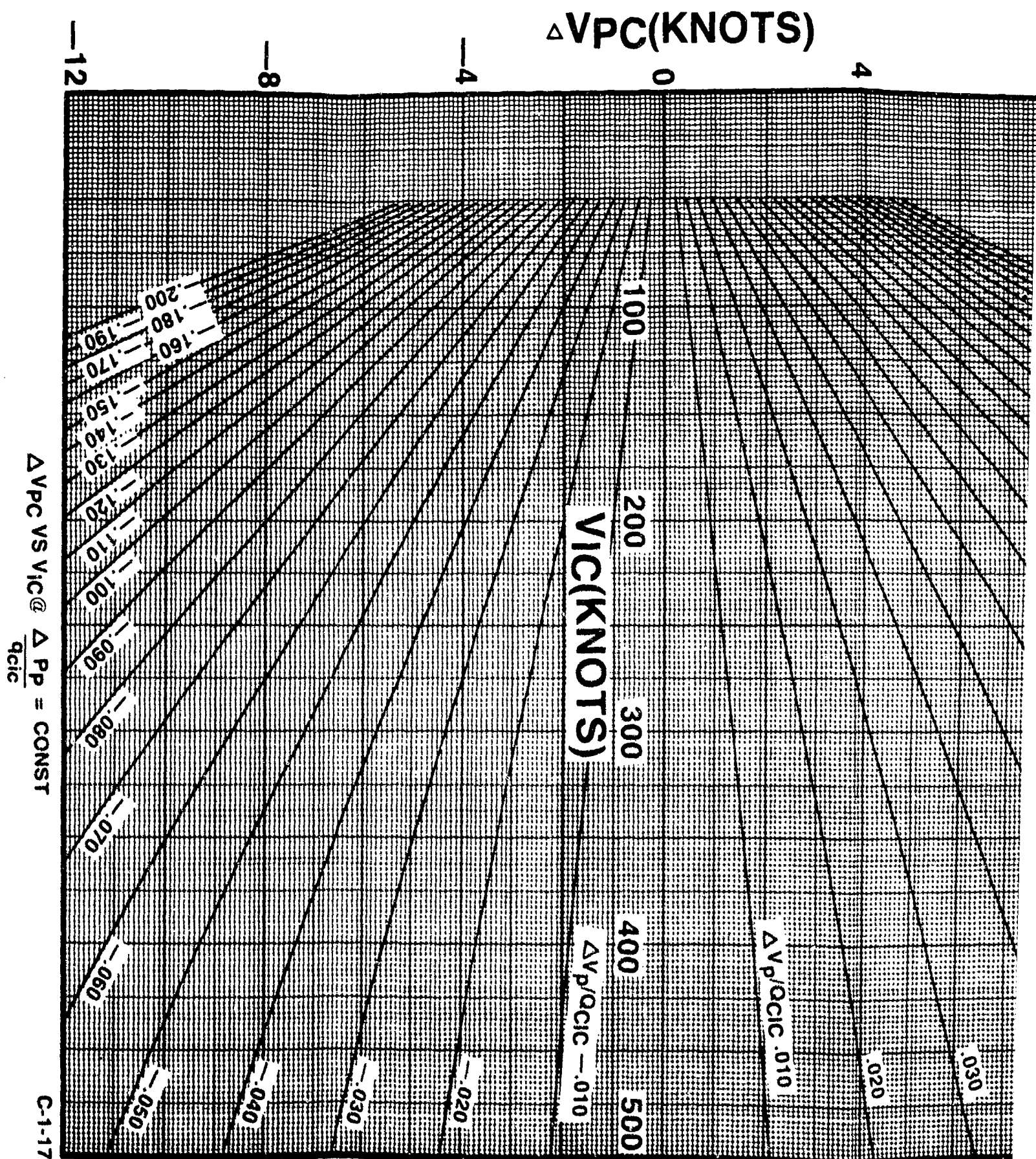
1.2

1.4

1.6

1.8

2.0



$\Delta V_{PC}(\text{KNOTS})$

8

-4

0

4

8

12

$VIC(\text{KNOTS})$

100

200

300

400

500

$\Delta V_{p/QCIC} .010$

$\Delta V_{p/QCIC} -.010$

-.020

.190 .200

.170 .180

.160

.150

.140

.130

.120

.110

.100

.090

.080

.070

.060

.050

.040

.030

.020

.010

.000

-.010

-.020

-.030

-.040

-.050

-.060

-.070

-.080

-.090

-.100

-.110

-.120

-.130

-.140

-.150

-.160

-.170

-.180

-.190

-.200

-.210

-.220

-.230

-.240

-.250

-.260

-.270

-.280

-.290

-.300

-.310

-.320

-.330

-.340

-.350

-.360

-.370

-.380

-.390

-.400

-.410

-.420

-.430

-.440

-.450

-.460

-.470

-.480

-.490

-.500

-.510

-.520

-.530

-.540

-.550

-.560

-.570

-.580

-.590

-.600

-.610

-.620

-.630

-.640

-.650

-.660

-.670

-.680

-.690

-.700

-.710

-.720

-.730

-.740

-.750

-.760

-.770

-.780

-.790

-.800

-.810

-.820

-.830

-.840

-.850

-.860

-.870

-.880

-.890

-.900

-.910

-.920

-.930

-.940

-.950

-.960

-.970

-.980

-.990

-1.000

-1.010

-1.020

-1.030

-1.040

-1.050

-1.060

-1.070

-1.080

-1.090

-1.100

-1.110

-1.120

-1.130

-1.140

-1.150

-1.160

-1.170

-1.180

-1.190

-1.200

-1.210

-1.220

-1.230

-1.240

-1.250

-1.260

-1.270

-1.280

-1.290

-1.300

-1.310

-1.320

-1.330

-1.340

-1.350

-1.360

-1.370

-1.380

-1.390

-1.400

-1.410

-1.420

-1.430

-1.440

-1.450

-1.460

-1.470

-1.480

-1.490

-1.500

-1.510

-1.520

-1.530

-1.540

-1.550

-1.560

-1.570

-1.580

-1.590

-1.600

-1.610

-1.620

-1.630

-1.640

-1.650

-1.660

-1.670

-1.680

-1.690

-1.700

-1.710

-1.720

-1.730

-1.740

-1.750

-1.760

-1.770

-1.780

-1.790

-1.800

-1.810

-1.820

-1.830

-1.840

-1.850

-1.860

-1.870

-1.880

-1.890

-1.900

-1.910

-1.920

-1.930

-1.940

-1.950

-1.960

-1.970

-1.980

-1.990

-2.000

-2.010

-2.020

-2.030

-2.040

-2.050

-2.060

-2.070

-2.080

-2.090

-2.100

-2.110

-2.120

-2.130

-2.140

-2.150

-2.160

-2.170

-2.180

-2.190

-2.200

-2.210

-2.220

-2.230

-2.240

-2.250

-2.260

-2.270

-2.280

-2.290

-2.300

-2.310

-2.320

-2.330

-2.340

-2.350

-2.360

-2.370

-2.380

-2.390

-2.400

-2.410

-2.420

-2.430

-2.440

-2.450

-2.460

-2.470

-2.480

-2.490

-2.500

-2.510

-2.520

-2.530

-2.540

-2.550

-2.560

-2.570

-2.580

-2.590

-2.600

-2.610

-2.620

-2.630

-2.640

-2.650

-2.660

-2.670

-2.680

-2.690

-2.700

-2.710

-2.720

-2.730

-2.740

-2.750

-2.760

-2.770

-2.780

-2.790

-2.800

-2.810

-2.820

-2.830

-2.840

-2.850

-2.860

-2.870

ΔV_{PC} (KNOTS)

8

0

4

8

12

500

600

700

800

900

1000

VIC (KNOTS)

.050

.045

.040

.035

.030

.025

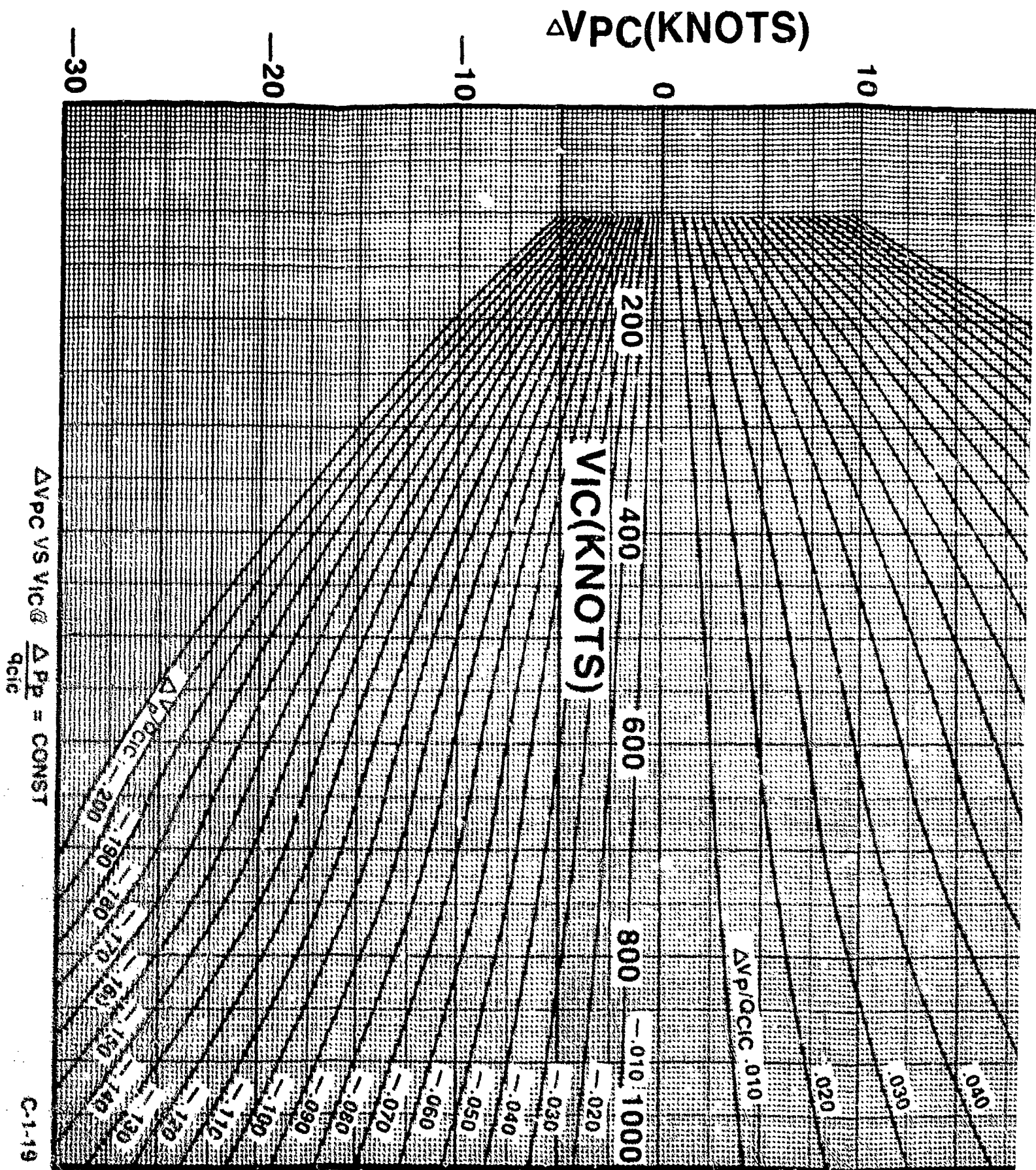
.020

.015

$\Delta V_{PC/CIC}$.010

$\Delta V_{PC/CIC} - .010$

2



$\Delta VPC(KNOTS)$

-10

0

10

20

30

200

400

600

800

1000

$VIC(KNOTS)$

.200

.190

.180

.170

.160

.150

.140

.130

.120

.110

.100

.090

.080

.070

.060

.050

.040

.030

.020

.010

.000

-.010

-.020

-.030

-.040

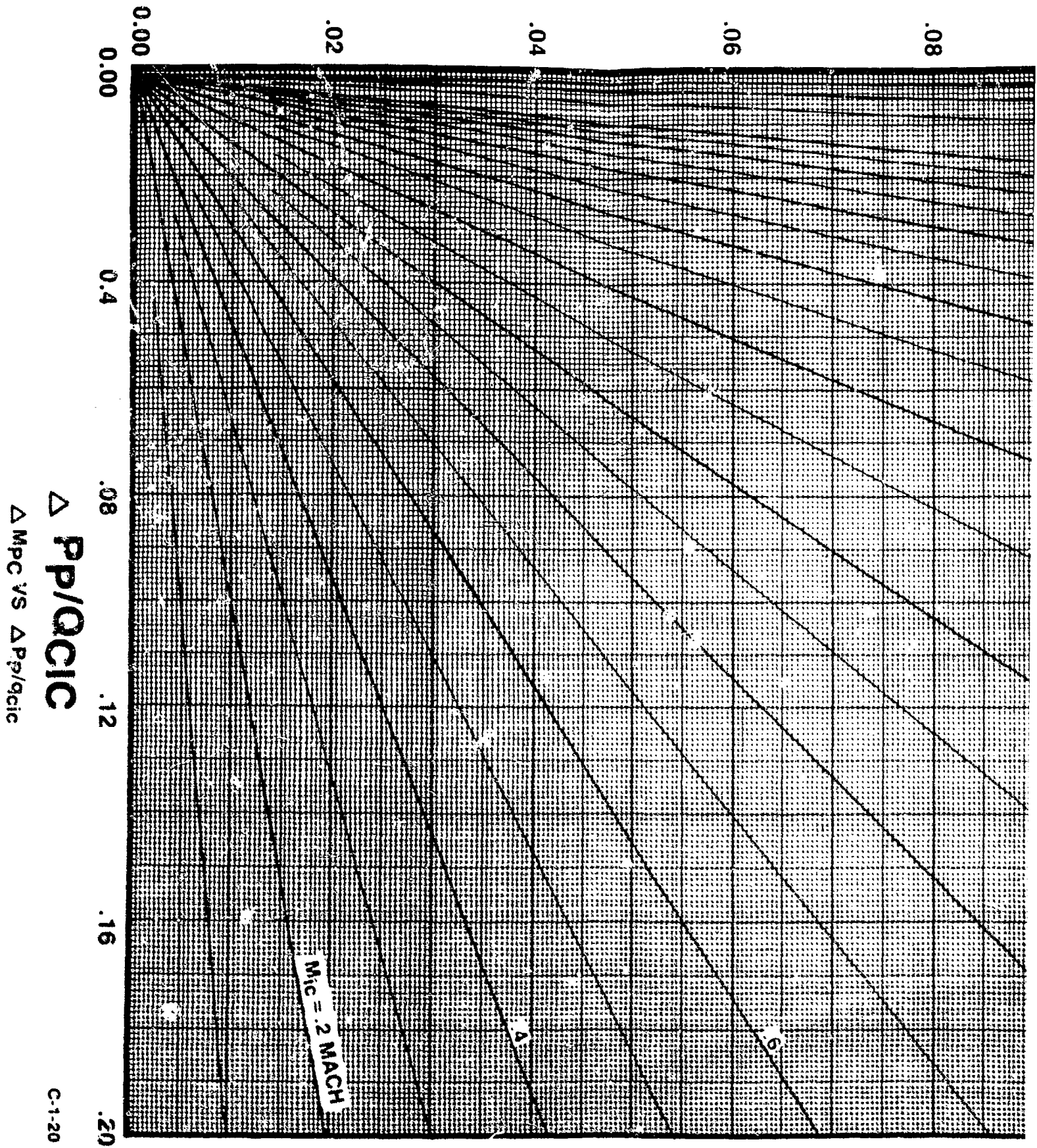
-.050

-.060

$\Delta P/QCIC .010$

2

ΔM_{PC} (MACH NO.)



C-1-20

AMPC (MACH NO.)

.06

.08

.10

.12

.14

4.0
3.0

2.0

1.8

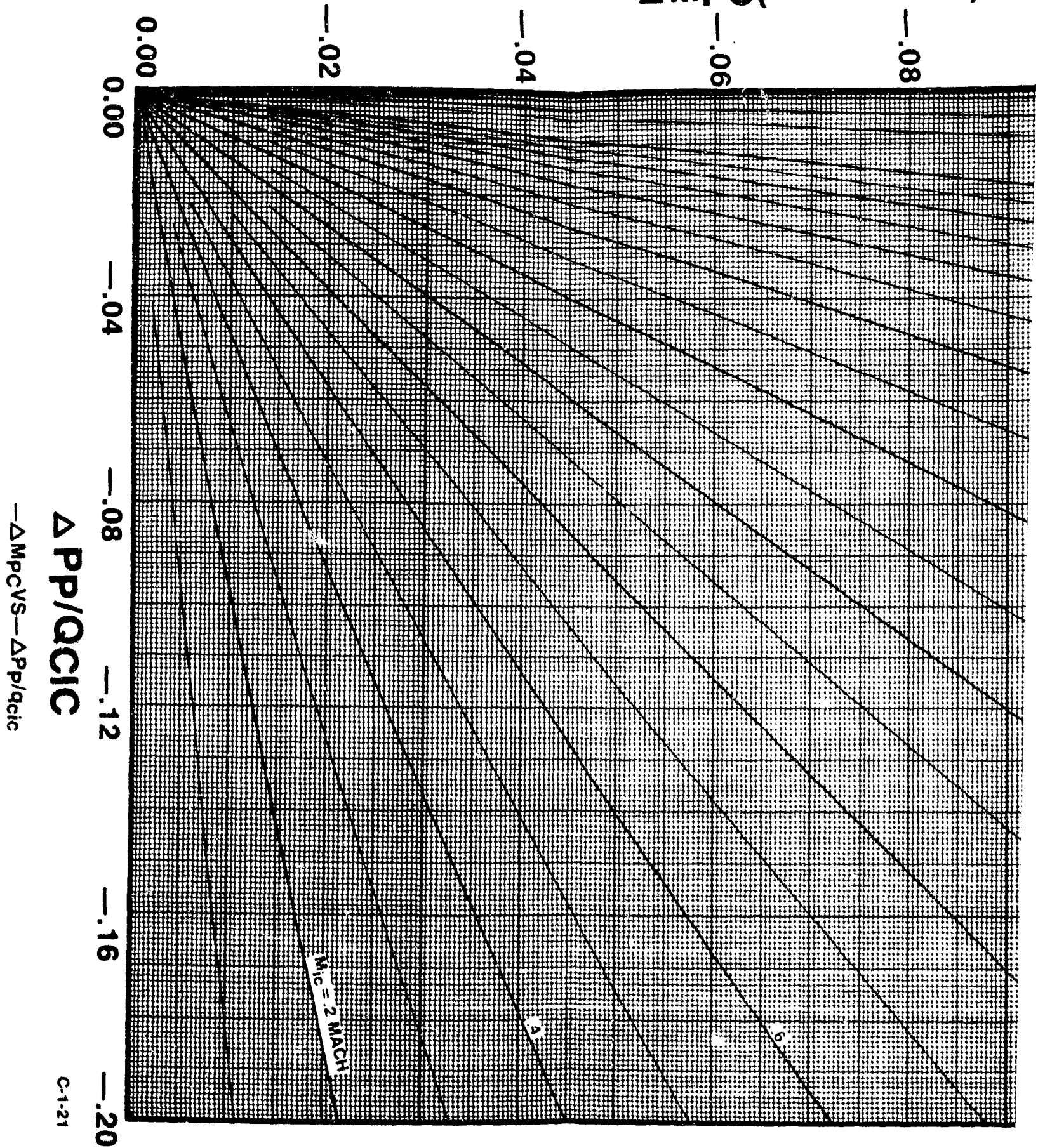
1.6

1.4

1.2

1.0

$\Delta MPC(MACH NO.)$



$\Delta MPC(MACH NO.)$

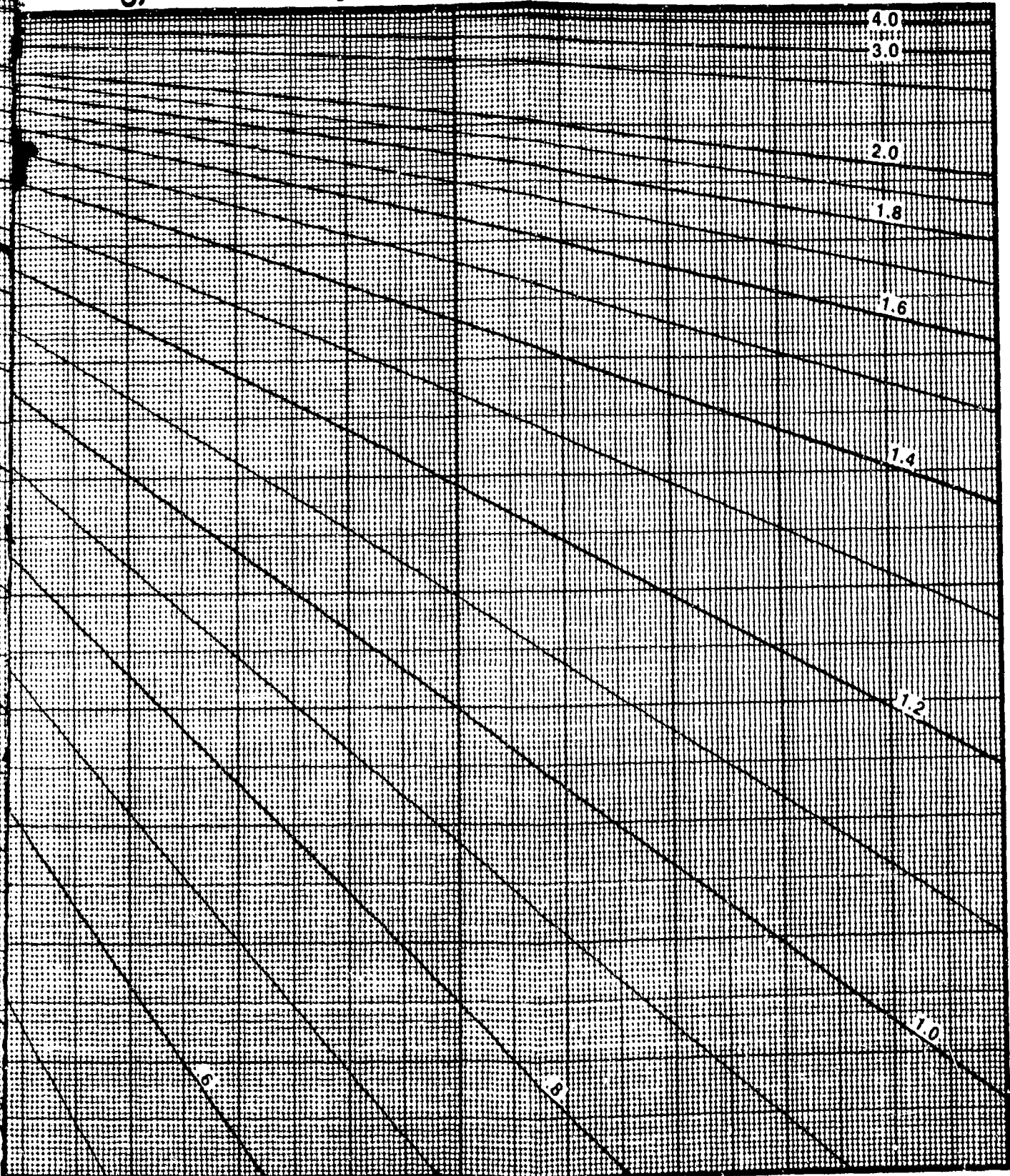
-.06

-.08

-.10

-.12

-.14



APPENDIX C-2
PITOT-STATIC CHARTS

APPENDIX C-2

PITOT-STATIC CHARTS

Mach Number M versus Calibrated Airspeed V_c for

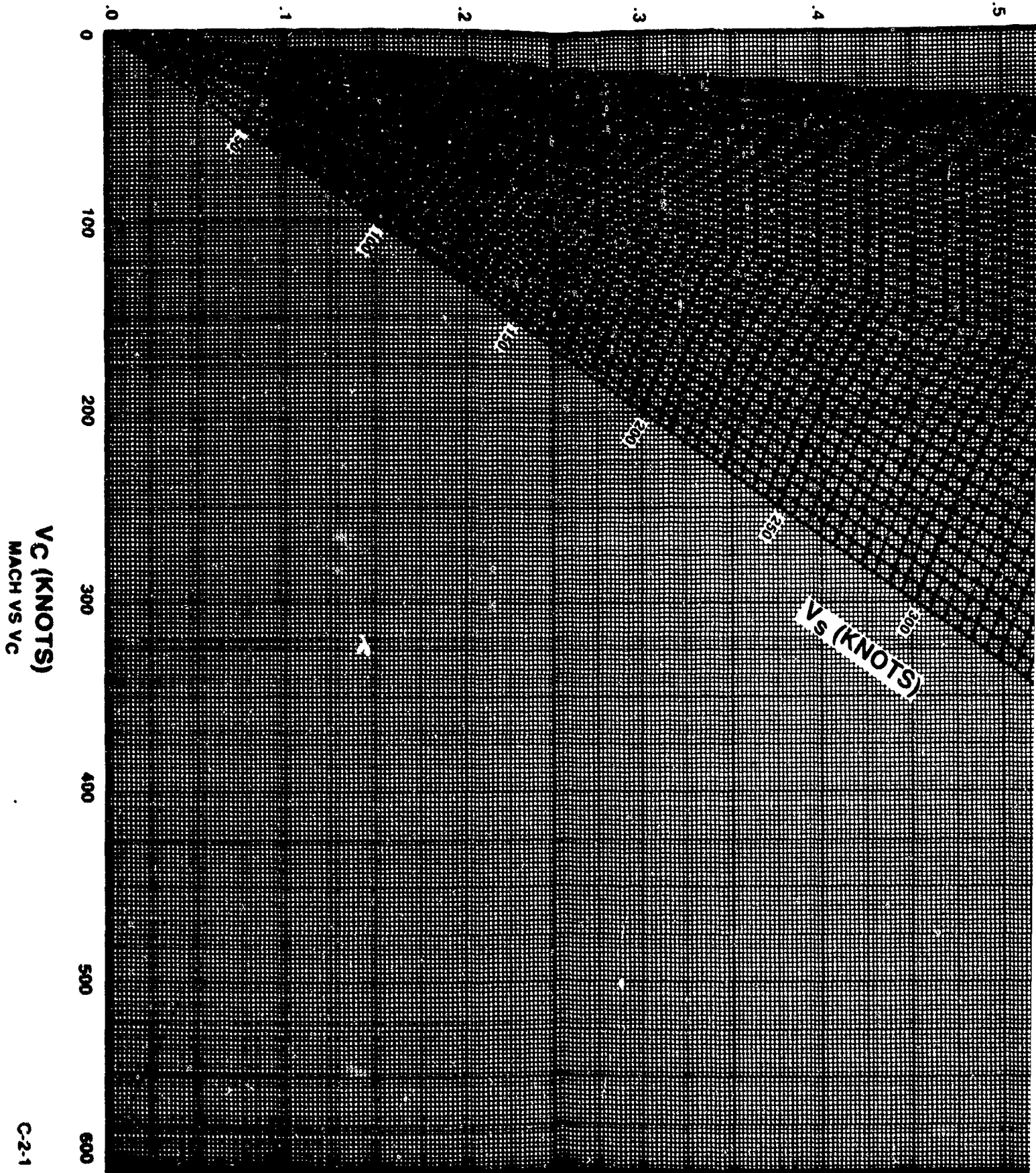
Pressure Altitude $H_c = \text{Constant}$ with Lines of

Standard Day True Speed $V_s = \text{Constant}$.

(Also M_{ic} versus V_{ic} for $H_{ic} = \text{Constant}$)

APRIL 1967

MACH M



VC (KNOTS)
MACH VS VC

C-2-1

MACH M

3

4

5

6

7

8

100000

90000

70000

60000

50000

40000

30000

20000

10000

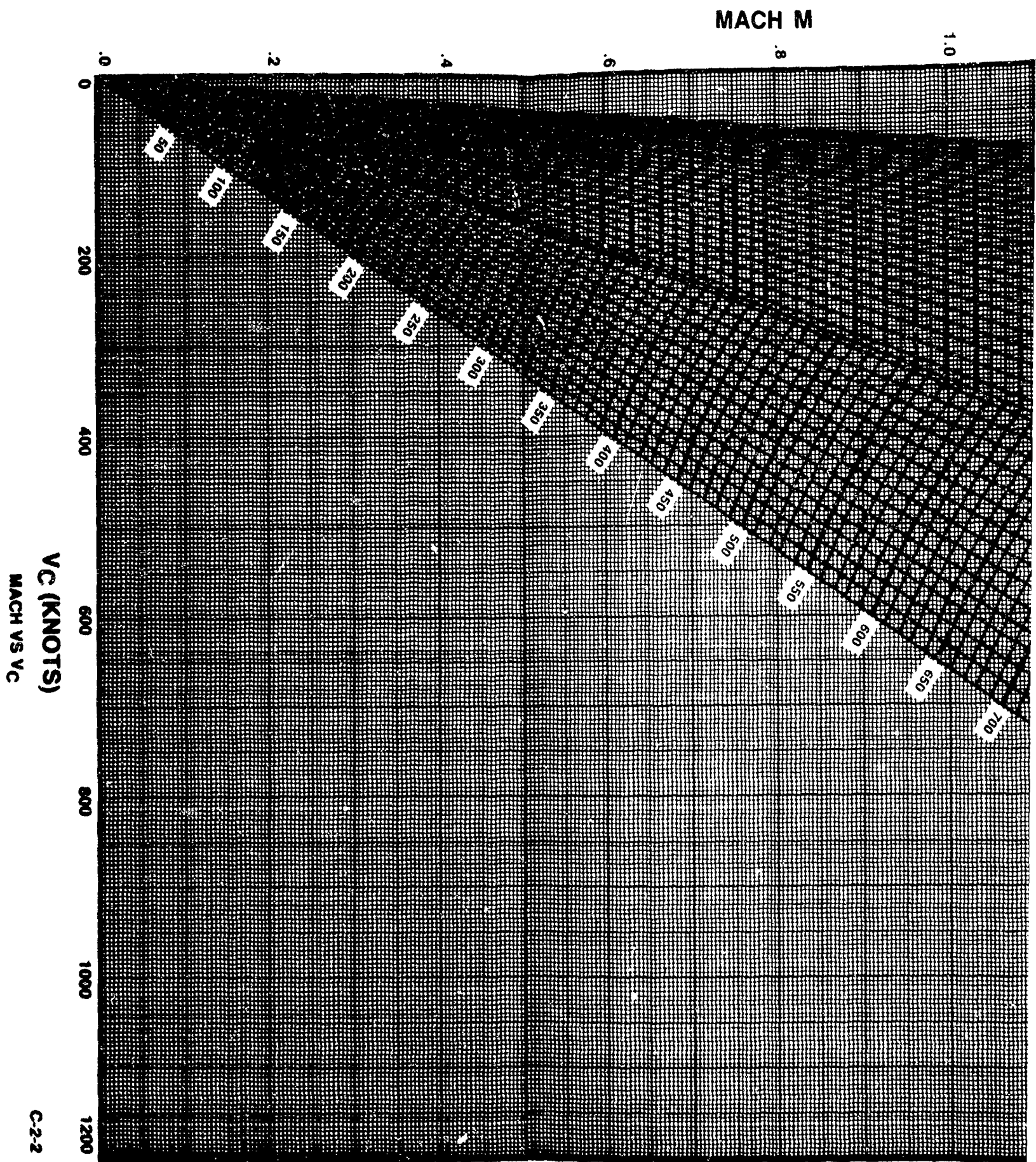
0

H_c = 0 FEET

V_s (KNOTS)

724

2



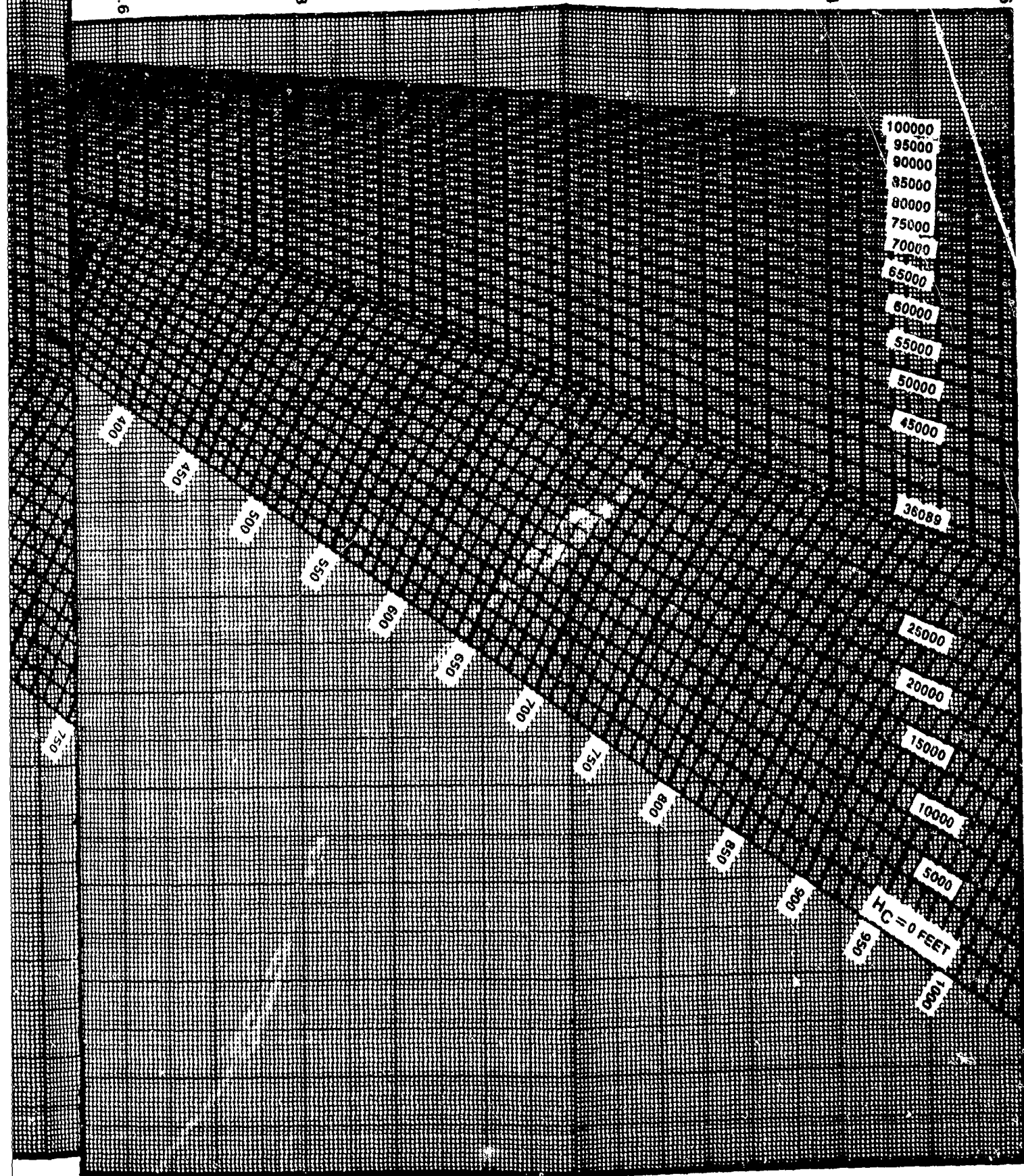
MACH M

1.0

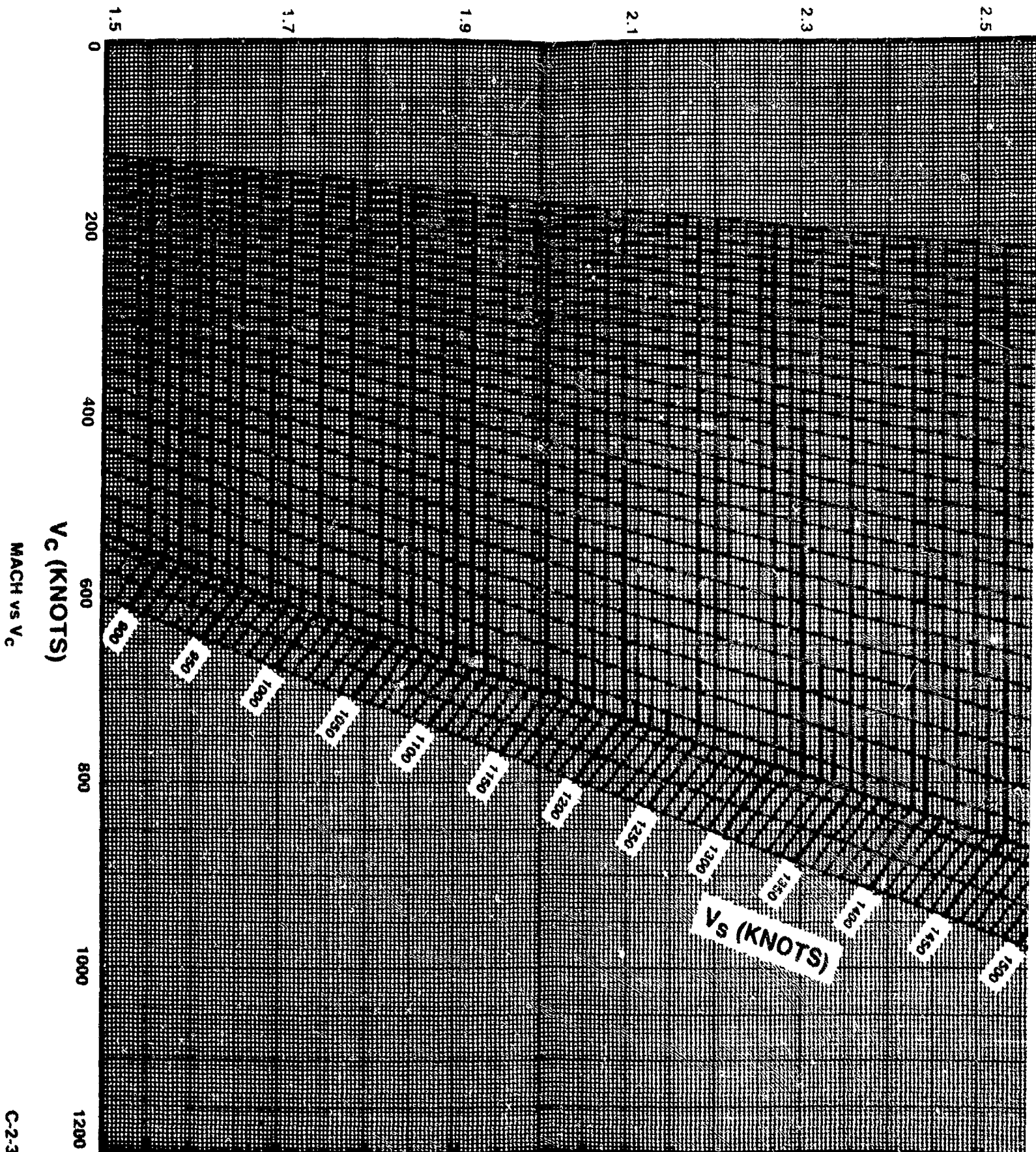
1.2

1.4

1.6



MACH M



Vc (KNOTS)
MACH VS Vc

C-23

MACH M

2.1

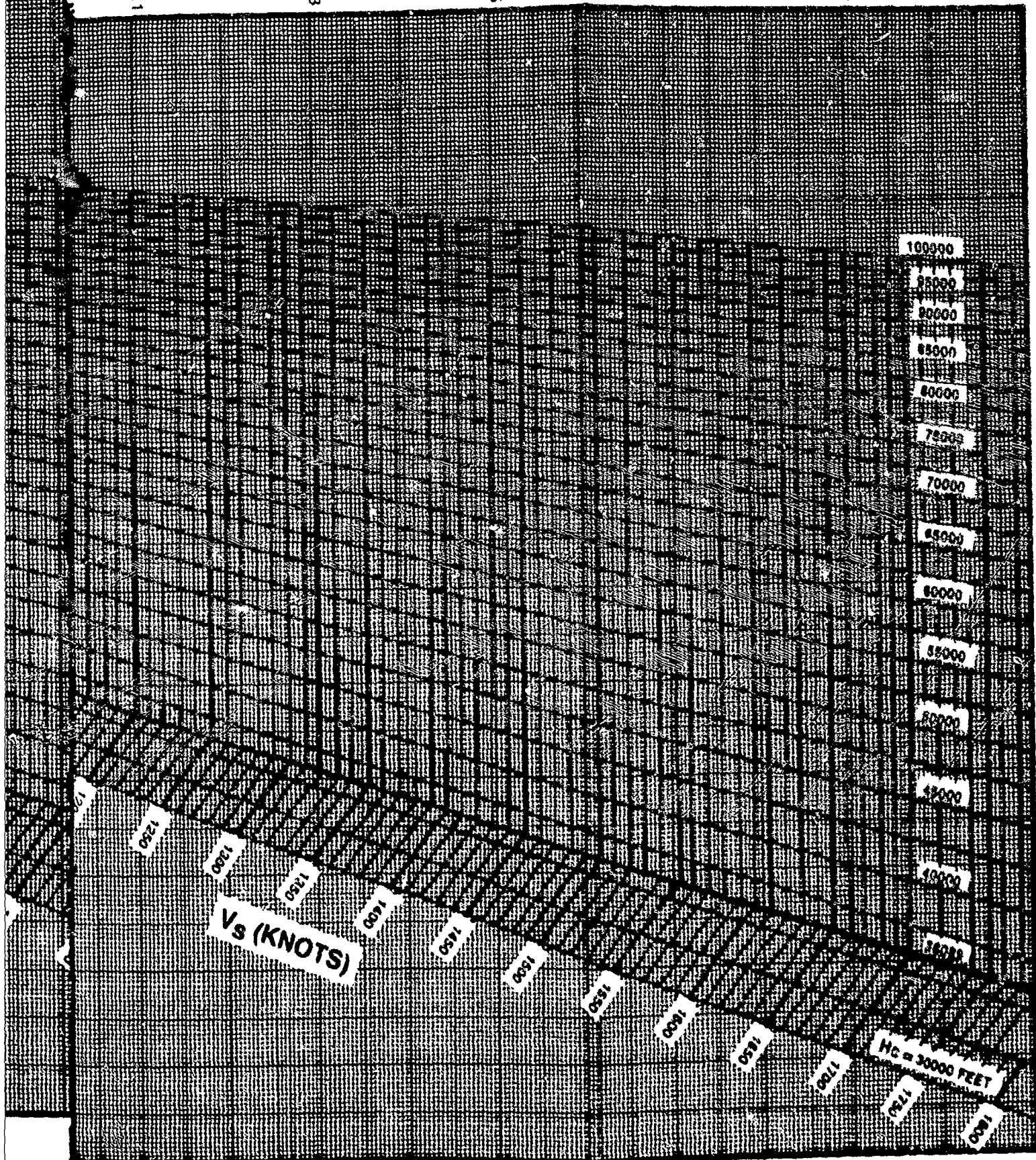
2.3

2.5

2.7

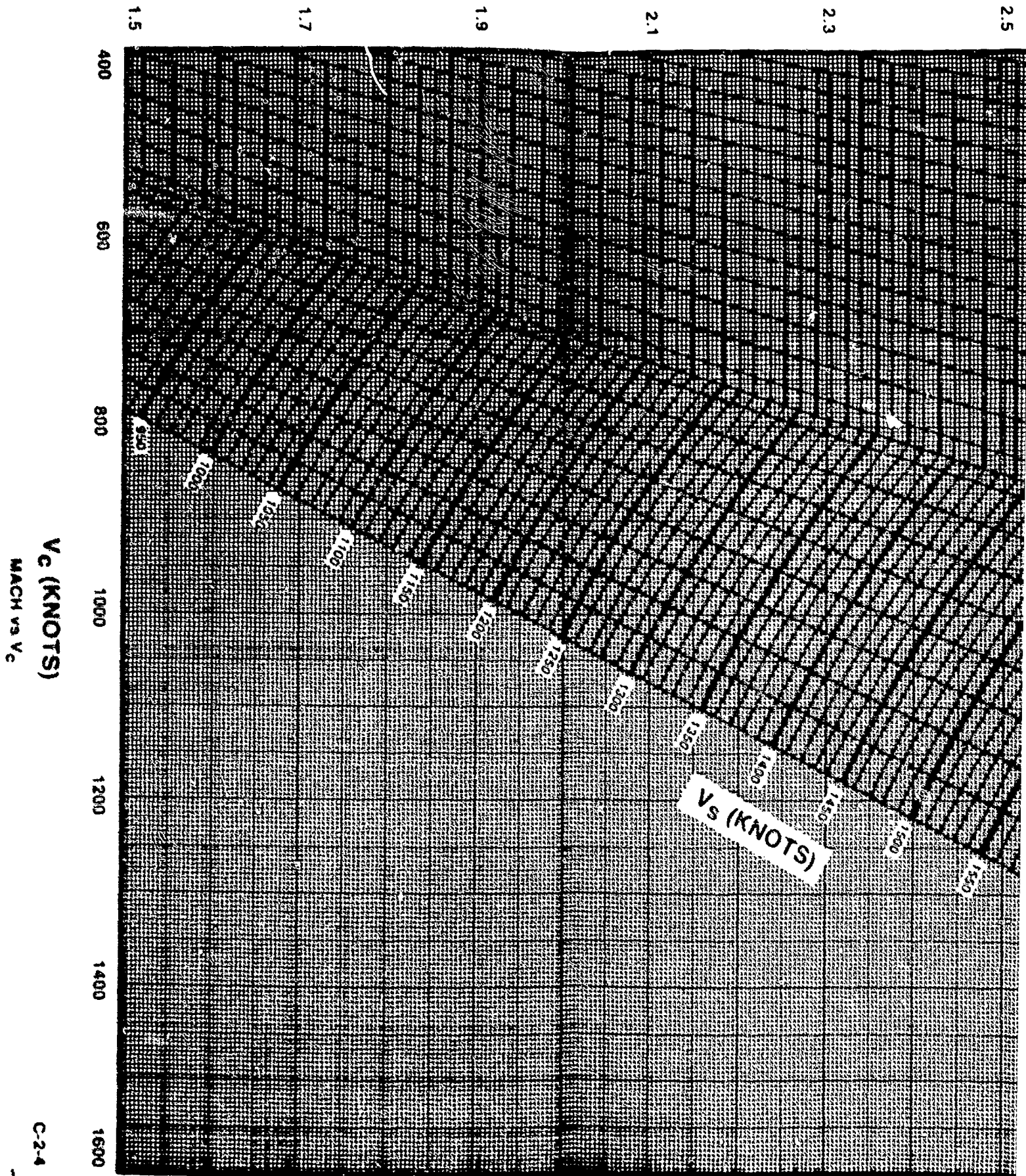
2.9

3.1



2

MACH NUMBER, M



Vc (KNOTS)

MACH VS Vc

C-2-4

MACH NUMBER, M

2.1

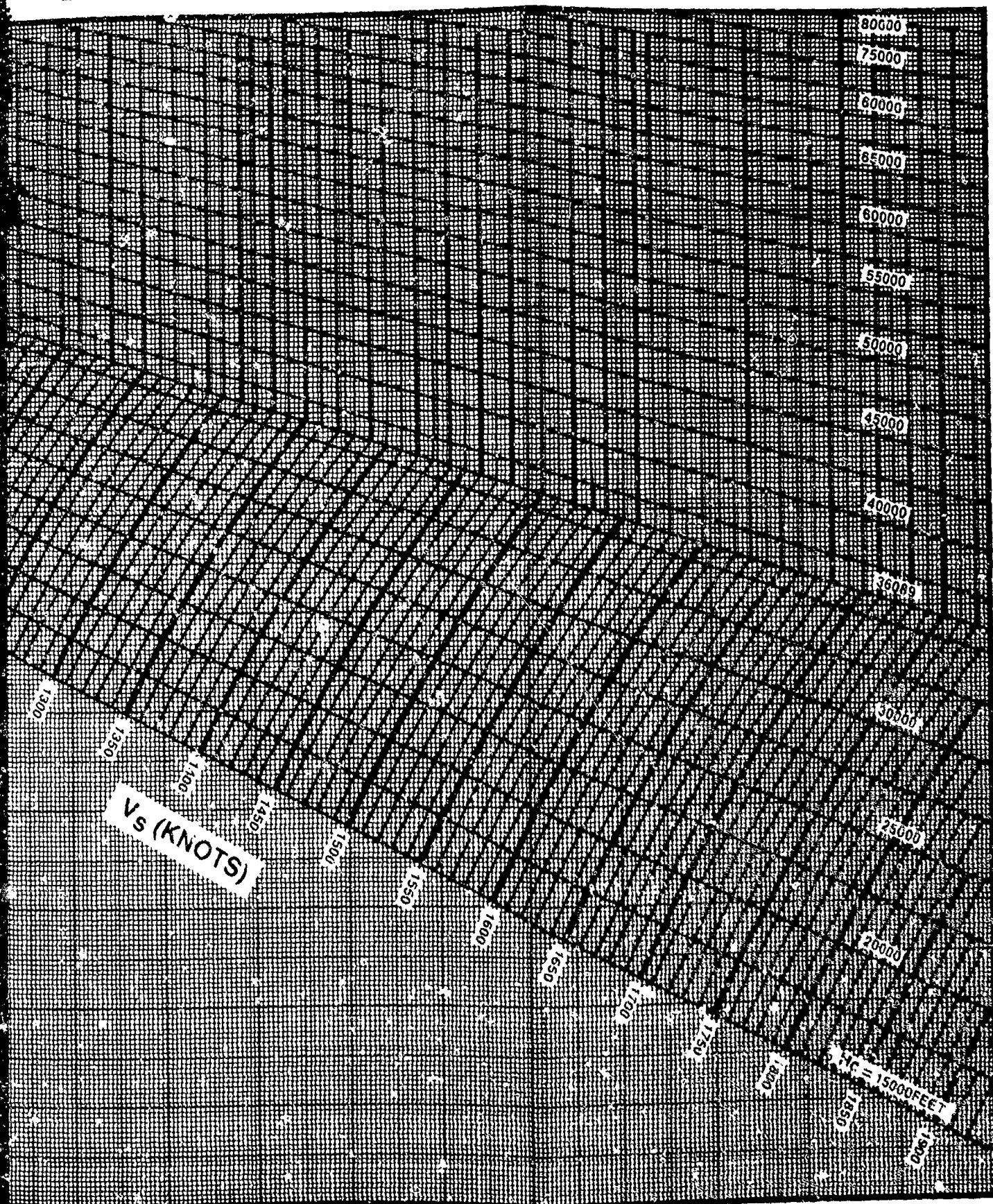
2.3

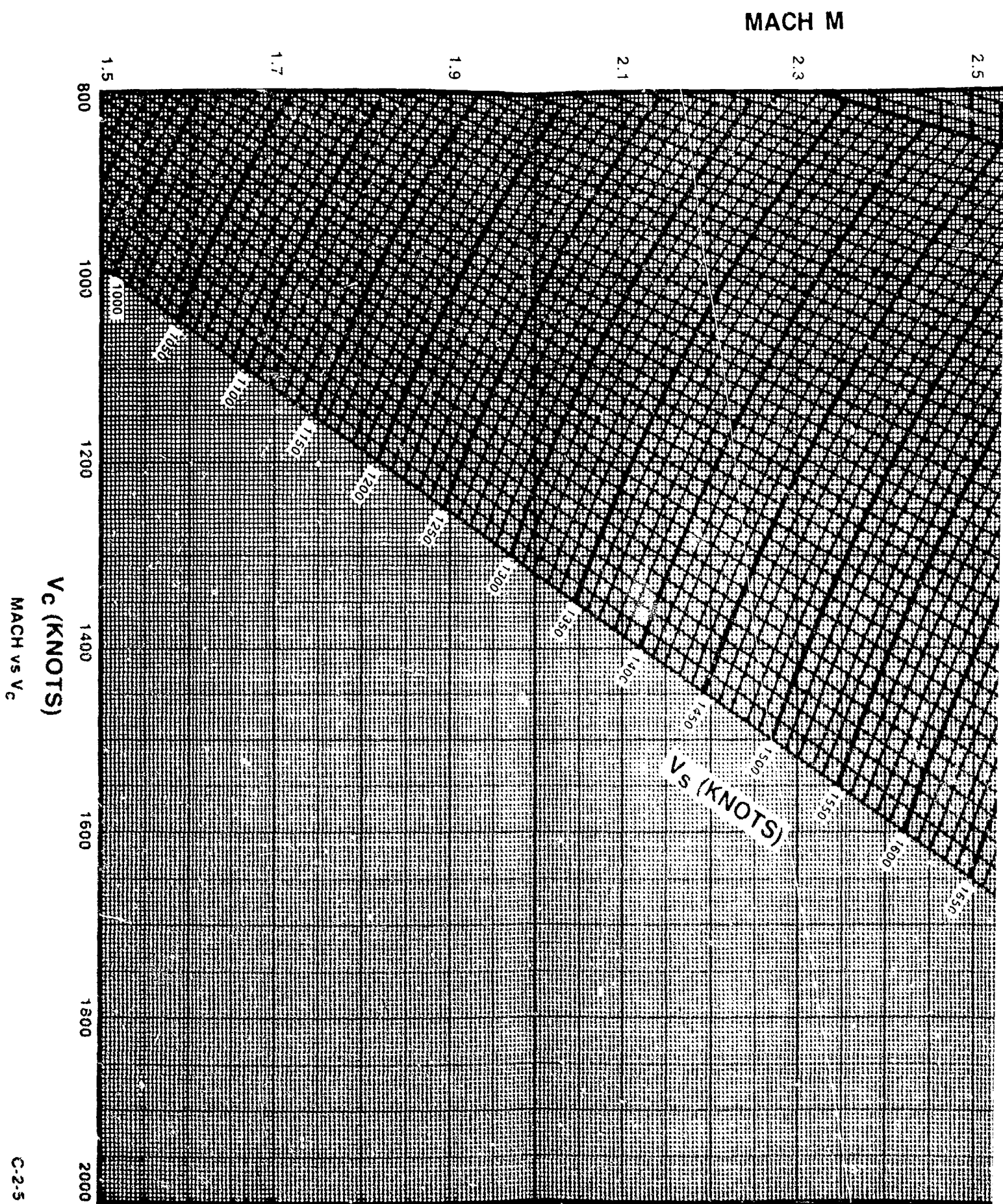
2.5

2.7

2.9

3.1





MACH M

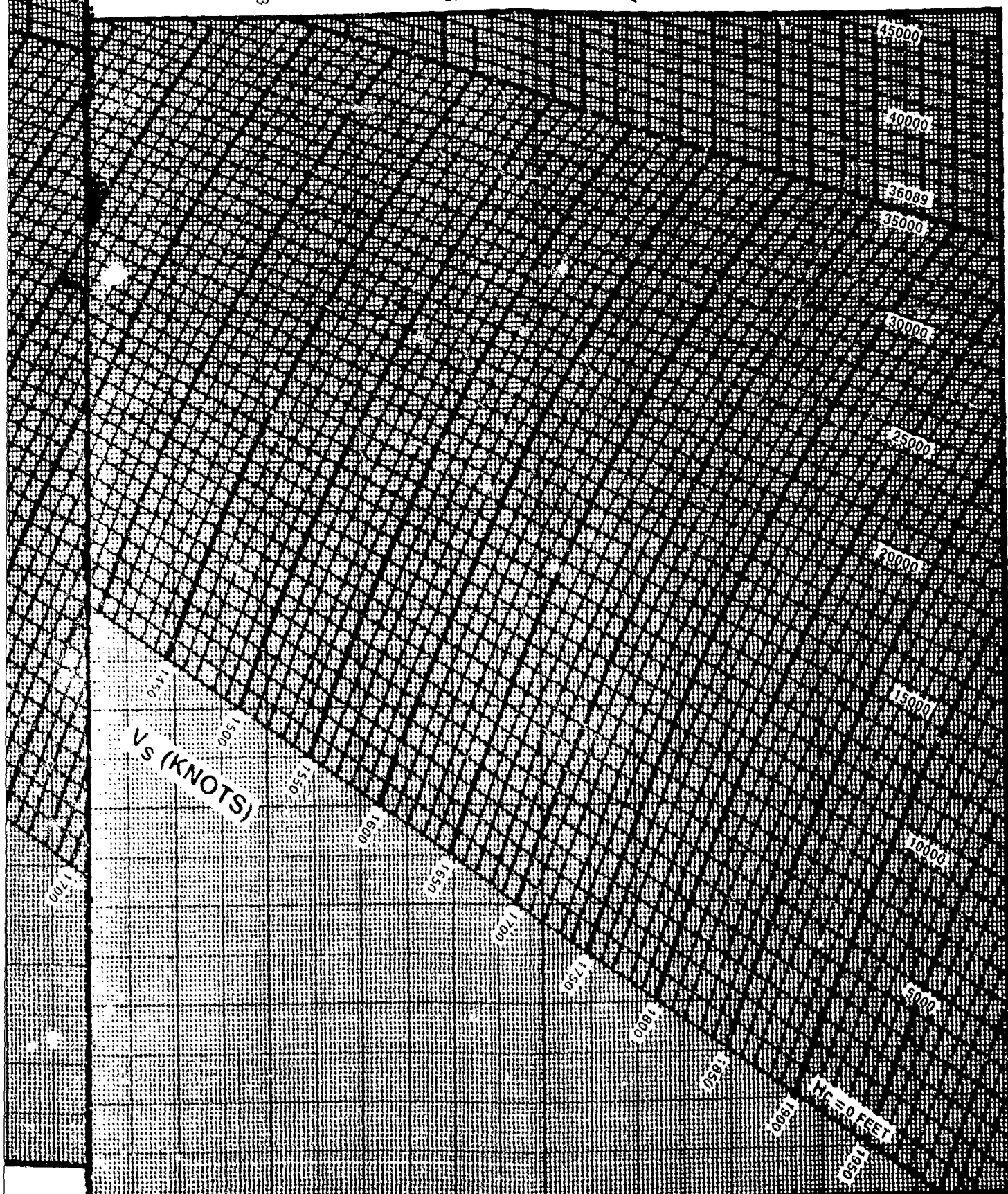
2.3

2.5

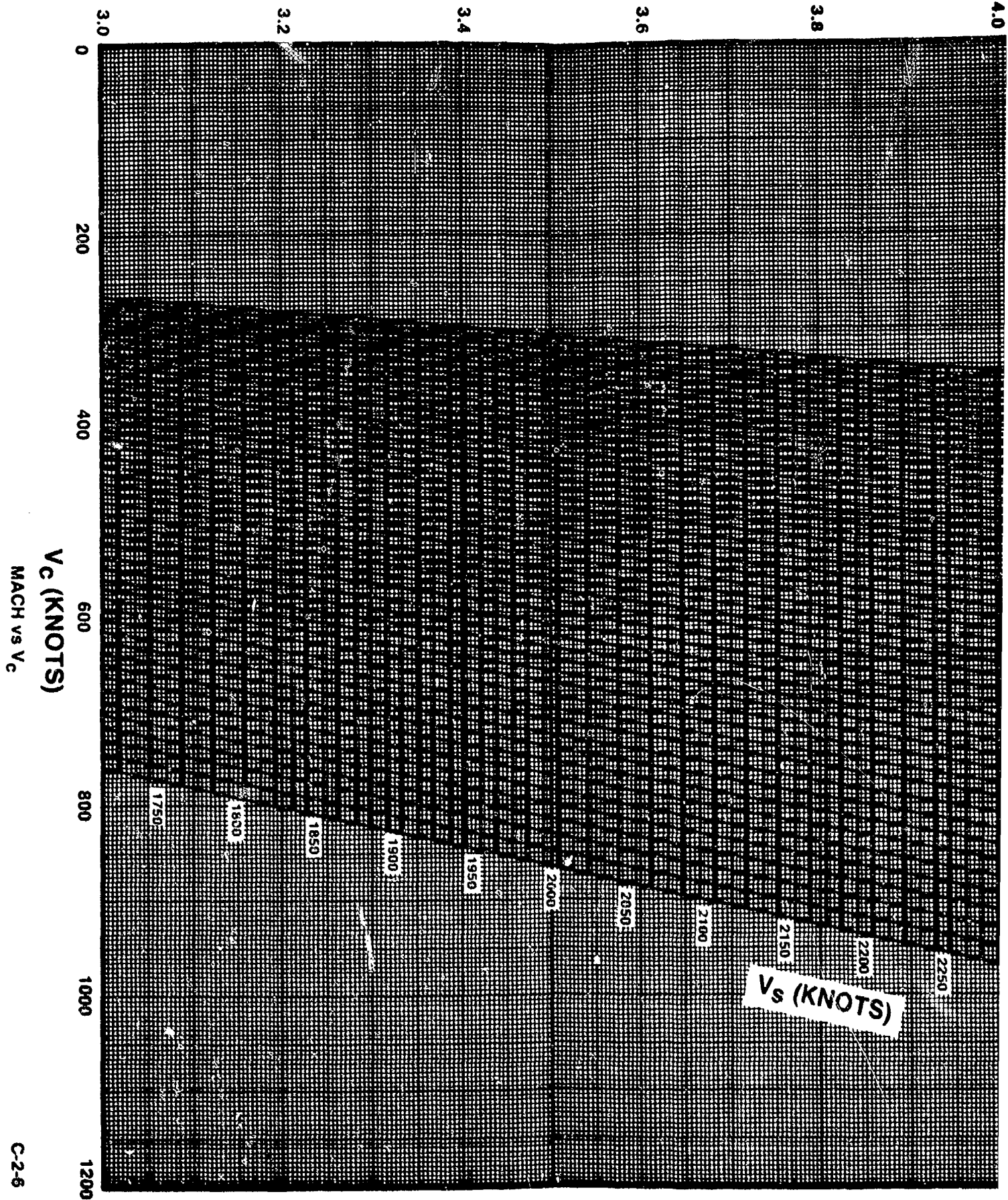
2.7

2.9

3.1



MACH M



Vc (KNOTS)

MACH vs Vc

C-26

MACH M

3.6

3.8

4.0

4.2

4.4

4.6

100000

95000

90000

85000

80000

75000

70000

65000

60000

55000

Hc = 80000 FEET

Vs (KNOTS)

2050

2100

2150

2200

2250

2300

2350

2400

2450

2500

2550

2600

2200

2

MACH M

4.0

3.8

3.6

3.4

3.2

3.0

600

800

1000

1200

1400

1600

1800

V_c (KNOTS)

MACH VS V_c

V_s (KNOTS)

C-2-7

MACH M

3.6

3.8

4.0

4.2

4.4

4.6

75000

70000

65000

60000

55000

50000

45000

40000

35000

30000

25000

20000

15000

10000

5000

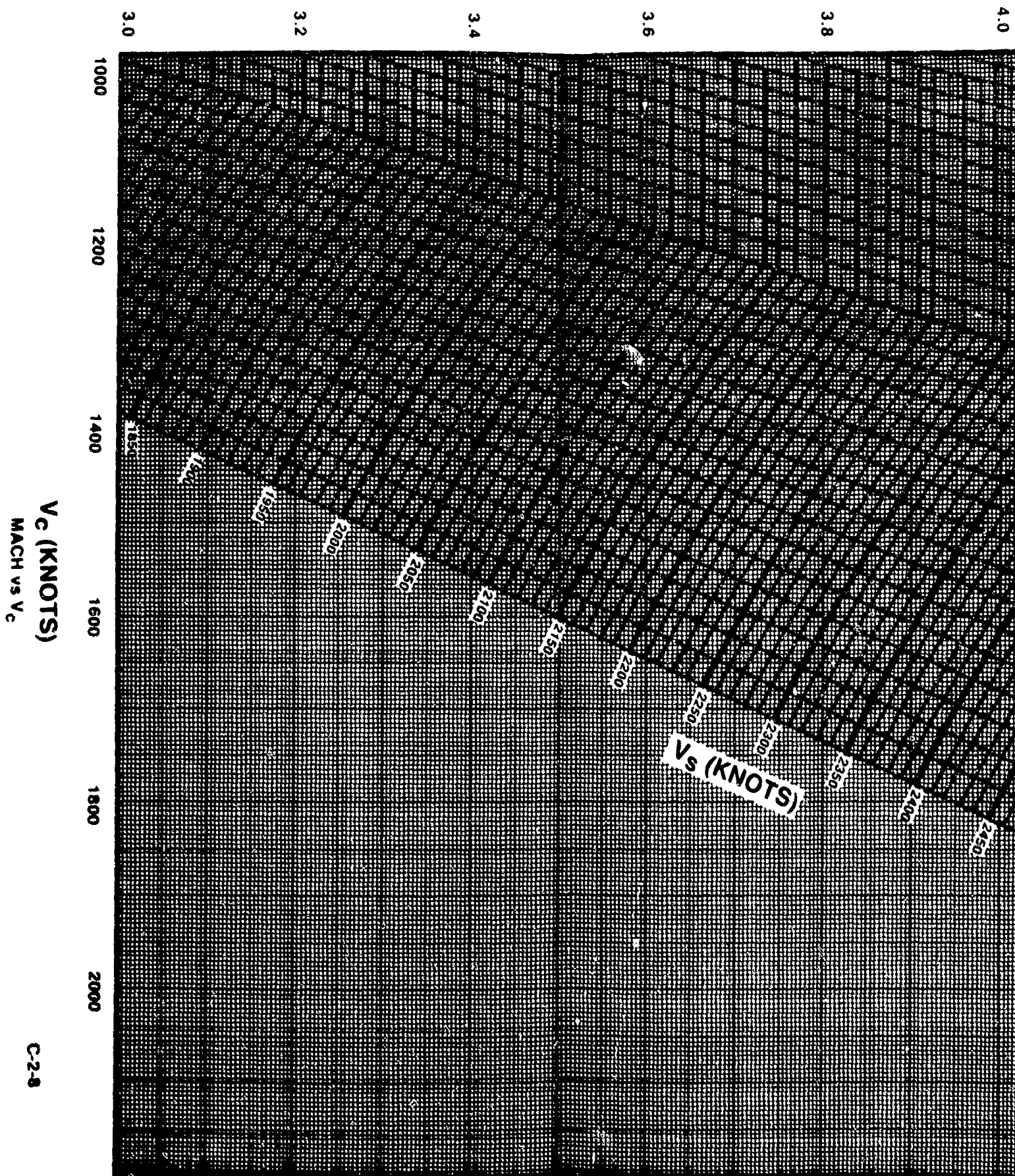
0

Vs (KNOTS)

MC = 60000 FEET

2

MACH M



Vc (KNOTS)

MACH vs Vc

Vs (KNOTS)

C-28

MACH M

3.6

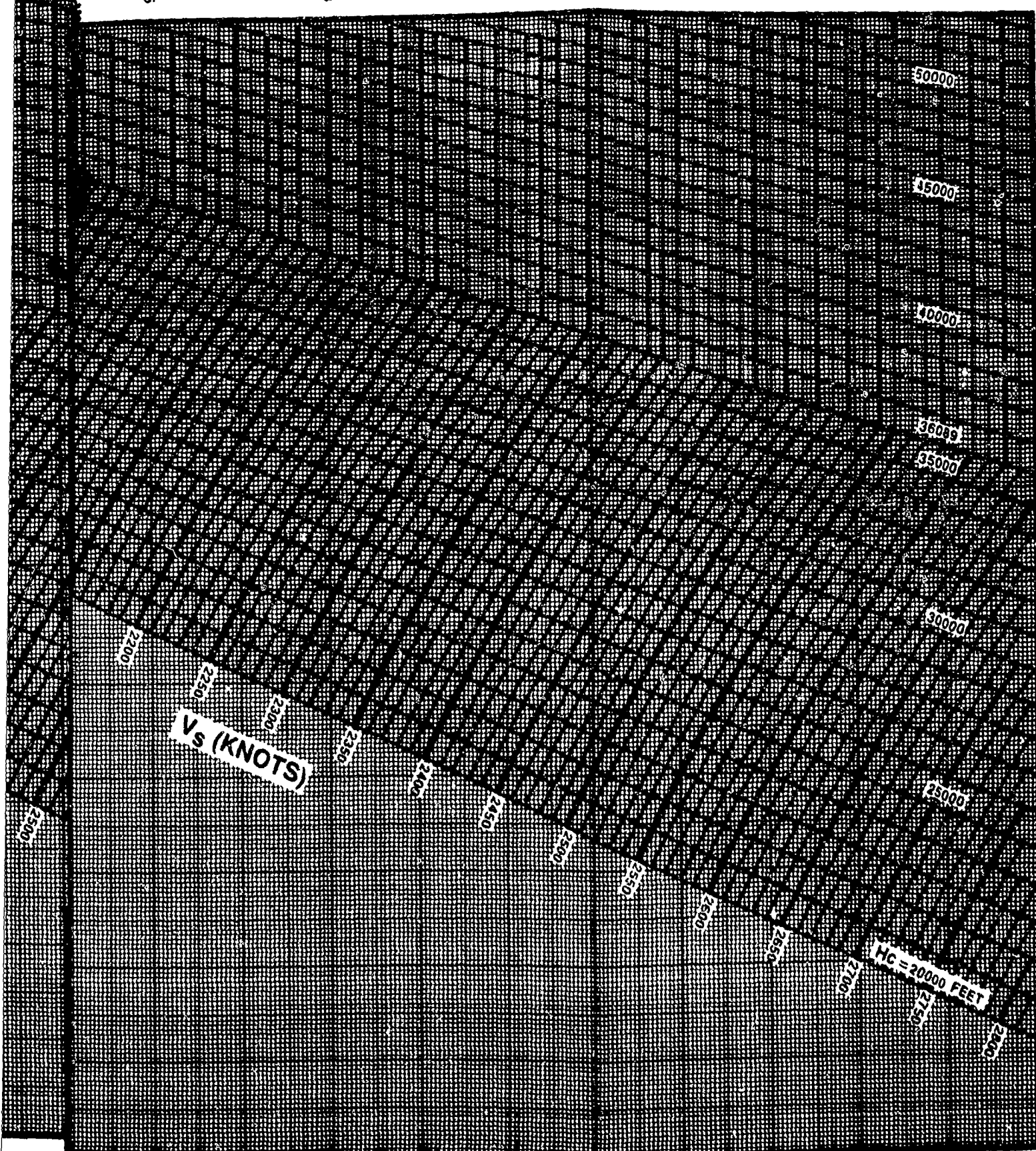
3.8

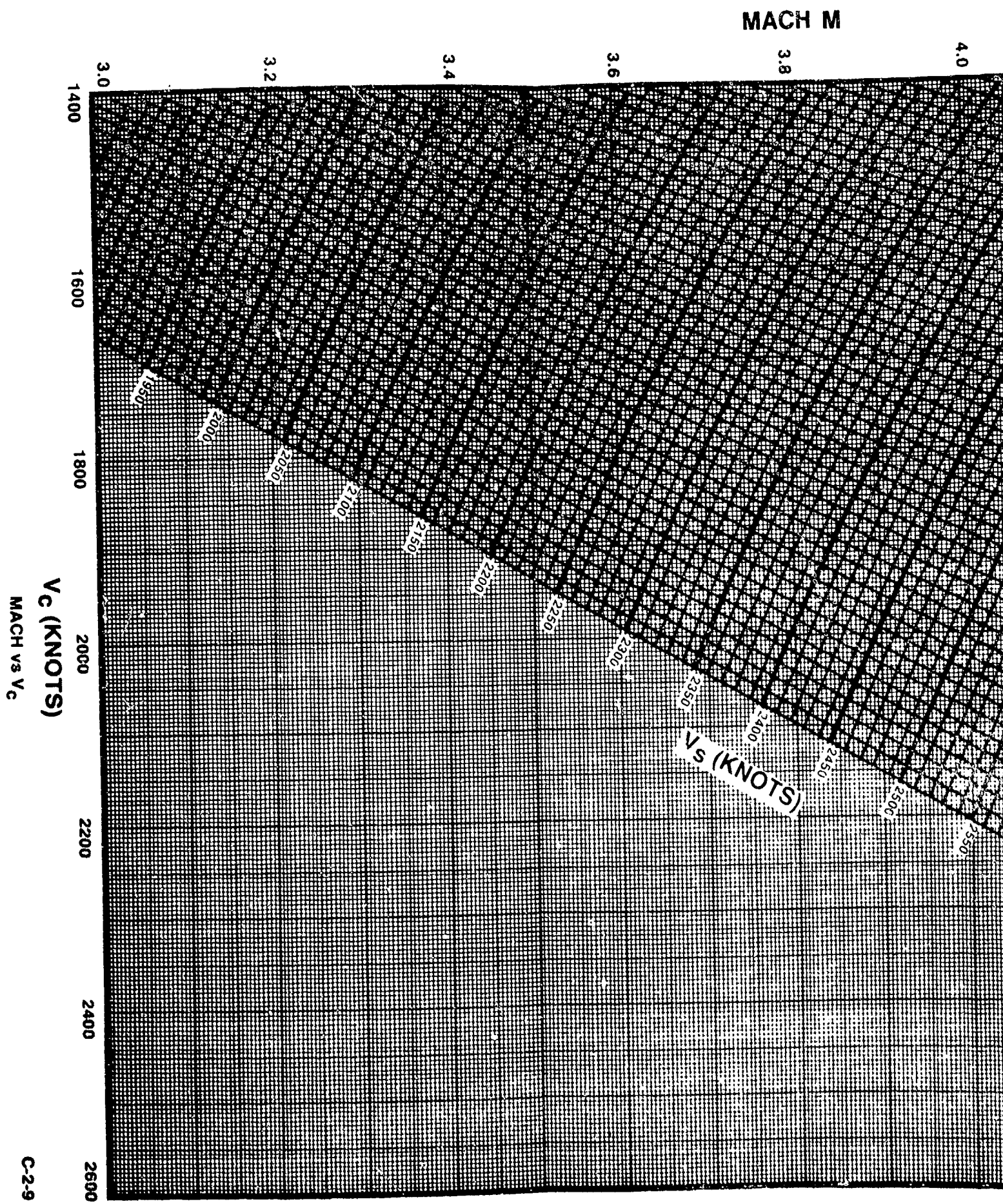
4.0

4.2

4.4

4.6





MACH M

3.6

3.8

4.0

4.2

4.4

4.6

36089
35000

30000

25000

20000

15000

Hc = 10000 FEET

2850
2900

Vs (KNOTS)

2350

2400

2450

2500

2550

2600

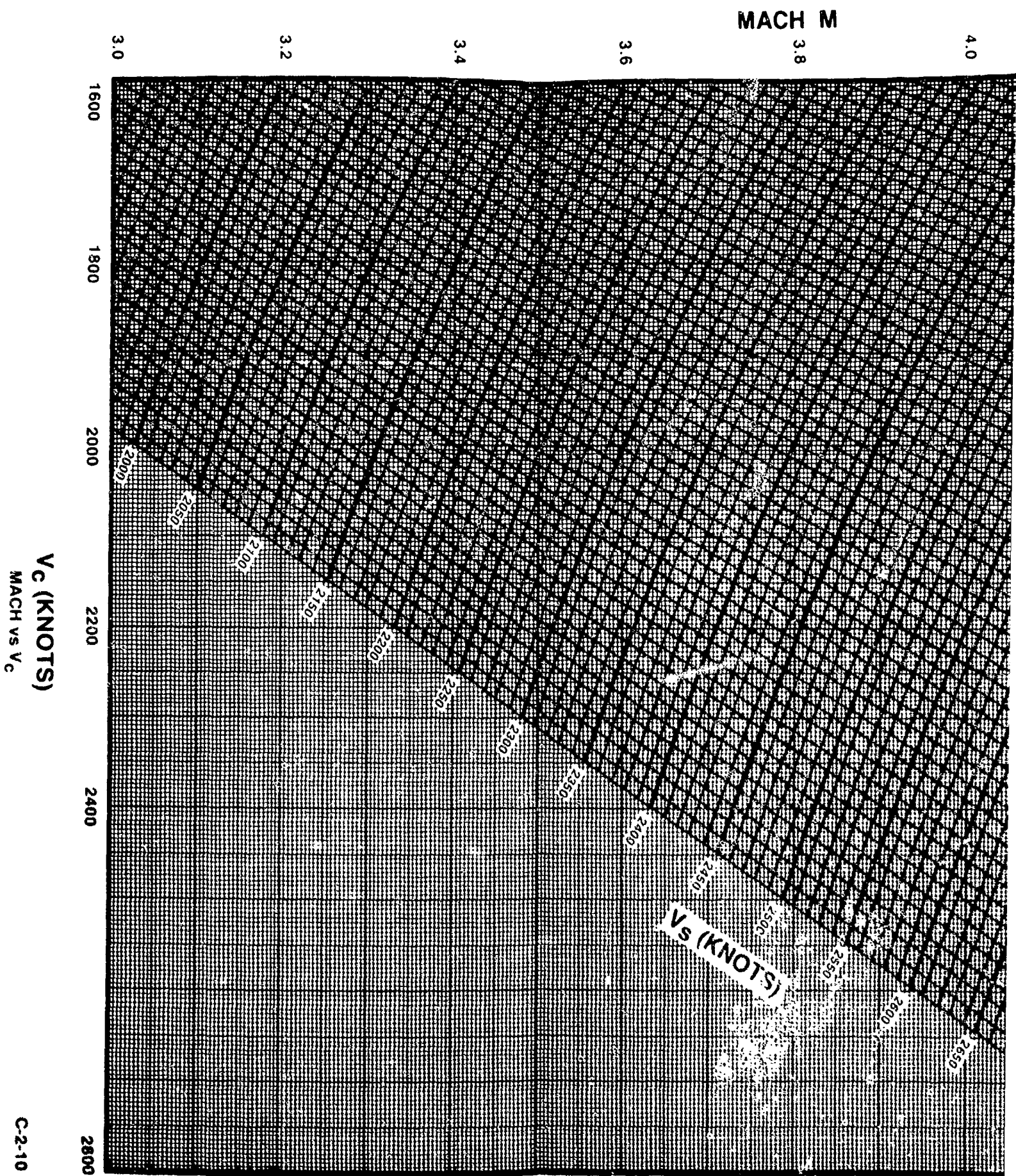
2650

2700

2750

2800

2



C-2-10

3.6

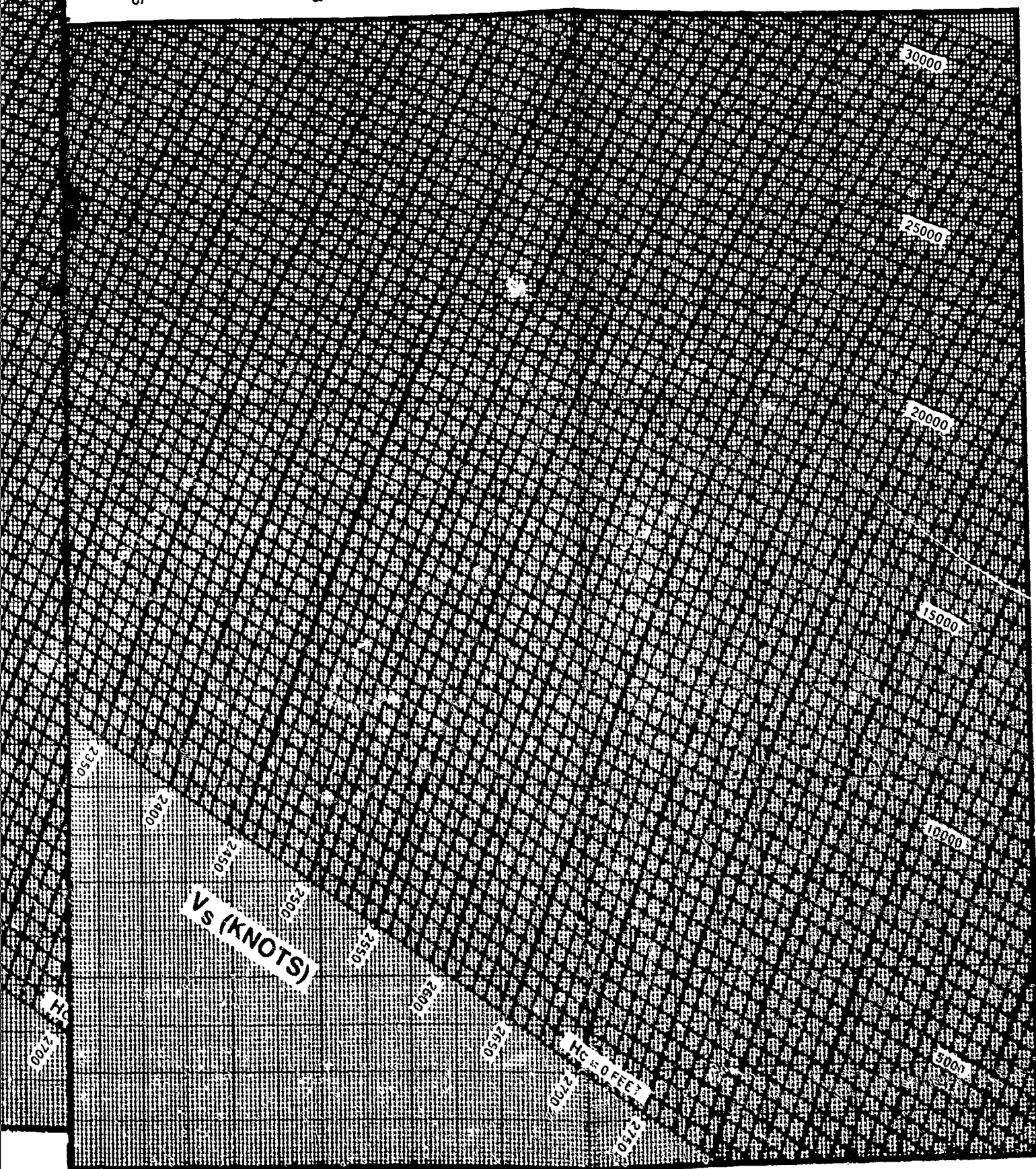
3.8

4.0

4.2

4.4

A.6



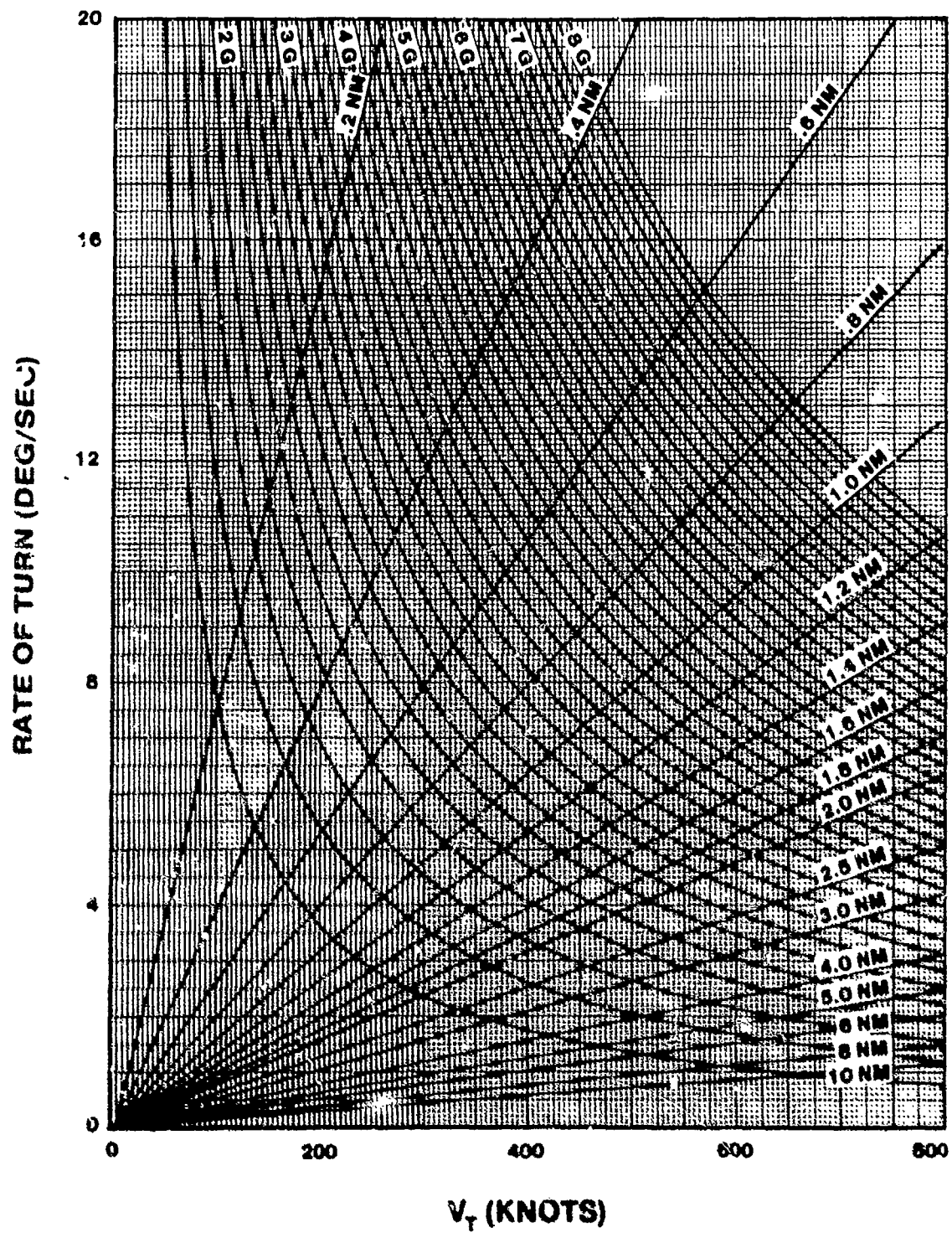
2

APPENDIX D
CHARTS OF INTEREST FOR THE USAF
TEST PILOT SCHOOL

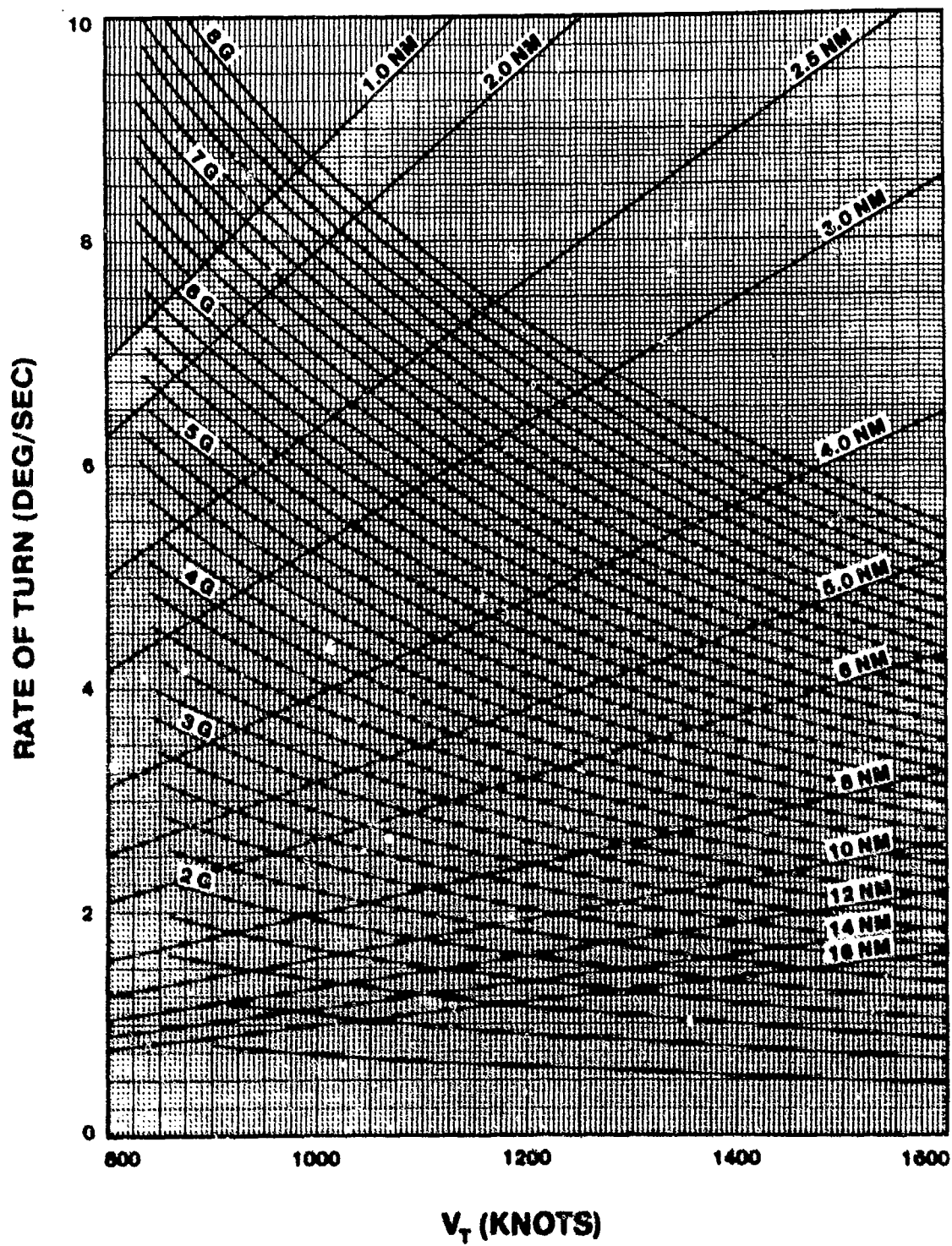
APPENDIX D
CHARTS OF INTEREST FOR THE
USAF TEXT PILOT SCHOOL

<u>PAGE NUMBER</u>	<u>TITLE</u>
D-1 - D-2	Rate of Turn vs V_{True}
D-3	Ram Pressure Ratio vs Mach
D-4	Delta Rate of Climb Factor for Turbojets ($.70 < n_r < 1.0$)
D-5 - D-6	Test Rate of Climb Acceleration Correction
D-7	A-37B Drag Polar
D-8	A-37B Thrust Curve
D-9	T-38A Drag Polar
D-10	T-38A Thrust Curve without Afterburn
D-11	T-38A Thrust Curve with Afterburn
D-12	RF-4C Drag Polar
D-13	T-38A Position Error Chart (Flight Test Nose Boom)
D-14	RF-4C Position Error Chart (Compensated Nose Boom)

RATE OF TURN VS V_{TRUE}



RATE OF TURN VS V_{TRUE}

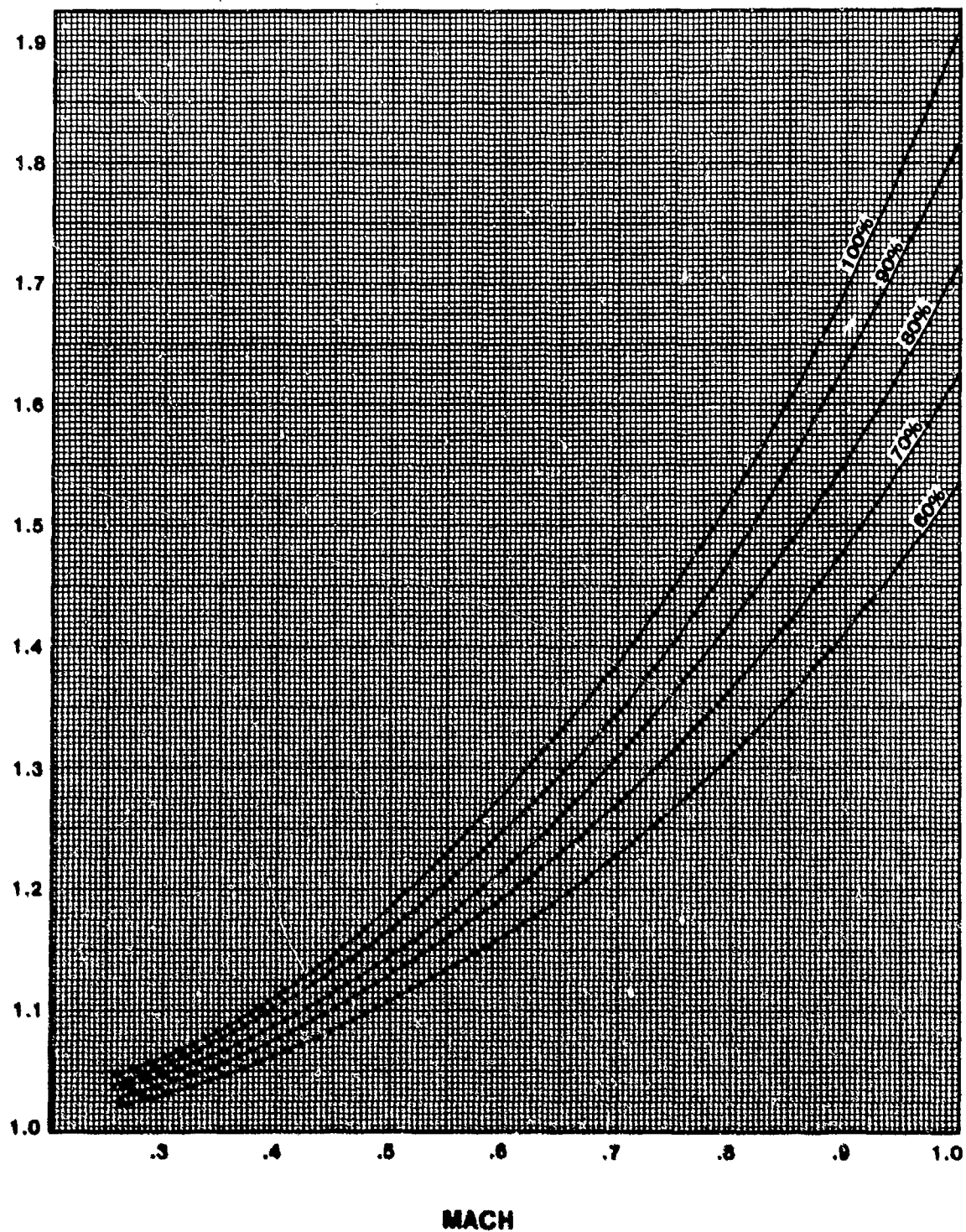


RAM PRESSURE RATIO VS MACH

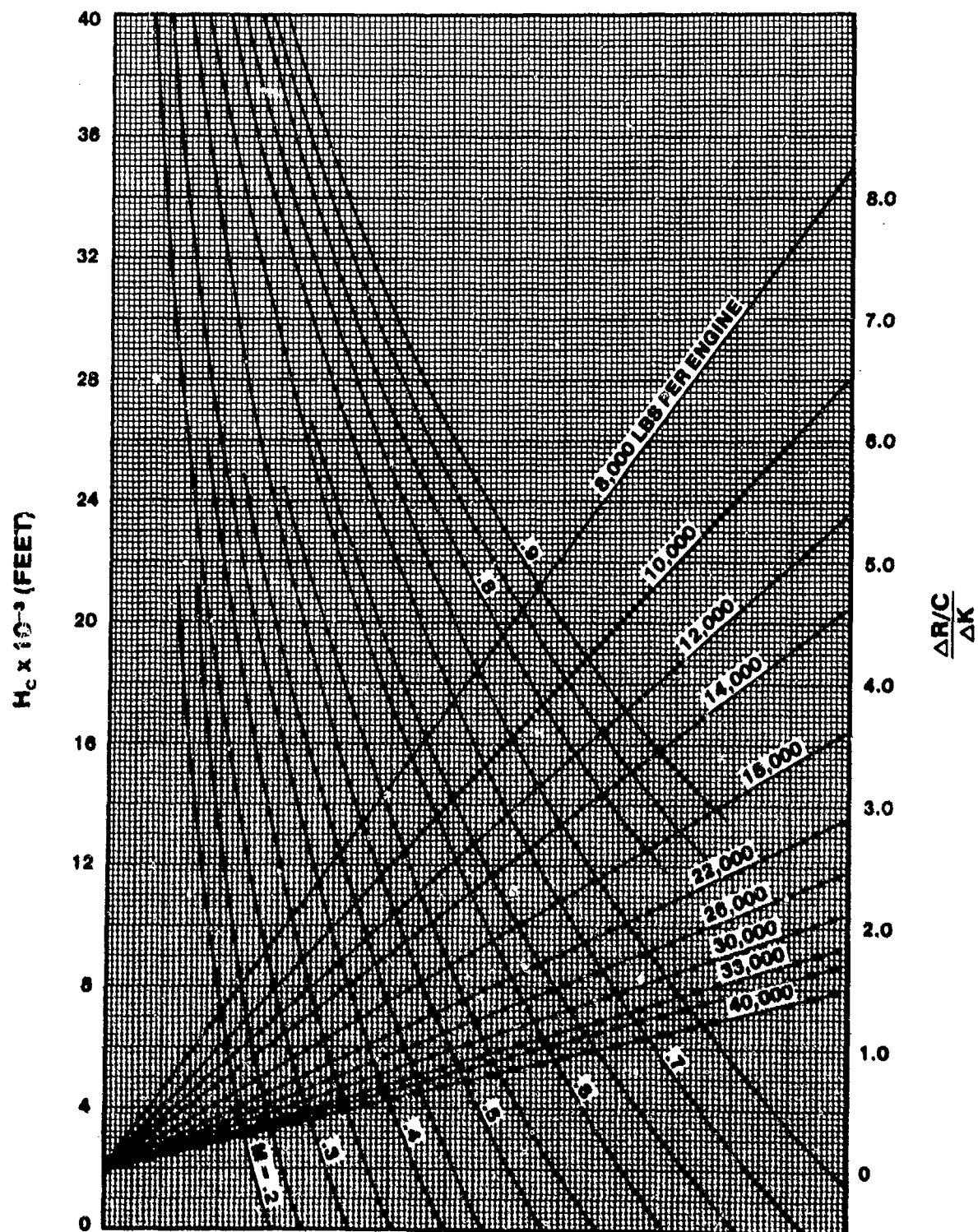
$$P_o/P_a = [1 + 0.2(M)^2]^{3.5}$$

$$\% \text{ RAM} = \frac{P_{o\text{ACT}} - P_a}{P_{o\text{THEO}} - P_a}$$

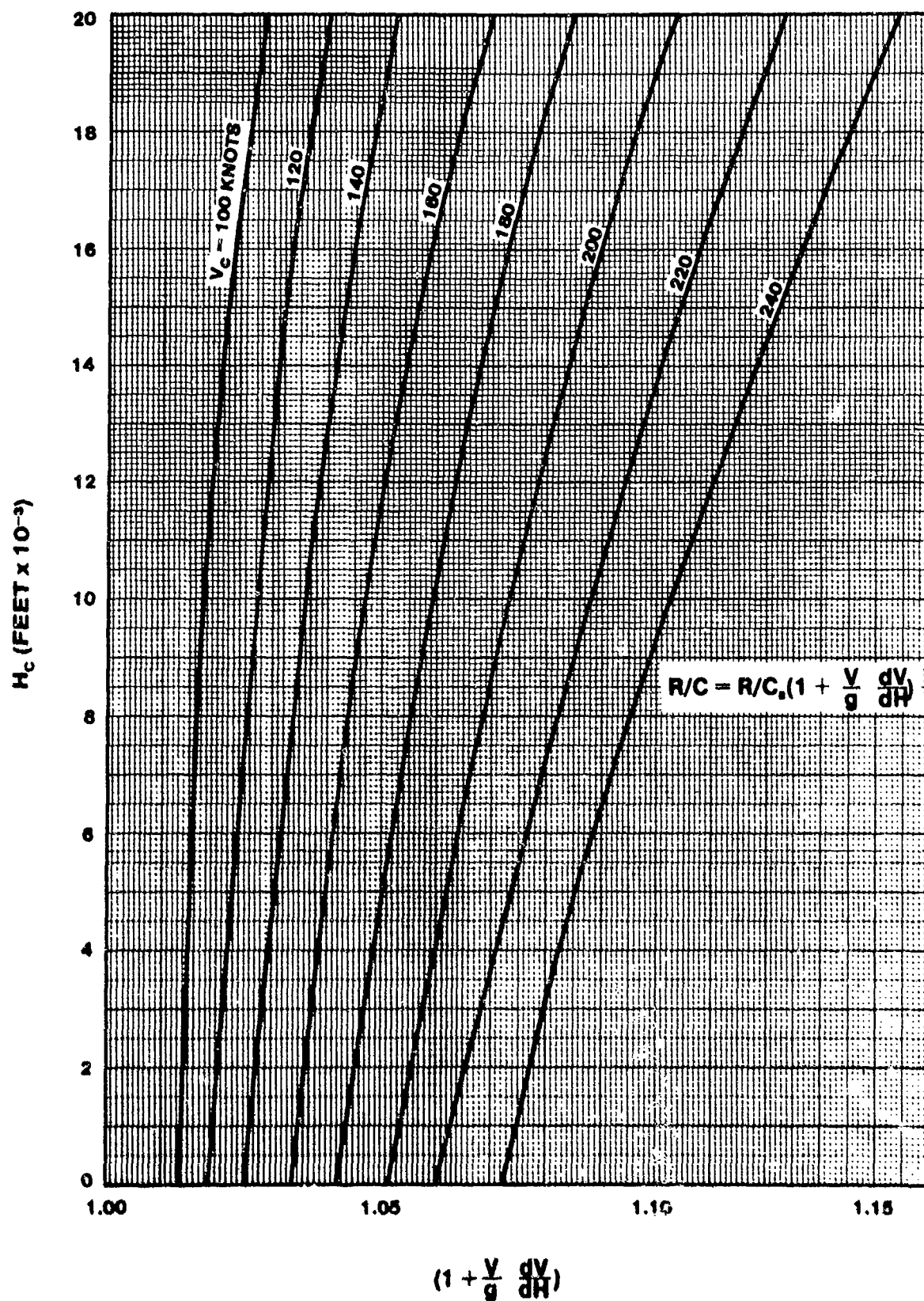
$P_{\text{RAM}}/P_{\text{AMB}} = P/P_a - P_o/P_a$

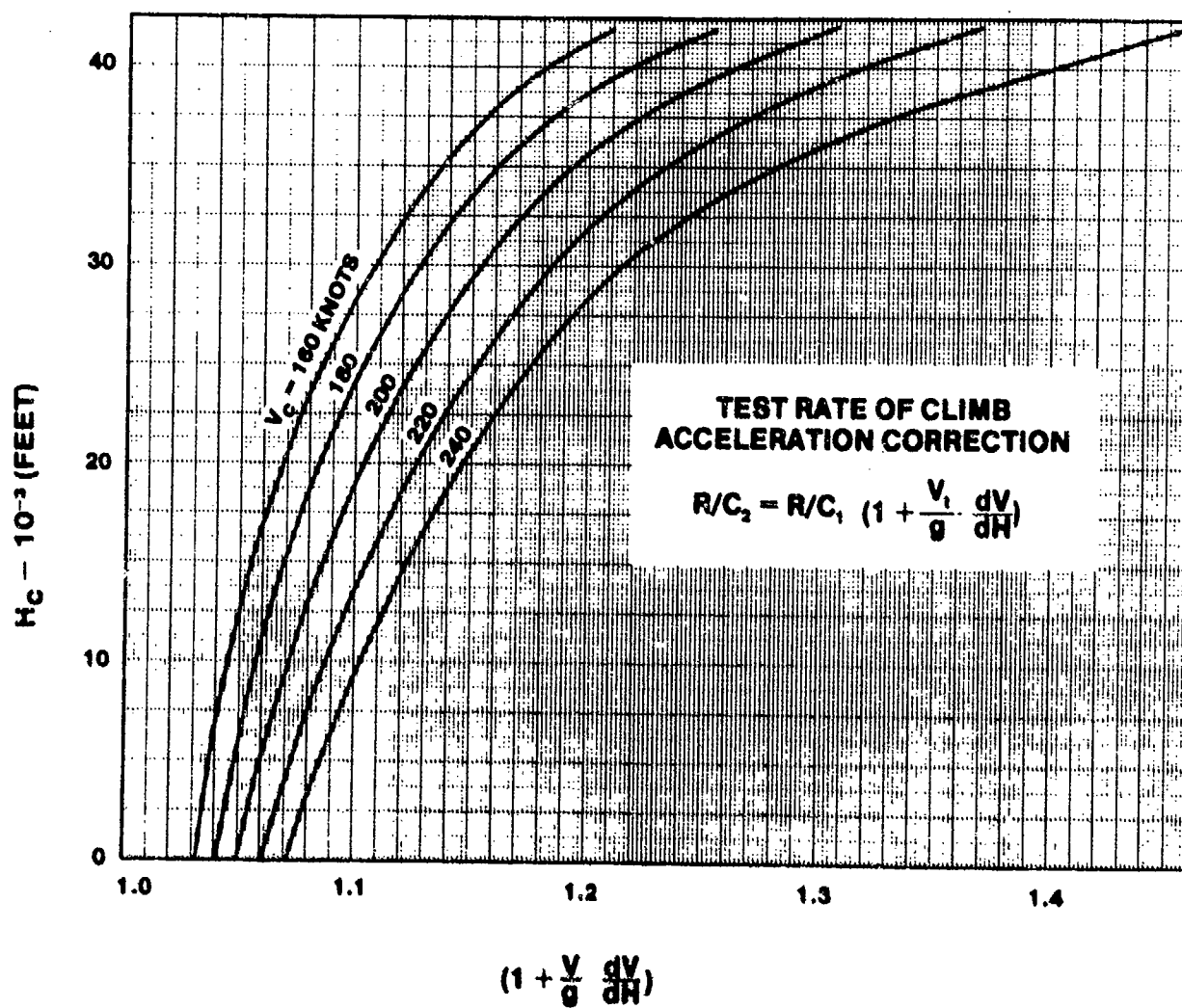


DELTA RATE OF CLIMB FACTOR FOR ALL TURBO-JET ENGINES WITH RAM EFFICIENCIES OF .70 TO 1.0

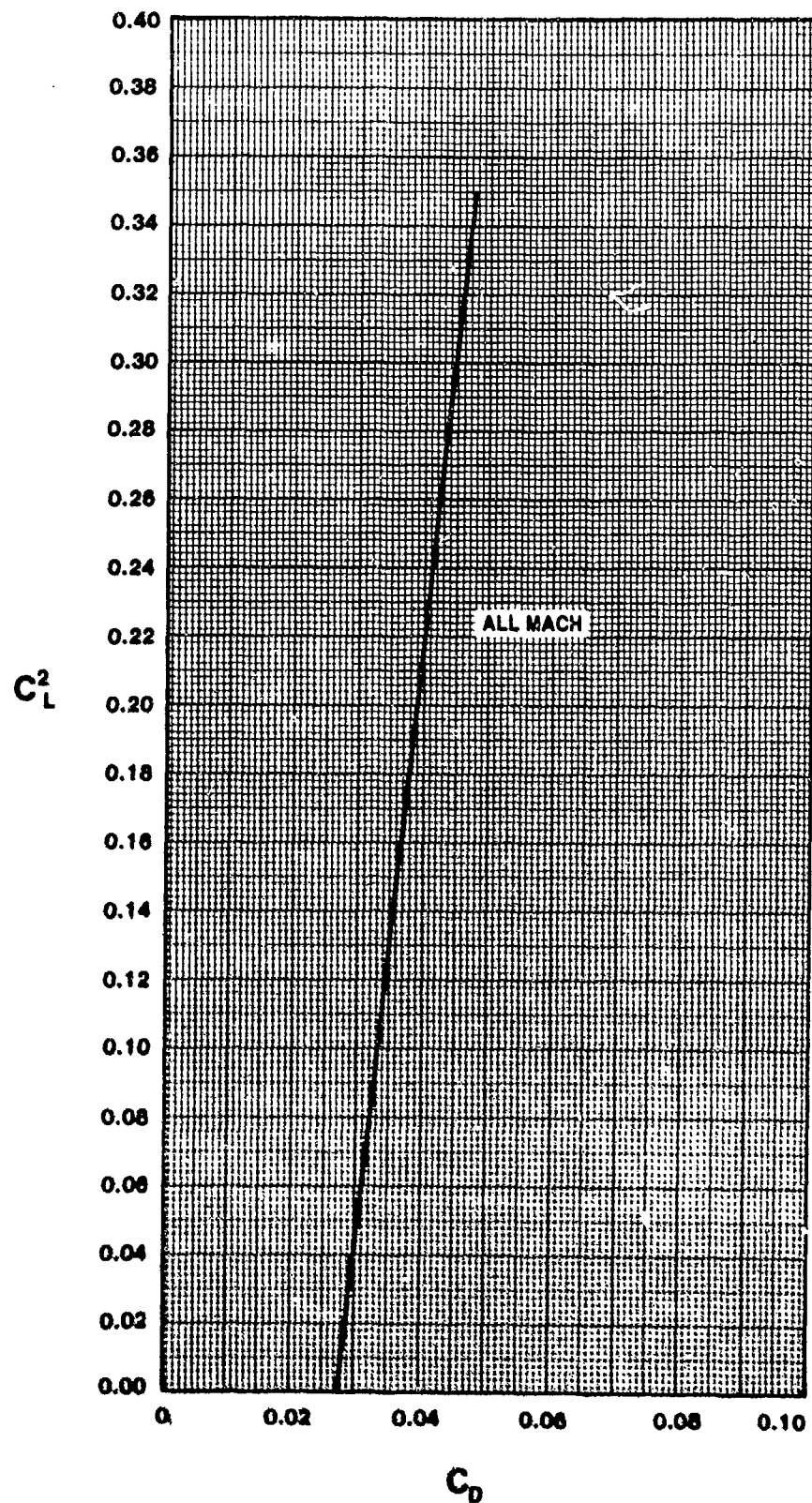


TEST RATE OF CLIMB ACCELERATION CORRECTION

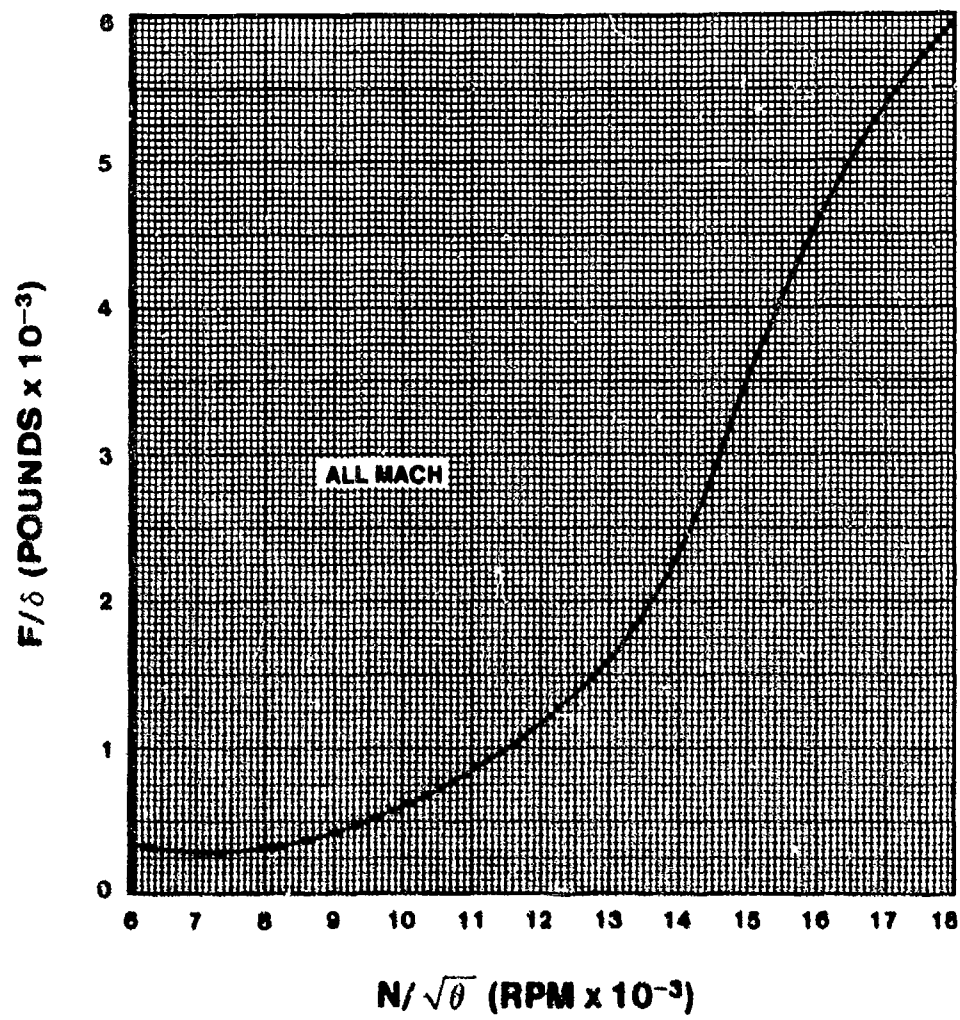




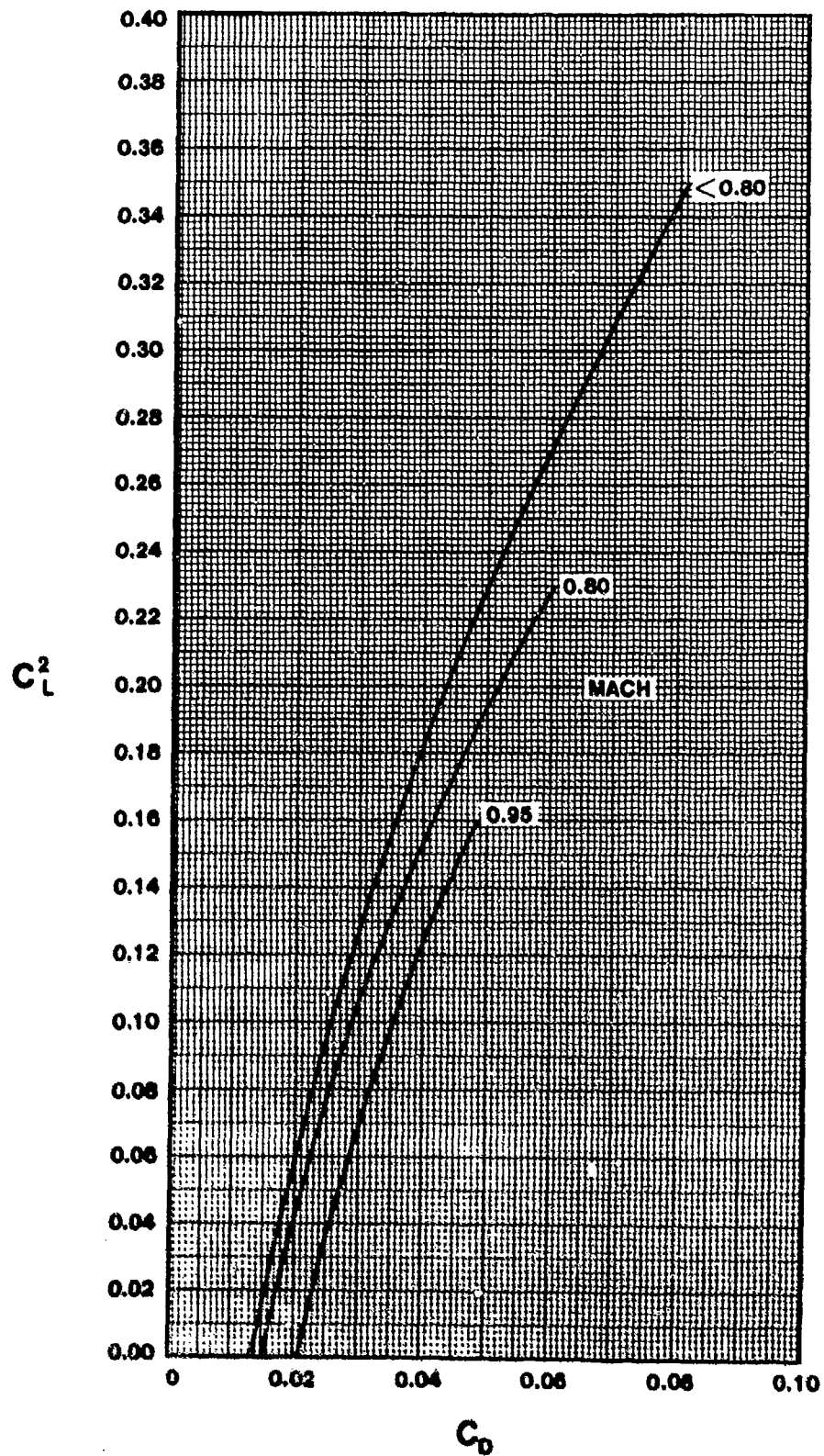
A-37B DRAG POLAR TWO J85-17A ENGINES CRUISE CONFIGURATION



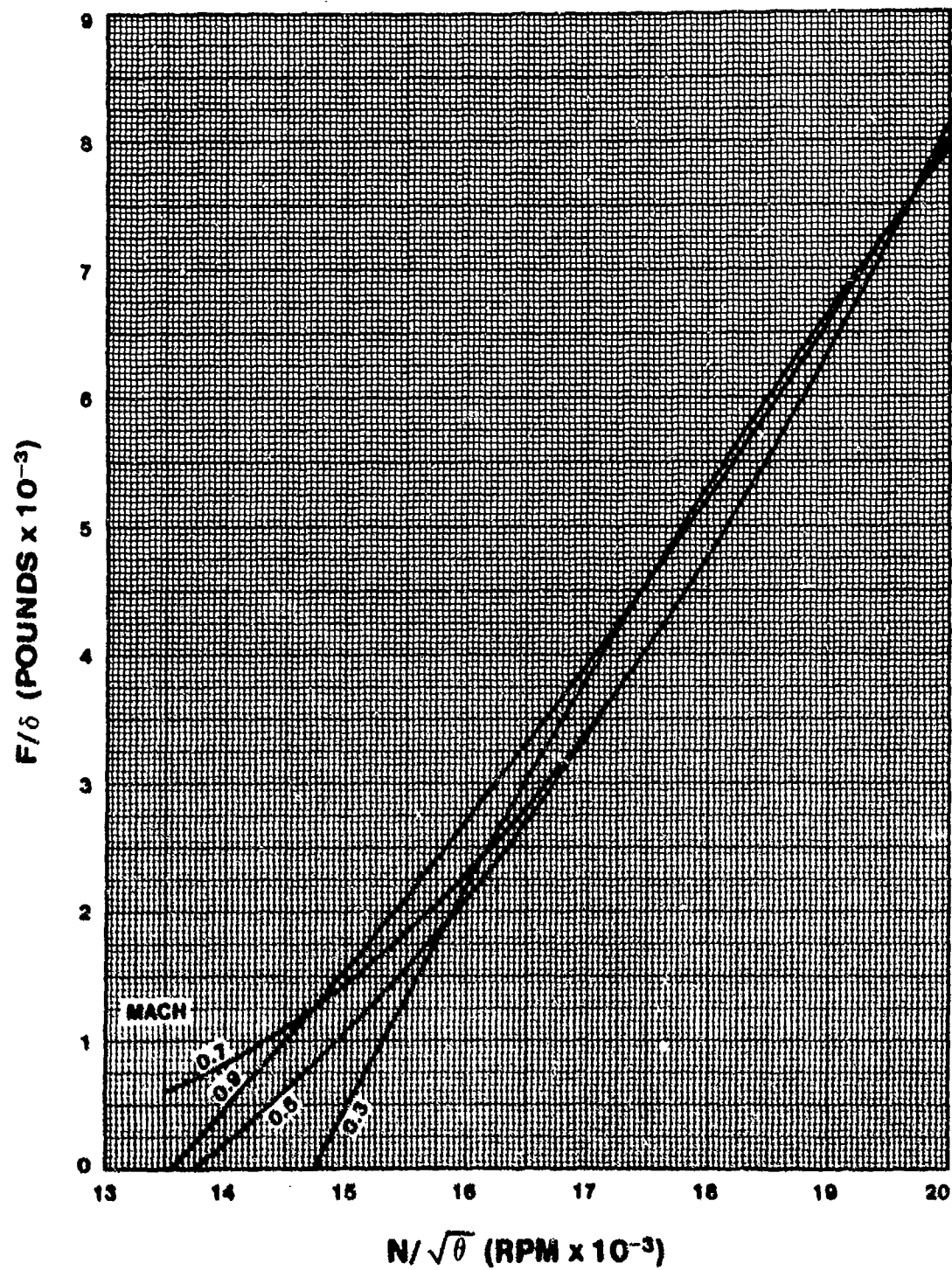
A-37B THRUST CURVE TWO J85-17A ENGINES



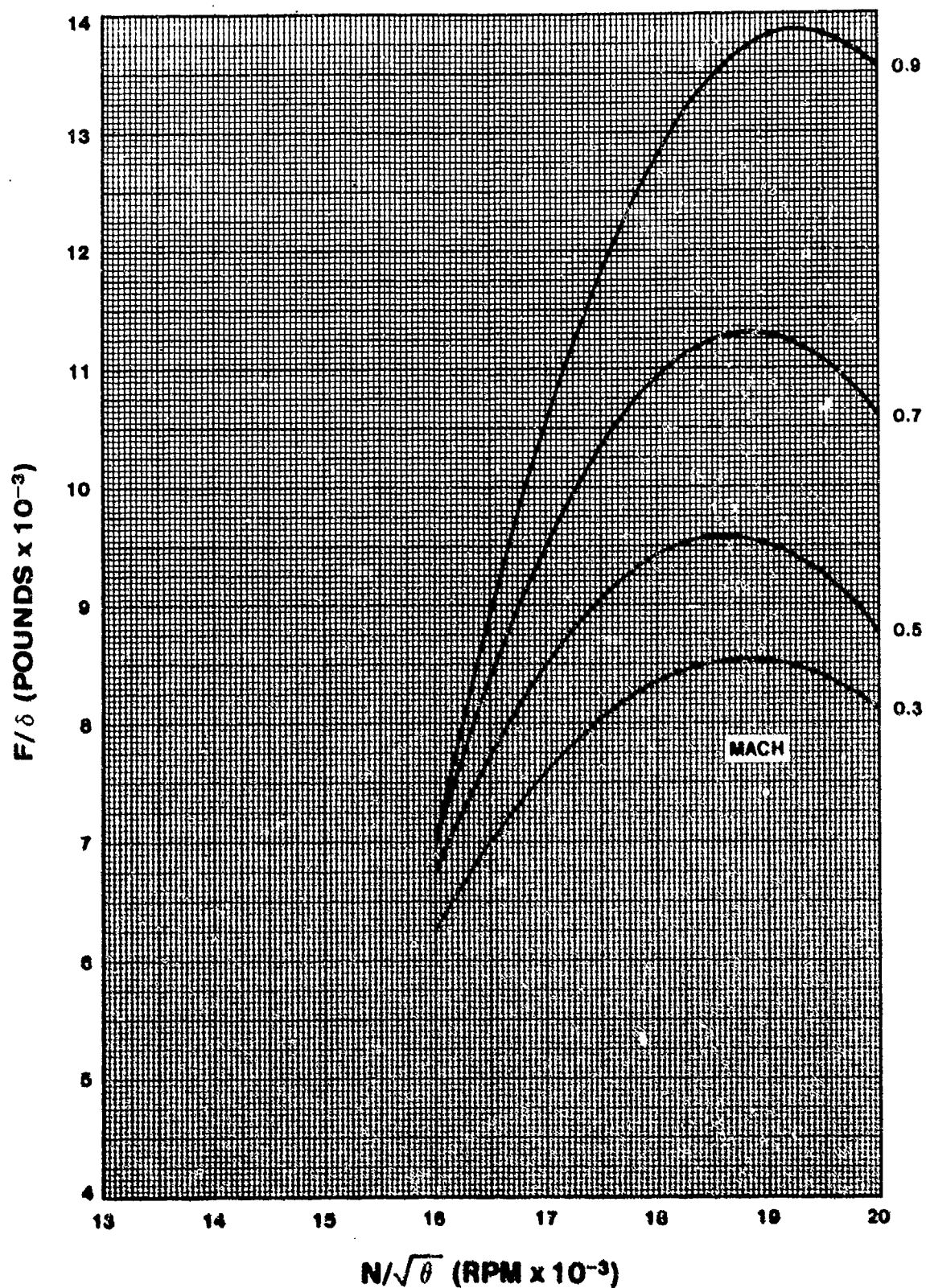
T-38A DRAG POLAR TWO J85-GE-5A ENGINES CRUISE CONFIGURATION



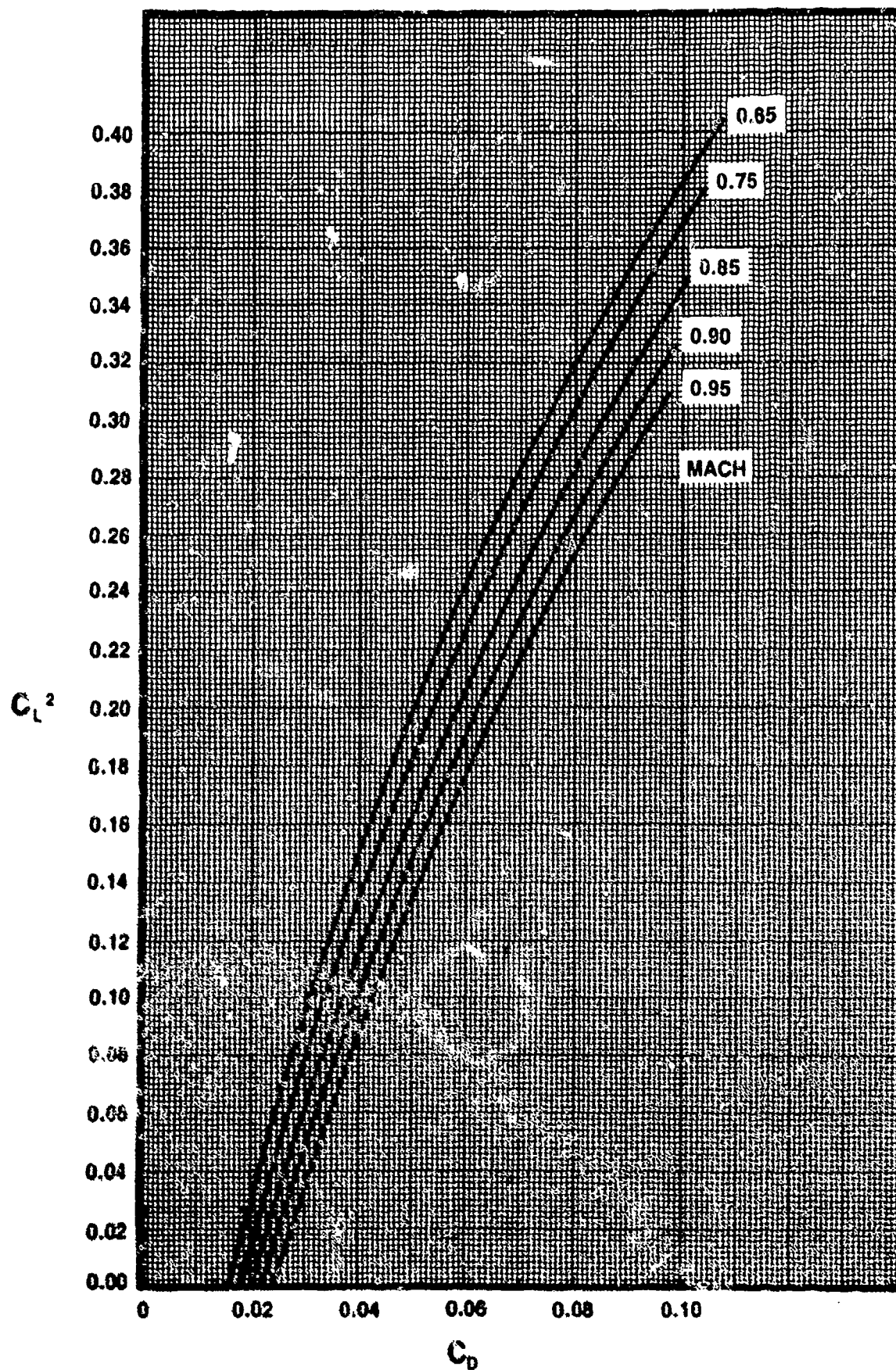
T-38A THRUST CURVE WITHOUT AFTERBURNER TWO J85-GE-5A ENGINES



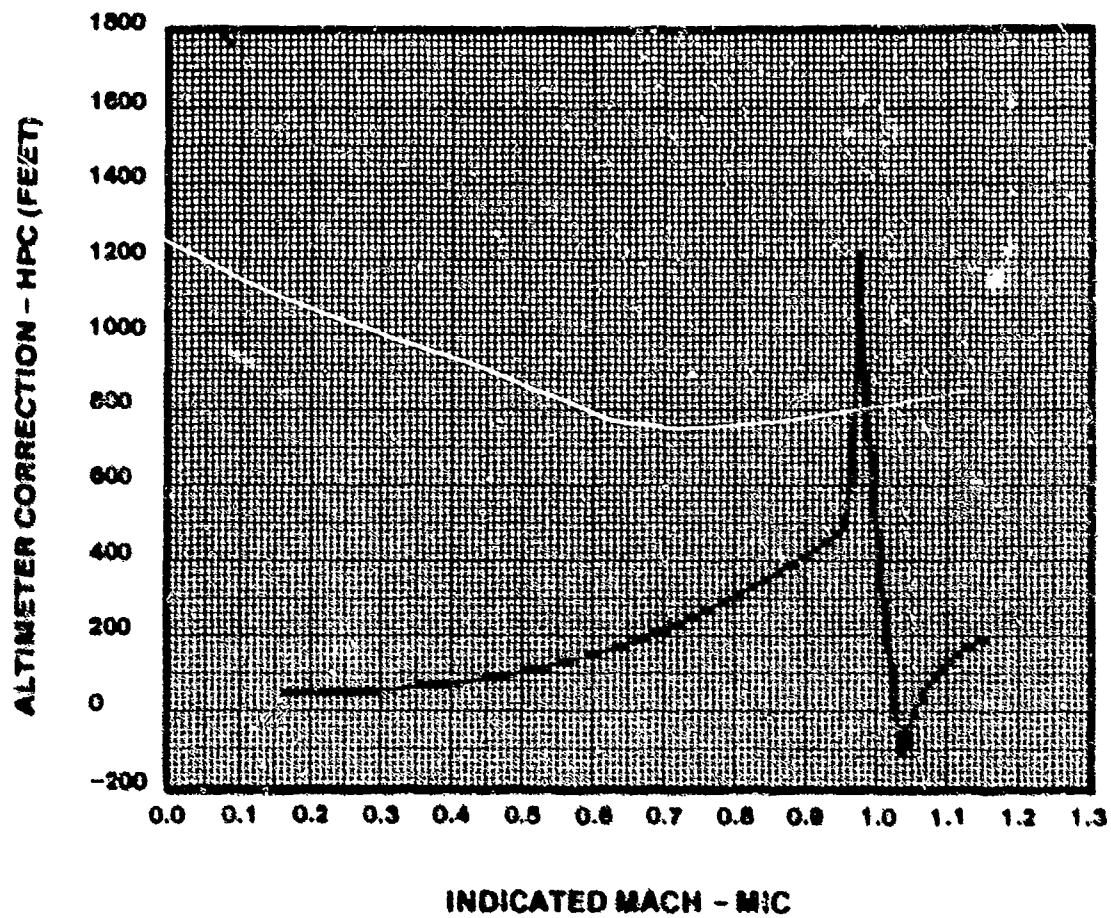
T-38A THRUST CURVE WITH AFTERBURNER TWO J85-GE-5A ENGINES



RF-4C DRAG POLAR PLOT

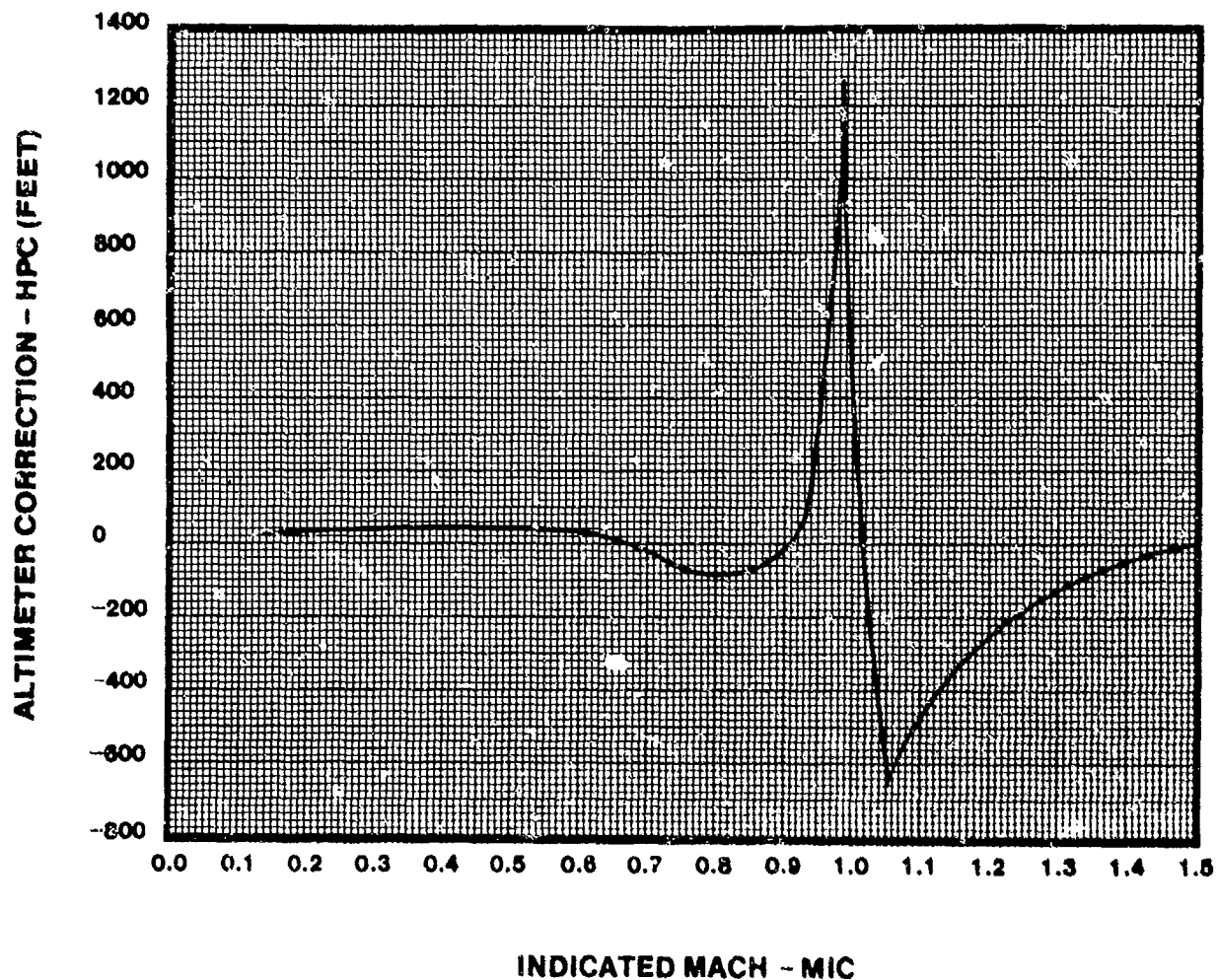


USAF TPS PITOT-STATIC CALIBRATION
T-38A AIRCRAFT
COCKPIT AND MAGTAPE
YAPS HEAD PITOT-STATIC SYSTEM



ALTIMETER POSITION ERROR CORRECTION

USAF TPS PITOT-STATIC CALIBRATION
 RF-4C AIRCRAFT
 COCKPIT AND MAGTAPE
 STANDARD PITOT-STATIC SYSTEM



ALTIMETER POSITION ERROR CORRECTION

APPENDIX E
DISTRIBUTION TABLES

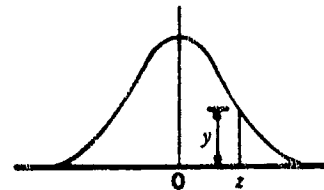
APPENDIX E
DISTRIBUTION TABLES

<u>PAGE</u>	<u>TITLE</u>
E-1	Ordinates (y) of the Standard Normal Curve at Z
E-2	Areas Under the Standard Normal Curve from 0 to Z
E-3	Percentile Values (t_p) for Student's t Distribution with ν Degrees of Freedom
E-4	Percentile Values (χ^2_p) for the Chi-Square Distribution with ν Degrees of Freedom
E-5	95th Percentile Values (0.05 Levels), F.95 for the F Distribution
E-6	99th Percentile Values (0.01 Levels), F.99, for the F Distribution
E-7	97.5th Percentile Values (0.025 Levels), F.975 for the F Distribution
E-8	90% and 95% Confidence Belts for Proportions
E-9	99% Confidence Belts for Proportions
E-10	Signed Rank Test Tables
E-11	Sample Size for Normal Test and for t - Test
E-12	Sample Size for χ^2 Test and for F Test

March 1979

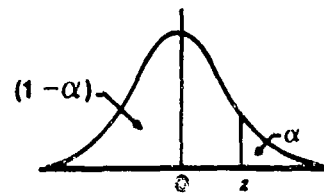
1417

**ORDINATES (y)
OF THE
STANDARD
NORMAL CURVE
AT z**



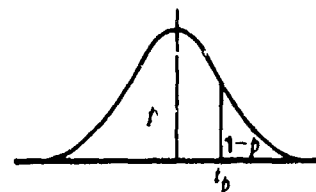
z	0	1	2	3	4	5	6	7	8	9
0.0	.3989	.3989	.3989	.3988	.3986	.3984	.3982	.3980	.3977	.3973
0.1	.3970	.3965	.3961	.3956	.3951	.3945	.3939	.3932	.3925	.3918
0.2	.3910	.3902	.3894	.3885	.3876	.3867	.3857	.3847	.3836	.3825
0.3	.3814	.3802	.3790	.3778	.3765	.3752	.3739	.3725	.3712	.3697
0.4	.3683	.3668	.3653	.3637	.3621	.3605	.3589	.3572	.3555	.3538
0.5	.3521	.3503	.3485	.3467	.3448	.3429	.3410	.3391	.3372	.3352
0.6	.3332	.3312	.3292	.3271	.3251	.3230	.3209	.3187	.3166	.3144
0.7	.3123	.3101	.3079	.3056	.3034	.3011	.2989	.2966	.2943	.2920
0.8	.2897	.2874	.2850	.2827	.2803	.2780	.2756	.2732	.2709	.2685
0.9	.2661	.2637	.2613	.2589	.2565	.2541	.2516	.2492	.2468	.2444
1.0	.2420	.2396	.2371	.2347	.2323	.2299	.2275	.2251	.2227	.2203
1.1	.2179	.2155	.2131	.2107	.2083	.2059	.2036	.2012	.1989	.1965
1.2	.1942	.1919	.1895	.1872	.1849	.1826	.1804	.1781	.1758	.1736
1.3	.1714	.1691	.1669	.1647	.1626	.1604	.1582	.1561	.1539	.1518
1.4	.1497	.1476	.1456	.1435	.1415	.1394	.1374	.1354	.1334	.1315
1.5	.1295	.1276	.1257	.1238	.1219	.1200	.1182	.1163	.1145	.1127
1.6	.1109	.1092	.1074	.1057	.1040	.1023	.1006	.0989	.0973	.0957
1.7	.0940	.0925	.0909	.0893	.0878	.0863	.0848	.0833	.0818	.0804
1.8	.0790	.0775	.0761	.0748	.0734	.0721	.0707	.0694	.0681	.0669
1.9	.0656	.0644	.0632	.0620	.0608	.0596	.0584	.0573	.0562	.0551
2.0	.0540	.0529	.0519	.0508	.0498	.0488	.0478	.0468	.0459	.0449
2.1	.0440	.0431	.0422	.0413	.0404	.0396	.0387	.0379	.0371	.0363
2.2	.0355	.0347	.0339	.0332	.0325	.0317	.0310	.0303	.0297	.0290
2.3	.0283	.0277	.0270	.0264	.0258	.0252	.0246	.0241	.0235	.0229
2.4	.0224	.0219	.0213	.0208	.0203	.0198	.0194	.0189	.0184	.0180
2.5	.0175	.0171	.0167	.0163	.0158	.0154	.0151	.0147	.0143	.0139
2.6	.0136	.0132	.0129	.0126	.0122	.0119	.0116	.0113	.0110	.0107
2.7	.0104	.0101	.0099	.0096	.0093	.0091	.0088	.0086	.0084	.0081
2.8	.0079	.0077	.0075	.0073	.0071	.0069	.0067	.0065	.0063	.0061
2.9	.0060	.0058	.0056	.0055	.0053	.0051	.0050	.0048	.0047	.0046
3.0	.0044	.0043	.0042	.0040	.0039	.0038	.0037	.0036	.0035	.0034
3.1	.0033	.0032	.0031	.0030	.0029	.0028	.0027	.0026	.0025	.0025
3.2	.0024	.0023	.0022	.0022	.0021	.0020	.0020	.0019	.0018	.0018
3.3	.0017	.0017	.0016	.0016	.0015	.0015	.0014	.0014	.0013	.0013
3.4	.0012	.0012	.0012	.0011	.0011	.0010	.0010	.0010	.0009	.0009
3.5	.0009	.0008	.0008	.0008	.0008	.0007	.0007	.0007	.0007	.0006
3.6	.0006	.0006	.0006	.0006	.0005	.0005	.0005	.0005	.0005	.0004
3.7	.0004	.0004	.0004	.0004	.0004	.0004	.0003	.0003	.0003	.0003
3.8	.0003	.0003	.0003	.0003	.0003	.0002	.0002	.0002	.0002	.0002
3.9	.0002	.0002	.0002	.0002	.0002	.0002	.0002	.0002	.0001	.0001

**AREAS
UNDER THE
STANDARD
NORMAL CURVE
FROM 0 TO z**



z	0	1	2	3	4	5	6	7	8	9
0.0	.0000	.0040	.0080	.0120	.0160	.0199	.0239	.0279	.0319	.0359
0.1	.0398	.0438	.0478	.0517	.0557	.0596	.0636	.0675	.0714	.0754
0.2	.0793	.0832	.0871	.0910	.0948	.0987	.1026	.1064	.1103	.1141
0.3	.1179	.1217	.1255	.1293	.1331	.1368	.1406	.1443	.1480	.1517
0.4	.1554	.1591	.1628	.1664	.1700	.1736	.1772	.1808	.1844	.1879
0.5	.1915	.1950	.1985	.2019	.2054	.2088	.2123	.2157	.2190	.2224
0.6	.2258	.2291	.2324	.2357	.2389	.2422	.2454	.2486	.2518	.2549
0.7	.2580	.2612	.2642	.2673	.2704	.2734	.2764	.2794	.2823	.2852
0.8	.2881	.2910	.2939	.2967	.2996	.3023	.3051	.3078	.3106	.3133
0.9	.3159	.3186	.3212	.3238	.3264	.3289	.3315	.3340	.3365	.3389
1.0	.3413	.3438	.3461	.3485	.3508	.3531	.3554	.3577	.3599	.3621
1.1	.3643	.3665	.3686	.3708	.3729	.3749	.3770	.3790	.3810	.3830
1.2	.3849	.3869	.3888	.3907	.3925	.3944	.3962	.3980	.3997	.4015
1.3	.4032	.4049	.4066	.4082	.4099	.4115	.4131	.4147	.4162	.4177
1.4	.4192	.4207	.4222	.4236	.4251	.4265	.4279	.4292	.4306	.4319
1.5	.4332	.4345	.4357	.4370	.4382	.4394	.4406	.4418	.4429	.4441
1.6	.4452	.4463	.4474	.4484	.4495	.4505	.4515	.4525	.4535	.4545
1.7	.4554	.4564	.4573	.4582	.4591	.4599	.4608	.4616	.4625	.4633
1.8	.4641	.4649	.4656	.4664	.4671	.4678	.4686	.4693	.4699	.4706
1.9	.4713	.4719	.4726	.4732	.4738	.4744	.4750	.4756	.4761	.4767
2.0	.4772	.4778	.4783	.4788	.4793	.4798	.4803	.4808	.4812	.4817
2.1	.4821	.4826	.4830	.4834	.4838	.4842	.4846	.4850	.4854	.4857
2.2	.4861	.4864	.4868	.4871	.4875	.4878	.4881	.4884	.4887	.4890
2.3	.4893	.4896	.4898	.4901	.4904	.4906	.4909	.4911	.4913	.4916
2.4	.4918	.4920	.4922	.4925	.4927	.4929	.4931	.4932	.4934	.4936
2.5	.4938	.4940	.4941	.4943	.4945	.4946	.4948	.4949	.4951	.4952
2.6	.4953	.4955	.4956	.4957	.4959	.4960	.4961	.4962	.4963	.4964
2.7	.4965	.4966	.4967	.4968	.4969	.4970	.4971	.4972	.4973	.4974
2.8	.4974	.4975	.4976	.4977	.4977	.4978	.4979	.4979	.4980	.4981
2.9	.4981	.4982	.4982	.4983	.4984	.4984	.4985	.4985	.4986	.4986
3.0	.4987	.4987	.4987	.4988	.4988	.4989	.4989	.4989	.4990	.4990
3.1	.4990	.4991	.4991	.4991	.4992	.4992	.4992	.4992	.4993	.4993
3.2	.4993	.4993	.4994	.4994	.4994	.4994	.4994	.4995	.4995	.4995
3.3	.4995	.4995	.4995	.4996	.4996	.4996	.4996	.4996	.4996	.4997
3.4	.4997	.4997	.4997	.4997	.4997	.4997	.4997	.4997	.4997	.4998
3.5	.4998	.4998	.4998	.4998	.4998	.4998	.4998	.4998	.4998	.4998
3.6	.4998	.4998	.4999	.4999	.4999	.4999	.4999	.4999	.4999	.4999
3.7	.4999	.4999	.4999	.4999	.4999	.4999	.4999	.4999	.4999	.4999
3.8	.4999	.4999	.4999	.4999	.4999	.4999	.4999	.4999	.4999	.4999
3.9	.5000	.5000	.5000	.5000	.5000	.5000	.5000	.5000	.5000	.5000

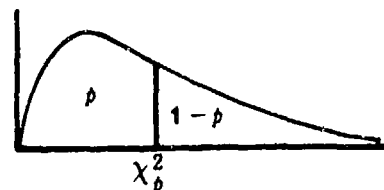
**PERCENTILE VALUES (t_p)
FOR
STUDENT'S t DISTRIBUTION
WITH ν DEGREES OF FREEDOM**



ν	$t_{.55}$	$t_{.60}$	$t_{.70}$	$t_{.75}$	$t_{.80}$	$t_{.90}$	$t_{.95}$	$t_{.975}$	$t_{.99}$	$t_{.995}$
1	.158	.325	.727	1.000	1.376	3.08	6.31	12.71	31.82	63.66
2	.142	.289	.617	.816	1.061	1.89	2.92	4.30	6.96	9.92
3	.137	.277	.584	.765	.978	1.64	2.35	3.18	4.54	5.84
4	.134	.271	.569	.741	.941	1.53	2.13	2.78	3.75	4.60
5	.132	.267	.559	.727	.920	1.48	2.02	2.57	3.36	4.03
6	.131	.265	.553	.718	.906	1.44	1.94	2.45	3.14	3.71
7	.130	.263	.549	.711	.896	1.42	1.90	2.36	3.00	3.50
8	.130	.262	.546	.706	.889	1.40	1.86	2.31	2.90	3.36
9	.129	.261	.543	.703	.883	1.38	1.83	2.26	2.82	3.25
10	.129	.260	.542	.700	.879	1.37	1.81	2.23	2.76	3.17
11	.129	.260	.540	.697	.876	1.36	1.80	2.20	2.72	3.11
12	.128	.259	.539	.695	.873	1.36	1.78	2.18	2.68	3.06
13	.128	.259	.538	.694	.870	1.35	1.77	2.16	2.65	3.01
14	.128	.258	.537	.692	.868	1.34	1.76	2.14	2.62	2.98
15	.128	.258	.536	.691	.866	1.34	1.75	2.13	2.60	2.95
16	.128	.258	.535	.690	.865	1.34	1.75	2.12	2.58	2.92
17	.128	.257	.534	.689	.863	1.33	1.74	2.11	2.57	2.90
18	.127	.257	.534	.688	.862	1.33	1.73	2.10	2.55	2.88
19	.127	.257	.533	.688	.861	1.33	1.73	2.09	2.54	2.86
20	.127	.257	.533	.687	.860	1.32	1.72	2.09	2.53	2.84
21	.127	.257	.532	.686	.859	1.32	1.72	2.08	2.52	2.83
22	.127	.256	.532	.686	.858	1.32	1.72	2.07	2.51	2.82
23	.127	.256	.532	.685	.858	1.32	1.71	2.07	2.50	2.81
24	.127	.256	.531	.685	.857	1.32	1.71	2.06	2.49	2.80
25	.127	.256	.531	.684	.856	1.32	1.71	2.06	2.48	2.79
26	.127	.256	.531	.684	.856	1.32	1.71	2.06	2.48	2.78
27	.127	.256	.531	.684	.855	1.31	1.70	2.05	2.47	2.77
28	.127	.256	.530	.683	.855	1.31	1.70	2.05	2.47	2.76
29	.127	.256	.530	.683	.854	1.31	1.70	2.04	2.46	2.76
30	.127	.256	.530	.683	.854	1.31	1.70	2.04	2.46	2.75
40	.126	.255	.529	.681	.851	1.30	1.68	2.02	2.42	2.70
60	.126	.254	.527	.679	.848	1.30	1.67	2.00	2.39	2.66
120	.126	.254	.526	.677	.845	1.29	1.66	1.98	2.36	2.62
∞	.126	.253	.524	.674	.842	1.28	1.645	1.96	2.33	2.58

Source: R. A. Fisher and F. Yates, *Statistical Tables for Biological, Agricultural and Medical Research*, published by Longman Group Ltd., London (previously published by Oliver and Boyd, Edinburgh), and by permission of the authors and publishers.

**PERCENTILE VALUES (χ^2_p)
FOR THE
CHI-SQUARE DISTRIBUTION
WITH ν DEGREES OF FREEDOM**



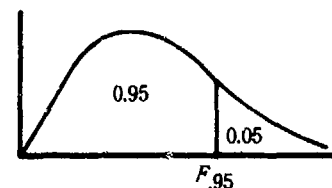
ν	$\chi^2_{.005}$	$\chi^2_{.01}$	$\chi^2_{.025}$	$\chi^2_{.05}$	$\chi^2_{.10}$	$\chi^2_{.25}$	$\chi^2_{.50}$	$\chi^2_{.75}$	$\chi^2_{.90}$	$\chi^2_{.95}$	$\chi^2_{.975}$	$\chi^2_{.99}$	$\chi^2_{.995}$	$\chi^2_{.999}$
1	.0000	.0002	.0010	.0039	.0158	.102	.455	1.32	2.71	3.84	5.02	6.63	7.88	10.8
2	.0100	.0201	.0506	.103	.211	.575	1.39	2.77	4.61	5.99	7.38	9.21	10.6	13.8
3	.0717	.115	.216	.352	.584	1.21	2.37	4.11	6.25	7.81	9.35	11.3	12.8	16.3
4	.207	.297	.484	.711	1.06	1.92	3.36	5.39	7.78	9.49	11.1	13.3	14.9	18.5
5	.412	.554	.831	1.15	1.61	2.67	4.35	6.63	9.24	11.1	12.8	15.1	16.7	20.5
6	.676	.872	1.24	1.64	2.20	3.45	5.35	7.84	10.6	12.6	14.4	16.8	18.5	22.5
7	.989	1.24	1.69	2.17	2.83	4.25	6.35	9.04	12.0	14.1	16.0	18.5	20.3	24.3
8	1.34	1.65	2.18	2.73	3.49	5.07	7.34	10.2	13.4	15.5	17.5	20.1	22.0	26.1
9	1.73	2.09	2.70	3.33	4.17	5.90	8.34	11.4	14.7	16.9	19.0	21.7	23.6	27.9
10	2.16	2.56	3.25	3.94	4.87	6.74	9.34	12.5	16.0	18.3	20.5	23.2	25.2	29.6
11	2.60	3.05	3.82	4.57	5.58	7.58	10.3	13.7	17.3	19.7	21.9	24.7	26.8	31.3
12	3.07	3.57	4.40	5.23	6.30	8.44	11.3	14.8	18.5	21.0	23.3	26.2	28.3	32.9
13	3.57	4.11	5.01	5.89	7.04	9.30	12.3	16.0	19.8	22.4	24.7	27.7	29.8	34.5
14	4.07	4.66	5.63	6.57	7.79	10.2	13.3	17.1	21.1	23.7	26.1	29.1	31.3	36.1
15	4.60	5.23	6.26	7.26	8.55	11.0	14.3	18.2	22.3	25.0	27.5	30.6	32.8	37.7
16	5.14	5.81	6.91	7.96	9.31	11.9	15.3	19.4	23.5	26.3	28.8	32.0	34.3	39.3
17	5.70	6.41	7.56	8.67	10.1	12.8	16.3	20.5	24.8	27.6	30.2	33.4	35.7	40.8
18	6.26	7.01	8.23	9.39	10.9	13.7	17.3	21.6	26.0	28.9	31.5	34.8	37.2	42.3
19	6.84	7.63	8.91	10.1	11.7	14.6	18.3	22.7	27.2	30.1	32.9	36.2	38.6	43.8
20	7.43	8.26	9.59	10.9	12.4	15.5	19.3	23.8	28.4	31.4	34.2	37.6	40.0	45.3
21	8.03	8.90	10.3	11.6	13.2	16.3	20.3	24.9	29.6	32.7	35.5	38.9	41.4	46.8
22	8.64	9.54	11.0	12.3	14.0	17.2	21.3	26.0	30.8	33.9	36.8	40.3	42.8	48.3
23	9.26	10.2	11.7	13.1	14.8	18.1	22.3	27.1	32.0	35.2	38.1	41.6	44.2	49.7
24	9.89	10.9	12.4	13.8	15.7	19.0	23.3	28.2	33.2	36.4	39.4	43.0	45.6	51.2
25	10.5	11.5	13.1	14.6	16.5	19.9	24.3	29.3	34.4	37.7	40.6	44.3	46.9	52.6
26	11.2	12.2	13.8	15.4	17.3	20.8	25.3	30.4	35.6	38.9	41.9	45.6	48.3	54.1
27	11.8	12.9	14.6	16.2	18.1	21.7	26.3	31.5	36.7	40.1	43.2	47.0	49.6	55.5
28	12.5	13.6	15.3	16.9	18.9	22.7	27.3	32.6	37.9	41.3	44.5	48.3	51.0	56.9
29	13.1	14.3	16.0	17.7	19.8	23.6	28.3	33.7	39.1	42.6	45.7	49.5	52.3	58.3
30	13.8	15.0	16.8	18.5	20.6	24.5	29.3	34.8	40.3	43.8	47.0	50.9	53.7	59.7
40	20.7	22.2	24.4	26.5	29.1	33.7	39.3	45.6	51.8	55.8	59.3	63.7	66.8	73.4
50	28.0	29.7	32.4	34.8	37.7	42.9	49.3	56.3	63.2	67.5	71.4	76.2	79.5	86.7
60	35.5	37.5	40.5	43.2	46.5	52.3	59.3	67.0	74.4	79.1	83.3	88.1	92.0	99.6
70	43.3	45.4	48.8	51.7	55.3	61.7	69.3	77.6	85.5	90.5	95.0	100	104	112
80	51.2	53.5	57.2	60.4	64.3	71.1	79.3	88.1	96.6	102	107	112	116	125
90	59.2	61.8	65.6	69.1	73.3	80.6	89.3	98.6	108	113	118	124	128	137
100	67.3	70.1	74.2	77.9	82.4	90.1	99.3	109	118	124	130	136	140	149

Source: E. S. Pearson and H. O. Hartley, *Biometrika Tables for Statisticians*, Vol. 1 (1966), Table A, pages 137 and 138, by permission.

**95TH PERCENTILE VALUES (0.05 LEVELS), $F_{.95}$,
FOR THE
F DISTRIBUTION**

ν_1 DEGREES OF FREEDOM IN NUMERATOR

ν_2 DEGREES OF FREEDOM IN DENOMINATOR



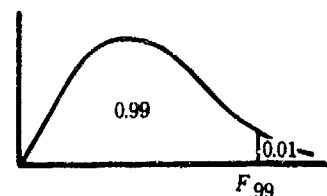
$\nu_2 \backslash \nu_1$	1	2	3	4	5	6	7	8	9	10	12	15	20	24	30	40	60	120	∞
1	161	200	216	225	230	234	237	239	241	242	244	246	248	249	250	251	252	253	254
2	18.5	19.0	19.2	19.2	19.3	19.3	19.4	19.4	19.4	19.4	19.4	19.4	19.4	19.5	19.5	19.5	19.5	19.5	19.5
3	10.1	9.55	9.28	9.12	9.01	8.94	8.89	8.85	8.81	8.79	8.74	8.70	8.66	8.64	8.62	8.59	8.57	8.55	8.53
4	7.71	6.94	6.59	6.39	6.26	6.16	6.09	6.04	6.00	5.96	5.91	5.86	5.80	5.77	5.75	5.72	5.69	5.66	5.63
5	6.61	5.79	5.41	5.19	5.05	4.95	4.88	4.82	4.77	4.74	4.68	4.62	4.56	4.53	4.50	4.46	4.43	4.40	4.37
6	5.99	5.14	4.76	4.53	4.39	4.28	4.21	4.15	4.10	4.06	4.00	3.94	3.87	3.84	3.81	3.77	3.74	3.70	3.67
7	5.59	4.74	4.35	4.12	3.97	3.87	3.79	3.73	3.68	3.64	3.57	3.51	3.44	3.41	3.38	3.34	3.30	3.27	3.23
8	5.32	4.46	4.07	3.84	3.69	3.58	3.50	3.44	3.39	3.35	3.28	3.22	3.15	3.12	3.08	3.04	3.01	2.97	2.93
9	5.12	4.26	3.86	3.63	3.48	3.37	3.29	3.23	3.18	3.14	3.07	3.01	2.94	2.90	2.86	2.83	2.79	2.75	2.71
10	4.96	4.10	3.71	3.48	3.33	3.22	3.14	3.07	3.02	2.98	2.91	2.85	2.77	2.74	2.70	2.66	2.62	2.58	2.54
11	4.84	3.98	3.59	3.36	3.20	3.09	3.01	2.95	2.90	2.85	2.79	2.72	2.65	2.61	2.57	2.53	2.49	2.45	2.40
12	4.75	3.89	3.49	3.26	3.11	3.00	2.91	2.85	2.80	2.75	2.69	2.62	2.54	2.51	2.47	2.43	2.38	2.34	2.30
13	4.67	3.81	3.41	3.18	3.03	2.92	2.83	2.77	2.71	2.67	2.60	2.53	2.46	2.42	2.38	2.34	2.30	2.25	2.21
14	4.60	3.74	3.34	3.11	2.96	2.85	2.76	2.70	2.65	2.60	2.53	2.46	2.39	2.35	2.31	2.27	2.22	2.18	2.13
15	4.54	3.68	3.29	3.06	2.90	2.79	2.71	2.64	2.59	2.54	2.48	2.40	2.33	2.29	2.25	2.20	2.16	2.11	2.07
16	4.49	3.63	3.24	3.01	2.85	2.74	2.66	2.59	2.54	2.49	2.42	2.35	2.28	2.24	2.19	2.15	2.11	2.06	2.01
17	4.45	3.59	3.20	2.96	2.81	2.70	2.61	2.55	2.49	2.45	2.38	2.31	2.23	2.19	2.15	2.10	2.06	2.01	1.96
18	4.41	3.55	3.16	2.93	2.77	2.66	2.58	2.51	2.46	2.41	2.34	2.27	2.19	2.15	2.11	2.06	2.02	1.97	1.92
19	4.38	3.52	3.13	2.90	2.74	2.63	2.54	2.48	2.42	2.38	2.31	2.23	2.16	2.11	2.07	2.03	1.98	1.93	1.88
20	4.35	3.49	3.10	2.87	2.71	2.60	2.51	2.45	2.39	2.35	2.28	2.20	2.12	2.08	2.04	1.99	1.95	1.90	1.84
21	4.32	3.47	3.07	2.84	2.68	2.57	2.49	2.42	2.37	2.32	2.25	2.18	2.10	2.05	2.01	1.96	1.92	1.87	1.81
22	4.30	3.44	3.05	2.82	2.66	2.55	2.46	2.40	2.34	2.30	2.23	2.15	2.07	2.03	1.98	1.94	1.89	1.84	1.78
23	4.28	3.42	3.03	2.80	2.61	2.53	2.44	2.37	2.32	2.27	2.20	2.13	2.05	2.01	1.96	1.91	1.86	1.81	1.76
24	4.26	3.40	3.01	2.78	2.62	2.51	2.42	2.36	2.30	2.25	2.18	2.11	2.03	1.98	1.94	1.89	1.81	1.79	1.73
25	4.24	3.39	2.99	2.76	2.60	2.49	2.40	2.34	2.28	2.24	2.16	2.09	2.01	1.96	1.92	1.87	1.82	1.77	1.71
26	4.23	3.37	2.98	2.74	2.59	2.47	2.39	2.32	2.27	2.22	2.15	2.07	1.99	1.95	1.90	1.85	1.80	1.75	1.69
27	4.21	3.35	2.96	2.73	2.57	2.46	2.37	2.31	2.25	2.20	2.13	2.06	1.97	1.93	1.88	1.84	1.79	1.73	1.67
28	4.20	3.34	2.95	2.71	2.56	2.45	2.36	2.29	2.24	2.19	2.12	2.04	1.96	1.91	1.87	1.82	1.77	1.71	1.65
29	4.18	3.33	2.93	2.70	2.55	2.43	2.35	2.28	2.22	2.18	2.10	2.03	1.94	1.90	1.85	1.81	1.75	1.70	1.64
30	4.17	3.32	2.92	2.69	2.53	2.42	2.33	2.27	2.21	2.16	2.09	2.01	1.93	1.89	1.84	1.79	1.74	1.68	1.62
40	4.08	3.23	2.84	2.61	2.45	2.34	2.25	2.18	2.12	2.08	2.00	1.92	1.84	1.79	1.74	1.69	1.64	1.58	1.51
60	4.00	3.15	2.76	2.53	2.37	2.25	2.17	2.10	2.04	1.99	1.92	1.84	1.75	1.70	1.65	1.59	1.53	1.47	1.39
120	3.92	3.07	2.68	2.45	2.29	2.18	2.09	2.02	1.96	1.91	1.83	1.75	1.66	1.61	1.55	1.50	1.43	1.35	1.25
∞	3.84	3.00	2.60	2.37	2.21	2.10	2.01	1.94	1.88	1.83	1.75	1.67	1.57	1.52	1.46	1.30	1.32	1.22	1.00

Source: E. S. Pearson and H. O. Hartley, *Biometrika Tables for Statisticians*, Vol. 2 (1972), Table 5, page 179, by permission.

**99TH PERCENTILE VALUES (0.01 LEVELS), $F_{.99}$,
FOR THE
F DISTRIBUTION**

ν_1 DEGREES OF FREEDOM IN NUMERATOR

ν_2 DEGREES OF FREEDOM IN DENOMINATOR



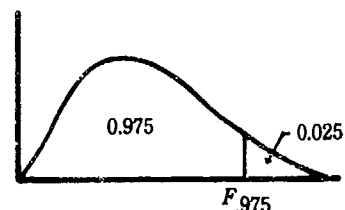
$\nu_2 \backslash \nu_1$	1	2	3	4	5	6	7	8	9	10	12	15	20	24	30	40	60	120	∞
1	4052	5000	5403	5625	5764	5859	5928	5981	6023	6056	6106	6157	6209	6235	6261	6287	6313	6339	6356
2	98.5	99.0	99.2	99.2	99.3	99.3	99.4	99.4	99.4	99.4	99.4	99.4	99.4	99.5	99.5	99.5	99.5	99.5	99.5
3	34.1	30.8	29.5	28.7	28.2	27.9	27.7	27.5	27.3	27.2	27.1	26.9	26.7	26.6	26.5	26.4	26.3	26.2	26.1
4	21.2	18.0	16.7	16.0	15.5	15.2	15.0	14.8	14.7	14.5	14.4	14.2	14.0	13.9	13.8	13.7	13.7	13.6	13.5
5	16.3	13.3	12.1	11.4	11.0	10.7	10.5	10.3	10.2	10.1	9.89	9.72	9.55	9.47	9.38	9.29	9.20	9.11	9.02
6	13.7	10.9	9.78	9.15	8.75	8.47	8.26	8.10	7.98	7.87	7.72	7.56	7.40	7.31	7.23	7.14	7.06	6.97	6.88
7	12.2	9.55	8.45	7.85	7.46	7.19	6.99	6.84	6.72	6.62	6.47	6.31	6.16	6.07	5.99	5.91	5.82	5.74	5.65
8	11.3	8.65	7.59	7.01	6.63	6.37	6.18	6.03	5.91	5.81	5.67	5.52	5.36	5.28	5.20	5.12	5.03	4.95	4.86
9	10.6	8.02	6.99	6.42	6.06	5.80	5.61	5.47	5.35	5.26	5.11	4.96	4.81	4.73	4.65	4.57	4.48	4.40	4.31
10	10.0	7.56	6.55	5.99	5.64	5.39	5.20	5.06	4.94	4.85	4.71	4.56	4.41	4.33	4.25	4.17	4.08	4.00	3.91
11	9.65	7.21	6.22	5.67	5.32	5.07	4.89	4.74	4.63	4.54	4.40	4.25	4.10	4.02	3.94	3.86	3.78	3.69	3.60
12	9.33	6.93	5.95	5.41	5.06	4.82	4.64	4.50	4.39	4.30	4.16	4.01	3.86	3.78	3.70	3.62	3.54	3.45	3.36
13	9.07	6.70	5.74	5.21	4.86	4.62	4.44	4.30	4.19	4.10	3.96	3.82	3.66	3.59	3.51	3.43	3.34	3.25	3.17
14	8.86	6.51	5.56	5.04	4.70	4.46	4.28	4.14	4.03	3.94	3.80	3.66	3.51	3.43	3.35	3.27	3.18	3.09	3.00
15	8.68	6.36	5.42	4.89	4.56	4.32	4.14	4.00	3.89	3.80	3.67	3.52	3.37	3.29	3.21	3.13	3.05	2.96	2.87
16	8.53	6.23	5.29	4.77	4.44	4.20	4.03	3.89	3.78	3.69	3.55	3.41	3.26	3.18	3.10	3.02	2.94	2.84	2.75
17	8.40	6.11	5.19	4.67	4.34	4.10	3.93	3.79	3.68	3.59	3.46	3.31	3.16	3.08	3.00	2.92	2.83	2.75	2.65
18	8.29	6.01	5.09	4.58	4.25	4.01	3.84	3.71	3.60	3.51	3.37	3.23	3.08	3.00	2.92	2.84	2.75	2.66	2.57
19	8.18	5.93	5.01	4.50	4.17	3.94	3.77	3.63	3.52	3.43	3.30	3.15	3.00	2.92	2.84	2.76	2.67	2.58	2.49
20	8.10	5.85	4.94	4.43	4.10	3.87	3.70	3.56	3.46	3.37	3.23	3.09	2.94	2.86	2.78	2.69	2.61	2.52	2.42
21	8.02	5.78	4.87	4.37	4.04	3.81	3.64	3.51	3.40	3.31	3.17	3.03	2.88	2.80	2.72	2.64	2.55	2.46	2.36
22	7.95	5.72	4.82	4.31	3.99	3.76	3.59	3.45	3.35	3.26	3.12	2.98	2.83	2.75	2.67	2.58	2.50	2.40	2.31
23	7.88	5.66	4.76	4.26	3.94	3.71	3.54	3.41	3.30	3.21	3.07	2.93	2.78	2.70	2.62	2.54	2.45	2.35	2.26
24	7.82	5.61	4.72	4.22	3.90	3.67	3.50	3.36	3.26	3.17	3.03	2.89	2.74	2.66	2.58	2.49	2.40	2.31	2.21
25	7.77	5.57	4.68	4.18	3.86	3.63	3.46	3.32	3.22	3.13	2.99	2.85	2.70	2.62	2.54	2.45	2.36	2.27	2.17
26	7.72	5.53	4.64	4.14	3.82	3.59	3.42	3.29	3.18	3.09	2.96	2.82	2.66	2.58	2.50	2.42	2.33	2.23	2.13
27	7.68	5.49	4.60	4.11	3.78	3.56	3.39	3.26	3.15	3.06	2.93	2.78	2.63	2.55	2.47	2.38	2.29	2.20	2.10
28	7.64	5.45	4.57	4.07	3.75	3.53	3.36	3.23	3.12	3.03	2.90	2.75	2.60	2.52	2.44	2.35	2.26	2.17	2.06
29	7.60	5.42	4.54	4.04	3.73	3.50	3.33	3.20	3.09	3.00	2.87	2.73	2.57	2.49	2.41	2.33	2.23	2.14	2.03
30	7.56	5.39	4.51	4.02	3.70	3.47	3.30	3.17	3.07	2.98	2.84	2.70	2.55	2.47	2.39	2.30	2.21	2.11	2.01
40	7.31	5.18	4.31	3.83	3.51	3.29	3.12	2.99	2.89	2.80	2.66	2.52	2.37	2.29	2.20	2.11	2.02	1.92	1.80
60	7.08	4.98	4.13	3.65	3.34	3.12	2.95	2.82	2.72	2.63	2.50	2.35	2.20	2.12	2.03	1.94	1.84	1.73	1.60
120	6.85	4.79	3.95	3.48	3.17	2.96	2.79	2.66	2.56	2.47	2.34	2.19	2.03	1.95	1.86	1.76	1.66	1.53	1.38
∞	6.63	4.61	3.78	3.32	3.02	2.80	2.64	2.51	2.41	2.32	2.18	2.04	1.88	1.79	1.70	1.59	1.47	1.32	1.00

Source: E. S. Pearson and H. O. Hartley, *Biometrika Tables for Statisticians*, Vol. 2 (1972), Table 5, page 180, by permission.

**97.5TH PERCENTILE VALUES (.025 LEVELS), $F_{.975}$,
FOR THE
F DISTRIBUTION**

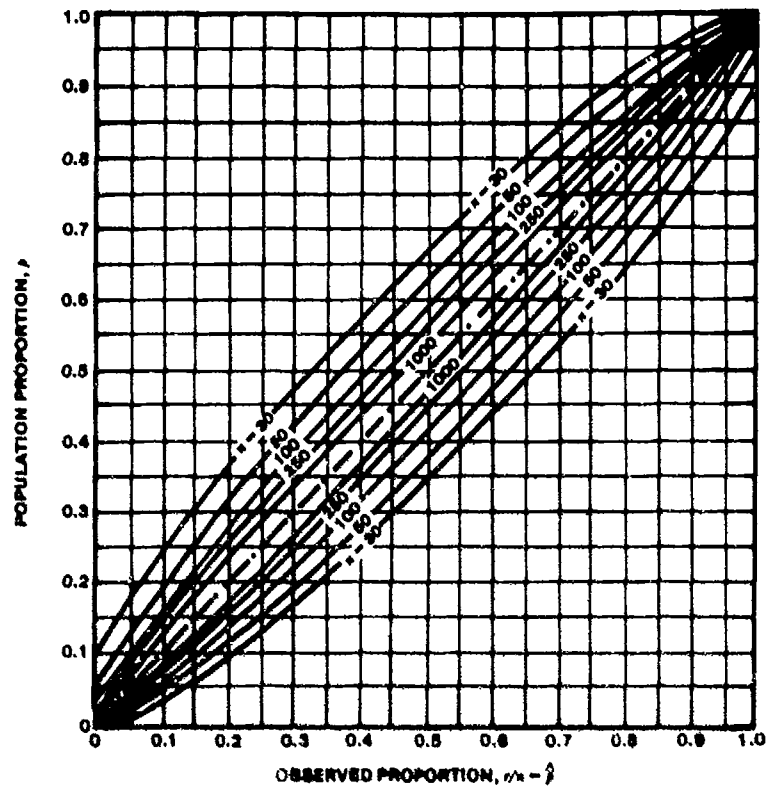
ν_1 DEGREES OF FREEDOM IN NUMERATOR

ν_2 DEGREES OF FREEDOM IN DENOMINATOR

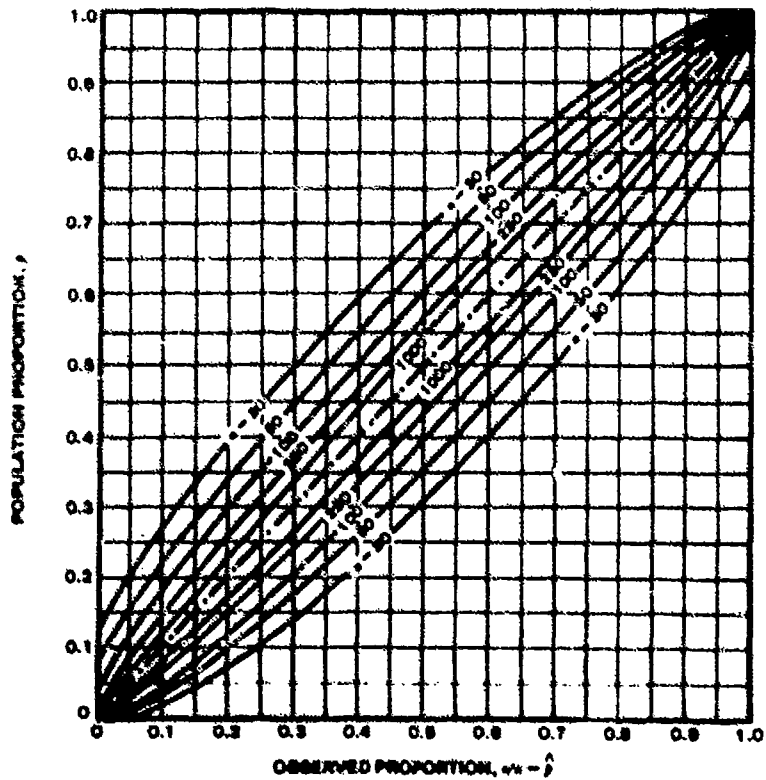


$\nu_1 \backslash \nu_2$	1	2	3	4	5	6	7	8	9	10	12	15	20	24	30	40	60	120	∞
1	647.8	799.5	864.2	899.6	921.8	937.1	948.2	956.7	963.3	968.6	976.7	984.9	993.1	997.2	1001	1006	1010	1014	1018
2	38.51	39.00	39.17	39.25	39.30	39.33	39.36	39.37	39.39	39.40	39.41	39.43	39.45	39.46	39.46	39.47	39.48	39.49	39.50
3	17.44	16.04	15.44	15.10	14.88	14.73	14.62	14.54	14.47	14.42	14.34	14.25	14.17	14.12	14.08	14.04	13.99	13.95	13.90
4	12.22	10.65	9.98	9.60	9.36	9.20	9.07	8.98	8.90	8.84	8.75	8.66	8.56	8.51	8.46	8.41	8.36	8.31	8.26
5	10.01	8.43	7.76	7.39	7.15	6.98	6.85	6.76	6.68	6.62	6.52	6.43	6.33	6.28	6.23	6.18	6.12	6.07	6.02
6	8.81	7.26	6.60	6.23	5.99	5.82	5.70	5.60	5.52	5.46	5.37	5.27	5.17	5.12	5.07	5.01	4.96	4.90	4.85
7	8.07	6.54	5.89	5.52	5.29	5.12	4.99	4.90	4.82	4.76	4.67	4.57	4.47	4.42	4.36	4.31	4.25	4.20	4.14
8	7.57	6.06	5.42	5.05	4.82	4.65	4.53	4.43	4.36	4.30	4.20	4.10	4.00	3.95	3.89	3.84	3.78	3.73	3.67
9	7.21	5.71	5.08	4.72	4.48	4.32	4.20	4.10	4.03	3.96	3.87	3.77	3.67	3.61	3.56	3.51	3.45	3.39	3.33
10	6.94	5.46	4.83	4.47	4.24	4.07	3.95	3.85	3.78	3.72	3.62	3.52	3.42	3.37	3.31	3.26	3.20	3.14	3.08
11	6.72	5.26	4.63	4.28	4.04	3.88	3.76	3.66	3.59	3.53	3.43	3.33	3.23	3.17	3.12	3.06	3.00	2.94	2.88
12	6.55	5.10	4.47	4.12	3.89	3.73	3.61	3.51	3.44	3.37	3.28	3.18	3.07	3.02	2.96	2.91	2.85	2.79	2.72
13	6.41	4.97	4.35	4.00	3.77	3.60	3.48	3.39	3.31	3.25	3.15	3.05	2.95	2.89	2.84	2.78	2.72	2.66	2.60
14	6.30	4.86	4.24	3.89	3.66	3.50	3.38	3.29	3.21	3.15	3.05	2.95	2.84	2.79	2.73	2.67	2.61	2.55	2.49
15	6.20	4.77	4.15	3.80	3.58	3.41	3.29	3.20	3.12	3.06	2.96	2.86	2.76	2.70	2.64	2.59	2.52	2.46	2.40
16	6.12	4.69	4.08	3.73	3.50	3.34	3.22	3.12	3.05	2.99	2.89	2.79	2.68	2.63	2.57	2.51	2.45	2.38	2.32
17	6.04	4.62	4.01	3.66	3.44	3.28	3.16	3.06	2.98	2.92	2.82	2.72	2.62	2.56	2.50	2.44	2.38	2.32	2.25
18	5.98	4.56	3.95	3.61	3.38	3.22	3.10	3.01	2.93	2.87	2.77	2.67	2.56	2.50	2.44	2.38	2.32	2.26	2.19
19	5.92	4.51	3.90	3.56	3.33	3.17	3.05	2.96	2.88	2.82	2.72	2.62	2.51	2.45	2.39	2.33	2.27	2.20	2.13
20	5.87	4.46	3.86	3.51	3.29	3.13	3.01	2.91	2.84	2.77	2.68	2.57	2.46	2.41	2.35	2.29	2.22	2.16	2.09
21	5.83	4.42	3.82	3.48	3.25	3.09	2.97	2.87	2.80	2.73	2.64	2.53	2.42	2.37	2.31	2.25	2.18	2.11	2.04
22	5.79	4.38	3.78	3.44	3.22	3.05	2.93	2.84	2.76	2.70	2.60	2.50	2.39	2.33	2.27	2.21	2.14	2.08	2.00
23	5.75	4.35	3.75	3.41	3.18	3.02	2.90	2.81	2.73	2.67	2.57	2.47	2.36	2.30	2.24	2.18	2.11	2.04	1.97
24	5.72	4.32	3.72	3.38	3.15	2.99	2.87	2.78	2.70	2.64	2.54	2.44	2.33	2.27	2.21	2.15	2.08	2.01	1.94
25	5.69	4.29	3.69	3.35	3.13	2.97	2.85	2.75	2.68	2.61	2.51	2.41	2.30	2.24	2.18	2.12	2.05	1.98	1.91
26	5.66	4.27	3.67	3.33	3.10	2.94	2.82	2.73	2.65	2.59	2.49	2.39	2.28	2.22	2.16	2.09	2.03	1.95	1.88
27	5.63	4.24	3.65	3.31	3.08	2.92	2.80	2.71	2.63	2.57	2.47	2.36	2.25	2.19	2.13	2.07	2.00	1.93	1.85
28	5.61	4.22	3.63	3.29	3.06	2.90	2.78	2.69	2.61	2.55	2.45	2.34	2.23	2.17	2.11	2.05	1.98	1.91	1.83
29	5.59	4.20	3.61	3.27	3.04	2.88	2.76	2.67	2.59	2.53	2.43	2.32	2.21	2.15	2.09	2.03	1.96	1.89	1.81
30	5.57	4.18	3.59	3.25	3.03	2.87	2.75	2.65	2.57	2.51	2.41	2.31	2.20	2.14	2.07	2.01	1.94	1.87	1.79
40	5.42	4.05	3.46	3.13	2.90	2.74	2.62	2.53	2.45	2.39	2.29	2.18	2.07	2.01	1.94	1.88	1.80	1.72	1.64
60	5.29	3.93	3.34	3.01	2.79	2.63	2.51	2.41	2.33	2.27	2.17	2.06	1.94	1.88	1.82	1.74	1.67	1.58	1.48
120	5.15	3.80	3.23	2.89	2.67	2.52	2.39	2.30	2.22	2.16	2.05	1.94	1.82	1.76	1.69	1.61	1.53	1.43	1.31
∞	5.02	3.69	3.12	2.79	2.57	2.41	2.29	2.19	2.11	2.05	1.94	1.83	1.71	1.64	1.57	1.48	1.39	1.27	1.00

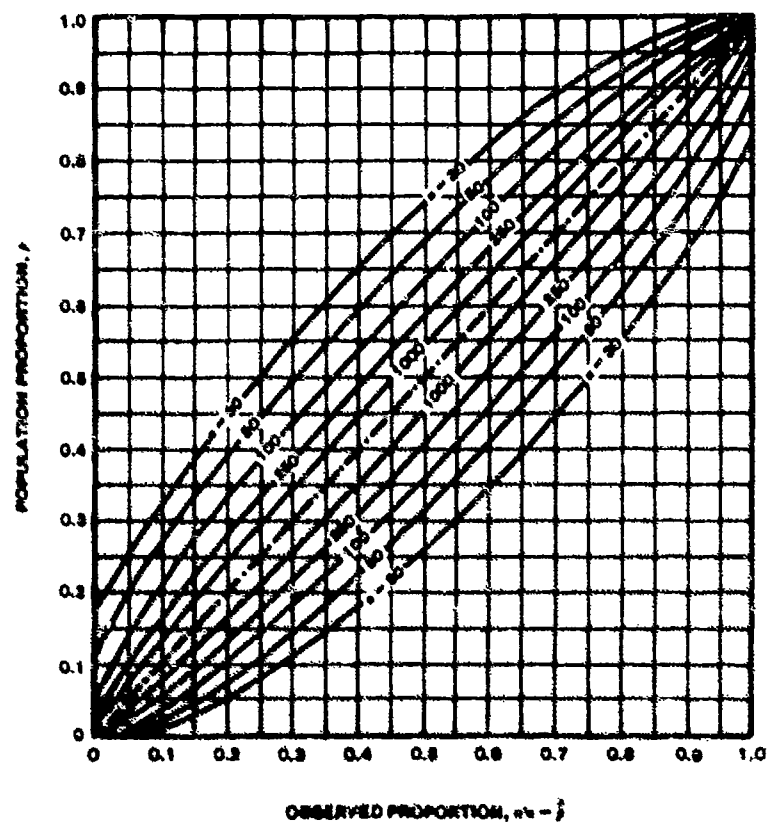
90% CONFIDENCE BELTS FOR PROPORTIONS



95% CONFIDENCE BELTS FOR PROPORTIONS



99% CONFIDENCE BELTS FOR PROPORTIONS

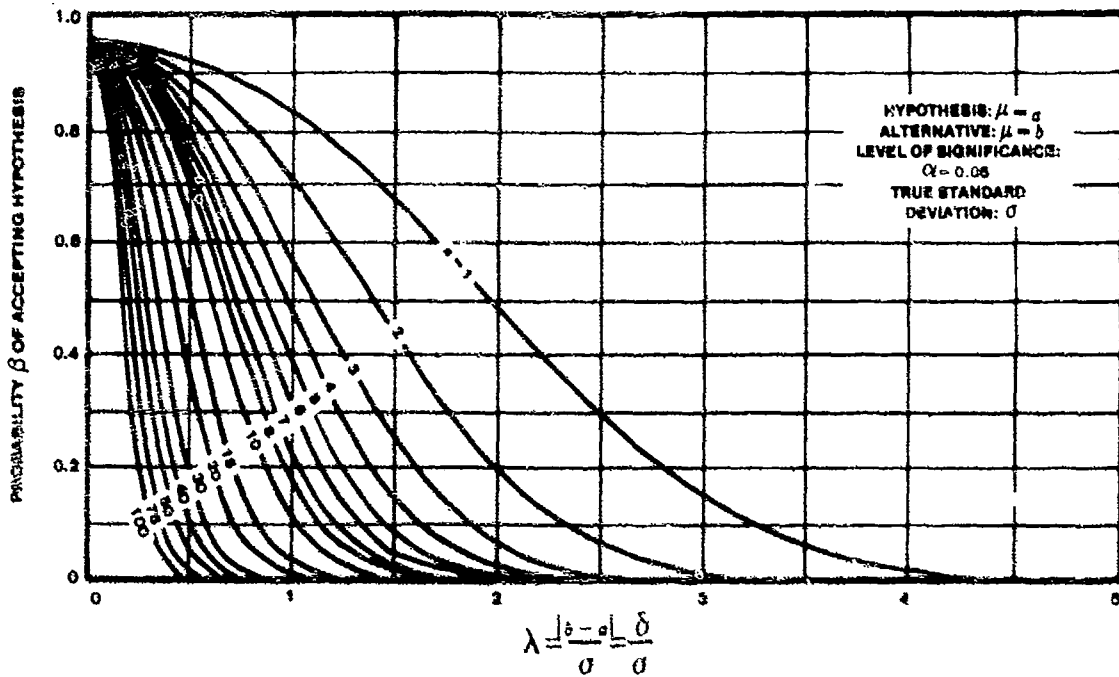
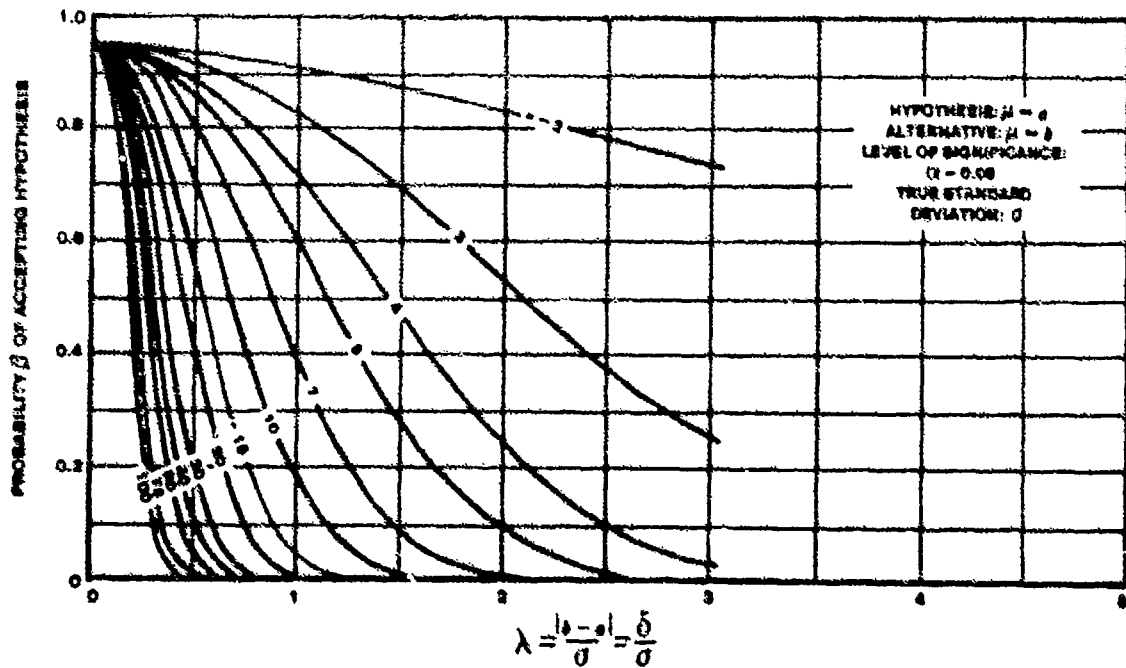


SIGNED RANK TEST

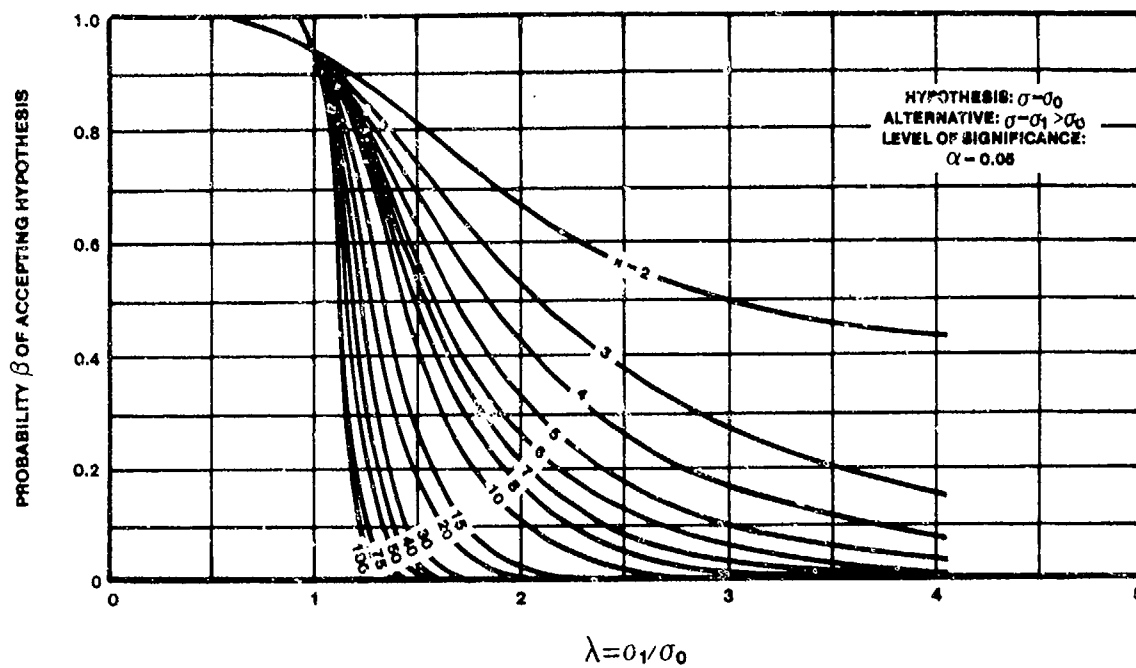
SIGNIFICANCE POINTS FOR THE ABSOLUTE VALUE OF THE SMALLER SUM OF SIGNED RANKS OBTAINED FROM PAIRED OBSERVATIONS.

n	5%	2%	1%
6	0	.	.
7	2	0	.
8	4	2	0
9	6	3	2
10	8	5	3
11	11	7	5
12	14	10	7
13	17	13	10
14	21	16	13
15	25	20	16
16	30	24	20
17	35	28	23
18	40	33	26
19	46	38	32
20	52	43	36
21	59	49	43
22	66	55	49
23	73	62	55
24	81	69	61
25	89	77	68

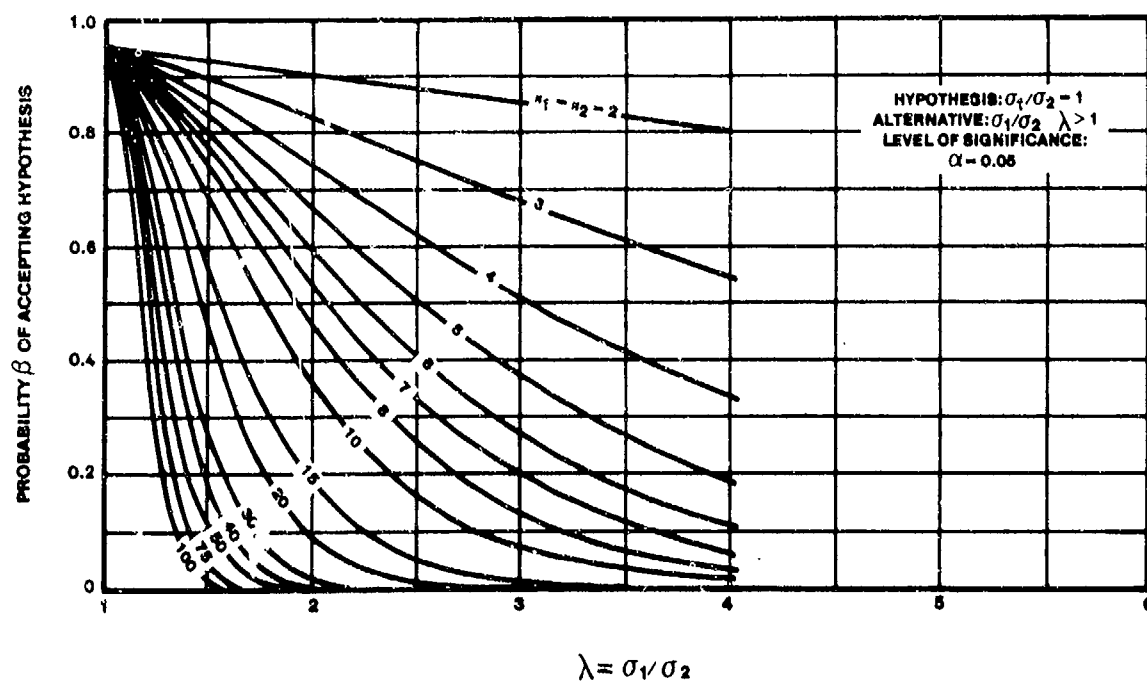
WHERE n = NUMBER OF PAIRED OBSERVATIONS.

OC CURVES FOR TESTING HYPOTHESIS $\mu = a$ BY THE EQUAL-TAILS NORMAL TESTOC CURVES FOR TESTING HYPOTHESIS $\mu = \mu_0$ BY THE EQUAL-TAILS t TEST

OC CURVES FOR TESTING THE HYPOTHESIS $\sigma = \sigma_0$ AGAINST $\sigma = \sigma_1 > \sigma_0$ BY THE χ^2 TEST



OC CURVES FOR TESTING THE HYPOTHESIS $\sigma = \sigma_0$ AGAINST $\sigma_1 > \sigma_0$ BY THE F TEST



APPENDIX F
DERIVATIONS

F.1 DERIVATION OF EULER EQUATION (Chapter 2)

Starting with Newton's Second Law

$$F = ma$$

for an element moving along a streamline with velocity V in the X direction

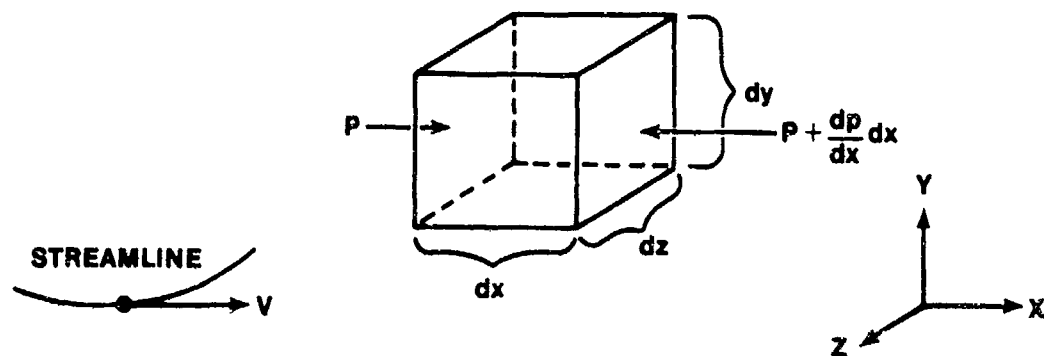


FIGURE F.1.1. FORCES ON A FLUID PARTICLE

$$\Sigma F_x = p dy dz - (p + \frac{dp}{dx} dx) dy dz$$

or

$$F_x = - \frac{dp}{dx} (dx dy dz)$$

$$\text{mass} = (\text{volume}) (\text{density})$$

i.e.,

$$m = \rho (dx dy dz)$$

$$a = \frac{dV}{dt} = \frac{dV}{dx} \frac{dx}{dt} = \frac{dV}{dx} V$$

$$\therefore - \frac{dp}{dx} (dx dy dz) = \rho (dx dy dz) V \frac{dV}{dx}$$

$$\boxed{dp = -\rho V dV}$$

F.2 DERIVATION OF STANDARD ATMOSPHERE RELATIONS (Chapter 5)

Beginning with Equation 5.4 from 5.7

$$\frac{dp_a}{p_a} = - \frac{G}{R} \frac{dH}{T_a}$$

Since $T_a = f(H)$ below 36,089 ft due to the lapse rate, L , we can substitute

$$T_a = T_{aSL} - LH = T_{aSL} \left(1 - \frac{L}{T_{aSL}} H \right)$$

Therefore,

$$\frac{dp_a}{p_a} = - \frac{G}{RT_{aSL}} \frac{dH}{\left(1 - \frac{L}{T_{aSL}} H \right)}$$

Upon integration we get

$$\int_{p_{aSL}}^{p_a} \frac{dp_a}{p_a} = \ln \frac{p_a}{p_{aSL}} \quad (F.2.1)$$

and

$$\begin{aligned} - \frac{G}{RT_{aSL}} \int_0^H \frac{dH}{\left(1 - \frac{L}{T_{aSL}} H \right)} &= - \frac{G}{RT_{aSL}} \left[- \frac{T_{aSL}}{L} \ln \left(1 - \frac{L}{T_{aSL}} H \right) - 0 \right] \\ &= \frac{G}{RL} \ln \left(1 - \frac{L}{T_{aSL}} H \right) \end{aligned} \quad (F.2.2)$$

Equate F.2.1 and F.2.2, the two sides of Equation 5.4

$$\ln \left(\frac{p_a}{p_{aSL}} \right) = \frac{G}{RL} \ln \left(1 - \frac{L}{T_{aSL}} H \right)$$

DERIVATION F.2 (Continued)

or

$$\frac{P_a}{P_{a_{SL}}} = \left(1 - \frac{L}{T_{a_{SL}}} H\right)^{G/RL}$$

$$= (1 - K_1 H)^{K_2}$$

Finally, since

$$P_a \propto \rho_a T_a$$

we can get the expression for ρ from

$$\sigma = \frac{\rho_a}{\rho_{a_{SL}}} = \frac{P_a}{T_a} \bigg/ \frac{P_{a_{SL}}}{T_{a_{SL}}} = \left(\frac{P_a}{P_{a_{SL}}}\right) \left(\frac{T_{a_{SL}}}{T_a}\right) = \delta/\theta$$

$$\sigma = \frac{(1 - K_1 H)^{K_2}}{(1 - K_1 H)}$$

$$\sigma = (1 - K_1 H)^{K_2 - 1}$$

Similar derivations can be done for $H > 36,089$ ft.

F.3 DERIVATION OF SPEED OF SOUND (Chapter 6)

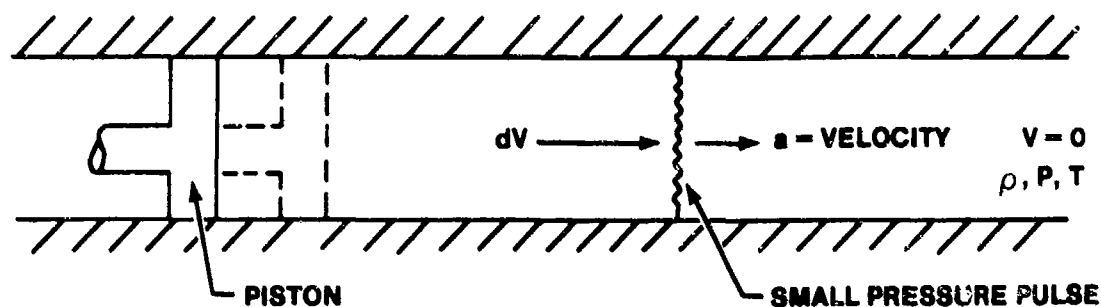


FIGURE F.3.1. PROPAGATION OF A SMALL PRESSURE PULSE IN A FRICTIONLESS PIPE

With the piston stationary the velocity in the pipe is zero, and the fluid has some density, pressure, and temperature. Displacing the piston to the dotted position (an infinitely small distance) causes a small pressure pulse (dP). This small dP travels down the pipe at a speed defined as the speed of sound, a , for the fluid in the pipe. This speed of an infinitely small pressure pulse is also known as acoustic velocity. Behind the pressure pulse the air has a small dV because the piston has displaced the fluid. While not obvious, this fact can be verified experimentally. To analyze this situation mathematically, a coordinate change will be made. Such a change is common in almost all fluid mechanics and aerodynamics courses and is the basis for wind tunnel testing. The math model in Figure F.3.2 transforms to that shown in Figure F.3.3. Notice that the pressure wave in Figure F.3.3 is stationary.

DERIVATION F.3 (Continued)

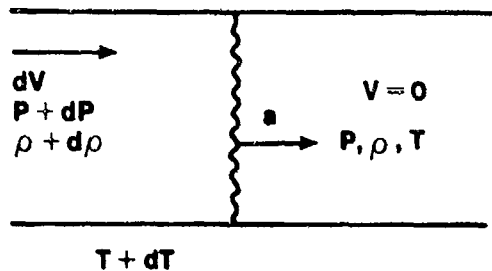


FIGURE F.3.2. MOVING WAVE

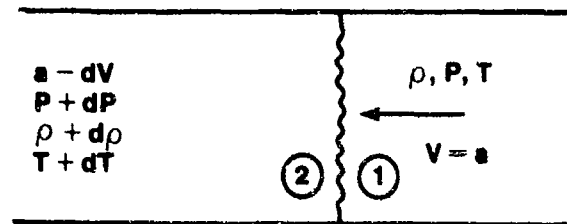


FIGURE F.3.3. STATIONARY WAVE

Evaluating the momentum equation across the pressure pulse from (2) to (1) in Figure F.3.3

$$dP + \rho V dV = 0$$

$$dP = P_2 - P_1 = P + dP - P = dP$$

$$dV = V_2 - V_1 = a - dV - a = -dV$$

Substituting

$$dP + \rho a (-dV) = 0$$

$$dP = \rho a dV \quad (F.3.1)$$

Evaluating the continuity equation across the pressure pulse from (2) to (1) gives

$$\rho AV = \text{Constant}$$

$$(\rho AV)_2 = (\rho AV)_1$$

$$(\rho + d\rho) (a - dV) = \rho a$$

$$\rho a - \rho dV + a d\rho - d\rho dV = \rho a$$

$$d\rho = (\rho/a) dV \quad (F.3.2)$$

DERIVATION F.3 (continued)

Dividing Equation F.3.1 by F.3.2

$$\frac{dP}{d\rho} = \frac{\rho a dV}{(\rho/a) dV}$$

$$\sqrt{\frac{dP}{d\rho}} = a$$

F.4 DERIVATION OF STEADY FLOW ENERGY EQUATION (Chapter 6)

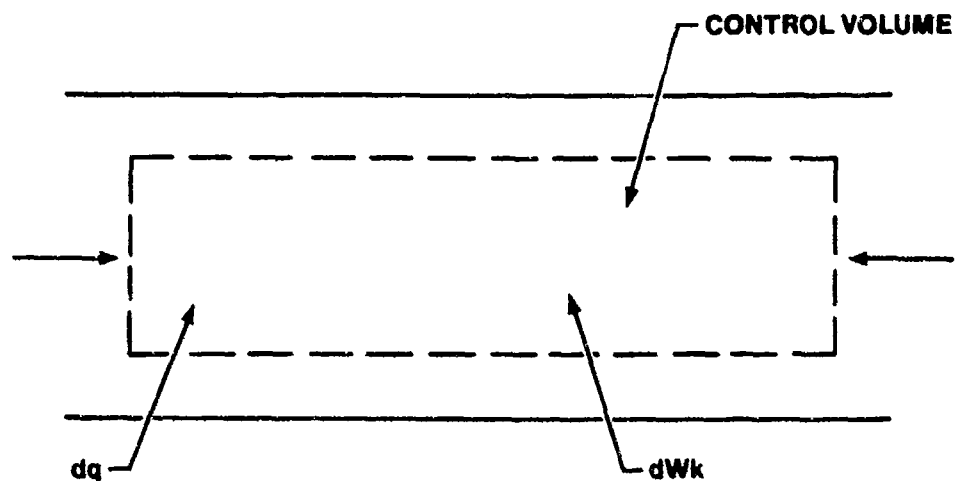


FIGURE F.4.1. CONTROL VOLUME FOR ENERGY BALANCE

$$de = dq - dW \quad (\text{First Law of Thermodynamics}) \quad (\text{F.4.1})$$

$$dW = \text{Work}$$

$$dW_k = \text{Shaft work}$$

$$dq = \text{Heat transfer}$$

$de =$ Energy (Capacity of flow to do work). Several types of energy are possible.

First kinetic energy:

$$KE = \frac{1}{2} mV^2$$

$$d(KE) = mVdV$$

or for a unit mass

$$d(KE) = VdV$$

DERIVATION F.4 (Continued)

A second type of energy is potential energy:

$$d(PE) = gdz$$

Internal energy is energy due to random motion of the molecules of the fluid. Consider the two fluid molecules in the accompanying sketch.

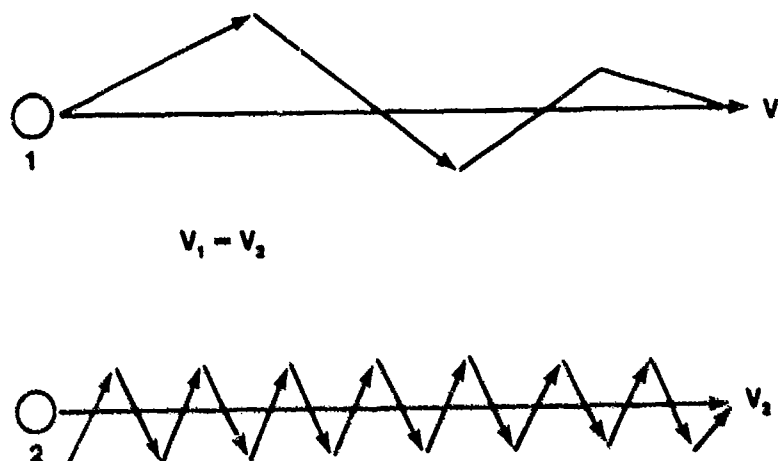


FIGURE F.4.2. MOLECULAR MOTION

The kinetic energy of each molecule is the same, because the average velocities V_1 and V_2 are equal. However, molecule 2 obviously has more random energy and therefore, more energy. This type of energy, called internal energy, u , is solely dependent on absolute temperature. This type of energy is a fluid property.

Expansion and flow work are separated from shaft work and will be written on the energy side of Equation F.4.1 by convention. Expansion work is the work done in order to expand or compress a unit mass of matter

$$d(\text{Expansion Work}) = PdV$$

Flow work is the work done in moving the unit mass of matter

$$D(\text{Flow work}) = v dP$$

DERIVATION F.4 (Continued)

Now, substituting all of these energy and work definitions into Equation F.4.1

$$VdV + gdz + du + Pdv + vdP = dq - dW_K \quad (F.4.2)$$

$$gdz + VdV + du + Pdv + vdP = dq - dW_K$$

But

$$Pdv + vdP = d(Pv) = d\left(\frac{P}{\rho}\right)$$

$$VdV + du + d\left(\frac{P}{\rho}\right) = gdz = dq - dW_K \quad (F.4.3)$$

Recalling the definition of enthalpy

$$h \equiv u + \frac{P}{\rho}$$

$$dh = du + d\left(\frac{P}{\rho}\right)$$

Substituting into Equation F.4.3

$$gdz + VdV = dh = dq - dW_K \quad (F.4.4)$$

Integrating

$$q - W_K = h_2 - h_1 + \frac{v_2^2 - v_1^2}{2} + g(z_2 - z_1) \quad (F.4.5)$$

Potential energy change in our problems can be considered negligible when compared to the kinetic and internal energy changes of our system. In the case of an adiabatic process with no shaft work, Equation F.4.5 reduces to

$$h_2 - h_1 + \frac{v_2^2 - v_1^2}{2} = 0$$

or

$$h + \frac{v^2}{2} = \text{constant} \quad (F.4.6)$$

F.5 RELATIONSHIP BETWEEN M AND M* (Chapter 6)

Starting with Equation F.4.6 in Derivation F.4

$$h + \frac{V^2}{2} = \text{constant}$$

Substituting for h

$$\frac{V^2}{2} + c_p T = c_p T_T = \frac{V^{*2}}{2} + c_p T^*$$

Using $a^2 = \gamma R T$ $a^{*2} = \gamma R T^*$

$$T = \frac{a^2}{\gamma R} \quad T^* = \frac{a^{*2}}{\gamma R} \quad R = c_p - c_v \quad \gamma = \frac{c_p}{c_v}$$

$$\therefore T = \frac{a^2}{\frac{c_p}{c_v} (c_p - c_v)} \quad T^* = \frac{a^{*2}}{\frac{c_p}{c_v} (c_p - c_v)}$$

Substituting into Equation (F.4.6)

$$\frac{V^2}{2} + \frac{\frac{c_p a^2}{\frac{c_p}{c_v} (c_p - c_v)}}{\frac{c_p}{c_v} (c_p - c_v)} = \frac{V^{*2}}{2} + \frac{\frac{c_p a^{*2}}{\frac{c_p}{c_v} (c_p - c_v)}}{\frac{c_p}{c_v} (c_p - c_v)}$$

$$\frac{V^2}{2} + \frac{a^2}{\left(\frac{c_p}{c_v} - 1\right)} = \frac{V^{*2}}{2} + \frac{a^{*2}}{\left(\frac{c_p}{c_v} - 1\right)}$$

For local sonic conditions $M = 1.0 = \frac{V^*}{a^*} \quad \therefore V^* = a^*$

$$\frac{V^2}{2} + \frac{a^2}{\gamma - 1} = \frac{a^{*2}}{2} + \frac{a^{*2}}{\gamma - 1} = \frac{(\gamma - 1) a^{*2} + 2a^{*2}}{2(\gamma - 1)}$$

DERIVATION F.5 (Continued)

Dividing by V^2

$$\frac{1}{2} + \frac{a^2}{V^2 (\gamma - 1)} = \frac{a^{*2} (\gamma - 1 + 2)}{V^2 2(\gamma - 1)} = \frac{a^{*2} (\gamma + 1)}{V^2 2(\gamma - 1)}$$

But

$$M \equiv \frac{V}{a} \quad M^* \equiv \frac{V}{a^*}$$

So

$$\frac{1}{2} + \frac{1}{M^2 (\gamma - 1)} = \frac{1}{M^{*2}} \frac{(\gamma + 1)}{2 (\gamma - 1)} \quad (\text{F.5.1})$$

Solving for M^2

$$\frac{1}{M^2 (\gamma - 1)} = \frac{1}{M^{*2}} \frac{\gamma + 1}{2 (\gamma - 1)} - \frac{1}{2} = \frac{\gamma + 1 - M^{*2} (\gamma - 1)}{2 (\gamma - 1) M^{*2}}$$

Or

$$M^2 = \frac{\frac{\gamma + 1}{2} M^{*2}}{\left[1 - \frac{\gamma - 1}{\gamma + 1} M^{*2} \right]}$$

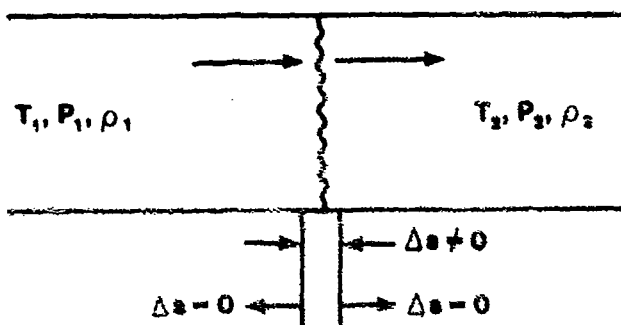
Now solve F.5.1 for M^{*2}

$$M^{*2} = \frac{(\gamma + 1) M^2}{M^2 (\gamma - 1) + 2}$$

$$\therefore \boxed{M^{*2} = \frac{\frac{\gamma + 1}{2} M^2}{1 + \frac{\gamma - 1}{2} M^2}}$$

F.6 NORMAL SHOCK RELATIONS (Chapter 6)

Assume: Adiabatic flow, thin shock, constant cross-sectional area, properties constant throughout area 1, and throughout area 2



$$\frac{T_{T1}}{T_1} = \left(1 + \frac{\gamma - 1}{2} M_1^2\right)$$

(F.6.1) Since process is adiabatic

$$T_{T1} = T_{T2} = T_T \text{. Divide}$$

(F.6.1) by (F.6.2)

$$\frac{T_{T2}}{T_2} = \left(1 + \frac{\gamma - 1}{2} M_2^2\right) \quad (\text{F.6.2})$$

$$\frac{T_2}{T_1} = \frac{1 + \frac{\gamma - 1}{2} M_1^2}{1 + \frac{\gamma - 1}{2} M_2^2} \quad (\text{F.6.3})$$

DERIVATION F.6 (Continued)

From continuity $\rho_1 AV_1 = \rho_2 AV_2$ or $\rho_1 V_1 = \rho_2 V_2$ (F.6.4)

From perfect gas law $P = \rho RT$ or $\frac{P}{RT} = \rho$ Substitute into F.6.4

$$\frac{P_1}{RT_1} V_1 = \frac{P_2}{RT_2} V_2$$

Or

$$\frac{T_2}{T_1} = \frac{P_2 V_2}{P_1 V_1}$$

But

$$M = \frac{V}{a}; V = Ma = M \sqrt{\gamma RT}$$

$$\frac{T_2}{T_1} = \frac{P_2 M_2 \sqrt{\gamma RT_2}}{P_1 M_1 \sqrt{\gamma RT_1}}$$

$$\frac{T_2}{T_1} = \left[\frac{P_2}{P_1} \frac{M_2}{M_1} \right]^2 \quad (F.6.5)$$

Equate (F.6.3) and (F.6.5)

$$\frac{P_2}{P_1} \frac{M_2}{M_1} = \frac{\sqrt{1 + \frac{\gamma-1}{2} M_1^2}}{\sqrt{1 + \frac{\gamma-1}{2} M_2^2}} \quad (F.6.6)$$

Use momentum Equation $dP + \rho V dV = 0$ and from continuity of $\rho V = \text{constant}$

$$P + \rho V^2 = \text{const}$$

DERIVATION F.6 (Continued)

$$P_1 + \rho_1 V_1^2 = P_2 + \rho_2 V_2^2$$

$$V = M \sqrt{\gamma RT} \quad \rho = \frac{P}{RT} \text{ again}$$

$$P_1 + M_1^2 \frac{\gamma RT_1 P_1}{RT_1} = P_2 + M_2^2 \frac{\gamma RT_2 P_2}{RT_2}$$

Factoring each side

$$P_1 [1 + \gamma M_1^2] = P_2 [1 + \gamma M_2^2]$$

$$\frac{P_2}{P_1} = \frac{1 + \gamma M_1^2}{1 + \gamma M_2^2} \quad (\text{F.6.6a})$$

Substitute into Equation F.6.6 and rearrange

$$\frac{1 + M_1^2}{1 + M_2^2} = \frac{M_1}{M_2} \frac{\sqrt{1 + \frac{\gamma - 1}{2} M_1^2}}{\sqrt{1 + \frac{\gamma - 1}{2} M_2^2}} \quad (\text{F.6.7})$$

Solving for M_2^2

$$M_2^2 = \frac{M_1^2 + \frac{2}{\gamma - 1}}{\frac{2\gamma}{\gamma - 1} M_1^2 - 1} \quad (\text{F.6.8})$$

Substituting Equation F.6.8 into Equation F.6.6a and Equation F.6.3 gives

DERIVATION F.6 (Continued)

$$\frac{P_2}{P_1} = \frac{2\gamma}{\gamma + 1} M_1^2 - \frac{\gamma - 1}{\gamma + 1} = \frac{1 - \gamma + 2\gamma M_1^2}{\gamma + 1}$$

$$\frac{T_2}{T_1} = \left[\frac{2\gamma}{\gamma + 1} M_1^2 - \frac{\gamma - 1}{\gamma + 1} \right] \left[\frac{\gamma - 1}{\gamma + 1} + \frac{2}{(\gamma + 1) (M_1^2)} \right] \quad (\text{F.6.9})$$

ρ_2/ρ_1 can be similarly attained with lots of algebra.

$$\frac{\rho_2}{\rho_1} = \frac{(\gamma + 1) M_1^2}{2 + (\gamma - 1) M_1^2} \quad (\text{F.6.10})$$

F.7 SHOCKS IN SUPERSONIC FLOW: (Chapter 6)

A shock has been described as a discontinuity between supersonic and subsonic flow. Nothing has been said concerning the conditions under which it can or cannot occur. First, the existence of a shock wave must be physically justified, and then the conditions that must exist before a shock will form must be determined.

It will be shown that a shock is a discontinuity between supersonic and subsonic flow and it will be shown that a shock can ONLY occur when flow goes from supersonic to subsonic conditions.

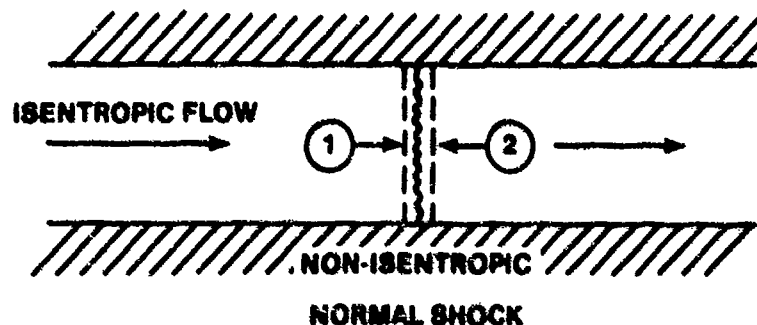


FIGURE F.7.1. NORMAL SHOCK

The mass flow rate through a shock is a constant, i.e., no mass is added or destroyed by the shock, and the cross-sectional area through the shock is assumed constant. Therefore, the continuity and momentum equations may be written

$$\dot{m} = \rho VA = \text{constant} \quad (\text{F.7.1})$$

$$\dot{m} = \rho_1 V_1 = \rho_2 V_2 = \text{constant}$$

$$dP + \rho V dV = 0 \quad (\text{F.7.2})$$

DERIVATION F.7 (Continued)

Evaluating Equation F.7.2 at Stations 1 and 2 (Figure F.7.1) and substituting m for ρV gives

$$P_2 - P_1 = \dot{m} V_1 - V_2$$

Dividing the momentum equation by the continuity equation:

$$\frac{P_2}{\rho_2 V_2} - \frac{P_1}{\rho_1 V_1} = V_1 - V_2 \quad (\text{F.7.3})$$

Multiplying Equation F.7.3 by γ and substituting $a^2 = \frac{\gamma P}{\rho}$

$$\frac{a_2^2}{V_2} - \frac{a_1^2}{V_1} = \gamma (V_1 - V_2) \quad (\text{F.7.4})$$

Writing the energy equation for a point in the free stream and at local sonic conditions:

$$\begin{aligned} c_p T_T &= c_p T + 1/2 V^2 \\ &= c_p T^* + 1/2 V^{*2} \end{aligned} \quad (\text{F.7.5})$$

Substitute the following values for $c_p T$ and V^* into Equation F.7.5:

$$c_p T = c_p \left(\frac{\gamma c_v}{c_p} \right) \left(\frac{R}{c_p - c_v} \right) T = \frac{a^2}{\gamma - 1}$$

$$c_p T^* = \frac{a^{*2}}{\gamma - 1}$$

$$V^* = a^*, \text{ since } M = 1$$

DERIVATION F.7 (Continued)

and solving for a^2

$$a^2 = \frac{\gamma + 1}{2} a^{*2} - \frac{\gamma - 1}{2} v^2 \quad (\text{F.7.6})$$

Substituting this equation into Equation F.7.4 and rearranging (since $a^*_2 = a^*_1 = a^*$)

$$\frac{a^{*2}}{v_1 v_2} (v_1 - v_2) = v_1 - v_2 \quad (\text{F.7.7})$$

If v_1 equals v_2 , Equation F.7.7 has a trivial solution, i.e., $0 = 0$, or that no velocity discontinuity exists in the flow. It is an experimental fact that v_1 does not equal v_2 across a shock and that shock waves are present under certain flow conditions. Dividing by $(v_1 - v_2)$ admits that there is a velocity discontinuity in the mathematical flow description and

$$a^{*2} = v_1 v_2 \quad (\text{F.7.8})$$

a^* is the speed of sound at local sonic conditions and can be shown to be a constant through the shock. The shock is assumed to be an adiabatic process, therefore

$$T_{t1} = T_{t2}$$

and

$$\frac{T^*}{T_t} = \text{constant} \quad (\text{F.7.9})$$

DERIVATION F.7 (Continued)

Therefore

$$T^*_1 = T^*_2$$

or

$$a^*_1 = a^*_2$$

From Equation F.7.8 it can be seen that if V_1 is greater than a^* , then V_2 must be less than a^* in order for the equality to hold. This can be written

$$\frac{V_1}{a^*} = \frac{a^*}{V_2}$$

and from definition of M^*

$$M^*_1 = \frac{1}{M^*_2} \quad (7.10)$$

Equation F.7.10 shows that if M^*_1 is greater than 1.0, then M^*_1 must be less than 1.0, i.e., if $M^*_1 = 2.0$, then $M^*_2 = .5$.

If there is a velocity discontinuity in the flow, then the velocity on one side of the discontinuity must be subsonic and on the other side must be supersonic. This relationship between M^*_1 and M^*_2 gives no insight as to which side of the shock is subsonic and which side is supersonic.

Supersonic side of shock:

Next it must be established which side of the shock must be supersonic. Experiments have proven that a shock occurs only when the upstream Mach is greater than 1.0, but why? In answer to this question, an equation for the change in entropy has been written

$$dS = c_p \frac{dT}{T} = R \frac{dP}{P}$$

DERIVATION F.7 (Continued)

Integrating and rearranging this expression

$$\frac{\Delta S}{R} = \frac{c_p}{R} \ln T \left| \begin{array}{c} 2 \\ 1 \end{array} \right| - \ln P \left| \begin{array}{c} 2 \\ 1 \end{array} \right| \quad (F.7.11)$$

where 1 and 2 refer to the stations upstream and downstream of the shock wave. Evaluating this equation with the stagnation properties at Stations 1 and 2.

$$\frac{\Delta S}{R} = \frac{c_p}{R} \ln \frac{T_{T2}}{T_{T1}} - \ln \frac{P_{T2}}{P_{T1}}$$

and since $T_{T2} = T_{T1}$, and $\ln 1 = 0$

$$\frac{\Delta S}{R} = - \ln \frac{P_{T2}}{P_{T1}} \quad (F.7.12)$$

The second law of thermodynamics states that entropy may only increase. Therefore ΔS in Equation F.7.12 is positive.

In P_{T2}/P_{T1} must be negative or $P_{T2}/P_{T1} < 1$. If an equation relating P_{T2}/P_{T1} to M_1 can be derived, the question of which side of a shock wave is supersonic will be solved.

Using Equation F.7.11 to equate the entropy change in terms of free stream conditions to the entropy change in terms of stagnation conditions:

$$- \ln \frac{P_{T2}}{P_{T1}} = \frac{c_p}{R} \ln \frac{T_2}{T_1} - \ln \frac{P_2}{P_1}$$

DERIVATION F.7 (Continued)

Rearranging

$$\frac{P_{T_2}}{P_{T_1}} = \frac{\frac{P_2}{P_1}}{\left(\frac{T_2}{T_1}\right)^{\frac{\gamma}{\gamma-1}}} = \left[\frac{\left(\frac{\rho_2}{\rho_1}\right)^{\frac{\gamma}{\gamma-1}}}{\frac{P_2}{P_1}} \right]^{\frac{1}{\gamma-1}}$$

Substituting in the normal shock equations for P_2/P_1 and ρ_1/ρ_2 and rearranging

$$\frac{P_{T_2}}{P_{T_1}} = \left[\frac{1}{\left(\frac{\gamma-1}{\gamma+1} + \frac{2}{(\gamma+1) M_1^2}\right)^{\frac{\gamma}{\gamma-1}} \left(\frac{2\gamma}{\gamma+1} M_1^2 - \frac{\gamma-1}{\gamma+1}\right)} \right]^{\frac{1}{\gamma-1}} \quad (\text{F.7.13})$$

Substituting into Equation F.7.12 the upstream conditions necessary for an increase in entropy can be determined.

$$\frac{\Delta S}{R} = -\ln \left[\frac{1}{\left(\frac{\gamma-1}{\gamma+1} + \frac{2}{(\gamma+1) M_1^2}\right)^{\frac{\gamma}{\gamma-1}} \left(\frac{2\gamma}{\gamma+1} M_1^2 - \frac{\gamma-1}{\gamma+1}\right)} \right]^{\frac{1}{\gamma-1}} \quad (\text{F.7.14})$$

when

$$M_1 = 1.0; \quad P_{T_2}/P_{T_1} = 1; \quad \Delta S = 0$$

$$M_1 > 1.0; \quad P_{T_2}/P_{T_1} < 1.0; \quad \Delta S \text{ is positive}$$

$$M_1 < 1.0; \quad P_{T_2}/P_{T_1} > 1.0; \quad \Delta S \text{ is negative}$$

The case where $M < 1.0$ is contrary to the requirement that entropy must always increase, consequently it is not possible for a shock to form when the flow goes from subsonic to supersonic velocity.

Notice that when $M = 1$, $\Delta S = 0$. This is the case of the isentropic sound wave or weakest possible normal shock since changes across it are so small that no entropy change is produced.

F.8 LINEAR THIN WING THEORY (ACKERET THEORY) (Chapter 6)

To develop the Ackeret Theory, the following must be satisfied:

1. Geometric and trigometric flow relations
2. Conservation of mass
3. Conservation of momentum

Geometric and Trigometric Relations:

The geometry of an expansion flow is shown in Figure F.8.1. The flow for a compression Mach wave is exactly the same except $d\delta$, dV , and dV_N are negative. Thus the expansion case equations will be valid for the compression case if the signs are reversed. Only the expansion case equations will be developed.

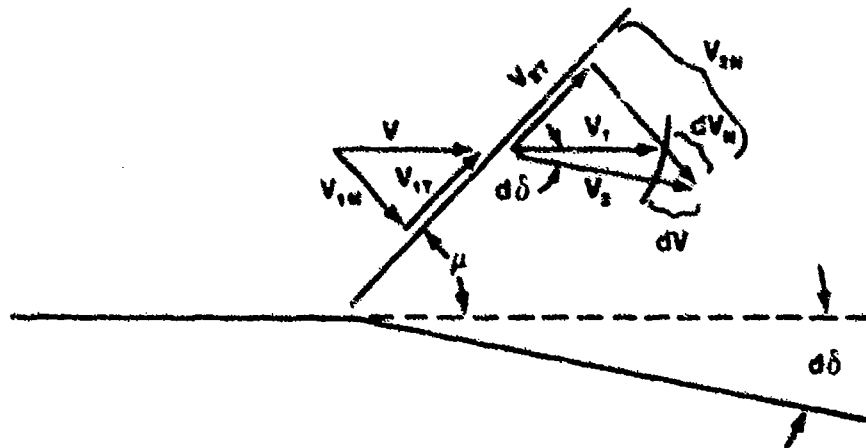


FIGURE F.8.1. EXPANSION FLOW

DERIVATION F.8 (Continued)

Since $d\delta$ is small then

$$dV = \text{change in magnitude of } V = dV_N \sin \mu$$

$$dV_N = \frac{dV}{\sin \mu} \quad (\text{F.8.1})$$

also

$$d\delta = \frac{dV_N \cos \mu}{V} \quad (\text{F.8.2})$$

Substituting Equation F.8.1 into Equation F.8.2

$$d\delta = \frac{dV}{V} \frac{\cos \mu}{\sin \mu} = \frac{dV}{V} \frac{1}{\tan \mu}$$

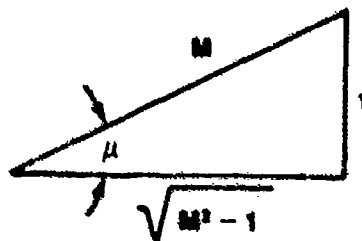


FIGURE F.8.2.

From definition of sine and

$$\sin \mu = \frac{1}{M} \quad (\text{F.8.3})$$

Figure F.8.2 can be constructed. From Figure F.8.2

$$\tan \mu = \frac{1}{\sqrt{M^2 - 1}} \quad (\text{F.8.4})$$

DERIVATION F.8 (Continued)

Since $d\delta$ is small then

$$dV = \text{change in magnitude of } V = dV_N \sin \nu$$

$$dV_N = \frac{dV}{\sin \nu} \quad (\text{F.8.1})$$

also

$$dV = dV_N \sin \nu$$

DERIVATION F.8 (Continued)

and

$$d\delta = \frac{dV}{V} \frac{1}{\sqrt{M^2 - 1}}$$

or

$$\frac{dV}{V} = \frac{d\delta}{\sqrt{M^2 - 1}} \quad (\text{F.8.5})$$

Conservation of Mass:

If we consider a constant area across the Mach wave then from the conservation of mass equation

$$\rho_1 V_{1N} = \rho_2 V_{2N} \quad (\text{F.8.6})$$

and

$$\rho_2 = \rho_1 + d\rho$$

$$V_{2N} = V_{1N} + dV_N$$

or

$$\rho_1 V_{1N} = (\rho_1 + d\rho)(V_{1N} + dV_N) \quad (\text{F.8.7})$$

Simplifying Equation 8.7 and dropping $d\rho dV_N$ as insignificant

$$V_{1N} d\rho + \rho_1 dV_N = 0 \quad (\text{F.8.8})$$

Conservation of Momentum:

Parallel to the Mach waves there are no pressure differential forces and thus no momentum flux change parallel to the Mach waves and the conservation of momentum equation becomes

$$(\rho_1 V_{1N}) V_{1T} = (\rho_2 V_{2N}) V_{2T} \quad (\text{F.8.9})$$

DERIVATION F.8 (Continued)

but from conservation of mass

$$\rho_1 V_{1N} = \rho_2 V_{2N} \quad (\text{F.8.6})$$

and

$$V_{1T} = V_{2T}$$

There is a pressure differential normal to the wave and by Newton's second law, this pressure differential per unit area must equal the rate of change of momentum

or

$$(\rho_1 V_{1N}) V_{1N} - (\rho_2 V_{2N}) V_{2N} = P_2 - P_1 \quad (\text{F.8.10})$$

but

$$\rho_1 V_{1N} = \rho_2 V_{2N} \quad (\text{F.8.6})$$

$$V_{2N} = V_{1N} + dV_N \quad (\text{F.8.11})$$

$$P_2 = P_1 + dP \quad (\text{F.8.12})$$

Substituting Equations F.8.6, F.8.11, and F.8.12 into Equation F.8.10 gives

$$V_{1N} dV_N + \frac{dP}{\rho_1} = 0$$

or

$$dV_N = - \frac{dP}{\rho_1 V_{1N}} \quad (\text{F.8.13})$$

DERIVATION F.8 (Continued)

Now we will combine the relationships of the three previous sections. Substituting Equation F.8.13 into Equation F.8.8 gives

$$V_{1N} d\rho - \rho_1 \frac{dP}{\rho_1 V_{1N}} = 0$$

rearranging gives

$$V_{1N}^2 = \frac{dP}{d\rho} = a^2$$

but

$$a^2 = \gamma R T_1 = \gamma \frac{P_1}{\rho_1}$$

Thus

$$V_{1N}^2 = \frac{\gamma P_1}{\rho_1}$$

or

$$\rho_1 = \frac{\gamma P_1}{V_{1N}^2} \quad (\text{F.8.14})$$

Substituting Equation F.8.14 into Equation F.8.13 and rearranging gives

$$dP = \frac{\gamma P_1}{V_{1N}^2} V_{1N} dV_N = - \frac{\gamma P_1}{V_{1N}} dV_N \quad (\text{F.8.15})$$

substituting Equations F.8.1 and F.8.3 into Equation F.8.15 gives

$$dP = - \frac{\gamma P_1}{V_{1N}} M dV$$

Multiply right side by V/V and substituting a for V_{1N} gives

$$dP = - \gamma P_1 M^2 \frac{dV}{V}$$

DERIVATION F.8 (Continued)

Substituting in Equation F.8.5 gives

$$dP = - \frac{\gamma P_1 M^2 d\delta}{\sqrt{M^2 - 1}} \quad (F.8.16)$$

Equation F.8.16 is valid for an expansion and for a compression the equation is

$$dP = - \frac{\gamma P_1 M^2 d\delta}{\sqrt{M^2 - 1}} \quad (F.8.17)$$

If $d\delta$ is small but not infinitesimal, then $d\delta$ becomes δ and dP becomes ΔP .
For an approximation

$$\Delta P = \pm \frac{\gamma P_1 M^2}{\sqrt{M^2 - 1}}$$

Defining a pressure coefficient

$$C_p \equiv \frac{\Delta P}{q} = \frac{2\delta}{\sqrt{M^2 - 1}} \quad (F.8.18)$$

F.9 DERIVATION OF THRUST EQUATION FOR A TURBOJET (Chapter 7)

The following equations from thermodynamics and physics will be required and are presented here for quick reference.

From gas dynamics for one-dimensional gas flow

$$\frac{T_{\text{TOTAL}}}{T_{\text{STATIC}}} = \frac{T_T}{T} = \left(1 + \frac{\gamma - 1}{\gamma} M^2\right)^{\frac{\gamma}{\gamma - 1}} \quad (\text{F.9.1})$$

$$\frac{P_{\text{TOTAL}}}{P_{\text{STATIC}}} = \frac{P_T}{P} = \left(1 + \frac{\gamma - 1}{2} M^2\right)^{\frac{\gamma}{\gamma - 1}} \quad (\text{F.9.2})$$

For an isentropic process

$$\left(\frac{P_1}{P_2}\right)^{\frac{\gamma - 1}{\gamma}} = \frac{T_1}{T_2} \quad (\text{F.9.3})$$

Mach

$$M = \frac{V}{\sqrt{\gamma R T}} \quad (\text{F.9.4})$$

General thrust equation

$$F_n = \frac{W}{g} (V_{10} - V_0) \quad (\text{F.9.5})$$

DERIVATION F.9 (Continued)

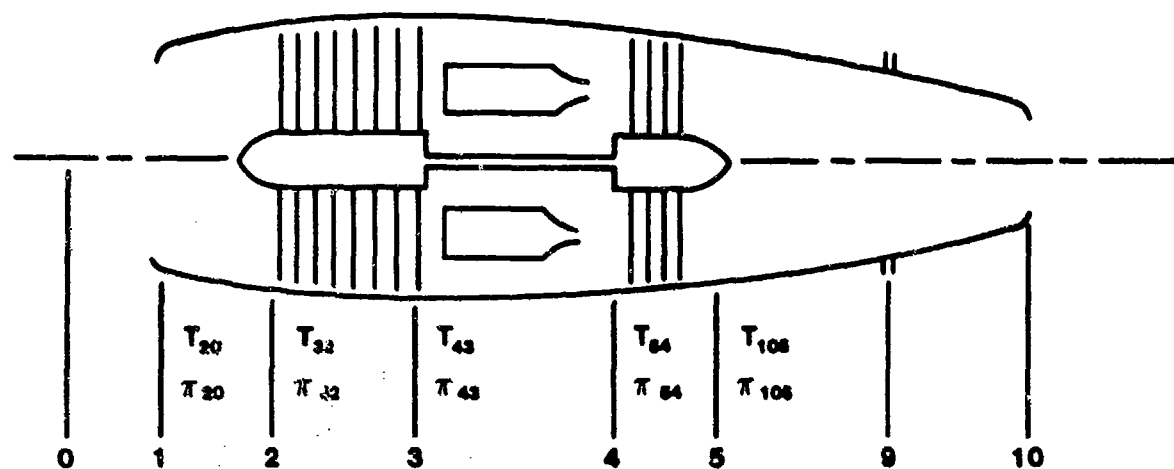


FIGURE F.9.1. STATION DESIGNATIONS AND PARAMETER DEFINITIONS

Define

$$T_{20} = \frac{T_{T2}}{T_0}$$

$$\pi_{20} = \frac{P_{T2}}{P_0}$$

$$T_{32} = \frac{T_{T3}}{T_{T2}}$$

$$\pi_{32} = \frac{P_{T3}}{P_{T2}}$$

$$T_{43} = \frac{T_{T4}}{T_{T3}}$$

$$\pi_{43} = \frac{P_{T4}}{P_{T3}}$$

$$T_{54} = \frac{T_{T5}}{T_{T4}}$$

$$\pi_{54} = \frac{P_{T5}}{P_{T4}}$$

$$T_{105} = \frac{T_{T10}}{T_{T5}}$$

$$\pi_{105} = \frac{P_{T10}}{P_{T5}}$$

NOTE:

$$T_{105} = \pi_{43} = \pi_{105} = 1$$

DERIVATION F.9 (Continued)

Required: $F_n = f$ (temperatures)

Solution:

Apply Equation F.9.1

$$T_{T10} = T_{10} \left(1 + \frac{\gamma-1}{2} M_{10}^2 \right) = T_{10} T_{10} T_{32} T_{43} T_{54} T_{105}$$

and note $T_{105} = 1$

Apply Equation F.9.6

$$P_{T10} = P_{10} = \left(1 + \frac{\gamma-1}{2} M_{10}^2 \right) = P_o \pi_{20} \pi_{32} \pi_{43} \pi_{54} \pi_{105} \quad (F.9.7)$$

and note $\pi_{43} = \pi_{105} = 1$

Assume the nozzle expands gas to ambient pressure so $P_{10} = P_o$.

Equation F.9.7 yields

$$\left(1 + \frac{\gamma-1}{2} M_{10}^2 \right) = \pi_{20} \pi_{32} \pi_{54} \frac{\gamma-1}{\gamma} \quad (F.9.8)$$

From Equation F.9.6

$$\frac{T_{10}}{T_o} = \frac{T_{20} T_{20} T_{32} T_{43} T_{54}}{\left(1 + \frac{\gamma-1}{2} M_{10}^2 \right)} \quad (F.9.9)$$

Combining Equations F.9.8 and F.9.10

$$T_{10} = \frac{\pi_{20} \pi_{32} \pi_{43} \pi_{54}}{\left(P_{20} P_{32} P_{54} \frac{\gamma-1}{\gamma} \right)} \quad (F.9.10)$$

DERIVATION F.9. (Continued)

From Equation F.9.3

$$\pi_{20} \frac{\gamma-1}{\gamma} = T_{20}, \quad \pi_{32} \frac{\gamma-1}{\gamma} = T_{32}, \quad \pi_{54} \frac{\gamma-1}{\gamma} = T_{54}$$

Substituting these expressions into Equation F.9.10

$$\frac{T_{10}}{T_0} = T_{43} \quad (\text{F.9.11})$$

Dividing Equation F.9.9 by Equation F.9.11

$$\left(1 + \frac{\gamma-1}{\gamma} M_{10}^2 \right) = T_{20} T_{32} T_{54}$$

Solve for M_{10}^2 :

$$M_{10}^2 = \left(\frac{2}{\gamma-1} \right) (T_{20} T_{32} T_{54} - 1) \quad (\text{F.9.12})$$

From Equation F.9.1

$$T_{20} = \left(1 + \frac{\gamma-1}{2} M_0^2 \right)$$

Solve for M_0^2 :

$$M_0^2 = \left(\frac{2}{\gamma-1} \right) T_{20} \quad (\text{F.9.13})$$

Dividing Equation F.9.13 by Equation F.9.12

$$\left(\frac{M_{10}^2}{M_0^2} \right) = \frac{T_{20} T_{32} T_{54} - 1}{T_{20} - 1} \quad (\text{F.9.14})$$

DERIVATION F.9 (Continued)

From Equation F.9.4

$$M_{10} = V_{10} \sqrt{\gamma R T_{10}}$$

$$M_0 = V_0 \sqrt{\gamma R T_0}$$

Hence

$$\left(\frac{M_{10}^2}{M_0^2} \right) = \left(\frac{V_{10}^2}{V_0^2} \right) \frac{T_{10}}{T_0} = \left(\frac{V_{10}}{V_0} \right)^2 T_{43} \quad (\text{F.9.15})$$

where Equation F.9.11 was used in the last step.

Combining Equations F.9.15 and F.9.16

$$\left(\frac{V_{10}}{V_0} \right)^2 = T_{43} \left(\frac{T_{20} T_{32} T_{54}}{T_{20} - 1} \right) - 1 \quad (\text{F.9.16})$$

Since $W_C = W_T$

$$h_{T3} - h_{T2} = h_{T4} - h_{T5}$$

$$T_{T3} - T_{T2} = T_{T4} - T_{T5}$$

$$T_{T2} (T_{32} - 1) = T_{T2} T_{32} T_{43} (1 - T_{54})$$

$$T_{54} = 1 - \frac{(T_{32} - 1)}{(T_{43} T_{32})} \quad (\text{F.9.17})$$

Substitute Equation F.9.17 into F.9.16

$$\frac{V_{10}}{V_0} = \sqrt{\frac{T_{20}}{(T_{20} - 1) (T_{43} - 1) (T_{32} - 1) + (T_{43})}} \quad (\text{F.9.18})$$

DERIVATION F.9 (Continued)

From Equation F.9.5

$$F_n = \frac{W}{g} (V_{10} - V_0)$$

$$= \frac{W}{g} V_0 \left(\frac{V_{10}}{V_0} - 1 \right) \quad (F.9.19)$$

Substituting Equation F.9.18 into F.9.19

$$F_n = \frac{W}{g} V_0 \left[\sqrt{\frac{T_{20}}{(T_{20} - 1)} (T_{43} - 1) (T_{32} - 1) + T_{43} - 1} \right] \quad (F.9.20)$$

Equation F.9.20 shows that net thrust is dependent only on three design parameters.

$$T_{43} = \frac{T_{T4}}{T_{T3}} \text{ proportional to fuel flow}$$

$$T_{32} = \frac{T_{T3}}{T_{T2}} \text{ proportional to compressor ratio}$$

$$T_{20} = \frac{T_{T2}}{T_0} \text{ proportional to Mach}$$

If T_{32} approaches 1, a ramjet results and Equation F.9.20 reduces to

$$F_n = \frac{W}{g} V_0 \left(\sqrt{T_{43}} - 1 \right) \quad (F.9.21)$$

What is the static thrust ($M = 0$) of the ramjet and turbojet?

Ramjet:

$$\lim_{M_0 \rightarrow 0} F_n = \lim_{M_0 \rightarrow 0} \left[\frac{W}{g} V_0 \left(\sqrt{T_{43}} - 1 \right) \right]$$

DERIVATION F.9 (Continued)

Note: $V_0 = a M_0$ where a is the speed of sound and T_{43} is independent of Mach

$$= \frac{W}{g} a \left(\sqrt{T_{43}} \right)^{-1} \lim_{M_0 \rightarrow 0} M_0 = 0$$

This, of course, is the expected result as a ramjet does not produce any static thrust.

Turbojet:

$$\lim_{M_0 \rightarrow 0} F_n = \lim_{M_0 \rightarrow 0} \frac{W}{g} V_0 \left[\sqrt{\frac{T_{20}}{(T_{20} - 1)} (T_{43} - 1) (T_{32} - 1) + T_{43} - 1} \right]$$

Since

$$T_{T2} = T_{T0}$$

$$T_{20} = \frac{T_{T2}}{T_0} = 1 + \frac{\gamma - 1}{2} M_0^2$$

and

$$\frac{T_{20}}{T_{20} - 1} = \frac{1 + \frac{\gamma - 1}{2} M_0^2}{\frac{\gamma - 1}{2} M_0^2}$$

Substituting and simplifying

$$= \frac{W}{g} a \lim_{M_0 \rightarrow 0} \sqrt{\frac{1 + \frac{\gamma - 1}{2} M_0^2}{\frac{\gamma - 1}{2} M_0^2} (T_{43} - 1) (T_{32} - 1) + T_{43} M_0^2 - M_0}$$

DERIVATION F.9 (Continued)

Thus

$$F_{n_{\text{STATIC}}} = \frac{W}{g} a \sqrt{\frac{2}{\gamma - 1} (T_{43} - 1) (T_{32} - 1)} \quad (\text{F.9.22})$$

which shows that unlike the ramjet, the turbojet produces thrust at zero velocity.

F.10 ALTERNATE DERIVATION OF IDEAL NET THRUST EQUATION FOR A TURBOJET
(Chapter 7)

Starting with

$$F_n = \frac{W_a}{g} (V_{10} - V_0) \quad (F.10.1)$$

We want to express F_n in terms of engine parameters and flight conditions.

From cycle analysis

$$V_{10}^2 = 2gJ (h_{T9} - h_{10}) \text{ where } h_{T5} = h_{T9} \quad (F.10.2)$$

$$V_0^2 = 2gJ (h_{T0} - h_0) \text{ where } h_{T0} = h_{T2} \quad (F.10.3)$$

Subtracting Equation F.10.3 from Equation F.10.2

$$V_{10}^2 - V_0^2 = 2gJ [h_{T5} - h_{10} - h_{T2} + h_0] \quad (F.10.4)$$

Since

$$W_c = h_{T3} - h_{T2} = W_T = h_{T4} - h_{T5}$$

then

$$h_{T5} - h_{T2} = h_{T4} - h_{T3} \quad (F.10.5)$$

Substituting Equation F.10.5 into Equation F.10.4

$$\begin{aligned} V_{10}^2 - V_0^2 &= 2gJ [(h_{T4} - h_{10}) - (h_{T3} - h_0)] \\ &= 2gJ C_p [(T_{T4} - T_{10}) - (T_{T3} - T_0)] \\ &= 2gJ C_p \left[T_{T4} \left(1 - \frac{T_{10}}{T_{T4}} \right) - T_0 \left(\frac{T_{T3}}{T_0} - 1 \right) \right] \quad (F.10.6) \end{aligned}$$

DERIVATION F.10 (Continued)

However for isentropic flow

$$\frac{T_{T3}}{T_{10}} = \left(\frac{P_{T3}}{P_0} \right)^{\frac{\gamma - 1}{\gamma}} \quad (F.10.7)$$

$$\frac{T_{T4}}{T_0} = \left(\frac{P_{T4}}{P_{10}} \right)^{\frac{\gamma - 1}{\gamma}} = \left(\frac{P_{T3}}{P_0} \right)^{\frac{\gamma - 1}{\gamma}} \quad (F.10.8)$$

since for an ideal process

$$P_{T3} = P_{T4}$$

and

$$P_{10} = P_0$$

Substituting Equations F.10.8 and F.10.7 into Equation F.10.6 and subtracting v_0^2 ,

$$v_{10}^2 = 2gJ C_p \left\{ T_{T4} \left[1 - \left(\frac{P_0}{P_{T3}} \right)^{\frac{\gamma - 1}{\gamma}} \right] - \left[T_0 \left(\frac{P_{T3}}{P_0} \right)^{\frac{\gamma - 1}{\gamma}} - 1 \right] \right\} v_0^2 \quad (F.10.9)$$

Note

$$\frac{P_{T3}}{P_0} = \frac{P_{T3}}{P_{T2}} \cdot \frac{P_{T2}}{P_{T1}} \cdot \frac{P_{T1}}{P_0} = CR \left(1 + \frac{\gamma - 1}{\gamma} M_0^2 \right) = CR f(M)$$

The last term is the ram recovery, $f(M)$

DERIVATION F.10 (Continued)

Solving for V_{10} ; $T_{T4} = TIT$ in Equation F.10.9,

$$V_{10} = \sqrt{2gJ C_p \left\{ TIT \left[1 - \left(\frac{1}{CR f(M)} \right)^{\frac{\gamma-1}{\gamma}} \right] - T_0 \left[\left(CR f(M) \right)^{\frac{\gamma-1}{\gamma}} - 1 \right] \right\} V_0^2} \quad (F.10.10)$$

Hence from Equations F.10.1 and F.10.10

$$F_n = \frac{W_a}{g} \left[\sqrt{2gJ C_p \left\{ TIT \left[1 - \left(\frac{1}{CR f(M)} \right)^{\frac{\gamma-1}{\gamma}} \right] - T_0 \left[\left(CR f(M) \right)^{\frac{\gamma-1}{\gamma}} - 1 \right] \right\} V_0^2} - V_0 \right] \quad (F.10.11)$$

$$= f(TIT, CR, M_0, T_0)$$